

Dissertation
zur Erlangung des Doktorgrades
der Fakultät für Chemie und Pharmazie
der Ludwig-Maximilians-Universität München



**Hydrogen Atom Transfer:
A Comprehensive Study on Phenoxy, Peptide, and N-Radicals**

Salavat Ashirbaev

aus

Sibai, Russland

2023

Erklärung

Diese Dissertation wurde im Sinne von § 7 der Promotionsordnung vom 28. November 2011 von Herrn Prof. Dr. Hendrik Zipse betreut.

Diese Dissertation wurde eigenständig und ohne unerlaubte Hilfe erarbeitet.

München, 06.09.23

Salavat Ashirbaev

Dissertation eingereicht am 06.09.23.

1. Gutachter: Prof. Dr. Hendrik Zipse
2. Gutachter: Prof. Dr. Oliver Trapp

Mündliche Prüfung am 31.10.23.

Acknowledgement

I would like to express my deepest gratitude to Prof. Dr. Henrik Zipse for an offered place in his research group back in 2018, for his scientific support and for the inspiration I got after hours of discussing our joint research projects (with a lot of coffee and cookies, for sure).

I am very thankful to my old and new colleagues, with whom I have travelled this path together, for their smart ideas as well as relevant criticism. In the end, it was a good time together.

I cannot express my gratitude in words to my family, for their love and support. It would not be possible without them, without all their help, so I dedicate this thesis to them all.

Contents

0. Summary	8
1. Combined <i>in silico</i> and <i>in vitro</i> Investigations of Hydrogen Atom Transfer Reactivity in the Amination of Pyrogallol-Based Polyphenols	11
1.1 Introduction.....	11
1.1.1. Flavonoids.....	11
1.1.2. Amination of Phenols	13
1.1.3. Polyphenol-Amine Oxidative Coupling	17
1.1.4. Flavonoids under Biomimetic Conditions	21
1.1.5. References.....	26
1.2. Combined <i>in silico</i> and <i>in vitro</i> Approaches to Uncover the Oxidation and Schiff Base Reaction of Baicalein as an Inhibitor of Amyloid Protein Aggregation.....	29
1.2.1. Supporting information.....	45
1.3. Combined <i>in silico</i> and <i>in vitro</i> Studies of the Amination of Baicalein and its Analogs ..	92
1.3.1. Introduction.....	93
1.3.2. Mechanistic Studies on the Oxidative Coupling.....	93
1.3.3. Variations of the Polyol Electrophile.....	97
1.3.4. Variations of the Amine Nucleophile	101
1.3.5. Conclusion	102
1.3.6. Outlook	103
1.3.7. Supporting information.....	105
2. Dipeptide C-H Bond Reactivity and Selectivity in Hydrogen Atom Transfer to Alkoxy Radicals	265
2.1. Introduction.....	266
2.2. Results and Discussions	271
2.2.1. Laser Flash Photolysis Experiments	271
2.2.2. Hydrogen Abstraction Reaction from Glycine and Alanine Dipeptide Models	274
2.2.3. Aliphatic Chain/Functional Groups Influence on HAT Reaction.....	285
2.3. Conclusions.....	287
2.4. Outlook	288
2.5. References.....	291
2.6. Supporting information.....	293
2.6.1. Synthesis of Oxidants, Reagents and Reaction Products.....	294
2.6.2. Laser Flash Photolysis Experiment.....	323
2.6.3. Oxidative Stress Reactions of AcGlyNMe (1a), AcAlaNMe (1b) and AcNMe (1c)	326

2.6.4. Oxidation Stress Reaction of Ac-AA-NMe (1d-g) and Ac-AA-OMe (14a-c).....	362
2.6.5. Analytical Data of the Oxidative Stress Reactions	371
2.6.6. NMR Spectra of the Synthesized Compounds.....	393
2.6.7. References.....	423
3. The Effects of Ring Annulation on the Regioselectivity of the Hydrogen Atom Transfer in the Hofmann-Löffler-Freytag Reaction	425
3.1. Introduction.....	426
3.2. Results and Discussions	428
3.3. Outlook	432
3.4. References.....	433
3.5. Supporting Information.....	434
3.5.1. Conformational Analysis and Reaction Energies	434
3.5.2. General Procedure for Fan Variation of HLF Reaction.....	460
3.5.3. Synthesis and Analytical Data for Reagents and Products	461
3.5.4. References:.....	478

List of Publications

Parts of this thesis have been published as follows:

S. S. Ashirbaev, N. F. Brás, H. Zipse, *Chem. Eur. J.* **2022**, 28, e202104240.

Other publications:

1. A. A. Zemtsov, S. S. Ashirbaev, V. V. Levin, V. A. Kokorekin, A. A. Korlyukov, A. D. Dilman, *J. Org. Chem.* **2019**, 84, 15745-15753.
2. S. S. Ashirbaev, V. V. Levin, M. I. Struchkova, A. D. Dilman, *J. Org. Chem.* **2018**, 83, 478-483.
3. S. S. Ashirbaev, V. V. Levin, M. I. Struchkova, A. D. Dilman, *Fluorine notes*, **2017**, 1-2.
4. S. S. Ashirbaev, V. V. Levin, M. I. Struchkova, A. D. Dilman, *J. Fluorine Chem.* **2016**, 191, 143-148
5. L. L. Fershtat, S. S. Ashirbaev, A. S. Kulikov, V. V. Kachala, N. N. Makhova, *Mendeleev Commun.* **2015**, 25, 257-259.

0. Summary

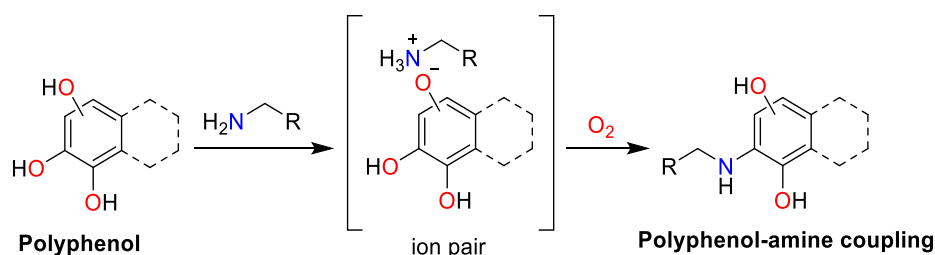
This thesis consists of three primary sections. In the first chapter, we examine the function of HAT in the interaction between polyphenols and amines. In the second chapter, we explore the selectivity of HAT in dipeptide models. Lastly, in the third chapter, we dive into the selectivity of HAT concerning N-radicals. Due to diversity of the given topics, each chapter starts with an introductory subchapter that helps to provide the reader with a solid foundation for the better understanding.

Chapter 1

Combined *in silico* and *in vitro* Investigations of Hydrogen Atom Transfer Reactivity in Amination of Polyphenols

Salavat S. Ashirbaev, Natércia F. Brás, Hendrik Zipse

Dept. Chemistry, LMU Muenchen, Butenandtstrasse 5-13, D-81377 Muenchen, Germany



Natural polyphenols have gained significant attention due to their wide range of biological activities, especially their role in the disaggregation of amyloid fibrils. In this study, we investigated the hydrogen atom transfer (HAT) reactivity in the amination of wide scope of different polyphenols, employing both *in silico* and *in vitro* approaches. Our aim was to show the underlying reaction mechanisms and identify important structural factors influencing the reactivity of these compounds with amines and amino acid as a peptide models. The results indicate the critical role of vicinal hydroxyl groups and the pyrogallol moiety in promoting the reactivity of the parent polyphenol. Also, the importance of electron-donating and withdrawing groups in the polyphenols was demonstrated. Our findings can provide valuable insights into the design of novel and more potent polyphenols targeting amyloid-related diseases.

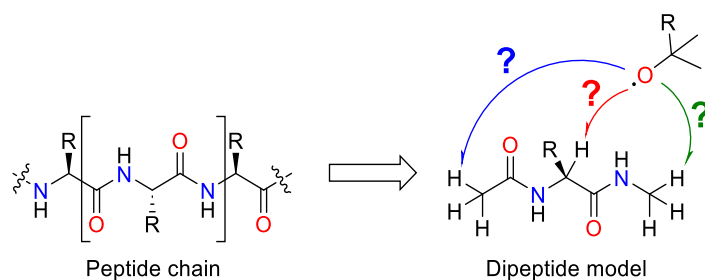
Chapter 2

Dipeptide C-H Bond Reactivity and Selectivity in Hydrogen Atom Transfer to Alkoxy Radicals

Salavat S. Ashirbaev^a, Harish Jangra^a, Michela Salamone^b, Massimo Bietti^b, Hendrik Zipse^a

^a*Dept. Chemistry, LMU Muenchen, Butenandtstrasse 5-13, D-81377 Muenchen, Germany*

^b*Dipartimento di Scienze e Tecnologie Chimiche, Università "Tor Vergata", Via della Ricerca Scientifica, 1, I-00133 Rome, Italy*



Understanding the C-H bond reactivity of amino acids within peptides is highly important for getting a general idea about protein stability, function, and possible chemical modification. In this study, we investigated the reactivity and selectivity of HAT reactions from dipeptide models to alkoxy radicals under controlled mild conditions. The results show that the C-H bond reactivity in dipeptide models is highly dependent on the steric effects, reaction media, and the nature of the alkoxy radical. Also, the C-H bond cleavage and recombination products were analyzed and identified with methods like GC-FID, NMR and HPLC. The structures of the obtained products were further confirmed by independent synthesis. Taken all together, these insights contribute to the fundamental understanding of dipeptide C-H bond reactivity and selectivity in HAT reactions from proteins.

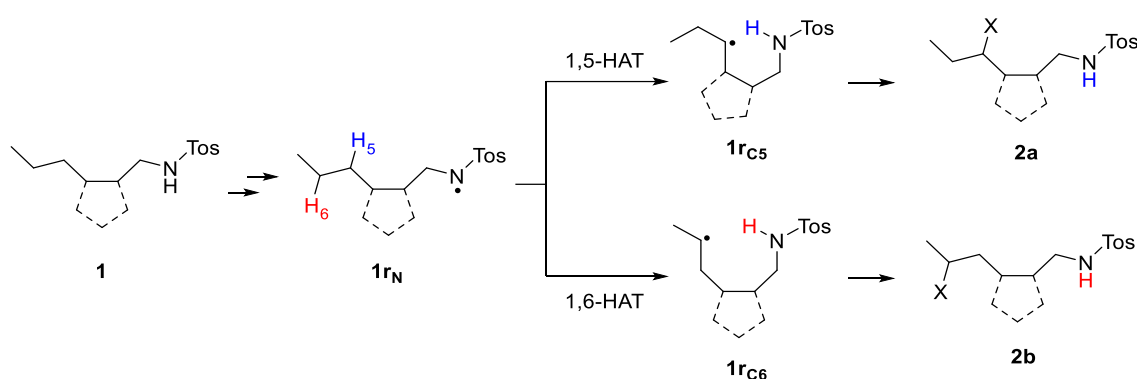
Chapter 3

The Effects of Ring Annulation on the Regioselectivity of the Hofmann-Löffler-Freytag Reaction

Salavat S. Ashirbaev^a, Davor Šakić^b, Hendrik Zipse^a

^aDept. Chemistry, LMU Muenchen, Butenandtstrasse 5-13, D-81377 Muenchen, Germany

^bUniversity of Zagreb, Faculty of Pharmacy and Biochemistry, Ante Kovačića 1, 10000 Zagreb, Croatia



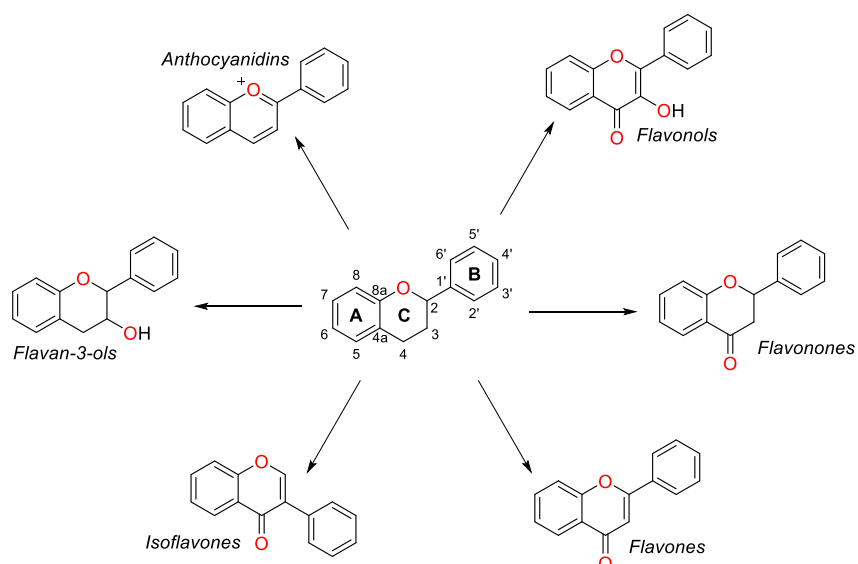
The Hofmann-Löffler-Freytag reaction provides an entry into aminyl-radical mediated C-H bond activation chemistry and has recently received renewed attention due to innovative methods for the generation of nitrogen-centered radicals. The reaction is particularly interesting in the functionalization of otherwise unfunctionalized substrates such as the sulfonamide **1**, where the initially generated N-centered radical **1r_N** is positioned such that hydrogen abstraction seems feasible at the C5- or C6-position. Currently known experimental results indicate a large kinetic preference for the 1,5-hydrogen atom transfer pathway. We now study here how this selectivity is affected by substituents positioned at the C3 and/or C4 positions, with particular emphasis on the effects of annulated ring systems along these positions.

1. Combined *in silico* and *in vitro* Investigations of Hydrogen Atom Transfer Reactivity in the Amination of Pyrogallol-Based Polyphenols

1.1 Introduction

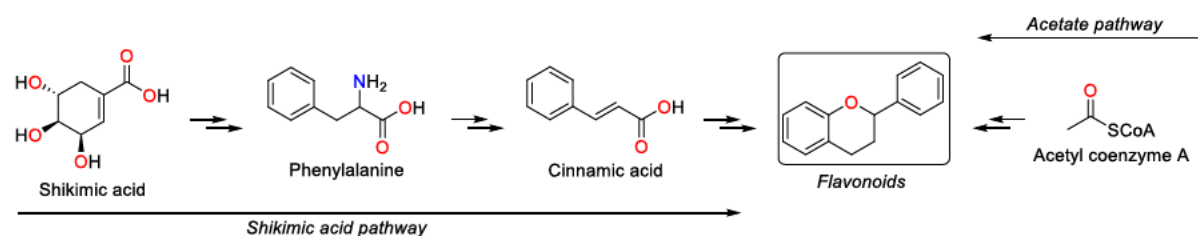
1.1.1. Flavonoids

Flavonoids, which have been known for their dyeing properties (from the Latin word *flavus*, meaning "yellow") for a long time, are a diverse class of natural low molecular weight polyphenolic compounds derived from various plant-based sources. Studies on flavonoids and their structure, properties and biological activities in living organisms were initiated in the 1930s, following the pioneering work of Albert Szent-Györgyi (Nobel Prize in Physiology or Medicine, 1937).^[1] So far, more than 8000 different types of flavonoids have been identified in the form of glycosides and aglycones.^[2] Flavonoids have a basic structure consisting of a 15-carbon skeleton, composed of two benzene rings (**A** and **B**) and a 3-carbon linking chain forming a heterocyclic pyran ring (**C**). Categorization of the flavonoids is based on the variations of the chemical structure: the presence of the double bond between the C2- and C3-atom and the carbonyl group located on C4, the attaching point of the ring **B**, and the degree of hydroxylation. Taking all of this into account, flavonoids can be divided in major subgroups: anthocyanidins, flavan-3-ols, isoflavones, flavanones, flavonols, and flavones (Scheme 1).



Scheme 1. Categorization of flavonoids based on chemical structure.

It is generally accepted that there are two basic pathways for the flavonoid backbone biosynthesis: the acetate and the shikimic acid pathways. Simple flavonoids are synthesized by plants, utilizing the acetate pathway, while the synthesis of more complex polyphenolic moieties requires the combination of both pathways (Scheme 2).^[3]



Scheme 2. Proposed mechanisms of flavonoid backbone biosynthesis.

Flavonoids are the most abundant group of polyphenolic compounds in the human/animal diet, that are commonly found in fruits/juices, vegetables, cereals, tea and wine.^[4] These polyphenols play a big role in biological reactions and their importance cannot be overestimated. Flavonoids act like "conventional" antioxidants, scavenging reactive oxygen species, and also influence the signal processing, due to specific interactions with regulatory proteins in living systems (Fig. 1).^[5]

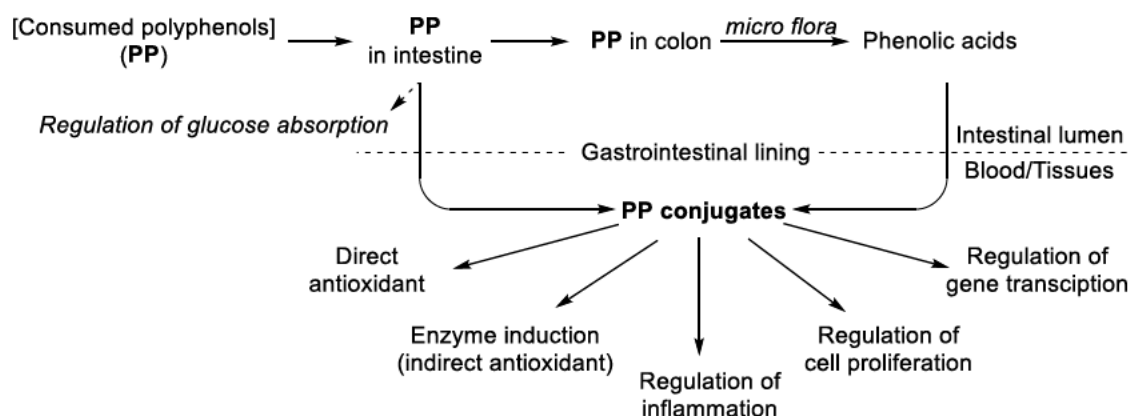
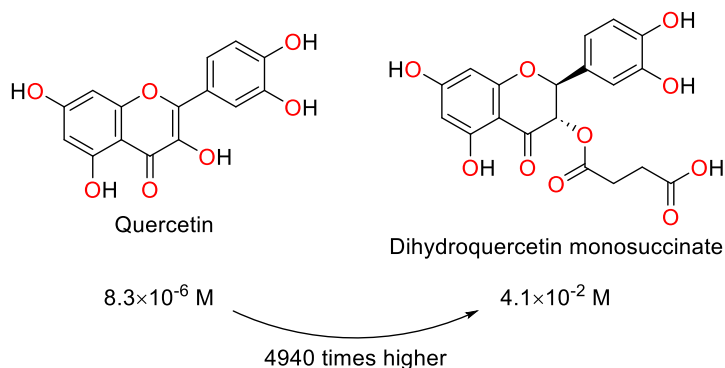


Fig. 1. Flavonoids and their metabolites are involved in various biological processes in living organisms.^[5]

Despite all the described beneficial properties of flavonoids, there are also some disadvantages of these compounds. Due to their low solubility in water, flavonoids and their glucosides have a short residence time in the intestine and limited absorption, which tend to minimize their potential medicinal and therapeutic effects. Therefore, increasing the oral bioavailability of insoluble flavonoids is one of the major topics in flavonoid-based drug design.^[6] For example, the water solubility of one of the most consumed flavonoids, quercetin

(25-50 mg/day), is only 8.3×10^{-6} M.^[7] Structural modification of this flavonoid significantly increases the water solubility and dihydroquercetin monosuccinate has a solubility ~5000 times higher than its parent flavonoid (4.1×10^{-2} M) (Scheme 3).^[8]

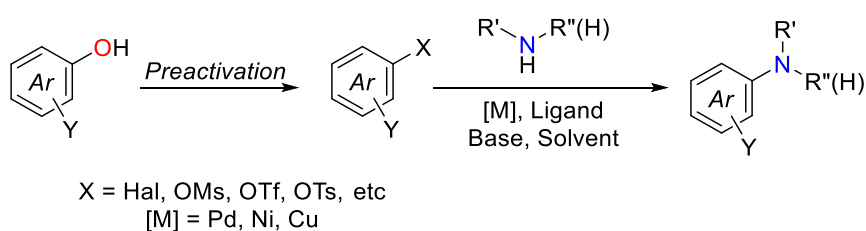


Scheme 3. Solubility of quercetin and its derivative, dihydroquercetin monosuccinate, in water.^[8]

Once flavonoids are digested, they have a high probability of cascade oxidation reactions and coupling with surrounding functional groups. In our studies, we have focused on various *N*-nucleophiles as models of the peptide environment surrounding a flavonoid and its metabolites. Understanding the reaction between flavonoids and peptide models can help to understand the fundamental chemical interactions happening in living organisms. But first, we have to review the existing literature information on the amination of phenols and small polyphenols as model substrates for flavonoids.

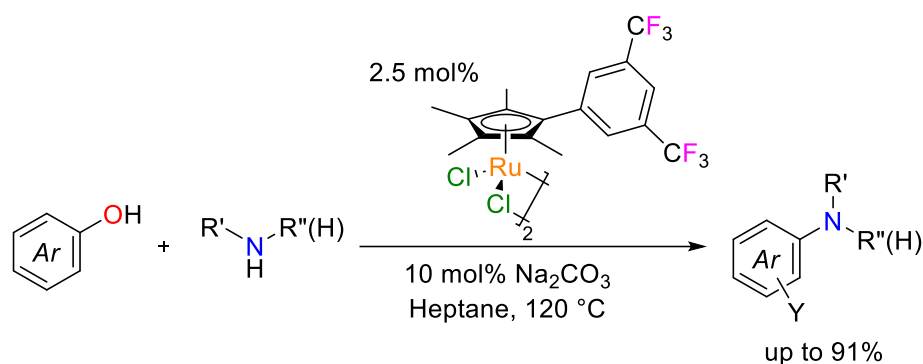
1.1.2. Amination of Phenols

The synthesis of anilines, commonly found in natural products, pharmaceuticals, functional materials, and agricultural chemicals, has become a significant area of interest in synthetic organic chemistry.^[9] Transition metal catalysed amination of aromatic compounds in various cross-coupling reactions was initiated by independent work of Buchwald and Hartwig in the 1990s.^[10] The wide scope of possible variations in reagents, metals, ligands, and other reaction parameters can be summarized in the general reaction (Scheme 4).^[11]



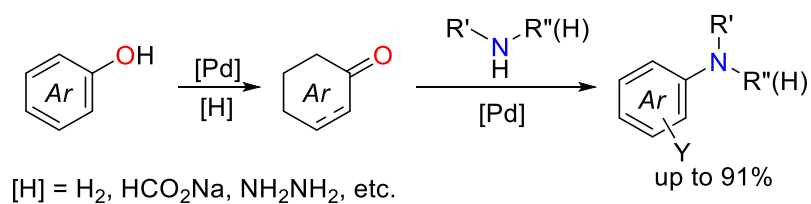
Scheme 4. Amination reaction mediated by transition metal catalysis.^[11]

Despite the significant progress made in the amination of aromatic compounds using transition metal catalysis for the last years, direct functionalization of phenols with amines is a challenging task. Phenols are mostly unsuitable for direct amination due to their oxidation, formation of stable transition metals complexes, and the high dissociation energy (>450 kJ/mol) of the Ph-OH bond.^[12] To overcome these difficulties, phenols have to be converted into more reactive functional groups, such as -OMs or -OTs, enabling further cross-coupling steps. Therefore, the most interesting reactions are those that directly functionalize phenols without any additional activation reactions or even without use of transition metals. The most interesting example of the first concept is the Ru-catalyzed direct amination reaction of phenols (Scheme 5).^[13]



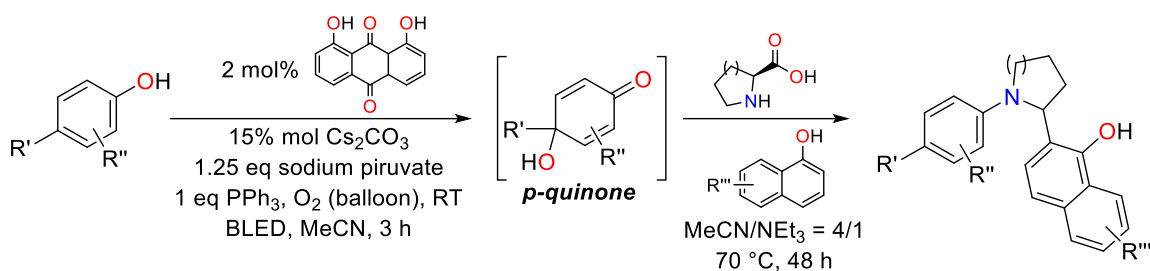
Scheme 5. Ru-catalysed direct amination of phenols.^[13]

Dearomatization/coupling/dehydrogenative aromatization strategy is an alternative approach for aniline synthesis directly from phenols.^[14] This method requires a transition metal catalyst (usually Pd), as well as the external source of hydrogen (Scheme 6).



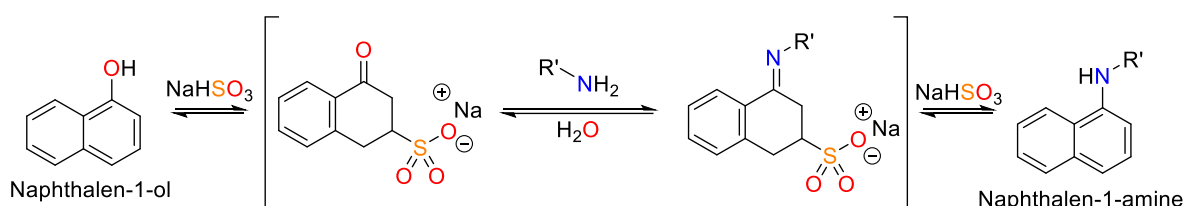
Scheme 6. Dearomatization/coupling/dehydrogenative aromatization synthesis of anilines.^[14]

Transition-metal-free dearomatization /coupling/dehydrogenative aromatization strategy has been reported for synthesizing a broad range of *p*-quinones, using an anthraquinone-based organophotocatalyst (Scheme 7).^[15]



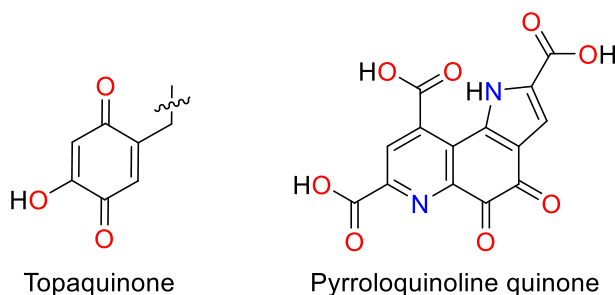
Scheme 7. Cross-coupling of phenols with amines via combined photooxidative dearomatization-rearomatization strategy.^[15]

Bucherer-Lepetit reaction is the well-known example of a phenol-amine coupling. The reaction does not require the use of transition metals or organocatalysts and involves only amine/ammonia and sodium bisulfite as reagents (Scheme 8). Although the Bucherer reaction is limited to naphthol derivatives, it has found general application in the preparation of a wide range of synthetic dyes.^[16]



Scheme 8. Bucherer-Lepetit reaction.^[16]

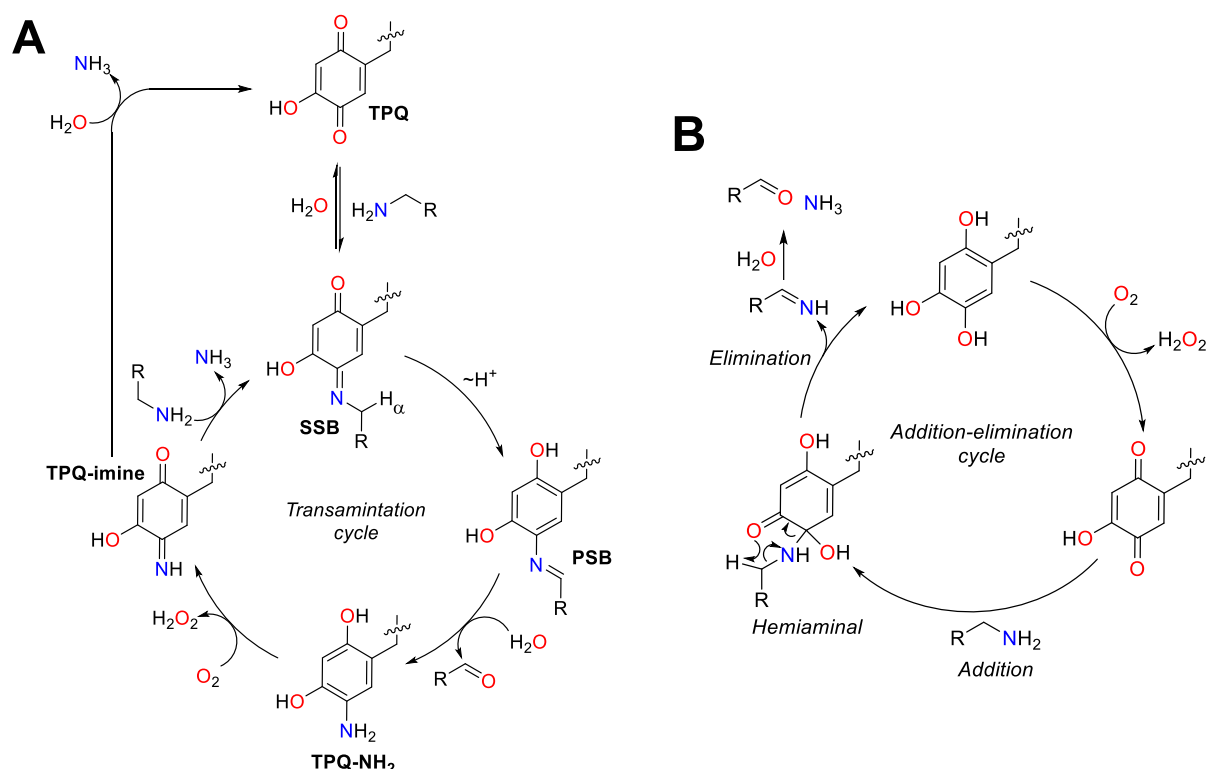
As was mentioned before, polyphenols are sensitive to oxidation. As a result, they can be easily converted into quinones, their oxidized forms, which have the potential to interact with neighboring functional groups.



Scheme 9. Structures of topaquinone (**TPQ**) and pyrroloquinoline quinone (**PQQ**).

In general, quinone cofactors like topaquinone (**TPQ**) and pyrroloquinoline quinone (**PQQ**) are found in various quinoproteins, which are involved in catalyzing the biological oxidation of amines and alcohols (Scheme 9).^[17]

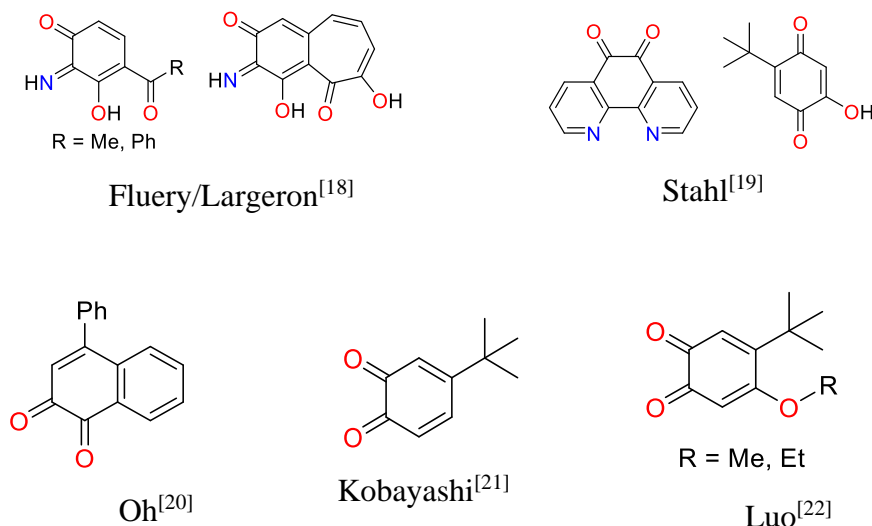
The following proposed mechanisms are represented in the example of **TPQ**. It is widely accepted that the primary amine oxidation mechanism proceeds *via* the transamination pathway **A**. Nucleophilic addition of an amine to **TPQ** forms the substrate Schiff base (**SSB**), which tautomerizes into the product Schiff base (**PSB**) after C $_{\alpha}$ -deprotonation. **PSB** then hydrolyses and releases an aldehyde and aminated adduct **TPQ-NH $_2$** , which is then oxidized to **TPQ-imine**. The formed **TPQ-imine** can then turn back into **TPQ** after a hydrolysis step or into **SSB** after an aminolysis process (Scheme 10).



Scheme 10. Two proposed mechanisms of **TPQ**-mediated amine oxidation.

One should keep in mind that there is an alternative pathway **B**, which involves the oxidation of the amine through a *hemiaminal intermediate* via an addition-elimination mechanism.^[17d] Therefore, it is important to consider both pathways during the investigation of the oxidation of amines in biological systems.

Significant effort has been made to mimic the reactivity of quinone cofactors *in vitro*, developing new series of synthetic quinones in organic synthesis (Scheme 11). The presented catalysts based on quinones are used in a wide range of organic reactions like amine or alcohol oxidation. Given the large number of articles on this topic, only selected references are given together with the corresponding catalysts shown in Scheme 11.

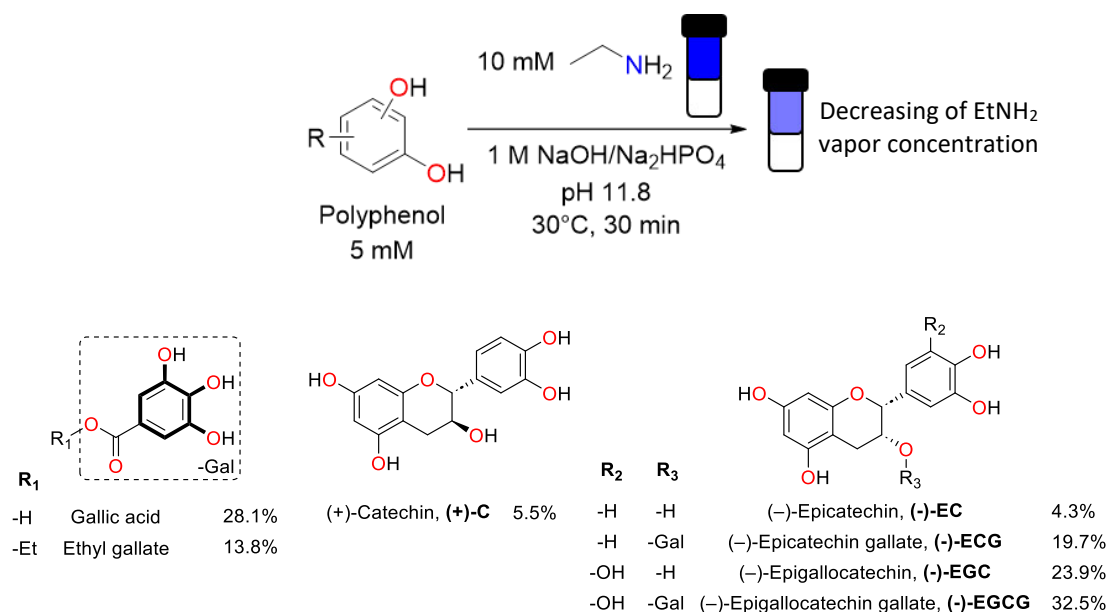


Scheme 11. Biomimetic quinone-based catalysts.

The literature analysis shows that the methods, reagents, and conditions used for phenol aminations lack the applicability to flavonoids and miss the biological relevance, therefore it is important to look for mild, transition metal-free and biomimetic reactions for flavonoid-peptide(amine) reactions. Polyphenol-amine reactions will be presented in the next chapter to get a better understanding of basic reactivity mechanism that has been already discovered.

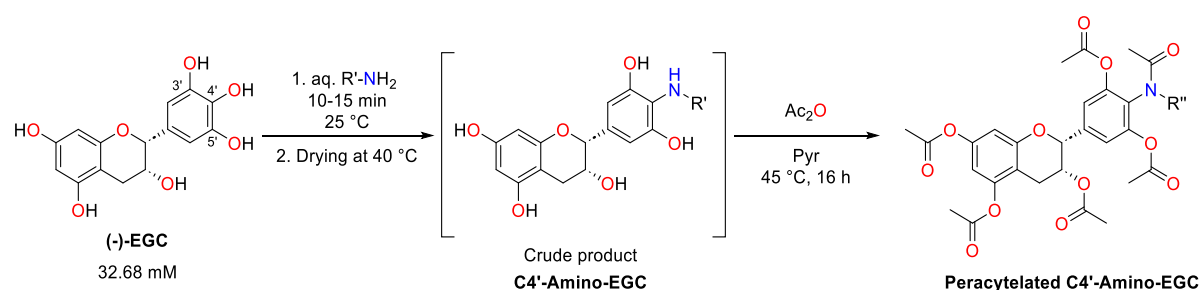
1.1.3. Polyphenol-Amine Oxidative Coupling

Deodorizing effects of polyphenols on amines have been tested in the past (Scheme 12).



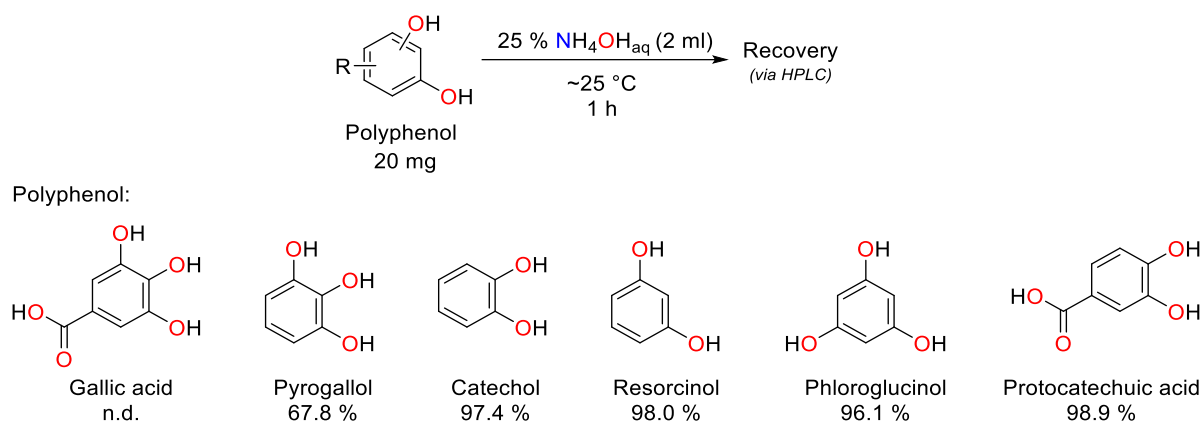
Scheme 12. Polyphenol structures. The pyrogallol moiety is shown in **bold**. Deodorizing activity on EtNH₂ is shown below the structures.^[23]

It was found that compounds with 1,2,3-trihydroxybenzene (*pyrogallol*), moiety in their structures show significantly higher deodorizing activity on EtNH₂ in 1 M NaOH/Na₂HPO₄ buffer solution (pH 11.8). Also, the represented catechins had no deodorizing activity on secondary and tertiary amines (e.g., Me₂NH or Et₃N).^[23] (-)-EGC, which showed relatively high deodorizing activity, was taken as a model compound, and treated respectively with excess of 40% MeNH₂, 70% EtNH₂, and 25% NH₄OH. The reaction was followed by HPLC, which showed the formation of one major product. Before isolation, the corresponding compounds (**C4'-amino-EGC**) were acetylated due to their high hydrophilicity. Analysis of the obtained peracetylated adduct showed that they all share the same C4'-regioselectivity (Scheme 13).^[23]



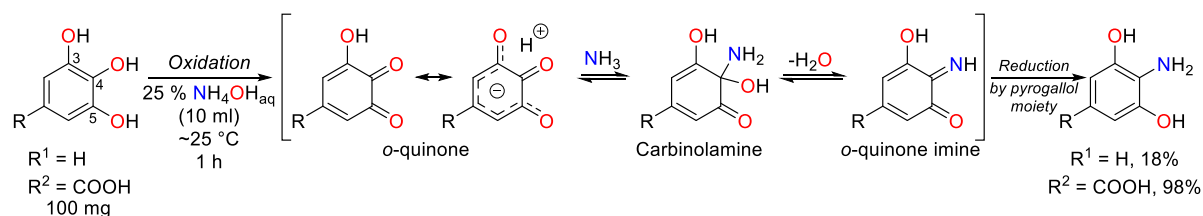
Scheme 13. Oxidative amination of (-)-EGC with aqueous solutions of ammonia and primary amines.^[23]

The importance of the pyrogallol moiety for the oxidative amination reaction was also demonstrated by *Ohara et al.*^[24] Various phenolic compounds were treated with excess of aqueous ammonia under air atmosphere and the percent recovery for each compound was tested (Scheme 14).



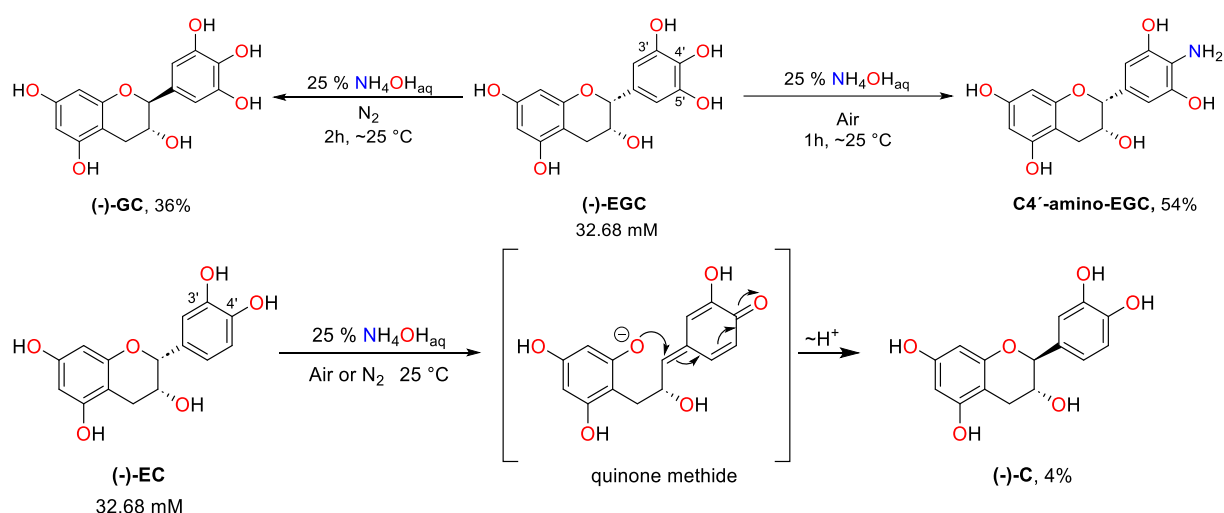
Scheme 14. Percent recovery of the phenolic compounds after NH₃ treatment under aerobic conditions.^[24]

The initial concentrations of gallic acid and pyrogallol were significantly affected by aqueous ammonia, in contrast to the other compounds, which showed a minor change. The main reaction products of gallic acid and pyrogallol were isolated and characterized. As well as in Scheme 13, the analysis showed the formation of C4'-amino adducts, 2-aminoresorcinol and 4-amino-3,5-dihydroxybenzoic acid, correspondingly (Scheme 15).



Scheme 15. Oxidative amination of gallic acid and pyrogallol in aqueous ammonia.^[24]

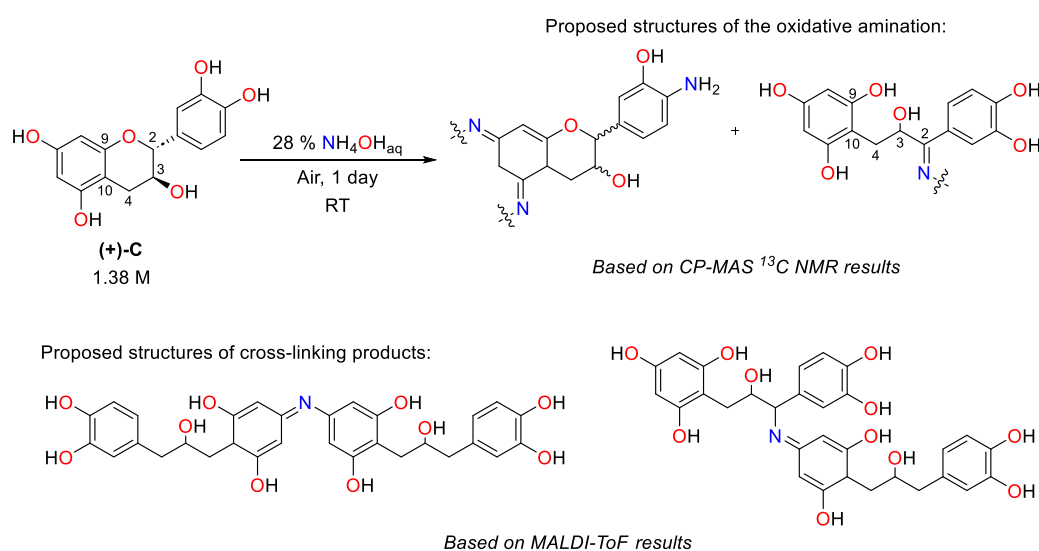
The proposed mechanism for the selective C4'-amination includes the formation of the *o*-quinone intermediate in the presence of nucleophile, NH₃, and oxidant, O₂. Regioselective nucleophilic attack of ammonia on the C4'-position of quinone forms a 4-carbinolamine intermediate, followed by water elimination to give the *o*-quinone imine. The next step is proposed to be a reducing reaction by another molecule of corresponding polyphenol, yielding C4'-amino adducts. The crucial role of oxygen was demonstrated in the article, because no C4'-amino adducts were detected under N₂ in independent experiments. More complex substances, (-)-EC and (-)-EGC, were treated with aqueous ammonia under the same conditions.



Scheme 16. Reactions of (-)-EC and (-)-EGC affected by aqueous ammonia.^[25]

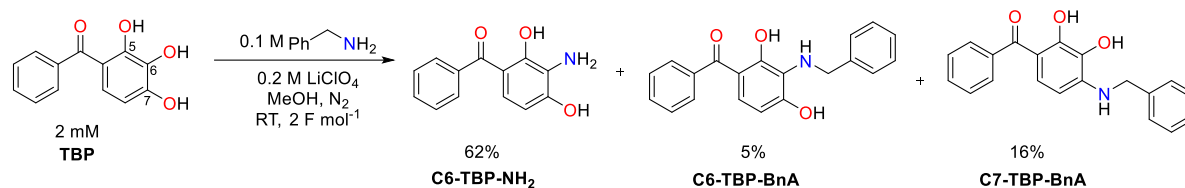
Similarly to gallic acid and pyrogallol, oxidative amination of (-)-EGC leads to formation of C4'-amino-epigallocatechin. It has been shown that (-)-EGC epimerizes process under inert gas atmosphere, forming (-)-galocatechin, (-)-GC. (-)-EC, on one side, does not form an amino adduct, but, on the other side, also epimerizes under basic conditions, giving (-)-catechin, (-)-C (Scheme 16). Observed epimerization reaction, on the example of compound (-)-EC, supposedly occurs through opening of the pyran ring, which gives a *quinone methide* intermediate, followed by intra- or intermolecular attack.^[25]

Products of the intermolecular coupling are detected in highly concentrated solutions of polyphenol, (+)-catechin, (+)-C, in concentrated aqueous ammonia.^[26] Unfortunately, the exact structures of the products are not provided, due to increased complexity of the formed amino adducts, but structural proposals have been made based on the combined results of solid-state ¹³C NMR and MALDI-ToF analysis (Scheme 17).



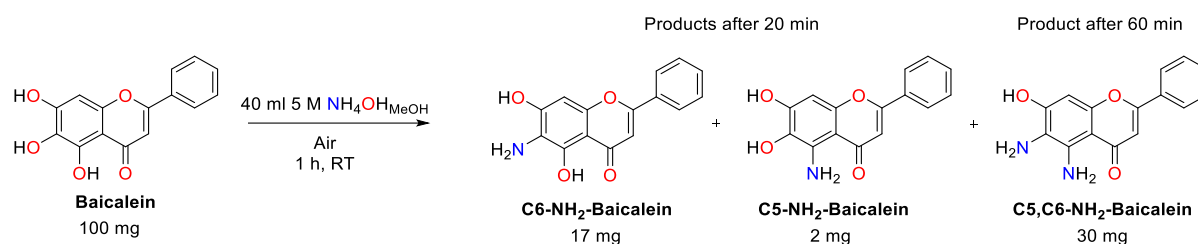
Scheme 17. Reactions of (+)-C with aqueous ammonia.^[26]

Electrochemical coupling of 2,3,4-trihydroxybenzophenone (**TBP**) with benzyl amine under the conditions of excessive oxidation has been studied. The product analysis showed that the main product was the result of C6-NH₂-functionalization. Also the formation of two minor by-products, **C6-TBN-BnA** and **C7-TBN-BnA**, were detected as a result of reductive coupling (Scheme 18).^[27]



Scheme 18. Electrochemical coupling of 2,3,4-trihydroxybenzophenone (TBP) with benzyl amine.^[27]

Studying the potential of baicalein to detoxify ammonia and treat ammonia-associated diseases, it was shown that baicalein forms three different products of oxidative coupling with ammonia (Scheme 19).^[28]



Scheme 19. Reactions of baicalein in methanolic solution of ammonia.

Literature analysis shows that polyphenols containing a pyrogallol moiety show enhanced reactivity towards primary amines. This could potentially explain the biological activity of certain natural polyphenolic compounds that extends beyond oxygen species scavenging activity or non-covalent interaction. The interaction of polyphenols with biologically relevant substrates will be discussed in the following chapter.

1.1.4. Flavonoids under Biomimetic Conditions

With thousands of flavonoids known to exist, each with unique structure and biological activities, it is impossible to study them all in details. Therefore, recent literature results will be reviewed in this chapter.

During amyloidosis, specific proteins misfold and aggregate, leading to the accumulation of insoluble fibrillar deposits known as amyloid fibrils in various tissues and organs. Amyloid fibril formation is linked to cellular dysfunction, tissue damage, and organ failure in numerous diseases, such as Alzheimer's, Parkinson's, type 2 diabetes, and systemic amyloidosis.^[29] For example, Fig. 2 illustrates the timeline of human islet amyloid polypeptide (hIAPP) fibril formation, which, in extreme cases, leads to the death of β -pancreatic cells and triggers severe symptoms associated with type 2 diabetes.^[30]

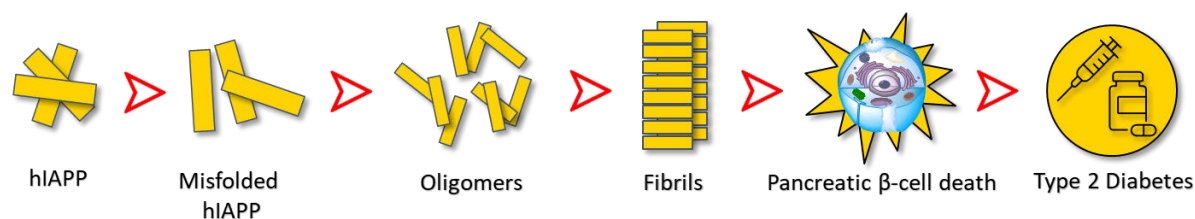
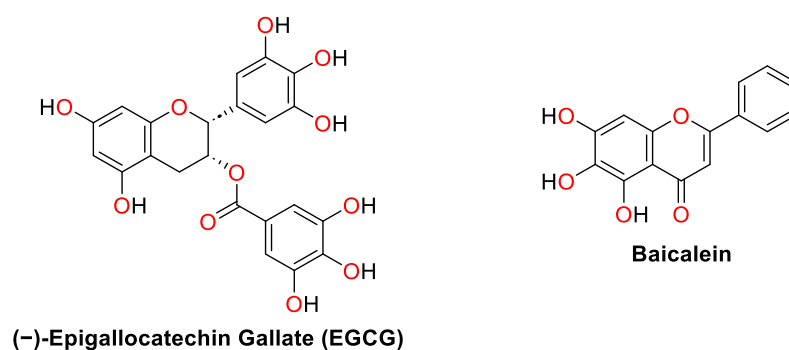


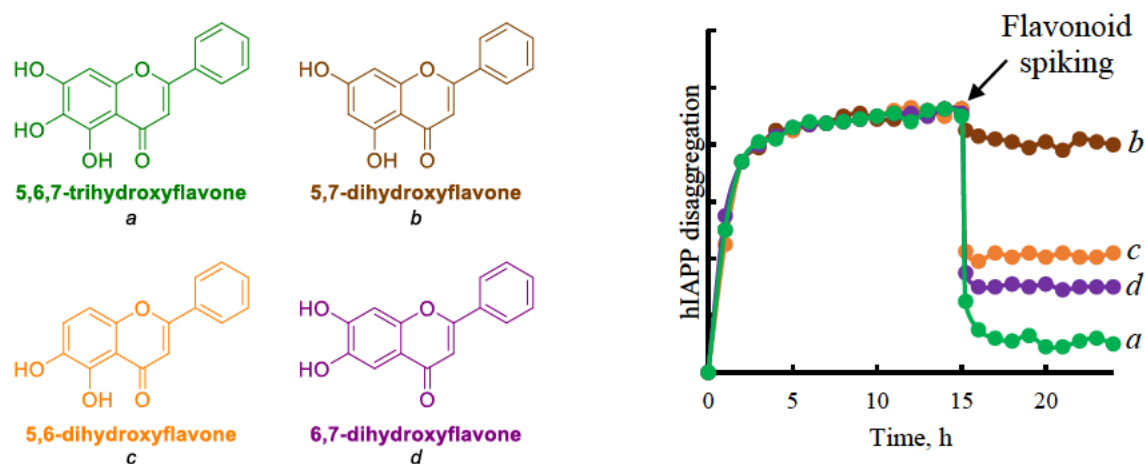
Fig. 2. Mechanism of amyloid formation on the example of **hIAPP**.^[30]

(-)-Epigallocatechin gallate, **EGCG**, has been found to show anti-amyloidogenic effects by inhibiting the formation of amyloid fibrils of **iAPP** and promoting the disaggregation of pre-formed fibrils (Scheme 20).^[31] These interactions are considered to be non-covalent, since the experiments on **EGCG** with another amyloidogenic proteins like α -synuclein/A β 42 show no formation of covalent adducts *via* ESI-MS analysis.^[32] It has been reported that baicalein, like **EGCG**, is a potent inhibitor of **hIAPP** amyloids.



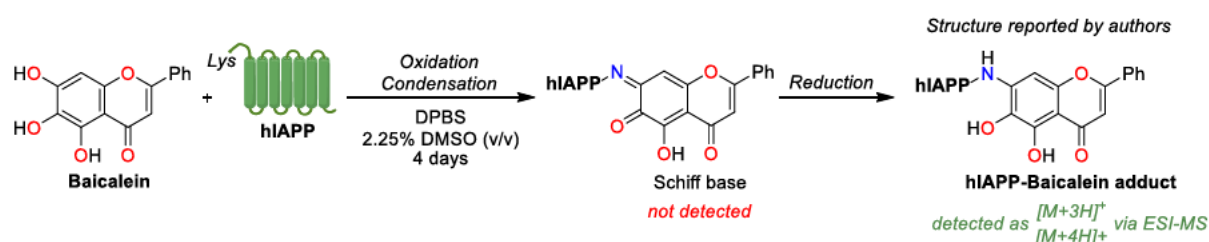
Scheme 20. The most potent natural flavonoids against **hIAPP** amyloidosis.

Baicalein and its analogues were compared for their ability to disaggregate the fibrils. In the experiment, **hIAPP** was allowed to form aggregates for 15 hours, then the incubated mixture was spiked with certain amounts of flavonoids (Scheme 21). Baicalein, **5,6,7-trihydroxyflavone**, showed almost complete disaggregation of the pre-formed fibrils (green line). **5,6-** and **6,7-dihydroxyflavones**, which can be oxidized to their o-quinone forms, showed moderate disaggregating properties (orange and purple lines, correspondingly), while **5,7-dihydroxyflavone** did not affect the fibrils (brown line). The results indicated that the vicinal phenoxy groups play a crucial role in the process of disaggregation.^[33]



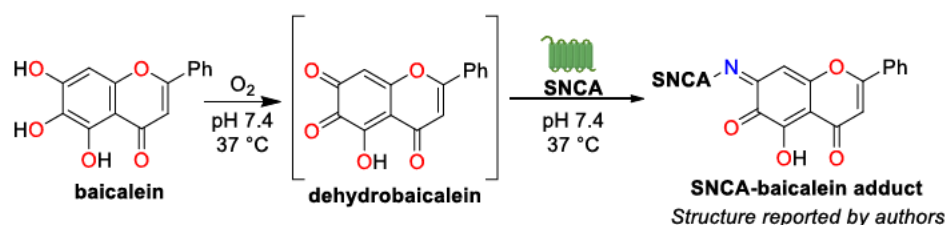
Scheme 21. Thioflavin T fluorescence-based assay showing amyloid formation and flavonoid spiking after 15 h and the resulting complete or partial disaggregation of the aggregates.^[33]

It has also been demonstrated that a covalent adduct is formed between **hIAPP** and baicalein via UPLC-ESI(MS) analysis (Scheme 22).^[33]



Scheme 22. Proposed reaction of baicalein-**hIAPP** interaction.^[33]

Baicalein can also inhibit fibrillation of α -synuclein, peptide associated with Parkinson disease. It inhibits the fibril formation, as well as disaggregates already existing ones, resulting in the formation of water-soluble oligomer of α -synuclein. It is hypothesized that oxidized baicalein covalently binds to the protein, forming a Schiff base with a lysine side chain, which disrupts the fibril folding (Scheme 23).^[34]



Scheme 23. Proposed mechanism of baicalein- α -synuclein interaction.^[34a]

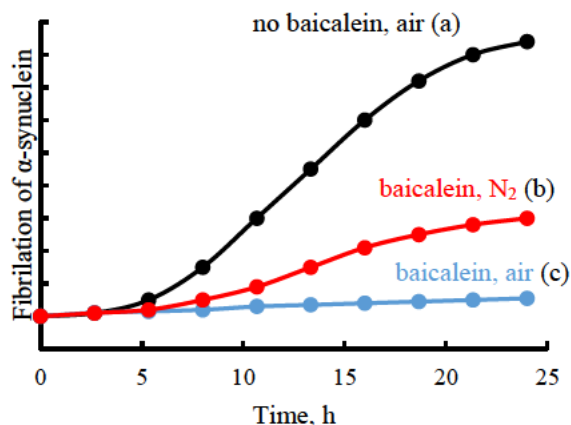
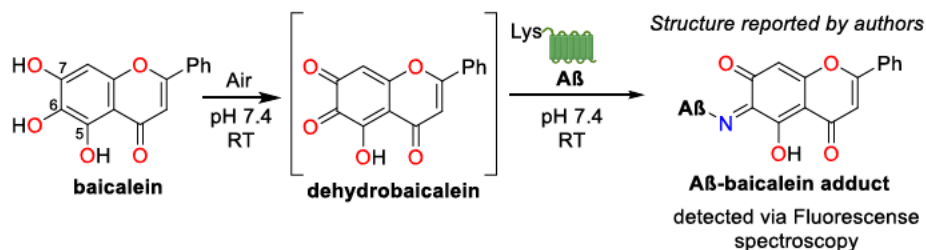


Fig. 3. Fibrillation of α -synuclein under different conditions. Fibril formation was monitored by the intensity of thioflavin T fluorescence.^[34a]

The role of baicalein oxidation has been investigated, which demonstrated that it was not baicalein itself inhibiting the fibril formation, but its oxidized form, dehydrobaicalein, because under anaerobic conditions (N_2 atmosphere, 10 min N_2 -bubbling), the efficiency of baicalein disaggregation property dramatically drops down (Fig. 3, black (a) vs red (b) line). While under air, no fibrillation was detected (blue (c) line).^[34a] These results were further confirmed in another study, which

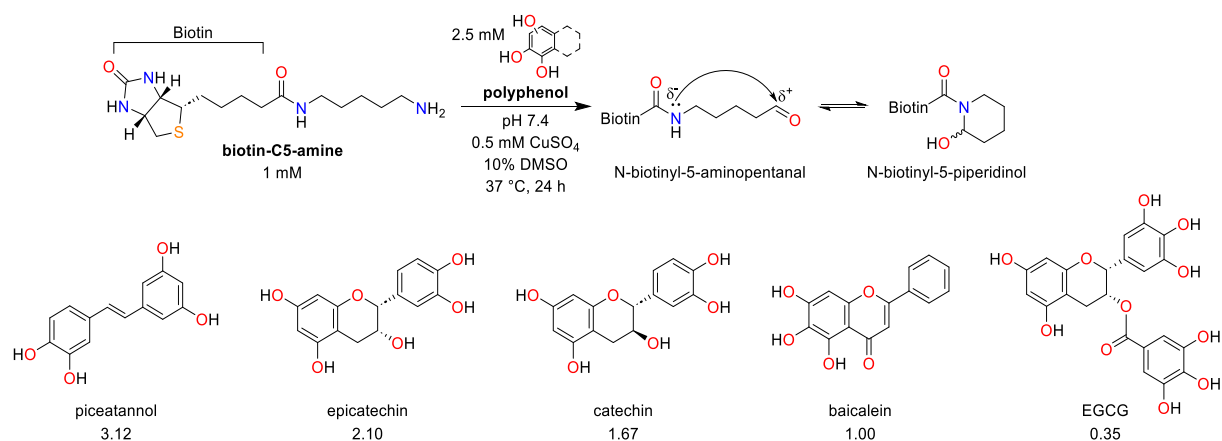
demonstrated that baicalein acts as an effective compound in the inhibition of fibrillation of α -synuclein and $A\beta_{1-42}$ in both early and late stages.^[35]

Schiff base formation between baicalein and lysine residue of $A\beta_{1-42}$ is considered to be detected by the methods of fluorescence and synchronous fluorescence.^[36] Unlike the other examples described above, the authors have speculated of the C6-regioselectivity of the $A\beta$ -baicalein adduct (Scheme 24).



Scheme 24. Possible interaction of lysine residue in $A\beta_{1-42}$ with baicalein.^[36]

The Cu^{2+} -mediated oxidative deamination activity of several polyphenols was investigated using LC-ESI-MS.^[37] Biotin-C5-amine was taken as a lysine model and it has been shown that picatannol had the biggest effect on its deamination process, followed by catechin, epicatechin and baicalein (Scheme 25).



Scheme 25. A proposed mechanism of the oxidative deamination of biotin-C5-amine by polyphenols. The most potent polyphenols are represented below with their relative efficiencies.^[37]

Surprisingly, **EGCG** showed only a small effect relatively to baicalein. Nevertheless, the authors stated that *o*-catechol-containing polyphenols have considerable lysyl-oxidase-like ability via a Cu²⁺/catechol driven mechanism.

In this introduction, we explore the complex interactions between polyphenols and amines. A comprehensive analysis of existing literature, we have identified knowledge gaps and inconsistencies, particularly concerning flavonoid and peptide interactions. Our study aims to provide significant insights into flavonoid-amine interactions, thereby contributing to a deeper understanding of their functional roles and implications in various chemical and biological conditions.

1.1.5. References

- [1] a) A. Bentsáth, S. T. Ruzsnyák, A. Szent-Györgyi, *Nature* **1936**, *138*, 798-798; b) S. T. Ruzsnyák, A. Szent-Györgyi, *Nature* **1936**, *138*, 27-27.
- [2] G. B. Gonzales, K. Raes, S. Coelus, K. Struijs, G. Smagghe, J. Van Camp, *J. Chromatogr. A* **2014**, *1323*, 39-48.
- [3] M. Wiciński, J. Gębalski, E. Mazurek, M. Podhorecka, M. Śniegocki, P. Szychta, E. Sawicka, B. Malinowski, *Nutrients*, *12*, **2020**, 350.
- [4] J. P. Spencer, *Br. J. Nutr.* **2008**, *99E (Suppl 1)*, 60-77.
- [5] D. E. Stevenson, R. D. Hurst, *Cell. Mol. Life Sci.* **2007**, *64*, 2900-2916.
- [6] J. Zhao, J. Yang, Y. Xie, *Int. J. Pharm.* **2019**, *570*, 118642.
- [7] a) K. Srinivas, J. W. King, L. R. Howard, J. K. Monrad, *J. Food Eng.* **2010**, *100*, 208-218; b) J. V. Formica, W. Regelson, *Food Chem. Toxicol.* **1995**, *33*, 1061-1080.
- [8] E. E. Zolotarev, A. V. Kashevskii, B. N. Bazhenov, B. L. Finkelshtein, A. Y. Safronov, *Electrochem. Commun.* **2014**, *45*, 23-26.
- [9] A. J. Burke, C. S. Marques, *Catalytic arylation methods: from the academic lab to industrial processes*, John Wiley & Sons, **2015**.
- [10] a) J. P. Wolfe, S. L. Buchwald, *J. Org. Chem.* **1997**, *62*, 1264-1267; b) J. Louie, M. S. Driver, B. C. Hamann, J. F. Hartwig, *J. Org. Chem.* **1997**, *62*, 1268-1273.
- [11] a) R. Jana, T. P. Pathak, M. S. Sigman, *Chem. Rev.* **2011**, *111*, 1417-1492; b) M. Marin, R. J. Rama, M. C. Nicasio, *Chem. Rec.* **2016**, *16*, 1819-1832; c) C. M. Lavoie, M. Stradiotto, *ACS Catal* **2018**, *8*, 7228-7250; d) R. Dorel, C. P. Grugel, A. M. Haydl, *Angew. Chem. Int. Ed.* **2019**, *58*, 17118-17129.
- [12] a) C. Di Bugno, M. Pasquali, P. Leoni, P. Sabatino, D. Braga, *Inorg. Chem.* **1989**, *28*, 1390-1394; b) J. Pedley, R. Naylor, S. Kirby, P. Francis, *Thermochemical data of organic compounds* (2nd edition), Elsevier, **1987**.
- [13] K. Chen, Q.-K. Kang, Y. Li, W.-Q. Wu, H. Zhu, H. Shi, *J. Am. Chem. Soc.* **2022**, *144*, 1144-1151.
- [14] a) T. Ichitsuka, I. Takahashi, N. Koumura, K. Sato, S. Kobayashi, *Angew. Chem. Int. Ed.* **2020**, *59*, 15891-15896; b) Z. Chen, H. Zeng, S. A. Girard, F. Wang, N. Chen, C.-J. Li, *Angew. Chem. Int. Ed.* **2015**, *54*, 14487-14491; c) Y. Lang, C.-J. Li, H. Zeng, *Synlett* **2020**, *32*, 429-435.
- [15] A. Afanasenko, A. Kavun, D. Thomas, C.-J. Li, *Chem. Eur. J.* **2022**, *28*, e202200309.
- [16] a) N. L. Drake, *Org. React.* **2004**, *1*, 63-90; b) H. Seeboth, *Angew. Chem. Int. Ed. Engl.* **1967**, *6*, 307-317.

- [17] a) C. Anthony, M. Ghosh, C. Blake, *Biochem. J.* **1994**, *304*, 665; b) A. Lang, J. P. Klinman, *eLS* **2001**; c) C. Anthony, *Biochem. J.* **1996**, *320*, 697-711; d) C. Qiao, K.-Q. Ling, E. M. Shepard, D. M. Dooley, L. M. Sayre, *J. Am. Chem. Soc.* **2006**, *128*, 6206-6219.
- [18] a) M. Largeton, M.-B. Fleury, *Chem. Eur. J.* **2017**, *23*, 6763-6767; b) M. Largeton, P. Deschamps, K. Hammad, M.-B. Fleury, *Green Chem.* **2020**, *22*, 1894-1905; c) M. Largeton, M.-B. Fleury, *Angew. Chem. Int. Ed.* **2012**, *51*, 5409-5412.
- [19] a) B. Li, A. E. Wendlandt, S. S. Stahl, *Org. Lett.* **2019**, *21*, 1176-1181; b) A. E. Wendlandt, S. S. Stahl, *Org. Lett.* **2012**, *14*, 2850-2853; c) A. E. Wendlandt, S. S. Stahl, *J. Am. Chem. Soc.* **2014**, *136*, 506-512.
- [20] a) T. Si, H. Y. Kim, K. Oh, *Chem. Eur. J.* **2021**, *27*, 18150-18155; b) T. Si, H. Cho, H. Y. Kim, K. Oh, *Org. Lett.* **2022**, *24*, 8531-8535; c) J. Baek, T. Si, H. Y. Kim, K. Oh, *Org. Lett.* **2022**, *24*, 4982-4986.
- [21] H. Yuan, W.-J. Yoo, H. Miyamura, S. Kobayashi, *J. Am. Chem. Soc.* **2012**, *134*, 13970-13973.
- [22] a) Y. Qin, L. Zhang, J. Lv, S. Luo, J.-P. Cheng, *Org. Lett.* **2015**, *17*, 1469-1472; b) R. Zhang, Y. Qin, L. Zhang, S. Luo, *Org. Lett.* **2017**, *19*, 5629-5632.
- [23] K. Kida, M. Suzuki, A. Takagaki, F. Nanjo, *Biosci. Biotechnol. Biochem.* **2002**, *66*, 373-377.
- [24] K. Hashida, R. Makino, S. Ohara, *Holzforchung* **2009**, *63*, 319-326.
- [25] a) K. Hashida, S. Ohara, *J. Wood Chem. Technol.* **2002**, *22*, 11-23; b) K. Hashida, S. Ohara, R. Makino, *J. Wood Chem. Technol.* **2003**, *23*, 227-232.
- [26] F. Braghiroli, V. Fierro, A. Pizzi, K. Rode, W. Radke, L. Delmotte, J. Parmentier, A. Celzard, *Ind. Crops Prod.* **2013**, *44*, 330-335.
- [27] M. Largeton, M.-B. Fleury, *J. Org. Chem.* **2000**, *65*, 8874-8881.
- [28] S. Zhang, R. Wang, Y. Zhao, F. S. Tareq, S. Sang, *Chem. Res. Toxicol.* **2020**, *33*, 2181-2188.
- [29] F. Chiti, C. M. Dobson, *Annu. Rev. Biochem* **2017**, *86*, 27-68.
- [30] P. Westermark, A. Andersson, G. T. Westermark, *Physiol. Rev.* **2011**, *91*, 795-826.
- [31] F. Meng, A. Abedini, A. Plesner, C. B. Verchere, D. P. Raleigh, *Biochemistry* **2010**, *49*, 8127-8133.
- [32] D. E. Ehrnhoefer, J. Bieschke, A. Boeddrich, M. Herbst, L. Masino, R. Lurz, S. Engemann, A. Pastore, E. E. Wanker, *Nat. Struct. Mol. Biol.* **2008**, *15*, 558-566.

- [33] P. Velander, L. Wu, W. K. Ray, R. F. Helm, B. Xu, *Biochemistry* **2016**, *55*, 4255-4258.
- [34] a) M. Zhu, S. Rajamani, J. Kaylor, S. Han, F. Zhou, A. L. Fink, *J. Biol. Chem.* **2004**, *279*, 26846-26857; b) D.-P. Hong, A. L. Fink, V. N. Uversky, *J. Mol. Biol.* **2008**, *383*, 214-223.
- [35] J.-H. Lu, M. T. Ardah, S. S. K. Durairajan, L.-F. Liu, L.-X. Xie, W.-F. D. Fong, M. Y. Hasan, J.-D. Huang, O. M. A. El-Agnaf, M. Li, *ChemBioChem* **2011**, *12*, 615-624.
- [36] S.-m. Song, Y.-x. Wang, L.-m. Xiong, L.-b. Qu, M.-t. Xu, *Chem. Res. Chin. Univ.* **2013**, *29*, 20-25.
- [37] K. Yamaguchi, M. Itakura, R. Kitazawa, S. Y. Lim, K. Nagata, T. Shibata, M. Akagawa, K. Uchida, *J. Biol. Chem.* **2021**, *297*, 101035.

1.2. Combined *in silico* and *in vitro* Approaches to Uncover the Oxidation and Schiff Base Reaction of Baicalein as an Inhibitor of Amyloid Protein Aggregation.

Salavat S. Ashirbaev, Natércia F. Brás, Hendrik Zipse

Dept. Chemistry, LMU Muenchen, Butenandtstrasse 5-13, D-81377 Muenchen, Germany

Author contributions

All experiments were performed by Salavat S. Ashirbaev, all the calculations were performed by Natércia F. Brás. The manuscript was written jointly by Salavat S. Ashirbaev, Natércia F. Brás and Hendrik Zipse.

Combined in Silico and in Vitro Approaches To Uncover the Oxidation and Schiff Base Reaction of Baicalein as an Inhibitor of Amyloid Protein Aggregation

Natércia F. Brás^{*,[a, b]} Salavat S. Ashirbaev^{+, [b]} and Hendrik Zipse^[b]

Abstract: The oxidized form of baicalein (BA) leads to covalent binding with human amyloid proteins. Such adducts hamper the aggregation and deposition of fibrils. A novel reaction of BA with pentylamine (PA) as a model for the lysine side chain is described. This is the first study addressing the atomistic details of a Schiff base reaction with the trihydroxylated moiety of BA. Nuclear magnetic resonance and mass spectrometry approaches clearly indicate the formation of dehydrobaicalein in solution as well as its

condensation with PA under aerobic conditions, yielding regioselectively C6-substituted products. The combined results suggest initial ion pair formation between BA and PA, followed by a redox chain reaction: the initiation by oxygen/air; an *o*-quinone-based chain involving oxidation and reduction steps; and extra off-chain formation of a doubly oxidized product. These mechanistic details support the anti-amyloid activity of BA and endorse its trihydroxyphenyl moiety as a pharmacophore for drug-design studies.

Introduction

Human islet amyloid polypeptide (hIAPP, also known as amylin) is a 37-residue neuroendocrine hormone co-expressed and co-secreted with insulin by pancreatic β -cells. Type 2 diabetes (T2D) patients have increased blood concentrations of hIAPP, causing its aggregation and deposition as toxic insoluble fibrils that significantly contribute to cell death.^[1] Because of this, the inhibition of hIAPP amyloidosis is an emerging target for the treatment of T2D. However, this is a challenging task due to the complexity of protein self-assembly and the poor knowledge of the molecular details of inhibition, despite the growing number of proposed mechanisms by which a drug can interfere with amyloids.^[2]

Many promising natural phenolic compounds have been reported as small inhibitors of protein misfolding and aggregation.^[3] The molecular structure of flavonoids enables

them to chemically bind to and avoid assembly of the hIAPP fibrils. Epigallocatechin gallate (EGCG), quercetin, myricetin, chrysin and baicalein (Scheme 1a) are some examples of flavonoids with recognized anti-amyloidogenic activity.^[4]

Previous studies proposed that these molecules interact with and stabilize the amyloidogenic peptides by covalent and/or noncovalent interactions.^[3b] Due to antioxidant properties and the propensity to undergo autooxidation (by enzymatic or nonenzymatic reactions), certain polyphenols can act as electrophiles and interfere with proteins through specific covalent contacts.^[3b,5] Indeed, chemical modifications by Schiff base and Michael addition reactions have been reported between nucleophilic amines and thiols of amyloid peptides and electrophilic reactive groups of *o*-quinones and aldehyde molecules.^[3b,4a,b,6] It has been proposed that EGCG oxidizes readily in solution and the oxidized forms can produce Schiff base adducts with hIAPP and β -amyloid peptide (A β).^[7] The inhibitory mechanism of A β aggregation by (+)-taxifolin also requires its autooxidation to form an *o*-quinone to react with lysine residues.^[8] Also, covalent adduct formation significantly affects anti-aggregation effects of quercetin on α -synuclein.^[6a] Recently, a study with tetramers of caffeic acid suggested that the greater the number of catechol moieties, the greater the inhibitory effect on IAPP aggregation.^[9]


Baicalein (BA, **1**) is a flavone isolated from the roots of the traditional Chinese herbal medicine *Scutellaria baicalensis* known to have plenty of pharmacological activities such as antioxidant, anti-inflammatory and anti-tumor properties^[10] as well as anti-amyloid abilities against A β ,^[11] amyloid precursor protein,^[12] α -synuclein,^[6b] insulin,^[13] calcitonin^[14] and hIAPP.^[4b]


Upon oxidation, BA forms several intermediates including the dehydrobaicalein (DBA) quinones, which are susceptible to nucleophilic attack through imine (Schiff base) formation by the side chain of Lys residues, leading to covalent modification. Velandar et al. identified Schiff base-mediated hIAPP:baicalein

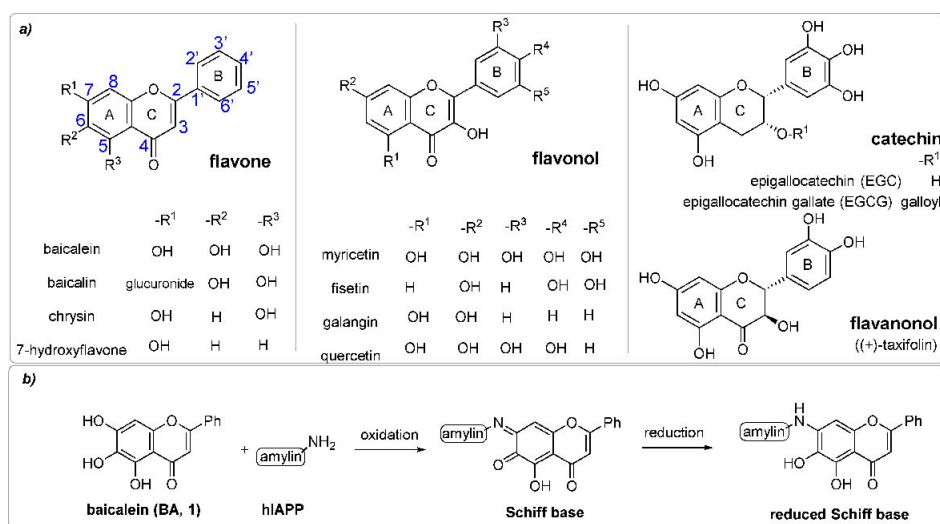
[a] Dr. N. F. Brás^{*}
LAQV, REQUIMTE
Departamento de Química e Bioquímica
Faculdade de Ciências, Universidade do Porto
Rua do Campo Alegre s/n, 4169-007 Porto (Portugal)
E-mail: nbras@fc.up.pt
natercia.braz@cup.uni-muenchen.de

[b] Dr. N. F. Brás,⁺ S. S. Ashirbaev,⁺ Prof. H. Zipse
Department Chemie
Ludwig-Maximilians-Universität Muenchen
81377 Muenchen (Germany)

[⁺] These authors contributed equally to this work.

 Supporting information for this article is available on the WWW under <https://doi.org/10.1002/chem.202104240>

 © 2022 The Authors. Chemistry - A European Journal published by Wiley-VCH GmbH. This is an open access article under the terms of the Creative Commons Attribution Non-Commercial NoDerivs License, which permits use and distribution in any medium, provided the original work is properly cited, the use is non-commercial and no modifications or adaptations are made.



Scheme 1. a) Molecular representations of the flavonoids mentioned in this work. b) The proposed reaction for baicalein–hIAPP conjugation based on mass spectrometric evidence is shown.

adducts by mass spectrometry (Scheme 1b).^[4b] They pointed out the importance of vicinal hydroxy groups in the A ring of BA (5,6,7-trihydroxyflavone) for its anti-amyloid inhibitory effects;^[4b] however, the underlying molecular details of the chemical reaction are not yet fully understood. Zhu et al. also demonstrated that the inhibition of α -synuclein is very sensitive to the oxidation state of BA.^[6b] While minor inhibitory effects could be observed under anaerobic conditions, stronger inhibition can only be observed in the presence of oxygen, highlighting the importance of the quinone forms and covalent modifications to prevent amyloid fibril formation. They also concluded that it is the interaction between the oxidized baicalein with both hIAPP and α -synuclein peptides that is responsible for the anti-amyloid activity (instead of the antioxidant potential of BA).^[6a,b] In addition, other studies pointed out that the amination of pyrogallol derivatives by ammonia/water treatment is a regioselective amino-substitution that proceeds under mild conditions (e.g., presence of molecular oxygen) without a catalyst.^[15]

Due to the occurrence of Schiff bases as transient intermediates in catalysis, chemical engineering and medicine, the nucleophilic attack of primary amines on quinones and aldehyde moieties is well studied in the literature.^[16] In general, it involves the formation of a carbinolamine, followed by a dehydration reaction that forms an imine. However, as the mechanistic pathways can depend on the intermediate species and environmental conditions such as chains of water molecules that act as proton transporters, this reaction can be far from straightforward.^[16c,17]

In addition to the critical role of Lys residues for Schiff base covalent inhibition mechanisms, they also are crucial hot spots for mechanisms involving both hydrophobic and electrostatic

interactions such as those present in Lys-specific tweezers.^[18] The unique Lys residue present in the hIAPP (the N-terminal residue-Lys1) has not been pointed out as a part of the fibril core structure; however, recent studies proposed that covalent modifications of Lys1 such as glycation and Schiff base reaction can significantly affect the aggregation and the hIAPP-membrane interactions.^[19] Therefore, Lys1 of hIAPP also plays a role in inhibitor binding, and the uncovering of its chemical modification with atomistic detail will be very helpful for amyloidosis events. Even though baicalein has been shown to covalently bind the Lys1 of hIAPP, its mechanism of action remains poorly understood.

This study proposes to clarify the atomistic details of the Schiff base reaction between the thermodynamically most favored dehydrobaicalein tautomers and the Lys1 of hIAPP (DBA–Lys covalent adduct). For this purpose, combined *in silico* (quantum mechanical calculations) and *in vitro* (NMR and HRMS) assays are employed to i) assess the oxidation and ionizable properties of baicalein in solution, and ii) to identify the preferable Schiff base adducts that are formed.

Experimental Section

Computational methods: The geometries of the various tautomeric forms (and respective rotamers) of BA and DBA were optimized using the hybrid B3LYP^[20] density functional associated with the empirical dispersion D3 correction of Grimme et al.^[21] in combination with the 6-31+G(d,p) basis set.^[22] The solvent effects were accounted for by the SMD solvation model.^[23] Harmonic vibrational frequency calculations were performed at the same level of theory to obtain the thermochemical corrections to the enthalpic and free

energies at 298.15 K. The charge distribution was analyzed by applying the NBO formalism.^[24]

To analyze the free energy of the various tautomeric forms of the reaction products, the potential energy surface (PES) of the interaction between a Lys side chain and each tautomer of dehydrobaicalein was explored by a linear transit scan along the dihedral angle that governs that N–C bond (a representative calculation is displayed in Figure S1 in the Supporting Information). Then, the enthalpic and free energies were obtained by optimization without constraints by using the same level of theory (SMD(water)/B3LYP-D3/6-31+G(d,p)).

The binding mode between the most stable tautomeric forms of DBA and the Lys1 of hIAPP (PDBID 2KB8) was obtained by molecular modelling and molecular dynamics (MD) simulations. Throughout the MD simulations, a constant force was used to restrain the *o*-quinone ring of DBA close to the amine side-chain of Lys1. The details of the MD procedure are provided in the Supporting Information. The prevalent conformations for each hIAPP:dehydrobaicalein complex obtained from clustering analysis revealed that the interaction between the side chain of Lys1 and the flavonoid is isolated from the remaining peptide residues (Figure S2). Because of this, and to directly compare with the current experiments, a reduced model system including DBA, 1-pentylamine as a mimic of the Lys1 side chain, and one water molecule was then used to explore the chemical reaction pathways. The truncated Lys1 residue is hereinafter referred to as pentylamine (3, PA) for simplicity. This molecule is an excellent model to represent the lysine side chain due to the great similarity of their experimental pK_a values (10.6^[25] and 10.5–10.7^[26] for PA and Lys, respectively). Previous studies also used truncated lysine models such as 1-butylamine, which also has a pK_a of 10.6, to represent this amino acid.^[27] Indeed, the use of aliphatic primary amines is often used to represent lysine residues in reaction mechanism studies using quantum chemical and/or quantum mechanics/molecular mechanics methods.^[6c,27b,28] Herein, the PA was used to maintain the topology from the alpha carbon atom which better characterizes the complete lysine side chain.

The geometries of reactants, transition states, intermediates and products were optimized at the B3LYP-D3/6-31+G(d,p) level of theory in conjunction with the SMD model. The reaction pathways were followed from the transition states to both the reactants and the products by using the intrinsic reaction coordinate (IRC) method. The nature of the stationary points was confirmed by calculating vibrational nuclear frequencies at the same level of theory. Thermochemical corrections to the free energies at 298.15 K were considered. Single-point energy calculations were carried out by using the DLPNO-CCSD(T) method combined with the larger cc-pVTZ basis set.^[29] The B3LYP calculations were performed by using the Gaussian 09 program package,^[30] whilst the DLPNO-CCSD(T) calculations were carried out by using the ORCA program package.^[31]

To determine the pK_a values of baicalein, a proton exchange computational approach^[32] was employed, using reference flavonoids with known pK_a , Chrysin and galangin (Scheme 1a) were used as reference molecules because the former is structurally similar, whereas the latter has the same number of ionizable groups of baicalein. Equation (1) was used to calculate the free energy for the deprotonation reaction ΔG_{sol}^* , which is then employed in the pK_a determination [Eqs. (2) and (3)].

$$\Delta G_{\text{sol}}^* = G_A + G_{\text{ref,H}^+} - G_{\text{HA}} + G_{\text{ref}} \quad (1)$$

$$\Delta pK_a = \frac{1}{2.303 RT} \Delta G_{\text{sol}}^* \quad (2)$$

$$pK_a(\text{HA}) = pK_a(\text{H}_{\text{ref}}) + \Delta pK_a(\text{HA}) \quad (3)$$

Experimental methods: All reactions sensitive to air and moisture were performed under a nitrogen atmosphere and the glassware as well as magnetic stir bars were dried overnight in a dry oven at 110 °C.

Solvents, reagents: All reagents and solvents were purchased from TCI, Sigma-Aldrich or Fisher Scientific. All air- or water-sensitive reagents were stored under nitrogen.

NMR spectroscopy: All ¹H NMR spectra were recorded by Bruker 400 in [D₆]DMSO at 400 MHz at 23 °C. All ¹³C NMR spectra were recorded, respectively, at 101 MHz. The chemical shifts are reported in ppm (δ), relative to the resonance of [D₆]DMSO at δ = 2.50 ppm for ¹H and for ¹³C{1H} relative to the resonance of [D₆]DMSO δ = 39.52 ppm. Spectra were imported and processed in the MestreNova 14.1.1 program. For ¹H NMR spectra the multiplicities (d = doublet, t = triplet, q = quartet, hept = heptet, dd = doublet of doublets, m = multiplet), coupling constants *J*, number of protons and assignment to the structure are reported. In ¹³C NMR spectra singular carbons are marked with (s).

Mass spectrometry: For electrospray ionization (ESI) spectra a Thermo Finnigan LTQ FT ultra Fourier transform ion cyclotron resonance mass spectrometer was utilized. Atmospheric pressure chemical ionization (APCI) measurements were performed on an Advion CMS instrument using positive ion mode.

Melting point: Melting points were measured on a BUCHI Melting Point M-560.

IR spectroscopy: IR spectra were measured on a PerkinElmer FTIR BX spectrometer mounting an ATR technology module.

UV/VIS spectroscopy: UV/VIS spectra were measured on UV/VIS Varian Cary 50 spectrometer.

More details about the experimental procedures are provided in the Supporting Information.

Deposition Number 2124561 (for the TAP–PA complex) contains the supplementary crystallographic data for this paper. These data are provided free of charge by the joint Cambridge Crystallographic Data Centre and Fachinformationszentrum Karlsruhe Access Structures service.

Results and Discussion

Due to their chemical structure, phenolic compounds such as BA can be oxidized to the respective quinone forms, whose electrophilic character provides the basis for reactions with nucleophiles such as the lysine residues of amyloidogenic proteins. However, different *o*-quinone species can differ in inhibitory activities and act by different mechanisms, suggesting that other properties of the molecules may also be relevant for inhibition. Thus, mechanistic studies with *o*-quinone species have attracted special interest to help optimize *o*-quinone-based drug candidates. Following this idea, in this paper, we assess the atomistic details of the reaction mechanism between several *o*-quinone–baicalein forms and PA through quantum chemical calculations. As previously mentioned, the primary

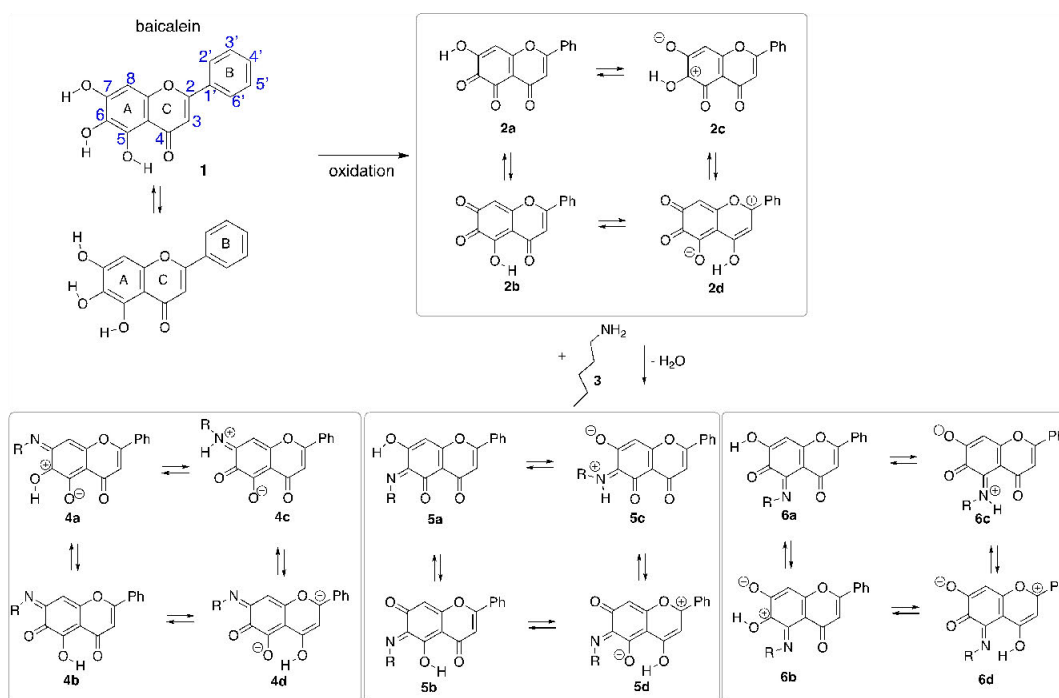
step of the Schiff base reaction between **BA** and **PA** must be the oxidation of the trihydroxylated moiety of **BA**. Therefore, prior to the mechanistic calculations, a deeper understanding of the structure, oxidation and ionization forms of **BA** is performed.

Theoretical analysis of baicalein and dehydrobaicalein (DBA) tautomers

Molecular structures of all possible conformers of **BA** were optimized at the SMD(water)/B3LYP-D3/6-31+G(d,p) level of theory (Table S1). Energies were subsequently refined through DLPNO-CCSD(T)/cc-pVTZ single point calculations and combined with thermochemical corrections to free energies and solvation energies for water to obtain free energies in water at 298.15 K. The subsequent discussion will focus on these high-level results, if not mentioned otherwise. The geometry with the three hydroxy groups in "anticlockwise" orientations is more stable by 18.5 kJ mol⁻¹ than the "clockwise" geometry (Figure S3 and Table S1). This is in agreement with previous results pointing out the "anticlockwise" conformer of **BA**. As the most stable, as it maximizes the number of H-bonds (C7–OH...O–C6 of 2.23 Å, C6–OH...O–C5 of 2.32 Å and C5–OH...O–C4 of 1.71 Å).^[33] Baicalein has a slightly nonplanar structure (C2–C1' length of 1.471 Å and a torsion angle around

this bond of 21.0°), which also agrees with previous X-ray and theoretical studies.^[33a,34] The conformational energy analysis of **BA** indicates a nonplanar conformation (torsion angle of 22.8°) as the lowest potential energy geometry.^[34] Upon oxidation, baicalein can form four different dehydrobaicalein (**DBA**) tautomers (**2a–2d**, Scheme 2), each of which comes in two different conformers with respect to the remaining hydroxy group (**2e–2h**, Scheme S1 and Table S2a and b). Tautomer **2a** is found to be most stable in an aqueous environment, followed by tautomer **2d** with an energy difference of 7.4 kJ mol⁻¹. This quite small energy difference suggests that both tautomers are populated at ambient temperature. Both molecules are *o*-quinones that are much more stable than the zwitterionic forms **2c/2g**. Interestingly, a different anti-amyloid activity is also observed for *o*- and *m*-quinones. The structure-activity relationship analyzed for the inhibition of hIAPP amyloid formation by baicalein and its analogues reveals that both *o*-quinones (5,6-dihydroxyflavone and 6,7-dihydroxyflavone) also have activity, while this is not so for 5,7-dihydroxyflavone.^[14b] The presence of vicinal hydroxy groups on the phenyl rings of polyphenolic molecules is also reported as essential for their inhibitory activity against human calcitonin aggregation.^[14]

As observed for **1**, both **2a** and **2d** have slightly nonplanar structures (torsion angles around the C2–C1' bond of 20.2° and 18.3°, respectively). In addition, both tautomers have intramolecular H bonds: in **2a** the C7–OH interacts with the



Scheme 2. Pathway from baicalein to dehydrobaicalein tautomers **2a–2d**, which will react with pentylamine to produce the covalently bound products **4a–4d**, **5a–5d** and **6a–6d**.

carbonyl group of C6 (2.25 Å), whilst in **2d** the proton of O4 orients to the neighboring C5–O, establishing a short interaction (1.77 Å) that anticipates an easy interconversion between **2d** and **2b** tautomers. Indeed, a relationship between the groups of C4 and C5 is also evidenced in studies in which the **BA** acts as a chelator and coordinates the metal by these adjacent groups.^[35] The conformational reaction of the tautomeric shift between **2d** and **2b**, in the presence of one explicit water molecule, has activation and reaction energies of 15.0 and 10.2 kJ mol⁻¹, respectively (Figure S4). This quite small barrier suggests that the tautomeric exchange between **2d** and **2b** follows the Curtin-Hammett principle, in which two tautomeric species are conformationally equilibrated when their interconversion is much faster than the reaction that they can be involved.

Theoretical dehydrobaicalein–pentylamine (DBA–PA) tautomeric analysis

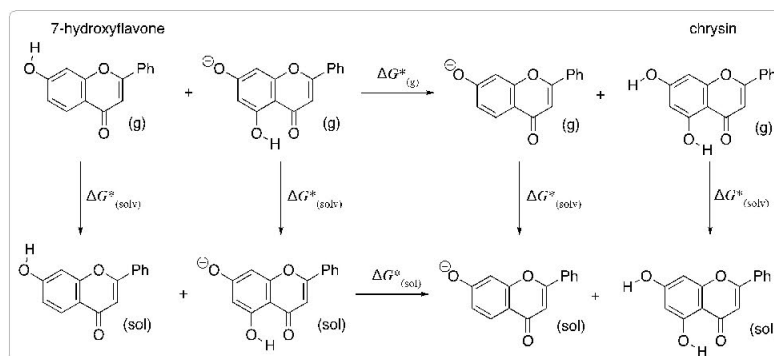
Because the nucleophilic attack of the amine group can occur at positions C7, C6 and C5 of the A ring, there are 12 different possibilities for formation of dehydrobaicalein–pentylamine adducts (**4a–4d**, **5a–5d** and **6a–6d** products of the reaction, Scheme 2). According to the relative energy values to the most stable tautomer (Table S3), the adduct formation at C7 (**4c**) is clearly favored, followed by C6 (**5a**, +23.5 kJ mol⁻¹) and C5 (**6c**, +24.7 kJ mol⁻¹) positions. It is interesting to note that two of these forms are zwitterionic in nature, where the iminium ion unit is actively involved in hydrogen bonding interactions with its direct neighbors. This energetic ordering is strongly impacted by aqueous solvation effects, and the predicted relative ordering in the gas phase can be thus substantially different.

Theoretical pK_a values of baicalein

Previous data obtained for fisetin (Scheme 1a) suggested a pH dependence for the regioselectivity and nature of the formed quinone adducts. At pH values below the pK_a for quinone protonation, they also observed the formation of water adducts in the C ring of the flavonoid (inexistent at pH > pK_a).^[5] Considering the structural similarities of fisetin and baicalein, the pK_a values of the latter were determined to assess possible effects of pH on the quinone chemistry and the regioselectivity of the formed adducts by this electrophilic molecule. A computational approach to calculate relative pK_a values using a reference molecule was carried out. The reference flavonoids with known experimental pK_a values used in this study are: chrysin (which belongs to the flavone class as does **BA**, but has only two ionizable groups), and galangin (with three ionizable groups as in **BA**, but belongs to the class of flavonols). To validate the employment of the proton exchange method to determine the pK_a values of flavonoids, we first calculate the pK_a value of the 7-hydroxyflavone using chrysin and galangin as reference compounds (Schemes 1a, S2 and S3). As example of the procedure, Scheme 3 illustrates the thermocycle for the deprotonation reaction of 7-hydroxyflavone using chrysin as reference molecule.

The experimental pK_a values determined for 7-hydroxyflavone vary between 7.39 and 8.48,^[36] which compares to the calculated pK_a values of 8.2 and 8.4 with the chrysin and galangin reference systems (Table 1). The same protocol based on the experimental pK_a values of chrysin (pK_{a1} = 8.0 and pK_{a2} = 11.9) and galangin (pK_{a1} = 7.6, pK_{a2} = 9.5 and pK_{a3} = 10.9) obtained by Musialik et al.^[36] is then used for the calculation of the pK_a values of **BA**.

The electronic energies of the optimized geometries of all possible mono-, di-, and tri-anion species of the three flavonoids are in Table S1. For **BA**, our calculations indicate the deprotonation of the C7–OH group as the most favorable, which agrees with earlier studies pointing to this group as the most acidic (pK_a between 7.5 and 8.5) and the most favored for heterolytic O–H breaking.^[33b,36] In addition, the di-anionic



Scheme 3. Thermodynamic cycle for the deprotonation of 7-hydroxyflavone with chrysin as reference molecule.

Table 1. Computed pK_a values of the ionizable groups of 7-hydroxyflavone and baicalein with chrysin and galangin as reference molecules.

Reference	Target	SMD(water)/ B3LYP-D3/6-31 + G(d,p)	DLPNO-CCSD(T)/ cc-pVTZ//SMD(water)/ B3LYP-D3/6-31 + G(d,p)
chrysin ($pK_{a1} = 8.0$; $pK_{a2} = 11.9$) ^[36]	pK_{a1} (7-hydroxyflavone at C7–OH)	8.2	8.2
	pK_{a1} (BA at C7–OH)	6.2	5.5
	pK_{a2} (BA–7O [−] at C5–OH)	11.8	12.1
	pK_{a3} (BA–7O [−] , 5O [−] at C6–OH)	17.3	28.2
galangin ($pK_{a1} = 7.6$; $pK_{a2} = 9.5$; $pK_{a3} = 10.9$) ^[36]	pK_{a1} (7-hydroxyflavone at C7–OH)	7.9	8.4
	pK_{a1} (BA at C7–OH)	6.0	5.6
	pK_{a2} (BA–7O [−] at C5–OH)	14.4	15.4
	pK_{a3} (BA–7O [−] , 5O [−] at C6–OH)	15.1	24.5

molecule with positions 7 and 5 deprotonated is marginally more stable than the dianion-7,6-baicalein molecule (difference of 23.8 kJ mol^{−1}), thus suggesting an acidity order of C7 > C5 > C6. Table 1 displays the pK_a values for BA (following Schemes S2 and S3). The computed pK_{a1} of BA is 5.5 or 5.6, which is slightly smaller than the usually estimated for flavonoids, indicating that a significant portion of baicalein would be dissociated at pH 7.4 as well as in the alkaline conditions required to act as antioxidant. Our predicted pK_{a2} of BA is 12.1 or 15.4, which are 0.2 and 5.9 pK_a units larger than the experimental value of the reference molecules (chrysin and galangin, respectively). The pK_{a2} of 12.1 should be more reliable because the deprotonated position in BA is the same as those in the reference chrysin molecule. However, the use of both reference molecules estimates a somewhat large pK_{a3} value for BA, being 16.3 and 13.6 pK_a units larger than the respective reference values. This discrepancy probably happens due to the distinct number of ionization groups in chrysin, as well as the different hydroxylation pattern in galangin: BA only has OH groups on its A ring, whilst galangin has the C3–OH group on the B ring that also establishes a hydrogen-bond with the carbonyl group at C4, decreasing the acidity of the C5–OH group. In addition, this structural difference can also influence the accuracy of the proton exchange method by introducing possible errors.^[32] Furthermore, there are possible limitations of the implicit solvation model used in the calculations that may provide a poor description of multi-anionic species. Indeed, past theoretical studies on successive deprotonation reactions in aqueous solution (using the same solvation model) of flavonols indicated much larger Gibbs free energy differences after the second deprotonation.^[37] Despite the error of the method, our results suggest large values for the second and third ionization, which can in turn influence the oxidation ability of baicalein to form quinone forms in alkaline environments.

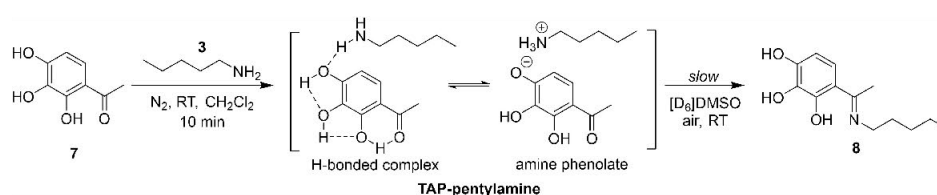
Experimental studies of baicalein and its reaction with pentylamine

Selected NMR and HRMS experiments were performed to characterize baicalein and its reactivity with pentylamine in solution, which is not known. The ¹H NMR spectrum of partially deuterated [D₂]BA reveals the loss of 6-OH and 7-OH peaks, although a weak 5-OH signal remains detectable for slightly

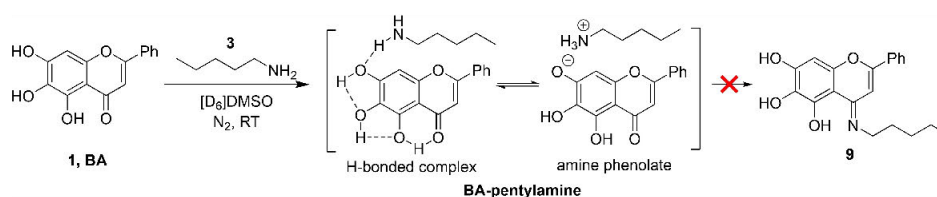
longer times, indicating a constrained proton position (Figure S5). This is in full agreement with earlier experiments, in which the alkylation of BA with *n*-propyl iodide in acetone generated a mixture of two products: one monoalkylated at position C6 (11%) and another molecule dialkylated at positions C6 and C7 (62%; Scheme S4).^[38] It was proposed that the 5-OH of BA forms an intramolecular H-bond with the keto group, which reduces its reactivity. Previous theoretical studies also pointed out the most stable radical tautomer was obtained by dehydrogenation of the C6–OH group of BA, whilst the most stable anion tautomer of BA was obtained by deprotonating the C7–OH.^[33b]

In order to explore the intrinsic reactivity of baicalein's A ring substructure, initial experiments with PA involve 2',3',4'-trihydroxyacetophenone (7, TAP) as a simplified model. Mixing TAP with PA in CH₂Cl₂ leads to the immediate formation of a yellow crystalline precipitate, whose characterization by NMR spectroscopy indicates a 1:1 ratio of the constituting reactants TAP and PA, but no signal correlations (and thus no covalent bonding) between the respective fragments. This is most easily understood through formation of the TAP-PA ammonium-phenolate ion pair shown in Scheme 4, whose assignment is also supported by the solid state structure of the precipitate (Figure S7 and Table S4, CCDC deposition number 2124561). This agrees with the well-known tendency of phenols to form rather stable hydrogen-bonded complexes with amines.^[39] On extended reaction times the TAP-PA complex was then observed to form imine 8 at room temperature (Scheme 4).

Due to its structural resemblance with TAP, we expect an analogous behavior for baicalein (1, BA) in its reaction with pentylamine. Due to the very low solubility of BA in CH₂Cl₂ these reactions have been performed in [D₂]DMSO under nitrogen atmosphere (see the Supporting Information for details). As anticipated, the ¹H,¹³C HSQC spectra shows the formation of BA-PA salt species; however, no formation of the imine condensation product could be observed even after 72 h at room temperature or after 5 h at 50 °C (Scheme 5). The proposed deprotonated BA[−] structure is based on the similar chemical shifts of TAP data, and indeed it is in line with the first deprotonation position (pK_{a1}) of BA predicted by QM calculations. The obtained BA-PA salt structure is also in line with the formation of ion pairs in the reaction of hexamethylenediamine with catechin (as model for tannin extracts).^[40]



Scheme 4. Reaction of TAP with PA.



Scheme 5. Reaction of BA with pentylamine under anaerobic conditions.

Therefore, these results suggest an effective role of oxygen as initiator of the reaction between the BA and PA. In fact, a past study also showed that the flavonoid epigallocatechin (EGC, Scheme 1) treated with aqueous ammonia solution under aerobic conditions forms a condensation adduct.^[15a] A similar behavior was also reported by Velander et al.^[46b] after incubating BA for 4 days with the hIAPP amyloid polypeptide in Dulbecco's phosphate buffer solution containing 2.25% DMSO (v/v). Even though the oxidized product species was not directly detected in these studies, they characterized the final product by LC-MS as reduced baicalin-hIAPP conjugate (Scheme 1b). They proposed that BA can be autoxidized to *o*-quinone that conjugates with hIAPP amine groups through a Schiff base mechanism with further reduction.^[46b]

To evaluate the impact of aerobic conditions in this reaction, the nitrogen atmosphere was replaced by pure oxygen, whereupon the solution promptly changes from orange to black, and then to deep red. Even the exposure to air during sample preparation for NMR analysis can trigger the reaction, supporting the role of oxygen/air to initiate the reaction. Also, it has been shown that when freeze-pump-thaw degassed solvents are used no condensation product is detected (see the Supporting Information for details). The APCI-MS analysis shows a $[M+H]^+$ peak at m/z 340 corresponding to an amine condensation product, and the $^1\text{H},^{13}\text{C}$ HMBC NMR analysis reveals that the regioselectivity is at C6 (C6-substituted BA derivative). The molecular geometry and energy of all tautomers and rotamers of the various BA-PA product ($[M+H]^+$ peak at m/z 340) were analyzed with the same theoretical methods as before. BA-PA **10 a** (C7-substituted) and **11 a** (C6-substituted) are found to be the most stable in an aqueous environment, and their very small energy difference (3.3 kJ mol^{-1}) suggests that both tautomers are populated at ambient temperature, which agrees with the observed experimentally.

Experiments on BA oxidation and dehydrobaicalein-pentylamine condensation reaction

Some studies indicated that baicalin (BA) exhibited antioxidant and free radical-scavenging activities (scavenged hydroxyl radical, 2,2-diphenyl-1-picrylhydrazyl (DPPH) radical and alkyl radicals in a dose-dependent manner in alkaline solution).^[41] The formation of DBA was also detected by previous UPLC/ESI-MS studies with baicalin, a glucuronide form of BA (Scheme 1a).^[42] However, previous experimental attempts of structural investigation of DBA in solution are not so widely known. Because of this, we assess the reactivity of baicalin with molecular oxygen through in situ oxidation of BA by a flow of pure O_2 for 15 h in $[\text{D}_6]\text{DMSO}$. However, no major differences could be observed in the analytical data after this treatment, which indicates that BA is stable under these conditions. This lack of reactivity is supported by a theoretically calculated reaction free energy of $+22.7 \text{ kJ mol}^{-1}$ for the reaction of triplet oxygen with BA to yield hydrogen peroxide and DBA. Afterwards, several experiments with increasing pH values were carried out (details in the Supporting Information). The obtained results are in line with earlier studies of Feng et al.,^[43] where it was shown that even under mild conditions BA tends to degrade at higher pH values. All this data reinforces the idea that the formation of BA-PA ion-pair species (H-bonded complex or ammonium phenolate) is a crucial step, since the deprotonated BA⁻ readily oxidizes and forms DBA as a transient intermediate. In order to assess the condensation reaction of the *o*-quinone dehydrobaicalein with PA in solution, a protocol with *o*-chloranil as an alternative oxidant to oxidize BA is used.^[44] APCI-MS analysis shows successful formation of DBA through its $[M+H]^+$ ion peak at m/z 269, whilst the $^1\text{H},^{13}\text{C}$ HMBC NMR analysis characterizes the structure of DBA as 6,7-dehydrobaicalein. Further, the formation of DBA was also examined by treating the obtained crude DBA with an excess

of *o*-phenylenediamine in MeOH with a catalytic amount of acetic acid in analogy to an established procedure by Morimoto and colleagues.^[45] The analytical data gathered by APCI-MS ($[M+H]^+$ signal at m/z 341) for the crude reaction products are in line with the already characterized 6,7-substituted BA phenazine derivative,^[45] which also supports the formation of DBA **2b** species throughout the reactions.

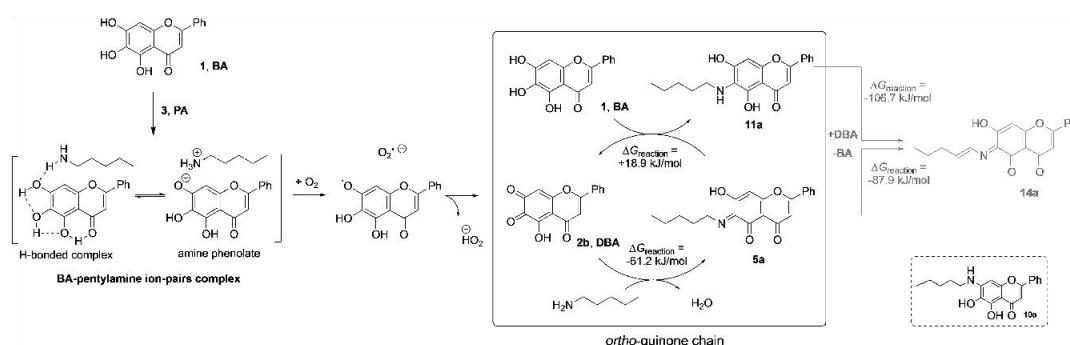
Afterwards, the obtained crude DBA was treated with PA in CH_2Cl_2 and with a catalytic amount of glacial acetic acid.^[44] The APCI-MS analysis indicates coupling products distributed in two $[M+H]^+$ ion peaks (at m/z 336 and m/z 340) with a ratio of $\sim 3/2$, as well as a peak of reduced baicalein species (m/z 271). However, these mass spectrometric peaks have a difference of about m/z 2 to the expected $[M+H]^+$ ion peak at m/z 338 for the imine adduct (**4a–4d**, **5a–5d** or **6a–6d** in Scheme 2). Overall, this data is consistent with a Schiff base reaction, in agreement with the baicalein–hIAPP covalent Schiff base conjugation proposed by Velandar et al.,^[4b] and discards the mechanistic hypothesis of the aza-Michael addition characterized for some *o*-quinone species of flavonoids.^[6c] Also, the molecular geometry and energies of the possible tautomers and rotamers of product with the $[M+H]^+$ peak at m/z 336 were analyzed with the same theoretical methods as before. Based on the results of this study, we propose the mechanism of the Schiff base reaction between BA and PA shown in Scheme 6. The reaction energies of the main mechanistic pathways, predicted by QM calculations using the experimentally observed tautomers, are displayed in Scheme S17.

According to Scheme 6, BA reacts anaerobically with PA to an ion pair intermediate with 1:1 composition. This ionic structure is very susceptible to oxidation by O_2 and thus reacts rapidly to **2b**, which subsequently forms the Schiff base condensation product (**5a**, $[M+H]^+$ at m/z 338) at the most electrophilic carbonyl (C6). However, this transient intermediate product is straightaway reduced by another BA molecule to afford the product **11a** with $[M+H]^+$ at m/z 340 and regenerates DBA. As the latter reaction is found to be endergonic at $+18.9$ kJ mol⁻¹, the driving force to obtain the main product observed experimentally (**11a**) is the formation of the transient intermediate **5a** (which is found to be largely

exergonic, $\Delta G_R = -61.2$ kJ mol⁻¹). Similar redox cycles have also been proposed for alike oxidative reactions,^[15b,16d] such as those between catechin derivatives and nucleophiles.^[15a] An important characteristic of this *ortho*-quinone chain mechanism is the requirement of only minute amounts of oxygen for the generation of the amine coupling product **11a**, which may also provide a rational basis for the observation of residual inhibitory activity of baicalein under formally anaerobic conditions.^[6b]

Furthermore, to uncover the further formation of product **14a** with $[M+H]^+$ at m/z 336, some control experiments (detailed description is provided in the Supporting Information) were carried out. On the one hand, the oxidation of the C6-substituted BA derivative **11a** ($[M+H]^+$ at m/z 340) leads to the formation of the highly oxidized adduct **14a**, while at the same time reducing DBA back to BA. Two molecules of DBA are needed for this coupling reaction that is found to be exergonic at -106.7 kJ mol⁻¹. On the other hand, not detecting of product **14a** ($[M+H]^+$ at m/z 336) in the experiments under a mild oxidant agent (e.g., air) suggests that this extra reactive pathway only occurs in the presence of strong oxidants such as *o*-quinones. All proposed reaction pathways are viable in a cell environment due to several oxidant and reactive species produced by enzymatic or nonenzymatic reactions that could assist in DBA formation. That at least two molecules of DBA are needed for the coupling reaction to yield **14a** ($[M+H]^+$ at m/z 336) suggests that the DBA amounts in solution (or in human physiological conditions) act as a regulator to thereby direct the redox chain reaction to form the product **11a** or **14a**.

Another rational mechanistic hypothesis would be the disproportionation of two molecules of **5a** to form products **11a** and **14a**. This reaction is found to be exergonic at -69.0 kJ mol⁻¹, which provides an additional argument for why direct detection of Schiff base product **5a** was not successful. All taken together the experiments clearly show the oxidation of baicalein in solution as well as the formation of the reduced and highly oxidized covalent dehydrobaicalein-amine adducts. The latter observations are particularly relevant to complement the computational study on the reaction mechanism for DBA–PA Schiff base formation.



Scheme 6. Proposed mechanism for the condensation reaction between BA and PA.

BA is known to be a strong iron chelator under physiological conditions, in which the O6 and O7 atoms constitute the iron-binding site.^[46] In general, in the presence of redox-active ions, the flavonoids might act as antioxidants or as pro-oxidants, affecting the metal-promoted Fenton chemistry and the redox state of cells. On the other hand, in the presence of amyloid peptides, the metal ions can interact with them and create hydroxyl radicals, which could accelerate the production of flavonoid–quinone species. Hence, the presence of transition metals could help the redox shuttling required for the BA–PA condensation reaction in an unspecific manner. Regarding the anti-amyloidogenic properties of the flavonoids in the presence of metals, it was observed that the Zn–EGCG complex significantly suppress hIAPP's amyloid aggregation and cellular toxicity,^[47] whilst the Al^{III}–EGCG complex inhibits hIAPP fibril formation more efficiently than the flavonoid alone.^[48] However, the underlying molecular details of these reactions are not yet fully understood. Grasso et al. also indicated that in an oxidative stress-related environment, Cu^{II} ions generally inhibit the Michael addition modification between the 4-hydroxy-2-nonenal and the His residues of A β . However, once it is formed, the metal still binds the peptide with high affinity, forming a ternary complex.^[49] Despite possible competition effects, these studies suggest that the BA–PA Schiff base reaction may progress in a medium with metal ions; however, all these processes merit further investigation.

Many studies reported that the covalent modifications of proteins by quinones may severely influence the properties of both reaction partners, which is particularly important when amyloid proteins are involved. In general, protein–flavonoid covalent complexes have higher stability and protect the phenolic compound from decomposition. The main molecular events of amyloid formation are the primary and secondary nucleation, fibril elongation and fibril fragmentation.^[2a] Zhu et al. showed that the BA- α -synuclein adducts affect the nucleation stage of aggregation by stabilizing stable and soluble oligomeric forms (off-pathway oligomers). The covalent binding of the DBA changed the secondary structure of the peptide, modifying the structural flexibility associated to the fibrils folding. Additionally, the covalently modified peptides were able to form oligomers with unmodified molecules.^[6b] The same authors also observed the formation of stable hydrophilic oligomers by covalent binding of the oxidized quercetin to α -synuclein, leading to the inhibition of fibrillization by preventing both nucleation and elongation molecular events.^[6a] Sato et al. suggested that the nucleophilic addition to the *o*-quinone form of the flavonoid (+)-taxifolin by the Lys residues of A β 42 interferes more in the elongation rather than the nucleation phase.^[8] As the structural flexibility and solvent exposure of lysine residues can facilitate their transitory deprotonation and favors the inhibition of amyloid aggregation by covalent binding,^[6c] an effective inhibition of hIAPP aggregation by DBA is expected because the Lys1 belongs to the flexible N-terminus.

Theoretical DBA–PA Schiff base reaction mechanisms

To assess the regioselectivity of the DBA–PA Schiff base reaction mechanisms, we provide a detailed atomistic description of the overall mechanistic pathways and energetic portrait to attain the 4c, 5a and 6c DBA–PA adducts. Throughout this discussion, all energies are those obtained at the DLPNO-CCSD(T)/cc-pVTZ//SMD(water)/B3LYP-D3/6-31+G(d,p) level of theory.

Formation of the 4c adduct

Considering that both 2d and 2b tautomeric forms (in conformational equilibrium) are those that provide possibilities for adduct formation at C7, we start our calculations by determining the tautomerization of the C4–OH group to a C4–keto group in the presence of pentylamine and one water molecule. The inclusion of an explicit solvent molecule assists the proton transfer leading to the final products, as has been described in previous studies.^[16c,17] Figure S21 illustrates the stationary points for this reactive step as well as their associated energies. The activation and reaction energy are similar to those obtained in the absence of the amine group (differences of -3.2 and -1.5 kJ mol⁻¹, respectively), reinforcing the ease of the tautomeric conversion between 2d and 2b, with the latter showing itself as the most favorable to continue the reaction. The reaction then follows the well-established mechanism for Schiff base formation through nucleophilic attack of pentylamine at the C7–keto group, accompanied by water-mediated proton transfer from the amine to the carbonyl oxygen. Figure 1a shows the geometries of the stationary points of this step. In the reactant complex (react), the N atom of pentylamine is placed at distances of 2.77 and 2.31 Å from the C7 and C6 atoms of the A ring, respectively. The preference of the amine group to be positioned below the C6 atom seems to occur due to a charge distribution effect. Indeed, the natural bond orbital (NBO) analysis of tautomer 2b (Figure S22) indicates that the charges of C6 and O6 (+0.498 and -0.508) are slightly higher than at C7 and O7 (+0.446 and -0.619), becoming more attractive for the nitrogen atom. The initially formed zwitterionic intermediate (react') then features an N–C7 distance of 1.57 Å and a largely pyramidalized carbonyl carbon atom. Hydrogen-bonded pre-reaction species were also observed in other studies on the reaction of amines and aldehydes.^[16a,c] In the current case the energy difference between react' and react amounts to +46.9 kJ mol⁻¹. The following transition state TS1 is destabilized by additional 28.5 kJ mol⁻¹ relative to adduct react' and characterized by an N–C7 distance of 1.52 Å and a short hydrogen bond of 1.47 Å between one of the amine protons and the water oxygen atom such that an energetically favorable six-membered ring arrangement is formed (Figure 1a). Starting from the resulting carbinolamine intermediate INT1 located +19.8 kJ mol⁻¹ higher than the reactant complex react, various alternative pathways for its dehydration to the corresponding Schiff base were assessed.

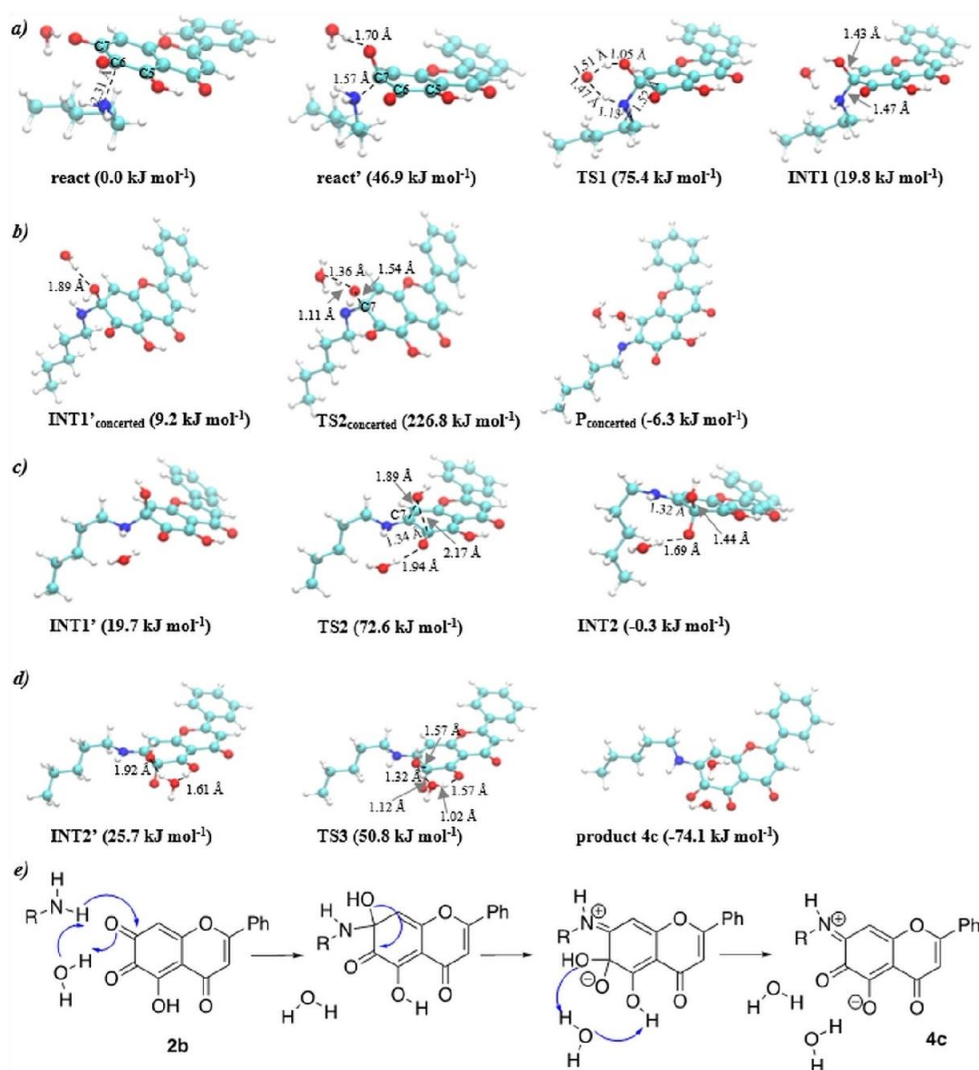


Figure 1. Representation of the mechanistic pathway to form the dehydrobaicalein–pentylamine adduct **4c**: a) carbinolamine formation, b), c) and d) dehydration/Schiff base formation, and e) 2D depiction of the complete reaction.

Firstly, the concerted release of the hydroxy group from C7 with the water-mediated transfer of one proton from the charged nitrogen, forming the neutral form of Schiff base (Figure 1b), is determined. The transition state TS2_{concerted} features a six-membered ring geometry and faces a barrier of 217.6 kJ mol⁻¹ relative to intermediate INT1'_{concerted}. In addition, the complete reaction is slightly exergonic ($\Delta G_R = -6.3$ kJ mol⁻¹ relative to react). Past studies pointed out the carbinolamine dehydration as the rate-limiting step, being in general, difficult and associated with large barriers (the inclusion of two water molecules still produces barriers of ca. 108 kJ mol⁻¹).^[17] How-

ever, these activation energies could be dropped by assistance of other molecules such as polar groups or large solvent chains that allow efficient charge delocalization by hydrogen-bond networks. For example, the presence and involvement of functional groups such as the pyridoxal 5'-phosphate (PLP), a key co-enzyme in the metabolism of amino acids and inhibition of glycation in membrane surfaces, is critical to reduce the energy barriers and lead to faster imine formation.^[16b,50] Therefore, our extremely high barrier means that this mechanistic path should be different than the usually postulated, or that additional solvent molecules are needed.

An alternative pathway for the dehydration reaction could be found, where the hydroxy group initially migrates from C7 to the neighboring C6 atom. The geometries of all stationary points are displayed in Figure 1c. INT1 and INT1' are conformational isomers of each other with different positions for the assisting water molecule. Similar variations associated with small energy differences were also reported in earlier studies such as the nitrogen inversion.^[17] Between INT1' and the transition state TS2 the C7–OH bond distance increases from 1.46 to 1.89 Å, being severely weakened, but not yet broken. At TS2, the hydroxy group is positioned 2.17 Å away from C6, being bound only at the final state of this step (INT2). Throughout this step, the water molecule plays a stabilizing role on the carbonyl group of C6, and we can also see the expected hybridization change from sp³ to sp² of the C7 atom. This step features a barrier of 52.9 kJ mol⁻¹ and a reaction free energy of 20.0 kJ mol⁻¹ relative to INT1. Then, in the last mechanistic step, the C5–OH transfers the proton to the assisting water molecule, which in turn donates its proton to the leaving hydroxy group (now bound at the nearby C6), yielding the protonated Schiff base and a second water molecule. As seen in Figure 1c, in the transition state TS3 the O5 is already deprotonated (O5–H distance of 1.57 Å), whilst the proton from the water is midway to the releasing hydroxy group (O_{wat}–H_{wat} and H_{wat}–OH distances of 1.12 Å and 1.32 Å, respectively), having the latter a HO–C6 distance of 1.57 Å. The TS3 is destabilized by 25.1 and 50.8 kJ mol⁻¹ relative to the INT2' and react states, respectively. Additionally, the product state is energetically favored relative to INT2' by -99.8 kcal mol⁻¹, which brings the overall reaction free energy to -74.1 kJ mol⁻¹.

As can be seen in the mechanistic summary in Figure 1e, the overall dehydration/Schiff base formation sequence occurs in two separated steps, which differs from that commonly expected for this reaction (concerted release of the hydroxy group with N=C formation). This difference can derive from the particular structure of the A–C rings (resonance effects) and could be a specific property of the dehydrobaicalein species.

To investigate the effect of more solvent molecules, additional calculations were performed on this reaction mechanism considering a second explicit water molecule (see the Supporting Information for details). The results support a similar reaction pathway as compared to that established for only one water molecule. However, the inclusion of an additional water molecule greatly facilitates all mechanistic steps by assisting the proton transfers or through a neighboring catalyst charge delocalization effect. As a consequence, the barriers of the carbinolamine and dehydration steps decreased by 16.2 and 12.7 kJ mol⁻¹. This is in agreement with previous calculations on imine formation from methylamine and formaldehyde, where the inclusion of two water molecules greatly reduced the barrier for carbinolamine formation.^[17] Several reaction coordinates were tested to establish the reported dehydration step through the energetically favored eight-membered ring transition states. However, all these attempts were unfruitful probably due to stereoelectronic effects of the bulky and strained A–C rings of dehydrobaicalein.

Formation of 5a adduct

Two reaction pathways were explored for the formation of 5a, one starting from tautomer 2a and the other starting from tautomer 2b. Figure 2 illustrates the geometries of key stationary points along the pathway that is similar to that described for 4c before.

Starting from 2a, the reactants feature a N–C6 distance of 2.20 Å that shortens to 1.54 Å in transition state TS1. This latter state resembles a six-membered ring with an internal CNH angle of 99.7°, the O6 is almost protonated (H_{wat}–O6 distance of 1.08 Å) and the amine is transferring its proton to the assisting water molecule (N–H and H–O_{wat} lengths of 1.14 Å and 1.45 Å). TS1 lies 43.7 kJ mol⁻¹ above the reactant complex, while the following carbinolamine intermediate INT1 lies 16.9 kJ mol⁻¹ below the reactants. The dehydration/imine formation step is, however, rather different to the one found previously for adducts 4c and 6c. It becomes simpler due to the neighboring C7–OH unit that can donate its proton to the leaving C6 hydroxy group that releases a water molecule and forms the protonated Schiff base. The assisting water plays a catalytic role by electrostatic stabilization of O7 the oxygen atom. The following transition state TS2 features C–O and N–C bond distances of 1.55 and 1.39 Å, whilst the H-transfer is already advanced, being the proton nearer to the hydroxy group (distance of 1.12 Å) than to the O7 (distance of 1.37 Å). The barrier for this step amounts to +69.1 kJ mol⁻¹ relative to INT1', whereas the formed intermediate 5c is favored by 27.1 kJ mol⁻¹ relative to the reactant complex. The sequence terminates through H-transfer to form product 5a. In the associated TS3, the proton from the nitrogen is already transferred to the water molecule (distances of 1.41 Å and 1.11 Å, respectively), whereas the other proton is being transferred to O7 (distance of 1.36 Å). The barrier for this step is +35.6 kJ mol⁻¹ in relation to INT2', and the complete reaction is exergonic by ΔG_R = -32.5 kJ mol⁻¹.

As expected, a similar reaction pathway can be found when starting from 2b (Scheme 7). The main difference between the two reactions is found in the energy profile, where the barriers for carbinolamine and Schiff base formation generated by the latter tautomer are higher by 16.3 and 12.7 kJ mol⁻¹, respectively.

Formation of 6c adduct

Scheme 8 portrays the reaction pathway for the formation of DBA–PA adduct 6c from the 2a. The complete reaction is exergonic at -49.0 kJ mol⁻¹. Despite the similarity of the reaction pathways leading to adducts 6c and 4c, there are some differences in the reaction energy profiles. The barrier for formation of the carbinolamine intermediate is much smaller in the formation of 6c than the formation of 4c with an energy differences of 48.5 kJ mol⁻¹; however, the latter adduct is thermodynamically more favorable by 16.2 kJ mol⁻¹.

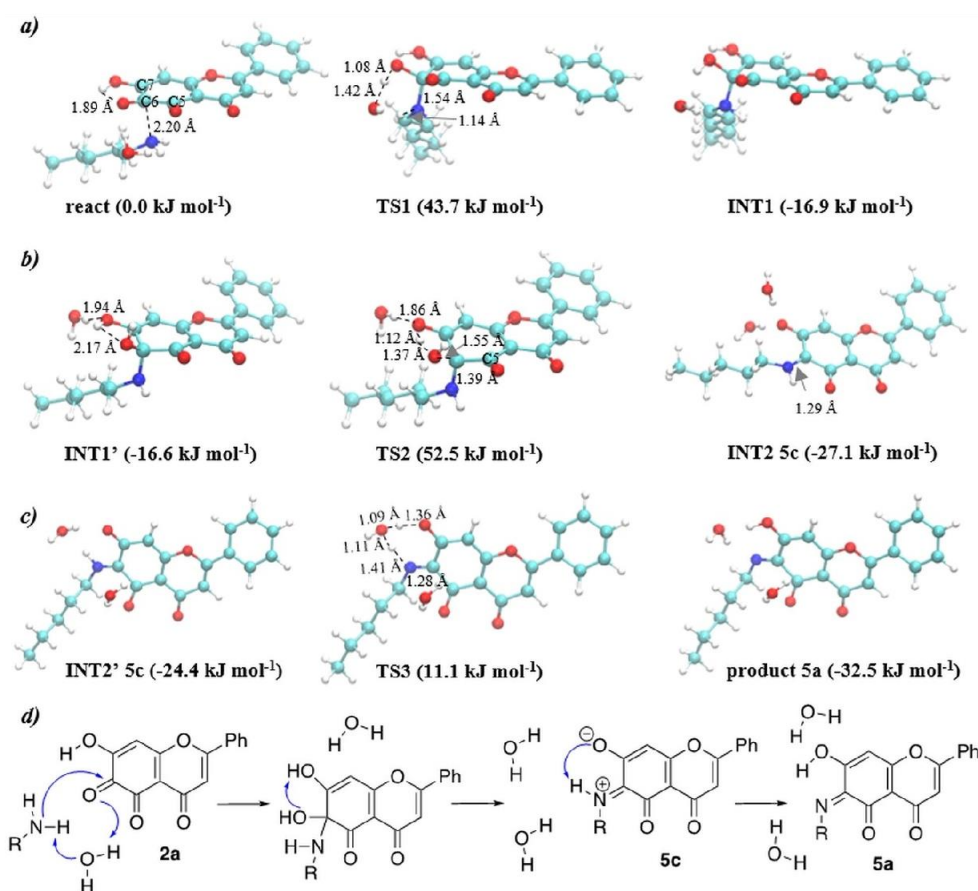
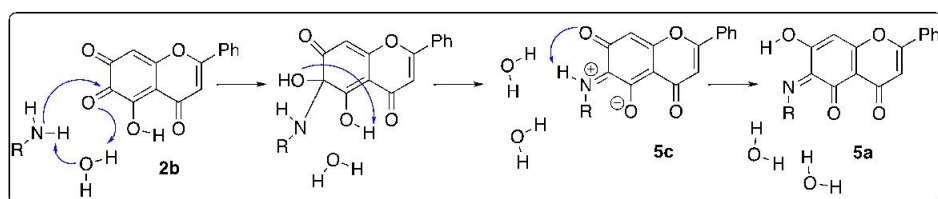


Figure 2. Representation of the mechanistic pathway to form the dehydrobaicalein–pentylamine adduct **5a** from **2a**: a) carbinolamine formation, b) dehydration/Schiff base formation, c) **5a** formation, and d) 2D depiction of the complete reaction.

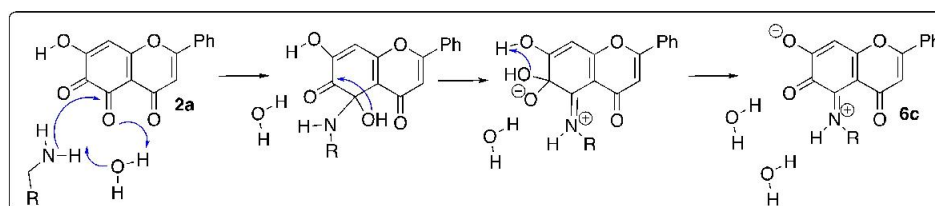


Scheme 7. Reaction pathway for the formation of dehydrobaicalein–pentylamine adduct **5a** from **2b**.

Energetic comparison of the reaction pathways to form the **4c**, **5a** and **6c** adducts

Figure 3 displays the energy profiles for the complete reaction pathways to form adducts **4c**, **5a** and **6c** in the presence of one water molecule as obtained at the DLPNO-CCSD(T)/cc-pVTZ//SMD(water)/B3LYP-D3/6-31+G(d,p) level of theory. For

the cases with two geometries of the same species (e.g., INT1 and INT1'), the most favored state is considered to compare the energies of the various mechanisms. These results show higher free energies for the dehydration step of all reactions (varying between 69.4 (**5a** path from **2a**) and 87.0 kJ mol⁻¹ (**6c** path)), thus indicating that this step should be rate-limiting. The exception is the path to form **4c** that, due to a charge



Scheme 8. Mechanistic pathway from **2a** to form the dehydrobaicalein–pentylamine adduct **6c**.

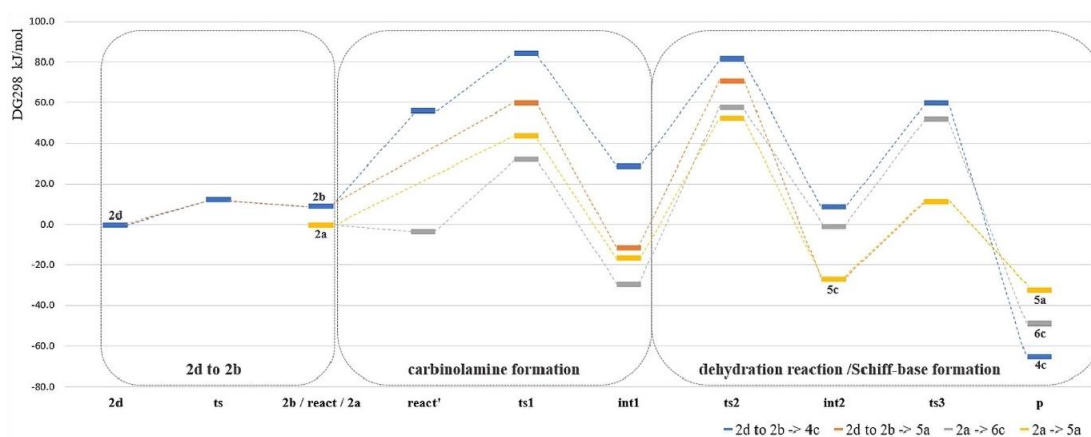


Figure 3. Energetic profiles of the Schiff base reaction of dehydrobaicalein tautomers **2a**, **2b** and **2d** with the nucleophile **3** to yield the dehydrobaicalein–pentylamine adducts **4c**, **5a** and **6c**.

delocalization effect on **2b** structure that provides a disadvantageous pre-reaction geometry, has similar barriers for carbinolamine and Schiff base formation (84.2 and 81.4 kJ mol⁻¹, respectively). This unfavorable effect is also reflected in the instability of the carbinolamine intermediate on the **4c**-path (28.6 kJ mol⁻¹ above the reactants) that is notoriously different to the energetically favored intermediates of the other reactions (−29.6 kcal mol⁻¹, −16.9 and −11.5 kJ mol⁻¹ for **6c** path, **5a** path (from **2d/2b**), respectively).

Overall, these mechanistic findings indicate energetically viable routes to form the various **DBA–PA** adducts, which could be responsible for the favored covalent inhibition mechanisms of baicalein targeting lysine residues of amyloid proteins. The formation of **5a** (C6-substituted **DBA**) is kinetically favored due to the overall lowest free energy barriers, while the formation of **4c** (C7-substituted **DBA**) is found to be the most thermodynamically favored (exergonic at −65.2 kJ mol⁻¹). The experiments only found the C6-substituted Schiff base product, which suggests kinetic control under these reaction conditions.

Furthermore, considering the higher stability of **4c**, future **DBA**-based drug-design strategies should focus on providing molecules with further positive charge character nearby the C7 (e.g., at C8) centers to improve the relative amine group C7

position, avoiding the formation of the unfavorable pre-reaction geometry that subsequently may decrease the barriers.

Conclusions

Amongst its physiological antioxidant benefits, the flavonoid baicalein exhibits inhibitory activity towards amyloid proteins such as hIAPP through covalent reactions with the pentylamine group of lysine residues that subsequently disturb the peptide aggregation. A combination of *in silico* and *in vitro* approaches is essential to clarify the oxidation state and reactivity of **BA** as well as its conjugation with the side chain of lysine residues in solution.

Based on these results, we conclude that: i) dehydrobaicalein species, namely 6,7-dehydrobaicalein **2b**, are formed in solution. ii) The reaction of **BA** and **PA** starts with the formation of a ion pair between the protonated amine group and the ionized **BA**[−] under anaerobic conditions that precedes a (low-oxygen) induced redox chain reaction. Thus, the presence of O₂ is crucial to generate the *o*-quinone **DBA** that promptly forms the intermediate **DBA–PA** (**5a**), which could be then reduced to yield the main **BA–PA** product (**11a**). Despite the fact that transient intermediate **5a** could not be detected under our

experimental conditions, we propose that its formation and further reduction is essential for the redox cycle. iii) The atomistic mechanistic studies uncovered an unusual pathway for the carbinolamine dehydration reaction, which focuses on the resonance ring effects of the dehydrobaicalein species. It involves an intramolecular rearrangement of the hydroxy leaving group that assists and reduces the barrier of this step. Also, the carbinolamine dehydration mechanistic step of all studied pathways is the rate-limiting step. iv) In agreement with the kinetically preferred pathway suggested by calculations, experiments show a regioselectivity of the Schiff base reaction for the middle position of the three hydroxy groups of BA. This may be attributed to the resonance-stabilized structure along the AC and B (with no substituents) rings. However, the theoretical mechanistic findings suggest feasible energetic profiles for all reactive pathways toward the formation of C6-, C7- and C5-substituted products. These many covalent mechanistic possibilities could be a specific property of baicalein that might contribute to its higher inhibition ability against amyloid formation as compared to other structurally related flavone molecules. The poor solubility of baicalein could limit its use as a therapeutic compound, but innovative strategies such as the use of baicalein–theophylline cocrystals have been proposed to overcome this hurdle and improve the bioavailability of baicalein.^[51] In addition, a baicalein- β -cyclodextrin combination was suggested as a promising therapeutic route to inhibit and remodel α -synuclein amyloids.^[52] These should be considered in designing novel baicalein-based molecules for inhibiting hIAPP amyloidogenesis in vivo. The pharmacological and wide structural properties of flavonoids as well as their lower toxicity compared to synthetic compounds gives them an advantage as future multitargeting therapeutic molecules. Hence, the currently uncovered mechanistic differences could be valuable to optimize and engineer future o-quinone–baicalein based drug candidates.

Acknowledgements

This work was supported by UIDB/50006/2020 with funding from FCT/MCTES – the Portuguese Foundation for Science and Technology through national funds. N.F.B. acknowledges support from the scientific employment stimulus – individual call of 2018 (CEECIND/02017/2018). Open Access funding enabled and organized by Projekt DEAL.

Conflict of Interest

The authors declare no conflict of interest.

Data Availability Statement

The data that support the findings of this study are available in the supplementary material of this article.

Keywords: autoxidation · computational chemistry · quinones · Schiff bases · transition states

- [1] X. X. Zhang, Y. H. Pan, Y. M. Huang, H. L. Zhao, *World J. Diabetes* **2016**, *7*, 189–197.
- [2] a) V. Armiento, A. Spanopoulou, A. Kapurniotu, *Angew. Chem. Int. Ed.* **2020**, *59*, 3372–3384; *Angew. Chem.* **2020**, *132*, 3396–3409; b) M. Stefani, S. Rigacci, *Int. J. Mol. Sci.* **2013**, *14*, 12411–12457.
- [3] a) Z. Dhoulfi, K. Cuanalo-Contreras, E. A. Hayouni, C. E. Mays, C. Soto, I. Moreno-Gonzalez, *Cell. Mol. Life Sci.* **2018**, *75*, 3521–3538; b) P. Velandier, L. Wu, F. Henderson, S. Zhang, D. R. Bevan, B. Xu, *Biochem. Pharmacol.* **2017**, *139*, 40–55.
- [4] a) P. Cao, D. P. Raleigh, *Biochemistry* **2012**, *51*, 2670–2683; b) P. Velandier, L. Wu, W. K. Ray, R. F. Helm, B. Xu, *Biochemistry* **2016**, *55*, 4255–4258; c) I. R. Sequeira, S. D. Poppitt, *Nutrients* **2017**, *9*, 788; d) A. A. Alkahtane, H. A. Alghamdi, B. Almutairi, M. M. Khan, M. S. Hasnain, M. M. Abdel-Daim, W. M. Alghamdi, S. Alkahtani, *Int. J. Med. Sci.* **2021**, *18*, 199–206.
- [5] H. M. Awad, M. G. Boersma, S. Boeren, P. J. van Bladeren, J. Vervoort, I. M. Rietjens, *Chem. Res. Toxicol.* **2001**, *14*, 398–408.
- [6] a) M. Zhu, S. Han, A. L. Fink, *Biochim. Biophys. Acta* **2013**, *1830*, 2872–2881; b) M. Zhu, S. Rajamani, J. Kaylor, S. Han, F. Zhou, A. L. Fink, *J. Biol. Chem.* **2004**, *279*, 26846–26857; c) T. Ginex, M. Trius, F. J. Luque, *Chem. Eur. J.* **2018**, *24*, 5813–5824.
- [7] F. L. Palhano, J. Lee, N. P. Grimster, J. W. Kelly, *J. Am. Chem. Soc.* **2013**, *135*, 7503–7510.
- [8] M. Sato, K. Murakami, M. Uno, Y. Nakagawa, S. Katayama, K. Akagi, Y. Masuda, K. Takegoshi, K. Irie, *J. Biol. Chem.* **2013**, *288*, 23212–23224.
- [9] J. Sun, T. Murata, H. Shigemori, *J. Nat. Med.* **2020**, *74*, 579–583.
- [10] E. O. Choi, J. W. Jeong, C. Park, S. H. Hong, G. Y. Kim, H. J. Hwang, E. J. Cho, Y. H. Choi, *Int. J. Mol. Med.* **2016**, *37*, 798–806.
- [11] S. M. Choi, B. C. Kim, Y. H. Cho, K. H. Choi, J. Chang, M. S. Park, M. K. Kim, K. H. Cho, J. K. Kim, *Chonnam. Med. J.* **2014**, *50*, 45–51.
- [12] S. Q. Zhang, D. Obregon, J. Ehrhart, J. Deng, J. Tian, H. Hou, B. Giunta, D. Sawmiller, J. Tan, *J. Neurosci. Res.* **2013**, *91*, 1239–1246.
- [13] R. Malisaukas, A. Botyriute, J. G. Cannon, V. Smirnovas, *PLoS One* **2015**, *10*, e0121231.
- [14] R. Lantz, B. Busbee, E. P. Wojcikiewicz, D. Du, *Chem. Eur. J.* **2020**, *26*, 13063–13071.
- [15] a) K. Hashida, R. Makino, S. Ohara, *Holzforchung* **2009**, *63*, 319–326; b) F. J. Wang, J. Y. Bae, A. R. Jacobson, Y. H. Lee, L. M. Sayre, *J. Org. Chem.* **1994**, *59*, 2409–2417.
- [16] a) Y. Q. Ding, Y. Z. Cui, T. D. Li, *J. Phys. Chem. A* **2015**, *119*, 4252–4260; b) B. Vilanova, J. M. Gallardo, C. Caldes, M. Adrover, J. Ortega-Castro, F. Munoz, J. Donoso, *J. Phys. Chem. A* **2012**, *116*, 1897–1905; c) C. Solis-Calero, J. Ortega-Castro, A. Hernandez-Laguna, F. Munoz, *Theor. Chem. Acc.* **2012**, *131*, 1263; d) M. LARGERON, A. Neudorffer, M. B. Fleury, *J. Chem. Soc. Perkin Trans. 2* **1998**, 2721–2727.
- [17] N. E. Hall, B. J. Smith, *J. Phys. Chem. A* **1998**, *102*, 4930–4938.
- [18] S. Sinha, D. H. Lopes, Z. Du, E. S. Pang, A. Shanmugam, A. Lomakin, P. Talbiersky, A. Tennstaedt, K. McDaniel, R. Bakshi, P. Y. Kuo, M. Ehrmann, G. B. Benedek, J. A. Loo, F. G. Klamer, T. Schrader, C. Wang, G. Bitan, *J. Am. Chem. Soc.* **2011**, *133*, 16958–16969.
- [19] a) M. H. Wu, A. C. Chan, L. H. Tu, *Biochimie* **2020**, *177*, 153–163; b) Y. H. Hsu, Y. W. Chen, M. H. Wu, L. H. Tu, *Biophys. J.* **2019**, *116*, 2304–2313.
- [20] A. D. Becke, *J. Chem. Phys.* **1993**, *98*, 5648–5652.
- [21] S. Grimme, J. Antony, S. Ehrlich, H. Krieg, *J. Chem. Phys.* **2010**, *132*, 154104.
- [22] P. C. Harihar, J. A. Pople, *Theor. Chim. Acta* **1973**, *28*, 213–222.
- [23] A. V. Marelich, C. J. Cramer, D. G. Truhlar, *J. Phys. Chem. B* **2009**, *113*, 6378–6396.
- [24] A. E. Reed, R. B. Weinstock, F. Weinhold, *J. Chem. Phys.* **1985**, *83*, 735–746.
- [25] Z. Jia, T. Ramstad, M. Zhong, *Electrophoresis* **2001**, *22*, 1112–1118.
- [26] a) D. S. Kristol, P. Krauthaim, S. Stanley, R. C. Parker, *Bioorg. Chem.* **1975**, *4*, 299–304; b) I. Andre, S. Linse, F. A. Mulder, *J. Am. Chem. Soc.* **2007**, *129*, 15805–15813.
- [27] a) N. F. Bras, M. A. Perez, P. A. Fernandes, P. J. Silva, M. J. Ramos, *J. Chem. Theory Comput.* **2011**, *7*, 3898–3908; b) P. Georgieva, F. Himo, *J. Comput. Chem.* **2010**, *31*, 1707–1714.
- [28] N. F. Bras, P. A. Fernandes, M. J. Ramos, S. D. Schwartz, *Chem. Eur. J.* **2018**, *24*, 1978–1987.
- [29] T. H. Dunning, *J. Chem. Phys.* **1989**, *90*, 1007–1023.
- [30] M. J. Frisch, G. W. Trucks, H. B. Schlegel, G. E. Scuseria, M. A. Robb, J. R. Cheeseman, G. Scalmani, V. Barone, G. A. Petersson, H. Nakatsuji, X. Li,

- M. Caricato, A. Marenich, J. Bloino, B. G. Janesko, R. Gomperts, B. Mennucci, H. P. Hratchian, J. V. Ortiz, A. F. Izmaylov, J. L. Sonnenberg, D. Williams-Young, F. Ding, F. Lipparini, F. Egidi, J. Goings, B. Peng, A. Petrone, T. Henderson, D. Ranasinghe, V. G. Zakrzewski, J. Gao, N. Rega, G. Zheng, W. Liang, M. Hada, M. Ehara, K. Toyota, R. Fukuda, J. Hasegawa, M. Ishida, T. Nakajima, Y. Honda, O. Kitao, H. Nakai, T. Vreven, K. Throssell, J. A. Montgomery, Jr., J. E. Peralta, F. Ogliaro, M. Bearpark, J. J. Heyd, E. Brothers, K. N. Kudin, V. N. Staroverov, T. Keith, R. Kobayashi, J. Normand, K. Raghavachari, A. Rendell, J. C. Burant, S. S. Iyengar, J. Tomasi, M. Cossi, J. M. Millam, M. Klene, C. Adamo, R. Cammi, J. W. Ochterski, R. L. Martin, K. Morokuma, O. Farkas, J. B. Foresman, D. J. Fox, *Gaussian v.09*, Gaussian, Inc., Wallingford CT, 2016.
- [31] F. Neese, F. Wennmohs, U. Becker, C. Riplinger, *J. Chem. Phys.* **2020**, *152*, 224108.
- [32] a) N. L. Haworth, Q. Wang, M. L. Coote, *J. Phys. Chem. A* **2017**, *121*, 5217–5225; b) P. G. Seybold, G. C. Shields, *Wiley Interdiscip. Rev.: Comput. Mol. Sci.* **2015**, *5*, 290–297.
- [33] a) M. Wolniak, J. Oszmianski, I. Wawer, *Magn. Reson. Chem.* **2008**, *46*, 215–225; b) Z. S. Markovic, J. M. Dimitric Markovic, D. Milenkovic, N. Filipovic, *J. Mol. Model.* **2011**, *17*, 2575–2584.
- [34] M. Rossi, R. Meyer, P. Constantinou, F. Caruso, D. Castelbuono, M. O'Brien, V. Narasimhan, *J. Nat. Prod.* **2001**, *64*, 26–31.
- [35] M. R. Fesen, Y. Pommier, F. Leteurtre, S. Hiroguchi, J. Yung, K. W. Kohn, *Biochem. Pharmacol.* **1994**, *48*, 595–608.
- [36] M. Musialik, R. Kuzmicz, T. S. Pawlowski, G. Litwinienko, *J. Org. Chem.* **2009**, *74*, 2699–2709.
- [37] R. Alvarez-Diduk, M. T. Ramirez-Silva, A. Galano, A. Merkoci, *J. Phys. Chem. B* **2013**, *117*, 12347–12359.
- [38] Y. Lee, H. Yeo, S. H. Liu, Z. Jiang, R. M. Savizky, D. J. Austin, Y. C. Cheng, *J. Med. Chem.* **2004**, *47*, 5555–5566.
- [39] a) T. Mizutani, H. Takagi, U. Yoshiyuki, T. Horiguchi, K. Yamamura, H. Ogoshi, *J. Phys. Org. Chem.* **1998**, *11*, 737–742; b) J. E. Barry, M. Finkelstein, S. D. Ross, *J. Org. Chem.* **1984**, *49*, 1669–1671.
- [40] F. J. Santiago-Medina, A. Pizzi, M. C. Basso, L. Delmotte, A. Celzard, *Polymer* **2017**, *9*, 37.
- [41] a) D. Wozniak, A. Drys, A. Matkowski, *Nat. Prod. Res.* **2015**, *29*, 1567–1570; b) Y. K. Han, H. Kim, H. Shin, J. Song, M. K. Lee, B. Park, K. Y. Lee, *Molecules* **2020**, *25*, 3617; c) Z. Gao, K. Huang, X. Yang, H. Xu, *Biochim. Biophys. Acta* **1999**, *1472*, 643–650.
- [42] C. Tang, J. Tan, J. Jin, S. Xi, H. Li, Q. Xie, X. Peng, *Rapid Commun. Mass Spectrom.* **2015**, *29*, 1863–1873.
- [43] Z. Feng, J. Zhou, X. Shang, G. Kuang, J. Han, L. Lu, L. Zhang, *Pharm. Biol.* **2017**, *55*, 1177–1184.
- [44] A. T. Garrison, Y. Abouelhassan, D. Kallifidas, F. Bai, M. Ukhanova, V. Mai, S. Jin, H. Luesch, R. W. Huigens 3rd, *Angew. Chem. Int. Ed.* **2015**, *54*, 14819–14823; *Angew. Chem.* **2015**, *127*, 15032–15036.
- [45] S. Morimoto, N. Tateishi, T. Matsuda, H. Tanaka, F. Taura, N. Furuya, N. Matsuyama, Y. Shoyama, *J. Biol. Chem.* **1998**, *273*, 12606–12611.
- [46] C. A. Perez, Y. Wei, M. Guo, *J. Inorg. Biochem.* **2009**, *103*, 326–332.
- [47] Y. H. Lee, Y. Lin, S. J. Cox, M. Kinoshita, B. R. Sahoo, M. Ivanova, A. Ramamoorthy, *Biochim. Biophys. Acta Proteins Proteomics* **2019**, *1867*, 529–536.
- [48] Z. X. Xu, Q. Zhang, G. L. Ma, C. H. Chen, Y. M. He, L. H. Xu, Y. Zhang, G. R. Zhou, Z. H. Li, H. J. Yang, P. Zhou, *J. Diabetes Res.* **2016**, *2016*, 1867059.
- [49] G. Grasso, H. Komatsu, P. H. Axelsen, *J. Inorg. Biochem.* **2017**, *174*, 130–136.
- [50] H. S. Fernandes, M. J. Ramos, N. M. F. S. A. Cerqueira, *Chem. Eur. J.* **2017**, *23*, 9162–9173.
- [51] W. Li, J. Pi, Y. Zhang, X. Ma, B. Zhang, S. Wang, D. Qi, N. Li, P. Guo, Z. Liu, *Fitoterapia* **2018**, *129*, 85–93.
- [52] S. Gautam, S. Karmakar, R. Batra, P. Sharma, P. Pradhan, J. Singh, B. Kundu, P. K. Chowdhury, *Biochim. Biophys. Acta Proteins Proteomics* **2017**, *1865*, 589–603.

Manuscript received: November 26, 2021
Accepted manuscript online: January 6, 2022
Version of record online: January 27, 2022

1.2.1. Supporting information

General methods: All reactions sensitive to air and moisture were performed under nitrogen atmosphere, and the glassware as well as magnetic stir bars were dried overnight in a dry oven at 110°C.

Solvents, reagents: All reagents and solvents were purchased from the companies TCI, Sigma Aldrich or Fisher Scientific. All air- or water-sensitive reagents were stored under nitrogen.

NMR spectroscopy: All ^1H NMR spectra were recorded by Bruker 400 in DMSO-*d*₆ at 400 MHz at 23 °C. All ^{13}C NMR spectra were recorded, respectively, at 101 MHz. The chemical shifts are reported in ppm (δ), relative to the resonance of DMSO-*d*₆ at $\delta = 2.50$ ppm for ^1H and for ^{13}C relative to the resonance of DMSO-*d*₆ $\delta = 39.52$ ppm. Spectra were imported and processed in the MestreNova 14.1.1 program. For ^1H NMR spectra multiplicity (s = singlet, d = doublet, t = triplet, q = quartet, quint = quintet, m = multiplet, dd = doublet of doublets, dt = doublet of triplets, td = triplet of doublets, and bs = broad signal.), coupling constants *J*, number of protons and assignment to the structure are reported. In ^{13}C NMR spectra singular carbons are marked with (s).

Mass spectrometry: For electrospray ionization (ESI) spectra a Thermo Finnigan LTQ FT Ultra Fourier Transform Ion Cyclotron Resonance Mass Spectrometer was utilized. For atmospheric pressure chemical ionization (APCI) a Advion CMS using positive mode was used.

Melting point. Melting points were measured using Buchi-560 and are not corrected.

Infrared spectroscopy. FT-IR spectra were measured using FT-IR Perkin Elmer Spectrum BXII/1000 with Smiths ATR.

Single-crystal X-ray diffraction. scXRD measurements were performed on a Bruker D8 Venture TXS diffractometer.

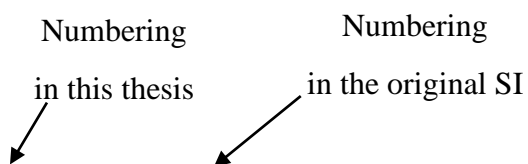
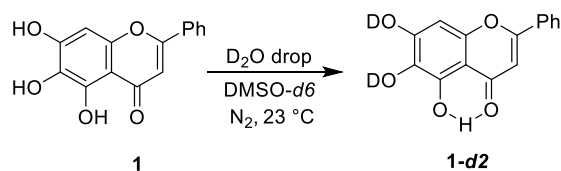


Fig. S1: [Figure S1]. Potential Energy Surface (PES) along the dihedral angle that governs the N-C bond of the **4c** adduct.

1.2.1.1. Experimental Part: Investigating Baicalein (1)-Pentylamine (3) Oxidative Coupling Reactions

Proton exchange experiment



Approximately 5 mg of baicalein (**1**) was placed in a J. Young NMR tube and dissolved in 0.75 ml of dry DMSO-*d*₆ under nitrogen atmosphere. ¹H NMR spectra of the obtained solution was taken, then one drop of D₂O was added to the sample, shaken and the analysis was performed again. The spectra comparison showed the absence of 6- and 7-OH peaks, whilst the 5-OH signal is still detected, due to slower proton-deuterium exchange (Fig. S1).

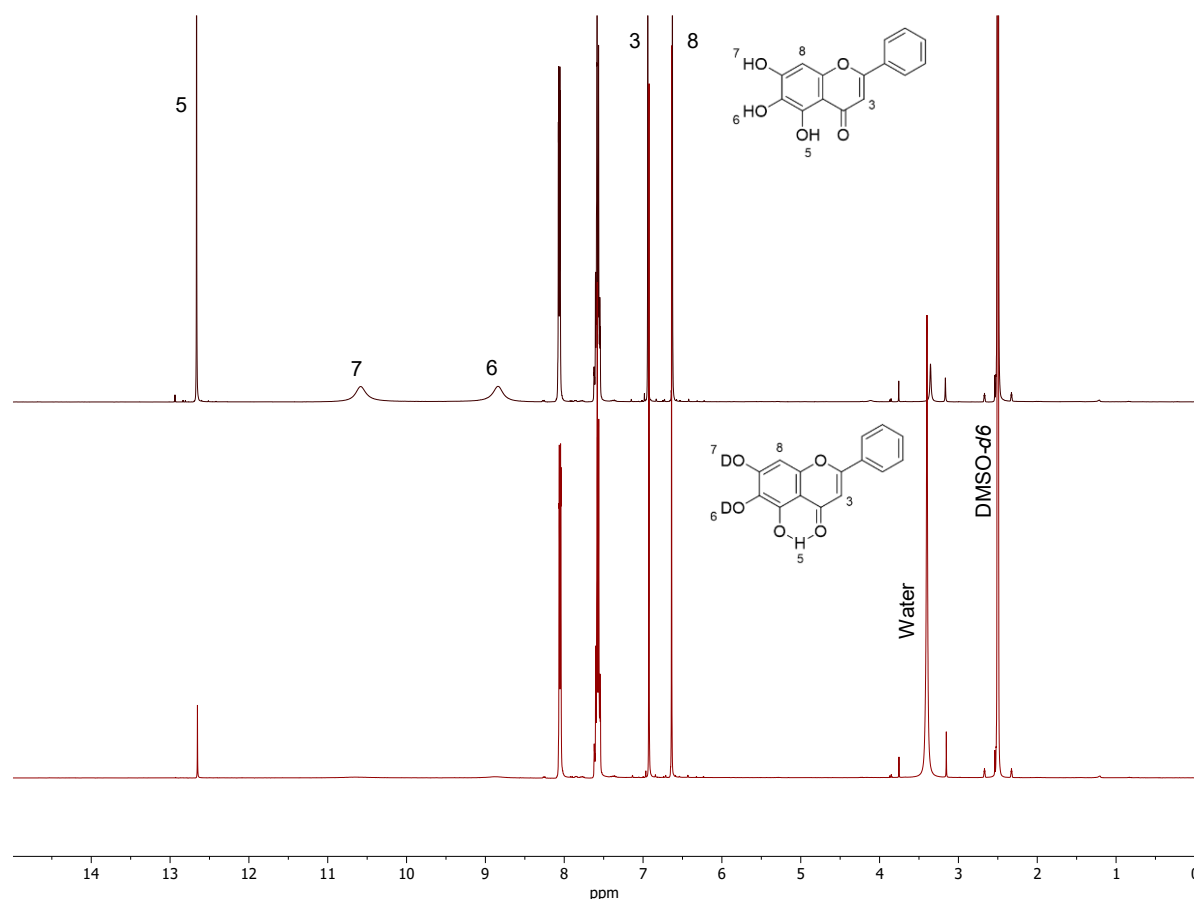
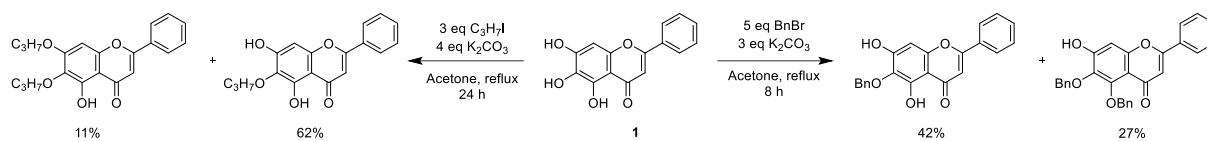


Fig. S1: [Figure S5]. ¹H NMR spectra of baicalein (**1**) in DMSO-*d*₆ and baicalein (**1**) in DMSO-*d*₆/D₂O, 400 MHz.

This observation is in the line with literature reports that alkylation of baicalein (**1**) with *n*-propyl iodide in acetone yields a mixture of monoalkylated (11%) and dialkylated (62%)

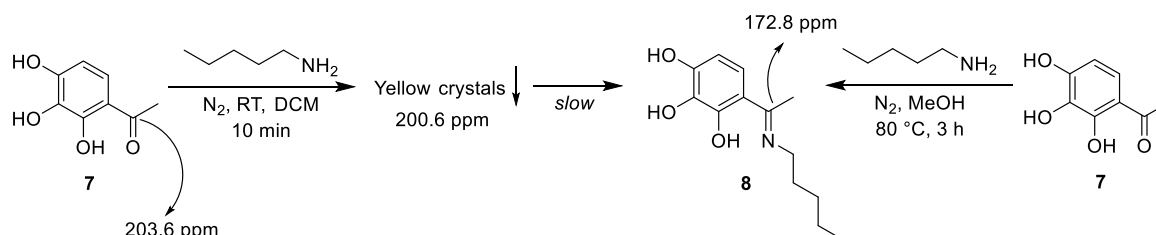
products, correspondingly (Scheme S1). The authors state that the 5-OH of baicalein (**1**) creates an intramolecular hydrogen bond with the keto group, making itself resistant to alkylation (6-OH > 7-OH > 5-OH).^[1]



Scheme S1: [Scheme S4]. Alkylation of baicalein **1** studied by Lee *et. al.*^[1]

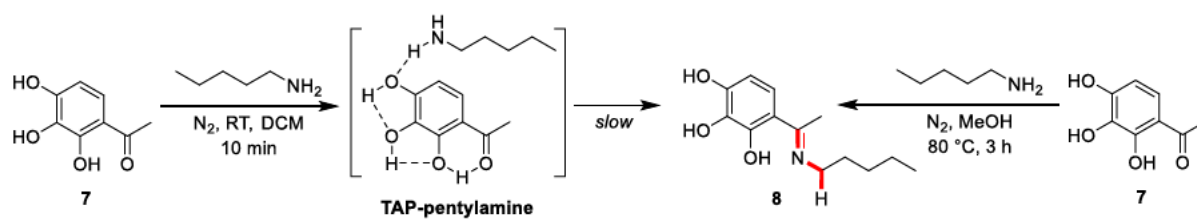
Experiment on TAP (7) with pentylamine (3)

When pentylamine (**3**) is mixed with TAP (**7**) in DCM under nitrogen atmosphere, yellow crystals are formed after short time. The precipitate was filtered off and recrystallized from *i*Hex/EtOAc. It would be obvious to assume that imine **8** is formed during the reaction, since ¹H NMR shows 1 to 1 content of TAP (**7**) and pentylamine (**3**). But ¹³C NMR analysis reveals the signal of the unaffected C=O bond (200.6 ppm). To prove the point, imine **8** was synthesised independently, using another synthetic approach (Scheme S2).



Scheme S2: [Scheme S5]. Preliminary observation on TAP (**7**) and pentylamine (**3**) reaction. ¹³C NMR chemical shifts are given for observed C=X bonds in DMSO-*d*₆ (X = O, N).

In ¹H-¹³C HMBC spectrum of the obtained precipitate, no multiple bond correlations were detected between protons of alkyl chain of the amine and carbon atoms of TAP (**7**), indicating the absence of a covalent bond. Whilst there is a correlation between the imine carbon in C=N bond and the protons of the α-CH₂-group in imine **8**. The imine signals in HMBC spectrum can be explained by slow conversion of the obtained precipitate in the solution to imine **8** during the NMR analysis (Fig. S2). Despite instability of obtained crystals, single crystal X-ray analysis was performed, revealing the true structure of the obtained precipitate (Fig. S3, Table S1).



Scheme S3: [Scheme S6]. TAP (7) reaction with pentylamine (3). ^1H - ^{13}C HMBC correlation in red shows the formation of imine 8.

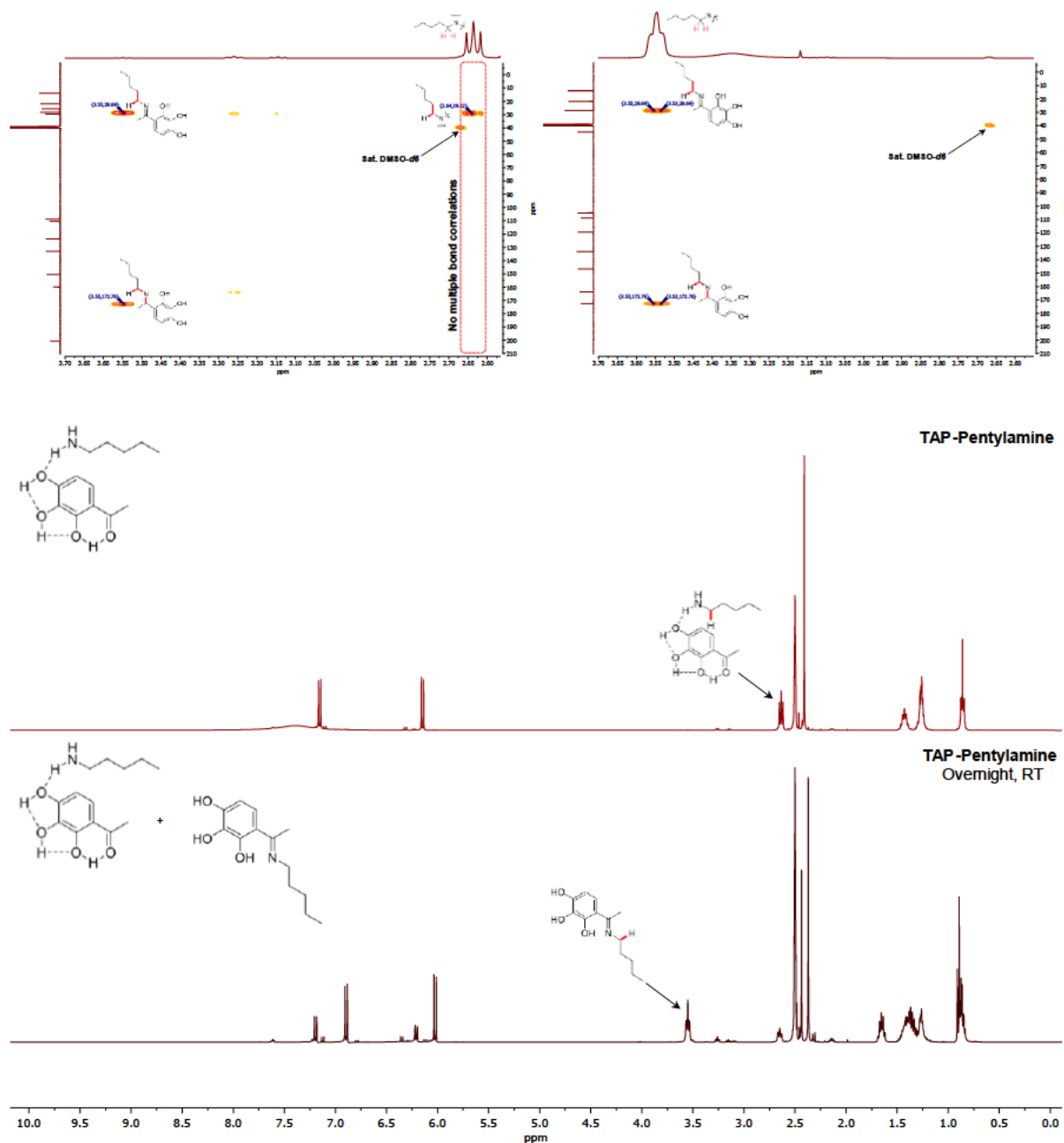


Fig. S2: [Figure S6]. ^1H - ^{13}C HMBC spectrum of TAP-pentylamine (left) and imine 8 (right). TAP-pentylamine slowly forms imine 8 in solution at RT.

When pentylamine (**3**) is mixed with TAP (**7**), TAP-pentylamine phenolate forms, which slowly turns into imine **8** at room temperature. Also, it is good to keep in mind, that amines and polyphenols also tend to form hydrogen-bonded complexes. In Scheme S3, the intermediate is represented as TAP-pentylamine complex for simplicity reasons. The similar chemical behaviour is expected when pentylamine (**3**) is mixed with baicalein, due to structural resemblance of the latter with TAP (**7**).

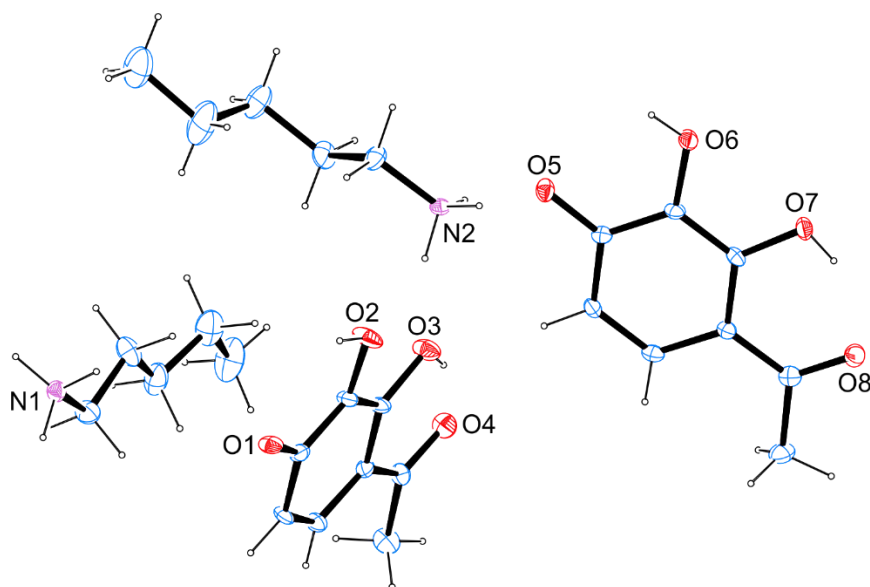


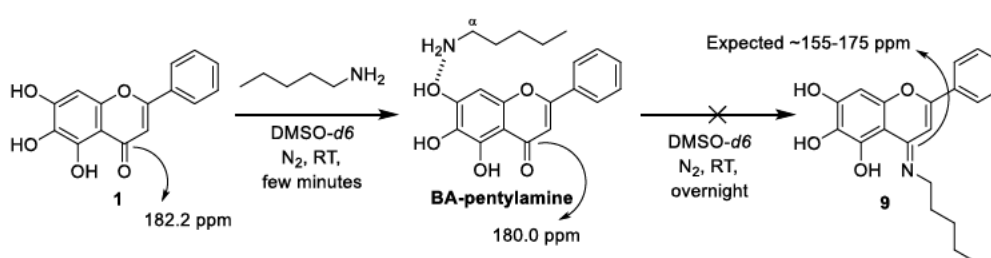
Fig. S3: [Figure S7]. X-ray crystal structure of TAP-pentylamine complex (CCDC Deposition Number 2124561).

Table S1: [Table S4]. Crystallographic data for TAP-pentylamine complex.

net formula	$C_{13}H_{21}NO_4$	transmission factor range	0.57–1.00
$M_r/g\ mol^{-1}$	255.31	refls. measured	4958
crystal size/mm	$0.250 \times 0.150 \times 0.020$	R_{int}	0.1266
T/K	173.(2)	mean $\sigma(I)/I$	0.1142
radiation	MoK α	θ range	2.573–25.348
diffractometer	Bruker D8 Venture TXS	observed refls.	3436
crystal system	triclinic	x, y (weighting scheme)	0, 5.1698
space group	P-1	hydrogen refinement	mixed
a/Å	11.359(2)	Flack parameter	?
b/Å	11.559(2)	refls in refinement	4958
c/Å	11.933(3)	parameters	408
α°	71.277(7)	restraints	54
β°	70.247(7)	$R(F_{obs})$	0.1026
γ°	80.087(7)	$R_w(F^2)$	0.2440
V/Å ³	1393.0(5)	S	1.172
Z	4	shift/error _{max}	0.001
calc. density/g cm ⁻³	1.217	max electron density/e Å ⁻³	0.558
μ/mm^{-1}	0.090	min electron density/e Å ⁻³	-0.357
absorption correction	Multi-Scan		

Experiment on Baicalein (1) with Pentylamine (3)

Due to insolubility of baicalein (1) in DCM, it was decided to switch to DMSO-*d*6 to perform *in situ* reactions. 20 mg of baicalein (1) (0.0741 mmol, 1 eq) in a J. Young NMR tube was evacuated and refilled with N₂ three times, dissolved in 0.75 ml of dry degassed (3×freeze-pump-thaw cycles) DMSO-*d*6, followed by addition of ~9 μl pentylamine (3) (7 mg, 0.0781, 1 eq). The yellow-green solution colour instantly turns orange. The analysis of the obtained ¹H-¹³C HSQC spectra shows the formation of BA-pentylamine complex (Scheme S4). The assumption is based on the similar chemical shifts of protons and carbon of the α-CH₂-group (Fig. S4).



Scheme S4: [Scheme S7]. Baicalein (1) reaction with pentylamine (3). ¹³C NMR chemical shifts are given for observed C=X bonds in DMSO-*d*6 (X = O, N).

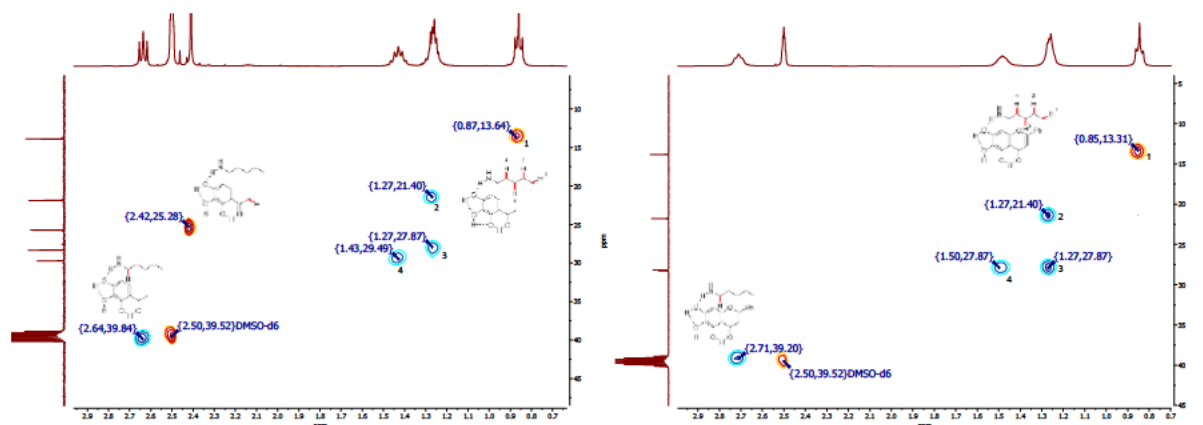


Fig. S4: [Figure S8]. Comparison of ¹H-¹³C HSQC spectra of TAP- and BA-pentylamine, DMSO-*d*6, 400 MHz.

Since TAP-pentylamine slowly turns into imine 8, the same reaction was expected from BA-pentylamine with formation of imine 9 through nucleophilic addition. The sample, mentioned above, was stored over 3 days at RT and ¹H NMR analysis was performed again, after 72 h. No major difference was detected between two measurements, after few minutes and after 72 h, correspondingly (Fig. S5).

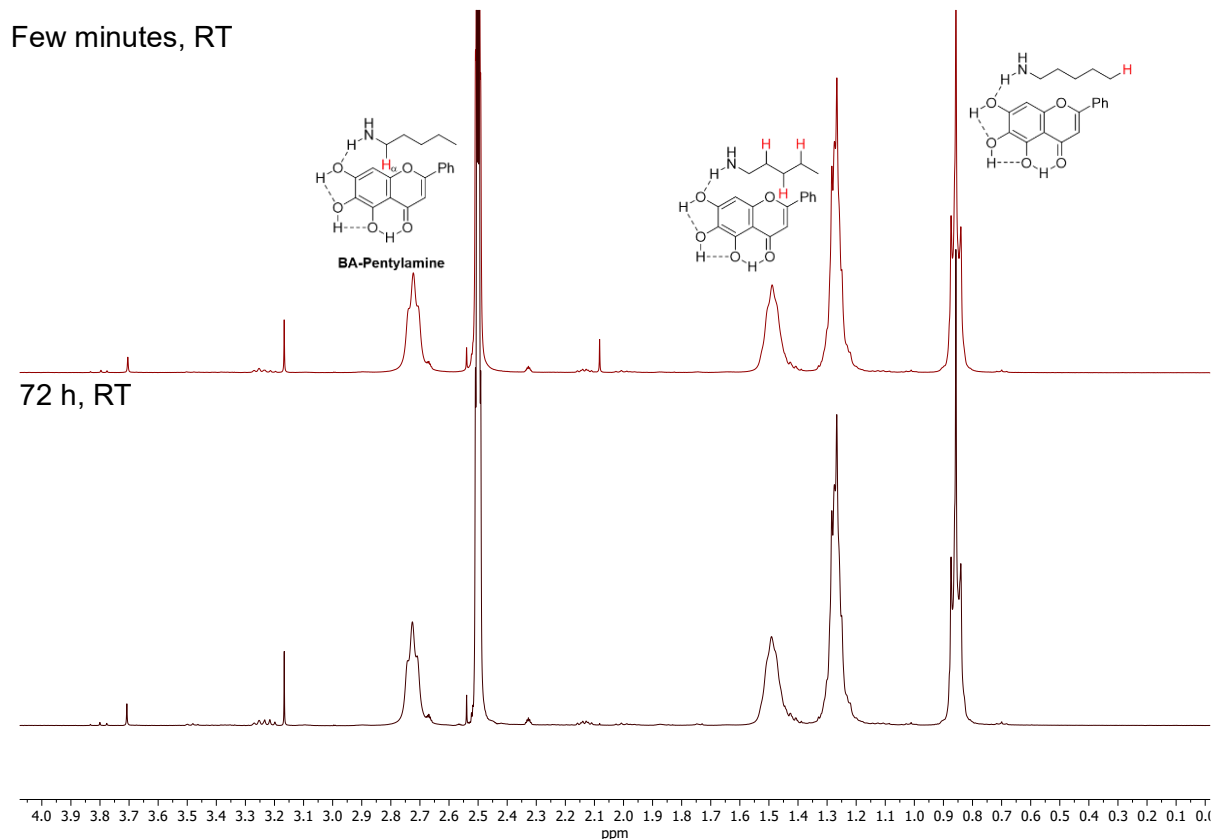


Fig. S5: [Figure S9]. BA-pentylamine after 72 h at RT, DMSO-d₆, 400 MHz

The same reaction was performed again, but with an addition of catalytic amount of acid to accelerate the possible condensation reaction. ¹H NMR spectrum of the obtained reaction mixture was taken. The sample showed no difference after staying for 5 days (120 h) at RT. The same results were obtained after heating the sample up to 50 °C for 5 h (Fig. S6). The absence of a product can be explained by anaerobic conditions during the reaction. To prove the point, nitrogen atmosphere in the J. Young NMR tube was carefully replaced by pure oxygen and the sample was shaken vigorously for a few seconds. The solution changes from clear orange color to black. Then the color of the solution changes from black to deep red after 1-2 minutes at RT (Fig. S7).

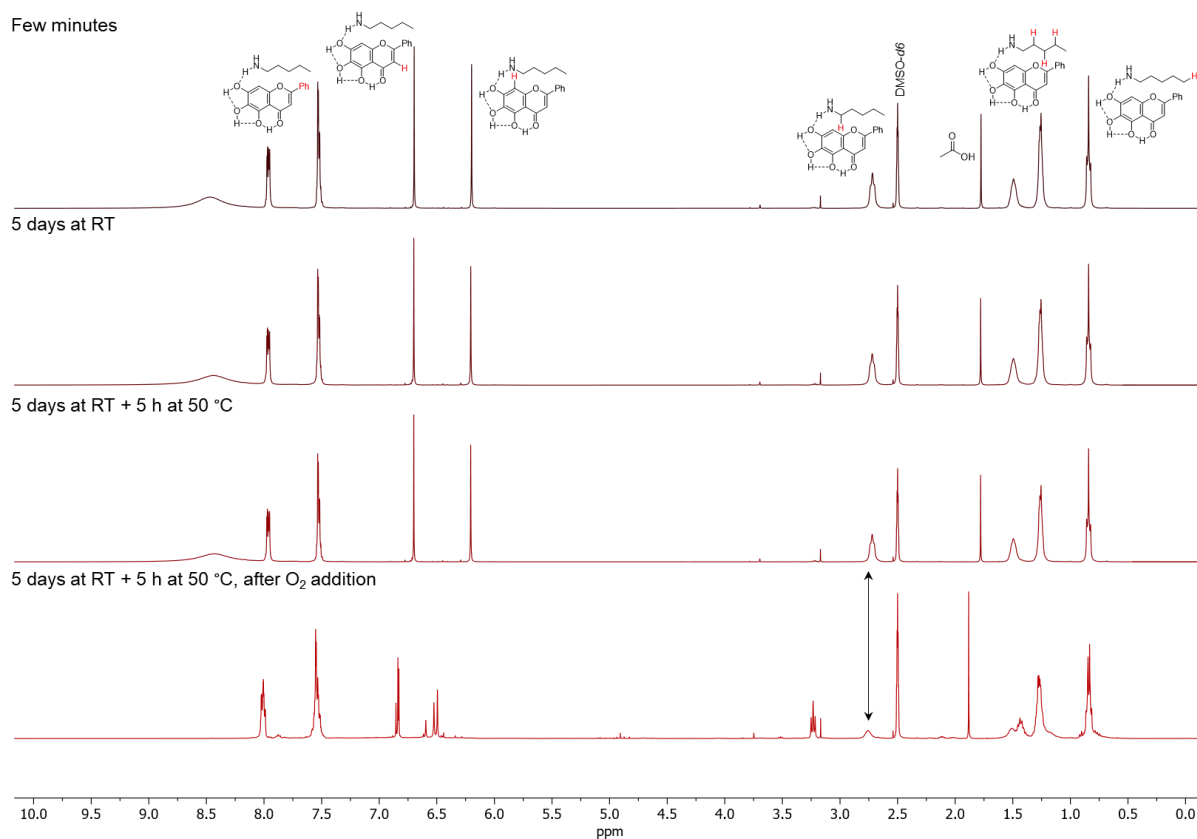


Fig. S6: [Figure S10]. BA-pentylamine with catalytic amount of AcOH, DMSO-*d*₆, 400 MHz.

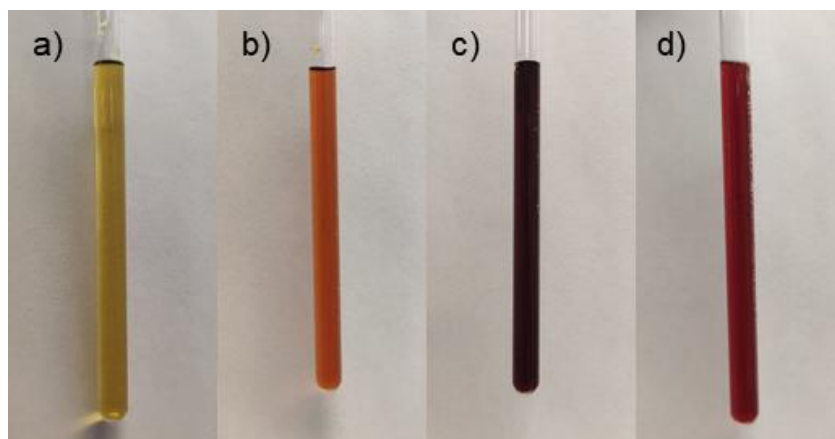


Fig. S7: [Figure S11]. a) BA, b) BA-pentylamine, c) BA-pentylamine + O₂(few seconds) d) BA-pentylamine + O₂ (1-2 minutes).

1 ml aliquot of prepared BA-pentylamine solution was exposed to air, while being transferred to another NMR tube, which was sealed with a plastic cap. The remaining 1 ml of prepared BA-pentylamine solution was stored under anaerobic conditions. ¹H NMR spectra was taken for both samples after 5 days (120 h). It was shown that even slight exposure to air during the sample preparation for NMR analysis can trigger the reaction (Fig. S8).

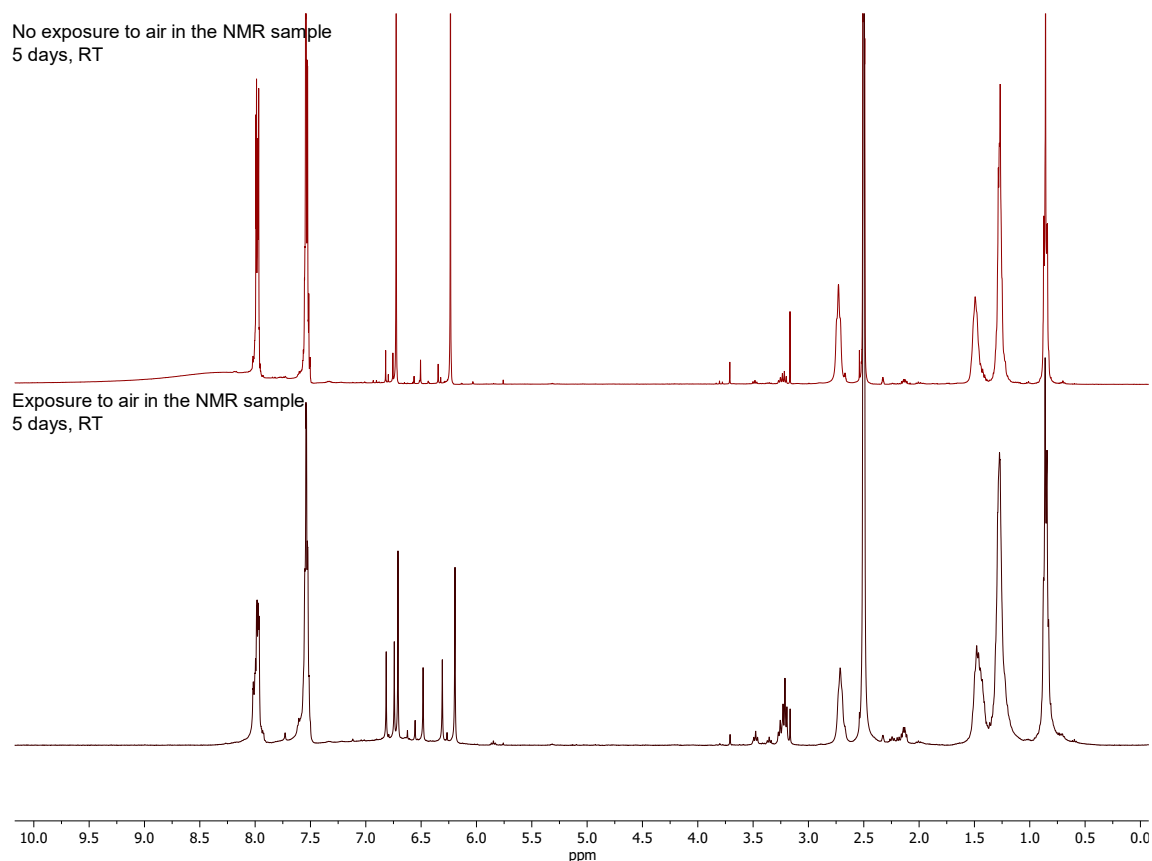


Fig. S8: [Figure S12]. BA-pentylamine, no exposure to air (top) and with exposure to air (bottom) after 5 days (120 h), DMSO-*d*₆, 400 MHz.

Preliminary Experiment on Baicalein (1) with Pentylamine (3)

Approximately 5 mg of baicalein (**1**) was placed in a GC vial and dissolved in 1 ml of dry DCM under air. A drop of pentylamine (**3**) was added to the stirring suspension, which turns clear yellow as soon as amine is well mixed in (Fig. S9). After 10 min of stirring at room temperature, APCI-MS analysis was performed, which shows the formation of a new $[M+H]^+$ peak at m/z 340, isomeric to condensation product with water molecule elimination. No condensation products were observed when *t*-butylamine was used instead of pentylamine.

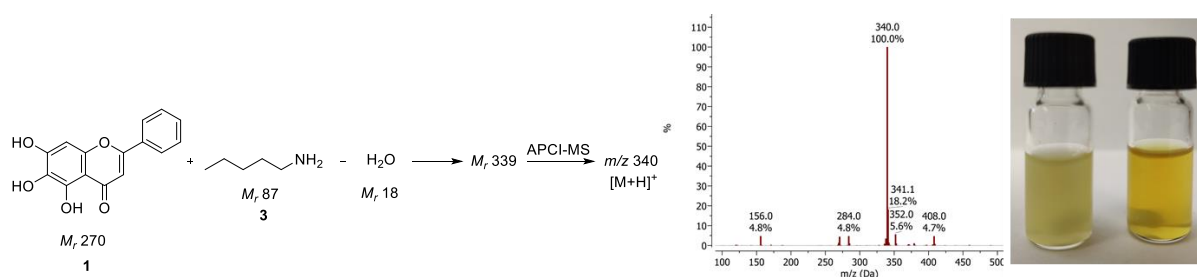


Fig. S9: [Figure S13]. BA suspension (left), BA solution with a drop of pentylamine (**3**) in DCM under air (right).

Influence of Oxygen Content on baicalein (1) with Pentylamine (3) Reaction

Since autooxidation processes can take place, a new batch of baicalein was used further. 50 mg BA (0.185 mmol, 1 eq) in an oven-dry 10 ml vial was evacuated and refilled with N₂ three times, dissolved in 3 ml of dry degassed (3 × freeze-pump-thaw cycles) DCM. 20 μl of pentylamine (15.8 mg, 0.182 mmol, 1 eq) were added to a stirring suspension. The reaction becomes clear yellow and after some time a precipitate starts to form, which dissolves in a short time. APCI-MS analysis was performed exactly after exposure to air (Fig. S10).

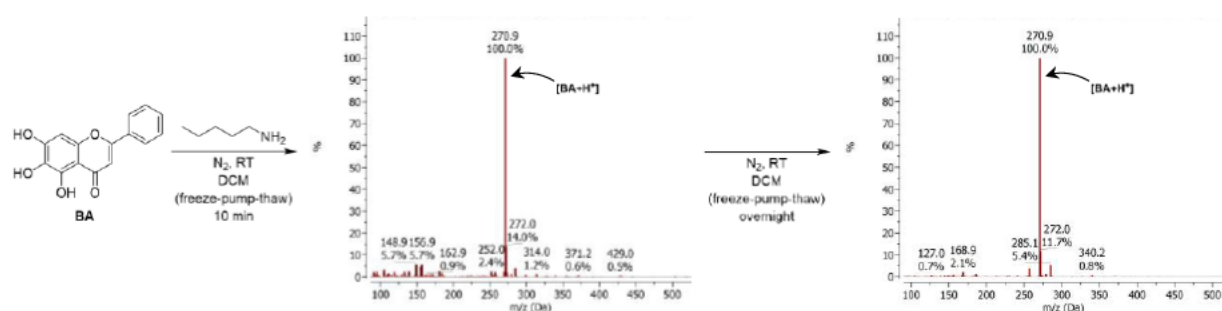


Fig. S10: [Figure S14]. APCI-MS spectra of BA with pentylamine (3) in DCM (3×freeze-pump-thaw cycles) under nitrogen atmosphere.

The same reaction was performed again with the key difference that non-degassed DCM was used. APCI-MS analysis was performed, which shows the formation of the [M+H]⁺ peak at m/z 340, indicating traces of oxygen are enough to trigger the condensation reaction (Fig. S11)

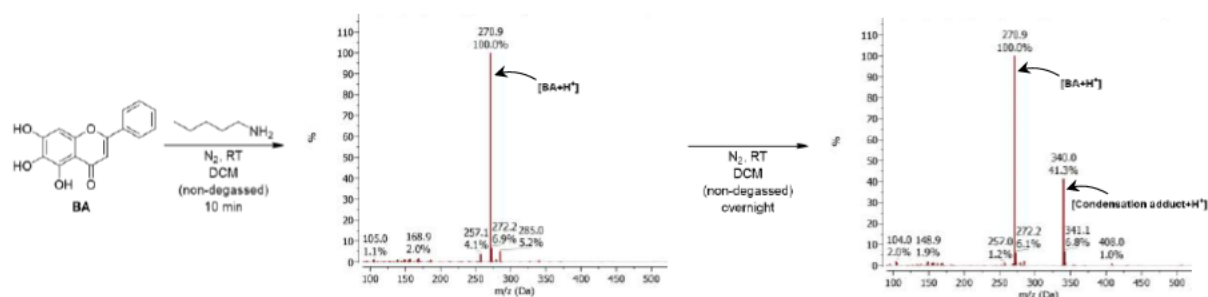
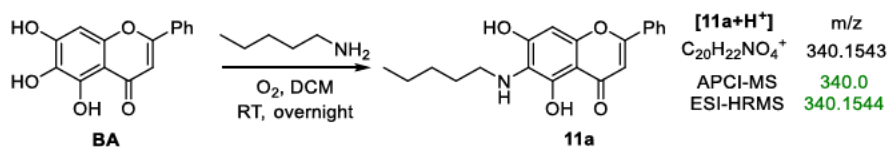


Fig. S11: [Figure S15]. APCI-MS spectra of BA with Pentylamine (3) in DCM (non-degassed) under nitrogen atmosphere.

Since oxygen plays a significant role in this reaction, it was decided to perform it under pure oxygen atmosphere. ¹³C and ¹H-¹³C HMBC NMR spectrum analysis showed that the condensation occurs at C6-position of BA, giving adduct **11a** (Fig. S12 and S13).



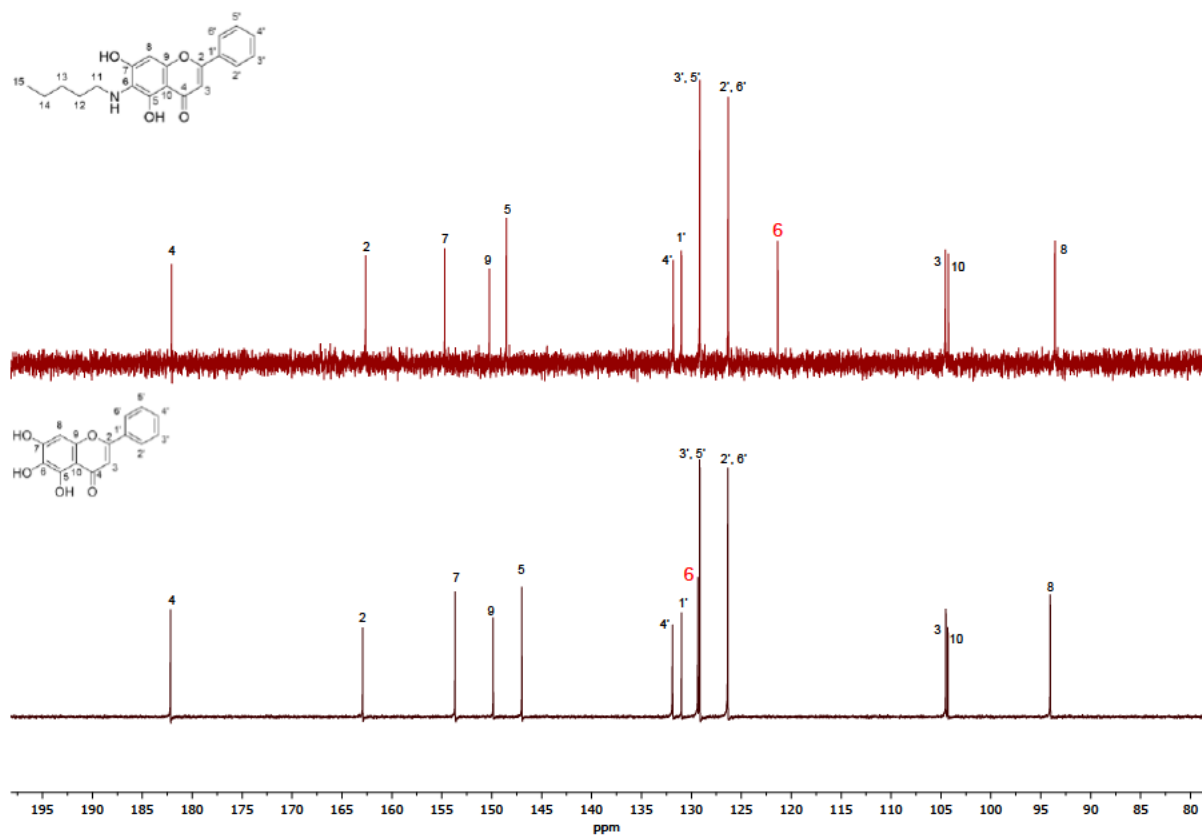


Fig. S12: [Figure S16]. ^{13}C NMR spectrum of coupling product **11a**, $\text{DMSO-}d_6$, 400 MHz.

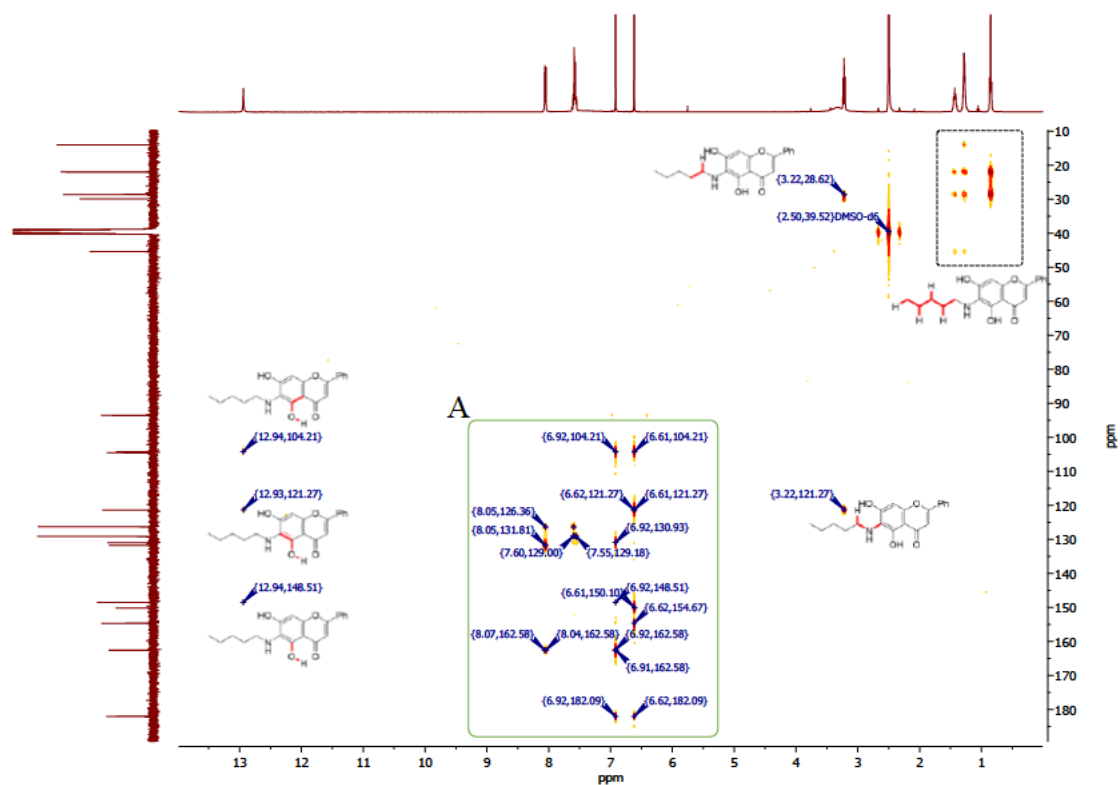


Fig. S13a: [Figure S17a]. ^1H - ^{13}C HMBC spectrum of coupling product **11a**, $\text{DMSO-}d_6$, 400 MHz.

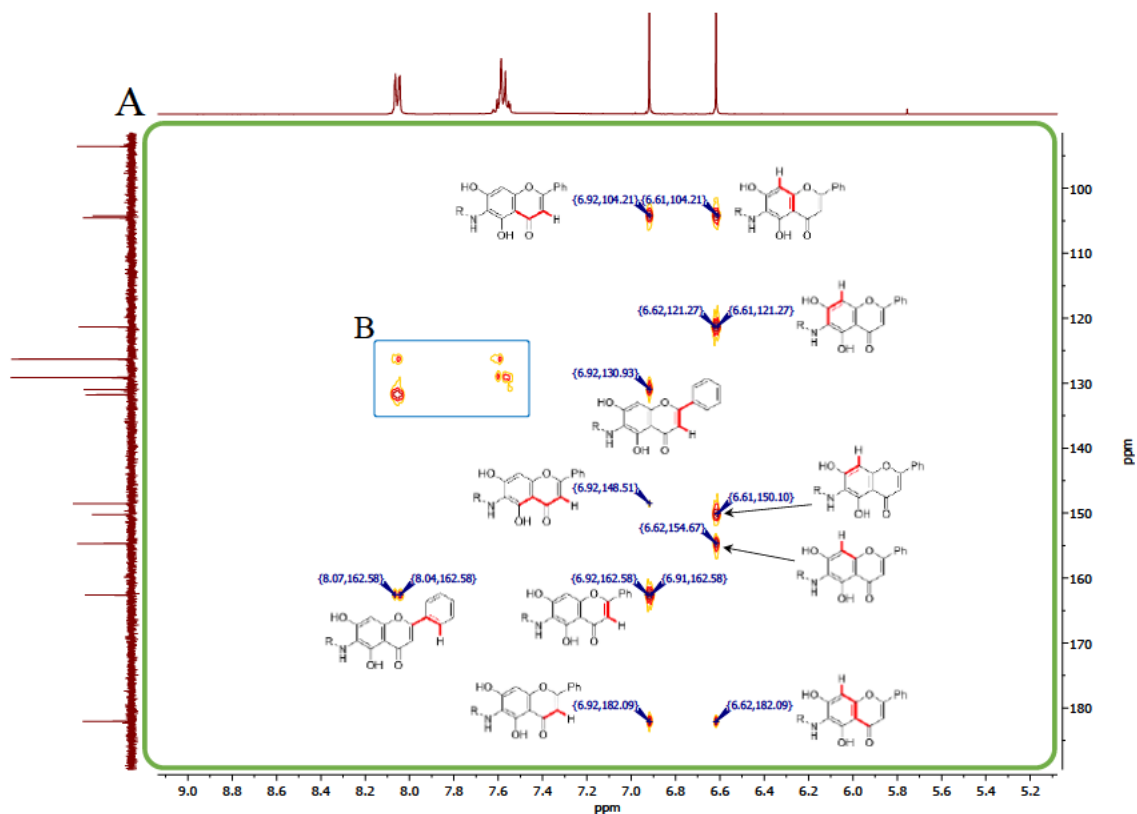


Fig. S13b: [Figure S17b]. ^1H - ^{13}C HMBC spectrum of coupling product **11a**, DMSO- d_6 , 400 MHz.

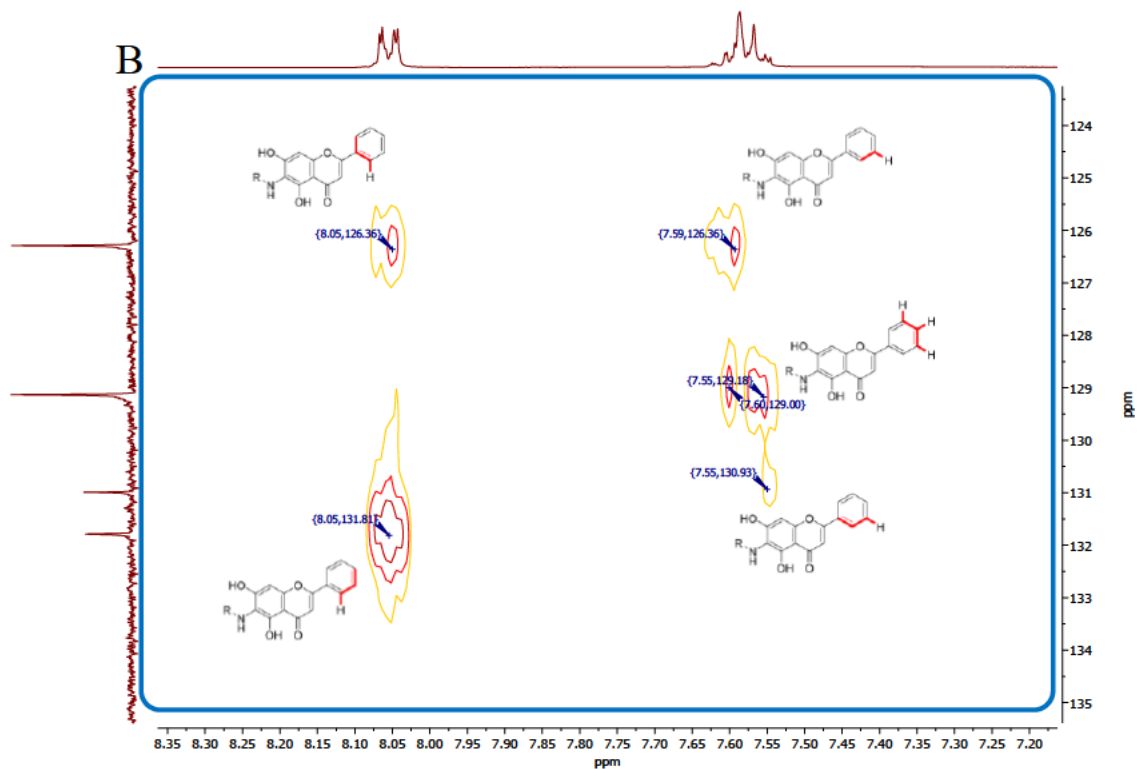
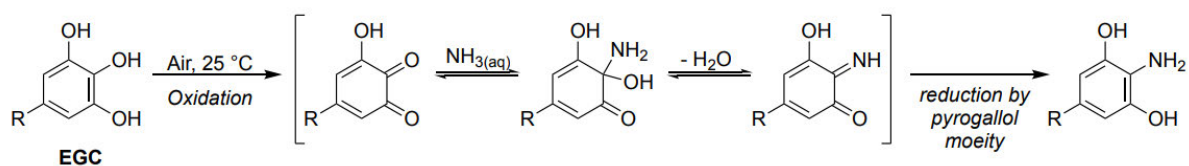
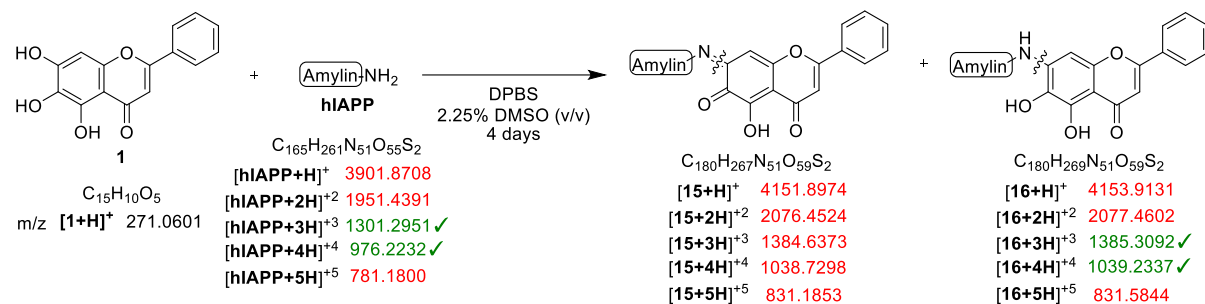


Fig. S13c: [Figure S17c]. ^1H - ^{13}C HMBC spectrum of coupling product **11a**, DMSO- d_6 , 400 MHz.

The literature analysis shows few similar examples:



Scheme S5: [Scheme S8]. Reaction of epigallocatechin (EGC) with ammonia in water under aerobic conditions.^[2]



Scheme S6: [Scheme S9]. Coupling reaction of baicalein (**1**, BA) with human amylin (**hIAPP**) studied by Velandar et. al., in which the reduced imine species were detected. Detected signals are marked at green.^[3]

Aerobic oxidation of baicalein (**1**):

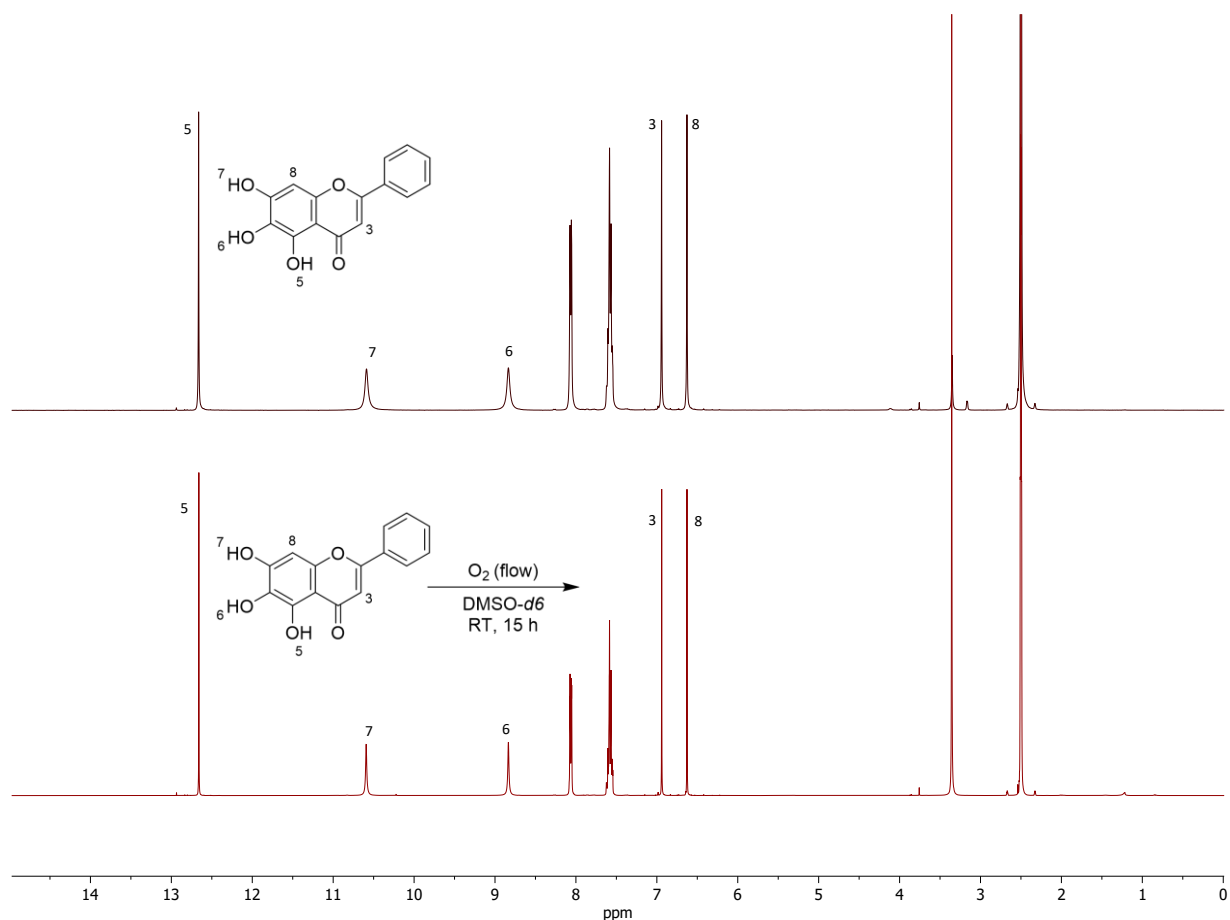


Fig. S14: [Figure S18]. ¹H NMR spectra of BA and BA after 15 h of O₂ bubbling, DMSO-*d*₆, 400 MHz.

O₂ was bubbled through a baicalein (**1**, 30 mg) solution in 3 ml of dry DMSO-*d*₆ for 15 h. An 0.5 ml aliquot was taken for NMR analysis, which showed no major difference from the reference **BA** spectrum (Fig. S14). The obtained data reflects the stability of **BA** against oxidation with O₂ under these conditions.

Aerobic Oxidation of Baicalein (**1**) under Basic Condition.

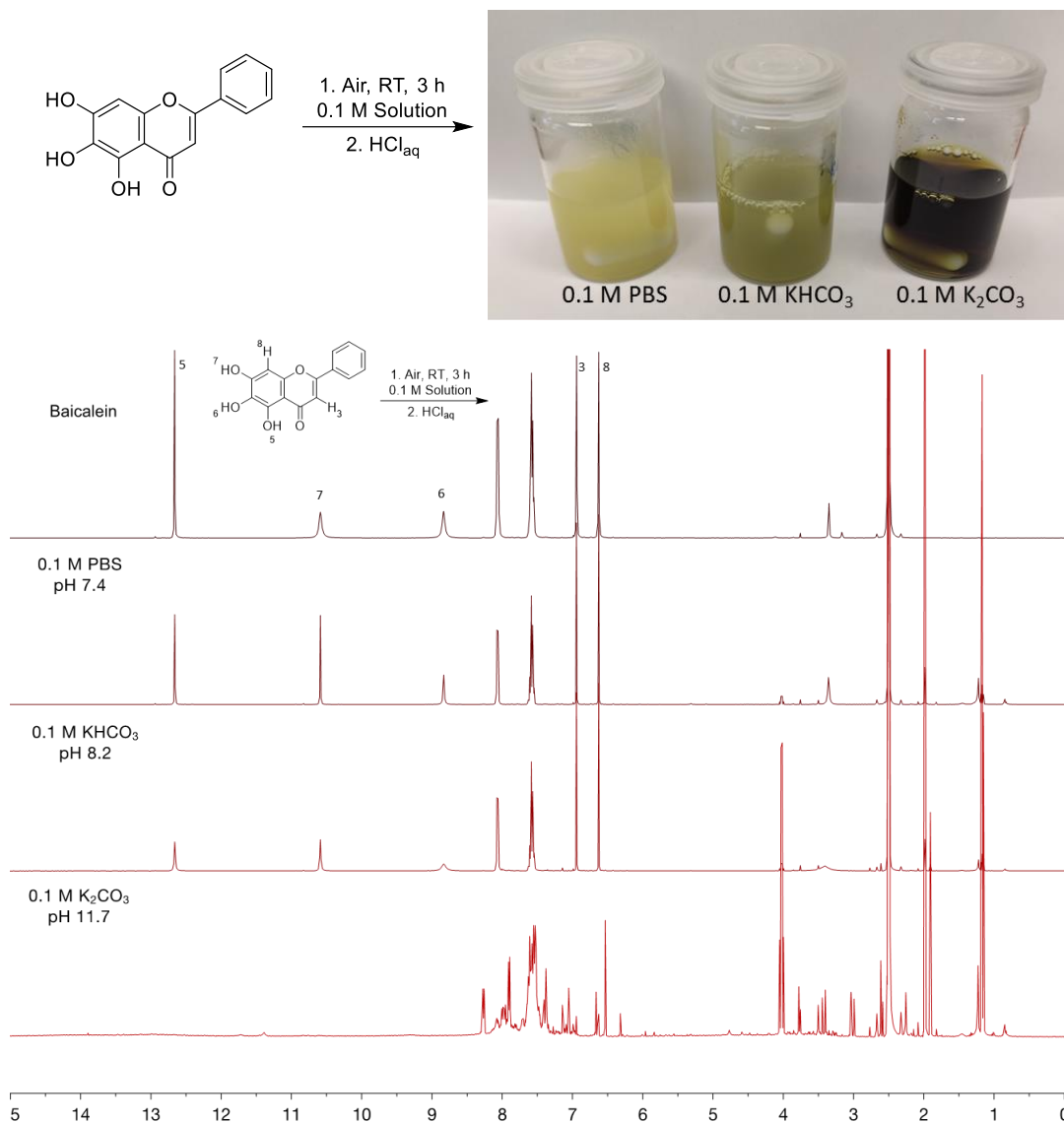


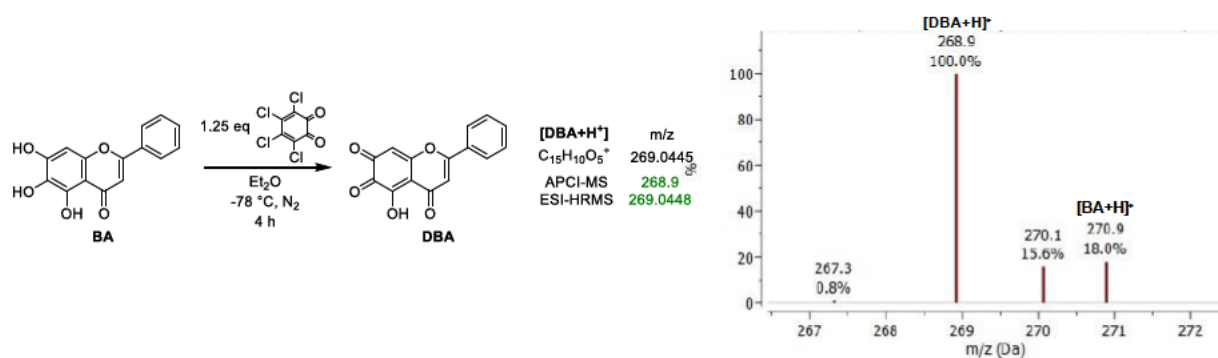
Fig. S15: [Figure S19]. ¹H NMR spectra of aerobic **BA** oxidation at different pH values, DMSO-*d*₆, 400 MHz.

A suspension of baicalein (**1**, 10 mg) in 10 ml of 0.1 M corresponding aqueous solution with certain pH value: phosphoric buffer solution, PBS, (pH 7.4), KHCO₃ (pH 8.2) and K₂CO₃ (pH 11.7), was vigorously stirred for 3 h at RT. Reaction mixtures were carefully acidified with 37% HCl to pH ~2 (colour changes to intensive red), extracted with EtOAc (3 × 5ml). The organic phases were combined and dried over MgSO₄. The solvent was evaporated under

reduced pressure at 25 °C. The crude material was dissolved in DMSO-*d*6 and ¹H NMR spectra was taken (Fig. S15). The obtained data shows higher degradation rates of BA for higher pH values under these conditions.^[4]



Scheme S7: [Scheme S12]. Mechanism of BA aerobic oxidation.



Scheme S8: [Scheme S13]. Oxidation of BA with *o*-chloranil.

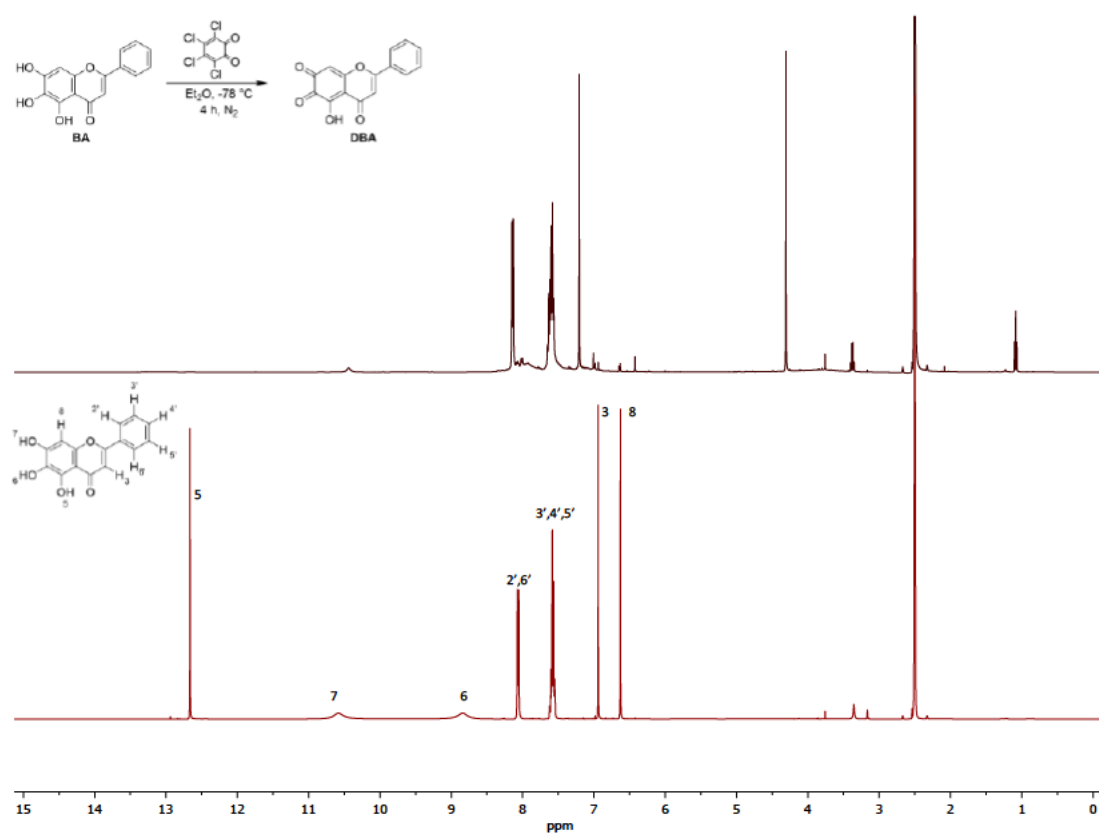
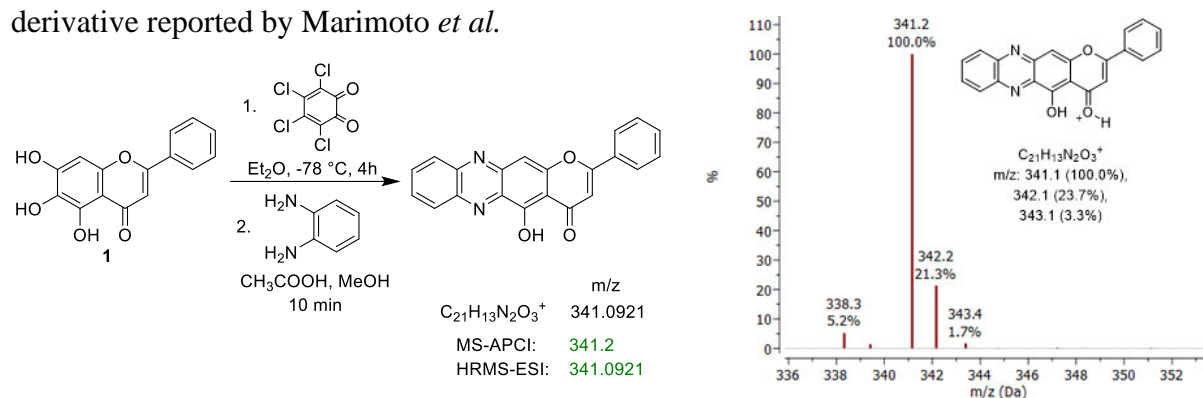


Fig. S16: [Figure S20]. ¹H NMR spectra of baicalein (1) oxidation with *o*-chloranil (top) and baicalein (1) (bottom), DMSO-*d*6, 400 MHz.

Coupling of Dehydrobaicalein (DBA) with *o*-Phenylenediamine

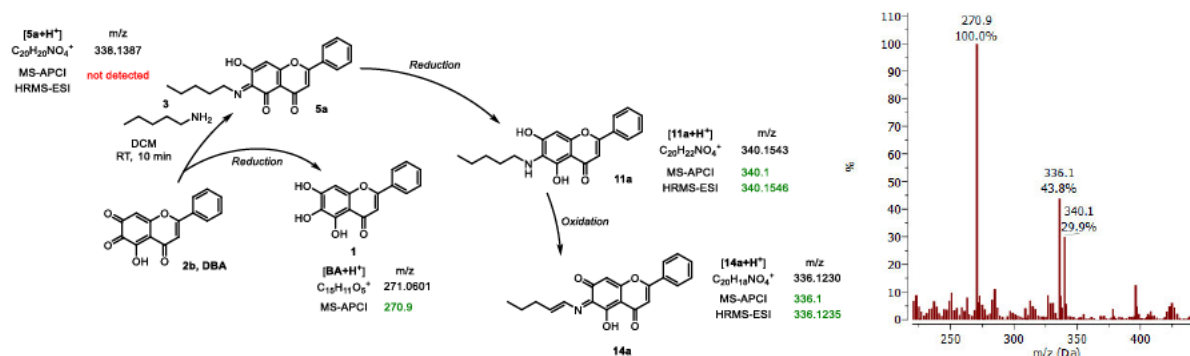
DBA formation was also chemically proven with a reaction described by *Marimoto et al.*^[5]

150 mg (1.39 mmol, 12.6 eq) of *o*-phenylenediamine was added to 30 mg (0.11 mmol, 1 eq) of obtained crude mixture in 100 ml of dry MeOH and 1 ml of acetic acid was added. The reaction mixture was stirred for 10 min at room temperature, upon completion of the reaction, all the volatiles were evaporated under reduced pressure at 25 °C. The crude product gives signals of m/z 341 in MS-APCI (Scheme S9), which was characterized as the phenazine derivative reported by *Marimoto et al.*



Scheme S9: [Scheme S14]. Reaction of DBA with *o*-phenylenediamine.

25 μl of amylamine (19 mg, 0.22 mmol) were added dropwise to the solution of crude material obtained above with one drop of glacial acetic acid in 10 ml of dry DCM. The resulting reaction mixture was allowed to stir for 24 h at RT. Upon completion of the reaction, all volatiles were evaporated under reduced pressure at 25 °C. Afterwards it was shown, that the reaction is over after 10 min without addition of a catalytic amount of glacial acetic acid. Instead of expected imine derivative **5a** with $[\text{M}+\text{H}]^+$ ion peak at m/z 338, peaks at m/z 336 and 340 were observed in APCI-MS (Scheme 10). Also, peak of reduced baicalein species, m/z 271, was detected.

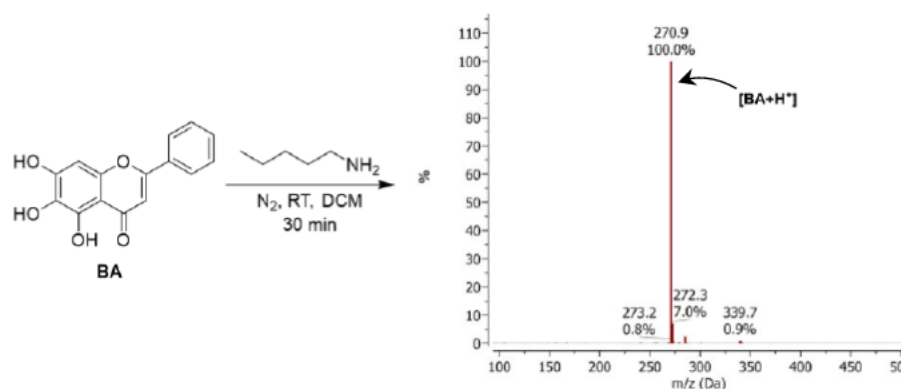


Scheme S10: [Scheme S15]. Condensation reaction between DBA (**2b**) and pentylamine (**3**). The detected signals are marked at green.

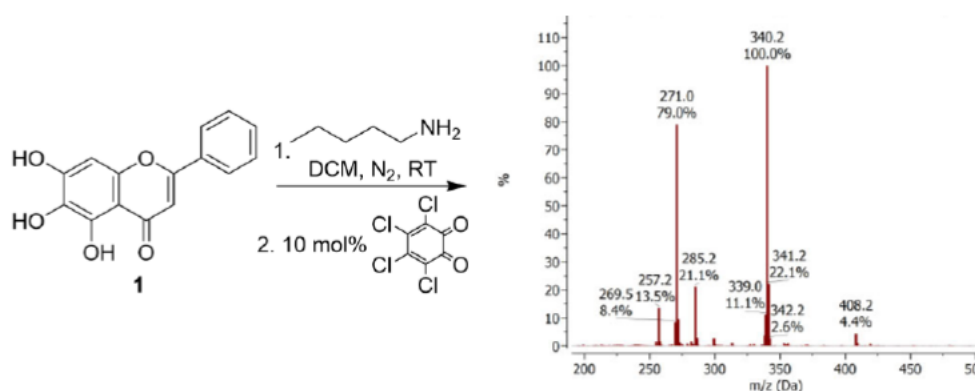
Control Experiments to Test Mechanistic Hypothesis.

Few control experiments were carried to test these assumptions.

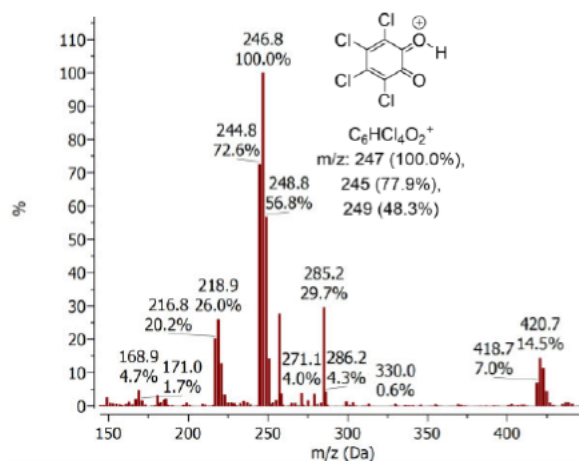
1. No coupling product of **BA** and pentylamine (**3**) was detected under anaerobic conditions in dry degassed DCM after 30 min.



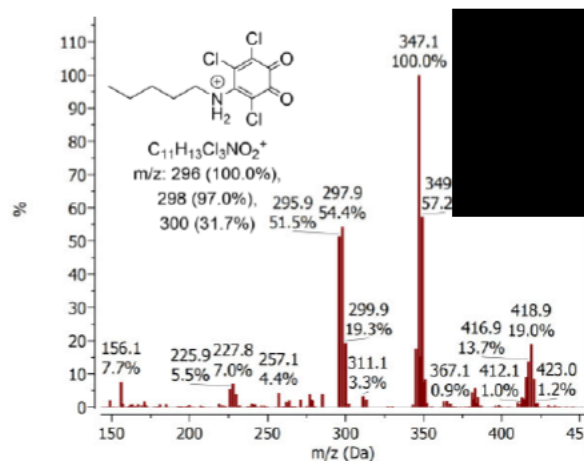
2. Addition of 10 mol% of *o*-chloranil to **BA**-pentylamine under anaerobic conditions leads to significant formation of C6-coupled product **11a** with mass peak at m/z 340.



Also, it has been shown that *o*-chloranil reacts with pentylamine (**3**), giving mono- and disubstituted derivatives.

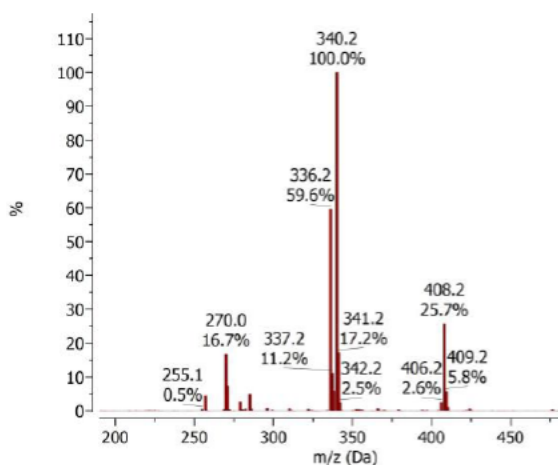
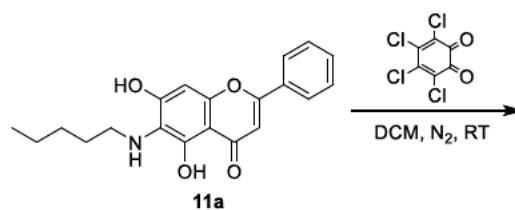


o-Chloranil

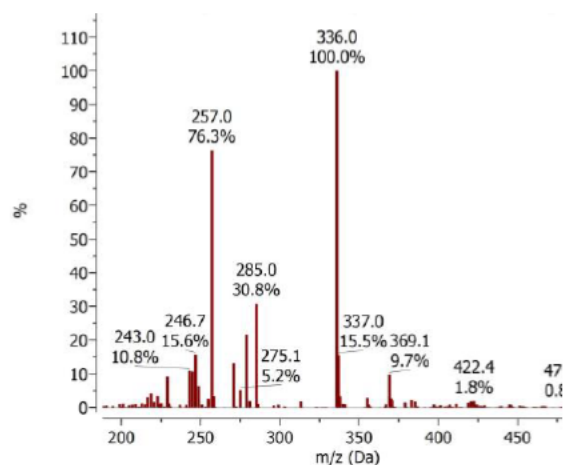


o-Chloranil + pentylamine (3)

3. C6-coupling product **11a** was mixed with an equimolar amount of *o*-chloranil in DCM at room temperature. APCI-MS analysis showed the formation of a peak at m/z 336, showing that it forms from the oxidation of the product with mass peak at m/z 340. Addition of excess of *o*-chloranil leads to only peak at m/z 336.

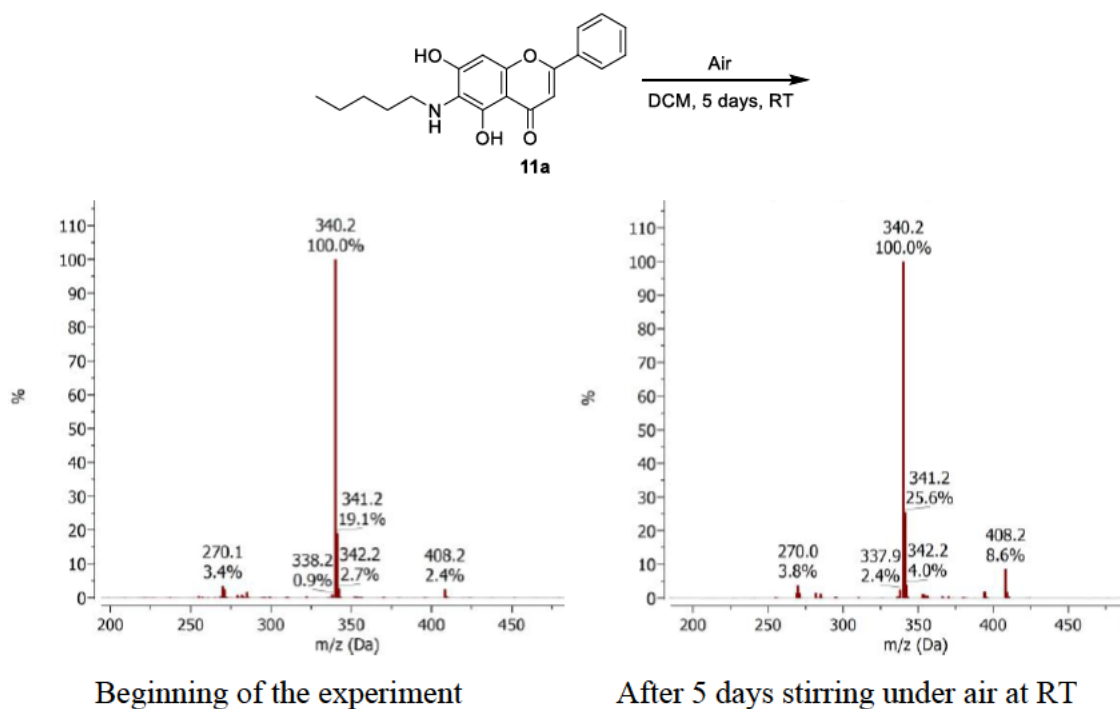


Addition of equimolar amount of *o*-chloranil

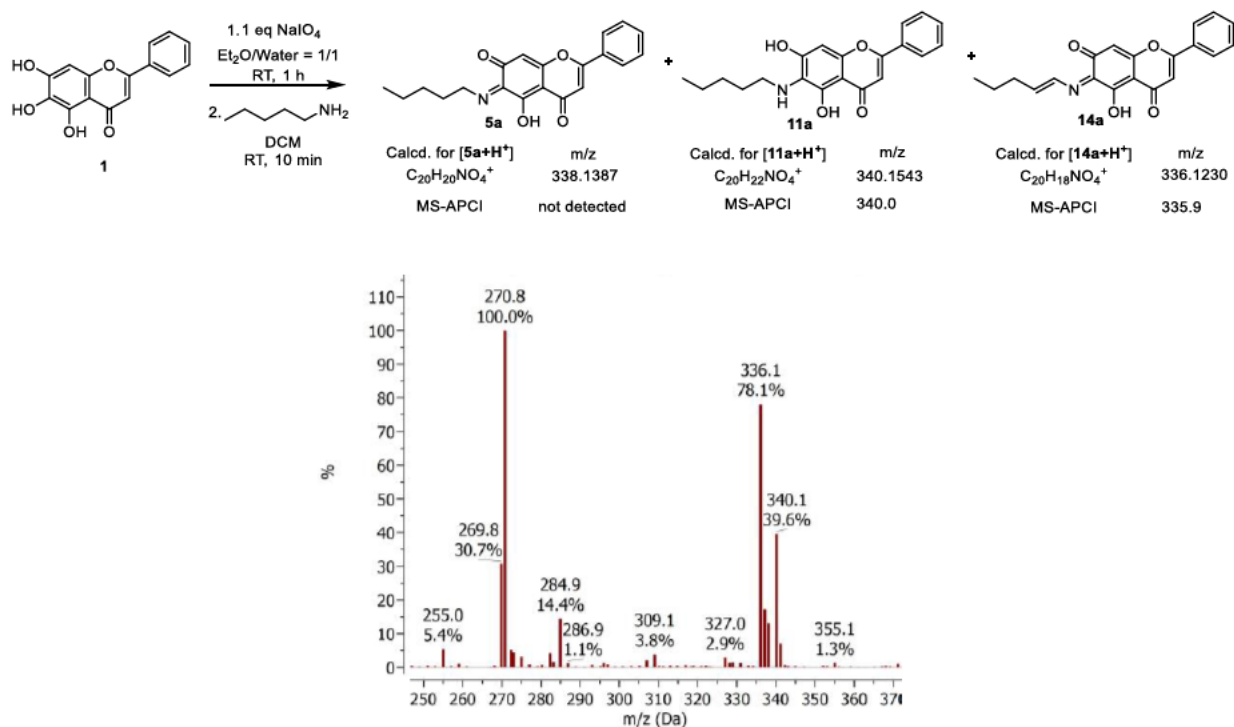


Addition of excess amount of *o*-chloranil

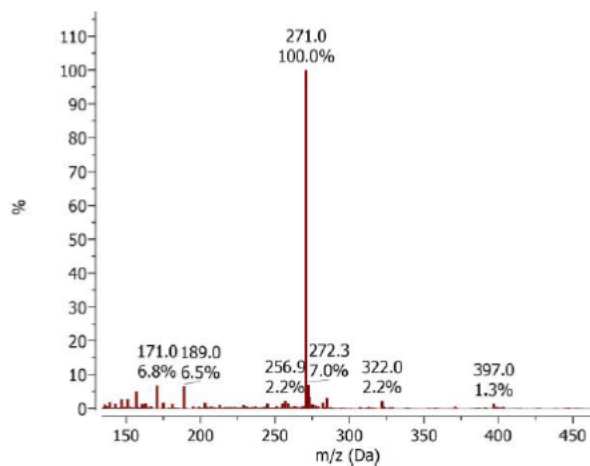
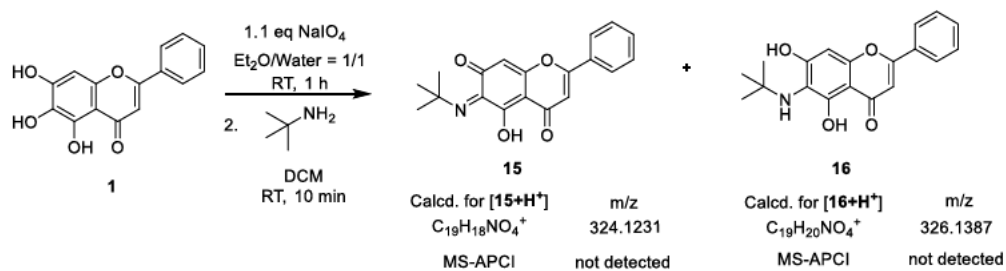
4. Stirring the solution of C6-coupling product **11a** under aerobic conditions for 5 days does not lead to formation of the product with peak at m/z 336.



5. NaIO_4 was used as an oxidant to get DBA (**2b**), which was mixed with pentylamine (**3**) and similar APCI-MS profile was obtained with peaks at m/z 336 and 340.

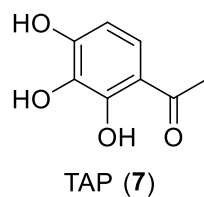


6. Sterically more hindered *tert*-butyl amine, on the other hand, show no peaks of expected coupling products with DBA (**2b**).



1.2.1.3. Analytical Data of Reagents and Reaction Products.

2',3',4'-Trihydroxyacetophenone (TAP, **7**)

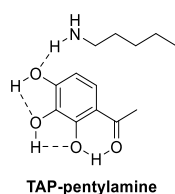


$^1\text{H NMR}$ (400 MHz, DMSO-*d*₆) δ 12.61 (s, 1H), 10.07 (s, 1H), 8.63 (s, 1H), 7.30 (d, *J* = 8.9 Hz, 1H), 6.40 (d, *J* = 8.8 Hz, 1H), 2.51 (s, 3H).

$^{13}\text{C NMR}$ (101 MHz, DMSO-*d*₆) δ 203.5, 152.6, 152.2, 132.3, 123.2, 113.2, 107.7, 26.4.

m.p. 170-172 °C

TAP-pentylamine complex



68.8 mg of TAP (0.41 mmol, 1 eq) was dissolved in 6 ml of dry DCM and 50 μl of pentylamine (38 mg, 0.42 mmol, 1 eq) were added under nitrogen atmosphere. Short time after, yellow precipitate starts to form. After 10 min of stirring, the reaction mixture was cooled down to 4 °C, the precipitate was

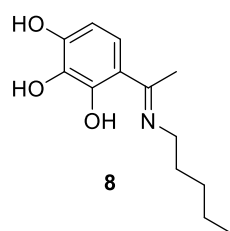
filtered off, dried and recrystallized from *i*-Hexane/EtOAc. Product was obtained as yellow crystals (70 mg).

$^1\text{H NMR}$ (400 MHz, DMSO-*d*₆) δ 7.37 (bs), 7.15 (d, *J* = 8.9 Hz, 1H), 6.15 (d, *J* = 8.9 Hz, 1H), 2.66 – 2.61 (m, 3H), 2.41 (s, 3H), 1.59 – 1.16 (m, 6H), 1.04 – 0.68 (m, 3H).

$^{13}\text{C NMR}$ (101 MHz, DMSO-*d*₆) δ 200.6, 159.9, 150.4, 132.9, 123.7, 110.3, 108.8, 29.7, 28.3, 25.7, 21.9, 13.9.

m.p. 111-112 °C (decomp)

Imine **8**



160 mg of TAP (**7**, 0.95 mmol, 1 eq) was dissolved in 3 ml of dry degassed MeOH under nitrogen atmosphere and 121 μl of pentylamine **3** (91 mg, 1.05 mmol, 1.1 eq) were added under nitrogen while stirring. The vial was tightly closed and heated up to 80 °C for 3 hours. After, reaction was cooled down to 4 °C, formed yellow precipitate was filtered off, washed with cold MeOH and dried under reduced pressure.

The imine **8** was obtained as yellow solid (52 mg, 23%).

$^1\text{H NMR}$ (400 MHz, DMSO-*d*₆) δ 8.93 (br), 7.65 (bs), 6.90 (d, *J* = 9.1 Hz, 1H), 6.02 (d, *J* = 9.1 Hz, 1H), 3.56 – 3.56 (m, 2H), 2.37 (s, 3H), 1.65 (p, *J* = 7.0 Hz, 2H), 1.44 – 1.29 (m, 4H), 0.89 (t, *J* = 7.0 Hz, 3H).

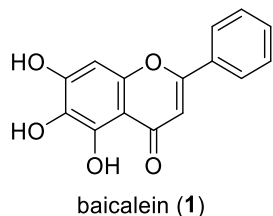
$^{13}\text{C NMR}$ (101 MHz, DMSO-*d*₆) δ 172.7, 164.0, 146.9, 133.9, 119.5, 108.8, 105.1, 44.7,

28.7, 28.6, 21.8, 14.0, 13.9.

HRMS (ESI): calcd for $C_{13}H_{20}NO_3$ $[M + H]^+$, 238.1438; found 238.1438.

m.p. 238-240 °C (decomp)

Baicalein (BA, **1**)

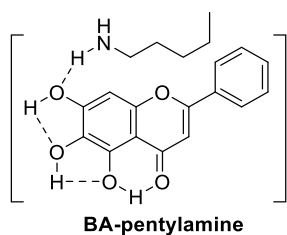


1H NMR (400 MHz, DMSO-*d*₆) δ : 12.66 (s, 1H), 10.57 (s, 1H), 8.85 (s, 1H), 8.41 – 7.88 (m, 2H), 7.82 – 7.37 (m, 3H), 6.94 (s, 1H), 6.63 (s, 1H).

^{13}C NMR (101 MHz, DMSO-*d*₆) δ : 182.2, 163.0, 153.7, 149.9, 147.0, 131.9, 131.0, 129.4, 129.2, 126.3, 104.5, 104.3, 94.1.

m.p. 269-271 °C (decomp)

BA-pentylamine complex

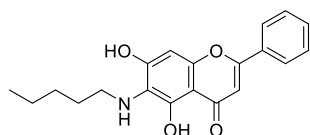


20 mg **BA** (0.0741 mmol, 1 eq) in a J. Young NMR tube was evacuated and refilled with N_2 three times, dissolved in 0.75 ml of dry degassed ($3 \times$ freeze-pump-thaw cycles) DMSO-*d*₆, followed by addition of $\sim 9 \mu\text{l}$ pentylamine (7 mg, 0.0781, 1 eq). After the sample preparation, various NMR experiments were performed (describe above).

1H NMR (400 MHz, DMSO-*d*₆) δ 8.15 (bs), 8.35 – 7.87 (m, 2H), 7.52 (m, 3H), 6.68 (s, 1H), 6.15 (s, 1H), 2.71 (t, $J = 7.4$ Hz, 2H), 1.61 – 1.09 (m, 6H), 1.01 – 0.74 (m, 3H).

^{13}C NMR (101 MHz, DMSO-*d*₆) δ 179.9, 164.5, 160.3, 152.1, 142.6, 131.7, 131.4, 131.0, 129.0, 125.8, 104.2, 100.7, 93.6, 28.3, 28.2, 21.8, 13.8.

Oxidative coupling of baicalein (**1**) and pentylamine (**3**)



45 μl of pentylamine (34 mg, 0.39 mmol, 1 eq) were added to a stirring suspension of 106 mg **BA** (0.39 mmol, 1 eq) in 5 ml of dry DCM under O_2 atmosphere (1 atm). The reaction was vigorously stirred overnight at room temperature. Solvent was evaporated under reduced pressure at 25 °C. Crude material was purified by column chromatography on silica gel (DCM/MeOH = 20/1, R_f 0.36). Product was obtained as orange solid (120 mg, 90%).

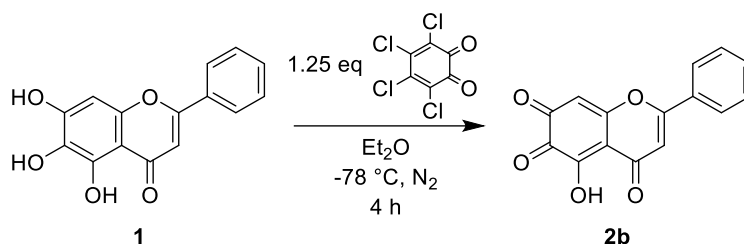
1H NMR (400 MHz, DMSO-*d*₆) δ 12.94 (s, 1H), 8.07 – 8.04 (m, 2H), 7.78 – 7.43 (m, 3H), 6.92 (s, 1H), 6.62 (s, 1H), 3.22 (t, $J = 7.0$ Hz, 2H), 1.55 – 1.19 (m, 6H), 0.98 – 0.76 (m, 3H).

^{13}C NMR (101 MHz, DMSO-*d*₆) δ 182.1, 162.6, 154.7, 150.2, 148.5, 131.8, 131.0, 129.1, 126.3, 121.4, 104.6, 104.2, 93.6, 45.4, 29.9, 28.6, 22.0, 14.0.

HRMS (ESI): calcd for C₂₀H₂₂NO₄ [M + H]⁺, 340.1544; found 340.1544.

m.p. 61-62 °C

Oxidation of baicalein (**1**) with *o*-chloranil:



o-Chloranil (178 mg, 0.69 mmol) was added to baicalein (**1**) suspension (150 mg, 0.56 mmol) in 3 ml of Et₂O at -78 °C under N₂ atmosphere and allowed to stir at -78 °C for 4 hours. The reaction mixture was then filtered, washed with Et₂O (3 x 5ml) and dried under reduced pressure to afford 115 mg of red powder (77% from starting **1**). Small amount of product was dissolved in MeOH and MS analysis was performed, which showed the formation of **2b**.

HRMS (ESI): calcd for C₁₅H₇O₅ [M - H]⁻, 267.0298; found 267.0299.

Oxidation of baicalein (**1**) with NaIO₄ and coupling with pentylamine (**3**)

NaIO₄ (19 mg, 0.09 mmol) was added to suspension of **1** (16 mg, 0.06 mmol) in 2 ml of Et₂O/Water = 1/1 solution. Mixture allowed to stir at room temperature for 1 hour. Solid material was separated by centrifuge, washed with water (3×1 ml) and dried under reduced pressure. Obtained red powder was dissolved in dry degassed DCM, followed by addition of 3 μl of pentylamine while stirring. After 10 min of stirring at room temperature, ACPI-MS analysis was performed.

Oxidation of baicalein (**1**) with NaIO₄ and coupling with *t*-butylamine

NaIO₄ (17 mg, 0.08 mmol) was added to suspension of **1** (16 mg, 0.06 mmol) in 2 ml of Et₂O/Water = 1/1 solution. Mixture allowed to stir at room temperature for 1 hour. Solid material was separated by centrifuge, washed with water (3×1 ml) and dried under reduced pressure. Obtained red powder was dissolved in dry degassed DCM, followed by addition of

2 μl of *t*-butylamine while stirring. After 10 min of stirring at room temperature, APCI-MS analysis was performed.

Oxidative Coupling of Baicalein (1) and Pentylamine (3) with 10 mol% of *o*-Chloranil

20 mg **1** (0.0741 mmol, 1 eq) in a J. Young NMR tube was evacuated and refilled with N_2 three times, dissolved in 0.75 ml of dry degassed $\text{DMSO-}d_6$, followed by addition of $\sim 9 \mu\text{l}$ pentylamine (7 mg, 0.0781, 1 eq). Yellow-green solution colour instantly turns orange while shaking. ^1H NMR spectrum was taken for the samples. After, 10 mol% of *o*-chloranil ($\sim 2 \text{ mg}$, 0.1 eq) was added to the reaction mixture and ^1H NMR spectrum was taken again. It was shown that small amount of oxidant can trigger the reaction (Fig. S17).

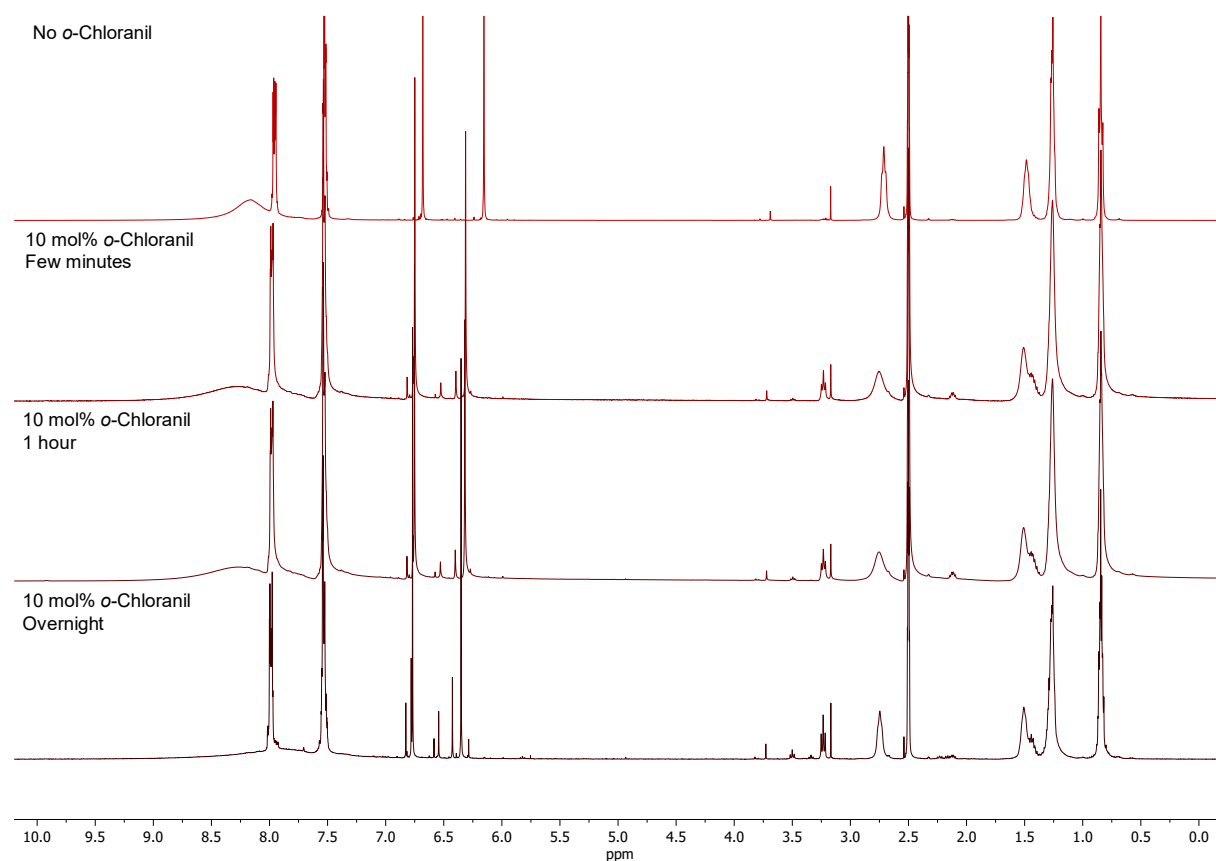


Fig. S17: [Figure S68]. Addition of 10 mol% of *o*-Chloranil to **BA-Pentylamine**, $\text{DMSO-}d_6$, 400 MHz

1.2.1.4. NMR spectra of reagents and reaction products

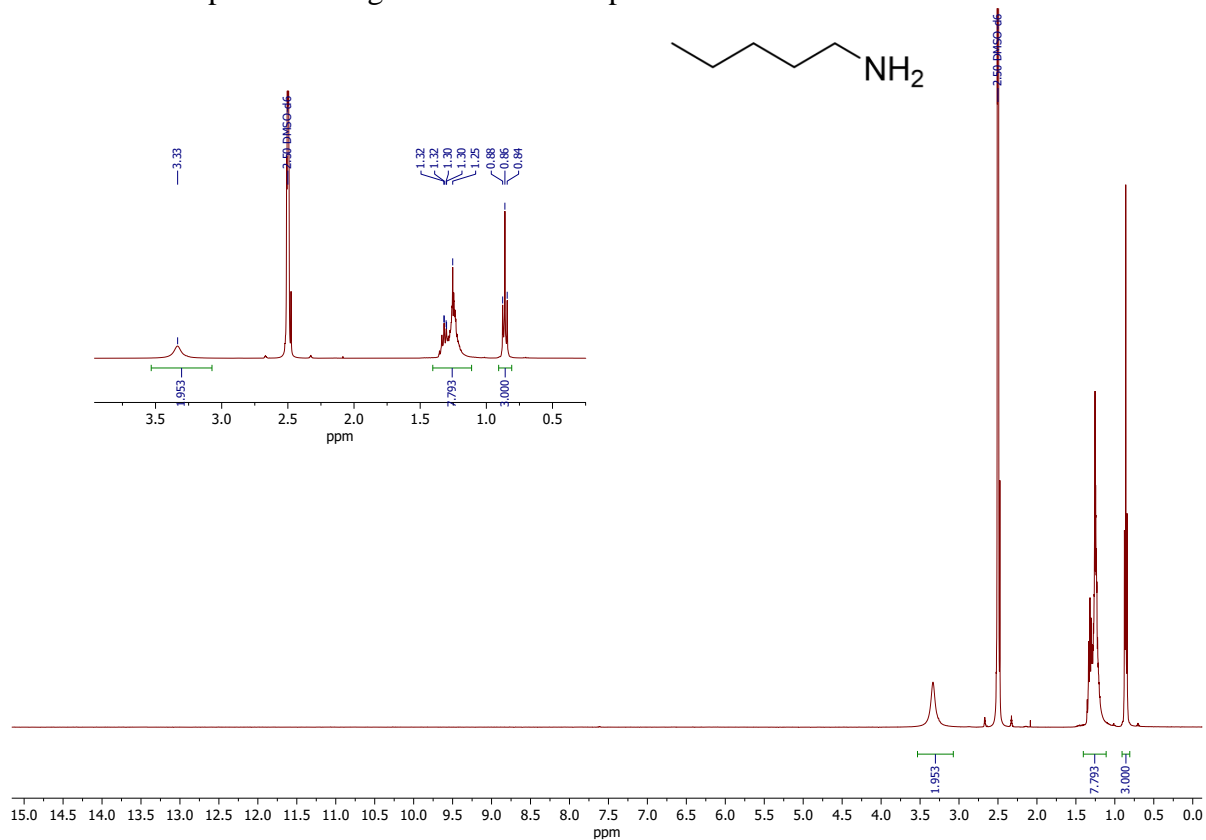


Fig. S18. ^1H NMR spectrum of pentylamine (3), DMSO- d_6 , 400 MHz.

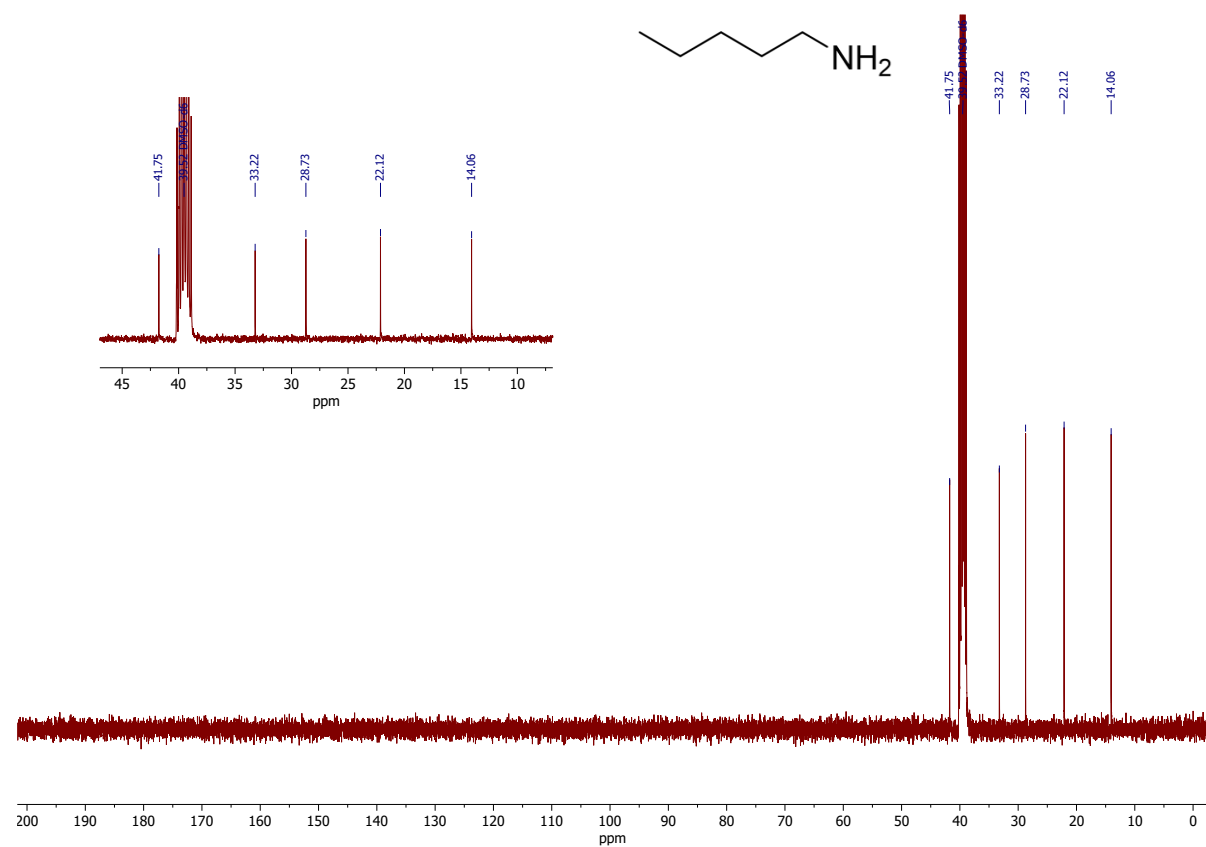


Fig. S19. ^{13}C NMR spectrum of pentylamine (3), DMSO- d_6 , 400 MHz.

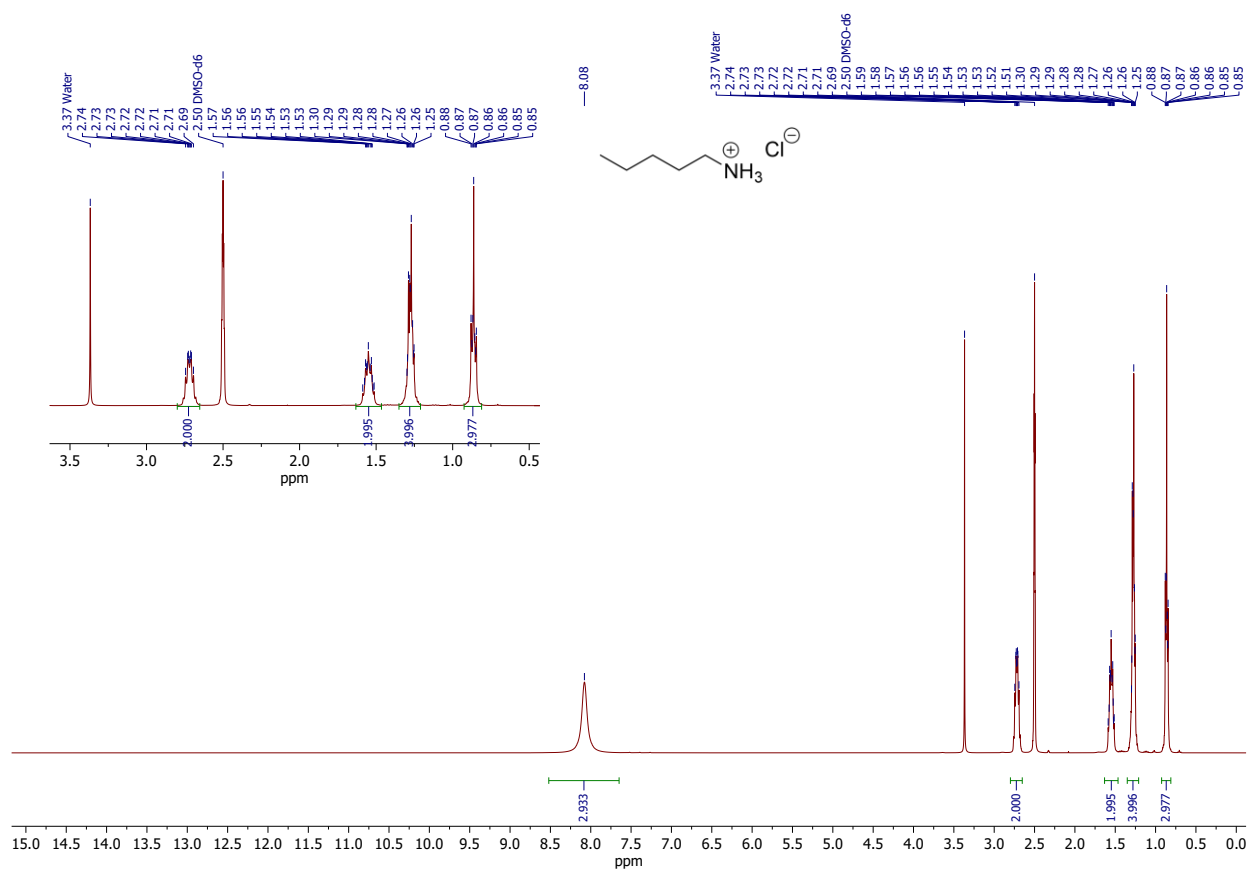


Fig. S20. ^1H NMR spectrum of pentylamine hydrochloride salt, $\text{DMSO-}d_6$, 400 MHz.

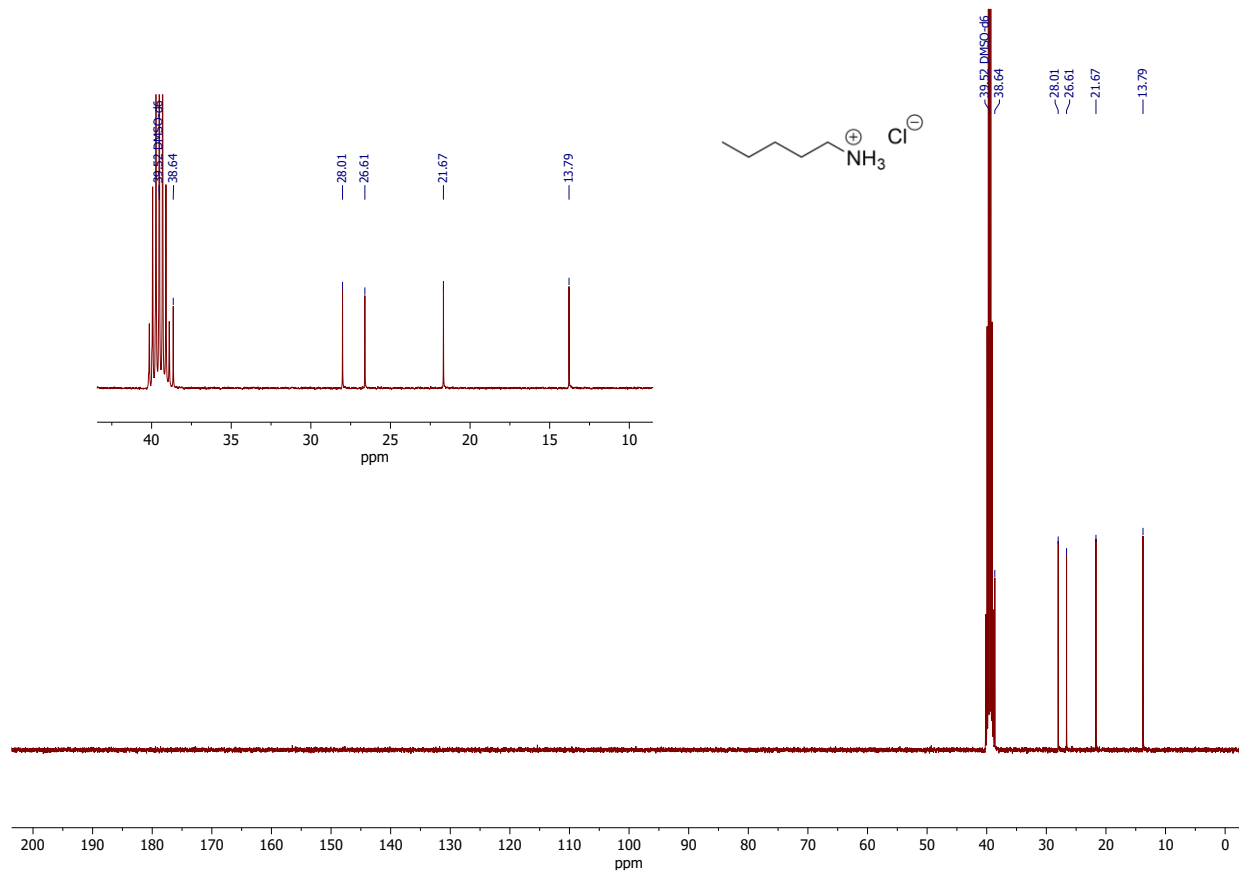


Fig. S21. ^{13}C NMR spectrum of pentylamine hydrochloride salt, $\text{DMSO-}d_6$, 101 MHz.

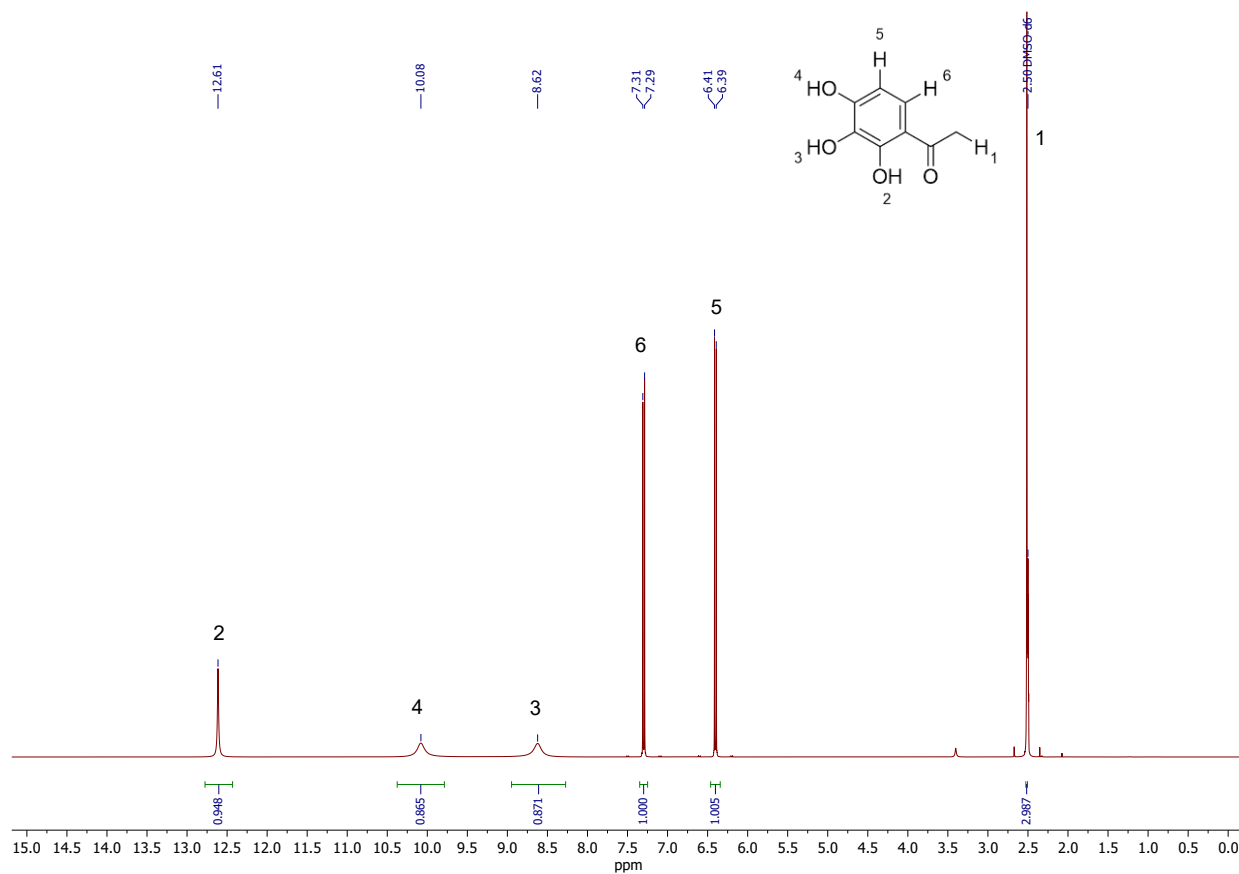


Fig. S22. ^1H NMR spectrum of TAP (7), DMSO- d_6 , 400 MHz.

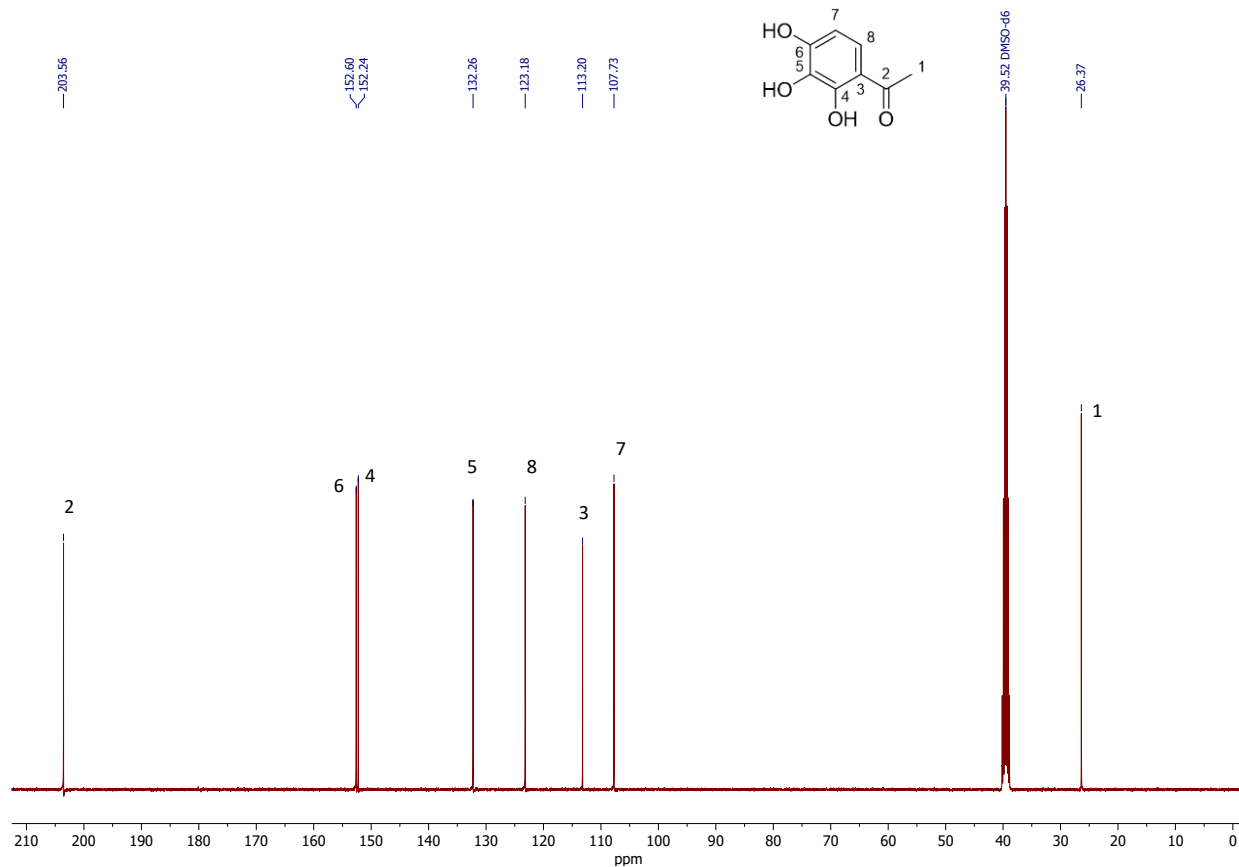


Fig. S23. ^{13}C NMR spectrum of TAP (7), DMSO- d_6 , 101 MHz.

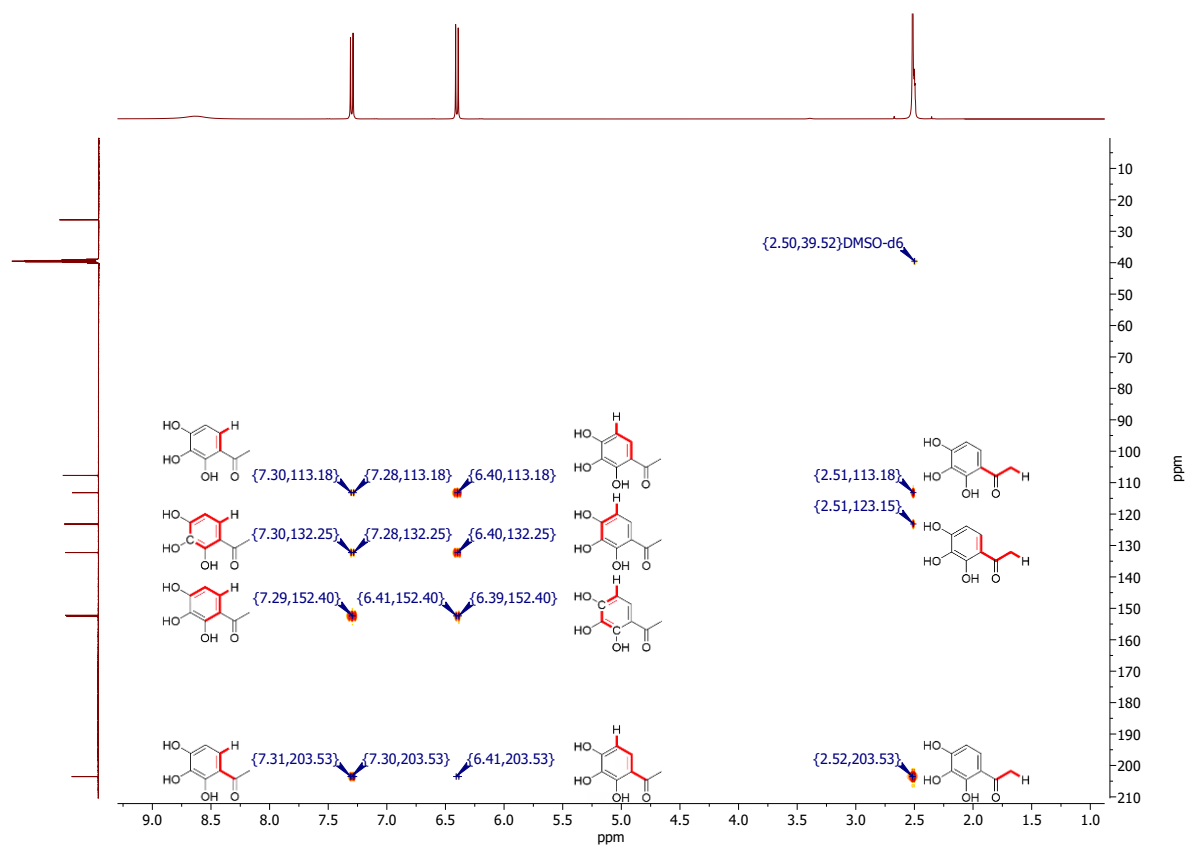


Fig. S24. ^1H - ^{13}C HMBC spectrum of TAP (7), $\text{DMSO-}d_6$, 400 MHz.

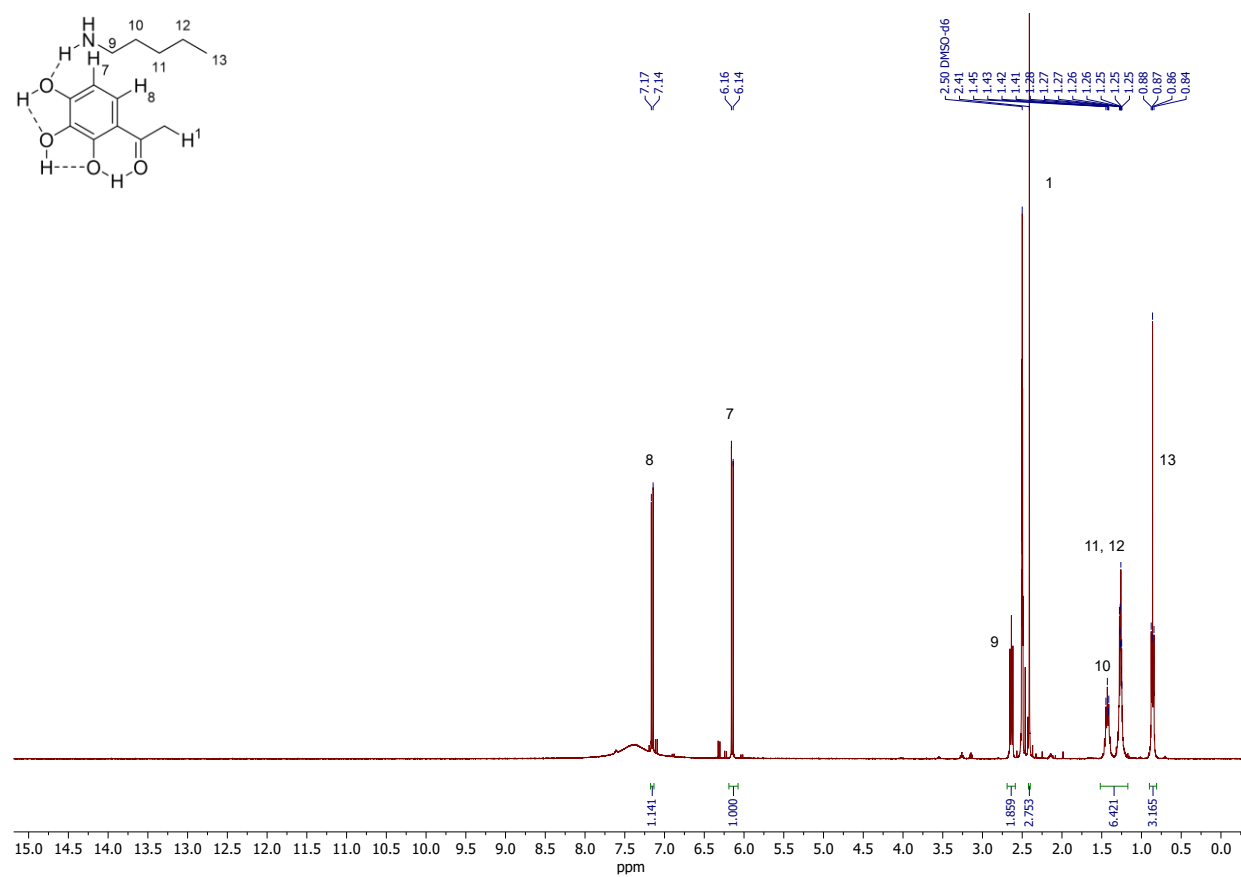


Fig. S25. ^1H NMR spectrum of TAP-pentylamine, $\text{DMSO-}d_6$, 400 MHz.

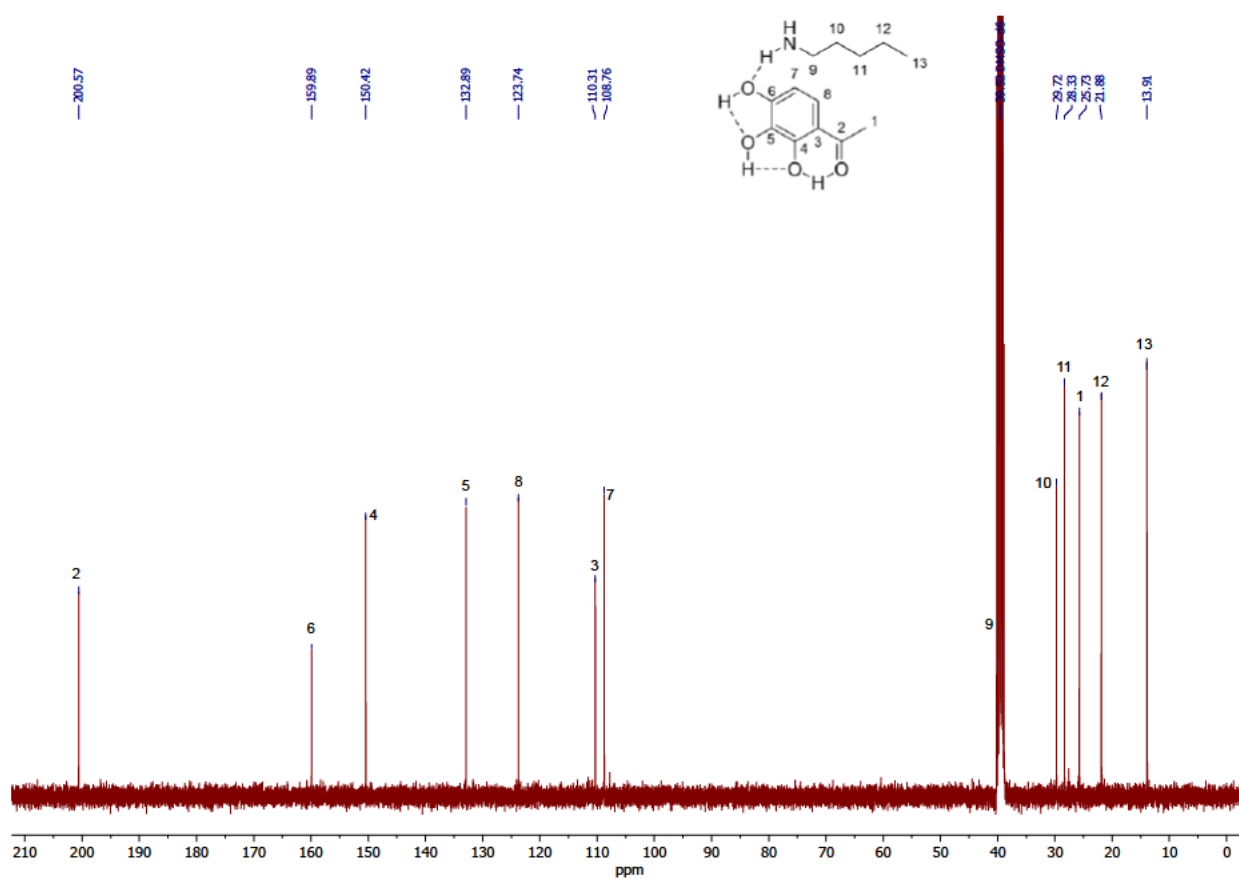


Fig. S26. ^{13}C NMR spectrum of TAP-pentylamine, $\text{DMSO-}d_6$, 101 MHz.

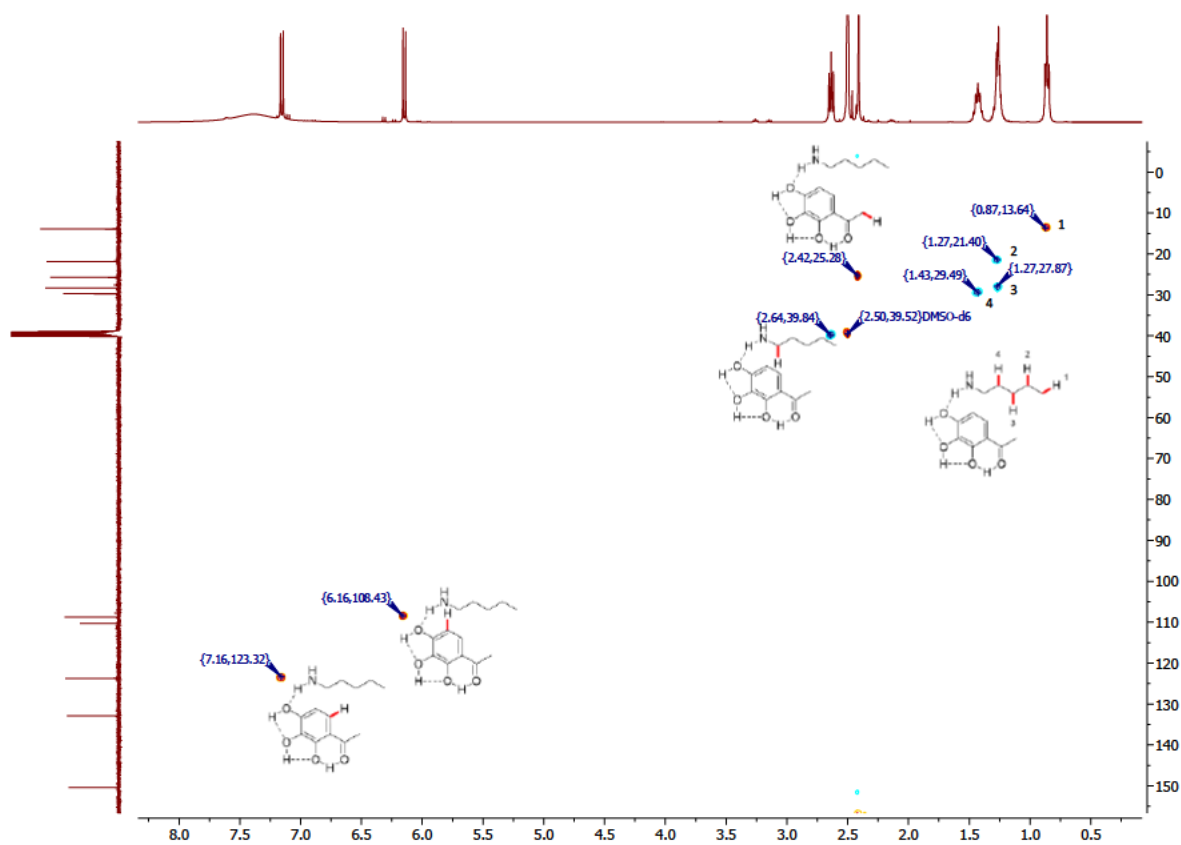


Fig. S27. $^1\text{H-}^{13}\text{C}$ HSQC spectrum of TAP-pentylamine, $\text{DMSO-}d_6$, 400 MHz

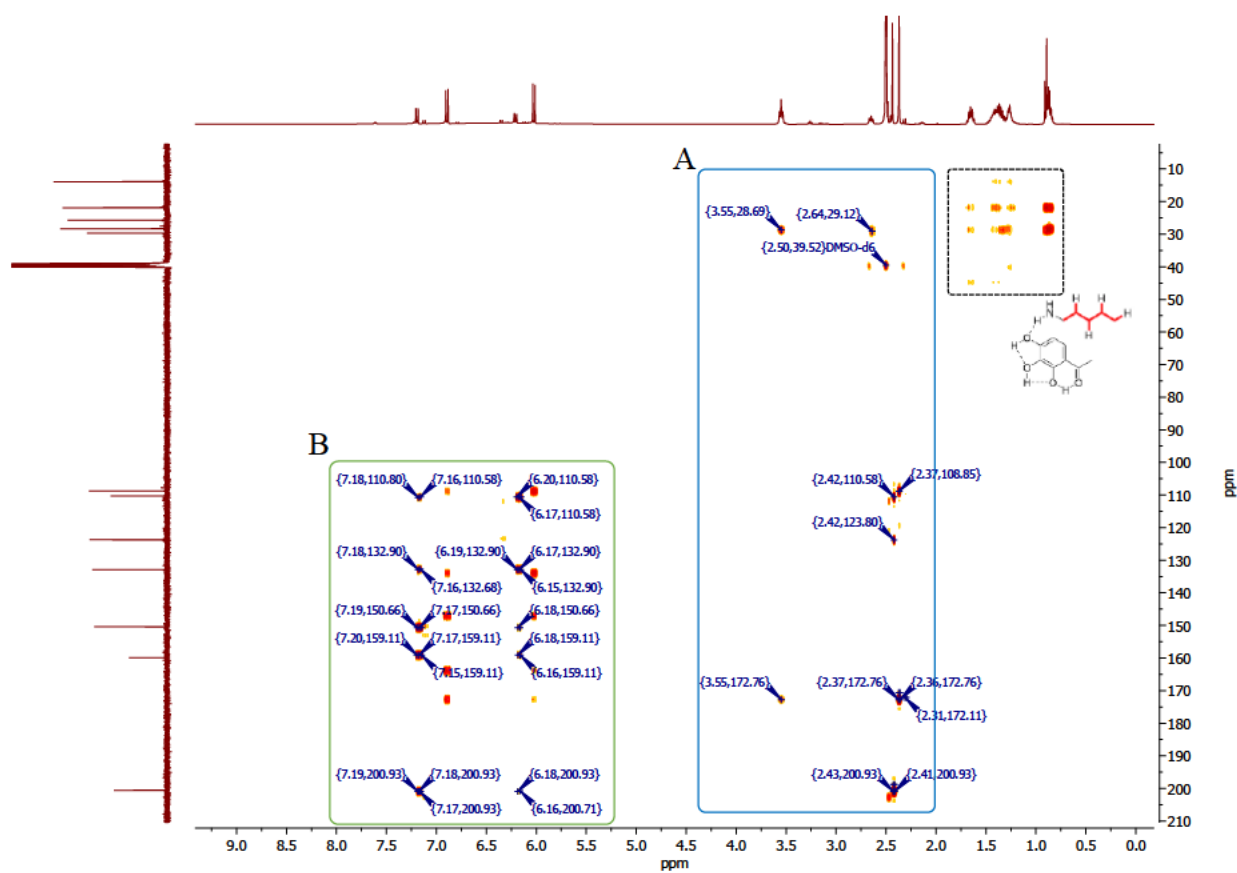


Fig. S28a. ^1H - ^{13}C HMBC spectrum of TAP-pentylamine, DMSO-d₆, 400 MHz.

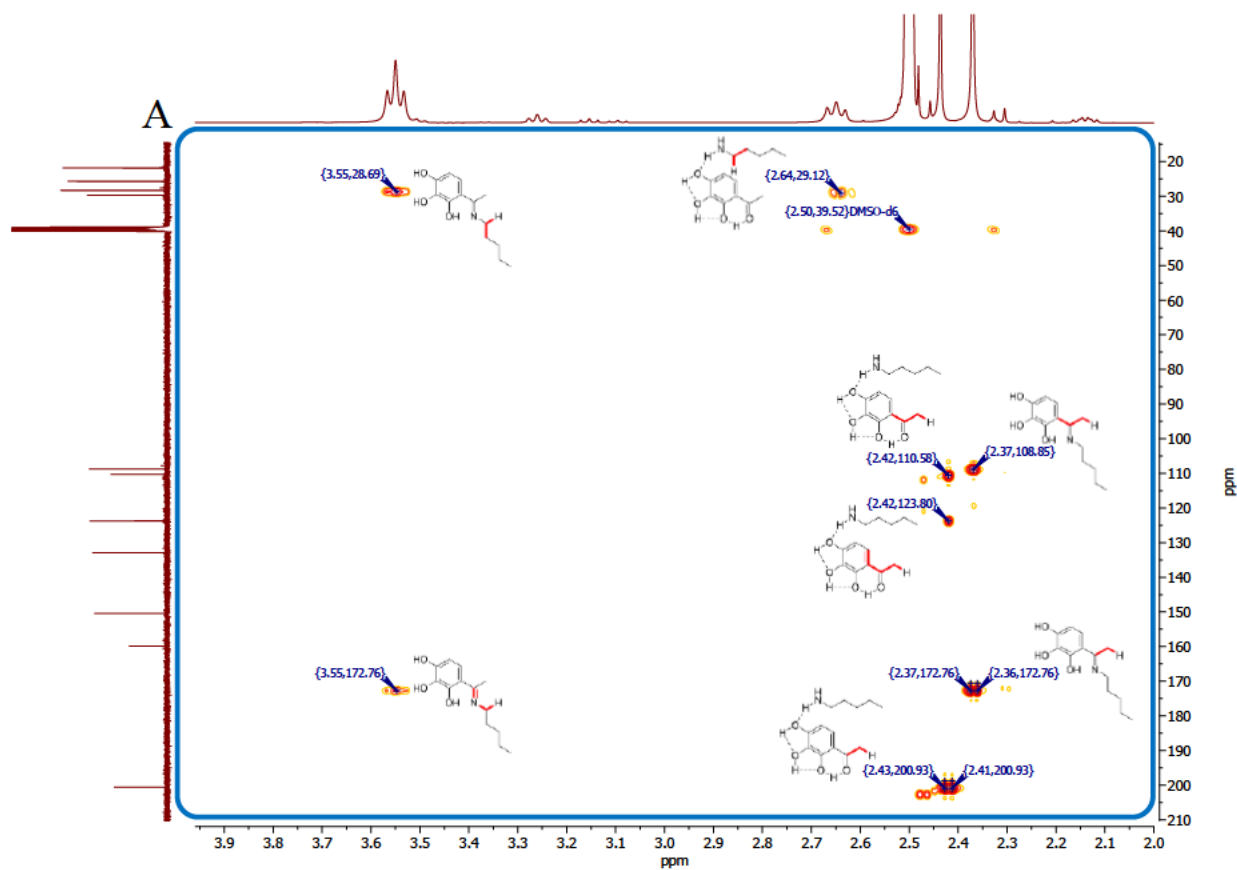


Fig. S28b. ^1H - ^{13}C HMBC spectrum of TAP-pentylamine, DMSO-d₆, 400 MHz.

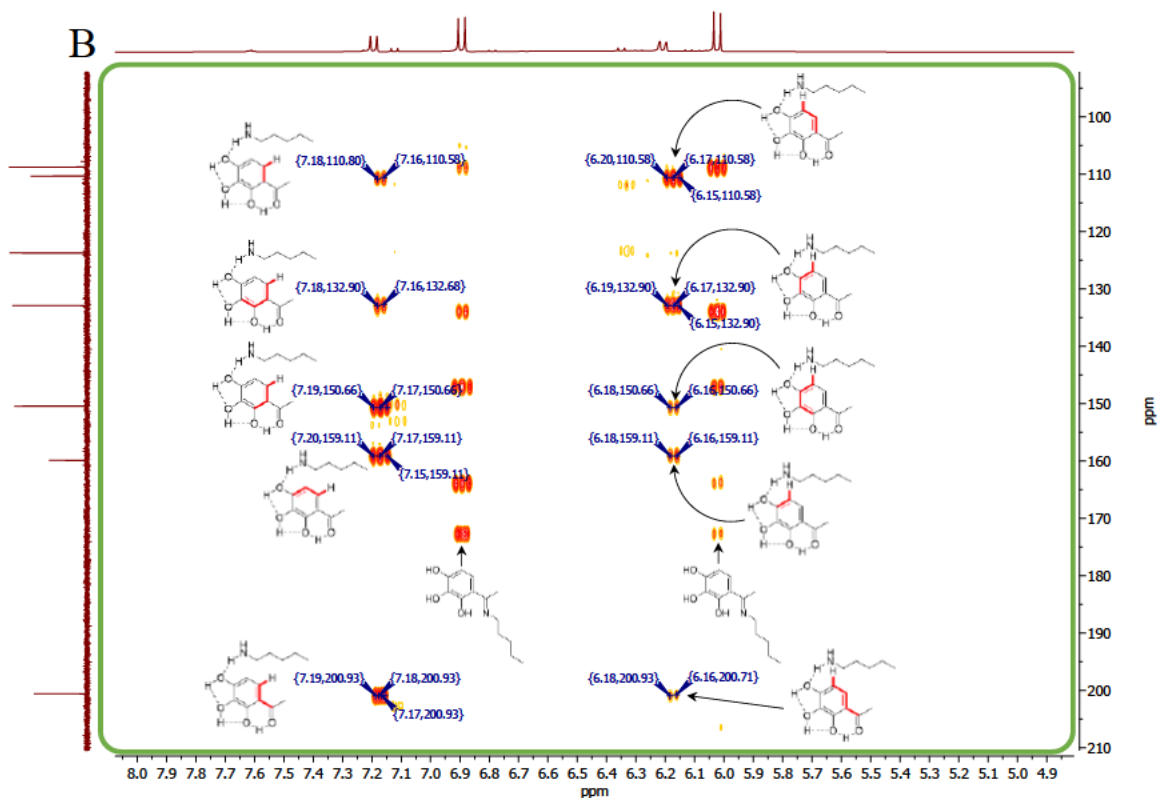


Fig. S28c. ^1H - ^{13}C HMBC spectrum of TAP-pentylamine, DMSO- d_6 , 400 MHz.

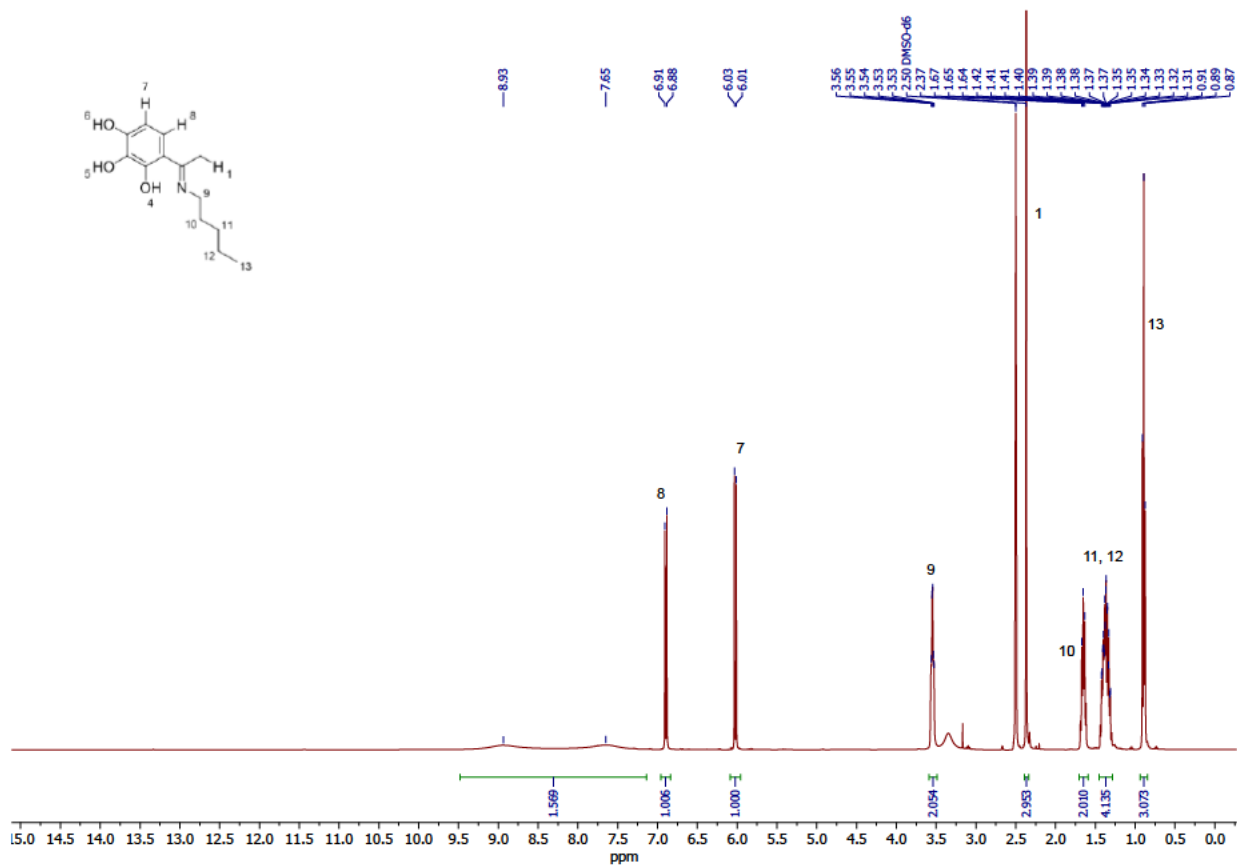


Fig. S29. ^1H NMR spectrum of imine **8**, DMSO- d_6 , 400 MHz.

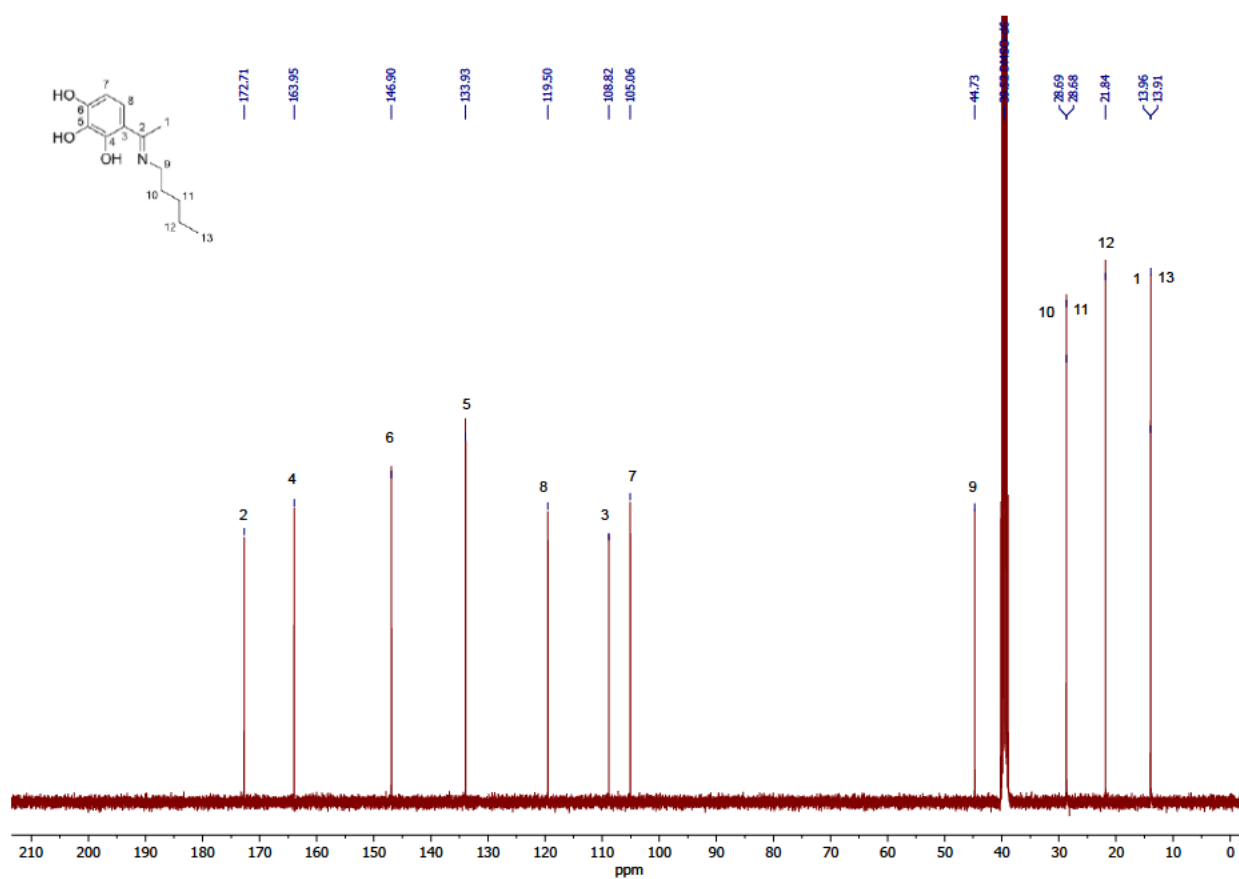


Fig. S30. ^{13}C NMR spectrum of imine **8**, $\text{DMSO-}d_6$, 101 MHz.

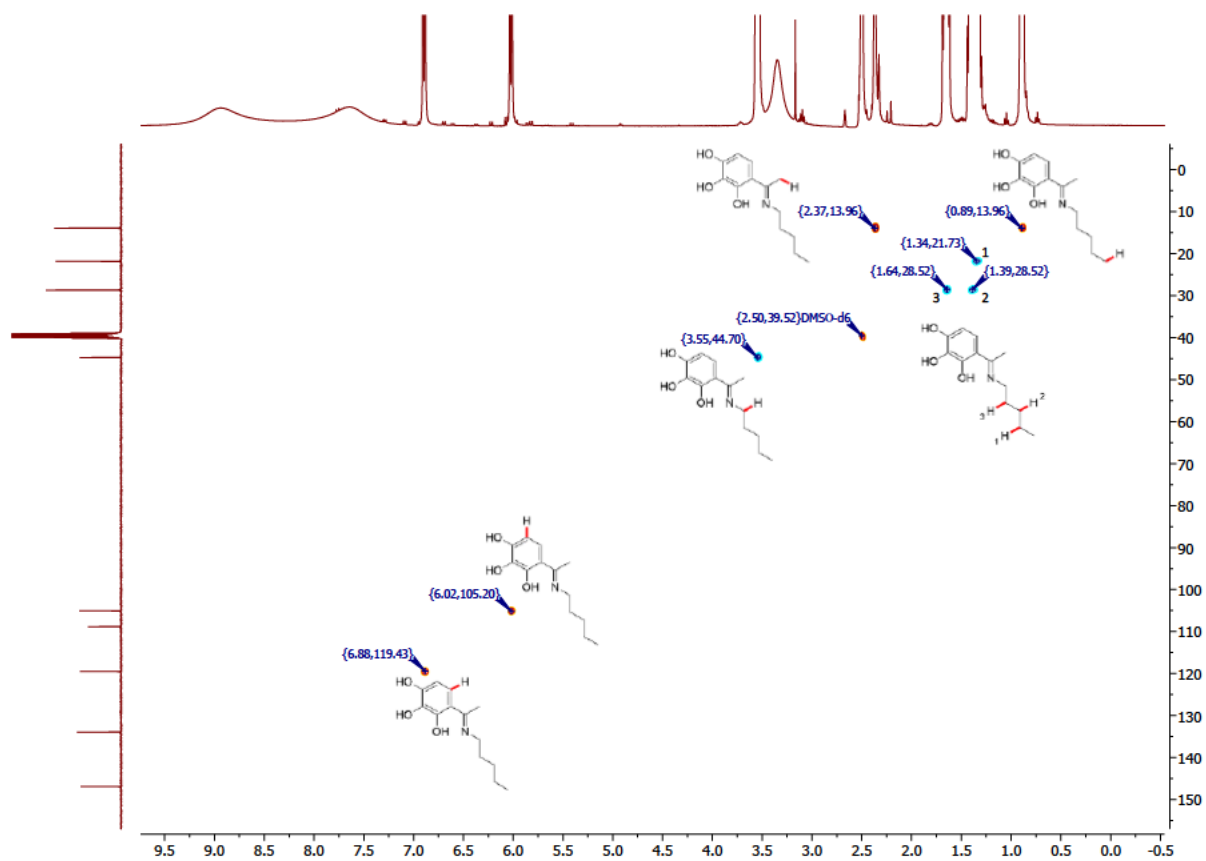


Fig. S31. $^1\text{H-}^{13}\text{C}$ HSQC spectrum of imine **8**, $\text{DMSO-}d_6$, 400 MHz.

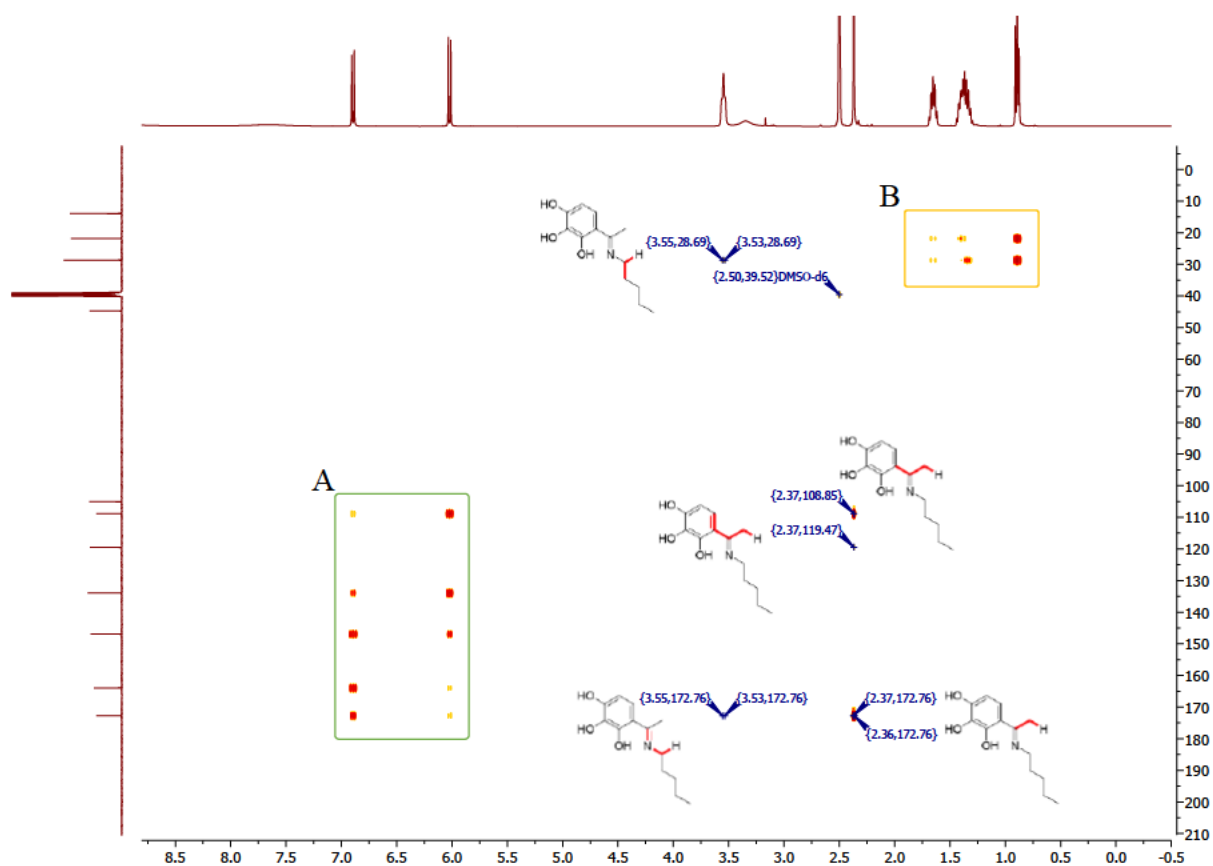


Fig. S32a. ^1H - ^{13}C HMBC spectrum of imine **8**, $\text{DMSO-}d_6$, 400 MHz.

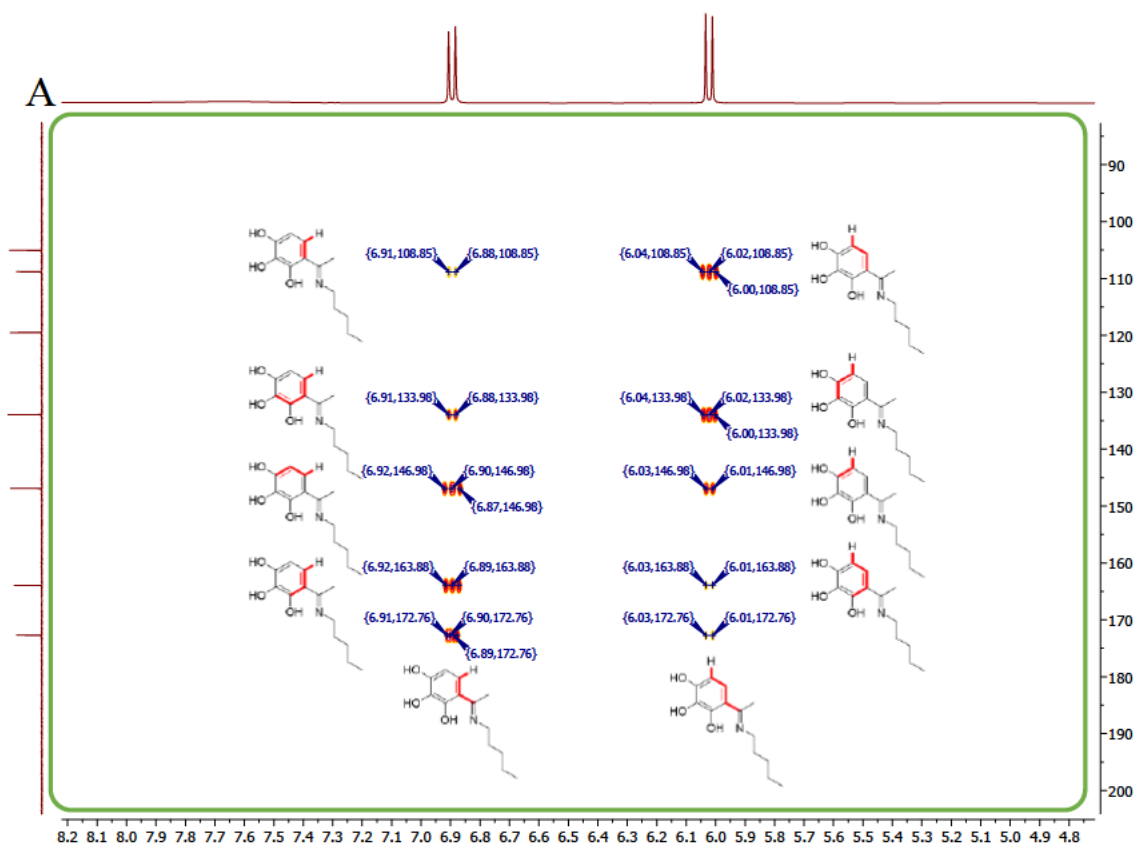


Fig. S32b. ^1H - ^{13}C HMBC spectrum of imine **8**, $\text{DMSO-}d_6$, 400 MHz.

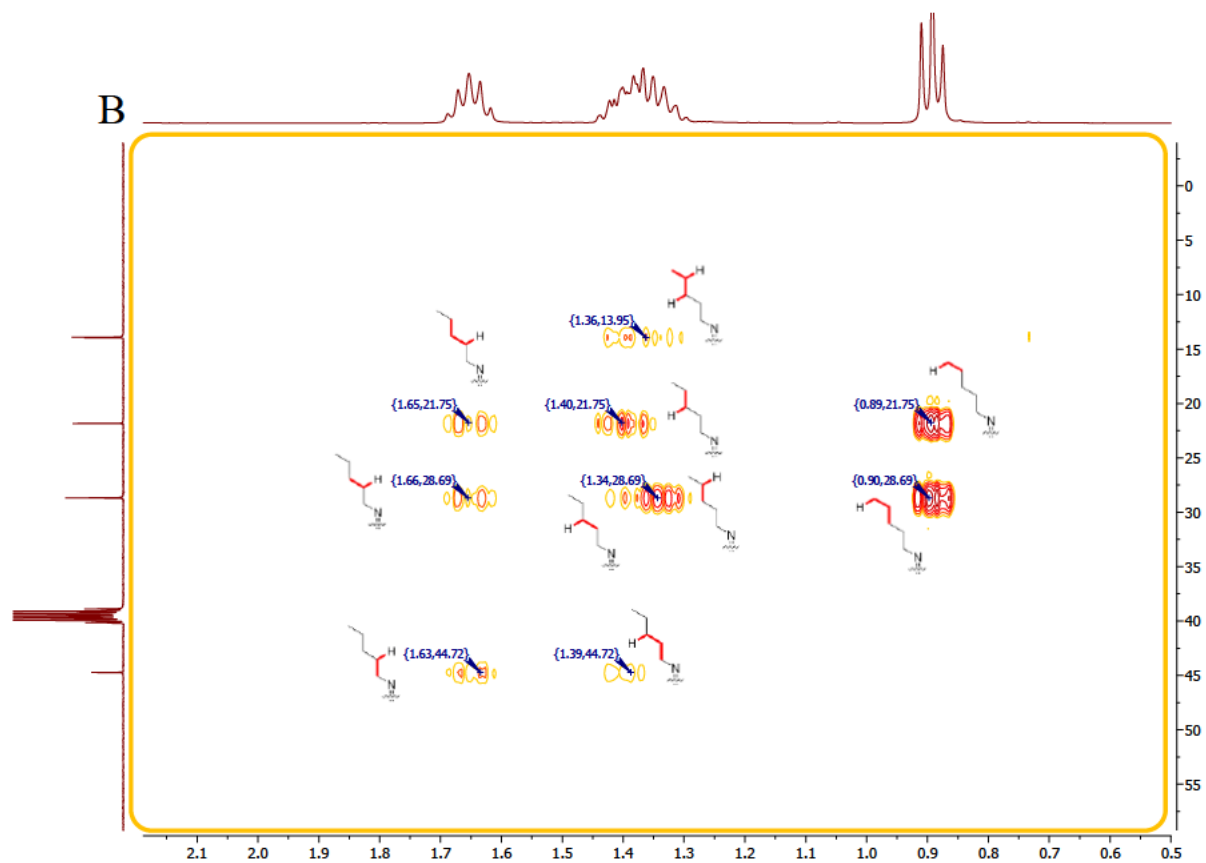


Fig. S32c. ^1H - ^{13}C HMBC spectrum of imine **8**, $\text{DMSO-}d_6$, 400 MHz.

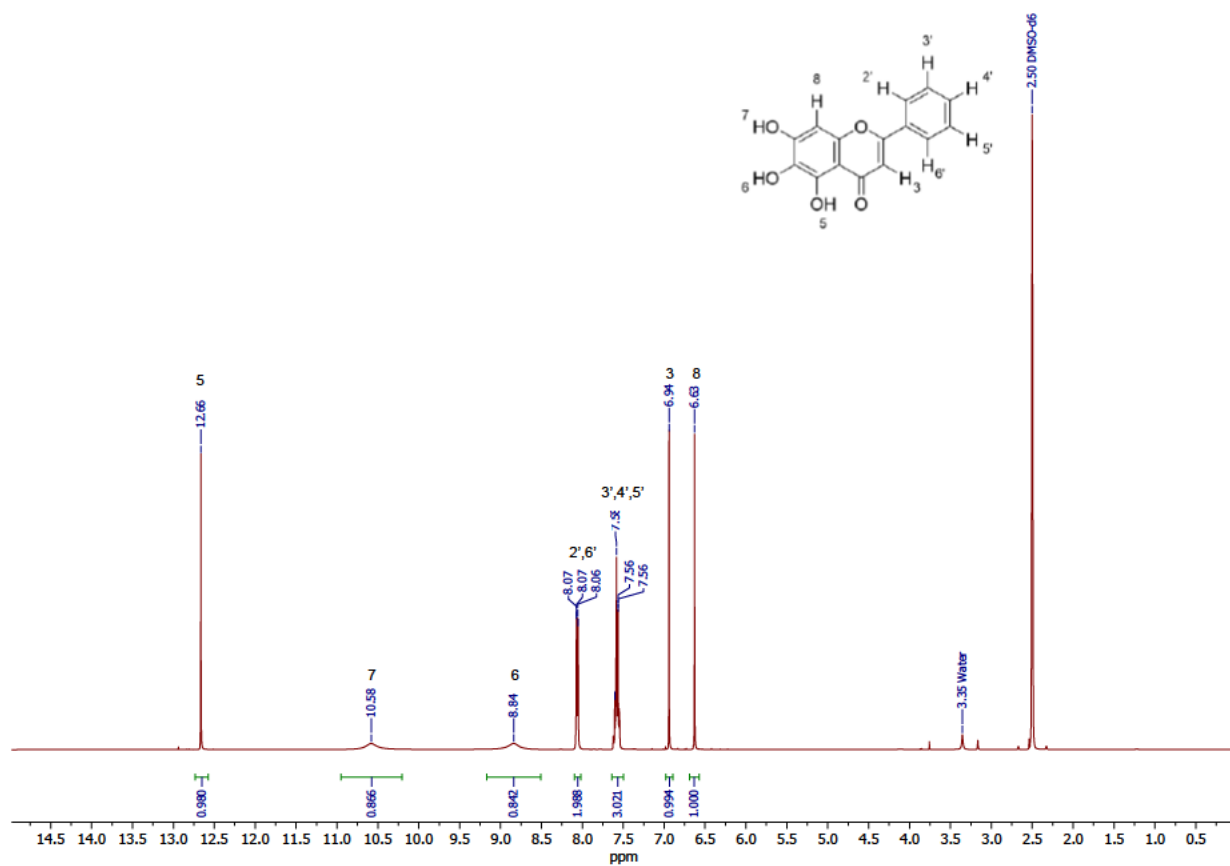


Fig. S33. ^1H NMR spectrum of BA (**1**), $\text{DMSO-}d_6$, 400 MHz.

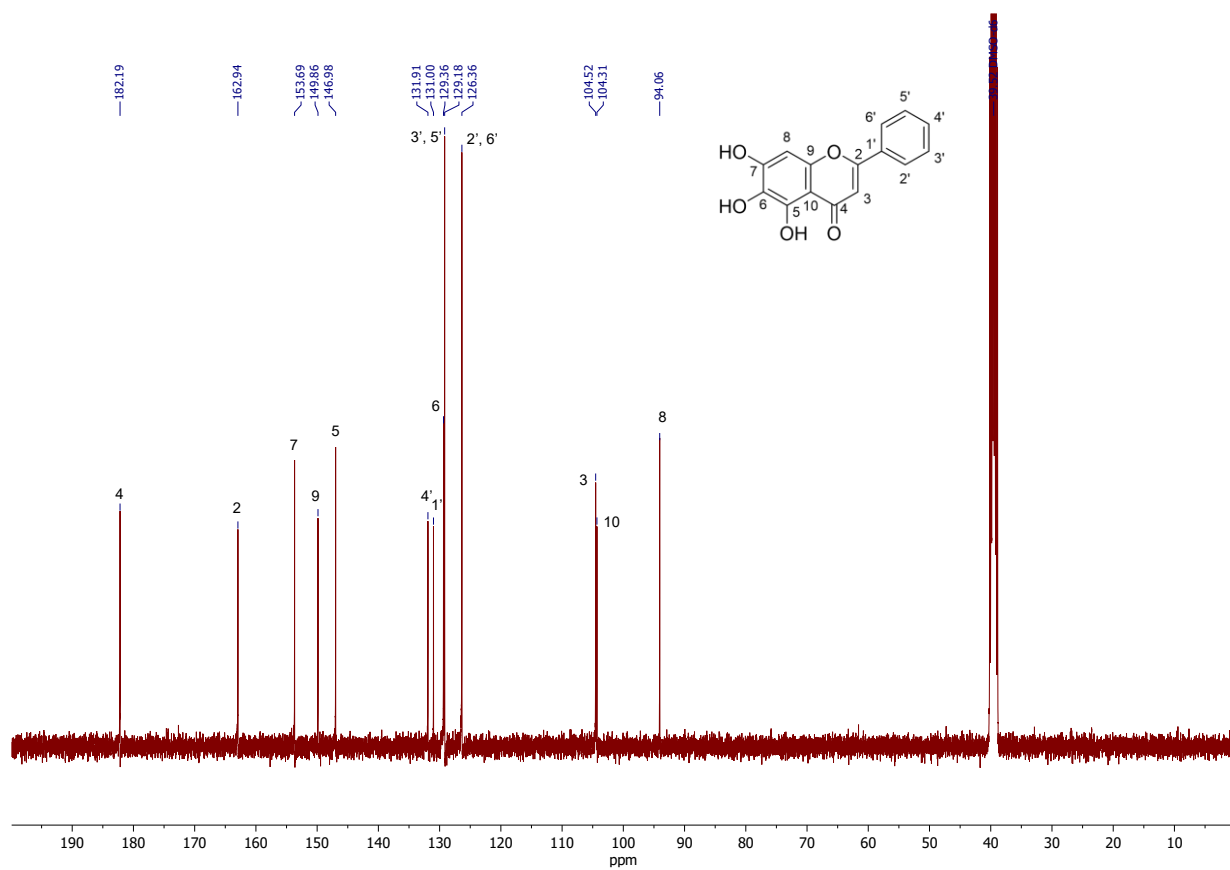


Fig. S34. ^{13}C NMR spectrum of BA (1), DMSO- d_6 , 101 MHz.

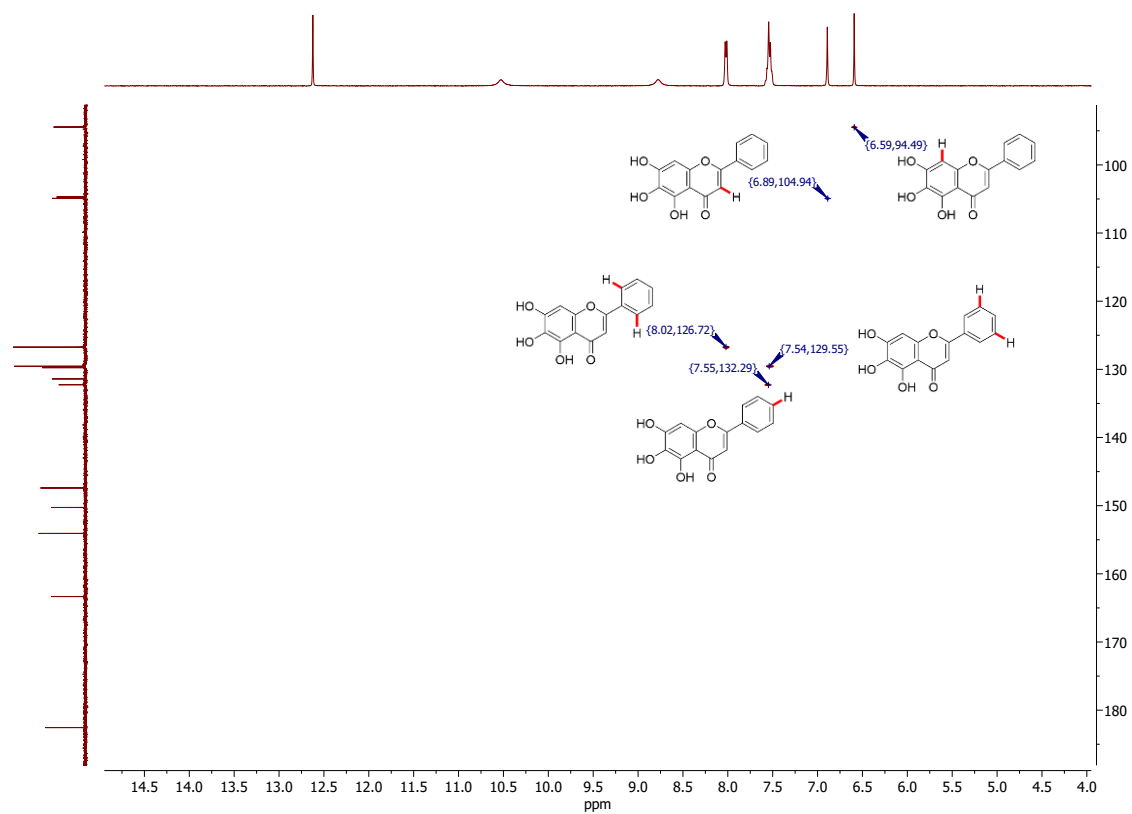


Fig. S35. ^1H - ^{13}C HSQC spectrum of BA (1), DMSO- d_6 , 400 MHz.

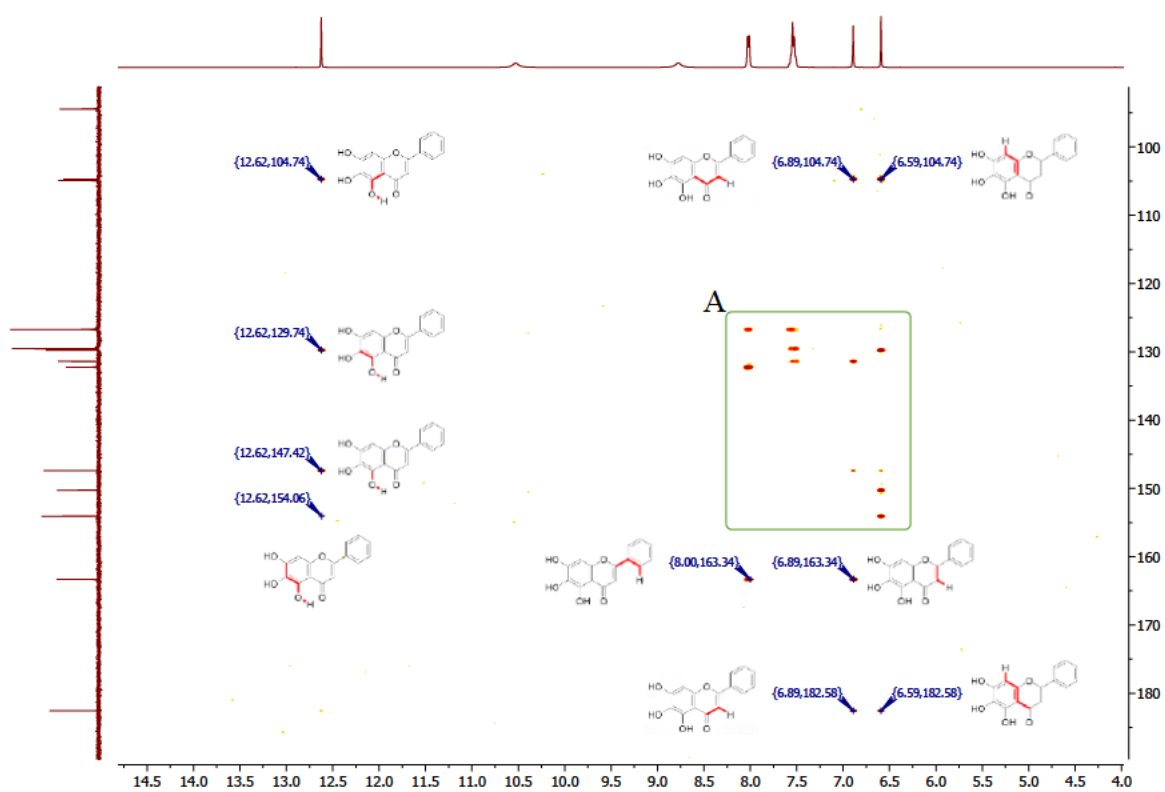


Fig. S36a. ^1H - ^{13}C HMBC spectrum of BA (1), $\text{DMSO-}d_6$, 400 MHz.

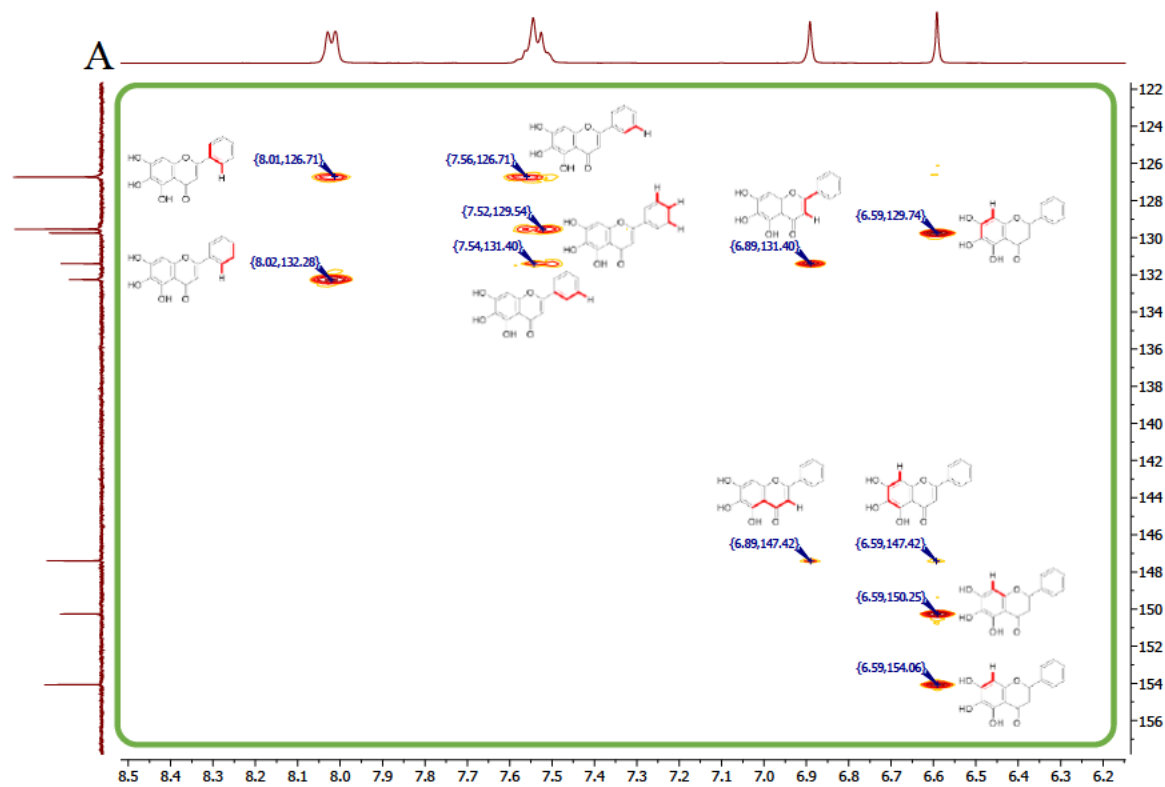


Fig. S36b. ^1H - ^{13}C HMBC spectrum of BA (1), $\text{DMSO-}d_6$, 400 MHz.

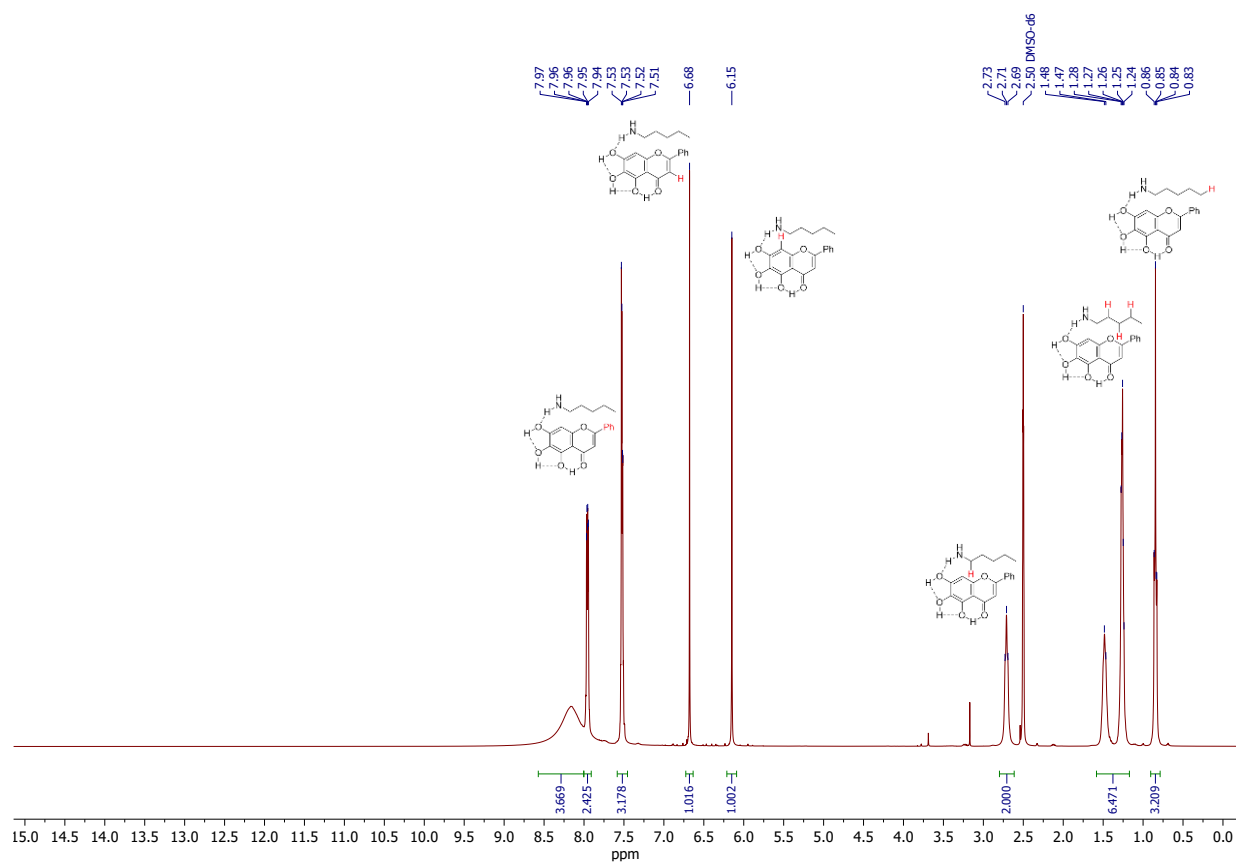


Fig. S37. ^1H NMR spectrum of BA-pentylamine complex, $\text{DMSO-}d_6$, 400 MHz.

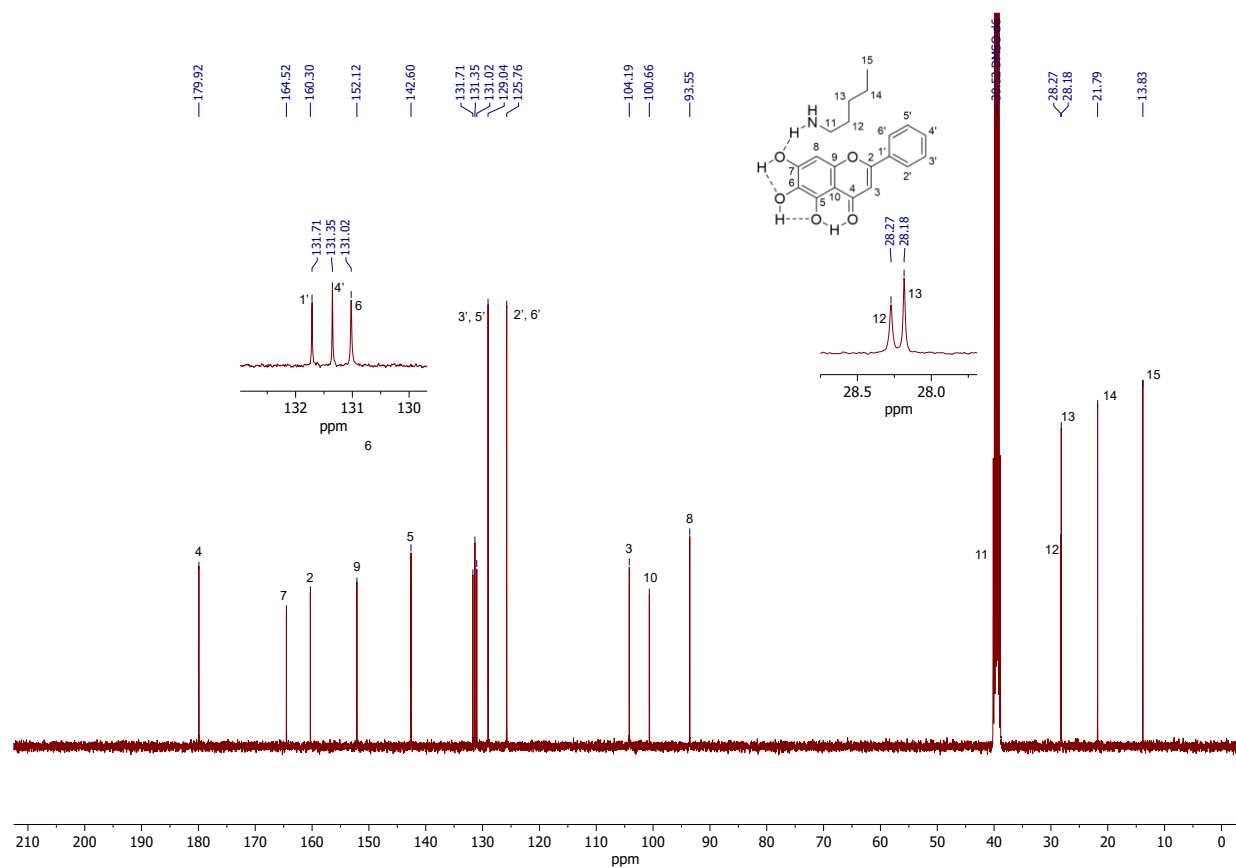


Fig. S38. ^{13}C NMR spectrum of BA-pentylamine complex, $\text{DMSO-}d_6$, 101 MHz.

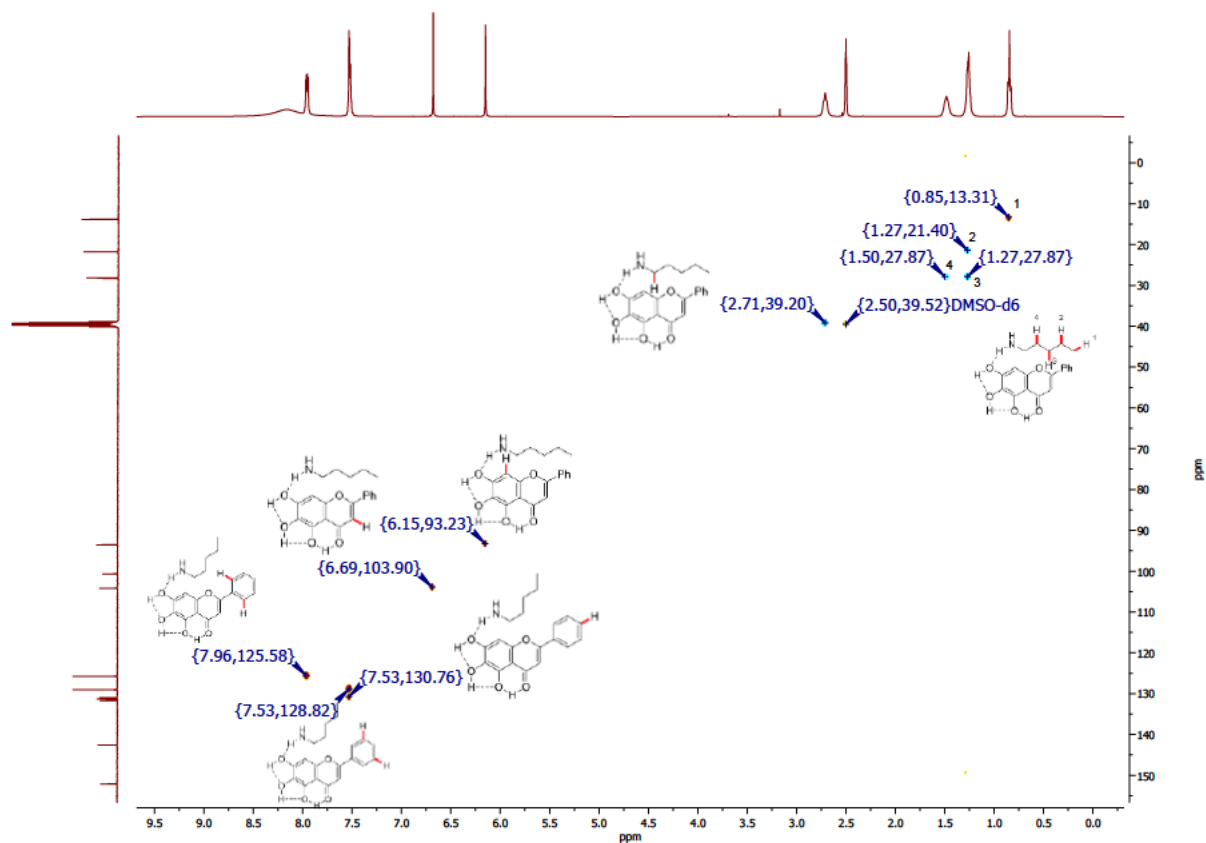


Fig. S39. ^1H - ^{13}C HSQC spectrum of BA-Pentylamine complex, DMSO-*d*₆, 400 MHz.

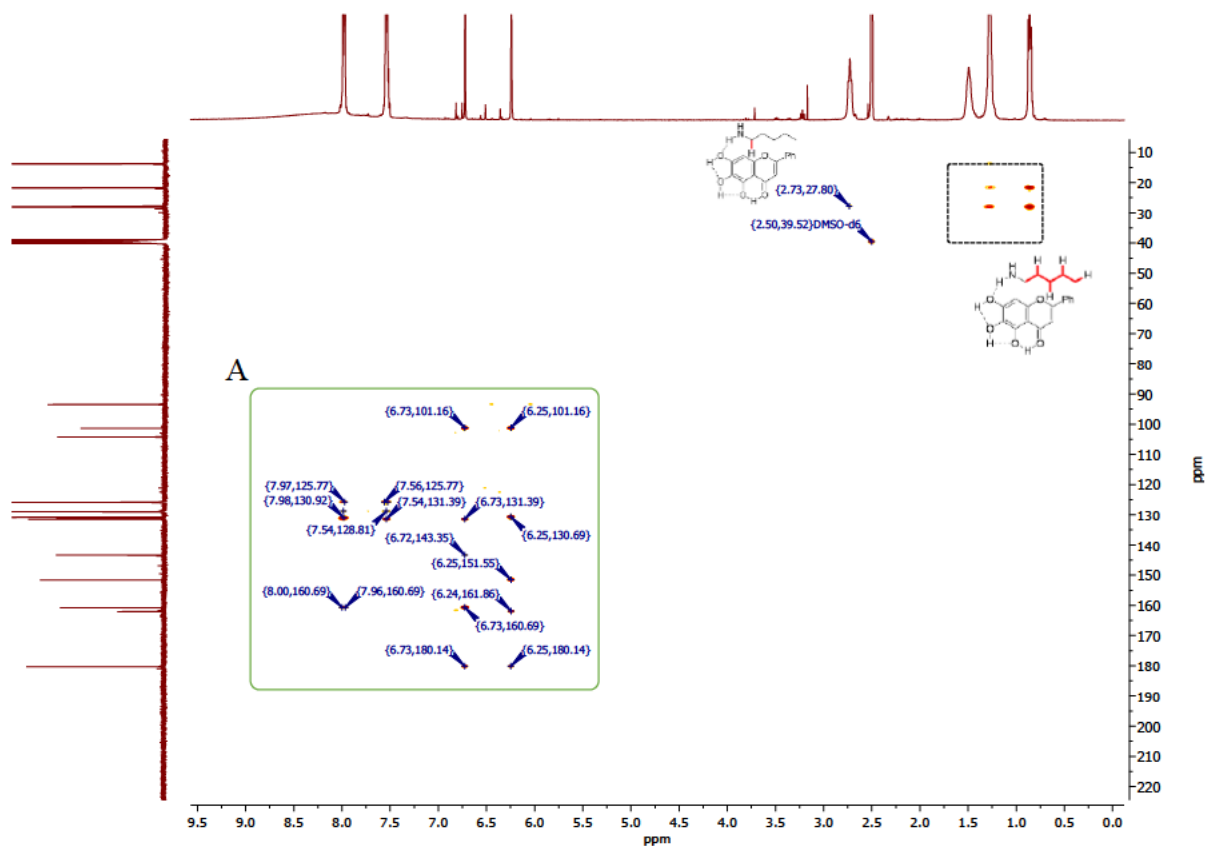


Fig. S40a. ^1H - ^{13}C HMBC spectrum of BA-pentylamine complex, DMSO-*d*₆, 400 MHz.

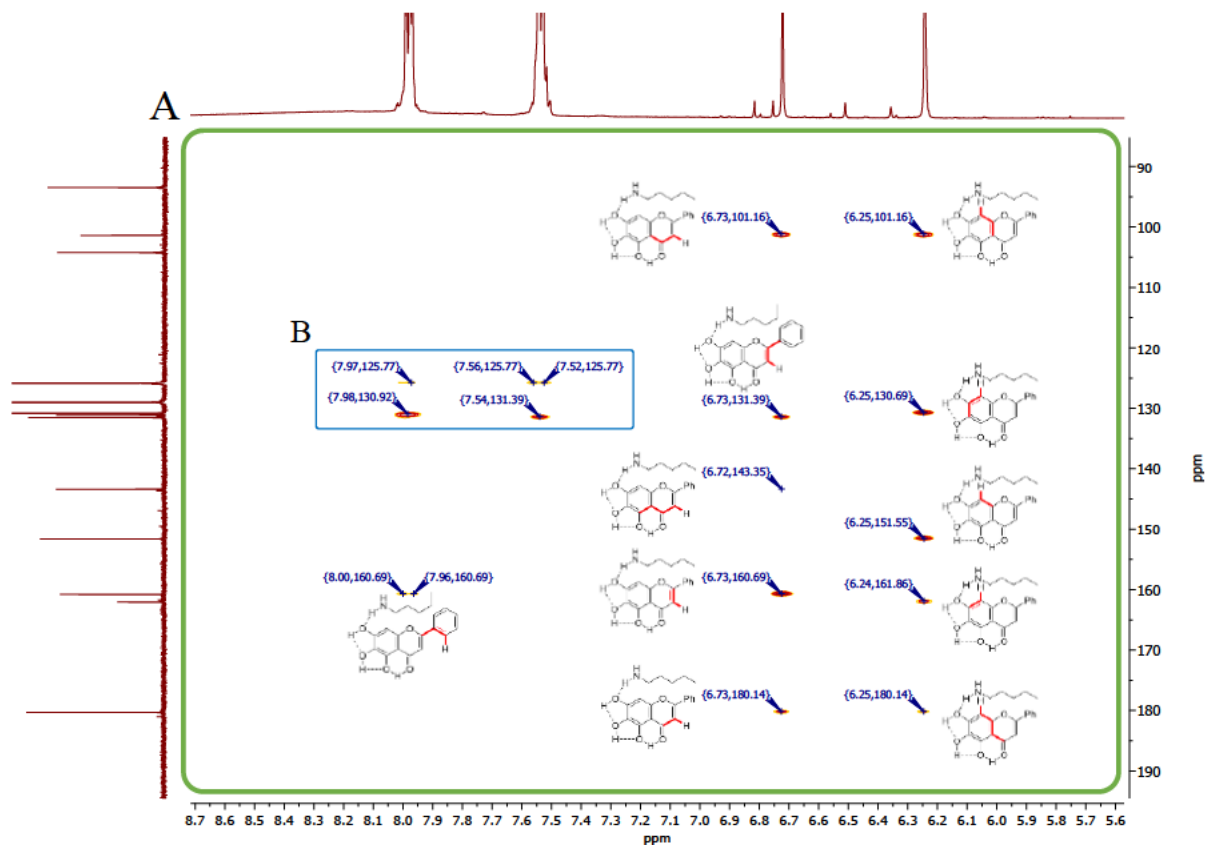


Fig. S40b. ^1H - ^{13}C HMBC spectrum of BA-pentylamine complex, DMSO- d_6 , 400 MHz.

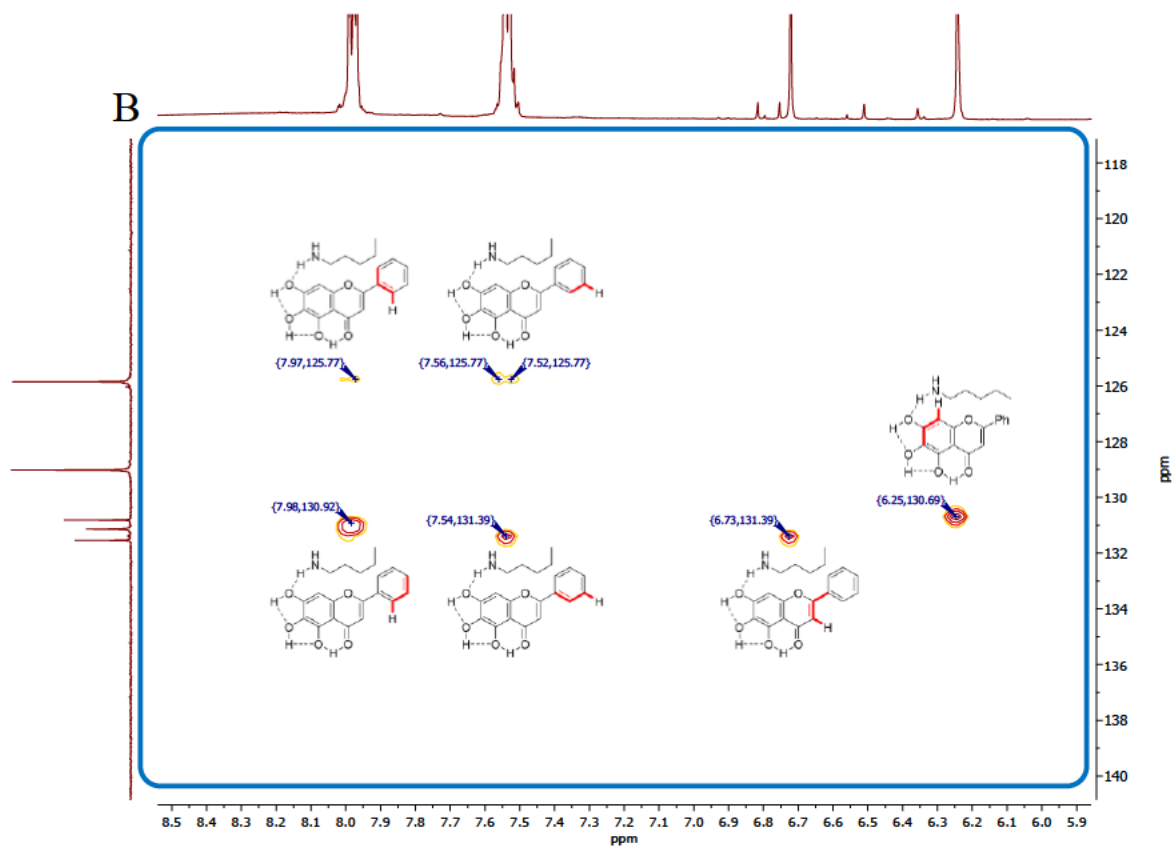


Fig. S40c. ^1H - ^{13}C HMBC spectrum of BA-pentylamine complex, DMSO- d_6 , 400 MHz.

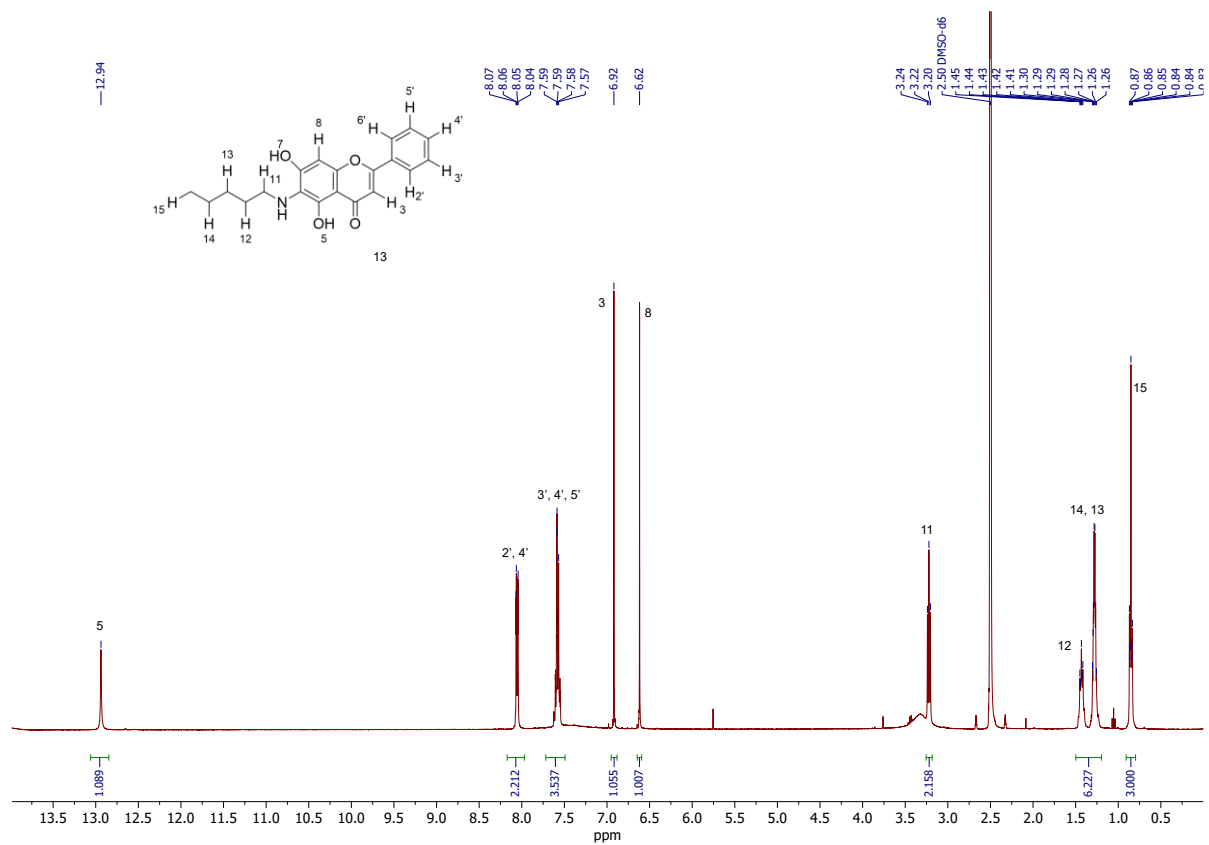


Fig. S41. ¹H NMR spectrum of coupling product **11a**, DMSO-*d*₆, 400 MHz.

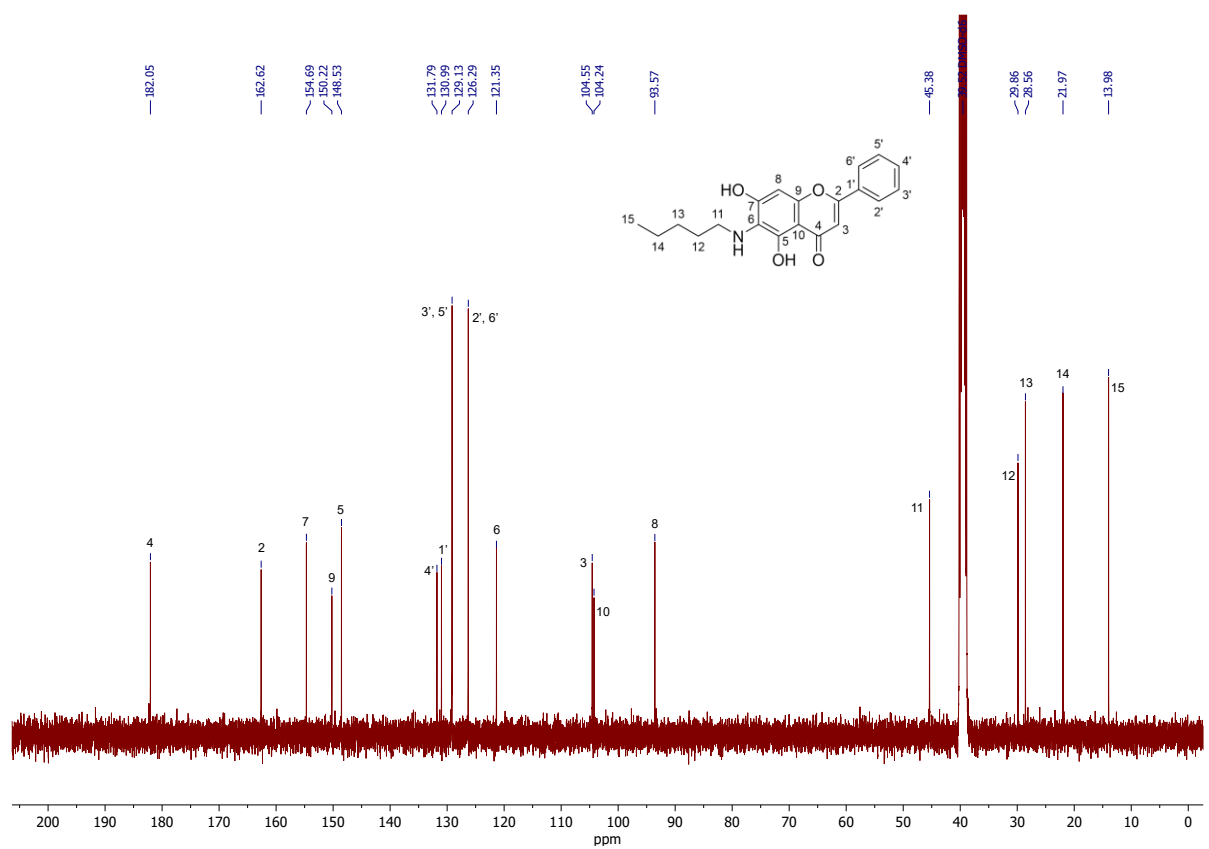


Fig. S42. ¹³C NMR spectrum of coupling product **11a**, DMSO-*d*₆, 101 MHz.

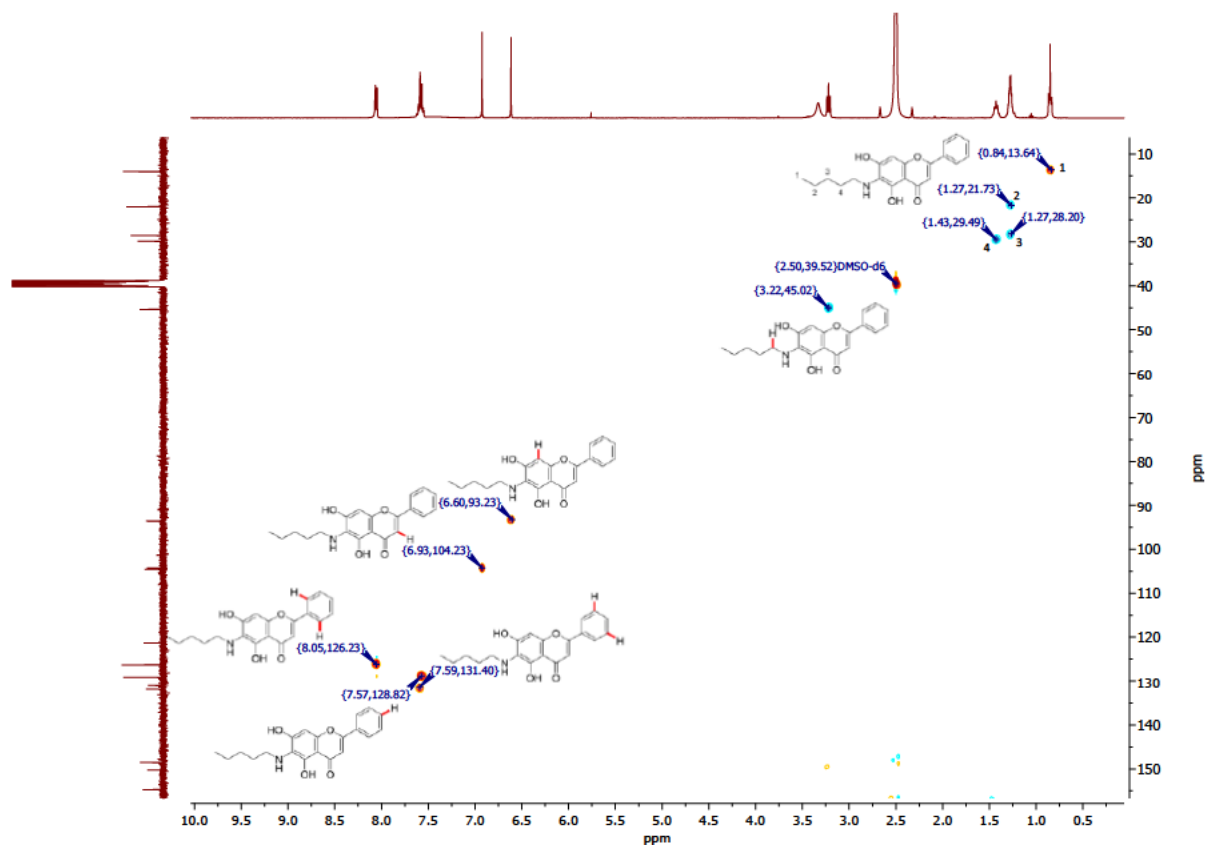


Fig. S43. ^1H - ^{13}C HSQC spectrum of product **11a**, $\text{DMSO-}d_6$, 400 MHz.

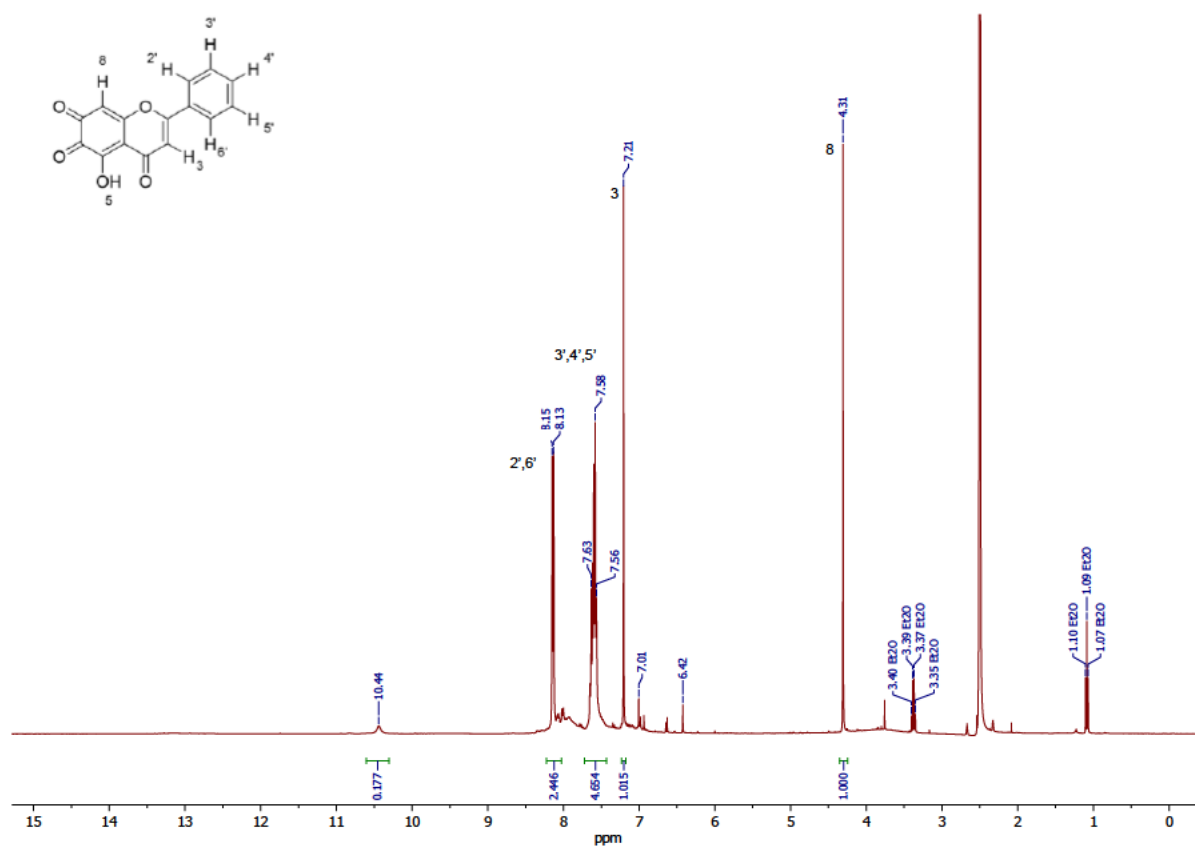


Fig. S44. ^1H NMR spectrum of crude **2b**, $\text{DMSO-}d_6$, 400 MHz.

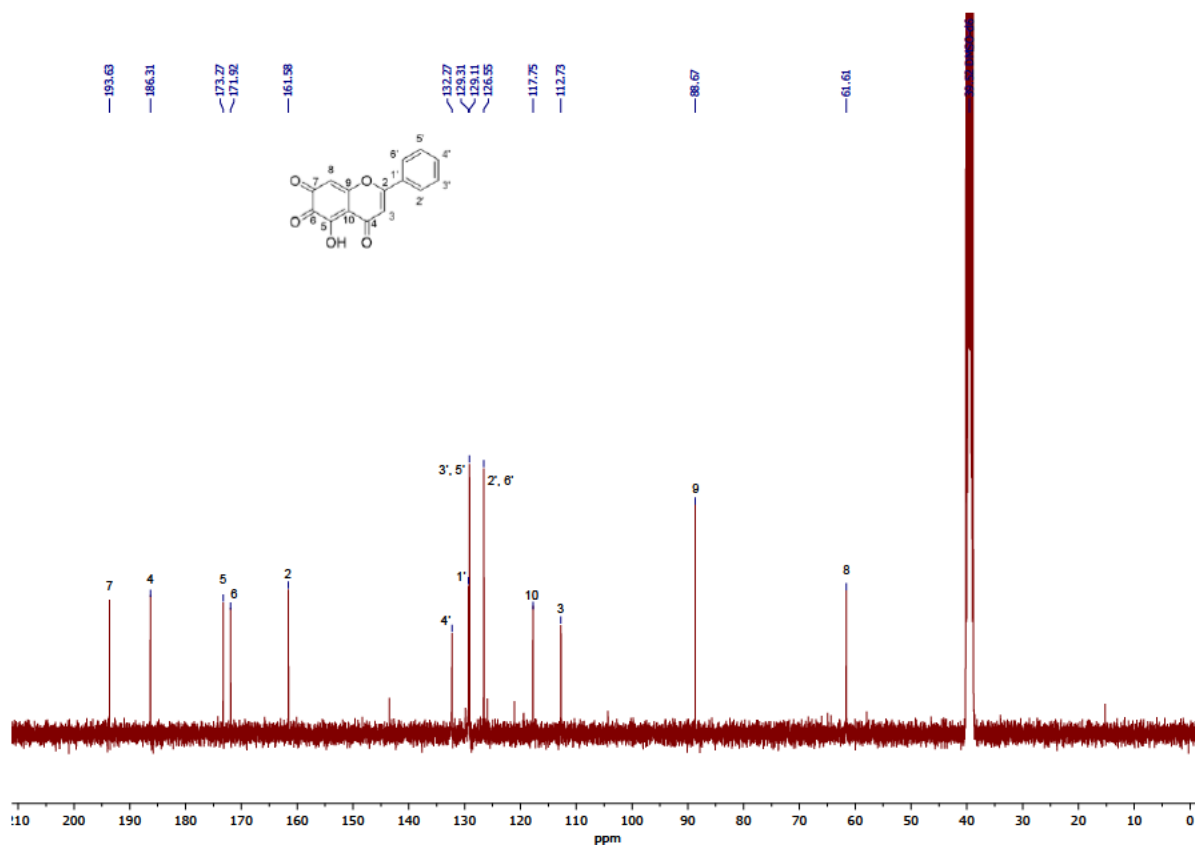


Fig. S45. ^{13}C NMR spectrum of crude **2b**, $\text{DMSO-}d_6$, 101 MHz.

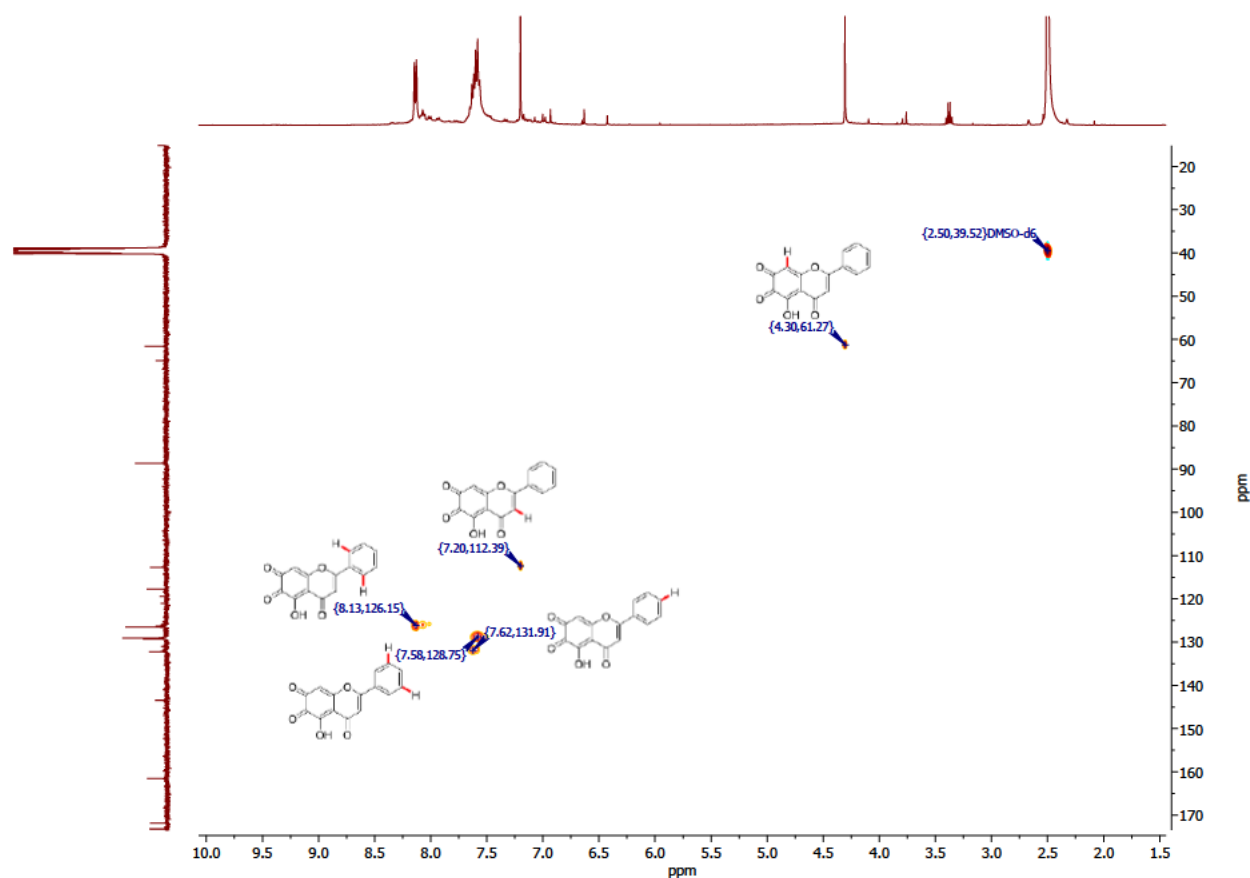


Fig. S46. ^1H - ^{13}C HSQC spectrum of **2b**, $\text{DMSO-}d_6$, 400 MHz.

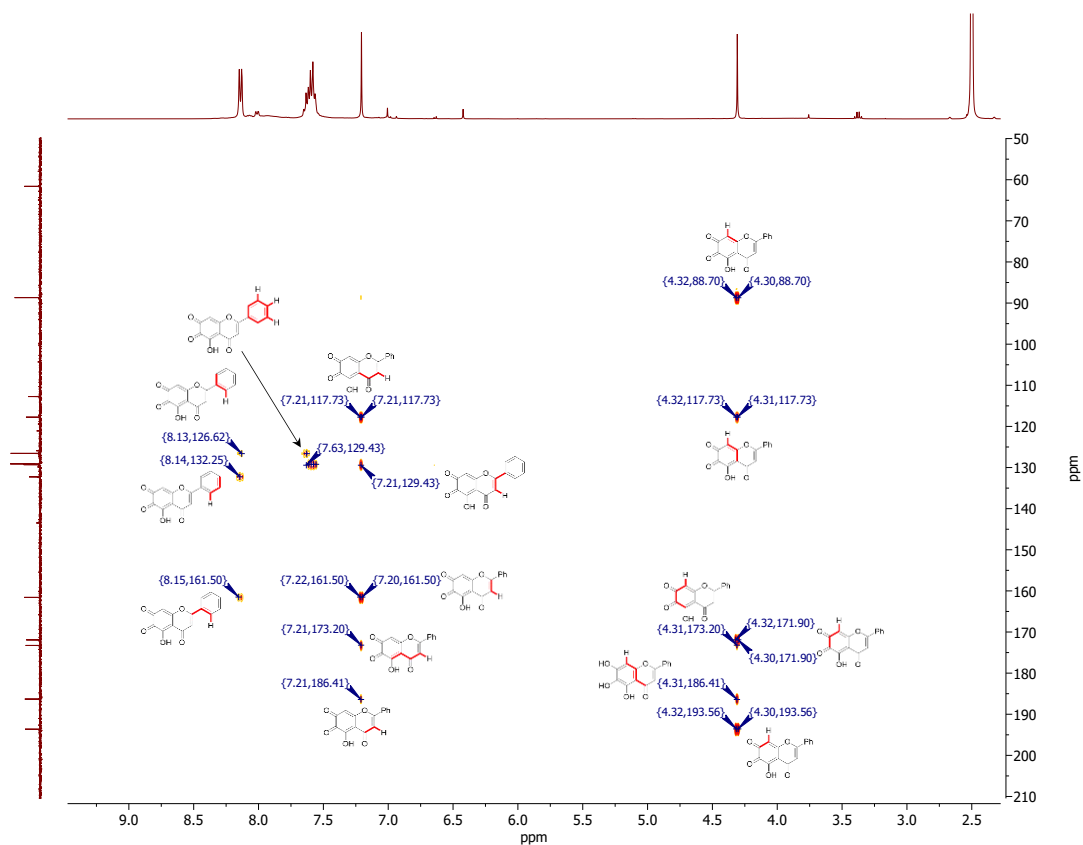


Fig. S47. ^1H - ^{13}C HMBC spectrum of **2b**, DMSO- d_6 , 400 MHz.

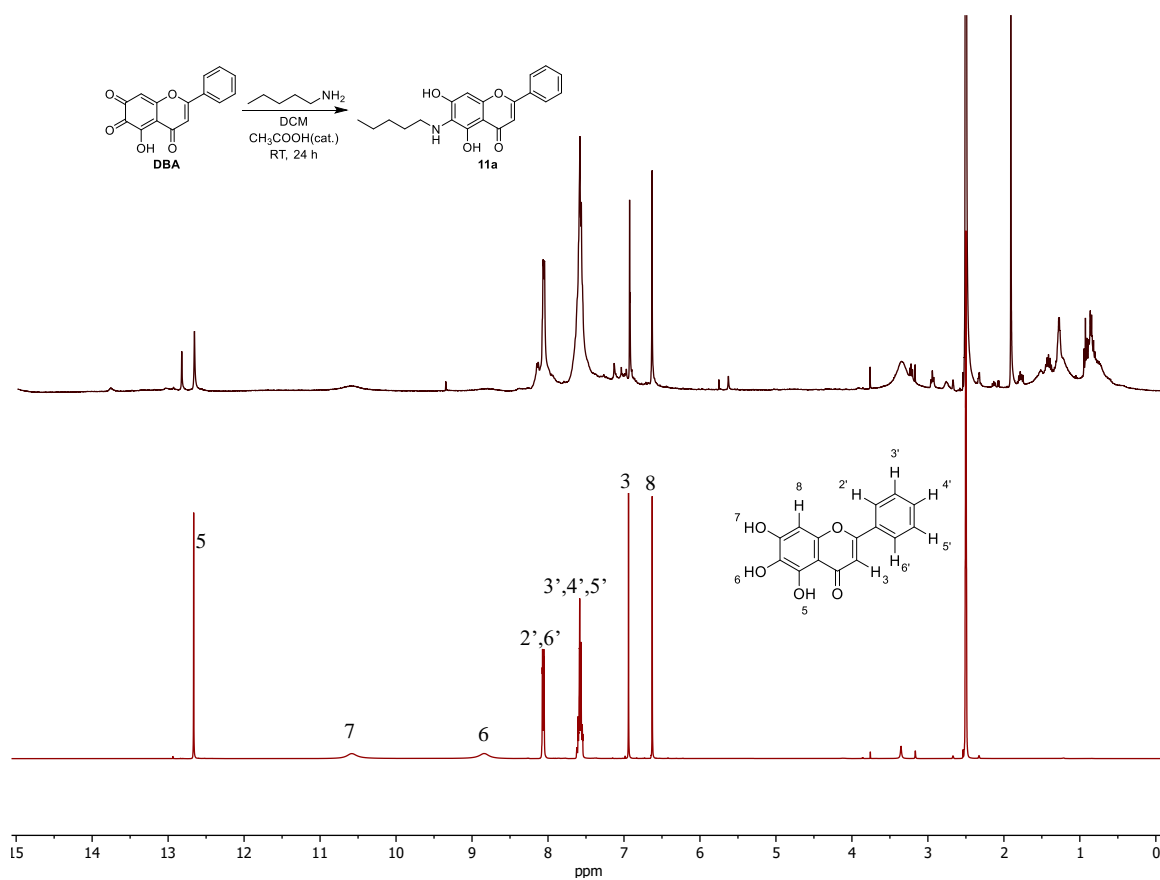


Fig. S48. ^1H NMR spectra of **2b**-pentylamine coupling product (**11a**) (top) and **BA** (**1**) (bottom), DMSO- d_6 , 400 MHz.

Mass spectrometry analysis of reaction products

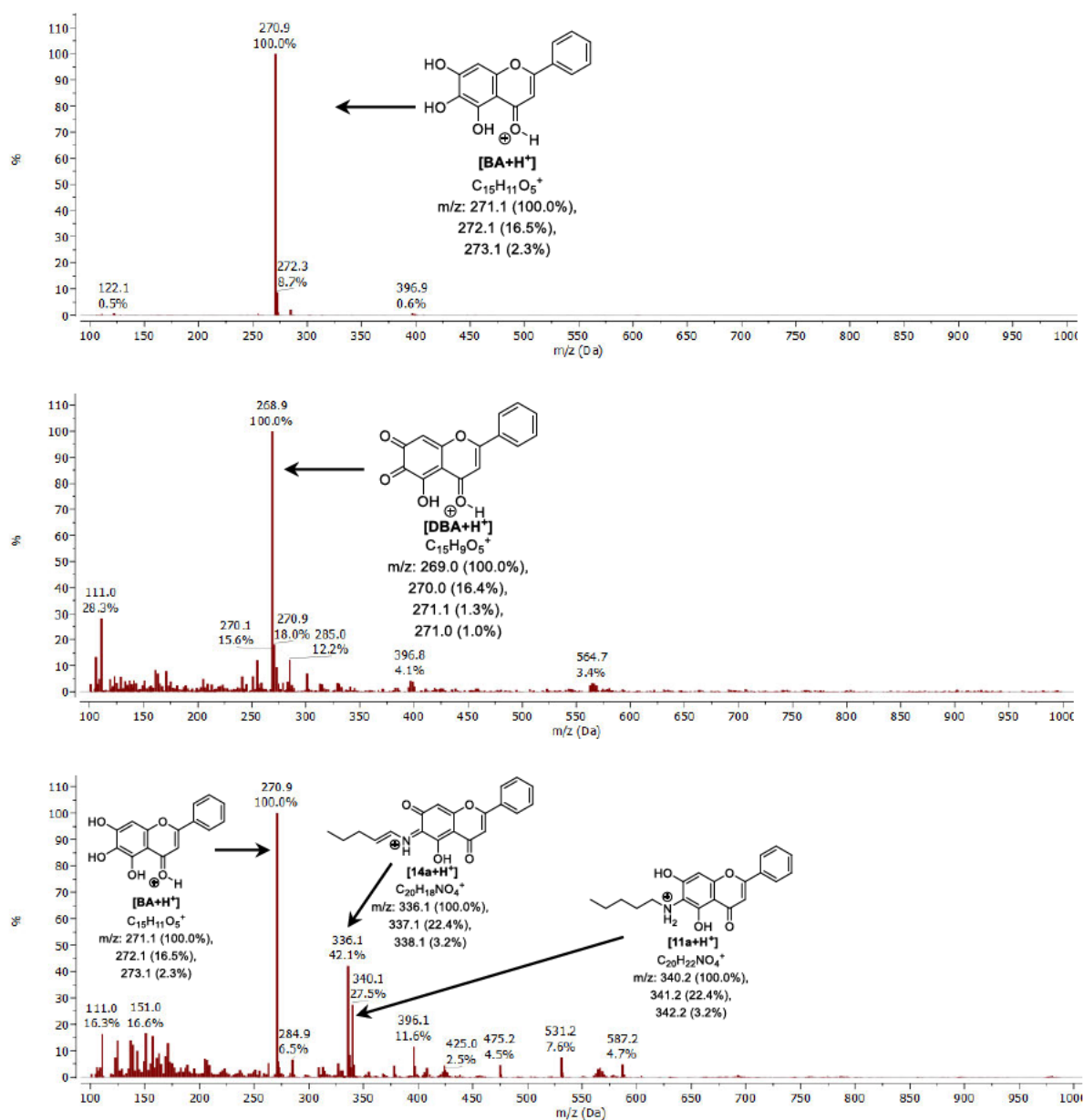


Fig. S49. APCI-MS spectra of baicalein (**1**), dehydrobaicalein (**2b**) and the coupling product of the reaction between DBA with pentylamine (**3**).

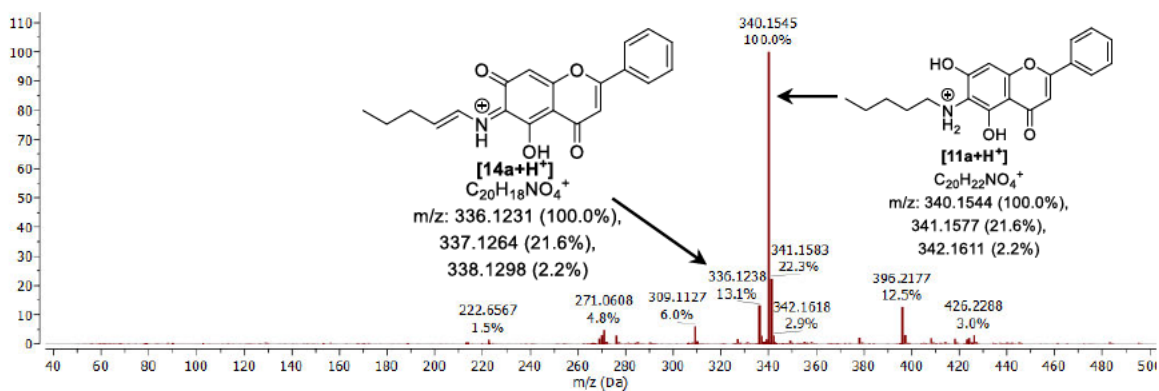


Fig. S50. HRMS-ESI spectrum of crude coupling product coupling product of the reaction between DBA and pentylamine (**3**).

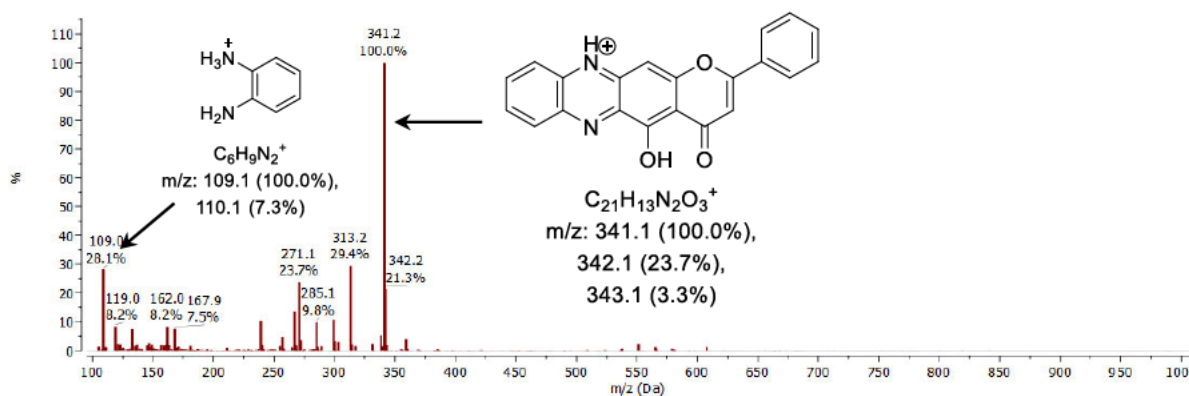
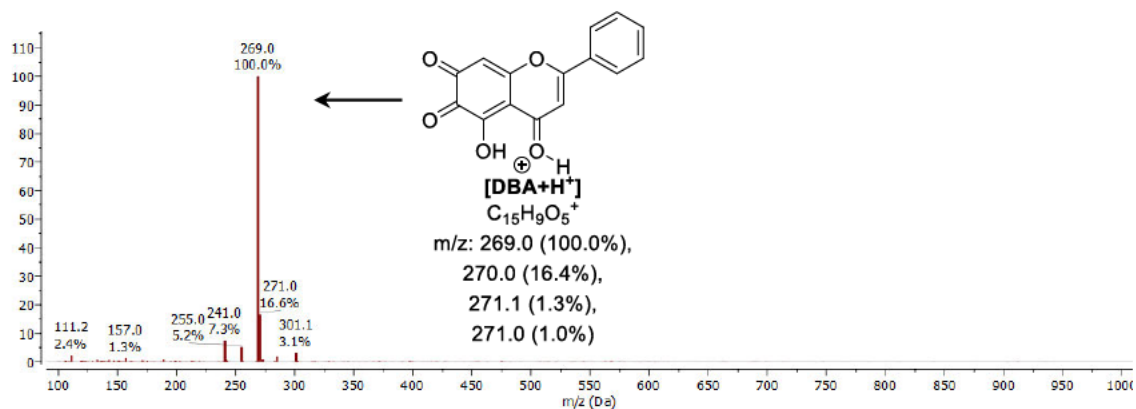
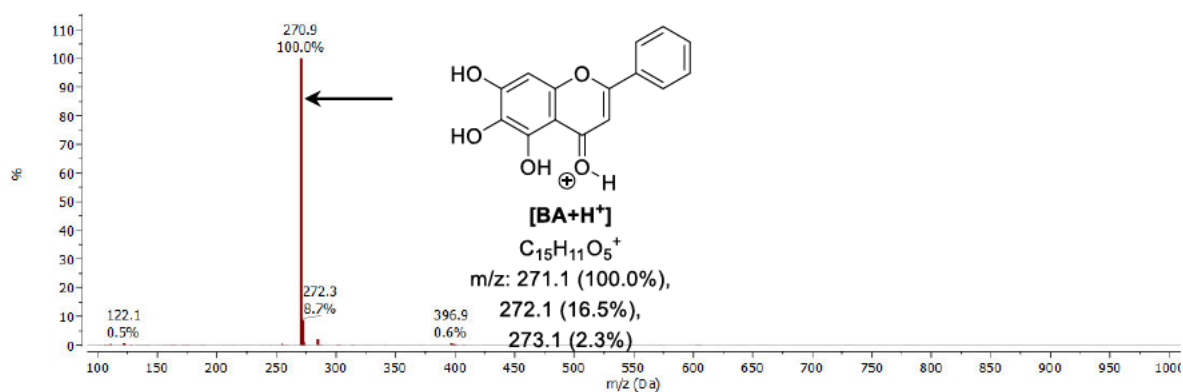


Fig. S51. MS-APCI spectra of baicalein (**1**), dehydrobaicalein (**2b**) and the coupling product 6,7-BA phenazine derivative.

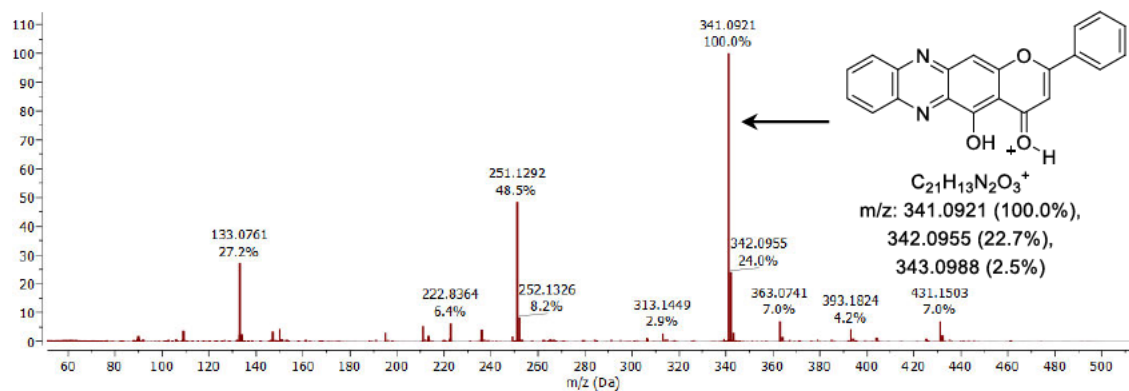


Fig. S52. HRMS-ESI spectrum of coupling product 6,7-BA phenazine derivative.

References:

- [1] Y. Lee, H. Yeo, S.-H. Liu, Z. Jiang, R. M. Savitzky, D. J. Austin, Y.-c. Cheng, *J. Med. Chem.* **2004**, *47*, 5555-5566.
- [2] K. Hashida, R. Makino, S. Ohara, *Holzforschung* **2009**, *63*, 319-326.
- [3] P. Velander, L. Wu, W. K. Ray, R. F. Helm, B. Xu, *Biochemistry* **2016**, *55*, 4255-4258.
- [4] Z. Feng, J. Zhou, X. Shang, G. Kuang, J. Han, L. Lu, L. Zhang, *Pharm. Biol.* **2017**, *55*, 1177-1184.
- [5] S. Morimoto, N. Tateishi, T. Matsuda, H. Tanaka, F. Taura, N. Furuya, N. Matsuyama, Y. Shoyama, *J. Biol. Chem.* **1998**, *273*, 12606-12611.

1.3. Combined *in silico* and *in vitro* Studies of the Amination of Baicalein and its Analogs

Salavat S. Ashirbaev, Natércia F. Brás, Hendrik Zipse

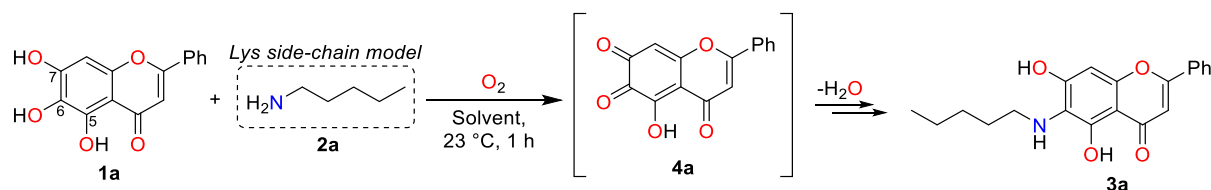
Dept. Chemistry, LMU Muenchen, Butenandtstrasse 5-13, D-81377 Muenchen, Germany

Author contributions

All experiments were performed by Salavat S. Ashirbaev and Kuangjie Liu under the supervision of Salavat S. Ashirbaev (for substrates **1h**, **1i** and **1l**), all the calculations were performed by Natércia F. Brás. The manuscript was written together by Salavat S. Ashirbaev, Natércia F. Brás and Hendrik Zipse.

1.3.1. Introduction

In the previous chapter it has been shown that flavonoid baicalein (**1a**) reacts with primary amine **2a**, forming a C6-covalent adduct **3a**. The overall reaction proceeds through transient generation of *o*-quinone intermediate **4a** as a main reactive species (Scheme 1). From our side, it was assumed that this might contribute to higher inhibition ability baicalein (**1a**) against fibril formation relative to other structurally related flavone molecules.

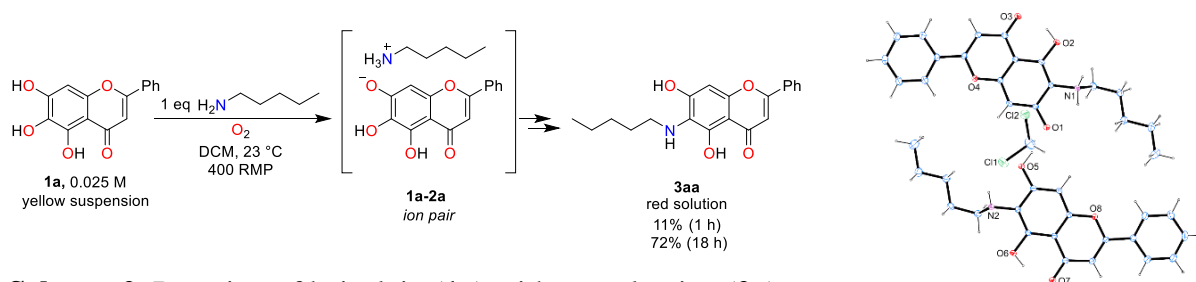


Scheme 1. The oxidative coupling of baicalein (**1a**) with pentylamine (**2a**).

It was decided to continue the investigation of the oxidative coupling reaction, not only within the context of the initially studied flavonoid baicalein (**1a**), but also with a scope of other polyphenols, both natural and synthetic in origin. The goal is to understand the mechanism of covalent interactions between these polyphenols and amines, from the structural perspective of the polyphenol.

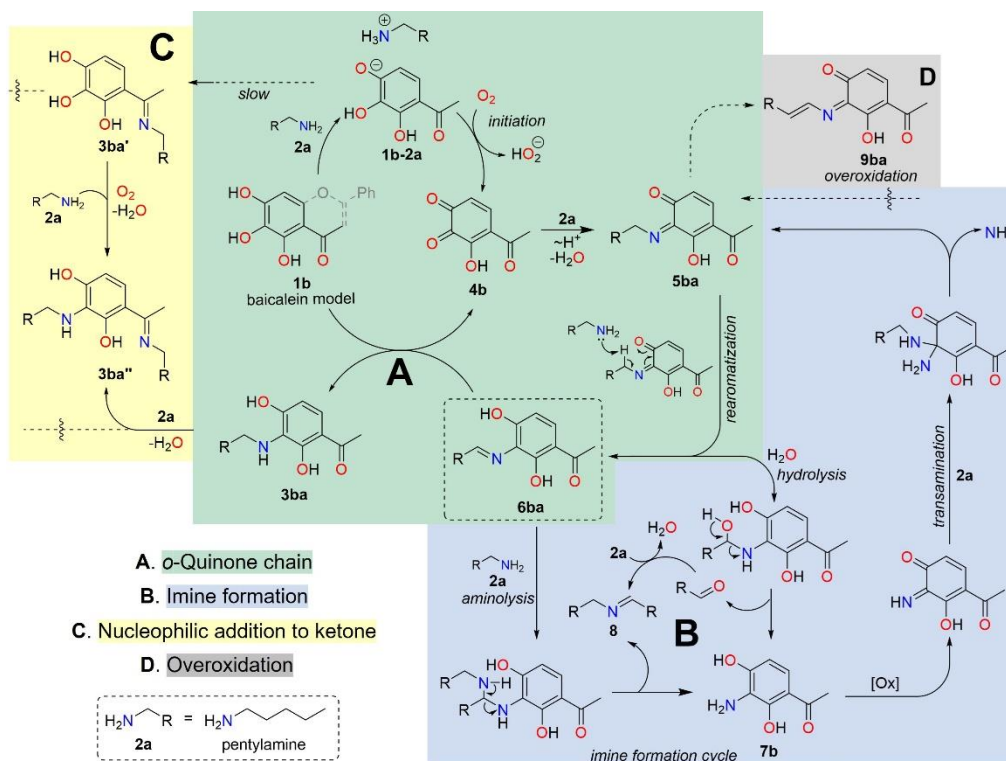
1.3.2. Mechanistic Studies on the Oxidative Coupling

Baicalein (**1a**), insoluble in DCM-*d*₂, readily reacts with amine **2a**, through ion pair formation, giving 11% and 72% yield of **3aa** in 1 h and 18 h, correspondingly, under O₂ atmosphere at 23 °C. After many attempts, it was possible to obtain a crystal suitable for scXRD analysis, which revealed the C6-regioselectivity of the product (Scheme 2). Detailed analysis of the obtained X-ray structure indicates that the two given molecules of **3aa** are not equivalent as one of the molecules of **3aa** in the unit cell is present as a zwitterion, while the second unit of **3aa** shows no internal charge separation.



Scheme 2. Reaction of baicalein (**1a**) with pentylamine (**2a**).

To assess the propensity of other substrates to undergo the amination reaction observed for **1a**, it is helpful to analyze the requirements of all stages of the proposed reaction mechanism. For the mechanistic insights, our focus was made on the reaction of 2,3,4-trihydroxyacetophenon (TAP, **1b**) as a baicalein (**1a**) model, with pentylamine (**2a**) (Scheme 3).



Scheme 3. Proposed mechanism of the oxidative coupling of **1b-2a**.

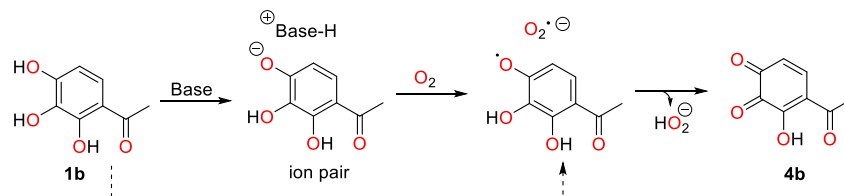
TAP (**1b**) was mixed with amine **2a** in various reaction media and reaction conditions to elucidate further the nature of this reaction and its role in the inhibition of **hiAPP** aggregation. As shown in Scheme 3, the overall reaction can be divided up into a *chain propagation* **A** and *imine formation* **B** pathways. The initiation of the reaction involves reaction of **2a** with **1b** such that a precipitate of a phenolate/ammonium ion pair **1b-2a** is formed, which was proven via single X-ray analysis in the previous chapter. It has been shown that the oxidative coupling with 3 eq of **2a** is very slow under air in DCM (only 4% for **1b**). Increasing the oxygen content, replacing air with O_2 has only a moderate effect (27% yield) on the reaction yield (Table 1, Entries 1 and 2). The low reactivity was explained by the insolubility of the reacting ion pair species in DCM. To demonstrate this, the reaction medium was spiked with 10% v/v DMSO-*d*₆, which significantly increased the rate of the oxidative coupling and gave 88% of **3ba** (Table 1, Entry 16).

Table 1. TAP (**1b**) and pentylamine (**2a**) oxidative coupling

#	Solvent	2a , eq	Yield, % ^a		
			3ba	7b	8
1 ^b	DCM	3.00	4	2	ND
2		3.00	27	2	ND
3		0.20	6	3	7
4		0.50	27	7	15
5				42	7
6 ^d			45	8	15
7 ^e		1.00	30	11	20
8 ^f			75	11	-
9 ^g			70	14	-
10 ^h	DCM-d2 ^c		34	ND	4
11		1.15	52	8	14
12		1.33	56	8	12
13		1.75	75	10	11
14		2.00	80	10	10
15 ^b		3.00	76	9	9
16		3.00	88	11	9
17		5.00	88	12	7
18	CDCl ₃ ^c	1.00	26	3	7
19			6	32	48
20 ⁱ	DMSO- <i>d</i> 6	1.00	6	32	-
21 ^b			7	32	51

^a Yields were determined by ¹H NMR analysis. ^b Air was used. ^c 10 vol% DMSO-*d*6. ^d Mixing. ^e 1 eq NEt₃. ^f 1 eq of *t*BuNH₂. ^g 0.1 eq of DBU. ^h 1 eq of **1e**. ⁱ 15 min.

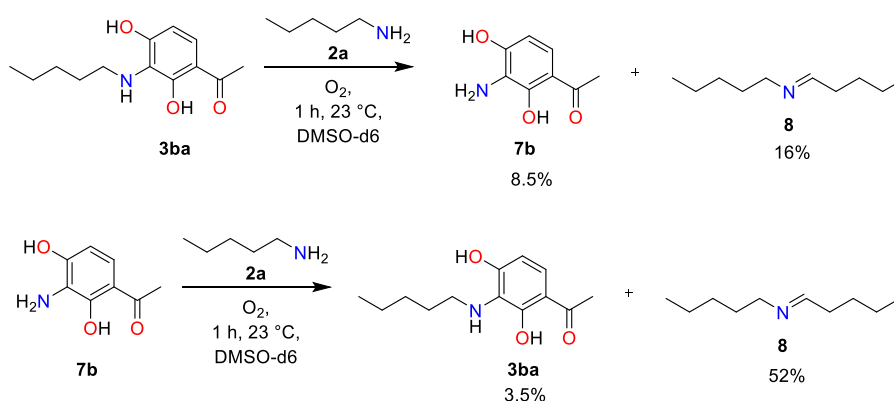
Once the phenolate ion pair **1b-2a** is dissolved, it can then react with air oxygen through single electron transfer (SET) to yield dioxygen radical anion and phenoxy radical complex, followed by a hydrogen atom transfer (HAT) step to yield hydroperoxide anion **HO₂⁻** and *o*-quinone **4b**. We note in passing that the stability of the respective phenoxy radical is directly related to the O-H bond dissociation energy (BDE) in polyphenol as indicated by the dotted arrow in Scheme 4.

**Scheme 4.** Step-by-step oxidation of pyrogallol-based polyphenol (Scheme 3, *initiation*).

Quinone **4b** is expected to react rapidly with amine **2a** to the respective imine **5ba**, followed by intramolecular or intermolecular isomerization to α -imine **6ba**, followed by the transfer-hydrogenation step with **1b** to complete the formation of amination product **3ba**. Most likely **2a** acts as a base in the rearomatization step, because it has been shown that the overall rate

of the reaction increases up to 2 eq of **2a** (80% yield, Table 1, Entry 11-17) and reaches the plateau or the addition of non-reacting amine, like 1 eq of tert-BuNH₂ or 0.1 eq of DBU, give the same amount of the product (75% and 70%, correspondingly) (Table 1, Entries 8-9).

Closer analysis shows that the addition of DMSO-*d*₆ leads the reaction in another pathway, the *imine formation B*, of polyphenol-amine interaction, giving minor product **7b** and the equimolar amount of dipentyl imine **8** (Scheme 3). These facts can be explained by taking in account the formation of **8** via extensive secondary processes of aminolysis/hydrolysis of the formed intermediate, **6ba**, and overoxidation of the product **3ba**. The reaction in pure DMSO-*d*₆ completely changes the pathways and leads to formation of **7b** and **8** as the major products, 32% and 48%, correspondingly, with minor 6% of **3b**. The control experiments showed that the final substrate **3ba** undergoes further oxidation, if treated with 1 eq of **2a**, giving imine **5ba** back. 8.5% of the **3ba** was converted into **7b** through this process, leading to the formation of an equimolar amount of **8** (16%). From the other side, only 3.5% of **7b** was converted to **3ba** under the same conditions, while 52% of **2a** was oxidized to imine **8** via extensive transamination process, releasing an ammonia molecule as a side product, which was proven by trapping NH₃ with TFA-*d*₁.

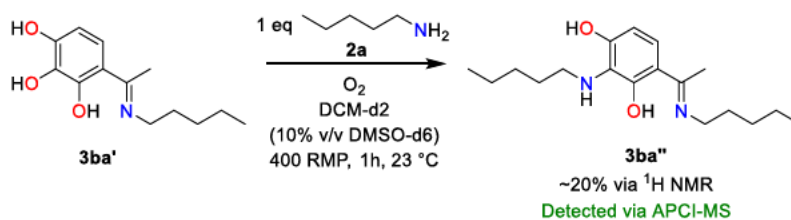


Scheme 5. **7b** has a greater potential in oxidative deamination of the amines.

This observation suggests that the physiological activity may not be attributed to the phenols themselves, but rather to aminophenols, like **7b**, which are products of their sequential oxidation, condensation with *N*-nucleophiles, and hydrolysis of the parent polyphenols.

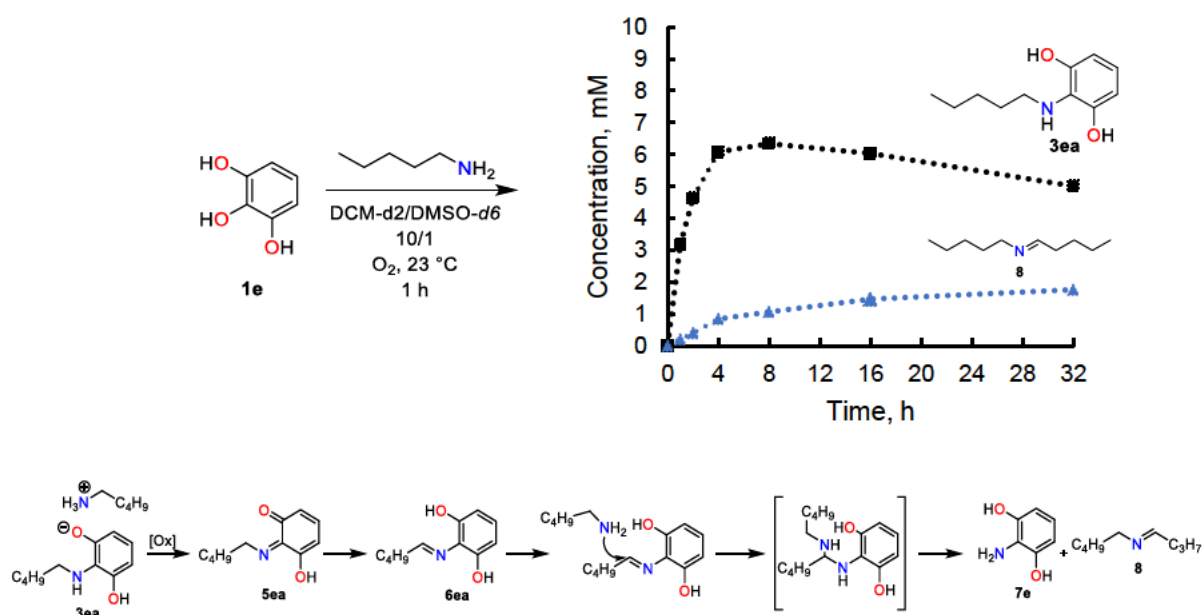
The distinctive feature of **1b** is the presence of an electrophilic carbonyl group which competes in conversion of the primary amine **2a** (*ketone condensation C*) and forms imines with both the polyphenol and the reaction products, **3ba'** and **3ba''**. The most interesting substrate is **3ba'**, as it contains a pyrogallol moiety that may still show reactive properties and

react further with amine **2a**. Indeed, it has been demonstrated that substrate **3ba'** forms a covalent product **3ba''** under aerobic conditions (Scheme 6).



Scheme 6. **3ba'** oxidative coupling with amine **2a**.

Additionally, it is also worth mentioning that a small fraction of product **3ba** undergoes further overoxidation, resulting in product **9ba**, which was detected *via* APCI-MS (overoxidation D pathway). The reaction of pyrogallol (**1e**) and amine **2a** serves as an excellent example to illustrate this phenomenon. It was observed that, for a certain period (~4 h), the concentration of the product **3ea** increases, but then the curve reaches a plateau and starts to consistently decrease (Scheme 7).



Scheme 7. The formation and overoxidation of the formed product **3ea** over the course of 32 h under aerobic conditions with a proposed reaction mechanism

1.3.3. Variations of the Polyol Electrophile

To find out which factors play a major role in polyphenol-amine coupling reaction, a set of different polyphenols with structural modifications was tested. 1 eq of **2a** was mixed with certain polyphenols under O_2 atmosphere and the product yields were measured after 1 hour of the reaction to consider the reactivity of the corresponding polyphenol (Table 2). It has

been demonstrated that polyphenols with vicinal phenol groups, *o*-catechol **1c** moiety, do not exhibit any reactivity towards amine **2a**. For this reaction, the presence of a pyrogallol ring is required. Pyrogallol **1e** shows low activity under the given conditions (13% yield of **3ea**), but it can be significantly tuned up if the electron-withdrawing group is attached to 4a-position of the pyrogallol ring. For example, a nitrile group at 4a-position (**1g**) increases the yield of covalent adduct **3ga** to 68%, while an ester group at 8a-position (**1h**) significantly decreases the reactivity, giving only 1.2% of covalent adduct **3ha**.

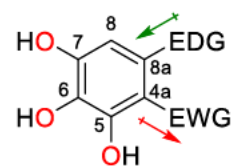


Table 2. Reaction of pentylamine (**2a**) with different polyphenols and their categorization by their ability to form a covalent amine adduct.

No reactivity

Low reactivity (1-25%)

Moderate reactivity (26-50%)

Good reactivity (51-75%)

High reactivity (>76%)

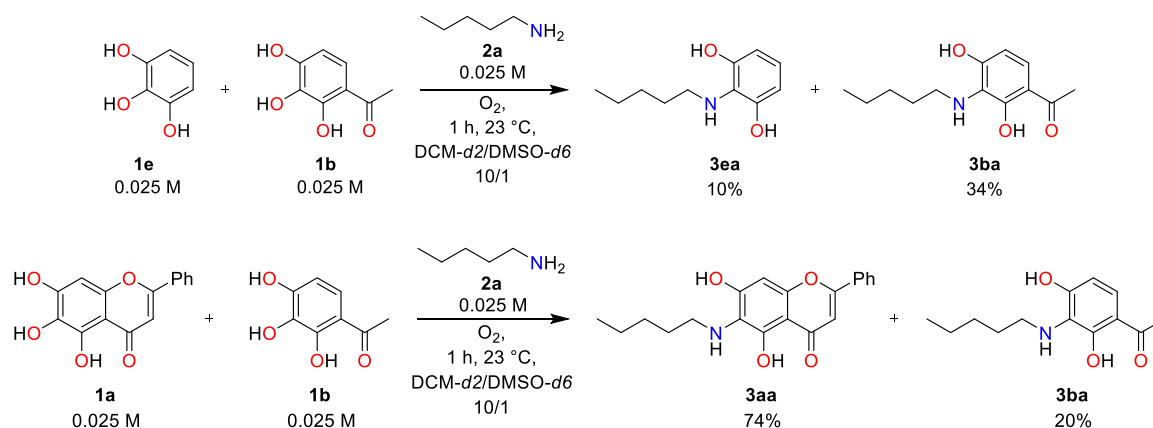
Yield, % ^a	1a	1b	1e	1g	1h	1i	1m	1o	1p	7b^b
3xa	80%	42%	13%	68%	1.2%	49%	66%	3%	45%	15%
7a	-	7%	-	4%	-	8%	-	-	-	-
8	5%	13%	5%	8%	-	17%	7%	-	4%	7%

^aYields were determined by ¹H NMR analysis. ^bin 24 hours

The addition of electron donating groups at 8a-position of the pyrogallol ring increases the yield of covalent addition (compare **1b** and **1m**, 41% vs 66% yield). The most interesting example is the unnatural flavonoid **1l**, which is fully isomeric with the most reactive compound **1a**, but having reversed electronic effects. Substrate **1l** demonstrates an almost complete absence of covalent product formation, which highlights the crucial role that electron-withdrawing groups at 4a-position and electron-donating groups at 8a-position play in this reaction. Baicalein (**1a**) shows remarkable reactivity, even among the highly reactive polyphenols, like **1j**, surpassing them in the rate of covalent adduct formation. This

observation might suggest that not only are the electronic effects of the donor or acceptor important, but also the extended π -conjugation system plays a significant role in the reactivity of the polyphenols. This hypothesis is supported by the experiment with unnatural flavonoid **1m**, which has similar backbone and the electronic effects as baicalein **1a** (EWG at 4a-position, EDG at 8a-position); however, its π -conjugation system is divided into two separate parts. The lower reactivity observed for substrate **1m** relative to **1a** (66% vs 80%, correspondingly) highlights the importance of the extended π -conjugation system in the reactivity of the given polyphenol.

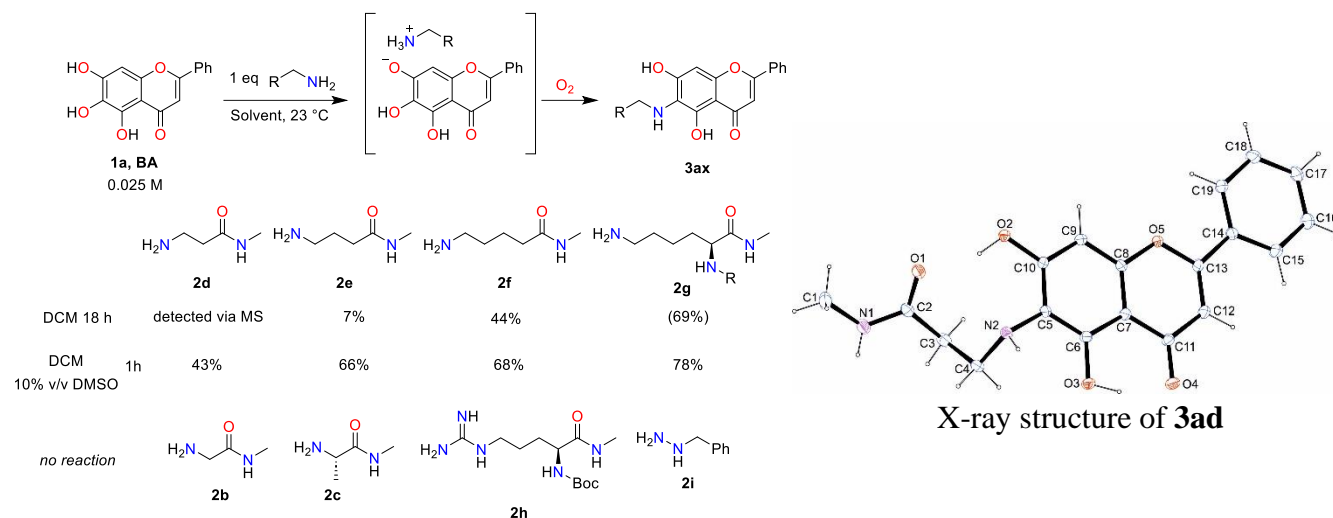
The relative reactivities has been established for polyphenols with low, moderate and high reactivities such as **1e**, **1b** and **1a**, respectively, by a 1 to 1 competition reaction (Scheme 8). These experiments showed that baicalein is 7.4 times more reactive toward amine **2a** than non-functionalized pyrogallol (**1e**) in the presence of **1b** under the similar conditions.



Scheme 8. 1 to 1 competition reactions of polyphenols **1a**, **1b** and **1e**.

The reaction between baicalein (**1a**) and amine **2a** occurs relatively fast under aerobic conditions, making it difficult to extract the necessary data about the polyphenol-amine coupling rate. It was decided to slow down the oxidative coupling by adding one extra step in the reaction equilibrium. Instead of free amine **2a**, pentylamine benzoic acid salt (**BzA**·**2a**) was used (Scheme 9). In this case, the amine, which is in equilibrium, acts like a ball being passed back and forth between two players, the acid and the polyphenol, thereby slowing down the overall reaction rate.

models, surprisingly, shows no oxidative coupling, even in the case of addition of external bases such as DIPEA or DBU (Scheme 10).



Scheme 10. Reaction of **1a** with different *N*-nucleophiles **2b-i**.

In the homologous series of *N*-methylamido-1-aminocarboxylic acids **2d-g**, we observe a gradual increase in the yield of C6-adducts **3ax**, which correlates with the pK_a values of these *N*-nucleophiles, reaching its maximum in the case of reactions with lysine derivatives (Fig. 2).

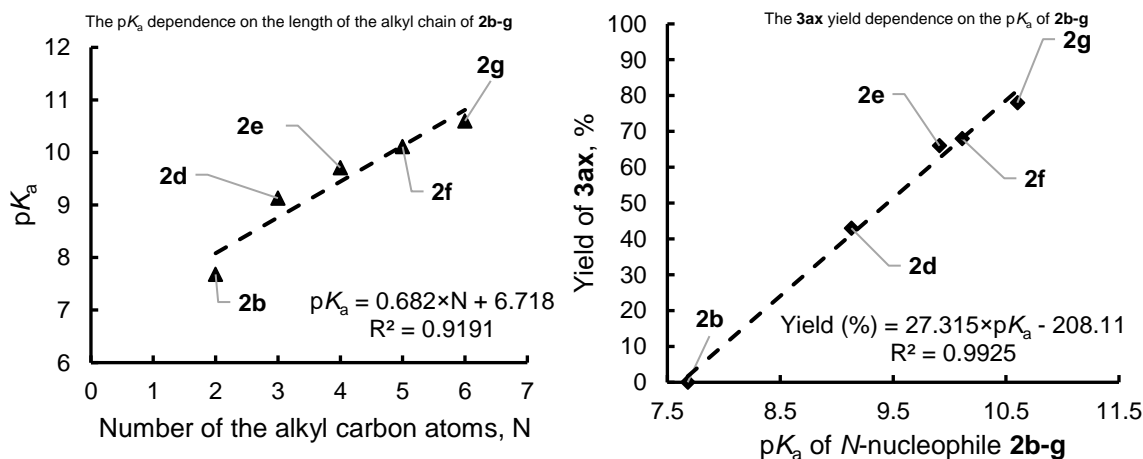
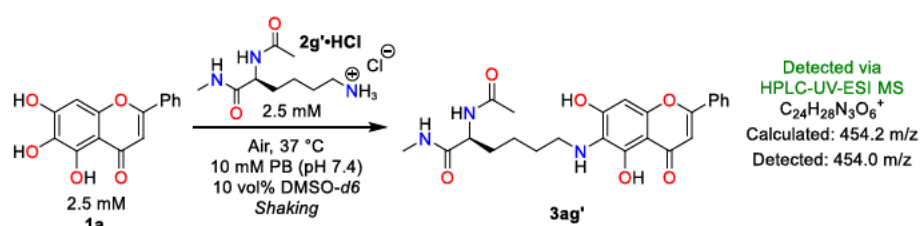


Fig. 2. The pK_a dependance on the length of the alkyl chain of **2b-g** (left) and the **3ax** yield dependance on the pK_a value of **2b-g** (right).

It was possible to grow a crystal for scXRD analysis for adduct **3ad** to demonstrate the regioselectivity of the oxidative coupling reaction. In attempts to understand the applicability of the oxidative coupling reaction, other *N*-nucleophiles, such as derivative of arginine **2h** or benzyl hydrazine **2i**, were tested, which, as has been shown, do not lead to the formation of covalently linked adducts.

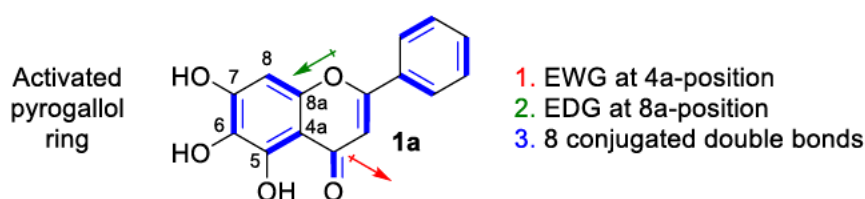
Even if an individual amino acid does not represent an entire polypeptide and may show entirely different properties, it was decided to perform the reaction of baicalein (**1a**) with lysine derivative **2g'** in an aqueous medium under controlled pH value and temperature. The possibility of this reaction was demonstrated using HPLC-UV-ESI MS analysis, which provided evidence for the formation of adduct **3ag'** in the reaction between the **1a** and lysine derivative **2g'** under the specified conditions, indicating the potential for interactions between the flavonoid and reactive sites within polypeptides in aqueous media (Scheme 11). This approach aims to show the reactivity between the flavonoid and amino acid moieties within a more biologically relevant context.



Scheme 11. Reaction of **1a** with lysine derivative **2g'** in phosphate buffer (pH 7.4) at 37 °C.

1.3.5. Conclusion

The reaction between polyphenols and various *N*-nucleophiles has been investigated, showing the key structural elements presented in polyphenols for this reaction. The structural elements are 1) the presence of a pyrogallol ring, 2) an electron-withdrawing group (EWG) at 4a position (also a preferably electron-donating group (EDG) at position 8a), and 3) an extensive π -conjugated system. All the required structural elements are present in baicalein **1a**, making it the most reactive polyphenol substrate in this study (Scheme 12).



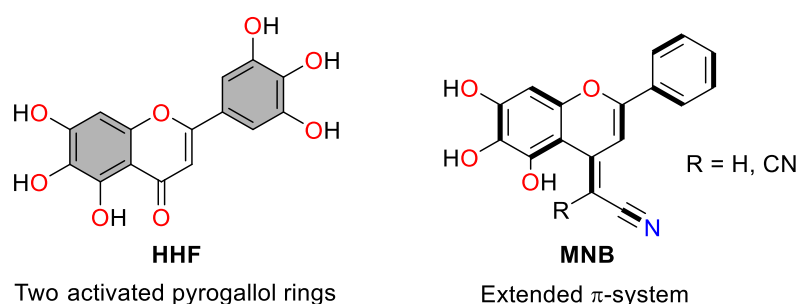
Scheme 12. Structural elements combined in baicalein (**1a**).

From the *N*-nucleophiles side, a necessary condition for the reaction is a value of $pK_a > 9$, which gives sufficient nucleophilicity and basicity for effective interaction with polyphenols as a base and a condensation partner. Also, it has been found that aminophenols, like **7b**, have higher ability than its parent polyphenol **1b** to oxidize the amine **2a** into imine **8**. The

observation suggests that the design of amino derivatives of polyphenols can be a promising target for anti-amyloid drug discovery in future.

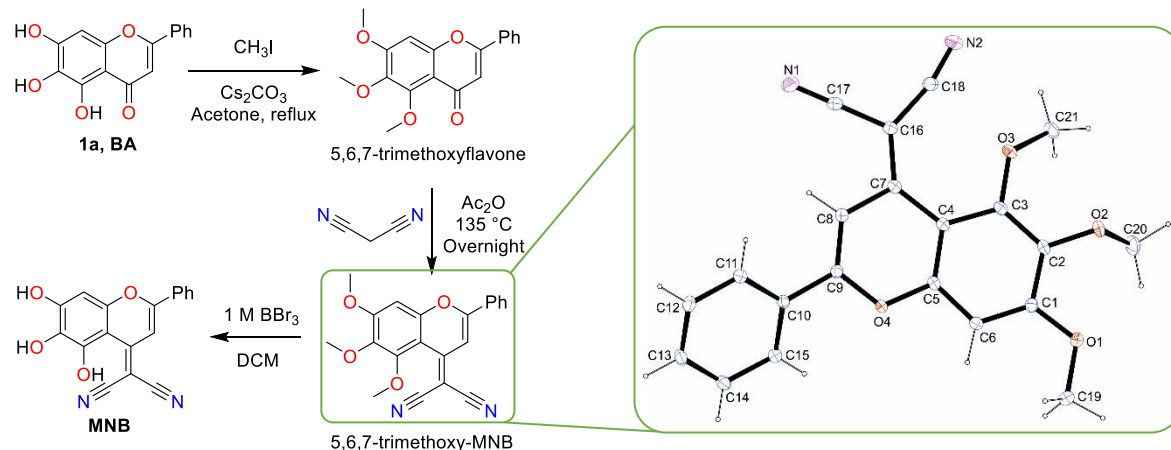
1.3.6. Outlook

There are two potential compounds that can surpass baicalein **1a** in reactivity with primary amines and in anti-amyloid activity. 3',4',5',5,6,7-hexahydroxyflavone, **HHF**, is based on the concept of increasing the number of activated pyrogallol rings. On the other hand, the reactivity of malononitrile baicalein, **MNB**, relies on the enlargement of the conjugated π -system, leaving the electron-withdrawing potential (Scheme 13).



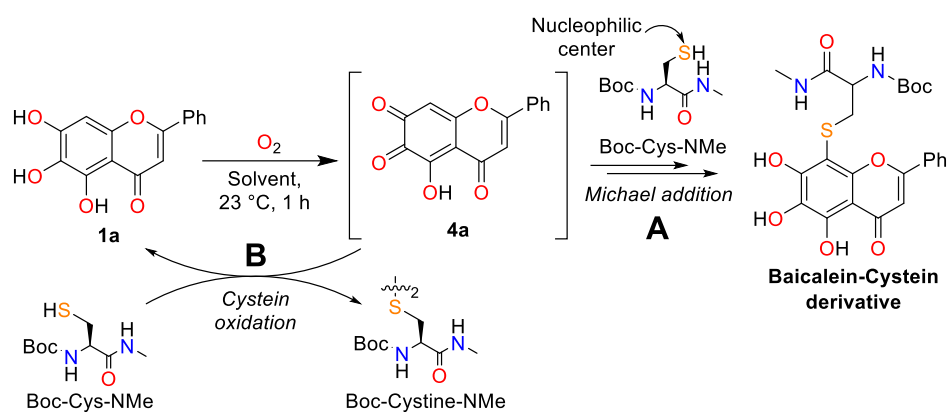
Scheme 13. Potential polyphenolic compounds, **HHF** and **MNB**.

MNB synthesis starts with protection of the phenolic groups of baicalein (**1a**) by using methyl iodide and cesium carbonate in refluxed acetone (Scheme 14). Afterwards, the Knoevenagel reaction was performed with the obtained 5,6,7-trimethoxyflavone and malononitrile in acetic anhydride at 135 °C, giving 5,6,7-trimethoxy-MNB. It was possible to obtain good quality crystals for scXRD analysis, which proved the formation of 5,6,7-trimethoxy-MNB. Deprotection of the phenolic groups is currently on development.



Scheme 14. Synthesis strategy of **MNB** and X-ray structure of 5,6,7-trimethoxy-MNB.

The study described in this chapter is based on the reactivity of polyphenols and various *N*-nucleophiles, but it can be significantly improved by adding the scope of *S*-nucleophiles. For example, reaction of baicalein with cysteine derivatives is a model representation of the interactions of sulfur-containing peptides with natural flavonoids (Scheme 15, A). Due to increased nucleophilicity, thiols might undergo a Michael addition with oxidized forms of polyphenols. From the other site, the oxidized forms of polyphenols, like **4a**, can act as a stoichiometric oxidant, turning cysteine-based substrates to cystine adducts (Scheme 15, B).



Scheme 15. Possible reaction of cysteine derivative with baicalein (**1a**).

1.3.7. Supporting information

1.3.7.1. General Methods and Procedures

General methods: All reactions sensitive to air and moisture were performed under nitrogen atmosphere, and the glassware as well as magnetic stir bars were dried overnight in a dry oven at 110°C.

Solvents, reagents: All reagents and solvents were purchased from the companies TCI, Sigma Aldrich or Fisher Scientific. All air- or water-sensitive reagents were stored under nitrogen.

NMR spectroscopy: All ^1H NMR spectra were recorded by Bruker 400 in DMSO-*d*₆/DCM-*d*₂ at 400 MHz at 23 °C. All ^{13}C NMR spectra were recorded, respectively, at 101 MHz. The chemical shifts are reported in ppm (δ), relative to the resonance of DMSO-*d*₆ at δ = 2.50/DCM-*d*₂ at δ = 5.32 ppm for ^1H and for ^{13}C relative to the resonance of DMSO-*d*₆ δ = 39.52 ppm. Spectra were imported and processed in the MestreNova 14.1.1 program. For ^1H NMR spectra multiplicity (s = singlet, d = doublet, t = triplet, q = quartet, quint = quintet, m = multiplet, dd = doublet of doublets, dt = doublet of triplets, td = triplet of doublets, and bs = broad signal.), coupling constants *J*, number of protons and assignment to the structure are reported. In ^{13}C NMR spectra singular carbons are marked with (s).

Mass spectrometry: For electrospray ionization (ESI) spectra a Thermo Finnigan LTQ FT Ultra Fourier Transform Ion Cyclotron Resonance Mass Spectrometer was utilized. For atmospheric pressure chemical ionization (APCI) a Advion CMS using positive mode was used.

Melting point. Melting points were measured using Buchi-560 and are not corrected.

Infrared spectroscopy. FT-IR spectra were measured using FT-IR Perkin Elmer Spectrum BXII/1000 with Smiths ATR.

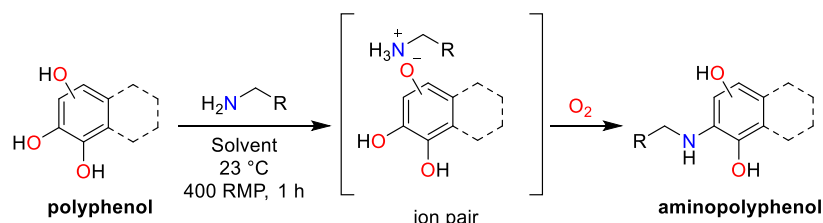
Powder X-ray diffraction. pXRD measurements were performed on a Stoe STADI P X-Ray powder diffractometer built up in Transmission/Debye-Scherrer geometry. Diffractograms were imported and processed in the WinXPOW 3.0.2.1 program.

Single-crystal X-ray diffraction. scXRD measurements were performed on a Bruker D8 Venture TXS diffractometer.

pH measurements. pH values were determined using HANNA HI-5221 pH-meter.

HPLC analysis: All HPLC spectra were measured on a Knauer Azura machine with P6.1L pump, autosampler AS6.1, column thermostat CT2.1 and diode array detector DAD2.1L. Eurospher II 250×4.6 mm C18 column was utilized. Data analysis was performed with ClarityChrom 7.4.1.

General procedures

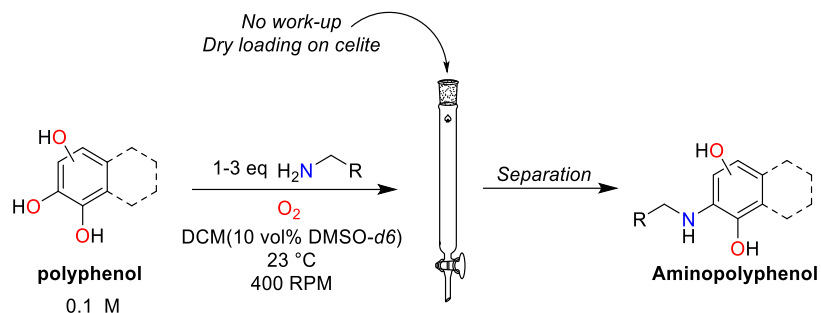


Procedure A: The polyphenol (0.125 mmol, 1 eq) in a 20 ml GC vial was evacuated and filled with O₂ three times. The GC vial was capped, and the polyphenol was dissolved in solution of 5 ml of solvent and 0.25 ml of dry DMSO-*d*₆, using a shaker at 400 RPM. While shaking, 250 μl of 0.5 M/1 M solution of amine (0.125 mmol/0.250 mmol, 1 eq/2 eq) in DMSO-*d*₆ were added. Shaking continued for 1 h, a certain amount of 1,3,5-trimethoxybenzene was added as an IS, and then 0.5 ml aliquot was taken. The aliquot was evaporated and dissolved in 0.75 ml of dry degassed DMSO-*d*₆ under nitrogen atmosphere to prevent oxidative coupling. ¹H NMR analysis was performed to establish the yield of the final products.

Procedure B (*in situ*, DCM-*d*₂/DMSO-*d*₆): A Young NMR tube was evacuated and filled with O₂ three times. 50 μl of 0.5 M polyphenol (0.025 mmol, 1 eq) solution with a defined amount of 1,3,5-trimethoxybenzene in dry DMSO-*d*₆ were added and diluted with 1 ml of DCM-*d*₂. 50 μl of 0.5 M solution of the *N*-nucleophile (0.025 mmol, 1 eq) in dry DMSO-*d*₆ were added, the NMR tube was capped and turned upside-down 10 times. After 1 h of reaction at 23 °C, ¹H NMR analysis was performed to establish the yield of the final products.

Procedure C (*in situ*, DMSO-*d*₆): It is necessary to mix the reaction when the oxidative coupling is performed in DMSO-*d*₆, otherwise uneven oxidation occurs. The 10 ml GC vial was evacuated and filled with O₂ three times. 2 ml of a 0.025 M solution polyphenol (0.05 mol, 1 eq) in DMSO-*d*₆ were added. The GC vial was capped and placed on a shaker at 400 RPM at 23 °C. While shaking, 100 μl of 0.5 M/1 M solution of amine (0.05 mol/0.1 mmol, 1 eq/2 eq) in dry DMSO-*d*₆ were added, that caused an instant color change of the reaction. Shaking continued for 1 hour, 50 μl of 1,3,5-trimethoxybenzene solution was added as an IS

and then 0.75 ml aliquot was taken for ^1H NMR analysis to establish the yield of the final products.



Procedure D (Product synthesis): A polyphenol was weighed in a 20 ml GC vial and evacuated and filled with O_2 three times. Dry DCM was added to obtain a suspension with a concentration of 0.1 M. To the stirring mixture of polyphenol in DCM, 1-3 eq of amine in dry DMSO- d_6 (10 vol%) was added. The GC vial was capped and placed on a shaker at 400 RPM for 1-24 h at 23 °C. Celite was added, all the volatiles were evaporated under reduced pressure at 25 °C and the crude material was purified using column chromatography. The exact amount, reaction times, eluents are given in the analytical section of the corresponding products. Please, observe that the aminophenol adducts show some level of instability under aerobic conditions, turning black over time. In addition, the products strongly bind to silica gel during the flash column purification, leading to lower yields (basic additives, for example, 2-3% NEt_3 , dissolve the silica gel at higher eluent polarities, like 5-10% MeOH in DCM).

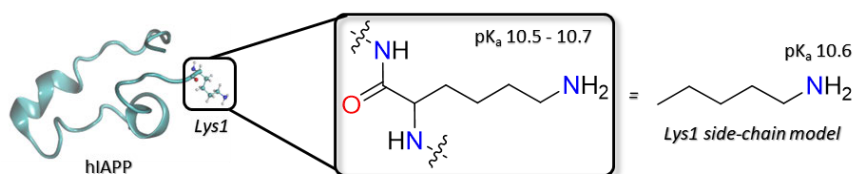


Fig. S2. Pentylamine (**2a**) representing the lysine side chain due to the similarity of their pK_a values.

The baicalein **1a**-pentylamine **2a** reaction (Procedure A) was monitored via ^1H NMR analysis (Fig. S3). It has been shown that the oxidative coupling was relatively slow in DCM (11% yield of **3aa** in 1 h) due to low solubility of the flavonoid **1a**. Increasing the reaction time up to 18 h, gave 72% yield of **3aa**. To dissolve the suspension, 10 vol% of DMSO- d_6 was added to the reaction mixture, resulting in a significant increase in the overall reaction rate (80% yield of **3aa** in 1 hour).

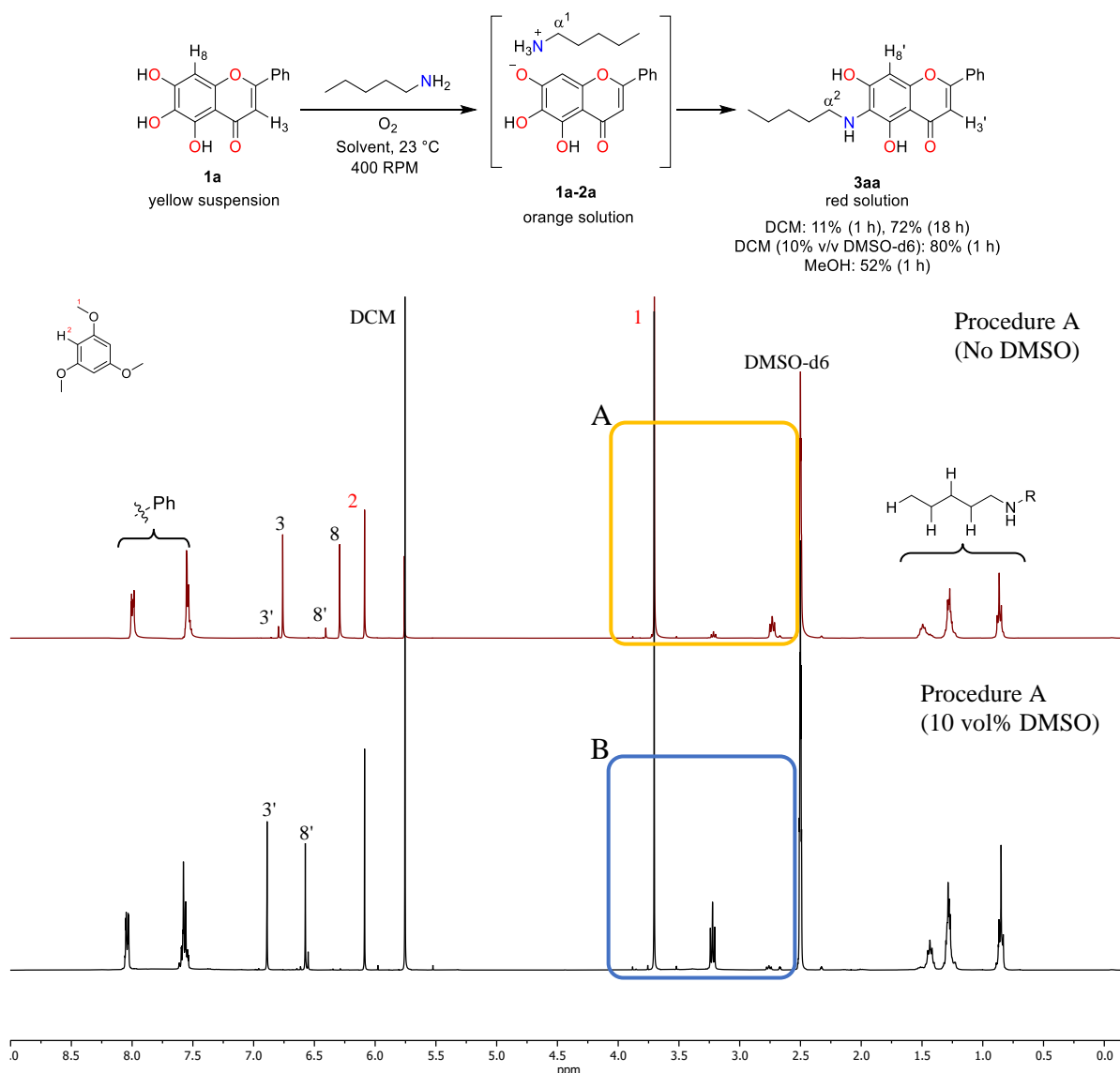


Fig. S3a. ^1H NMR spectra of **1a/2a** reaction in DCM (top) and DCM with 10 vol% DMSO- d_6 (bottom)

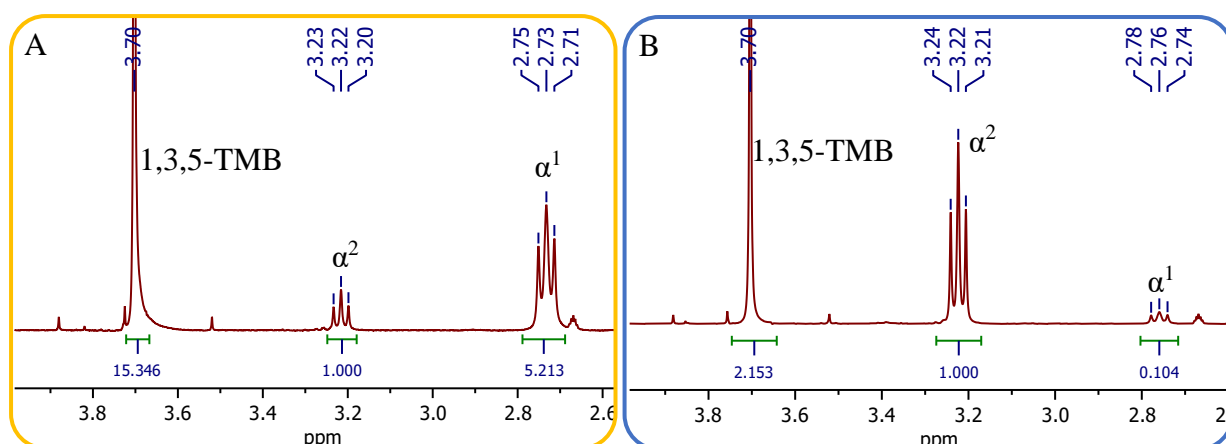


Fig. S3b. Zoomed-in ¹H NMR spectra of **1a/2a** reaction in DCM (left) and DCM with 10 vol% of DMSO-*d*₆ (right).

To find out, if the yield is affected during the evaporation/concentration, the parallel experiments were performed (Procedure A). These experiments (**A** and **B**) showed that no accelerated reaction occurs during the evaporation process (Fig. S4).

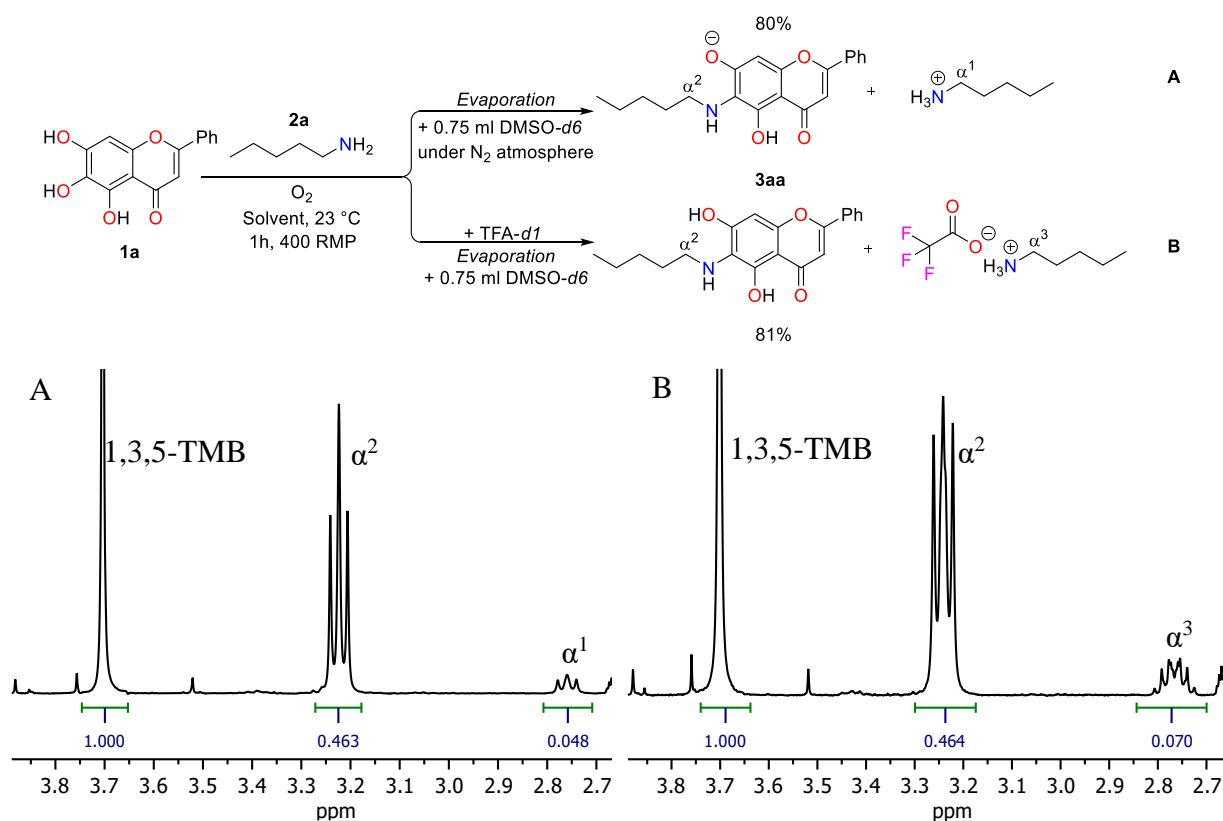


Fig. S4. ¹H NMR spectra of the **1a/2a** reaction without TFA quenching (A) and with TFA quenching (B). The integrals of the IS (1,3,5-TMB) and the product (α²) are the same with/without TFA quenching.

A) 100 μl of 0.250 M TFA solution were added to the aliquot to quench free **2a** in the solution. Then all the volatiles were evaporated under reduced pressure, diluted with 0.75 ml of DMSO-*d*₆ and ¹H NMR analysis was performed. ω(**3aa**) = 81%

B) The aliquot was evaporated under reduced pressure, diluted with 0.75 ml of DMSO-*d*6 under N₂ atmosphere and ¹H NMR analysis was performed. ω(**3aa**) = 80%.

To check for the formation of possible volatile products, we performed *in situ* experiments, the same reaction of **1a-2a** oxidative coupling was performed in DCM-*d*2/DMSO-*d*6 = 10/1 with 1 and 2 eq of **2a** (Procedure B, Fig. S5). A little formation of dipentyl imine **8** was detected in the experiment. The significant increase in imine **8** formation is detected when the reaction is performed in DMSO-*d*6 (Procedure C, Fig. S5).

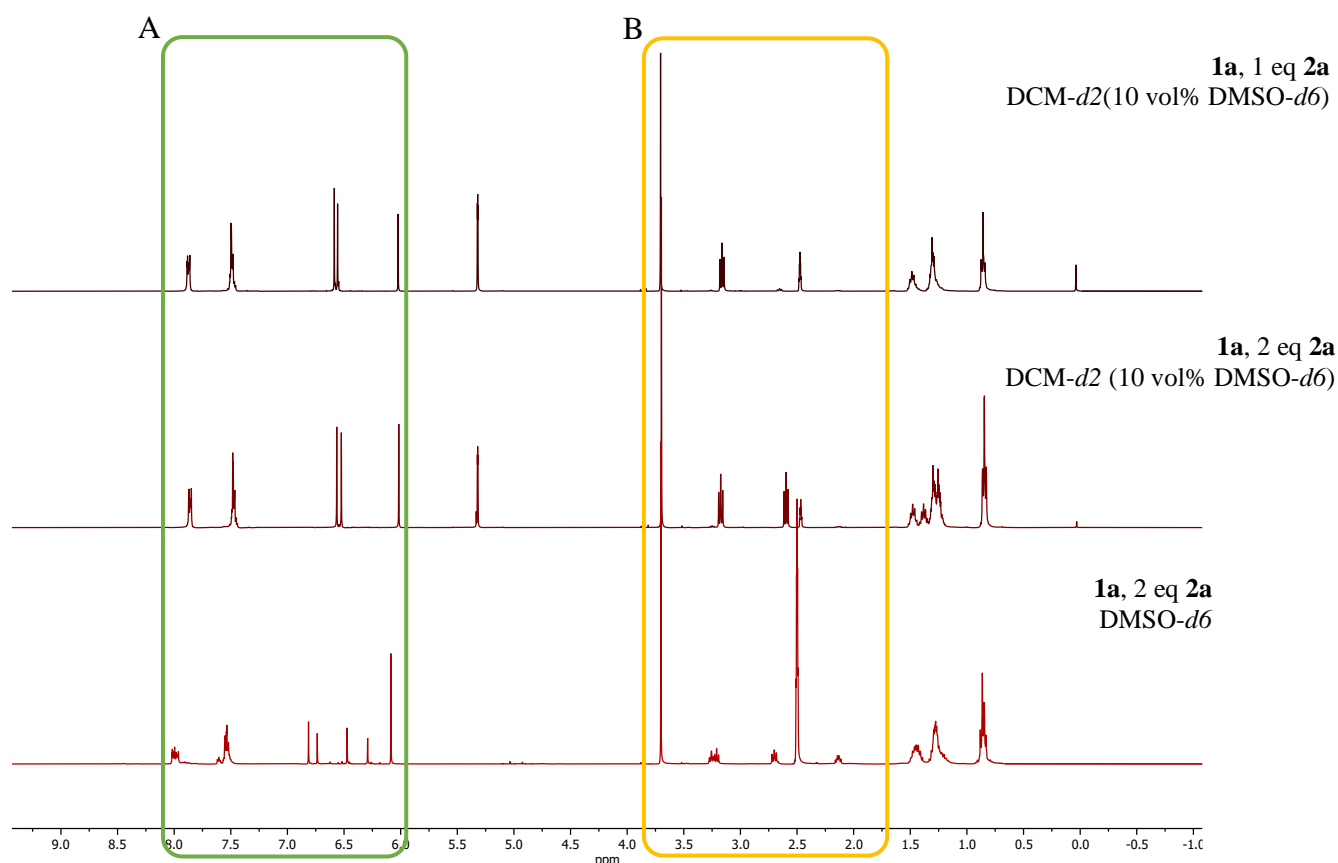
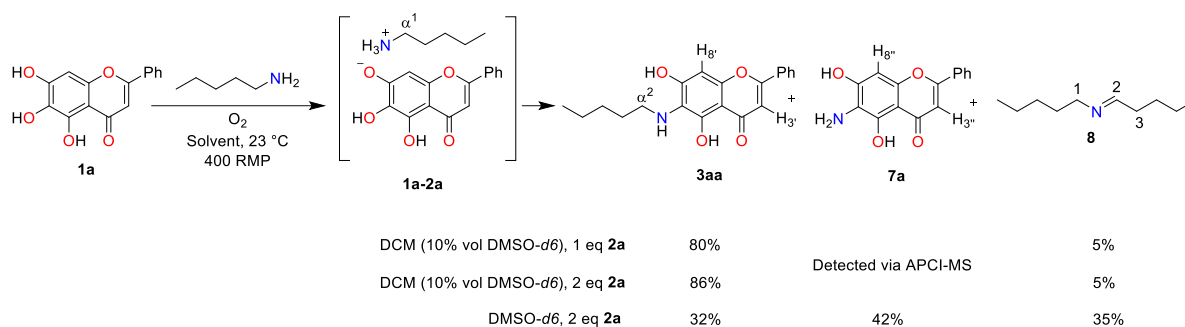


Fig. S5a. *in situ* ¹H NMR spectra of the **1a/2a** oxidative coupling, 400 MHz.

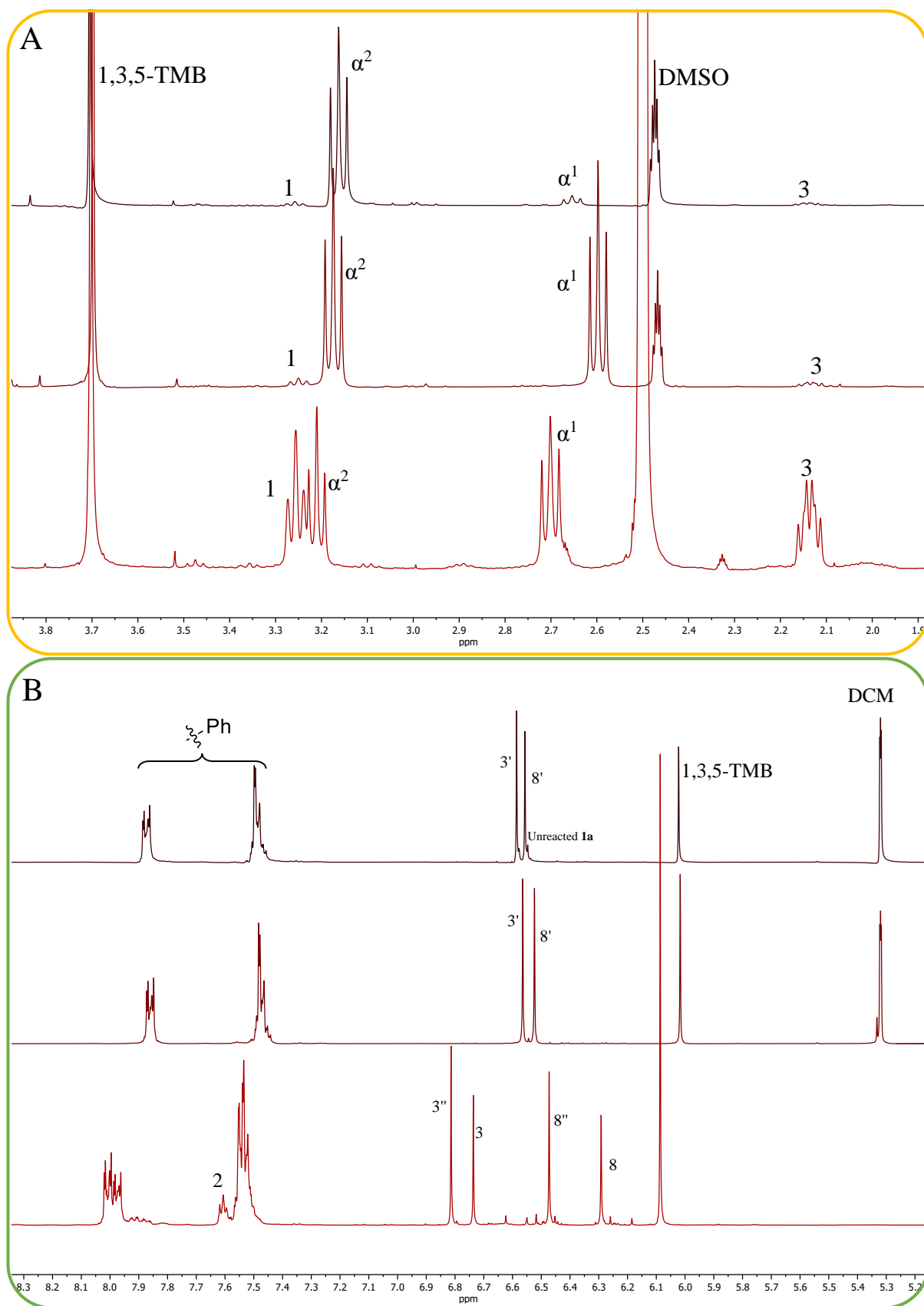


Fig. S5b. Close-up *in situ* ^1H NMR spectra of the **1a/2a** oxidative coupling, 400 MHz.

Imine **8** formation was proven by independent *in situ* synthesis from pentylamine **2a** and pentanal (1/1) in DMSO-*d*₆ (Fig. S6).

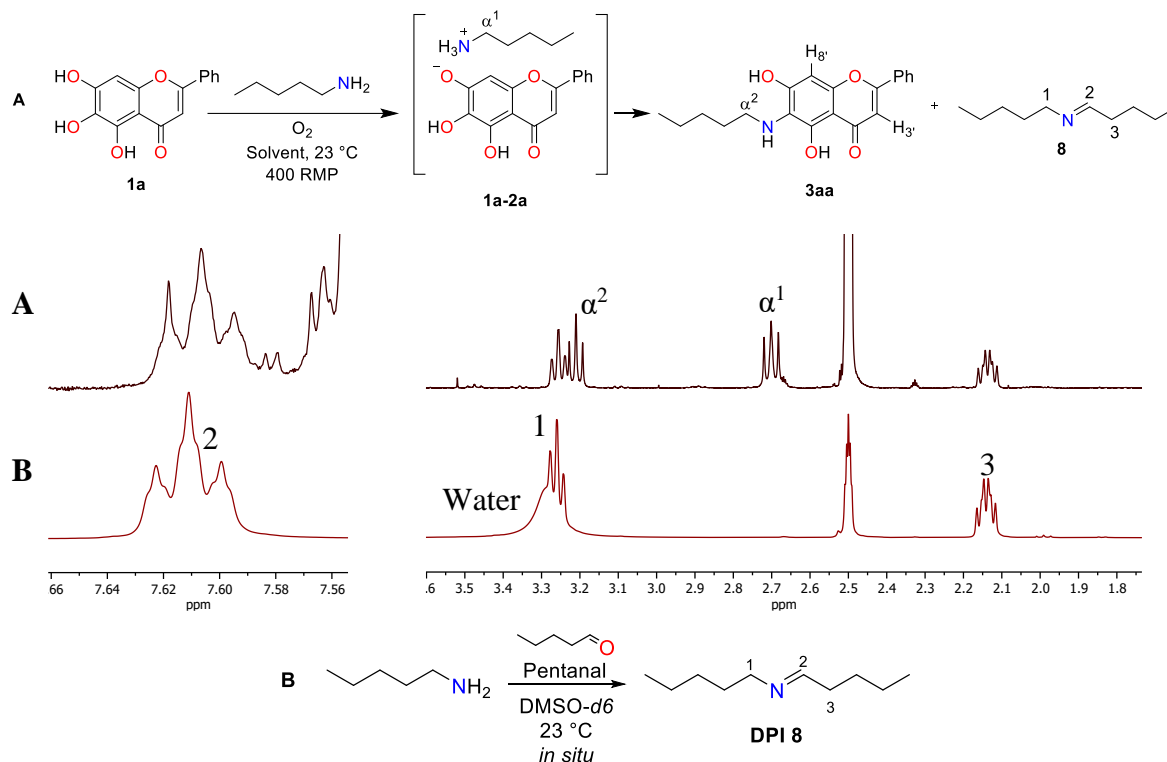


Fig. S6. ¹H NMR spectrum comparison of **1a/2eq 2a** oxidative coupling reaction with independently synthesized imine **8**, DMSO-*d*₆, 400 MHz.

APCI-MS analysis of the crude material in DMSO-*d*₆ shows full conversion of **1a**, no peak at *m/z* 271 (Fig. S7). Instead of this, a signal at *m/z* 270 is detected, which only can be related to **7a**. Also, peak of **3a** is observed at *m/z* 340 together with its by-products of overoxidation **9aa** (*m/z* 336 and 338). The same peaks were observed during oxidation of **3aa** with strong oxidants such as *o*-chloranil.^[1]

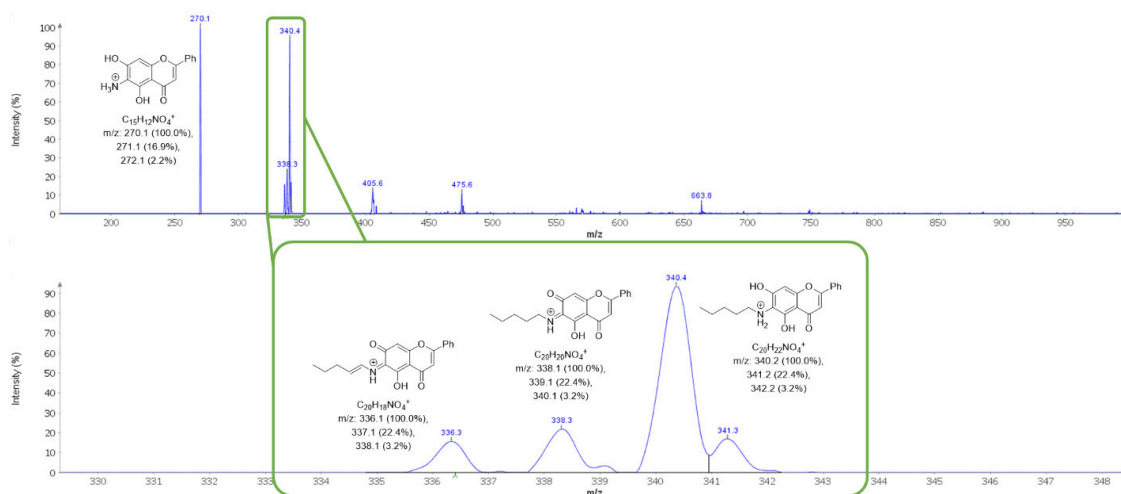
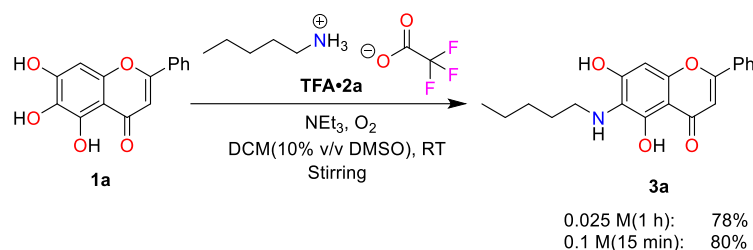


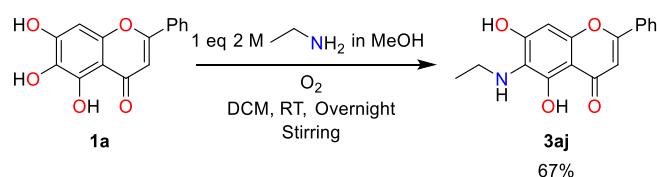
Fig. S7. APCI-MS of the **1a/2eq 2a** oxidative coupling reaction in DMSO-*d*₆.

Commercially available amino acids are typically present in the form of salts of inorganic (HCl) and organic acids (TFA) as obtained by deprotecting, for example, of the respective BOC derivatives, under acidic conditions. The potential of using amine salts for synthetic purposes was investigated. Procedure A was slightly modified, 1 eq of pentylamine trifluoroacetate **TFA**×**2a** was used instead of free **2a**. 2 eq of triethylamine was added as an external base. It has been shown that the yields of the final product are not different if a free amine had been used instead, 78% (Scheme S1).



Scheme S1. Ammonium salt gives the same yield as free amine in the oxidative coupling.

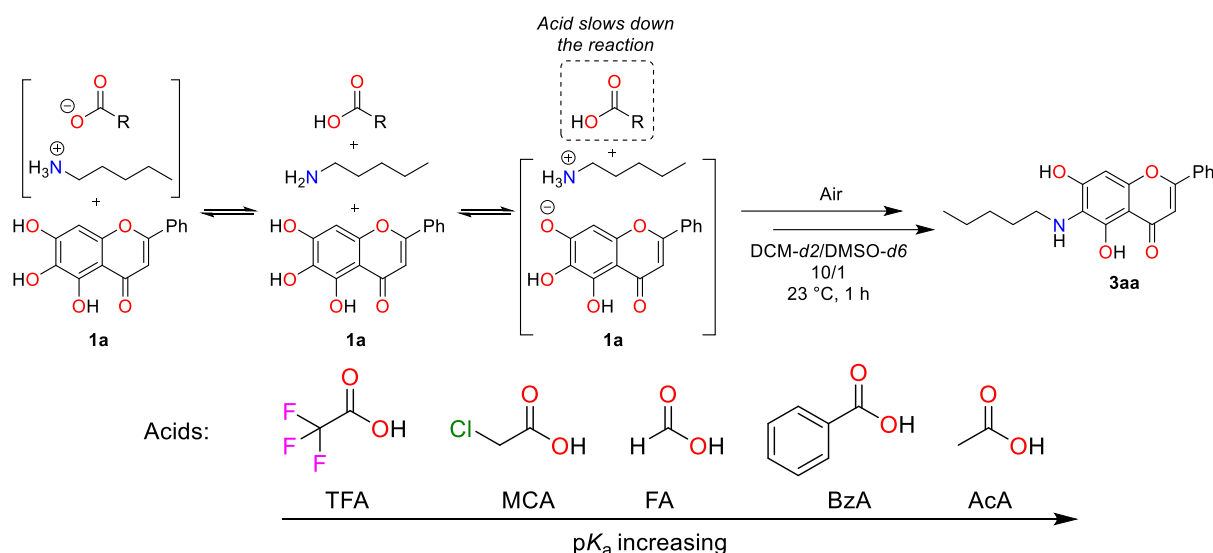
Also, the possibility of the utilization of alcoholic solutions of amines has been investigated. 1 eq of ethylamine **2j** in methanol was taken instead of **2a**. After the completion, 67% of **3aj** was isolated and characterized (Scheme S2).



Scheme S2. Alcoholic solutions of amine are also suitable for the oxidative coupling reactions with **1a**.

1.3.7.3. Baicalein (**1a**)-pentylamine salt (**Acid**×**2a**)

The reaction between **1a** and **2a** occurs relatively fast under aerobic conditions, making it difficult to extract the necessary data about polyphenol-amine coupling rate. It was decided to slow down the oxidative coupling by adding one extra step in the reaction equilibrium. Instead of free **2a**, pentylamine salt (**Acid**×**2a**) was used. In this case, the amine, which is in equilibrium, acts like a tennis ball being passed back and forth between two players, the acid and the polyphenol, thereby slowing down the overall reaction rate (Scheme S3). Initially, a series of organic acids in ascending order of their pK_a were tested to find out a suitable counter-ion for the amine.



Scheme S3. Oxidative coupling of pentylamine salt with baicalein.

As expected, pentylamine salt of stronger acids, like TFA or MCA, showed no conversion via ¹H NMR, indicating the equilibrium is drastically shifted to the left (Table S1, Entries 1 and 2).

Table S1. Dependence of **3aa** yield from counter-ion of **2a**.

№	Acid	p <i>K</i> _{a, water} ^a	ω(3aa), 1h, %
1	TFA	0.23	ND
2	MCA	2.86	ND
3	FA	3.77	25
4	BzA	4.20	19
5	AcA	4.76	73
6	No acid	-	80

^a Aqueous p*K*_a compilation by R. Williams (document compiled by W.P. Jencks, added to by F. H. Westheimer).

From the other side, the strength of AcA is not high enough to show big difference from the experiments with free pentylamine (73% yield from **AcA**×**2a** vs 80% yield from free **2a**, Table S1, Entries 5 and 6). **FA**×**2a** and **BzA**×**2a** show almost the same reactivity (25% and 19%, correspondingly, Table S1, Entries 3 and 4), but **FA**×**2a** shows almost no reaction with less active polyphenol **1b** (only 3% conversion after 12 h). Taking the above into consideration, **BzA**×**2a** was used as a model compound for oxidative coupling (Procedure B). The concentrations of the product (**3aa**) and amine (**BzA**×**2a**) and were monitored via ¹H NMR analysis using 1,3,5-TMB as an IS (Table S2 and Fig. S8). The obtained data was plotted on a graph to visualize the relationship between **1a** concentration over time in the **1a/BzA**×**2a** oxidative coupling reaction (Fig. S9). As expected, the linearization approach

using zero- and first-order integrated rate laws does not provide a linear slope (Fig. S9a, A and B). Considering the concentration decline of **BzA**×**2a** during the reaction, including its concentration in the second-order integrated rate law gives improved results (Fig. S9a, C and D).

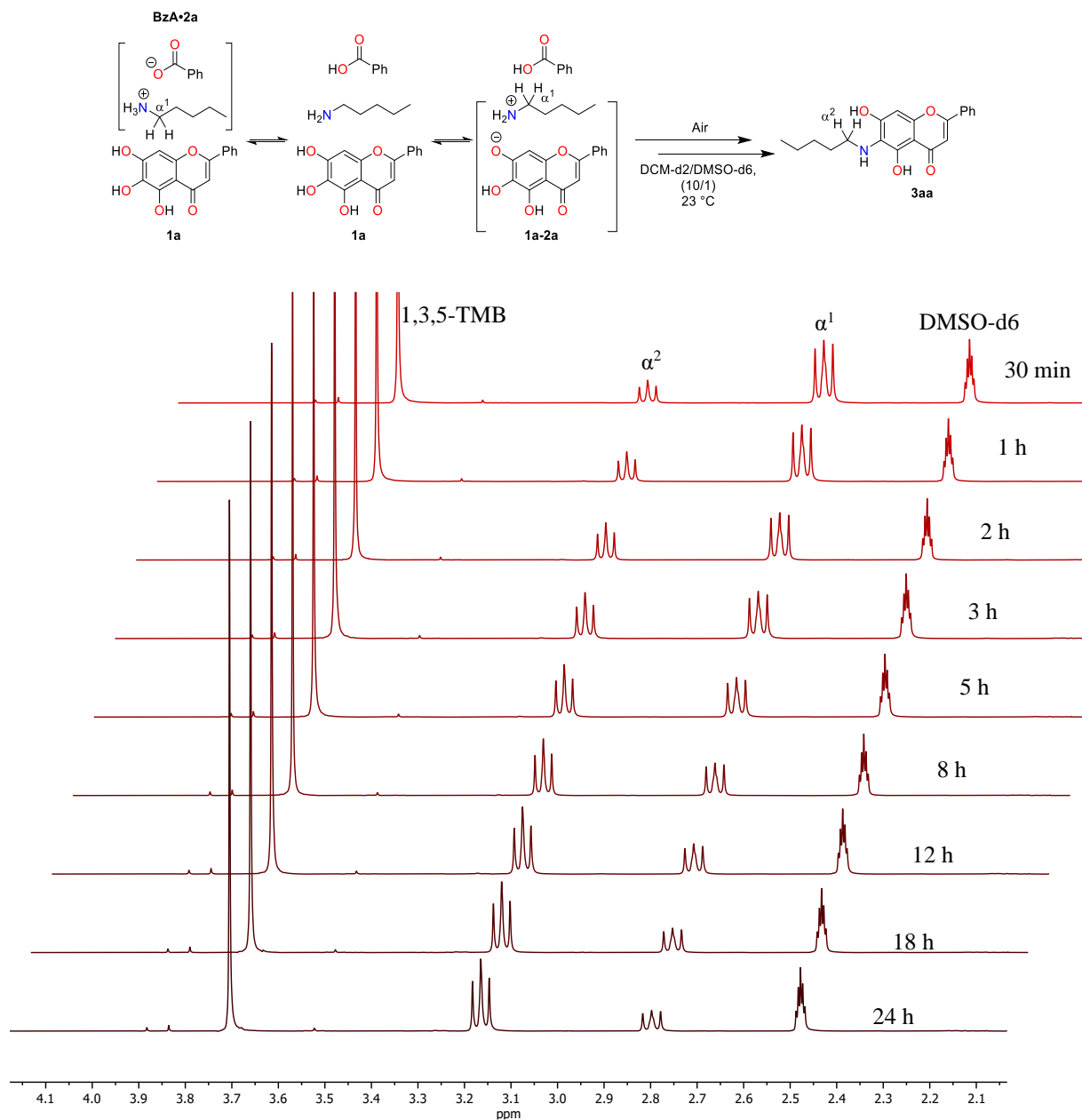
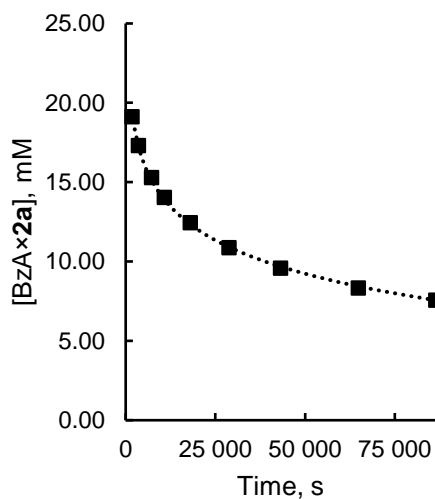


Fig. S8. *in situ* ¹H NMR spectra of **1a**/**BzA**×**2a** oxidative coupling, DCM-*d*2/DMSO-*d*6, 400 MHz.

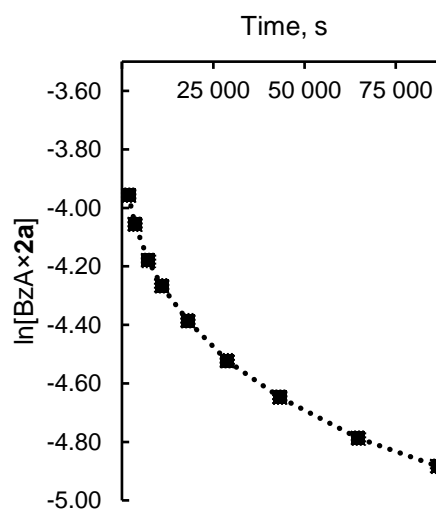
Table S2. Monitored integrals of α¹ and α² over time in the **1a**/**BzA**×**2a** oxidative coupling via ¹H NMR.

Time, s	[3aa], mM	[BzA × 2a], mM	[1a], mM	[BzA × 2a] conv, %	ln[BzA × 2a]	1/[BzA × 2a], 1/M	1/[1a][BzA × 2a], 1/M ²
1800	5.83	19.13	19.03	24.2	-3.96	52.3	2746
3600	7.54	17.30	17.16	31.4	-4.06	57.8	3367
7200	9.40	15.30	15.11	39.1	-4.18	65.4	4325
10800	10.82	14.03	13.70	45.0	-4.27	71.3	5200

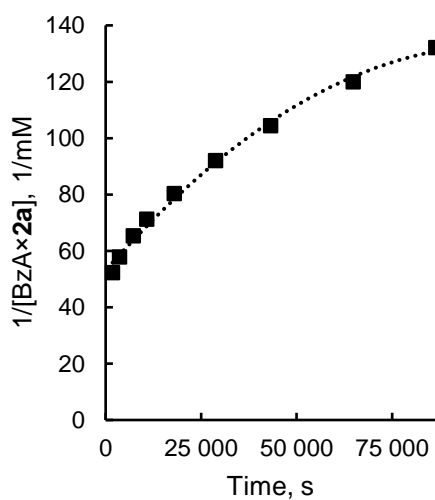
18000	12.25	12.45	12.06	51.0	-4.39	80.3	6662
28800	13.61	10.86	10.48	56.6	-4.52	92.0	8781
43200	14.90	9.58	9.10	62.0	-4.65	104.3	11467
64800	16.13	8.34	7.76	67.1	-4.79	119.9	15459
86400	16.70	7.57	6.93	69.5	-4.88	132.1	19062



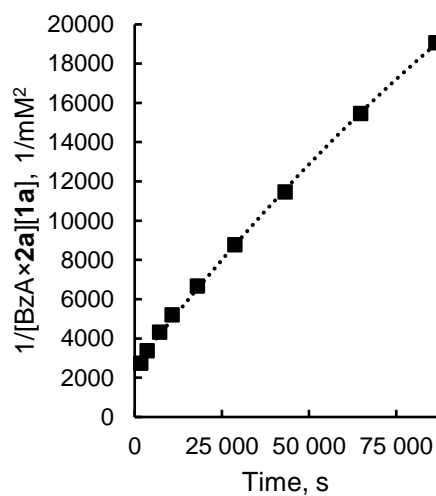
a) Zero order, $[BzA \times 2a]$ vs time, s



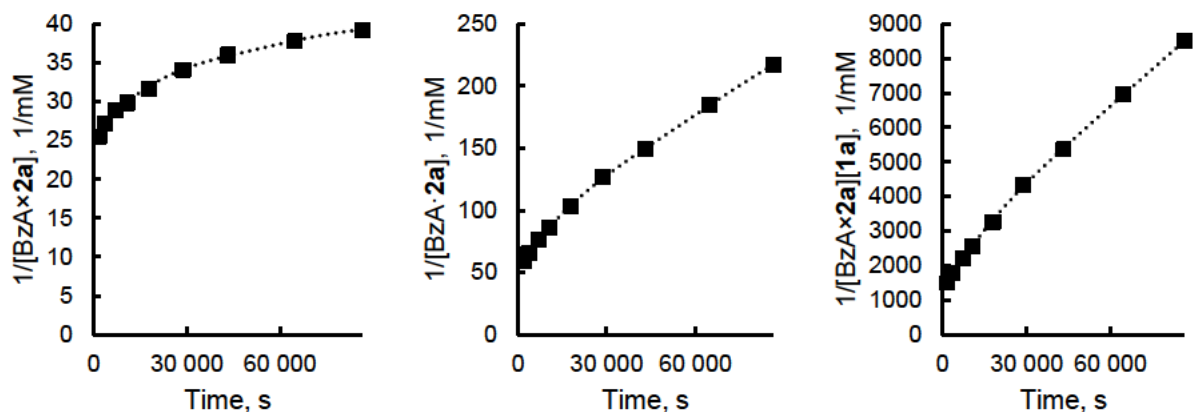
b) First order, $\ln[BzA \times 2a]$ vs time, s



c) Second order, $1/[BzA \times 2a]$ vs time, s



d) Second order, $1/[1a][BzA \times 2a]$ vs time, s



1/[BzA×2a] vs time, s

1/[1a] vs time, s

1/[1a][BzA×2a] vs time, s

e) 2 eq of BzOH·2a

Fig. S9a. Graphical representation of the curves obtained from the integrated rate laws.

However, the experiment with 2 eq of **BzA×2a** shows that the reaction deviates from the 2nd order integrated laws (Fig. S9a, E). To get better understanding about the rate law of the oxidative coupling reaction, CoPaSi (CoPaSi CoMplex PAThway SimulatoR) software was used (Fig. S9b).

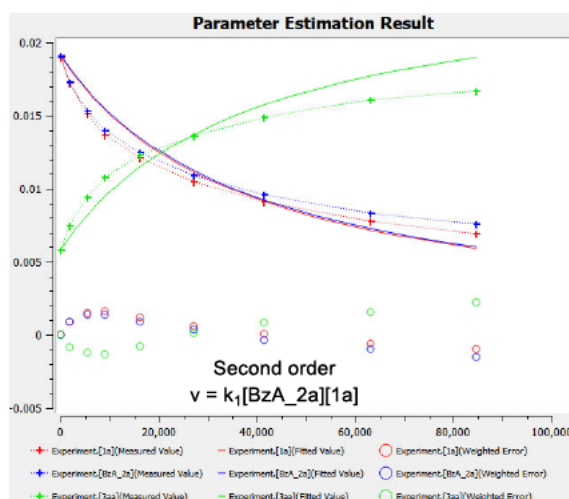
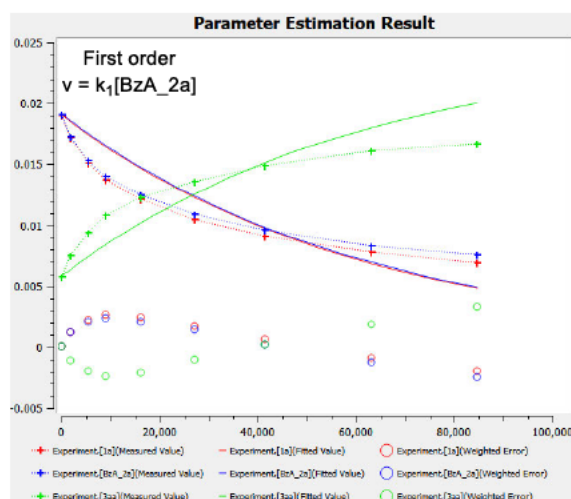


The concentrations of the reagents/product were taken from Table S2

The rate law k_1 was tuned to optimally fit the experimental data curve

Order	RMSE value		
	1a	BzA_2a	3aa
First	0.001750214	0.001696707	0.001861574
Second	0.000997281	0.000996241	0.001196822
Third	0.000471839	0.000452432	0.000681643
Fourth	0.000350938	0.000116335	0.000351734

A lower Root Mean Square Error (RMSE) value indicates a better fit to the experimental data.



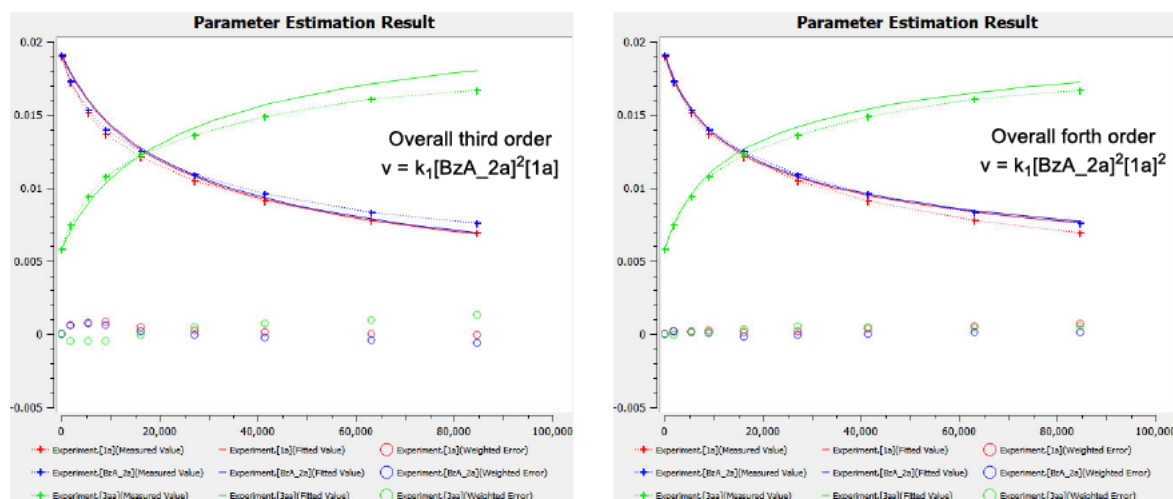


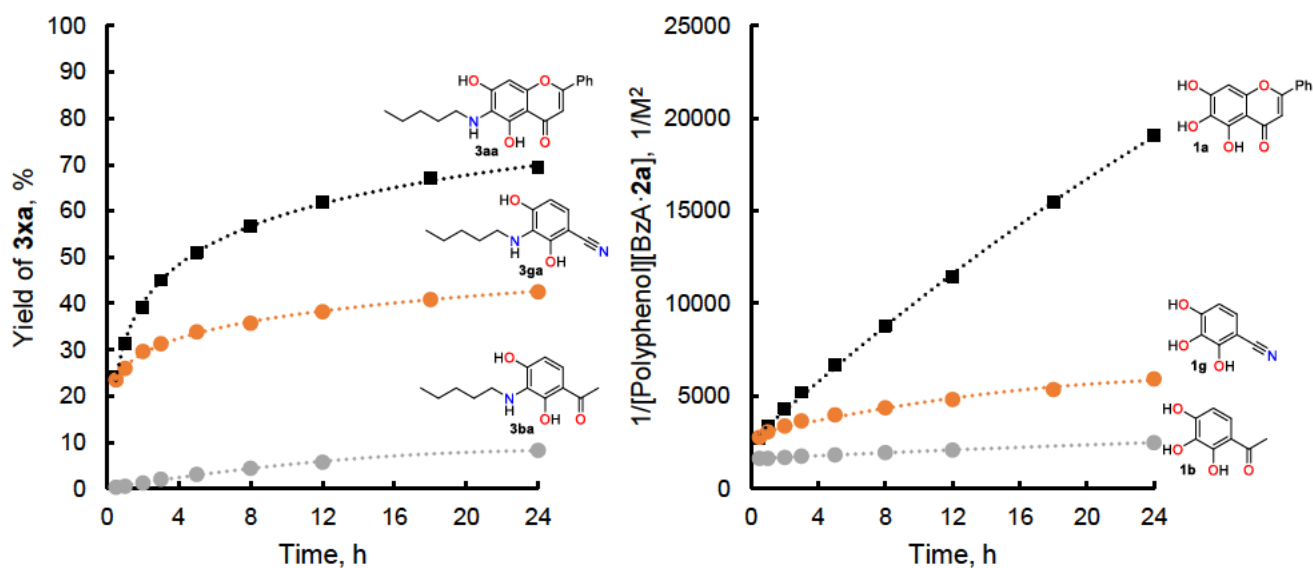
Fig. S9b. CoPaSi software parameter estimation of the oxidative coupling of **1a**/**BzA**×**2a**.

Simulations show that the best fit is achieved when a 4th overall order reaction rate is implemented, because an additional equivalent of amine is needed as a base for rearomatization step, and an extra equivalent of baicalein **1a** serves as a reductant in *o*-quinone chain. (Fig. S9b and 47). Also, testing other less active polyphenols (like **1g** and **1b**) indicated that in these cases, the curve deviated significantly from a linear slope in the early stages of the reaction (**1g**), or the conversion rates were too low (8% in 24 h, **1b**) (Table S3 and Fig. S10). It would be possible to consider only the first 8-12 h, during which the curve aligns more or less with a straight line, but this approach does not provide an explanation for the underlying reasons of such chemical behavior. Therefore, it was decided to focus on different approaches for further investigations.

Table S3. Obtained reactivity data for different polyphenols (**1a**, **1b**, **1j**).

Time, h	[1a] ₀ = 26 01 mM		[1g] ₀ = 24 99 mM		[1b] ₀ = 26 46 mM	
	[3aa], mM	[BzA×2a], mM	[3ga], mM	[BzA×2a], mM	[3ba], mM	[BzA×2a], mM
0	-	24.04	-	24.69	-	23.13
1800	5.83	19.13	5.80	18.89	0.08	23.13
3600	7.54	17.30	6.42	17.74	0.13	23.03
7200	9.40	15.30	7.32	16.86	0.28	22.65
10800	10.82	14.03	7.73	16.07	0.48	22.26
18000	12.25	12.45	8.37	15.32	0.72	21.80
28800	13.61	10.86	8.83	14.36	1.03	21.06
43200	14.90	9.58	9.44	13.50	1.33	20.28

64800	16.13	8.34	10.09	12.72	-	-
86400	16.70	7.57	10.50	11.79	1.91	18.42



Yield of **3ax**(%) vs time, h

1/[Polyphenol][BzA·2a] vs time, h

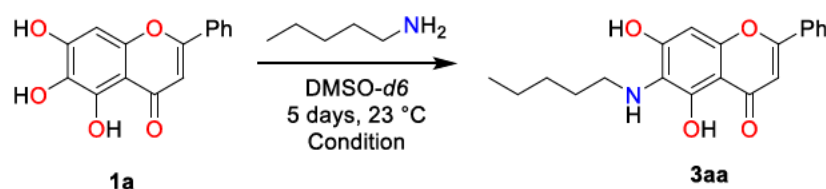
Fig. S10. The reactivity of polyphenols **1b** and **1g** relative to baicalein (**1a**).

1.3.7.4. Baicalein (**1a**) + pentylamine (**2a**) under different levels of oxygen concentrations

13 mg of **1a** (0.048 mmol, 1 eq) were placed in a J. Young NMR tube and dissolved in 0.5 ml of DMSO-*d*₆ under different conditions:

1. Non-degassed solvent, under air,
2. Non-degassed solvent, under N₂
3. Degassed solvent (bubbling N₂ for 1 h), under N₂
4. Degassed solvent (3 × freeze-pump-thaw), under N₂

6 μl of **2a** (0.052 mmol, 1.1 eq) were added to the resulting solution. The samples were incubated at 23 °C for 5 days and ¹H NMR analysis was performed afterwards (Fig. S11).



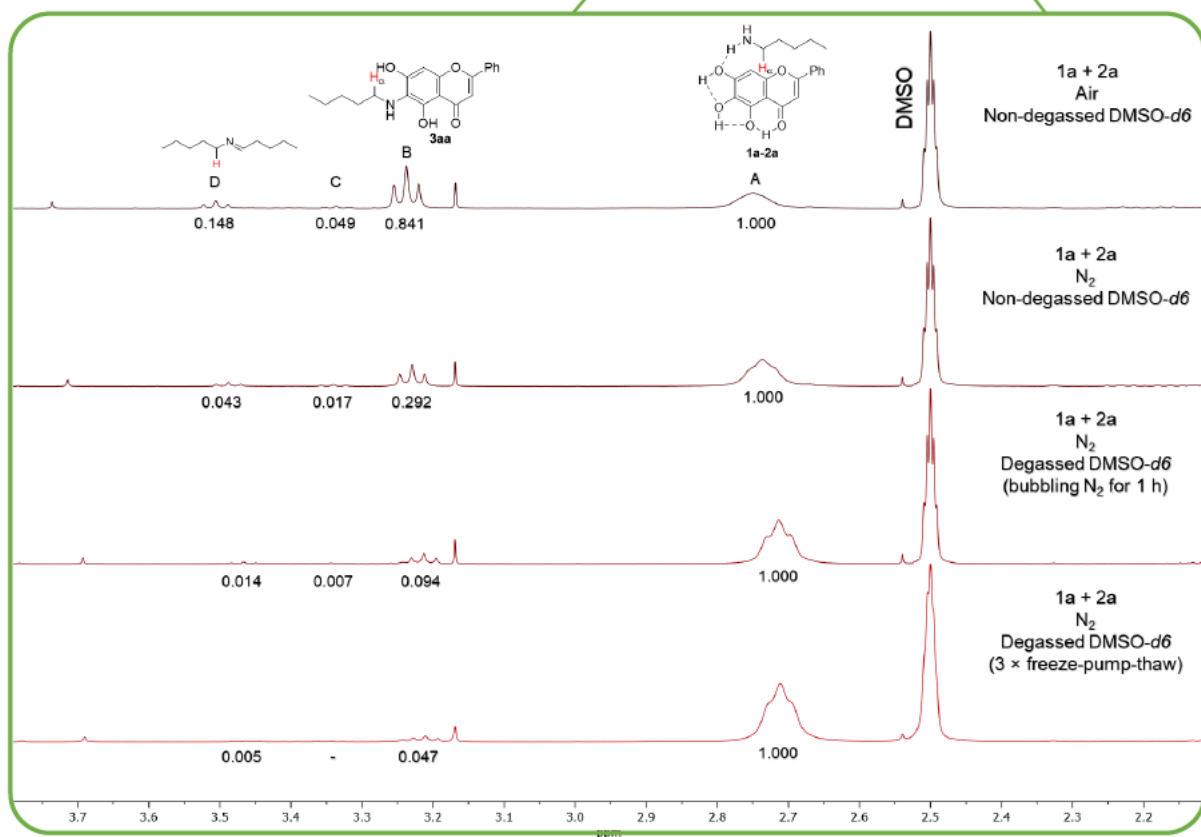
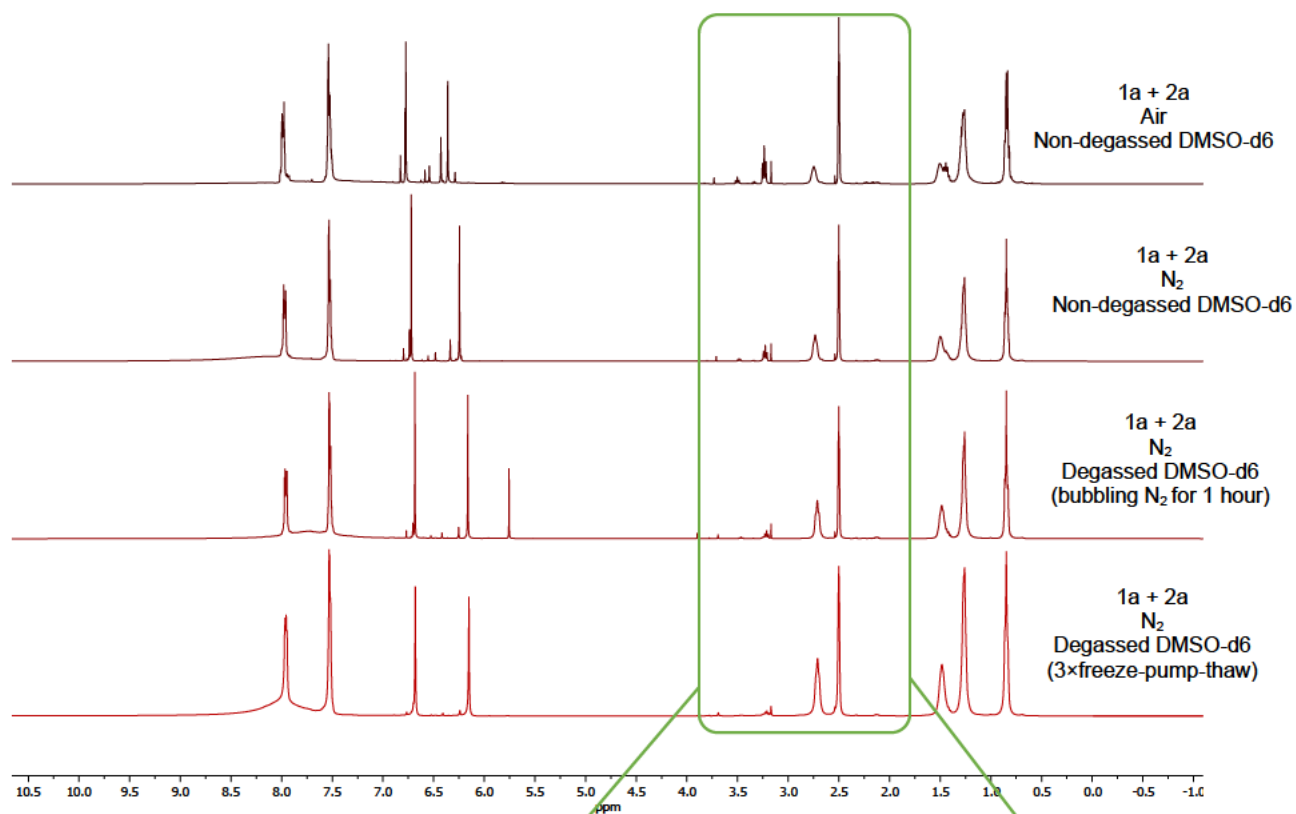


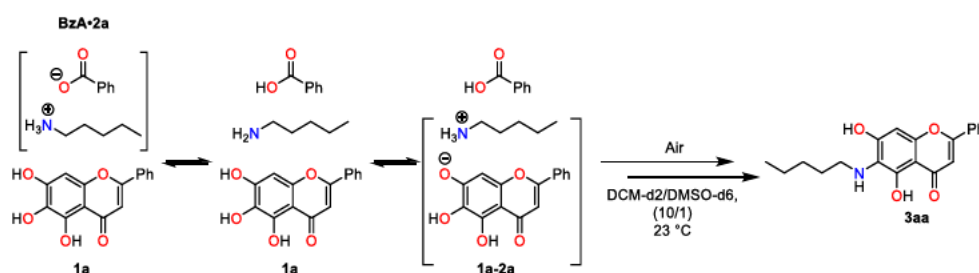
Fig. S11. A close-up of the ¹H NMR spectra of **1a** and **2a** at different O₂ in DMSO-d₆, 400 MHz. (Numbers indicate the integral value of the signal)

It was shown that oxygen acts as an oxidant and plays a significant role in this reaction. It was furthermore demonstrated that even traces of oxygen (for example, dissolved in the solvent) trigger the coupling reaction. Bubbling N₂ for 1 h through the solvent, as one of the widely used degassing techniques, was proven to be not sufficient to remove all oxygen traces, whilst the sample with the freeze-pump-thaw degassed DMSO-*d*6 shows the lowest oxidation state of **1a**.

Table S4. Reactivity level of **1a-2a** at different levels of oxygen concentrations.

No	Condition	Conversion of 2a , %
1	Air, non-degassed DMSO- <i>d</i> 6	52
2	N ₂ , non-degassed DMSO- <i>d</i> 6	25
3	N ₂ , degassed DMSO- <i>d</i> 6 (bubbling N ₂ for 1 h)	10
4	N ₂ , degassed DMSO- <i>d</i> 6 (3 × freeze-pump-thaw)	5

The same approach was also applied with **BzA×2a** to demonstrate the importance of the amount of oxygen in the reaction vessel.



The previously mentioned results are shown in gray (a) in Fig S12 (1 eq **BzA×2a** under air atmosphere). Under these conditions, the product yield is 70%. Using pure oxygen instead of air significantly accelerates the reaction, and the product yield curve reaches a plateau earlier (83%, green curve (b)). The same level of oxidative coupling is reached when 2 eq of **BzA×2a** is used (82%, yellow curve (c)). Worth to mention that oxygen concentration dissolved in the solvents (DCM-*d*2 and DMSO-*d*6) is enough to keep the reacti-

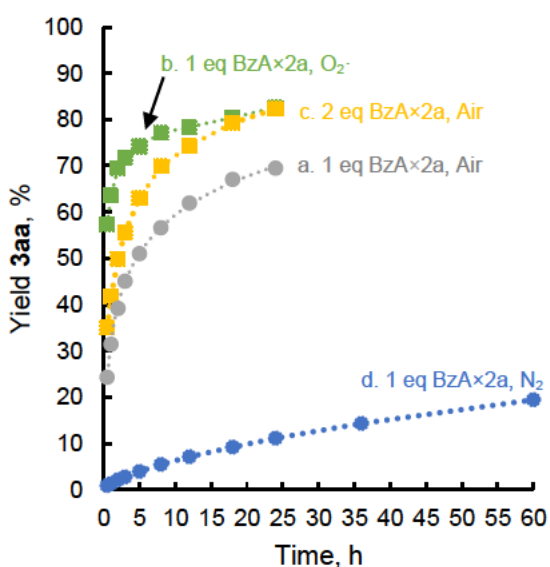
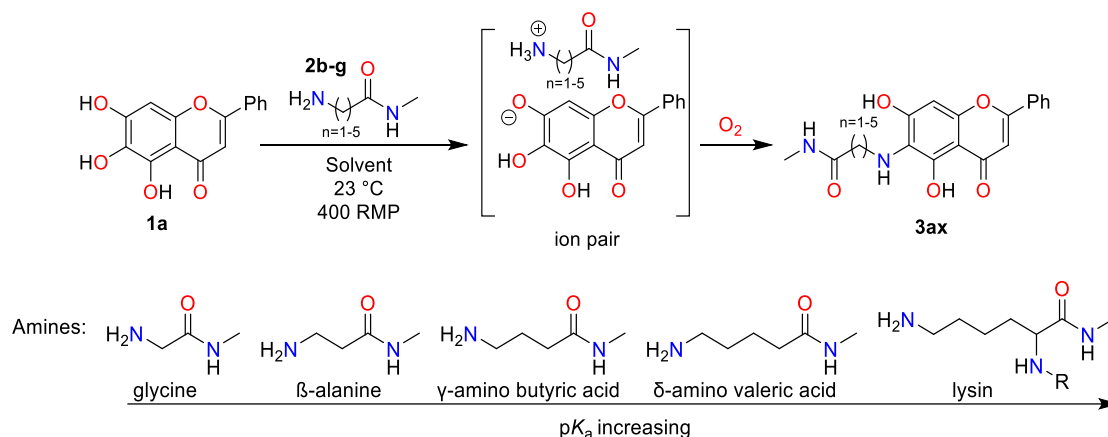


Fig. S12. Oxidative coupling of **1a/BzA×2a** under different conditions.

on running (blue curve (d)). The reaction is slowly reaching 19% after 60 h of incubation at 23 °C.

1.3.7.5. Oxidative coupling of baicalein (**1a**) with various *N*-nucleophiles **2b-i**

pK_a values for the amino group of a homologous series of amino acids are presented on the Table S5. It was decided to use *N*-methyl amides **2b-g** for these amino acids for further reactions to mimic a real peptide (Scheme S4):



Scheme S4. Oxidative coupling of *N*-methyl amides **2b-g** with baicalein (**1a**).

Table S5. Dependence of yield of **3ax** from pK_a of *N*-nucleophiles **2b-g**

№	Amino acid	pK_a	Yield of 3ax , %	
			DCM	DCM- <i>d</i> 2/DMSO- <i>d</i> 6
1	Glycine ^[3]	7.68*	X	X
2	β-Alanine ^[4]	9.13*	Detected in APCI MS	
3	γ-amino butyric acid ^[5]	9.91*	7	66
4	δ-amino valeric acid ^[5]	10.10*	44	68
5	Lysin ^[1]	10.6	69	78
6	Pentylamine 2a	10.6	72	80

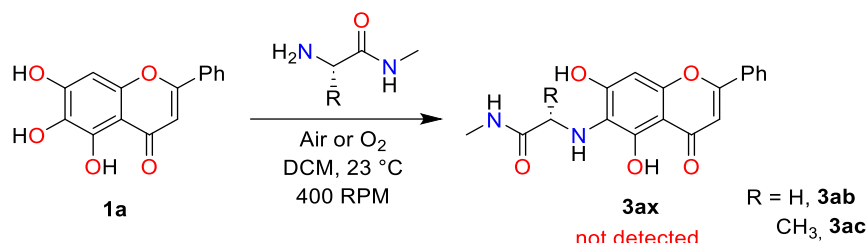
* Given for amino acid methyl/ethyl ester

Because of the low solubility of *N*-methyl amides **2b-g** in DCM procedure A was slightly modified. Instead of adding defined amount of calibrated DCM solution of a *N*-nucleophile, amino acid derivatives **2b-g** were weighed on the inner side of the vial cap. Due to the high surface tension, the droplet remains in place upon closing the vial. Afterwards, the GC vial was placed upside down on a shaker at 400 RPM. Shaking continued for 18 h at 23 °C, then followed by APCI-MS analysis. If APCI-MS analysis indicated the formation of a product, a defined amount of 1,3,5-trimethoxybenzene was added as an IS. 0.5 ml Aliquot was

evaporated and dissolved in 0.75 ml of dry degassed DMSO-*d*6 under nitrogen atmosphere to prevent oxidative coupling. ¹H NMR analysis was performed to establish the yield of the final products.

H-Gly-NMe (2b) and H-Ala-NMe (2c).

a) In DCM



The reaction was performed according to the modified Procedure A, described at the beginning of the chapter. No homogenization and color change of the reaction mixture were observed as before, when **2a** was used as a reactant.^[1] After 10 min, APCI-MS analysis was performed, showing no coupling. The reaction was allowed to shake for 18 h at 23 °C with no product formation via APCI-MS. The reactions were repeated but under O₂ atmosphere, giving the same result (Fig. S13). The absence of reactivity can be explained by relatively low *pK_a* value of the selected *N*-nucleophiles.

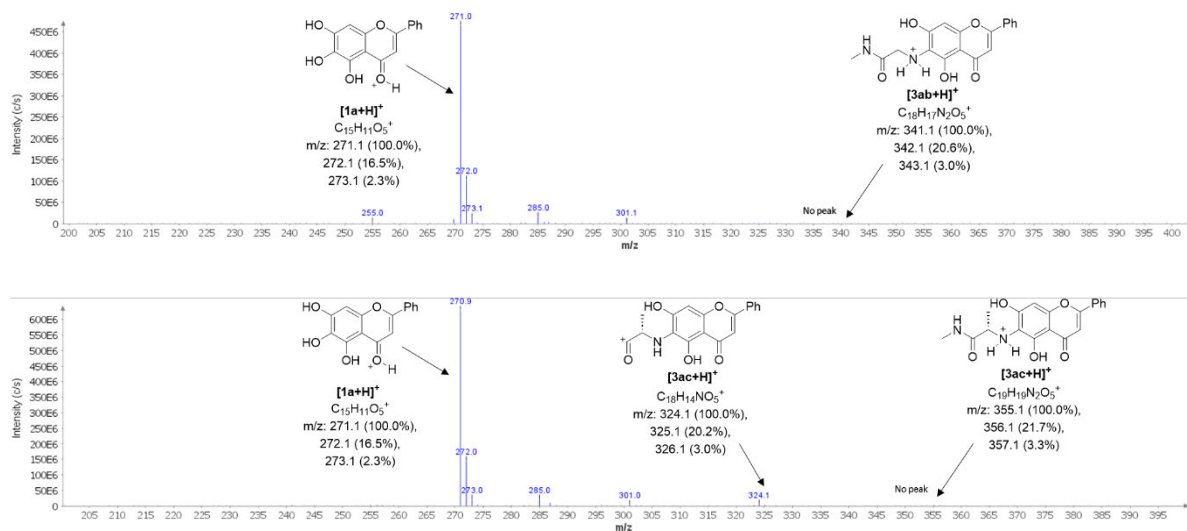
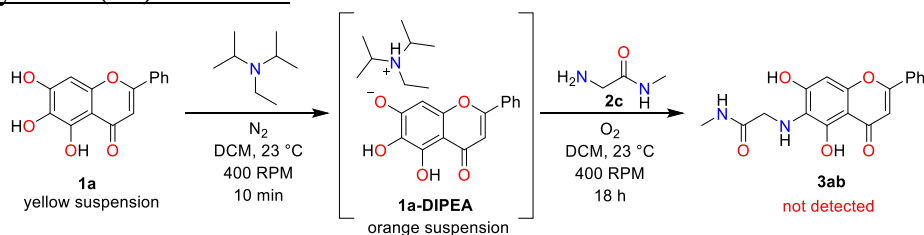


Fig. S13. APCI MS spectra of the reaction of **1a** with H-Gly-NMe **2b** (top) and H-Ala-NMe **2c** (bottom).

1a + H-Gly-NMe (2b) + DIPEA.



In our assumption, the formation of the ion pair is the crucial step. Procedure A was modified and 20 or 100 mol% DIPEA was used to deprotonate **1a** under inert atmosphere, forming the orange **1a-DIPEA** complex. The ion pair was treated with 1 eq of H-Gly-NMe **2b** under molecular oxygen. The reaction was shaken for 18 h at 23 °C with no product formation via APCI MS (Fig. S14).

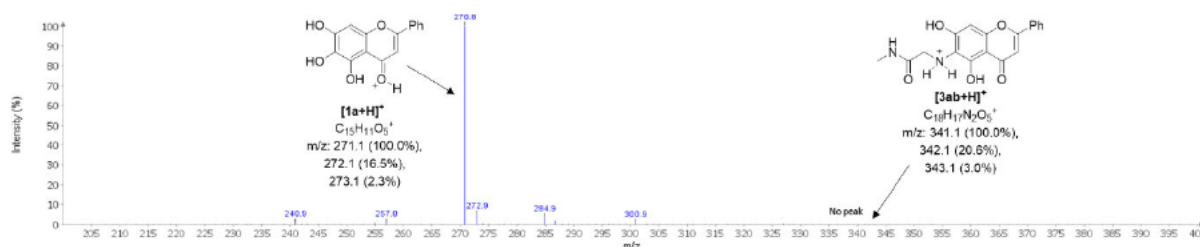
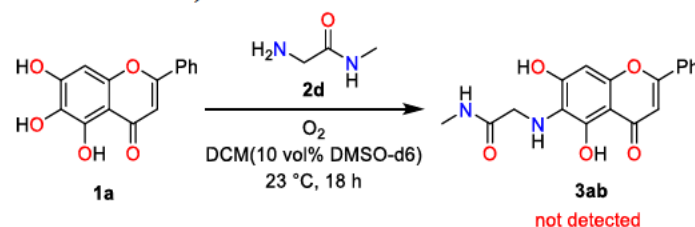


Fig. S14. APCI-MS spectra of the reaction of **1a** with H-Gly-NMe **2b** and 100 mol% DIPEA addition.

b) DCM (10 vol% DMSO-*d*6)



The reaction was performed according to Procedure B. No color change was observed. The reaction was allowed to stir 18 h at 23 °C with no product formation via APCI-MS (Fig. S15).

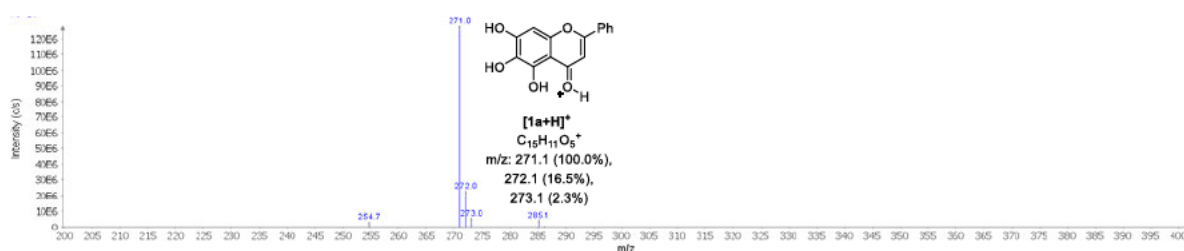
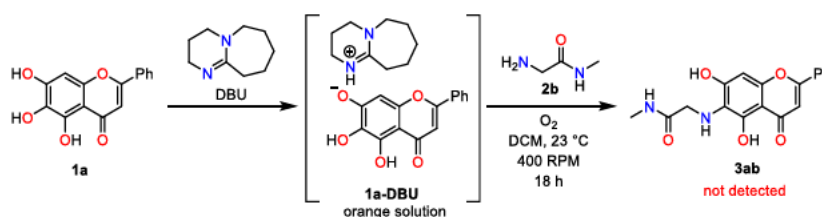


Fig. S15. APCI MS spectra of the reaction of **1a** with H-Gly-NMe (**2b**) in DCM (10 vol% DMSO-*d*6).

In order to obtain the product **3ab**, 10 and 100% mol DBU was added as an auxiliary base. The reaction was allowed to shake 18 h at 23 °C with no product formation via APCI-MS (Fig. S16).



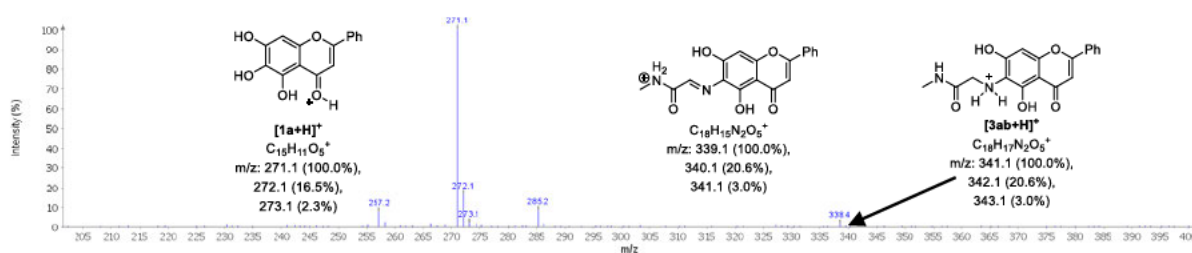
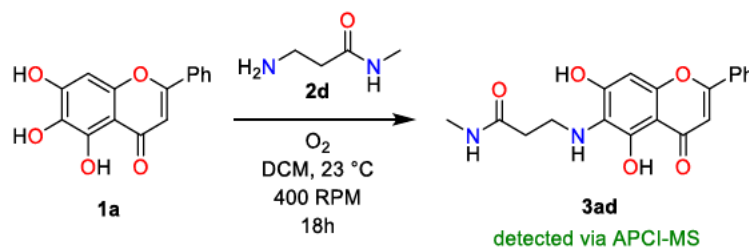


Fig. S16. APCI MS spectra of the reaction of H-Gly-NMe (**2b**) with 10% mol DBU in DCM (10 vol% DMSO-*d*6).

H-β-Ala-NMe **2d**

a) In DCM



The reaction was performed according to the modified procedure A described at the beginning of the chapter. No homogenization and color change of the reaction mixture were observed as before. The reaction was allowed to shake for 18 h at 23 °C with showing a minor product formation via APCI-MS (Fig. S17).

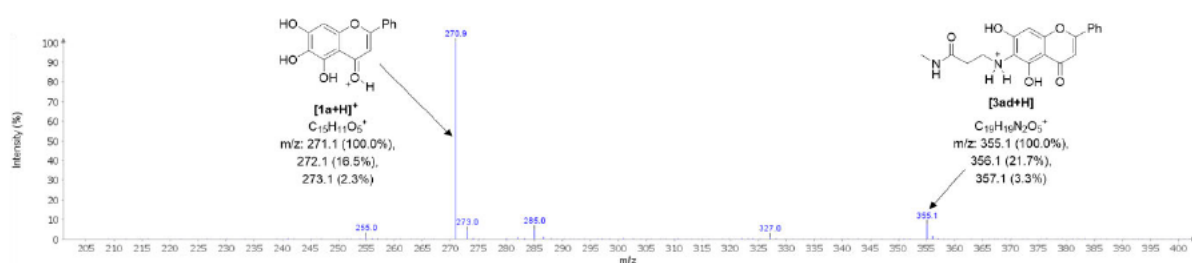
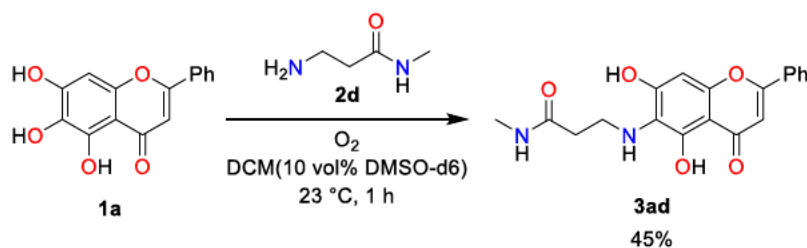


Fig. S17. APCI MS spectra of the reaction of **1a** with H-β-Ala-NMe **2d** in DCM.

b) DCM (10 vol% DMSO-*d*6).

The reaction was performed according to procedure B. An instant color change was observed upon the addition of amine **2d**. ¹H NMR analysis was performed after 1 h at 23 °C, where APCI MS showed the formation of a significant amount of the product (Fig. S18).



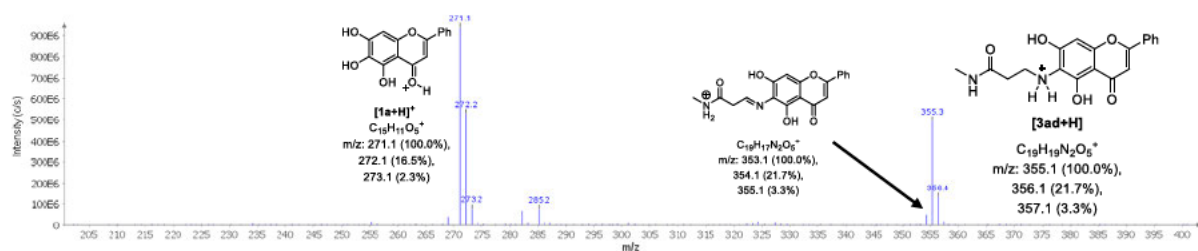


Fig. S18. APCI MS spectra of the reaction of **1a** with H- β -Ala-NMe (**2d**) in DCM (10 vol% DMSO-*d*6).

It was shown that **3ad** was formed with 45% yield (average yield from 2 independent experiments), according to the obtained ^1H NMR spectra (Fig. S19). The C6-regioselectivity of **3ad** was proven by scXRD analysis.

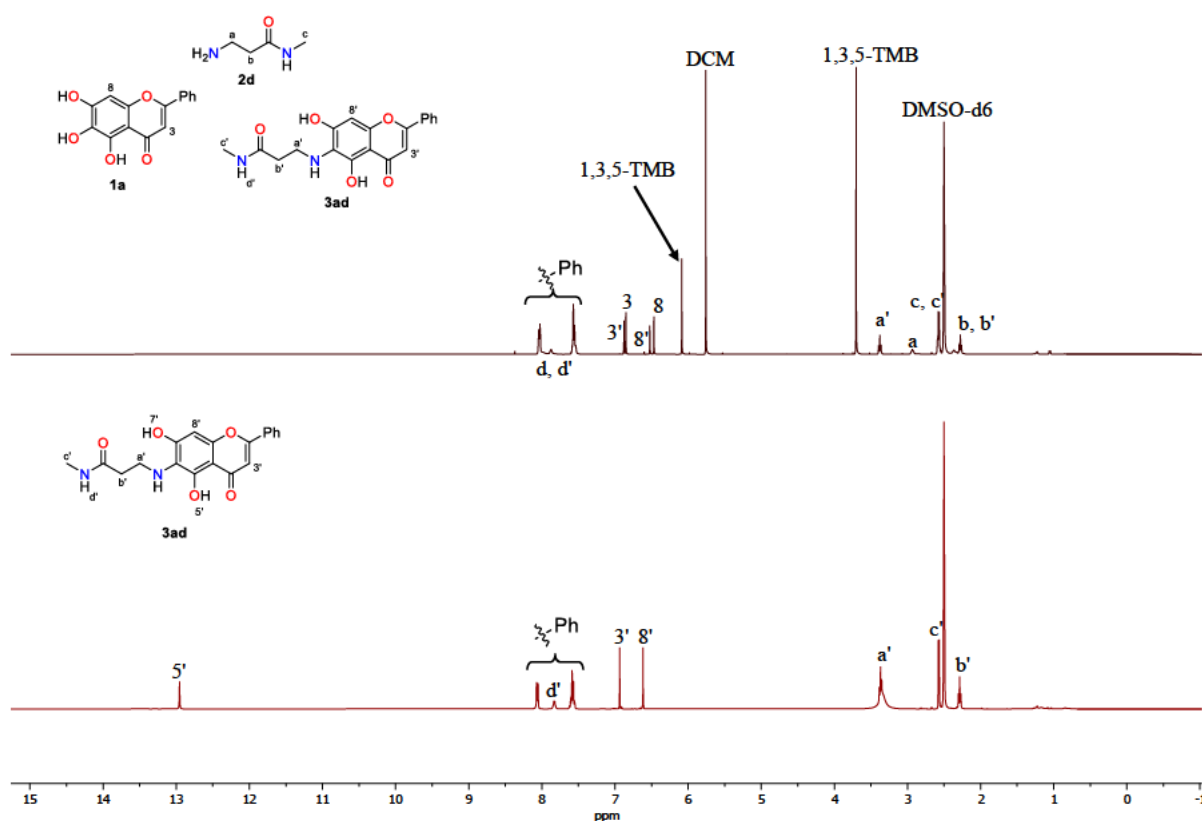
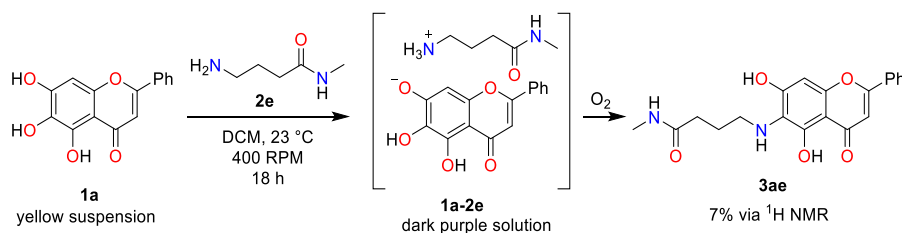


Fig. S19. ^1H NMR spectra of the crude reaction mixture (top) compared with those of the isolated product **3ad** (bottom), 400 MHz, DMSO-*d*6.

The reaction was repeated according to Procedure A. 1,3,5-TMB was added as an IS, a small aliquot was taken in an NMR tube, the solvent was evaporated under reduced pressure, and the crude material was dissolved in DMSO-*d*6 for further analysis indicating a yield of 43%.

H-Gaba-NMe 2e

a) In DCM



The reaction was performed according to the modified Procedure A, described at the beginning of the chapter. The stirring yellow suspension of **1a** immediately turned dark purple on the addition of amine **2e**. The reaction was allowed to stir for 18 h at 23 °C with no further change in color and the coupling product was detected via APCI-MS analysis (Fig. S20).

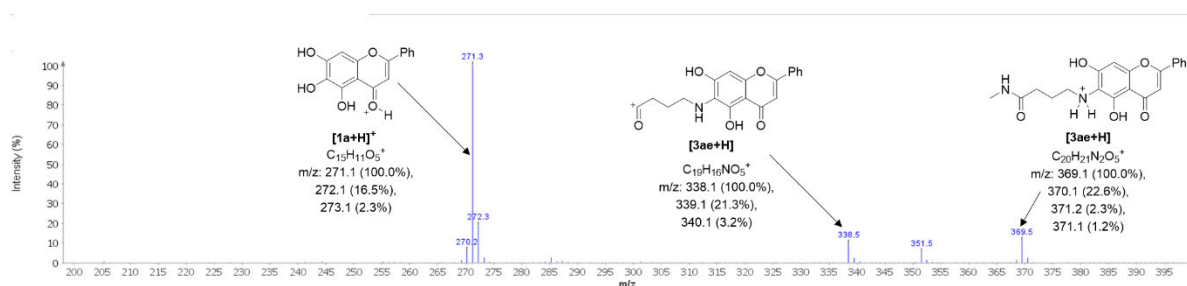
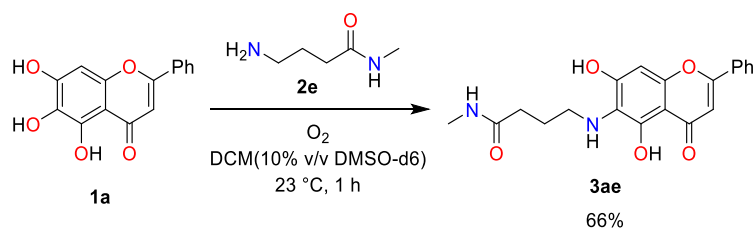


Fig. S20. APCI MS spectra of the reaction of **1a** with H-Gaba-NMe (**2e**).

1,3,5-TMB was added as an IS, small aliquot was taken in an NMR tube, the solvent was evaporated under reduced pressure, and the crude material was dissolved in DMSO-*d*₆ for further analysis (the dark purple crude material gives an orange solution). It was shown that **3ae** was formed with 7% yield, according to the obtained ¹H NMR spectra.

b) DCM (10 vol% DMSO-*d*₆)

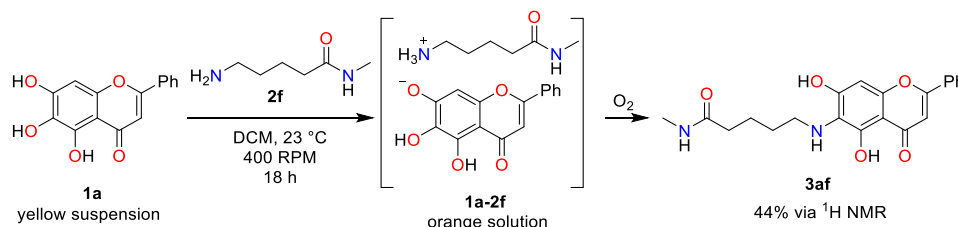


The reaction was performed according to Procedure B. An instant color change was observed on addition of amine **2e**. The ¹H NMR analysis was performed after 1 h at 23 °C. It was shown that **3ae** was formed with 66% yield (average yield from 2 independent experiments), according to the obtained ¹H NMR spectra (Fig. S21).

The reaction was repeated according to Procedure A (0.25 mmol scale). After quenching with 1.25 eq of TFA-*dl*, 1,3,5-TMB was added as an IS, a small aliquot was taken in an NMR tube, the solvent was evaporated under reduced pressure, and the crude material was dissolved in DMSO-*d*₆ for further analysis indicating a yield of 66% (Fig. S22).

H-Ava-NMe (**2f**)

a) In DCM



The reaction was performed according to the modified Procedure A described at the beginning of the chapter. The stirring yellow suspension immediately turns orange on addition of amine **2f** and the coupling product is detected after 10 min via APCI-MS analysis (Fig. S23).

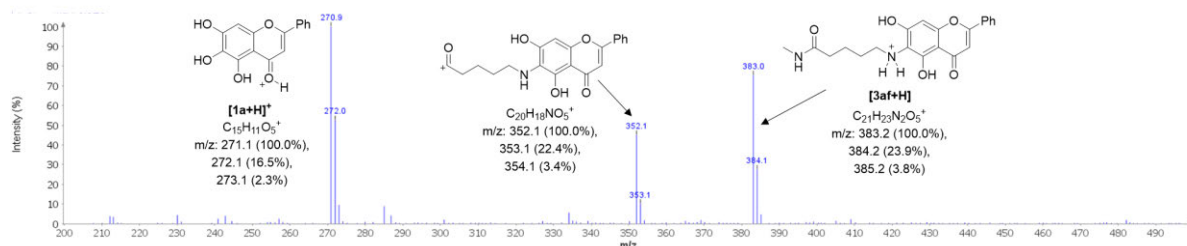
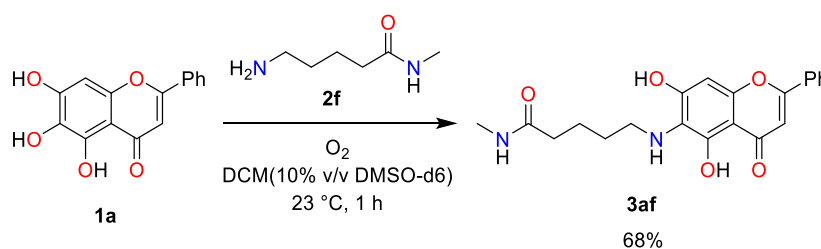


Fig. S23. APCI MS spectra of the reaction of **1a** with H-Ava-NMe (**2f**) in DCM.

The reaction was allowed to shake for 18 h at 23 °C, when 1,3,5-TMB was added as an IS, small aliquot was taken in an NMR tube, the solvent was evaporated under reduced pressure, and the crude material was dissolved in DMSO-*d*₆ for further analysis. It was shown that **3af** was formed with 44% yield, according to the obtained ¹H NMR spectrum. The reaction was repeated on 0.2 mmol scale, and the crude product was purified by preparative TLC chromatography (28 mg, 37%).

b) DCM (10 vol% DMSO-*d*₆)



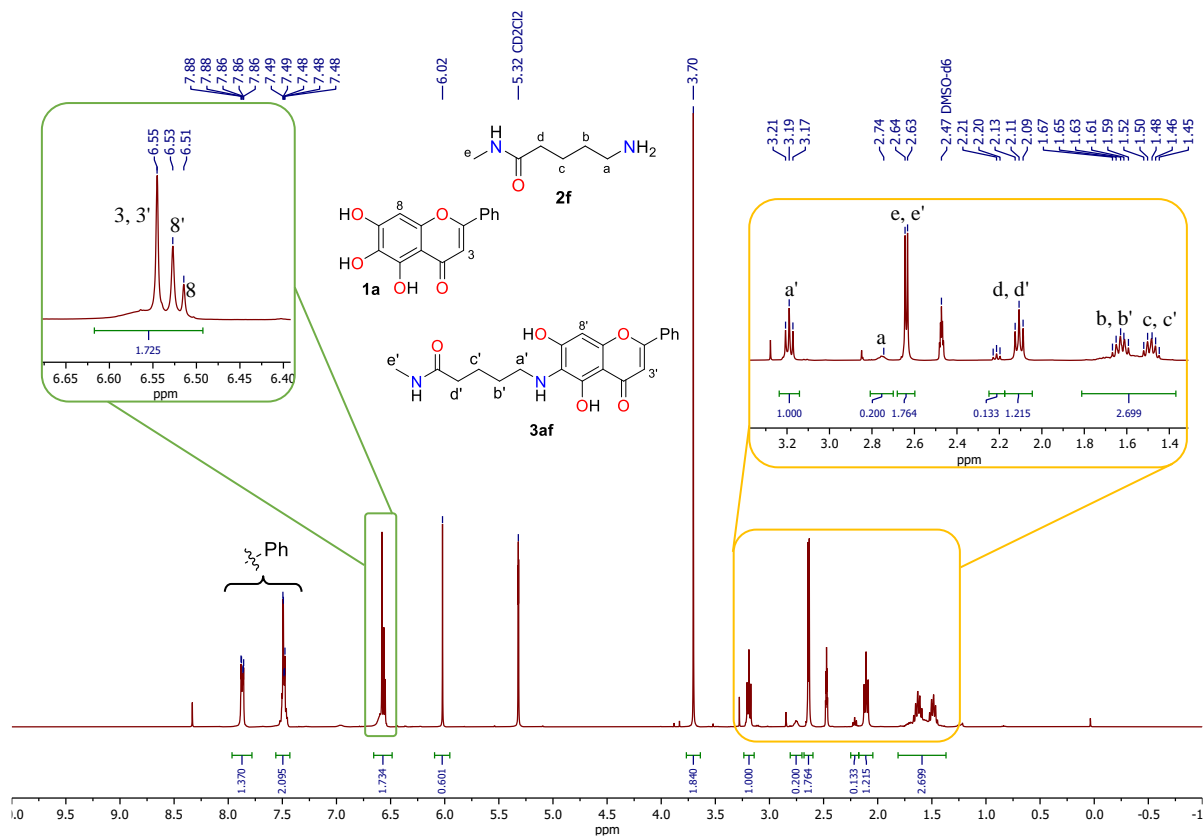


Fig. S24. *In situ* ^1H NMR spectrum of **1a/2f** oxidative coupling, 400 MHz, DCM- d_2 /DMSO- d_6 .

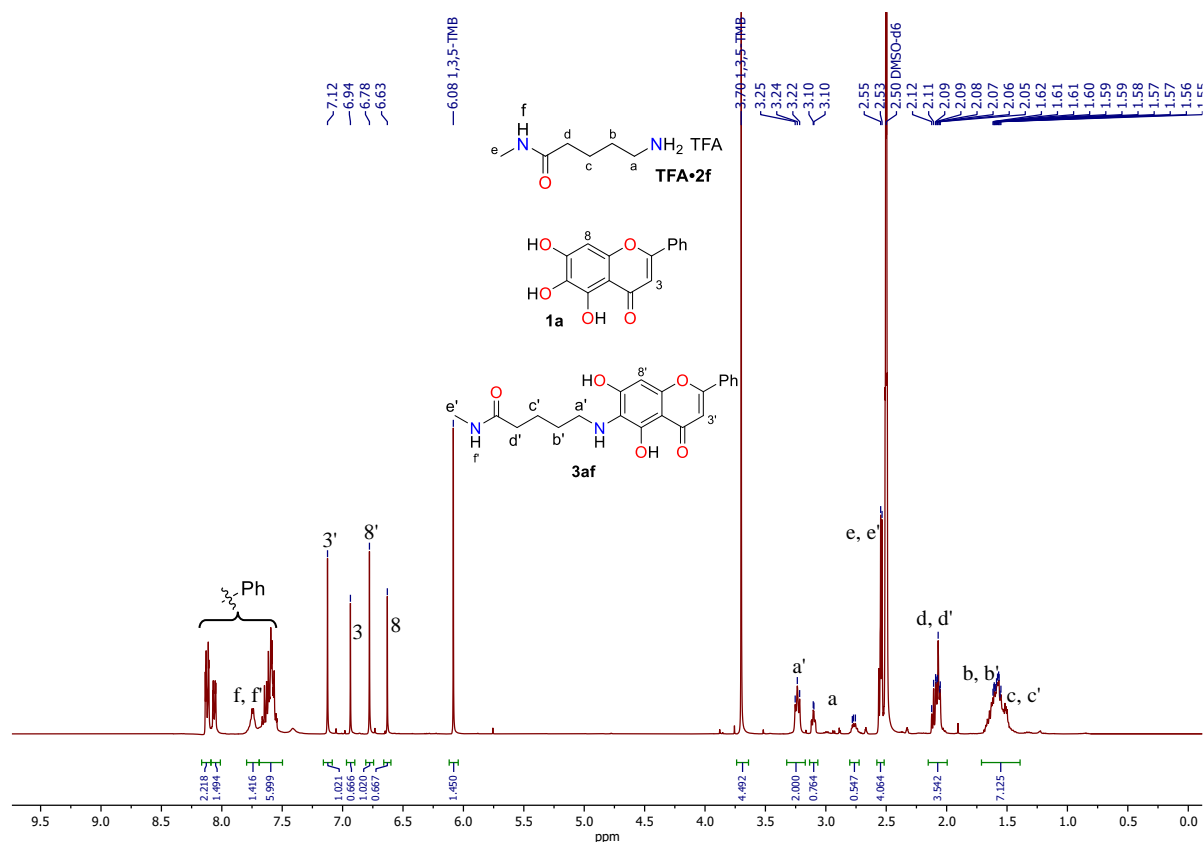


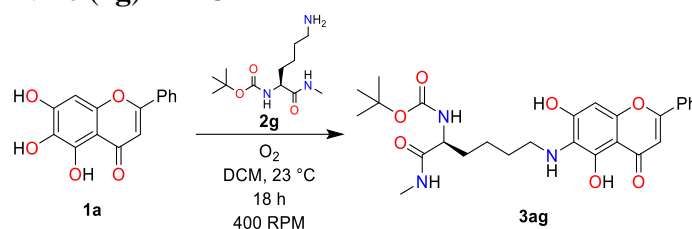
Fig. S25. ^1H NMR spectrum of **1a/2f** oxidative coupling, TFA quenching, 400 MHz, DMSO- d_6 .

The reaction was performed according to Procedure B. An instant color change was observed on addition of amine **2f**. ^1H NMR analysis was performed after 1 h at 23 °C. It was shown that **3af** was formed with 68% yield (average yield from 2 independent experiments), according to the obtained ^1H NMR spectra (Fig. S24).

The reaction was repeated according to Procedure A (0.25 mmol scale), quenched with 1.25 eq of TFA-*d*1, 1,3,5-TMB was added as an IS, a small aliquot was taken in an NMR tube, the solvent was evaporated under reduced pressure, and the crude material was dissolved in DMSO-*d*6 for further analysis with 60% yield (Fig. S25).

Lysine derivatives **2g** and **2g'**

a) N_α -Boc-Lys-NMe (**2g**) in DCM



The reaction was performed according to the modified Procedure A, described at the beginning of the chapter. Instant homogenization and color change of the reaction mixture from yellow to green and then to orange were observed. After 10 min, APCI MS analysis was performed showing the coupling product (Fig. S26).

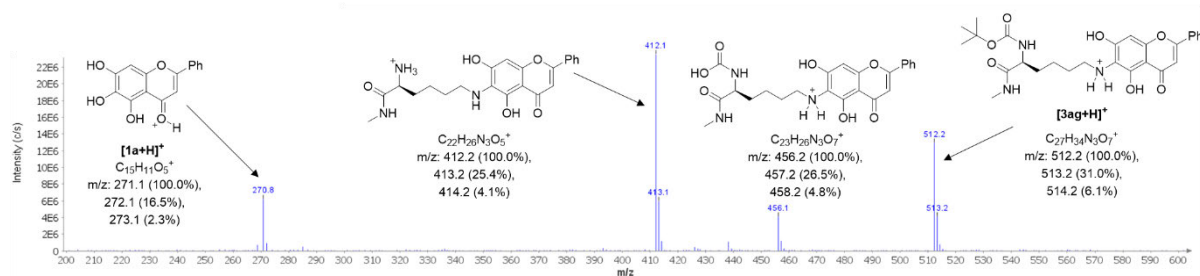


Fig. S26. APCI MS spectra of the reaction of **1a/2g** in DCM.

The reaction was shaken for 18 h at 23 °C. The crude product was purified by column chromatography to obtain the orange solid (35 mg, 69%). The product was identified as C6-Lys-functionalized **1a** via ^1H and ^{13}C NMR analysis (Fig. S27).

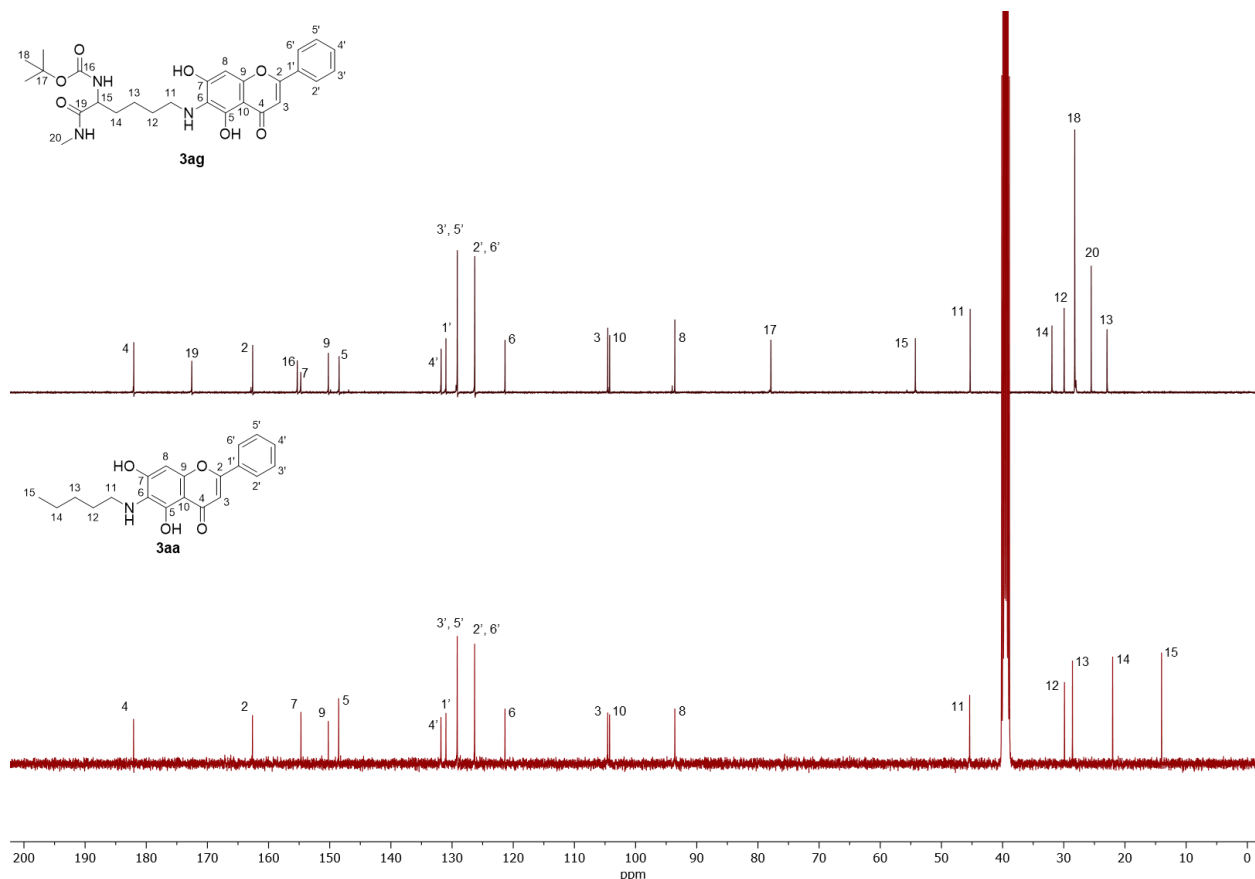
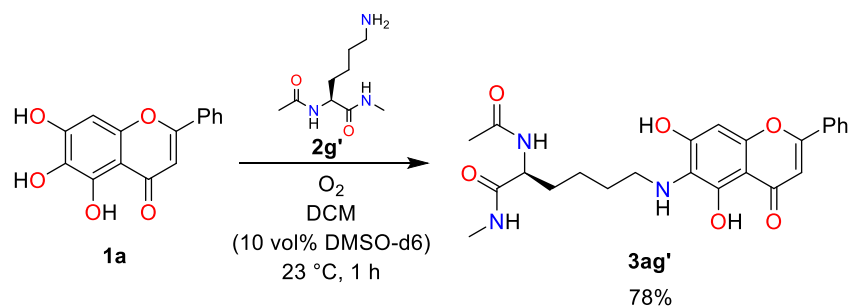


Fig. S27. Comparison of ¹³C NMR spectra of **3aa** (101 MHz) with the obtained **3ag** (201 MHz), DMSO-*d*₆.

b) N_α-Ac-Lys-NMe (**2g'**) in DCM (10 vol% DMSO-*d*₆)



The reaction was performed according to Procedure B. An instant color change was observed on addition of amine **2g'**. ¹H NMR analysis was performed after 1 h at 23 °C. It was shown that **3ag'** was formed with 78% yield (average yield from 2 independent experiments), according to the obtained ¹H NMR spectra (Fig. S28).

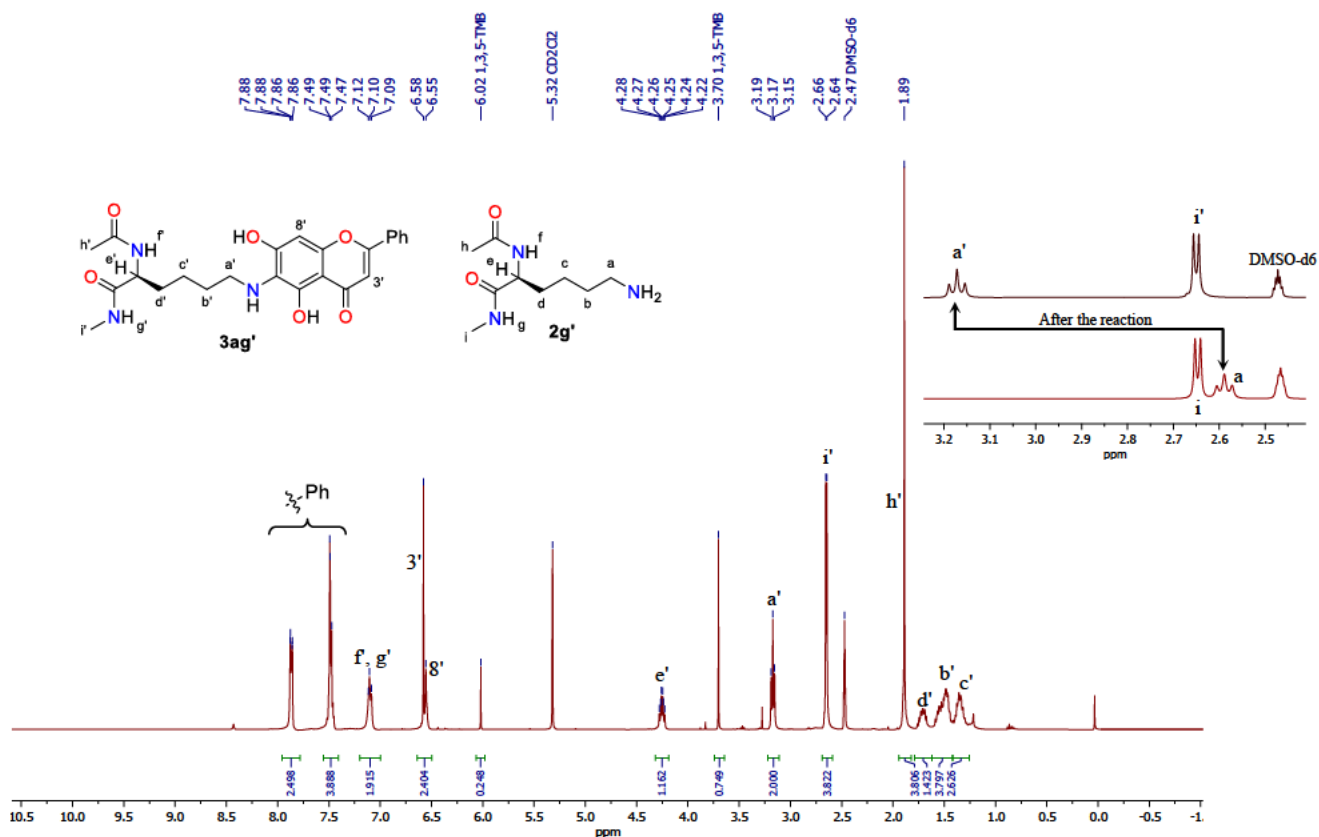


Fig. S28. *in situ* ^1H NMR spectrum of **1a/2g'** oxidative coupling, 400 MHz, DCM/DMSO- d_6 .

c) In aqueous media

The yellow suspension of **1a** (25 mM) in water slowly changes colors from yellow-green to brown on addition of amine **2a**. The reaction was quenched with 1.25 eq of TFA-*d1*, the precipitate was centrifuged and washed 3 times with water. APCI MS of the crude material showed a minor formation of the product **3aa** (9% via ^1H NMR) (Fig. S29 and S30).

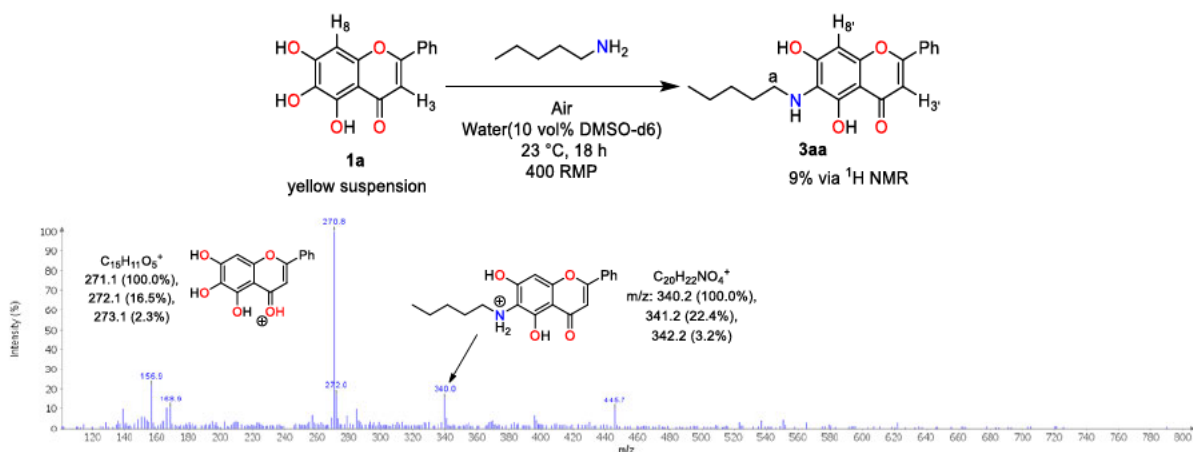


Fig. S29. APCI MS spectrum of the precipitate obtained from the **1a/2a** oxidative coupling in $\text{H}_2\text{O}/\text{DMSO} = 10/1$.

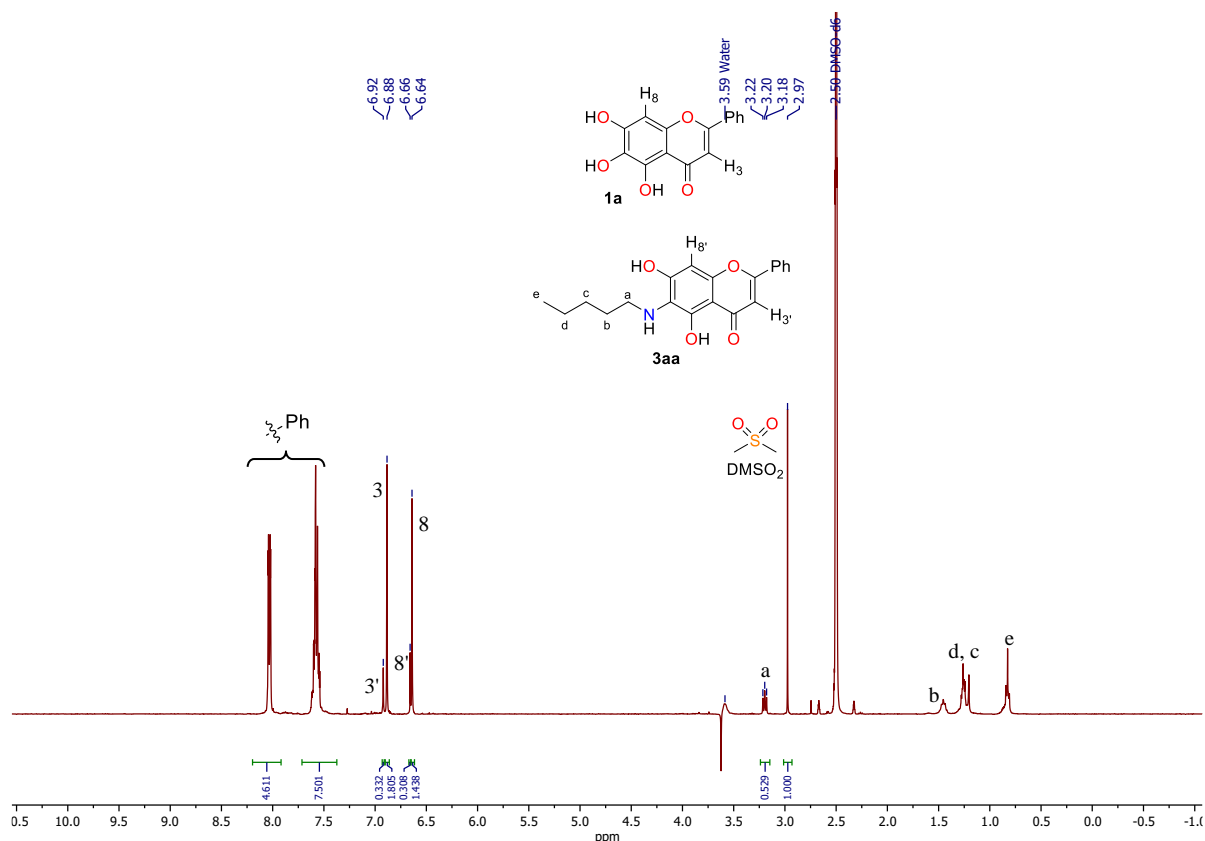


Fig. S30. ¹H NMR spectrum of the precipitate obtained from the **1a/2a** oxidative coupling in H₂O/DMSO = 10/1, 400 MHz, DMSO-*d*₆ (water suppression pulse sequence).

The addition of amine **2a** changes the pH value of the reaction mixture due to its basic properties. It has been demonstrated, an aqueous solution of **2a** (0.025 M) has a pH value of 11.53, which significantly deviates from the standard pH range observed in biological systems. Therefore, the phosphate buffer (**PB**) was selected to maintain a specific pH value in the reaction mixture. And the changes in pH values of the **PB** solution caused by the addition of amine were measured using a pH-meter (Table S6).

Table S6. The final pH values of the aqueous solutions of pentylamine derivatives

	Solvent	Amine	C[Amine], [M]	Final pH value	ΔpH
1	HPLC Water	2a	0.025	11.53	-
2	0.1 M Phosphate Buffer (pH 7.40)	2a	0.025	10.03	2.63
3	0.1 M Phosphate Buffer (pH 7.40)	2a	0.0125	8.00	0.60
4	0.1 M Phosphate Buffer (pH 7.44)	2a	0.0025	7.50	0.06
5	0.5 M Phosphate Buffer (pH 7.40)	2a	0.025	7.70	0.30
6	1.0 M Phosphate Buffer (pH 7.40)	2a	0.025	7.50	0.10
7	HPLC Water	BzA× 2a	0.025	7.85	-
8	0.1 M Phosphate Buffer (pH 7.35)	BzA× 2a	0.025	7.34	0.01

9	0.1 M Phosphate Buffer (pH 7.35)	TFA× 2a	0.025	7.35	0.00
10	0.1 M Phosphate Buffer (pH 7.35)	TFA× 2a	0.100	7.35	0.00

It has been shown that typical concentrations (0.025 M) of **2a** have a significant effect on the pH of the PB solution (Table S6, Entry 1 and 2). Only low concentrations of amine **2a** can be introduced to PB without significant changes in the pH value of the solution (Table S6, Entry 3 and 4). Taking these facts into account, the reaction was carried out following the procedure A. 25 mM suspension of **1a** was allowed to react with 2.5 mM of **2a** in 100 mM PB (10 vol% DMSO-*d*6) at 37 °C for 48 h. After the completion, APCI-MS analysis shows the formation of a trace amount of product (Fig. S31).

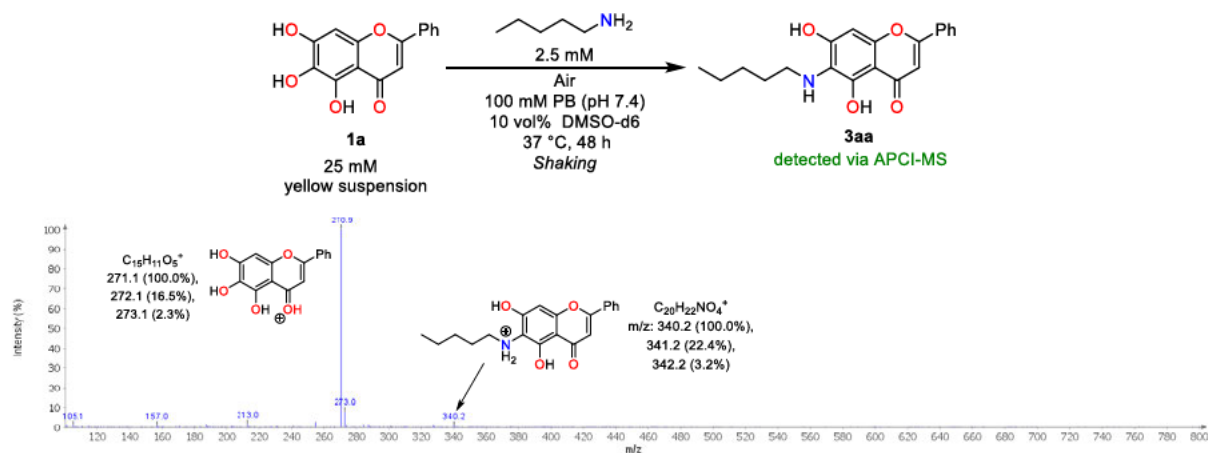


Fig. S31. APCI MS of **1a/2a** oxidative coupling in 100 mM PB, 37 °C, 48 h.

On the other hand, it has been found that the addition of pentylamine salts does not cause any pH changes (Table S6, Entries 8-10).

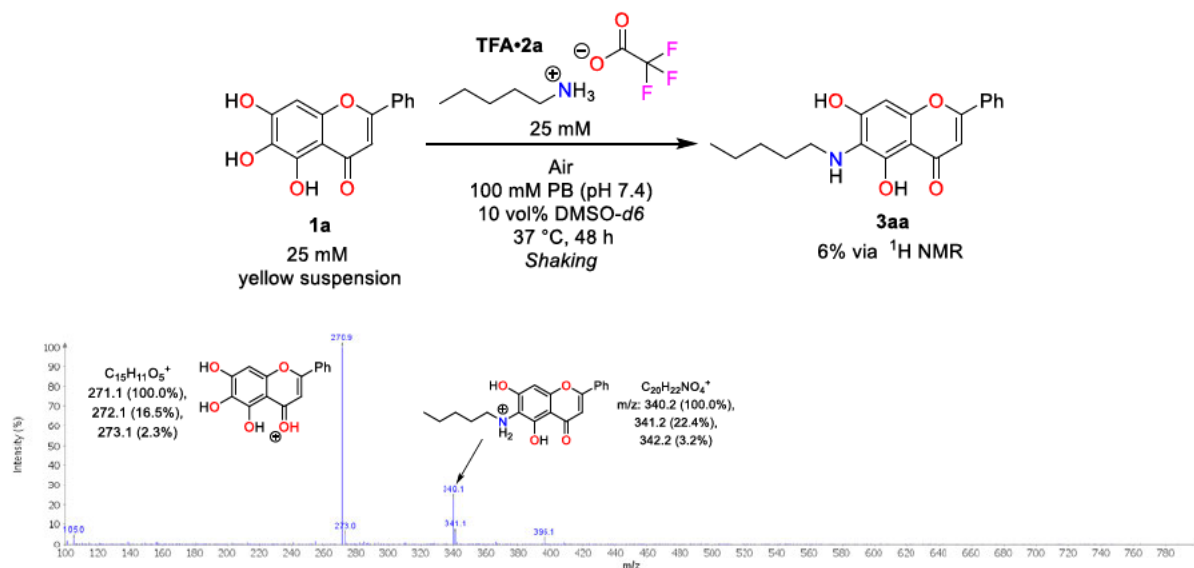
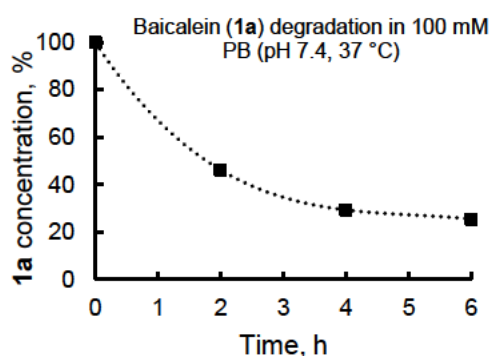


Fig. S32. APCI MS of **1a/TFA·2a** oxidative coupling in 100 mM PB, 37 °C, 48 h.

Additionally, as it was mentioned before, commercially available amino acids are typically present in the form of salts of inorganic (HCl) and organic acids (TFA) as obtained by deprotecting the respective BOC derivative, under acidic conditions. Therefore, the same reaction has been repeated using **Acid**×**2a** instead of free **2a**. A 25 mM suspension of **1a** was allowed to react with 25 mM of **2a** in 100 mM **PB** (10 vol% DMSO-*d6*) at 37 °C for 48 h. After the completion, APCI-MS analysis shows the formation of a higher amount of the product (6% via ¹H NMR) (Fig. S32).

Since **1a** shows limited solubility in aqueous media, it was decided to lower the starting concentration from 25 mM to 2.5 mM (maximum solubility). First, possible **1a** degradation products were checked. 2.5 mM solution of **1a** was shaken in 100 mM **PB** (10 vol% DMSO-*d6*) at 37 °C and its concentration was checked, using chrysin as an IS.



It was found that ~70% of **1a** is degraded within first 4 h under these conditions (Fig. S33). It has been shown, that **1a** exhibits relatively low stability under basic conditions: the $\tau_{1/2}[\mathbf{1a}] = 0.53$ h at pH 7.4 and $T = 40^\circ\text{C}$.^[6]

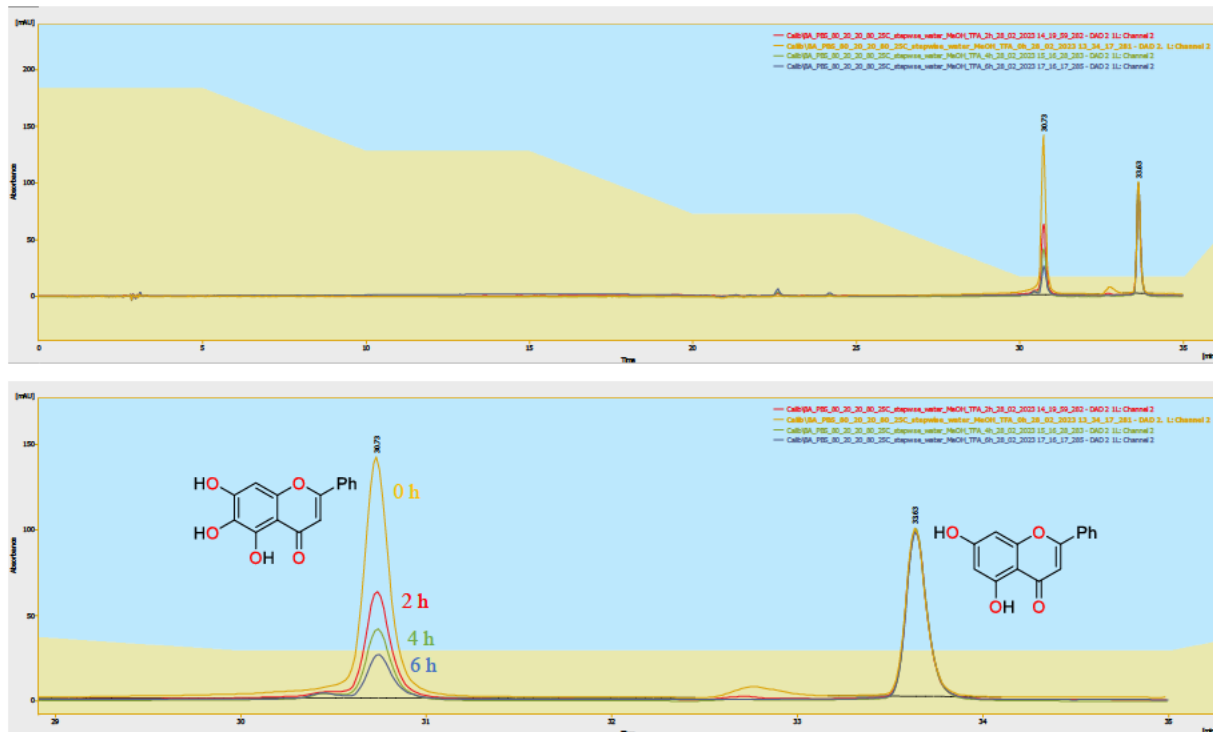


Fig. S33. HPLC-UV spectra of **1a** degradation in 100 mM phosphate buffer (pH 7.4, 37 °C) over 6 hours.

2.5 mM solution of **1a** was allowed to react with a 2.5 mM of **HCl**×**2ag'** in 10 mM PB (10 vol% DMSO-*d6*) at 37 °C for 4 h. The formation of covalent adduct of **1a** and lysine derivative **HCl**×**2ag'** was detected via HPLC-UV-ESI(MS) (Fig. S34). 50 µl of 0.05M solution of **HCl**×**2ag'** in DMSO-*d6* was added to 1 ml of freshly prepared 10 mM sodium phosphate buffer in 2 ml Eppendorf tube and mixed. 50 µl of 0.05M solution of baicalein **1a** in DMSO-*d6* was added to the resulting solution, the Eppendorf tube was closed and incubated at 37 °C while being shaken at 800 RPM. The reaction was quenched by adding 300 µL of cold methanol/0.5 M hydrochloric acid (10:1, v/v)^[6], 50 µl of 0.05M solution of daidzein in DMSO-*d6* was added as an IS and the resulting mixture was passed through a 0.2 µm syringe filter. For the analysis, AZURA® HPLC Plus HPG/LPG with a DAD 2.1L detector was coupled with the Advion MS (positive ESI mode). An aliquot of 25 µL was injected and chromatographic separation was performed on a Knauer C18 column (5 µm, 4.6×250 mm ID) at 25 °C. The detection wavelength was 320 nm. The mobile phase consists of water:0.1% (v/v) TFA and MeOH:0.1% (v/v) TFA. The flow rate was set to 1 ml/min.

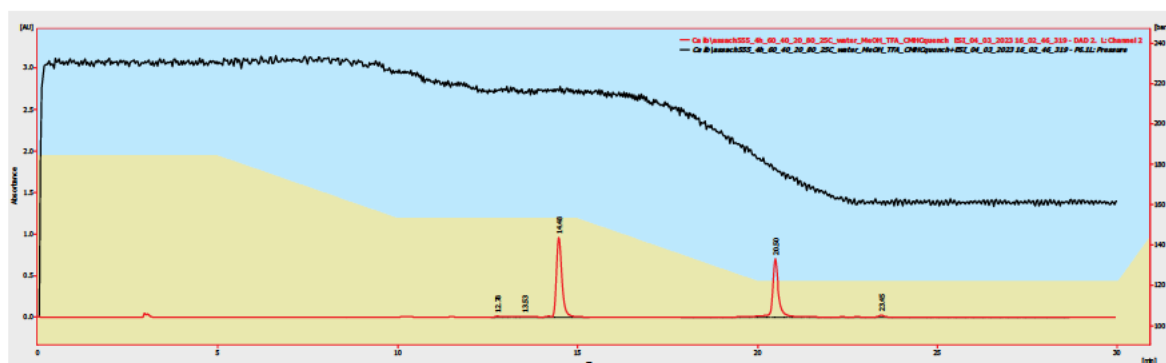
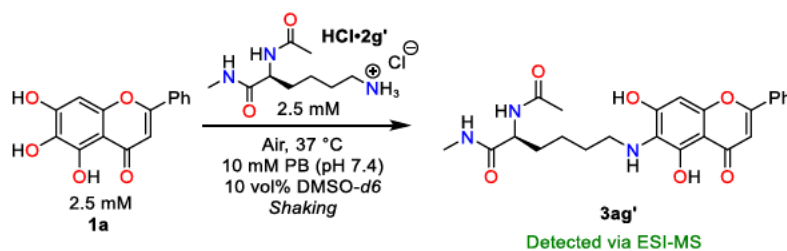
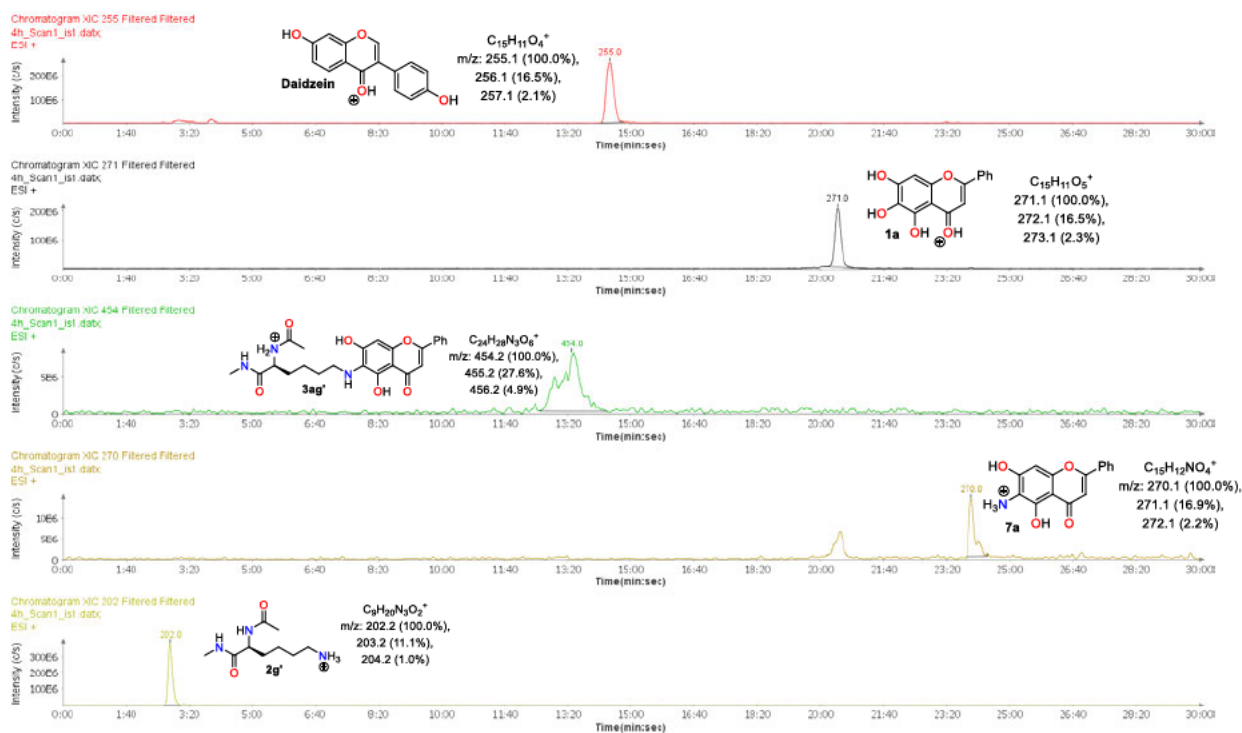
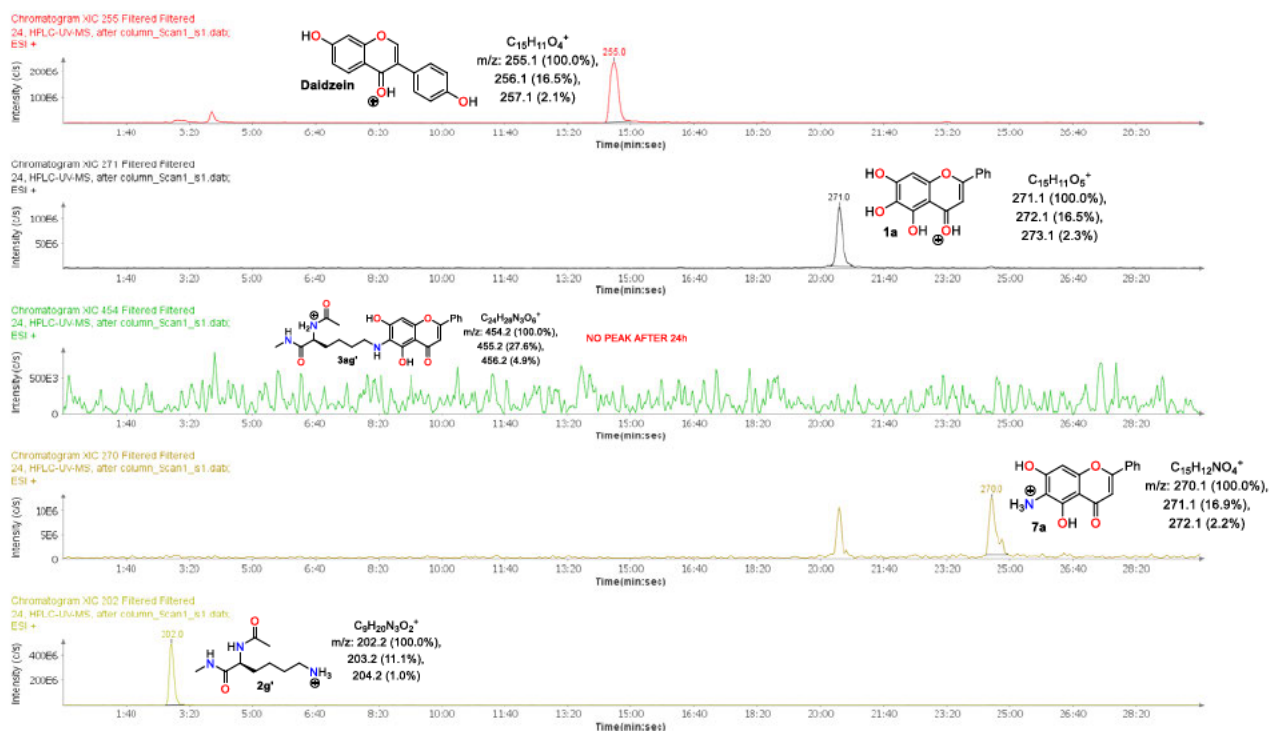


Fig. S34a. HPLC-UV analysis of **1a**/**2g'** reaction in 10 mM Phosphate buffer (pH 7.4).

a) ESI-MS profile of the reaction of **1a** with **2g'** after 4 h.



b) ESI-MS profile of the reaction of **1a** with **2g'** after 24 h (no **3ag'** is detected)



c) Independent synthesis of **3ag'** (**7a** is detected as the product of oxidative hydrolysis)

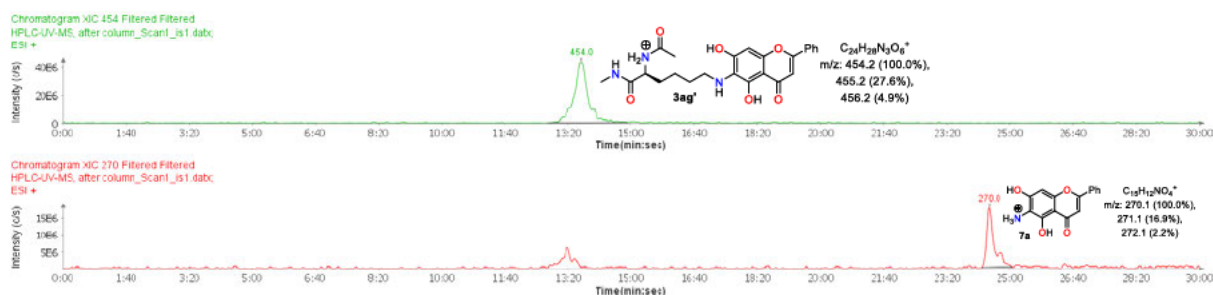


Fig. S34b. HPLC-ESI(MS) detection of **3ag'** in 10 mM Phosphate buffer (pH 7.4).

N α -Boc-Arg-NMe 2h

iAPP also contains the reactive arginine residue (Arg11)^[2], so it was decided to test if there is a covalent interaction between **1a** and arginine derivatives, such as N α -Boc-Arg-NMe (**2h**). The reaction was carried out according to the procedure B. No covalent interaction was observed via APCI MS under these conditions (Fig. S35).

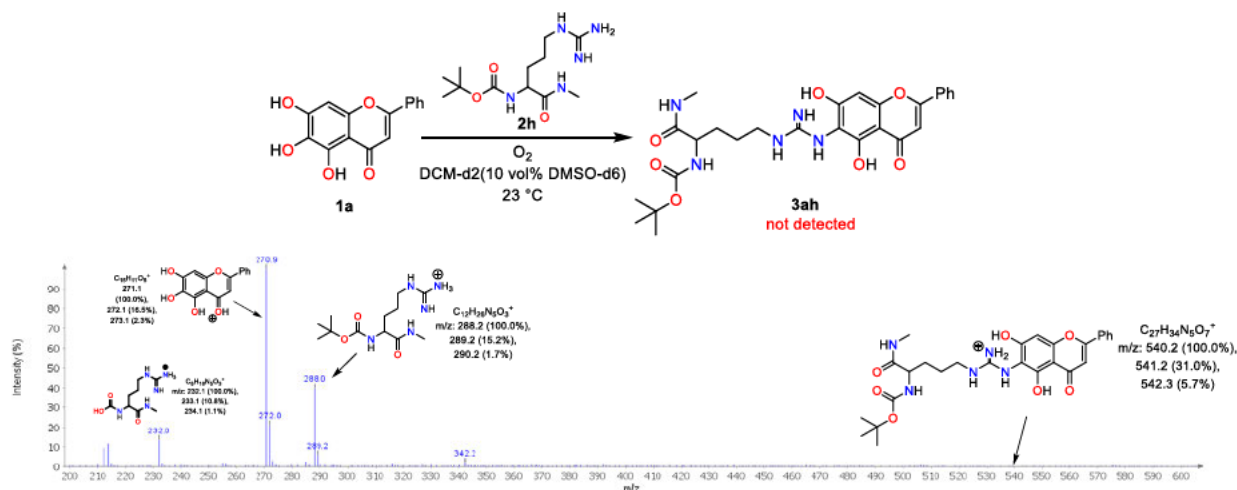


Fig. S35. APCI MS spectrum of **1a/2h** oxidative coupling.

To obtain the coupling product, **1a** was oxidized to **4a** using *o*-Chloranil.^[1] The reaction with crude **4a** was carried out according to the procedure B. No covalent interaction was observed via APCI MS under these conditions (Fig. S36).

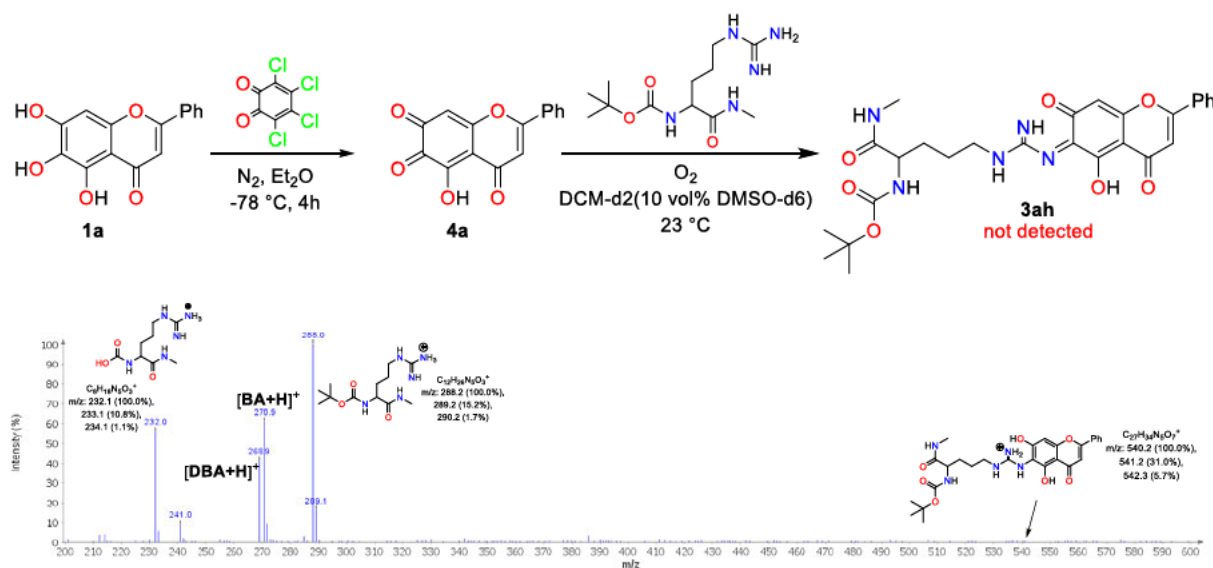
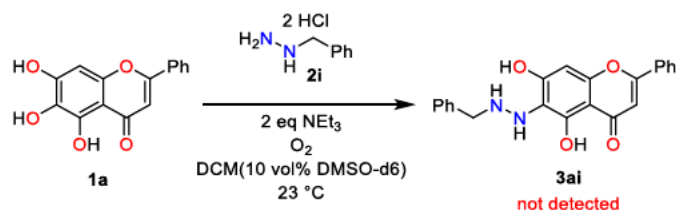


Fig. S36. APCI MS spectrum of 4a/2h oxidative coupling.

Benzylhydrazine (2i)



Benzylhydrazine (2i) was employed to examine additional *N*-nucleophiles. The reaction was performed according to the procedure B with minor changes. Due to the presence of 2i in the form of dihydrochloride, 2 eq of NEt_3 was added as a deprotonating agent. The reaction was monitored via ^1H NMR and APCI MS analysis, showing no product formation (Fig. S37 and S38).

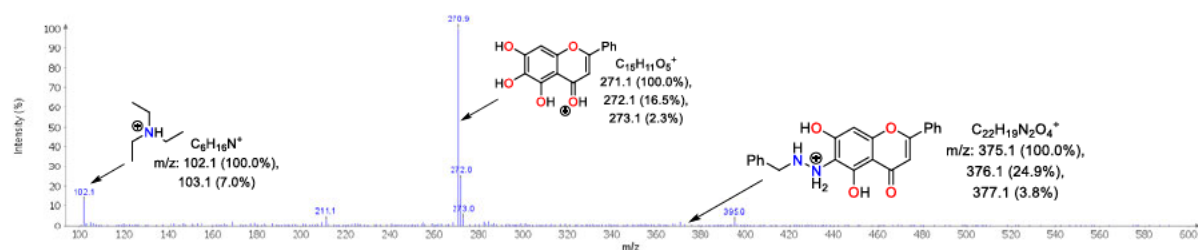


Fig. S37. APCI MS of the crude 1a/2i coupling reaction.

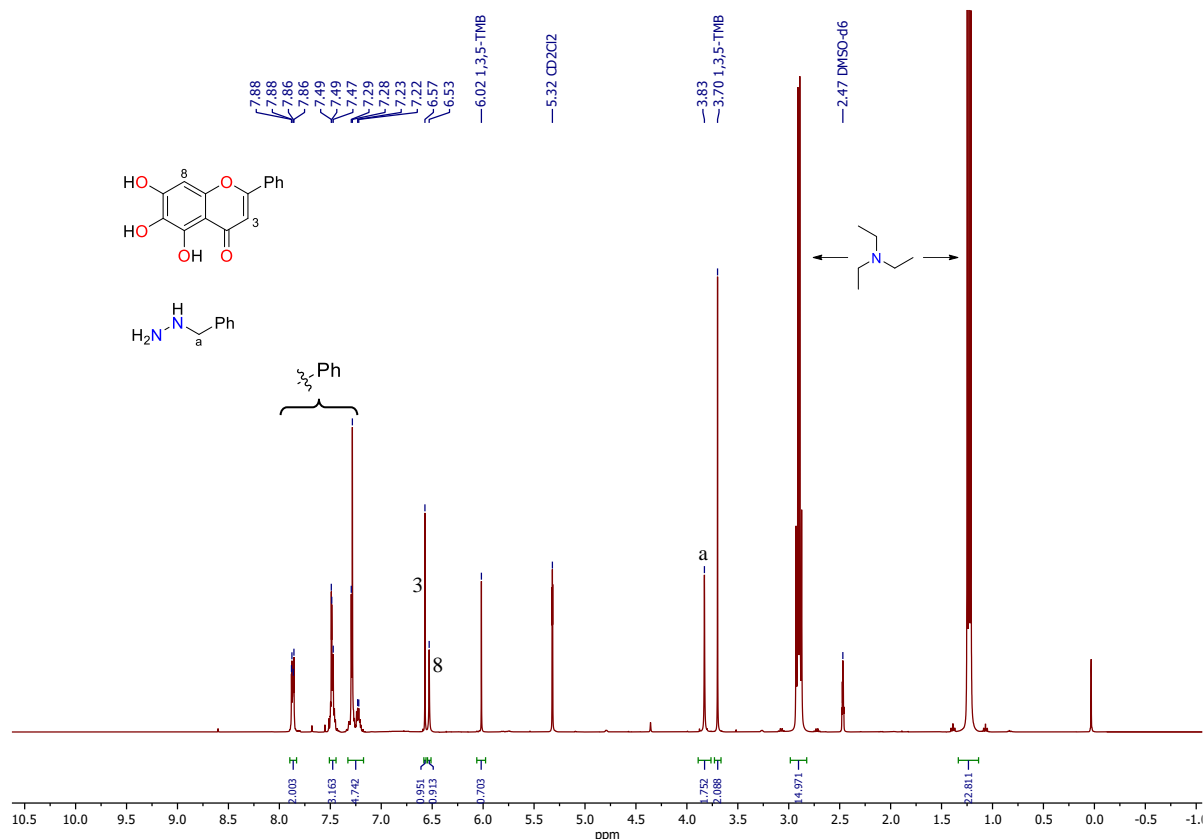
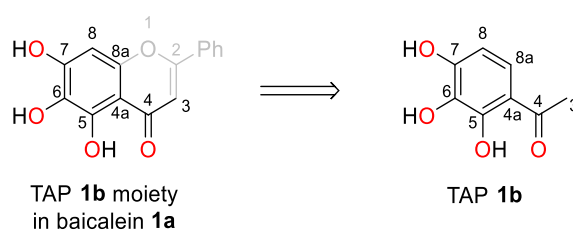


Fig. S38. *in situ* ^1H NMR spectra of **1a/2i** coupling reaction, $\text{DCM-}d_2/\text{DMSO-}d_6$, 400 MHz.

1.3.7.6. Oxidative coupling of pentylamine **2a** with various polyphenols

2,3,4-Tryhydroxyacetophenone (TAP, **1b**)

The reasoning behind the substrate selection is that 2,3,4-trihydroxyacetophenone (TAP) shares structural similarities with **1a** (Scheme S5)



Scheme S5. TAP (**1b**) moiety is present in the baicalein (**1a**) structure.

Amine **2a** was added to a shaking suspension of **1b** in dry solvent under O_2 atmosphere (1 atm). The reaction mixture immediately turns yellow (after a short time a yellow precipitate forms in DCM). The reaction was shaken (400 RPM) for 18 h at 23 °C. During this time, the precipitate dissolves and the reaction color changes to orange. A defined amount of the IS 1,3,5-TMB is added, small aliquot is taken in an NMR tube, evaporated at RT, and dissolved in $\text{DMSO-}d_6$ under N_2 atmosphere for further ^1H NMR analysis (for non-deuterated solvents) (Table S7).

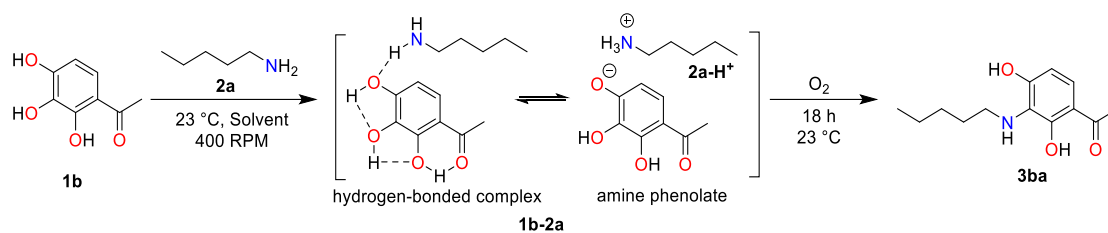


Table S7. Optimization of the **1b-2a** oxidation process^a

№	Solvent	1b , M	2a , eq	3ba , %
1	DCM	0.083	0.50	24
2	DCM	0.083	0.75	72
3	DCM	0.083	1.00	(63)
4	DCM	0.083	1.33	84(80)
5	DCM	0.083	1.75	86
6	DCM	0.025	1.33	88
7 ^b	DCM	0.025	1.33	26
8	DCM	0.025	2.00	>99
9	MeOH-d ₄	0.083	1.33	51
10	MeOH-d ₄	0.083	2.00	50

^a The yield was determined by ¹H NMR analysis of the crude reaction mixture using 1,3,5-trimethoxybenzene as an IS. Isolated yields are presented in brackets. ^b Air was used instead of O₂.

Increasing the **2a** equivalents to 1.33 gave 84% yield. The crude product was purified by column chromatography on silica gel. The pure product was obtained as a pale-yellow solid (95 mg, 80%). Single crystal X-ray analysis showed that product is the C6-functioniled **3ba**.

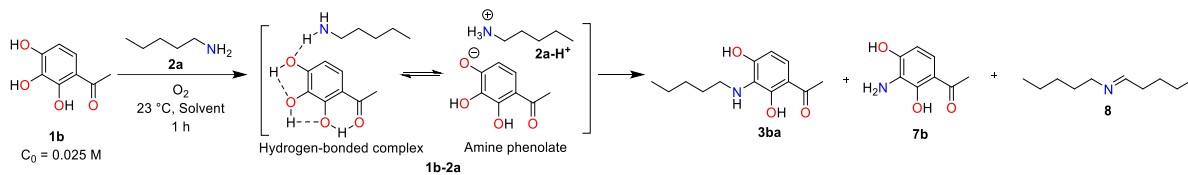
To find out, whereas the yield is affected through the evaporation, the 2 experiments were performed. The reaction 5 (Table S8) was repeated on a larger scale, using DCM/DMSO-*d*₆ = 10/1 solvent system (Procedure A). Shaking continued for 1 hour, 1,3,5-TMB was added, and then 2 × 0.5 ml aliquots were taken:

A) The first aliquot was evaporated under reduced pressure, diluted with 0.75 ml of DMSO-*d*₆ and ¹H NMR analysis was performed. ω(**3ba**) = 42%, what corresponds to the result obtained in the Table S8 (Entry 5).

B) 100 μl of 0.250 M TFA solution were added to the second aliquot to quench free **2a** in the solution. Then all volatiles were evaporated under reduced pressure, diluted with 0.75 ml of DMSO-*d*₆ and ¹H NMR analysis was performed. ω(**3ba**) = 40%

These experiments (**A** and **B**) showed that no accelerated reaction occurs during evaporation process.

Table S8. Optimization table of **1b/2a** oxidation reaction^a



No	Solvent	2a , eq	Comment	2a-H⁺ , %	1b , %	3b , %	7b , %	8 , %
1	DCM	3.00	Air	-	97	4	2	-
2		3.00		-	77	27	2	-
3	DCM- <i>d</i> ₂ ^b	0.20		86	95	6	3	7
4		0.50		51	82	27	7	15
5				40	49	42	7	13
6		Mixing		38	47	45	8	15
7		1 eq tBuNH ₂		-	7	75	11	-
8		1 eq NEt ₃		51	56	30	11	20
9		0.1 eq DBU		-	17	70	14	-
10		0.1 eq 1c		43	49	42	7	13
11		0.1 eq 4-Methyl <i>o</i> -catechol		53	57	35	6	11
12		1 eq of 1f		57	65	34	2	4
13		1.15		34	39	52	8	14
14		1.33		39	36	56	8	12
15		1.75		38	10	75	10	11
16		2.00		43	11	80	10	10
10	Air		50	19	76	9	9	
17	3.00		64	n.d.	88	11	9	
18	5.00		-	n.d.	88	12	7	
19	CDCl ₃ ^b	1.00		68	71	26	3	7
20	DMSO- <i>d</i> ₆	1.00		-	41	6	32	48
21		1.00	Air	-	45	7	32	51
22		1.00	15 min	-	45	6.5	32	-
23		2.00		-	-	10	69	52

a) The yield was determined by ¹H NMR analysis of the crude reaction mixture using 1,3,5-trimethoxybenzene as an IS. b) 10 vol% DMSO-*d*₆.

It was shown that that yield of **3ba** reached its maximum at 2 eq of added **2a** (Fig. S39).

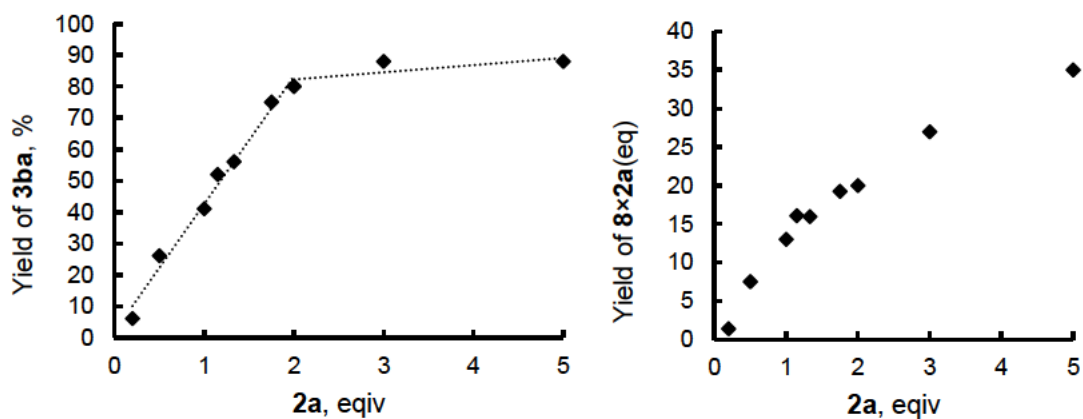


Fig. S39. Yield of **3ba** (left) and yield of **8** (right) as a function of added amounts of **2a** in DCM-*d*₂/DMSO-*d*₆ = 10/1.

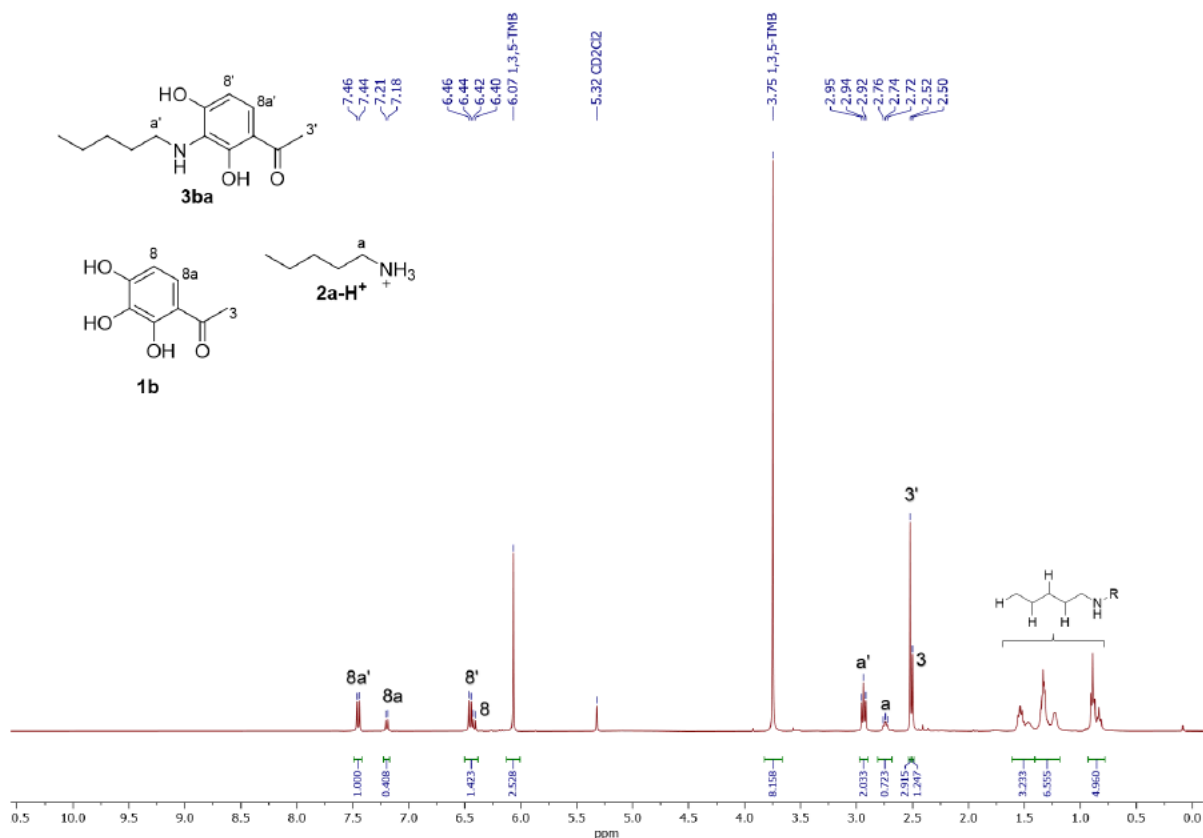


Fig. S40. *in situ* ¹H NMR spectrum of **1b/2a** oxidative coupling (Table S7, Entry 2), DCM-*d*₂, 400 MHz. No **7b** formation is detected.

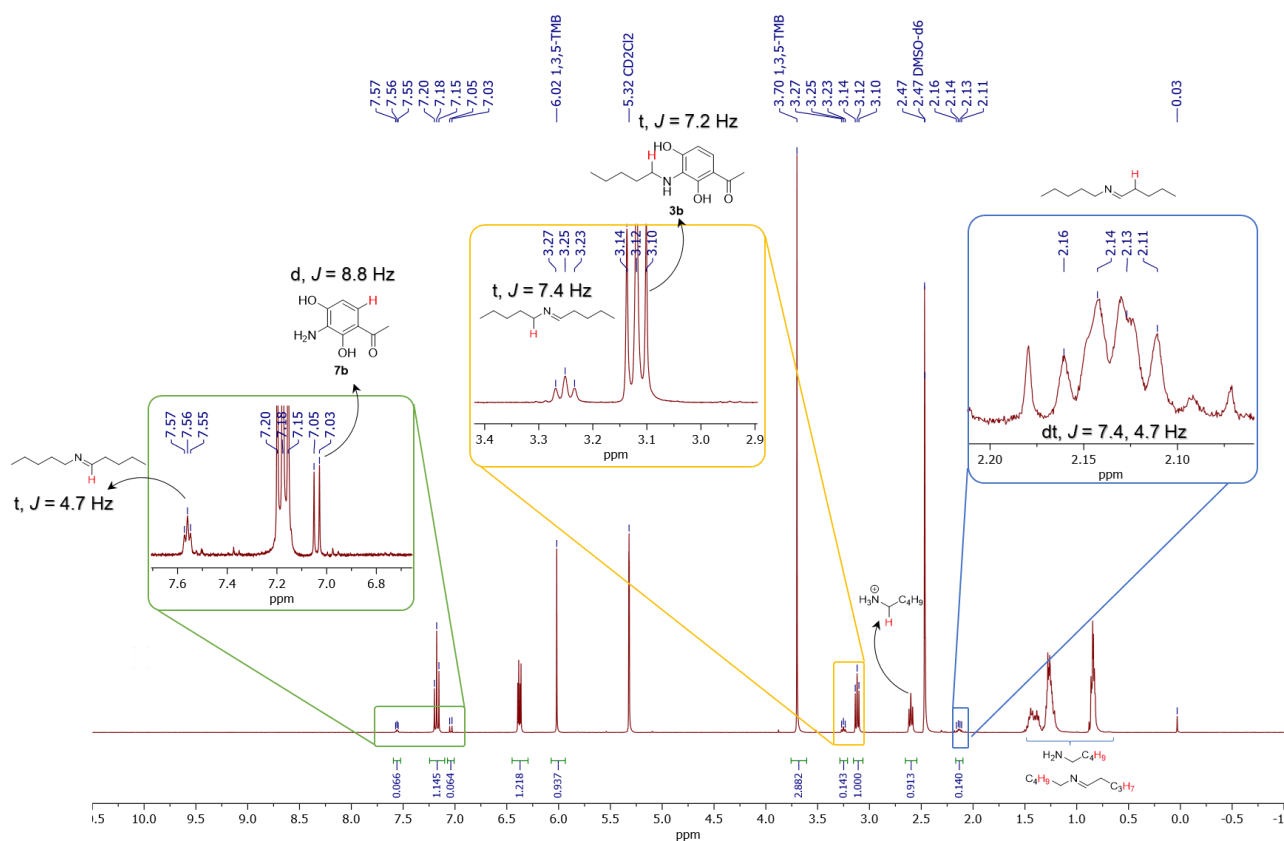


Fig. S41. *in situ* ¹H NMR spectrum of **1b/2a** oxidation (Table S8, Entry 5), DCM-*d*₂/DMSO-*d*₆ = 10/1, 400 MHz.

To investigate the possibility of further reaction of the initially formed products, a solution of **3ba** was treated with 1 eq **2a** under O₂ atmosphere in DMSO-*d*₆. It has been demonstrated that the main pathway involves nucleophilic addition to the carbonyl group, resulting in the formation of imine **3ba''** (Fig. S42).

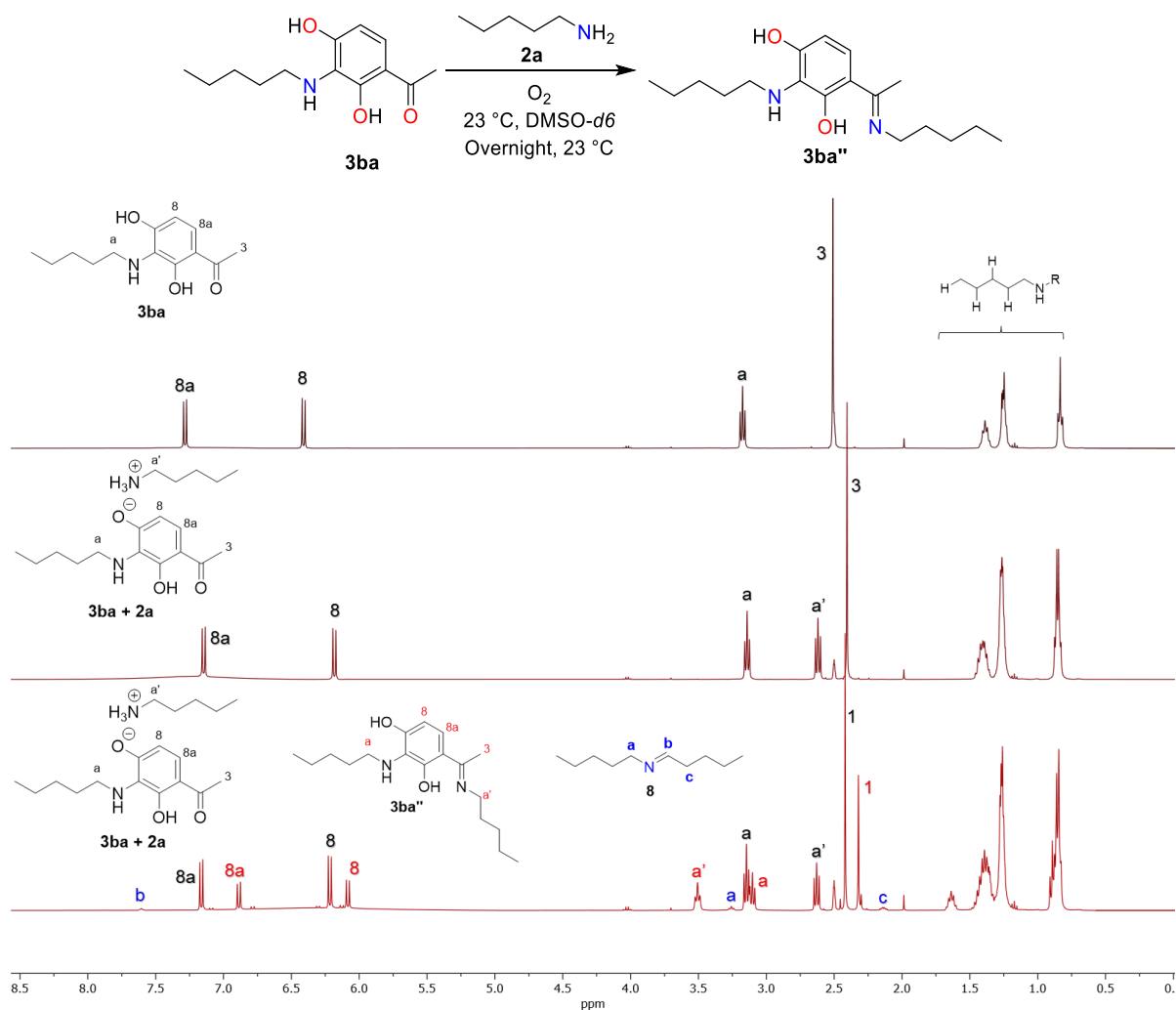


Fig. S42. *in situ* ¹H NMR spectra of the formation of **3ba''** under O₂ at RT, DMSO-*d*₆, 400 MHz.

7b slowly turns into **3ba** (15% conv. in 24 h) when treated with 1 eq of **2a** under O₂ atmosphere through the oxidative transamination reaction (Fig. S43 and S44). The reaction was performed according to the general procedure **B**.

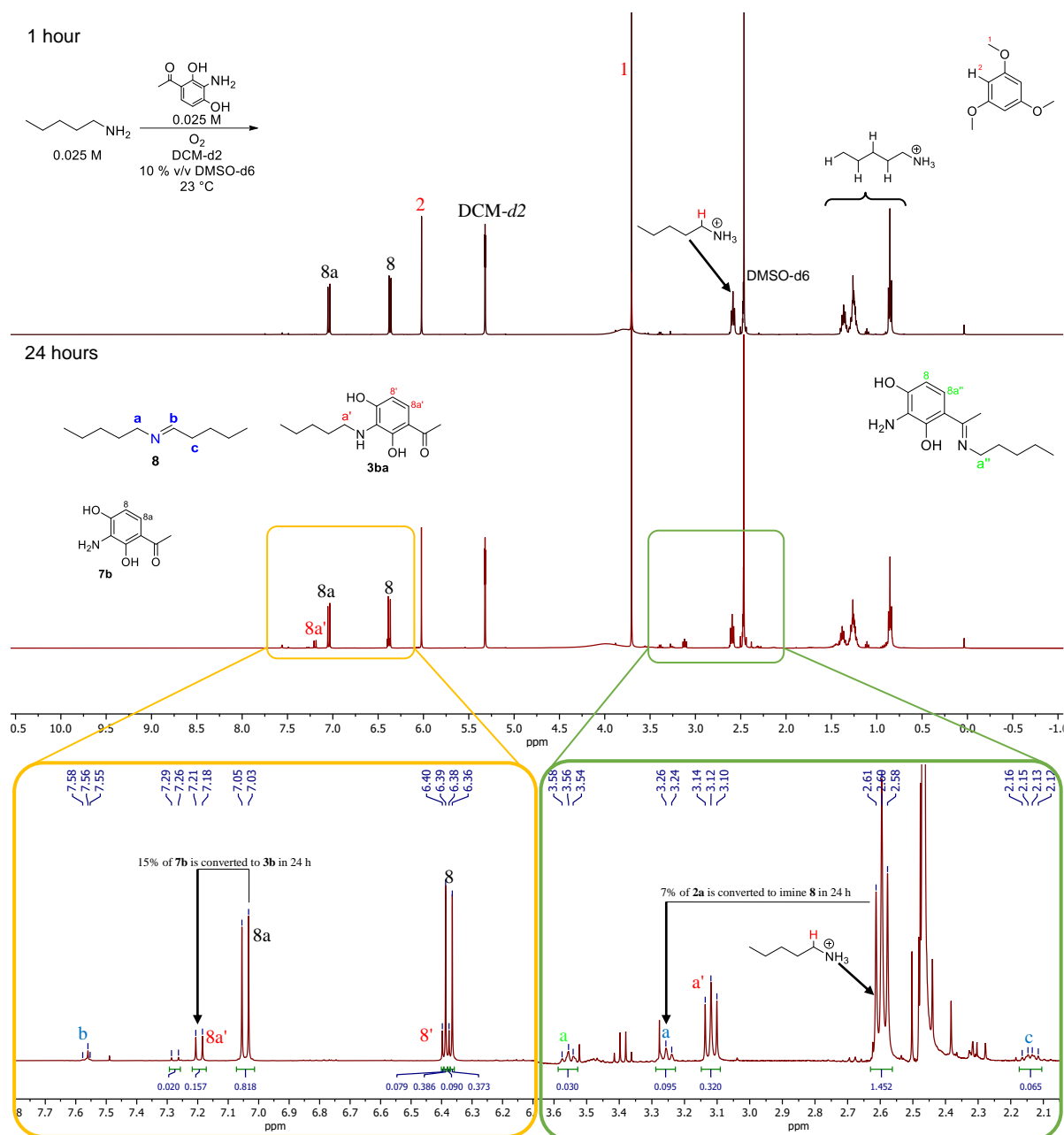


Fig. S43. *in situ* ^1H NMR spectrum of **7b/2a** oxidative coupling after 1 hour (top) and 24 h (bottom), DCM-*d*2/DMSO-*d*6, 400 MHz.

Also, **7b** acts as active species in the process of oxidative deamination of **2a**, leading to formation of imine **8** (52% yield) in DMSO-*d*6. The addition of 1 equivalent of TFA-*d*1 to the reaction mixture helped to quantify the formation of ammonia (NH_3) as the generated byproduct (Fig. S45). Under identical conditions, **3ba** forms equimolar amount of imine **8** (16%) and **7b** (8.5%), through the aminolysis reaction.

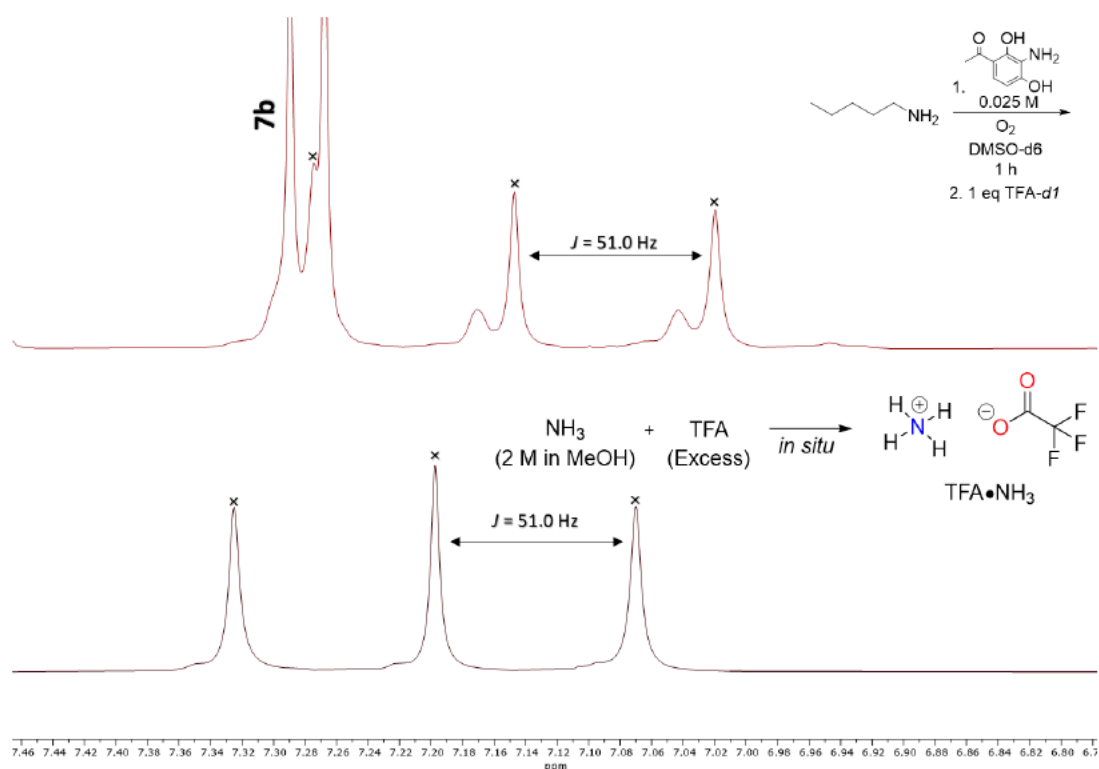


Fig. S45. Detection of NH_3 as a byproduct of **3ba** aminolysis, in form of its TFA salt, DMSO-d_6 , 400 MHz.

The reactivity of C4-imine of TAP, **3ba'**, with **2a** was also investigated. The reaction was performed according to the general procedure A. APCI-MS analysis of the reaction showed the product of the oxidative coupling with **2a** (m/z 307, 20% via ^1H NMR analysis) the product of oxidative aminolysis **3ba'''** (m/z 237). Another major peak at m/z 456 can presumably be attributed to the condensation product of **3ba'''** and **3ba'** (Fig. S46).

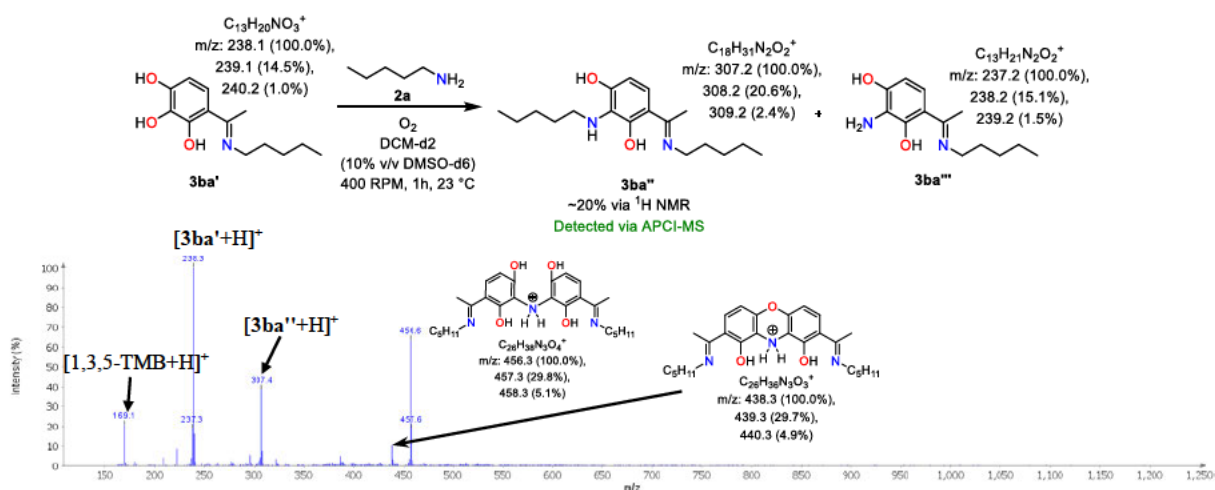


Fig. S46a. APCI-MS spectrum of **3ba'/2a** oxidative coupling.

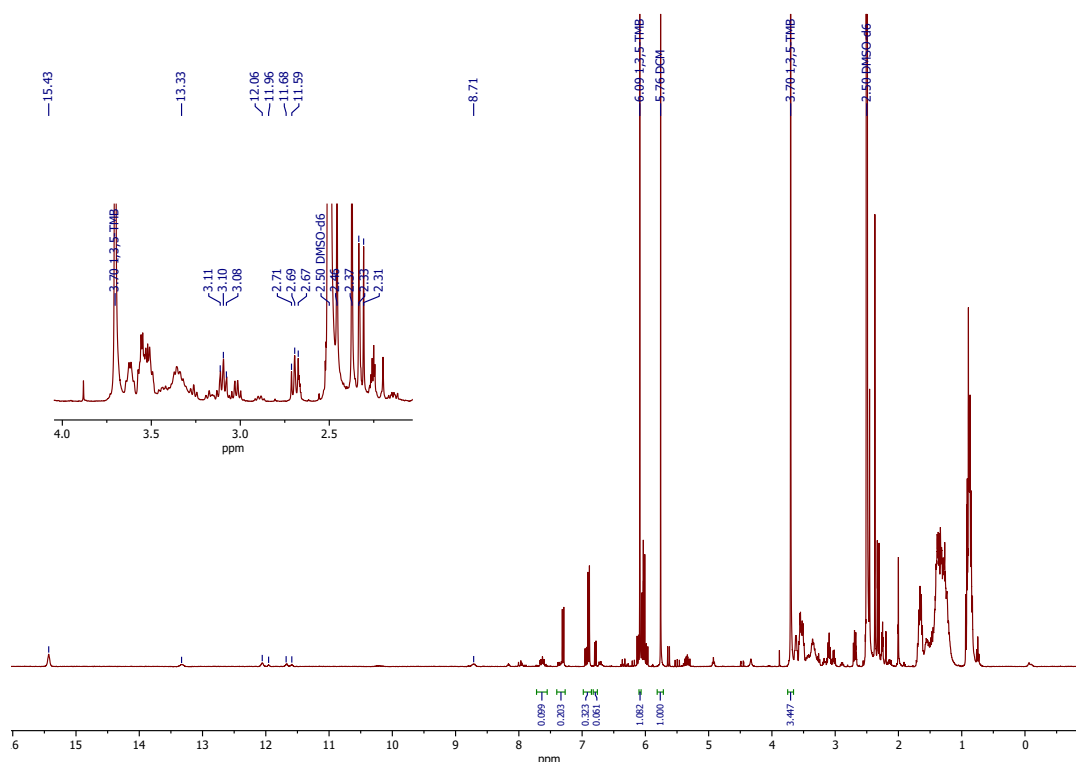


Fig. S46b. *in situ* ^1H NMR spectrum of **3ba'**/**2a** oxidative coupling, DCM-*d*₂/DMSO-*d*₆, 400 MHz.

Considering all the details provided above, it is possible to draw a comprehensive reaction mechanism of the oxidative coupling of pyrogallol-based polyphenol with primary amines (Fig. S47).

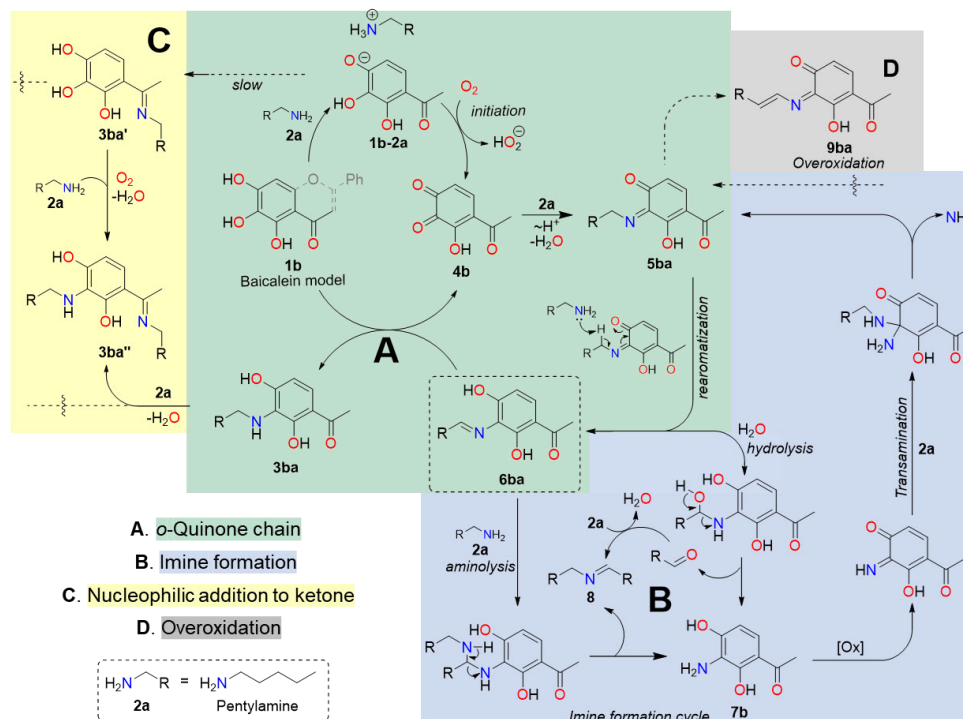
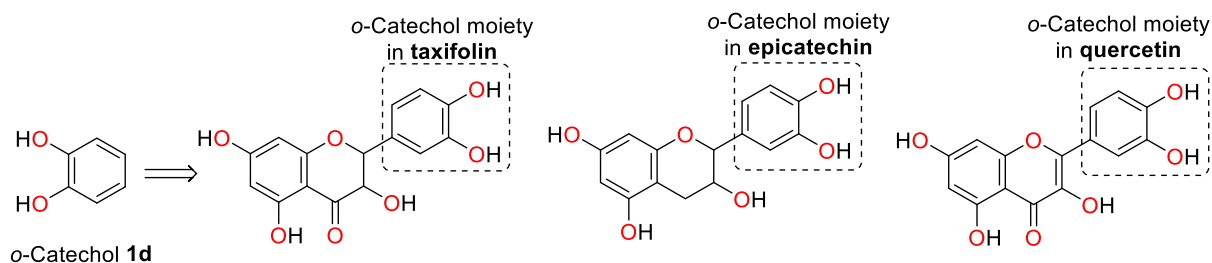


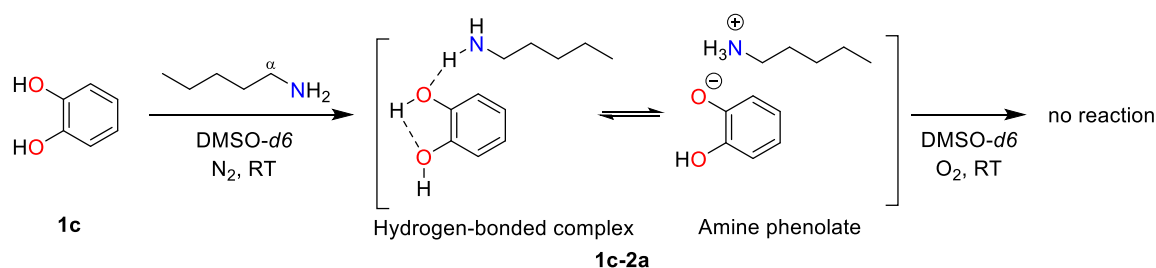
Fig. S47. Proposed mechanism of **1b/2a** reaction under aerobic conditions.

o-Catechol (*o*-Cat, **1c**)

Substrate selection: *o*-Catechol (**1c**) was chosen because the B-ring of several flavonoids is a substituted *o*-catechol moiety (Scheme S6). We found it interesting to examine the reactivity of the unmodified *o*-catechol ring.



Scheme S6. *o*-catechol **1c** moiety is present in the structure of several flavonoids.



10 mg of *o*-catechol (**1c**) (0.091 mmol, 1 eq) in an Young NMR tube was evacuated and refilled with N₂ three times, dissolved in 0.75 ml of dry degassed (3 x freeze-pump-thaw cycles) DMSO-*d*6, followed by addition of ~11 μ l pentylamine (**2a**) (8 mg, 0.092 mmol, 1 eq). No significant shift for α -methylene protons of **2a** was observed in ¹H NMR spectrum. Since the $pK_a(\mathbf{1c}) = 9.34^{[7]}$, it is more likely that the **1c-2a** complex exists as a hydrogen-bounded complex rather than the amine phenolate like **1a-2a** and **1b-2a** complexes, described in our previous work.^[1] The formation of an initial ion pair is the crucial step for following oxidation and coupling reactions of polyphenols with *N*-nucleophiles such as **2a** in our case. The absence of **1c-2a** distinct ion pair led to the hypothesis that **1c** will not react with **2a** under aerobic conditions. The assumption was confirmed replacing N₂ inert atmosphere with O₂ in the J. Young NMR tube. No significant changes were observed even after 5 days at RT, indicating the low activity of **1c** toward **2a** and molecular oxygen (Fig. S48).

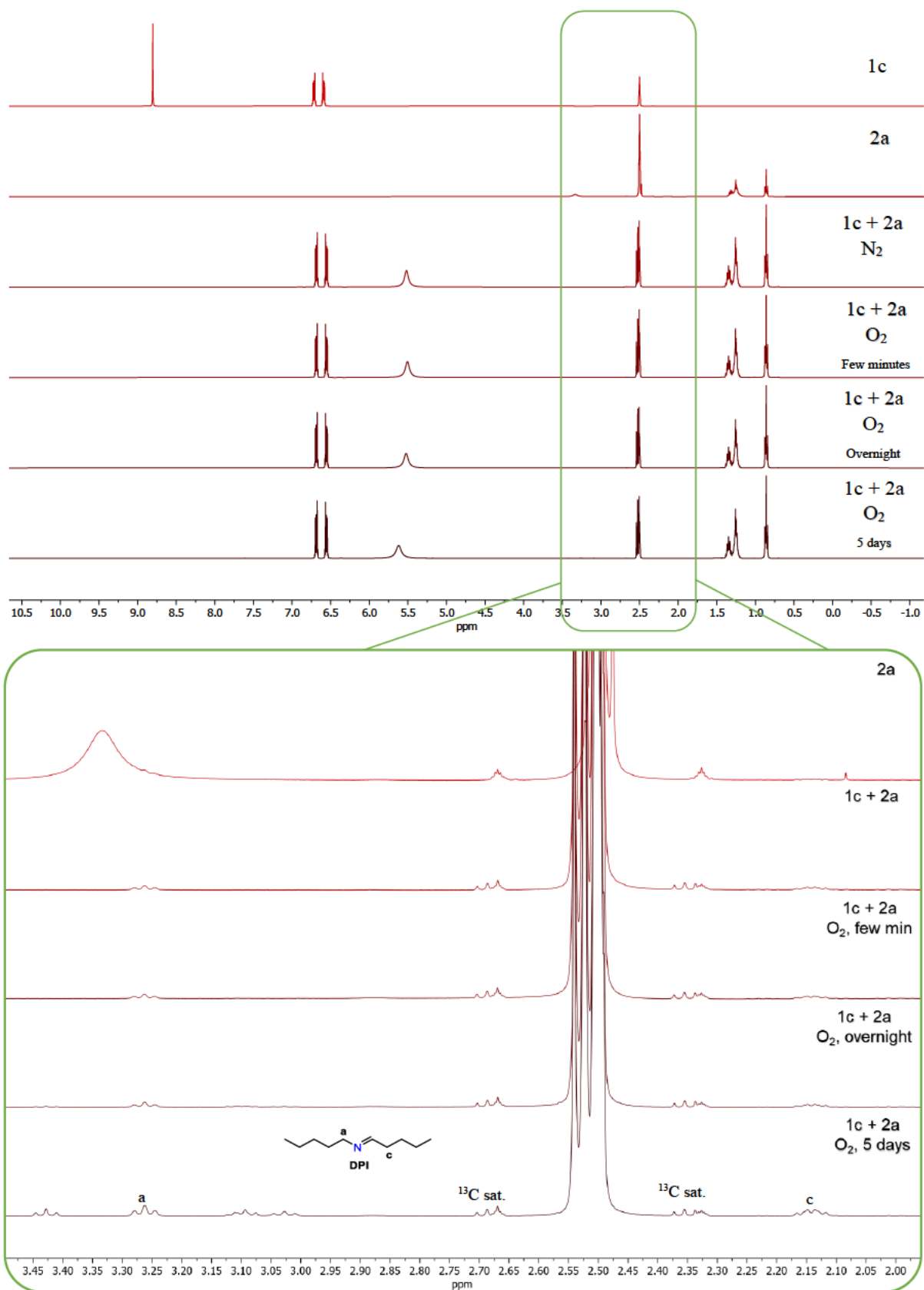
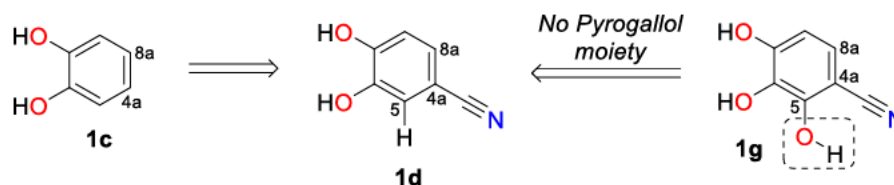


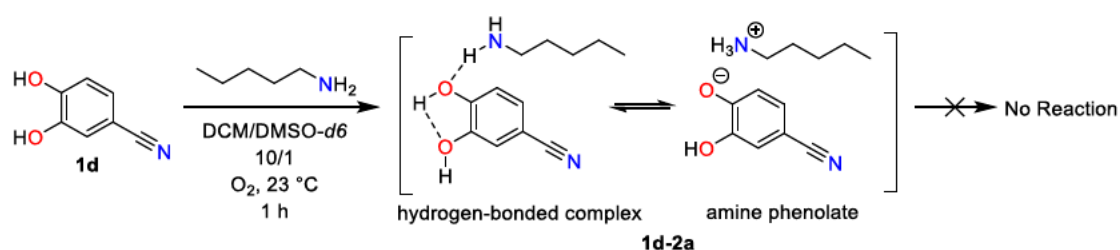
Fig. S48. *in situ* ^1H NMR spectra of **1c-2a** oxidation, DMSO-*d*₆, 400 MHz

6,7-dihydroxybenzonitrile (6,7-DBN, **1d**)

Substrate selection: The effects of EWG at the C4a-position of the catechol moiety were checked in experiments with 6,7-DBN (Scheme S7).



Scheme S7. 6,7-DBN **1d** has the EWG group at 4a-position, and unlike TBD **1g** has no pyrogallol moiety.



The reaction was carried according to procedure B. No reaction was observed between **1e** and amine **2a** under these conditions (Fig. S49), only a trace amount of imine **8** was detected (smaller than ¹³C satellites peaks).

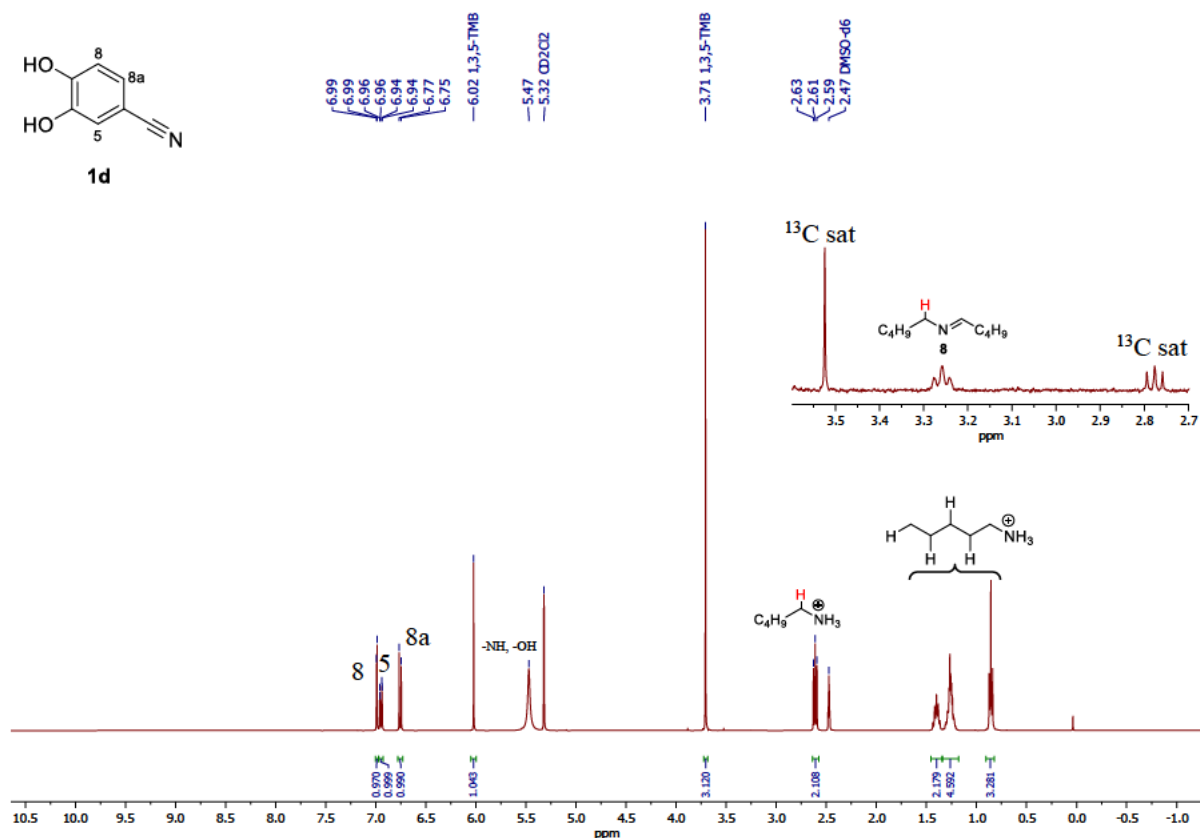
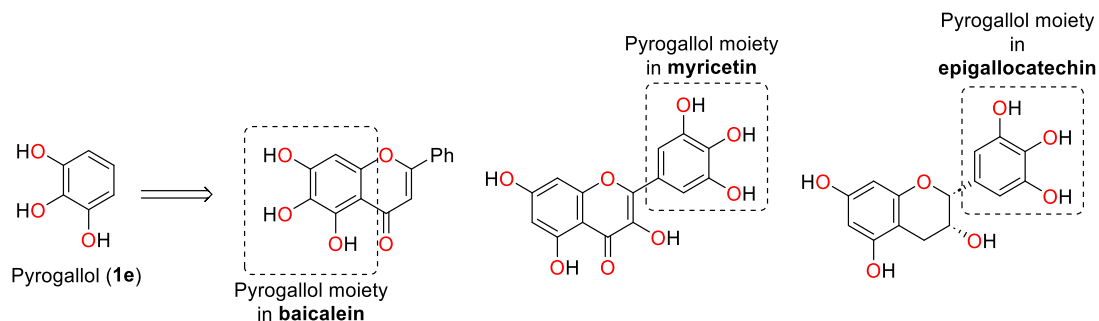


Fig. S49. *in situ* ¹H NMR spectrum of **1d/2a** oxidative coupling, DCM-*d*₂/DMSO-*d*₆, 400 MHz.

Pyrogallol (Pyr, **1e**)

Substrate selection: Pyrogallol (**1e**) was chosen because the A-ring of baicalein and B-ring in myricetin/epicatechin contain pyrogallol substructure (Scheme S8). We found it interesting to examine the reactivity of the unmodified pyrogallol ring.



Scheme S8. The pyrogallol moiety is present in the structure of several flavonoids.

a) DCM

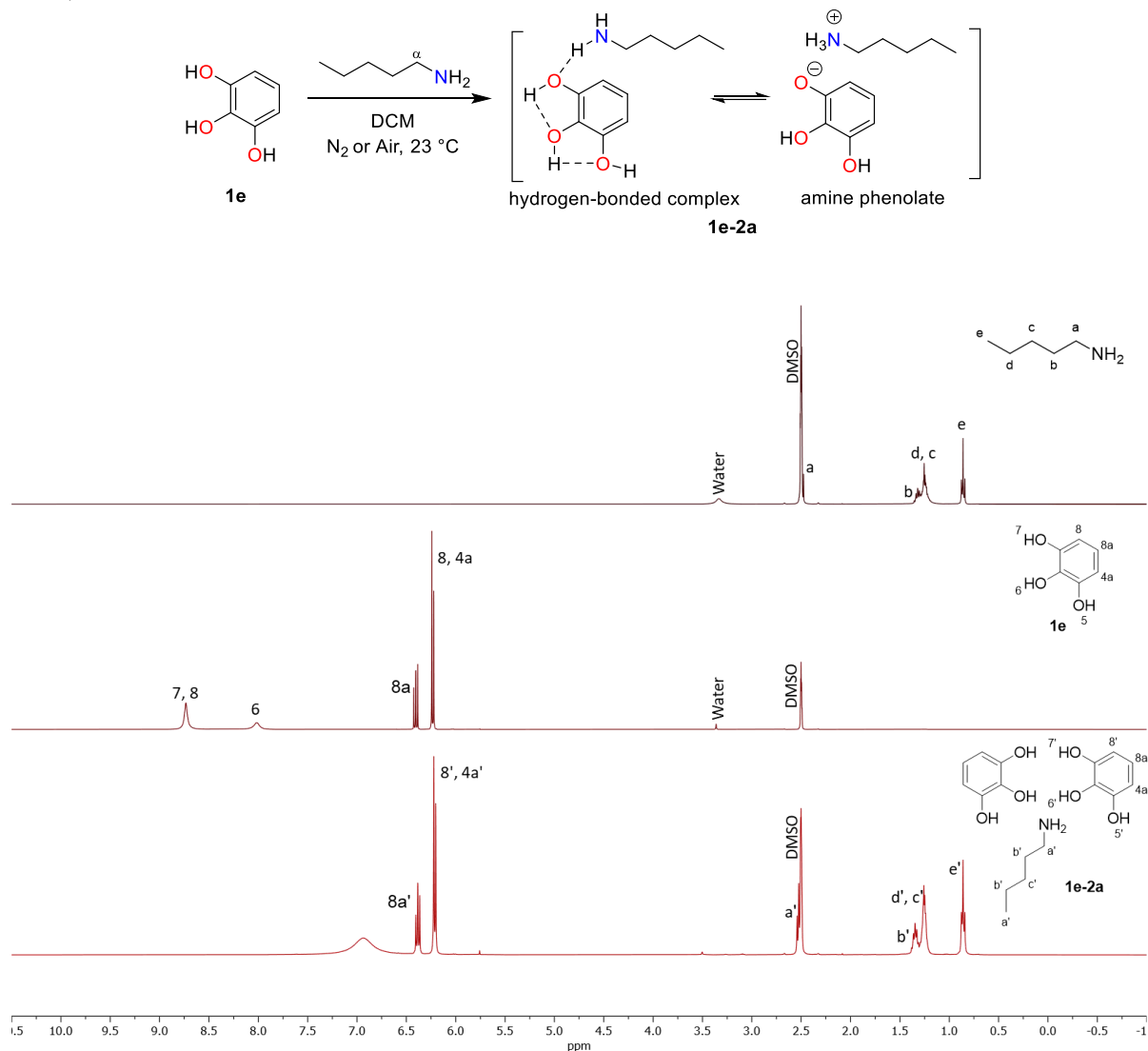


Fig. S50. ¹H NMR spectra of **2a**, **1e** and the obtained white precipitate, DMSO-*d*₆, 400 MHz.

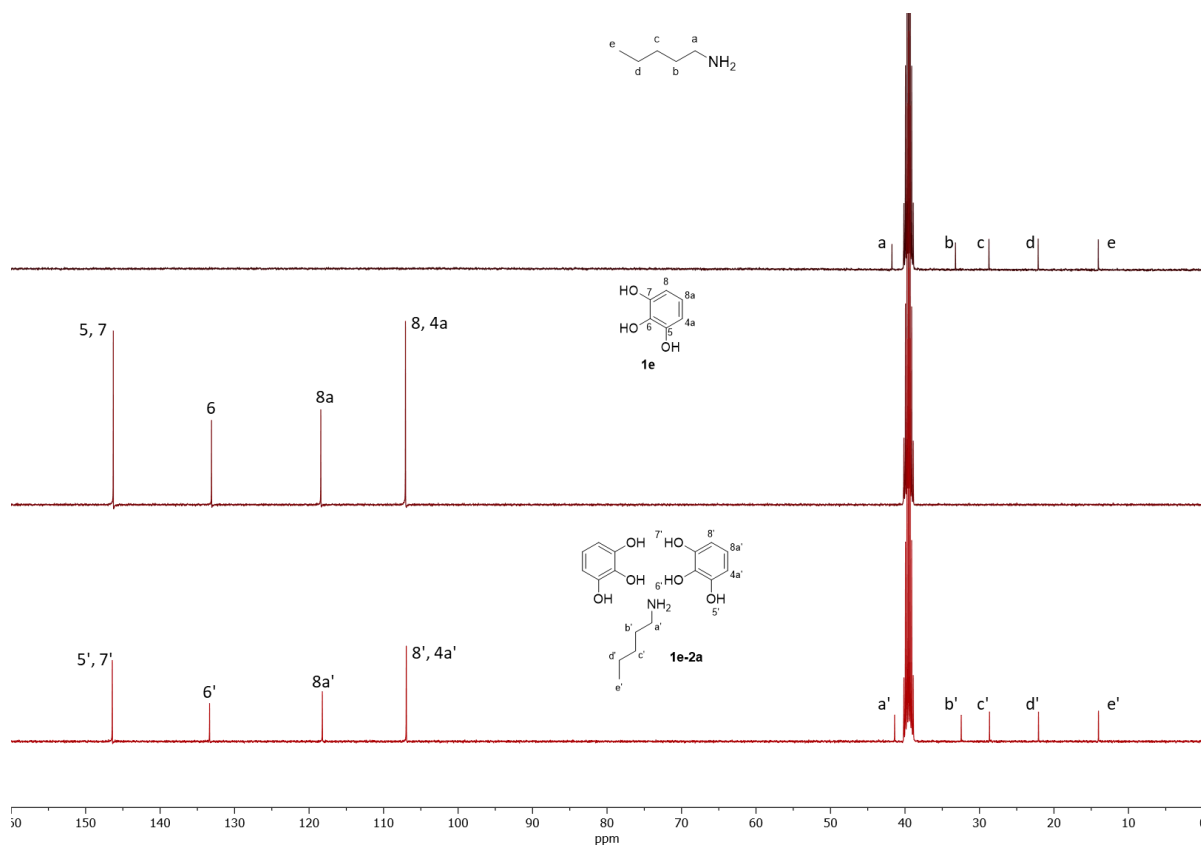
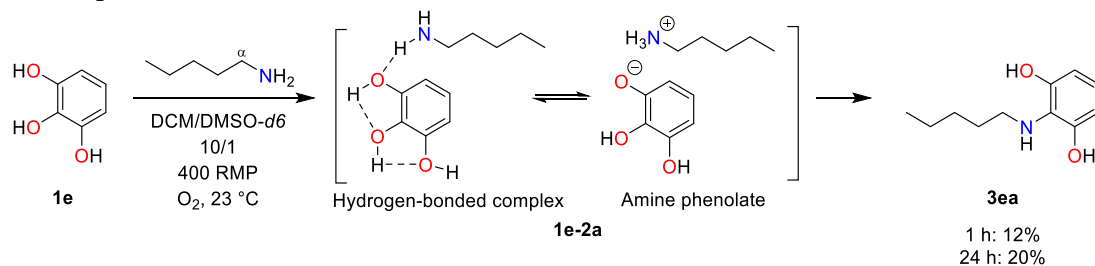


Fig. S51. ^{13}C NMR spectra of **2a**, **1e** and the obtained white precipitate, $\text{DMSO-}d_6$, 101 MHz.

First, the formation of the **1e-2a** ion pair was checked by mixing 60 mg of **1e** (0.48 mmol, 1 eq) with 55 μl of **2a** (43 mg, 0.5 mmol, 1 eq) in 6 ml of dry degassed DCM ($3 \times$ freeze-pump-thaw cycle) under nitrogen atmosphere. The resulting suspension was stirred vigorously and after a short time a white precipitate formed. The reaction was allowed to stir overnight at RT. The precipitate was filtered off (29 mg). ^1H NMR showed that the precipitate consists of two parts of **1e** and one part of **2a** (Fig. S50). ^{13}C NMR spectra showed no new signals as if the precipitate was a mixture of **1e** and **2a** (Fig. S51).

b) DCM (10 vol% $\text{DMSO-}d_6$)

1) 1 eq of **2a**



The reaction was performed according to Procedure A (Fig. S52). It has been shown that yields of **3ea** were 12% and 20% after 1 h and 24 h, correspondingly, using 1,3,5-TMB as an IS (5.9 mg). Also, after 24 h reaction, time the by-product **7e** (~40%), was detected (Fig.

S53). The regioselectivity of the products were proven by independent synthesis of **3ea** and **7e**.

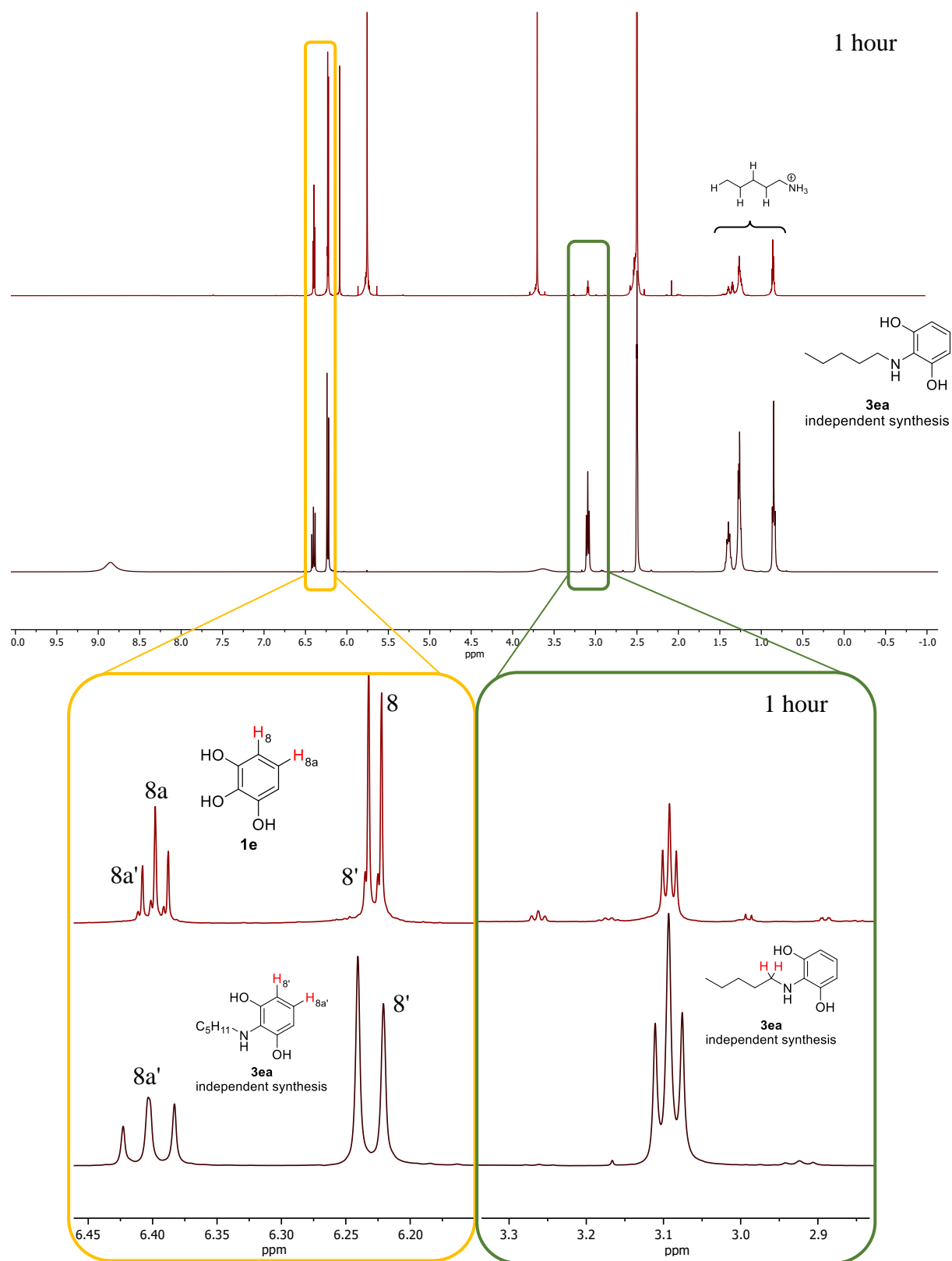


Fig. S52. ¹H NMR spectrum comparison of **1e/2a** oxidative coupling reaction after 1 hour (800 MHz) with independently synthesized **3ea** (400 MHz), DMSO-*d*₆.

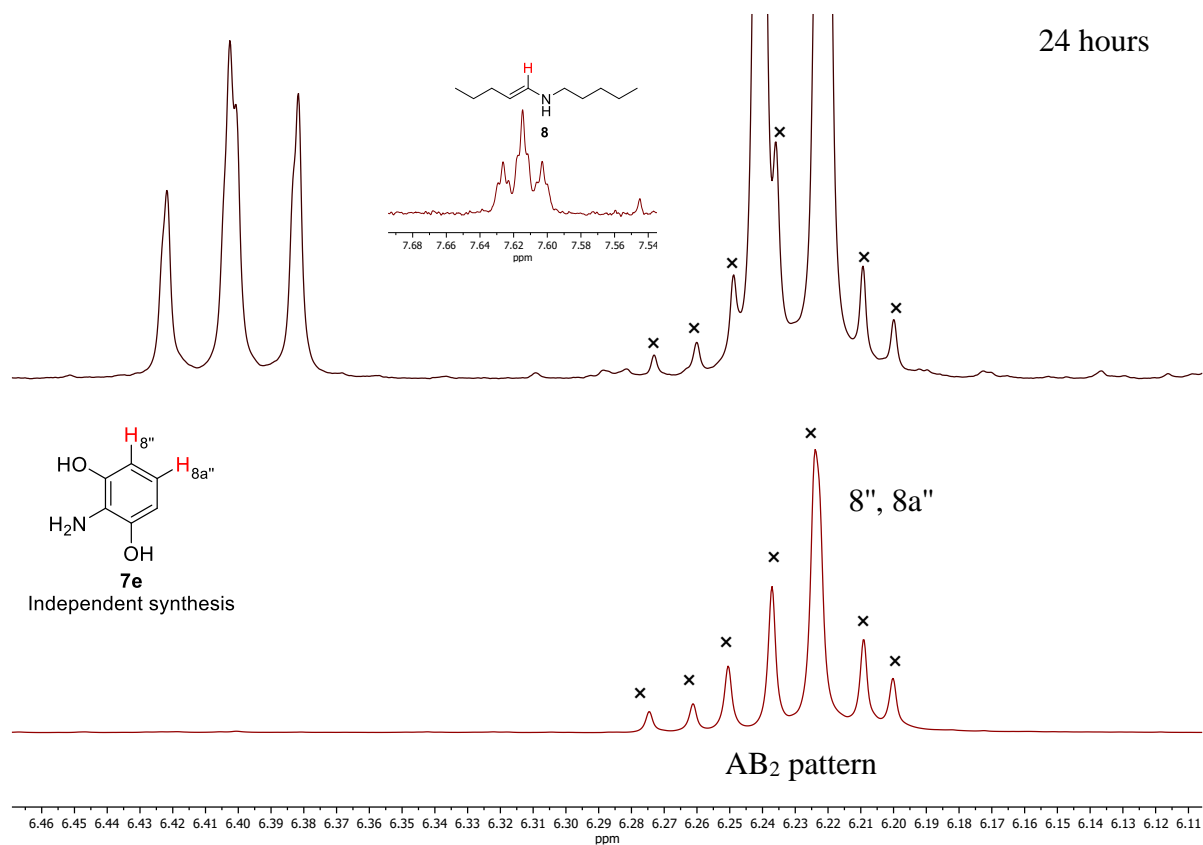
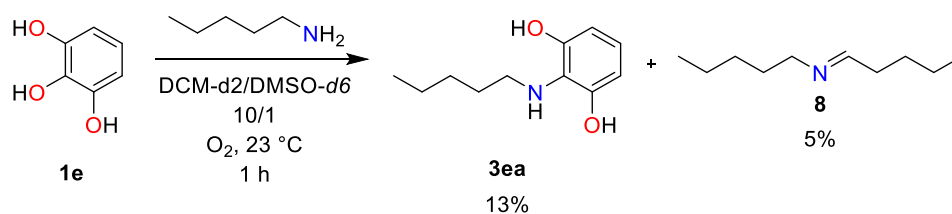


Fig. S53. ¹H NMR spectra comparison of **1e/2a** oxidative coupling reaction after 24 h with independently synthesized **7e**, DMSO-*d*₆, 400 MHz.

a) 1 eq of **2a**, *in situ*



The reaction was performed according to the general procedure B. It has been shown that yields of **3ea** and **8** were 13% and 5%, correspondingly, using 1,3,5-TMB (0.56 mg) as an IS (Fig. S54).

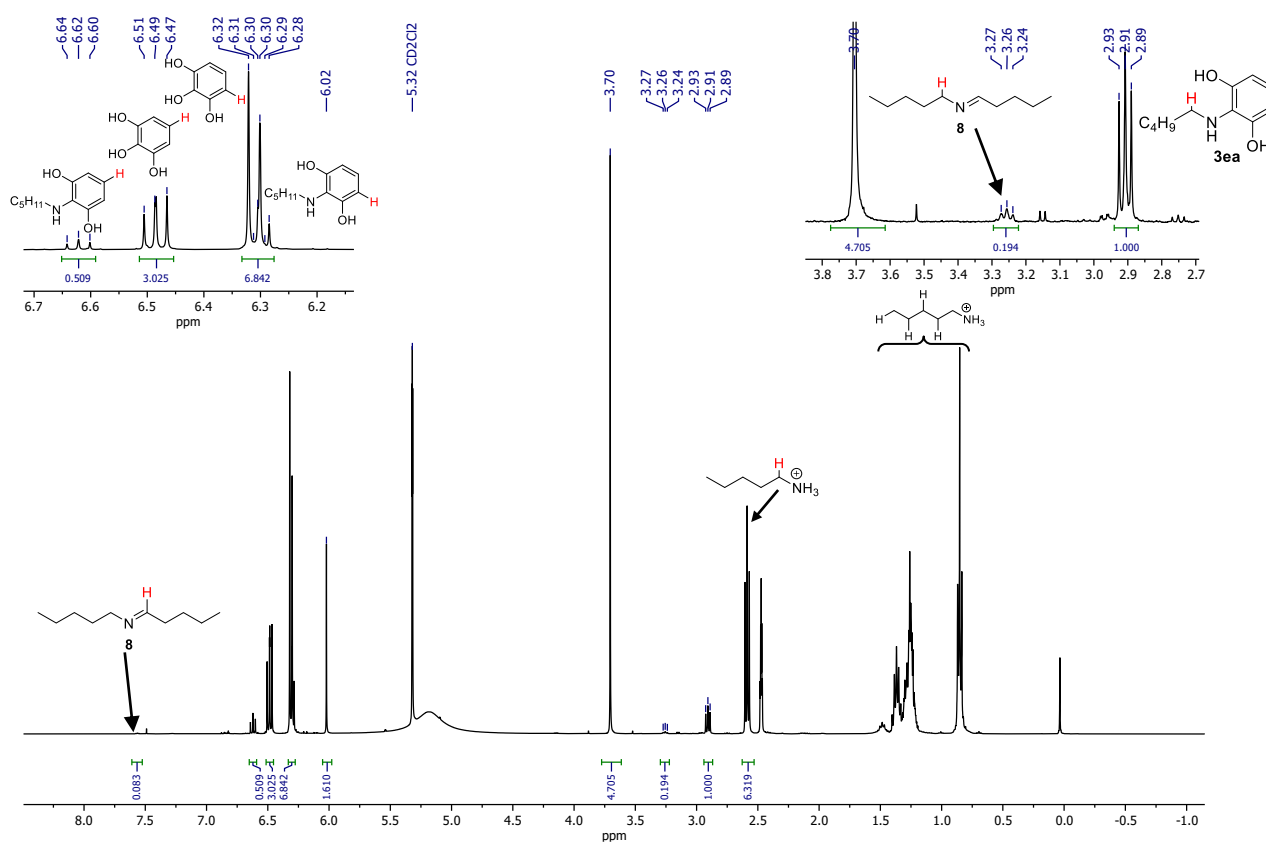


Fig. S54a. *in situ* ¹H NMR spectrum of **1e/2a** oxidative coupling reaction after 1 hour, DCM-d₂/DMSO-d₆, 400 MHz.

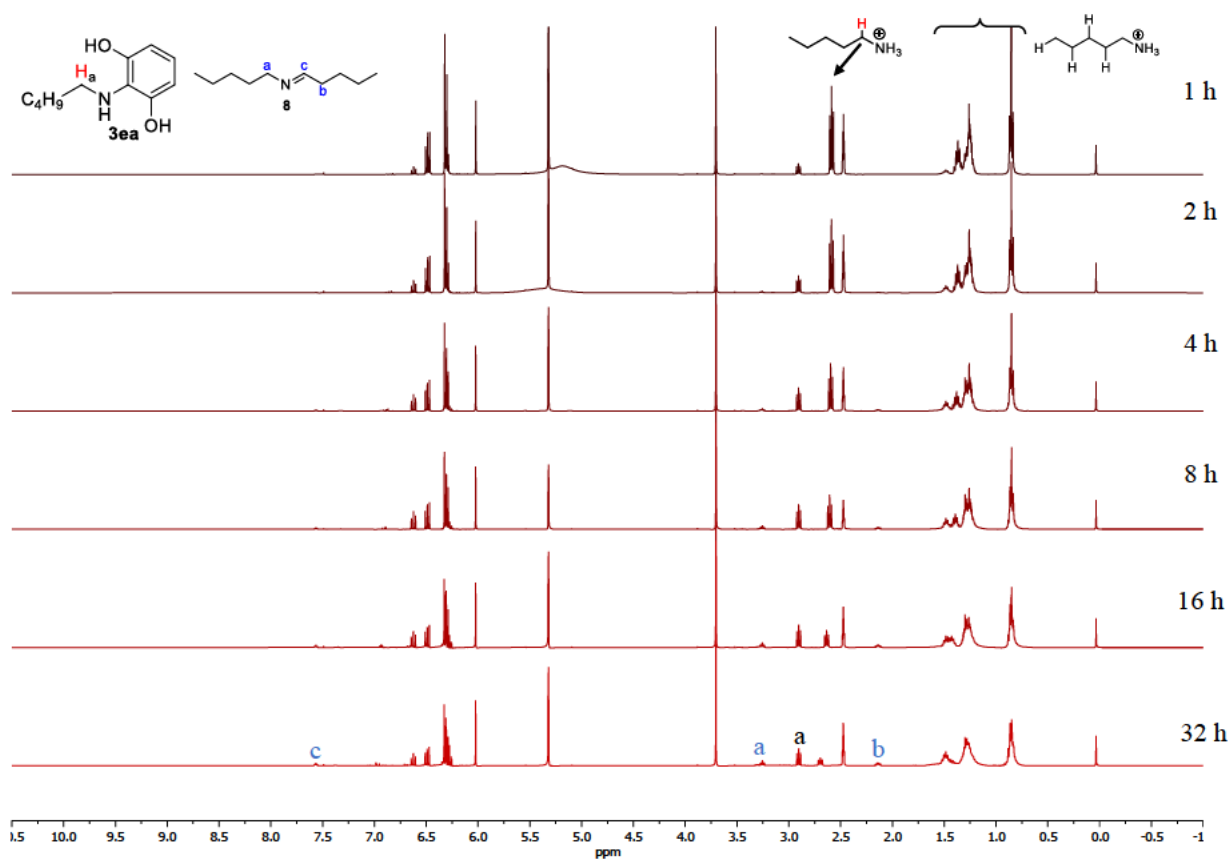


Fig. S54b. *in situ* ^1H NMR spectrum of **1e/2a** oxidative coupling reaction over 32 h, $\text{DCM-}d_2/\text{DMSO-}d_6$, 400 MHz.

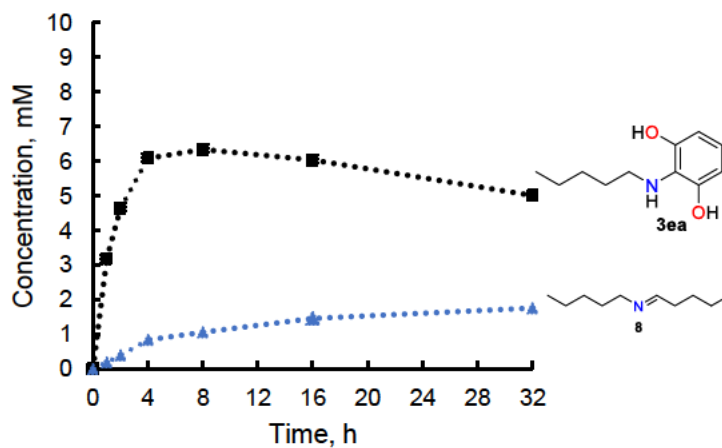


Fig. S55. Yield monitoring of **3ea** and imine **8** over 32 h, $\text{DCM-}d_2/\text{DMSO-}d_6$.



Scheme S9. Proposed mechanism of the step-by-step oxidation/aminolysis of **3ea** to **7e**.

2) 2 eq of **2a**

The reaction was performed according to Procedure A. It has been shown that the yield of **3ea** was 38% after 1 h, using 1,3,5-TMB as an IS (7.45 mg). No significant amount of **7e** was detected (Fig. S56).

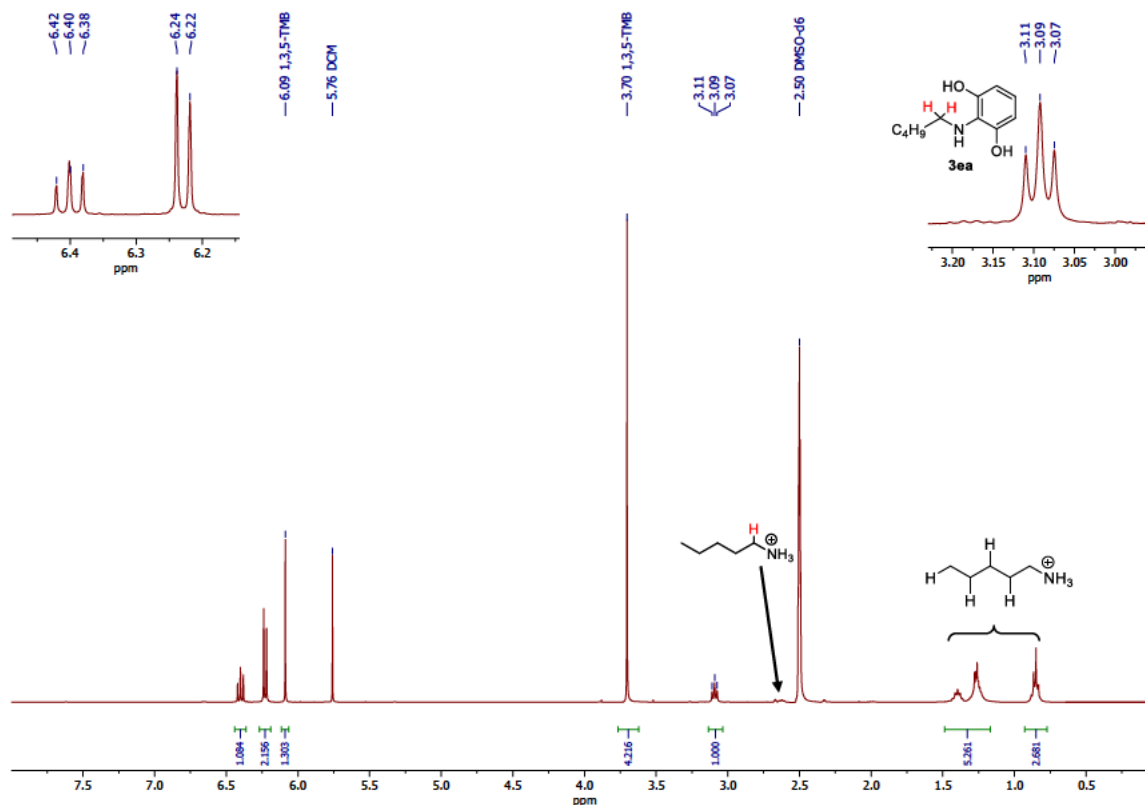
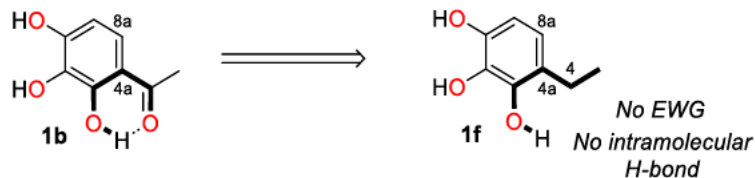


Fig. S56. ^1H NMR spectrum of **1e**/2 eq **2a** oxidative coupling reaction after 1 hour, DMSO-*d*₆, 400 MHz.

Ethyl Pyrogallol (EtPyr, **1f**)

Substrate selection: The importance of the EWG at C4a-position and the intramolecular hydrogen bond were checked in the experiment with EtPyr (**1f**) (Scheme S10).



Scheme S10. **1f** has no EWG group at 4a-position and no intramolecular hydrogen bond.

The reaction was carried according to procedure B. No reaction was observed between **1f** and amine **2a** under these conditions (Fig. S57).

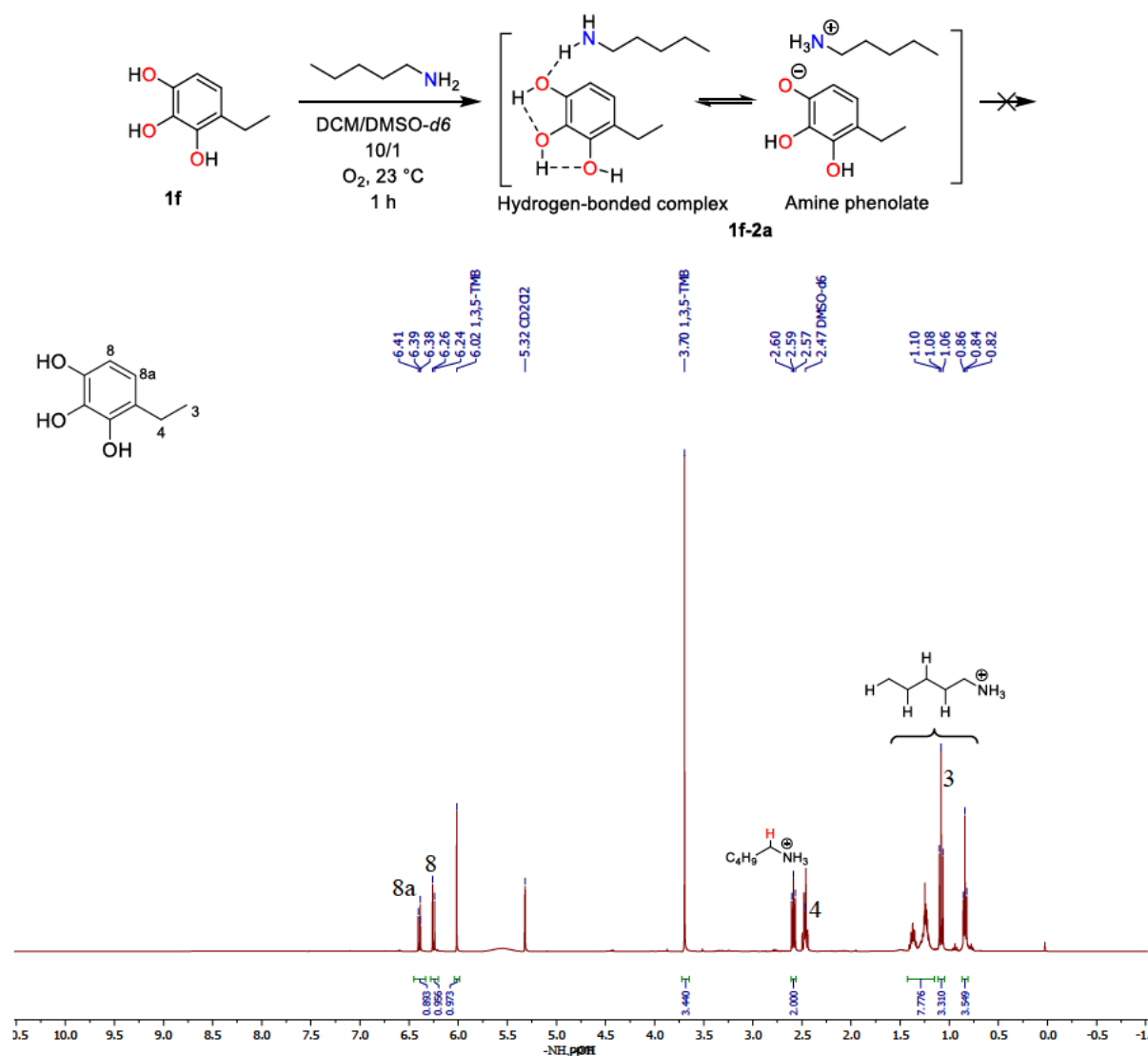


Fig. S57. *in situ* ¹H NMR spectrum of **1f/2a** oxidative coupling reaction after 1 hour, 400 MHz, DCM-*d*₂/DMSO-*d*₆.

Important note: EtPyr **1f**, unlike the other polyphenols mentioned in this study, slowly undergoes autoxidation during storage time. The conclusion was made after analysis of the mass spectrum of the polyphenol some time after its synthesis (Fig. S58).

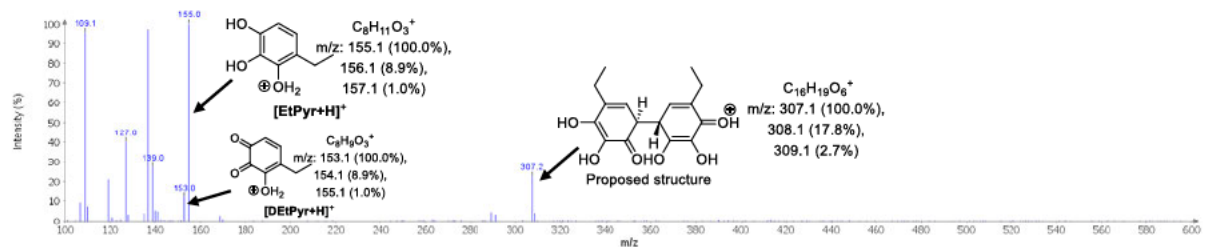
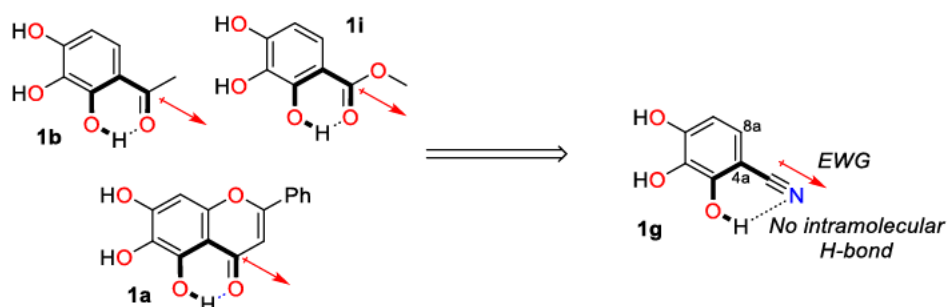


Fig. S58. APCI-MS spectrum of EtPyr **1f** autoxidation.

2,3,4-trihydroxybenzonitrile (TBN, **1g**)

Substrate selection: The importance of an EWG at C4a-position and of an intramolecular hydrogen bond were checked in the experiment with **1g** (Scheme S11).



Scheme S11. TBN **1g** has the EWG group at 4a-position, but no intramolecular H-bond.

The reaction was carried according to procedure B. The yields of **3ga**, **8** and **7g** were 68%, 8% and 4%, correspondingly, using 1,3,5-TMB (0.352 mg) as an IS (Fig. S59) (Average from 2 independent experiments). The regioselectivity of **3g** was proven by scXRD analysis.

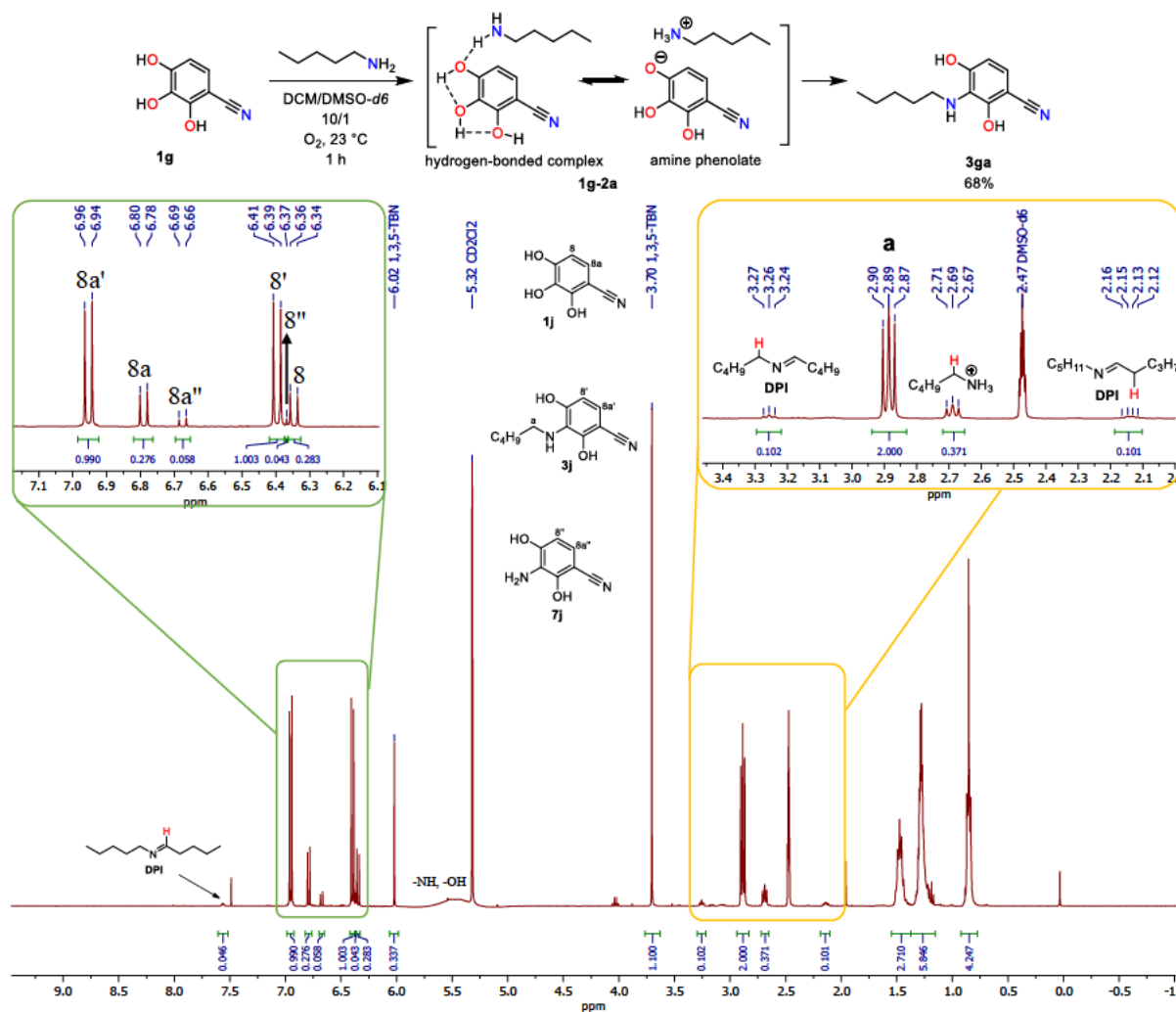
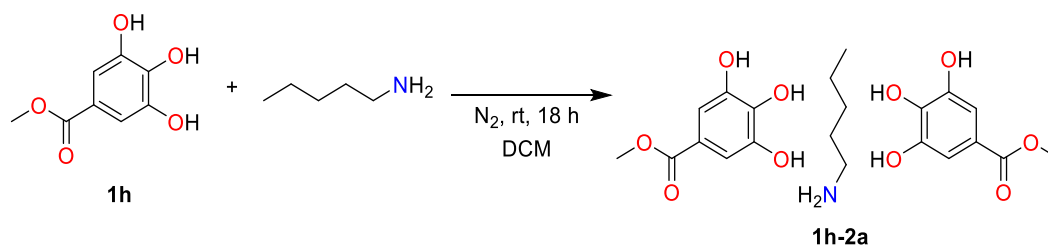


Fig. S59. *In situ* ¹H NMR spectrum of **1g/2a** oxidative coupling reaction after 1 hour, 400 MHz, DCM-*d*2/DMSO-*d*6.

addition of **2a**, the clear colorless solution became immediately white and turbid. The resulting mixture was stirred at RT for 18 h. The reaction mixture was concentrated in vacuo to afford a white solid, which was then recrystallized in *i*Hex with dropwise addition of EtOAc to afford thin white needle crystals.^[1] A 2:1 ratio of MetGal **1h** to **2a** was found in the ¹H NMR spectrum (Scheme S13, Fig. S61)



Scheme S13. Formation of **1h-2a** complex.

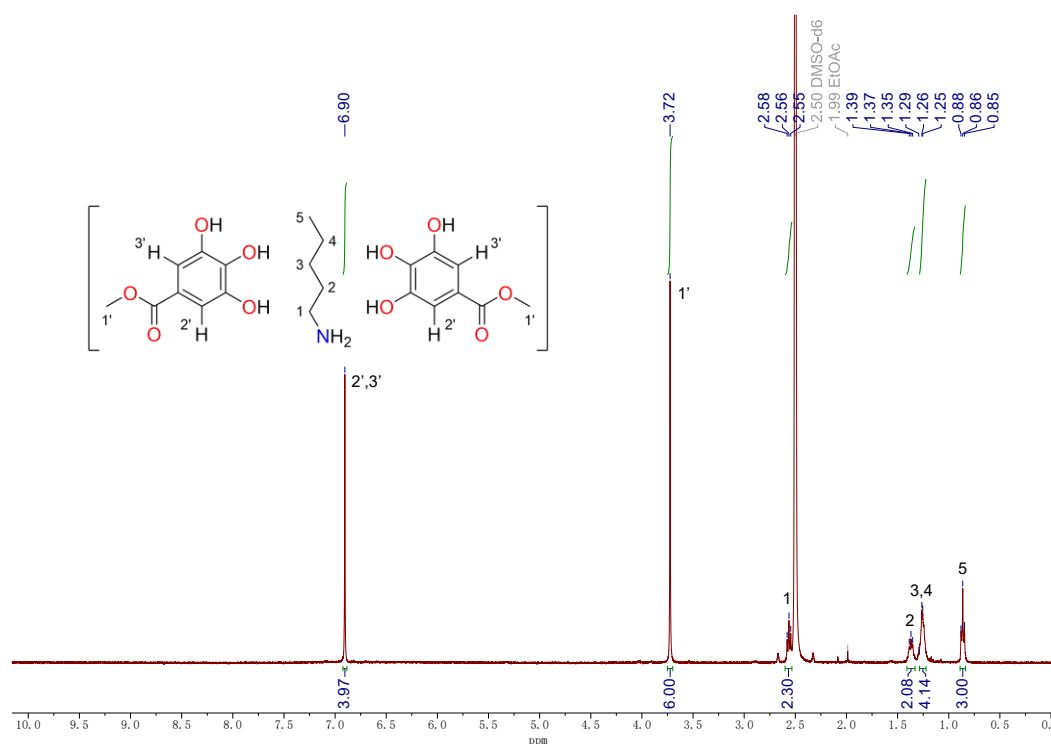


Fig. S61. ¹H NMR spectrum of **1h-2a** complex, DMSO-*d*₆, 400 MHz.

To characterize the complex and to determine the crystal property along with a potential crystal structure, pXRD experiment of the freshly recrystallized dry product were performed (Fig. S62). As comparison, the diffractogram of **1h** was measured. The diffractogram showed that it is isotropic in the white **1h-2a** complex, which means that even though the white solids appeared to have a needle crystal-like structure after recrystallization, the product is not a crystal. Nevertheless, there has been research showing methyl gallate **1h** could be used as co-former for co-crystallization in the pharmaceutical industry^[8], for example methyl gallate

build 1:1 co-crystals with theophylline anhydrate^[9] and 1:1 co-crystals with caffeine with improved mechanical properties as a result of modification of overall crystal packing^[10].

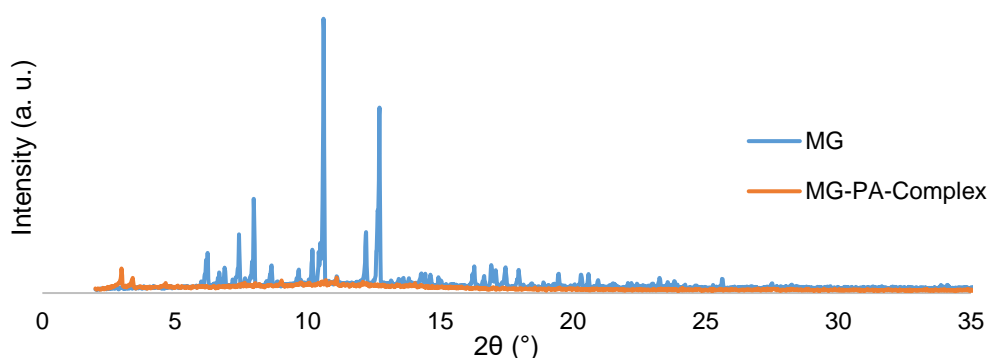
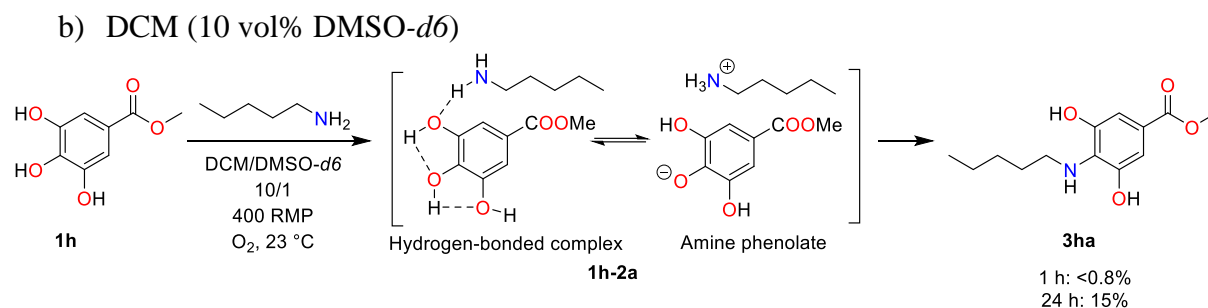


Fig. S62. pXRD diffractogram of Methyl gallate (**1h**) and methyl gallate-pentylamine complex (**1h-2a**).



The reaction was carried according to procedure A. It has been shown that the yields of **3ha** were <math><0.8\%</math> and 15% after 1 h and 24 h, correspondingly, using 1,3,5-TMB as an IS (8.0 mg) (Fig. S63). The regioselectivity of the product was proven by independent synthesis of **3ha**.

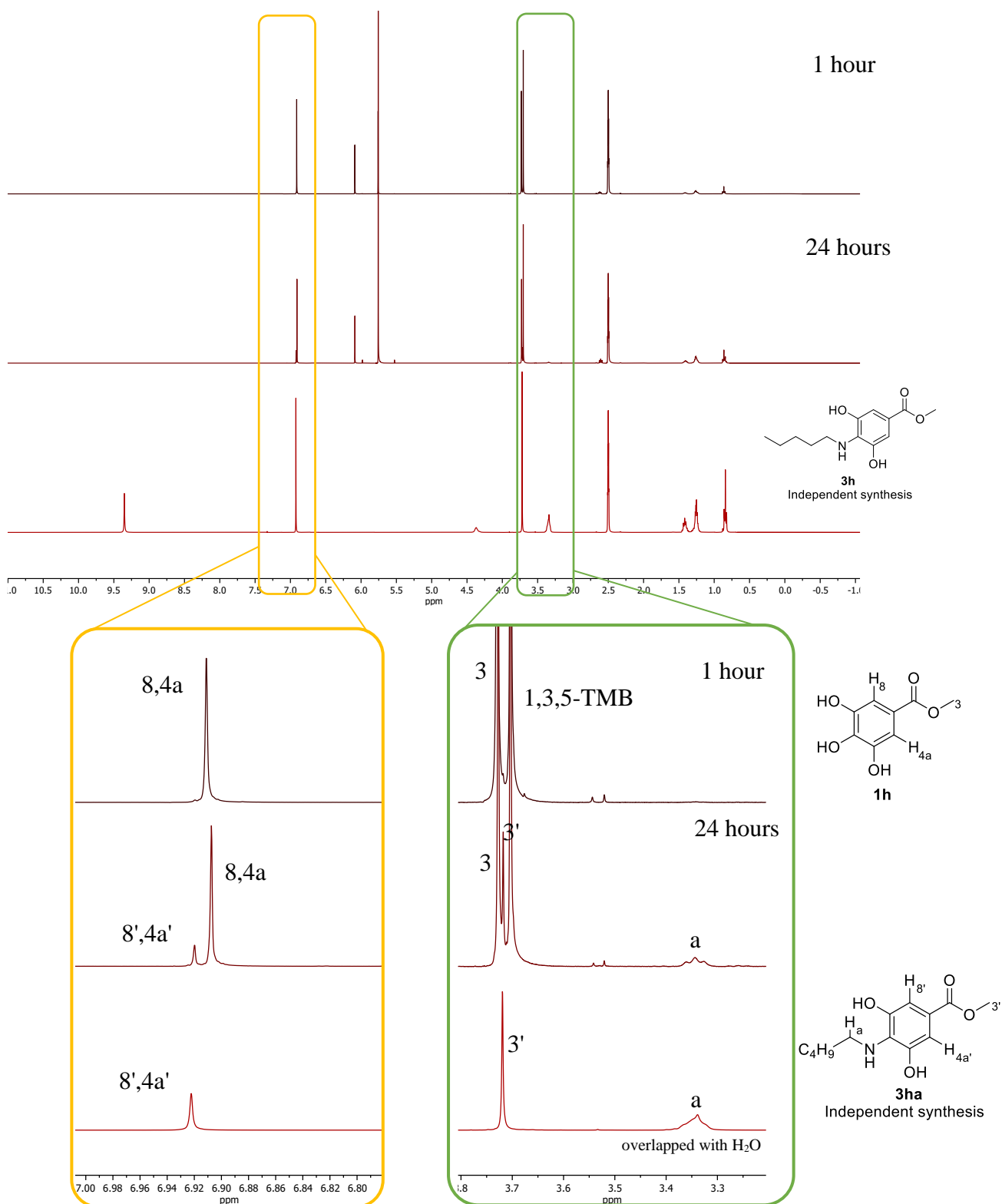


Fig. S63. ¹H NMR spectrum comparison of **1h/2a** oxidative coupling reaction after 1 hour, 24 h with independently synthesized **3ha**, 400 MHz, DMSO-*d*₆.

The reaction was carried according to procedure B. The yield of **3ha** was 1.2% after 1 h, using 1,3,5-TMB as an IS (0.60 mg) (Fig. S64 and S65).

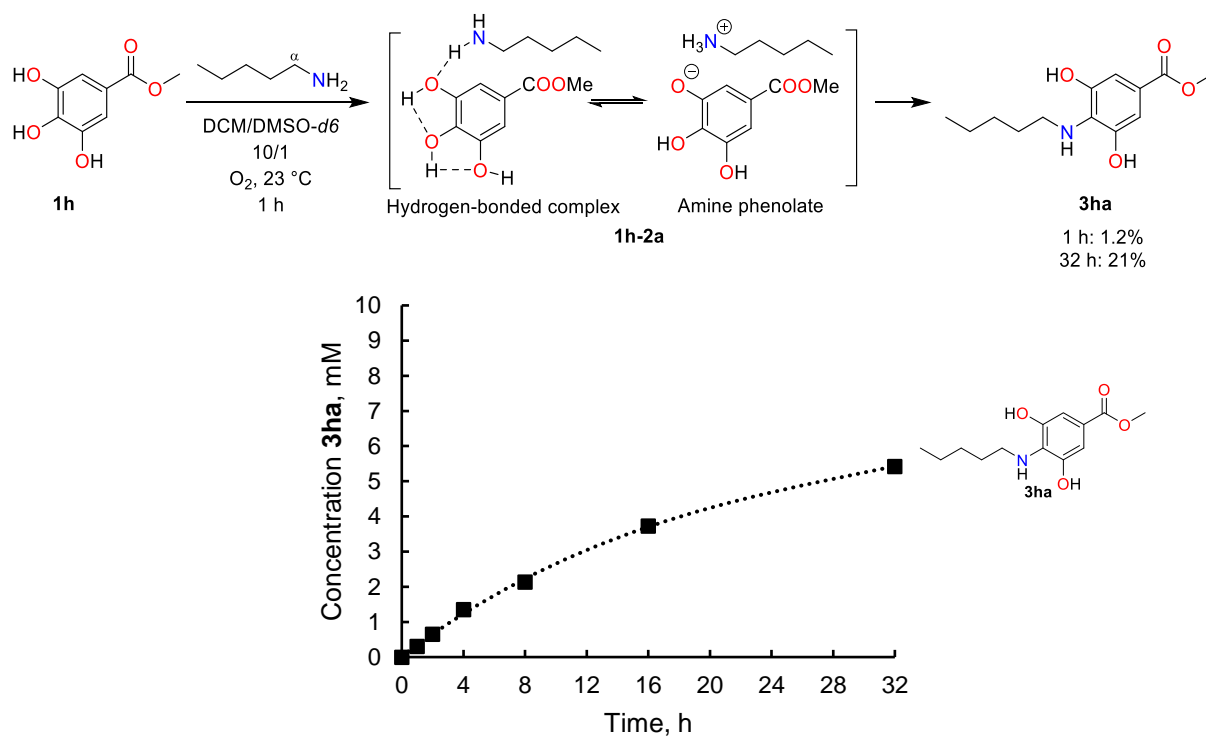


Fig. S64. Yield monitoring of **3ha** formation during 32 h, DCM-*d*2/DMSO-*d*6.

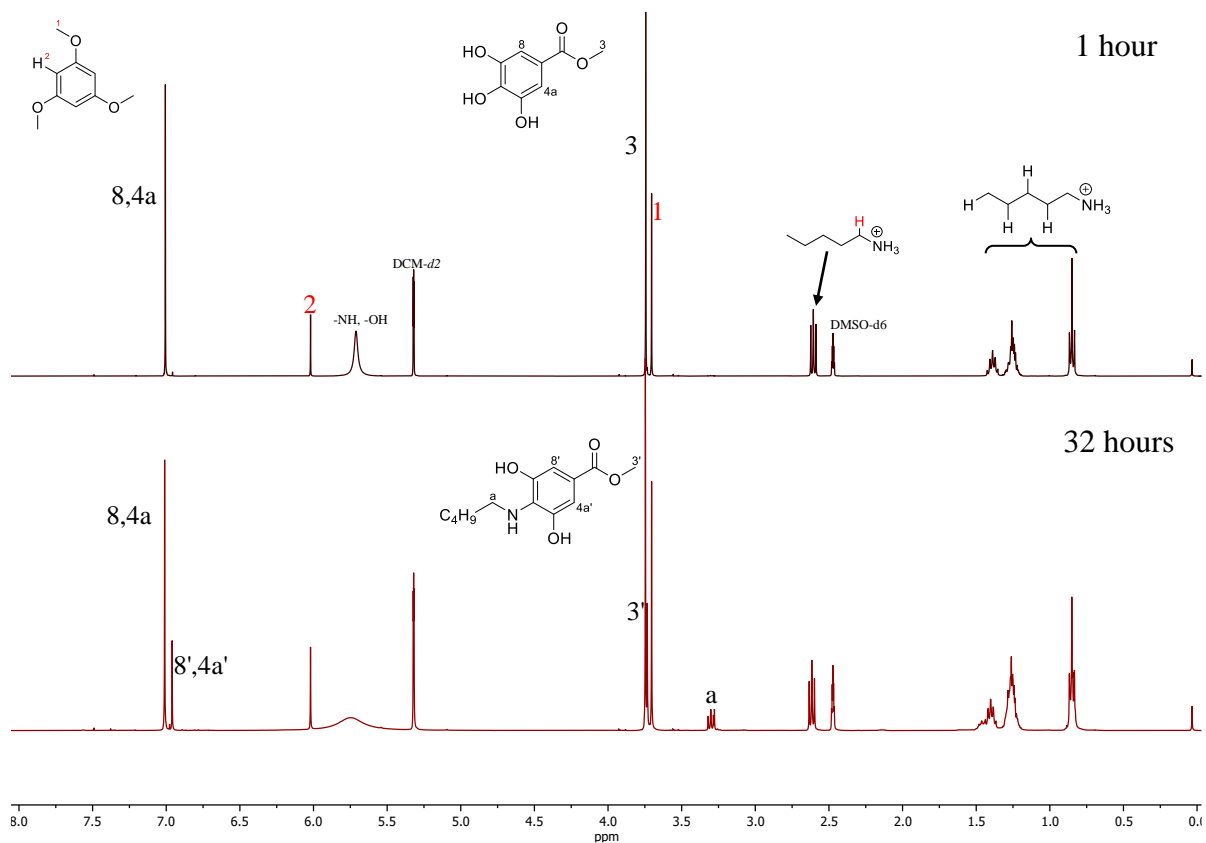


Fig. S65. *in situ* ¹H NMR spectrum comparison of **1h/2a** oxidative coupling after 1 hour, 32 h 400 MHz, DCM-*d*2/DMSO-*d*6.

Addition of 2 mol% of CuMeSal in the reaction mixture^[11] does not result in a significant increase in the rate of product formation. Instead, a larger amount of MeOH, compared to other experiments, was detected by ¹H NMR analysis, indicating that the reaction proceeds via a nucleophilic attack on the ester group, resulting in the formation of an amide and elimination of MeOH (Fig. S66).

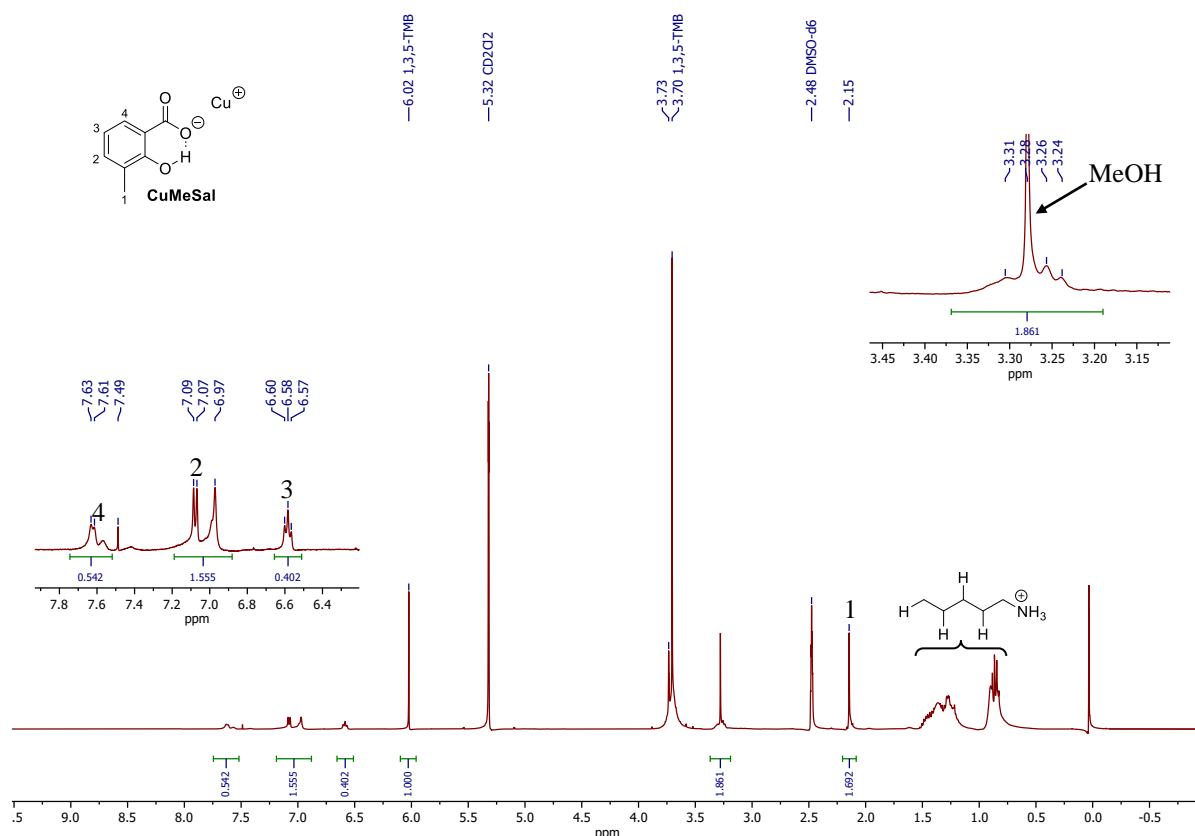
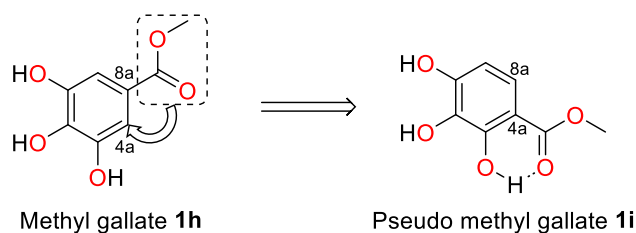


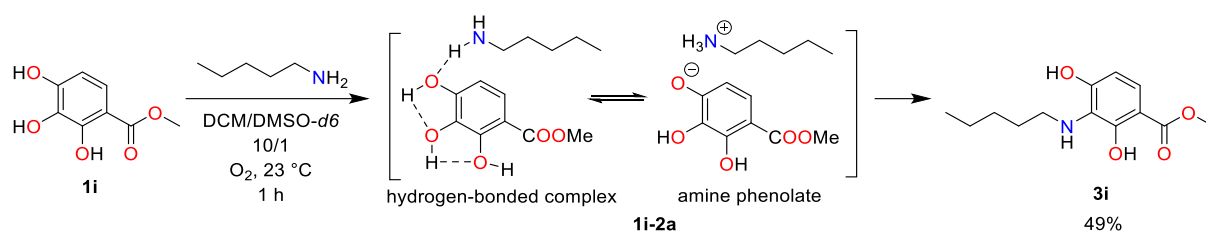
Fig. S66. *in situ* ¹H NMR spectrum of **1h/2a** oxidative coupling with 2 mol% CuMeSal after 16 h 400 MHz, DCM-*d*2/DMSO-*d*6.

Pseudo Methyl Gallate (psMetGal, **1i**)

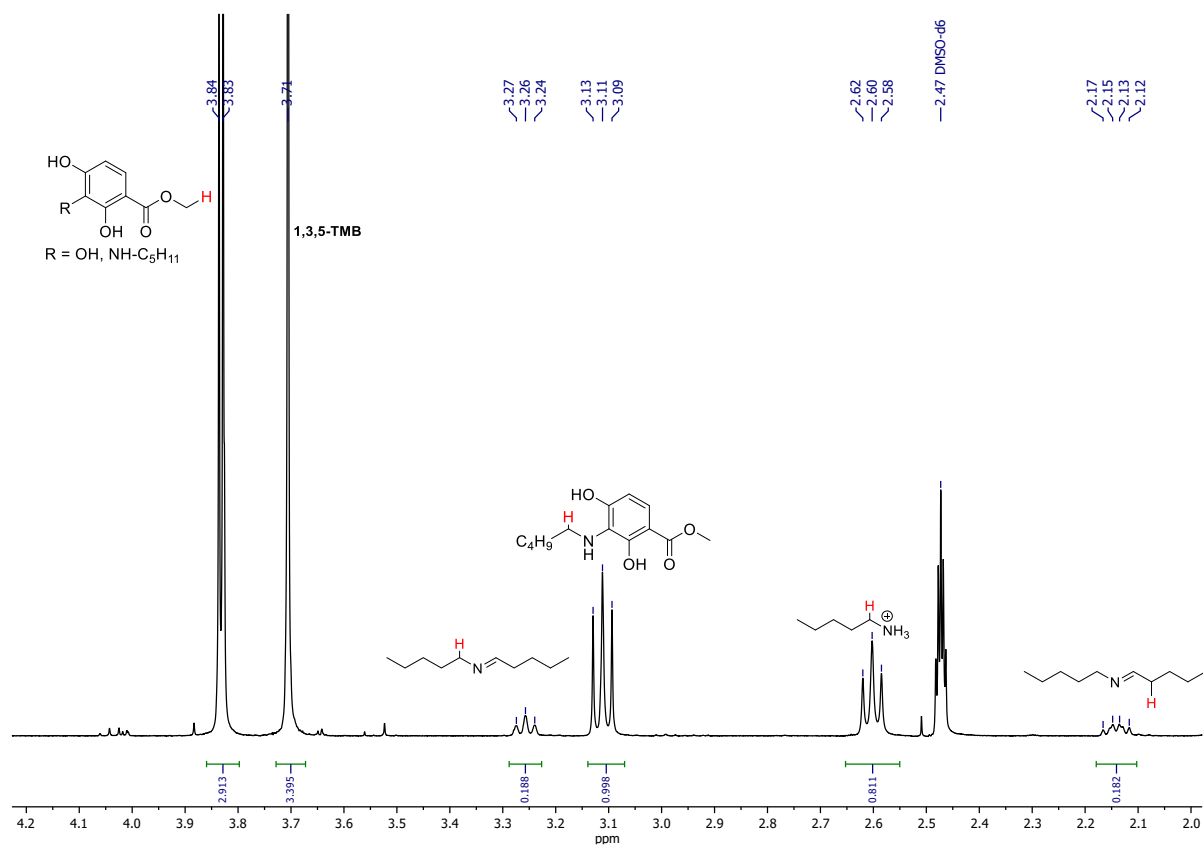
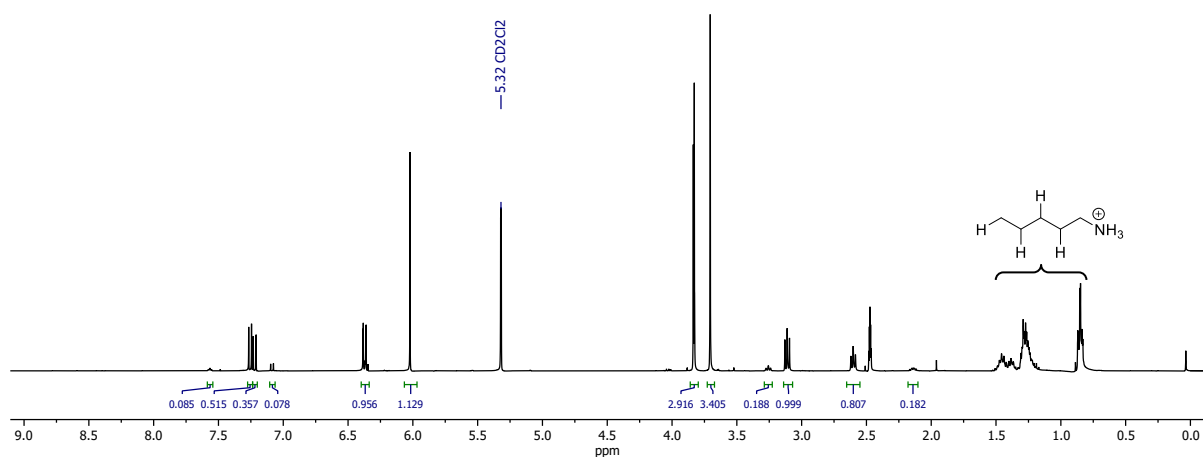
Substrate selection: pseudo methyl gallate (**1i**) is an isomer of methyl gallate (**1h**), but with a structural modification, the methyl ester group has been moved to C4a-position from C8a-position (Scheme S14).



Scheme S14. Structural difference between methyl gallate(**1h**) and pseudo methyl gallate(**1i**).



The reaction was carried according to procedure B. The yield of **3ia**, **7i** and **8** were 49%, 8.5% and 17%, correspondingly, using 1,3,5-TMB as an IS (Fig. S67) (1.56 mg). The regioselectivity of the **3ia** was proven via scXRD analysis.



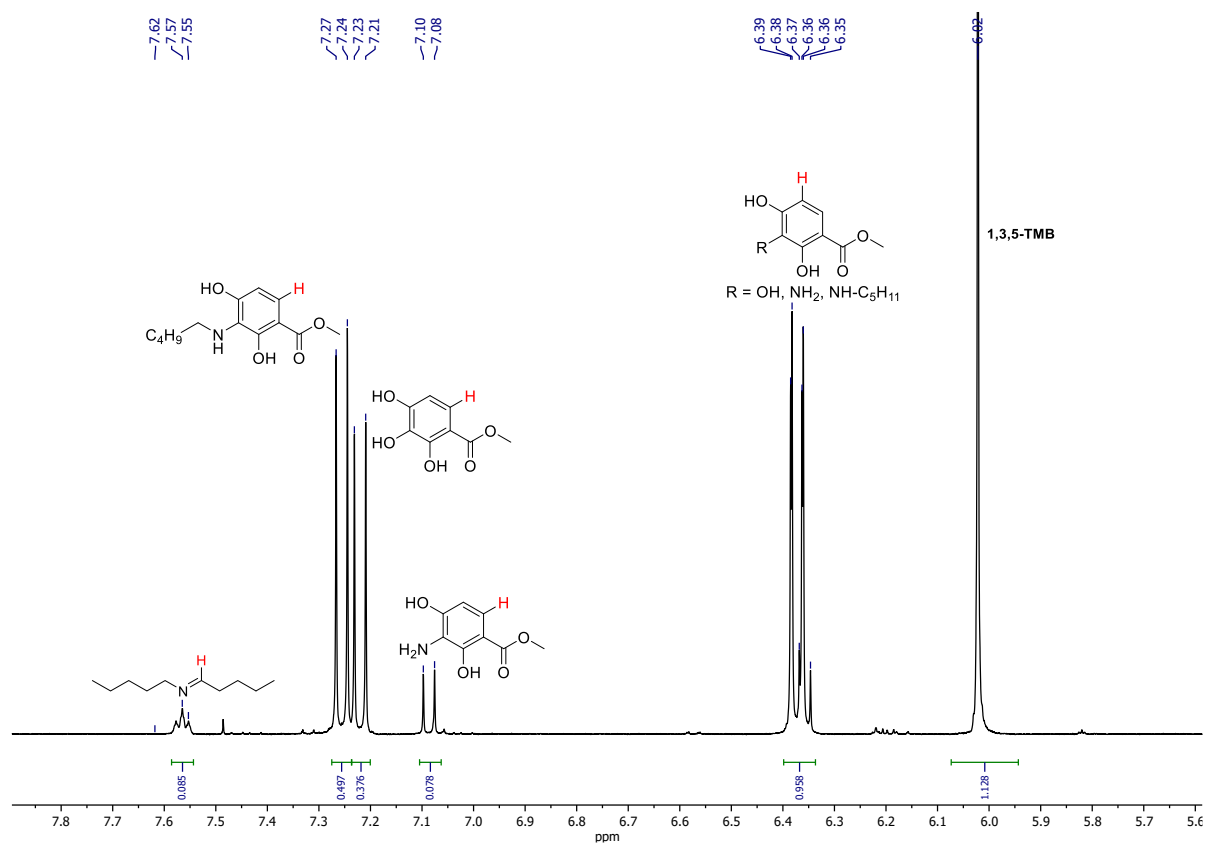
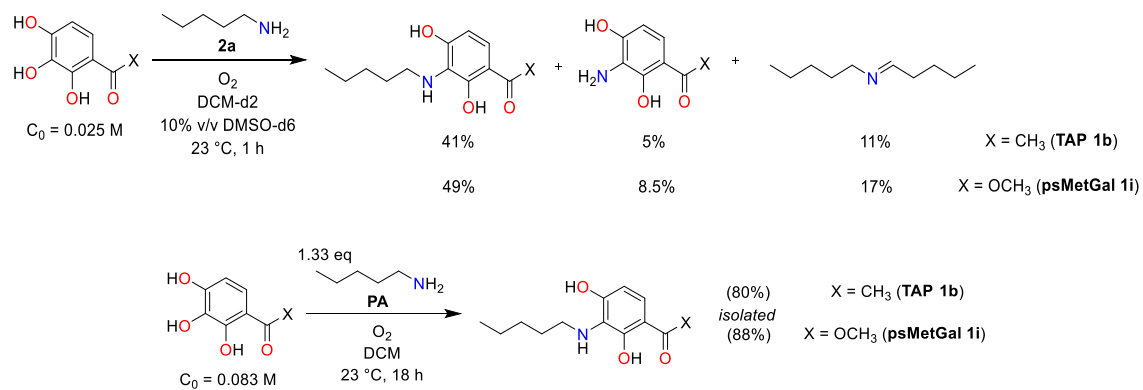


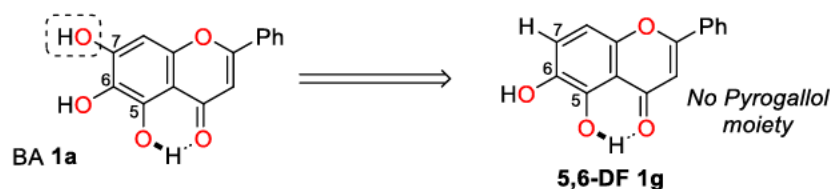
Fig. S67. *in situ* 1H NMR spectrum of **1i/2a** oxidative coupling reaction after 1 hour, 400 MHz, DCM- d_2 /DMSO- d_6 .



Scheme S15. Comparison of TAP **1b** and psMetGal **1i** reactivity.

5,6-dihydroxyflavone (5,6-DF, **1j**)

Substrate selection: Baicalein **1a** first deprotonation occurs preferentially at 7-OH position.^[1] It was decided to “remove” 7-OH to check the effect of this functional group (Scheme S16).



Scheme S16. 5,6-DF (**1j**) has no 7-OH group.

The reaction was carried according to procedure C, because no reactivity was detected in DCM/DMSO mixture, similar to the example with 7,8-DF (**1k**). No reaction was observed between 5,6-DF **1j** and pentylamine **2a** under these conditions (Fig. S68).

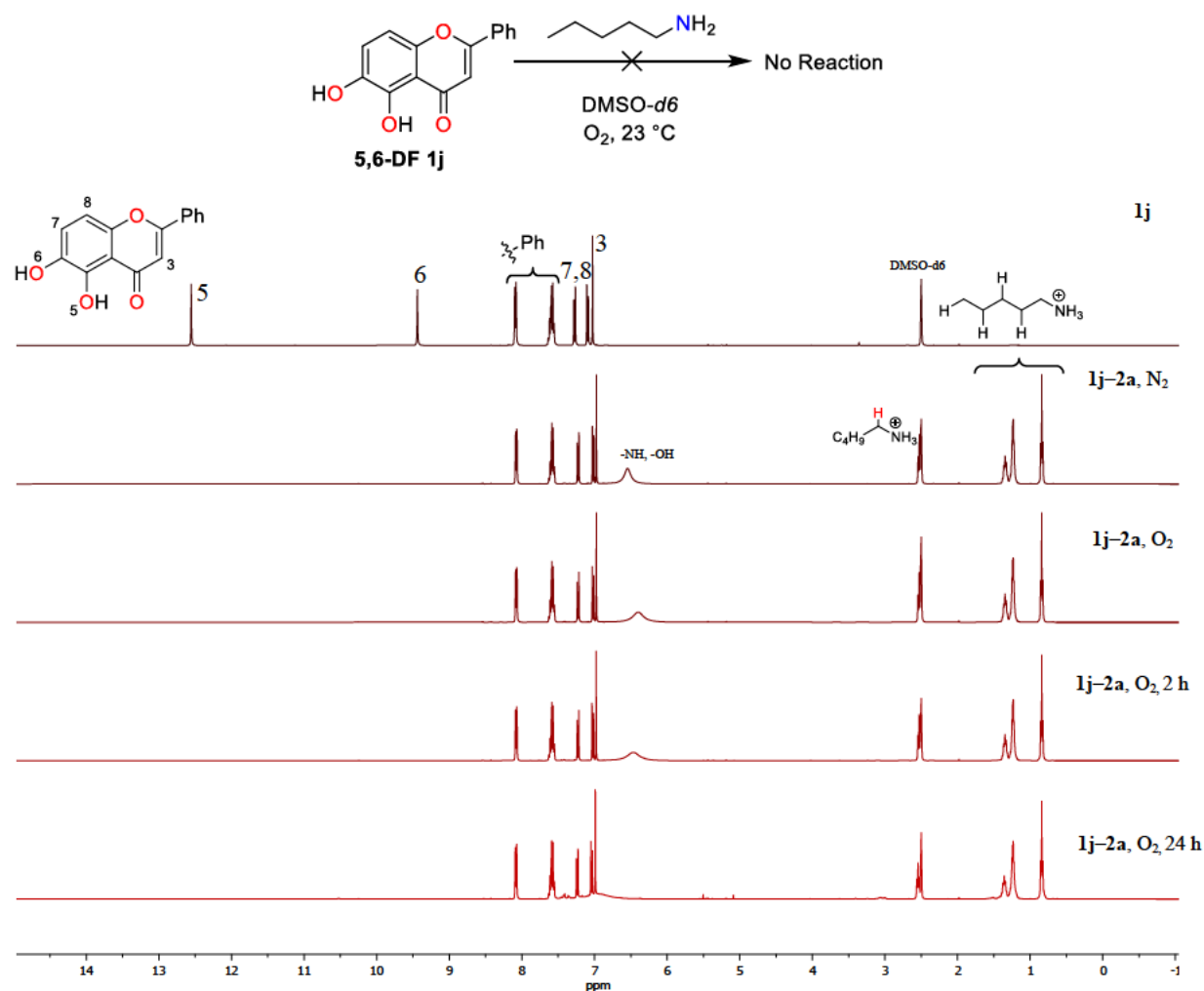
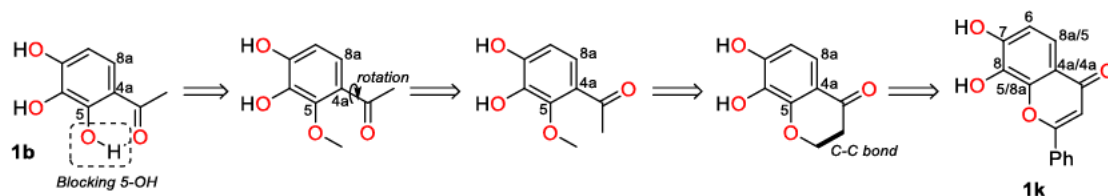


Fig. S68. *in situ* ¹H NMR spectra of **1j/2a** oxidative coupling over 24 h, DMSO-*d*₆, 400 MHz.

7,8-dihydroxyflavone (7,8-DF, **1k**)

Substrate selection: Blocking of the 5-OH substituent of TAP (**1b**) was considered as an interesting idea. Methylation of 5-OH would require 3 step synthesis.^[12] 7,8-dihydroxyflavone (**1k**) was used as a model of TAP **1b** with blocked 5-OH phenoxy group (Scheme S17).



Scheme S17. 7,8-DF **1k** is a model compound of **1b** with blocked 5-OH group.

The reaction was carried according to procedure B. No reaction was observed between 7,8-DF **1k** and pentylamine (**2a**) under these conditions (Fig. S69).

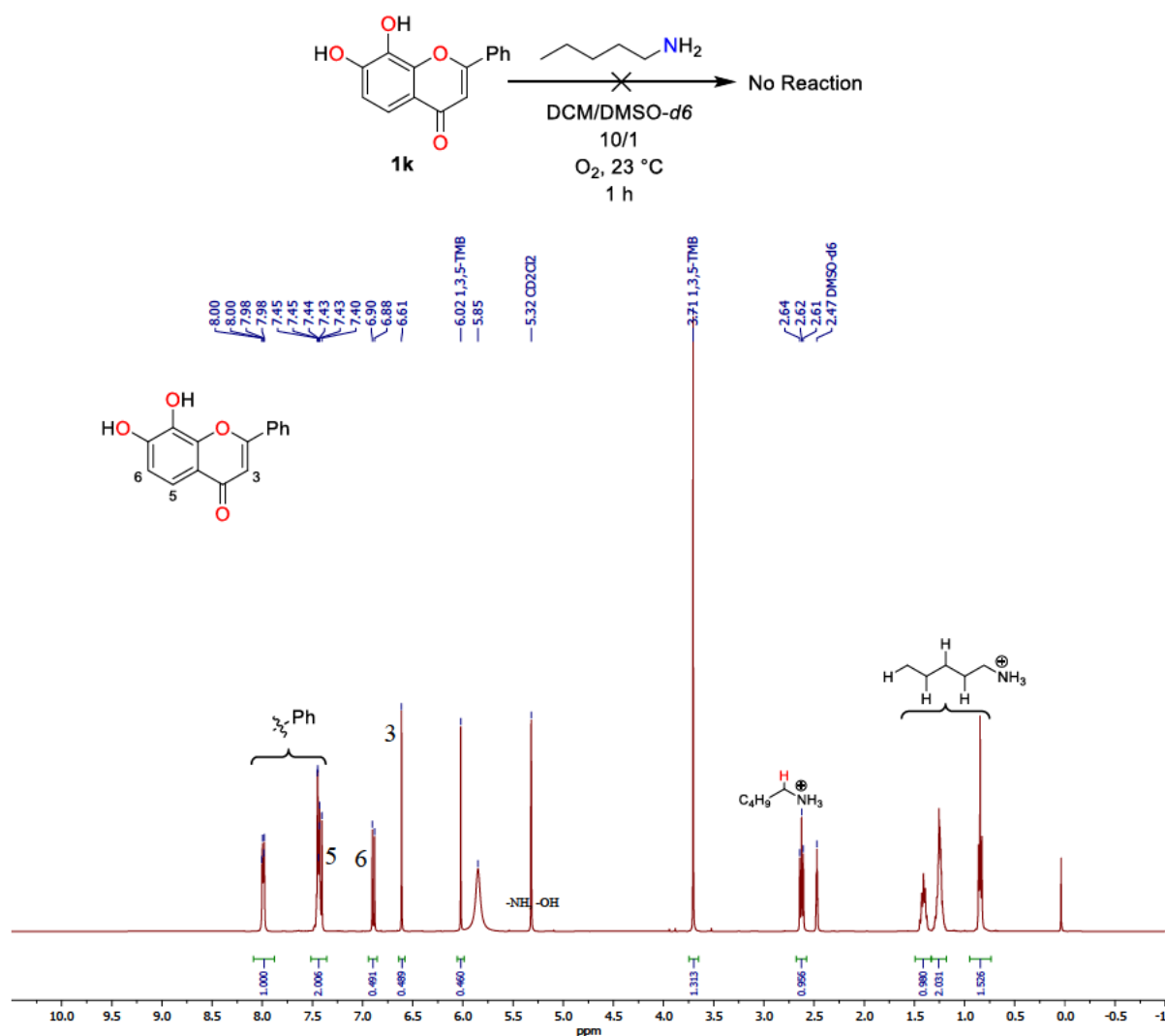
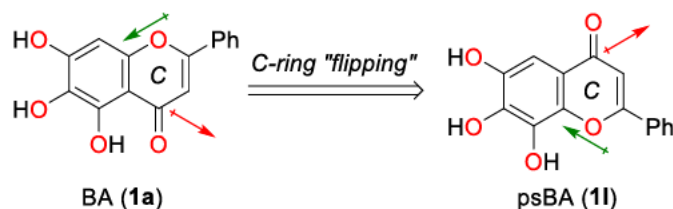


Fig. S69. *in situ* ¹H NMR spectrum of **1k/2a** oxidative coupling, DCM-d₂/DMSO-d₆, 400 MHz.

Pseudo baicalein (psBA, **11**)

Substrate selection: Baicalein (**1a**) shows high reactivity with amine **2a**. It was decided to "flip" the C-ring of baicalein **1a** to obtain reverse electron withdrawing and donating effects (Scheme S18).



Scheme S18. **11** has "reverse" electron withdrawing and donating effects relative to **1a**.

The reaction was carried according to procedure B. No reaction was observed between **11** and amine **2a** under these conditions (Fig. S70 and S71).

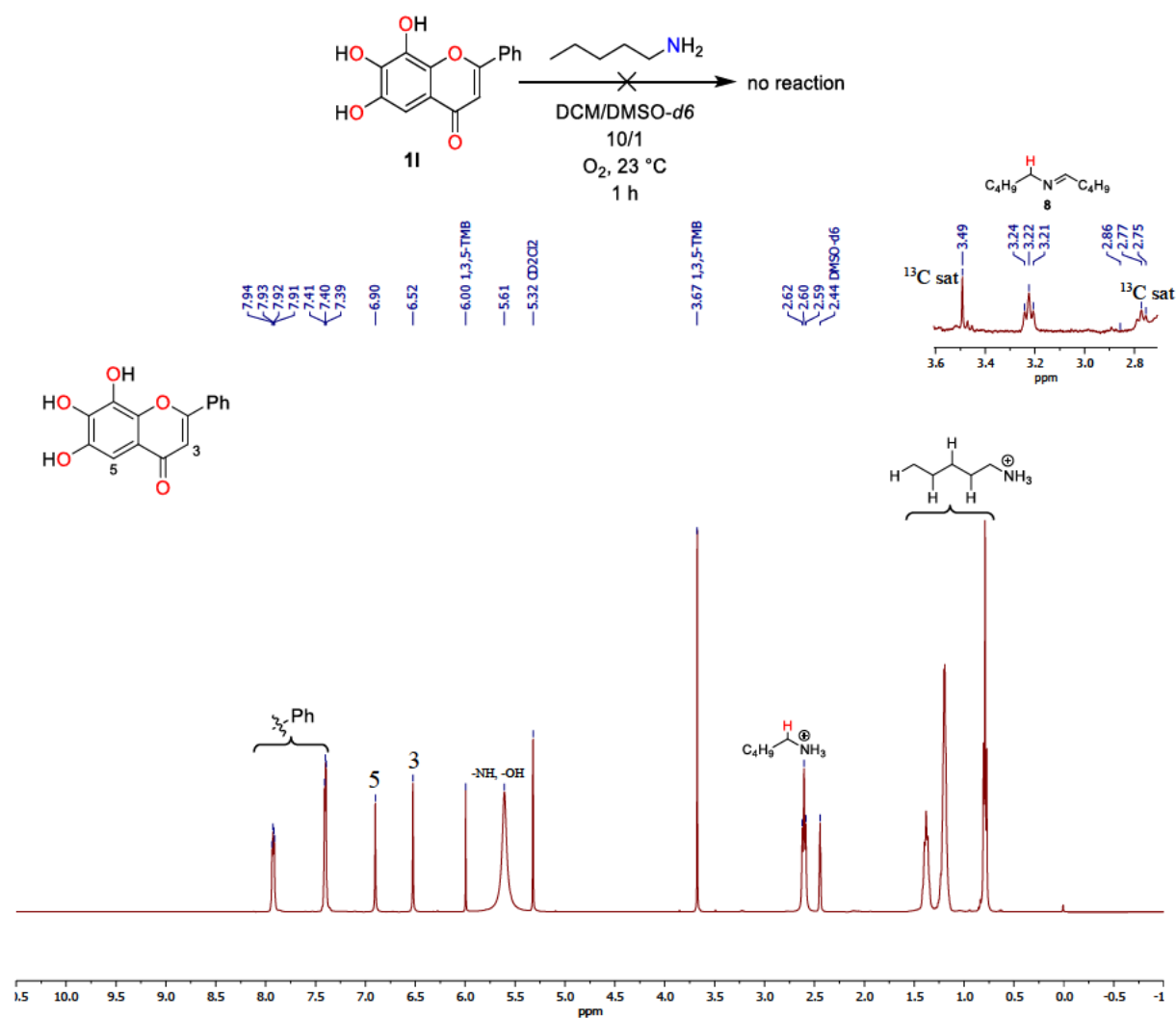


Fig. S70. *in situ* ¹H NMR spectrum of **11/2a** oxidative coupling after 1 hour, DCM-*d*₂/DMSO-*d*₆, 400 MHz.

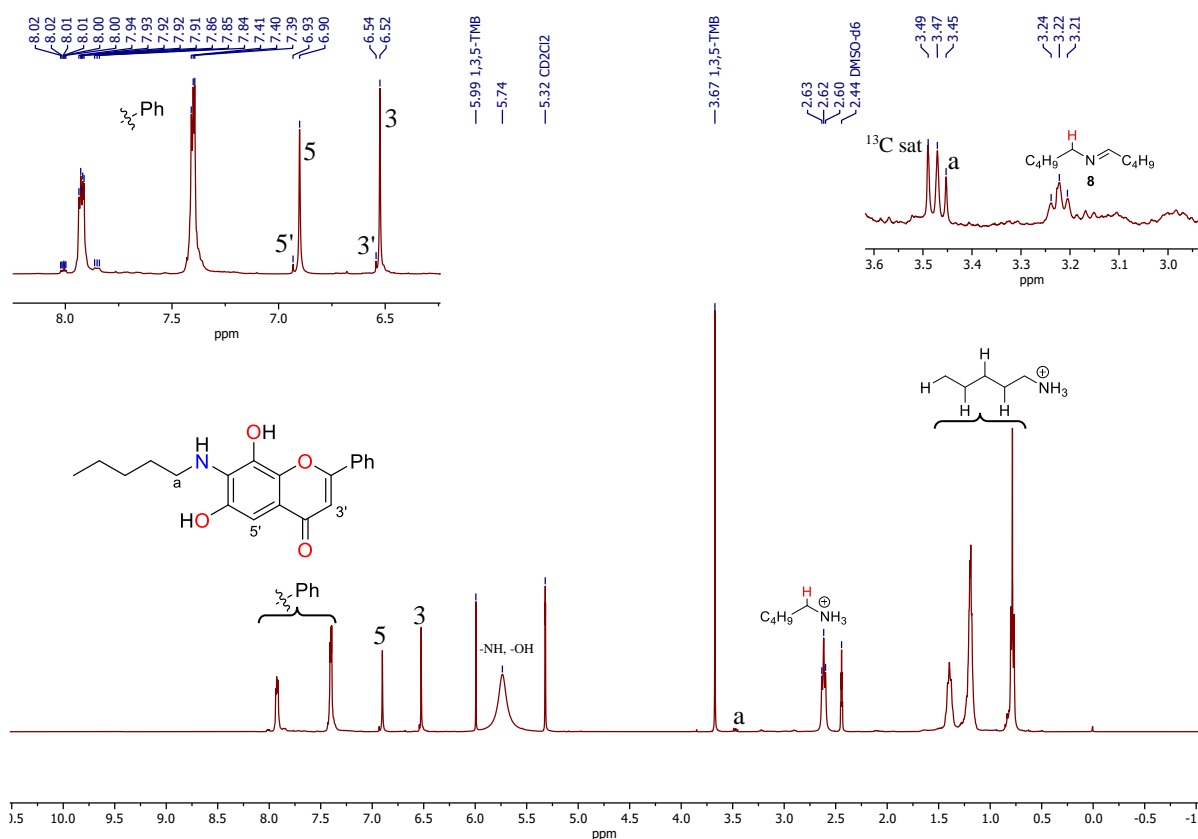


Fig. S71. *in situ* ¹H NMR spectrum of **11/2a** oxidative coupling, 24 h, DCM-*d*₂/DMSO-*d*₆, 400 MHz.

In order to verify the production of even small amount of product, the reaction was repeated using higher concentrations of substrates in DMSO-*d*₆. Upon the addition of amine **2a**, the colour of the solution immediately changed from light yellow to brown and turned red after exchange of the gas atmosphere from N₂ to O₂. The colour slowly turns dark red in the end. The ¹H NMR spectra were measured directly after the addition and before the gas exchange, and then after 2 h, 24 h, 96 h, and 144 h (Fig. S72).

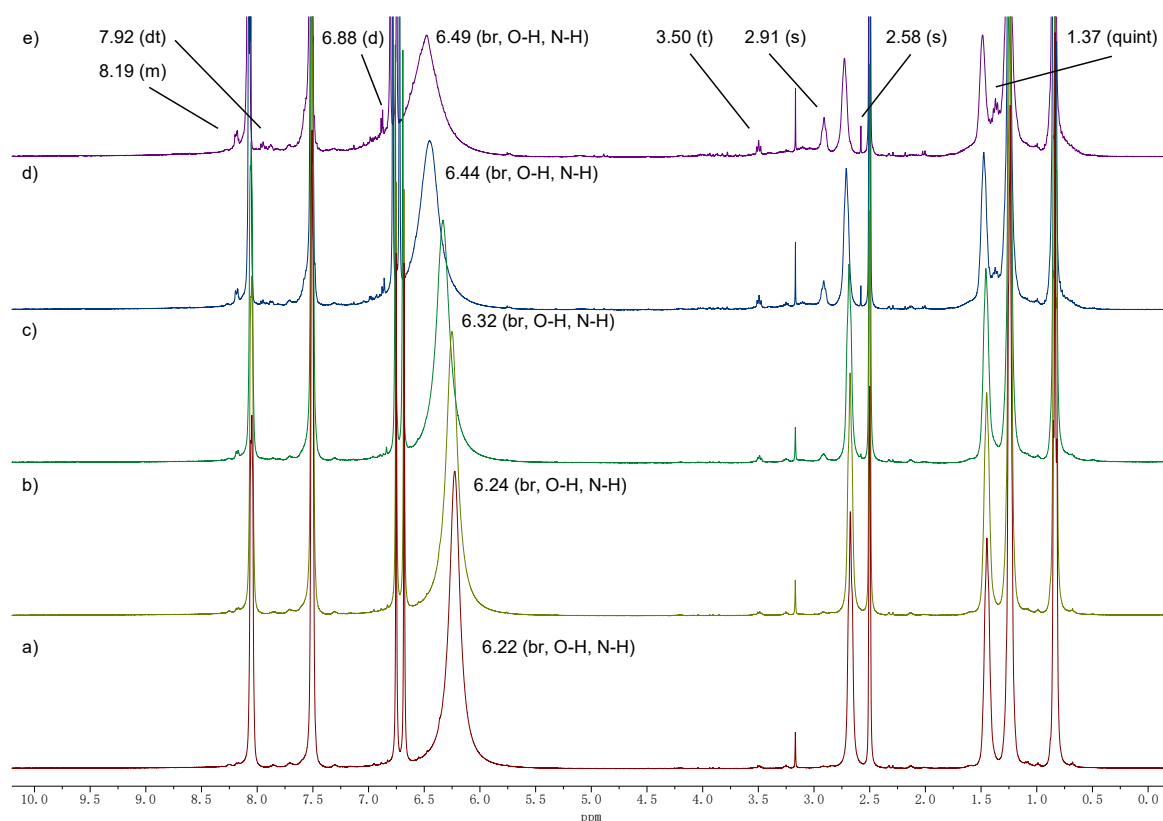
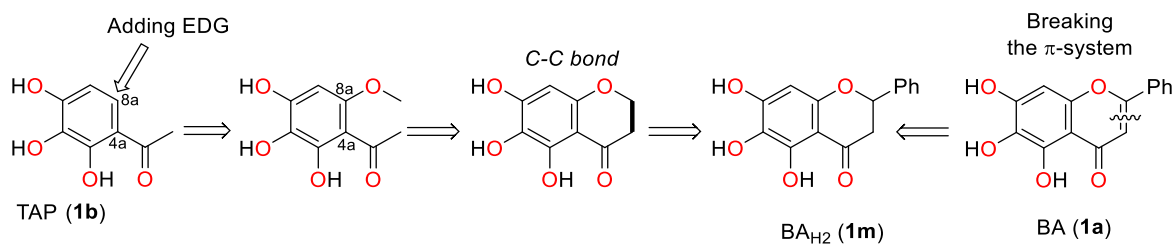


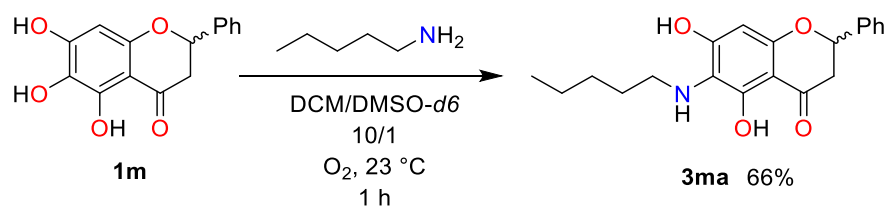
Fig. S72. *in situ* ^1H NMR spectra of the reaction of **11** and **2a** in a 1:1 ratio at 23 °C, $\text{DMSO-}d_6$, 400 MHz: a) under N_2 ; after gas exchange to O_2 for b) 2 h, c) 24 h, d) 96, e) 144 h.

2,3-Dihydrodaicaein (BA_{H_2} , **1m**)

Substrate selection: **1m** can be considered as a model of TAP (**1b**) with an EDG at C8a-position. On the other hand, **1m** represent baicalein (**1a**) with a split π -system of conjugated double bonds (Scheme S19).



Scheme S19. **1m** is a model of **1b** with EDG at C8a-position or a model of **1a** with a split π -system.



The reaction was carried according to procedure A. It has been shown that the yield of **3ma** was 66% using 1,3,5-TMB as an IS (average from 3 independent experiments). The reaction was quenched with 1.25 eq TFA-*d*1 (inactivating **2a** to **TFA**×**2a**), dried and dissolved again in DMSO-*d*6 (resolving the overlapping peaks of H³- and H^a-protons) (Fig. S73). Yield of **8** (7%) was established from independent *in situ* reaction according to the general procedure B (Fig. S74).

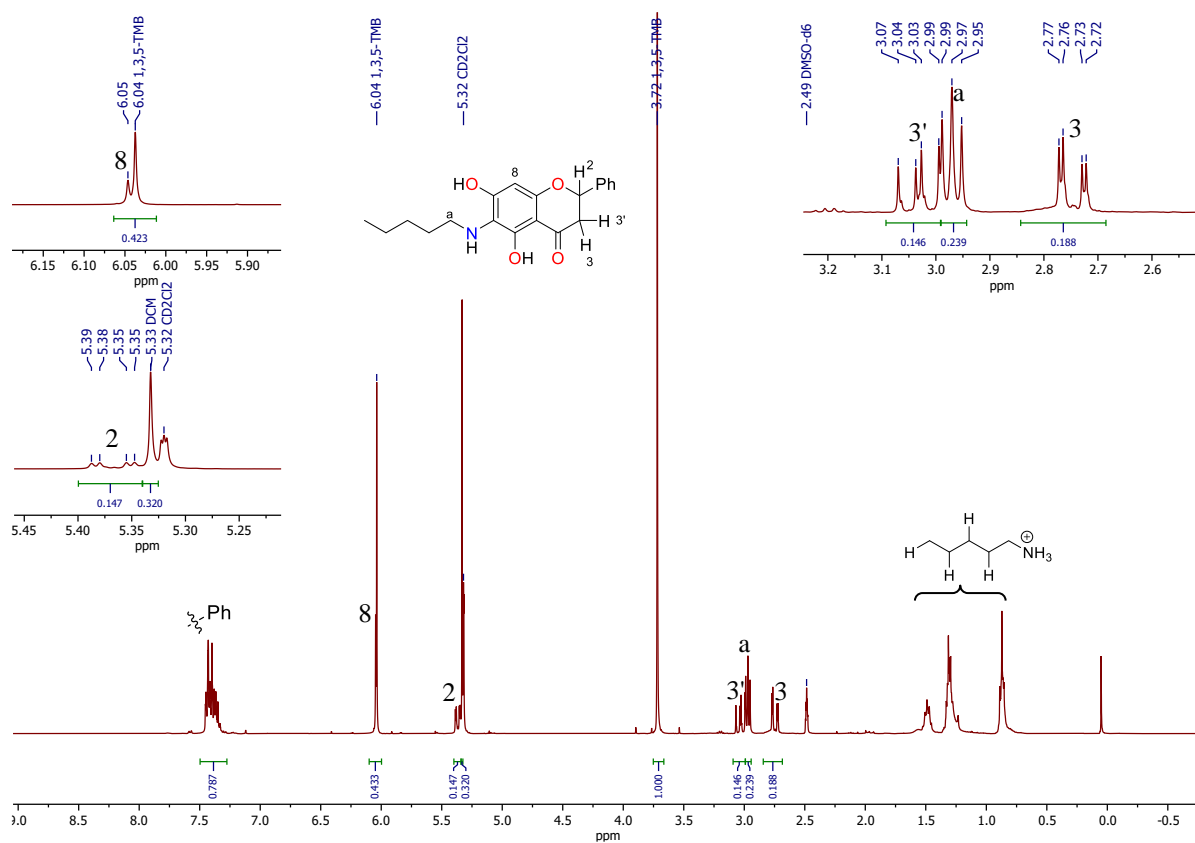


Fig. S73a. ¹H NMR spectrum of **1m/2a** oxidative coupling, DCM-*d*2/DMSO-*d*6, 400 MHz.

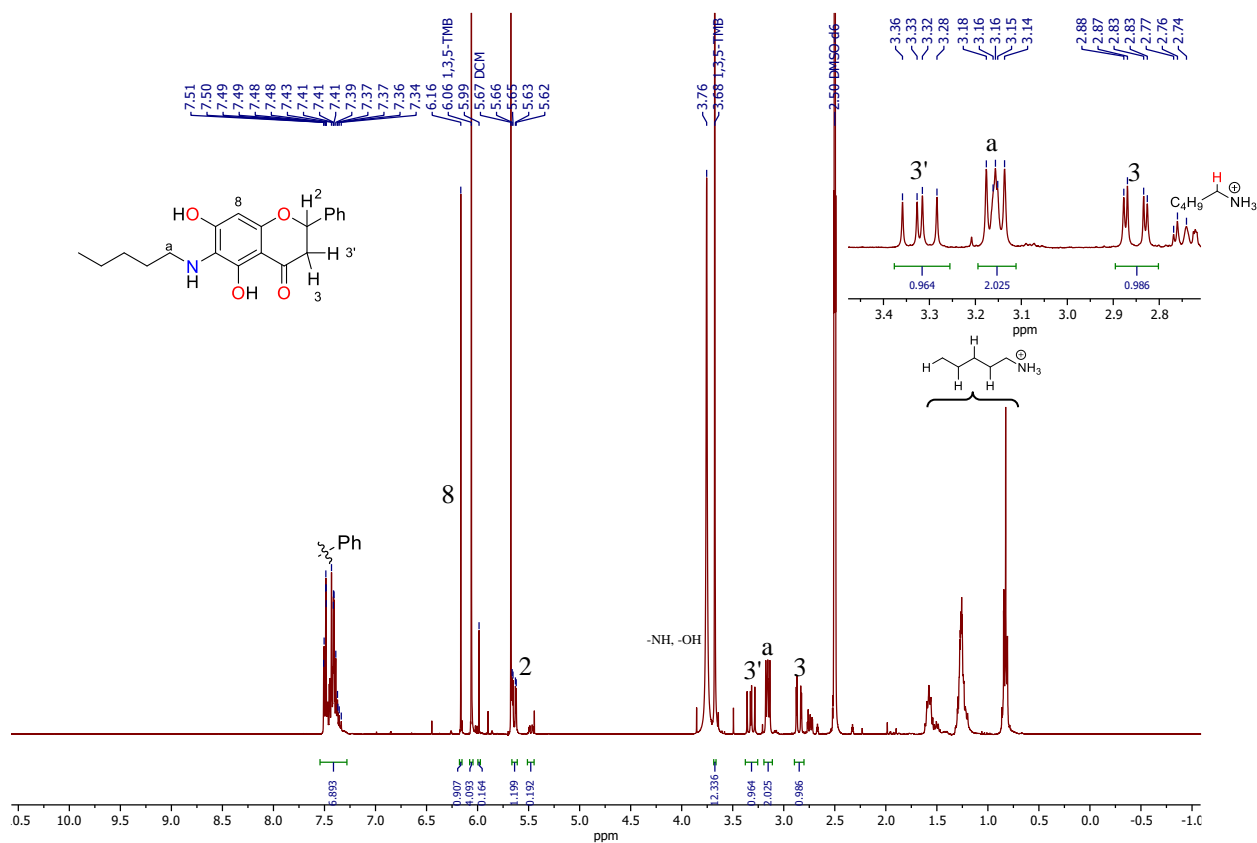


Fig. S73b. ^1H NMR spectrum of **1m/2a** oxidative coupling, TFA quenching (peaks resolving), $\text{DMSO-}d_6$, 400 MHz.

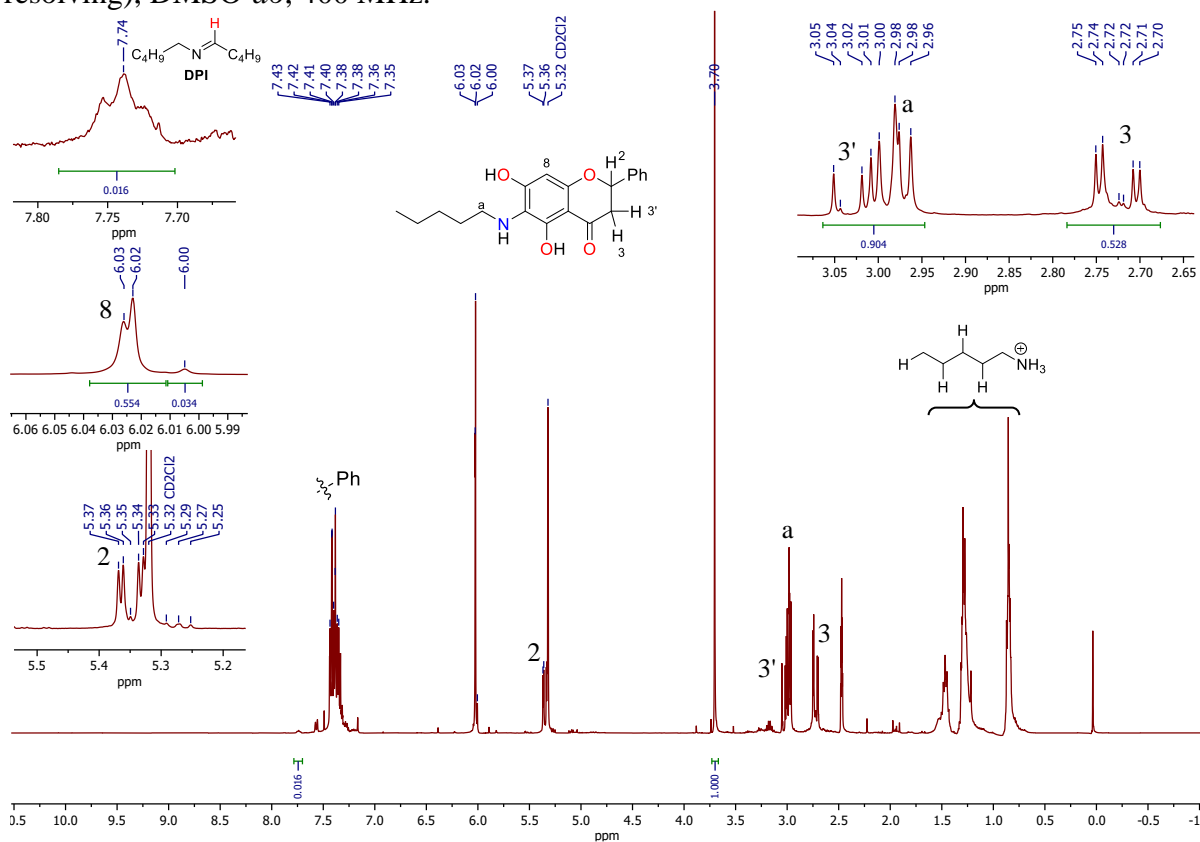
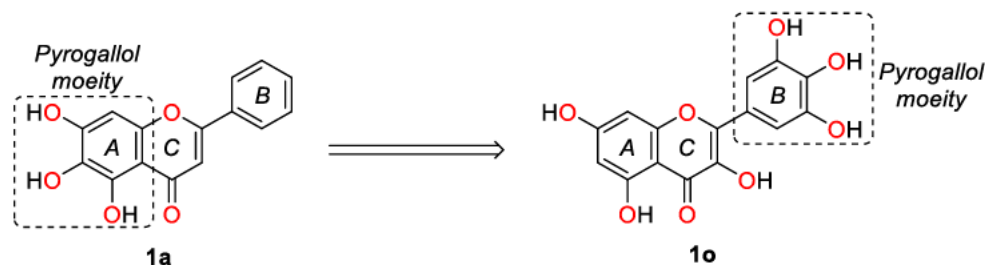


Fig. S74. *in situ* ^1H NMR spectrum of **1m/2a** oxidative coupling, $\text{DCM-}d_2/\text{DMSO-}d_6$, 400 MHz.

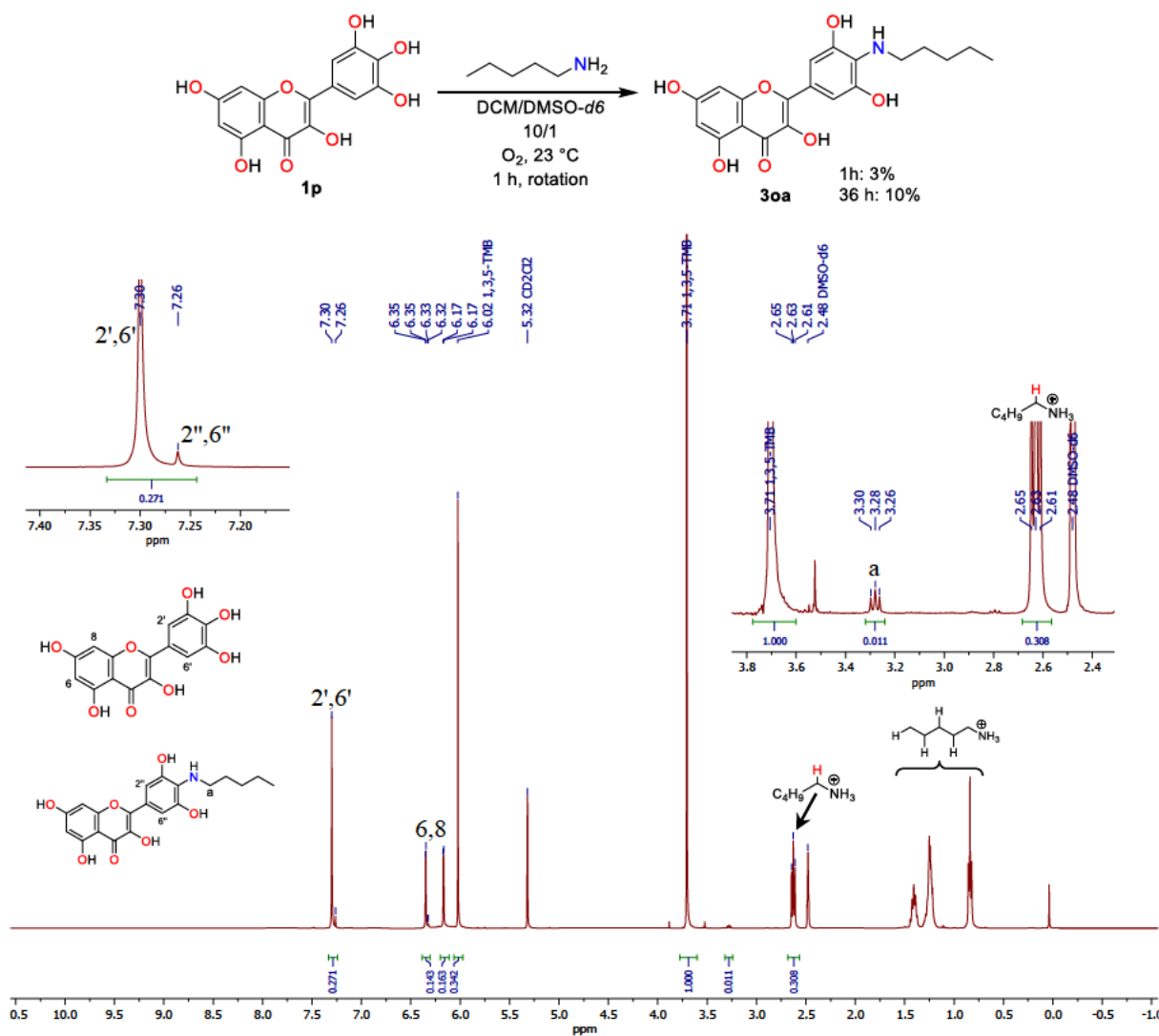
Myricetin (Myr, **1o**)

Substrate selection: Myricetin **1o** has almost the same flavonoid backbone as baicalein (**1a**), but pyrogallol moiety is on the B-ring (Scheme S20).



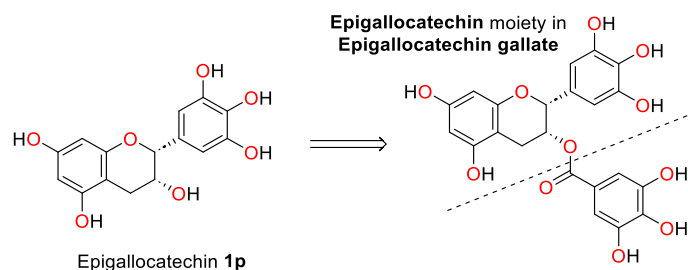
Scheme S20. Myricetin **1o** has a pyrogallol moiety on B-ring of the flavonoid backbone.

The reaction was carried according to procedure B. Yield of **3oa** was 3%, using 1,3,5-TMB as an IS (Fig. S75) (2.81 mg) (average from 2 independent experiments).



Epigallocatechin gallate (EGC, **1p**)

Substrate selection: Epigallocatechin (**1p**) was chosen because epigallocatechin gallate is an ester of epigallocatechin and gallic acid (Scheme S21).



Scheme S21. Epigallocatechin (**1p**) moiety in epigallocatechin gallate

The reaction was carried according to procedure B. It has been shown that the yields of **3pa** and **8** were 45% and 4%, correspondingly, using 1,3,5-TMB as an IS (Fig. S76) (average from 2 independent experiments). The reaction has to be mixed, because EGC **11** was not soluble in a DCM/DMSO mixture.

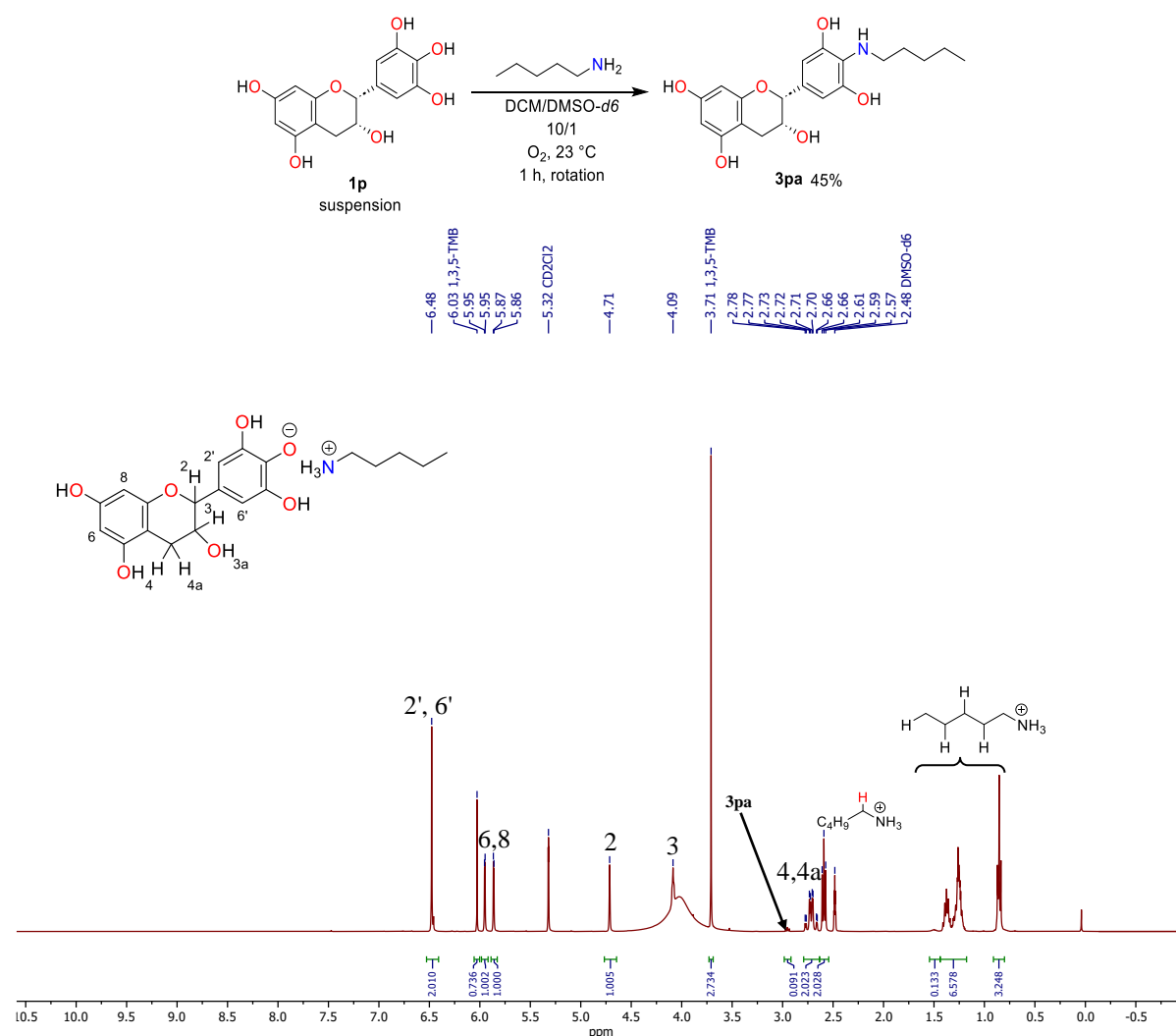


Fig. S76a. *in situ* ¹H NMR spectrum of **1p/2a** ion pair under N₂, DCM-*d*2/DMSO-*d*6, 400 MHz.

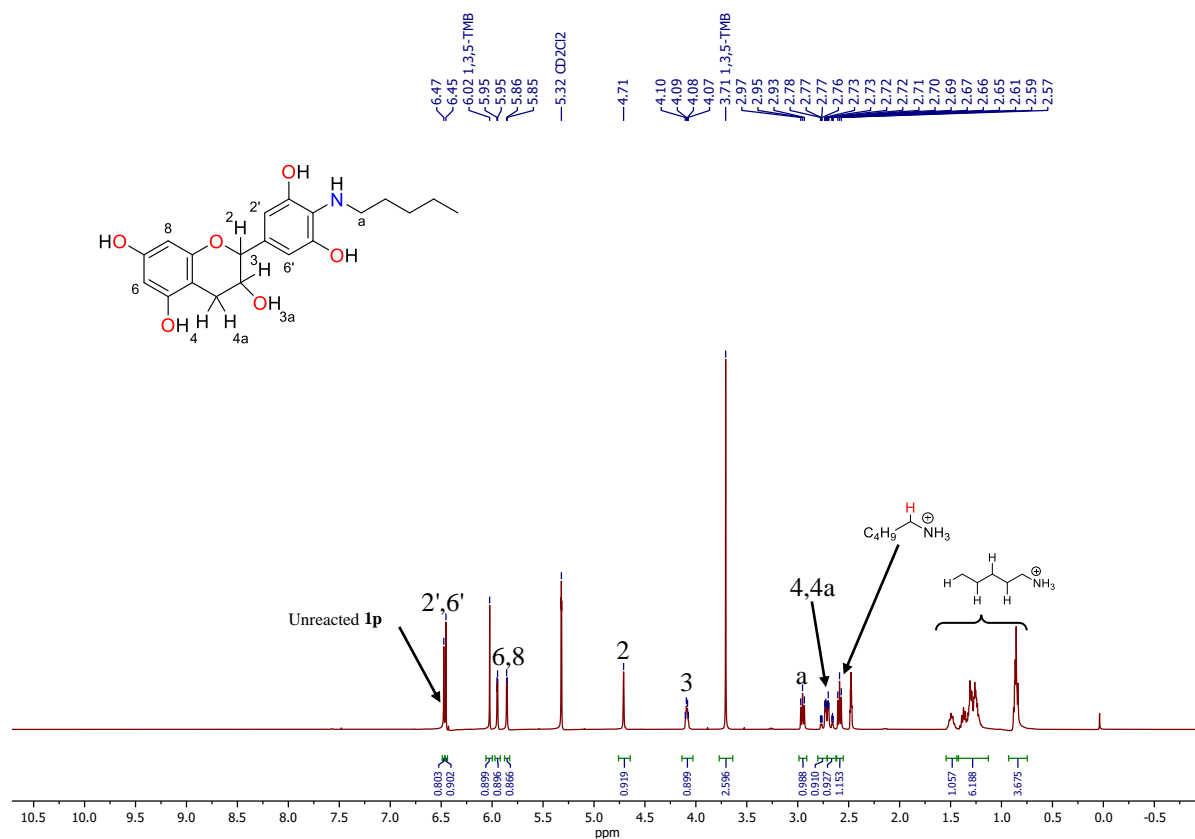
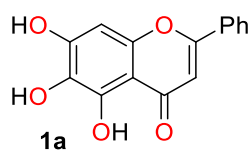


Fig. S76b. *in situ* ¹H NMR spectrum of **1p/2a** oxidative coupling after 1 hour, DCM-*d*₂/DMSO-*d*₆, 400 MHz.

1.3.7.7. Synthesis and analytical data of polyphenols **1a-q**

Important note: Purchased or synthesized flavonoids might be represented in a form of stable hydrate complexes. If the excessive water peak is detected in ^1H NMR spectrum of the certain flavonoid in dry $\text{DMSO-}d_6$, the elemental analysis of the flavonoid was performed to confirm the composition ($\text{Flavonoid} \times n \text{H}_2\text{O}$). If the flavonoid is in its hydrate form, it is shown next to the corresponding flavonoid in the text below.

5,6,7-trihydroxyflavone (BA, **1a**).^[1]



^1H NMR (400 MHz, $\text{DMSO-}d_6$) δ 12.65 (s, 1H), 10.55 (s, 1H), 8.81 (s, 1H), 8.11 – 8.01 (m, 2H), 7.65 – 7.56 (m, 3H), 6.93 (s, 1H), 6.63 (s, 1H).

^{13}C NMR (101 MHz, $\text{DMSO-}d_6$) δ : 182.2, 163.0, 153.7, 149.9, 147.0, 131.9, 131.0, 129.4, 129.2, 126.3, 104.5, 104.3, 94.1.

IR $\tilde{\nu}$ = 3408(m, -OH), 1656(s, C=O), 1617(s), 1578(s), 1505(s), 1470(s), 1419(s), 1385(s), 1339(s), 1296(s), 1212(m), 1182(w), 1160(vs), 1103(m), 1085(s), 1032(m), 1021(m), 916(w), 897(m), 852(m), 826(m), 782(vw), 776(w), 733(m), 714(w), 705(w), 681(m) cm^{-1} .

Elem. Calcd for $\text{C}_{15}\text{H}_{10}\text{O}_5$: C 66.67, H 3.73. Found: C 66.45, H 3.75.

Crystals of **1a** were obtained by slow evaporation of n-butanol solution.

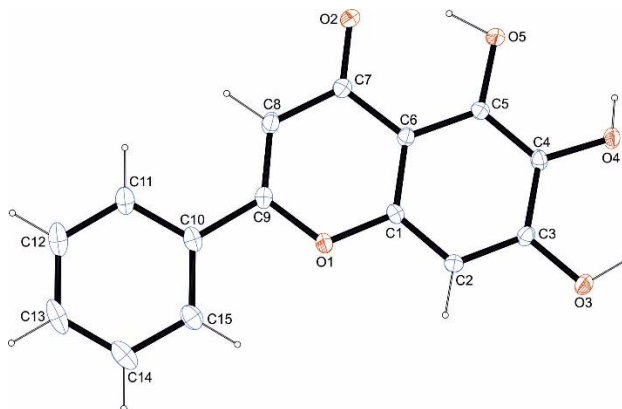


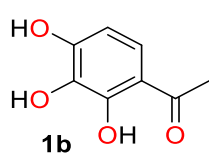
Fig. S77. X-ray structure of **1a**.

Table S9. Crystallographic data for **1a**

net formula	$\text{C}_{15}\text{H}_{10}\text{O}_5$	transmission factor range	0.93-0.99
$M_r/\text{g mol}^{-1}$	270.23	refls. measured	23593
crystal size/mm	$0.110 \times 0.080 \times 0.070$	R_{int}	0.0426
T/K	173.(2)	mean $\sigma(I)/I$	0.0203
radiation	MoK α	θ range	3.063–26.372
diffractometer	Bruker D8 Venture TXS	observed refls.	2029
crystal system	Monoclinic	x, y (weighting scheme)	0.0464, 0.4175
space group	P 1 21/c 1	hydrogen refinement	mixed
a/ \AA	7.8165(4)	Flack parameter	?

b/Å	13.2981(6)	refls in refinement	2411
c/Å	11.5748(5)	parameters	193
α /	90	restraints	0
β /	100.768(2)	R(F _{obs})	0.0387
γ /	90	R _w (F ²)	0.1033
V/Å ³	1181.95(10)	S	1.079
Z	4	shift/error _{max}	0.001
calc. density/g cm ⁻³	1.519	max electron density/e Å ⁻³	0.234
μ /mm ⁻¹	0.115	min electron density/e Å ⁻³	-0.174
absorption correction	Multi-Scan		

2,3,4-Trihydroxyacetophenone (TAP, **1b**).^[1]



¹H NMR (400 MHz, DMSO-*d*₆) δ 12.61 (s, 1H), 10.07 (bs, 1H), 8.63 (bs, 1H), 7.30 (d, *J* = 8.8 Hz, 1H), 6.40 (d, *J* = 8.8 Hz, 1H), 2.51 (s, 3H).

¹³C NMR (101 MHz, DMSO-*d*₆) δ 203.5, 152.6, 152.2, 132.3, 123.2, 113.2, 107.7, 26.4.

IR $\tilde{\nu}$ = 3348(m, -OH), 1643(s, C=O), 1598(s), 1507(s), 1463(m), 1370(s), 1319(vs), 1289(vs), 1246(s), 1226(s), 1182(m), 1138(w), 1045(s), 1025(m), 898(m), 813(m), 791(vs), 679(m) cm⁻¹.

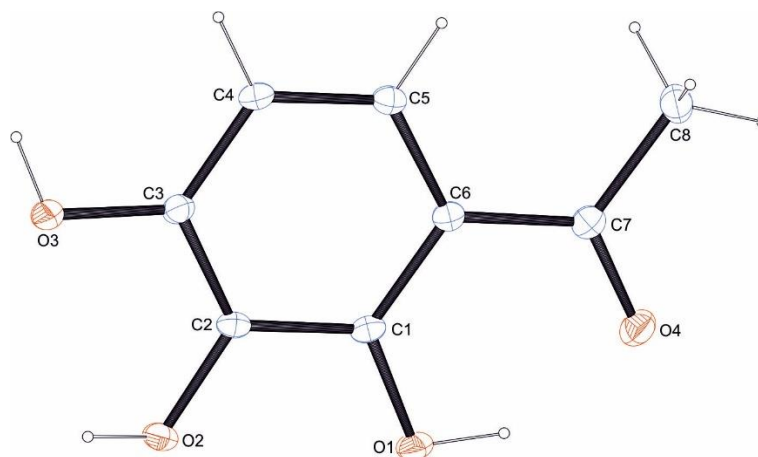


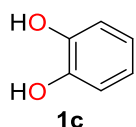
Fig. S78. X-ray structure of **1b**.

Table S10. Crystallographic data for **1b**.

net formula	C ₈ H ₈ O ₄	transmission factor range	0.97-0.99
M _r /g mol ⁻¹	168.14	refls. measured	32672
crystal size/mm	0.140 × 0.100 × 0.080	R _{int}	0.0431
T/K	173.(2)	mean σ (I)/I	0.0180
radiation	MoK α	θ range	3.104–27.477
diffractometer	Bruker D8 Venture TXS	observed refls.	1548
crystal system	orthorhombic	x, y (weighting scheme)	0.0408, 0.9348
space group	'P b c a'	hydrogen refinement	mixed
a/Å	10.2848(6)	Flack parameter	?
b/Å	11.7842(8)	refls in refinement	1707
c/Å	12.3377(8)	parameters	122

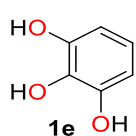
$\alpha/$	90	restraints	0
$\beta/$	90	$R(F_{\text{obs}})$	0.0371
$\gamma/$	90	$R_w(F^2)$	0.0991
$V/\text{\AA}^3$	1495 31(17)	S	1.077
Z	8	shift/error _{max}	0.001
calc. density/ g cm^{-3}	1.494	max electron density/ e \AA^{-3}	0.275
μ/mm^{-1}	0.121	min electron density/ e \AA^{-3}	-0.230
absorption correction	Multi-Scan		

o-Catechol (*o*-Cat, **1c**)



$^1\text{H NMR}$ (400 MHz, DMSO-*d*₆) δ 8.80 (s, 2H), 6.72 (dd, $J = 5.9, 3.6$ Hz, 2H), 6.59 (dd, $J = 5.9, 3.6$ Hz, 2H).

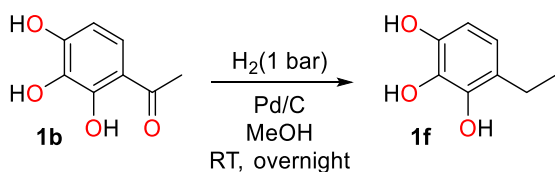
1,2,3-Trihydroxybenzene (Pyr, **1e**)



$^1\text{H NMR}$ (400 MHz, DMSO-*d*₆) δ 8.73 (bs, 2H), 8.02 (bs, 1H), 6.40 (dd, $J = 8.3, 7.5$ Hz, 1H), 6.23 (d, $J = 8.3$ Hz, 2H).

$^{13}\text{C NMR}$ (101 MHz, DMSO-*d*₆) δ 146.29, 133.10, 118.42, 107.06.

4-ethyl pyrogallol (EtPyr, **1f**.^[13])



To the stirring suspension of 10% w/w Pd/C (25 mg) in 30 ml of MeOH was added 336 mg of TAP (**1b**) (2 mmol) under nitrogen atmosphere, which after was replaced by H₂

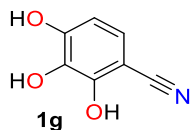
gas. The resulting reaction mixture was stirred overnight at RT. The reaction mixture was filtered through a Celite pad, and all the volatiles were evaporated under reduced pressure give EtPyr (**1f**) as colorless solid (300 mg, 97%).

$^1\text{H NMR}$ (400 MHz, DMSO-*d*₆) δ 8.74 (bs, 1H), 8.12 (bs, 1H), 8.00 (bs, 1H), 6.32 (d, $J = 8.2$ Hz, 1H), 6.19 (d, $J = 8.2$ Hz, 1H), 2.41 (q, $J = 7.5$ Hz, 2H), 1.05 (t, $J = 7.5$ Hz, 3H).

$^{13}\text{C NMR}$ (101 MHz, DMSO-*d*₆) δ 144.0, 143.9, 132.8, 121.6, 118.1, 106.2, 22.5, 14.8.

MS (APCI) calcd for C₈H₁₁O₃ [M + H]⁺, 155.1; found 155.0

2,3,4-trihydroxybenzonitrile (TBN, **1g**)^[14]



Modified literature procedure.^[15]

170 mg of $\text{NH}_2\text{OH}\cdot\text{HCl}$ (2.44 mmol, 1.05 eq) were added to a solution of 2,3,4-trihydroxybenzaldehyde (356 mg, 2.3 mmol, 1 eq) in 2 ml of dry DMSO under N_2 atmosphere. The reaction was stirred at 90 °C for 2 h, quenched with 10 ml of water, extracted with *n*-BuOH (3×10 ml). The organic phases were combined and dried over MgSO_4 . All the volatiles were evaporated under reduced pressure and the crude material was purified by column chromatography, followed by 3×recrystallization from *i*Hex/EtOAc. The title compound **1g** was obtained as pale brown solid (230 mg, 65%).

^1H NMR (400 MHz, $\text{DMSO-}d_6$) δ 10.22 (bs, 1H), 9.88 (bs, 1H), 8.93 (bs, 1H), 6.89 (d, $J = 8.5$ Hz, 1H), 6.40 (d, $J = 8.5$ Hz, 1H).

^{13}C NMR (101 MHz, $\text{DMSO-}d_6$) δ 150.9, 150.1, 133.3, 123.4, 117.9, 108.2, 90.7.

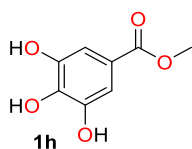
HRMS (ESI) m/z calcd for $\text{C}_7\text{H}_4\text{NO}_3$ $[\text{M} - \text{H}]^-$, 150.0196; found 150.0197.

IR $\tilde{\nu} = 3214(\text{w})$, 2234(s, $\text{C}\equiv\text{N}$), 1630(s), 1508(s), 1485(m), 1311(vs), 1227(s), 1052(s), 949(s), 796(s), 743 (w).

R_f 0.39 (*i*Hex/[EtOAc/EtOH=3/1] = 1/1)

M.p. 168 °C

Methyl 3,4,5-trihydroxybenzoate (MetGal, **1h**)



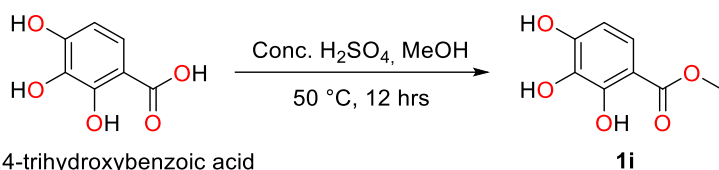
^1H NMR (400 MHz, $\text{DMSO-}d_6$) δ 9.16 (bs, 3H), 6.93 (s, 1H), 3.74 (s, 3H).

^{13}C NMR (101 MHz, $\text{DMSO-}d_6$) δ 166.4, 145.7, 138.5, 119.4, 108.6, 51.7.

IR $\tilde{\nu} = 3291(\text{s})$, 1669(s, $\text{C}=\text{O}$), 1610(s), 1540(s), 1464(m), 1436(s), 1372(m), 1304(vs), 1258(s), 1190(s), 1034(s), 1002(s), 917(w), 879(m), 806(w), 772(s), 751(m) cm^{-1} .

M.p. 208 °C

Methyl 2,3,4-trihydroxybenzoate (psMetGal, **1i**)^[16]



To a stirred solution of 2,3,4-trihydroxybenzoic acid (0.86 g, 5.06 mmol, 1.0 eq) in MeOH

(10 mL) was added conc H₂SO₄ (2 mL). The resultant mixture was stirred at 60 °C for 12 h overnight. The reaction mixture was diluted with H₂O (20 mL) and the aqueous phase was extracted with EtOAc (3×50 mL). The combined organic extract was dried over anhydrous MgSO₄, filtered, and concentrated in *vacuo* to afford a brown solid. The residue was recrystallized twice from *i*Hex/EtOAc mixture and then purified by flash column chromatography to afford a dark solid, which is further recrystallized again from *i*Hex/EtOAc under N₂ atmosphere to afford **1i** (0.28 g, 1.54 mmol, 30%) as pale-yellow needle crystals.

(10 mL) was added conc H₂SO₄ (2 mL). The resultant mixture was stirred at 60 °C for 12 h overnight. The reaction mixture was diluted with H₂O (20 mL) and the aqueous phase was extracted with EtOAc (3×50 mL). The combined organic extract was dried over anhydrous MgSO₄, filtered, and concentrated in *vacuo* to afford a brown solid. The residue was recrystallized twice from *i*Hex/EtOAc mixture and then purified by flash column chromatography to afford a dark solid, which is further recrystallized again from *i*Hex/EtOAc under N₂ atmosphere to afford **1i** (0.28 g, 1.54 mmol, 30%) as pale-yellow needle crystals.

¹H NMR (400 MHz, DMSO-*d*₆) δ 10.64 (s, 1H), 9.93 (s, 1H), 8.61 (s, 1H), 7.18 (d, *J* = 8.7 Hz, 1H), 6.39 (d, *J* = 8.8 Hz, 1H), 3.84 (s, 3H)

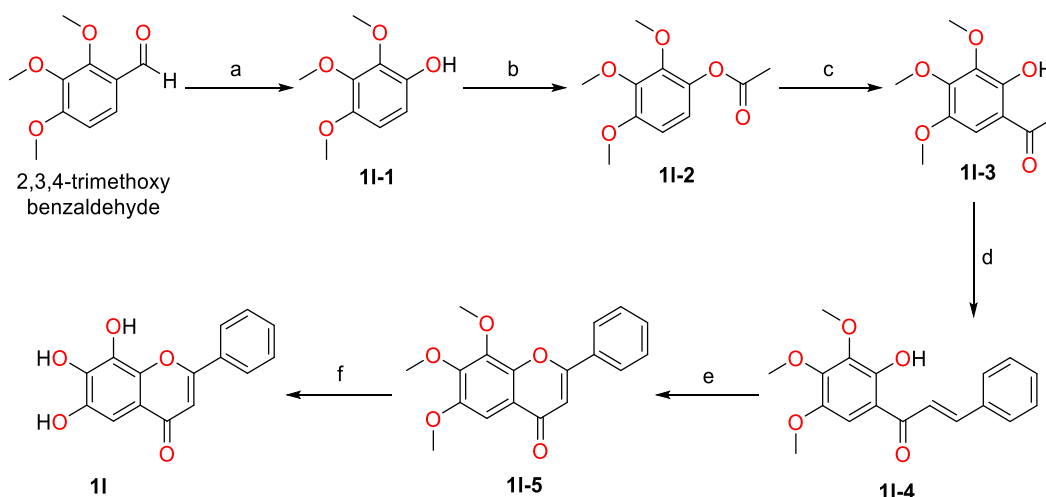
¹³C NMR (101 MHz, DMSO-*d*₆) δ 170.1, 151.8, 150.9, 132.6, 120.7, 107.9, 104.4, 52.1

IR $\tilde{\nu}$ = 3400(m, -OH), 3328(m), 1653(s, C=O), 1519(w), 1437(s), 1268(s), 1199(s), 1144(s), 1042(s), 986(s), 779(s), 732(s), 698(m) cm⁻¹.

HRMS (ESI) *m/z* calcd for C₈H₇O₅ [M - H]⁻, 183.0299; found 183.0299.

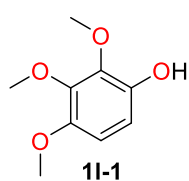
R_f 0.60 (DCM/MeOH/AcOH = 100/10/1)

Synthetic route to 6,7,8-trihydroxyflavone psBA (**1i**)



Scheme S22. Synthesis of **1i**. Reagents and conditions of reaction: (a) 30% aq. H₂O₂, conc H₂SO₄, MeOH, N₂, RT, 12 h; (b) Ac₂O, Pyridine, DMAP, CHCl₃, RT, 12 h; (c) BF₃·OEt₂, N₂, 100 °C, 1 h; (d) benzaldehyde, 50% aq. NaOH, MeOH, 48 h; (e) I₂, DMSO, 180 °C, 2 h; (f) 1M BBr₃, DCM, reflux, 20 h.

a. 2,3,4-Trimethoxyphenol **11-1**



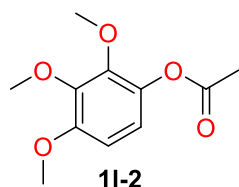
Modified literature procedure.^[17]

To a stirred solution of the starting material 2,3,4-trimethoxybenzaldehyde (4.80 g, 24.46 mmol, 1.0 eq) in MeOH (50 mL), 30% H₂O₂ aqueous solution (3.4 mL, 31.80 mmol, 1.3 eq) was added under N₂ atmosphere. Catalytic amount of concentrated H₂SO₄ (0.5 mL) was added at 0°C over 5 min and the reaction mixture was warmed up to RT and further stirred for 12 h. The reaction was quenched with saturated NaHCO₃ aqueous solution (50 mL). The aqueous layer was extracted with DCM (3×50 mL). The DCM layers were combined, washed with brine (50 mL), dried over anhydrous MgSO₄, concentrated in *vacuo* to afford 2,3,4-trimethoxyphenol (**11-1**) (4.51 g, 24.48 mmol, 100%) as a brown oil, which was pure according to ¹H NMR analysis and it was used without further purification. Spectral data are in agreement with literature value.¹⁸

¹H NMR (400 MHz, CDCl₃) δ 6.63 (d, *J* = 9.0 Hz, 1H), 6.55 (d, *J* = 9.0 Hz, 1H), 5.36 (s, 1H), 3.96 (s, 3H), 3.89 (s, 3H), 3.81 (s, 3H).

MS (APCI) calcd for C₉H₁₃O₄ [M + H]⁺, 185.1; found 185.1.

b. 2,3,4-Trimethoxyphenyl acetate (**11-2**)



Modified literature procedure.^[18]

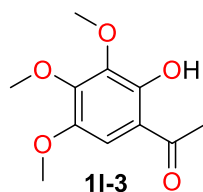
To a stirred solution of 2,3,4-trimethoxyphenol (**11-1**) (4.51 g, 24.48 mmol, 1.0 eq) and pyridine (59.2 mL, 734.40 mmol, 30.0 eq) in CHCl₃ (80 mL), Ac₂O (8.1 mL, 85.68 mmol, 3.5 eq) and DMAP (cat) were added at RT under N₂ atmosphere. After stirring for 12 h at RT, the reaction mixture was quenched with H₂O (200 mL) and extracted with DCM (3 × 50 mL). The combined organic layers were washed with saturated KHSO₄ aqueous solution (200 mL), washed with brine (200 mL), then washed with saturated NaHCO₃ aqueous solution (200 mL), and washed with brine (200 mL). The organic layer was dried over anhydrous MgSO₄ and concentrated in *vacuo* to yield 2,3,4-trimethoxyphenylacetate (**11-2**) (5.23 g, 23.12 mmol, 95%) as a brown oil, which was pure according to ¹H NMR analysis and it was used without further purification. Spectral data are in agreement with literature value.^[18]

¹H NMR (400 MHz, CDCl₃) δ 6.74 (d, 1H, *J* = 9.0 Hz), 6.62 (d, 1H, *J* = 9.0 Hz), 3.89 (s, 3H), 3.88 (s, 3H), 3.85 (s, 3H), 2.31 (s, 3H).

MS (APCI) calcd for C₁₁H₁₅O₅ [M + H]⁺, 227.1; found 227.1.

c. 1-(2-Hydroxy-3,4,5-trimethoxyphenyl)ethan-1-one (**11-3**)

Modified literature procedure.^[18]

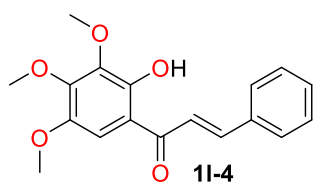


To the 2,3,4-trimethoxyphenyl acetate (**11-2**) (2.27 g, 10.03 mmol, 1.0 eq) $\text{BF}_3 \cdot \text{Et}_2\text{O}$ (25.3 mL, 200.68 mmol, 20.0 eq) was added dropwise at 0 °C under N_2 atmosphere. The reaction mixture was then heat up to 100 °C and stirred for 1 h. The reaction was quenched with H_2O (100 mL) and the resulting mixture was extracted with DCM (3×50 mL). The organic layers were combined and washed with saturated NaHCO_3 aqueous solution (100 mL), brine (100 mL), dried over anhydrous MgSO_4 , and concentrated in *vacuo* to afford 1-(2-hydroxy-3,4,5-trimethoxyphenyl)ethan-1-one (**11-3**) (2.27 g, 100%) as brown crystals. Spectral data are in agreement with literature value.^[18]

$^1\text{H NMR}$ (400 MHz, CDCl_3) δ 12.44 (s, 1H), 6.92 (s, 1H), 4.04 (s, 3H), 3.92 (s, 3H), 3.86 (s, 3H), 2.59 (s, 3H).

MS (APCI) calcd for $\text{C}_{11}\text{H}_{15}\text{O}_5$ $[\text{M} + \text{H}]^+$, 227.1; found 227.1.

d. 1-(2-Hydroxy-3,4,5-trimethoxyphenyl)-3-phenylprop-2-en-1-one (**11-4**)



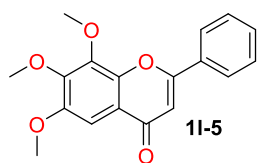
Modified literature procedure.^[19]

To a stirred solution of 1-(2-hydroxy-3,4,5-trimethoxyphenyl)ethan-1-one (**11-3**) (1.97 g, 8.71 mmol, 1.0 eq) and freshly distilled acetophenone (1.0 mL, 9.58 mmol, 1.1 eq) in MeOH (25 mL) was added a 50% w/v NaOH aqueous solution (6 mL) dropwise at 0 °C, upon which the reaction mixture immediately turned dark brown. The reaction mixture was then warmed up to RT and stirred for 48 h. It was quenched with 2M HCl (40 mL) and extracted with DCM (3×50 mL). The combined organic layers were dried over anhydrous MgSO_4 and concentrated in *vacuo*. The crude material was purified by flash column chromatography (*i*Hex/EtOAc = 10/1 \rightarrow 5/1; *i*Hex/EtOAc = 5/1, R_f 0.40) to afford 1-(2-hydroxy-3,4,5-trimethoxyphenyl)-3-phenylprop-2-en-1-one (**11-4**) (2.02 g, 6.43 mmol, 74%) as blood-red crystals.

$^1\text{H NMR}$ (400 MHz, CDCl_3) δ 13.08 (s, 1H), 7.92 (d, $J = 15.4$ Hz, 1H), 7.69 – 7.65 (m, 2H), 7.53 (d, $J = 15.4$ Hz, 1H), 7.46 – 7.44 (m, 3H), 7.11 (s, 1H), 4.07 (s, 3H), 3.96 (s, 3H), 3.90 (s, 3H).

MS (APCI) calcd for $\text{C}_{18}\text{H}_{19}\text{O}_5$ $[\text{M} + \text{H}]^+$, 315.1; found 315.1.

e. 6,7,8-Trimethoxyflavone (**11-5**)



Modified literature procedure.^[20]

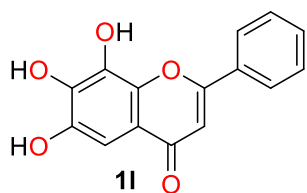
To a stirred solution of 1-(2-hydroxy-3,4,5-trimethoxyphenyl)-3-phenylprop-2-en-1-one (**11-4**) (1.90 g, 6.05 mmol 1.0 eq) in dry DMSO (40 mL) was added I₂ (0.15 g, 0.60 mmol, 0.1 eq) under N₂ atmosphere.

The resulting mixture was stirred for 2 h at 180 °C in a sand bath. The reaction was cooled down to RT, quenched with H₂O (60 mL). The resulting black suspension was treated with 1 g Na₂S₂O₃ and extracted with DCM (3×50 mL). The organic layers were combined, washed with brine (6×100 mL) to remove remaining DMSO, dried over anhydrous MgSO₄, and concentrated under reduced pressure to afford 6,7,8-trimethoxyflavone (**11-5**) (1.64 g, 5.26 mmol, 87%) as dark brown crystals, which was pure according to ¹H NMR analysis and it was used without further purification.

¹H NMR (400 MHz, CDCl₃) δ 7.98 – 7.91 (m, 2H), 7.58 – 7.49 (m, 3H), 7.40 (s, 1H), 6.81 (s, 1H), 4.10 (s, 3H), 4.05 (s, 3H), 3.97 (s, 3H)

MS (APCI) calcd for C₁₈H₁₇O₅ [M + H]⁺, 313.1; found 313.1.

f. 6,7,8-trihydroxyflavone (psBA, **11**)



Modified literature procedure.^[21]

To a stirred solution of 6,7,8-trimethoxy-2-phenyl-4H-chromen-4-one (**11-5**) (0.62 g, 2.00 mmol, 1.0 eq) in dry DCM (10 mL) was added 1M BBr₃ solution in DCM (30 mL, 30.00 mmol, 15.0 eq) dropwise at 0 °C under N₂ atmosphere and the obtained solution was stirred for 30 min at 0 °C. The reaction mixture was then warmed up and stirred under reflux for 20 h. After being cooled to 0 °C, MeOH (60 mL) was added, and the reaction mixture was further stirred for 2 h at RT to quench the remaining BBr₃. The reaction mixture was concentrated in *vacuo* to afford a dark brown solid. The residue was recrystallized twice from H₂O/MeOH = 2/1 solution and dried at 120 °C in *vacuo* for 2 h to afford 6,7,8-trihydroxyflavone (**11**) (0.25 g, 0.92 mmol, 46%) as a beige powder.

¹H NMR (400 MHz, DMSO-*d*₆) δ 9.61 (s, 3H), 8.12 (dd, *J* = 6.4, 2.7 Hz), 7.57 (m, 3H), 6.92 (s, 1H), 6.84 (s, 1H)

¹³C NMR (101 MHz, DMSO-*d*₆) δ 176.6, 161.2, 144.6, 141.4, 140.2, 134.0, 131.8, 131.3, 129.0, 126.2, 115.8, 105.6, 98.3

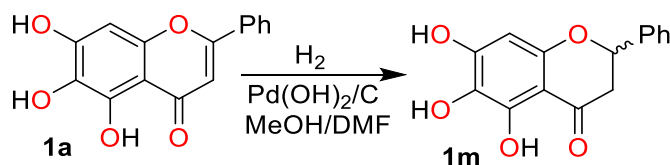
HRMS (ESI) *m/z* calcd for C₁₅H₉O₅ [M - H]⁻, 269.0455; found 269.0455.

IR $\tilde{\nu}$ = 3473(w), 3065(w), 1624 (w), 1573(s, C=O), 1552(s), 1484(s), 1448(m), 1404(s),

1345(s), 1254(m), 1235(m), 1182(s), 1110(s), 1059(w), 1036(m), 938(vw), 923(vw), 870(m), 841(w), 774 (m), 680(m), 656(w) cm^{-1} .

Elem. Calcd for $\text{C}_{15}\text{H}_{10}\text{O}_8$: C 66.67, H 3.73. Found: C 66.30, H 3.74.

5,6,7-trihydroxy-2-phenylchroman-4-one (BA_{H_2} , **1m**)^[22]



Modified literature procedure.^[23]

270 mg of Baicalein (**1a**, 1 mmol) and 25 mg of 50% $\text{Pd}(\text{OH})_2/\text{C}$ were stirred in 15 ml MeOH under H_2 atmosphere.

The resulting mixture was stirred for 3 h, and a small aliquot was taken for MS analysis, which showed no product formation. After addition of 6 ml of dry DMF, the reaction mixture was stirred for 18 h under H_2 atmosphere. The reaction mixture was filtered through a Celite pad and evaporated under reduced pressure. The crude product was purified by flash column chromatography (iHex/[EtOAc/EtOH=3/1] = 1/1). The title compound **1m** was obtained as yellow solid (230 mg, 85%).

^1H NMR (400 MHz, $\text{DMSO}-d_6$) δ 11.97 (s, 1H), 10.43 (s, 1H), 8.26 (s, 1H), 7.55 – 7.47 (m, 2H), 7.47 – 7.32 (m, 3H), 5.98 (s, 1H), 5.51 (dd, $J = 12.6, 3.0$ Hz, 1H), 3.22 (dd, $J = 17.1, 12.7$ Hz, 1H), 2.76 (dd, $J = 17.1, 3.1$ Hz, 1H).

^{13}C NMR (101 MHz, $\text{DMSO}-d_6$) δ 196.6, 155.8, 155.0, 150.2, 139.0, 128.5, 128.5, 126.6, 126.4, 101.7, 94.8, 78.5, 42.4.

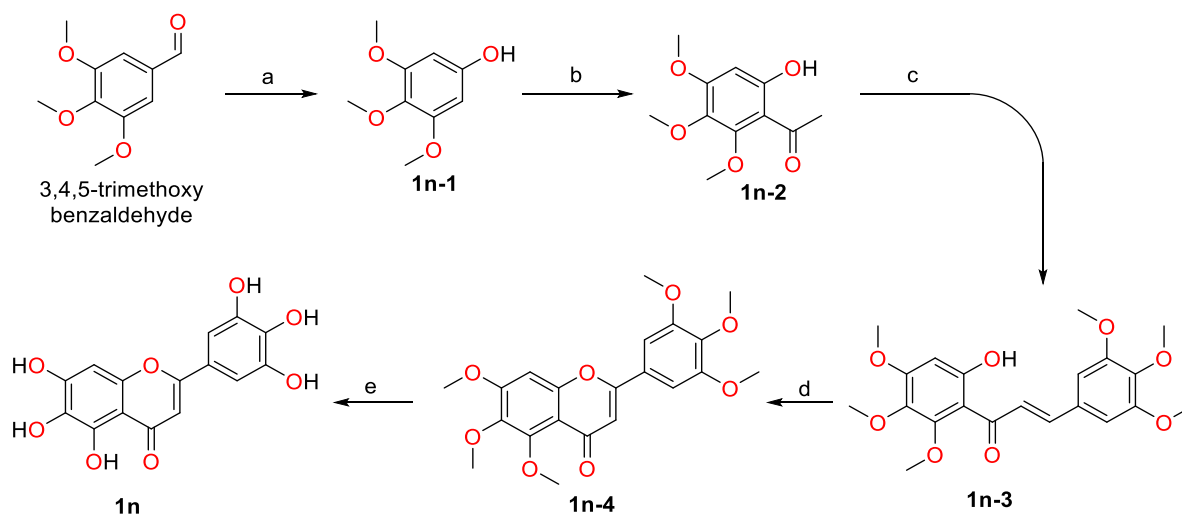
IR $\tilde{\nu}$ = 3225(w, -OH), 1626 (s, C=O), 1593(s), 1465(s), 1362(m), 1338(w), 1270(s), 1203(s), 1152(s), 1058(s), 992(w), 906(w), 853(vw), 824 (w), 763(m).

HRMS (ESI) m/z calcd for $\text{C}_{15}\text{H}_{11}\text{O}_5$ [$\text{M} - \text{H}$]⁻, 271.0611; found 271.0612.

R_f 0.61 (iHex/[EtOAc/EtOH=3/1] = 1/1)

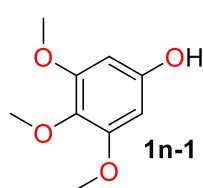
M.p 148 °C (decomp)

Synthetic route to 2',3',5',5,6,7-hexahydroxyflavone (HHF, **1n**)



Scheme S23. Synthesis of **1n**. Reagents and conditions of reaction: (a) *m*-CPBA, NaHCO₃, 1 h, RT; then K₂CO₃, MeOH, 1 h, RT (b) AcCl, AlCl₃, N₂, 100 °C, 3 h; (c) 3,4,5-trimethoxybenzaldehyde, 50% aq. NaOH, MeOH, 72 h, RT; (d) I₂, DMSO, 180 °C, 2 h; (e) 47% HBr, AcOH, N₂, 135 °C, 48 h.

a. 3,4,5-Trimethoxyphenol (**1n-1**)

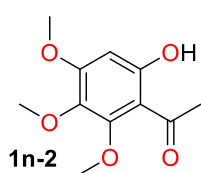


Modified literature procedure.^[24]

To a stirred solution of 3,4,5-trimethoxybenzaldehyde (2.1 g, 10.7 mmol, 1.0 eq) in 100 ml of dry DCM, 4.41 g of NaHCO₃ was added under N₂ atmosphere. Then *m*-CPBA (4.55 g, 20.3 mmol, 1.9 eq) was added to the suspension, and the reaction was allowed to stir for 1 h at RT. After, the reaction was quenched with saturated aqueous solution of Na₂S₂O₃ and extracted with DCM (3×25 mL). The combined organic layers were washed with saturated aqueous NaHCO₃ solution and dried over MgSO₄. The crude material obtained after evaporation was dissolved in 50 mL of MeOH and treated with K₂CO₃ (5 g, 36.3 mmol) to hydrolyze the remaining formate ester. The reaction was allowed to stir for an additional hour, diluted with water and extracted with diethyl ether (3×50 mL). The combined organic phases were washed with brine, dried over MgSO₄, filtered and evaporated under reduced pressure. The product **1n-1** was obtained as colourless solid (1 g, 51%).

¹H NMR (400 MHz, DMSO-*d*₆) δ 9.20 (s, 1H), 6.04 (s, 2H), 3.69 (s, 6H), 3.54 (s, 3H).

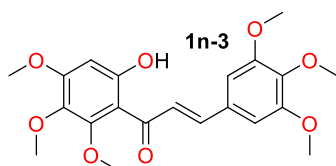
b. 1-(6-hydroxy-2,3,4-trimethoxyphenyl)ethan-1-one (**1n-2**)



The compound was synthesized following the modified literature procedure.^[25] The crude product was purified on a silica gel column (iHex/EtOAc = 10:1 → 2/1) to yield 0.92 g of the desired product as a pale-yellow solid (76%).

¹H NMR (400 MHz, DMSO-*d*6) δ 13.02 (s, 1H), 6.35 (s, 1H), 3.90 (s, 3H), 3.84 (s, 3H), 3.67 (s, 3H), 2.58 (s, 3H).

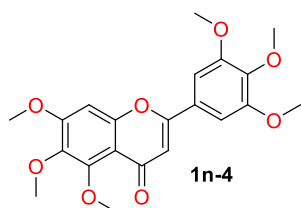
c. *E*-1-(6-hydroxy-2,3,4-trimethoxyphenyl)-3-(3,4,5-trimethoxyphenyl)prop-2-en-1-one (**1n-3**)



The compound was synthesized following the procedure given above (**11-4**). The title compound was obtained as an orange solid (1.1 g, 67%). Spectral data are in agreement with literature value.^[26]

¹H NMR (400 MHz, CDCl₃) δ 13.70 (s, 1H), 7.85 (d, *J* = 15.5 Hz, 1H), 7.76 (d, *J* = 15.5 Hz, 1H), 6.87 (s, 2H), 6.30 (s, 1H), 3.93 (s, 3H), 3.92 (s, 6H), 3.91 (s, 3H), 3.90 (s, 3H), 3.84 (s, 3H).

d. 3',4',5',5,6,7-trimethoxyflavone (**1n-4**)

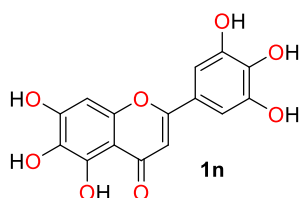


The compound was synthesized following the procedure given above (**11-5**). The title compound was obtained as a yellow solid (0.93 g, 84%). The product was pure according to ¹H NMR spectrum to be used for the next step without further purification.

Spectral data are in agreement with literature value.^[27]

¹H NMR (400 MHz, CDCl₃) δ 7.07 (s, 2H), 6.80 (s, 1H), 6.62 (s, 1H), 3.99 (s, 6H), 3.95 (s, 6H), 3.92 (s, 6H).

e. 3',4',5',5,6,7-trihydroxyflavone **1n** (HHF, **1n**)



Modified literature procedure.^[28]

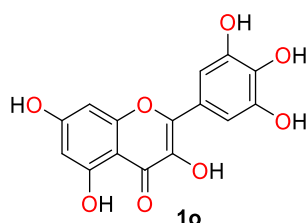
200 mg of **1n-4** were refluxed in a solution of 8 mL of 47% HBr and 10 mL of AcOH under a N₂ atmosphere for 48 h. The reaction was then cooled to RT and extracted with n-butanol (3×10 mL). The organic phases were combined, dried over Na₂SO₄, and concentrated under reduced pressure to yield a black crude material (105 mg). The crude material was purified by recrystallization from MeOH/Water, resulting in the isolation of a small amount (15 mg) of yellow solid for further FRAP/ORAC assays. Spectral data are in agreement with literature value.^[28]

¹H NMR (400 MHz, DMSO-*d*₆) δ 12.80 (s, 1H), 10.48 (bs, 1H), 9.36 (bs, 2H), 9.08 (bs, 1H), 8.73 (bs, 1H), 6.95 (s, 2H), 6.50 (s, 1H), 6.49 (s, 1H).

¹³C NMR (101 MHz, DMSO-*d*₆) δ 182.3, 164.3, 153.7, 150.1, 147.5, 146.8, 138.1, 129.6, 121.1, 106.0, 104.4, 102.7, 94.1.

APCI MS: calcd for C₁₅H₁₁O₈ [M + H]⁺, 319.0, found 319.3.

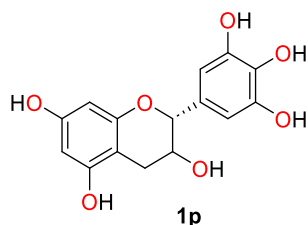
Myricetin (Myr, **1o**)



¹H NMR (400 MHz, DMSO-*d*₆) δ 12.50 (s, 1H), 10.79 (bs, 1H), 9.35 (bs, 1H), 9.23 (bs, 2H), 8.83 (bs, 1H), 7.24 (s, 2H), 6.37 (d, *J* = 2.0 Hz, 1H), 6.18 (d, *J* = 2.0 Hz, 1H).

Elem. Calcd for C₁₅H₁₀O₈ × H₂O: C 53.58, H 3.60. Found: C 53.52, H 3.62.

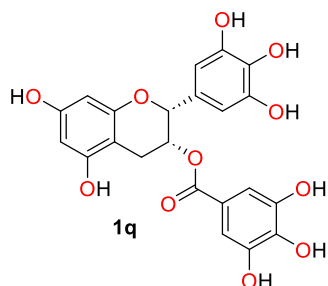
(-)-Epigallocatechin (EGC, **1p**)



¹H NMR (400 MHz, DMSO-*d*₆) δ 9.10 (bs, 1H), 8.89 (bs, 1H), 8.71 (bs, 2H), 7.95 (bs, 1H), 6.37 (s, 2H), 5.88 (d, *J* = 2.3 Hz, 1H), 5.70 (d, *J* = 2.3 Hz, 1H), 4.65 (bs, 1H), 4.62 (d, *J* = 4.5 Hz, 1H), 3.97 (qd, *J* = 4.2, 1.6 Hz, 1H), 2.66 (dd, *J* = 16.4, 4.5 Hz, 1H), 2.44 (d, *J* = 3.6 Hz, overlapped with DMSO-*d*₆ peak).

Elem. Calcd for C₁₅H₁₄O₇ × H₂O: C 55.56, H 4.97. Found: C 55.27, H 4.96.

(-)-Epigallocatechin gallate (EGCG, **1q**)

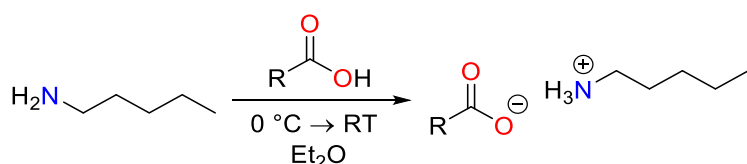


¹H NMR (400 MHz, DMSO-*d*₆) δ [9.29 (bs), 9.04 (bs), 8.74 (bs), 8.06 (bs), 8H], 6.81 (s, 2H), 6.39 (s, 2H), 5.92 (d, *J* = 2.3 Hz, 1H), 5.82 (d, *J* = 2.3 Hz, 1H), 5.35 (bs, 1H), 4.95 (s, 1H), 2.92 (dd, *J* = 17.3, 4.7 Hz, 1H), 2.64 (d, *J* = 16.4 Hz, 1H).

Elem. Calcd for C₂₂H₁₈O₁₁ × H₂O: C 55.47, H 4.23. Found: C 55.35, H 4.19.

1.3.7.8. Synthesis and analytical data of *N*-nucleophiles **2a-g**

Pentylamine salts **Acid·2a**

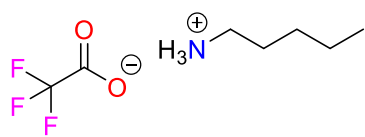


1 ml of pentylamine (0.755 g, 8.68 mmol, 1.05 eq) was dissolved in 10 ml of Et₂O at 0 °C. 1 eq of certain carboxylic

acid was added and the reaction mixture was stirred for 15 min at RT. The mixture was evaporated under reduced pressure and dried in vacuo. The product was obtained (>99%).

a) Pentylamine trifluoroacetate (**TFA**×**2a**)

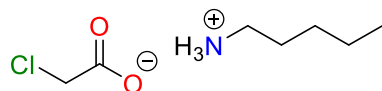
White powder



$^1\text{H NMR}$ (400 MHz, DMSO-*d*₆) δ 7.71 (bs, 3H), 3.26 – 2.68 (m, 2H), 1.58 – 1.46 (m, 2H), 1.32 – 1.24 (m, 4H), 0.94 – 0.81 (m, 3H).

b) Pentylamine monochloroacetate (**MCA**×**2a**)

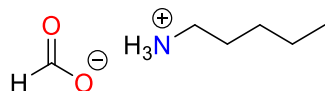
Yellow oil



$^1\text{H NMR}$ (400 MHz, CDCl₃) δ 8.22 (bs, 3H), 4.00 (s, 2H), 2.92 – 2.84 (m, 2H), 1.74 – 1.60 (m, 2H), 1.40 – 1.27 (m, 4H), 0.96 – 0.83 (m, 3H).

c) Pentylamine formate (**FA**×**2a**)

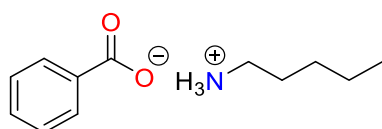
Colorless oil



$^1\text{H NMR}$ (400 MHz, DMSO-*d*₆) δ 8.45 (s, 1H), 2.74 – 2.66 (m, 2H), 1.57 – 1.45 (m, 2H), 1.35 – 1.20 (m, 4H), 0.93 – 0.81 (m, 3H).

d) Pentylamine benzoate (**BzA**×**2a**)

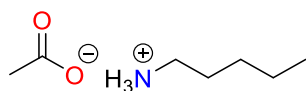
White powder



$^1\text{H NMR}$ (400 MHz, DMSO-*d*₆) δ 8.23 (bs, 3H), 7.88 – 7.83 (m, 2H), 7.49 – 4.81 (m, 3H), 2.74 (t, *J* = 7.4 Hz, 2H), 1.56 – 1.49 (m, 2H), 1.30 – 1.25 (m, 4H), 0.87 – 0.84 (m, 3H).

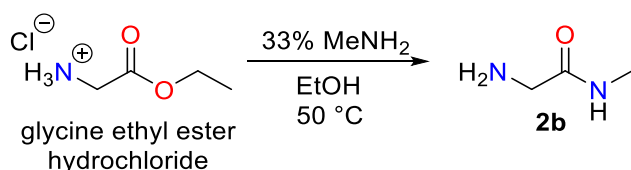
e) Pentylamine acetate (**AcA**×**2a**)

Colorless oil



$^1\text{H NMR}$ (400 MHz, DMSO-*d*₆) δ 6.88 (bs, 3H), 2.65 – 2.57 (m, 2H), 1.74 (s, 3H), 1.50 – 1.38 (m, 2H), 1.35 – 1.18 (m, 4H), 0.92 – 0.81 (m, 3H).

Glycine-*N*-methylamide (H-Gly-NMe, **2b**)



Modified literature procedure^[29]

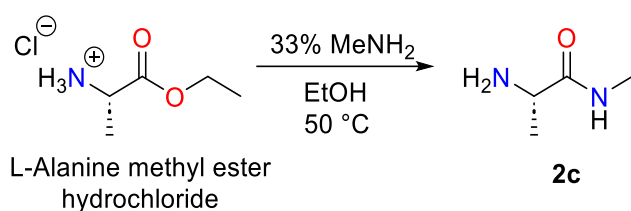
1 g of glycine ethyl ester hydrochloride (7.2 mmol, 1 eq) was stirred in 5 ml of 33% of MeNH₂ at 50 °C for 1 h and

overnight at RT. Afterwards 1 g of NaOH was added and stirring continued for 10 min. The mixture was evaporated under reduced pressure to then extracted with ethyl acetate (3×10 mL), which was filtered and dried in *vacuo*. The product was obtained as yellowish oil (323 mg, 52%). Spectral data are in agreement with literature value.^[29]

¹H NMR (400 MHz, DMSO-*d*₆) δ 7.75 (bs, 1H), 3.04 (s, 2H), 2.60 (d, *J* = 4.8 Hz, 3H), 1.74 (bs, 2H).

¹³C NMR (101 MHz, DMSO-*d*₆) δ 173.4, 44.8, 25.3.

L-Alanine-N-methylamide (H-Ala-NMe, **2c**)



Modified literature procedure^[29]

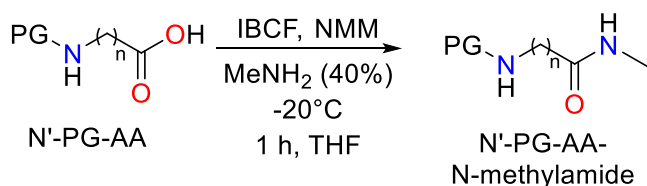
1 g of *L*-alanine methyl ester hydrochloride (7.2 mmol, 1 eq) was stirred in 10 ml of 33% of MeNH₂ at 50

°C for 1 h and overnight at RT. After 2 g of NaOH was added and stirring continued for 10 min. The mixture was evaporated under reduced pressure to then extracted with DCM (3×10 mL), which was filtered and dried in *vacuo*. The product was obtained as colorless oil (70 mg, 10%). Spectral data are in agreement with literature value.^[30]

¹H NMR (400 MHz, DMSO-*d*₆) δ 7.74 (bs, 1H), 3.20 (q, *J* = 6.9 Hz, 1H), 2.58 (d, *J* = 4.7 Hz, 3H), 1.09 (d, *J* = 6.9 Hz, 3H).

¹³C NMR (101 MHz, DMSO-*d*₆) δ 176.2, 50.3, 25.4, 21.7.

General synthesis of AA-N-methylamides for $n \geq 2$



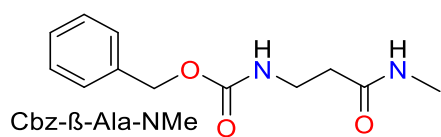
Modified literature procedure^[31]

1.21 ml of NMM (N-Methylmorpholine, 11 mmol, 1.11 g, 1.1 eq), then 1.43 ml of IBCF (isobutyl

chloroformate, 11 mmol, 1.5 g, 1.1 eq) were successively added to a solution of N'-PG-AA (10 mmol) in dry THF (50 mL) at -20 — -15 °C (Ice/salt = 3/1). After 5 min of activation, 0.85 ml of 40 % aqueous methylamine (11 mmol, 1.1 eq) was added, and the resulting solution was stirred for 1 hour at -20 °C. The reaction was quenched with 100 mL of 5% NaHCO₃ and stirred additionally for 1 hour at RT. The aqueous phase was extracted with DCM (3×50 mL). The combined organic phases were washed with 5 % NaHCO₃ (2×50 mL), dried over MgSO₄. Solvents were evaporated under reduced pressure; the crude product was

recrystallized from *i*-Hex/EtOAc.

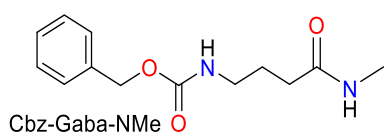
Benzyl (3-(methylamino)-3-oxopropyl)carbamate (Cbz-β-Ala-NMe, **Z-2d**)



White solid, yield 77%

¹H NMR (400 MHz, DMSO-*d*₆) δ 7.79 (q, *J* = 4.6 Hz, 1H), 7.38 – 7.28 (m, 5H), 7.25 (t, *J* = 5.9 Hz, 1H), 5.00 (s, 2H), 3.18 (q, *J* = 7.0 Hz, 2H), 2.55 (d, *J* = 4.6 Hz, 3H), 2.23 (t, *J* = 7.3 Hz, 2H).

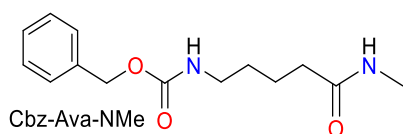
Benzyl (4-(methylamino)-4-oxobutyl)carbamate (Cbz-Gaba-NMe, **Z-2e**)



White solid, yield 78%

¹H NMR (400 MHz, DMSO-*d*₆) δ 7.71 (d, *J* = 5.8 Hz, 1H), 7.39 – 7.28 (m, 5H), 7.26 (t, *J* = 5.7 Hz, 1H), 5.00 (s, 2H), 2.96 (q, *J* = 6.9 Hz, 2H), 2.54 (d, *J* = 4.6 Hz, 3H), 2.04 (t, *J* = 7.5 Hz, 2H), 1.61 (p, *J* = 7.3 Hz, 2H).

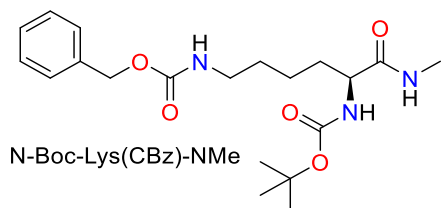
Benzyl (5-(methylamino)-5-oxopentyl)carbamate (Cbz-β-Ava-NMe, **Z-2f**)



White powder, yield 81%

¹H NMR (400 MHz, CDCl₃) δ 7.39 – 7.28 (m, 5H), 5.54 (bs, 1H), 5.09 (s, 2H), 4.89 (bs, 1H), 3.21 (q, *J* = 6.6 Hz, 2H), 2.78 (d, *J* = 4.8 Hz, 3H), 2.19 (t, *J* = 7.4 Hz, 2H), 1.71 – 1.63 (m, 2H), 1.53 (p, *J* = 6.9 Hz, 2H).

N-Boc-L-Lys(Cbz)-NMe (**Z-2g**)



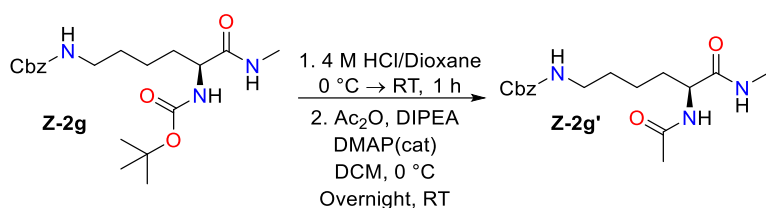
Recrystallized from EtOAc.

White powder, yield 70%

¹H NMR (400 MHz, DMSO-*d*₆) δ 7.72 (q, *J* = 4.6 Hz, 1H), 7.41 – 7.26 (m, 5H), 7.24 (t, *J* = 5.8 Hz, 1H), 6.78 (d, *J* = 8.1 Hz, 1H), 5.00 (s, 2H), 3.80 (td, *J* = 8.7, 5.1 Hz, 1H), 2.95 (q, *J* = 6.6 Hz, 2H), 2.56 (d, *J* = 4.6 Hz, 3H), 1.65 – 1.17 (m, 6H), 1.34 (s, 9H)
¹³C NMR (101 MHz, DMSO-*d*₆) δ 172.6, 156.1, 155.4, 137.3, 128.4, 127.8, 77.9, 65.1, 54.3, 40.1, 31.7, 29.1, 28.2, 25.5, 22.9.

MS (APCI): calcd for C₂₀H₃₂N₃O₅ [M + H]⁺, 394.2; found 394.1.

N-Ac-L-Lys(Cbz)-NMe (**Z-2g'**)



1.1 g (2.8 mmol, 1 eq) of N-Boc-L-Lys(Cbz)-NMe **Z-2g** in 10 mL of DCM was cooled to 0 °C. Then, 5 mL of 4 M HCl

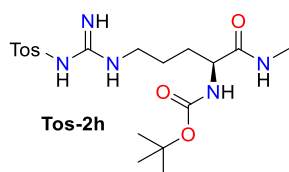
in 1,4-dioxane was added dropwise to the solution. The ice bath was removed, and the reaction was stirred at RT for 1 h. All the volatiles were evaporated under reduced pressure. The crude material was dissolved in 20 ml of DCM and cooled down to 0 °C under N₂. 1.46 ml of DIPEA (1.06 ml, 8.4 mmol, 3 eq) was added dropwise, followed by dropwise addition of 0.53 ml of Ac₂O (0.57 g, 5.6 mmol, 2 eq). The reaction mixture was diluted with additional 20 ml DCM and catalytic amount of DMAP was added after. The ice bath was removed, and the reaction was allowed to stir overnight at RT. After it was quenched with 100 ml of saturated NaHCO₃ and extracted with DCM (3×50 ml). All the volatiles were evaporated under reduced pressure. The crude material was recrystallized from EtOAc/EtOH, resulting in a yield of 0.52 mg white solid of the final product (55%).

¹H NMR (400 MHz, DMSO-*d*₆) δ 7.93 (d, *J* = 8.1 Hz, 1H), 7.80 (q, *J* = 4.5 Hz, 1H), 7.38 – 7.27 (m, 5H), 7.22 (t, *J* = 5.7 Hz, 1H), 5.00 (s, 2H), 4.12 (td, *J* = 8.5, 5.4 Hz, 1H), 2.95 (q, *J* = 6.6 Hz, 2H), 2.55 (d, *J* = 4.6 Hz, 3H), 1.83 (s, 3H), 1.64 – 1.52 (m, 1H), 1.51 – 1.33 (m, 3H), 1.32 – 1.12 (m, 2H).

¹³C NMR (101 MHz, DMSO-*d*₆) δ 172.2, 169.2, 156.1, 137.3, 128.4, 127.8, 52.5, 31.8, 29.2, 25.5, 22.8, 22.6.

MS (APCI): calcd for C₁₇H₂₆N₃O₄ [M + H]⁺, 336.2, found 336.1.

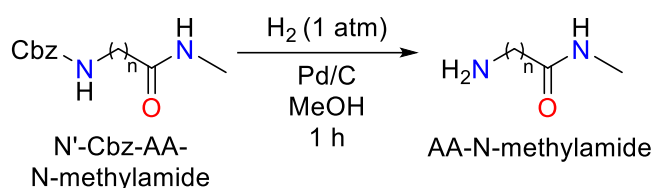
Boc-Arg(Tos)-NMe (**Tos-2h**)



Purified by column chromatography (DCM → DCM/MeOH = 10/1(R_f0.36))
White solid, 75%

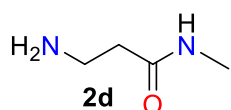
¹H NMR (400 MHz, DMSO-*d*₆) δ 7.76 (q, *J* = 4.5 Hz, 1H), 7.63 (d, *J* = 8.0 Hz, 2H), 7.29 (d, *J* = 8.0 Hz, 2H), 7.04 (bs, 1H), 6.81 (d, *J* = 8.2 Hz, 1H), 6.78 (bs, 1H, overlapped), 6.56 (bs, 1H), 3.85 – 3.80 (m, 1H), 3.02 (bs, 2H), 2.57 (d, *J* = 4.5 Hz, 3H), 2.35 (s, 3H), 1.59 – 1.50 (m, 1H), 1.46 – 1.33 (m, 3H), 1.38 (s, 9H).

MS (APCI): calcd for C₁₉H₃₂N₅O₅S [M + H]⁺, 442.2, found 442.3.



The obtained N'-Cbz-AA was stirred overnight with 200 mg 10% Pd/C in 50 ml of MeOH under H₂ atmosphere at RT. The reaction mixture was filtered through a Celite pad and evaporated under reduced pressure.

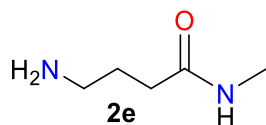
3-amino-N-methylpropanamide (H-β-Ala-NMe, **2d**)



Colorless oil, yield >99%

¹H NMR (400 MHz, DMSO-*d*₆) δ 7.78 (bs, 1H), 2.70 (t, *J* = 6.6 Hz, 2H), 2.55 (d, *J* = 4.6 Hz, 3H), 2.12 (t, *J* = 6.6 Hz, 2H), 1.38 (bs, 2H).

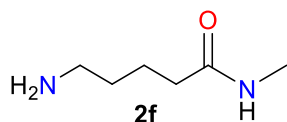
4-amino-N-methylbutanamide (H-Gaba-NMe, **2e**)



Colorless amorphous solid, yield >99%

¹H NMR (400 MHz, DMSO-*d*₆) δ 7.74 (bs, 1H), 2.54 (d, *J* = 4.6 Hz, 3H), 2.47 (t, overlapped with the solvent peak), 2.06 (t, *J* = 7.5 Hz, 2H), 1.54 (p, *J* = 7.2 Hz, 2H).

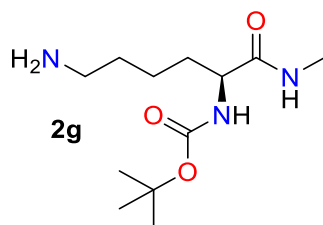
5-amino-N-methylpentanamide (H-Ava-NMe, **2f**)



White solid, yield >99%

¹H NMR (400 MHz, CDCl₃) δ 5.56 (bs, 1H), 2.80 (d, *J* = 4.9 Hz, 3H), 2.71 (t, *J* = 6.9 Hz, 2H), 2.19 (t, *J* = 7.5 Hz, 2H), 1.72 – 1.64 (m, 2H), 1.52 – 1.41 (m, 4H).

Tert-butyl (S)-(6-amino-1-(methylamino)-1-oxohexan-2-yl)carbamate (N-Boc-*L*-Lys-NMe, **2g**)



Colorless amorphous glass, >99%

Major conformer

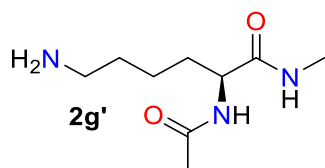
¹H NMR (400 MHz, DMSO-*d*₆) δ 7.78 (q, *J* = 4.6 Hz, 1H), 6.82 (d, *J* = 8.2 Hz, 1H), 3.82 (td, *J* = 8.6, 5.1 Hz, 1H), 2.97 (br s, 2H), 2.56 (d, *J* = 4.6 Hz, 3H), 2.52 (d, *J* = 4.6 Hz, overlapped), 1.61 – 1.14 (m, 6H), 1.37 (s, 9H)

¹³C NMR (101 MHz, DMSO-*d*₆) δ 172.6, 155.3, 77.9, 54.3, 41.0, 32.1, 31.9, 28.2, 25.5, 22.9.

MS (APCI): calcd for C₁₂H₂₆N₃O₃ [M + H]⁺, 260.2; found 260.1.

(S)-2-acetamido-6-amino-N-methylhexanamide (N-Ac-L-Lys-NMe, **2g'**)

White solid, >99%

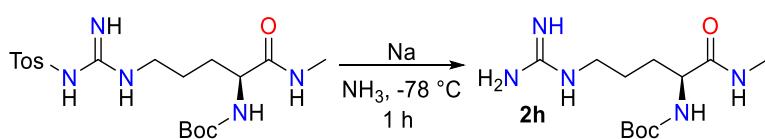


¹H NMR (400 MHz, DMSO-*d*₆) δ 7.99 (d, *J* = 8.1 Hz, 1H), 7.85 (q, *J* = 4.6 Hz, 1H), 4.12 (td, *J* = 8.5, 5.4 Hz, 1H), 2.55 (d, *J* = 4.6 Hz, 3H), 2.48 (t, overlapped with solvent peak), 1.83 (s, 3H), 1.65 – 1.50 (m, 1H), 1.49 – 1.38 (m, 1H), 1.37 – 1.12 (m, 4H).

¹³C NMR (101 MHz, DMSO-*d*₆) δ 172.3, 169.2, 52.6, 41.2, 32.5, 32.0, 25.5, 22.9, 22.6.

MS (APCI): calcd for C₉H₂₀N₃O₂ [M + H]⁺, 202.2, found 202.1.

Boc-Arg-NMe (**2h**)



The reaction (0.5 mmol scale) was performed following a known procedure^[32].

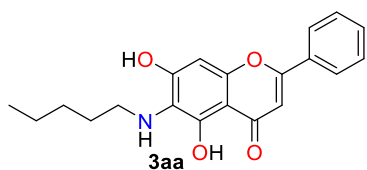
The obtained colorless amorphous glass mostly contained free Boc-Arg-NMe and was used without further purification.

¹H NMR (400 MHz, MeOH-*d*₄) δ 4.02 – 3.99 (m, 1H), 3.23 – 3.13 (m, 2H), 2.74 (s, 3H), 1.84 – 1.58 (m, 4H), 1.45 (s, 9H).

MS (APCI): calcd for C₁₂H₂₅N₅O₃ [M + H]⁺, 288.2, found 288.0.

1.3.7.9. Synthesis and analytical data of products **3xx** and **7x**

5,7-dihydroxy-6-(pentylamino)-2-phenyl-4H-chromen-4-one (**3aa**)



The compound was synthesized according to the procedure described before.^[1]

¹H NMR (400 MHz, DMSO-*d*₆) δ 12.94 (s, 1H), 8.07 – 8.04 (m, 2H), 7.78 – 7.43 (m, 3H), 6.92 (s, 1H), 6.62 (s, 1H), 3.22 (t, *J* = 7.0 Hz, 2H), 1.55 – 1.19 (m, 6H), 0.87 – 0.82 (m, 3H).

¹³C NMR (101 MHz, DMSO-*d*₆) δ 182.1, 162.6, 154.7, 150.2, 148.5, 131.8, 131.0, 129.1, 126.3, 121.4, 104.6, 104.2, 93.6, 45.4, 29.9, 28.6, 22.0, 14.0.

IR $\tilde{\nu}$ = 3068(vw), 2931(w), 2854(w), 1652(s), 1577(s), 1495(w), 1449(m), 1379(s), 1280(m), 1250(m), 1091(s), 1037(m), 872(s), 853(s), 816(vs), 766(s).

R_f 0.36 (DCM/MeOH = 20/1)

A DCM solution of **3aa** was allowed to evaporate slowly during several days at RT. The formed yellow crystals were carefully separated and quickly washed with DCM. The composition of the obtained crystals was **2×3aa×DCM**.

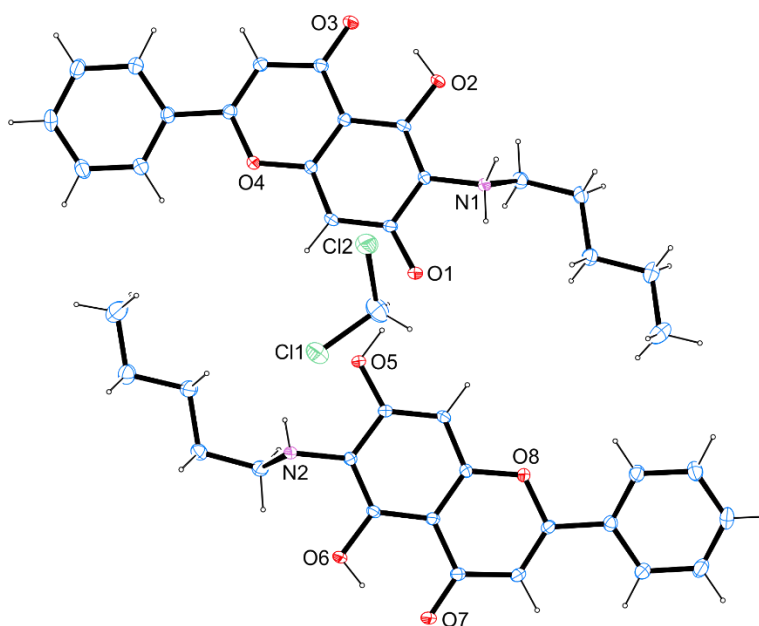


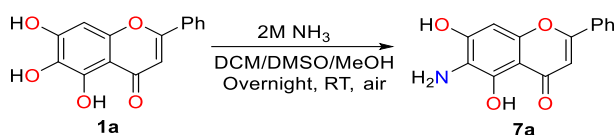
Fig. S79. X-ray crystal structure of **3aa**.

Table S11. Crystallographic data for **3aa**.

net formula	C ₄₁ H ₄₄ Cl ₂ N ₂ O ₈	transmission factor range	0.96-0.99
M _r /g mol ⁻¹	763.68	refls. measured	67492
crystal size/mm	0.120 × 0.090 × 0.050	R _{int}	0.0554
T/K	173.(2)	mean σ(I)/I	0.0298
radiation	MoKα	θ range	2.869–26.730

diffractometer	Bruker D8 Venture TXS	observed refls.	6370
crystal system	monoclinic	x, y (weighting scheme)	0.0516, 3.6222
space group	P 1 21/n 1	hydrogen refinement	mixed
a/Å	16.6356(7)	Flack parameter	?
b/Å	14.0673(6)	refls in refinement	8031
c/Å	17.2270(7)	parameters	504
α /	90	restraints	0
β /	109.9530(10)	R(F _{obs})	0.0533
γ /	90	R _w (F ²)	0.1377
V/Å ³	3789.4(3)	S	1.049
Z	4	shift/error _{max}	0.001
calc. density/g cm ⁻³	1.339	max electron density/e Å ⁻³	0.834
μ /mm ⁻¹	0.227	min electron density/e Å ⁻³	-0.940
absorption correction	Multi-Scan		

6-amino-5,7-dihydroxy-2-phenyl-4H-chromen-4-one (**7a**)



33.75 mg of **1a** (0.125 mmol, 1 eq) was dissolved in 5 ml of dry DCM (10 vol% of dry DMSO-d₆). 0.25 ml of 2 M NH₃ in

MeOH was added to the resulting solution of **1a**. The addition of NH₃ resulted in the formation of a yellow precipitate. The reaction mixture was placed on a shaker at 400 RPM and allowed to react overnight at RT. The precipitate dissolved over the course of the reaction to form a red solution. The reaction was quenched with 10 ml of water, causing the formation of a yellow precipitate. The resulting mixture was centrifuged (3×5 ml of water) to isolate the precipitate. The obtained product was dried under reduced pressure to obtain a yellow solid (16 mg, 48%). ¹H and ¹³C NMR spectra match the data reported in the literature.^[33]

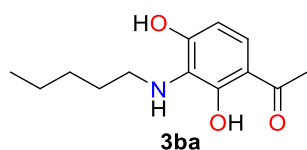
¹H NMR (400 MHz, DMSO-*d*₆) δ 12.65 (s, 1H), 8.11 – 8.03 (m, 2H), 7.65 – 7.55 (m, 3H), 6.93 (s, 1H), 6.64 (s, 1H).

¹³C NMR (101 MHz, DMSO-*d*₆) δ 181.9, 162.6, 151.5, 148.8, 144.6, 131.8, 131.1, 129.2, 126.3, 120.2, 104.5, 104.2, 93.4.

IR $\tilde{\nu}$ = 3425(vw), 3343(vw), 3067(m), 1654(s, C=O), 1621(m), 1576(s), 1498(s), 1450(s), 1407(m), 1366(vs), 1300(m), 1241(m), 1194(vs), 1018 (m), 912(w), 825(s), 764(s).

MS (APCI): calcd for C₁₅H₁₂NO₄ [M + H]⁺, 270.1; found 270.1.

2,4-dihydroxy-3-(pentylamino)acetophenone (**3ba**)



The synthesis was described above (Table S7, Entry 4).

Yellow solid (95 mg, 80%)

$^1\text{H NMR}$ (400 MHz, DMSO-*d*₆) δ 7.29 (d, $J = 8.8$ Hz, 1H), 6.41 (d, $J = 8.8$ Hz, 1H), 3.18 (t, $J = 7.0$ Hz, 2H), 2.51 (s, 3H), 1.43 – 1.34 (m, 2H), 1.33 – 1.18 (m, 4H), 0.84 (t, $J = 6.9$, 3H)

$^{13}\text{C NMR}$ (101 MHz, DMSO-*d*₆) δ 203.6, 154.1, 154.0, 124.0, 123.3, 112.7, 107.5, 45.4, 29.9, 28.6, 26.2, 22.0, 14.0.

HRMS (ESI): calcd for C₁₃H₂₀NO₃ [M + H]⁺, 238.1438; found 238.1437.

IR $\tilde{\nu}$ = 2952(m), 2929(m), 2865(w), 1608(vs, C=O), 1363(s), 1271(m), 1048(s), 1023(s), 861(s), 799(vs).

R_f 0.46 (DCM/MeOH = 10/1)

M.p 94 °C

Pure **3ba** was dissolved in DCM/iHex mixture, and the solvents were slowly evaporated at RT for several days. The formed yellow crystals were separated, quickly washed with iHex and analyzed via scXRD analysis.

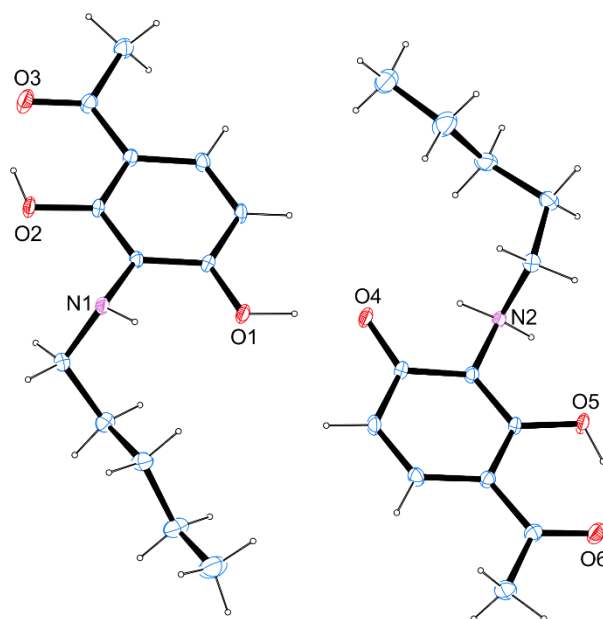


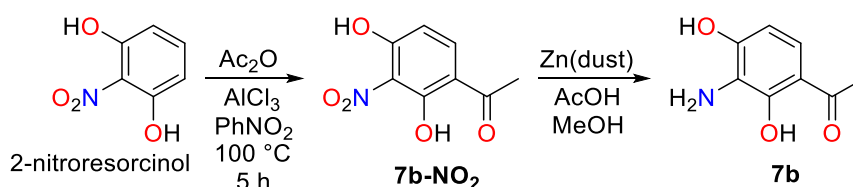
Fig. S80. X-ray structure of **3ba**.

Table S12. Crystallographic data for **3ba**.

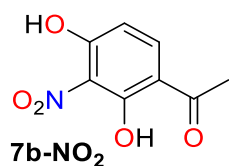
net formula	C ₁₃ H ₁₉ NO ₃	transmission factor range	0.97–0.99
M _r /g mol ⁻¹	237.29	refls. measured	22627
crystal size/mm	0.150 × 0.120 × 0.070	R _{int}	0.0347
T/K	173.(2)	mean $\sigma(I)/I$	0.0333
radiation	MoK α	θ range	2.319–27.481

diffractometer	Bruker D8 Venture TXS	observed refls.	4636
crystal system	triclinic	x, y (weighting scheme)	0.0583, 0.4036
space group	P -1	hydrogen refinement	mixed
a/Å	9.8014(3)	Flack parameter	?
b/Å	10.2955(3)	refls in refinement	5797
c/Å	13.7201(4)	parameters	335
α /	72.2560(10)	restraints	1
β /	74.5520(10)	R(F _{obs})	0.0440
γ /	89.0200(10)	R _w (F ²)	0.1248
V/Å ³	1267.90(7)	S	1.034
Z	4	shift/error _{max}	0.001
calc. density/g cm ⁻³	1.243	max electron density/e Å ⁻³	0.274
μ /mm ⁻¹	0.088	min electron density/e Å ⁻³	-0.216
absorption correction	Multi-Scan		

Synthetic route to **7b**



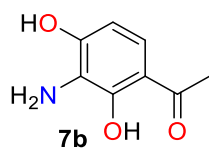
2,4-dihydroxy-3-nitroacetophenone (**7b-NO₂**)



The compound was synthesized using literature procedure.^[34]

¹H NMR (400 MHz, DMSO-*d*₆) δ 13.32 (s, 1H), 12.33 (bs, 1H), 7.98 (d, $J = 9.0$ Hz, 1H), 6.62 (d, $J = 9.0$ Hz, 1H), 2.59 (s, 3H).

2,4-dihydroxy-3-aminoacetophenone (**7b**)



The compound was synthesized using literature procedure^[35]

Yellow solid, yield 55%

¹H NMR (400 MHz, DMSO-*d*₆) δ 7.15 (d, $J = 8.7$ Hz, 1H), 6.40 (d, $J = 8.7$ Hz, 1H), 2.51 (s, 3H).

¹³C NMR (101 MHz, DMSO-*d*₆) δ 203.6, 150.3, 123.3, 120.4, 112.7, 107.0, 26.2.

M.p 200 °C (decomp)

The crystals of **7b** were obtained by slow evaporation from a Toluene/MeOH mixture.

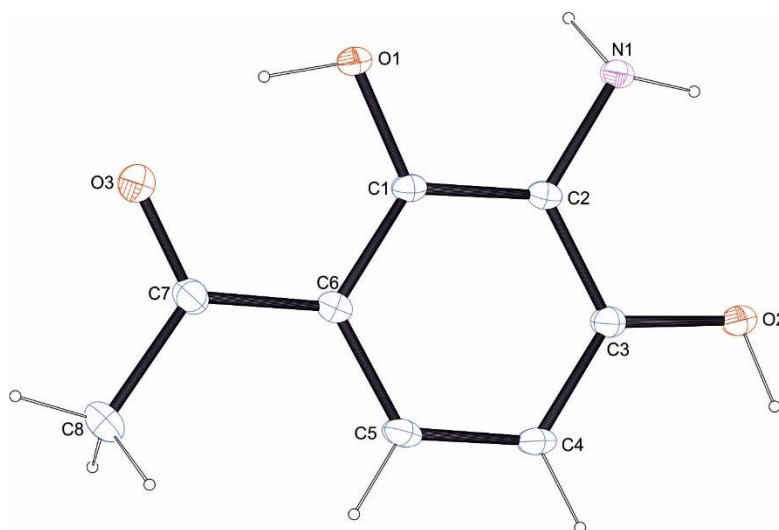
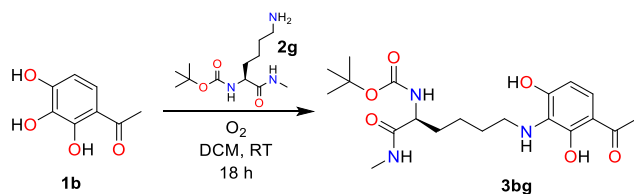


Fig. S81. X-ray structure of **7b**.

Table S13. Crystallographic data for **7b**.

net formula	C ₈ H ₉ NO ₃	transmission factor range	0.96-0.99
M _r /g mol ⁻¹	167.16	refls. measured	30304
crystal size/mm	0.120 × 0.090 × 0.070	R _{int}	0.0369
T/K	173.(2)	mean σ(I)/I	0.0136
radiation	MoKα	θ range	3.396–27.463
diffractometer	Bruker D8 Venture TXS	observed refls.	1575
crystal system	tetragonal	x, y (weighting scheme)	0.0514, 2.6071
space group	I 41/a	hydrogen refinement	mixed
a/Å	14.4301(3)	Flack parameter	?
b/Å	14.4301(3)	refls in refinement	1773
c/Å	14.8323(3)	parameters	126
α/°	90	restraints	1
β/°	90	R(F _{obs})	0.0381
γ/°	90	R _w (F ²)	0.1039
V/Å ³	3088.50(14)	S	1.044
Z	16	shift/error _{max}	0.001
calc. density/g cm ⁻³	1.438	max electron density/e Å ⁻³	0.284
μ/mm ⁻¹	0.111	min electron density/e Å ⁻³	-0.212
absorption correction	Multi-Scan		

Tert-butyl (S)-(6-((3-acetyl-2,6-dihydroxyphenyl)amino)-1-(methylamino)-1-oxohexan-2-yl)carbamate **3bg**



121 mg of N-Boc-Lys-NMe (**2g**) (0.465 mmol, 1.0 eq) was dissolved in 20 ml dry DCM under O₂ atmosphere. 80 mg of TAP (**1b**) (0.476 mmol, 1 eq) was added

was added to the stirring solution. The reaction immediately became green. The solution was

vigorously stirred for 18 h at RT. The solvent was evaporated under reduced pressure at 25 °C. Crude material was purified by column chromatography on silica gel (DCM → DCM/MeOH = 20/1). Product was obtained as yellow green glass (60 mg, 30%). NMR analysis showed the formation of **3bg** adduct.

¹H NMR (400 MHz, DMSO-*d*₆) δ 12.95 (bs, 1H), 7.70 (q, *J* = 4.6 Hz, 1H), 7.28 (d, *J* = 8.8 Hz, 1H), 6.74 (d, *J* = 8.2 Hz, 1H), 6.41 (d, *J* = 8.8 Hz, 1H), 3.81 (td, *J* = 8.5, 5.1 Hz, 1H), 3.15 (t, *J* = 6.9 Hz, 2H), 2.56 (d, *J* = 4.6 Hz, 3H), 2.51 (s, 3H), 1.62 – 1.39 (m, 2H), 1.37 (s, overlapped, 9H), 1.34 – 1.17 (m, overlapped, 4H).

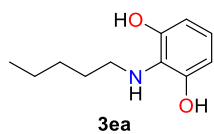
¹³C NMR (101 MHz, DMSO-*d*₆) δ 203.6, 172.5, 155.3, 154.0, 124.0, 123.3, 112.7, 107.5, 77.9, 54.3, 45.4, 31.9, 29.9, 28.2, 26.2, 25.5, 22.9.

HRMS (ESI): calcd for C₂₀H₃₂N₃O₆ [M + H]⁺, 410.2286; found 410.2287

IR $\tilde{\nu}$ = 3300(s, -OH), 2973(s), 2939(s), 1651(s), 1626(vs, C=O), 1508(s), 1437(s), 1366(vs), 1298(vs), 1165(s), 1055(s), 956(vw), 800(w), 711(w) cm⁻¹.

R_f 0.15 (DCM/MeOH = 20/1)

2-(pentylamino)benzene-1,3-diol (**3ea**)



The title compound (87 mg, 45%) was obtained as a colorless solid following the General Procedure D (1 mmol scale, 3 eq of Pentylamine **2a**) in 24 h after purification by flash chromatography (iHex/[EtOAc/

EtOH=3/1] = 7/3). Due to high reactivity, the compound becomes black on exposure to air.

¹H NMR (400 MHz, DMSO-*d*₆) δ 8.85 (bs, 2H), 6.40 (dd, *J* = 8.0, 7.5 Hz, 1H), 6.23 (d, *J* = 8.0 Hz, 2H), 3.64 (bs, 1H), 3.09 (t, *J* = 7.0 Hz, 2H), 1.43 – 1.36 (m, 2H), 1.33 – 1.19 (m, 4H), 0.91 – 0.78 (m, 3H).

¹³C NMR (101 MHz, DMSO-*d*₆) δ 148.6, 124.8, 119.1, 106.9, 46.1, 30.0, 28.7, 22.1, 14.0.

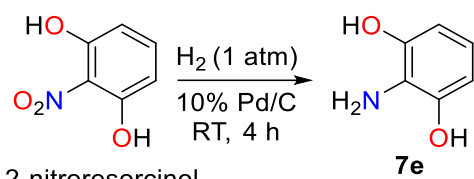
HRMS (ESI) calcd for C₁₁H₁₆NO₂ [M - H]⁻, 194.1186, found 194.1186.

R_f 0.27 (iHex/[EtOAc/EtOH=3/1] = 7/3)

M.p 104 °C

IR $\tilde{\nu}$ = 2928(m, -OH), 1606(m), 1458(s), 1307(m), 1241(m), 1043(m), 783(s), 732(m), 703(m) cm⁻¹.

2-aminoresorcinol (**7e**)

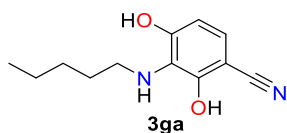


Modified literature procedure^[36]

To a stirring suspension of 10% w/w Pd/C (20 mg) in 25 ml of MeOH was added 310 mg of 2-nitroresorcinol under nitrogen atmosphere, which then was replaced by H₂ gas. The resulting reaction mixture was stirred for 4 h at RT. The reaction mixture was filtered through a Celite pad, and all the volatiles were evaporated under reduced pressure give **7e** as dark solid (237 mg, 95%). ¹H NMR spectrum matches literature data.^[36]

¹H NMR (400 MHz, DMSO-*d*₆) δ 8.83 (bs, 2H), 6.27 – 6.20 (m, 3H), 3.81 (bs, 2H).

2,4-dihydroxy-3-(pentylamino)benzonitrile (**3ga**)



The title compound (33 mg, 46%) was obtained as a red brown solid following the General Procedure D (0.33 mmol scale, 2 eq of amine **2a**) in 24 h after purification by flash chromatography (iHex/[EtOAc/EtOH=3/1] = 7/3). Unlike the other cases, the

reaction mixture did not homogenize. Due to high reactivity the compound becomes darker on the exposure to air.

¹H NMR (400 MHz, DMSO-*d*₆) δ 6.94 (d, *J* = 8.4 Hz, 1H), 6.42 (d, *J* = 8.5 Hz, 1H), 3.01 (t, *J* = 7.1 Hz, 2H), 1.45 – 1.35 (m, 2H), 1.33 – 1.21 (m, 4H), 0.87 – 0.83 (m, 3H).

¹³C NMR (101 MHz, DMSO-*d*₆) δ 154.1, 152.3, 126.0, 124.9, 118.3, 108.5, 92.0, 46.4, 29.6, 28.6, 22.0, 14.0.

HRMS (ESI): calcd for C₁₂H₁₅N₂O₂ [M - H]⁻, 219.1139; found 219.1139.

R_f 0.18 (iHex/[EtOAc/EtOH=3/1] = 7/3)

M.p 154 °C

IR $\tilde{\nu}$ = 2921(m, -OH), 2212(m, C≡N), 1616(m), 1558(s), 1506(w), 1457(s), 1356(s), 1286(m), 1244(vs), 1165(w), 1062(s), 880(w), 791(m), 746(m).

Pure **3ga** was dissolved in Heptan/EtOAc/EtOH mixture, and the solvents were slowly evaporated at RT for several days. The formed yellow crystals were separated, quickly washed with Heptane, and analyzed via scXRD analysis.

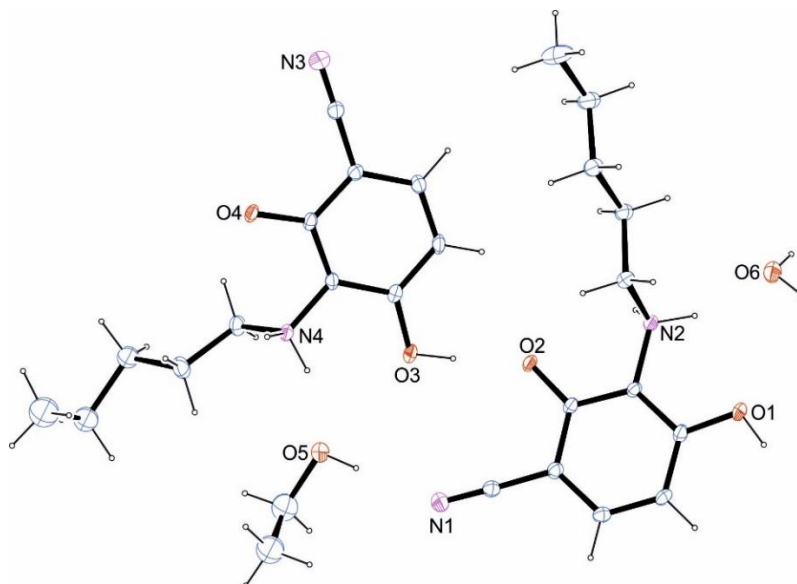
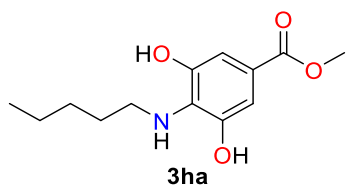


Fig. S82. X-ray structure of **3ga**.

Table S14. Crystallographic data for **3ga**.

net formula	C ₂₆ H ₄₀ N ₄ O ₆	transmission factor range	0.94–1.00
M_r /g mol ⁻¹	504.62	refls. measured	23996
crystal size/mm	0.130 × 0.090 × 0.030	R_{int}	0.0428
T/K	173.(2)	mean $\sigma(I)/I$	0.0385
radiation	MoK α	θ range	2.943–26.372
diffractometer	Bruker D8 Venture TXS	observed refls.	4586
crystal system	triclinic	x, y (weighting scheme)	0.0609, 1.3724
space group	P -1	hydrogen refinement	mixed
a/Å	8.2748(6)	Flack parameter	?
b/Å	13.4646(9)	refls in refinement	5706
c/Å	13.5690(10)	parameters	364
α /	76.263(2)	restraints	6
β /	72.472(2)	$R(F_{obs})$	0.0615
γ /	88.924(2)	$R_w(F^2)$	0.1572
V/Å ³	88.924(2)	S	1.039
Z	2	shift/error _{max}	0.001
calc. density/g cm ⁻³	1.199	max electron density/e Å ⁻³	0.451
μ /mm ⁻¹	0.085	min electron density/e Å ⁻³	-0.411
absorption correction	Multi-Scan		

Methyl 3,5-dihydroxy-(3-pentylamino)-benzoate (**3ha**)



The title compound (48 mg, 19%) was obtained as a colorless solid following the General Procedure D (1 mmol scale, 3 eq of amine **2a**) in 24 h after purification by flash chromatography (iHex/[EtOAc/EtOH=3/1] = 7/3). Due to high reactivity, the

compound becomes slightly red on exposure to air.

¹H NMR (400 MHz, DMSO-*d*₆) δ 9.35 (s, 2H), 6.92 (s, 2H), 4.37 (bs, 1H), 3.72 (s, 3H), 3.34 (t, overlapped with H₂O signal, 2H), 1.48 – 1.35 (m, 2H), 1.35 – 1.18 (m, 4H), 0.87 – 0.79 (m, 3H).

¹³C NMR (101 MHz, DMSO-*d*₆) δ 166.4, 145.8, 130.5, 117.3, 108.4, 51.4, 44.8, 30.4, 28.5, 22.0, 14.0.

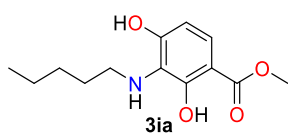
HRMS (ESI): calcd for C₁₃H₂₀NO₄ [M + H]⁺, 254.1387; found 254.1387.

R_f 0.40 (iHex/[EtOAc/EtOH=3/1] = 7/3)

M.p 150 °C

IR: ν̃ = 3385(m, -OH), 2956(w), 2861(w), 1686(s, C=O), 1607(m), 1467(m), 1424(s), 1355(s), 1290(m), 1248(vs), 1202(s), 1130(m), 1084(w), 1058(s), 1048(s), 1009(s), 982(w), 937(w), 867(m), 818(w), 766(s).

Methyl 3,5-dihydroxy-(3-pentylamino)-benzoate **3ia**



To a suspension of 92 mg of pseudo methyl gallate (0.5 mmol, 1.0 eq) in 10 ml of anhydrous DCM was added pentylamine (~76 μL, 0.66 mmol, 1.3 eq) under O₂ atmosphere. The resultant

mixture was stirred at RT for 12 h. The residue was concentrated in *vacuo* at 25 °C and purified by flash column chromatography (iHex/EtOAc = 3/1) to afford the title compound as a white solid (110 mg, 88%). Due to high reactivity the compound becomes darker on exposure to air.

¹H NMR (400 MHz, DMSO-*d*₆) δ 10.97 (bs, 1H), 7.17 (d, *J* = 8.7 Hz, 1H), 6.40 (d, *J* = 8.7 Hz, 1H), 3.84 (s, 3H), 3.17 (t, *J* = 7.0 Hz, 2H), 1.40 (p, *J* = 7.0 Hz, 2H), 1.27 – 1.24 (m, 4H), 0.86 – 0.82 (m, 3H).

¹³C NMR (101 MHz, DMSO-*d*₆) δ 170.6, 153.3, 152.7, 124.4, 120.8, 107.7, 104.0, 52.1, 48.6, 45.5, 29.9, 28.6, 14.0.

HRMS (ESI) *m/z* calcd for C₁₃H₁₈NO₄ [M - H]⁻, 252.1242; found 252.1242.

R_f 0.55 (iHex/EtOAc = 3/1)

M.p 66 °C

IR ν̃ = 2925(m, -OH), 1650(vs, C=O), 1436(s), 1269(s), 1192(s), 1140(s), 1062(s), 990(s),

789(vs) cm^{-1} .

Pure **3ia** was dissolved in DCM/iHex mixture, and the solvents were slowly evaporated at RT for several days. The formed yellow crystals were separated, quickly washed with iHex and analyzed via scXRD analysis.

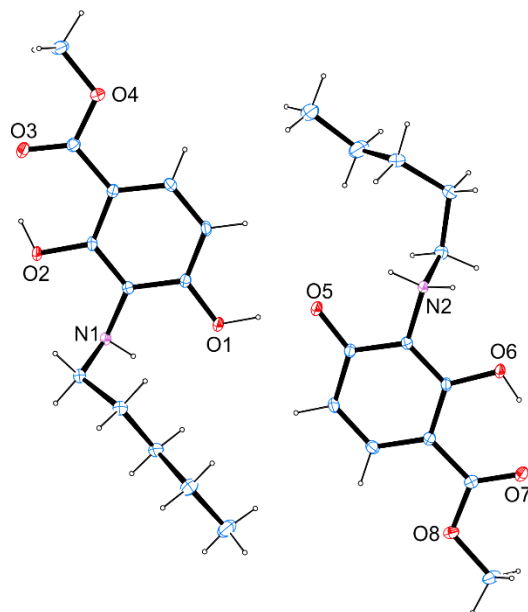
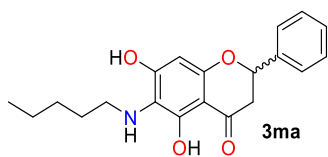


Fig. S83. X-ray structure of **3ia**.

Table S15. Crystallographic data for **3ia**.

net formula	C ₁₃ H ₁₉ NO ₄	transmission factor range	0.96-0.99
$M_r/\text{g mol}^{-1}$	253.29	refls. measured	22392
crystal size/mm	0.130 × 0.090 × 0.050	R_{int}	0.0377
T/K	173.(2)	mean $\sigma(I)/I$	0.0355
radiation	MoK α	θ range	2.361–27.103
diffractometer	Bruker D8 Venture TXS	observed refls.	4407
crystal system	triclinic	x, y (weighting scheme)	0.0678, 0.4467
space group	P -1	hydrogen refinement	mixed
a/Å	10.1321(4)	Flack parameter	?
b/Å	10.1321(4)	refls in refinement	5683
c/Å	13.2548(4)	parameters	353
$\alpha/^\circ$	107.7820(10)	restraints	1
$\beta/^\circ$	99.5030(10)	$R(F_{\text{obs}})$	0.0476
$\gamma/^\circ$	99.5030(10)	$R_w(F^2)$	0.1368
V/Å ³	1291.55(8)	S	1.046
Z	4	shift/error _{max}	0.001
calc. density/g cm ⁻³	1.303	max electron density/e Å ⁻³	0.292
μ/mm^{-1}	0.096	min electron density/e Å ⁻³	-0.310
absorption correction	Multi-Scan		

5,7-Dihydroxy-6-(pentylamino)-2-phenylchroman-4-one (**3ma**)



The title compound (42 mg, 49%) was obtained as a yellow green solid following general procedure A after purification by preparative TLC (Heptane/[EtOAc/EtOH=3/1] = 4/1). Due to its

high reactivity the compound becomes darker under aerobic conditions.

¹H NMR (400 MHz, DMSO-*d*₆) δ 12.37 (bs, 1H), 7.51 – 7.47 (m, 2H), 7.46 – 7.35 (m, 3H), 5.90 (s, 1H), 5.48 (dd, *J* = 12.7, 3.07 Hz, 1H), 3.17 (dd, *J* = 17.1, 12.7 Hz, 1H), 3.03 (t, *J* = 7.1 Hz, 2H), 2.71 (dd, *J* = 17.1, 3.5 Hz, 1H), 1.41 (p, *J* = 7.1 Hz, 2H), 1.28 – 1.23 (m, 4H), 0.89 – 0.83 (m, 3H).

¹³C NMR (101 MHz, DMSO-*d*₆) δ 195.8, 159.5, 156.4, 152.9, 139.1, 128.5, 128.4, 126.6, 117.3, 101.1, 94.8, 78.3, 46.3, 42.3, 29.3, 28.6, 22.0, 14.0.

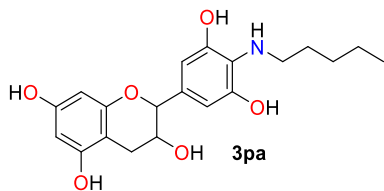
HRMS (ESI): calcd for C₂₀H₂₄NO₄ [M + H]⁺, 342.1700; found 342.1700.

IR $\tilde{\nu}$ = 2927(w), 1634(s, C=O), 1536(m), 1465(s), 1450(s), 1367(s), 1342(s), 1288(s), 1174(s), 1084(s), 822(m), 762(m).

R_f 0.17 (Heptane/[EtOAc/EtOH=3/1] = 4/1)

M.p. 70 °C (decomp)

2-(3,5-Dihydroxy-4-(pentylamino)phenyl)chromane-3,5,7-triol (**3pa**)



The title compound (50 mg, 53%) was obtained as a grey solid following general procedure A (0.25 mmol scale, 2 eq of amine **2a**) in 18 h after purification by flash chromatography (iHex/[EtOAc/EtOH=3/1] = 1/3). Due to

high reactivity the compound becomes darker under aerobic conditions.

¹H NMR (400 MHz, DMSO-*d*₆) δ 9.10 (bs, 1H), 8.89 (bs, 3H), 6.38 (s, 2H), 5.88 (d, *J* = 2.3 Hz, 1H), 5.70 (d, *J* = 2.3 Hz, 1H), 4.63 (s, 1H), 3.98 (d, *J* = 4.3 Hz, 1H), 3.09 (t, *J* = 7.0 Hz, 2H), 2.67 (dd, *J* = 16.4, 4.5 Hz, 1H), 2.47 (overlapped, 1H), 1.41 (p, *J* = 7.0 Hz, 2H), 1.30 – 1.23 (m, 4H), 0.91 – 0.81 (m, 3H).

¹³C NMR (101 MHz, DMSO-*d*₆) δ 156.5, 156.2, 155.8, 147.8, 130.7, 123.6, 105.9, 98.5, 95.0, 94.0, 78.2, 65.0, 46.1, 29.9, 28.7, 28.3, 22.1, 14.0.

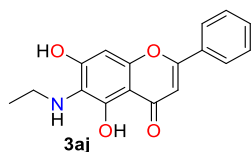
HRMS (ESI): calcd for C₂₀H₂₆NO₆ [M + H]⁺, 376.1755; found 376.1754.

IR: 3300(m), 2927(m), 2858(m), 1602(s, C=O), 1513(m), 1464(s), 1427(s), 1364(s), 1202(s), 1138(vs), 1094(s), 1042(s), 1012(s), 880(m), 818(s), 714(m), 674(m) cm⁻¹.

R_f 0.69 (EtOAc/EtOH = 3/1)

M.p. 141 °C (decomp)

6-(Ethylamino)-5,7-dihydroxy-2-phenyl-4H-chromen-4-one (**3aj**)



The title compound (25 mg, 67%) was obtained as an orange solid following general procedure D (0.125 mmol scale, 1 eq of 1 eq of ethylamine (2M in MeOH), overnight, RT) after purification by flash chromatography (DCM/MeOH = 20/1 → 10/1).

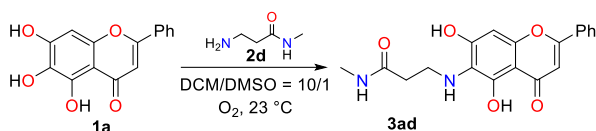
¹H NMR (400 MHz, DMSO-*d*₆) δ 12.95 (bs, 1H), 8.10 – 8.02 (m, 2H), 7.65 – 7.52 (m, 3H), 6.92 (s, 1H), 6.62 (s, 1H), 3.26 (q, *J* = 7.1 Hz, 2H), 1.06 (t, *J* = 7.1 Hz, 3H).

¹³C NMR (101 MHz, DMSO-*d*₆) δ 182.0, 162.6, 155.0, 150.4, 148.8, 131.8, 131.0, 129.1, 126.3, 121.2, 104.6, 104.2, 93.6, 40.1, 16.0.

HRMS (ESI): calcd for C₁₇H₁₆O₄N [M + H]⁺, 298.1074; found 298.1072.

R_f 0.43 (DCM/MeOH = 20/1)

3-((5,7-Dihydroxy-4-oxo-2-phenyl-4H-chromen-6-yl)amino)-N-methylpropanamide (**3ad**)



The title compound (50 mg, 41%) was obtained as a yellow solid following general procedure D (0.34 mmol scale, 2 eq of **2d**) in 24 h after purification by flash

chromatography (iHex/[EtOAc/EtOH=3/1]).

¹H NMR (400 MHz, DMSO-*d*₆) δ 12.95 (s, 1H), 8.12 – 8.00 (m, 2H), 7.83 (q, *J* = 4.6 Hz, 1H), 7.65 – 7.52 (m, 3H), 6.94 (s, 1H), 6.62 (s, 1H), 3.37 (t, *J* = 6.5 Hz, 2H), 2.57 (d, *J* = 4.6 Hz, 3H), 2.29 (t, *J* = 6.5 Hz, 2H).

¹³C NMR (101 MHz, DMSO-*d*₆) δ 182.1, 171.8, 162.7, 155.5, 150.7, 149.3, 131.9, 131.0, 129.2, 126.3, 120.9, 104.6, 104.2, 93.7, 42.0, 35.8, 25.5.

HRMS (ESI): calcd for C₁₉H₁₈N₂O₅Na [M + Na]⁺, 377.1108; found 377.1112.

R_f 0.27 (iHex/[EtOAc/EtOH=3/1] = 1/4)

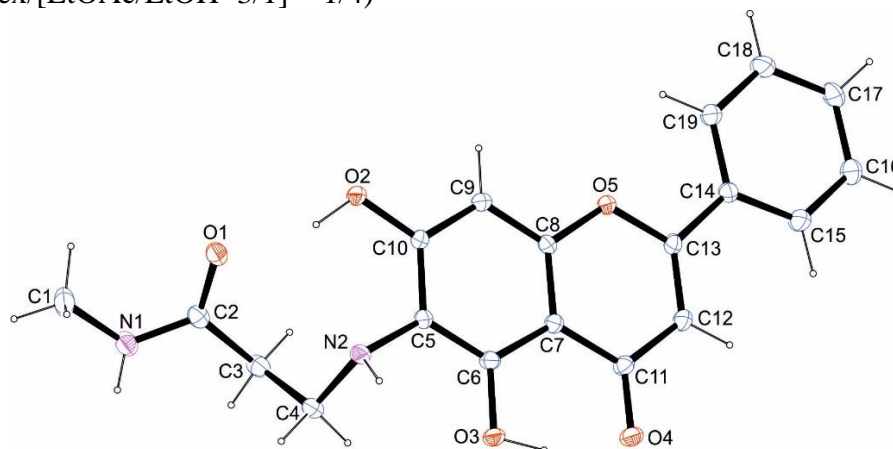
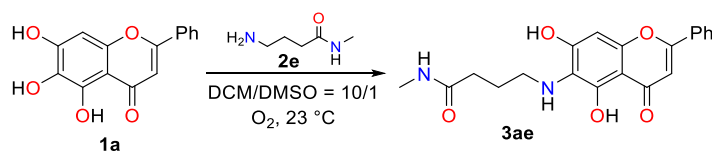


Fig. S84. X-ray crystal structure of **3ad**.

Table S16. Crystallographic data for **3ad**.

net formula	C ₁₉ H ₁₈ N ₂ O ₅	transmission factor range	0.96-1.00
M _r /g mol ⁻¹	354.35	refls. measured	27645
crystal size/mm	0.120 × 0.080 × 0.020	R _{int}	0.0397
T/K	173.(2)	mean σ(I)/I	0.0235
radiation	MoKα	θ range	2.393–26.368
diffractometer	Bruker D8 Venture TXS	observed refls.	3178
crystal system	monoclinic	x, y (weighting scheme)	0.0426, 0.8454
space group	P 1 21/c 1	hydrogen refinement	Mixed
a/Å	5.4488(2)	Flack parameter	?
b/Å	8.5460(3)	refls in refinement	3514
c/Å	35.8339(12)	parameters	253
α/°	90	restraints	0
β/°	94.3210(10)	R(F _{obs})	0.0461
γ/°	90	R _w (F ²)	0.1077
V/Å ³	1663.88(10)	S	1.095
Z	4	shift/error _{max}	0.001
calc. density/g cm ⁻³	1.415	max electron density/e Å ⁻³	0.215
μ/mm ⁻¹	0.104	min electron density/e Å ⁻³	-0.158
absorption correction	Multi-Scan		

4-((5,7-Dihydroxy-4-oxo-2-phenyl-4H-chromen-6-yl)amino)-N-methylbutanamide (**3ae**)

The title compound (59 mg, 64%) was obtained as an orange-red solid following general procedure D (0.25 mmol scale, 1.33 eq of **2e**) in 3 hours

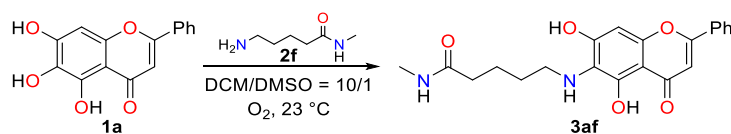
after purification by flash chromatography (DCM/MeOH = 20/1 → 10/1).

¹H NMR (400 MHz, DMSO-*d*₆) δ 12.95 (s, 1H), 8.09 – 8.03 (m, 2H), 7.72 (q, *J* = 4.7 Hz, 1H), 7.65 – 7.52 (m, 3H), 6.93 (s, 1H), 6.62 (s, 1H), 3.20 (t, *J* = 7.0 Hz, 2H), 2.54 (d, *J* = 4.6 Hz, 3H), 2.09 (t, *J* = 7.3 Hz, 2H), 1.63 (p, *J* = 7.3 Hz, 2H).

¹³C NMR (101 MHz, DMSO-*d*₆) δ 182.1, 172.4, 162.7, 154.8, 150.3, 148.7, 131.8, 131.0, 129.2, 126.3, 121.1, 104.6, 104.3, 93.6, 45.1, 32.9, 26.6, 25.5.

HRMS (ESI): calcd for C₂₀H₂₀N₂O₅Na [M + Na]⁺, 391.1264; found 391.1264.

R_f 0.31 (DCM/MeOH = 10/1)

5-((5,7-dihydroxy-4-oxo-2-phenyl-4H-chromen-6-yl)amino)-N-methylpentanamide (**3af**)

The title compound (50 mg, 52%) was obtained as an orange solid following general procedure D

(0.25 mmol scale, 1.33 eq of **2f**) in 2 h after purification by flash chromatography.

¹H NMR (400 MHz, DMSO-*d*₆) δ 12.94 (bs, 1H), 8.07 – 8.04 (m, 2H), 7.69 (q, *J* = 4.5 Hz, 1H), 7.62 – 7.55 (m, 3H), 6.93 (s, 1H), 6.62 (s, 1H), 3.21 (t, *J* = 7.1 Hz, 2H), 2.52 (t, *J* = 4.5,

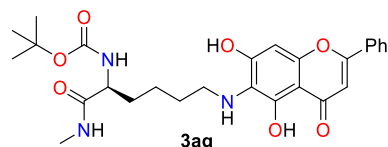
3H), 2.04 (t, $J = 7.1$ Hz, 2H), 1.55 – 1.48 (m, 2H), 1.42 – 1.35 (m, 2H).

^{13}C NMR (101 MHz, DMSO- d_6) δ 182.1, 172.5, 162.6, 154.7, 150.3, 148.5, 131.9, 131.0, 129.2, 126.3, 121.3, 104.6, 104.3, 93.6, 45.1, 35.2, 29.9, 25.4, 22.7.

HRMS (ESI): calcd for $\text{C}_{21}\text{H}_{21}\text{N}_2\text{O}_5$ [$\text{M} - \text{H}$] $^-$, 381.1456; found 381.1453

R_f 0.17 (DCM/MeOH = 10/1)

Tert-butyl (S)-6-((5,7-dihydroxy-4-oxo-2-phenyl-4H-chromen-6-yl)amino)-1-(methylamino)-1-oxohexan-2-yl)carbamate (**3ag**)



Procedure A (described in **3bg**). Orange solid (35 mg, 69%). To get crystals suitable for X-ray analysis, more of the title compound was synthesized: 130 mg of N-Boc-Lys-

NMe **2g** (0.5 mmol, 1.0 eq) was dissolved in 6 ml dry DCM under O_2 atmosphere. 135 mg of **1a** (0.5 mmol, 1 eq) was added to the stirring solution. The reaction immediately became green. The solution was vigorously stirred for 18 h at RT. Crude material was purified by column chromatography on silica gel (DCM \rightarrow DCM/MeOH = 10/1). Product was obtained as yellow green glass (170 mg, 67%).

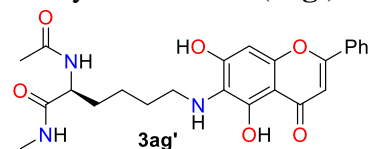
^1H NMR (400 MHz, DMSO- d_6) δ 12.94 (s, 1H), 8.07 – 8.04 (m, 2H), 7.72 (q, $J = 4.6$ Hz, 1H), 7.65 – 7.52 (m, 3H), 6.92 (s, 1H), 6.78 (d, $J = 8.2$ Hz, 1H), 6.61 (s, 1H), 3.82 (td, $J = 8.6, 5.1$ Hz, 1H), 3.20 (t, $J = 6.9$ Hz, 2H), 2.56 (d, $J = 4.6$ Hz, 3H), 1.63 – 1.18 (m, 6H), 1.36 (s, 9H).

^{13}C NMR (101 MHz, DMSO- d_6) δ 182.1, 172.6, 162.6, 155.3, 154.7, 150.2, 148.5, 131.8, 131.0, 129.2, 126.3, 121.3, 104.6, 104.2, 93.6, 77.9, 54.3, 45.3, 32.0, 30.0, 28.2, 25.5, 22.9.

HRMS (ESI): calcd for $\text{C}_{27}\text{H}_{34}\text{N}_3\text{O}_7$ [$\text{M} + \text{H}$] $^+$, 512.2392; found 512.2393.

R_f 0.32 (DCM/MeOH = 10/1)

(S)-2-acetamido-6-((5,7-dihydroxy-4-oxo-2-phenyl-4H-chromen-6-yl)amino) -N-methylhexanamide (**3ag'**)



The title compound (35 mg, 60%) was obtained as an orange solid following general procedure A after purification by flash chromatography (DCM/MeOH = 20/1 \rightarrow 5/1).

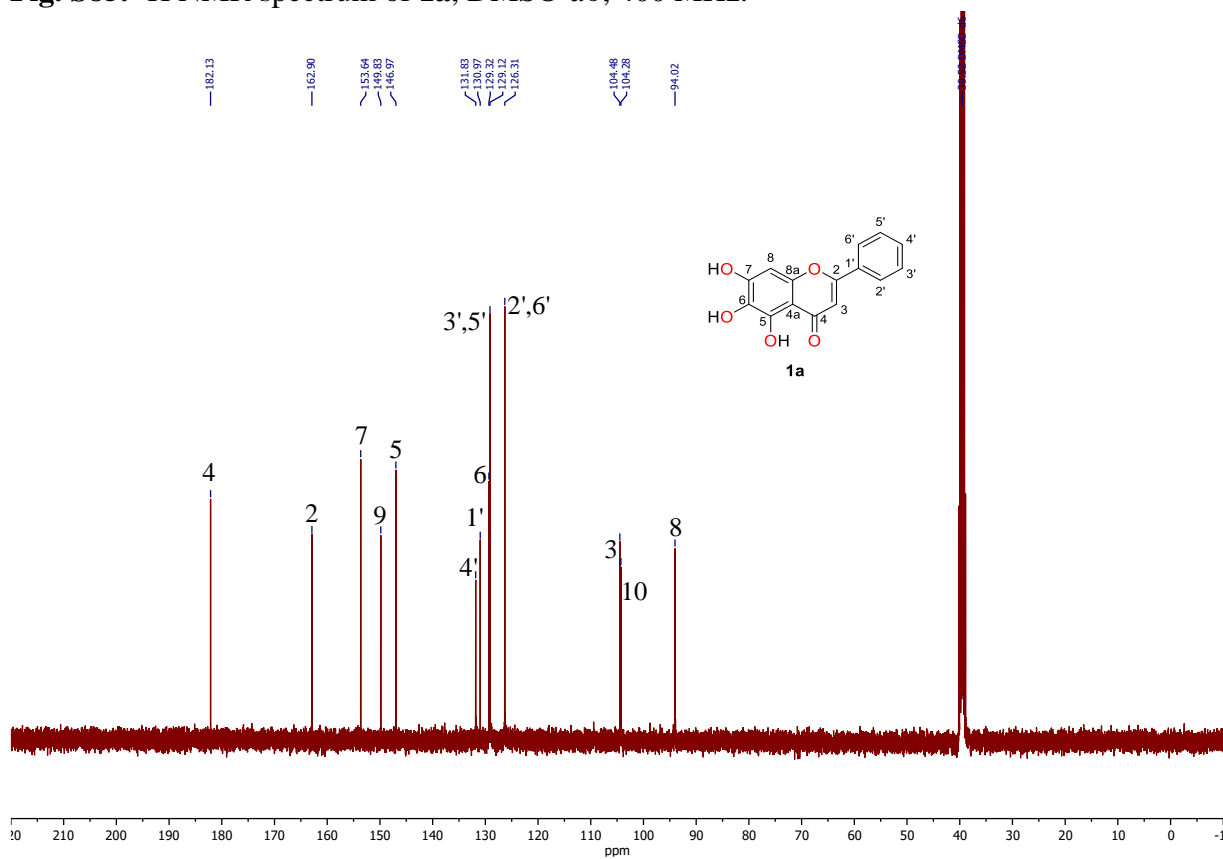
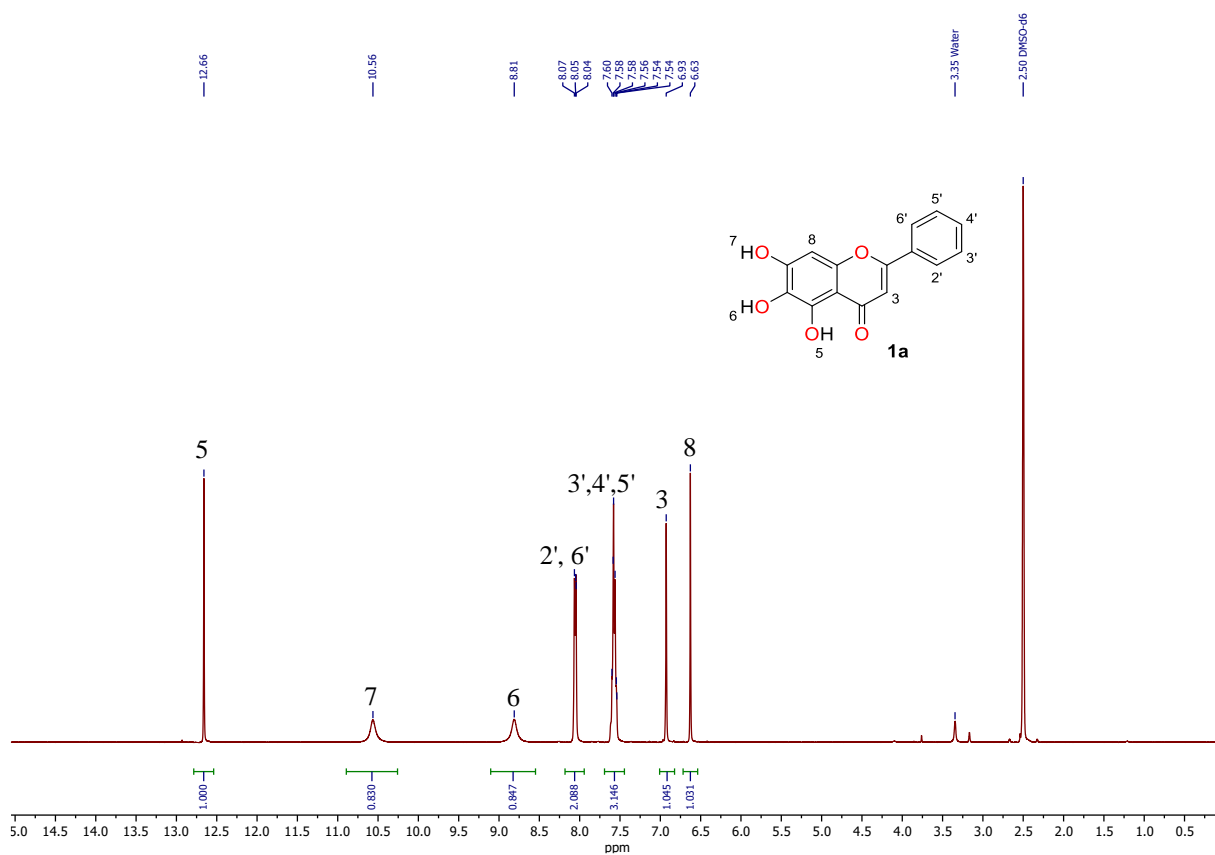
^1H NMR (400 MHz, MeOH- d_4) δ 8.50 – 7.83 (m, 2H), 7.64 – 7.46 (m, 3H), 6.72 (s, 1H), 6.55 (s, 1H), 4.23 (dd, $J = 8.9, 5.3$ Hz, 1H), 3.25 (td, $J = 7.1$, 2H), 2.71 (s, 3H), 1.98 (s, 4H), 1.87 – 1.70 (m, 1H), 1.70 – 1.51 (m, 3H), 1.51 – 1.34 (m, 1H).

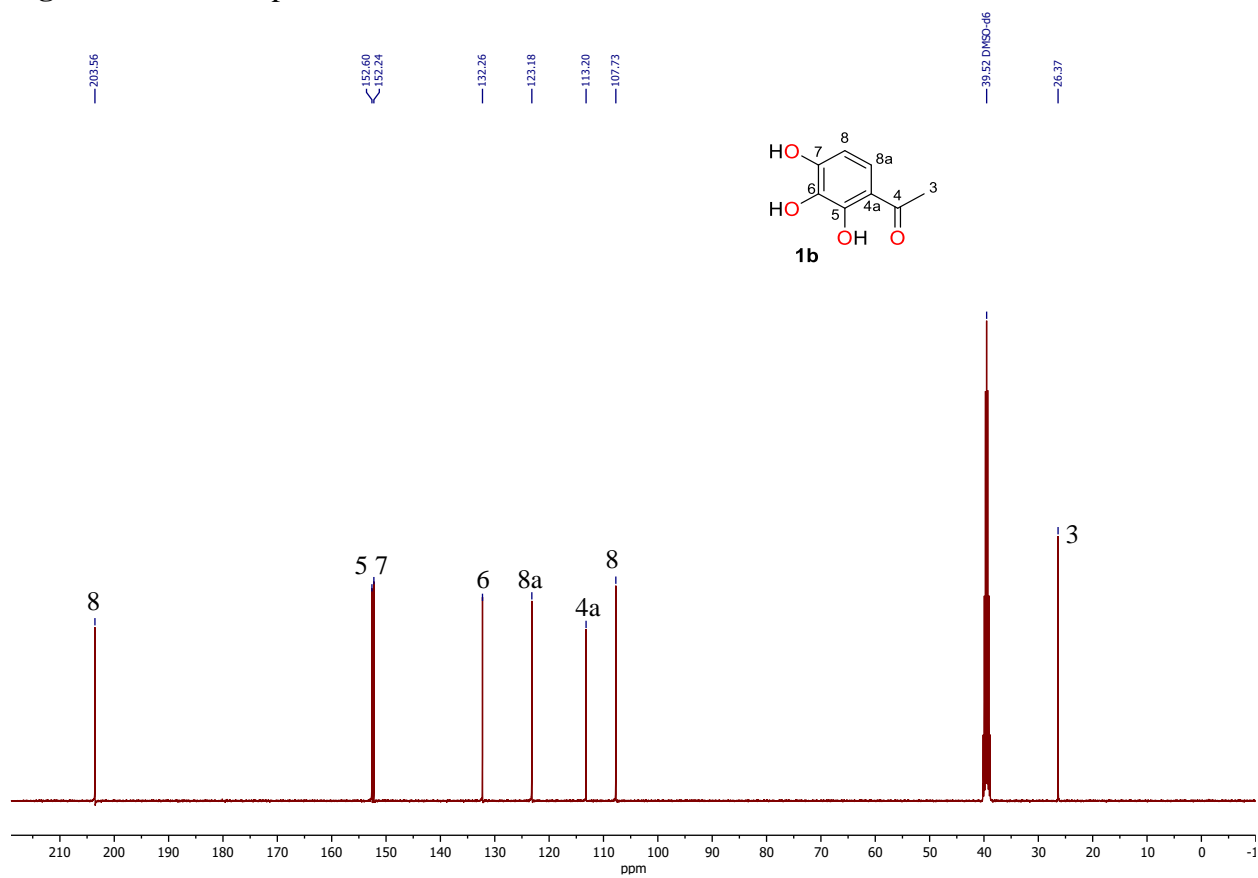
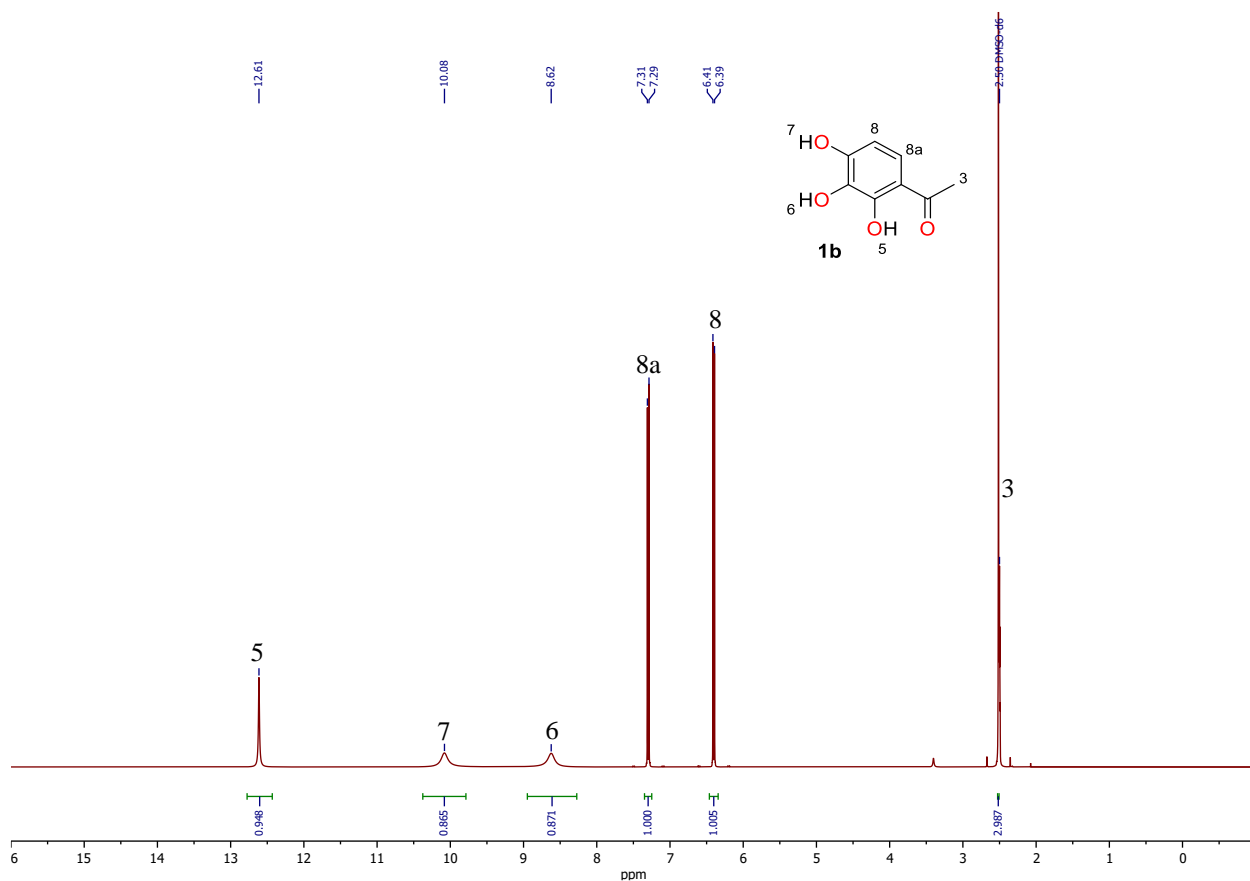
^{13}C NMR (101 MHz, MeOH- d_4) 184.0, 175.1, 173.4, 165.3, 158.9, 154.4, 152.4, 132.9, 132.7, 130.2, 127.4, 120.5, 105.6, 105.3, 94.9, 54.9, 47.7, 32.9, 30.4, 26.3, 24.3, 22.5.

HRMS (ESI): calcd for $\text{C}_{24}\text{H}_{26}\text{N}_3\text{O}_6$ [$\text{M} - \text{H}$] $^-$, 452.1827; found 452.1826.

R_f <0.05 (DCM/MeOH = 10/1)

1.3.7.10. NMR spectra of polyphenols **1a-q**





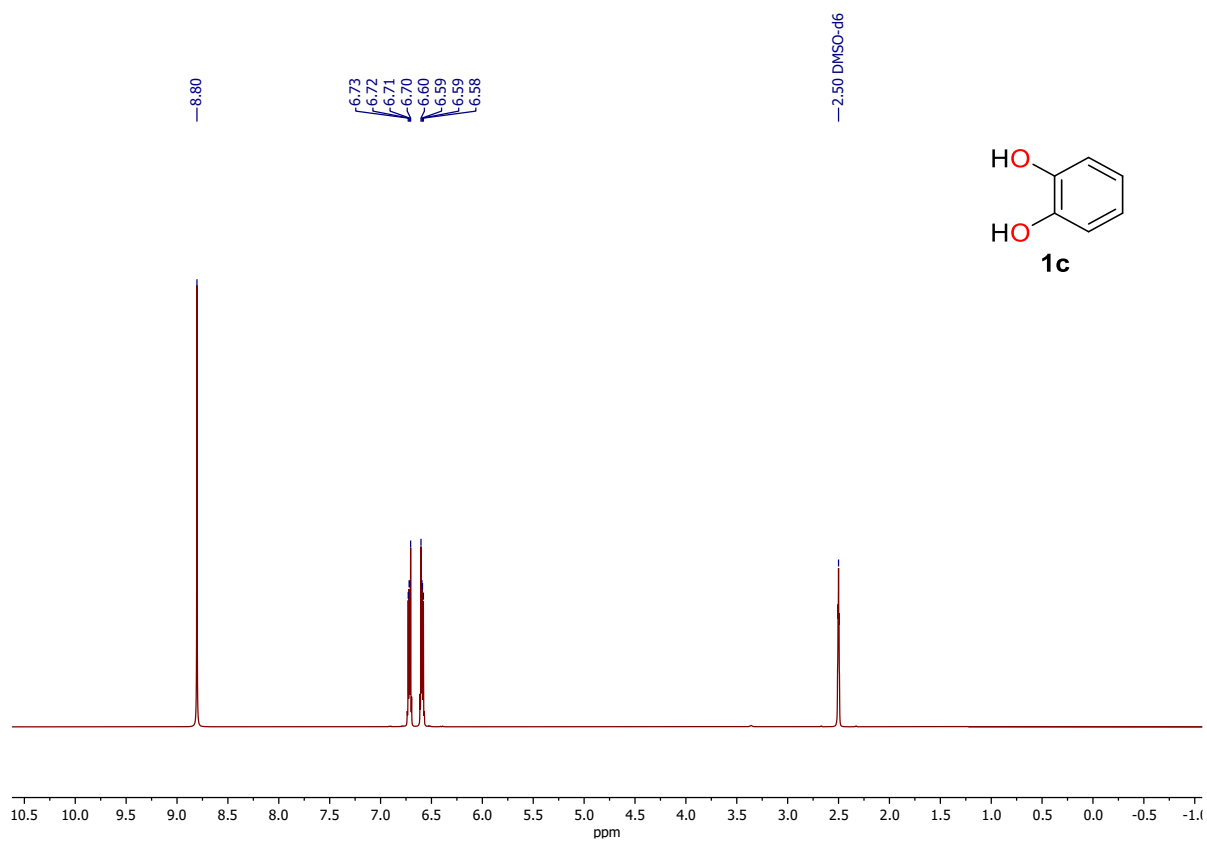


Fig. S89. ^1H NMR spectrum of **1c**, DMSO- d_6 , 400 MHz.

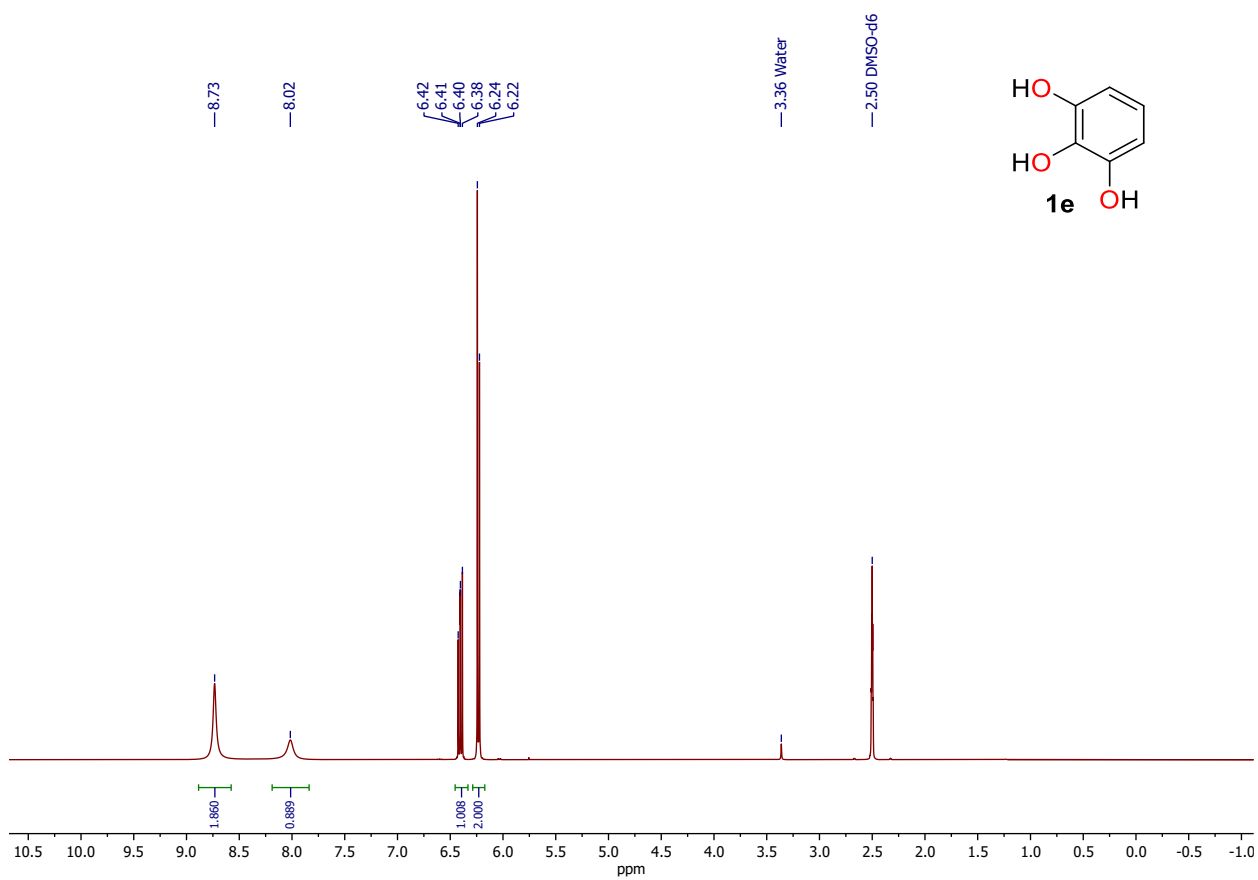


Fig. S90. ^1H NMR spectrum of **1e**, DMSO- d_6 , 400 MHz.

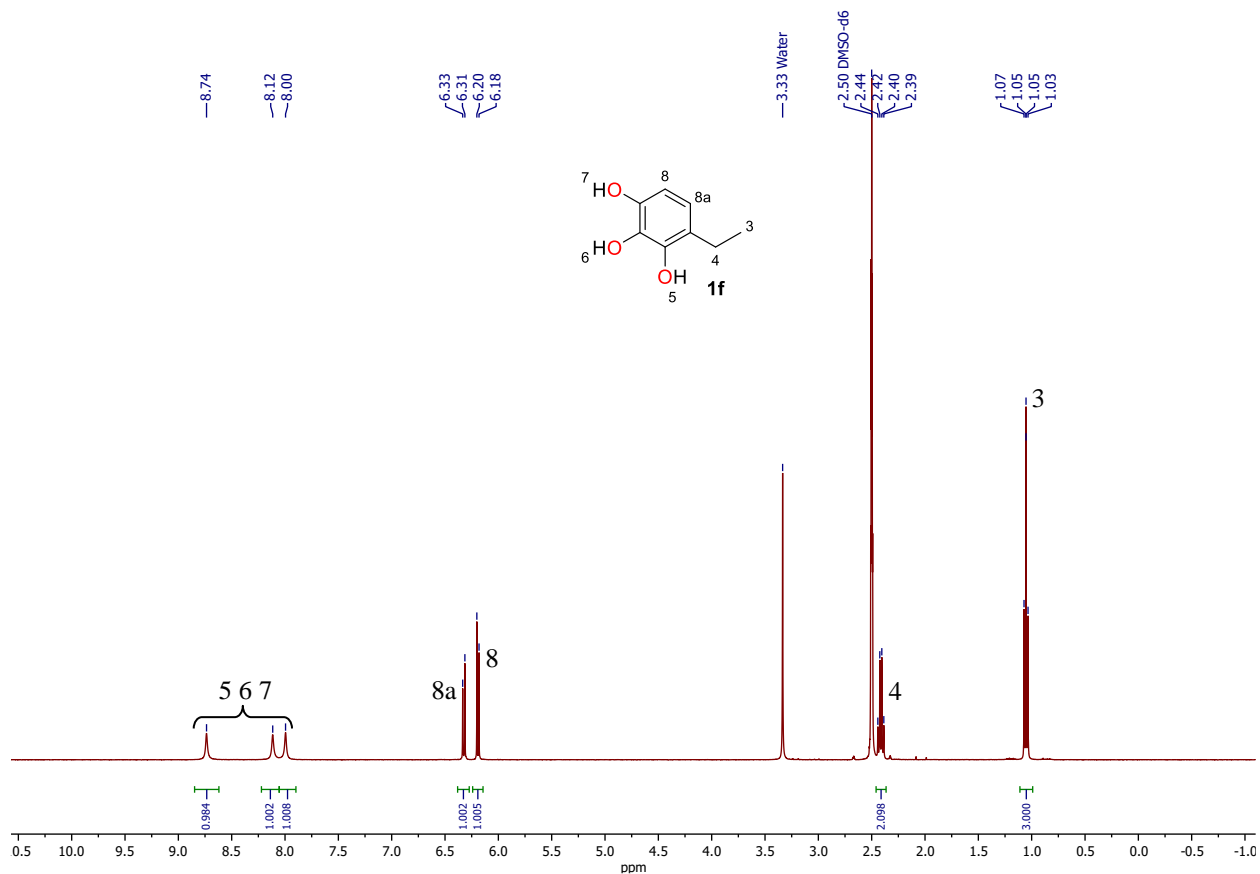


Fig. S91. ^1H NMR spectrum of **1f**, $\text{DMSO-}d_6$, 400 MHz.

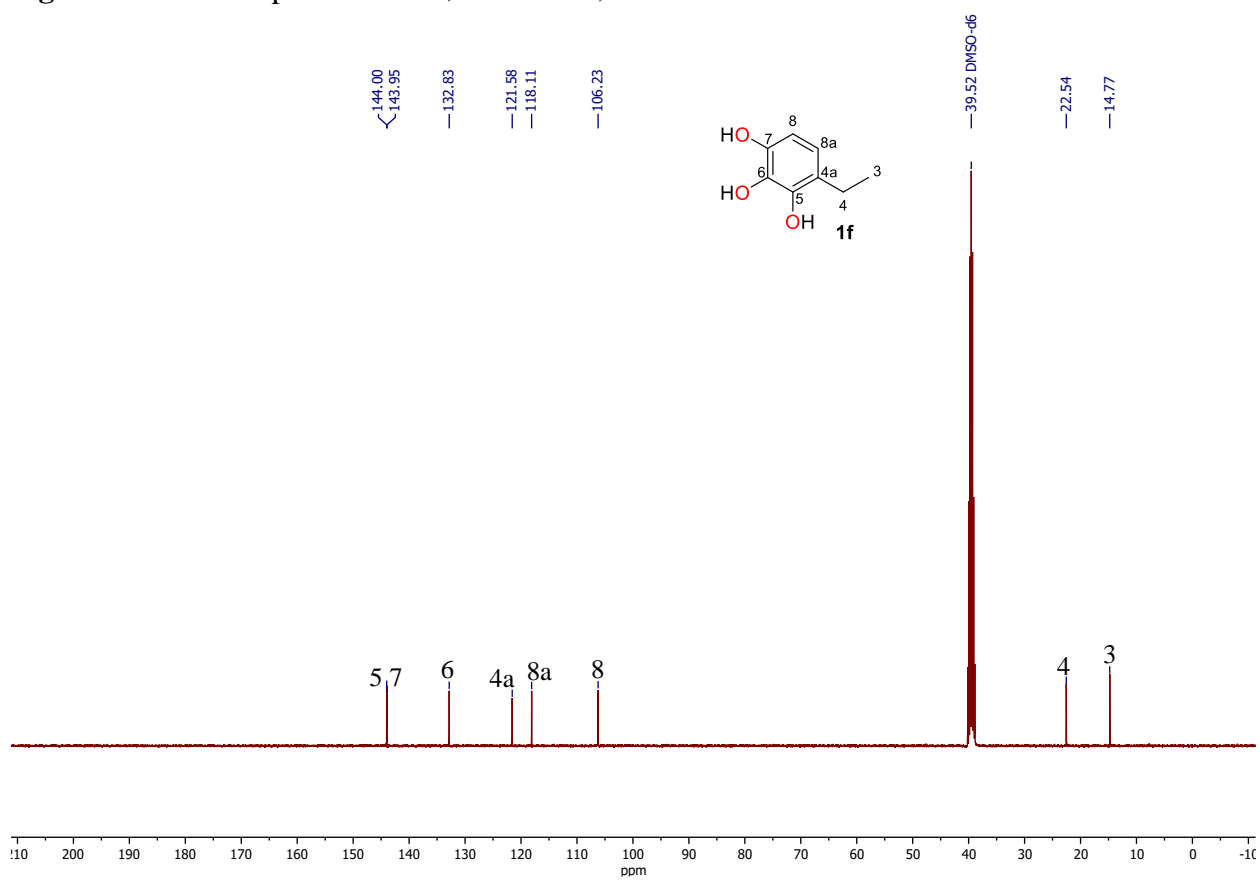


Fig. S92. ^{13}C NMR spectrum of **1f**, $\text{DMSO-}d_6$, 101 MHz.

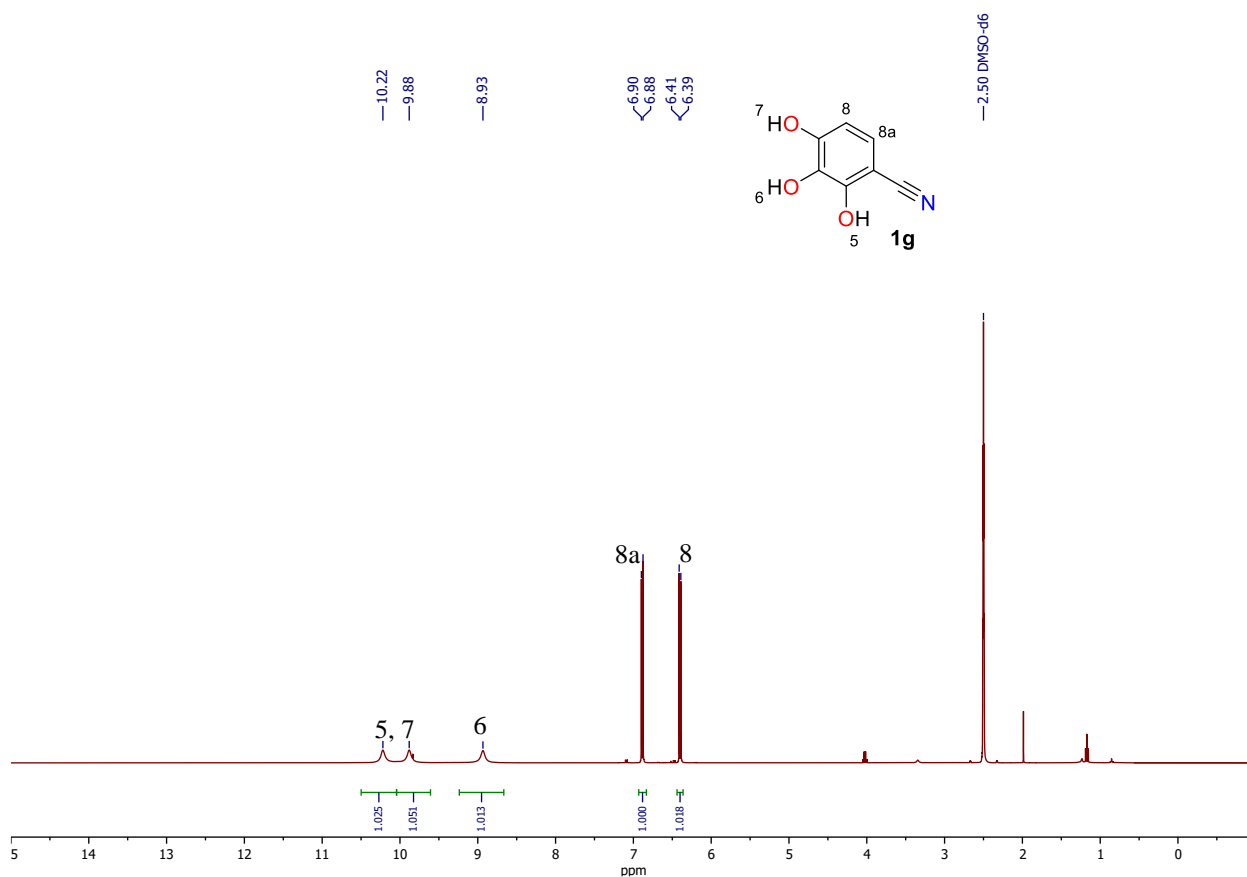


Fig. S93. ^1H NMR spectrum of **1g**, DMSO- d_6 , 400 MHz.

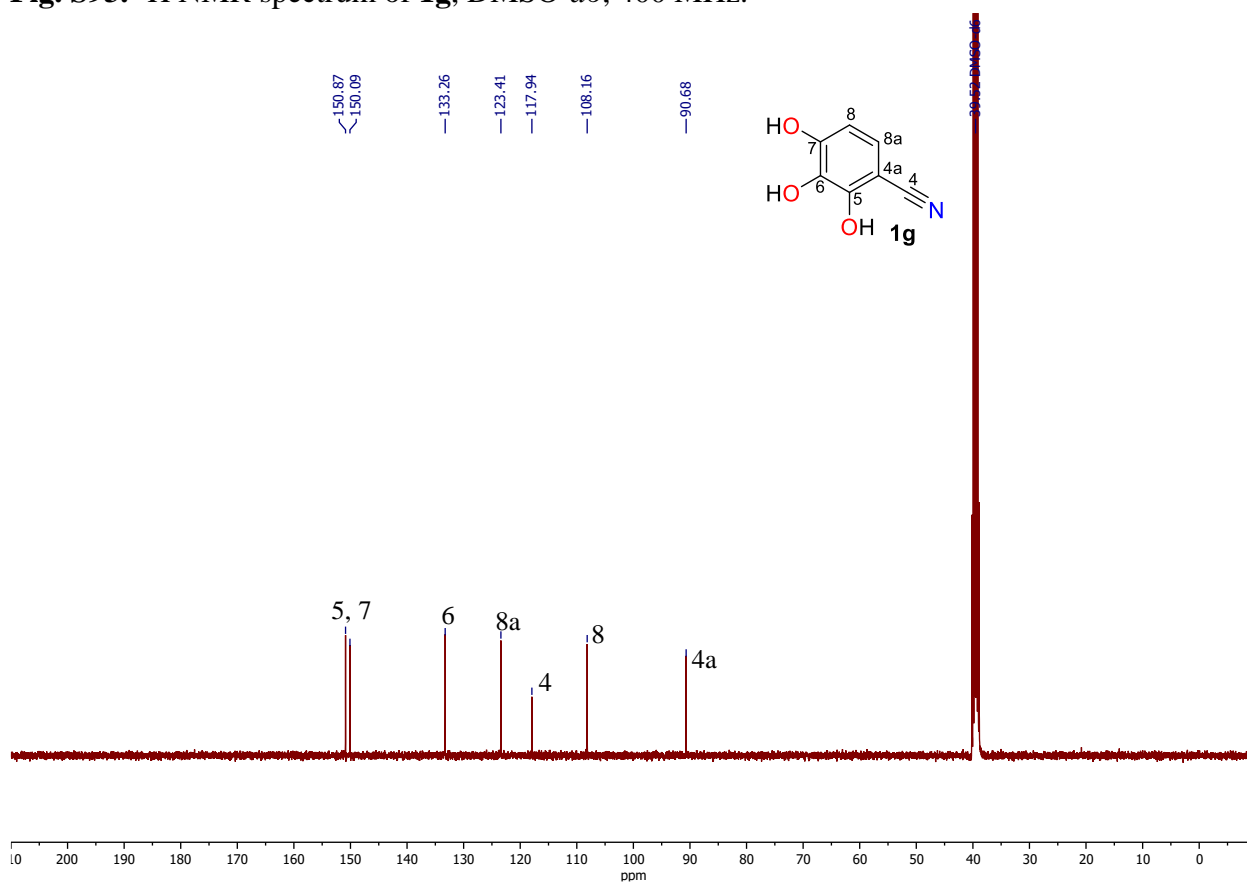


Fig. S94. ^{13}C NMR spectrum of **1g**, DMSO- d_6 , 101 MHz.

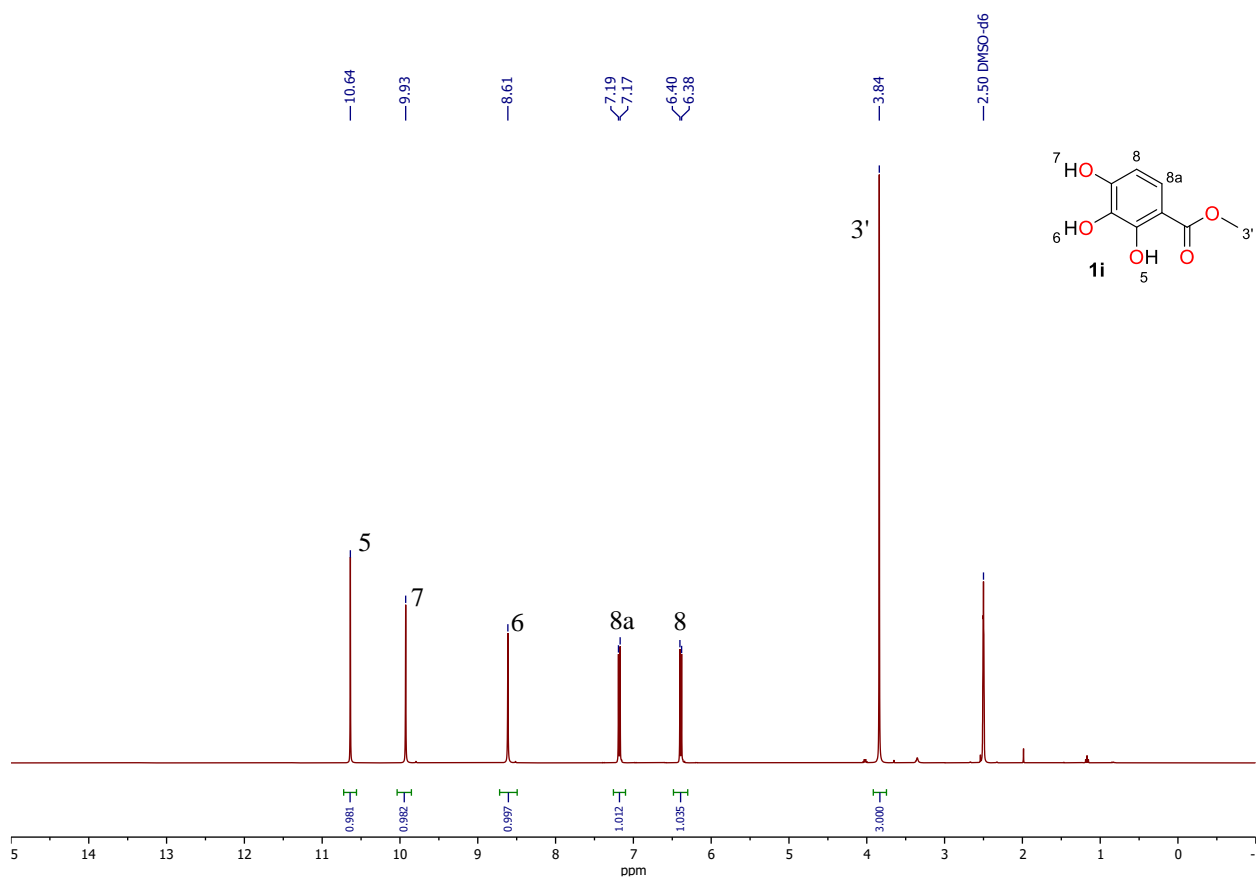


Fig. S95. ^1H NMR spectrum of **1i**, $\text{DMSO-}d_6$, 400 MHz.

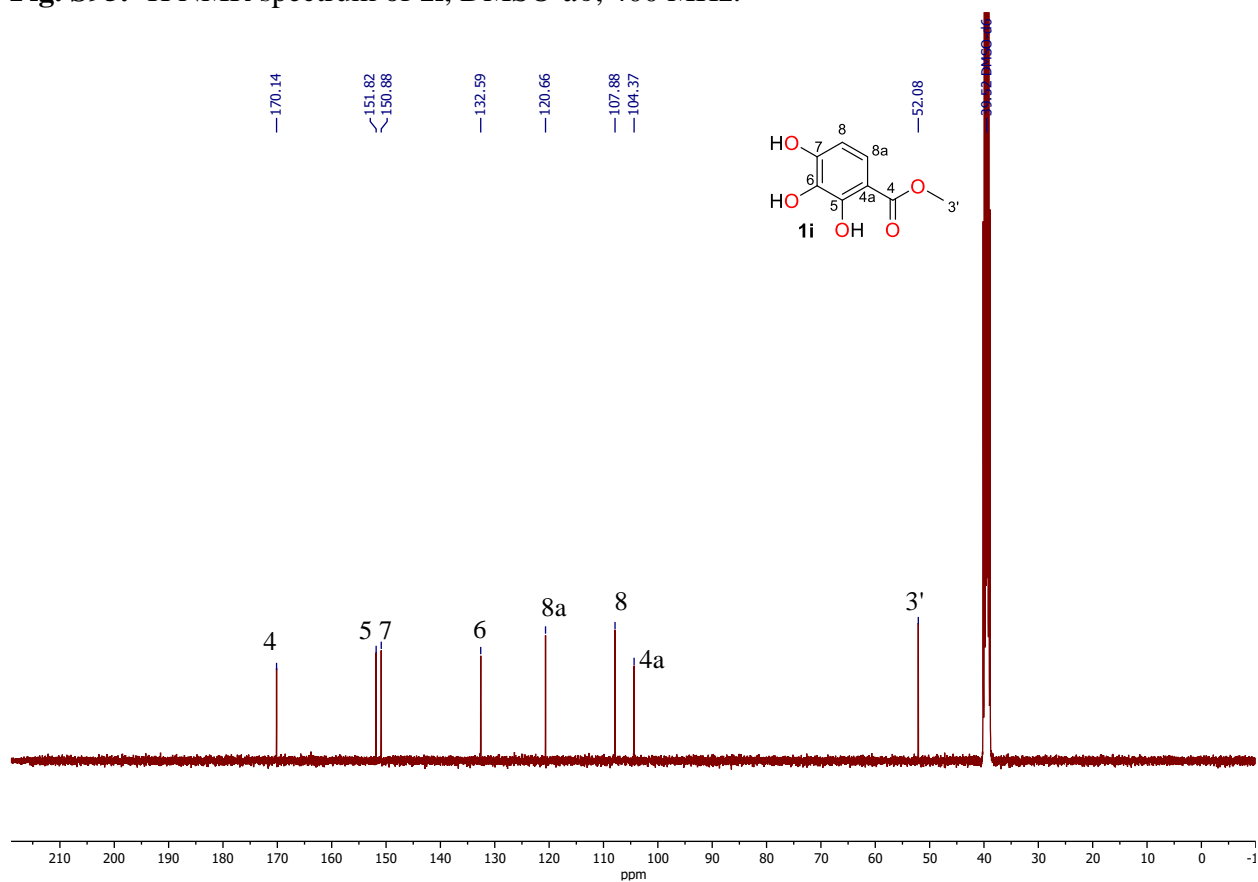


Fig. S96. ^{13}C NMR spectrum of **1i**, $\text{DMSO-}d_6$, 101 MHz.

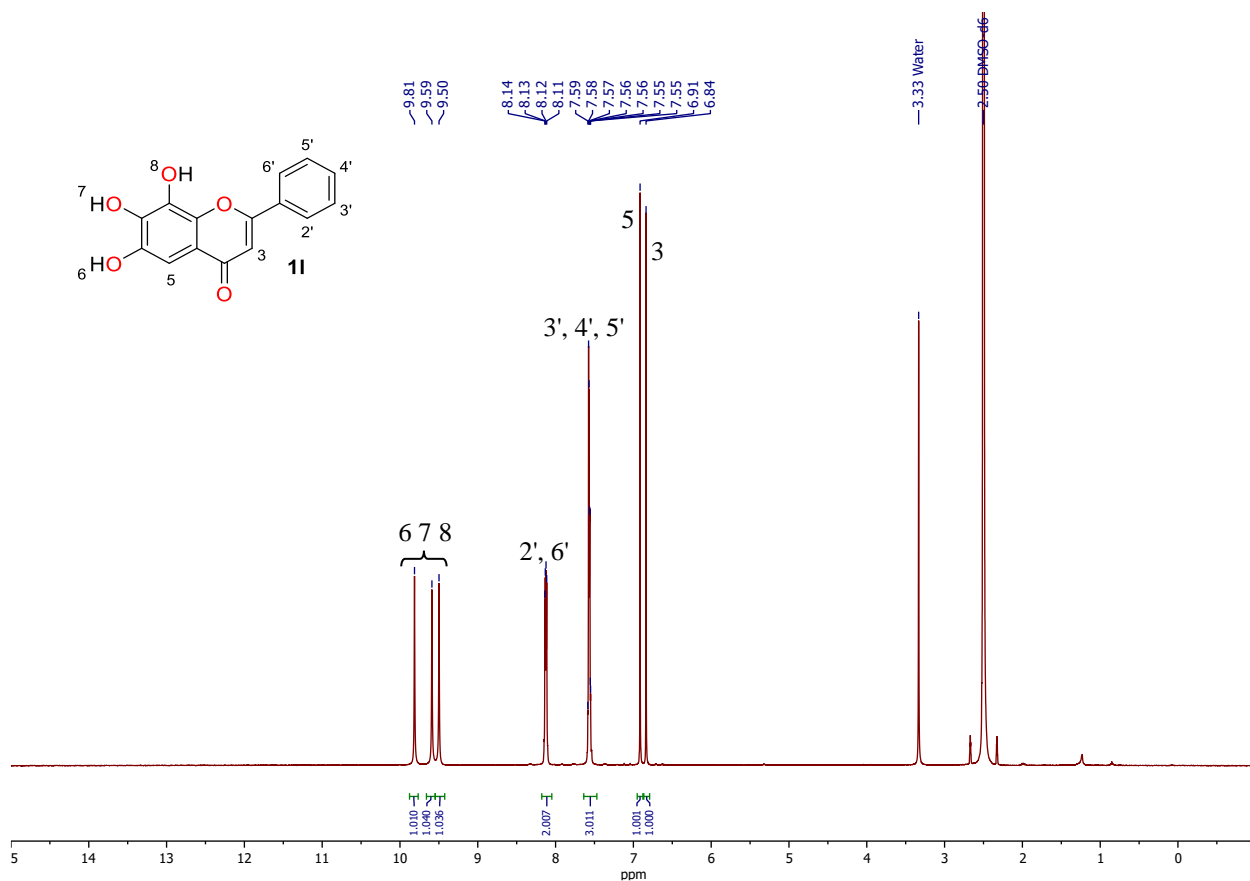


Fig. S97. ^1H NMR spectrum of **11**, $\text{DMSO-}d_6$, 400 MHz.

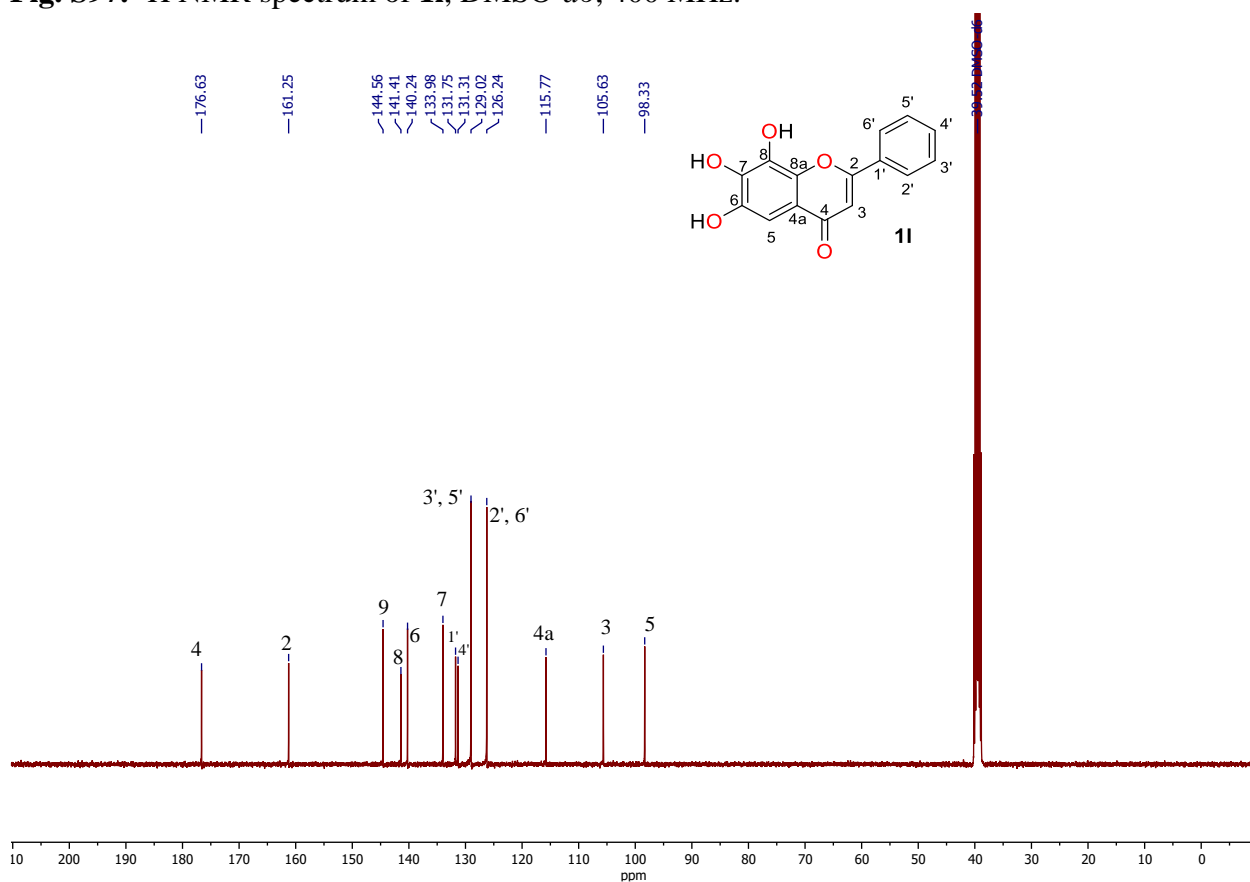


Fig. S98. ^{13}C NMR spectrum of **11**, $\text{DMSO-}d_6$, 101 MHz.

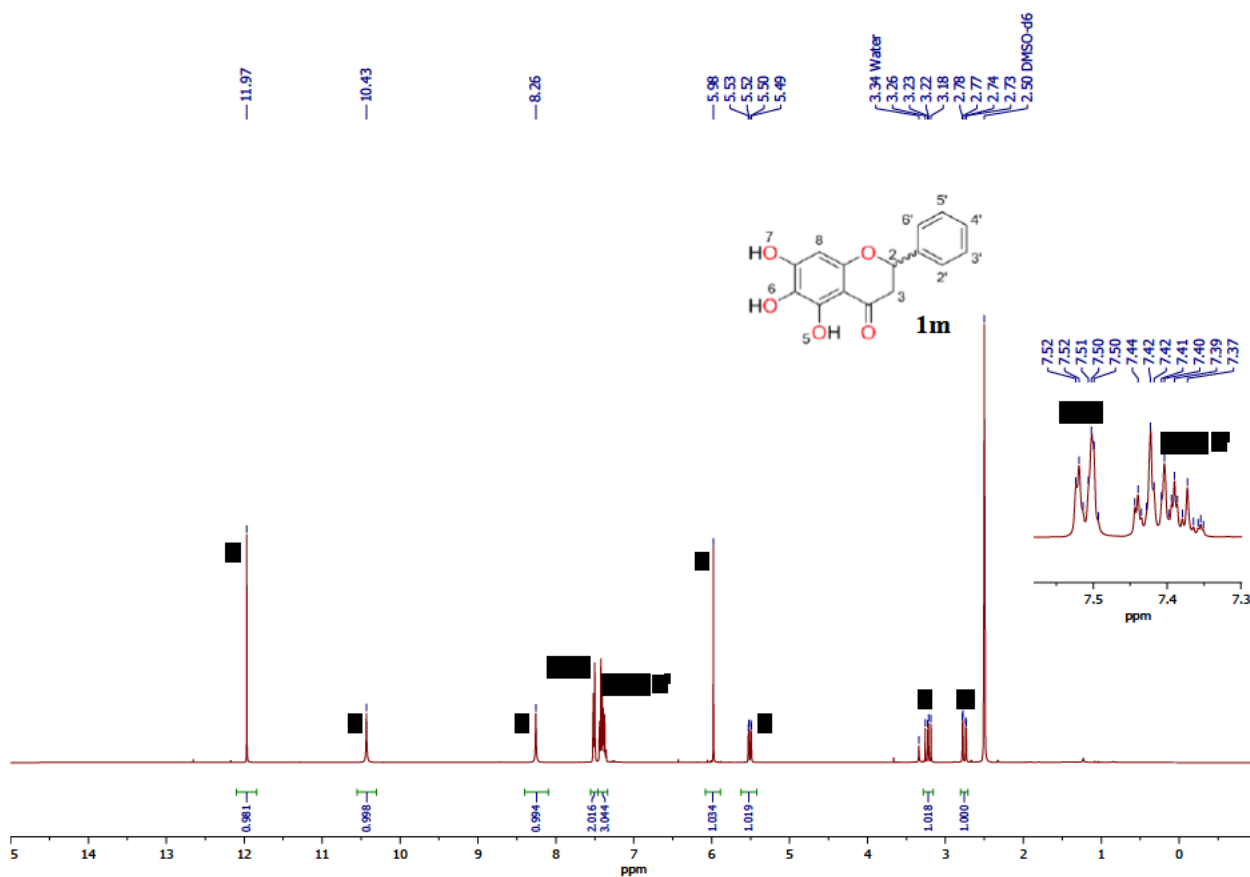


Fig. S99. ¹H NMR spectrum of **1m**, DMSO-*d*₆, 400 MHz.

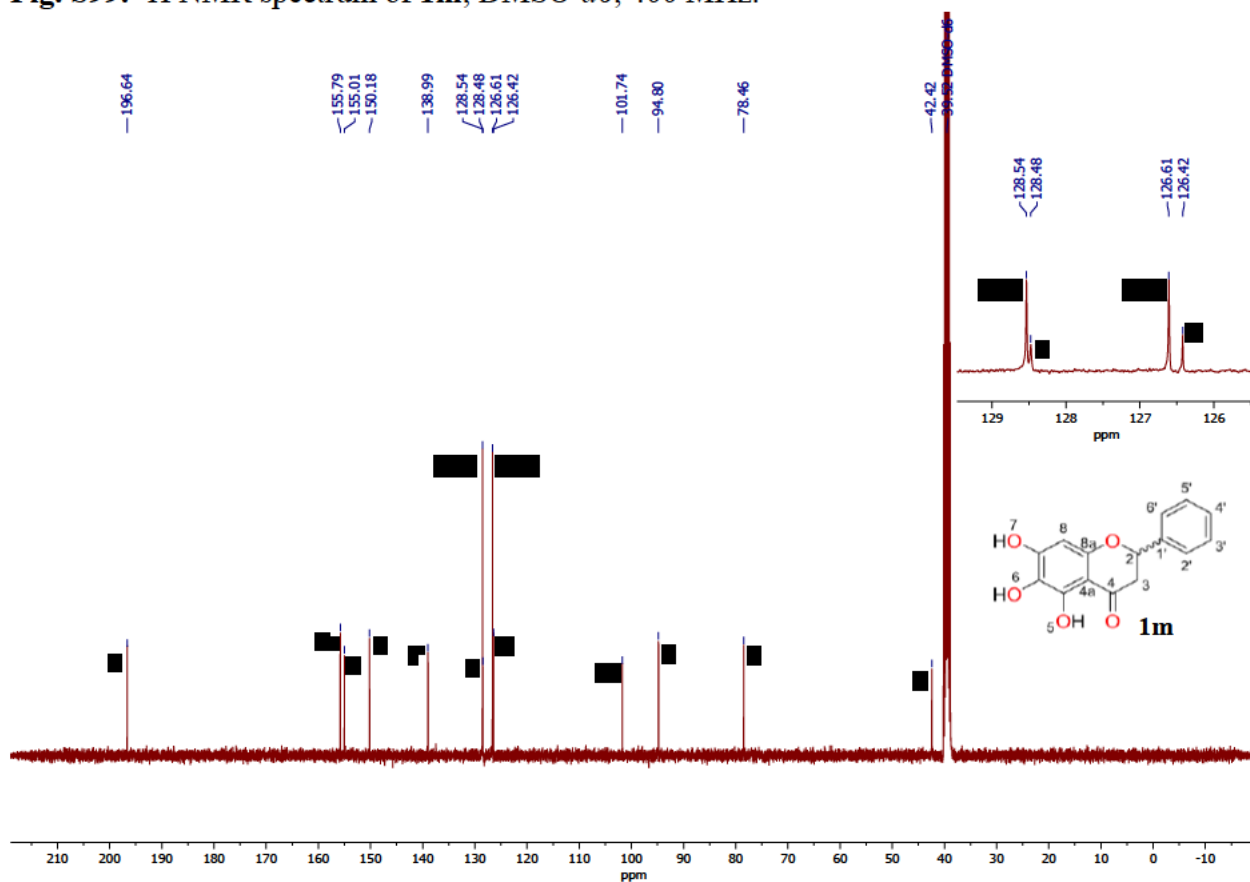
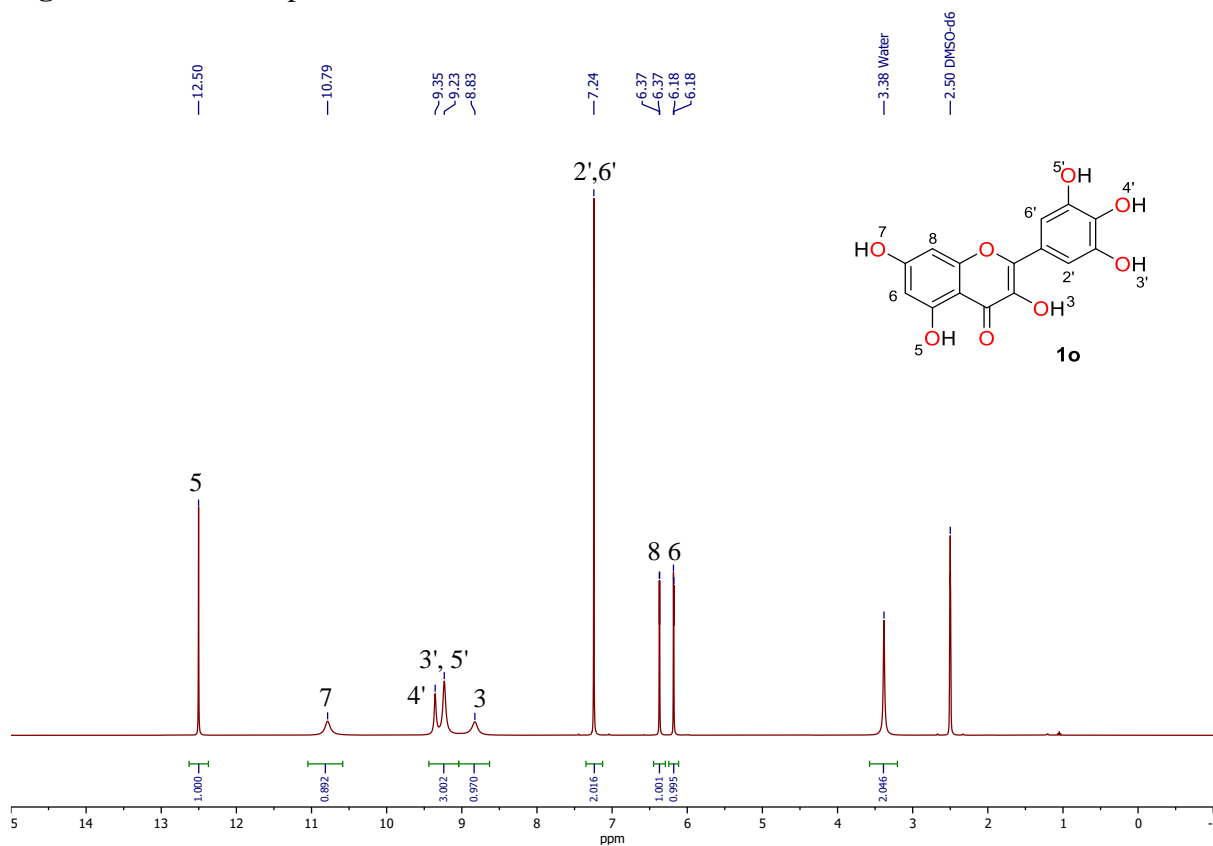
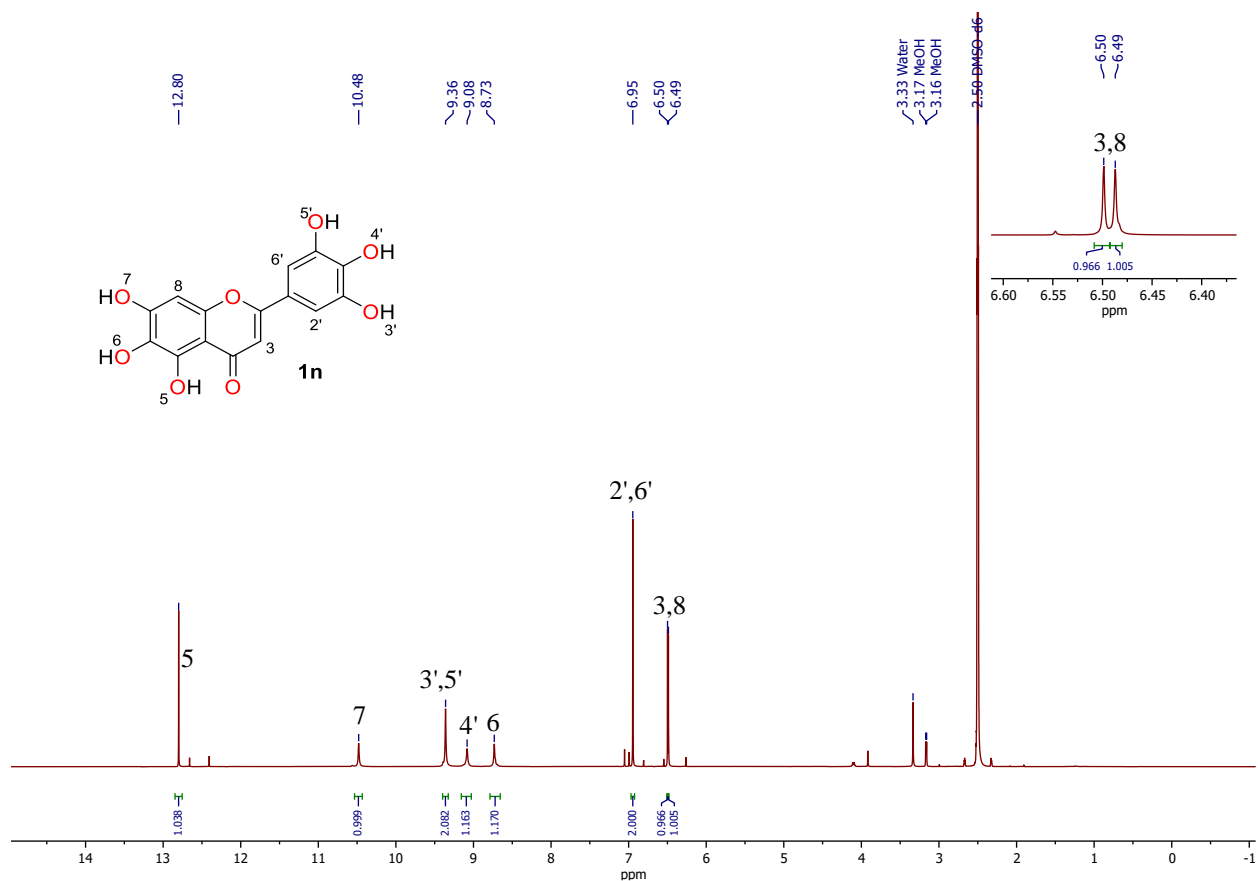
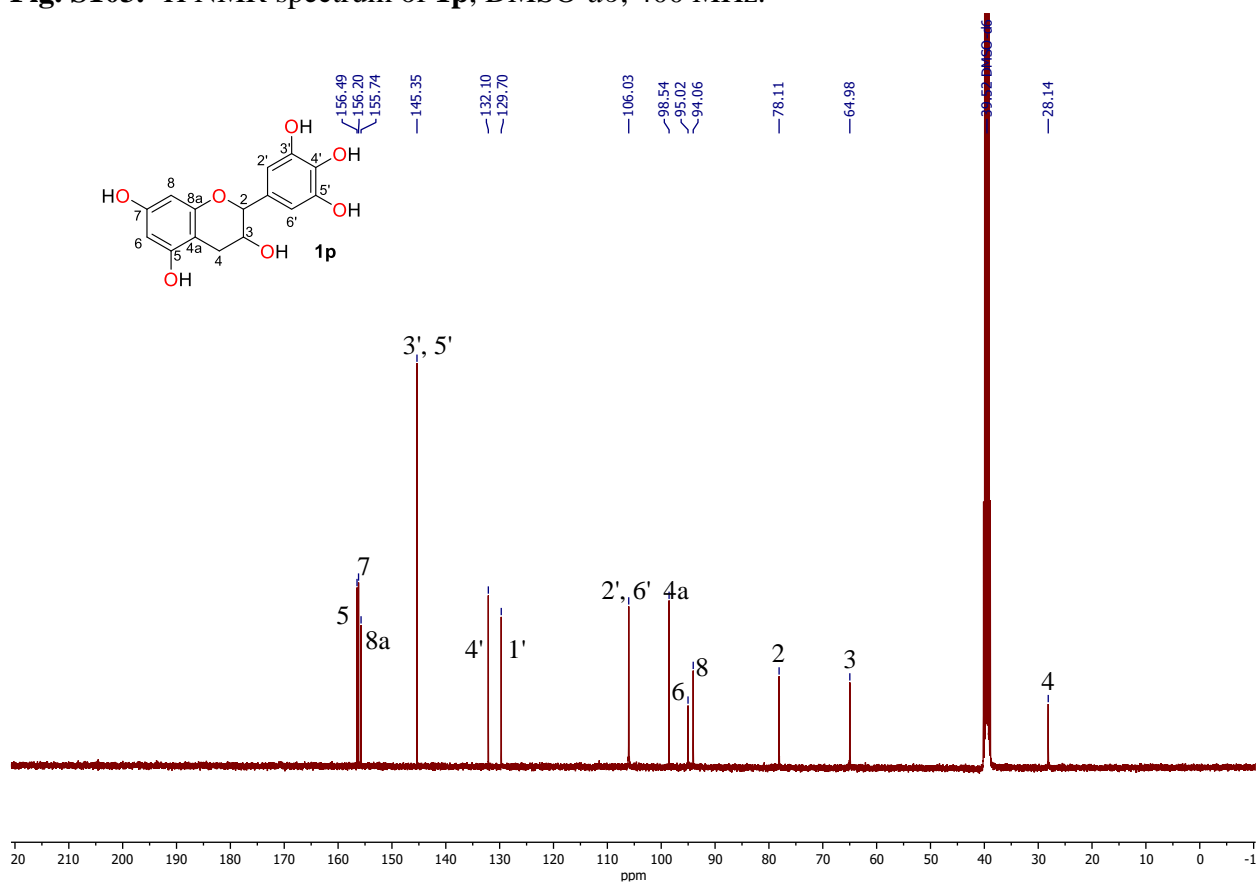
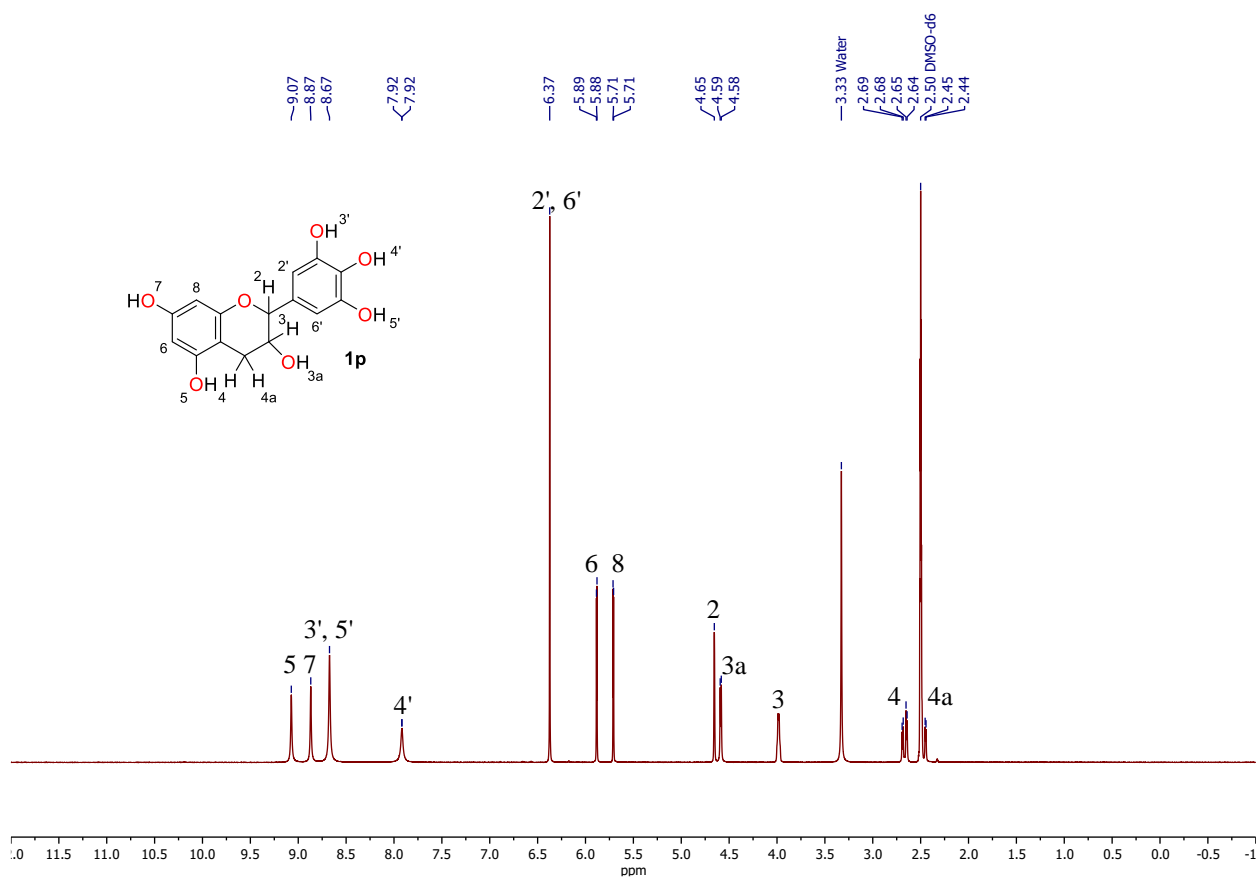


Fig. S100. ¹³C NMR spectrum of **1m**, DMSO-*d*₆, 101 MHz.





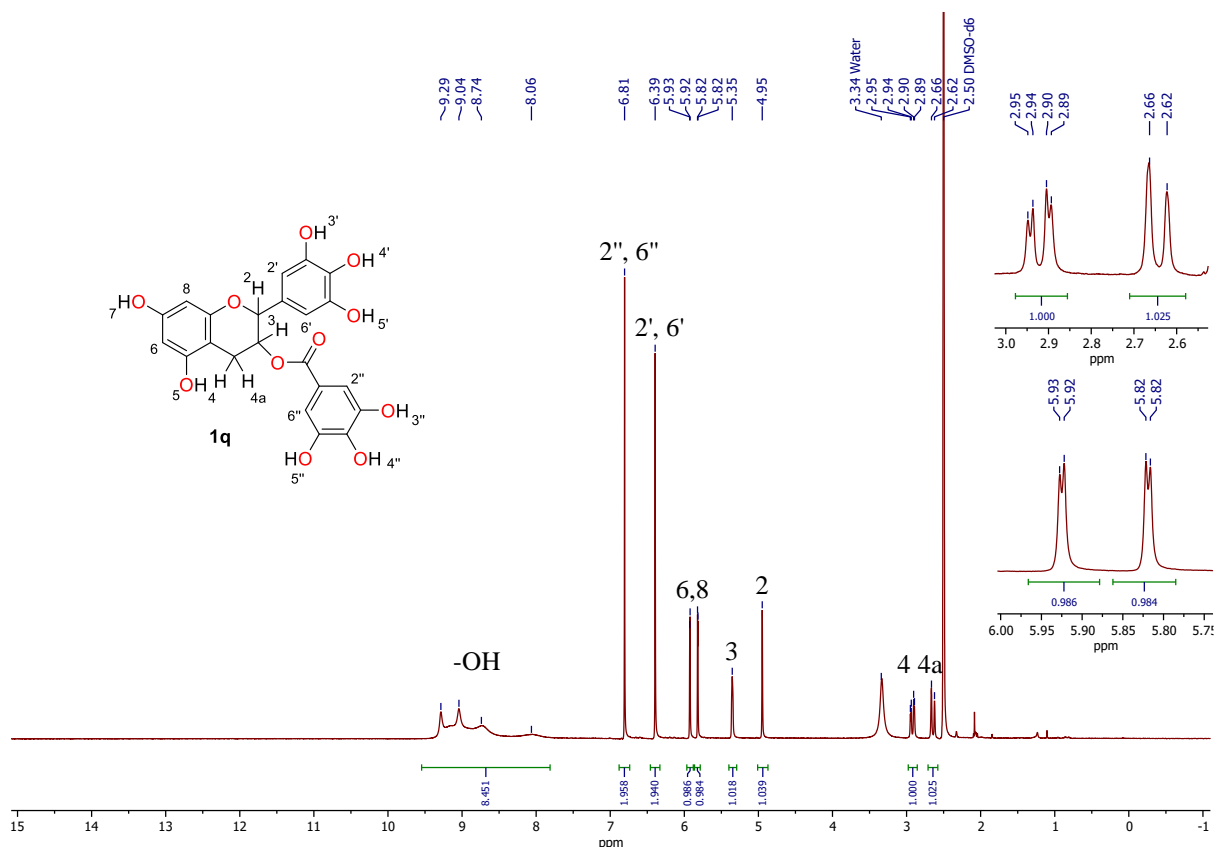


Fig. S105. ^1H NMR spectrum of **1q**, $\text{DMSO-}d_6$, 400 MHz.

1.3.7.11. NMR Spectra of *N*-nucleophiles **2a-g**

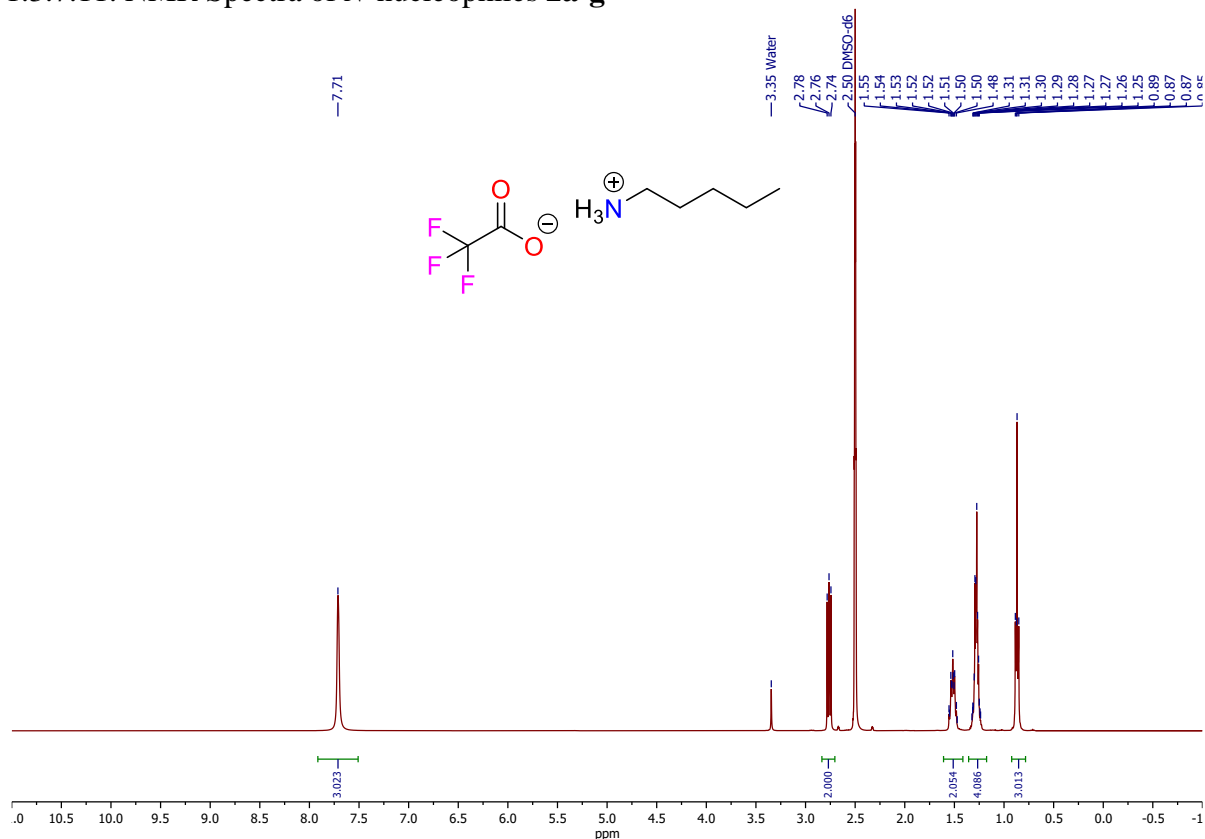


Fig. S106. ^1H NMR spectrum of pentylamine trifluoroacetate **TFA** $\times 2\mathbf{a}$, DMSO- d_6 , 400 MHz.

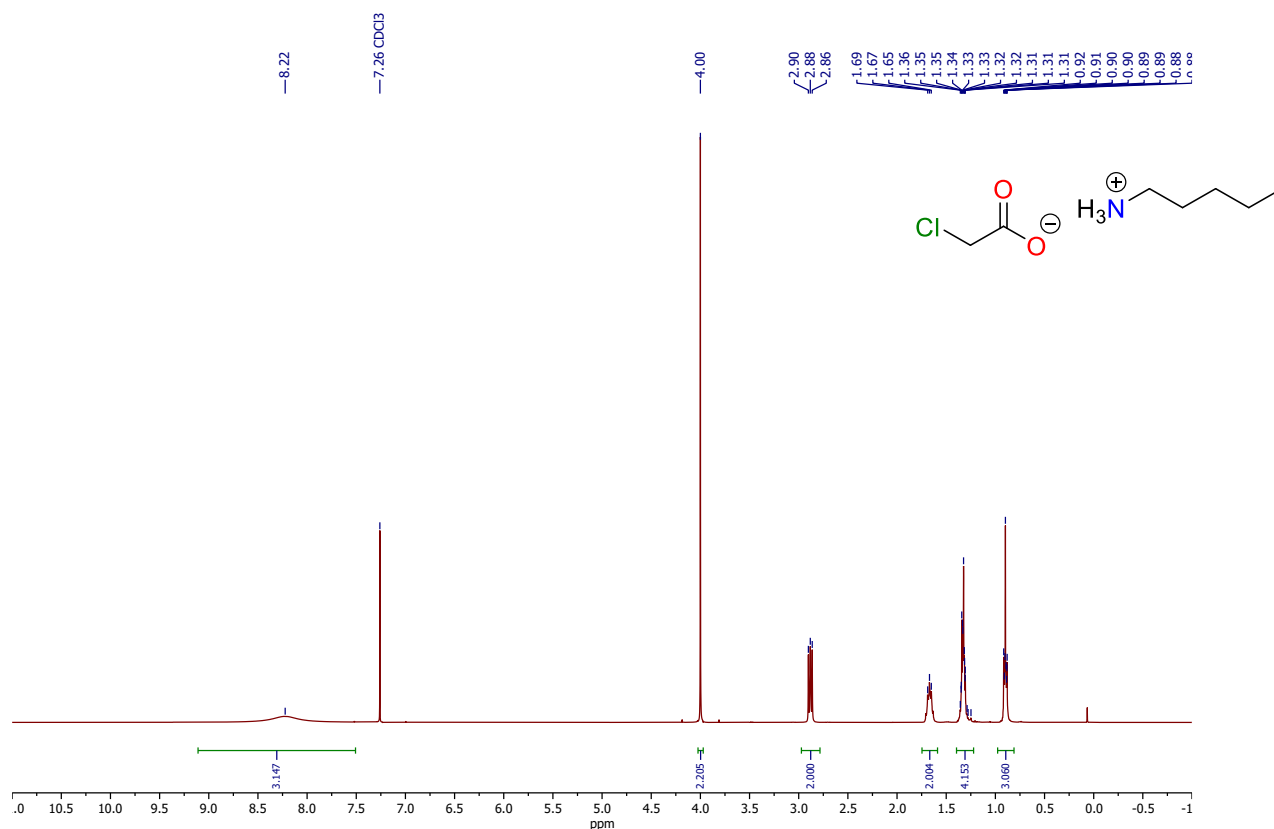


Fig. S107. ^1H NMR spectrum of pentylamine monochloroacetate **MCA** $\times 2\mathbf{a}$, CDCl $_3$, 400 MHz.

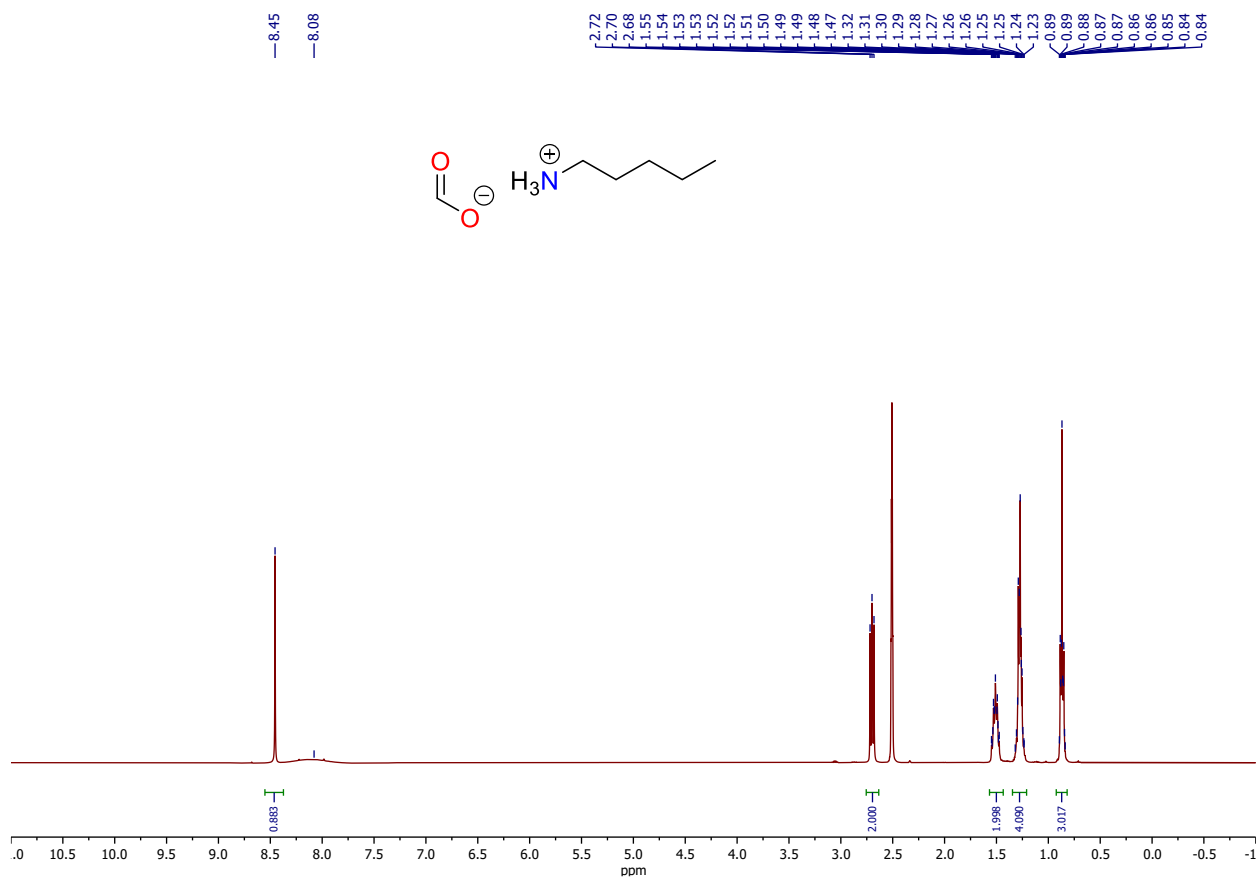


Fig. S108. ^1H NMR spectrum of pentylamine formate **FA** \times **2a**, DMSO- d_6 , 400 MHz.

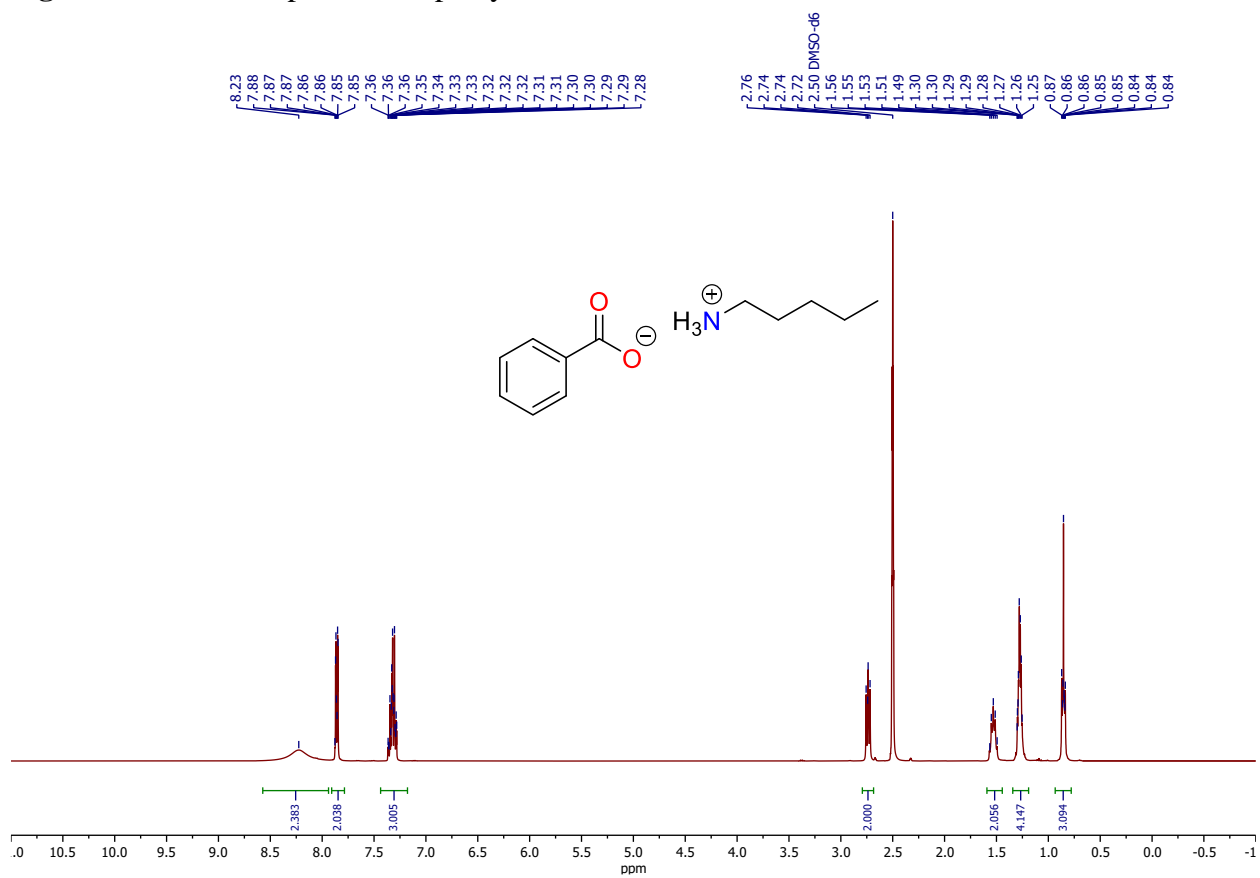


Fig. S109. ^1H NMR spectrum of pentylamine benzoate **BzA** \times **2a**, DMSO- d_6 , 400 MHz.

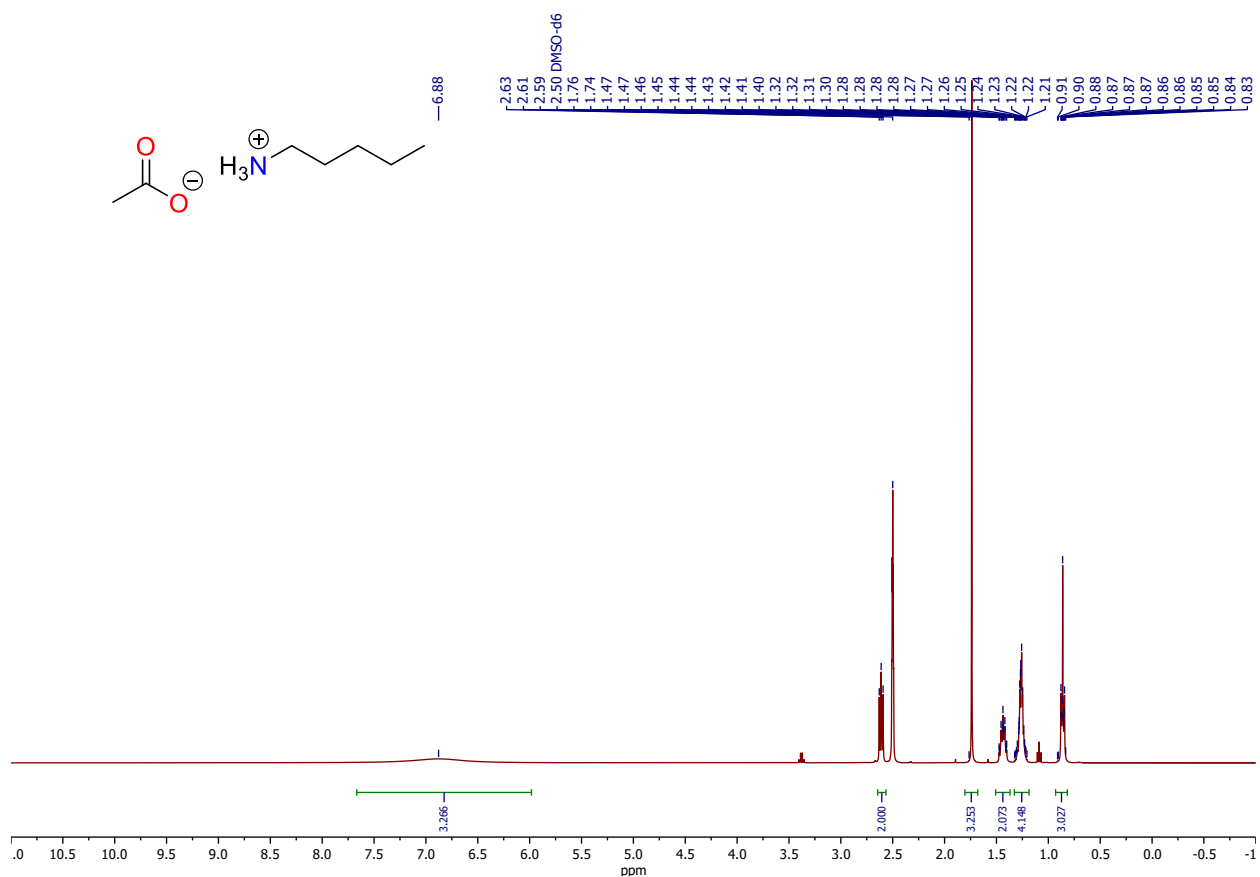


Fig. S110. ^1H NMR spectrum of pentylamine acetate $\text{AcA} \times 2\mathbf{a}$, $\text{DMSO-}d_6$, 400 MHz.

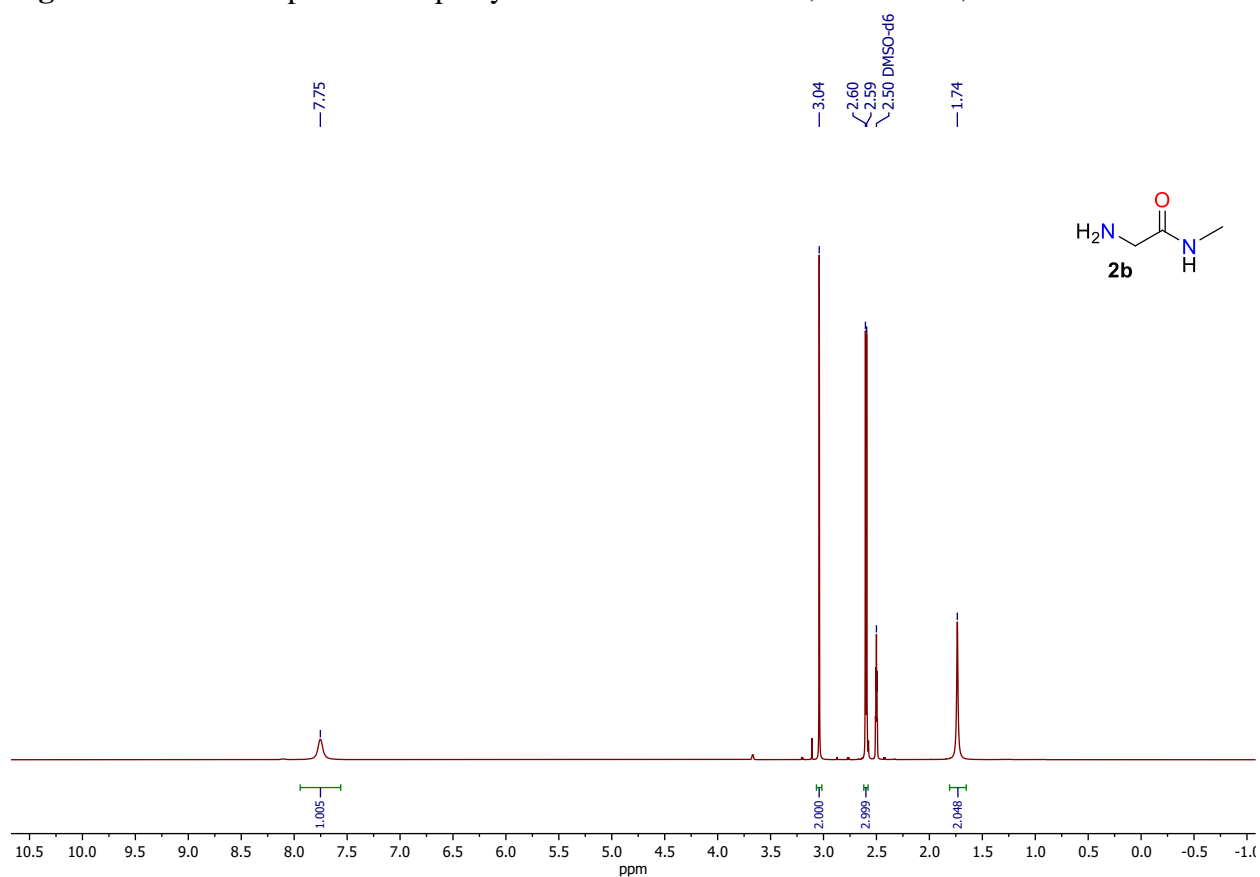


Fig. S111. ^1H NMR spectrum of H-Gly-NMe ($\mathbf{2b}$), $\text{DMSO-}d_6$, 400 MHz.

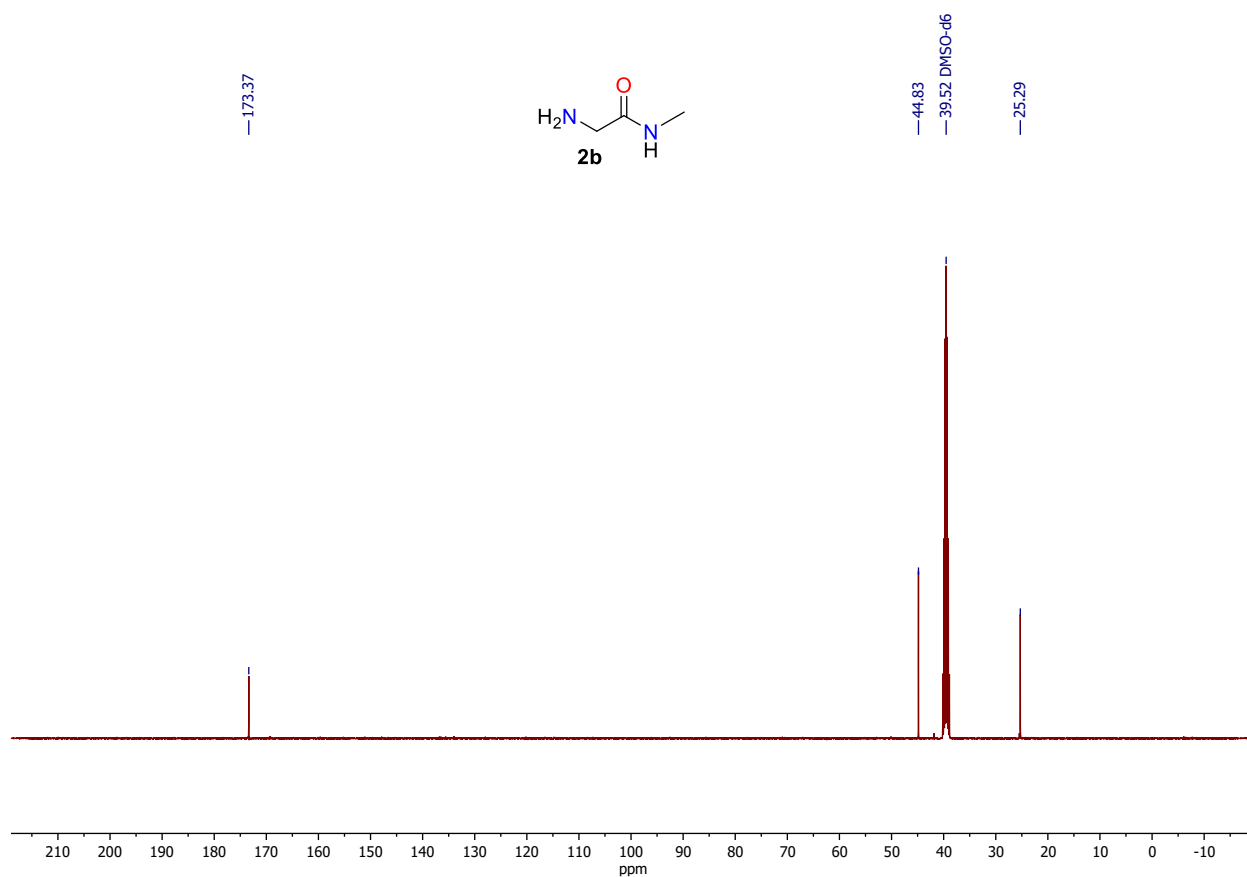


Fig. S112. ^{13}C NMR spectrum of H-Gly-NMe (**2b**), DMSO-*d*₆, 101 MHz.

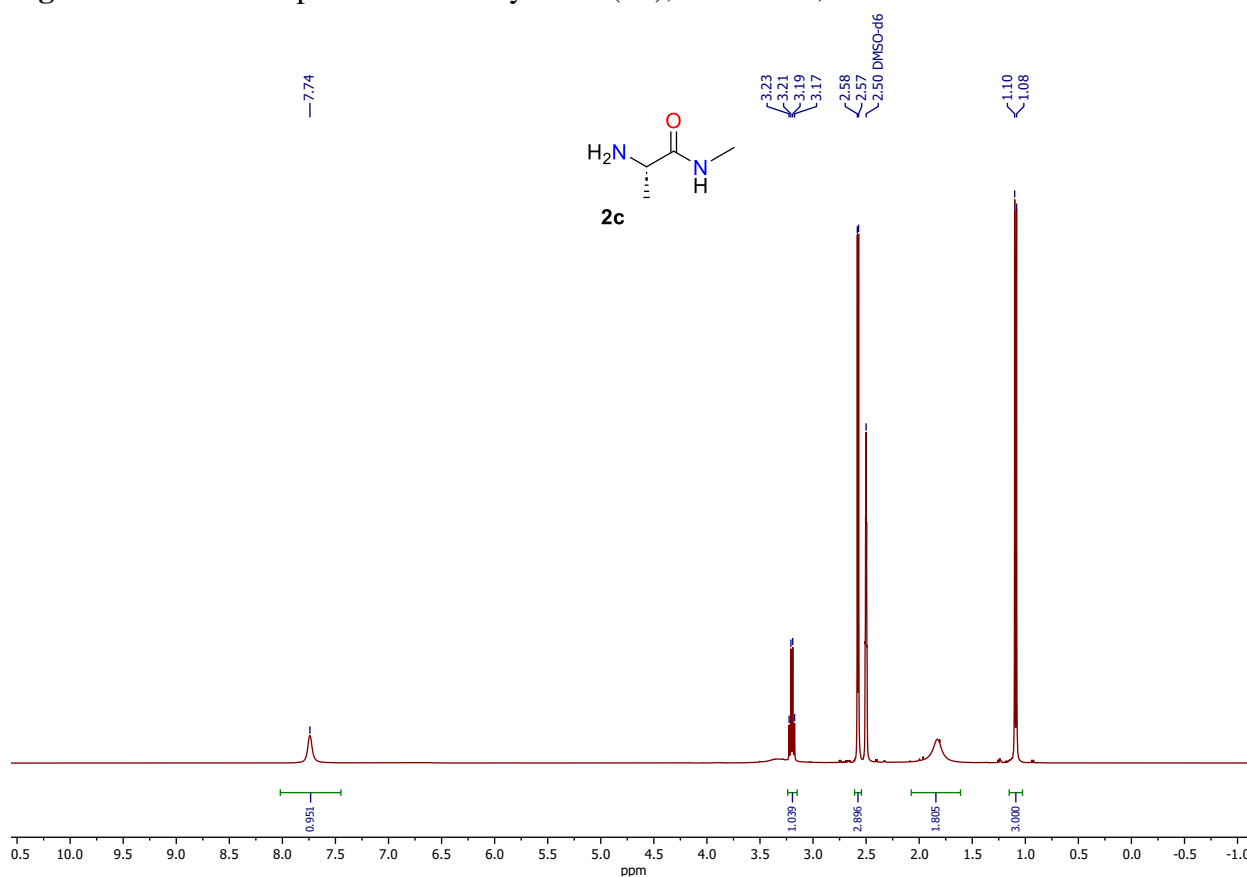


Fig. S113. ^1H NMR spectrum of H-*L*-Ala-NMe **2c**, DMSO-*d*₆, 400 MHz.

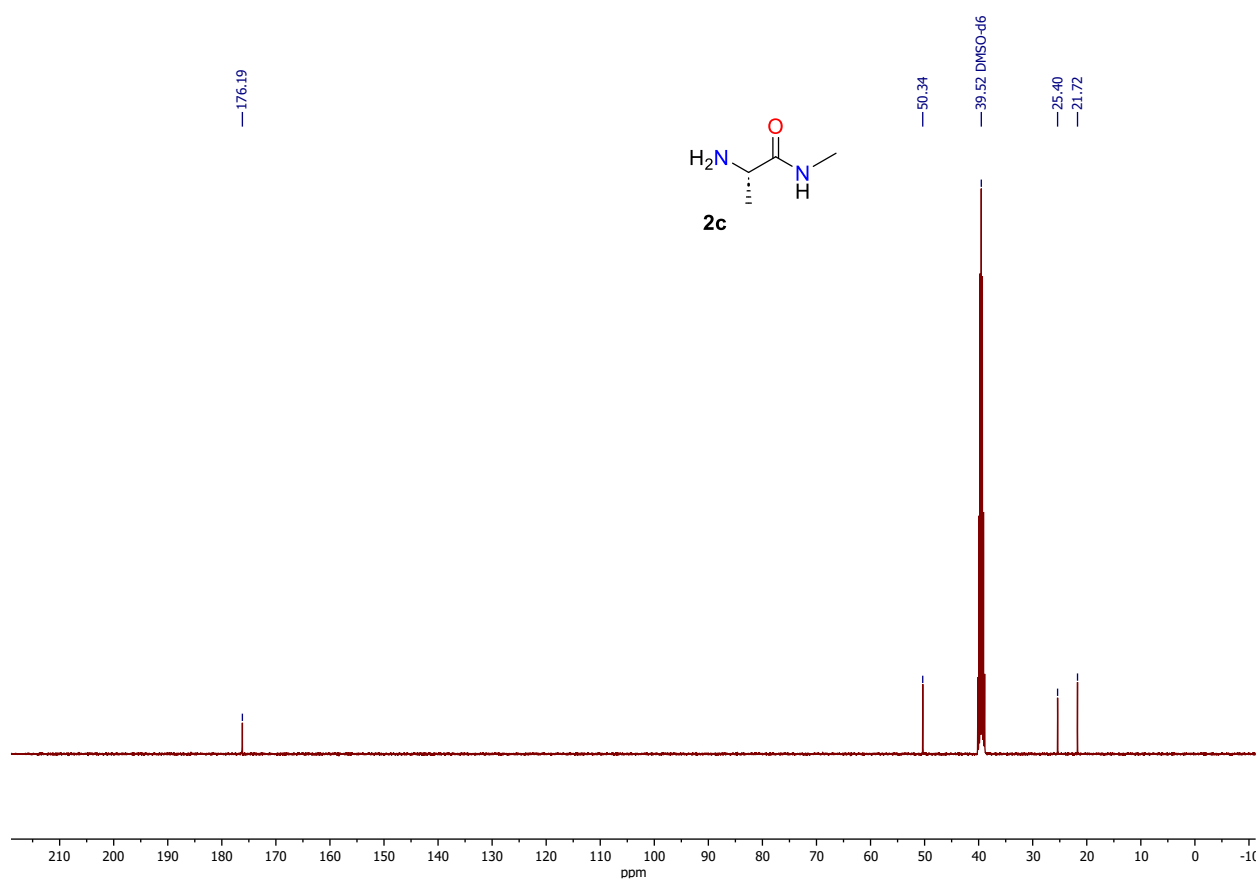


Fig. S114. ¹³C NMR spectrum of H-L-Ala-NMe (**2c**), DMSO-*d*₆, 101 MHz.

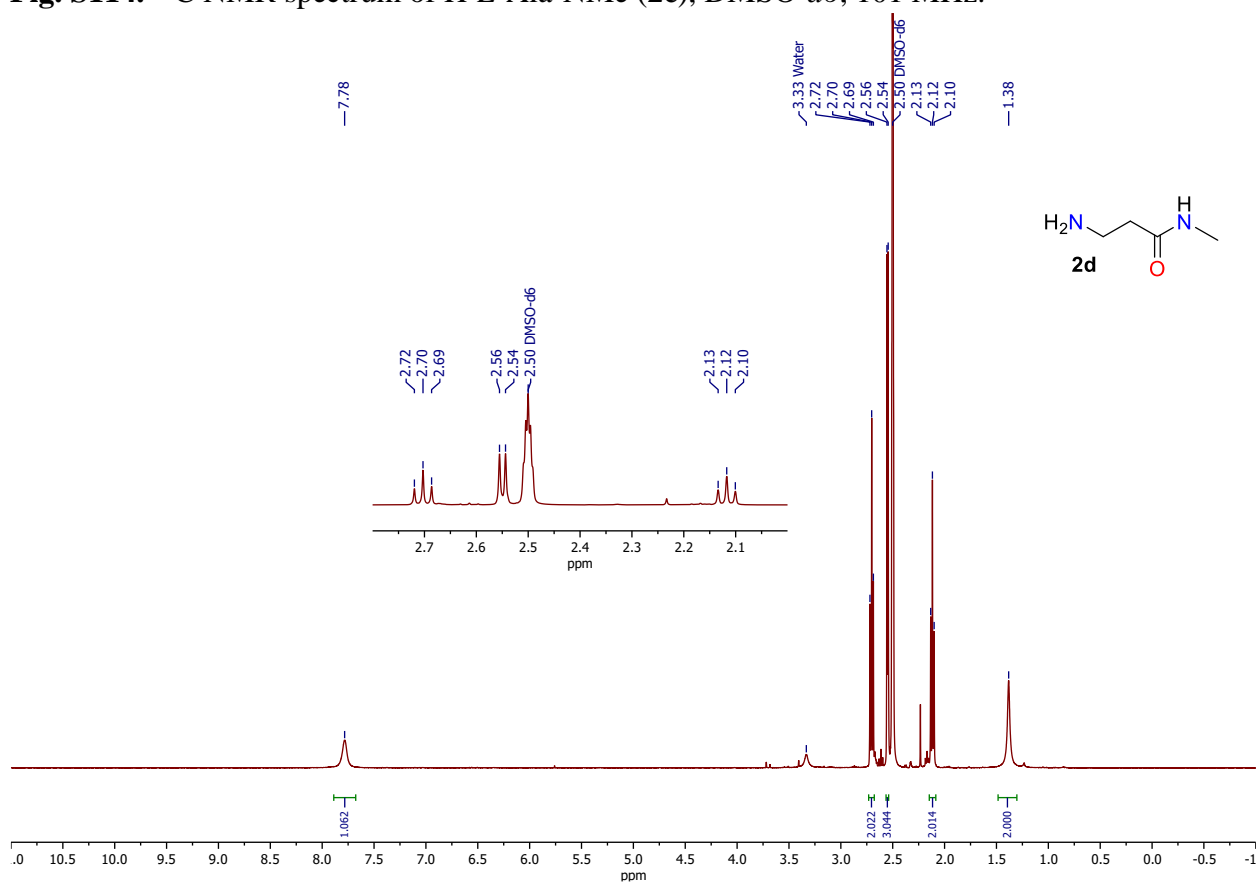


Fig. S115. ¹H NMR spectrum of H-β-Ala-NMe (**2d**), DMSO-*d*₆, 400 MHz.

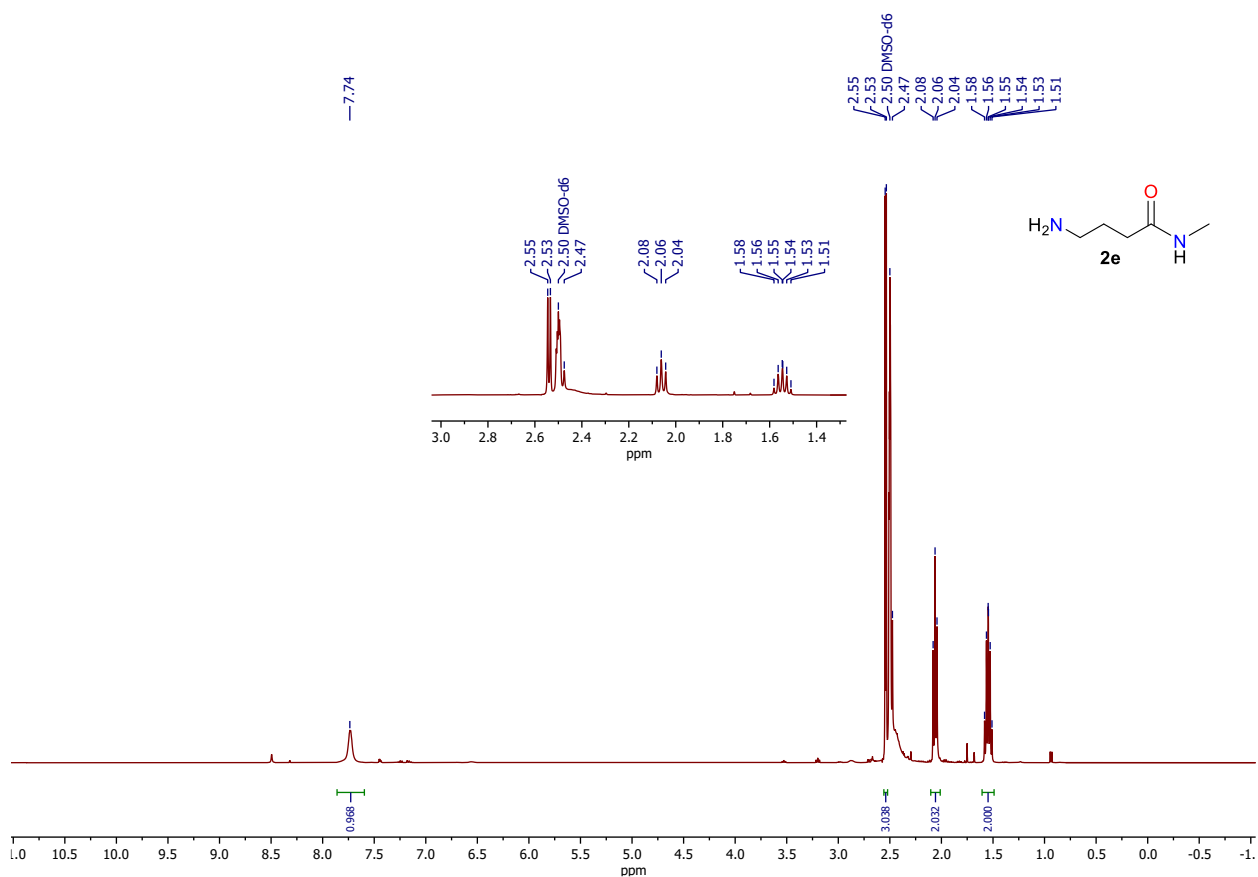


Fig. S116. ^1H NMR spectrum of H-GABA-NMe (2e), DMSO- d_6 , 400 MHz.

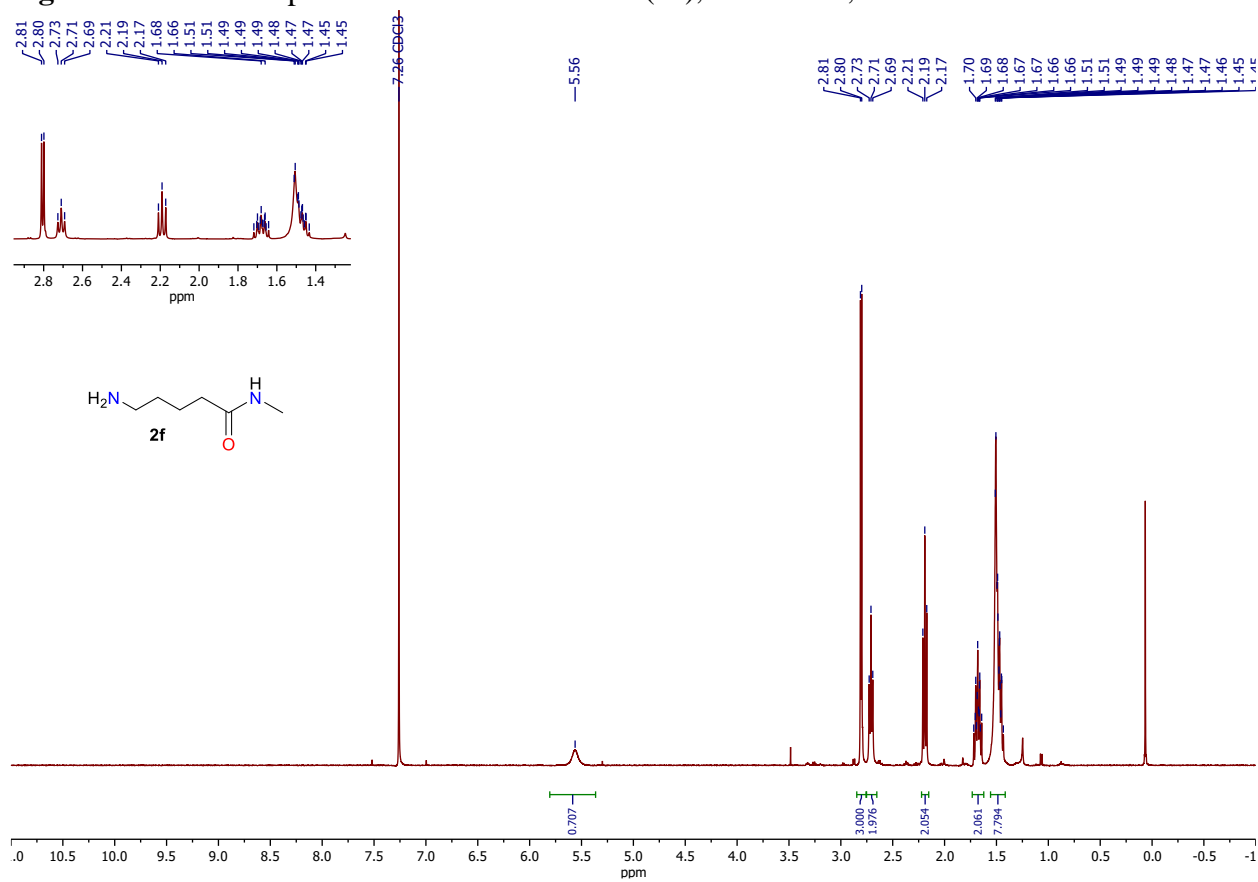


Fig. S117. ^1H NMR spectrum of H-Ava-NMe (2f), CDCl_3 , 400 MHz.

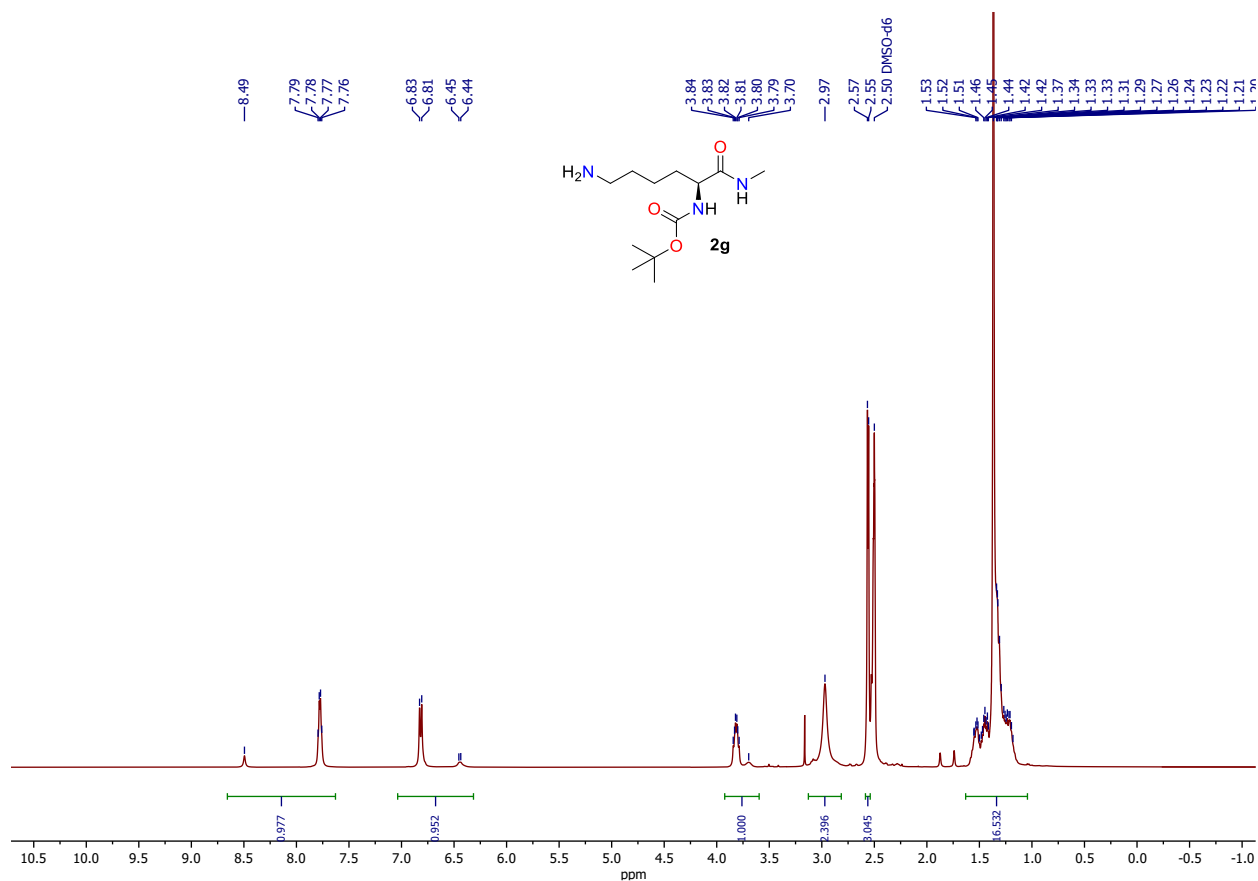


Fig. S118. ¹H NMR spectrum of N-Boc-Lys-NMe (**2g**), DMSO-*d*₆, 400 MHz.

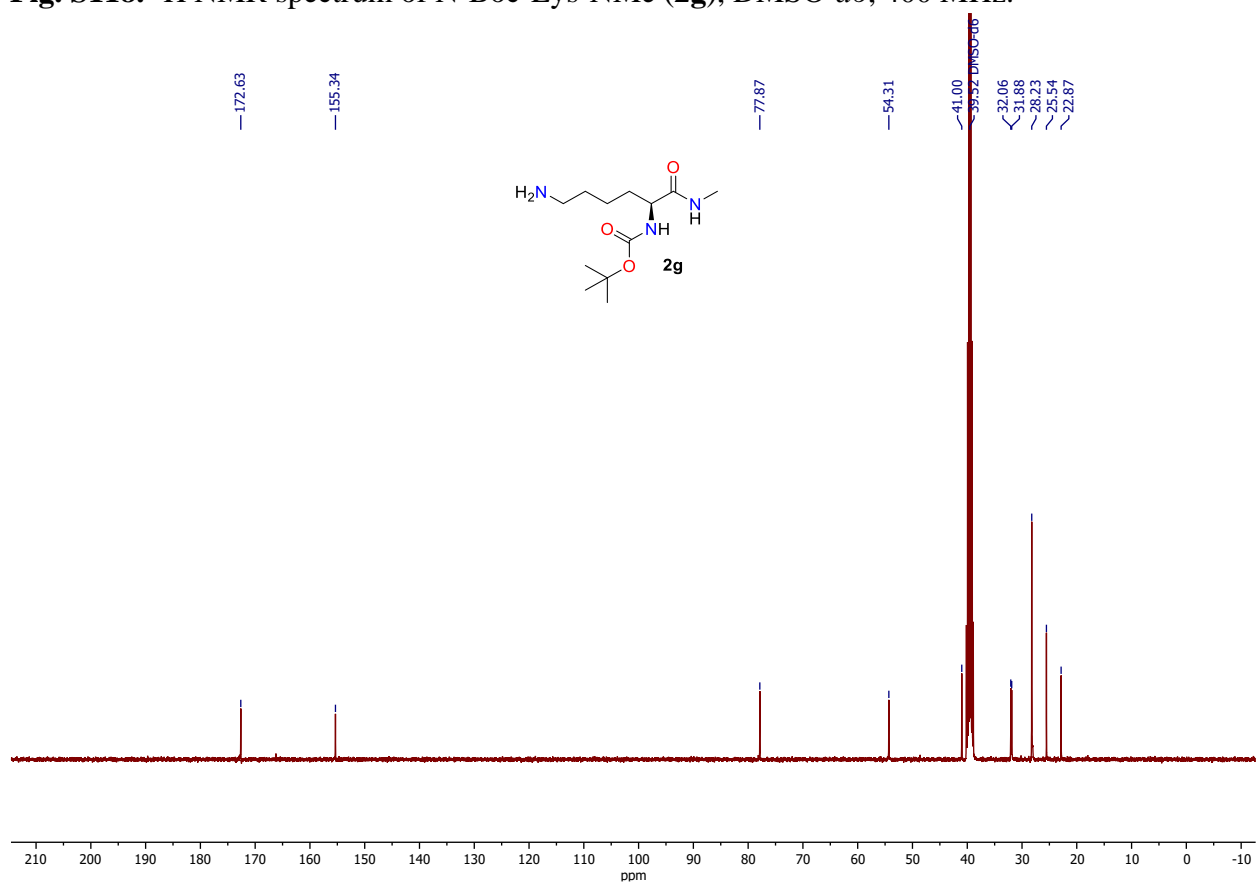


Fig. S119. ¹³C NMR spectrum of N-Boc-Lys-NMe (**2g**), DMSO-*d*₆, 101 MHz.

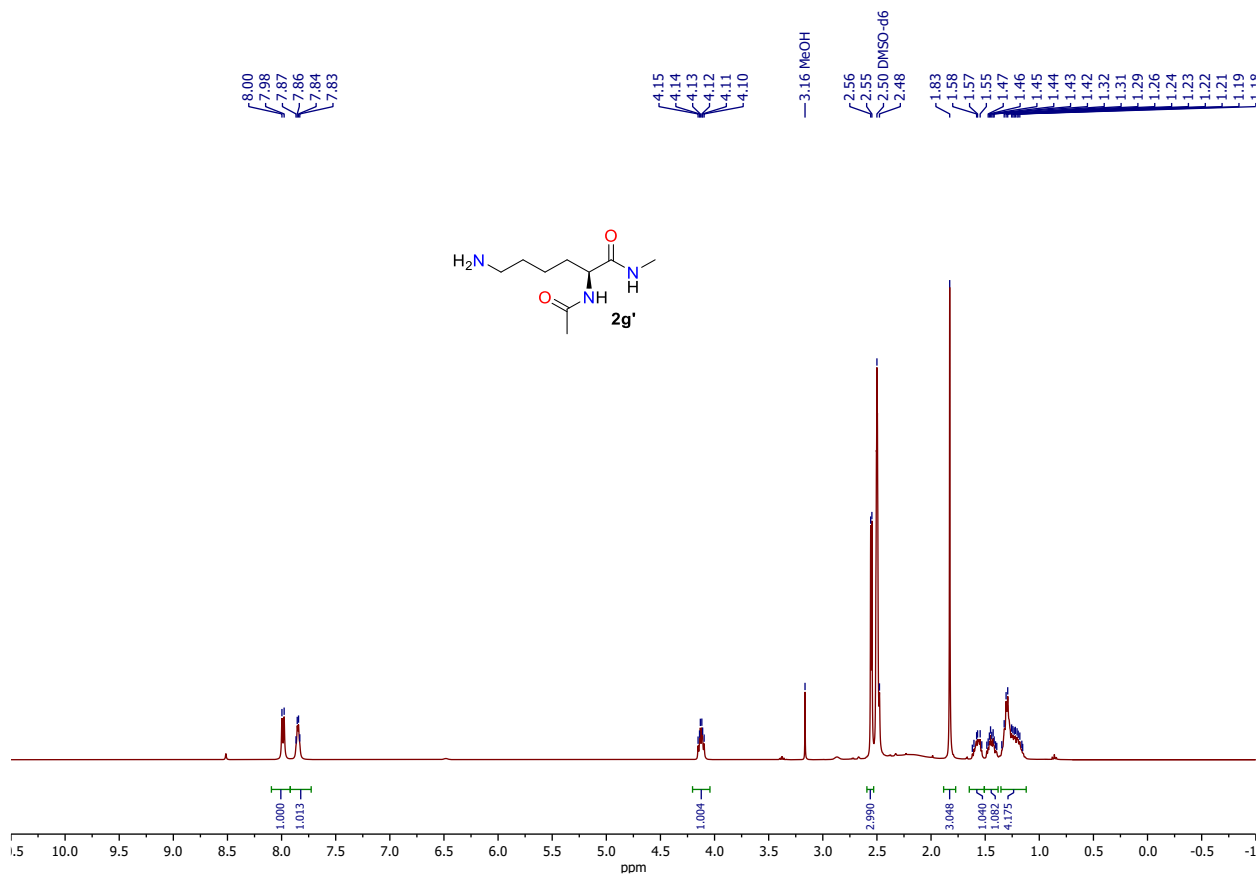


Fig. S120. ¹H NMR spectrum of N-Ac-Lys-NMe (**2g'**), DMSO-*d*₆, 400 MHz.

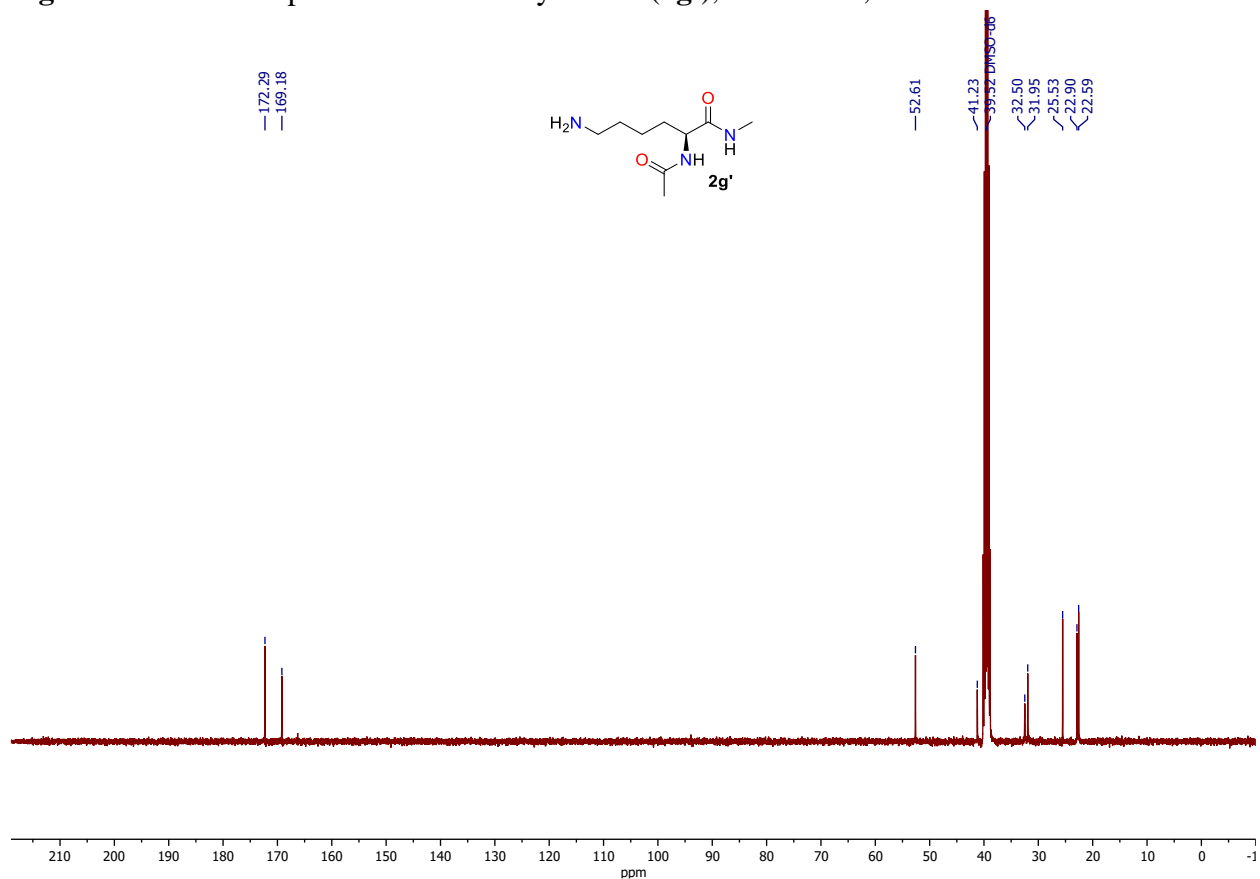


Fig. S121. ¹³C NMR spectrum of N-Ac-Lys-NMe (**2g'**), DMSO-*d*₆, 101 MHz.

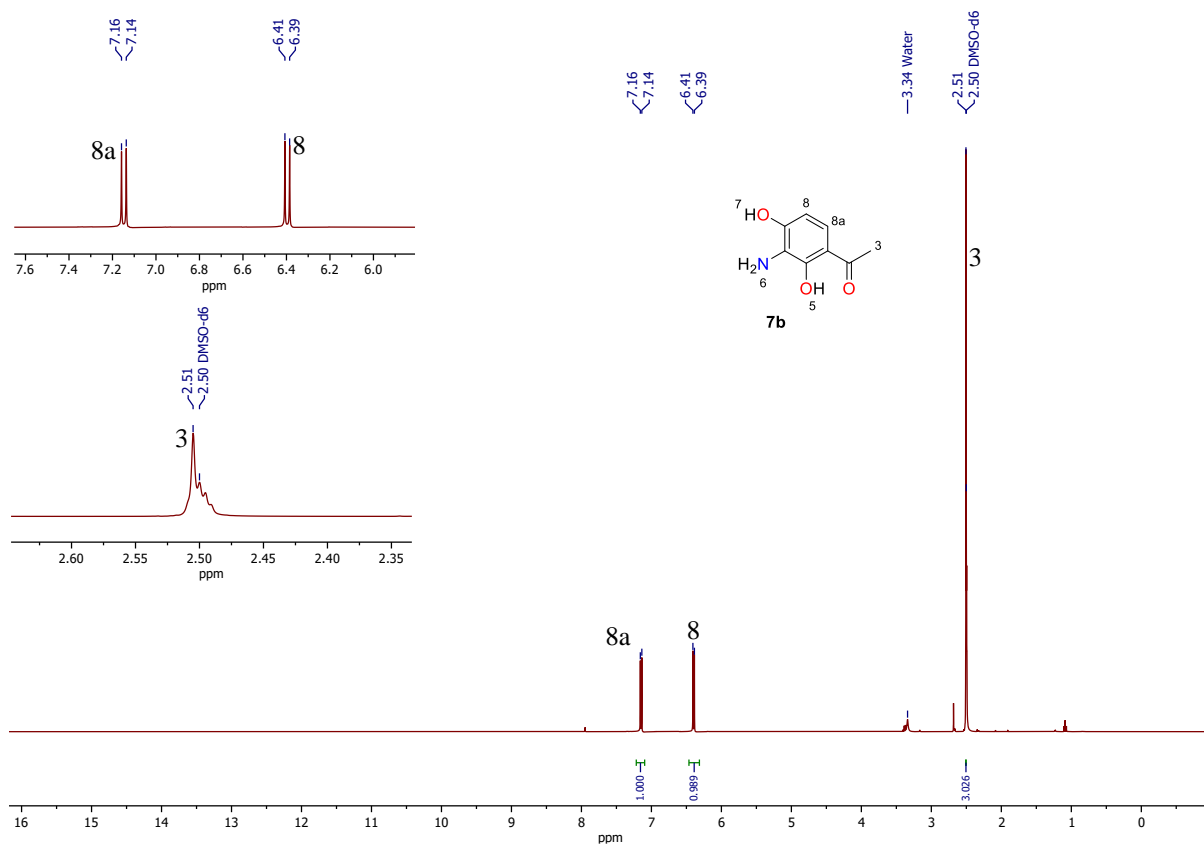


Fig. S124. ¹H NMR spectrum of **7b**, DMSO-*d*₆, 400 MHz.

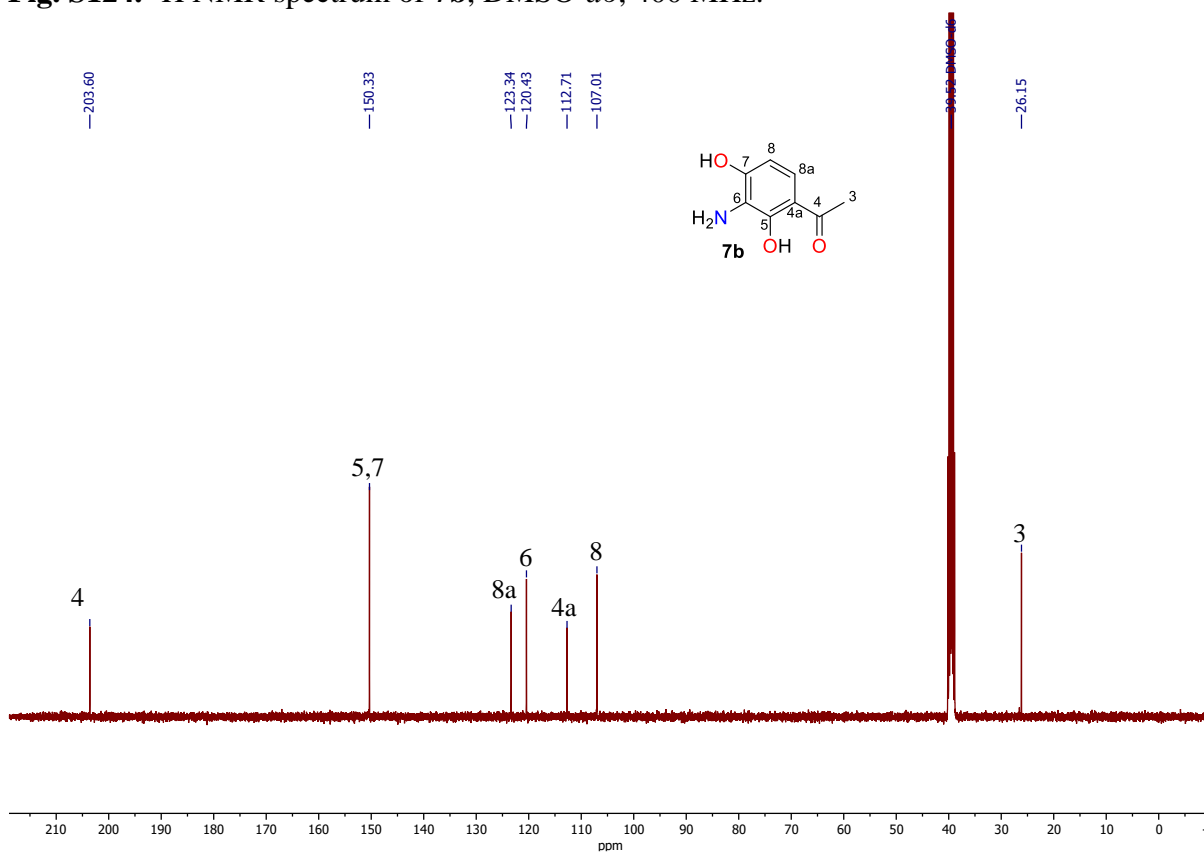


Fig. S125. ¹³C NMR spectrum of **7b**, DMSO-*d*₆, 101 MHz.

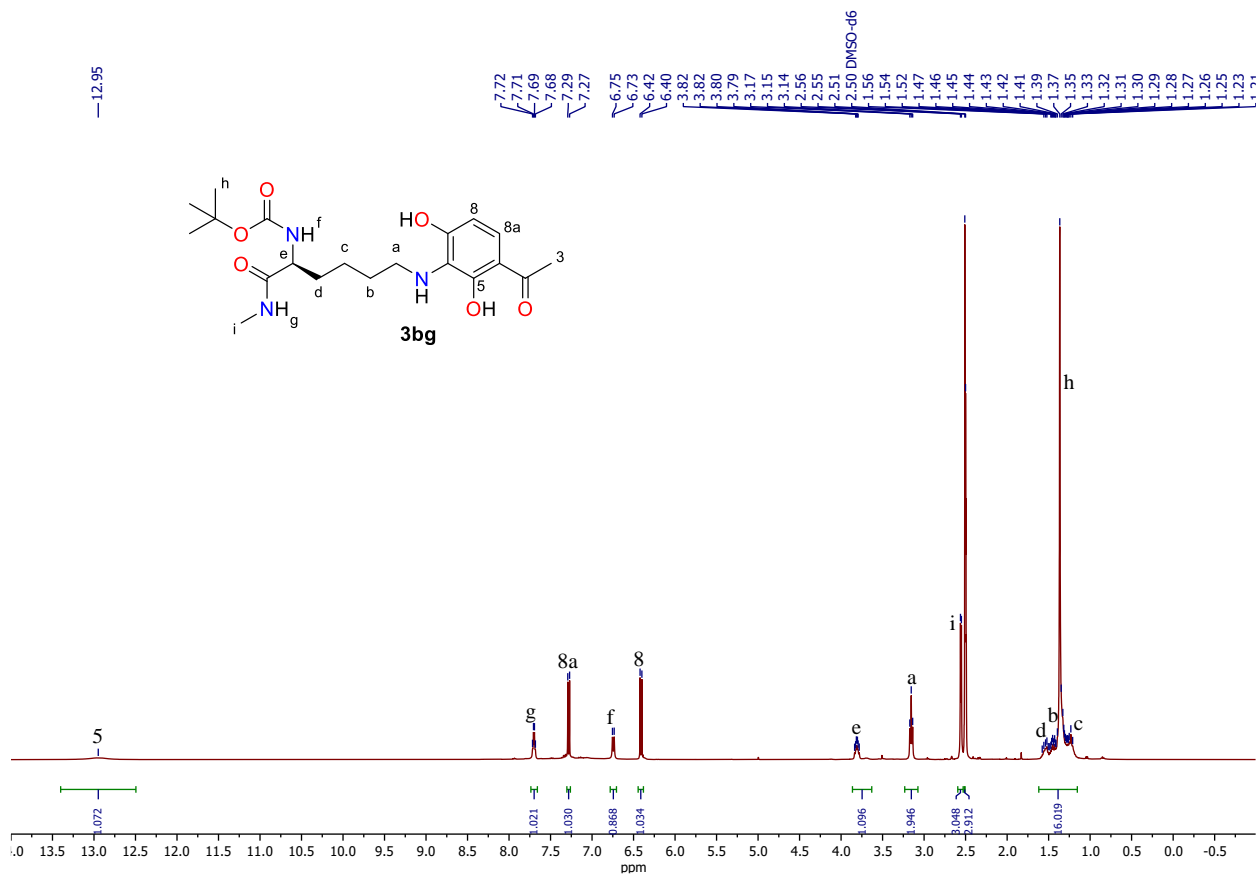


Fig. S126. ^1H NMR spectrum of **3bg**, DMSO- d_6 , 400 MHz.

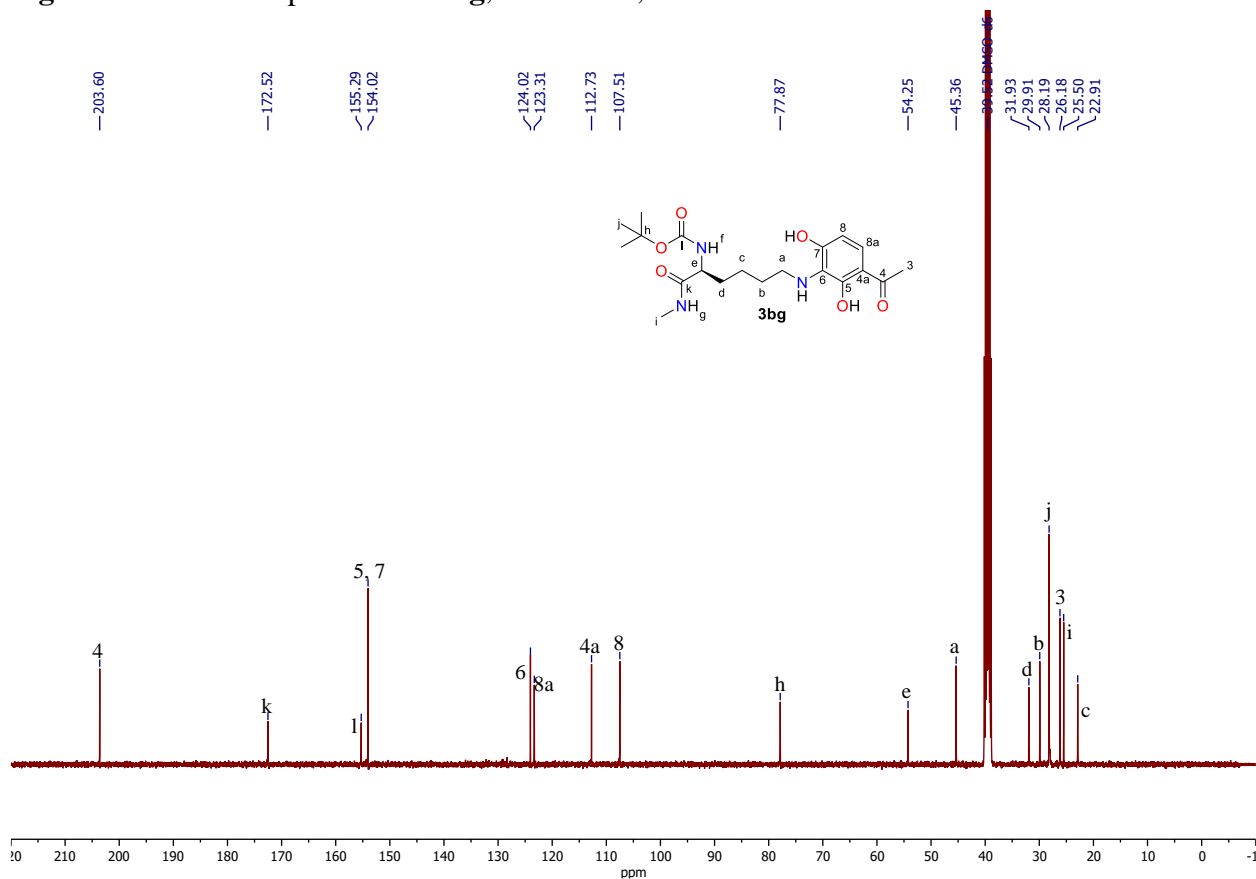


Fig. S127. ^{13}C NMR spectrum of **3bg**, DMSO- d_6 , 101 MHz.

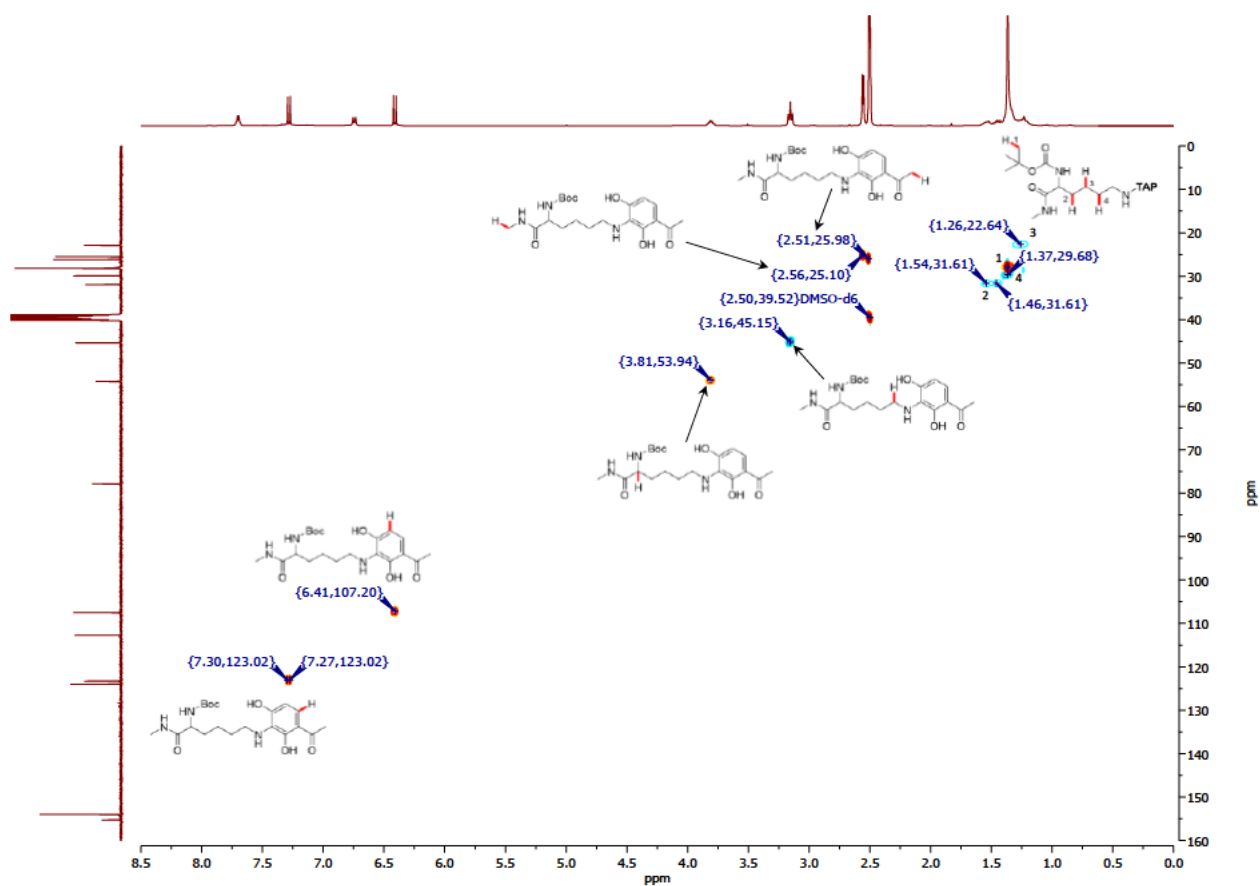


Fig. S128. ^1H - ^{13}C HSQC spectra of the obtained **3bg**, DMSO-*d*₆, 400 MHz.

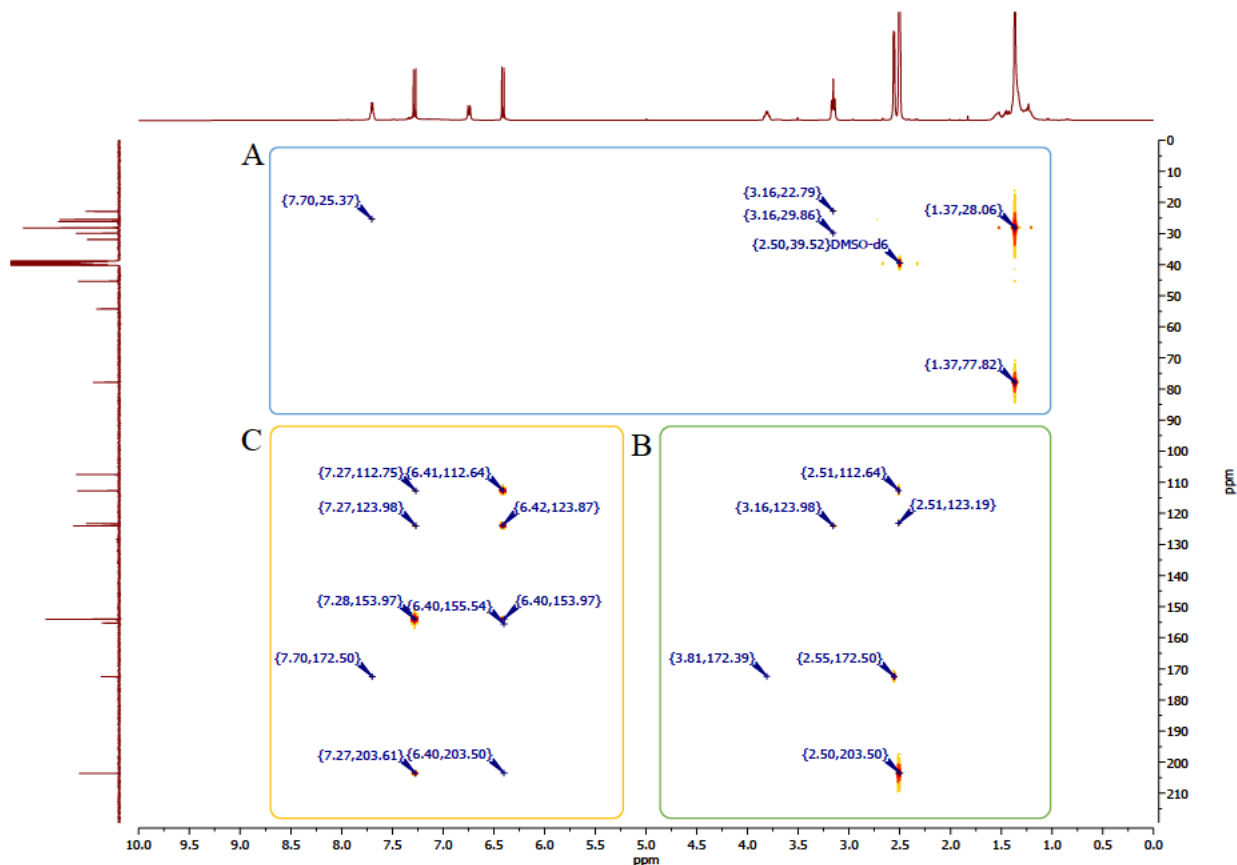


Fig. S129a. ^1H - ^{13}C HMBC spectra of the obtained **3bg**, DMSO-*d*₆, 400 MHz.

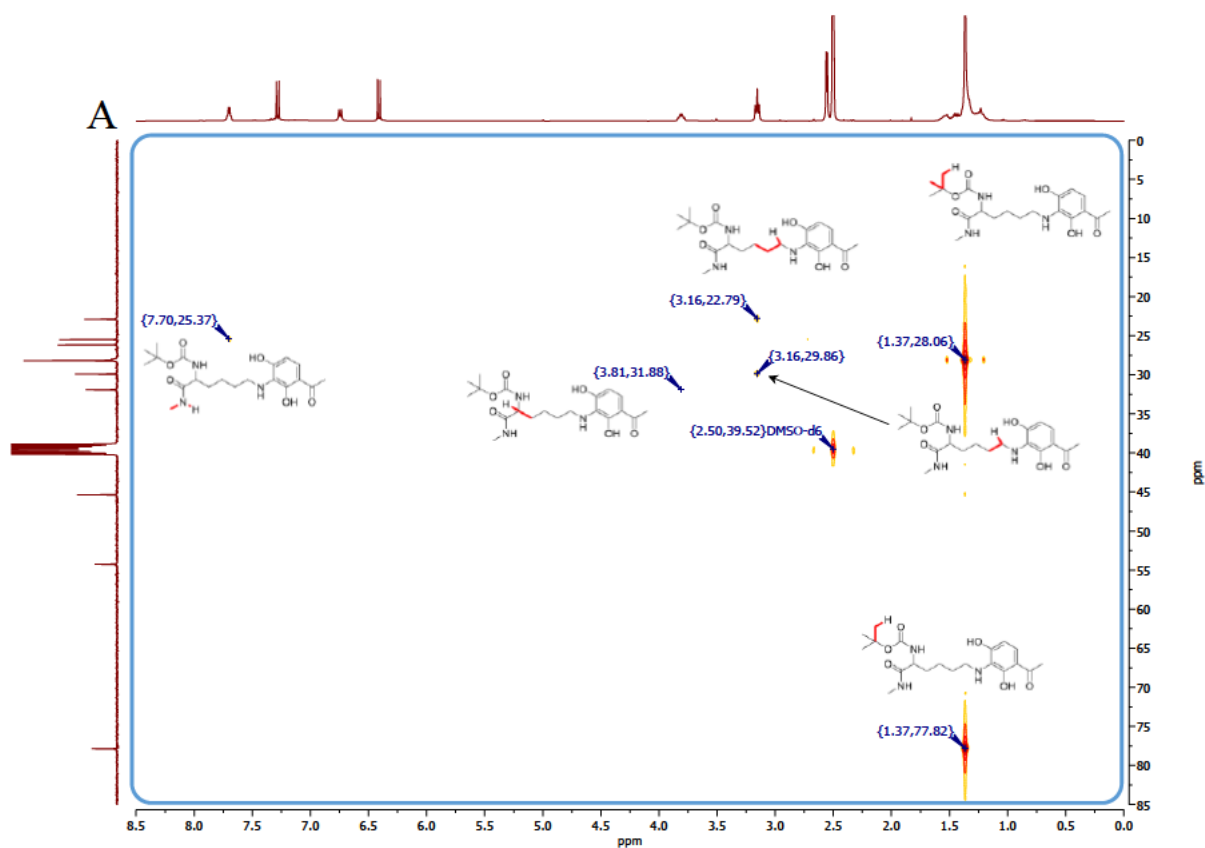


Fig. S129b. ^1H - ^{13}C HMBC spectra of the obtained **3bg**, DMSO- d_6 , 400 MHz.

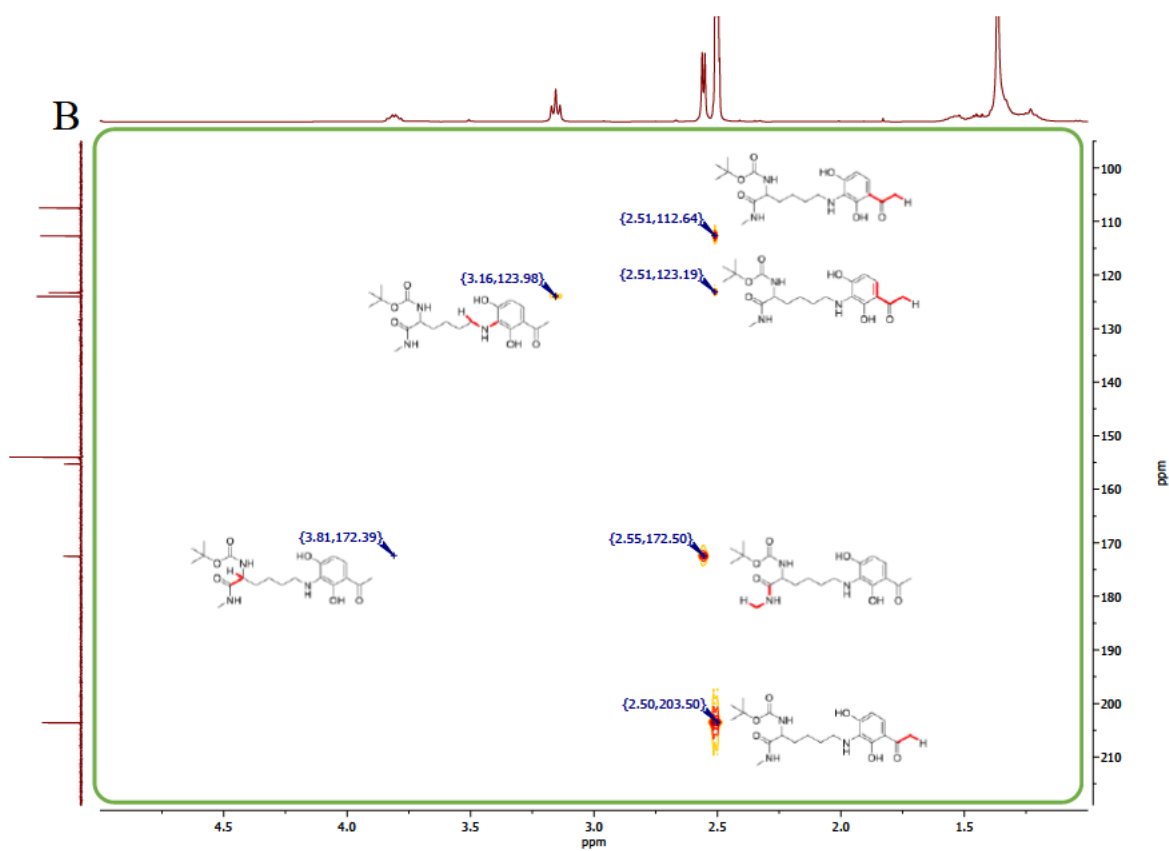


Fig. S129c. ^1H - ^{13}C HMBC spectra of the obtained **3bg**, DMSO- d_6 , 400 MHz.

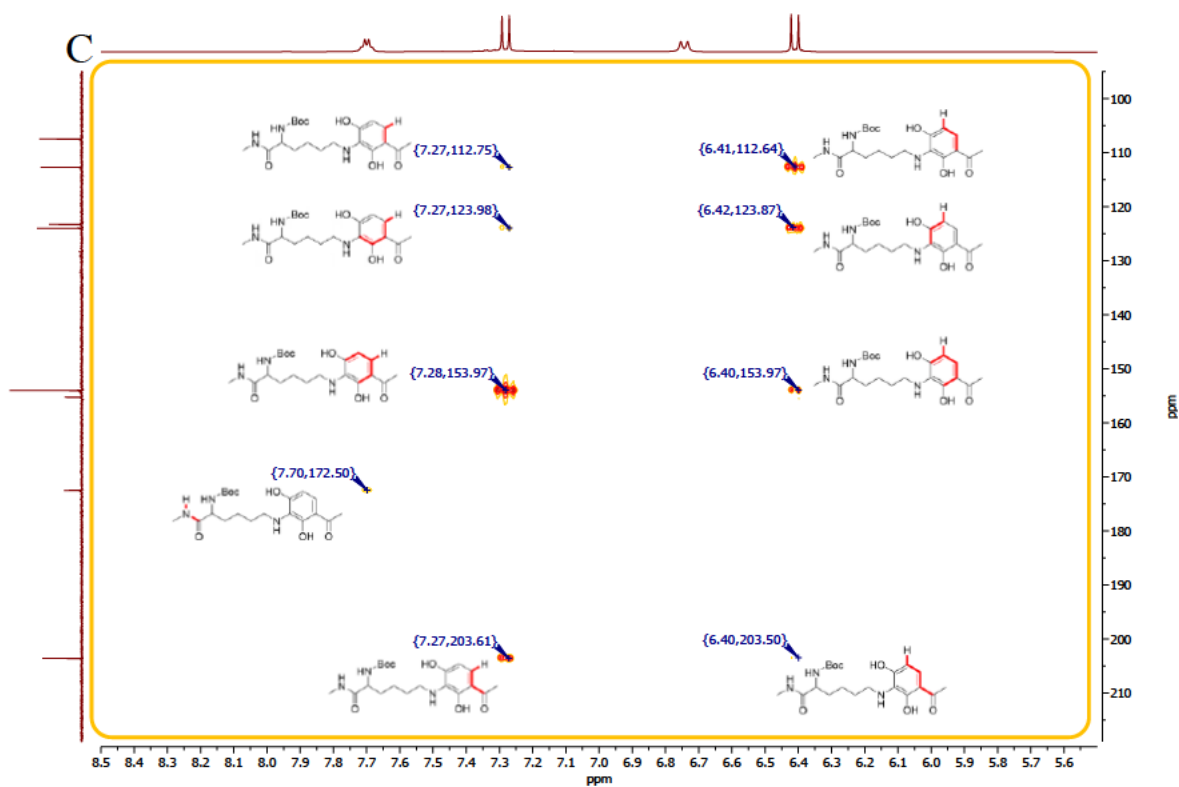


Fig. S129d. ^1H - ^{13}C HMBC spectra of the obtained **3bg**, DMSO-*d*₆, 400 MHz.

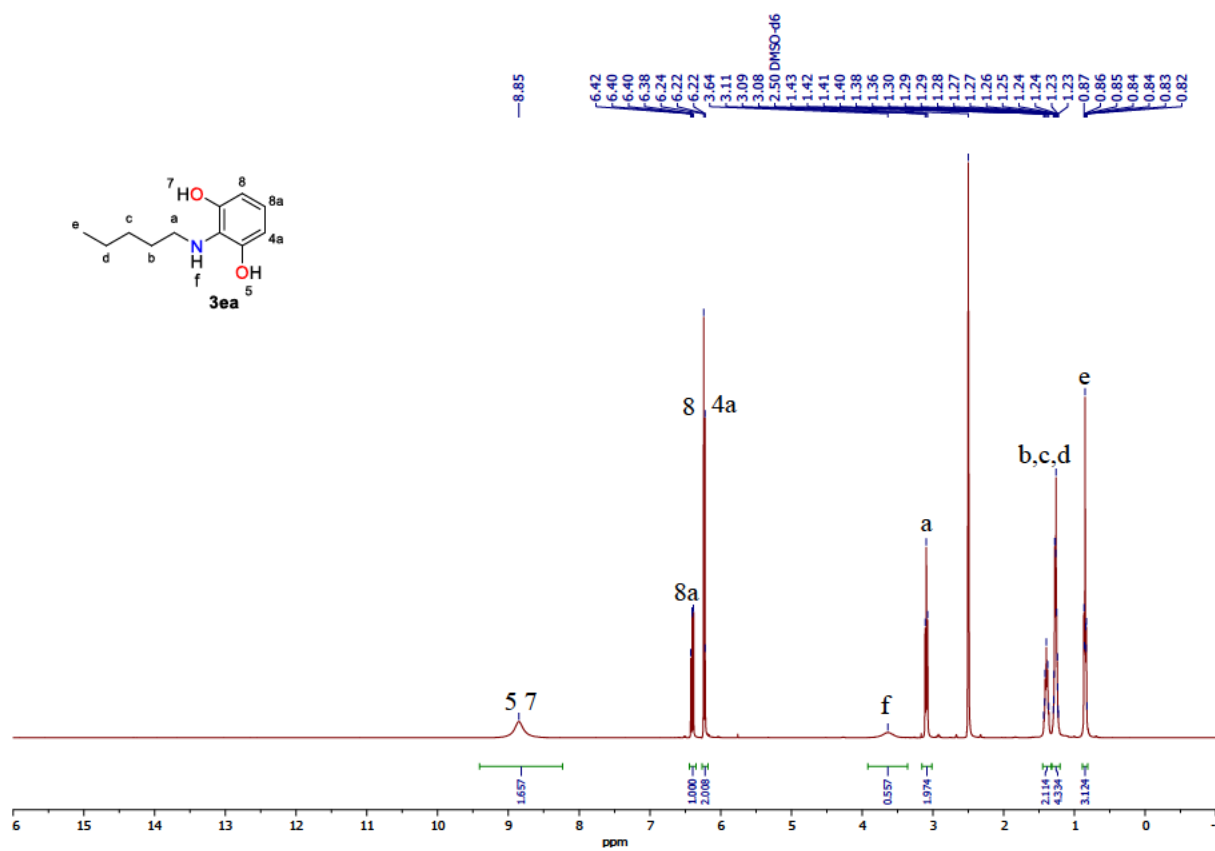


Fig. S130. ^1H NMR spectrum of **3ea**, DMSO-*d*₆, 400 MHz.

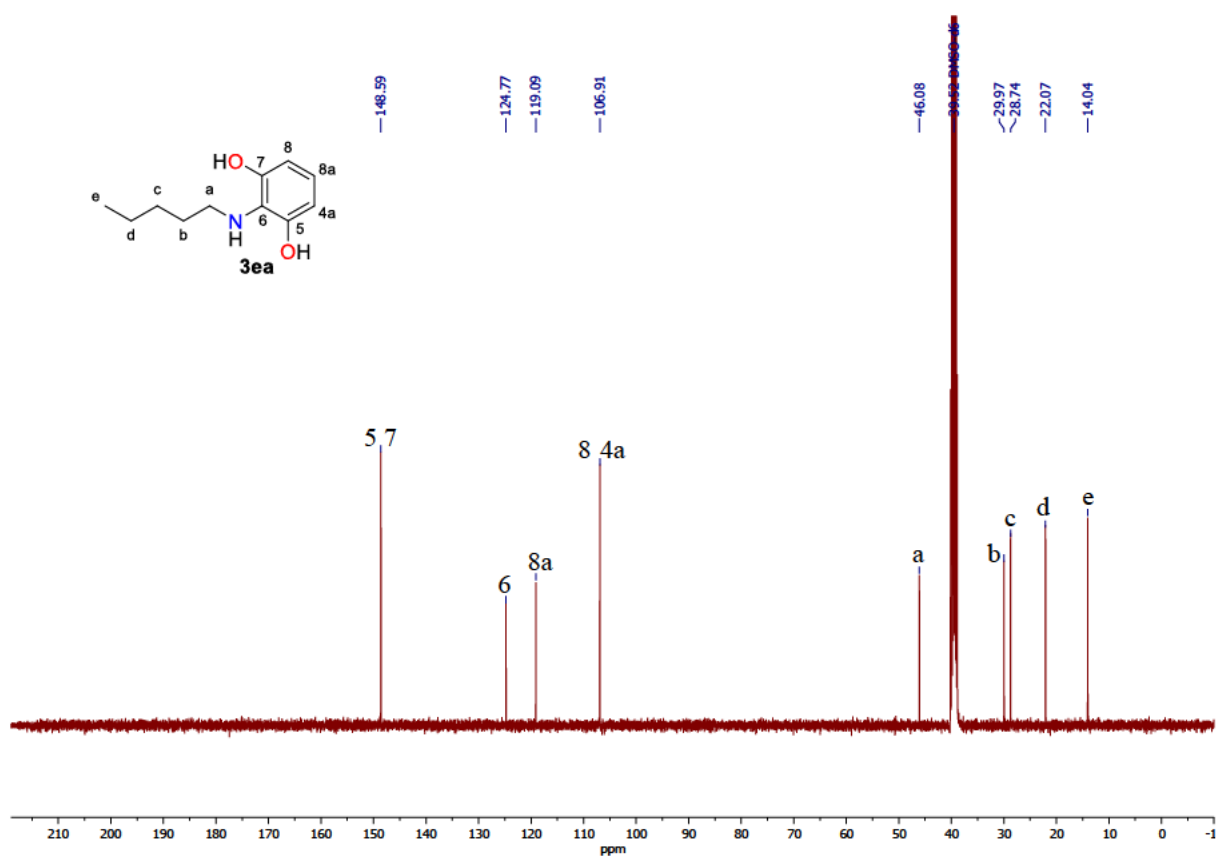


Fig. S131. ^{13}C NMR spectrum of **3ea**, DMSO- d_6 , 101 MHz.

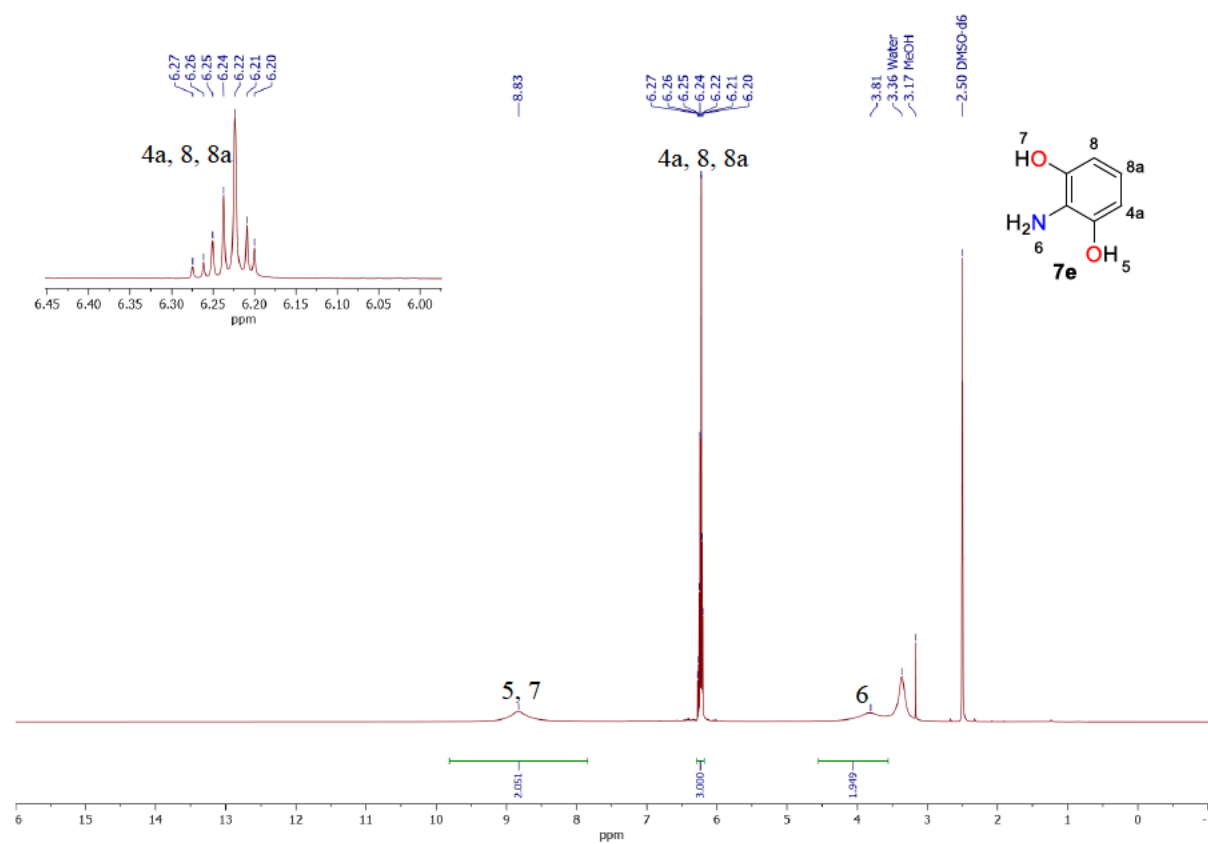


Fig. S132. ^1H NMR spectrum of **7e**, DMSO- d_6 , 400 MHz.

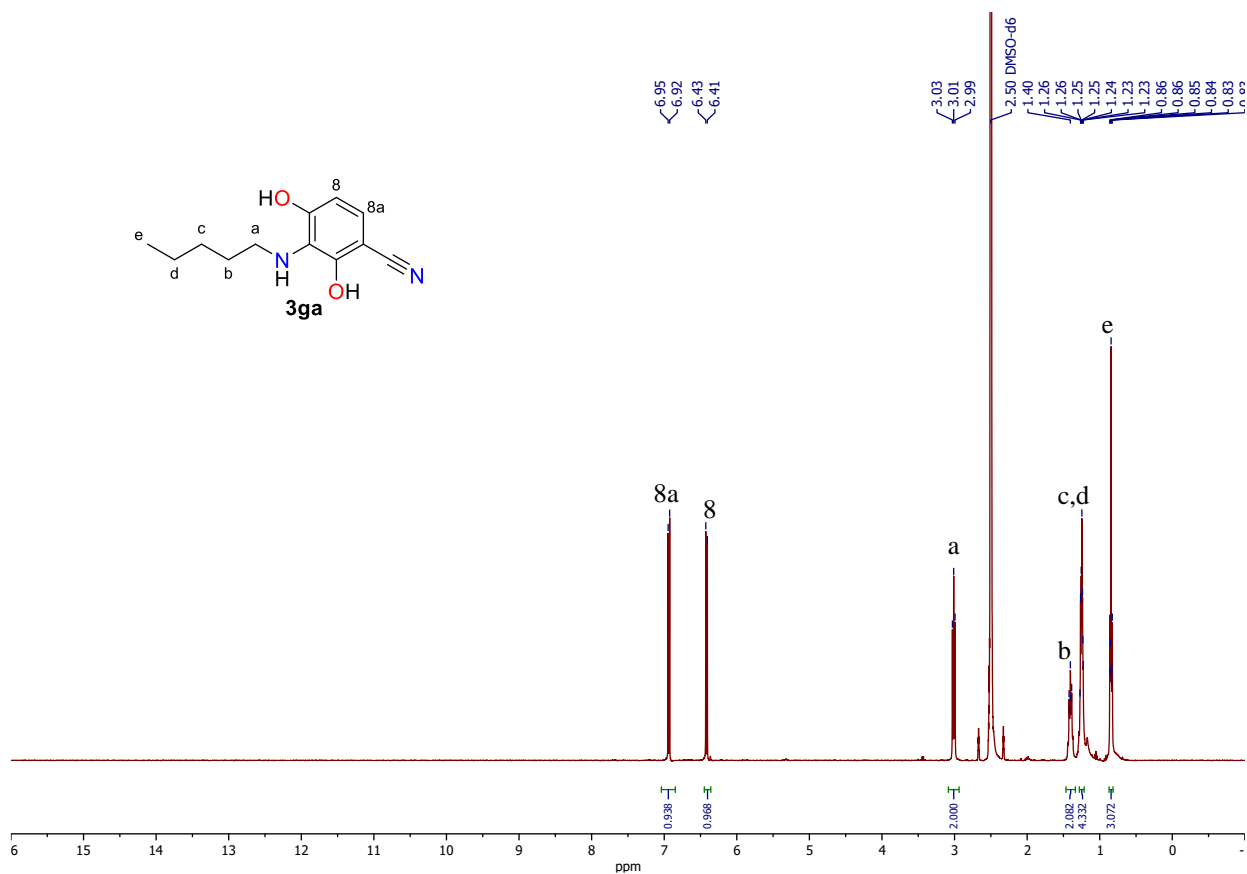


Fig. S133. ¹H NMR spectrum of **3ga**, DMSO-*d*₆, 400 MHz.

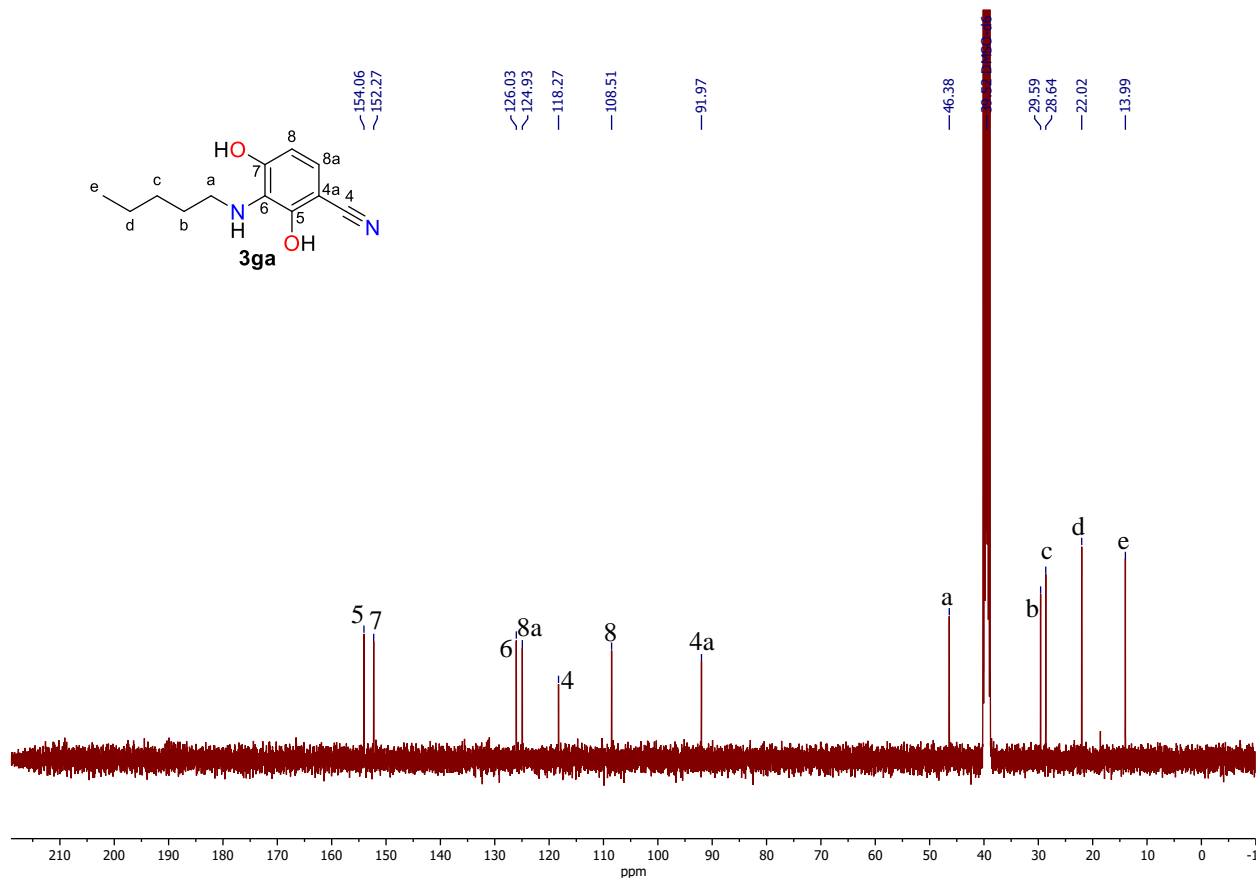


Fig. S134. ¹³C NMR spectrum of **3ga**, DMSO-*d*₆, 101 MHz.

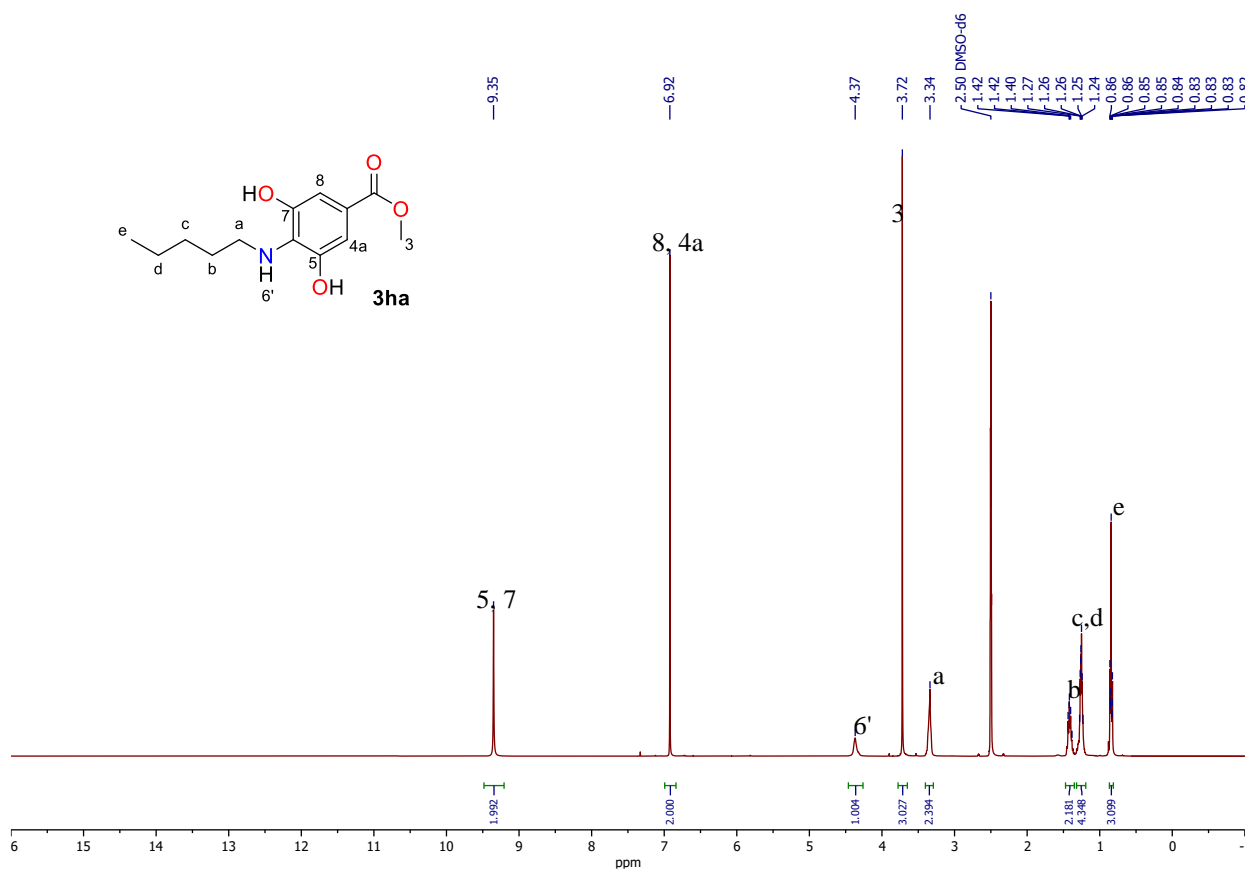


Fig. S135. ¹H NMR spectrum of **3ha**, DMSO-*d*₆, 400 MHz.

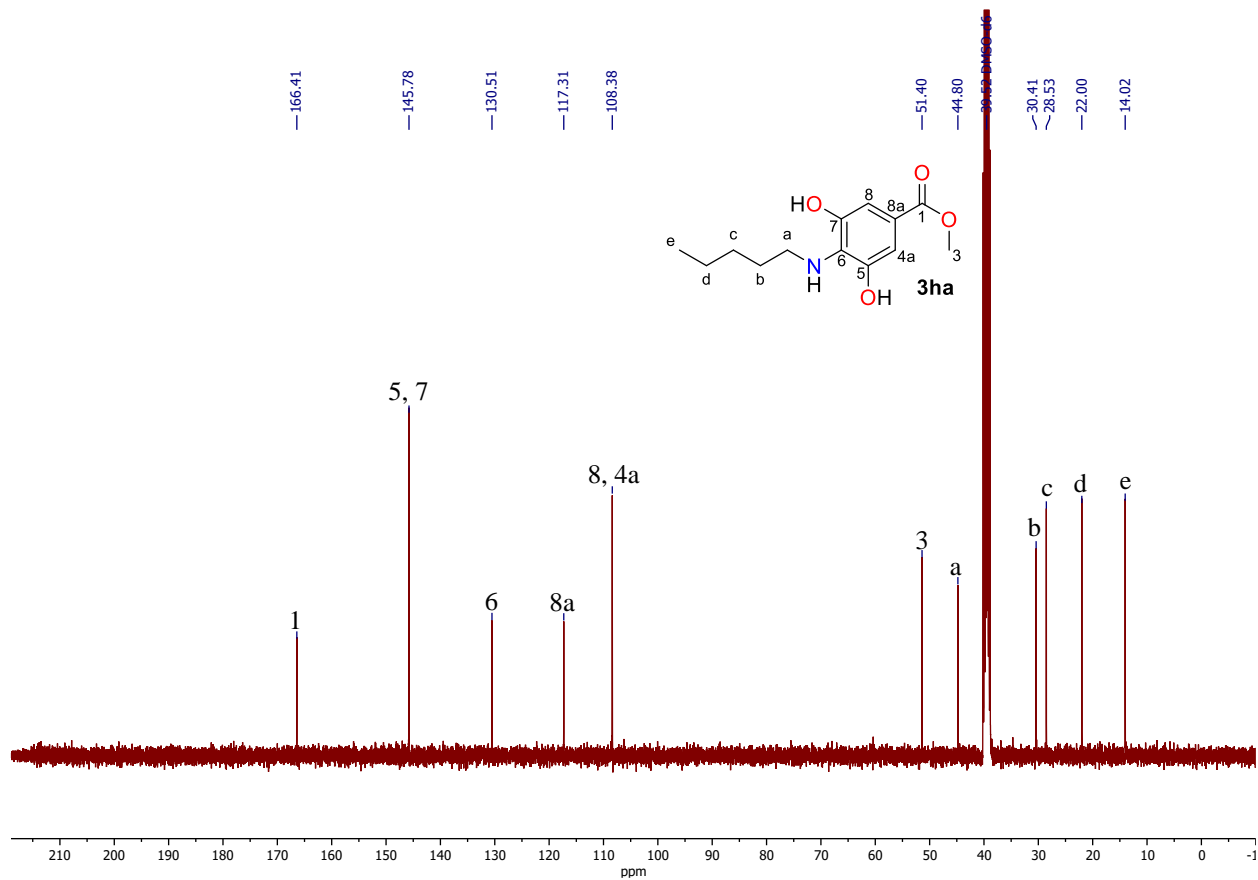


Fig. S136. ¹³C NMR spectrum of **3ha**, DMSO-*d*₆, 101 MHz.

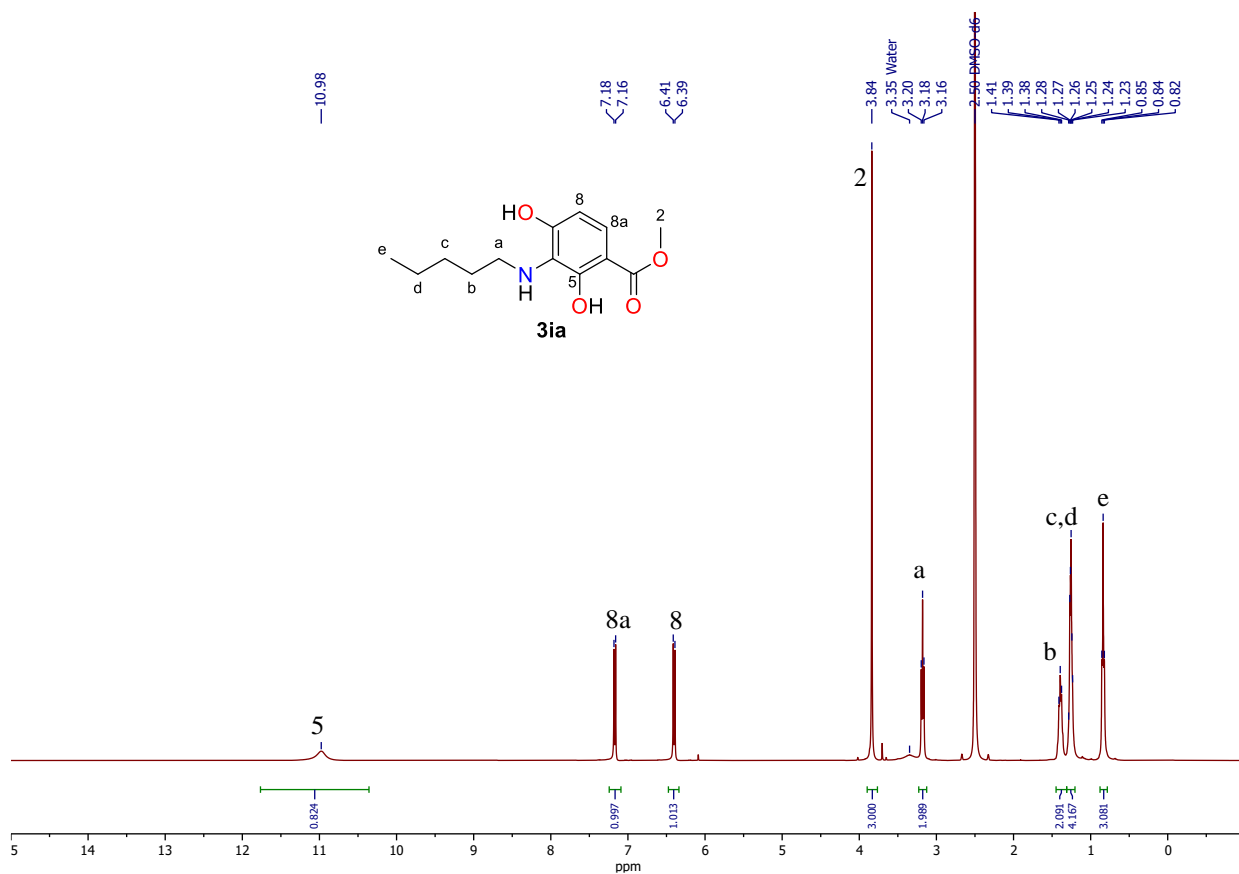


Fig. S137. ¹H NMR spectrum of **3ia**, DMSO-*d*₆, 400 MHz.

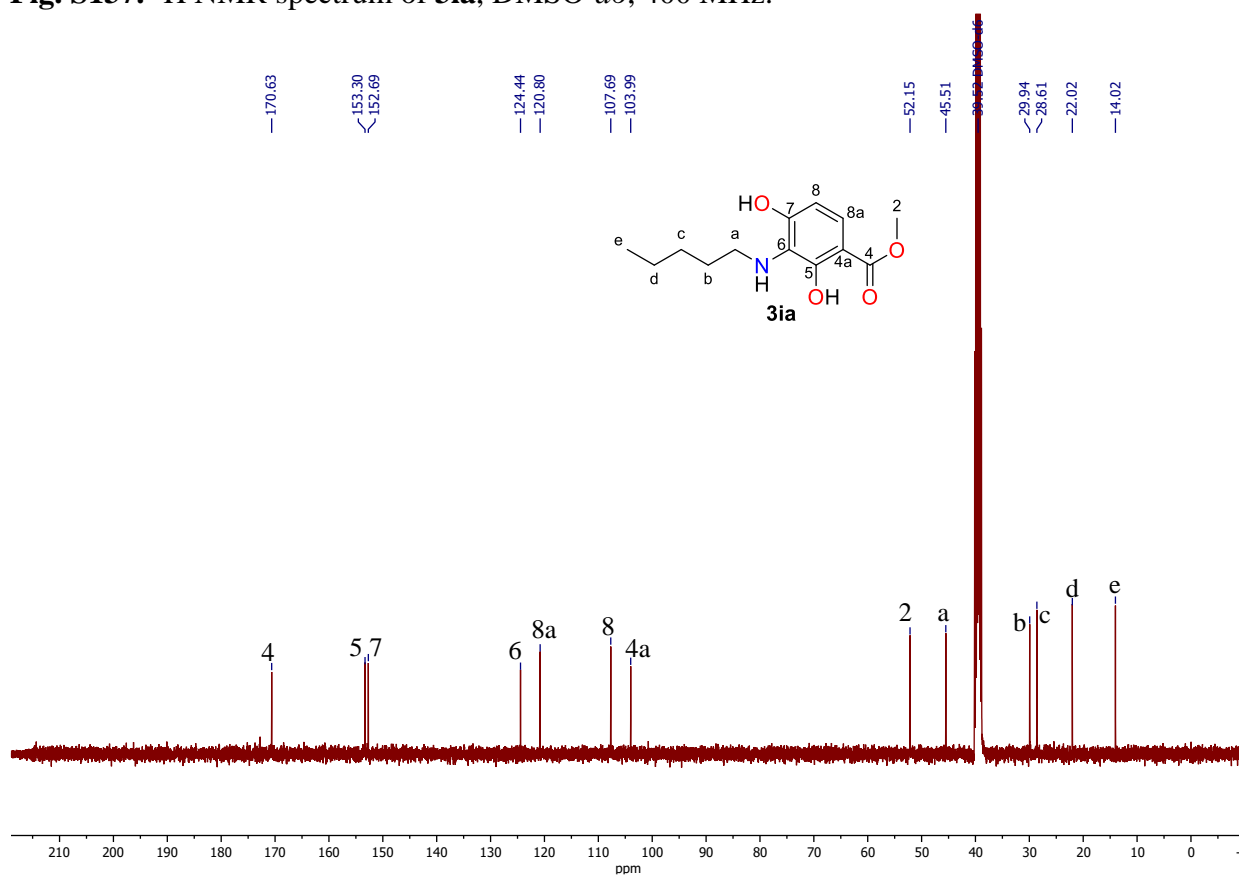


Fig. S138. ¹³C NMR spectrum of **3ia**, DMSO-*d*₆, 101 MHz.

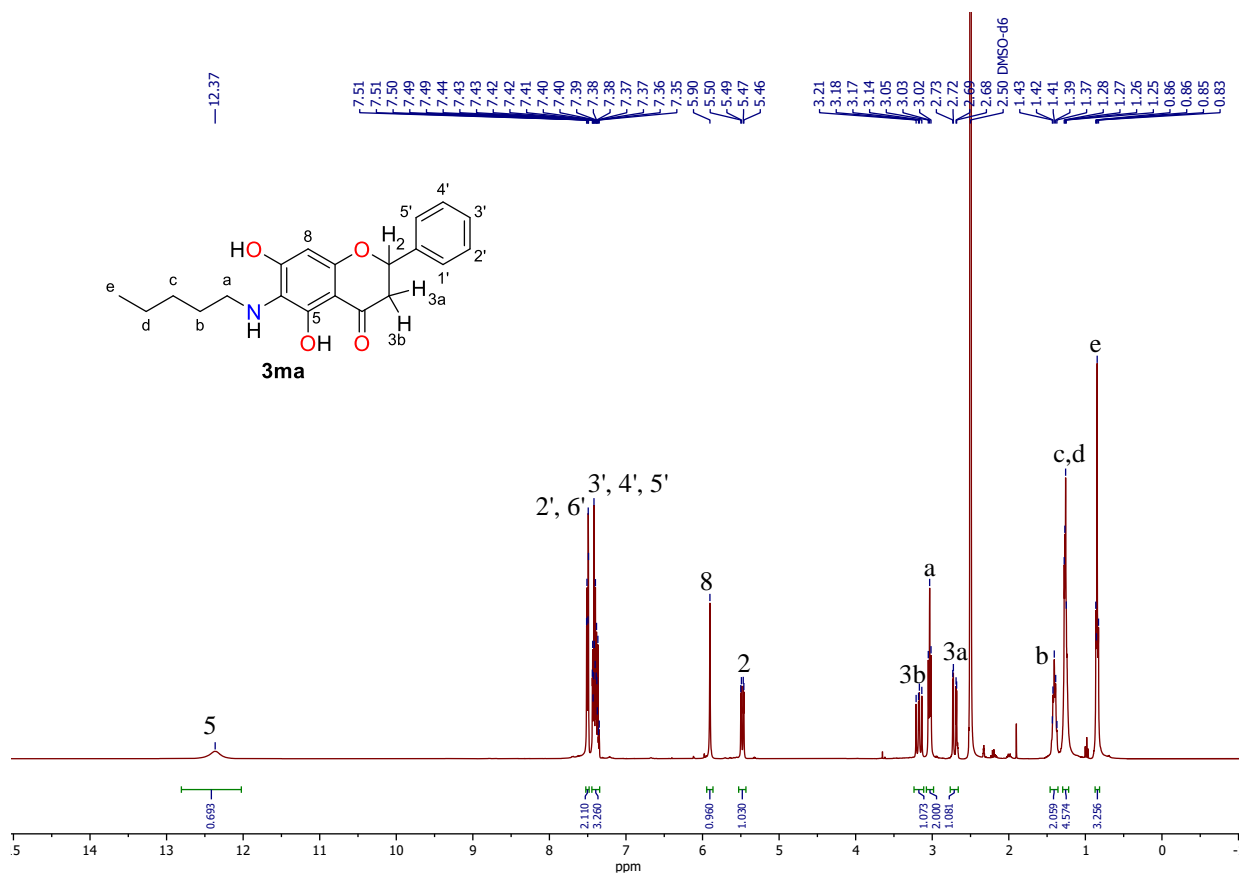


Fig. S139. ¹H NMR spectrum of **3ma**, DMSO-*d*₆, 400 MHz.

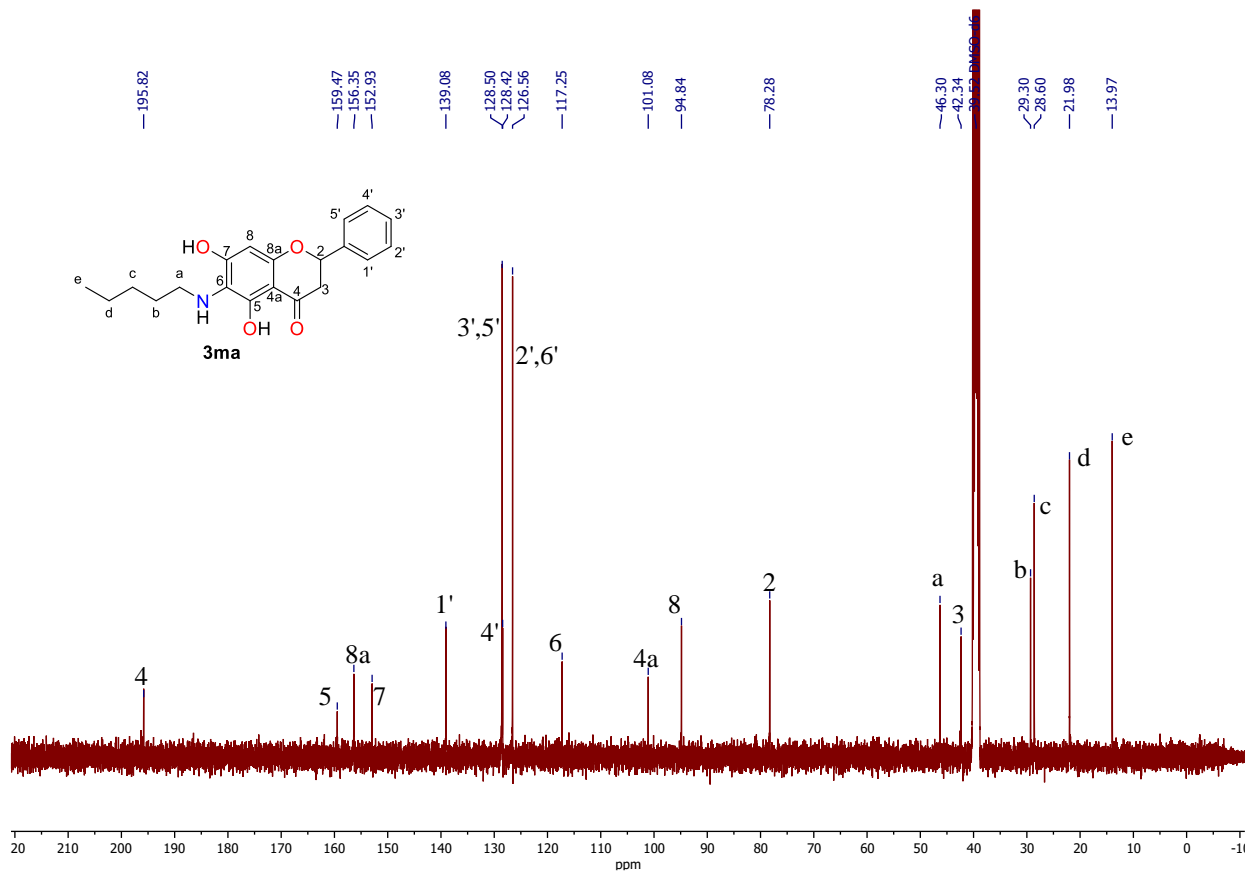


Fig. S140. ¹³C NMR spectrum of **3ma**, DMSO-*d*₆, 101 MHz.

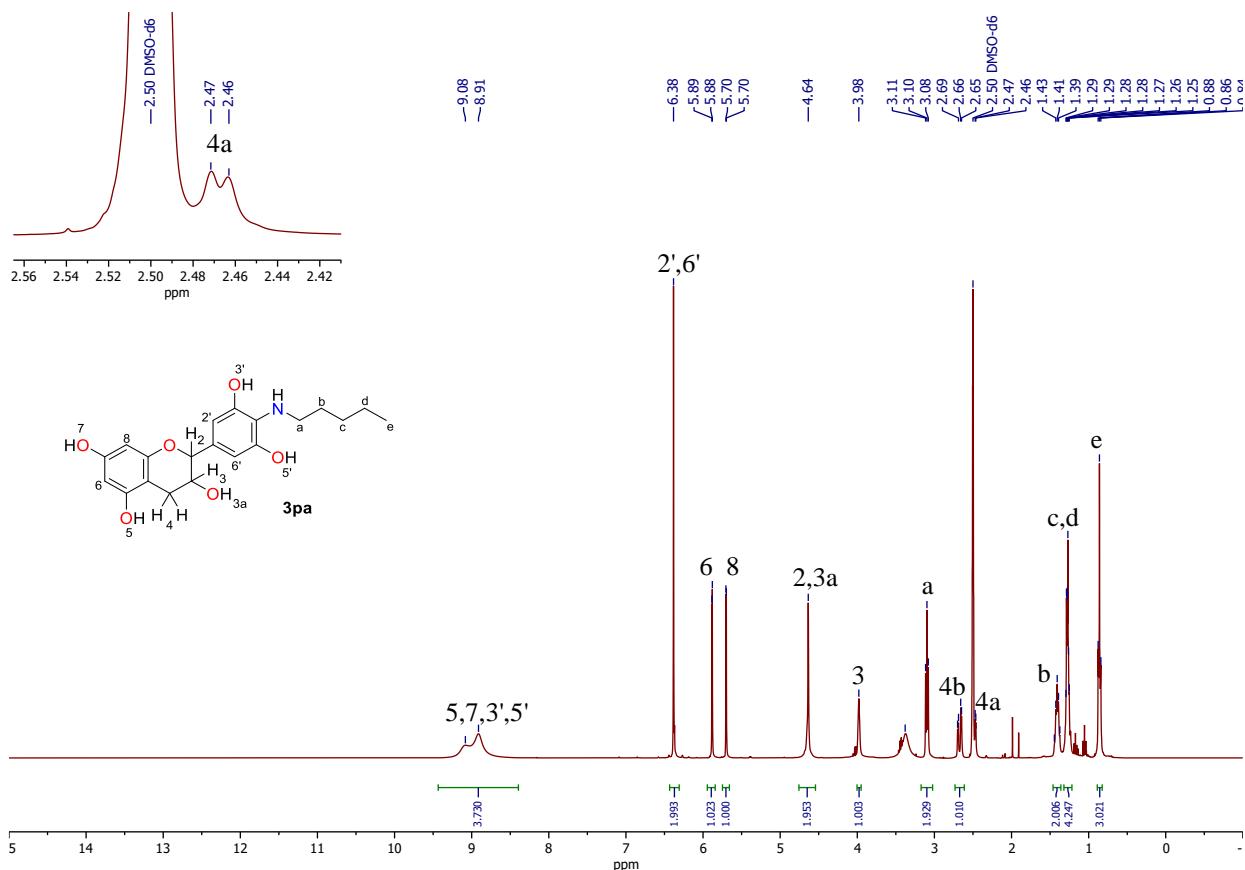


Fig. S141. ¹H NMR spectrum of **3pa**, DMSO-*d*₆, 400 MHz.

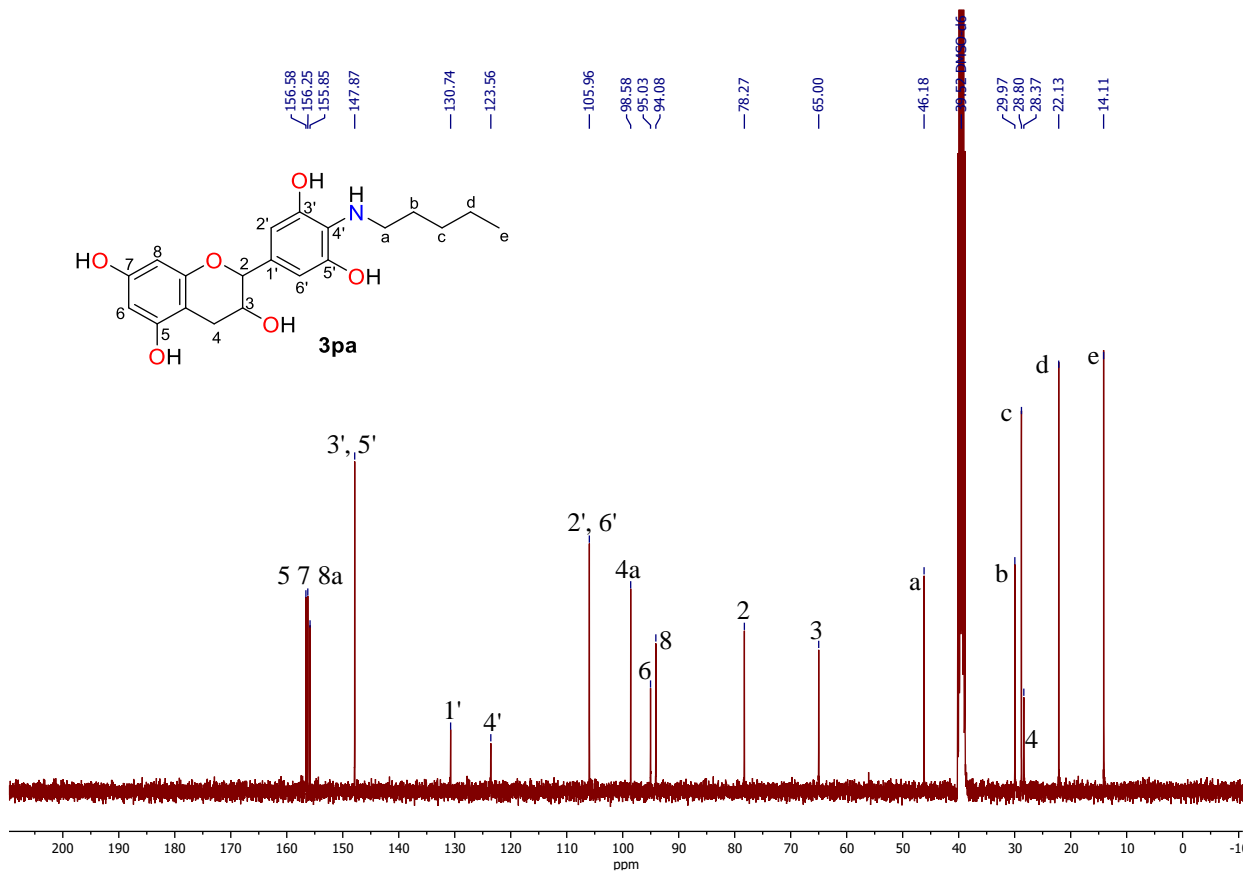


Fig. S142. ¹³C NMR spectrum of **3pa**, DMSO-*d*₆, 101 MHz.

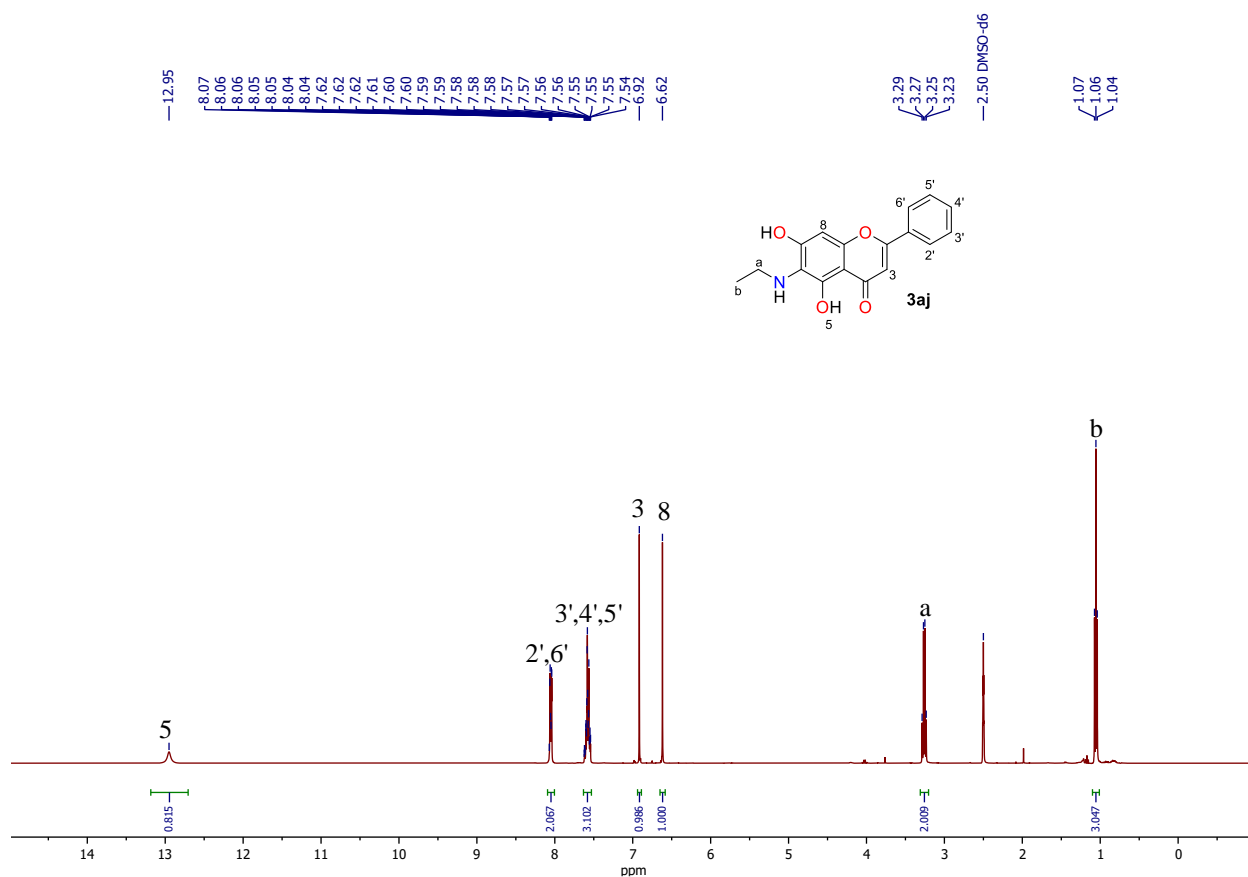


Fig. S143. ¹H NMR spectrum of **3aj**, DMSO-*d*₆, 400 MHz.

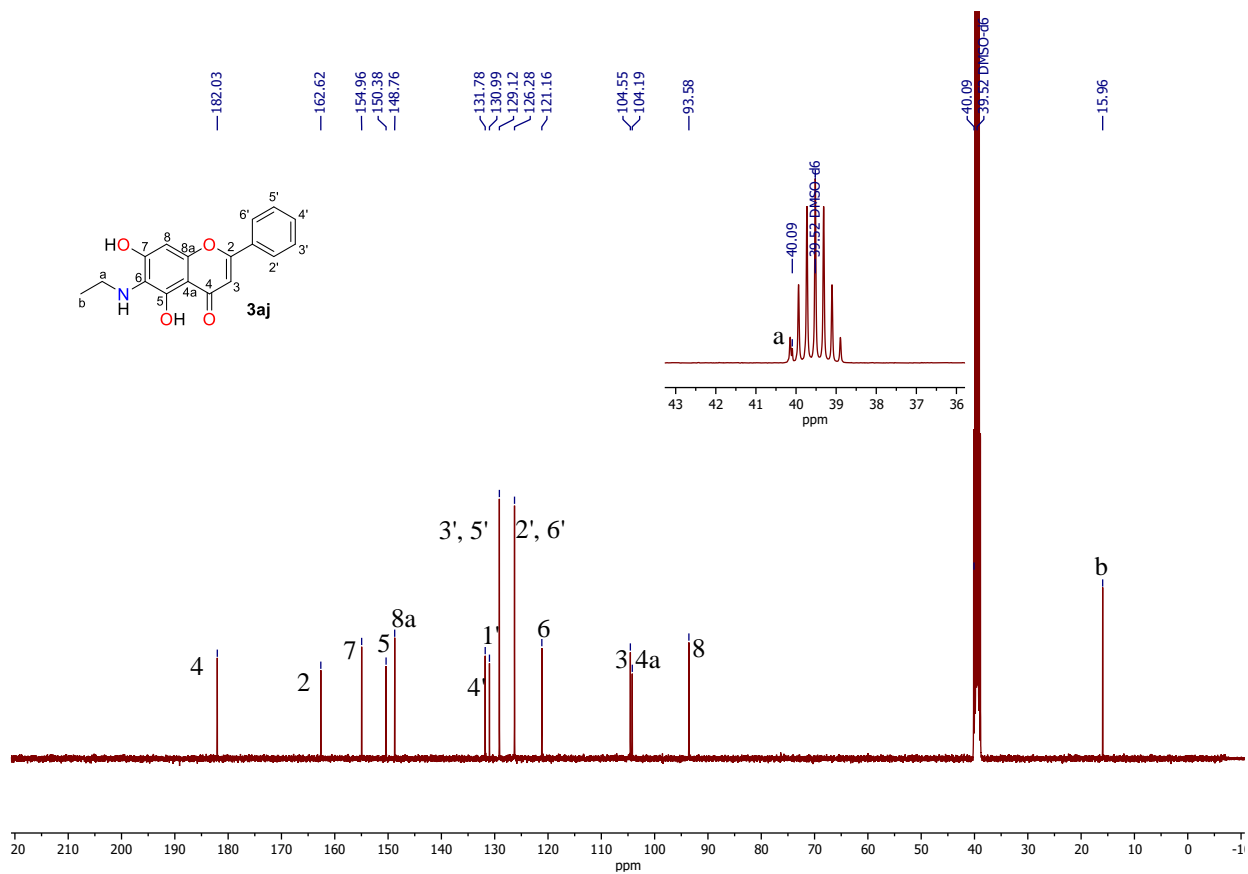
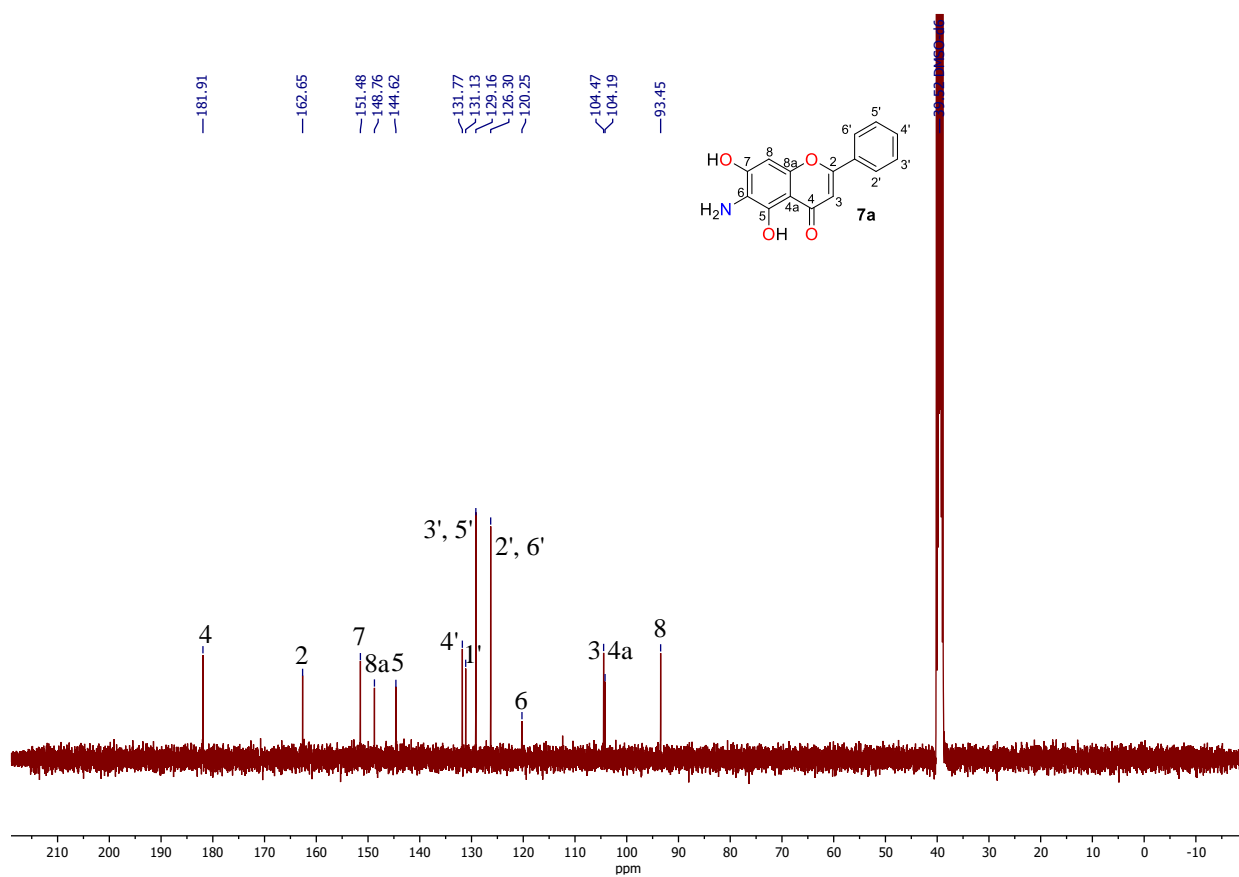
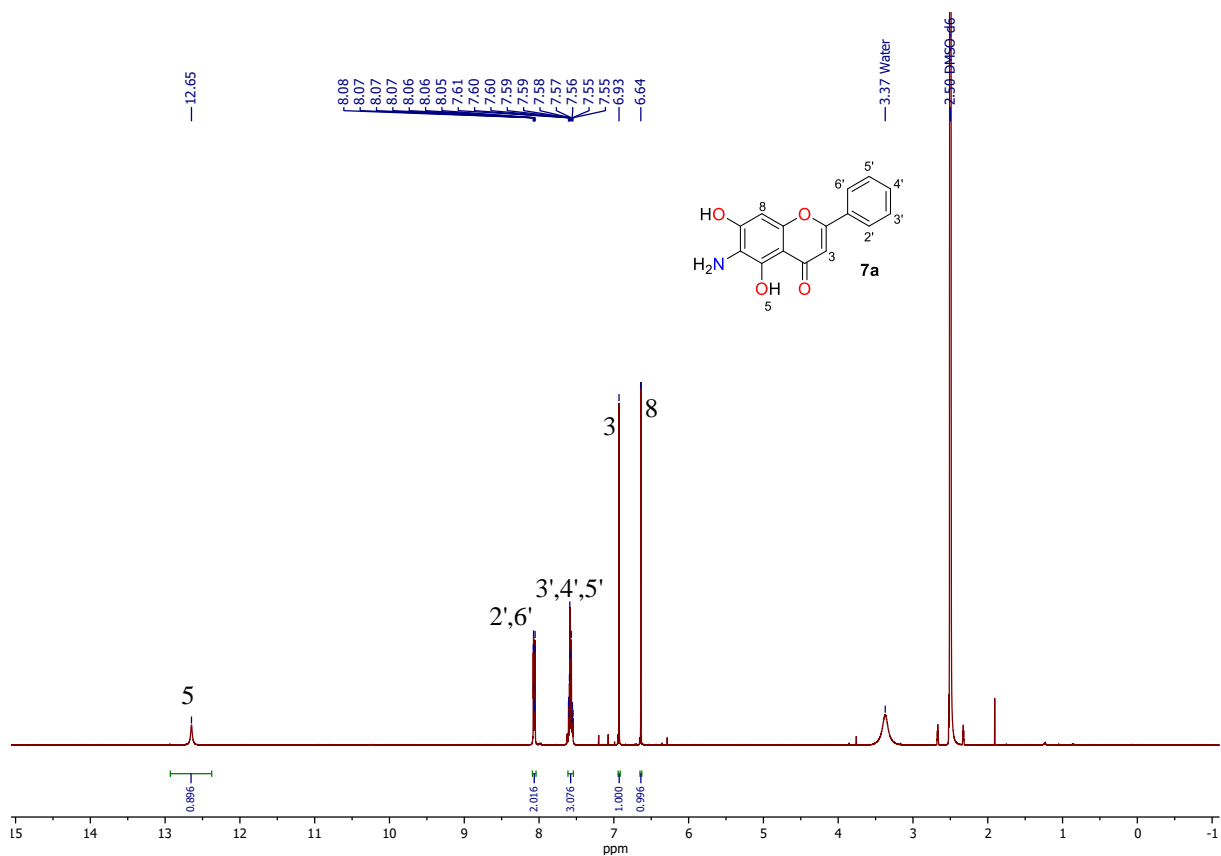


Fig. S144. ¹³C NMR spectrum of **3aj**, DMSO-*d*₆, 101 MHz.



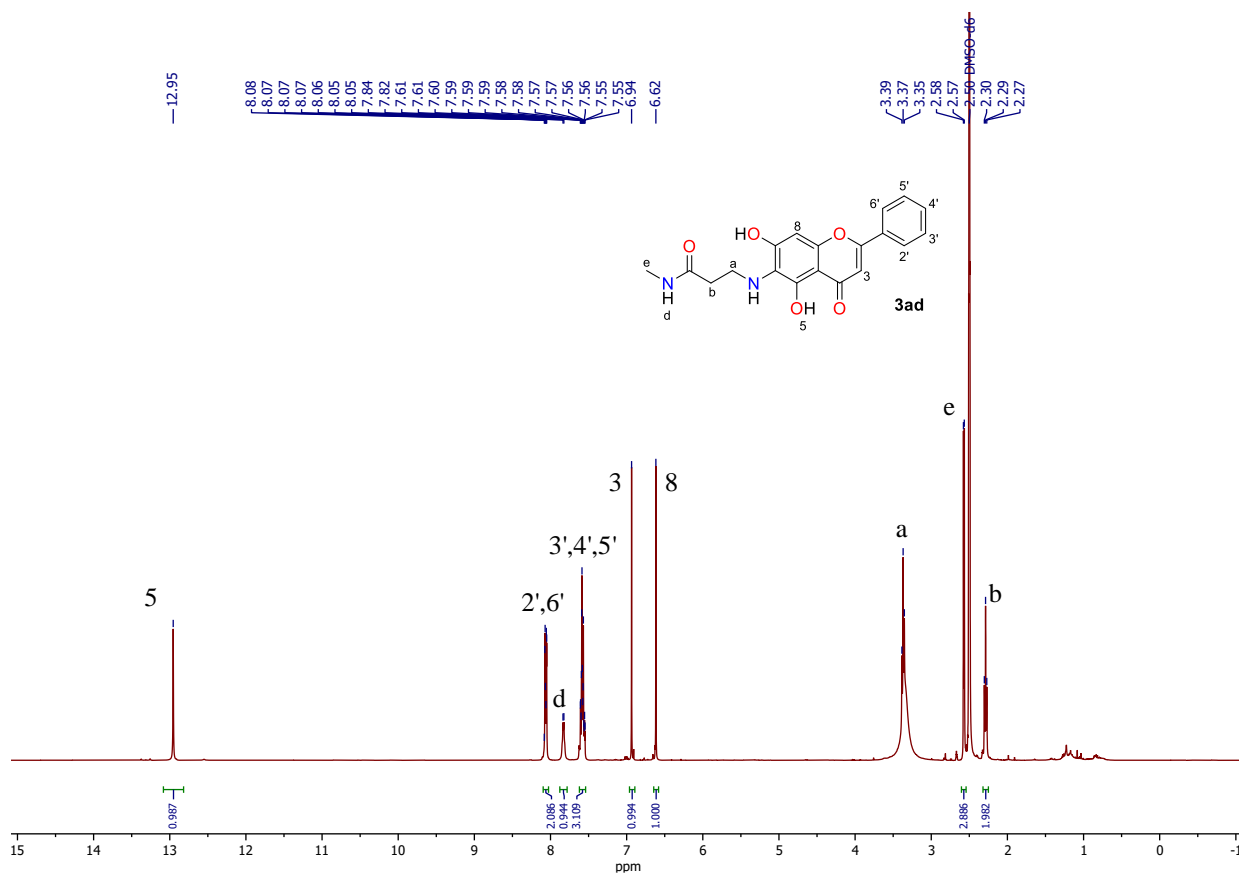


Fig. S147. ¹H NMR spectrum of **3ad**, DMSO-*d*₆, 400 MHz.

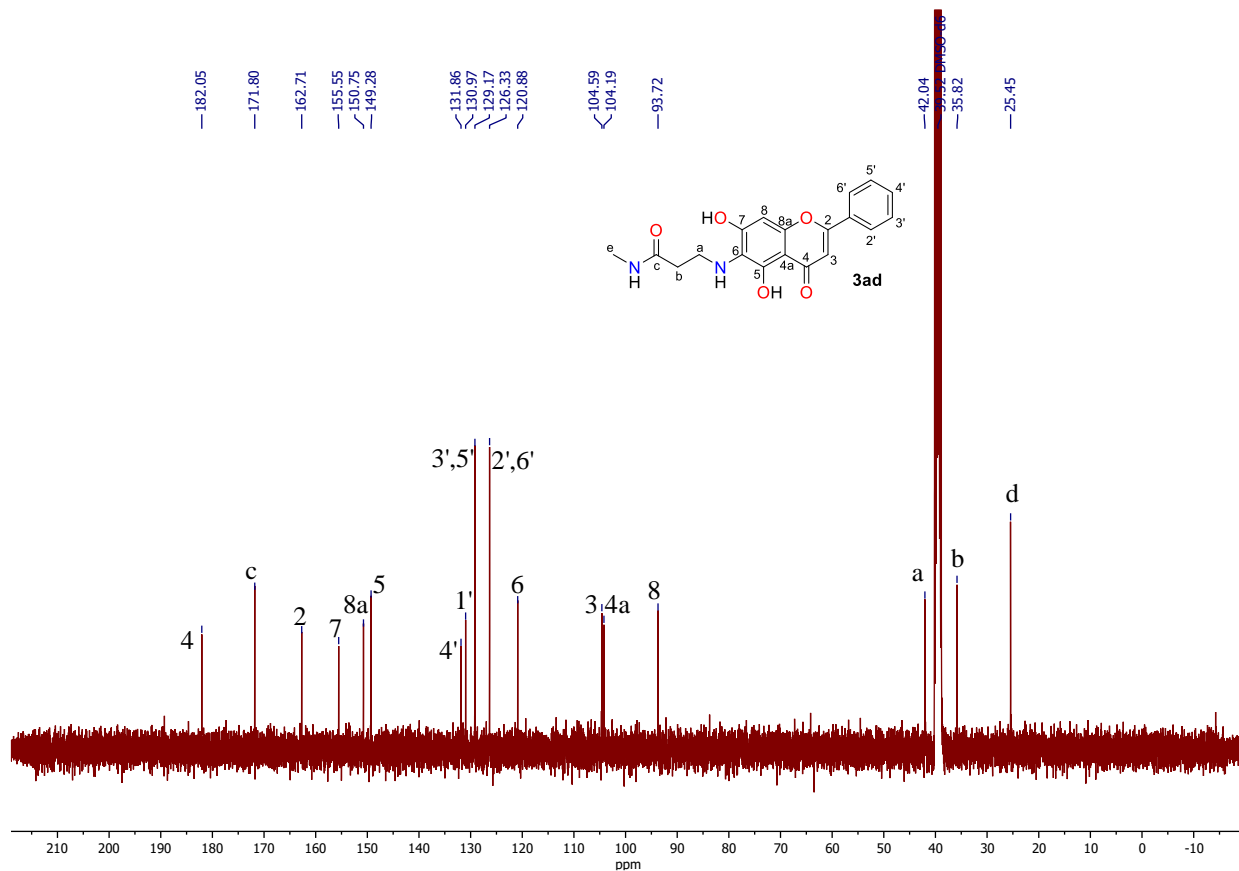


Fig. S148. ¹³C NMR spectrum of **3ad**, DMSO-*d*₆, 101 MHz.

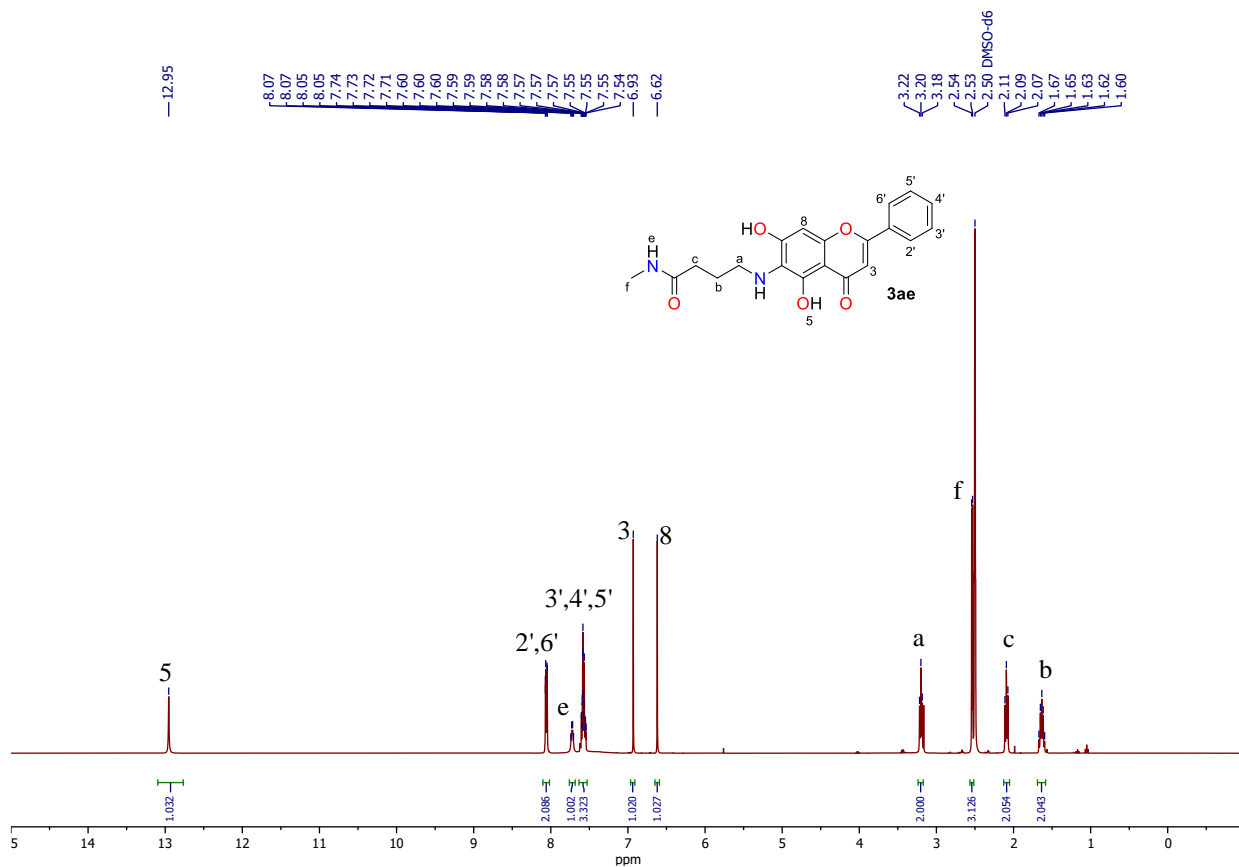


Fig. S149. ¹H NMR spectrum of **3ae**, DMSO-*d*₆, 400 MHz.

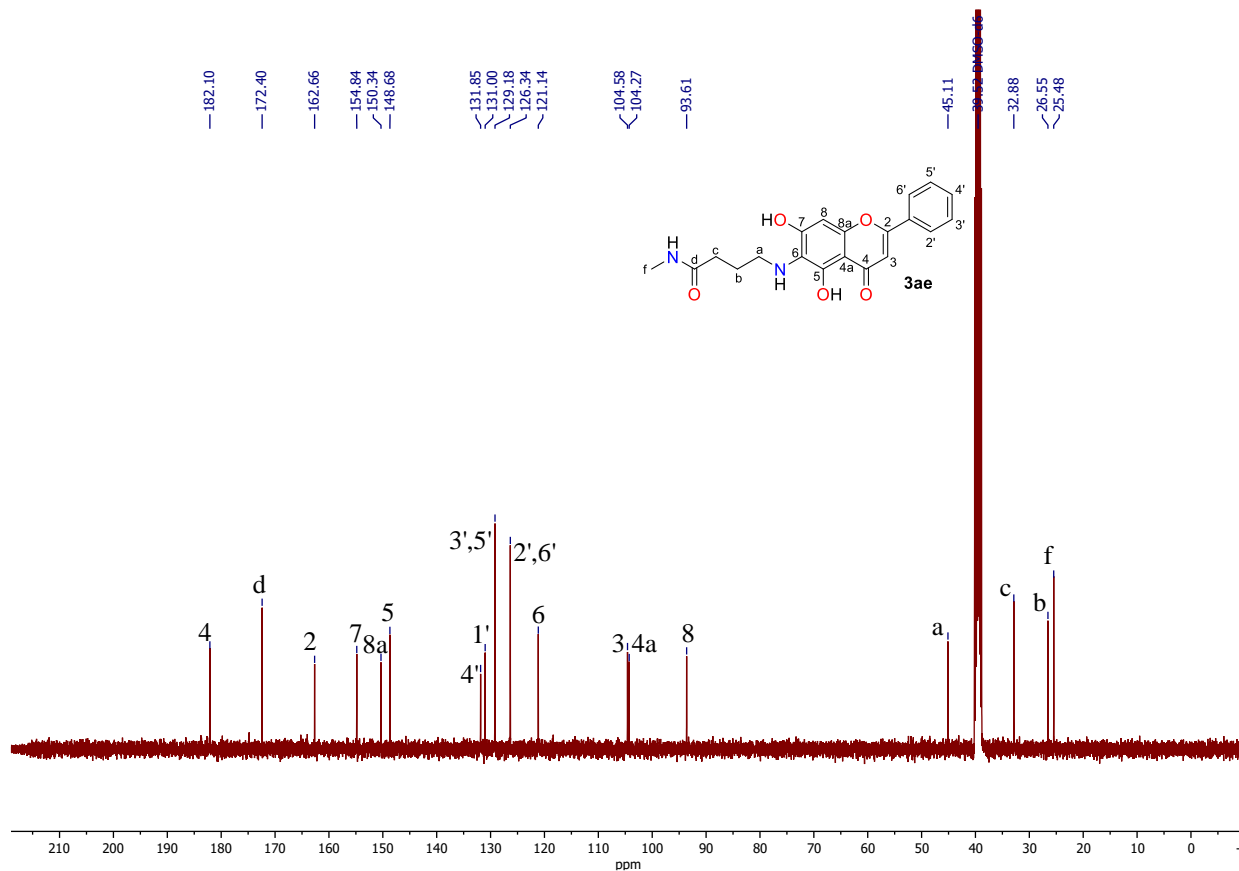


Fig. S150. ¹³C NMR spectrum of **3ae**, DMSO-*d*₆, 101 MHz.

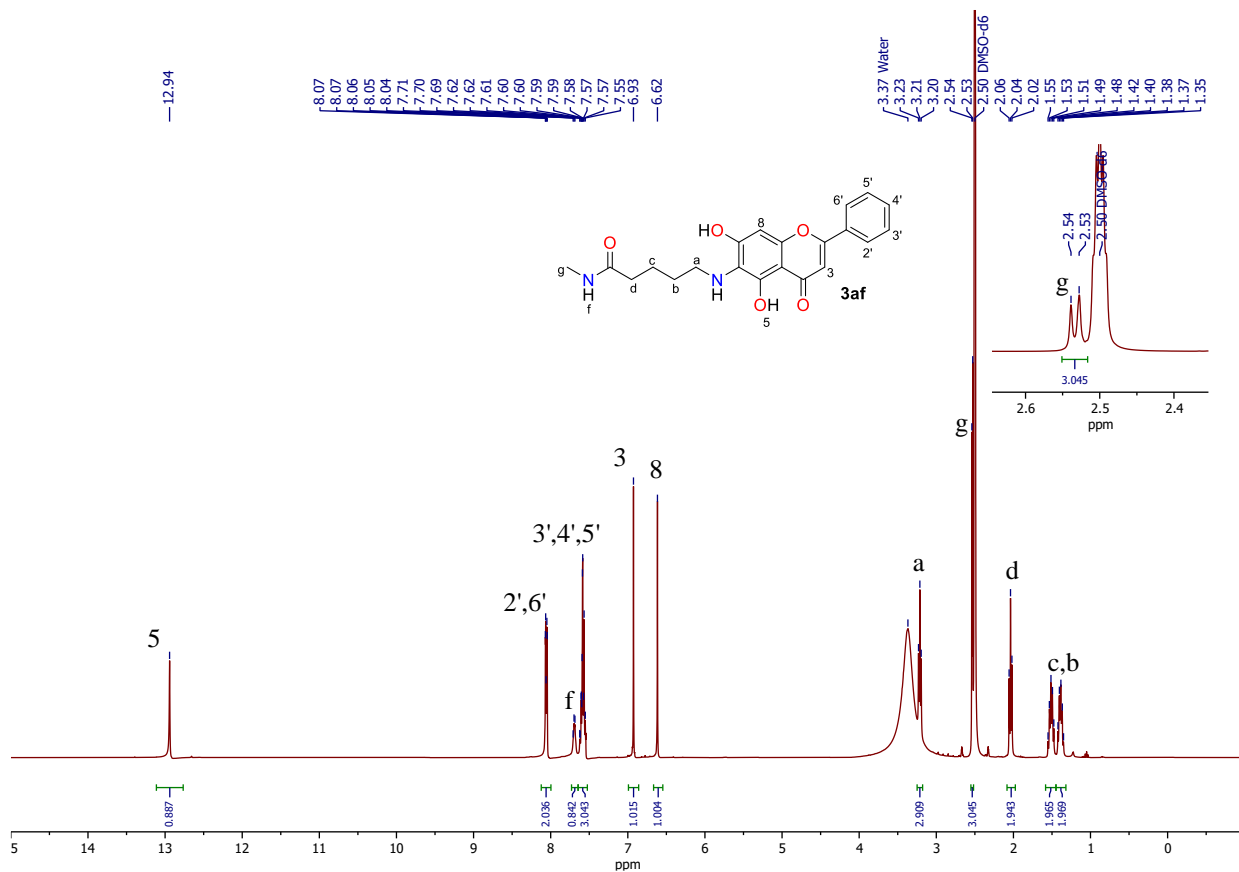


Fig. S151. ¹H NMR spectrum of **3af**, DMSO-*d*₆, 400 MHz.

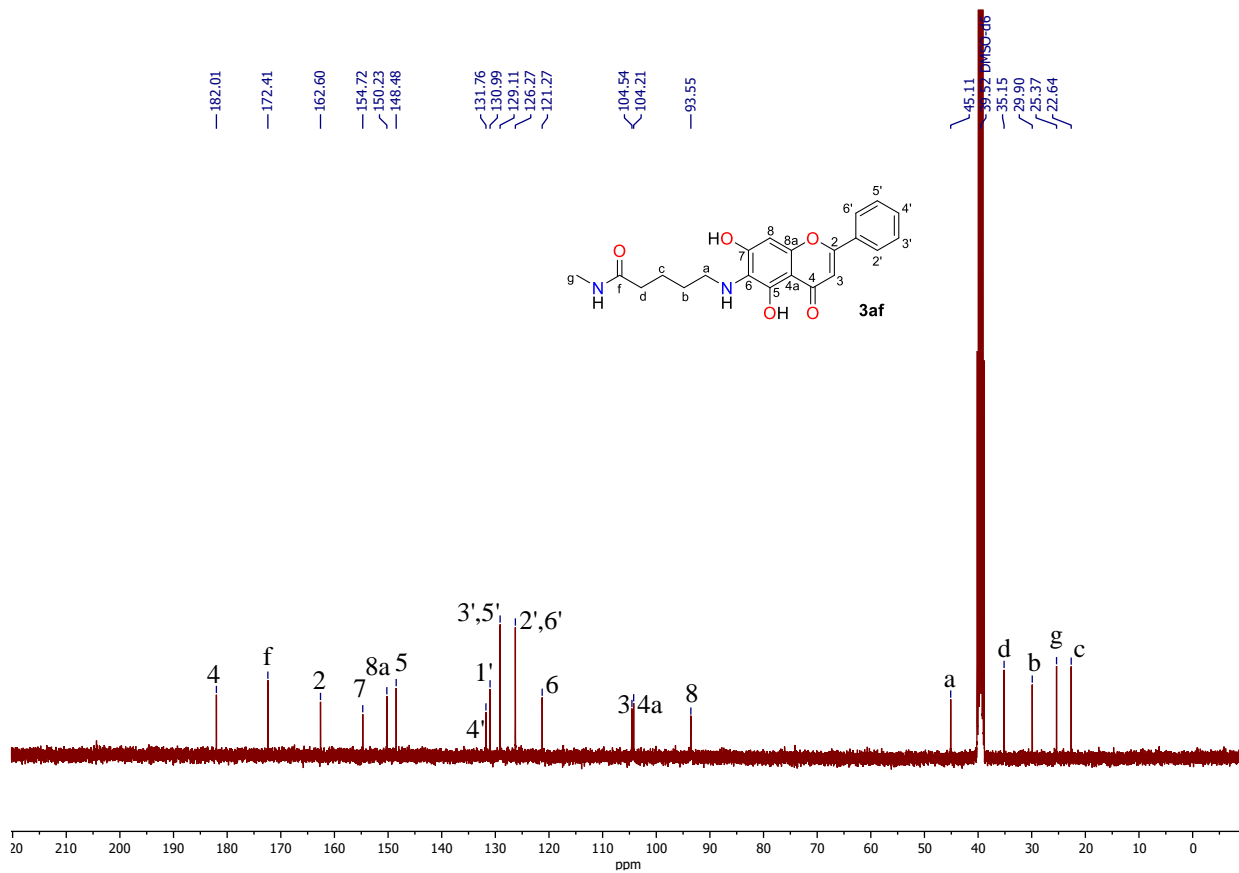


Fig. S152. ¹³C NMR spectrum of **3af**, DMSO-*d*₆, 101 MHz.

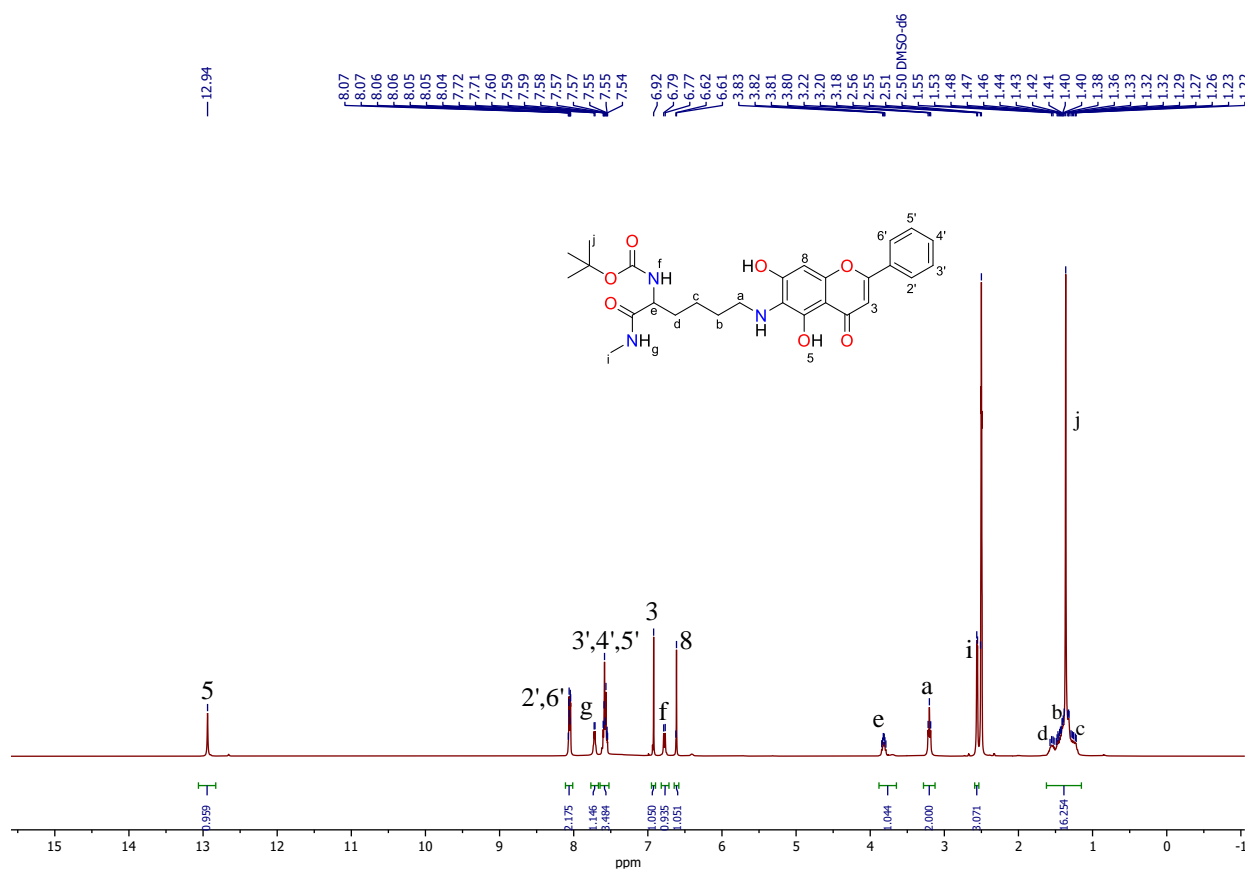


Fig. S153. ¹H NMR spectra of **3ag**, DMSO-*d*₆, 400 MHz.

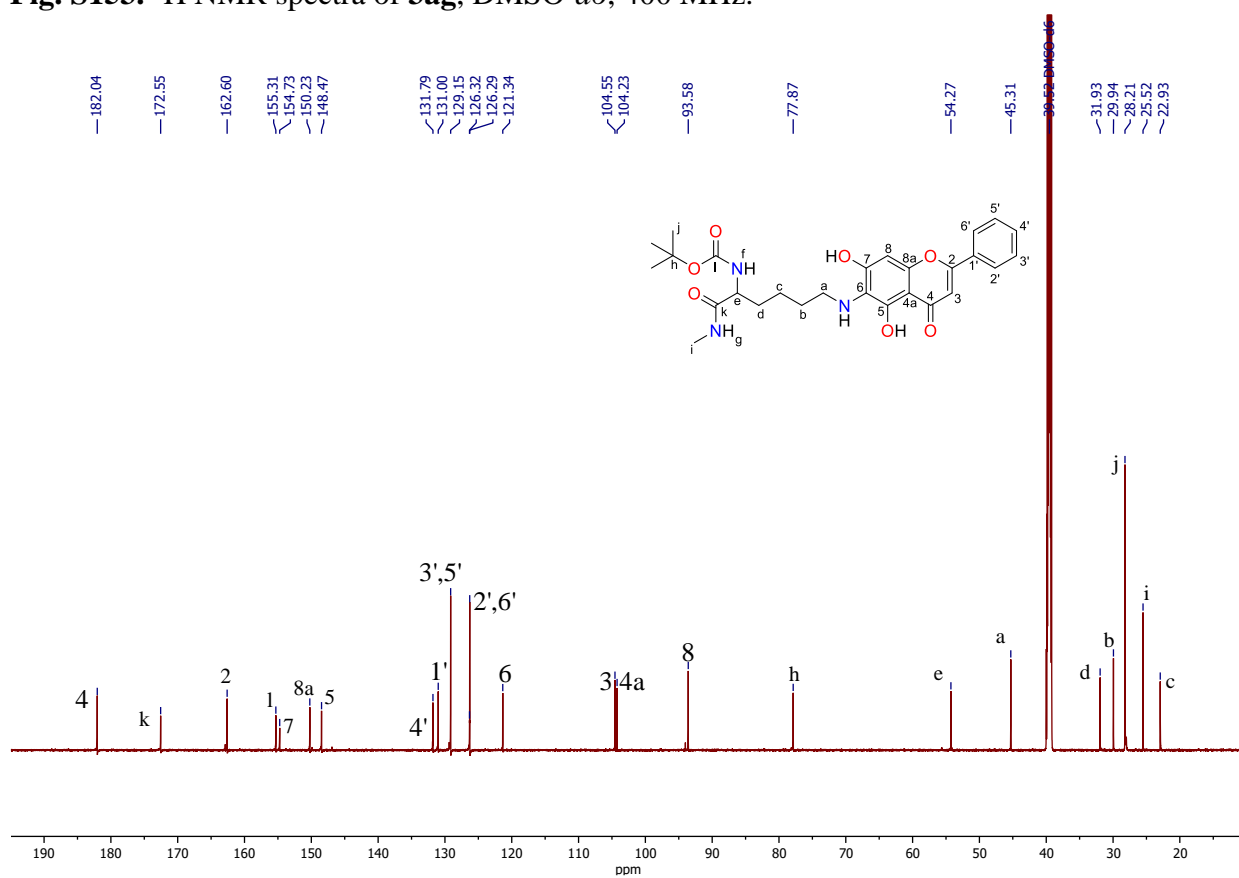


Fig. S154. ¹³C NMR spectrum of **3ag**, DMSO-*d*₆, 101 MHz.

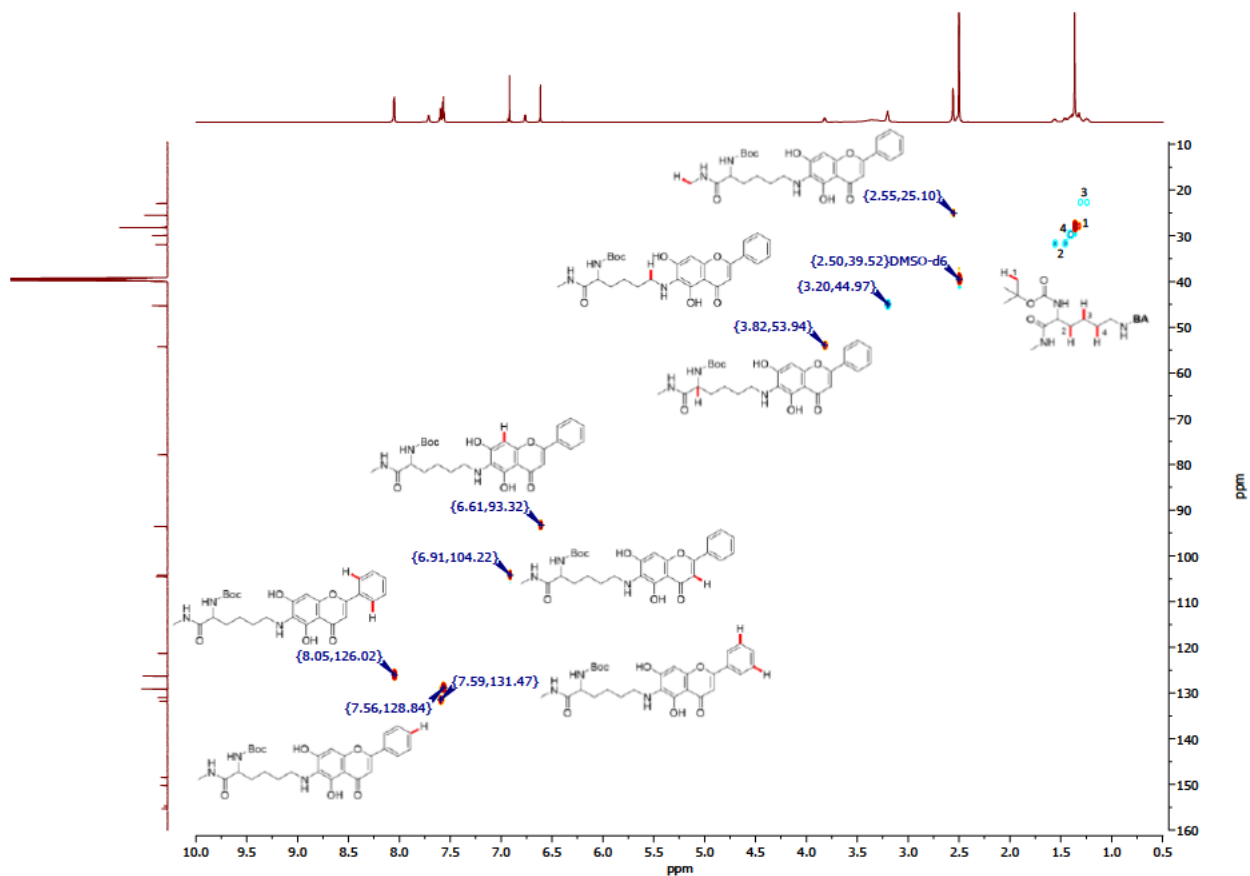


Fig. S155. ^1H - ^{13}C HSQC spectra of the obtained **3ag**, $\text{DMSO-}d_6$, 800 MHz.

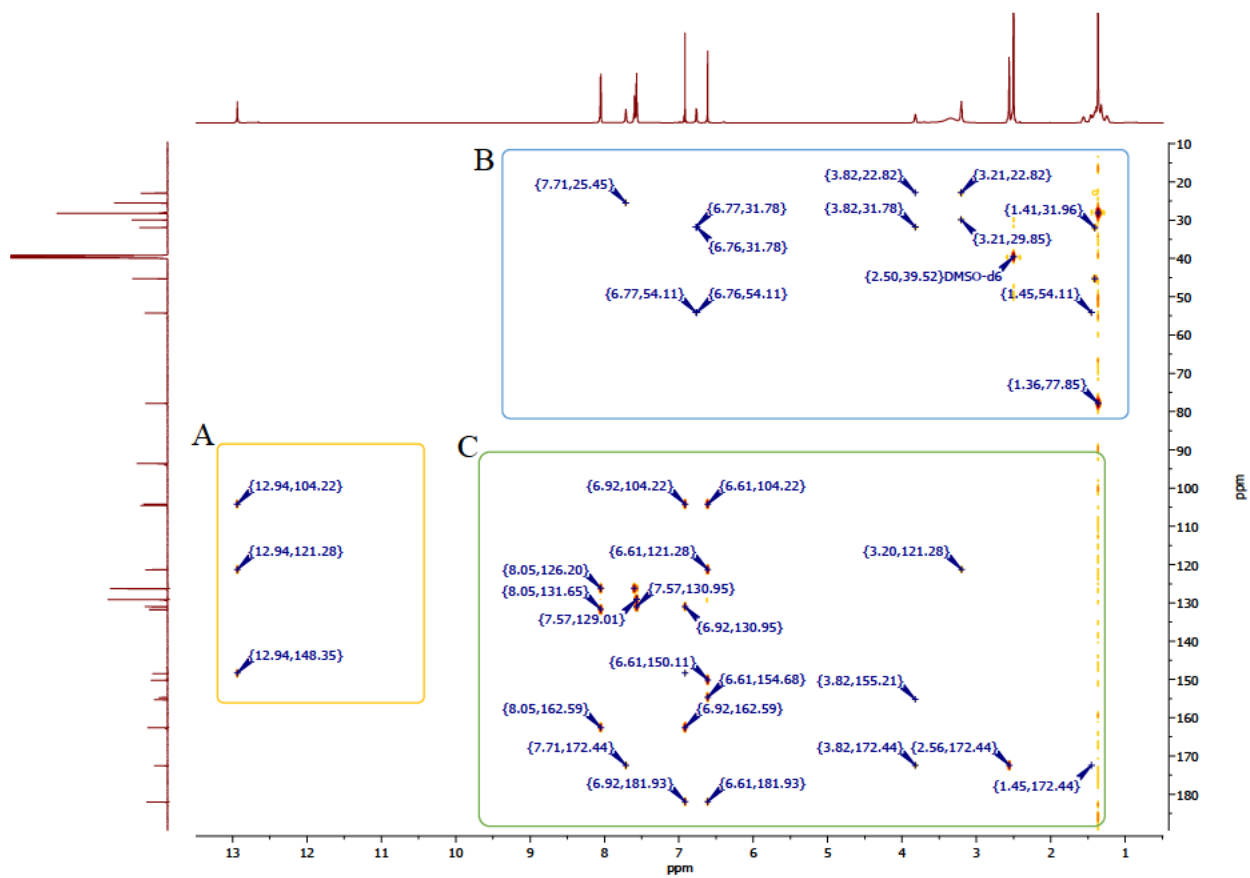


Fig. S156a. ^1H - ^{13}C HMBC spectra of the obtained **3ag**, $\text{DMSO-}d_6$, 800 MHz.

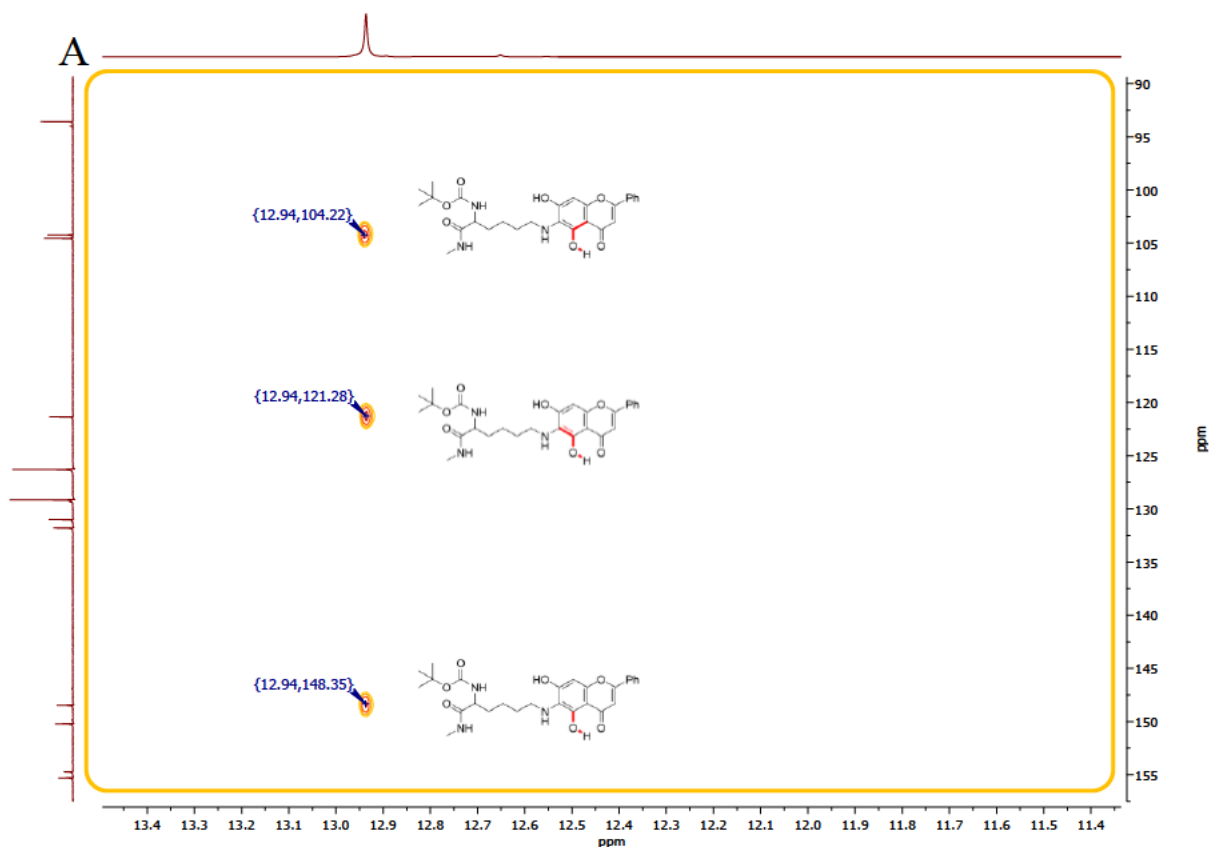


Fig. S156b. Close-up for ^1H - ^{13}C HMBC spectra of the obtained **3ag**, $\text{DMSO-}d_6$.

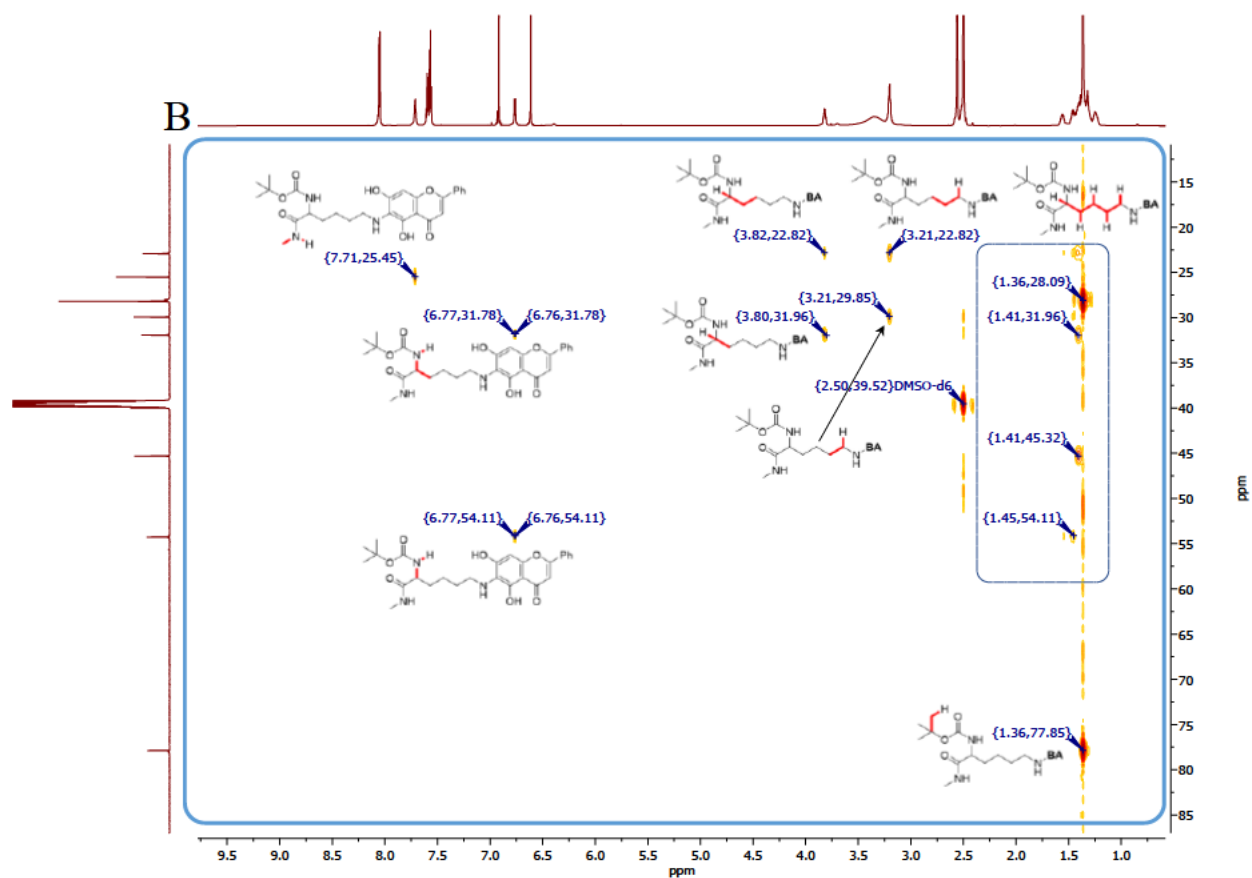


Fig. S156c. Close-up for ^1H - ^{13}C HMBC spectra of the obtained **3ag**, $\text{DMSO-}d_6$.

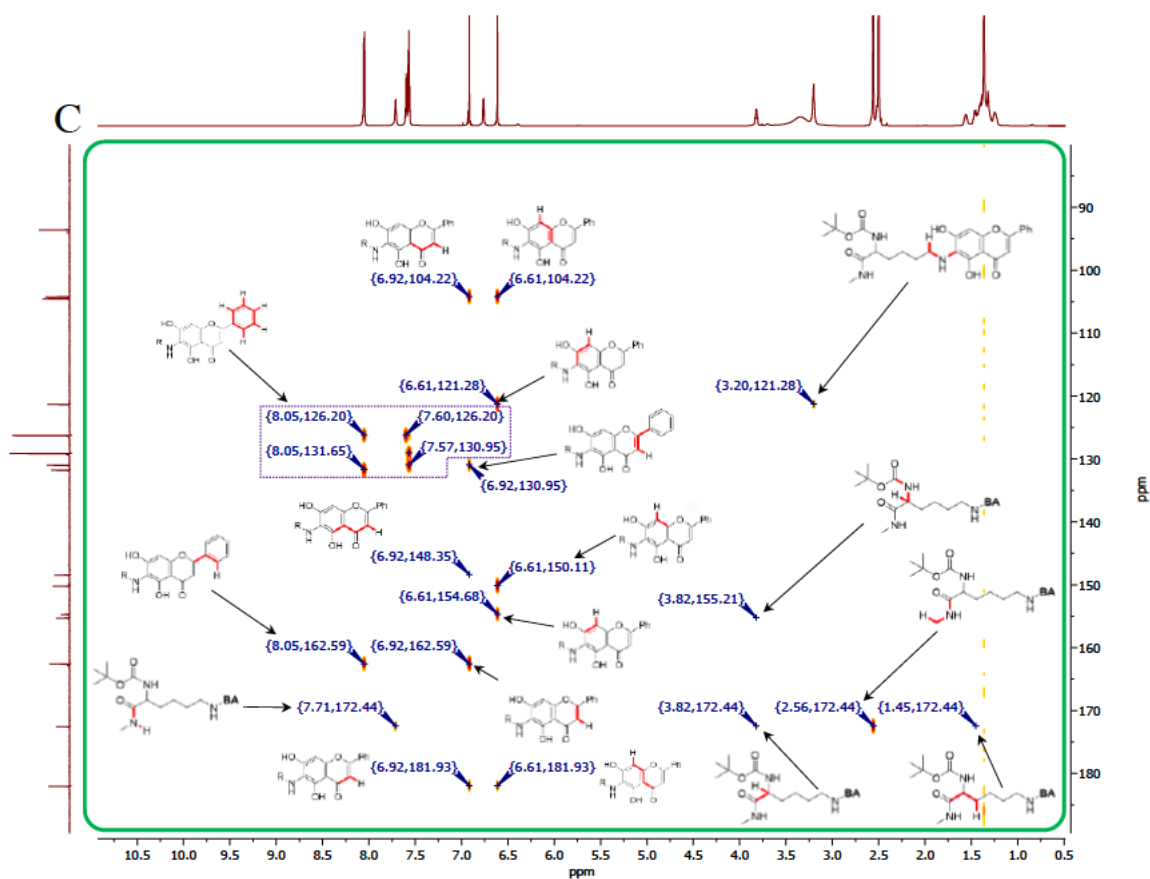


Fig. S156d. Close-up for ^1H - ^{13}C HMBC spectra of the obtained **3ag**, $\text{DMSO-}d_6$.

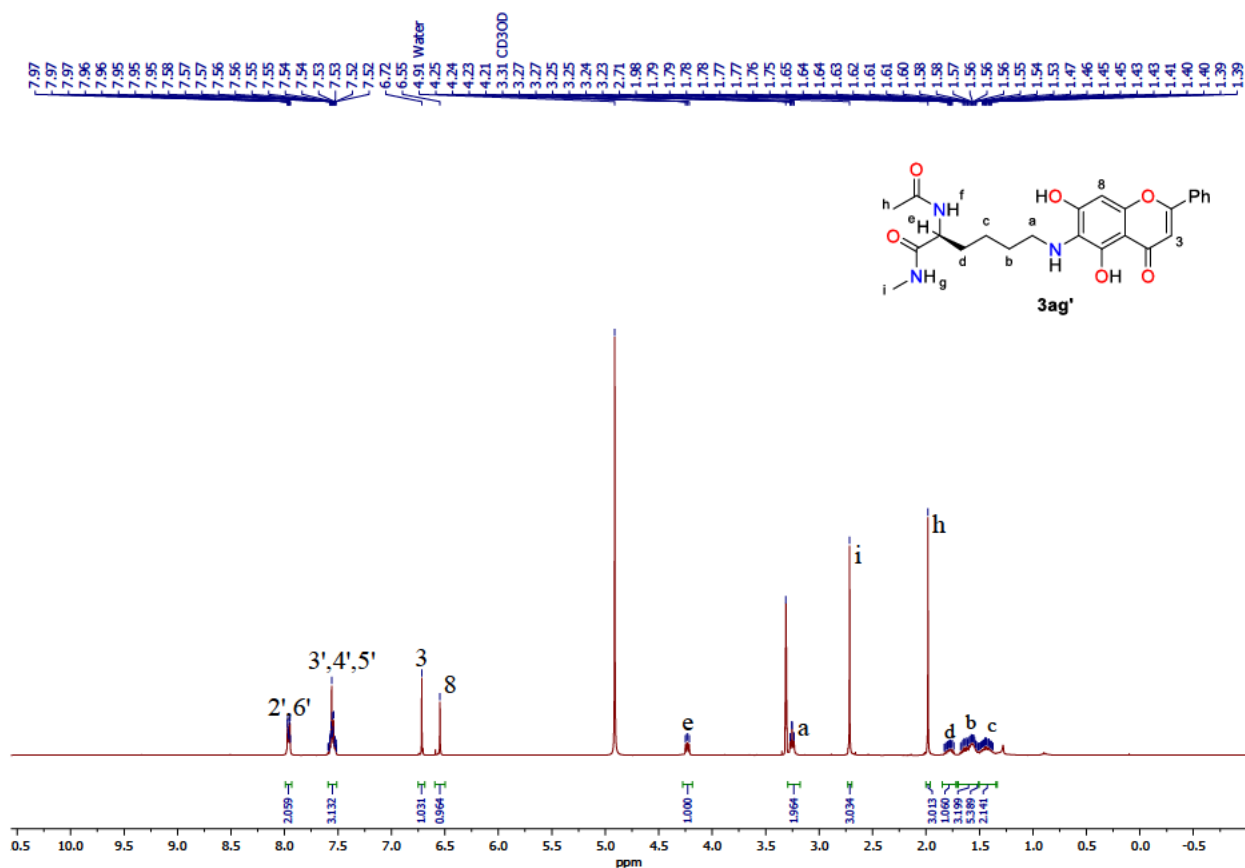


Fig. S157. ^1H NMR spectrum of **3ag'**, $\text{MeOH-}d_4$, 400 MHz.

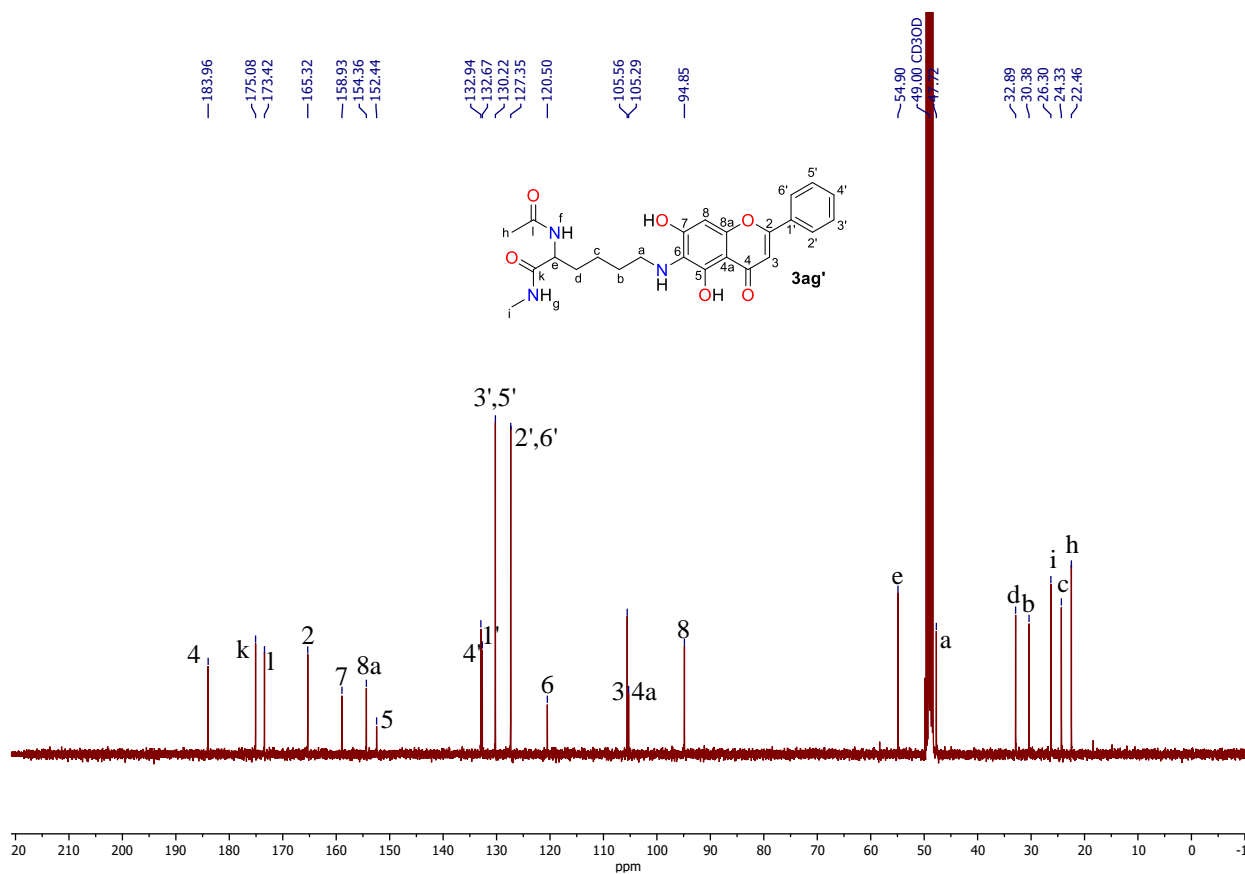


Fig. S158. ^{13}C NMR spectrum of **3ag'**, $\text{MeOH-}d_4$, 101 MHz.

1.3.7.13. NMR spectra of Intermediate Products

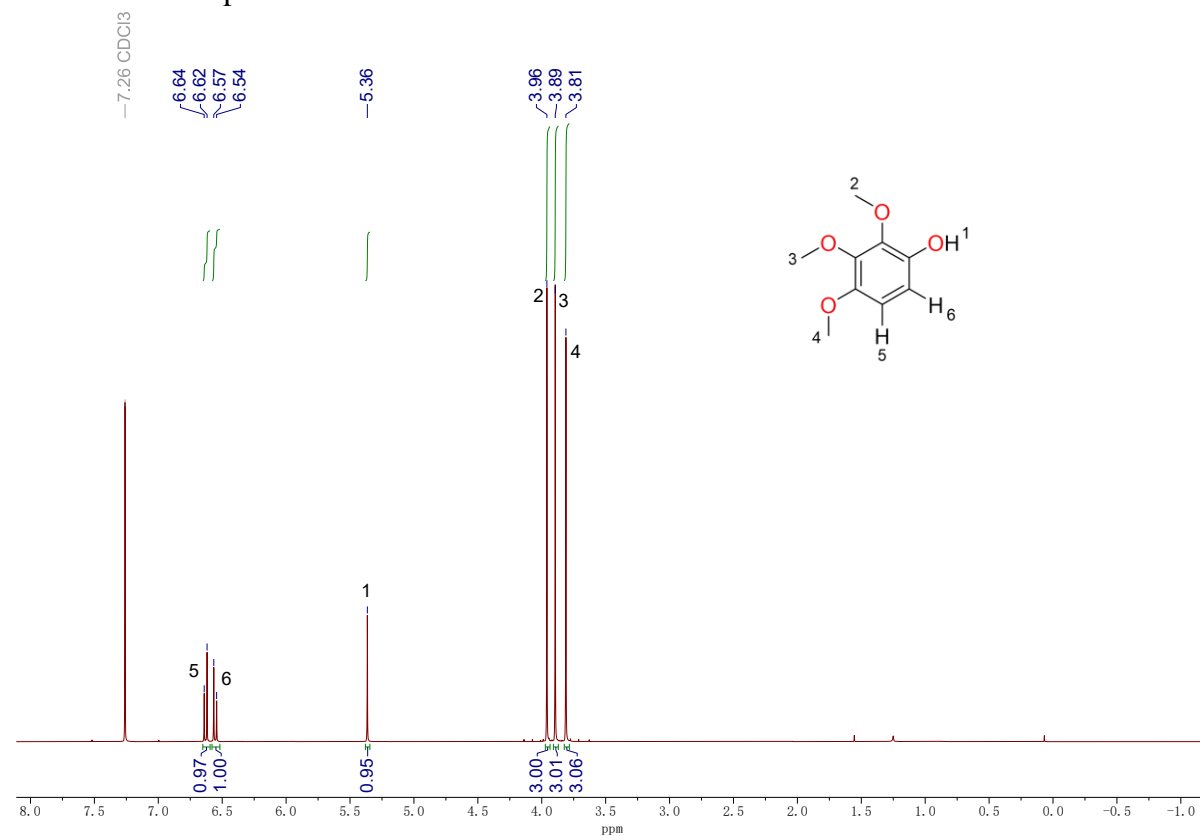


Fig. S159. ^1H NMR spectrum of 2,3,4-trimethoxyphenol (**11-1**), CDCl_3 , 400 MHz.

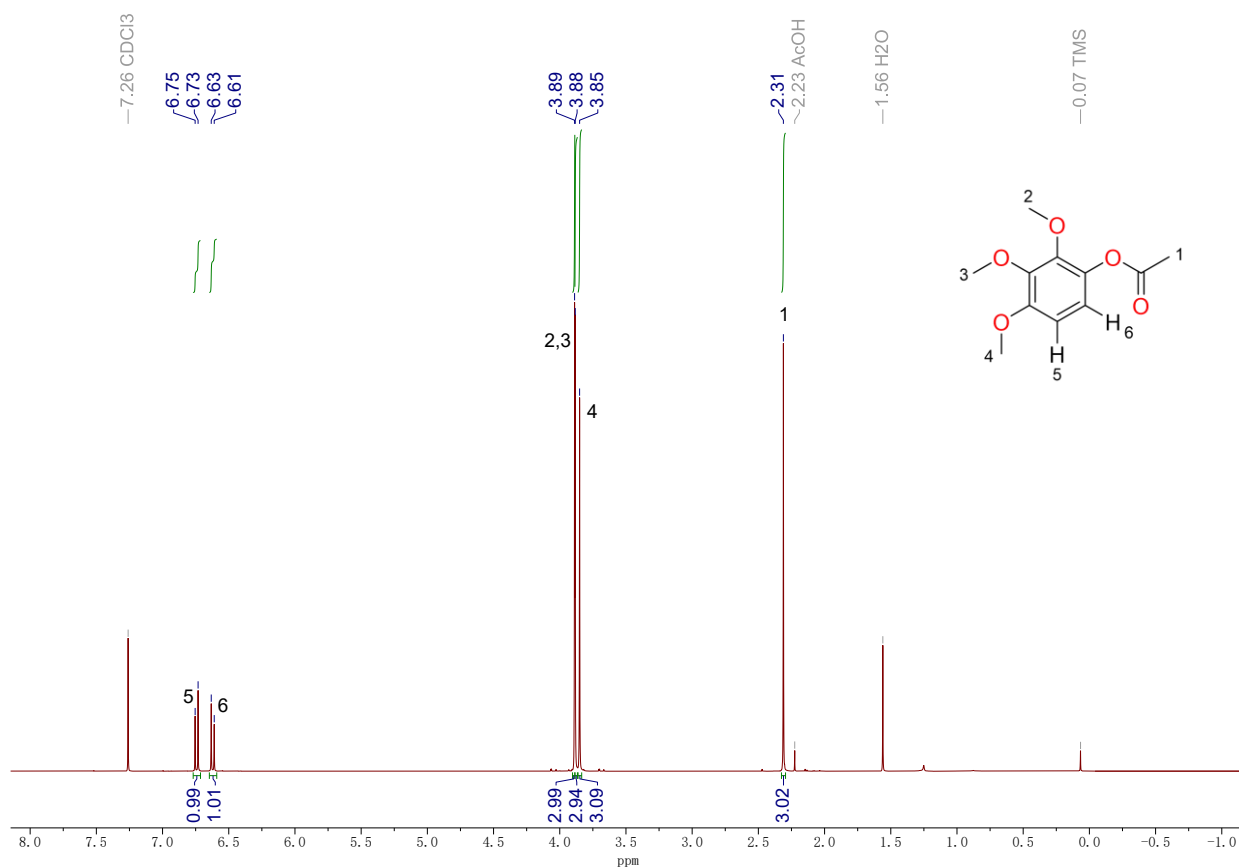


Fig. S160. ^1H NMR spectrum of 2,3,4-trimethoxyphenylacetate (**11-2**), CDCl_3 , 400 MHz.

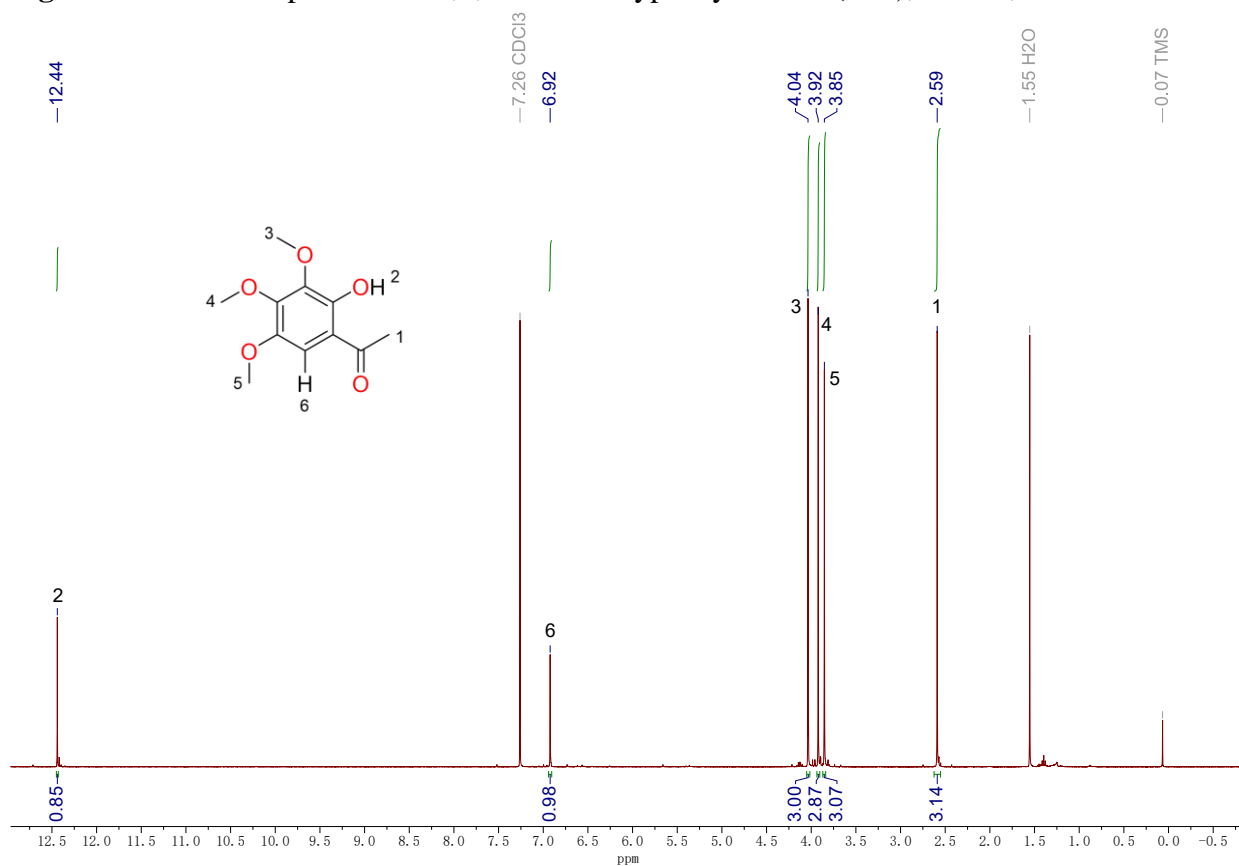


Fig. S161. ^1H NMR spectrum of 1-(2-hydroxy-3,4,5-trimethoxyphenyl)ethan-1-one (**11-3**), CDCl_3 , 400 MHz.

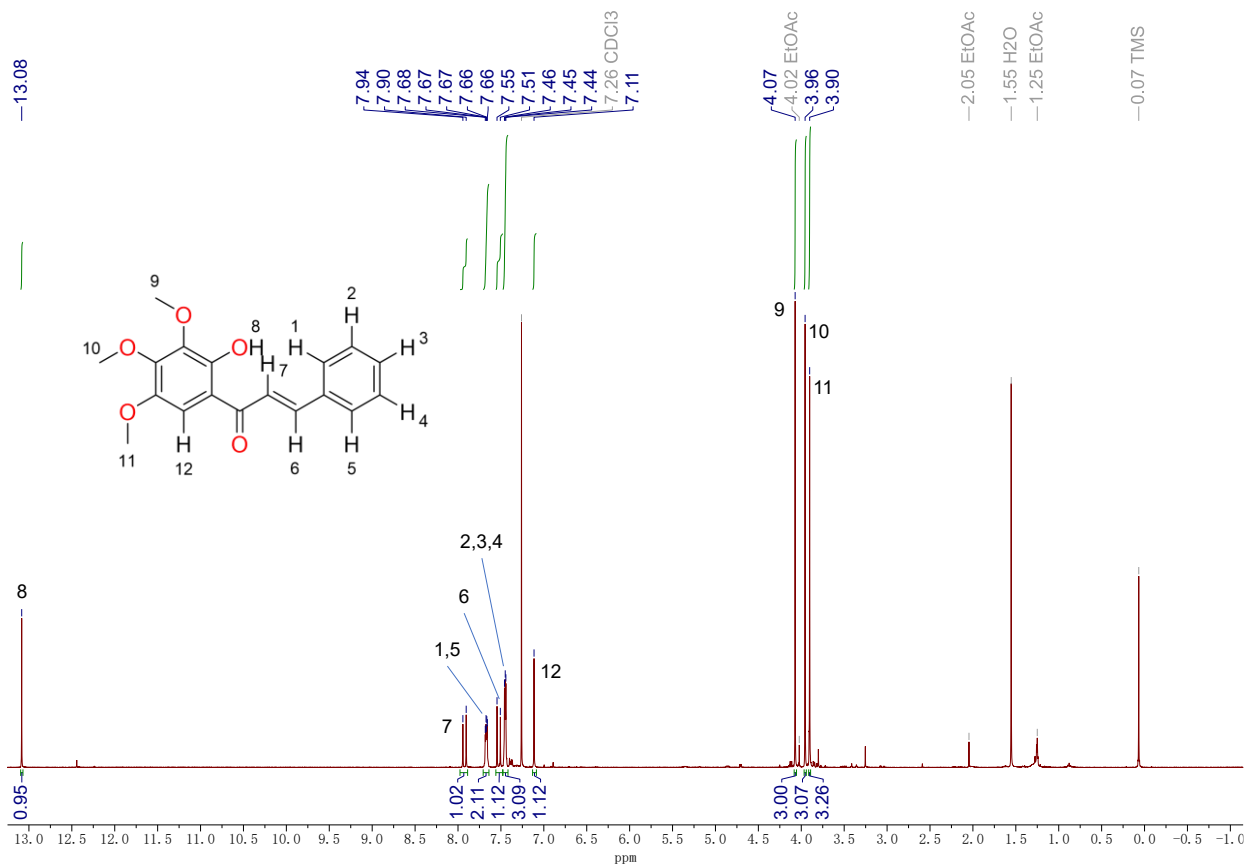


Fig. S162. ¹H NMR spectrum of 1-(2-hydroxy-3,4,5-trimethoxyphenyl)-3-phenylprop-2-en-1-one (**11-4**), CDCl₃, 400 MHz.

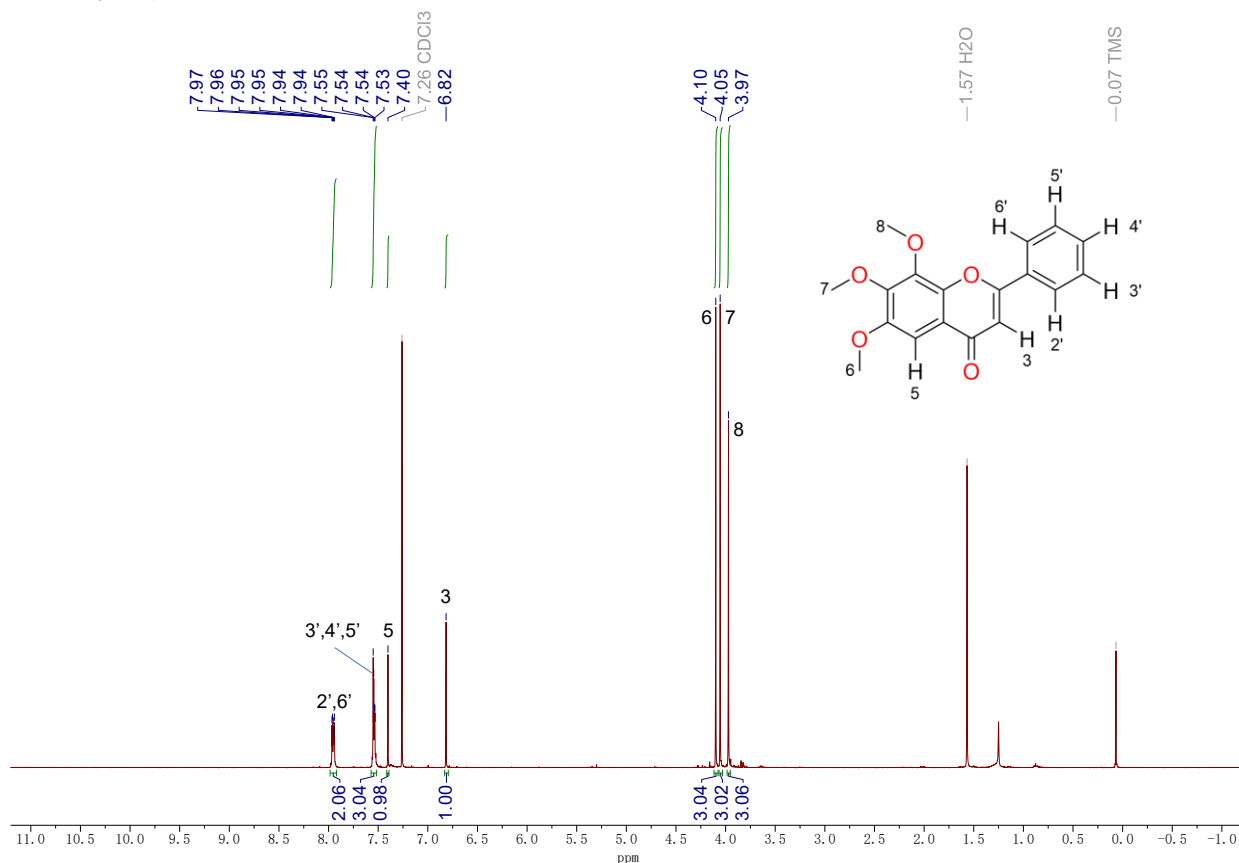


Fig. S163. ¹H NMR spectrum of 6,7,8-trimethoxyflavone (**11-5**), DMSO-*d*₆, 400 MHz.

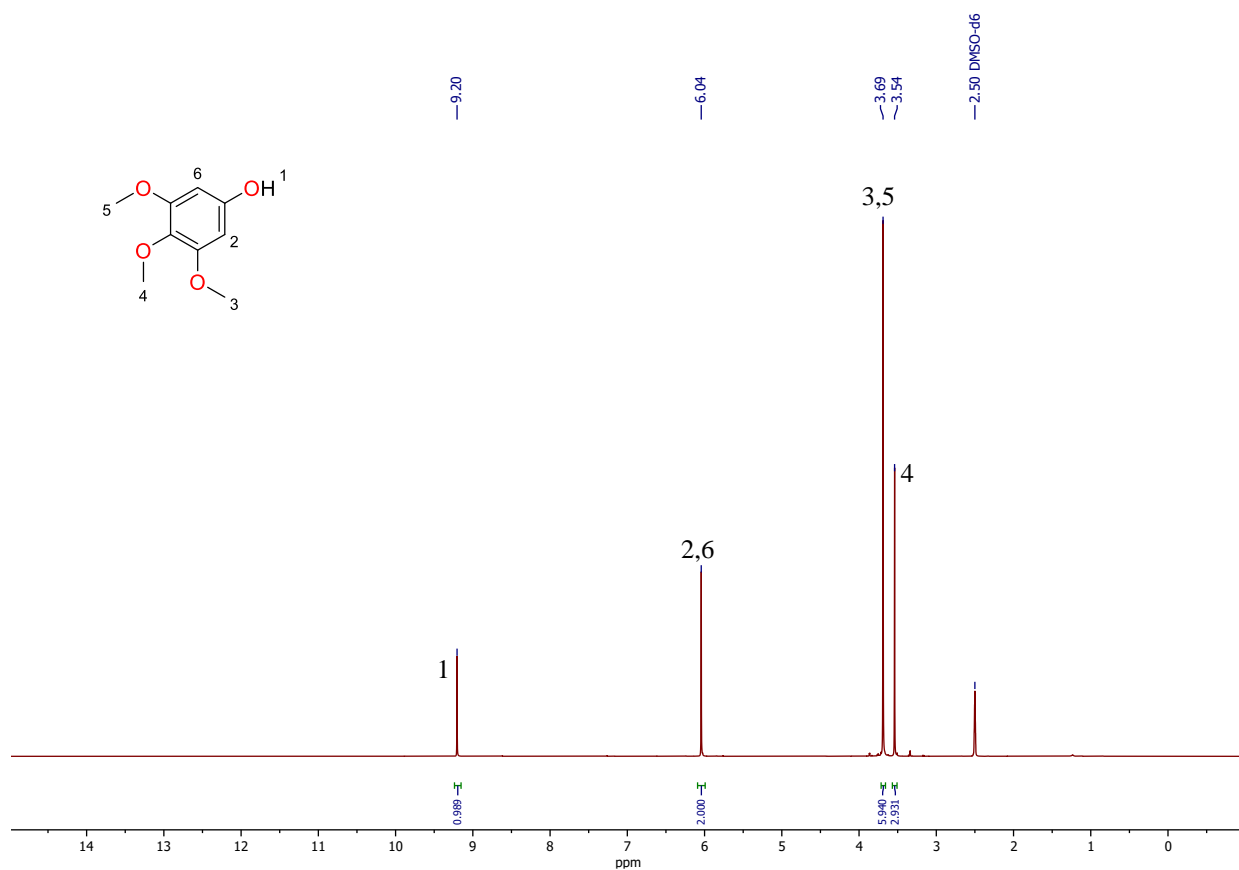


Fig. S164. ¹H NMR spectrum of 3,4,5-trimethoxyphenol (**1n-1**), DMSO-*d*₆, 400 MHz.

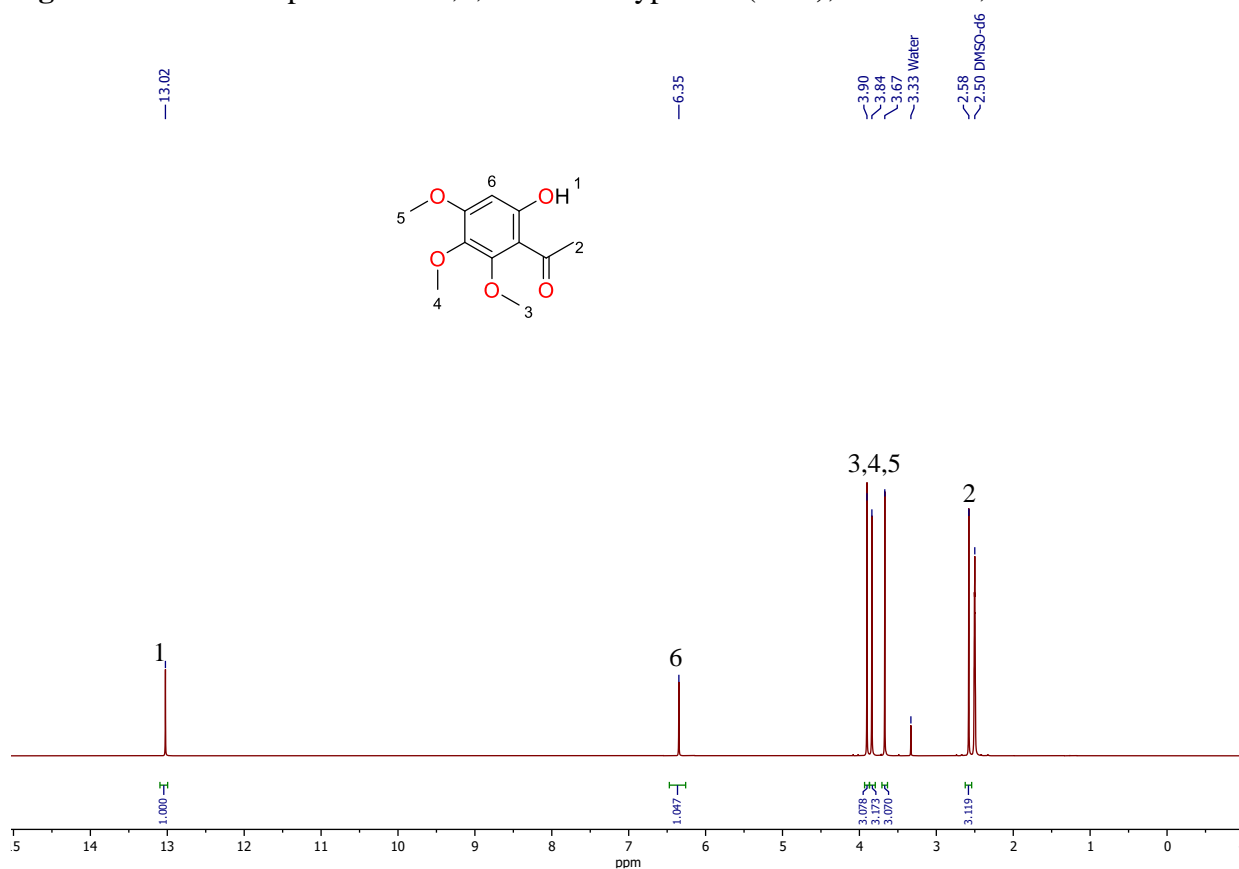


Fig. S165. ¹H NMR spectrum of 1-(6-hydroxy-2,3,4-trimethoxyphenyl)ethan-1-one (**1n-2**), DMSO-*d*₆, 400 MHz.

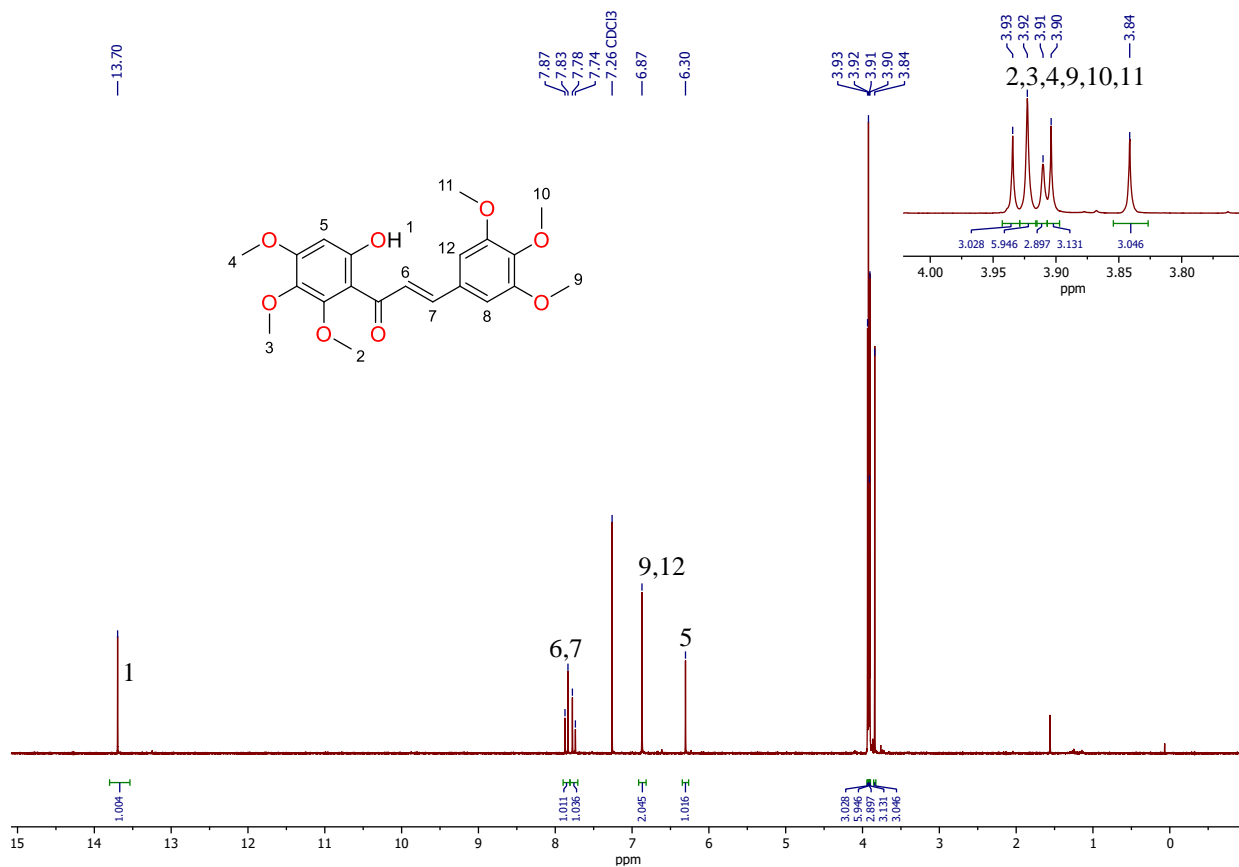


Fig. S166. ¹H NMR spectrum of (E)-1-(6-hydroxy-2,3,4-trimethoxyphenyl)-3-(3,4,5-trimethoxyphenyl)prop-2-en-1-one (**1n-3**), CDCl₃, 400 MHz.

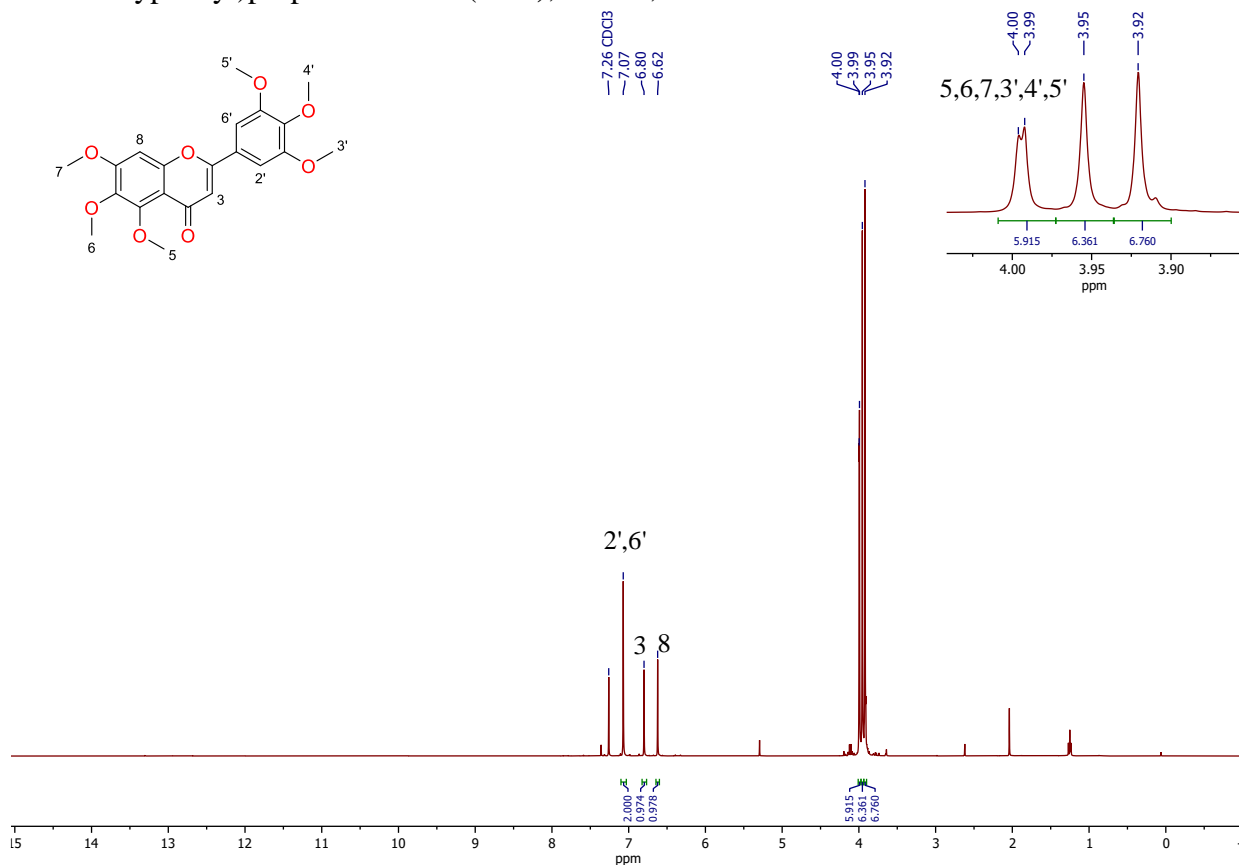


Fig. S167. ¹H NMR spectrum of 3',4',5',5,6,7-trimethoxyflavone (**1n-4**), CDCl₃, 400 MHz.

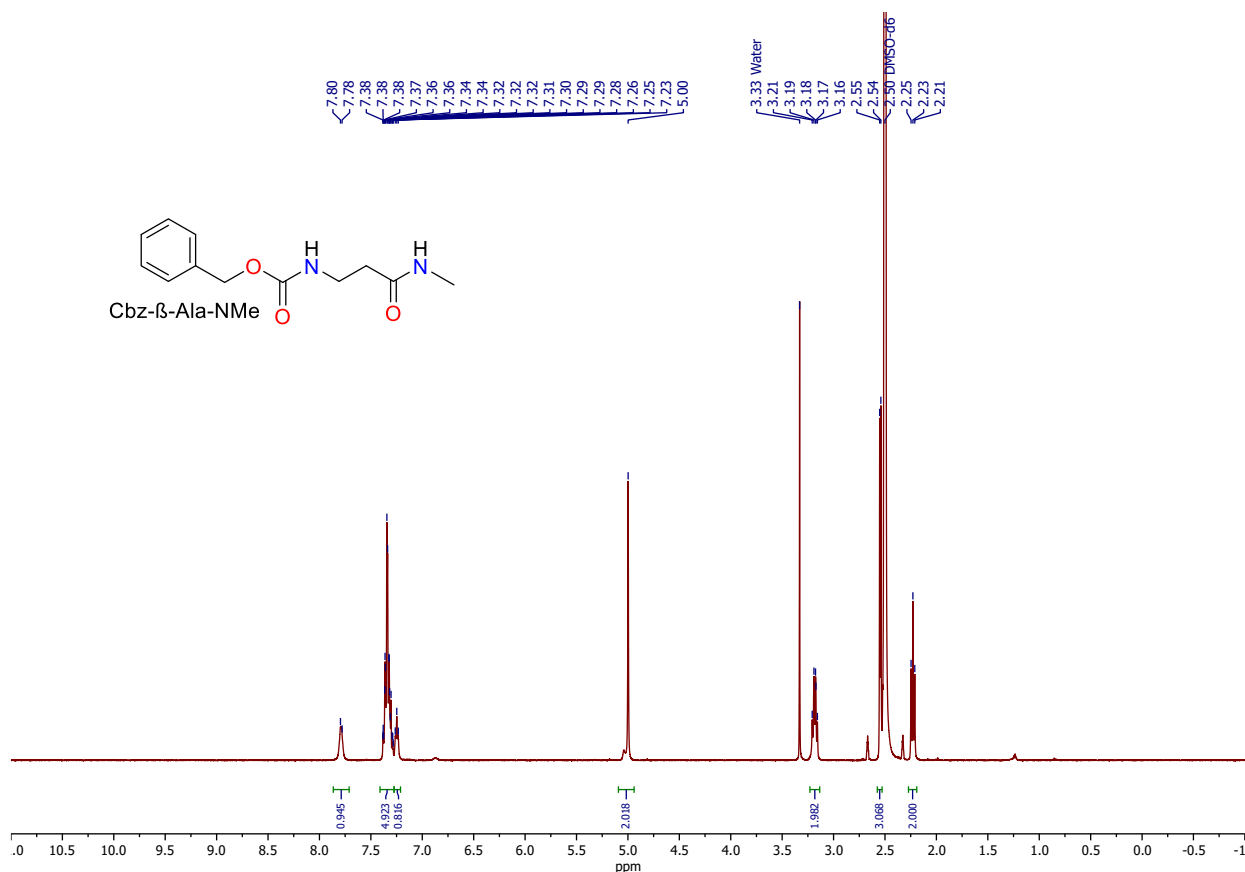


Fig. S168. ¹H NMR spectrum of Cbz-β-Ala-NMe (Z-2d), DMSO-*d*₆, 400 MHz.

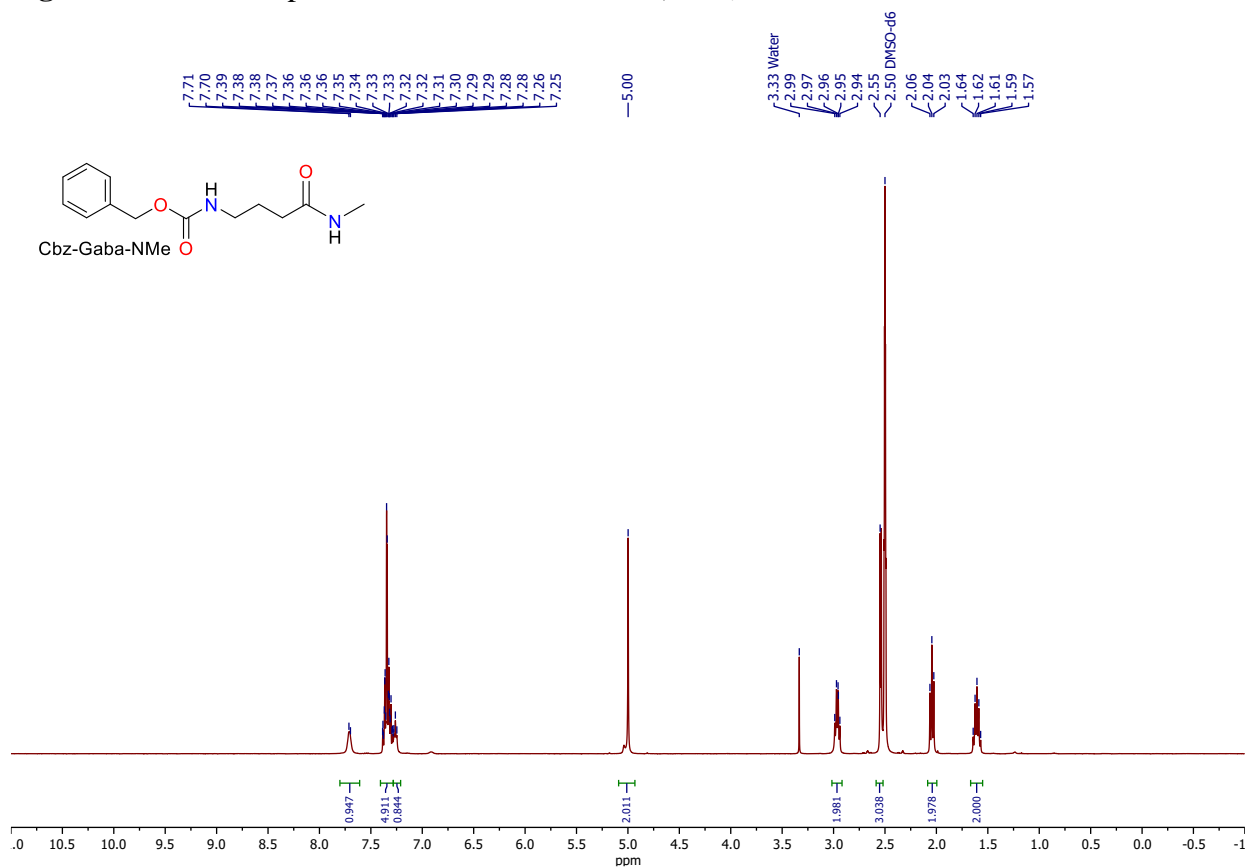


Fig. S169. ¹H NMR spectrum of Cbz-Gaba-NMe (Z-2e), DMSO-*d*₆, 400 MHz.

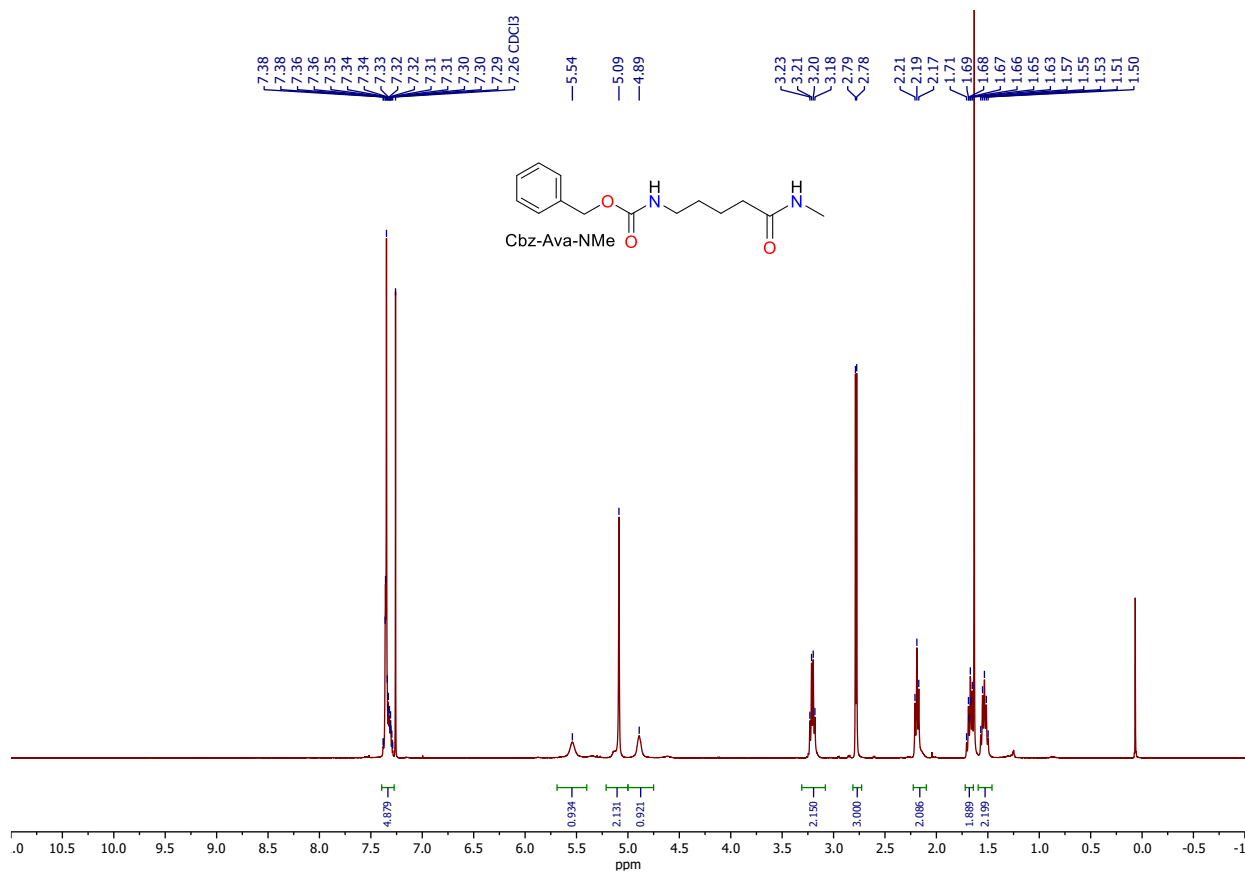


Fig. S170. ¹H NMR spectrum of Cbz-Ava-NMe (Z-2f), CDCl₃, 400 MHz.

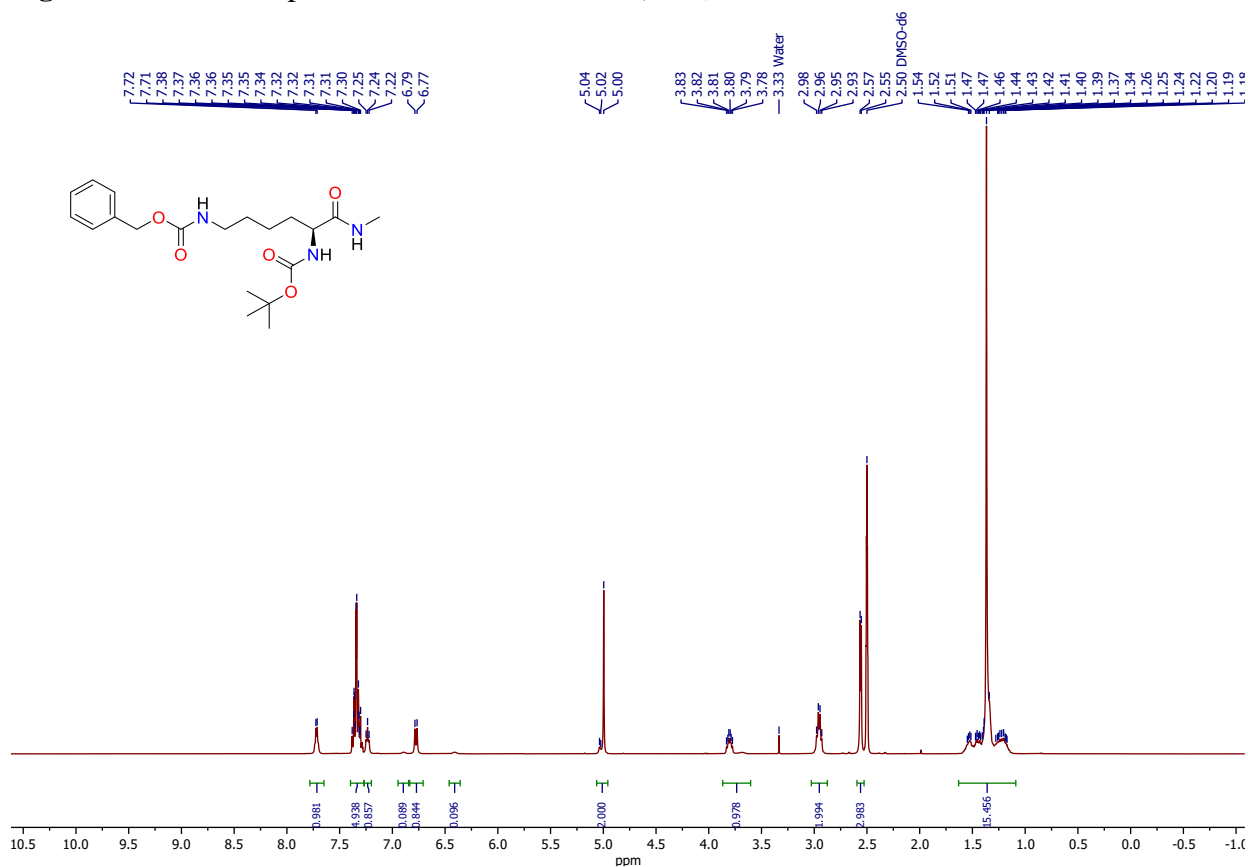


Fig. S171. ¹H NMR spectra of N-Boc-Lys(Cbz)-NMe (Z-2g), DMSO-d₆, 400 MHz.

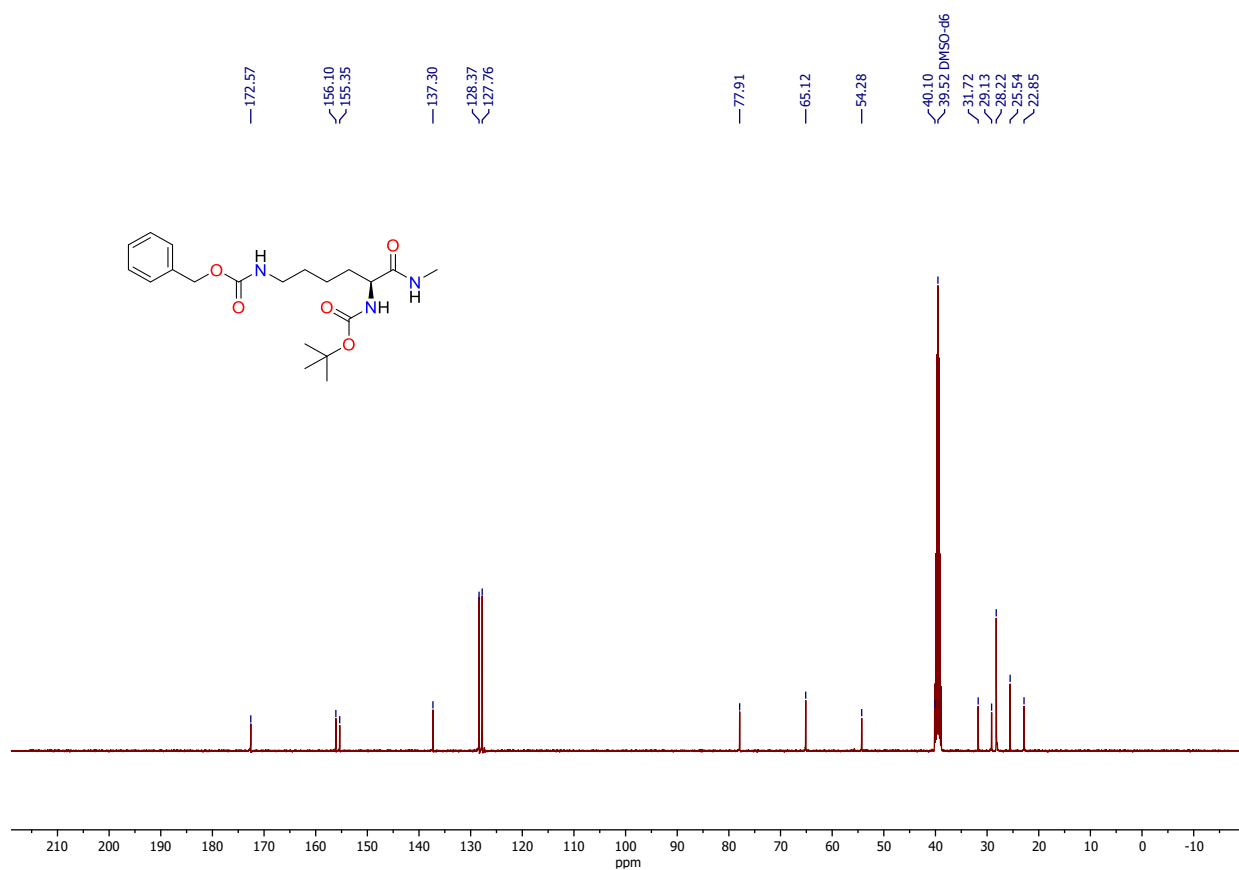


Fig. S172. ¹³C NMR spectra of N-Boc-Lys(Cbz)-NMe (Z-2g), DMSO-*d*₆, 101 MHz.

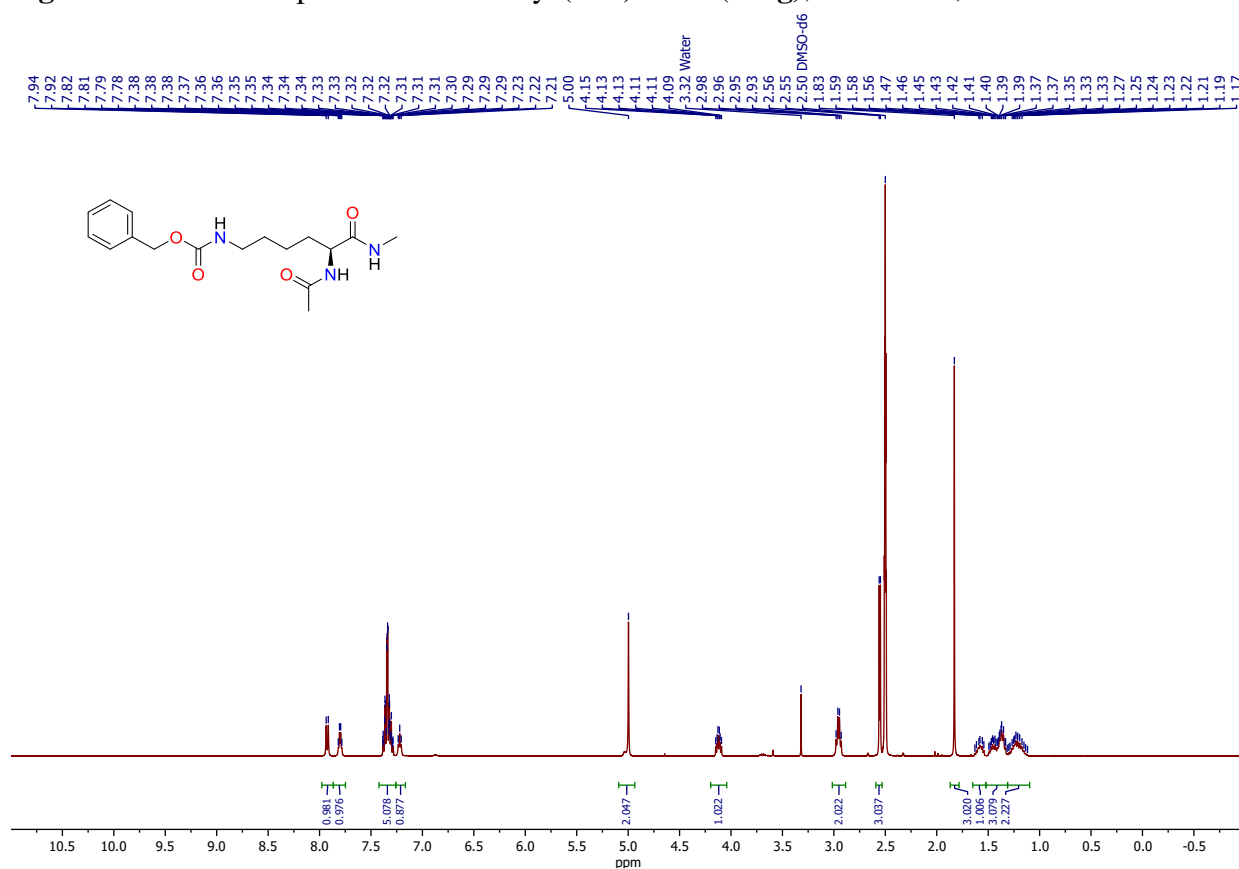


Fig. S173. ¹H NMR spectrum of N-Ac-Lys(Cbz)-NMe (Z-2g'), DMSO-*d*₆, 400 MHz.

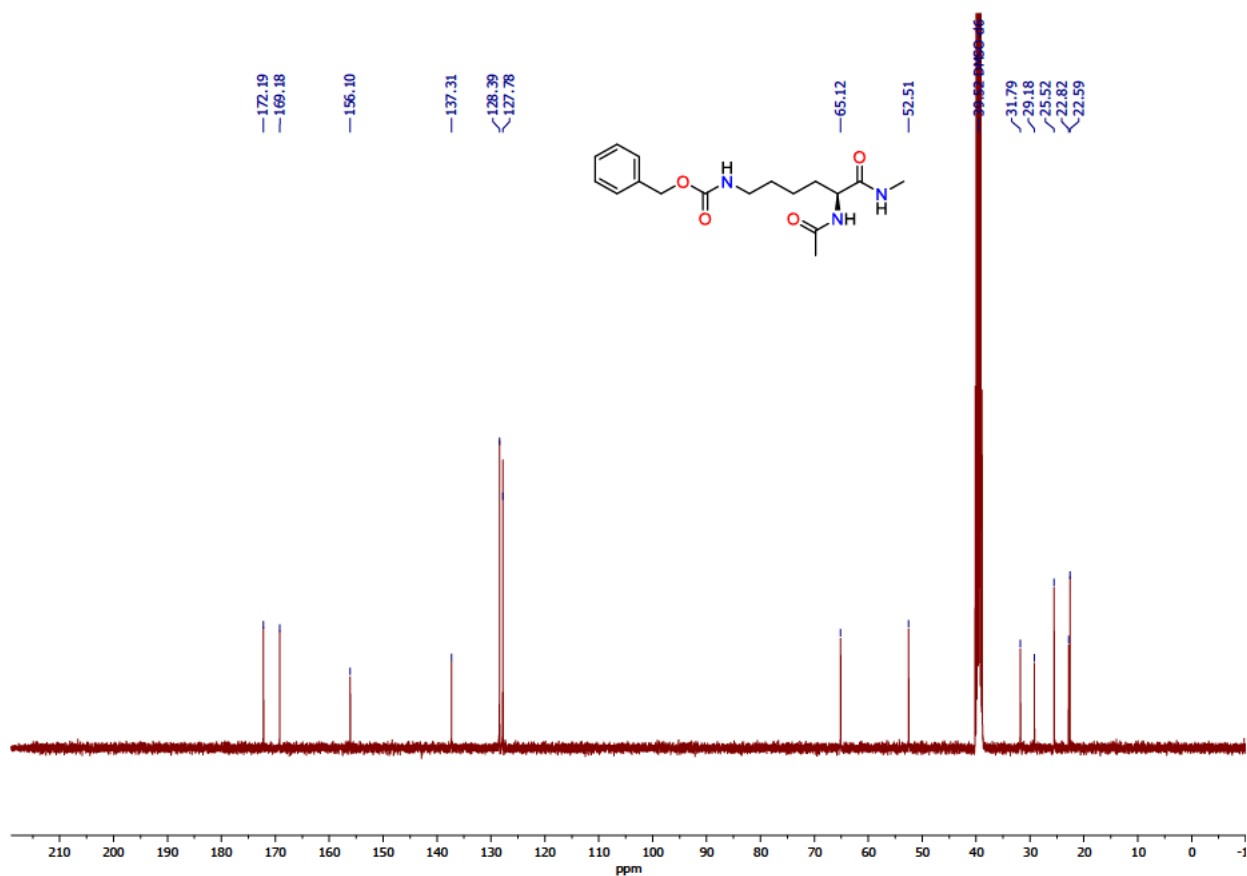


Fig. S174. ^{13}C NMR spectrum of N-Ac-Lys(Cbz)-NMe (**Z-2g'**), DMSO- d_6 , 400 MHz.

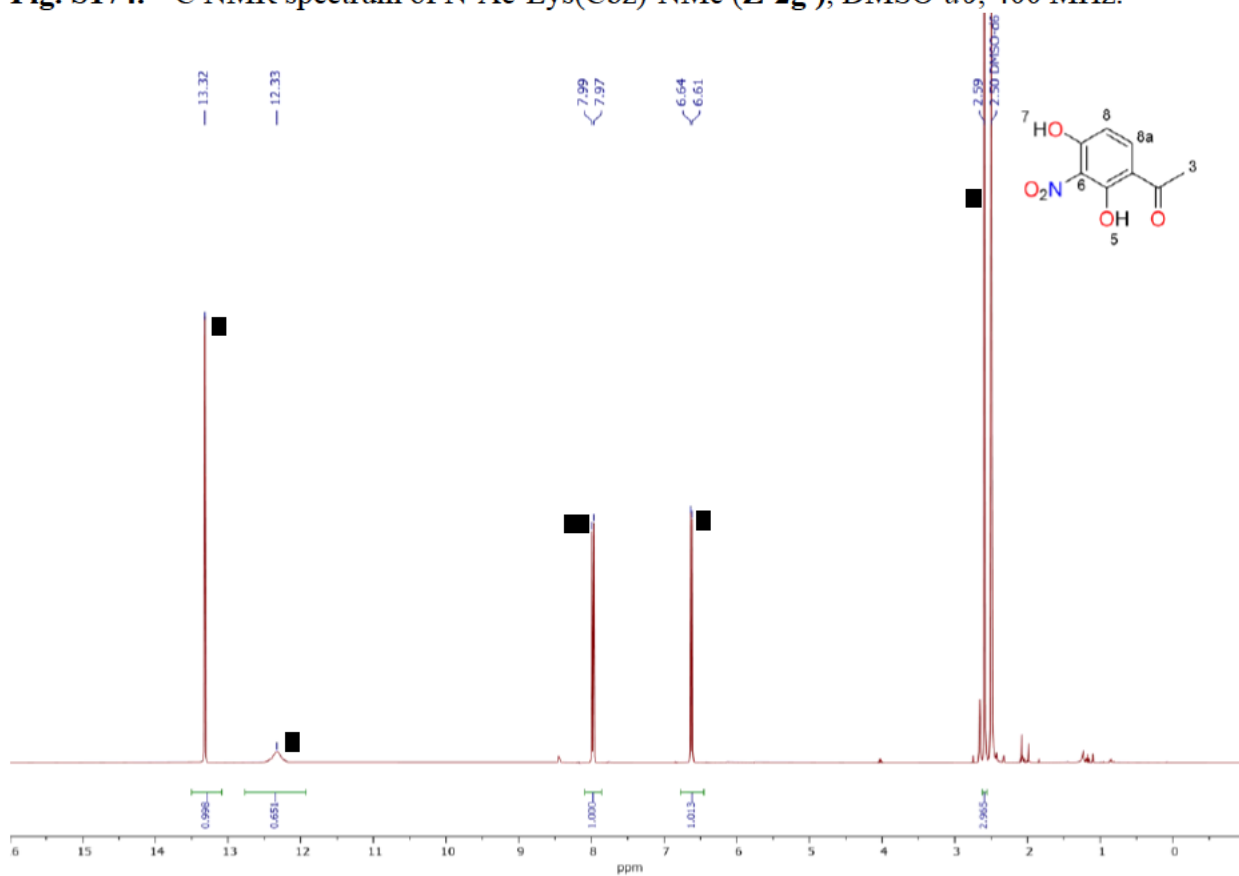


Fig. S175. ^1H NMR spectrum of **7b-NO2**, DMSO- d_6 , 400 MHz.

1.3.7.14. References

- [1] N. F. Brás, S. S. Ashirbaev, H. Zipse, *Chem. Eur. J.* **2022**, 28, e202104240.
- [2] G. Milordini, E. Zacco, M. Percival, R. Puglisi, F. Dal Piaz, P. Temussi, A. Pastore, *Front. Mol. Biosci.* **2020**, 7, 1-13.
- [3] I.-H. Um, E. Y. Kim, H.-R. Park, S.-E. Jeon, *J. Org. Chem.* **2006**, 71, 2302-2306.
- [4] H. K. Hall, Jr., *J. Am. Chem. Soc.* **1957**, 79, 5441-5444.
- [5] R. B. Martin, A. Parcell, R. I. Hedrick, *J. Am. Chem. Soc.* **1964**, 86, 2406-2413.
- [6] Z. Feng, J. Zhou, X. Shang, G. Kuang, J. Han, L. Lu, L. Zhang, *Pharm. Biol.* **2017**, 55, 1177-1184.
- [7] J. M. Herrero-Martínez, M. Sanmartin, M. Rosés, E. Bosch, C. Ràfols, *ELECTROPHORESIS* **2005**, 26, 1886-1895.
- [8] a) I. Miroshnyk, S. Mirza, N. Sandler, *Expert Opin. Drug. Deliv.* **2009**, 6, 333-341; b) G. Bolla, A. Nangia, *Chem. Commun.* **2016**, 52, 8342-8360.
- [9] S. Chatteraj, L. Shi, C. C. Sun, *CrystEngComm* **2010**, 12, 2466-2472.
- [10] C. C. Sun, H. Hou, *Cryst. Growth Des.* **2008**, 8, 1575-1579.
- [11] M. LARGERON, M.-B. Fleury, *Angew. Chem. Int. Ed.* **2012**, 51, 5409-5412.
- [12] S. Saito, J. Kawabata, *Tetrahedron* **2005**, 61, 8101-8108.
- [13] G. Baisch, B. Wagner, R. Öhrlein, *Tetrahedron* **2010**, 66, 3742-3748.
- [14] M. K. Srinatha, S. Poppe, G. Shanker, M. Alaasar, C. Tschierske, *J. Mol. Liq.* **2020**, 317, 114244.
- [15] J. K. Augustine, A. Bombrun, R. N. Atta, *Synlett* **2011**, 2011, 2223-2227.
- [16] X. Qin, L. Yang, P. Liu, L. Yang, L. Chen, L. Hu, M. Jiang, *Bioorg. Chem.* **2021**, 110, 104743.
- [17] a) C. Li, T. Chen, B. Li, G. Xiao, W. Tang, *Angew. Chem. Int. Ed.* **2015**, 54, 3792-3796; b) M. Matsumoto, K. Kobayashi, Y. Hotta, *J. Org. Chem.* **1984**, 49, 4740-4741.
- [18] K. Ishikawa, K. Takahashi, S. Hosoi, H. Takeda, H. Yoshida, D. Wakana, M. Tsubuki, F. Sato, M. Tojo, T. Hosoe, *J. Antibiot.* **2019**, 72, 71-78.
- [19] M. Satyanarayana, P. Tiwari, B. K. Tripathi, A. K. Srivastava, R. Pratap, *Biorg. Med. Chem.* **2004**, 12, 883-889.
- [20] Y. Huang, G. Sun, P. Wang, R. Shi, Y. Zhang, X. Wen, H. Sun, C. Chen, *Bioorg. Med. Chem. Lett.* **2018**, 28, 2957-2960.
- [21] B. B. Park, J. W. Choi, D. Park, D. Choi, J. Paek, H. J. Kim, S.-Y. Son, A. U.

- Mushtaq, H. Shin, S. H. Kim, Y. Zhou, T. Lim, J. Y. Park, J.-Y. Baek, K. Kim, H. Kwon, S.-H. Son, K. Y. Chung, H.-J. Jeong, H.-M. Kim, Y. W. Jung, K. Lee, K. Y. Lee, Y. Byun, Y. H. Jeon, *Sci. Rep.* **2019**, *9*, 8762.
- [22] H. Gao, J. Kawabata, *Biorg. Med. Chem.* **2005**, *13*, 1661-1671.
- [23] Z.-P. Xiao, Z.-Y. Peng, J.-J. Dong, J. He, H. Ouyang, Y.-T. Feng, C.-L. Lu, W.-Q. Lin, J.-X. Wang, Y.-P. Xiang, H.-L. Zhu, *Eur. J. Med. Chem.* **2013**, *63*, 685-695.
- [24] M. Y. Zhang, R. A. Barrow, *Org. Lett.* **2017**, *19*, 2302-2305.
- [25] L. K. Tsou, M. Lara-Tejero, J. RoseFigura, Z. J. Zhang, Y.-C. Wang, J. S. Yount, M. Lefebvre, P. D. Dossa, J. Kato, F. Guan, W. Lam, Y.-C. Cheng, J. E. Galán, H. C. Hang, *J. Am. Chem. Soc.* **2016**, *138*, 2209-2218.
- [26] J. Hierold, S. Baek, R. Rieger, T.-G. Lim, S. Zakpur, M. Arciniega, K. W. Lee, R. Huber, L. F. Tietze, *Chem. Eur. J.* **2015**, *21*, 16887-16894.
- [27] J.-N. Yang, J.-Y. Yang, J. Cao, X.-Q. Zhou, W. Mian, Y. Hui, W.-H. Chen, *Chem. Nat. Compd.* **2020**, *56*, 539-541.
- [28] H. Gao, J. Kawabata, *Biosci. Biotechnol. Biochem.* **2004**, *68*, 1858-1864.
- [29] L. Samulis, N. C. O. Tomkinson, *Tetrahedron* **2011**, *67*, 4263-4267.
- [30] T. Morack, C. Mück-Lichtenfeld, R. Gilmour, *Angew. Chem. Int. Ed.* **2019**, *58*, 1208-1212.
- [31] D. M. Shendage, R. Fröhlich, G. Haufe, *Org. Lett.* **2004**, *6*, 3675-3678.
- [32] A. R. Ekkati, A. A. Campanali, A. I. Abouelatta, M. Shamoun, S. Kalapugama, M. Kelley, J. J. Kodanko, *Amino Acids* **2010**, *38*, 747-751.
- [33] S. Zhang, R. Wang, Y. Zhao, F. S. Tareq, S. Sang, *Chem. Res. Toxicol.* **2020**, *33*, 2181-2188.
- [34] R. F. Sweis, Z. Wang, M. Algire, C. H. Arrowsmith, P. J. Brown, G. G. Chiang, J. Guo, C. G. Jakob, S. Kennedy, F. Li, D. Maag, B. Shaw, N. B. Soni, M. Vedadi, W. N. Pappano, *ACS Med. Chem. Lett.* **2015**, *6*, 695-700.
- [35] D. Xu, A. Chiaroni, M.-B. Fleury, M. LARGERON, *J. Org. Chem.* **2006**, *71*, 6374-6381.
- [36] R. Pasceri, D. Siegel, D. Ross, C. J. Moody, *J. Med. Chem.* **2013**, *56*, 3310-3317.

2. Dipeptide C-H Bond Reactivity and Selectivity in Hydrogen Atom Transfer to Alkoxy Radicals

Salavat S. Ashirbaev^a, Harish Jangra^a, Michela Salamone^b, Massimo Bietti^b, Hendrik Zipse^a

^a*Dept. Chemistry, LMU Muenchen, Butenandtstrasse 5-13, D-81377 Muenchen, Germany*

^b*Dipartimento di Scienze e Tecnologie Chimiche, Università "Tor Vergata", Via della Ricerca Scientifica, 1, I-00133 Rome, Italy*

Authors contribution:

All experiments were performed by Salavat S. Ashirbaev, Julie Van Hooste (for substrate **1b**)/Andreas Neuer (synthesis of **13a/b**) under the supervision of Salavat S. Ashirbaev, all the calculations were performed by Harish Jangra. The laser flash photolysis experiments were performed with a help of Professor Massimo Bietti and Professor Michela Salamone. The manuscript is written together by Salavat S. Ashirbaev and Hendrik Zipse.

2.1. Introduction

Hydrogen atom transfer (HAT) from peptide units to free radical species is a critical event, which can lead to backbone fragmentation, side chain functionalization or cross-linking reactions of proteins. As a result, proteins undergo significant structural changes and loss of important functions.^[1] It has been shown that these processes induce cellular damage, and as a consequence free radical species have been implicated in some pathological conditions.^[2] Also, HAT processes from amino acids can lead to the modification or even selective functionalization of protein building blocks, which can be useful in different biochemical investigations. A lot of effort has been applied to understand HAT processes from peptides using protected and unprotected amino acids or oligopeptides as simple models of protein moieties due to the complexity of natural substrates. Among the different species used in this kind of studies, oxygen-centered radicals gained a lot of attention. The most popular ones are *t*-butoxyl (*t*-BuO•) and cumyloxyl (CumO•) radicals due to their ease of generation under UV conditions from available peroxides.^[3] For example, time-resolved kinetic studies on the reactions of CumO• with different secondary amides have been performed, which showed that the main HAT process occurs from *N*-alkyl side chain, instead of the acyl moiety (Table 1).^[3c, 3d]

Table 1. Relative rates for HAT processes from secondary amides to CumO•.^[3c, 3d]

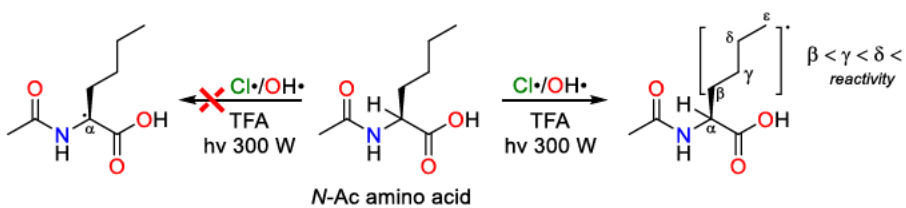
Reaction scheme: N-alkyl amide + CumO• $\xrightarrow[\text{266 nm, 25 }^\circ\text{C}]{\text{MeCN}}$ N-alkyl amide radical + CumOH. The amide hydrogen is labeled as 'susceptible to HAT'.

N-Alkyl amides								
	MA	EA	iPrA	tBuA	MPVA	EPVA	iPrPVA	tBuPVA
$k_{\text{H}}(\text{MA})/$ $k_{\text{H}}(\text{N-alkyl})^{\text{a}}$	1.0	0.5	2.0	17.7	1.0	0.6	5.2	>30

To approach the reactivity of real peptide systems, various amino acid derivatives were treated with wide scope of radical species. A series of amino acids were photolyzed in Cl_2 -saturated trifluoroacetic acid (Table 2).^[4] It has been shown, •Cl/•OH tend to abstract hydrogen from the distant, γ , δ , ϵ , positions on the alkyl chain of free and *N*-acetyl α -amino acids neither from backbone α - or adjacent β -positions (Table 2, Entry 1). The results have

been attributed to the repulsion of the incoming chlorine radical from carboxyl, protonated amino and acetoamido moieties of the amino acids.

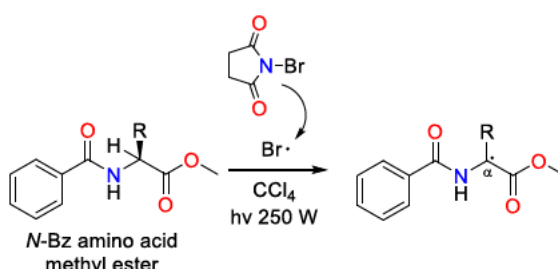
Table 2. Relative rate constants for reaction of the $\bullet\text{Cl}$ and $\bullet\text{OH}$ with different α -amino acids.^[4]



	Ac-Gly-OH	Ac-Ala-OH	Ac-Abu-OH	Ac-Val-OH	Ac-Tle-OH	Ac-Leu-OH	Ac-Nle-OH
$k_{\text{Rel}}(\bullet\text{Cl})$	1.0	0.25	5.5	8.75	11.25	47.5	55.0
$k_{\text{Rel}}(\bullet\text{OH})$	1.0	1.1	4.0	3.7	4.3	9.1	10.3

$\bullet\text{Br}$ radicals, in contrast, abstract hydrogen atoms directly from the α -position of amino acid derivatives. The relative reactivity of the Bz- α -amino acid methyl esters decrease as the size of the side chain increases (Table 3). The steric effects can be illustrated using *t*-leucine (Bz-Tle-OMe), which is fully resistant to radical formation.^[5]

Table 3. Relative rate constants for the reaction of $\bullet\text{Br}$ radicals with different Bz α -amino acids methyl esters.^[5]

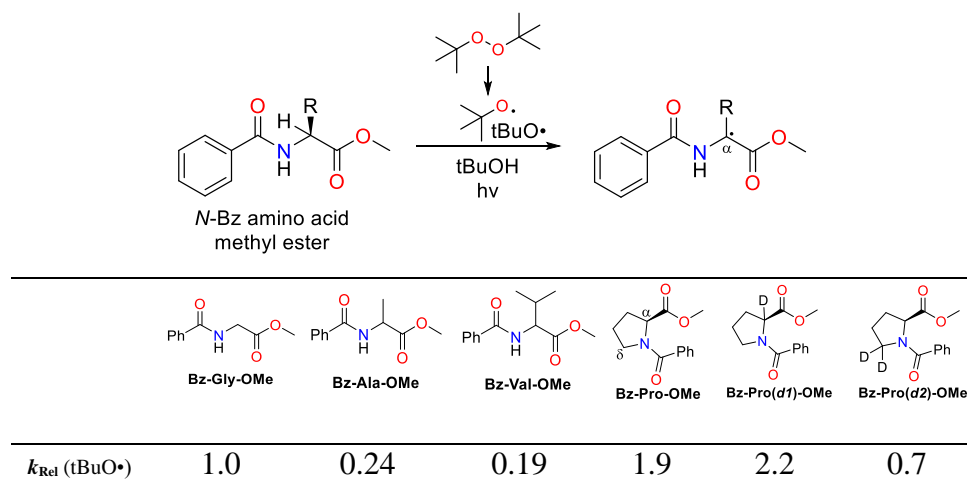


	Bz-Gly-OMe	Bz-Gly(d2)-OMe	Bz-Ala-OMe	Bz-Val-OMe	Bz-Tle-OMe	Bz-Pro-OMe	Bz-Pro(d1)-OMe	Bz-Pro(d2)-OMe
$k_{\text{Rel}}(\bullet\text{Br})$	1.0	0.32	0.33	0.04	<0.0004	1.4	1.2	0.42

Surprisingly, proline derivative Bz-Pro-OMe was more reactive than the corresponding glycine derivative. In deuterium labelling experiment it was shown that α -labelling has a minor effect on the reactivity of proline, while δ -labelling significantly slows down the

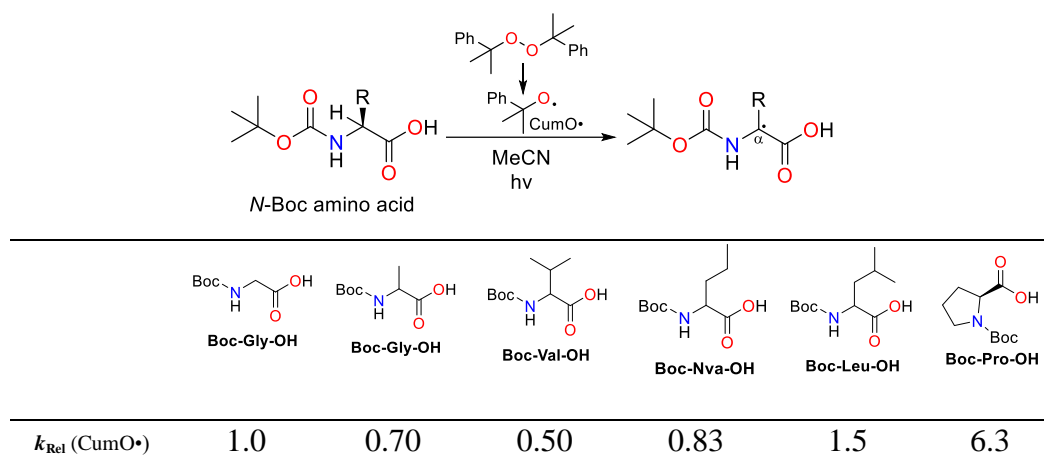
reactivity. The results suggests that main HAT process in proline occurs at the δ -position. Similar reactivity patterns of amino acid derivatives were obtained for tBuO• radicals, indicating that the HAT reaction also takes place at C $_{\alpha}$ -position (Table 4).^[5b]

Table 4. Relative rate constants for reaction of the tBuO• with different Bz α -amino acids methyl esters.^[5b]



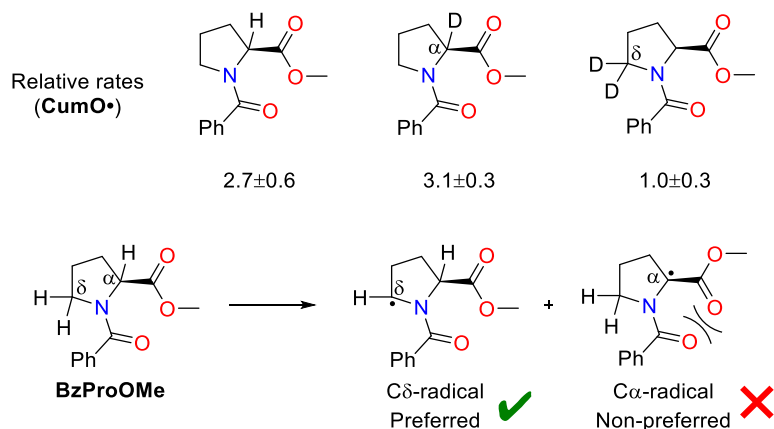
Studies on HAT from *N*-Boc α -amino acids to CumO•, which was generated under laser flash photolysis (LFP) conditions, showed that also HAT occurs from the C $_{\alpha}$ -position (Table 5). Also, like in the previous results, increased reactivity was obtained for proline derivative (6-fold increase from glycine to proline).^[3b]

Table 5. Relative rate constants for reaction of the CumO• with different *N*-Boc α -amino acids.^[3b]



It was found that deuteration at the α -position did not affect the HAT rates to CumO•, while deuteration of the δ -position significantly lowered the reactivity (by a factor of 3, Scheme 1).

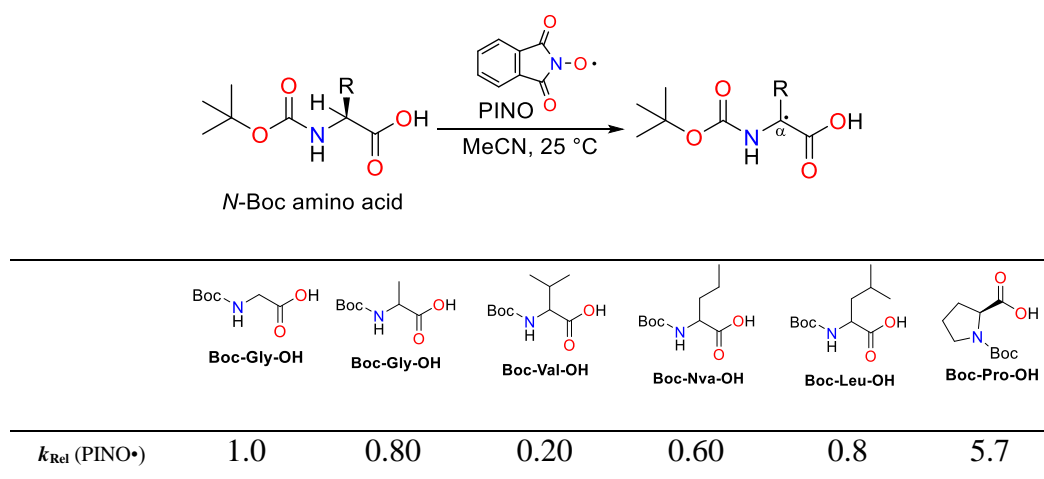
It was attributed to the constrained structure of the resulting C α -radical, which is a highly unfavorable process. These findings suggest that the primary process of HAT occurs at the δ -position rather than the α -position, as it was stated in the results with tBuO• radicals.^[3b]



Scheme 1. HAT from Bz-Pro-OMe derivatives to CumO• radical.

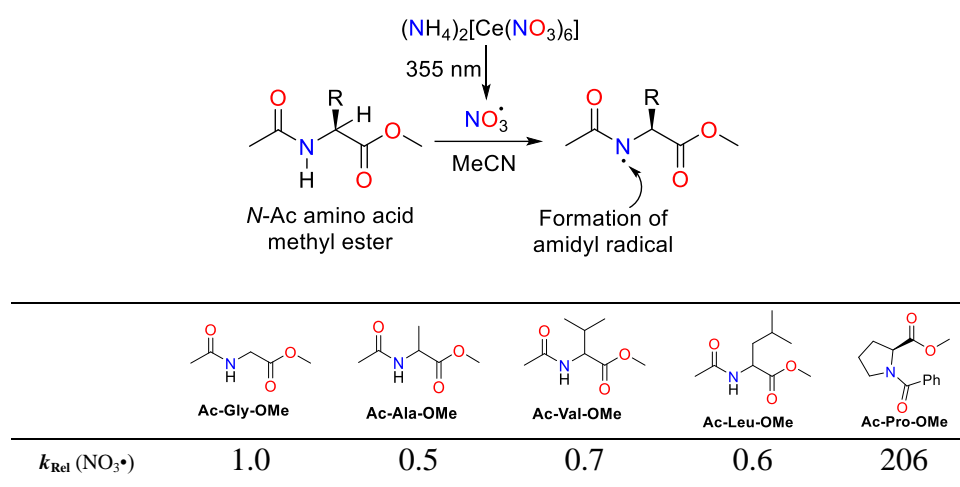
Studies which involve another similar sort of oxygen species, phthalimide *N*-oxyl (PINO) radicals, can be found in the literature (Table 6).

Table 6. Relative rate constants for reaction of PINO• radicals with different *N*-Boc α -amino acids.^[6]



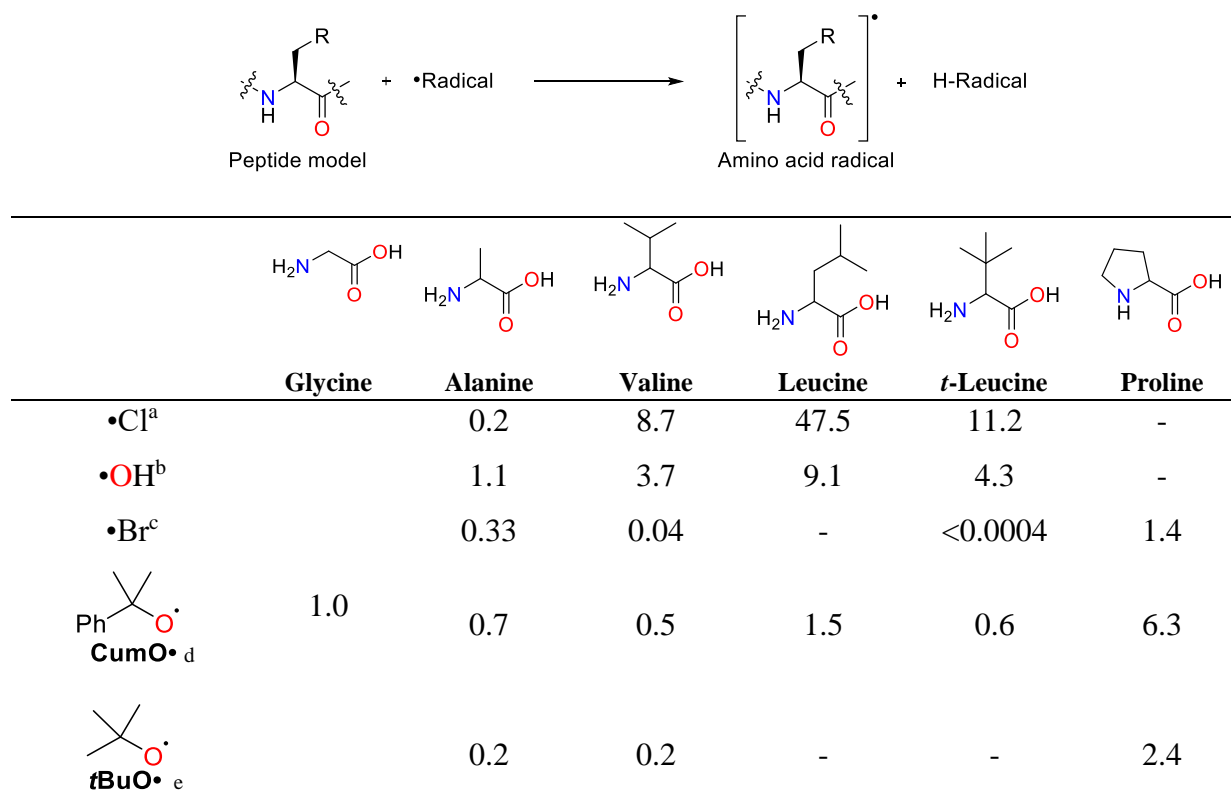
Oxidation of different peptide models has been investigated with nitrate radical, •NO₃, under laser flash photolysis conditions. These studies showed that •NO₃ is strong enough to abstract hydrogen not only from the C α - or activated side chain positions, but also from the amide *N*-H bond (Table 7).^[7] In this case, the proline derivative is 2-3 magnitudes more reactive toward •NO₃ than acyclic *N*-Ac amino acids.

Table 7. Relative rate constants for reaction of NO_3^\bullet with different *N*-Boc α -amino acid methyl esters.^[7]



Based on a comprehensive review of the literature, it has been shown that glycine and proline amino acid derivatives have the highest rates of oxidation by different radicals. This observation suggests that these residues are particularly prone to undergo radical-mediated modifications in real peptides. A short summary of the amino acid reactivities to various radicals is represented in Table 8.

Table 8. Relative rates for HAT processes from amino acids to different radical species.





	0.8	0.2	0.8	0.1	5.7
$\bullet\text{NO}_3^g$	0.5	0.7	0.6	-	206

^a *N*-acetyl α -amino acids, Cl_2 in TFA, for 1-20 min under 300W sunlamp.^[4]

^b *N*-acetyl α -amino acids, D_2O_2 in TFA, for 20-60 min under 254 nm lamp.^[4]

^c *N*-Bz α -amino acid methyl esters, NBS in CCl_4 , reflux for 9h under 300W sunlamp.^[5]

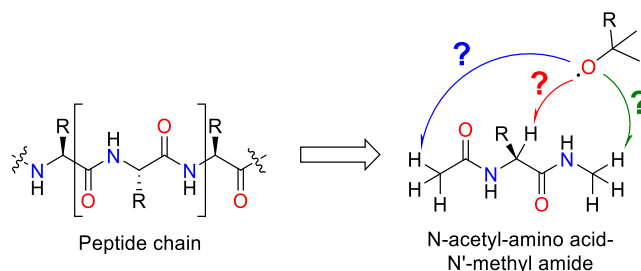
^d *N*-Boc α -amino acids, dicumyl peroxide in MeCN, 266 nm laser flash photolysis, $T = 25^\circ\text{C}$.^[3b]

^e *N*-Bz α -amino methyl esters, di-*tert*-butyl peroxide in *t*BuOH, reflux under 350 nm lamp.^[5b]

^f *N*-Boc α -amino acids, *N*-hydroxyphthalimide, cerium (IV) ammonium nitrate in MeCN, $T = 25^\circ\text{C}$.^[6]

^g *N*-Boc α -amino acid methyl esters, cerium (IV) ammonium nitrate, 355 nm laser flash photolysis, MeCN, $T = 25^\circ\text{C}$.^[7]

Although this literature review provides valuable information about various amino acids, reaction constants, and general patterns of radical oxidation, our work focuses on the radical oxidation of specific substrates without light excitation at mild temperatures (23°C). Additionally, while previous studies may have only examined the reactivity of the C_α -center or *N*-terminal part of the peptide separately, our dipeptide model incorporates two reactive centers, similar to those found in real peptide chains (Scheme 2).



Scheme 2. *N*-acetyl-amino acid-*N'*-methyl amide is a model substrate for oxidative stress.

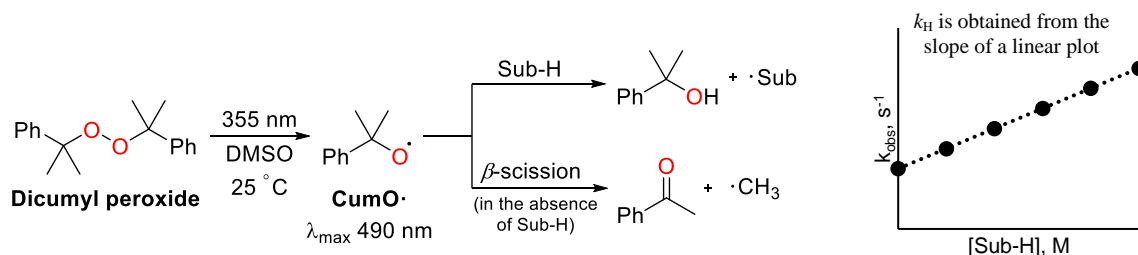
2.2. Results and Discussions

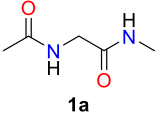
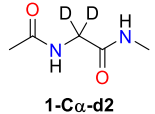
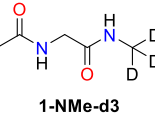
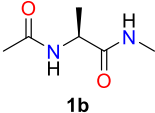
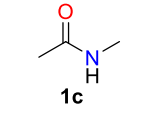
2.2.1. Laser Flash Photolysis Experiments

To understand the HAT process to cumyloxyl radical, $\text{CumO}\bullet$, LFP experiments were performed with AcGlyNMe (**1a**) and its derivatives. First attempts to perform the LFP measurements in MeCN were unsuccessful because of the limited solubility of dipeptide **1a** and its deuterated derivatives. Second order rate constants were obtained in DMSO as an alternative solvent. $\text{CumO}\bullet$ was generated by 355 nm laser irradiation of argon-saturated dicumyl peroxide solutions at 25°C . In the presence of hydrogen atom donor substrates (S-H), there is a competition process between β -scission and HAT as described in Table 9. The time-resolved kinetic studies were performed monitoring the decay of the $\text{CumO}\bullet$ visible band at 490 nm as a function of the concentration of added substrate. When the observed rate

constants (k_{obs}) were plotted against substrate concentration, excellent linear relationships were observed and the second-order rate constants for HAT to CumO^\bullet (k_{H}) were derived from the slopes of these plots. The k_{obs} vs [substrate] plots for the reactions of CumO^\bullet with dipeptide models **1a**, **1-C α -d2**, **1-NMe-d3**, AcAlaNMe (**1b**) and AcNMe (**1c**), as the simplest peptide model, measured in DMSO solution are shown in Table. 9.

Table 9. Second order rate constants (k_{H}) for reaction of the cumyloxyl radical (CumO^\bullet) with different peptide models, measured in DMSO at $T = 25^\circ\text{C}^a$.



No	Substrate	$k_{\text{H}} \times 10^5 / \text{M}^{-1} \text{s}^{-1}$	$k_{\text{H}}(\text{Relative})$
1	 1a	7.70 ± 0.37	1.00
2	 1-Cα-d2	4.53 ± 0.16	0.59
3	 1-NMe-d3	4.64 ± 0.18	0.60
4	 1b	3.39 ± 0.07	0.44
5	 1c	5.31 ± 0.06	0.69

^a CumO^\bullet has been generated by 355 nm LFP of argon saturated DMSO solutions ($T = 25^\circ\text{C}$) containing 1.0 M dicumyl peroxide. The k_{H} values have been obtained from the slope of the k_{obs} vs [substrate] plots where in turn, the k_{obs} values have been obtained following the decay of the CumO^\bullet visible absorption band ($\lambda_{\text{max}} = 490 \text{ nm}$) at the different substrate concentrations.

For the reference compound AcGlyNMe (**1a**) the second-order rate constants for HAT to CumO^\bullet is $k_{\text{H}}(\mathbf{1a}) = (7.70 \pm 0.37) \times 10^5 \text{ M}^{-1} \text{ s}^{-1}$, in comparison, $k_{\text{H}}(\text{BocGlyOH}) = (2.80 \pm 0.10) \times 10^5 \text{ M}^{-1} \text{ s}^{-1}$.^[3b] Decreased k_{H} values for deuterated samples were obtained because of the primary kinetic isotope effect. For example, the derivative with deuterated C α -

position, **1-C α -d2**, is 1.7 times less active than dipeptide **1a**. Surprisingly, **1-NMe-d3** shows the same reactivity as **1-C α -d2**. Addition of a methyl group to the C α -position as in AcAlaNMe (**1b**), decreases the reactivity even more. Dipeptide **1a** is 2.3 times more reactive than dipeptide **1b** but in this case 2-fold increase can be explained on the basis of the twofold higher number of C α -hydrogen bonds in **1a**. The simplest peptide bond model, *N*-methyl acetamide (**1c**), shows slightly higher reactivity towards CumO• than deuterated samples, **1-C α -d2**, **1-NMe-d3**.

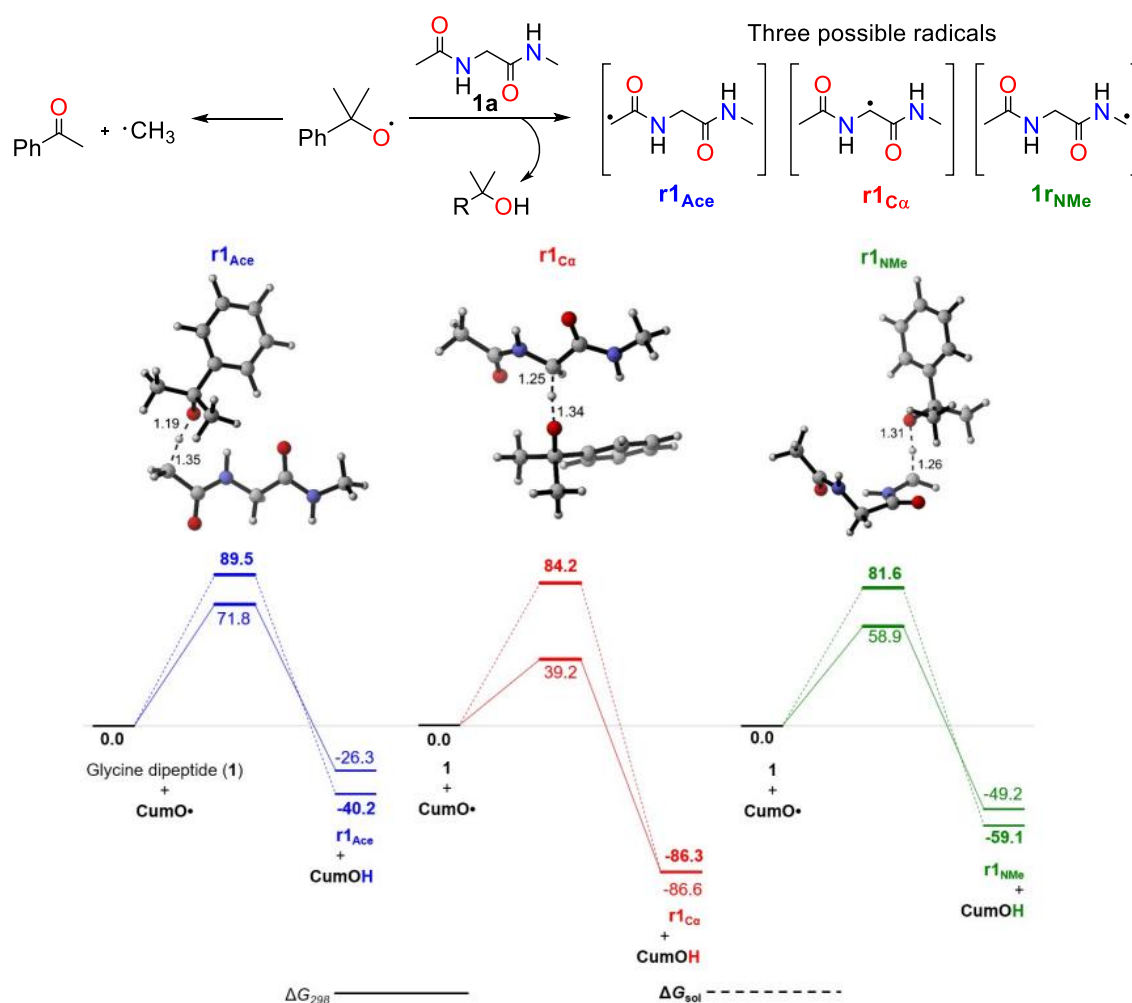


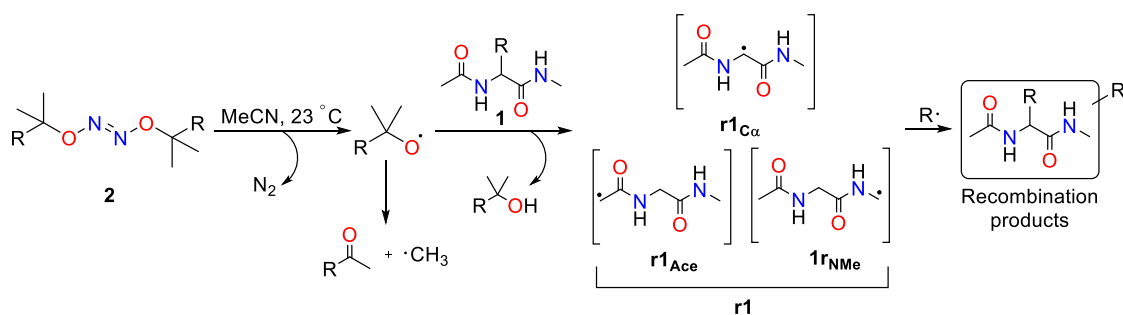
Fig. 1. Gas (ΔG_{298}) and solution phase (ΔG_{sol}) free energy surfaces (in kJ/mol) for hydrogen abstraction reaction from different carbon centres of **1a** calculated at G3(MP2)-RAD level of theory. Solvation energies are obtained at the PCM(acetonitrile)/HF/6-31G(d)/(U)B3LYP/6-31G(d) level of theory. Distances are given in Å. [A permission was obtained from the author of this image, Dr. Harish Jangra, to include it in this work]

Summing up the results, two active sites of the model compound **1a**, C α - and NMe-positions, have the same tendency for HAT to CumO• in DMSO at 25 °C. To explain the reactivity,

theoretical calculations of the reaction barriers have been performed for all three positions in substrate **1a** in their reaction with CumO radicals (Fig. 1). Once the CumO radical is formed, it can abstract hydrogen from three different positions, forming three distinct dipeptide radicals (Fig. 1). It has been demonstrated that abstraction from the C α center shows the lowest energy barrier (+39.2 kJ/mol) and is also the most exergonic (-86.6 kJ/mol). HAT from the NMe-moiety is higher (+58.9 kJ/mol) and less exergonic (-49.2 kJ/mol), while abstraction from the acyl group, as expected, is the least favorable HAT process (+71.8 kJ/mol, -26.3 kJ/mol). The gas phase calculations indicate that the C α -H bond is the weakest in the system and the most preferable for HAT by CumO. To estimate the solvent effect, the gas phase free energies were corrected using single-point solvation energy calculations. These calculations showed that the solvent, acetonitrile, described by the polarizable continuum model (PCM), significantly destabilizes the transition states relative to the reactants/products in such a way that now the abstraction from the NMe-moiety becomes slightly more favorable (+81.6 kJ/mol) compared to the HAT from the C α -position (+84.2 kJ/mol). It suggests that the hydrogen abstraction by CumO radical from the NMe-moiety has nearly the same rate as abstraction from the C α -center of dipeptide **1a**. These calculations are in agreement with the LFP experiments, since the experiments with selective site deuteration demonstrate that the rate of HAT from the C α -center is nearly the same as the HAT rate from the NMe-site of **1a**. (4.64 vs 4.53 $\times 10^5$ M $^{-1}$ s $^{-1}$, Table 9, Entries 2 and 3).

2.2.2. Hydrogen Abstraction Reaction from Glycine and Alanine Dipeptide Models

In an attempt to investigate the reaction that occurs during the LFP experiments, but without laser excitation of the model systems, alkyl hyponitrites **2** were chosen as good alternative, since they are well-known low-temperature alkoxy radical sources.^[8] (Scheme 3)

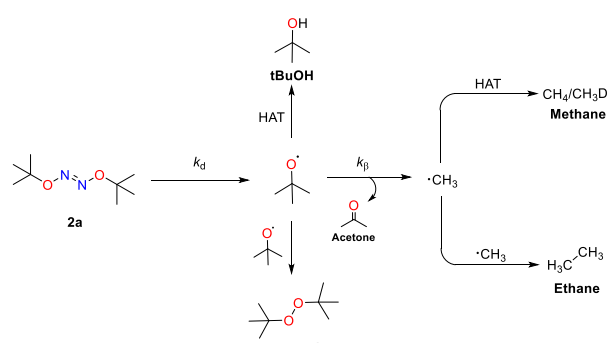


Scheme 3. Low temperature dipeptide model oxidation using alkyl hyponitrites **2**.

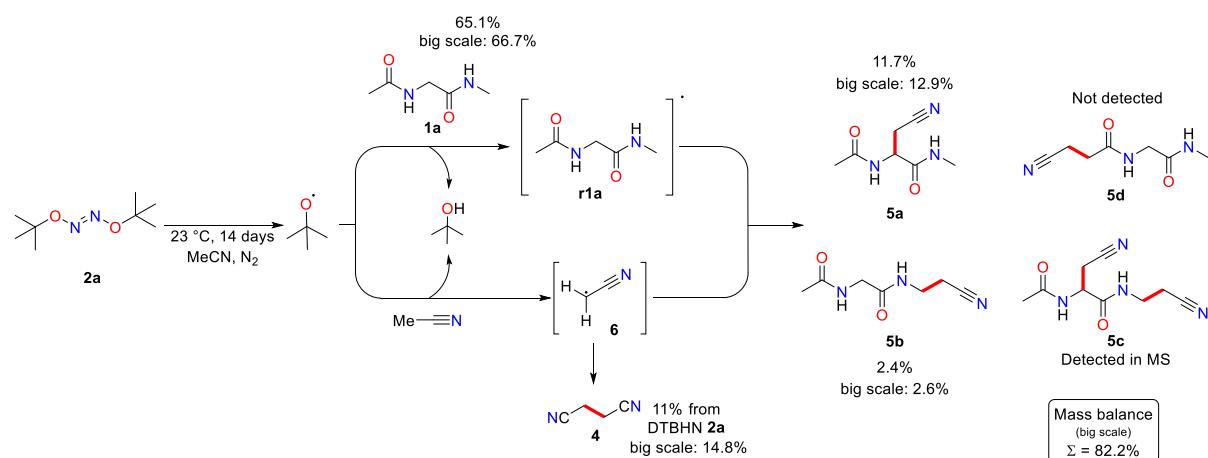
This approach opens the pathway to study the oxidative stress reactions through the analysis and characterization of the final recombination products of the formed dipeptide radicals **r1**. Due to its lower risk of explosion and established synthesis procedure, di-tert butyl hyponitrite (**2a**, DTBHN) was chosen as a model oxidant in our research. Since no information is available on its decomposition in solvents like MeCN, which is suitable not only for dissolving our dipeptide model, but also for column purification afterwards, the decomposition rates of **2a** and the decomposition products were initially determined using ¹H NMR analysis (Table 10).

Table 10. Decomposition rates of hyponitrite **2a** in MeCN-*d*3 at different temperatures.

First-order reaction rate law		
$v = k_d \times [2a]$		
T, °C	k_d , s ⁻¹	$\tau_{1/2}$, s (h)
65	$(2.32 \pm 0.17) \times 10^{-4}$	2994 (0.83)
40	$(7.38 \pm 0.34) \times 10^{-6}$	94102 (26.1)
23	$(0.675 \pm 0.52) \times 10^{-6}$	1031210 (286.4)
E_a , kJ	122.3 ± 3.2	



After DTBHN (**2a**) decomposition kinetic studies, a small-scale oxidative stress reaction was performed with 0.1 M concentration of AcGlyNMe (**1a**) and oxidant **2a** at 23 °C in dry degassed MeCN under N₂ atmosphere (no light exposure). Within 14 days, ~50% of DTBHN (**2a**) decomposes under these conditions. The oxidative stress reaction of dipeptide **1a** leads to formation of unknown white precipitate **3**, whose separation was unsuccessful due to its low amount and fine dispersion. Product analysis shows that a major part of crude material consists of recovered dipeptide **1a** (65.1%, Scheme 4).

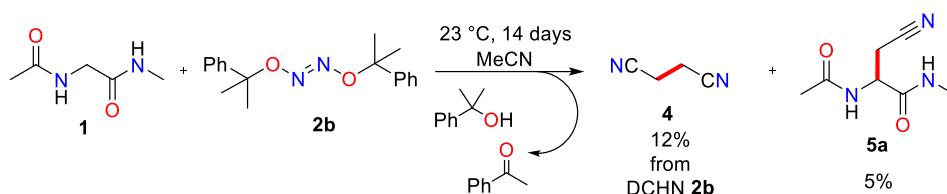


Scheme 4. Oxidative stress of AcGlyNMe (**1a**) with DTBHN (**2a**) for 14 days in MeCN.

GC-FID and ^1H NMR analysis show the formation of succinonitrile **4** (11% from DTBHN **2a**), the main oxidation products **5a** (11.7%) and **5b** (2.4%), adducts of cyanomethylation of initial dipeptide model **1a** at C_α and N -Me positions, correspondingly.

Also, MS analysis of crude material shows a trace amount of adduct **5c**, the double cyanomethyl functionalization of initial dipeptide **1**. This implies that acetonitrile acts as a hydrogen donor towards alkoxy radicals giving cyanomethyl radical **6**. It is well-known that cyanomethyl radical is a useful building block in wide range of organic reactions.^[9] As expected, the cyanomethylation adduct **5d** was not detected, indicating that the HAT process at the acetyl group moiety of **1a** is highly unfavorable.

After performing the reaction with di-cumyl hyponitrite (**2b**, DCHN), a white precipitate was formed again, and analysis of the supernatant showed that most of the crude material was the recovered dipeptide **1a**, with only a small part being oxidized during the reaction. The only oxidation products detected were compound **5a** (5%) and succinonitrile **4** (12%) (Scheme 5).

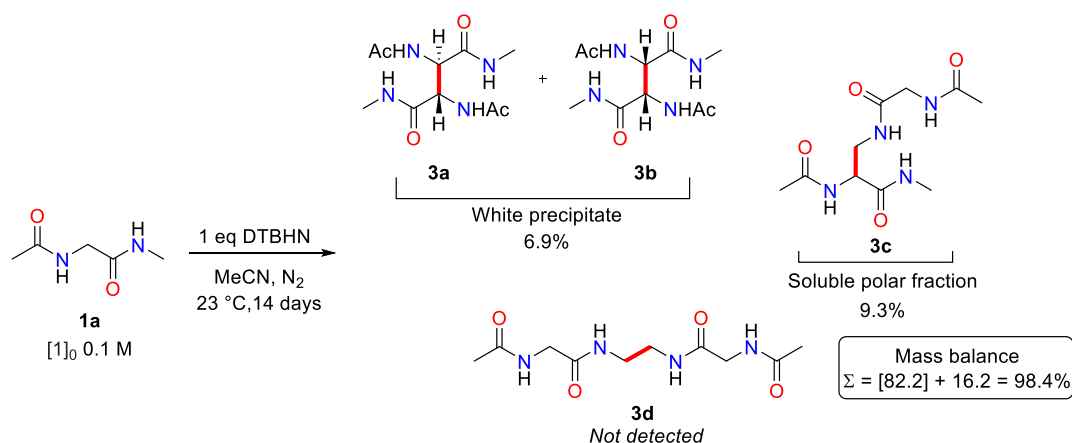


Scheme 5. Oxidative stress of AcGlyNMe (**1a**) with DCHN (**2b**) for 14 days in MeCN.

The lower yield observed can be attributed to the properties of the alkoxy radicals formed in the reaction mixture. Rates of HAT process acetonitrile to $\text{CumO}\cdot$ and its β -scission have been measured at 20 °C, $k_{s(\text{obs})}$, $\text{CumO}\cdot = 2.4 \times 10^5 \text{ s}^{-1}$ (pseudo first order) and β -scission rate, k_{β} , $\text{CumO}\cdot$, is $3.6 \times 10^5 \text{ s}^{-1}$, correspondingly.^[10] While formed $t\text{BuO}\cdot$ is more stable and has life time, k_{β} , $t\text{BuO}\cdot$, is $6.4 \times 10^4 \text{ s}^{-1}$ at 22 °C and k_{s} , $t\text{BuO}\cdot \times [\text{MeCN}] = 2.5 \times k_{\beta}$, $t\text{BuO}\cdot = 1.6 \times 10^5 \text{ s}^{-1}$ in neat acetonitrile.^[11] Summing up this information, $t\text{BuO}\cdot$ is 3.75 times more stable than $\text{CumO}\cdot$, and HAT from MeCN to $t\text{BuO}\cdot$ is 2.25 times slower than $\text{CumO}\cdot$, which means that the most important decay pathway of the formed $\text{CumO}\cdot$ is represented by C- CH_3 β -scission and HAT process from acetonitrile. In an attempt to increase the turnover of future reactions, it was decided to continue the experiments with di-tert butyl hyponitrite (**2a**).

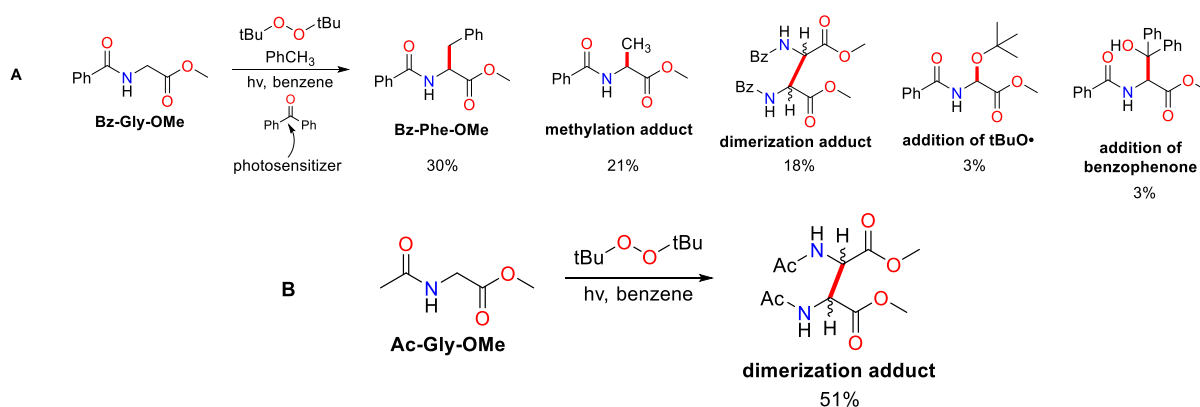
The reaction was scaled up to 1 mmol and repeated in order to isolate the white precipitate **3**. During the reaction, the clear reaction mixture becomes slightly yellow and the white precipitate forms during the reaction as before. The precipitate was centrifuged out, washed with acetonitrile, and further analyzed via NMR and HRMS, which gave the structure of

isomeric **3a** and **3b** (~1/1), the dimerization adducts of dipeptide **1a** at C α -position (6.9%). Another dimerization adduct of oxidative stress reaction was found after column separation of the crude mixtures in highly polar fractions (pure MeOH). Based on the ¹H NMR analysis, it was concluded that the structure of the compound includes unsymmetrical dimer **3c** (Scheme 6). To prove the assumption, independent synthesis of compound **3c** was performed. The obtained polar fractions were also analyzed using RP HPLC-UV, which showed that it consisted only of dimer **3c** (yield 9.3%).



Scheme 6. Structures of the obtained dimers **3a-c** formed during the oxidative stress experiment of **1a**.

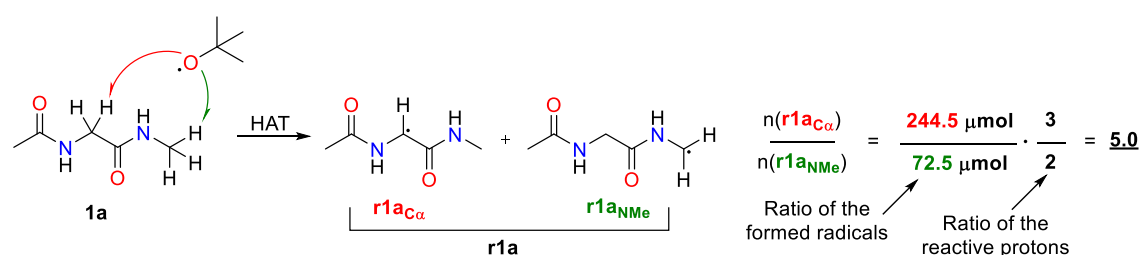
The radical mediated dimerization of amino acids has been reported in literature. For example, the synthesis of phenylalanines from glycine derivatives in the presence of toluene was performed (Scheme 7, A).^[3a] The reaction performed in the absence of the alkylating reagent leads to the formation of amino acid dimers (Scheme 7, B).^[3f]



Scheme 7. Radical functionalization of amino acids.

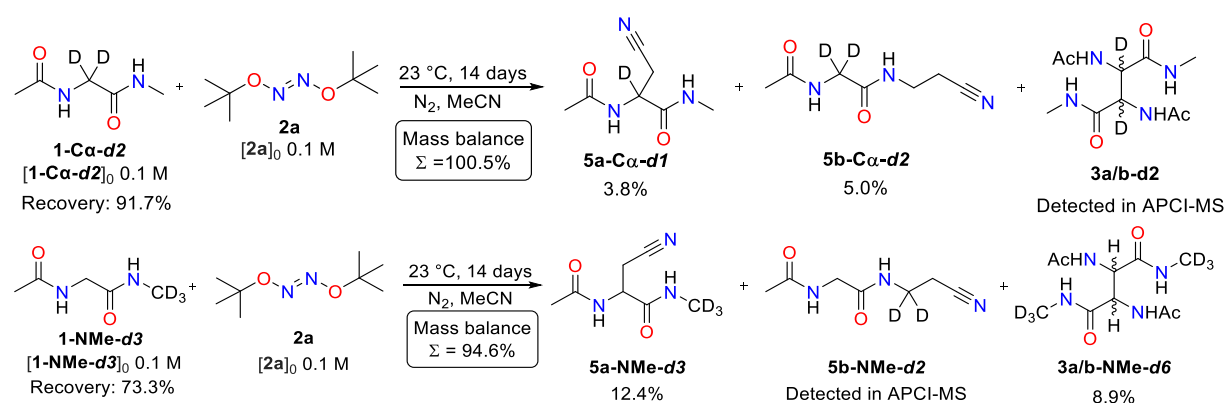
The overall mass balance of the reaction was 98.4% if the yield of the products **3a-c** and **5a-c** was combined with the recovery of AcGlyNMe (**1a**). By examining the product distribution, the reactivity of C α - and N-Me sites of the dipeptide **1a** was calculated (Table 11). It was found that the C-H bond at C α -position are 5.0 times more reactive than the C-H bond at N-Me moiety.

Table 11. C α - and N-Me sites reactivity of dipeptide **1a** under oxidative stress in MeCN



Product	5a	3a/b	3c	5b
Reactivity channel	C α -center	C α -center	C α -center and N-Me	N-Me
Yield, %	12.9	6.9	9.3	2.6
Yield, μmol	129	34.5	46.5	26
r1a formed, μmol	129	69	93	26
r1aCα and r1NMe formed, μmol	244.5			72.5

To investigate the reactivities of deuterated analogues of dipeptide **1a**, the reactions were performed under similar conditions as described in Scheme 8.



Scheme 8. Oxidative stress of deuterium labelled dipeptides **1-C α -d2** and **1-NMe-d3**

It has been shown that labelling the C α -position significantly decreases the overall turnover with only 8.8% of **1-C α -d2** turnover (vs 34.9% turnover of **1a**, 3.96 times less). Labelling the C α -position in **1a** did not result in an increased reactivity of the NMe-moiety (only 5.0% vs 2.6% with **1a**). Isotopic labeling of the NMe group in **1a** caused a small reduction in overall

turnover (26.7% compared to 34.9% with unlabeled **1a**), resulting in selective C α -modification and predominantly producing C α -functionalized adducts, such as **5a-NMe-d3** or **3a/b-NMe-d6**.

The calculated KIE values for different carbon centers in **1a** indicate that its deuterated analogs react 5.8-7.5 times slower (Fig. 2).

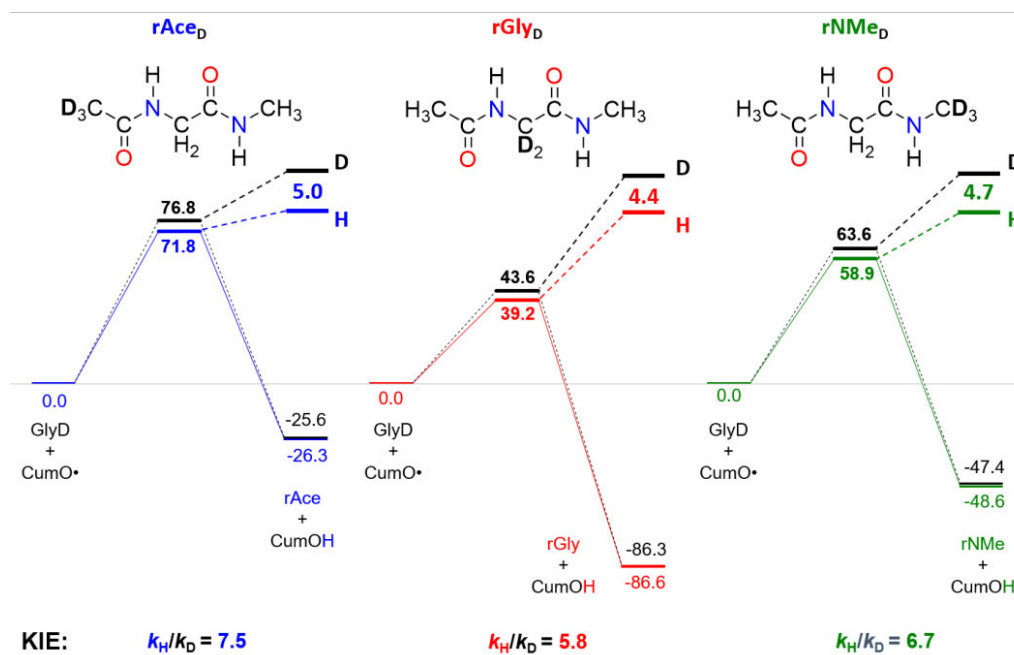
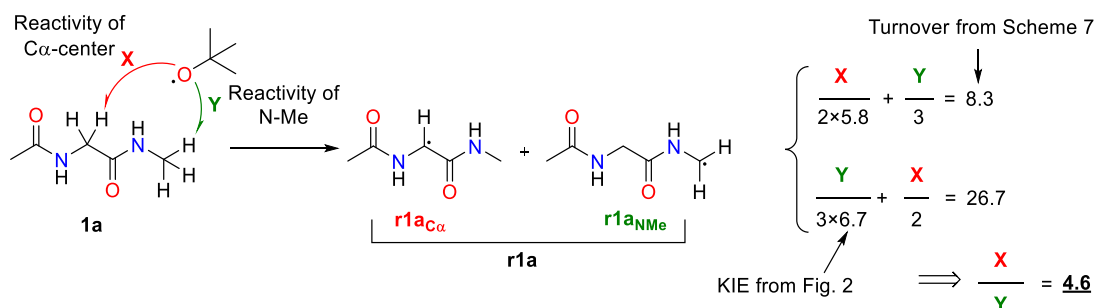


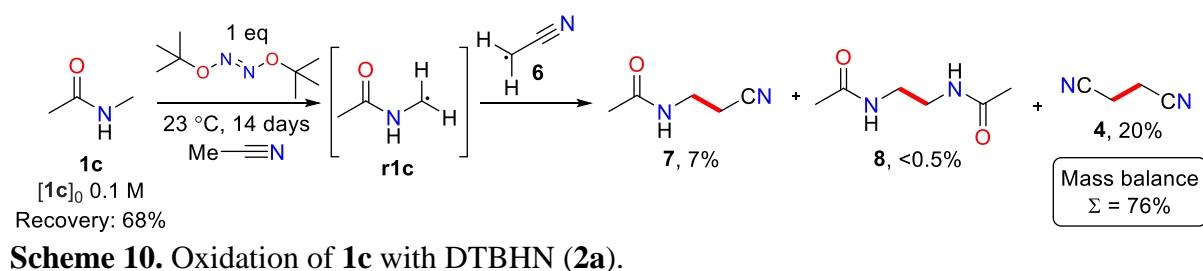
Fig 2. Classical deuterium kinetic isotope effects (KIE) on gas phase free energy surfaces (ΔG_{298} , in kJ/mol) for hydrogen abstraction reaction from different carbon centres of **1a** by calculated at G3(MP2)-RAD level. [A permission was obtained from the author of an image, Dr. Harish Jangra, to include it in this work]

An estimate of the relative reactivity based on the calculated KIE values and the obtained turnover rates suggests that the C α -center is approximately 4.6 times more reactive than the N-Me moiety, using the isotope labelled substrates (Scheme 9).



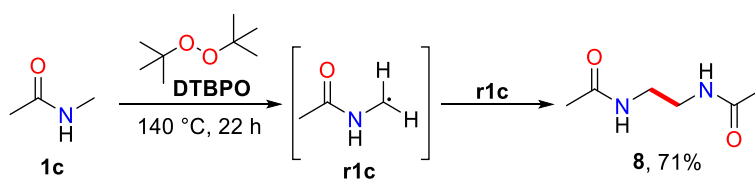
Scheme 9. C α - and N-Me sites reactivity of labelled dipeptide **1a** under oxidative stress.

Unexpectedly, during the analysis of the crude material of **1-Ca-d2**, in which the NMe-group is activated and forced to react, no symmetric dimer **3d** was detected. To test the possibility of symmetric *N*-dimer formation, the same reaction was performed using *N*-methyl acetamide (**1c**). The concept of this approach is to generate the radical **r1c**, which has only two possible recombination pathways: either with another **r1c** or with the cyanomethyl radical **6** that is inevitably formed during the reaction (Scheme 10). The GC-FID analysis showed that the main product of oxidation is the adduct of cyanomethylation **7** (7%) and trace amount of dimerization **8** (<0.5%), which tells about unfavorable process of symmetrical dimerization of NCH₂-radicals.



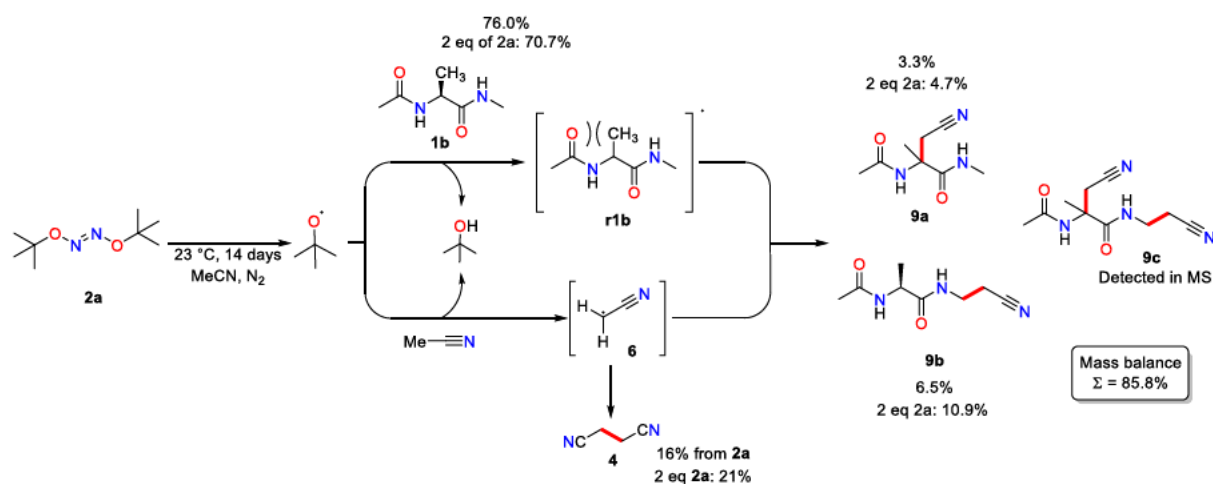
Scheme 10. Oxidation of **1c** with DTBHN (**2a**).

It is worth mentioning that the recovery of **1c** was 68%, indicating the possibility of unaccounted oxidative stress reactions such as oligomerization or decomposition, which may lead to the formation of volatile products, since the mass balance of the reaction in this case is only 76%. To test the first assumption, APCI MS analysis of the crude mixture was performed, which showed no formation of oligomers. The radical functionalization of *N*-methyl acetamide (**1c**) using di *t*-butyl peroxide (**DTBPO**) has been previously reported (Scheme 11).^[12]



Scheme 11. Radical dimerization of **1c**.^[12]

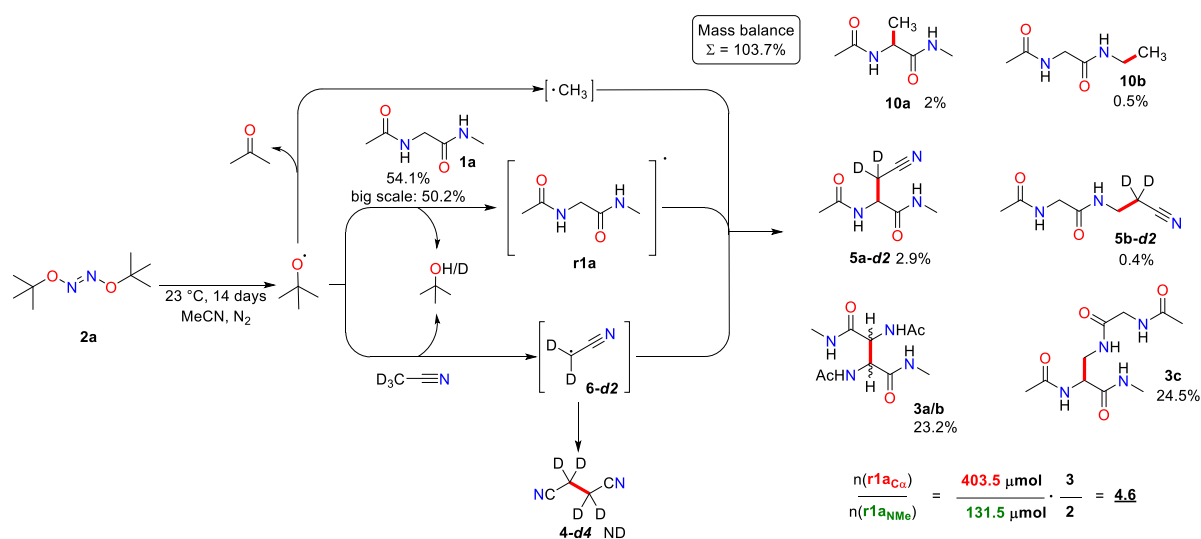
The oxidative stress reaction of AcAlaNMe (**1b**) was studied next (Scheme 12). A small-scale reaction was performed with 0.1 M concentration of AcAlaNMe (**1b**) and 1 eq **2a** at 23 °C in dry degassed MeCN under N₂ atmosphere (no light exposure).



Scheme 12. Oxidative stress reaction of AcAlaNMe (**1b**) with DTBHN (**2a**) for 14 days in MeCN.

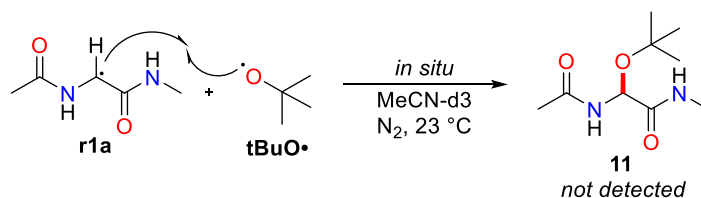
In this case, no formation of a precipitate was detected. The analysis of the supernatant showed a significant decrease in the reactivity of the C α -center, leading to an increased reactivity at the N-Me site of the dipeptide model **1b**. This can be attributed to the number of the reactive protons (now only one proton is present instead of two, as in the case of AcGlyNMe (**1a**)) and the steric hindrance created by the methyl group. GC-FID and ^1H NMR analysis showed the formation of succinonitrile **4** (16% from DTBHN **2a**). The main oxidation products **9a** (3.3%) and **9b** (6.5%) are adducts of cyanomethylation of initial dipeptide model **1b** at C α and N-Me positions, correspondingly. As before, MS analysis of the crude material shows the trace amounts of double cyanomethylation adduct **9c**. Increasing the amount of oxidant to 2 eq does not lead to a significant increase in the rate of oxidation of dipeptide **1b**, but results in a higher turnover of solvent oxidation (16% vs 21%). It was decided to switch to using a deuterated solvent, MeCN- d_3 , in further investigations as the reaction with the solvent was found to be unfavorable. Changing the solvent to deuterated analog, MeCN to MeCN- d_3 , has a significant influence due to large KIE values for HAT reactions, which almost cuts out the solvent participation in this reaction, giving new oxidation products **10a** and **10b**, the result of recombination of methyl radical ($\cdot\text{CH}_3$) from β -scission process and dipeptide radical after HAT, 2.0 and 0.5%, correspondingly (Table 12).

Table 12. C α - and N-Me sites reactivity of dipeptide **1a** under oxidative stress in MeCN-d₃.



Product	5a-d2 / 10a	3a/b	3c	5b-d2 / 10b
Reactivity channel	C α -center	C α -center	C α -center and N-Me	N-Me
Yield, %	2.9 / 2	23.2	24.5	0.5 / 0.4
Yield, μmol	49	116	122.5	9
r1a formed, μmol	49	232	245	9
r1a _{Cα} and r1a _{NMe} formed, μmol	403.5			131.5

Since the reaction is carried out in a deuterated solvent, direct ^1H NMR analysis of the reaction mixture is possible, allowing for the potential observation of product **11**, resulting from the recombination of the dipeptide radical **r1a** with *tert*-butoxy radical (Scheme 13). To confirm this, the possible product **11** was synthesized, however, ^1H NMR and MS analysis showed that the product was not formed in the oxidative stress reaction.

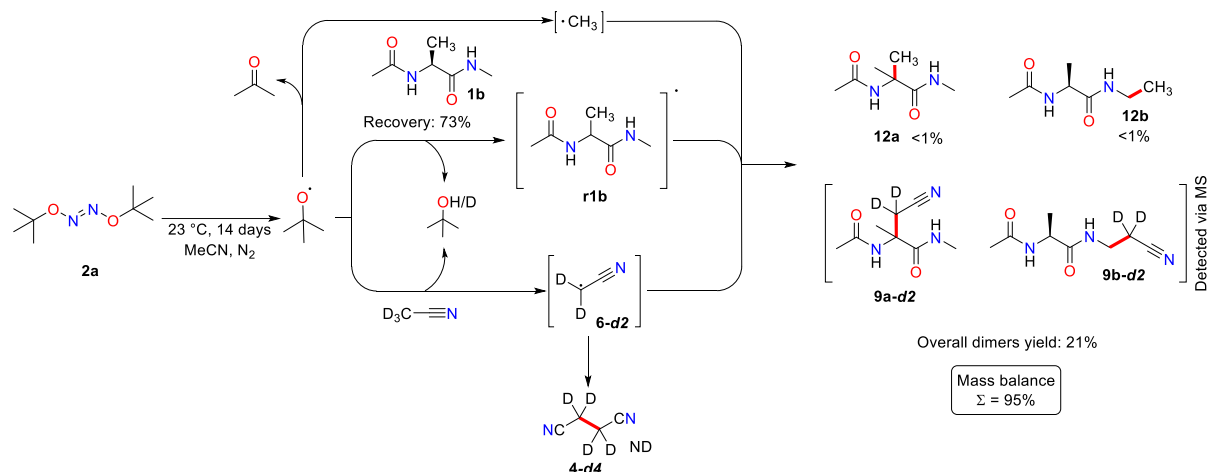


Scheme 13. Recombination product of dipeptide radical with tBuO \cdot was not detected.

Since the solvent reactivity was suppressed, the formed dipeptide radicals **r1a** had a higher probability of recombining with each other, resulting in an increased yield of the products of oxidative dimerization **3a/b** and **3c**, as observed in our study. However, despite the increased yield of products of oxidative dimerization, further analysis by HPLC-UV showed no

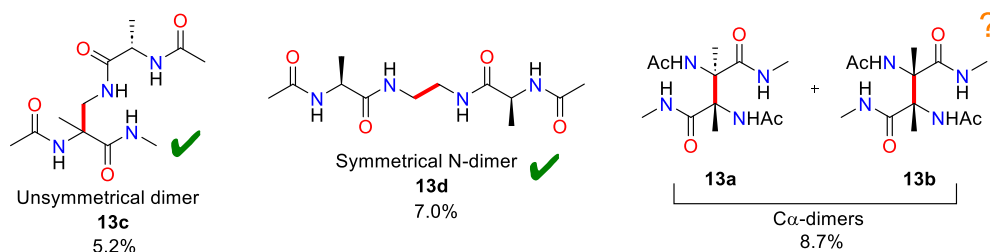
formation of the symmetric *N*-dimer **3d**. The overall mass balance of the reaction was 103.7% if the yield of the products **3a-c**, **5a-b** and **10a-b** was combined with the recovery of AcGlyNMe **1a**. It was found that the reactivity of the C α -center is 4.6 times higher than that of the *N*-Me moiety in MeCN-*d*₃, which is consistent with the value obtained in MeCN (5.0 vs 4.6). This finding makes sense because the intrinsic reactivity of the moieties does not depend on the level of solvent deuteration.

Similar reactions were expected for AcAlaNMe **1b** (73% recovery), but analysis of the supernatant showed the absence of cyanomethylation adducts (only detected by APCI MS), and a small amount of methylation adducts **12a-b** (Scheme 14). It was challenging to determine the exact yield due to overlapping GC-FID peaks, but the yield of the methylation adducts **12a-b** were negligible (<2%).



Scheme 14: Analysis of the supernatant from the reaction of AcAlaNMe (**1b**) with DTBHN (**2a**) in MeCN-*d*₃ for 14 days.

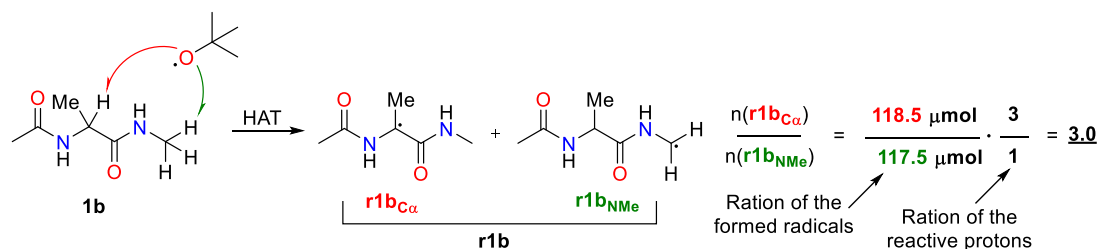
A complex mixture of several dimers **13** (yielding 21% overall) was obtained in highly polar (pure MeOH) fractions by column chromatography. Unsymmetrical dimer **13c** and symmetrical *N*-dimer **13d** were identified through independent syntheses of each compound (Scheme 15).



Scheme 15. Structures of the dimers **13a-d** formed during the oxidative stress of **1b**.

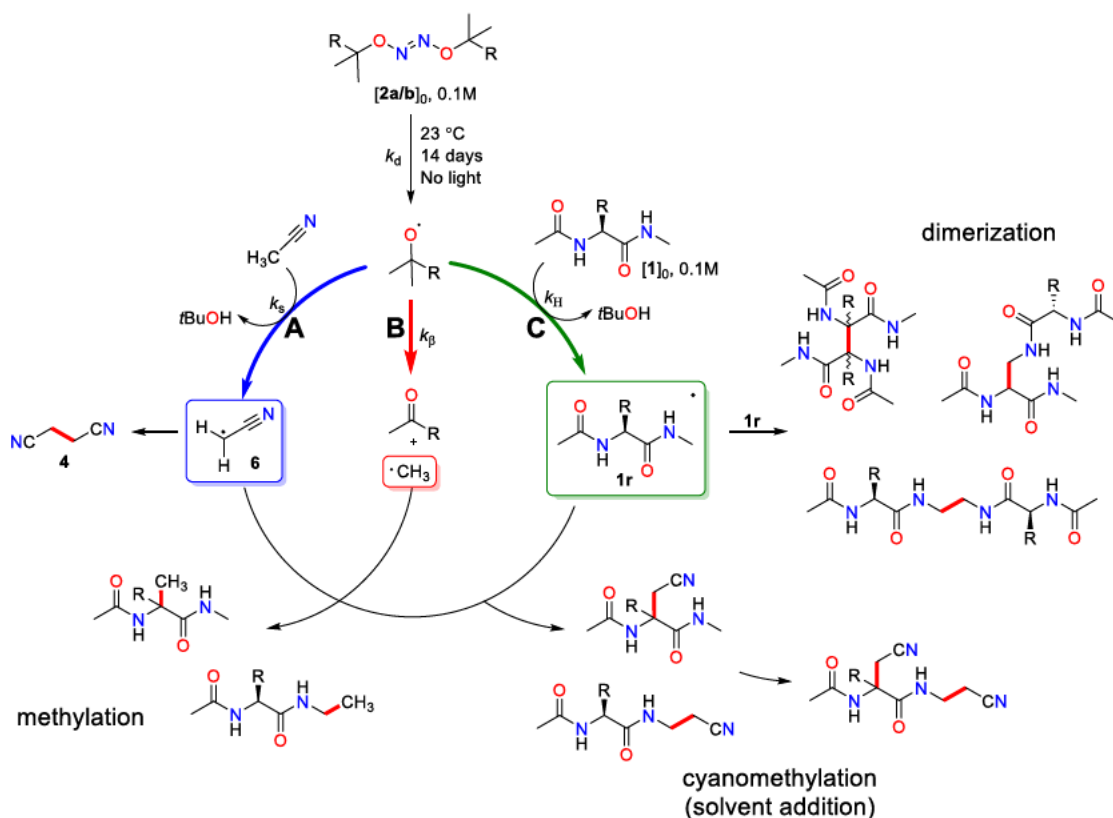
The unidentified peaks observed in the ^1H NMR spectra could potentially correspond to the C_α -dimers **13a/b**, which are difficult to synthesize due to the presence of two highly sterically hindered quaternary centers. The proposed synthesis of the dimer **13a/b** is given in the outlook chapter. By using the assumption of dimer **13** distributions based on the ^1H NMR and HPLC-UV spectrum, it is possible to determine the reactivity of C_α - and N-Me sites of the dipeptide **1b** in the same way as carried out for dipeptide **1a** (Table 13). It was found that the C_α -center is at most 3 times more reactive than the N-Me moiety. A significant decrease in reactivity was observed compared to the glycine derivative **1a**; however, the obtained value requires more accurate determination in the future.

Table 13. C_α - and N-Me site reactivities of dipeptide **1b** under oxidative stress in $\text{MeCN-}d_3$.



Product	12a	13a/b	13c	13d	12b
Reactivity channel	C_α -center	C_α -center	C_α -center and N-Me	N-Me	N-Me
Yield, %	1	6.7	8.3	1	6.6
Yield, μmol	10	33.5	41.5	1	33
r1b formed, μmol	10	67	83	10	66
r1b$_{\text{C}\alpha}$ and r1b$_{\text{NMe}}$ formed, μmol	118.5		117.5		

Summing up all the obtained information, the proposed oxidative stress mechanism of the dipeptide models can be drawn. The slow decay of the hyponitrite **2a/b** generates the alkoxy radicals, $\text{RO}\cdot$, following first-order kinetics. The radicals can undergo three main pathways: solvent abstraction A, β -scission B, and abstraction from a dipeptide C (Scheme 16). All three pathways generate secondary radicals: cyanomethyl radical **6**, methyl radical and dipeptide radical **1r**. These radicals recombine with each other, leading to three main channels of product formation: dimerization, cyanomethylation (solvent addition) and methylation. It is also possible that the obtained products may undergo further interactions with the formed radicals, resulting in the formation of secondary oxidation products. This is supported by the detection of products of double cyanomethylation or cyanomethylated dimers via APCI-MS analysis.



Scheme 16. Proposed mechanism of the oxidative stress of dipeptide models.

2.2.3. Aliphatic Chain/Functional Groups Influence on HAT Reaction.

The next step was an oxidative stress reaction of the set of *N*-acetyl-*N'*-methyl amido acids **1a-g** and *N*-acetyl amino acid methyl esters **14a-c**, which was prepared and oxidized under similar conditions. Due to the increased complexity of the formed products, the turnover of initial substrate was measured and taken as a stability parameter/side chain influence towards alkoxy radicals (Table 14). Due to the lack of solubility in MeCN-*d*3 observed for some dipeptide models such as AcPheNMe (**1e**) and AcSerNMe (**1g**), it was decided to repeat the oxidative stress reaction for the entire set using DMSO-*d*6 as the solvent. To accomplish this, the decomposition rate of DTBHN (**2a**) in DMSO-*d*6 at 23 °C was first measured, showing a half-life of 250 h, which is comparable to the value obtained in MeCN-*d*3 (286 h).

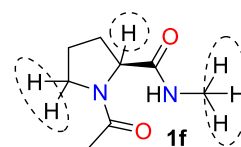
Almost no difference in reaction turnover was found among the dipeptide models containing the side chains: AcAlaNMe (**1b**), AcLeuNMe (**1d**), AcPheNMe (**1e**), and AcSerNMe (**1g**), indicating that the reaction is not dependent on the specific side chain of the chosen amino acids. Based on this information, we can make the assumption that the HAT reaction to tBuO occurs not along the sidechain (especially in the case of AcPheNMe (**1e**), which has susceptible benzylic protons) but rather from the C α -center and N-Me moiety of the dipeptide models.

Table 14. Influence of a side chain/C-terminal group on turnover rates under oxidative stress.

N-Methyl Amides				Methyl esters
50% / 61%	23% / 39%	50% / 63%	27% / 33%	47%
30% / 34%	12%* / 37%	52% / 51%	23%* / 35%	20%
				52%

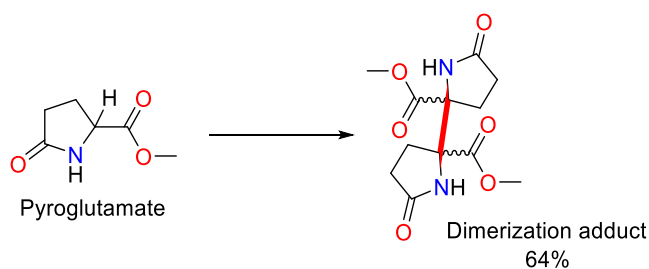
*Heterogeneous reactions

In the oxidative stress experiment, it was observed that the turnover rate for **1-C α -d2** was almost half of that for non-deuterated **1a** (23% vs 50%), whereas **1-NMe-d3** showed the same turnover rate as **1a** (50%). The most interesting example in this study is AcProNMe (**1f**), because it shows the same level of turnover as AcGlyNMe (**1a**, 52% vs 50% in MeCN-d3 or 51% vs 61% in DMSO-*d*₆, correspondingly). Such a great reactivity can be attributed to the fact, that the dipeptide model **1f** contains three positions with 6 protons, labile to HAT reactions. This observation is in line with previous experimental data (Tables 3 and 4).



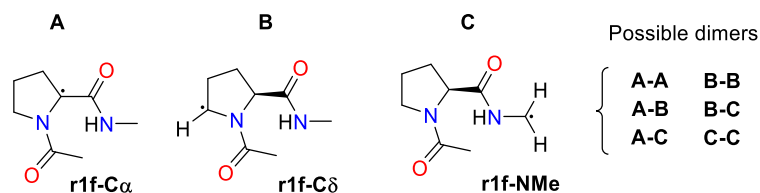
6 reactive protons!

Also, the radical dimerization of structurally similar pyroglutamate derivative has been reported.^[3f] The product analysis showed the formation of two diastereomeric dimers (Scheme 17).



Scheme 17. Radical dimerization of pyroglutamate.

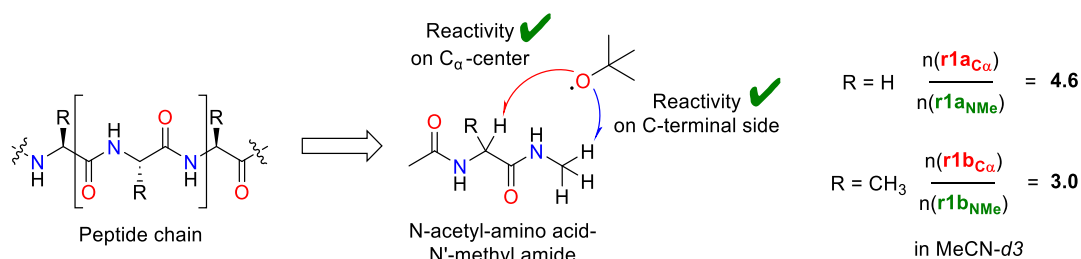
But in our case, substrate **1f** can form 3 different radicals that can recombine with each other. This free recombination leads to the formation of 6 different regioisomeric dimers (Scheme 18).



Scheme 18. Radical dimerization of Ac-Pro-NMe (**1f**).

2.3. Conclusions

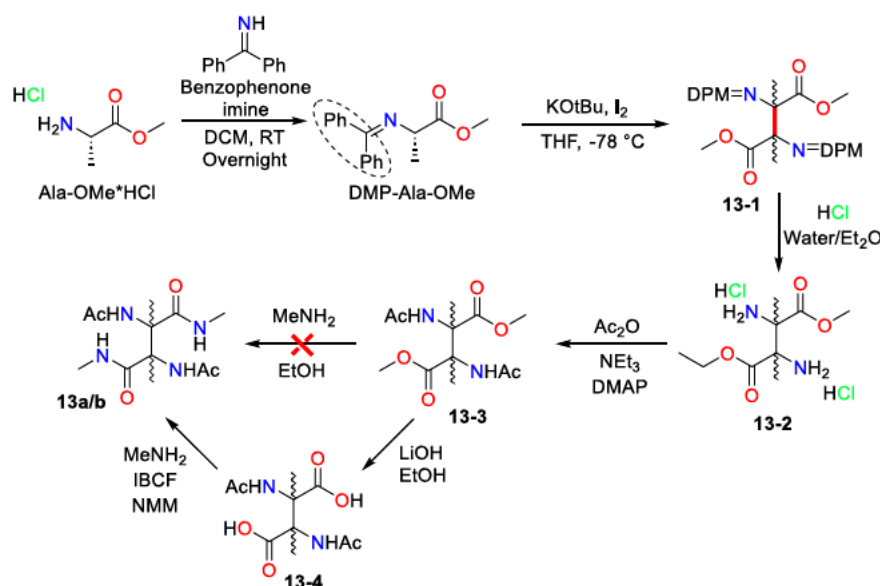
The oxidative stress of dipeptide models using alkyl hyponitrites as a mild source of alkoxy radicals was performed and investigated. Alkyl hyponitrites were shown to be mild oxidants towards dipeptides, which allows to use them in the model of oxidative stress processes. The determination of the distribution of oxidative recombination products indicates that the reactivity of C α -centers is several times (3-5) higher than that of NMe-moiety of the dipeptide, while LFP experiments with deuterated dipeptide substrates suggest almost the same reactivity.



It has been shown that dipeptide models tend to dimerize, recombine with solvent or methyl radicals under the oxidative stress conditions. It has been demonstrated that KIE can be successfully utilized by replacing the solvent with its deuterated analogue, allowing the reaction to proceed through certain reactivity channels, in our case, oxidative dimerization of the dipeptide models. It has been demonstrated that for a selected group of dipeptide models, the side chain does not have a significant impact on the overall rate of turnover, except in the case of glycine and proline derivatives, which unlike other dipeptide models, are prone to oxidation by alkoxy radicals.

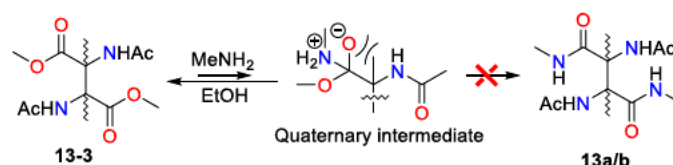
2.4. Outlook

The synthesis of dimers **13a/b** is complicated due to the presence of two highly sterically hindered quaternary centers. The synthesis route outlined in Scheme 19 is currently in progress. The synthesis of **13a/b** as a reference compound is an important step for confirming its formation during the oxidative stress reaction of dipeptide **1b**. With the reference compound in hand, it becomes possible to compare spectroscopic and analytical data to those obtained from the crude reaction mixture. This validation is essential in establishing the exact reactivity ratio of the C α -center and the NMe-moiety of dipeptide **1b** as it was described in Table 13.



Scheme 19. Proposed synthesis of C α -dimers **13a/b**.

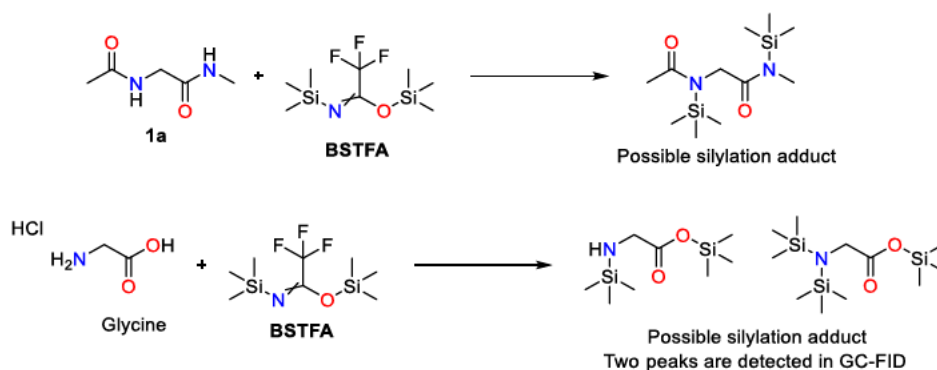
The synthesis begins with methyl alanine ester hydrochloride, H-Ala-OMe \times HCl, where the amino group is protected by benzophenone imine to eliminate all labile protons. The choice of the benzophenone imine protection group is important, because the following step involves deprotonation of the C α -center of DMP-Ala-OMe, using a strong base (KOtBu). This deprotonation is then followed by oxidative dimerization, forming the backbone structure **13-1** for the C α -dimer **13a/b**. The next steps involve deprotection of **13-1** under mild acidic conditions and the obtained dihydrochloride salt **13-2** is acylated. However, the step of amidation of **13-3** with MeNH $_2$ was unsuccessful (even under elevated temperatures, >100 °C), which was attributed to the huge steric hindrance in the formed quaternary intermediate (Scheme 20).



Scheme 20. Failed amidation step of **13-3**.

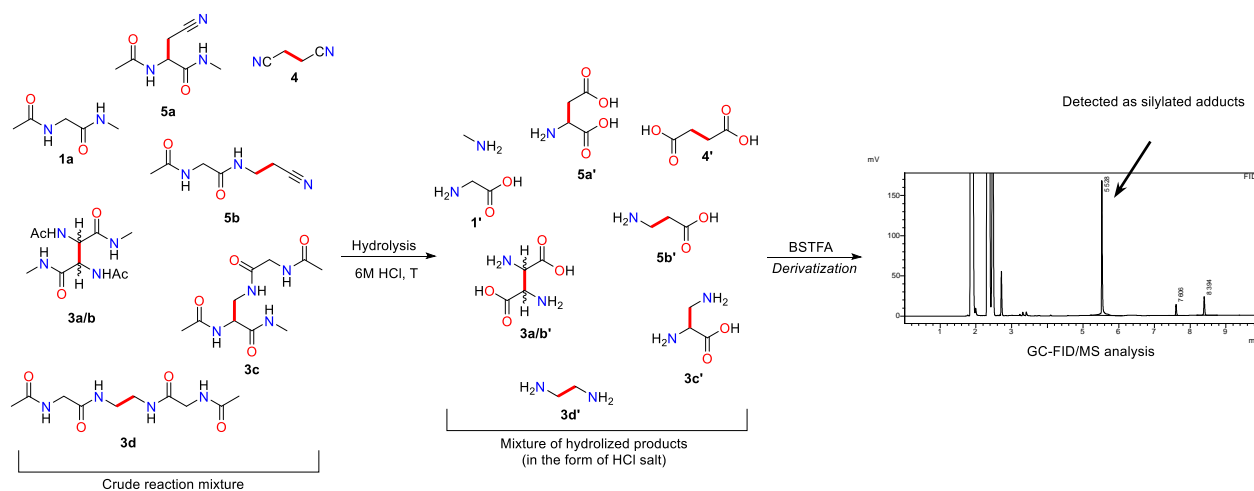
Therefore, it is necessary to first hydrolyze the formed methyl ester **13-3** into a carboxylic acid **13-4**, using LiOH. Then the carboxylic acid **13-4** can be activated, enabling the subsequent amidation to occur more readily and successfully. This modified approach helps to overcome the steric hindrance encountered in the initial method, ultimately yielding the desired product **13a/b**.

All the described product determination (Table 11, 12 and 13) can be adapted to detect not the products themselves but their derivatized products. For example, silylation, using reagents like N,O-Bis(trimethylsilyl)trifluoroacetamide or BSTFA (Scheme 21). This method is much better, since it allows to detect not only dipeptides themselves or cyanomethylation adducts, but also dimers, using GC methods.



Scheme 21. Derivatization of dipeptide models with BSTFA.

Unfortunately, our attempts showed that silylated dipeptide **1a** tends to give inconsistent broad signal in GC-FID analysis (Supporting information), which can be attributed to the thermal decomposition during the analysis, while the glycine hydrochloride itself gives sharp and well-resolved signal in GC-FID.^[13] This led to the idea of modifying the analytical concept (Scheme 22). After the oxidative stress reaction, the reaction mixture is subjected to hydrolysis using a standard hydrolysis protocol. The resulting amino acids are then derivatized with BSTFA and subsequently analyzed using GC-FID/MS.



Scheme 22. Potential acid hydrolysis product of the crude oxidative stress reaction.

This approach significantly reduces the complexity of the resulting products by breaking them down into small, unique building blocks that can be easily traced back to their parent compound and quantified (for example, detection of ethylenediamine **3d'** is evidence for symmetric *N*-dimer **3d** formation). It should also be noted that most of the hydrolysis products can be easily purchased or synthesized through fewer steps. This accessibility simplifies the process of obtaining reference compounds, which can then be used to verify the identity of the products generated in the reaction. The main challenge in this approach is the use of elevated temperatures for both acid hydrolysis and derivatization. Temperatures of 110 °C for 24 hours or 150 °C for 1 hour were tested and found to successfully hydrolyze the test sample of dipeptide **1a**. Additionally, for derivatization with BSTFA, temperatures of 150 °C for 15 minutes or 80 °C for 45 minutes both yielded consistent signals for the silylated adduct. Since only ~50% of DTBHN (**2a**) is decomposed after 14 days, the remaining **2a** should be extracted from the reaction before the hydrolysis step or hyponitrite **2b** should be used, because 14 days are sufficient for ~99% of it to decompose. The approach of derivatization of hydrolyzed products might help to detect the products of complex functionalization in their more simplified forms.

2.5. References

- [1] a) Michael J. Davies, *Biochem. J.* **2016**, *473*, 805-825; b) M. J. Davies, S. Fu, R. T. Dean, *Biochem. J.* **1995**, *305*, 643-649; c) W. M. Garrison, *Chem. Rev.* **1987**, *87*, 381-398; d) C. L. Hawkins, M. J. Davies, *Biochim. Biophys. Acta - Bioenerg.* **2001**, *1504*, 196-219; e) G. Xu, M. R. Chance, *Chem. Rev.* **2007**, *107*, 3514-3543.
- [2] a) E. R. Stadtman, *Science* **1992**, *257*, 1220-1224; b) S. P. Hussain, L. J. Hofseth, C. C. Harris, *Nat. Rev. Cancer* **2003**, *3*, 276-285; c) M. P. Mattson, *Nature* **2004**, *430*, 631-639; d) M. J. Davies, " *The pathology of protein oxidation*" **1997**, 207-218; e) K. B. Beckman, B. N. Ames, *Physiol. Rev.* **1998**, *78*, 547-581; f) Andrew R. Pitt, Corinne M. Spickett, *Biochem. Soc. Trans.* **2008**, *36*, 1077-1082.
- [3] a) H. S. Knowles, K. Hunt, A. F. Parsons, *Tetrahedron Lett.* **2000**, *41*, 7121-7124; b) M. Salamone, F. Basili, M. Bietti, *J. Org. Chem.* **2015**, *80*, 3643-3650; c) M. Salamone, F. Basili, R. Mele, M. Cianfanelli, M. Bietti, *Org. Lett.* **2014**, *16*, 6444-6447; d) M. Salamone, M. Milan, G. A. DiLabio, M. Bietti, *J. Org. Chem.* **2014**, *79*, 7179-7184; e) M. Salamone, M. Bietti, *Acc. Chem. Res.* **2015**, *48*, 2895-2903; f) N. Obata, K. Nimura, *J. Chem. Soc., Chem. Commun.* **1977**, 238-239; g) D. Elad, J. Sperling, *J. Chem. Soc. D* **1969**, 234-234.
- [4] a) H. Wang, D. Ge, Z. Cheng, N. Zhu, H. Yuan, Z. Lou, *J. Hazard. Mater.* **2020**, *387*, 121702; b) B. Chan, C. J. Easton, L. Radom, *J. Phys. Chem. A* **2018**, *122*, 1741-1746; c) Z. I. Watts, C. J. Easton, *J. Am. Chem. Soc.* **2009**, *131*, 11323-11325; d) B. Chan, R. J. O'Reilly, C. J. Easton, L. Radom, *J. Org. Chem.* **2012**, *77*, 9807-9812; e) R. J. O'Reilly, B. Chan, M. S. Taylor, S. Ivanic, G. B. Bacskay, C. J. Easton, L. Radom, *J. Am. Chem. Soc.* **2011**, *133*, 16553-16559; f) E. Hayon, T. Ibata, N. N. Lichtin, M. Simic, *J. Am. Chem. Soc.* **1970**, *92*, 3898-3903.
- [5] a) A. K. Croft, C. J. Easton, L. Radom, *J. Am. Chem. Soc.* **2003**, *125*, 4119-4124; b) V. A. Burgess, C. J. Easton, M. P. Hay, *J. Am. Chem. Soc.* **1989**, *111*, 1047-1052.
- [6] a) M. Bietti, V. Forcina, O. Lanzalunga, A. Lapi, T. Martin, M. Mazzonna, M. Salamone, *J. Org. Chem.* **2016**, *81*, 11924-11931; b) M. Bietti, O. Lanzalunga, A. Lapi, T. Martin, M. Mazzonna, M. Polin, M. Salamone, *J. Org. Chem.* **2017**, *82*, 5761-5768; c) B. Ticconi, M. Mazzonna, O. Lanzalunga, A. Lapi, *Tetrahedron* **2019**, *75*, 3579-3585.
- [7] a) J. G. Nathanael, U. Wille, *J. Org. Chem.* **2019**, *84*, 3405-3418; b) J. G. Nathanael, A. N. Hancock, U. Wille, *Chem. Asian J.* **2016**, *11*, 3188-3195; c) J. G. Nathanael, J.

- M. White, A. Richter, M. R. Nuske, U. Wille, *Organic & Biomolecular Chemistry* **2020**, *18*, 6949-6957.
- [8] a) L. Dulog, P. Klein, *Chem. Ber.* **1971**, *104*, 895-901; b) J. A. Howard, J. H. B. Chenier, *Can. J. Chem.* **1976**, *54*, 382-389; c) D. V. Avila, K. U. Ingold, A. A. Di Nardo, F. Zerbetto, M. Z. Zgierski, J. Luszyk, *J. Am. Chem. Soc.* **1995**, *117*, 2711-2718; d) S. Coseri, G. D. Mendenhall, K. U. Ingold, *J. Org. Chem.* **2005**, *70*, 4629-4636.
- [9] X.-Q. Chu, D. Ge, Z.-L. Shen, T.-P. Loh, *ACS Catal* **2018**, *8*, 258-271.
- [10] a) L. Grossi, S. Strazzari, *J. Org. Chem.* **2000**, *65*, 2748-2754; b) D. V. Avila, C. E. Brown, K. U. Ingold, J. Luszyk, *J. Am. Chem. Soc.* **1993**, *115*, 466-470.
- [11] a) Y. P. Tsentalovich, L. V. Kulik, N. P. Gritsan, A. V. Yurkovskaya, *J. Phys. Chem. A* **1998**, *102*, 7975-7980; b) H. Paul, R. D. Small, Jr., J. C. Scaiano, *J. Am. Chem. Soc.* **1978**, *100*, 4520-4527.
- [12] L. Friedman, H. Shechter, *Tetrahedron Lett.* **1961**, *2*, 238-242.
- [13] C. W. Gehrke, K. Leimer, **1970**.

2.6. Supporting information

General methods: All reactions sensitive to air and moisture were performed under nitrogen atmosphere, and the glassware as well as magnetic stir bars were dried overnight in a dry oven at 110°C.

Solvents, reagents: All reagents and solvents were purchased from the companies TCI, Sigma Aldrich or Fisher Scientific. All air- or water-sensitive reagents were stored under nitrogen.

NMR spectroscopy: All ^1H NMR spectra were recorded by Bruker 400 in DMSO-*d*6/MeOH-*d*4 at 400 MHz at 23 °C. All ^{13}C NMR spectra were recorded, respectively, at 101 MHz. The chemical shifts are reported in ppm (δ), relative to the resonance of DMSO-*d*6 at $\delta = 2.50$ /MeOH-*d*4 at $\delta = 3.31$ ppm for ^1H and for ^{13}C relative to the resonance of DMSO-*d*6 $\delta = 39.52$ /MeOH-*d*4 $\delta = 49.15$ ppm. Spectra were imported and processed in the MestreNova 14.1.1 program. For ^1H NMR spectra multiplicity (s = singlet, d = doublet, t = triplet, q = quartet, quint = quintet, m = multiplet, dd = doublet of doublets, dt = doublet of triplets, td = triplet of doublets, and bs = broad signal.), coupling constants *J*, number of protons and assignment to the structure are reported. In ^{13}C NMR spectra singular carbons are marked with (s).

Mass spectrometry: For electrospray ionization (ESI) spectra a Thermo Finnigan LTQ FT Ultra Fourier Transform Ion Cyclotron Resonance Mass Spectrometer was utilized. For atmospheric pressure chemical ionization (APCI) a Advion CMS using positive mode was used.

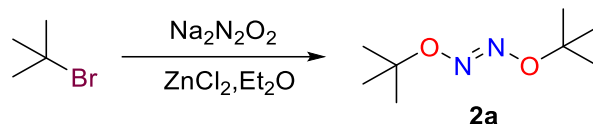
Single-crystal X-ray diffraction. scXRD measurements were performed on a Bruker D8 Venture TXS diffractometer.

HPLC analysis: All HPLC spectra were measured on a Knauer Azura machine with P6.1L pump, autosampler AS6.1, column thermostat CT2.1 and diode array detector DAD2.1L. Eurospher II 250×4.6 mm C8A or C18A column were utilized. Data analysis was performed with ClarityChrom 7.4.1.

2.6.1. Synthesis of Oxidants, Reagents and Reaction Products

2.6.1.1. Synthesis of alkyl hyponitrites

Synthesis of di-tert-butyl hyponitrite (DTBHN, **2a**):

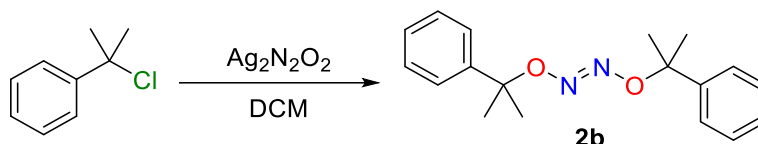


337 mg of dry ZnCl_2 (2.5 mmol, 1 eq) was dissolved in a mixture of 2.5 ml t-BuBr and 2 ml of dry Et_2O . Then 265 mg of dry $\text{Na}_2\text{N}_2\text{O}_2$ (2.5 mmol, 1 eq) was added portion wise while stirring. Reaction mixture was stirred for 2 h at RT, then was allowed to cool at 4 °C for additional 2 h. Inorganic salts were removed by filtration, washed with Et_2O . The organic phases were collected, washed several times with water and dried over MgSO_4 . The solvents were evaporated under reduced pressure. DTBHN was recrystallized from methanol at -78 °C. Pure product was obtained as white crystals (246 mg, 56%). Spectral data are in agreement with literature values.^[1]

$^1\text{H NMR}$ (400 MHz, CDCl_3) δ 1.39 (s, 18H)

Elem. Calcd for $\text{C}_8\text{H}_{18}\text{N}_2\text{O}_2$: C 55.15, N 16.08, H 10.41. Found: C 54.89, N 15.88, H 10.30.

Dicumyl hyponitrite (DCHN, **2b**):

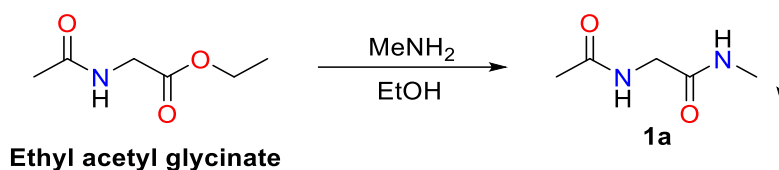


1 g of dry $\text{Ag}_2\text{N}_2\text{O}_2$ (3.63 mmol, 1 eq) was added portion-wise to a solution of 1.4 g of α,α -dimethylbenzyl chloride in 10 ml of dry DCM over 20 min at 0°C. The reaction was then stirred for 40 min at 0 °C. Inorganic salts were removed by filtration and washed with DCM. The organic phases were collected, washed several times with water, dried over MgSO_4 and the solvent was evaporated under reduced pressure. DCHN was recrystallized from methanol at -78 °C. Pure product was obtained as white powder (287 mg, 26%). Spectral data are in agreement with literature values.^[2]

$^1\text{H NMR}$ (400 MHz, CDCl_3) δ 7.36 – 7.23 (m, 10H), 1.72 (s, 12H).

2.6.1.2. Synthesis of *L*-Ac-AA-NMe and *L*-Ac-AA-OMe

2-acetamido-*N*-methylacetamide (AcGlyNMe, **1a**):



6.05 ml of 33% ethanol solution of methyl amine (64.5 mmol, 4.67 eq) was added dropwise to ethyl acetyl glycinate (2 g, 13.8 mmol, 1 eq) at 0 °C. Then the external cooling was removed and the reaction mixture was allowed to stir for 4 hours at RT. After removing the solvent under reduced pressure, the crude product was purified by column chromatography on silica (CH₂Cl₂/MeOH = 10/1, R_f 0.30). Pure 2-acetamido-*N*-methylacetamide (**1a**) was isolated as white crystals (1.56 g, 12 mmol, 87%). Spectral data are in agreement with literature values.^[3]

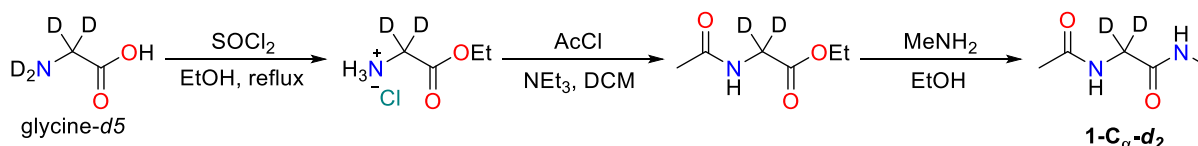
¹H NMR (600 MHz, DMSO-*d*₆) δ 8.06 (bs, 1H), 7.72 (bs, 1H), 3.61 (d, *J* = 5.9 Hz, 2H), 2.57 (d, *J* = 4.6 Hz, 3H), 1.85 (s, 3H).

¹³C NMR (150 MHz, DMSO-*d*₆) δ 169.70, 169.44, 42.16, 25.48, 22.56.

Elem. Calcd for C₅H₁₀N₂O₂: C 46.14, N 21.52, H 7.75. Found: C 46.05, N 21.53, H 7.61.

HRMS (ESI): calcd for C₅H₁₁N₂O₂ [M + H]⁺, 131.0815; found 131.0815.

2-acetamido-*N*-methylacetamide-2,2-*d*₂ (**1-C_α-d₂**):



1.5 g of glycine-*d*₅ (18.75 mmol, 1 eq) was dissolved in 50 ml of ethanol. The solution was cooled to 0 °C, then 3.4 ml of SOCl₂ (5.58 g, 2.5 eq) were added dropwise. After refluxing for 1 hour, all volatiles were removed under reduced pressure. Ethyl glycidate-2,2-*d*₂ hydrochloride was obtained as a white solid (2.65 g, quant.). The resulting solid (18.73 mmol, 1 eq) was dissolved in 50 ml of DCM, the solution was cooled down to 0 °C, and 5.22 ml of NEt₃ (3.78 g, 2 eq) was added dropwise. 1.33 ml of acetyl chloride (1.47 g, 1 eq) was added dropwise. Then the external cooling was removed. The reaction mixture was stirred for 4 hours, quenched with 100 ml of brine and extracted with EtOAc (3 × 50ml). The solvent was evaporated under reduced pressure. Then 10.3 ml of 33% ethanol solution of methyl amine (88 mmol, 4.67 eq) was added dropwise to the crude product at 0 °C. After 5 minutes the external cooling was removed and the reaction mixture was allowed to stir for 4 hours at RT. After

removing all residues of solvents under reduced pressure, the crude product was purified by recrystallization from EtOAc/EtOH and by column chromatography on silica (CH₂Cl₂/MeOH = 10/1, R_f 0.30). Pure product was isolated as white crystals (2.31 g, 93%).

¹H NMR (600 MHz, DMSO-*d*₆) δ 8.05 (s, 1H), 7.73 (s, 1H), 2.57 (d, *J* = 4.8 Hz, 3H), 1.84 (s, 3H).

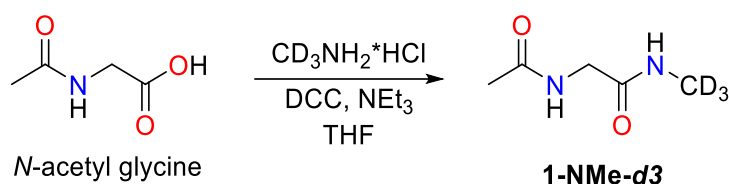
¹³C NMR (150 MHz, DMSO-*d*₆) δ 169.68, 169.43, 25.45, 22.54.

Elem. Calcd for C₅H₈D₂N₂O₂: C 45.44, N 21.20, H 9.15. Found: C 45.46, N 21.30, H 9.13

HRMS (ESI): calcd for C₅H₉D₂N₂O₂ [M + H]⁺, 133.0940; found 133.0941.

Deuterium content: 96.5%

2-acetamido-*N*-(methyl-*d*₃)acetamide (**1-NMe-*d*₃**):



20 ml THF were added to a mixture of *N*-acetyl glycine (1 g, 8.5 mmol, 1.2 eq) and methyl amine-*d*₃ hydrochloride (0.5 g, 7.1 mmol, 1 eq). Then NEt₃ (1.2 ml, 0.86 g, 8.5 mmol, 1.2 eq) was added dropwise to the stirring reaction mixture. After 10 min the reaction was cooled down to 0 °C by an ice bath. DCC (1.5 g, 7.1 mmol, 1 eq) was added portion-wise and the reaction mixture was stirred for 1 hour at 0 °C. Then it was warmed up to RT and stirring was continued for 2 hours. After that the solvent were evaporated, 5 ml MeOH were added, and DCU was filtered off and washed with MeOH (3×5 ml). NaOH (340 mg, 8.5 mmol, 1.2 eq) was dissolved in the obtained solution. All solvents were evaporated in *vacuo*, and the product was purified by column chromatography on silica (CH₂Cl₂/MeOH = 10/1, R_f 0.30). The pure product was isolated as white crystals (605 mg, 64%).

¹H NMR (600 MHz, DMSO-*d*₆) δ 8.11 (s, 1H), 7.73 (s, 1H), 3.60 (d, *J* = 5.9 Hz, 2H), 1.84 (s, 3H).

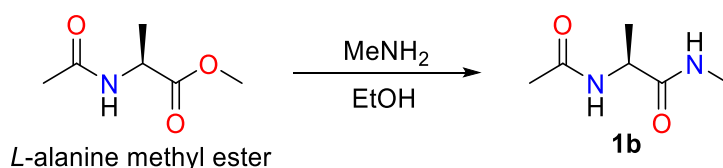
¹³C NMR (150 MHz, DMSO-*d*₆) δ 169.75, 169.53, 42.18, 22.63.

Elem. Calcd for C₅H₇D₃N₂O₂: C 45.10, N 21.04, H 9.84. Found: C 45.09, N 21.1, H 9.80.

HRMS (ESI): calcd for C₅H₈D₃N₂O₂ [M + H]⁺, 134.1003; found 134.1003.

Deuterium content: >99%

(S)-2-acetamido-*N*-methylpropanamide (*L*-AcAlaNMe, **1b**):



2 g of *N*-acetyl *L*-alanine methyl ester (13.8 mmol, 1 eq) was dissolved in 6 ml of 33% ethanol solution of methyl amine (64.5 mmol, 4.67 eq) was added dropwise at 0 °C. After 5 minutes the external cooling was removed. The reaction mixture was allowed to stir for 4 hours at RT. After removing all residues of solvent under reduced pressure, the crude product was purified by recrystallization from EtOAc/EtOH. The pure product **1b** was isolated as white crystals (1.71 g, 86%). Spectral data are in agreement with literature values.^[4]

¹H NMR (400 MHz, DMSO-*d*₆) δ 8.00 (d, *J* = 7.7 Hz, 1H), 7.77 (d, *J* = 4.6 Hz, 1H), 4.18 (p, *J* = 7.2 Hz, 1H), 2.56 (d, *J* = 4.6 Hz, 3H), 1.82 (s, 3H), 1.15 (d, *J* = 7.2 Hz, 3H).

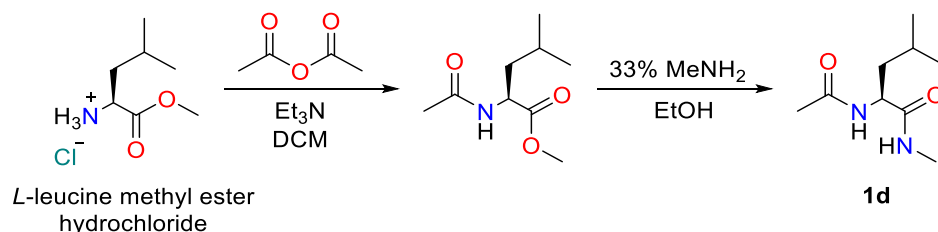
¹³C NMR (101 MHz, DMSO-*d*₆) δ 172.72, 168.95, 48.10, 25.55, 22.58, 18.29.

Elem. Calcd for C₆H₁₂N₂O₂: C 49.99, N 19.43, H 8.39. Found: C 49.96, N 19.57, H 8.25

[α]²⁰_D = -52.0 (c = 1.00 in EtOH)^[5]

HRMS (ESI): calcd for C₆H₁₃N₂O₂ [M + H]⁺, 145.0975; found 145.0972.

(S)-2-acetamido-*N*,4-dimethylpentanamide (*L*-AcLeuNMe, **1d**):



1.81 g of *L*-leucine methyl ester hydrochloride (10 mmol, 1 eq) was dissolved in 20 ml of dry DCM, the solution was cooled down to 0 °C, and 2.8 ml of NEt₃ (2.0 g, 20 mmol, 2 eq) were added dropwise. 1 ml of acetic anhydride (1.12 g, 11 mmol, 1.1 eq) was added dropwise. Then the external cooling was removed. The reaction mixture was stirred overnight, quenched with 50 ml of brine and extracted with EtOAc (3×25 ml). The combined organic layers were dried over MgSO₄. The solvent was evaporated under reduced pressure. Then 6 ml of 33% ethanol solution of methyl amine (50 mmol, 5 eq) was added dropwise to the crude product at 0 °C. After 5 minutes the external cooling was removed, and the reaction mixture was allowed to stir for 4 hours at RT. After removing all residues of solvents under reduced pressure, the crude

product was purified by recrystallization from EtOAc. The pure product was isolated as white crystals (1.35 g, 68%). Spectral data are in agreement with literature values.^[6]

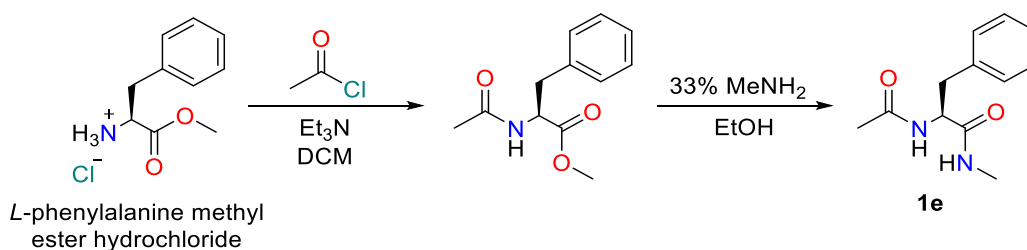
¹H NMR (400 MHz, DMSO-*d*₆) δ 7.96 (d, *J* = 8.3 Hz, 1H), 7.86 (q, *J* = 4.6 Hz, 1H), 4.21 (td, *J* = 8.3, 6.8 Hz, 1H), 2.55 (d, *J* = 4.6 Hz, 3H), 1.82 (s, 3H), 1.58 – 1.46 (m, 1H), 1.45 – 1.34 (m, 2H), 0.86 (d, *J* = 6.6 Hz, 3H), 0.82 (d, *J* = 6.6 Hz, 3H).

¹³C NMR (101 MHz, DMSO-*d*₆) δ 172.59, 169.14, 50.92, 41.06, 25.57, 24.29, 23.00, 22.59, 21.66.

[α]²⁵_D = -37.9 (c = 1.03 in EtOH)^[7]

Elem. Calcd for C₉H₁₈N₂O₂: C, 58.04; H, 9.74; N, 15.04; Found: C 57.75, H 9.75, N 15.11

(*S*)-2-acetamido-*N*-methyl-3-phenylpropanamide (*L*-AcPheNMe, **1e**):



2.15 g of *L*-phenylalanine methyl ester hydrochloride (10 mmol, 1 eq) was dissolved in 50 ml of dry DCM, the solution was cooled down to 0 °C and 3.1 ml of NEt₃ (2.2 g, 22 mmol, 2.2 eq) were added dropwise. 0.78 ml of freshly distilled acetyl chloride (0.86 g, 11 mmol, 1.1 eq) were added dropwise. Then the external cooling was removed. The reaction mixture was stirred for 2 h at RT, quenched with 50 ml of brine and extracted with DCM (3×25 ml). The combined organic layers were dried over MgSO₄, and the solvent was evaporated under reduced pressure. Then 6 ml of 33% ethanol solution of methyl amine (50 mmol, 5 eq) was added dropwise to the crude product at 0 °C. After 5 minutes the external cooling was removed. The reaction mixture was allowed to stir for 4 hours at RT. After removing the solvent under reduced pressure, the crude product was purified by recrystallization from EtOAc/*i*PrOH. The pure product was isolated as white crystals (1.58 g, 72%).

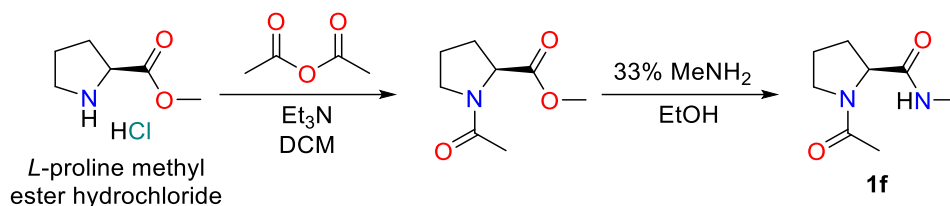
¹H NMR (400 MHz, DMSO-*d*₆) δ 8.12 (d, *J* = 8.5 Hz, 1H), 7.91 (q, *J* = 4.5 Hz, 1H), 7.51 – 7.15 (m, 5H), 4.39 (ddd, *J* = 9.7, 8.4, 5.0 Hz, 1H), 2.94 (dd, *J* = 13.7, 5.0 Hz, 1H), 2.71 (dd, *J* = 13.7, 9.7 Hz, 1H), 2.55 (d, *J* = 4.5 Hz, 3H), 1.75 (s, 3H).

¹³C NMR (101 MHz, DMSO-*d*₆) δ 171.68, 169.09, 138.22, 129.10, 128.09, 126.26, 54.14, 37.83, 25.57, 22.55.

[α]²⁵_D = +21.2 (c = 1.03 in EtOH)^[5]

Elem. Calcd for C₁₂H₁₆N₂O₂: C, 65.43; H, 7.32; N, 12.72; Found: C 65.38, H 7.28, N 12.70.

(S)-1-acetyl-N-methylpyrrolidine-2-carboxamide (*L*-AcProNMe, **1f**):



2.64 g of *L*-proline methyl ester hydrochloride (16 mmol, 1 eq) was dissolved in 30 ml of dry DCM, the solution was cooled down to 0 °C and 4.46 ml of NEt₃ (3.23 g, 32 mmol, 2 eq) were then added dropwise. 1.66 ml of acetic anhydride (1.79 g, 17.5 mmol, 1.1 eq) was then added dropwise. Then the external cooling was removed and reaction mixture was stirred overnight at RT, quenched with 50 ml of brine and extracted with DCM (3×25 ml). The combined organic layers were dried over MgSO₄, and the solvent was evaporated under reduced pressure. Then 10 ml of 33% ethanol solution of methyl amine (83 mmol, 8.3 eq) were added dropwise to the crude product at 0 °C. After 5 minutes the external cooling was removed, and the reaction mixture was allowed to stir overnight at RT. After removing the solvent under reduced pressure, the crude product was purified by recrystallization from *i*Hex/EtOAc. The pure product was isolated as white crystals (2.09 g, 76%). Spectral data are in agreement with literature values.^[8]

Major conformer:

¹H NMR (400 MHz, DMSO-*d*₆) δ 7.71 (br, 1H), 4.17 (dd, *J* = 8.6, 2.9 Hz, 1H), 3.56-3.49 (m, 1H), 3.46-3.37 (m, 1H), 2.54 (d, *J* = 4.6 Hz, 3H), 2.00-1.90 (m, 1H), 1.96 (s, 3H), 1.89-1.66 (m, 3H)

¹³C NMR (101 MHz, DMSO-*d*₆) δ 172.15, 168.71, 59.40, 47.48, 29.65, 25.56, 24.20, 22.45.

Minor conformer:

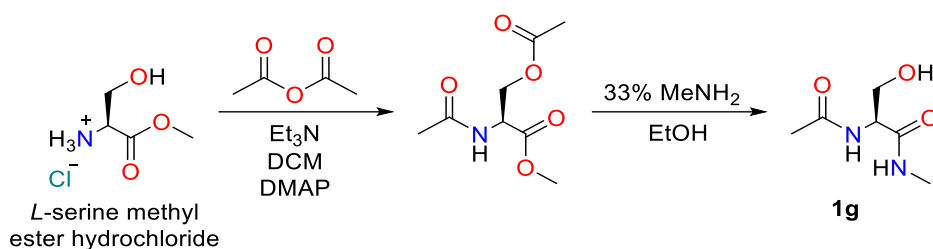
¹H NMR (400 MHz, DMSO-*d*₆) δ 7.97 (bs, 1H), 4.26 (dd, *J* = 8.6, 3.0 Hz, 1H), 3.46-3.67 (m, 2H), 2.60 (d, *J* = 4.6 Hz, 3H), 2.19-1.08 (m, 1H), 1.90-1.66 (m, 3H), 1.80 (s, 3H).

¹³C NMR (101 MHz, DMSO-*d*₆) δ 172.22, 168.63, 60.67, 46.19, 31.69, 25.76, 22.54, 22.11.

[α]²⁵_D = -85.9 (c = 1.003 in EtOH)^[9]

Elem. Calcd for C₈H₁₄N₂O₂: C, 56.45; H, 8.29; N, 16.46; Found: C 56.21, H 8.08, N 16.30

(S)-2-acetamido-3-hydroxy-*N*-methylpropanamide (*L*-AcSerNMe, **1g**):



1.55 g of *L*-serine methyl ester hydrochloride (10 mmol, 1 eq) was dissolved in 30 ml of dry DCM, the solution was cooled down to 0 °C, 4.2 ml of NEt_3 (3.0 g, 30 mmol, 3 eq) were added dropwise, followed by addition of a catalytic amount of DMAP. 4.7 ml of acetic anhydride (5.1 g, 50 mmol, 5 eq) were added dropwise. Then the external cooling was removed. The reaction mixture was stirred overnight, quenched with 50 ml of brine and extracted with DCM (3×25 ml). The combined organic layers were dried over MgSO_4 , and the solvent was evaporated under reduced pressure. Then 6 ml of 33% ethanol solution of methyl amine (50 mmol, 5 eq) was added dropwise to the crude product at 0 °C. After 5 minutes the external cooling was removed, and the reaction mixture was allowed to stir for 4 hours at RT. After removing the solvent under reduced pressure, the crude product was purified by recrystallization from EtOAc/*i*PrOH. The pure product was isolated as white solid (1.10 g, 69%). Spectral data are in agreement with literature values.^[10]

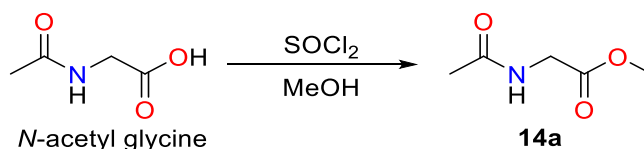
^1H NMR (400 MHz, $\text{DMSO-}d_6$) δ 7.88 (d, J = 8.1 Hz, 1H), 7.78 (q, J = 4.6 Hz, 1H), 4.85 (t, J = 5.6 Hz, 1H), 4.19 (dt, J = 8.1, 5.6 Hz, 1H), 3.52 (t, J = 5.6 Hz, 2H), 2.56 (d, J = 4.6 Hz, 3H), 1.85 (s, 3H).

^{13}C NMR (101 MHz, $\text{DMSO-}d_6$) δ 170.60, 169.42, 61.69, 55.22, 25.67, 22.73.

$[\alpha]^{23}_D$ = -18.9 (c = 1.059 in MeOH)^[11]

Elem. Calcd for $\text{C}_6\text{H}_{12}\text{N}_2\text{O}_3$: C, 44.99; H, 7.55; N, 17.49; Found: C 44.98, H 7.65, N 14.75.

Methyl acetylglycinate (AcGlyOMe, **14a**):



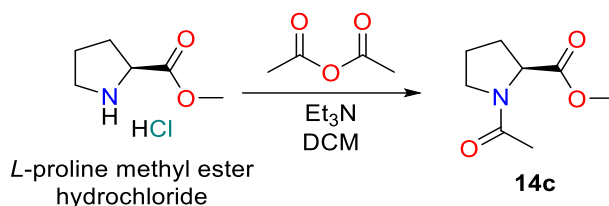
1.46 ml of SOCl_2 (2.4 g, 20 mmol, 2 eq) was added dropwise to 1.18 g of *N*-acetyl glycine (10 mmol, 1 eq) in 6 ml of dry MeOH at 0 °C. Then the external cooling was removed and the reaction mixture was allowed to stir overnight at RT. After removing all residues of solvent

under reduced pressure, the crude product was purified on a short silica column chromatography (CH₂Cl₂/MeOH = 20/1). Pure AcGlyOMe was isolated as a colorless solid (0.51 g, 3.9 mmol, 39%). Spectral data are in agreement with literature values.^[6]

¹H NMR (400 MHz, DMSO-*d*₆) δ 8.30 (t, *J* = 6.0 Hz, 1H), 3.80 (d, *J* = 6.0 Hz, 2H), 3.62 (s, 3H), 1.85 (s, 3H).

Elem. Calcd for C₅H₉NO₃: C 45.80, N 10.68, H 6.92. Found: C 45.85, N 7.19, H 6.92.

Methyl acetyl-*L*-prolinate (AcProOMe, **14c**):



L-proline methyl ester hydrochloride (1.0 g, 6.04 mmol) was dissolved in 50 mL dry DCM under nitrogen atmosphere at 0 °C. 0.7 ml of NEt₃ (1 ml, 12.08 mmol, 2 eq) was added to the mixture and then 0.6 ml of acetic anhydride (0.65 g, 6.64 mmol, 1.1 eq) was added dropwise. The reaction mixture was stirred overnight, quenched with 50 ml of brine and extracted with DCM (3×25 ml). The combined organic layers were dried over MgSO₄ and the solvent was evaporated under reduced pressure. The product was purified by column chromatography on silica (EtOAc/iHexane = 1:1→1:0). The product was obtained as a colorless liquid (0.86 g, 83 %). Spectral data are in agreement with literature values.^[12]

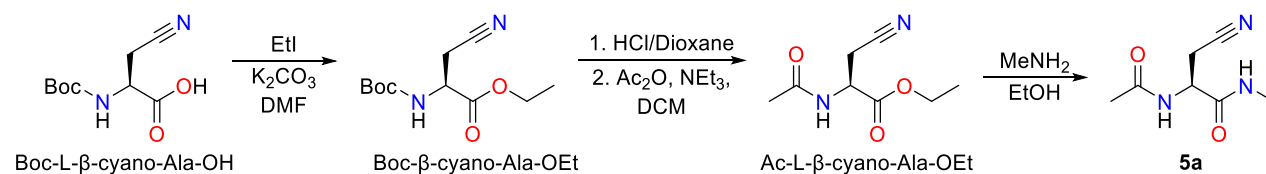
Major conformer:

¹H NMR (400 MHz, DMSO-*d*₆) δ 4.25 (dd, *J* = 8.7, 4.2 Hz, 1H), 3.60 (s, 3H), 3.57 – 3.46 (m, 2H), 2.22 – 2.08 (m, 1H), 1.97 (s, 3H), 1.96 – 1.86 (m, 2H), 1.86 – 1.78 ppm (m, 1H).

Elem. Calcd for C₈H₁₃NO₃: C, 56.13; H, 7.65; N, 8.18; Found: C 56.14, H 7.77, N 8.29.

2.6.1.3. Synthesis of cyanomethylation adducts of AcGlyNMe (**1a**)

(*S*)-2-acetamido-3-cyano-*N*-methylpropanamide (AcAla(CN)NMe, **5a**)



To 2.12 g Boc-*L*-β-cyano-Ala-OH (9.9 mmol, 1 eq) in DMF (20 mL) was added 1.37 g of K₂CO₃ (9.9 mmol, 1 eq). The reaction mixture was cooled down to 0 °C and then 2.4 ml of

ethyl iodide were added dropwise (4.6 g, 29.7 mmol, 3 eq). After stirring at RT for 18 h, the reaction mixture was quenched with brine (100 mL) and extracted with EtOAc (2×50 mL). The combined organic layers were washed with brine (50 mL), dried over MgSO₄ and concentrated in *vacuo*. The crude product was purified by flash chromatography (*i*Hex/EtOAc = 3/1, R_f 0.29) to give 1.55 g of Boc-β-cyano-Ala-OEt (6.4 mmol, 65%) as a white solid. Spectral data are in agreement with literature values.^[13]

¹H NMR (400 MHz, CDCl₃) δ 5.46 (d, *J* = 7.2 Hz, 1H), 4.49 (dt, *J* = 7.2, 5.0 Hz, 1H), 4.30 (qd, *J* = 7.2, 3.9 Hz, 2H), 3.01 (dd, *J* = 16.9, 5.4 Hz, 1H), 2.93 (dd, *J* = 16.9, 4.8 Hz, 1H), 1.46 (s, 9H), 1.33 (t, *J* = 7.2 Hz, 3H).

1.55 g of Boc-β-cyano-Ala-OEt (6.4 mmol, 1 eq) was dissolved in 4M HCl/Dioxane, stirred for 1 hour at RT and concentrated in *vacuo*. To a suspension of the hydrochloride salt in 50 ml of dry DCM were added 2.5 ml of NEt₃ (1.93 g, 19.2 mmol, 3 eq) and 3 ml of Ac₂O (3.26 g, 32.0 mmol, 5 eq). After stirring at RT for 2 h, the reaction mixture was quenched with H₂O (50 mL) and extracted with DCM (2×25 mL). The combined organic layers were washed with brine (50 mL), dried over MgSO₄ and concentrated in *vacuo*. The crude product was purified by flash chromatography (DCM/MeOH = 20/1, R_f 0.31) to give 810 mg of Ac-*L*-β-cyano-Ala-OEt (4.4 mmol, 74%) as a white solid.

¹H NMR (400 MHz, CDCl₃) δ 6.48 (s, 1H), 4.72 (ddd, *J* = 6.6, 5.3, 4.3 Hz, 1H), 4.32 (qq, *J* = 10.8, 7.1 Hz, 2H), 3.09 (dd, *J* = 16.9, 5.3 Hz, 1H), 2.94 (dd, *J* = 16.9, 4.3 Hz, 1H), 2.08 (s, 3H), 1.34 (t, *J* = 7.1 Hz, 3H).

¹³C NMR (101 MHz, CDCl₃) δ 170.39, 168.95, 116.29, 63.02, 49.18, 23.08, 21.45, 14.18.

250 mg of Ac-β-cyano-Ala-OEt (1.36 mmol, 1 eq) was treated with 1 ml of MeNH₂ (33%, EtOH) for 30 min at RT. The reaction mixture was concentrated in *vacuo*. The residue was purified by flash chromatography (CH₂Cl₂/MeOH = 10/1, R_f 0.37) to give 149 mg of **5a** (0.88 mmol, 65%) as a white solid. Spectral data are in agreement with literature values.^[14]

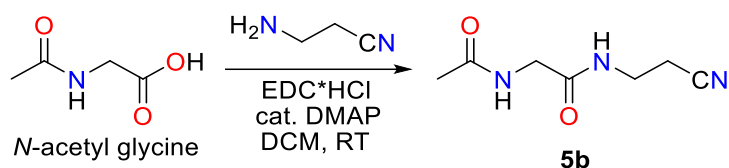
¹H NMR (400 MHz, CDCl₃) δ 7.01 (d, *J* = 8.2 Hz, 1H), 6.95 (br, 1H), 4.85 (dt, *J* = 8.3, 6.5 Hz, 1H), 2.88 (dd, *J* = 16.8, 6.5 Hz, 1H), 2.84 (d, *J* = 4.8 Hz, 3H), 2.79 (dd, *J* = 16.8, 6.5 Hz, 1H), 2.07 (s, 3H).

¹³C NMR (101 MHz, CDCl₃) δ 171.02, 169.16, 116.98, 49.32, 26.65, 23.18, 21.26.

Elem. Calcd for C₇H₁₁N₃O₂ (169.1811) C 49.70, N 24.84, H 6.55. Found: C 49.86, N 24.62, H 6.30.

HRMS (ESI): calcd for C₇H₁₂N₃O₂ [M + H], 170.0924; found 170.0925.

2-acetamido-*N*-(2-cyanoethyl)acetamide (AcGlyNEtCN, **5b**):



To a solution of *N*-acetyl glycine (117 mg, 1 mmol), DMAP (7.5 mg, 0.05 mmol) and EDC·HCl (193 mg, 1.1 mmol) in DCM (10 mL) was added 3-aminopropionitrile (75 μ l, 1 mmol). The reaction mixture was stirred at RT overnight and then evaporated in *vacuo*. The residue was purified by flash chromatography (CH₂Cl₂/MeOH= 10/1, R_f 0.25) to give **5b** (132 mg, 80%) as a white solid.

¹H NMR (400 MHz, DMSO-*d*₆) δ 8.20 (t, *J* = 5.7 Hz, 1H), 8.14 (t, *J* = 5.9 Hz, 1H), 3.65 (d, *J* = 5.9 Hz, 2H), 3.29 (q, *J* = 6.4 Hz, 2H), 2.63 (t, *J* = 6.4 Hz, 2H), 1.85 (s, 3H).

¹³C NMR (101 MHz, DMSO-*d*₆) δ 169.66, 169.59, 119.30, 41.96, 34.83, 22.54, 17.57.

Elem. Calcd for C₇H₁₁N₃O₂ (169.1811) C 49.70, N 24.84, H 6.55. Found: C 49.45, N 24.62, H 6.25.

HRMS (ESI): calcd for C₇H₁₂N₃O₂ [M + H]⁺, 170.0924; found 170.0924.

scXRD:

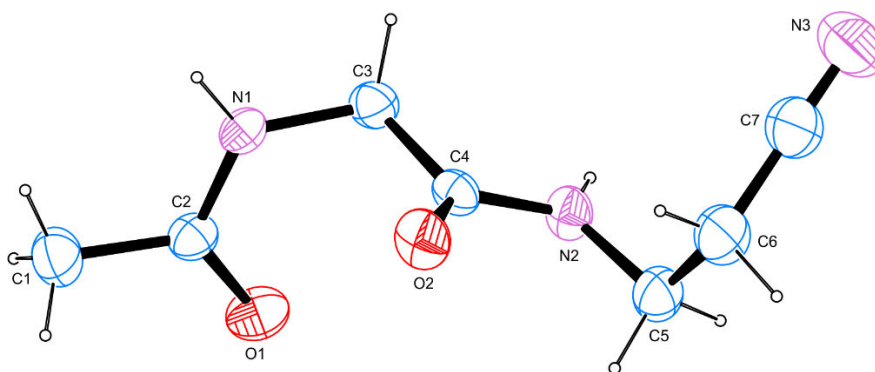


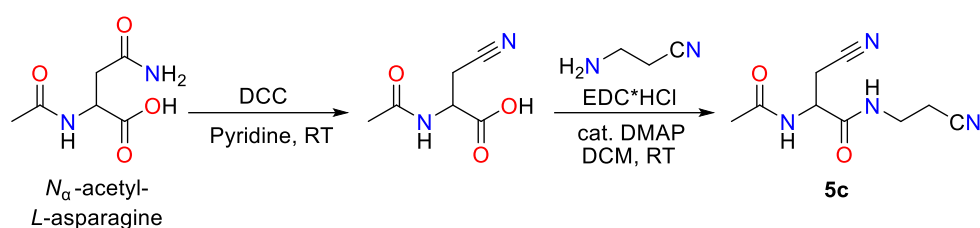
Fig. S1. X-ray structure of **5b**.

Table S1. Crystallographic data for **5b**.

net formula	C ₇ H ₁₁ N ₃ O ₂	transmission factor range	0.89–1.00
M _r /g mol ⁻¹	169.19	refls. measured	8596
crystal size/mm	0.080 × 0.040 × 0.030	R _{int}	0.0271
T/K	298.(2)	mean σ (I)/I	0.0223
radiation	MoK α	θ range	2.800–25.346
diffractometer	Bruker D8 Venture TXS	observed refls.	1398
crystal system	monoclinic	x, y (weighting scheme)	0.0572, 0.6642
space group	P 1 21/n 1	hydrogen refinement	constr

$a/\text{\AA}$	8.1185(4)	Flack parameter	?
$b/\text{\AA}$	5.0815(2)	refls in refinement	1678
$c/\text{\AA}$	22.4396(11)	parameters	138
$\alpha/^\circ$	90	restraints	23
$\beta/^\circ$	97.461(2)	R(F_{obs})	0.0625
$\gamma/^\circ$	90	R_w(F²)	0.1691
$V/\text{\AA}^3$	917.89(7)	S	1.160
Z	4	shift/error_{max}	0.001
calc. density/g cm⁻³	1.224	max electron density/e \AA^{-3}	0.154
μ/mm^{-1}	0.092	min electron density/e \AA^{-3}	-0.157
absorption correction	Multi-Scan		

2-acetamido-3-cyano-*N*-(2-cyanoethyl)propenamide (AcAla(CN)NEtCN, **5c**):



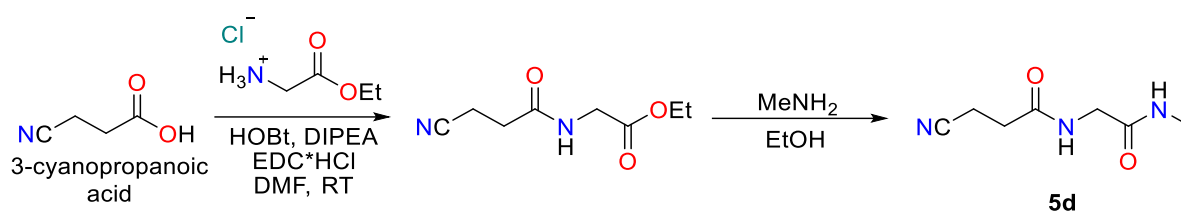
To *N* α -acetyl-*L*-asparagine (174 mg, 1 mmol) in 3 mL of dry pyridine was added DCC (206 mg, 1 mmol). The resulting mixture was stirred for 3 hours at RT. Then the DCU precipitate was filtered off and washes with acetone. The filtrate was concentrated in *vacuo* and the crude material was used further without purification. To a solution of the crude material, DMAP (7.5 mg, 0.05 mmol) and EDC·HCl (193 mg, 1.1 mmol) in DCM (10 mL) was added, followed by 3-aminopropionitrile (75 μ l, 1 mmol). The reaction mixture was stirred at RT overnight and then evaporated in *vacuo*. The residue was purified by flash chromatography (CH₂Cl₂/MeOH= 10/1, R_f 0.25) to give **5c** (172 mg, 83%) as a colorless oil.

¹H NMR (400 MHz, MeOH-*d*₄) δ 4.69 (dd, J = 8.2, 5.6 Hz, 1H), 3.46 (t, J = 6.6 Hz, 2H), 2.97 (dd, J = 17.0, 5.6 Hz, 1H), 2.86 (dd, J = 17.0, 8.2 Hz, 1H), 2.67 (t, J = 6.6 Hz, 2H), 2.04 (s, 3H).

¹³C NMR (101 MHz, MeOH-*d*₄) δ 173.50, 171.33, 119.27, 118.19, 50.87, 36.71, 22.46, 20.88, 18.29.

HRMS (ESI): calcd for C₉H₁₃N₄O₃ [M + H]⁺, 209.1033; found 209.1035.

3-cyano-*N*-(2-(methylamino)-2-oxoethyl)propenamide **5d**:



To a mixture of 3-cyanopropanoic acid (99 mg, 1 mmol) and HOBt (168 mg, 1.1 mmol) in 5 mL of dry DMF were added DIPEA (392 μ L, 2.2 mmol) followed by the addition of EDC \cdot HCl (211 mg, 1.1 mmol). The resulting mixture was stirred for 5 min, and then glycine ethyl ester hydrochloride (153.5 mg, 1.1 mmol) was added. The reaction was stirred overnight at RT. The mixture was washed with brine, extracted with EtOAc (3 \times 5 ml), and the organic layers were concentrated under vacuum to give crude material, which was used further without purification. It was treated with excess of MeNH₂ (33%, EtOH) for 1 hour at RT. The reaction mixture was concentrated in *vacuo*. The residue was purified by recrystallization from *i*Hex/EtOAc to give **5d** (105 mg, 62%) as a white solid.

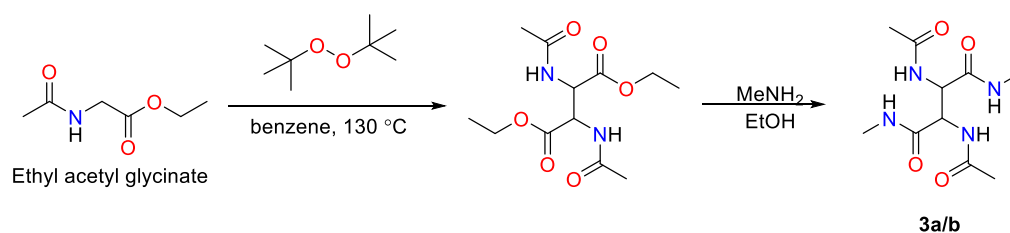
¹H NMR (400 MHz, DMSO-*d*₆) δ 8.29 (d, *J* = 5.8 Hz, 1H), 7.79 (br, 1H), 3.66 (d, *J* = 5.8 Hz, 2H), 2.63 (td, *J* = 7.0, 1.0 Hz, 2H), 2.58 (d, *J* = 4.6 Hz, 3H), 2.52 (s, 2H).

¹³C NMR (101 MHz, DMSO-*d*₆) δ 169.60, 169.07, 120.47, 42.10, 30.21, 25.48, 12.43.

HRMS (ESI): calcd for C₇H₁₂N₃O₂ [M + H]⁺, 170.0924; found 170.0925.

2.6.1.4. Synthesis of dimerization adducts of AcGlyNMe (**1a**)

2,3-diacetamido-*N*¹,*N*⁴-dimethylsuccinamide (**3a/b**):



3.5 ml of di-tert butyl peroxide (19 mmol, 5 eq) was added to 550 mg of ethyl acetyl glycinate (3.8 mmol, 1 eq) in 4 ml of dry degassed benzene. The reaction tube was sealed and heated up to 130 °C for 15 hours. Then all volatiles were removed under reduced pressure, and the crude product was treated with excess of MeNH₂ (33%, EtOH) for 4 hours. The white precipitate was separated by centrifuge, washed with MeCN (3 \times 1 ml) and dried in *vacuo* (144 mg, 29%).

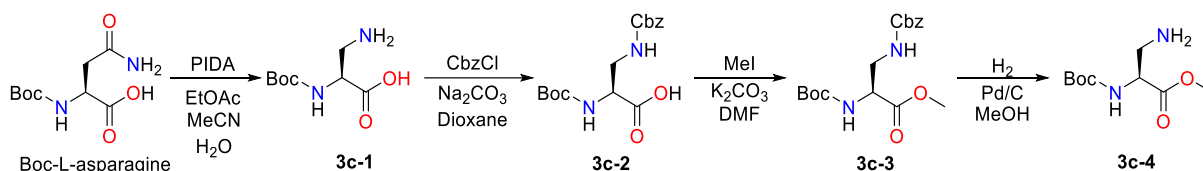
¹H NMR (400 MHz, D₂O) δ 4.82 (s, 1H), 2.68 (s, 3H), 2.67 (s, 3H), 1.99 (s, 6H).

^{13}C NMR (101 MHz, D_2O) δ 174.17, 174.13, 170.46, 170.26, 54.21, 53.61, 25.85, 25.79, 21.69, 21.67.

HRMS (ESI): calcd for $\text{C}_{10}\text{H}_{18}\text{N}_4\text{O}_4\text{Na}$ $[\text{M} + \text{Na}]^+$, 281.1220; found 281.1220.

Elem. Calcd for $\text{C}_{10}\text{H}_{18}\text{N}_4\text{O}_4$: C 46.50, N 21.69, H 7.02. Found: C 46.26, N 21.48, H 6.83.

2-acetamido-3-(2-acetamidoacetamido)-*N*-methylpropanamide (**3c**):



Modified literature procedure^[15]

To a stirring slurry of 2.32 g Boc-*L*-asparagine (10 mmol, 1 eq) in 12 mL EtOAc, 12 mL MeCN, and 3 mL H₂O at 10 °C, 3.22 g of PIDA (12 mmol, 1.2 eq) were added portion-wise. The reaction was stirred at 10 °C for 30 minutes, after which the temperature was allowed to reach RT, and the reaction was stirred for an additional 4 hours. Subsequently, the reaction was cooled using an ice bath and filtered. The filter cake was washed with EtOAc and dried under reduced pressure. **3c-1** was obtained as a white powder (1.42 g, 72%)

^1H NMR (400 MHz, MeOH-*d*₄) δ 4.06 (t, J = 6.5 Hz, 1H), 3.21 – 3.10 (m, 2H), 1.46 (s, 9H).

Modified literature procedure (US2006189806)

1.0 g of **3c-1** (4.9 mmol, 1 eq) was dissolved in a 10% aqueous solution of Na₂CO₃ (1.14 g, 10.74 mmol, 2.2 eq.) and 10 mL of 1,4-dioxane. Then, 0.76 mL of benzyl chloroformate (5.36 mmol, 1.1 eq.) was added dropwise, and the solution was stirred at RT for 3 hours. The reaction mixture was quenched with water and washed with diethyl ether (50 mL). The aqueous phase was acidified to pH 2 using 6M HCl, and the resulting mixture was extracted with EtOAc (3×50 mL). The organic layers were combined, washed with brine, and dried over MgSO₄. The solvent was removed under reduced pressure to yield a pale-yellow oil of **3c-2** (1.60 g, 97%). The crude material was used without further purification. Spectral data are in agreement with literature values.^[16]

^1H NMR (400 MHz, DMSO-*d*₆) δ 12.63 (bs, 1H), 7.40 – 7.26 (m, 6H), 6.97 (d, J = 8.2 Hz, 1H), 5.02 (s, 2H), 4.06 – 4.01 (m, 1H), 3.36 – 3.21 (m, 2H), 1.38 (s, 9H).

Modified literature procedure.^[16]

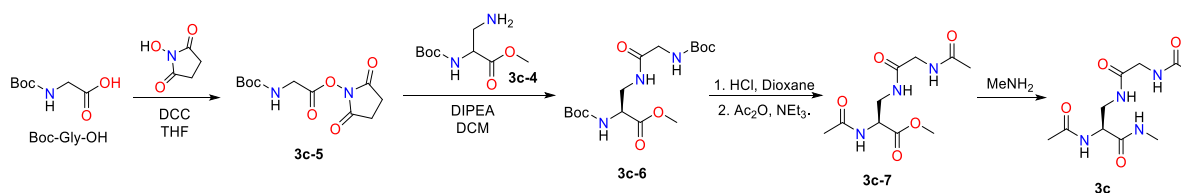
A suspension of **3c-2** (1.6 g, 4.9 mmol, 1.0 eq) and K₂CO₃ (6.73 g, 48.8 mmol, 10.0 eq) in 20 mL of dry DMF was stirred at 10 °C. MeI (6.1 mL, 13.86 g, 97.6 mmol, 20 eq) was added slowly, and the reaction mixture was stirred at RT overnight. The solvent was evaporated, and the residue was dissolved in water and extracted with EtOAc (3×50 mL). The organic layers were combined and dried over MgSO₄. The solvent was evaporated, and the residue was purified by column chromatography (EtOAc/iHex = 1/1, R_f 0.64) to yield **3c-3** as a colorless oil (1.54 g, 90%). Spectral data are in agreement with literature values.^[17]

¹H NMR (400 MHz, CDCl₃) δ 7.38 – 7.28 (m, 5H), 5.44 (d, *J* = 7.5 Hz, 1H), 5.15 (bs, 1H), 5.09 (s, 2H), 4.45 – 4.32 (m, 1H), 3.73 (s, 3H), 3.64 – 3.55 (m, 2H), 1.43 (s, 9H).

Modified literature procedure.^[16]

A suspension of **3c-3** (1.54 g), obtained from previous step, and 10% Pd/C (200 mg) was stirred in methanol (50 mL) under a H₂ atmosphere at RT overnight. After filtration through a Celite pad and washing with methanol, the solvent was evaporated under reduced pressure, and the residue was dried in vacuo to yield **3a-4** as a colorless oil (0.88 g, 88%). Spectral data are in agreement with literature values.^[17]

¹H NMR (400 MHz, CDCl₃) δ 5.42 (bs, 1H), 4.33 – 4.28 (m, 1H), 3.75 (s, 3H), 3.04 (d, *J* = 4.6 Hz, 2H), 1.44 (s, 9H).



Modified literature procedure.^[18]

Boc-Gly-OH (1.05 g, 6 mmol, 1 eq) and *N*-hydroxysuccinimide (1.03 g, 9 mmol, 1.5 eq) were dissolved in 24 ml of dry THF and stirred at RT. DCC (2.47 g, 12 mmol, 2 eq) was added to the reaction mixture, which was then stirred overnight at RT. Then, a few drops of glacial acetic acid were added, and the mixture was stirred for an additional hour. DCU was filtered off and the filter cake washed with THF. The solvent was removed under reduced pressure, and the crude material was recrystallized from isopropanol, yielding a white solid of **3c-5**. (1.54 g, 95%). Spectral data are in agreement with literature values.^[18]

Major conformer:

¹H NMR (400 MHz, CDCl₃) δ 5.02 (bs, 1H), 4.28 (d, *J* = 5.9 Hz, 2H), 2.84 (s, 4H), 1.45 (s, 9H).

878 mg of **3c-4** (4 mmol, 1 eq) and 0.7 ml of DIPEA (4 mmol, 1 eq) were added to 1.1 g of **3c-5** (4 mmol, 1 eq) in 50 ml of dry DCM. The reaction mixture was stirred overnight at RT. All the volatiles were evaporated, and the crude material was purified by column chromatography (EtOAc/*i*Hex = 3/1, R_f 0.46). 1.05 g of Boc-protected peptide **3c-6** was obtained as a white solid (2.8 mmol, 70%).

$^1\text{H NMR}$ (400 MHz, CDCl_3) δ 6.61 (bs, 1H), 5.50 (d, $J = 7.4$ Hz, 1H), 5.08 (bs, 1H), 4.38 (q, $J = 6.6$ Hz, 1H), 3.76 – 3.50 (m, 7H), 1.46 (s, 9H), 1.44 (s, 9H).

Boc-deprotection of **3c-6** has performed by treating of 375 mg of the obtained solid (1 mmol, 1 eq) with 4M HCl in dioxane for 1 hour at RT. Then all the volatiles were evaporated, the hydrochloride salt was mixed with 0.95 ml of acetic anhydride (10 mmol, 10 eq) and 835 μl of triethylamine (6 mmol, 6 eq). The reaction was allowed to stir overnight, the white precipitate was filtered off, washed with DCM (3 \times 2 ml) and dried in *vacuo*. 217 mg of **3c-7** as white solid was obtained (0.84 mmol, 84%).

$^1\text{H NMR}$ (400 MHz, MeOH-*d*4) δ 4.54 (dd, $J = 6.7, 5.4$ Hz, 1H), 3.80 (s, 2H), 3.73 (s, 3H), 3.66 (dd, $J = 13.8, 5.4$ Hz, 1H), 3.50 (dd, $J = 13.8, 6.7$ Hz, 1H), 2.01 (s, 3H), 1.99 (s, 3H).

$^{13}\text{C NMR}$ (101 MHz, MeOH-*d*4) δ 173.93, 173.39, 172.38, 172.06, 53.69, 52.97, 43.54, 41.28, 22.44, 22.42.

HRMS (ESI): calcd for $\text{C}_{10}\text{H}_{17}\text{N}_3\text{O}_5\text{Na}$ [$\text{M} + \text{Na}$] $^+$, 282.1060; found 282.1061.

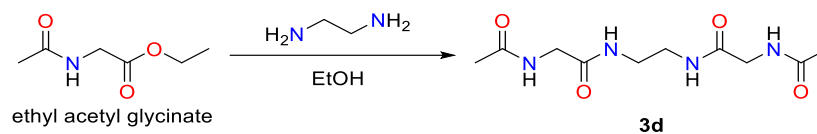
100 mg of obtained material was mixed with an excess of MeNH_2 (33%, EtOH) for 2 h at RT. Then all the volatiles were evaporated, and compound **3c** was obtained as a white powder (97 mg, 97%).

$^1\text{H NMR}$ (400 MHz, DMSO-*d*6) δ 8.11 (t, $J = 5.7$ Hz, 1H), 7.91 (d, $J = 8.0$ Hz, 1H), 7.82 – 7.77 (m, 2H), 4.23 (td, $J = 7.8, 5.7$ Hz, 1H), 3.67 – 3.57 (m, 2H), 3.40 – 3.35 (ddd, overlapped with solvent), 3.18 (ddd, $J = 13.3, 7.6, 5.7$ Hz, 1H), 2.57 (s, 1H), 2.56 (s, 2H), 1.85 (s, 3H), 1.84 (s, 3H).

$^{13}\text{C NMR}$ (101 MHz, MeOH-*d*4) δ 174.01, 173.50, 172.58, 172.53, 54.68, 43.65, 41.86, 26.42, 22.66, 22.45.

HRMS (ESI): calcd for $\text{C}_{10}\text{H}_{18}\text{N}_4\text{O}_4\text{Na}$ [$\text{M} + \text{Na}$] $^+$, 281.1220; found 281.1221.

(*N,N'*-(ethane-1,2-diyl)bis(2-acetamidoacetamide) (**3d**):



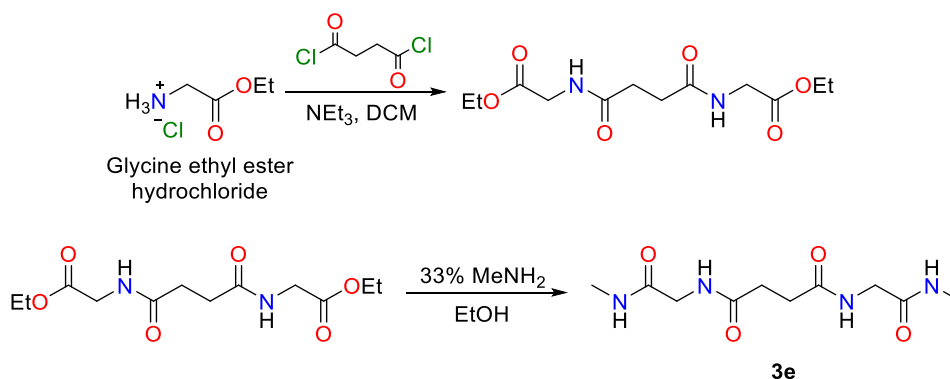
0.218 ml of ethylenediamine (3.3 mmol, 1 eq) was added dropwise to ethyl acetyl glycinate (1 g, 6.9 mmol, 2.1 eq), dissolved in 1 ml of EtOH, at 0 °C. After 5 minutes the external cooling was removed. The reaction mixture was stirred for 4 h at RT. The precipitate was filtered off, washed with EtOH (3×2 ml) and dried in *vacuo*. The pure product was isolated as a white solid (341 mg, 40%).

¹H NMR (600 MHz, D₂O) δ 3.79 (s, 4H), 3.27 (s, 4H), 1.99 (s, 6H).

¹³C NMR (150 MHz, D₂O) δ 174.70, 171.71, 42.37, 38.42, 21.56.

HRMS (ESI): calcd for C₁₀H₁₈N₄O₄Na [M + Na]⁺, 281.1220; found 281.1220.

*N*¹,*N*⁴-bis(2-(methylamino)-2-oxoethyl)succinimide (**3e**):



After 4 g of glycine ethyl ester hydrochloride (28.8 mmol, 2 eq) were dissolved in 70 ml of DCM, 8 ml of NEt₃ (5.8 g, 57.5 mmol, 4 eq) were added dropwise. The solution was cooled down to -25 °C, and 1.58 ml of succinyl chloride (14.4 mmol, 2.23 g, 1 eq) were then added dropwise. The reaction mixture was stirred for 2 h at -25 °C, slowly warmed up to RT and stirred 2 h additionally. The solvent was removed in *vacuo*. The solid was dissolved in 100 ml of EtOAc, and the organic phase was washed with 1N HCl (3×50 ml) and with brine. The solvent was removed under reduced pressure. The product was isolated as a white solid (2.5 mg, 60%) and was used without further purification. 10.8 ml of 33% ethanol solution of methylamine (87 mmol, 5 eq) was added dropwise at 0 °C. After 5 minutes the external cooling was removed. Reaction mixture was allowed to stir for 4 h at RT. After removing the solvent under

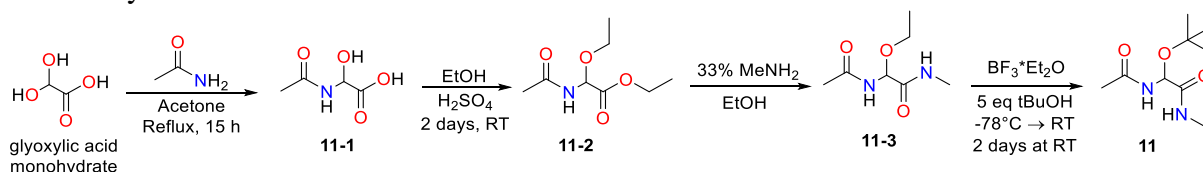
reduced pressure, the crude product was purified by recrystallization from EtOH/H₂O. Pure product was isolated as a white solid (1.8 g, 71%).

¹H NMR (600 MHz, D₂O) δ 3.73 (s, 4H), 2.59 (s, 6H), 2.51 (s, 4H).

¹³C NMR (150 MHz, D₂O) δ 175.59, 171.92, 42.34, 30.15, 25.58.

HRMS (ESI): calcd for C₁₀H₁₈N₄O₄Na [M + Na]⁺, 281.1220; found 281.1220.

2.6.1.5. Synthesis of the recombination adduct **11**



Acetamide (5 g, 84.7 mmol, 1 eq) and glyoxylic acid monohydrate (8.6 g, 93.2 mmol, 1.1 eq) were dissolved in 150 mL of dry acetone. The reaction mixture was refluxed for 15 hours. Then, the reaction mixture was concentrated under reduced pressure, and compound **11-1** was obtained as an amorphous glass (88%). Concentrated H₂SO₄ (2 mL) was added to an ice-cooled solution of **11-1** in 100 mL of EtOH. The reaction mixture was stirred for 48 hours at RT. The reaction was then quenched with an ice-cooled saturated NaHCO₃ solution (100 mL). The mixture was extracted with EtOAc (3×100 ml), and the combined organic layers were dried over MgSO₄ and evaporated under reduced pressure. The crude material was purified by vacuum distillation to yield compound **11-2** as a white solid (7.9 g, 45% yield).

¹H NMR (600 MHz, CDCl₃) δ 6.57 (t, *J* = 9.2 Hz, 1H), 5.56 (d, *J* = 9.2 Hz, 1H), 4.31 – 4.18 (m, 2H), 3.76 – 3.62 (m, 2H), 2.05 (s, 3H), 1.31 (t, *J* = 7.2 Hz, 3H), 1.21 (t, *J* = 7.0 Hz, 3H).

475 mg of **11-2** (2.5 mmol, 1 eq) was dissolved in 1.4 ml of 33% ethanol solution of methyl amine (11.7 mmol, 4.67 eq) at 0 °C. After 5 minutes the external cooling was removed, and the reaction mixture allowed to stir for 4 h at RT. After removing the solvent under reduced pressure, the crude product was purified by recrystallization from EtOAc/EtOH. The pure product **11-3** was isolated as a white solid (305 mg, 86%).

¹H NMR (400 MHz, CDCl₃) δ 6.87 – 6.76 (m, 2H), 5.53 (d, *J* = 8.7 Hz, 1H), 3.72 (dq, *J* = 9.2, 7.0 Hz, 1H), 3.62 (dq, *J* = 9.4, 7.0 Hz, 1H), 2.84 (d, *J* = 4.9 Hz, 3H), 2.06 (s, 3H), 1.21 (t, *J* = 7.0 Hz, 3H).

200 μL of BF₃·Et₂O (1.6 mmol, 1.6 eq) was added to a stirring suspension of 174 mg **11-3** (1 mmol, 1 eq) in 5 mL of Et₂O at -78 °C under an N₂ atmosphere. 474 μL of *t*-BuOH (5 mmol,

5 eq) were added dropwise, and the external cooling was removed. The reaction was allowed to slowly warm up to RT and then stirred for 48 hours. Afterwards, the reaction was carefully quenched with 5 ml of saturated aqueous NaHCO₃ solution and extracted with EtOAc (3×10 ml). The organic layers were combined and dried over MgSO₄. All volatiles were evaporated under reduced pressure, and the crude material was purified by column chromatography (DCM/MeOH = 10/1, R_f 0.40). Product **11** was obtained as a colorless oil (97 mg, 48%).

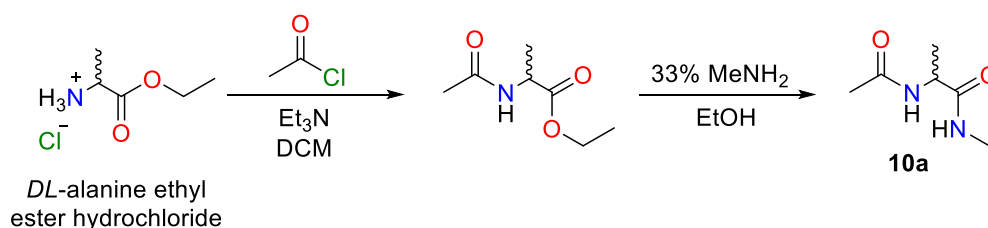
¹H NMR (400 MHz, CDCl₃) δ 7.28 (d, *J* = 9.1 Hz, 1H), 7.07 (q, *J* = 5.0 Hz, 1H), 5.56 (d, *J* = 9.2 Hz, 1H), 2.74 (d, *J* = 4.9 Hz, 3H), 1.92 (s, 3H), 1.19 (s, 9H).

¹³C NMR (101 MHz, CDCl₃) δ 170.43, 170.27, 76.16, 73.00, 28.10, 26.06, 23.21.

HRMS (ESI): calcd for C₉H₁₈N₂O₃K [M + K]⁺, 241.0949; found 241.0950

2.6.1.6. Synthesis of methylation adducts of AcGlyNMe **1a**

2-acetamido-*N*-methylpropanamide (*DL*-Ala-NMe, **10a**):

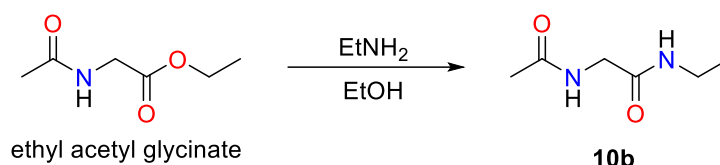


1 g of *DL*-alanine ethyl ester hydrochloride (6.5 mmol, 1 eq) was dissolved in 30 ml of dry DCM, the solution was cooled down to 0 °C, and 1.83 ml of NEt₃ (1.32 g, 13.1 mmol, 2 eq) was added dropwise, followed by 0.46 ml of freshly distilled acetyl chloride (0.51 g, 6.5 mmol, 1 eq). Then the external cooling was removed, and the reaction mixture was stirred for 2 h at RT, quenched with 50 ml of brine and extracted with DCM (3×25 ml). The combined organic layers were dried over MgSO₄, and the solvent were evaporated under reduced pressure. Then 2.5 ml of 33% ethanol solution of methyl amine (26 mmol, 4.67 eq) was added dropwise to the crude product at 0 °C. After 5 minutes the external cooling was removed and the reaction mixture allowed to stir overnight at RT. After removing all residues of solvents under reduced pressure, the crude product was purified by recrystallization from EtOAc/EtOH. The pure product was isolated as white crystals (0.49 g, 52%).

¹H NMR (400 MHz, DMSO-*d*₆) δ 8.00 (d, *J* = 7.6 Hz, 1H), 7.77 (d, *J* = 5.7 Hz, 1H), 4.18 (p, *J* = 7.2 Hz, 1H), 2.56 (d, *J* = 4.6 Hz, 3H), 1.82 (s, 3H), 1.15 (d, *J* = 7.1 Hz, 3H).

¹³C NMR (101 MHz, DMSO-*d*₆) δ 172.74, 168.96, 48.10, 25.55, 22.58, 18.29.

2-acetamido-*N*-ethylacetamide (AcGlyNEt, **10b**):



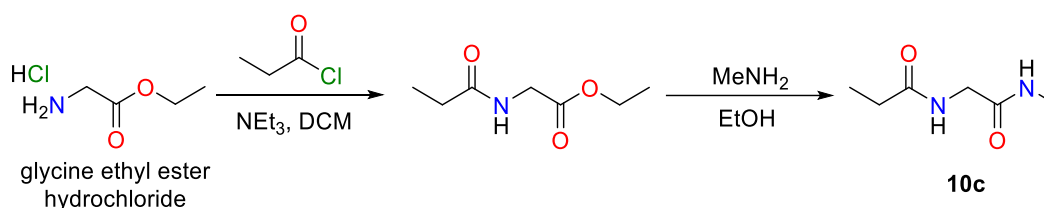
0.33 ml of ethyl amine (5 mmol, 5 eq) was added dropwise to ethyl acetyl glycinate (145 mg, 1 mmol, 1 eq) in 2 ml of EtOH at 0 °C. After 5 minutes the external cooling was removed and the reaction mixture allowed to stir overnight at RT. After removing all residues of solvent under reduced pressure, the crude product was recrystallized from EtOAc/EtOH mixture. Pure **10b** was isolated as white crystals (120 mg, 83%).

¹H NMR (400 MHz, DMSO-*d*₆) δ 8.07 (bs, 1H), 7.83 (bs, 1H), 3.60 (d, *J* = 5.9 Hz, 2H), 3.06 (qd, *J* = 7.2, 5.5 Hz, 2H), 1.84 (s, 3H), 0.99 (t, *J* = 7.2 Hz, 3H).

¹³C NMR (101 MHz, DMSO-*d*₆) δ 169.57, 168.62, 42.09, 33.37, 22.58, 14.80.

HRMS (ESI): calcd for C₆H₁₃N₂O₂ [M + H]⁺, 145.0972; found 145.0973.

N-(2-(methylamino)-2-oxoethyl)propionamide (PpGlyNMe, **10c**):

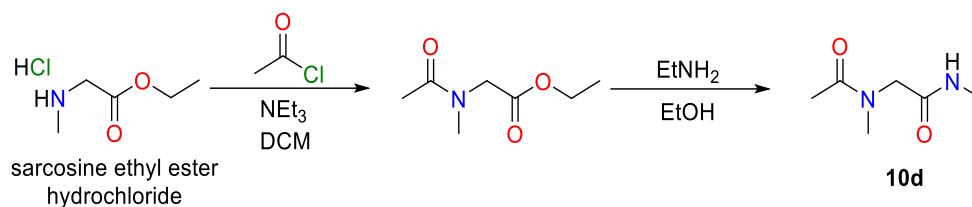


139.5 mg of glycine ethyl ester hydrochloride (1 mmol, 1 eq) were dissolved in 10 ml of dry DCM, the solution was cooled down to 0 °C, and 0.28 ml of NEt₃ (0.2 g, 2 mmol, 2 eq) were added dropwise, followed by 88 μl of freshly distilled propionyl chloride (0.925 g, 1 mmol, 1 eq). Then the external cooling was removed, the reaction mixture was stirred for 2 h at RT, and then quenched with 50 ml of brine and extracted with DCM (3×25 ml). The combined organic layers were dried over MgSO₄, and the solvent were evaporated under reduced pressure. Then 2 ml of 33% ethanol solution of methyl amine was added dropwise to the crude product at 0 °C. After 5 minutes the external cooling was removed. Reaction mixture was allowed to stir for 2 h at RT. Afterwards, the solvent was removed under reduced pressure, the crude product was purified by recrystallization from EtOAc/iPrOH. The pure product **10c** was isolated as white crystals (80 mg, 56%).

¹H NMR (400 MHz, DMSO-*d*₆) δ 7.99 (t, *J* = 5.9 Hz, 1H), 7.75 – 7.71 (m, 1H), 3.61 (d, *J* = 5.9 Hz, 2H), 2.57 (d, *J* = 4.6 Hz, 3H), 2.13 (q, *J* = 7.6 Hz, 2H), 0.98 (t, *J* = 7.6 Hz, 3H).

¹³C NMR (101 MHz, DMSO) δ 173.23, 169.46, 42.04, 28.27, 25.48, 9.68.

N-methyl-2-(*N*-methylacetamido)acetamide (AcSarNMe, **10d**):



1.54 g of sarcosine ethyl ester hydrochloride (10 mmol, 1 eq) were dissolved in 20 ml of dry DCM, the solution was cooled down to 0 °C, and 2.8 ml of NEt₃ (2.0 g, 20 mmol, 2 eq) was added dropwise, followed by 0.72 ml of freshly distilled acetyl chloride (0.79 g, 10 mmol, 1 eq). Afterwards, the external cooling was removed, and the reaction mixture was stirred overnight at RT, quenched with 50 ml of brine and extracted with EtOAc (3×25 ml). The combined organic layers were dried over MgSO₄, and the solvent was evaporated under reduced pressure. Then 2.4 ml of 33% ethanol solution of methyl amine (26 mmol, 4.67 eq) was added dropwise to 318 mg of the crude product at 0 °C. After 5 minutes the external cooling was removed and the reaction mixture allowed to stir overnight at RT. Afterwards, the solvent was removed under reduced pressure, the crude product was purified by short silica plug (DCM/MeOH = 20/1). The pure product was isolated as yellow oil (0.25 g, 87%).

Major conformer:

¹H NMR (400 MHz, DMSO-*d*₆) δ 7.72 (s, 1H), 3.83 (s, 2H), 2.96 (s, 3H), 2.57 (d, *J* = 4.6 Hz, 3H), 2.01 (s, 3H).

¹³C NMR (101 MHz, DMSO-*d*₆) δ 170.34, 168.66, 50.12, 37.01, 25.44, 21.51.

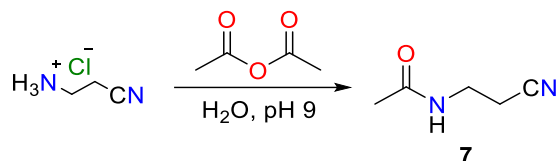
Minor conformer:

¹H NMR (400 MHz, DMSO-*d*₆) δ 7.95 (s, 1H), 3.90 (s, 1H), 2.75 (s, 1H), 2.61 (d, *J* = 4.6 Hz, 2H), 1.91 (s, 1H).

¹³C NMR (101 MHz, DMSO-*d*₆) δ 170.46, 168.46, 52.93, 34.04, 25.57, 21.25.

2.6.1.7. Synthesis of adducts of AcNMe (**1c**)

N-(2-cyanoethyl)acetamide (**7**):



Modified literature procedure^[19]

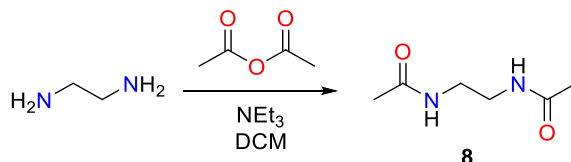
Aminonitrile hydrochloride (5 mmol) was dissolved in H_2O (50 ml) and the solution was adjusted to pH 9.0 with NaOH. 1.5 g of acetic anhydride (1.42 mL, 15 mmol) was added dropwise over 5 min, whilst maintaining the solution at pH 9 with NaOH/HCl. The reaction mixture was then acidified to pH 7 and all the volatiles were evaporated under reduced pressure. The crude material was dissolved in 20 ml of DCM, filtered through short silica pad and dried in *vacuo*. 459 mg of **7** (4.1 mmol, 82%) was obtained as a white solid.

¹H NMR (400 MHz, CDCl_3) δ 6.59 (bs, 1H), 3.46 (q, $J = 6.2$ Hz, 2H), 2.60 (t, $J = 6.3$ Hz, 2H), 1.99 (s, 3H).

¹³C NMR (101 MHz, CDCl_3) δ 171.08, 118.49, 35.75, 23.06, 18.47.

HRMS (EI): calcd for $\text{C}_5\text{H}_9\text{N}_2\text{O}$ $[\text{M}+\text{H}]^+$, 112.0632; found 112.6031.

N,N'-(ethane-1,2-diyl)diacetamide (**8**):



To 4.70 ml of Ac_2O (5.1 g, 50 mmol, 10 eq) in 10 ml of dry DCM, 333 ml of ethylenediamine (300 mg, 5 mmol, 1 eq) and 3.5 ml of triethylamine (2.52 g, 25 mmol, 5 eq) were added. The reaction mixture was stirred overnight at RT, and then quenched with 50 ml of water. The organic phase was separated and dried under vacuum. The crude material was recrystallized from EtOAc/EtOH mixture. Pure **8** was obtained as colorless crystals (0.64 g, 89 %).

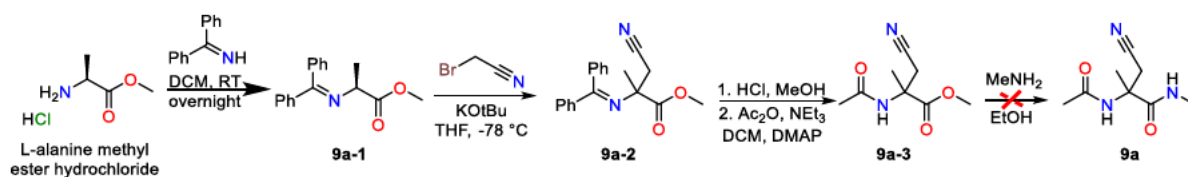
¹H NMR (400 MHz, $\text{DMSO-}d_6$) δ 7.87 (bs, 2H), 3.08 – 3.01 (m, 4H), 1.78 (s, 6H).

¹³C NMR (101 MHz, $\text{DMSO-}d_6$) δ 169.33, 38.40, 22.68.

HRMS (ESI): calcd for $\text{C}_6\text{H}_{12}\text{N}_2\text{O}_2\text{Na}$ $[\text{M} + \text{Na}]^+$, 167.0791; found 167.0792.

2.6.1.8. Synthesis of cyanomethylation adducts of AcAlaNMe (**1b**)

Ac-(α -Me)-Ala(CN)-NMe (**9a**):



Modified literature procedure.^[20]

Benzophenone imine (6.7 g, 37 mmol, 1 mmol) was added to *L*-alanine methyl ester (5.2 g, 37 mmol, 1 eq) in 80 mL of DCM and stirred overnight at RT. The reaction was then filtered, the volatiles were evaporated, and the crude material was recrystallized from an EtOAc/iHex mixture. The product **9a-1** was obtained as white crystals with a yield of 8.1 g (81%). Spectral data are in agreement with literature values.^[21]

¹H NMR (400 MHz, CDCl₃) δ 7.73 – 7.63 (m, 2H), 7.52 – 7.29 (m, 6H), 7.23 – 7.18 (m, 2H), 4.18 (q, J = 6.7 Hz, 1H), 3.72 (s, 3H), 1.42 (d, J = 6.7 Hz, 3H).

Modified literature procedure.^[22]

9a-1 (534 mg, 2 mmol) was added to a solution of KOtBu (246 mg, 2.2 mmol) in 5 mL anhydrous THF at 0 °C. Bromoacetonitrile (262 mg, 2.2 mmol) in 1 mL of THF was added dropwise at 0 °C. The reaction was stirred for 30 min at 0 °C, followed by overnight stirring at RT. The reaction was then quenched with 10 mL brine and extracted with EtOAc (3 \times 5 mL). The combined organic layers were dried over MgSO₄ and concentrated under reduced pressure. The crude product was purified by column chromatography (iHex/EtOAc = 4/1, R_f 0.43). Pure **9a-2** was obtained as white solid (427 mg, 70%).

¹H NMR (400 MHz, CDCl₃) δ 7.59 – 7.55 (m, 2H), 7.45 – 7.28 (m, 6H), 7.16 – 7.11 (m, 2H), 3.35 (s, 3H), 2.99 (d, J = 16.3 Hz, 1H), 2.87 (d, J = 16.3 Hz, 1H), 1.64 (s, 3H).

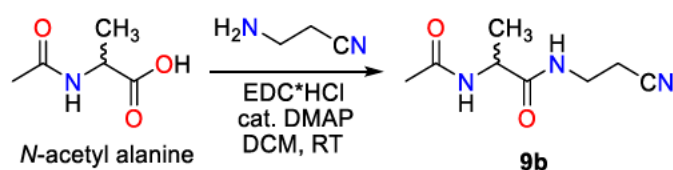
9a-2 (427 mg, 1.4 mmol, 1 eq) was dissolved in 5 mL of MeOH and treated with 1 eq of concentrated aqueous HCl for 20 min at RT. All volatiles were removed under reduced pressure, and the solids were washed multiple times with Et₂O. The crude material was used without further purification. The crude product was then treated with 145 μ L Ac₂O (157 mg, 1.53 mmol, 1.1 mmol), 214 μ L NEt₃ (155 mg, 1.53, 1.1 eq), and a catalytic amount of DMAP in 5 mL of dry DCM. The reaction was stirred overnight at RT, quenched with 10 mL brine, and extracted with DCM (3 \times 10 mL). The combined organic layers were dried over MgSO₄,

and the crude material was purified by passing through a short silica plug. Pure **9a-3** was isolated as a pale-yellow solid. (152 mg, 59%)

¹H NMR (400 MHz, CDCl₃) δ 6.14 (bs, 1H), 3.79 (s, 3H), 3.39 (d, *J* = 17.0 Hz, 1H), 3.20 (d, *J* = 17.0 Hz, 1H), 2.04 (s, 3H), 1.55 (s, 3H).

Then excess of 33% ethanol solution of methyl amine was added dropwise to 152 mg of **9a-3** at 0 °C. After 5 minutes the external cooling was removed and the reaction mixture allowed to stir overnight at RT. No product **9a** was detected *via* APCI MS analysis.

DL-AcAla(CN)NEtCN (**9b**)



To a solution of *N*-acetyl alanine (262 mg, 2 mmol, 1 eq), DMAP (15 mg, 0.1 mmol) and EDC·HCl (384 mg, 2.2 mmol) in DCM (10 mL) was added 3-aminopropionitrile (150 μL, 1 mmol). The reaction mixture was stirred at RT overnight and then evaporated in *vacuo*. The residue was purified by flash chromatography (CH₂Cl₂/MeOH= 10/1, R_f 0.27) to give **9b** (347 mg, 95%) as a white solid.

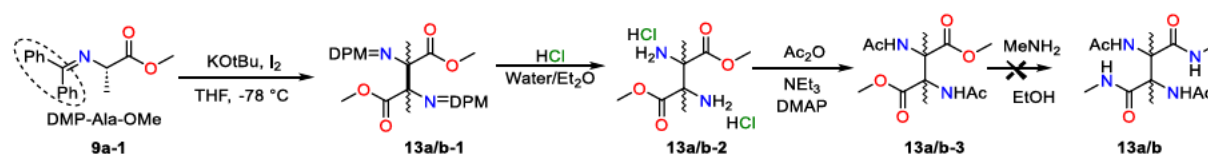
¹H NMR (400 MHz, DMSO-*d*₆) δ 8.22 (t, *J* = 5.8 Hz, 1H), 8.06 (d, *J* = 7.5 Hz, 1H), 4.21 (p, *J* = 7.2 Hz, 1H), 3.35 – 3.21 (m, 2H), 2.62 (td, *J* = 6.5, 1.4 Hz, 2H), 1.83 (s, 3H), 1.18 (d, *J* = 7.1 Hz, 3H).

¹³C NMR (101 MHz, DMSO-*d*₆) δ 172.96, 169.03, 119.18, 48.15, 34.74, 22.54, 18.29, 17.50.

Elem. Calcd for C₈H₁₃N₃O₂: C 52.54, N 22.94, H 7.15. Found: C 52.28, N 22.78, H 6.89.

2.6.1.9. Synthesis of dimerization adducts of *L*-AcAlaNMe (**1b**)

2,3-diacetamido-N1,N4,2,3-tetramethylsuccinamide (**13a/b**):



Modified literature procedure.^[23]

A solution of **9a-1** (2 g, 7.5 mmol, 1 eq) in dry THF (6 mL) was added dropwise to a solution of KOtBu (922 mg, 8.24 mmol, 1.1 mol) in 10 ml of THF at -78 °C, and the mixture was stirred for 1 h at -78 °C. A solution of I₂ (0.953 mg, 3.75 mmol, 0.5 eq) in 10 ml of THF was dropwise

added at $-78\text{ }^{\circ}\text{C}$ with vigorous stirring. The temperature was slowly raised to RT and the mixture stirred overnight. The reaction mixture was quenched with 10 ml of brine. The organic layer was extracted with EtOAc and the combined organic extracts were dried over MgSO_4 . The crude material was purified by hot filtration from *i*Hex/EtOAc=10/1 mixture. **13a/b-1** (dr = 1.1) was obtained as pale-yellow solid (1.05 g, 52%). Spectral data are in agreement with literature values.^[24]

Major isomer:

$^1\text{H NMR}$ (400 MHz, CDCl_3) δ 7.57 – 7.54 (m, 4H), 7.41 – 7.38 (m, 6H), 7.36 – 7.30 (m, 2H), 7.25–7.23 (m, 4H), 7.17 (m, 4H), 3.36 (s, 6H), 1.63 (s, 6H)

Minor isomer:

$^1\text{H NMR}$ (400 MHz, CDCl_3) δ 7.65 – 7.57 (m, 4H), 7.42 – 7.38 (m, 6H), 7.36 – 7.30 (t, 2H), 7.29 – 7.22 (m, 4H), 7.18 – 7.14 (m, 4H), 3.42 (s, 6H), 1.45 (s, 6H)

533 mg of **13a/b-1** in 5 mL Et_2O was treated with 3 mL of 1 N HCl at 0°C . The reaction was allowed to reach RT. After 1 h, 1 mL of MeOH was added to dissolve the solids, and the mixture was stirred for an additional hour. The reaction was extracted with Et_2O , and the aqueous phase was evaporated under reduced pressure to obtain **13a/b-2**, which was used without further purification.

Major isomer:

$^1\text{H NMR}$ (400 MHz, $\text{DMSO-}d_6$) δ 3.78 (s, 6H), 3.49 (bs, 6H), 1.59 (s, 6H).

Minor isomer:

$^1\text{H NMR}$ (400 MHz, $\text{DMSO-}d_6$) δ 3.79 (s, 1H), 3.49 (bs, 6H), 1.62 (s, 6H).

13a/b-2 was mixed with 950 μl Ac_2O (10 mmol, 10 eq), 835 μl NEt_3 (5 mmol, 6 eq) and 244 mg DMAP (2 mmol, 2 eq) in 10 ml of dry DCM. The reaction was allowed to stir overnight, quenched with 10 ml of saturated aqueous NaHCO_3 solution. The mixture was extracted with DCM ($3 \times 25\text{ mL}$), and the organic layers were collected and dried over MgSO_4 . After removing the volatiles under reduced pressure, the crude material was subjected to a short silica column (*i*Hex/EtOAc = 4/1). The volatiles were again evaporated, and the crude material was recrystallized from *i*Hex/EtOAc mixture. **13a/b-3** was obtained as white solid (70 mg, 24%). Spectral data are in agreement with literature values.^[25]

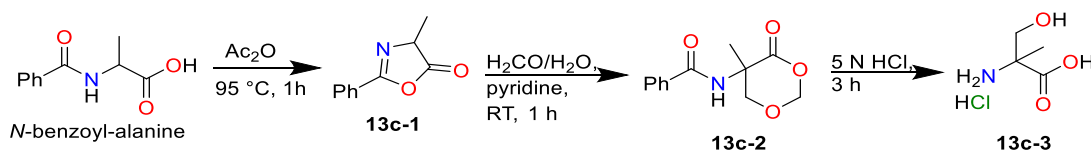
$^1\text{H NMR}$ (400 MHz, $\text{MeOH-}d_4$) δ 3.68 (s, 6H), 1.98 (s, 6H), 1.64 (s, 6H).

^{13}C NMR (101 MHz, MeOH-*d*4) δ 173.34, 172.48, 65.30, 53.23, 22.90, 18.44.

MS (APCI): calcd for $\text{C}_{12}\text{H}_{21}\text{N}_2\text{O}_6$ $[\text{M} + \text{H}]^+$, 289.1; found 289.0.

Then excess of 33% ethanol solution of methyl amine was added dropwise to 70 mg of **13a/b-3** at 0 °C. After 5 minutes the external cooling was removed and the reaction mixture allowed to stir overnight at RT. No product **13a/b** was detected *via* APCI MS analysis. The reaction mixture was transferred to a pressure tube and tightly sealed. The vessel was heated to 100 °C for 4 hours, cooled to RT. APCI MS analysis showed little product **13a/b** formation.

2-acetamido-3-((*S*)-2-acetamidopropanamido)-*N*,2-dimethylpropanamide (**13c**)



Modified literature procedure.^[26]

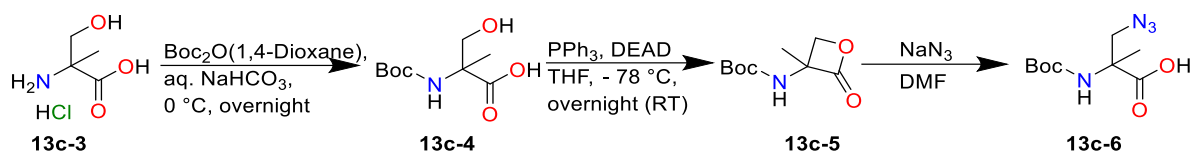
The oxazolone **13c-1** was prepared from *N*-benzoyl-alanine (10 g, 52 mmol) by dehydration with acetic anhydride (50 mL, 520 mmol). The reaction mixture was stirred at 95 °C for 1 h. The excess of acetic anhydride was removed under reduced pressure. With the assumption of 100 % conversion, it was used without further purification. **13c-1** was dissolved in 10 mL pyridine and treated with aqueous formaldehyde (35 %, 40 mL). The mixture was stirred at RT for 1 h. The mixture was filtered, and the solid material was washed with water. The solid material was dried under reduced pressure, obtaining a white powder of **13c-2**.

^1H NMR (400 MHz, CDCl_3) δ 7.79–7.76 (m, 2H), 7.58–7.52 (m, 1H), 7.47–7.41 (m, 2H), 6.52 (s, 1H), 5.68 (d, $J = 5.2$ Hz, 1H), 5.46 (dd, $J = 5.2, 1.7$ Hz, 1H), 4.35 (dd, $J = 10.8, 1.0$ Hz, 1H), 3.94 (dd, $J = 10.8, 1.7$ Hz, 1H), 1.74 (s, 3H).

Modified literature procedure.^[26]

13c-2 was refluxed in 100 mL 5 N HCl for 5 h. The reaction mixture was cooled and filtered, before evaporation. The residue was purified by flash chromatography (MeOH/DCM=1:10→100% MeOH). Pure **13c-3** was isolated as a pale-yellow solid (4.15 g, 52 %)

^1H NMR (DMSO-*d*6, 400 MHz) δ 13.75 (s, 1H), 8.41 (bs, 3H), 5.77 (s, 1H), 3.71 (d, $J = 11.1$ Hz, 1H), 3.60 (d, $J = 11.1$ Hz, 1H), 1.34 (s, 3H).



Modified literature procedure.^[27]

For the Boc protection, **13c-3** (4.15 g, 27 mmol) was diluted in 20 mL of NaHCO₃ saturated solution and cooled to 0 °C. 9 mL Boc₂O was mixed with 20 mL dioxane and added to the stirred solution of the hydrochloride. The reaction mixture was stirred at RT overnight. The pH was adjusted to 2 by 1 M HCl solution and 100 mL of brine was added. The compound was extracted with EtOAc (3×50 mL) and the organic layers were combined and dried over MgSO₄. The organic phase was evaporated under reduced pressure. The residue was purified by flash chromatography using DCM/MeOH = 10/11 as eluent. Pure **13c-4** (1.58 g, 7.2 mmol, 27 %) was obtained as brown oil. Spectral data are in agreement with literature values.^[27]

¹H NMR (CDCl₃, 400 MHz) δ 5.49 (bs, 1H), 3.93 (d, *J* = 11.6 Hz, 1H), 3.81 (d, *J* = 11.5 Hz, 1H), 1.51 (s, 3H), 1.46 (s, 9H).

Modified literature procedure.^[28]

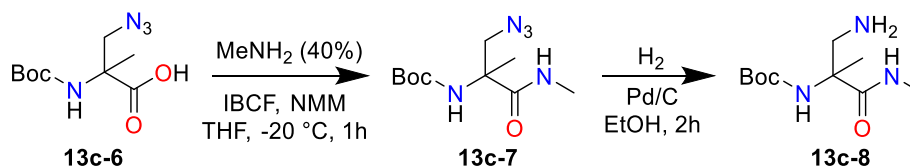
For the synthesis of the **13c-5**, a solution of triphenylphosphine (1.89 g, 7.21 mmol) in 30 mL of dry THF was prepared and a 2.2 M solution of diethyl azodicarboxylate in toluene (3.3 mL, 7.21 mmol) was added dropwise at -78 °C. The mixture was stirred for 20 min. The Boc-protected α-methyl-serine (1.58 g, 7.21 mmol) was dissolved in 3 mL of dry THF and added to the prepared solution. The reaction mixture was stirred at -78 °C for 1 h. The dry ice bath was removed, and the mixture was stirred at RT overnight. The solvents were removed under reduced pressure. The residue was purified by column chromatography (100% DCM, R_f 0.23). The solvent was evaporated under reduced pressure, giving **13c-5** (1.15 g, 79 %) as a white solid. Spectral data are in agreement with literature values.^[29]

¹H NMR (CDCl₃, 400 MHz) δ 4.95 – 4.55 (m, 2H), 4.12 (d, *J* = 4.6 Hz, 1H), 1.61 (s, 3H), 1.46 (s, 9H).

Sodium azide (482 mg, 7.41 mmol) was added to a solution of **13c-5** (1.14 g, 2.47 mmol) dissolved in 10 mL dry DMF. The mixture was stirred overnight. DMF was removed under reduced pressure at RT. The residue was dissolved in water, the pH was adjusted to 3 with 1 N NaHSO₄ solution and extracted with EtOAc (3×25 ml). The combined organic phase was washed with brine and dried over MgSO₄. The solvent was removed under reduced pressure at

RT. 1.34 g of **13c-6** (96 %) was obtained as a white solid. Spectral data are in agreement with literature values.^[30]

¹H NMR (CDCl₃, 400 MHz) δ 5.36 (bs, 1H), 4.36 – 4.16 (m, 1H), 3.81 – 3.78 (m, 1H), 1.55 (s, 3H), 1.45 (s, 9H).

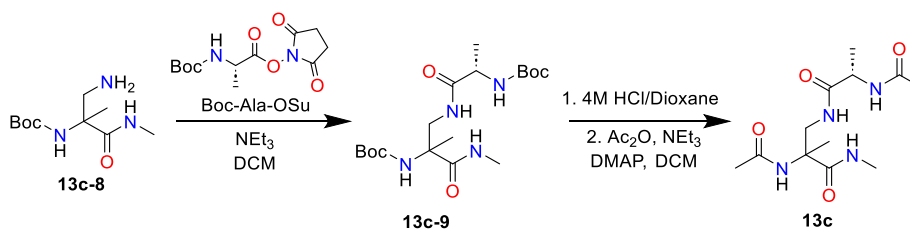


222 μl ml of NMM (2.02 mmol, 1.1 eq), and then 261 μl of IBCF (2.02 mmol, 1.1 eq) were successively added to a solution of **13c-6** (1.84 mmol, 1 eq) in dry THF (4 mL) at -20 – -18 °C (ice/salt = 3/1). After 5 min of activation, 156 μl of 40 % aqueous methylamine (2.02 mmol, 1.1 eq) were added, and the resulting solution was stirred for 1 hour at -20 – -18 °C. The reaction was quenched with 10 mL of 5% NaHCO₃ and stirred additionally for 30 min at RT. The aqueous phase was extracted with DCM (3×25 mL). The combined organic phases were washed with 5 % NaHCO₃ (2 × 50 mL), dried over MgSO₄. The solvent was evaporated under reduced pressure and the crude product was purified by column chromatography (*i*Hex/EtOAc = 1/1, R_f 0.15). 210 mg of **13c-7** (45 %) were obtained as a white solid.

¹H NMR (400 MHz, CDCl₃) δ 6.48 (bs, 1H), 5.15 (bs, 1H), 4.02 (d, *J* = 12.5 Hz, 1H), 3.58 (d, *J* = 12.5 Hz, 1H), 2.83 (d, *J* = 4.8 Hz, 3H), 1.47 (s, 3H), 1.45 (s, 9H).

¹³C NMR (101 MHz, CDCl₃) δ 173.05, 154.76, 81.00, 59.72, 55.21, 28.42, 26.69, 22.58.

A suspension of **13c-7** obtained from the previous step and 10% Pd/C (20 mg) was stirred in absolute ethanol (10 mL) under a H₂ atmosphere at RT for 2 h. After filtration through a Celite pad and washing with methanol, the solvent was evaporated under reduced pressure, and the residue was dried in *vacuo* to yield **13a-8** as a colorless oil (190 mg, >99%). The compound was used without further purification.



235 mg of *L*-Boc-Ala-OSu (0.82 mmol, 1 eq) and 115 μl of NEt₃ (0.82 mmol, 1 eq) were added to 190 mg of **13c-8** (0.82 mmol, 1 eq) in 10 ml of dry DCM. The reaction mixture was stirred

overnight at RT. All volatiles were evaporated, and the crude material was purified by column chromatography (100% EtOAc, R_f 0.27). 170 mg of **13c-9** (as a mixture of 2 diastereomers) was obtained as a white solid (51%).

^1H NMR (400 MHz, MeOH- d_4) δ 4.06 – 3.94 (m, 1H), 3.58 – 3.42 (m, 2H), 2.72 – 2.71 (m, 3H), 1.51 – 1.40 (m, 18H), 1.38 – 1.37 (m, 3H), 1.31 – 1.28 (m, 3H).

^{13}C NMR (101 MHz, MeOH- d_4) δ 177.21 (bs), 176.79 (bs), 176.20 (bs), 157.82, 157.73, 156.48 (bs), 80.67, 61.36 (bs), 52.16, 51.83, 46.14 (bs), 28.78, 28.74, 28.69, 28.66, 26.67, 26.65, 21.45 (bs), 18.20, 17.82.

MS (APCI): calcd for $\text{C}_{18}\text{H}_{35}\text{N}_4\text{O}_6$ $[\text{M} + \text{H}]^+$, 403.3, found 403.1

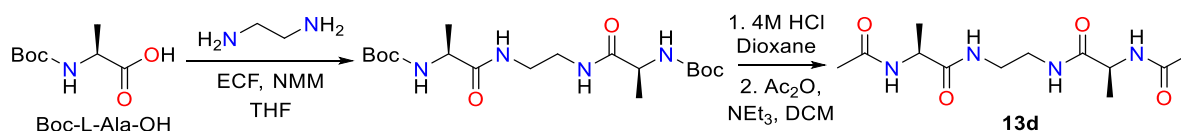
Boc-deprotection of **13c-9** has been done by treating of 150 mg of obtained **13c-9** (0.373 mmol, 1 eq) with 4M HCl in dioxane for 1 hour at RT. Then the volatiles were evaporated under reduced pressure, the hydrochloride salt was mixed with 353 μl of acetic anhydride (3.73 mmol, 10 eq), 312 μl of triethylamine (2.24 mmol, 6 eq) and 1 eq DMAP in 8 ml of dry DCM. The reaction was allowed to stir overnight, and the white slurry was filtered off, washed with DCM (3 \times 2 ml) and dried in *vacuo*. The crude material was purified by short column chromatography (DCM/MeOH = 10/1). 62 mg of **13c** was obtained as colorless solid (58%).

^1H NMR (400 MHz, MeOH- d_4) δ 4.29 – 4.18 (m, 1H), 3.71 – 3.52 (m, 2H), 2.71 – 2.70 (m, 3H), 1.99 (s, 3H), 1.95 – 1.94 (m, 3H), 1.38 – 1.36 (m, 3H), 1.35 – 1.32 (m, 3H).

^{13}C NMR (101 MHz, MeOH- d_4) δ 176.49, 176.28, 175.77, 175.68, 173.35, 173.33, 173.30, 173.19, 61.70, 61.68, 61.49, 61.47, 51.07, 50.88, 45.27, 45.07, 26.76, 26.75, 26.63, 26.61, 23.22, 23.21, 22.42, 22.36, 21.93, 21.89, 17.88, 17.64.

HRMS (ESI): calcd for $\text{C}_{12}\text{H}_{21}\text{N}_4\text{O}_4$ $[\text{M}-\text{H}]$, 285.1568; found 285.1568.

(2S,2'S)-N,N'-(ethane-1,2-diyl)bis(2-acetamidopropanamide) (**13d**)



To 567 mg Boc-*L*-Ala-OH (3 mmol, 2.5 eq) in 10 ml of dry THF was added 0.33 ml of *N*-methyl morpholine (NMM, 303 mg, 3 mmol, 2.5 eq) and 0.29 ml of ethyl chloroformate (ECF, 326 mg, 3 mmol, 2.5 eq) at -20 °C. After 5 minutes of activation, 80 μl of ethylenediamine (72 mg, 1.2 mmol, 1 eq) was added dropwise. The reaction mixture was allowed to stir for 1 h at -20 °C, then the mixture was quenched with 5% NaHCO_3 aqueous solution (50 mL) and

extracted with DCM (3×25 mL). The combined organic layers were washed with brine (50 mL), dried over MgSO₄ and concentrated in *vacuo*. The crude product was used without further purification. 5 ml of 4M HCl in dioxane was added dropwise to the obtained crude material at 0 °C. The reaction mixture was allowed to stir for 1 h at RT and the volatiles were evaporated under reduced pressure. 2.51 ml of NEt₃ (1.82 g, 18 mmol, 6 eq) was added dropwise to the crude product in 20 ml of dry DCM at 0 °C, followed by addition of 2.83 ml of Ac₂O (3.06 g, 30 mmol, 10 eq). The external cooling was removed, the reaction mixture was allowed to stir overnight at RT. The precipitate was filtered off, washed with DCM (3×5 ml) and dried under reduced pressure. The product was obtained as white solid (286 mg, 83%).

¹H NMR (400 MHz, MeOH-*d*4) δ 4.25 (q, *J* = 7.2 Hz, 2H), 3.30 – 3.24 (m, overlapped with the solvent peak, 4H), 1.99 (s, 6H), 1.33 (s, 3H), 1.31 (s, 3H).

¹³C NMR (101 MHz, DMSO-*d*6) δ 172.61, 169.04, 48.25, 38.29, 22.59, 18.26.

HRMS (ESI): calcd for C₁₂H₂₁N₄O₄ [M - H]⁻, 285.1568; found 285.1569.

2.6.2. Laser Flash Photolysis Experiment

LFP experiments were carried out with a laser kinetic spectrometer using the third harmonic (355 nm) of a Q-switched Nd:YAG laser, delivering 8 ns pulses. The laser energy was adjusted to ≤ 10 mJ/pulse by the use of the appropriate filter. A 3.5 mL Suprasil quartz cell (10 mm \times 10 mm) was used in all experiments. Argon saturated DMSO solutions of dicumyl peroxide (1 M) were employed. All the experiments were carried out at $T = 25 \pm 0.5$ °C under magnetic stirring. The observed rate constants (k_{obs}) were obtained following the decay of the cumyloxy radical (CumO^\bullet) visible absorption band (490 nm) at different substrate concentrations. The k_{obs} values obtained from the decay traces are the average of 2-3 individual values and were reproducible to within 5%. Correlation coefficients were in all cases > 0.99 . The rate constants displayed in Table 1 are the average of at least two independent experiments, typical errors being ≤ 10 %.

a) k_{obs} vs [AcGlyNMe (**1a**)] plot

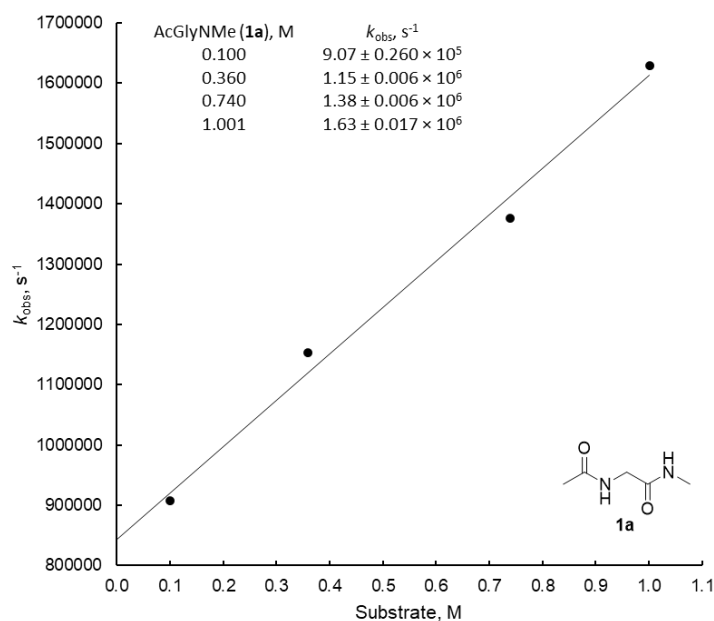


Fig. S2. Plots of the average observed rate constant (k_{obs}) against [substrate] for the reactions of the cumyloxy radical (CumO^\bullet) with AcGlyNMe (**1a**), measured in argon-saturated DMSO solution at $T = 25$ °C by following the decay of CumO^\bullet at 490 nm. From the linear regression analysis: $\text{CumO}^\bullet + \mathbf{1a}$, intercept = $8.43 \times 10^5 \text{ s}^{-1}$, $k_{\text{H}} = 7.70 \times 10^5 \text{ M}^{-1} \text{ s}^{-1}$, $r^2 = 0.9900$.

b) k_{obs} vs [1-C α -d2] plot

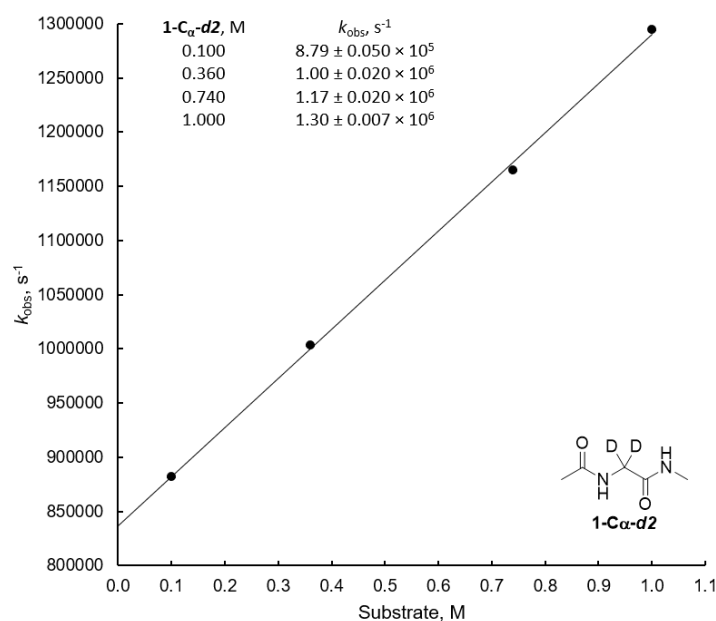


Fig. S3. Plots of the average observed rate constant (k_{obs}) against [substrate] for the reactions of the cumyloxy radical (CumO \cdot) with **1-C α -d2**, measured in argon-saturated DMSO solution at $T = 25$ °C by following the decay of CumO \cdot at 490 nm. From the linear regression analysis: CumO \cdot + **1-C α -d2**, intercept = $8.37 \times 10^5 \text{ s}^{-1}$, $k_{\text{H}} = 4.53 \times 10^5 \text{ M}^{-1} \text{ s}^{-1}$, $r^2 = 0.9991$.

c) k_{obs} vs [1-NMe-d3] plot

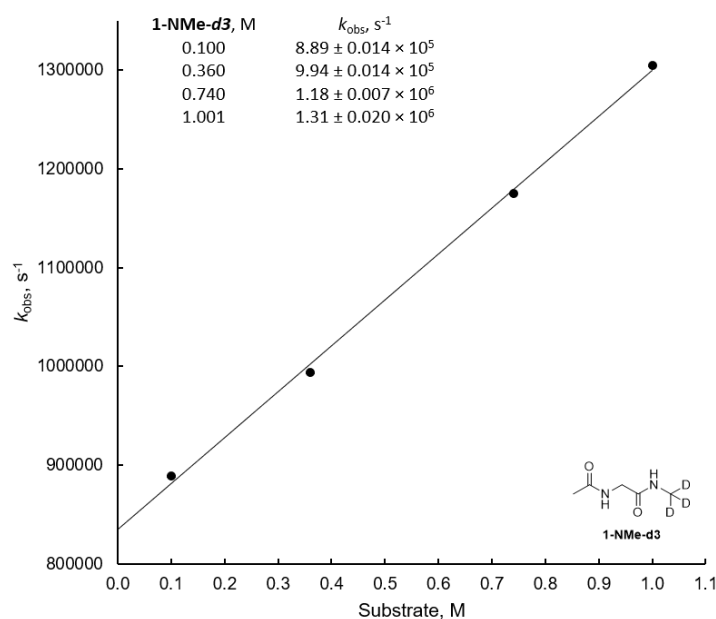


Fig. S4. Plots of the average observed rate constant (k_{obs}) against [substrate] for the reactions of the cumyloxy radical (CumO \cdot) with **1-NMe-d3**, measured in argon-saturated DMSO solution at $T = 25$ °C by following the decay of CumO \cdot at 490 nm. From the linear regression analysis: CumO \cdot + **1-NMe-d3**, intercept = $8.35 \times 10^5 \text{ s}^{-1}$, $k_{\text{H}} = 4.64 \times 10^5 \text{ M}^{-1} \text{ s}^{-1}$, $r^2 = 0.9984$.

d) k_{obs} vs [AcAlaNMe (**1b**)] plot

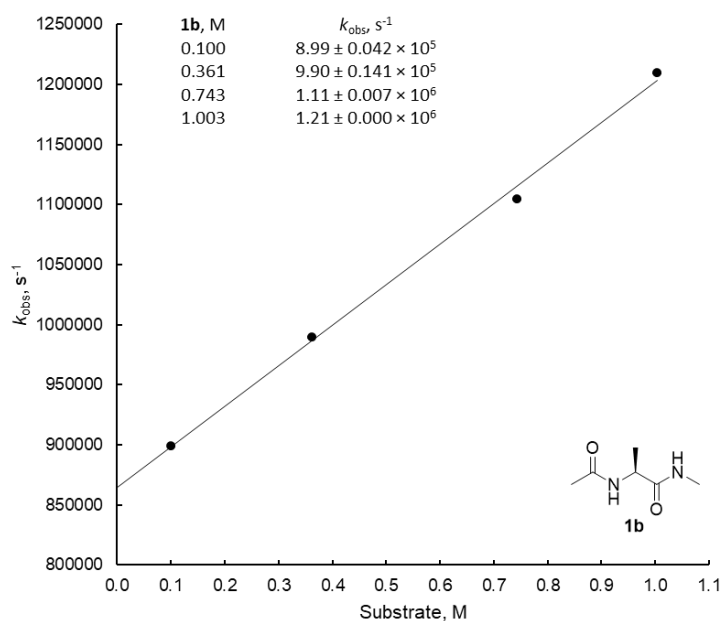


Fig. S5. Plots of the average observed rate constant (k_{obs}) against [substrate] for the reactions of the cumyloxy radical (CumO^\bullet) with **1b**, measured in argon-saturated DMSO solution at $T = 25^\circ\text{C}$ by following the decay of CumO^\bullet at 490 nm. From the linear regression analysis: $\text{CumO}^\bullet + \mathbf{1b}$, intercept = $8.64 \times 10^5 \text{ s}^{-1}$, $k_{\text{H}} = 3.93 \times 10^5 \text{ M}^{-1} \text{ s}^{-1}$, $r^2 = 0.9971$

e) k_{obs} vs [AcNMe (**1c**)] plot

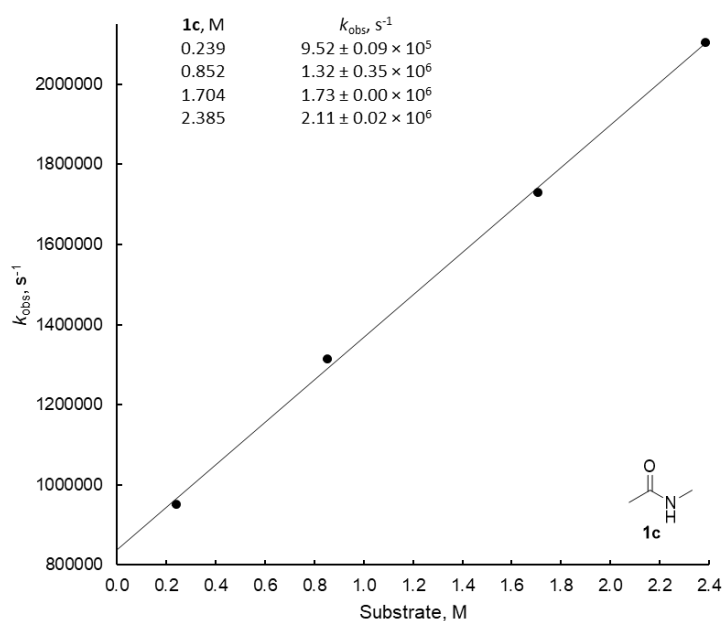
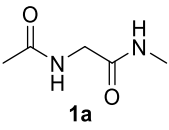
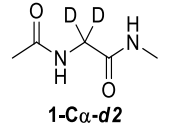
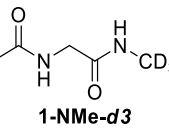
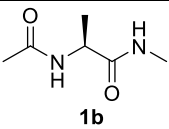
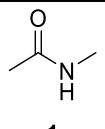


Fig. S6. Plots of the average observed rate constant (k_{obs}) against [substrate] for the reactions of the cumyloxy radical (CumO^\bullet) with **1c**, measured in argon-saturated DMSO solution at $T = 25^\circ\text{C}$ by following the decay of CumO^\bullet at 490 nm. From the linear regression analysis: $\text{CumO}^\bullet + \mathbf{1c}$, intercept = $8.38 \times 10^5 \text{ s}^{-1}$, $k_{\text{H}} = 5.30 \times 10^5 \text{ M}^{-1} \text{ s}^{-1}$, $r^2 = 0.9987$.

Table S2. Second order rate constants (k_H) for reaction of the cumyloxyl radical (CumO•) with different amino acids, measured in DMSO at $T = 25\text{ }^\circ\text{C}$.^a

substrate	$k_H / \text{M}^{-1} \text{s}^{-1}$
 1a	$7.8 \pm 0.3 \times 10^5$
 1-Cα-d2	$4.6 \pm 0.1 \times 10^5$
 1-NMe-d3	$4.7 \pm 0.1 \times 10^5$
 1b	$3.3 \pm 0.2 \times 10^5$
 1c	$5.3 \pm 0.05 \times 10^5$

^aCumO• has been generated by 355 nm LFP of argon-saturated DMSO solutions ($T = 25\text{ }^\circ\text{C}$) containing 1.0 M dicumyl peroxide. The k_H values have been obtained from the slope of the k_{obs} vs [substrate] plots where in turn, the k_{obs} values have been obtained following the decay of the CumO• visible absorption band ($\lambda_{\text{max}} = 490\text{ nm}$) at the different substrate concentrations.

2.6.3. Oxidative Stress Reactions of AcGlyNMe (**1a**), AcAlaNMe (**1b**) and AcNMe (**1c**)

2.6.3.1. Measurement properties.

Gas chromatograph: Shimadzu GC-2010

Injection Port SPL1:	
Injection mode	Split
Temperature	280 °C
Carrier gas	N ₂
Flow control mode	Velocity
Carrier gas pressure	70.9 kPa
Total flow	24.2 ml/min
Column flow	0.96 ml/min
Linear velocity	27.4 cm/s
Purge flow	3 ml/min
Split ratio	21
Primary pressure	429 kPa

Detector channel 1 FID1:	
Temperature	305 °C
Signal acquire	Yes
Sampling rate	40 ms
Stop time	17.50 min
Delay time	0.00 min
Subtract detector	None
Makeup gas	N ₂
Makeup flow	30 ml/min
H ₂ flow	40 ml/min
Air flow	400 ml/min

Column oven:

Column	OPTIMA 1701
Length	25 m
Inner diameter	0.25 mm
Film Thickness	0.25 μm

Rate ($^{\circ}\text{C}/\text{min}$)	Temperature ($^{\circ}\text{C}/\text{min}$)	Hold time, min
-	70	2
15	130	0
100	280	10

2.6.3.2. Derivatization attempts on AcGlyNMe (**1a**)

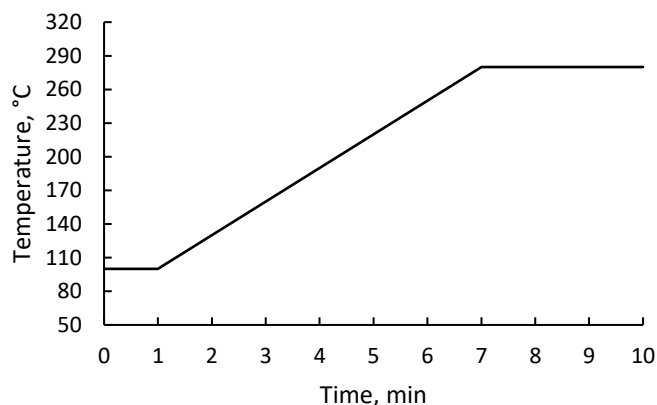


Fig. S7. Graphical representation of the temperature along the time of the GC analysis. Injection at 250 $^{\circ}\text{C}$

To 250 μl of the calibrated solution of AcGlyNMe (**1a**) in dry MeCN was added 250 μl BSTFA + 1% TMSCl under nitrogen atmosphere. The vial was tightly closed and incubated at 80 $^{\circ}\text{C}$ for 15 minutes. After, the solution was injected in GC-FID for further analysis, which showed that silylated product of AcGlyNMe (**1a**) has multiple inconsistent broad peaks at 5.52 min (Fig. S8 and S9). To avoid this problem in the future, it was decided to analyze the oxidative stress mixtures without additional derivatization step.

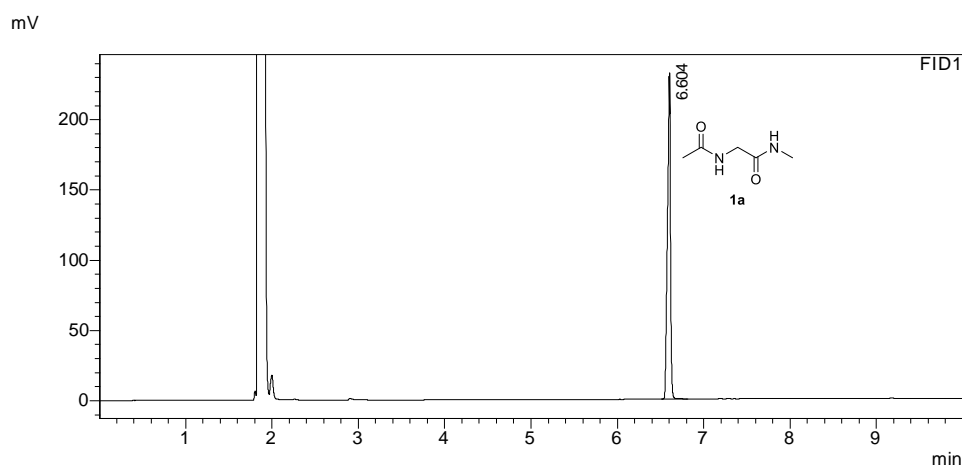


Fig. S8. GC-FID of AcGlyNMe (**1a**) before derivatization.

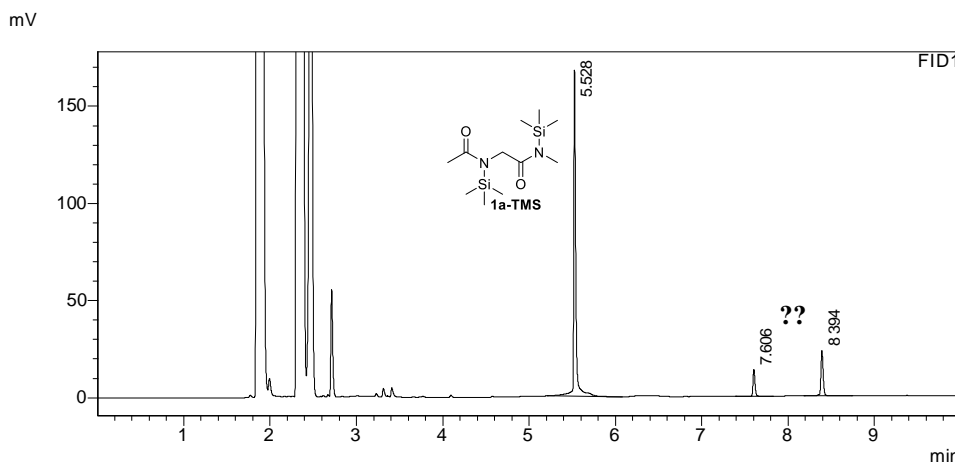


Fig. S9. GC-FID of AcGlyNMe (**1a**) before/after derivatization with BSTFA + 1% TMSCl.

2.6.3.3. Standard addition method

For GC analysis of small-scale reactions, calibration curves were measured for the single substances using standard addition method (Fig. S10). Therefore, 0.10, 0.25 and 0.50 ml of calibrated solutions of pure compounds were added to equal aliquots of calibrated crude reaction mixture and used for GC measurement. Linear response of the FID detector was estimated, so obtained peak area was multiplied by dilution factor to get normalized peak area of a certain compound. The linear equation $S_N = A \times C + B$, obtained from these measurements, was extrapolated to $S_N = 0$. Obtained concentrations and yields are the average of at least two independent measurements. Errors are given at 95% confidence level.

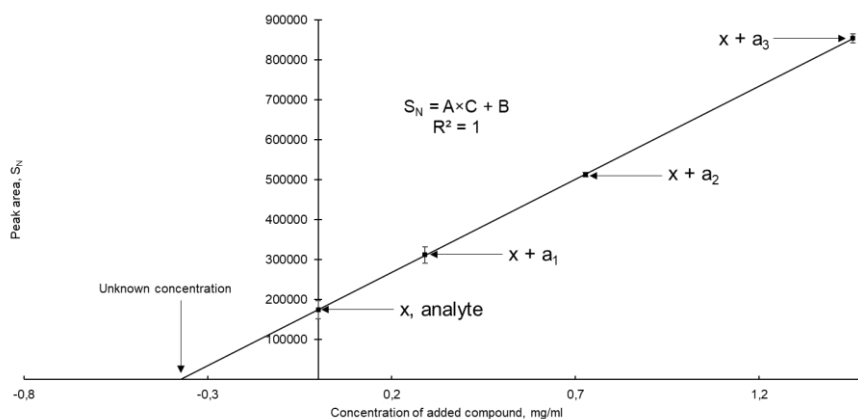


Fig. S10. Graphical explanation of standard addition method.

2.6.3.4. Applicability of GC-FID method

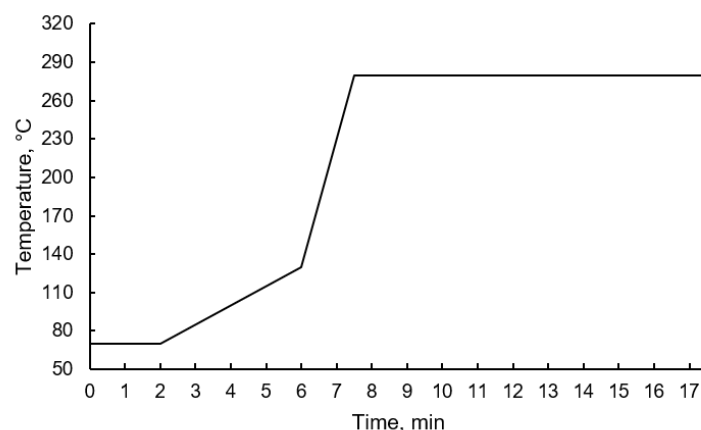


Fig. S11. Graphical representation of the temperature program used in GC analysis (injection at 280 °C).

Applicability of the GC method was tested before the investigation. For this purpose, a known concentration of AcGlyNMe (**1a**) was validated using the standard addition method. Before the analysis, a blank measurement of pure iPrOH was made to detect peaks of impurities in the solvent (Fig. S12).

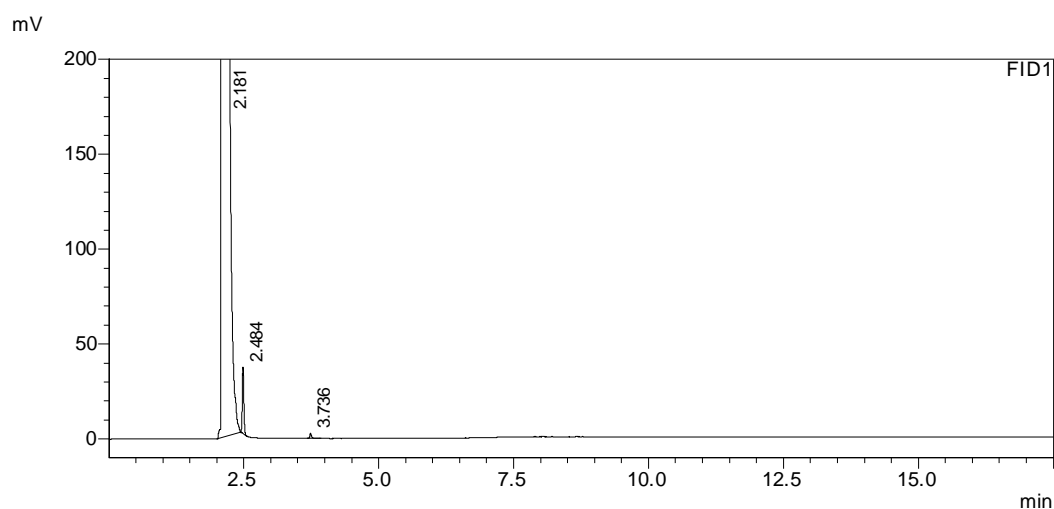


Fig. S12. GC-FID spectra of iPrOH.

The testing solution of AcGlyNMe (**1a**) was prepared with concentration $[\mathbf{1a}]_0 = 103.1$ mM in MeCN (Fig. S13). 1 ml of testing solution was diluted up to 5 ml with iPrOH, giving final $[\mathbf{1a}] = 20.62$ mM. To 0.5 ml of the obtained mixture (10.31 μ mol), the certain volume of a stock solution of AcGlyNMe (**1a**) in iPrOH with concentration $[\mathbf{1a}]_{\text{Stock}} = 32.23$ mM during two independent measurements for one data point. The results are represented in Table S3. GC-FID, as expected, shows linear behaviour ($R^2=1.000$) during used concentration range and good reproducibility of the measurements. The concentration of AcGlyNMe (**1a**) obtained, $[\mathbf{1a}]$, is

100.2 mM with 3% of innaccuracy. These measurements show that GC-FID is suitable method for quantitative analysis of dipeptide model **1a**.

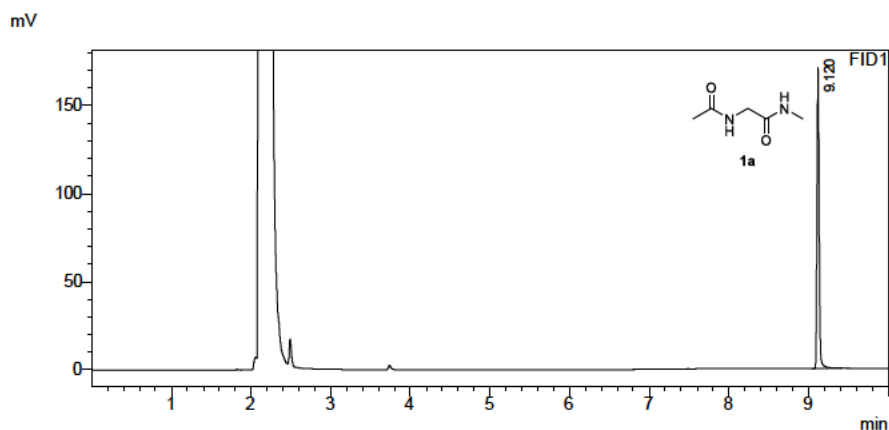


Fig. S13. GC-FID spectra of the calibrated solution of $[1a] = 20.62 \text{ mM}$.

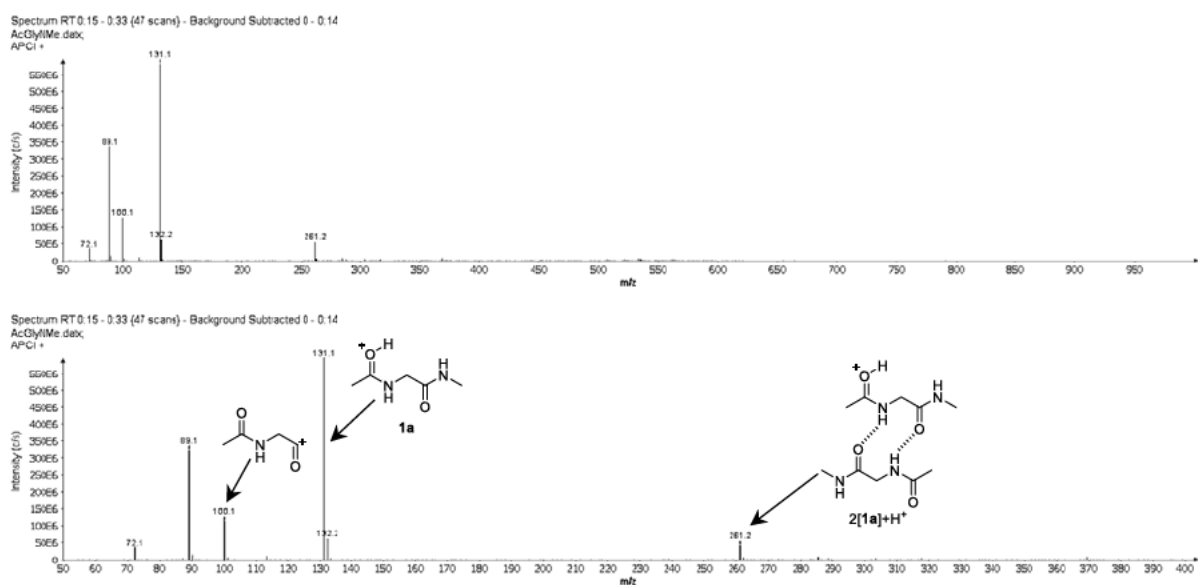
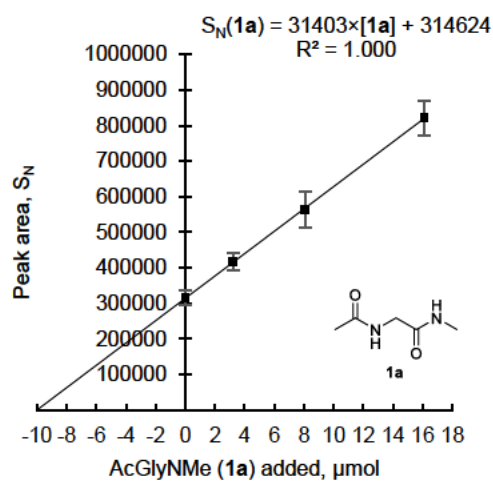


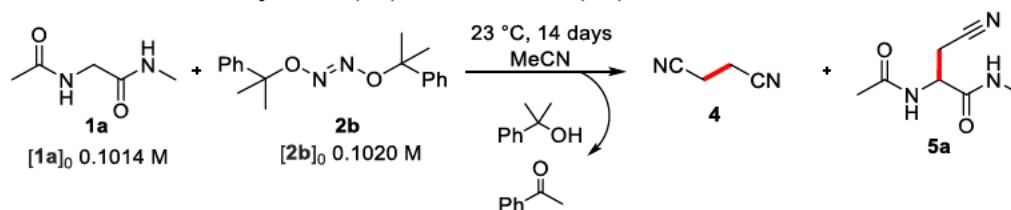
Fig. S14. APCI MS spectrum profile of AcGlyNMe (**1a**).

Table S3. Quantitative analysis of the testing solution of AcGlyNMe (**1a**).



$[1a]_{\text{stock}} = 32.23 \text{ mM}$	$\mu\text{mol added}$	Average peak area, S	DF	Normalized peak area, S_N	Confidence interval, P 0.95
	+ 0.00 ml	0.00	315400	1.00	315400 ± 21410
	+ 0.10 ml	3.22	378907	1.10	416798 ± 24006
	+ 0.25 ml	8.06	451656	1.25	564569 ± 50895
	+ 0.50 ml	16.12	548028	1.50	822041 ± 48265
Linear regression equation				$S_N(1a) = 31403 \times C[1a] + 314624$	
Obtained concentration, $[1a]$				If $S_N(1a) = 0$, then $C[1a] = \frac{314624}{31403} \times \frac{5}{0.5 \text{ ml}} = 100.2 \text{ mM}$	
Stated concentration, $[1a]_0$				103.1 mM	
Inaccuracy, $[1a]/[1a]_0$				-3 %	

2.6.3.5. Oxidation of AcGlyNMe (1a) with DCHN (2b)



152 mg (0.5101 mmol) of DCHN (**2b**) were dissolved in a 5 ml solution of AcGlyNMe (**1a**) (0.1014 M) in dry degassed acetonitrile. 1 ml of the prepared mixture was sealed in a vial under nitrogen atmosphere, wrapped in foil and set in cryostat at 23 °C for 14 days. The vial was then opened with caution because of the increased pressure inside, and the content diluted up to 10 ml with iPrOH. Yields were obtained by addition of an exact amount of known compounds to 0.5 ml aliquot of crude solution. Results are represented in Figure S15-16 and Table S3-5.

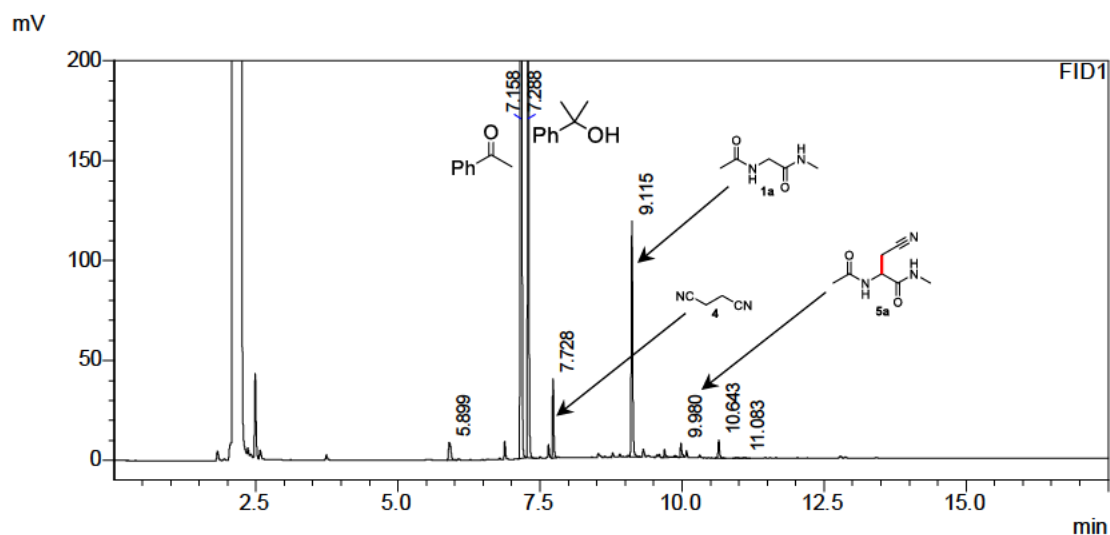


Fig. S15. GC-FID spectra of the oxidative stress reaction of AcGlyNMe (**1a**) with (**2b**).

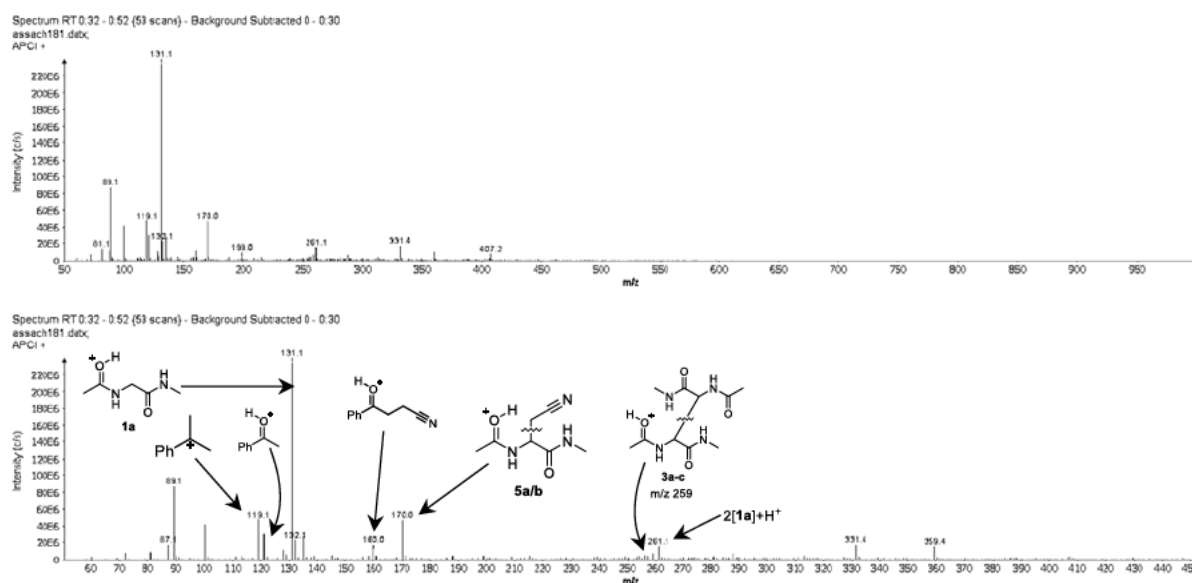
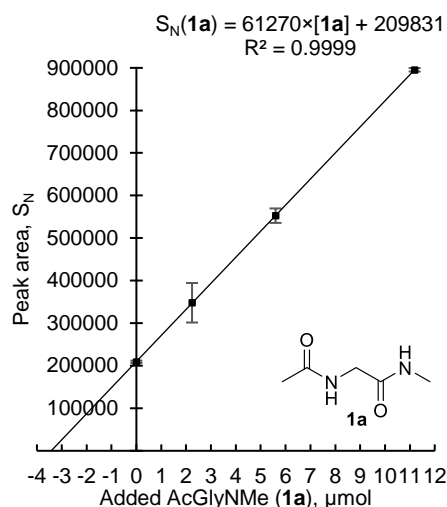


Fig. S16. APCI MS spectrum profile of the oxidative stress reaction of **1a** with **2b**.

Table S4a. Products distribution for oxidation of AcGlyNMe (**1a**) with DCHN (**2b**).

a) Recovery of AcGlyNMe (**1a**)



$[\mathbf{1a}]_{\text{Stock}} = 22.38 \text{ mM}$	μmol added	Average peak area, S	DF	Normalized peak area, S_N	Confidence interval, P 0.95
+ 0.00 ml	0.00	209133	1.00	209133	± 2656
+ 0.10 ml	2.24	217446	1.60	347913	± 46447
+ 0.25 ml	5.60	221046	2.50	552615	± 17001
+ 0.50 ml	11.19	223861	4.00	895444	± 4066
Linear regression equation				$S_N(\mathbf{1a}) = 61270 \times [\mathbf{1a}] + 209831$	
Obtained concentration, $[\mathbf{1a}]$				If $S_N(\mathbf{1a}) = 0$, $[\mathbf{1a}] = \frac{209831}{61270} \times \frac{10}{0.5 \text{ ml}} = 68.5 \text{ mM}$	
Stated concentration, $[\mathbf{1a}]_0$				101.4 mM	
Recovery of 1a , $[\mathbf{1a}]/[\mathbf{1a}]_0$				68 %	

b) Recovery of AcGlyNMe (**1a**, with internal standard)

To check if the obtained number is correct, AcGlyOEt (**1-IS**) was chosen as an internal standard, since the standard should be structurally similar to the analyte. Known amount of AcGlyOEt was added to reaction mixture and GC-FID was taken (Fig. S17). Average from two measurements was taken for final calculations (Table S4b).

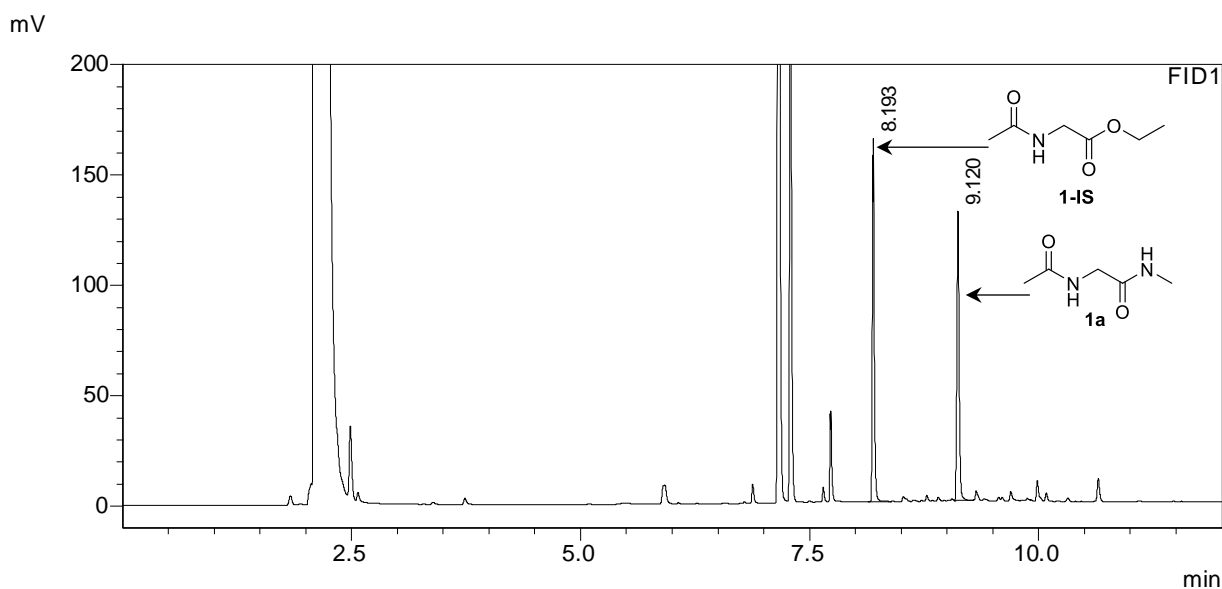
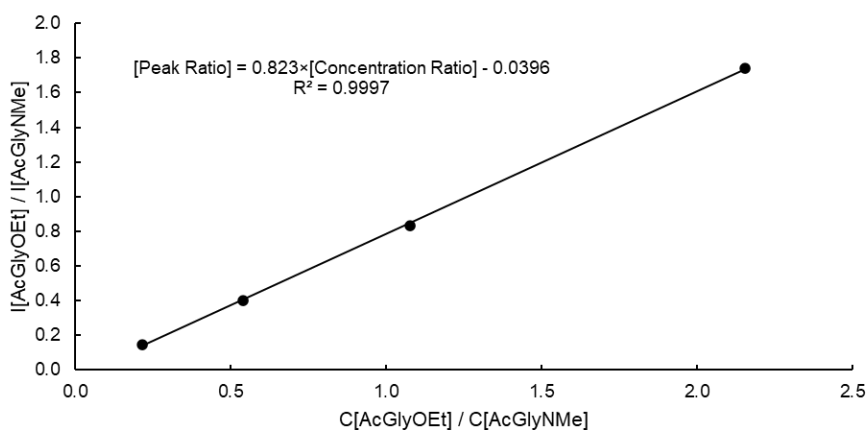


Fig. S17. GC-FID spectra of the oxidative stress reaction of **1a** with **5a** with AcGlyOEt **1-IS**.

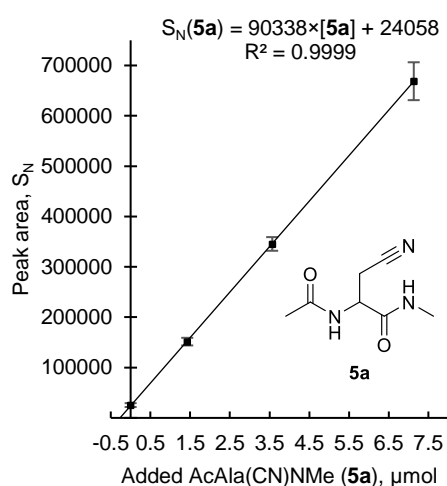
Table S4b. Recovery of AcGlyNMe (**1a**, with internal standard).



Calibration curve						
	C[1-IS], M	I[1-IS], S	C[1a], M	I[1a], S	C[1-IS] / C[1a]	I[1-IS] / I[1a]
1	0.01043	436317	0.00562	175488	0.54	0.40
2	0.00521	208772	0.00562	173367	1.08	0.83
3	0.00521	211441	0.01123	368047	2.15	1.74
4	0.01303	567572	0.00281	83965	0.22	0.15
Crude reaction mixture + 1-IS						
	C[1-IS], M	I[1-IS], S	C[1a], M	I[1a], S	C[1-IS] / C[1a]	I[1-IS] / I[1a]
1	0.00557	234444	-	225157	-	0.96
2	0.00557	226419	-	211542	-	0.93
Linear regression equation				[Peak Ratio] = 0.823 × [Concentration Ratio] - 0.0396		
Obtained concentration, [1a]				If [Peak Ratio] = 0.95, [1a] = $\frac{0.945+0.0396}{0.823} \times 5.57 \text{ mM} \times 10 = 66.6 \text{ mM}$		
Initial concentration, [1a] ₀				101.4 mM		
Recovery, [1a]/[1a] ₀				66 %		

Obtained value of recovery of C(**1a**) = 66% with +2% of difference from the recovery gained above(68%). These measurements show that both quantitative GC-FID analyses give similar results.

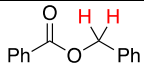
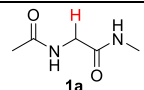
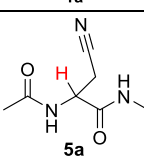
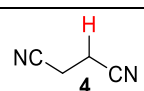
a) Yield of cyanomethylation adduct Ac-Ala(CN)-NMe (**5a**)



[5a] _{Stock} = 14.26 mM	μmol added	Average peak area, S	DF	Normalized peak area, S _N	Confidence interval, P 0.95
+ 0.00 ml	0.00	25460	1.00	25460	± 3850
+ 0.10 ml	1.43	94681	1.60	151490	± 7573
+ 0.25 ml	3.57	138220	2.50	345550	± 13557
+ 0.50 ml	7.13	167188	4.00	668752	± 37635
Linear regression equation				S _N (5a) = 90338 × [5a] + 24058	
Obtained concentration				If S _N (5a) = 0, [5a] = $\frac{24508}{90338} \times \frac{10}{0.5 \text{ ml}} = 5.3 \text{ mM}$	
Initial concentration, [1a] ₀				101.4 mM	
Yield 5a , [5a]/[1a] ₀				5 %	

Table S5. Quantitative ¹H NMR for the oxidative stress reaction of **1a** with DCHN (**2b**).

0.5 ml of calibrated benzyl benzoate solution (1.99 mg/ml) was added to 2.5 ml of calibrated solution of the crude mixture. All the volatiles were evaporated under reduced pressure; the crude material was redissolved in MeOH-*d*₄ and ¹H NMR spectra was taken.

Compound	Peak area	Moles, μmol	Mass, mg	Yield, %
	1.000	4.7	1.00	-
	6.256	73.8	9.59	73
	0.381 (overlapping)	8.98	1.52	9
	1.986	11.7	0.94	12*

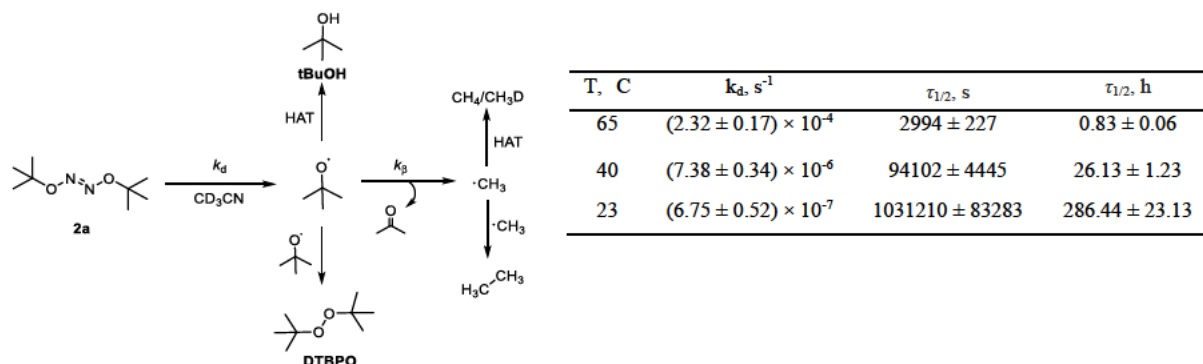
*from DCHN **2b** amount

2.6.3.6. DTBHN (**2a**) decomposition. Kinetic study

To clarify the reaction time, hyponitrite **2a** decomposition experiments have been done first. Decomposition products and the concentration of hyponitrite **2a** were established by ¹H NMR using 1,3,5-methoxybenzene as an internal standard. Kinetic studies were made in dry degassed MeCN-*d*₃ at three different temperatures, 65, 40 and 23 °C. In each case, hyponitrite **2a** decomposition showed first order behavior, as expected. The obtained decomposition rates at different temperatures allowed us to establish the energy of activation of this reaction. Also, it has been showed, that the addition of the equimolar amount of the hydrogen donor,

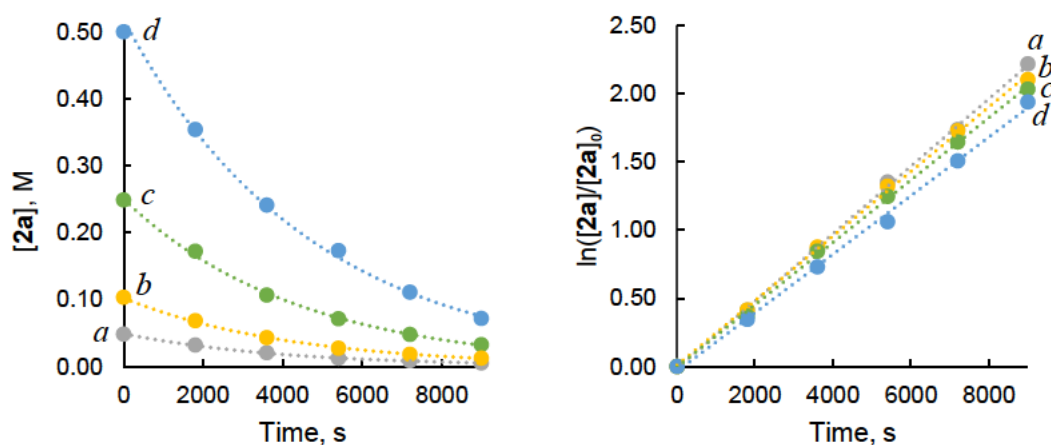
AcGlyNMe (**1a**), does not affect the decomposition rate of hyponitrite **2a**. Results are represented in Table S6.

Table S6. Decomposition rates of DTBHN (**2a**) in MeCN-*d*3 at different temperatures.



1) Decomposition of DTBHN (**2a**) at 65 °C

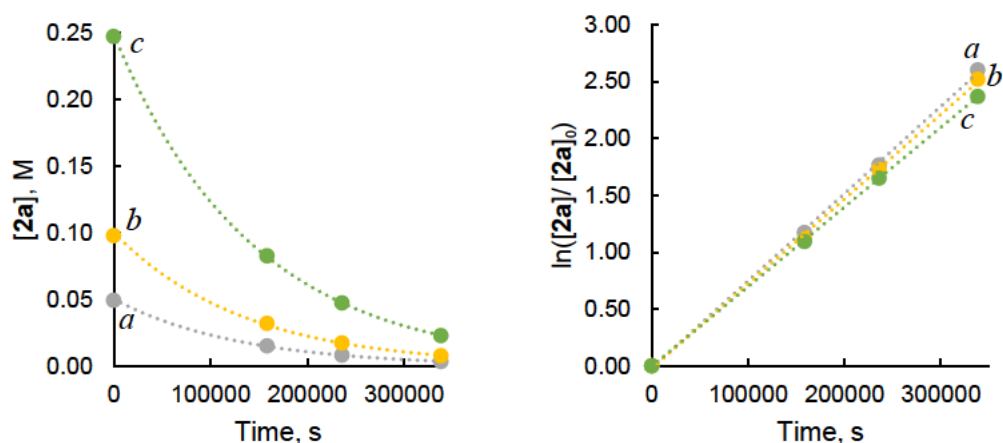
Table S7. Plots of the observed DTBHN (**2a**) concentrations or $\ln([2a]/[2a]_0)$ against time for the reaction of the DTBHN (**2a**) decomposition, measured in nitrogen-saturated MeCN-*d*3 solution at 65 °C followed via ¹H NMR analysis.



Time, s	[2a], M				$\ln([2a]/[2a]_0)$			
	a	b	c	d	a	b	c	d
0	0.048	0.103	0.249	0.500	0.000	0.000	0.000	0.000
1800	0.032	0.068	0.172	0.354	0.413	0.414	0.370	0.345
3600	0.020	0.043	0.107	0.241	0.860	0.875	0.846	0.729
5400	0.013	0.028	0.072	0.173	1.352	1.322	1.246	1.060
7200	0.009	0.018	0.048	0.111	1.737	1.727	1.644	1.506
9000	0.005	0.013	0.033	0.072	2.216	2.102	2.032	1.938
[2a] ₀ , M	Exponential equation			Linear equation			R ²	
d	$[2a] = 0.518 \times \exp(-2.1 \times 10^{-4} \times t)$			$\ln(C[2a]/C_0[2a]) = (2.1 \times 10^{-4}) \times t - 0.03492$			0.9973	
c	$[2a] = 0.250 \times \exp(-2.3 \times 10^{-4} \times t)$			$\ln(C[2a]/C_0[2a]) = (2.3 \times 10^{-4}) \times t - 0.00453$			0.9990	
b	$[2a] = 0.102 \times \exp(-2.4 \times 10^{-4} \times t)$			$\ln(C[2a]/C_0[2a]) = (2.4 \times 10^{-4}) \times t + 0.00936$			0.9989	
a	$[2a] = 0.049 \times \exp(-2.5 \times 10^{-4} \times t)$			$\ln(C[2a]/C_0[2a]) = (2.5 \times 10^{-4}) \times t - 0.01388$			0.9993	

2) Decomposition of DTBHN (**2a**) at 40 °C

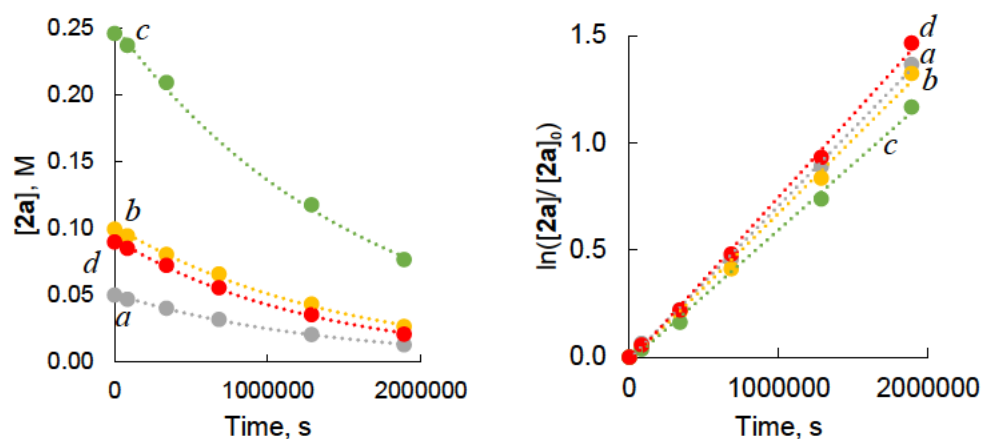
Table S8. Plots of the observed DTBHN (**2a**) concentrations or $\ln([2a]/[2a]_0)$ against time for the reaction of the DTBHN (**2a**) decomposition, measured in nitrogen-saturated MeCN-*d*₃ solution at 40 °C followed via ¹H NMR analysis.



Time, s	[2a], M			$\ln([2a]/[2a]_0)$		
	<i>a</i>	<i>b</i>	<i>c</i>	<i>a</i>	<i>b</i>	<i>c</i>
0	0.049	0.098	0.247	0.000	0.000	0.000
158460	0.015	0.032	0.083	1.171	1.116	1.094
236040	0.008	0.017	0.047	1.764	1.725	1.650
338340	0.004	0.008	0.023	2.603	2.520	2.369
[2a] ₀ , M	Exponential equation		Linear equation		R ²	
<i>c</i>	$[2a] = 0.248 \times \exp([-7.00 \times 10^{-6}] \times t)$		$\ln(C[2a]/C_0[2a]) = (7.00 \times 10^{-6} \times t) - 0.00535$		0.9999	
<i>b</i>	$[2a] = 0.102 \times \exp([-7.45 \times 10^{-6}] \times t)$		$\ln(C[2a]/C_0[2a]) = (7.45 \times 10^{-6} \times t) - 0.02384$		0.9991	
<i>a</i>	$[2a] = 0.049 \times \exp([-7.67 \times 10^{-6}] \times t)$		$\ln(C[2a]/C_0[2a]) = (7.67 \times 10^{-6} \times t) - 0.02038$		0.9999	

3) Decomposition of DTBHN (**2a**) at 23 °C

Table S9. Plots of the observed DTBHN (**2a**) concentrations or $\ln([2a]/[2a]_0)$ against time for the reaction of the DTBHN (**2a**) decomposition, measured in nitrogen-saturated MeCN-*d*₃ solution at 23 °C followed via ¹H NMR analysis.



Time, s	[2a], M				ln ([2a]/[2a] ₀)			
	a	b	c	d	a	b	c	d
0	0.050	0.099	0.246	0.090	0.000	0.000	0.000	0.000
82800	0.047	0.094	0.237	0.085	0.064	0.053	0.037	0.057
338400	0.040	0.080	0.209	0.072	0.221	0.212	0.162	0.219
682200	0.032	0.066	-	0.056	0.458	0.412	-	0.481
1285200	0.021	0.043	0.118	0.035	0.890	0.835	0.737	0.932
1890000	0.013	0.026	0.077	0.021	1.366	1.323	1.167	1.465

[2a] ₀ , M	Exponential equation	Linear equation	R ²
d ^a	[2a] = 0.092 × exp([-7.7 × 10 ⁻⁷] × t)	ln(C[2a]/C ₀ [2a]) = (7.7 × 10 ⁻⁷) × t - 0.02334	0.9977
c	[2a] = 0.251 × exp([-6.2 × 10 ⁻⁷] × t)	ln(C[2a]/C ₀ [2a]) = (6.2 × 10 ⁻⁷) × t - 0.02232	0.9973
b	[2a] = 0.101 × exp([-6.9 × 10 ⁻⁷] × t)	ln(C[2a]/C ₀ [2a]) = (6.9 × 10 ⁻⁷) × t - 0.02111	0.9964
a	[2a] = 0.050 × exp([-7.2 × 10 ⁻⁷] × t)	ln(C[2a]/C ₀ [2a]) = (7.2 × 10 ⁻⁷) × t - 0.01167	0.9988

^a The sample with equimolar amount of 1a is marked as Conc.4.

Analysis of the decomposition products of DTBHN (2a) showed that the temperature decreasing leads to a greater content of tBuOH (the HAT product), relative to acetone (β -scission product). This products distribution can be explained by lower k_{β} , tBuO \cdot at lower temperatures (Fig. S18).

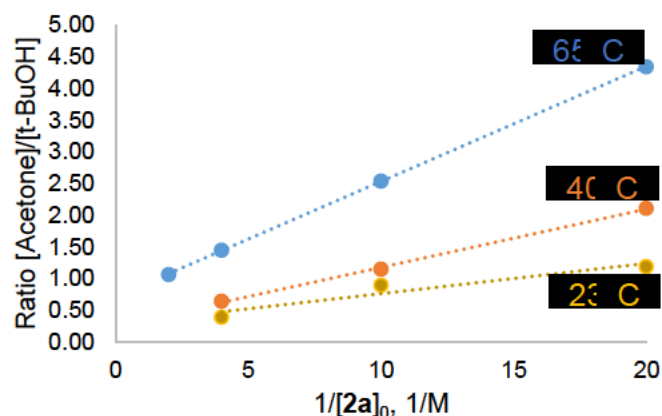


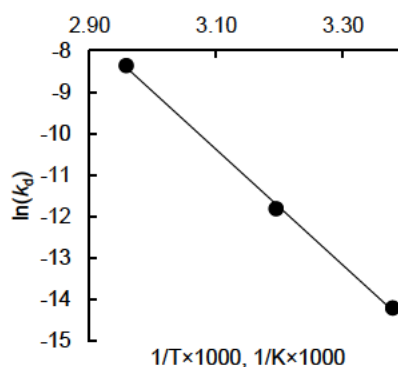
Fig. S18. Ration of decomposition products of DTBHN (2a) at different temperatures.

Also, the activation energy of the decomposition reaction was obtained from the reaction rates obtained at 65°, 40° and 23 °C, using the Arrhenius plot equation (Table S10).

Table S10. Activation energy of the decomposition of DTBHN (2a) in MeCN-*d*₃.

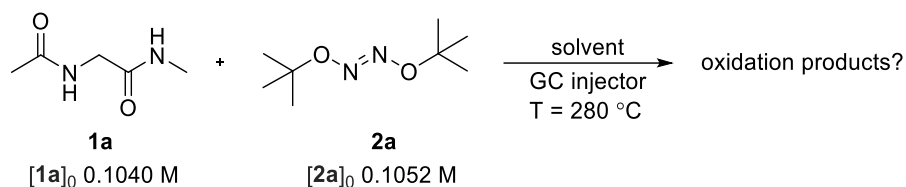
T, °C	T, K	1/T, 1/K	Average k_d s ⁻¹	Average ln(k_d)
65	338	2.96 × 10 ⁻³	6.8 × 10 ⁻⁷	-8.4
40	313	3.19 × 10 ⁻³	7.4 × 10 ⁻⁶	-11.8
23	296	3.38 × 10 ⁻³	2.3 × 10 ⁻⁴	-14.2

$$\ln(k_d) = -14.697 \times \frac{1}{T} + 35.120, R^2 = 1.0000$$

$$E_A = 14.697 \times 8.314 \text{ J} \cdot \text{K}^{-1} \cdot \text{mol}^{-1} = 122 \text{ kJ}$$


2.6.3.7. Possible in-line oxidation during GC-FID analysis

DTBHN (**2a**) is more stable than DCHN (**2b**), and there is some unreacted DTBHN (**2a**) even after 14 days. Since GC vaporizes the analyte samples, the possibility of chemical reactions during the injection was checked.



18.3 mg of DTBHN (**2a**) was dissolved in 1 ml of testing solution of AcGlyNMe (**1a**), [1a]_{Stock} = 101.5 mM. 1 ml of the solution was diluted up to 5 times with iPrOH, giving a final concentration [1a]₀ = 20.30 mM of AcGlyNMe (**1a**) and [DTBHN]₀ = 21.03 mM (Fig. S19). Results are represented in Table S11.

mV

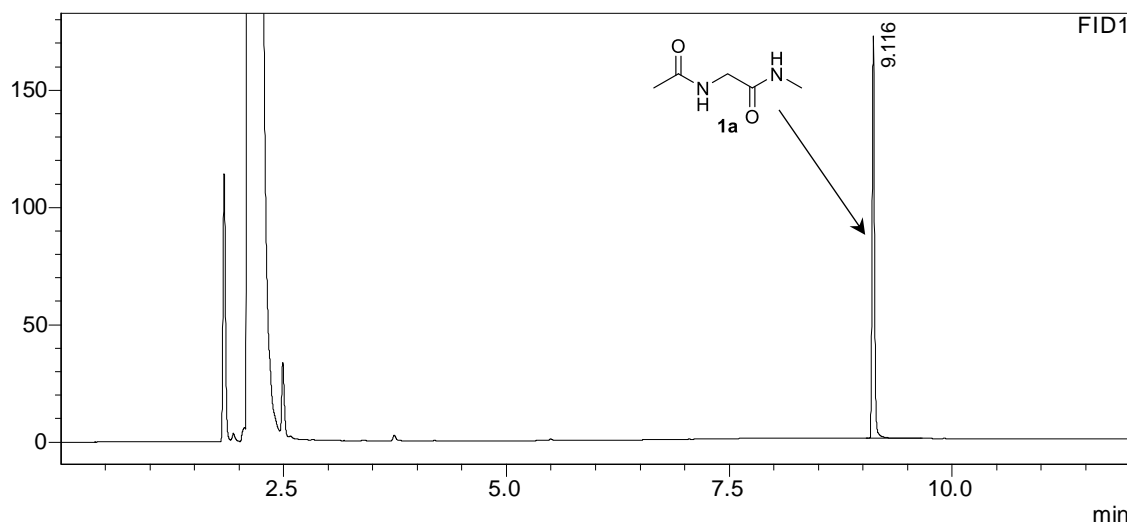
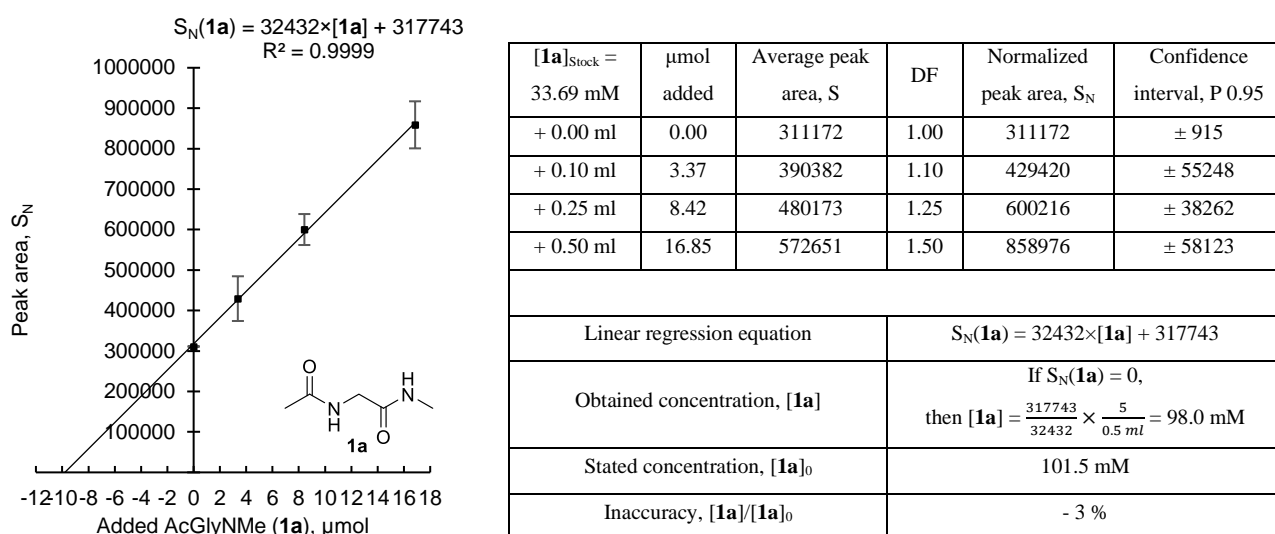


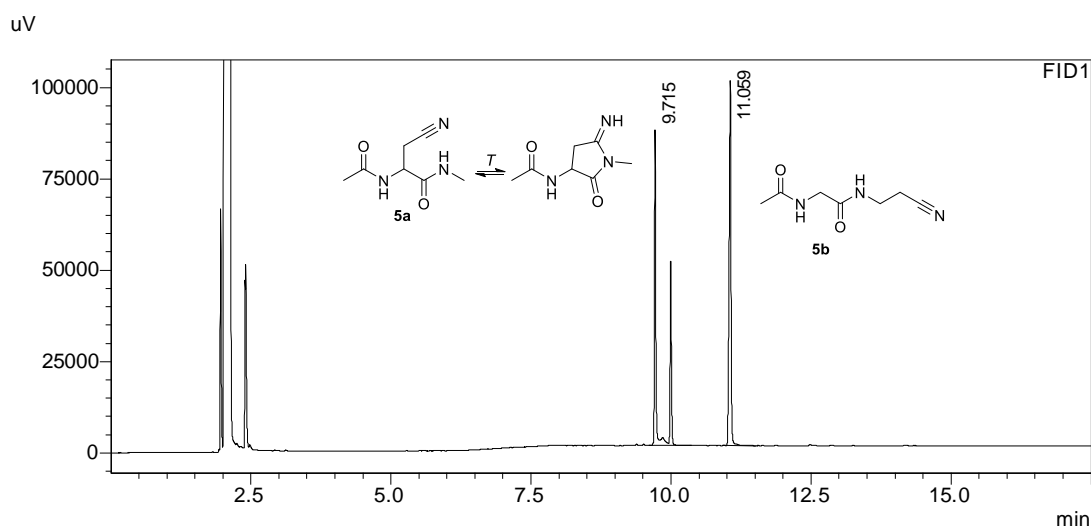
Fig. S19. GC-FID spectra of the calibrated mixture of [1a]₀ = 20.30 mM and [2a]₀ = 21.03 mM.

Table S11. Quantitative analysis of the testing mixture of AcGlyNMe (**1a**) with DTBHN (**2a**)

No DTBHN (**2a**) peak is observed in the GC-FID spectra, which indicates that DTBHN (**2a**) decomposes during the analysis. Obtained value of [1a] = 98.0 mM is within -3% of the stated [1a]₀. These measurements show that GC-FID is a suitable method for quantitative analysis of hyponitrite stress reactions.

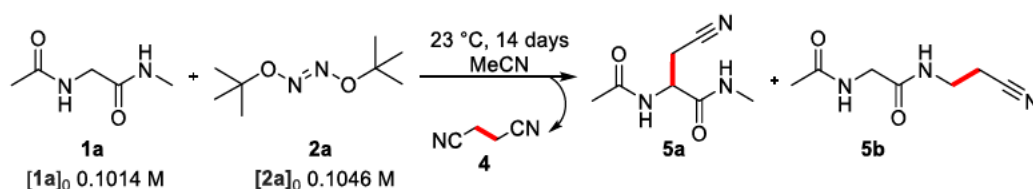
2.6.3.8. GC-FID response on isomers **5a** and **5b**

The solution of **5a** and **5b** with concentrations 10.18 and 10.71 mM, correspondingly, was prepared in EtOH to test the FID response on the isomeric compounds. The obtained difference in the peak ratio, 3.6%, was considered neglectable, which means that isomeric compounds have the same detector response (Table S12).

Table S12. GC-FID spectra of the equimolar solutions of **5a** and **5b**

Concentration	Peak area, S	Detector response, $S(5x)/C(5x)$	Response ratio	Δ , %
$C(5a) = 10.18 \text{ mM}$	230308	22623.6 mM^{-1}	1.036	+ 3.6
$C(5b) = 10.71 \text{ mM}$	233871	21836.7 mM^{-1}		

2.6.3.9. Oxidation of AcGlyNMe (**1a**) with DTBHN (**2a**)



91 mg (0.523 mmol) of DTBHN (**2a**) were dissolved in 5 ml solution of AcGlyNMe (**1a**, 0.1014 M) in dry degassed acetonitrile. 1 ml of the prepared mixture was sealed in a vial under nitrogen atmosphere, wrapped in foil and set in a cryostat at 23 °C for 14 days. Afterwards, the vials were opened with caution because of increased pressure inside, and the contents were diluted up to 5 ml with iPrOH. Yields were obtained by the addition of certain amount of known compounds to 1 ml aliquot of crude solution (Fig. S20 and S21). The results are represented in Table S13.

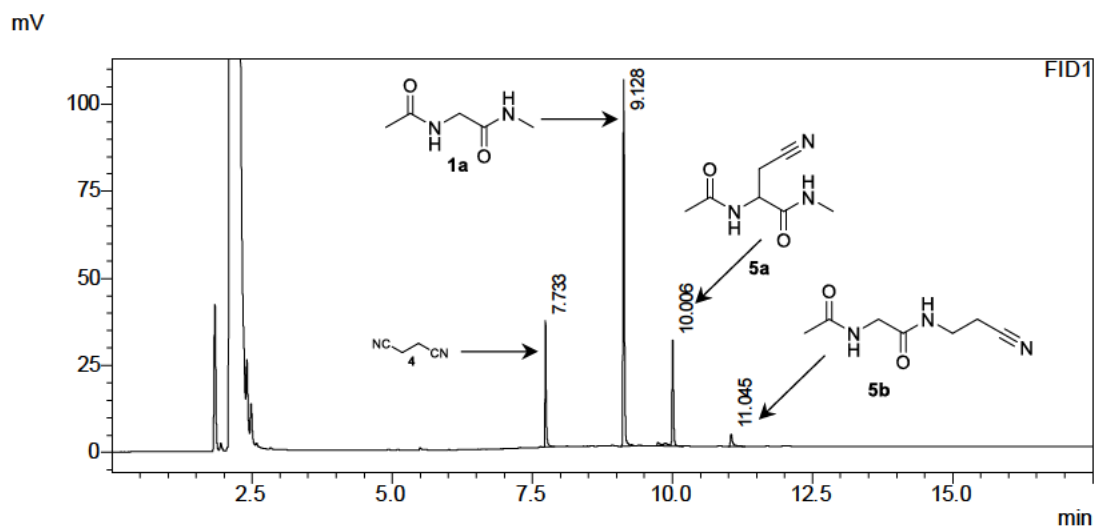
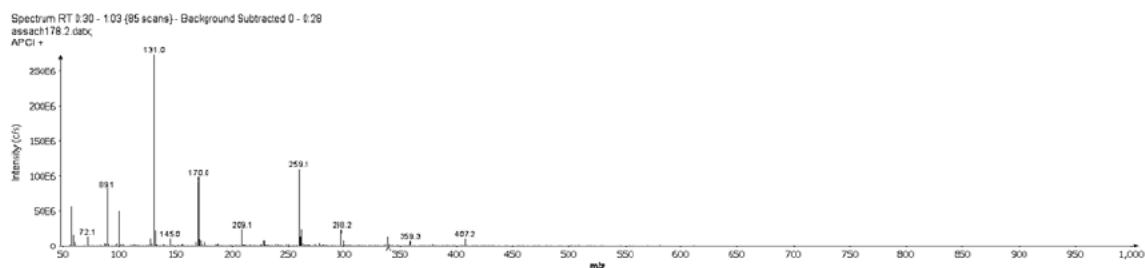


Fig. S20. GC-FID spectra of the oxidative stress reaction of AcGlyNMe (**1a**) with **2a**



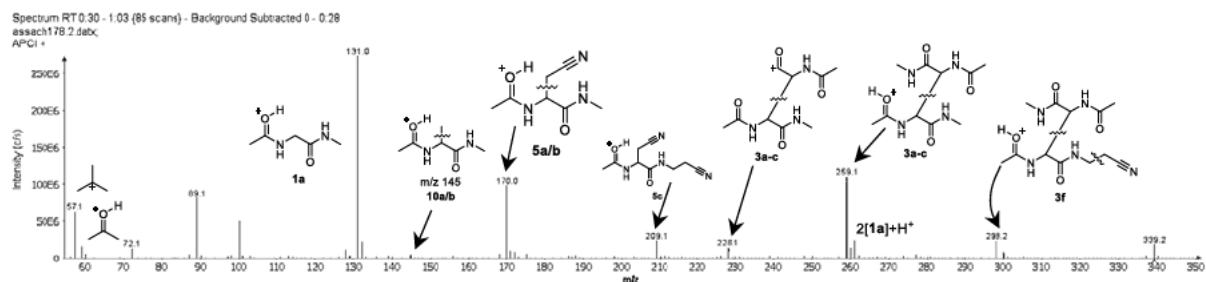


Fig. S21. APCI MS spectrum profile of the oxidative stress reaction of **1a** with **2a**.

Table S13. Products distribution for oxidation of AcGlyNMe (**1a**) with 1 eq of **2a**.

a) Recovery of AcGlyNMe (**1a**)

[1a] _{Stock} = 13.69 mM	μmol added	Average peak area, S	DF	Normalized peak area, S _N	Confidence interval, P 0.95
+ 0.00 ml	0.00	182035	1.0	182035	-
+ 0.25 ml	3.42	229176	1.0	229176	-
Obtained concentration, [1a]				66.05 mM	
Initial concentration [1a] ₀				101.4 mM	
Recovery 1a , [1a]/[1a] ₀				65.1 %	

b) Yield of cyanomethylation adduct AcGlyNEtCN (**5b**)

[5b] _{Stock} =7.35 mM	μmol added	Average peak area, S	DF	Normalized peak area, S _N	Confidence interval, P 0.95
+ 0.00 ml	0.00	9708	1.0	9708	-
+ 0.25 ml	1.84	45694	1.0	45694	-
Obtained concentration, [5b]				2.48 mM	
Initial concentration, [1a] ₀				101.4 mM	
Yield 5b , [5b]/[1a] ₀				2.4 %	

c) Yield of cyanomethylation adduct AcAla(CN)NMe (**5a**)

[5b] _{Stock} =7.35 mM	μmol added	Average peak area, S	DF	Normalized peak area, S _N	Confidence interval, P 0.95
+ 0.00 ml	0.00	46231	1.0	46231	-
Obtained concentration, [5a]				11.82 mM	
Initial concentration, [1a] ₀				101.4 mM	
Yield 5a , [5a]/[1a] ₀				11.7 %	

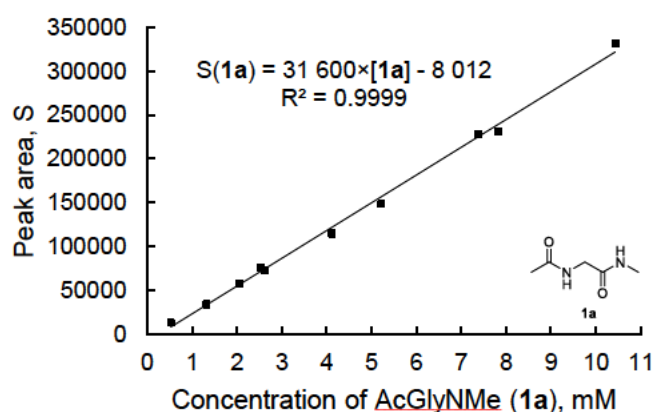
2.6.3.10. General procedure of oxidative stress reaction (1 mmol scale)

174 mg of hyponitrite **2a** (1 mmol, 1 eq) were added to 1 mmol of dipeptide (1 eq) in 10 ml of dry degassed MeCN under nitrogen atmosphere. The vessel was tightly closed, wrapped in foil

to cover the reaction mixture from light and placed in a thermostat at 23 °C. Afterwards, the reaction vessel was opened with caution, the formed white precipitate of **3a/b** was separated via centrifuge, washed with MeCN (3×1 ml), and the organic fractions were dried in *vacuo* at RT. The crude material was diluted up to 15 times in EtOH for further GC-FID analysis (Fig. S22). Yields of the oxidation products were obtained using absolute calibration curves (Table S14). Afterwards, all organic phases were combined and concentrated in *vacuo*. The crude material was separated on a silica column (DCM/MeOH = 10/1) for further NMR analysis, which shows that these fractions consist of solvent dimer **4**, adduct **5a**, dipeptide **1a**, adduct **5b** and dimerization adduct **3c** (in order of appearance during the column separation). Yields of succinonitrile (**4**), dipeptide **1a**, adducts **5a** and **5b** were obtained from quantitative GC-FID analysis, yields of dimerization products **3a/b** and **3c** were obtained from gravimetric measurements.

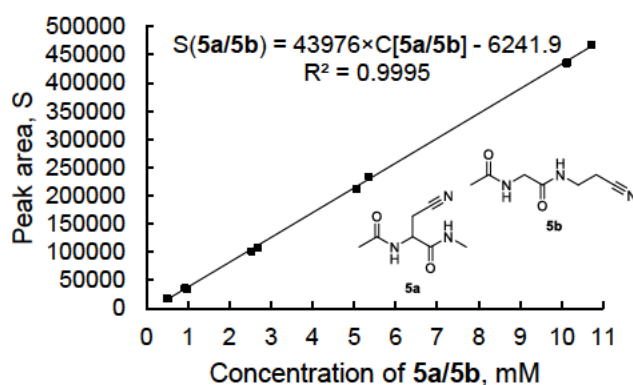
Table S14. Absolute calibration curves for oxidative stress reaction of AcGlyNMe (**1a**).

a) Calibration curve for AcGlyNMe (**1a**)



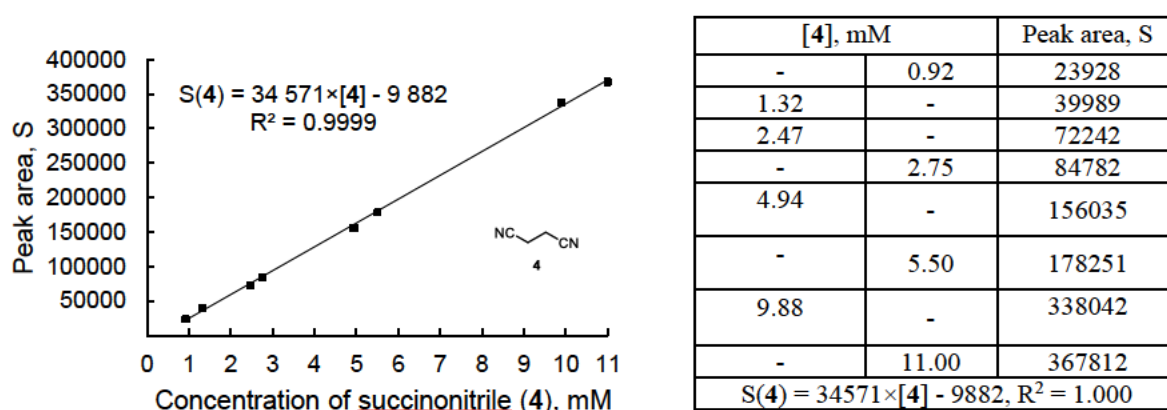
Concentration 1a , mM		Peak area, S
0.52	-	13217
1.30	-	34544
-	2.05	58314
2.61	-	73099
-	2.53	76060
-	4.10	114918
5.22	-	148745
-	7.38	228105
7.82	-	230947
10.43	-	330939
S(1a) = 31600 × [1a] - 8012, R ² = 1.000		

b) Calibration curve for AcAla(CN)NMe (**5a**) and AcGlyNEtCN (**5b**)



Concentration, mM		Peak area, S
5a	5b	
0.48	-	19088
-	0.51	17355
0.92	-	36412
-	0.97	34333
2.53	-	101959
-	2.68	107771
5.06	-	211853
-	5.36	234323
10.12	-	436018
-	10.71	468245
S(5a/5b) = 43976 × C[5a/5b] - 6241, R ² = 0.9995		

c) Calibration curve for succinonitrile (**4**)



Oxidative stress of AcGlyNMe (**1a**) with DTBHN (**2a**) at 23°C (1 mmol scale)

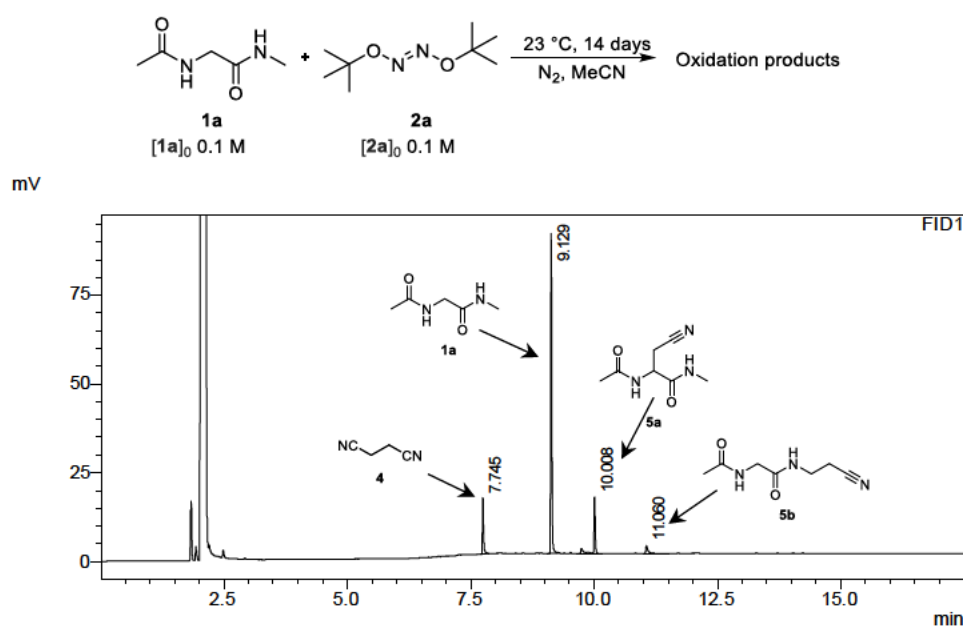


Fig. S22. GC-FID spectra of the oxidative stress reaction of **1a** with **2a** at 23°C.

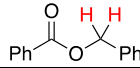
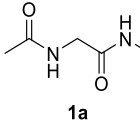
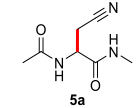
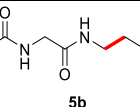
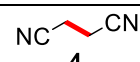
Table S15. Quantitative GC-FID of the oxidative stress reaction of **1a** with **2a** at 23 °C.

Peak area, S	-	24139	132470	31554	6285	-
Conc., M	-	0.014	0.067	0.013	0.003	-
Mole, mmol	-	0.147	0.667	0.129	0.026	-
Mass, mg	8.9	11.8	86.7	21.8	7.6	12.0
Yield, %	6.9	14.8*	66.7	12.9	2.6	9.3
Mass balance, %	98.4 %					

* from DTBHN **2a** amount

Table S16. Quantitative ^1H NMR the oxidative stress reaction of **1a** with **2a**

65.0 mg of benzyl benzoate solution was added to crude material, which was dissolved in $\text{MeOH-}d_4$ and ^1H NMR spectra was taken.

Compound	Peak area	Moles, μmol	Mass, mg	Yield, %
	1.000	30.7	65.0	-
 1a	2.374	72.8	94.6	72.8
 5a	0.187	11.5	19.4	11.5
 5b	0.113	3.5	5.9	3.5
 4	0.663	10.1	8.1	10*

*from DTBHN **2a** amount

Oxidative stress of AcGlyNMe (**1a**) with DTBHN (**2a**) at 40°C (1 mmol scale)

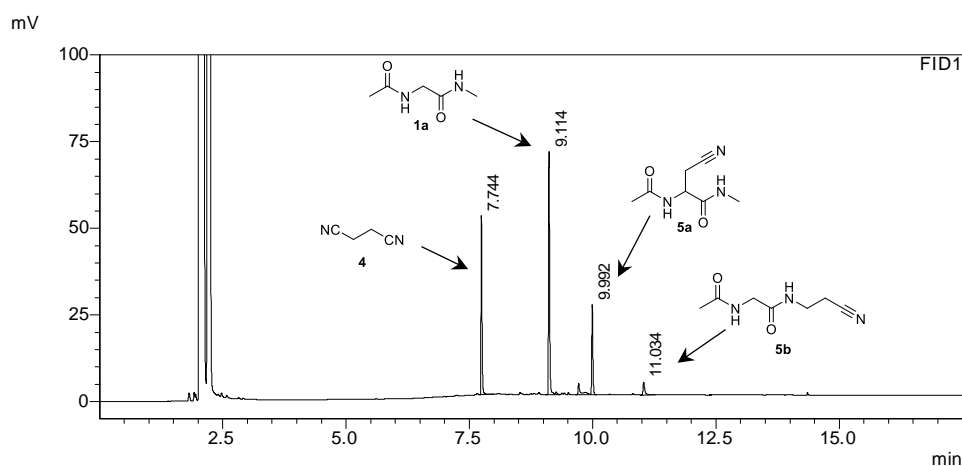
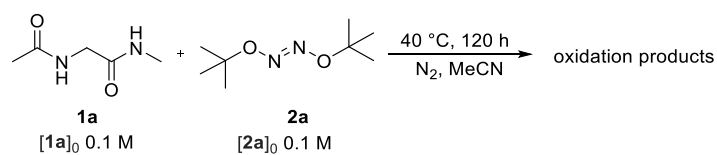
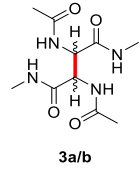
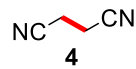
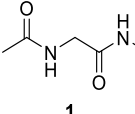
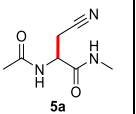
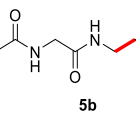
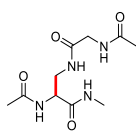
**Fig. S23.** GC-FID spectra of the oxidative stress reaction of **1a** with **2a** at 40°C .

Table S17. Quantitative GC-FID of the oxidative stress reaction of **1a** with **2a** at 40 °C

						
Peak area, S	-	70387	109259	53342	9055	-
Conc., M	-	0.035	0.056	0.020	0.005	-
Mole, mmol	-	0.349	0.556	0.203	0.052	-
Mass, mg	9.5	27.9	72.3	34.3	8.8	20.2
Yield, %	7.4	34.9*	55.6	20.3	5.2	15.7
Mass balance, %	104.2					

* from DTBHN **2a** amount

Oxidative stress of AcGlyNMe (**1a**) with DTBHN (**2a**) at 65 °C (1 mmol scale).

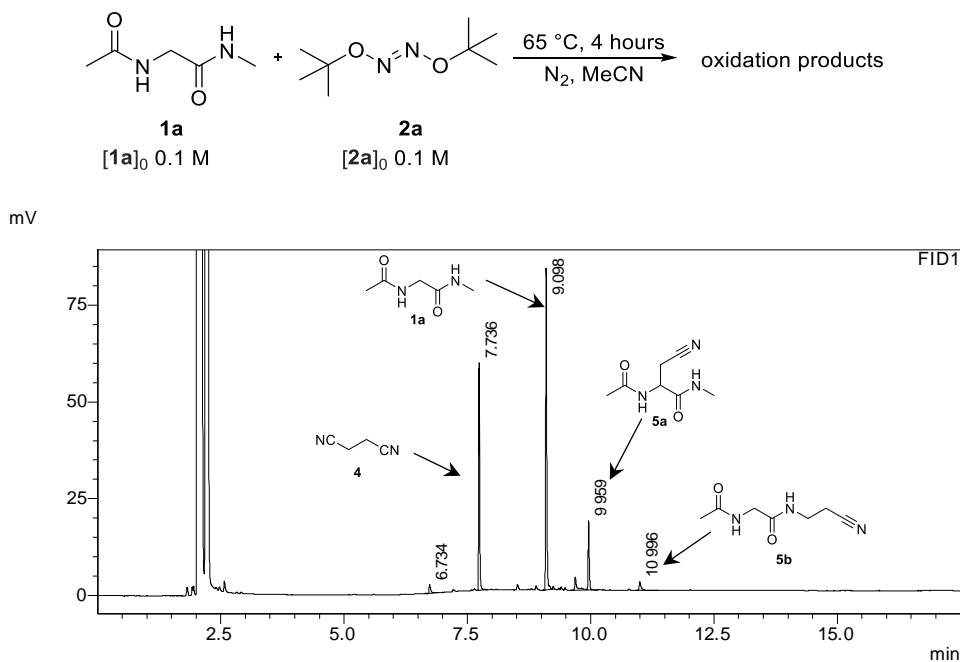
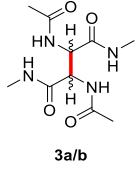
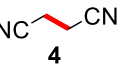
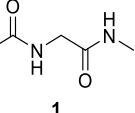
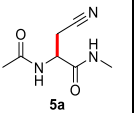
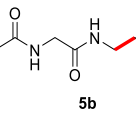
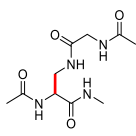


Fig. S24. GC-FID spectra of the oxidative stress reaction of **1a** with **2a** at 65 °C.

Table S18. Quantitative GC-FID of the oxidative stress reaction of **1a** with **2a** at 65 °C.

						
Peak area, S	-	79888	128519	39281	6143	-
Conc., M	-	0.039	0.065	0.015	0.004	-
Mole, mmol	-	0.390	0.648	0.155	0.042	-

Mass, mg	4.5	31.2	84.2	26.2	7.1	12.8
Yield, %	3.5	39.0*	64.8	15.5	4.2	9.9
Mass balance, %	97.9					

* from DTBHN 2a amount

Oxidative stress of 1-Ca-d2 with DTBHN (2a) at 23°C.

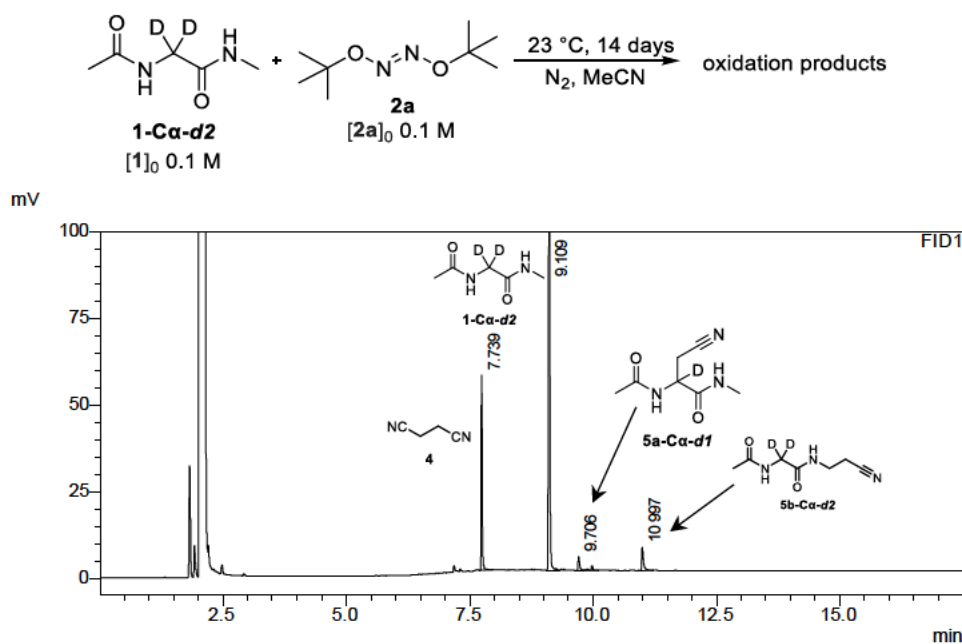
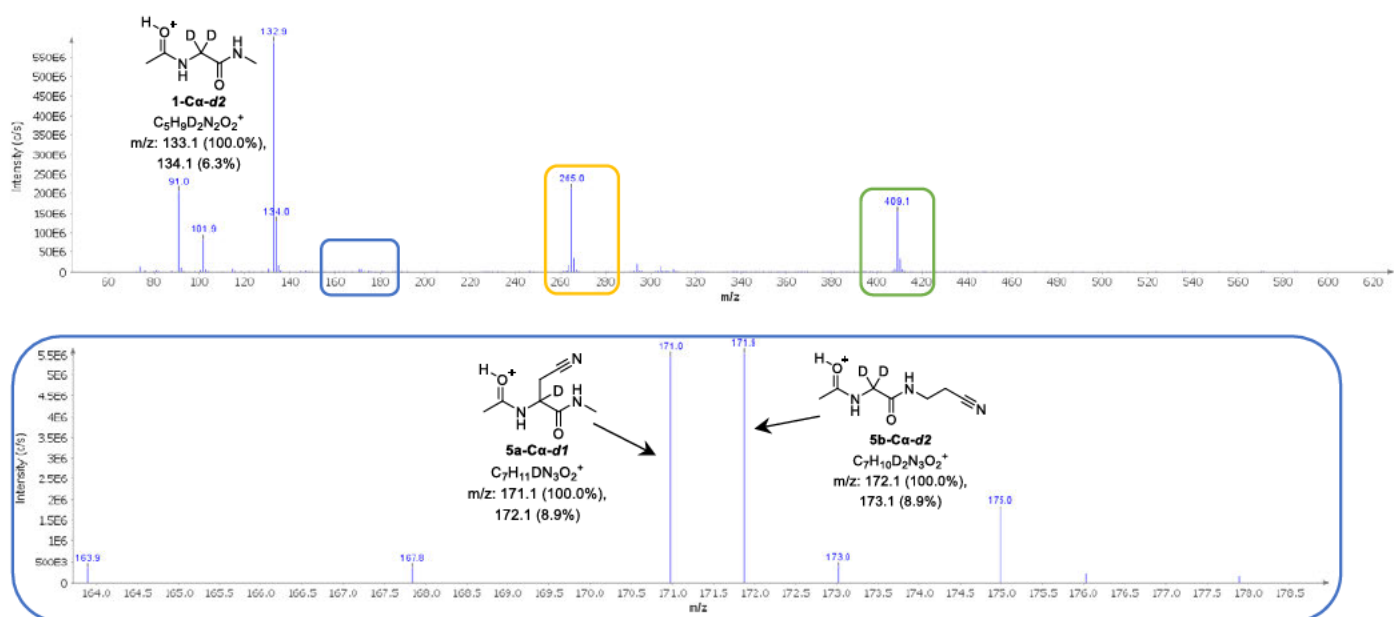


Fig. S25. GC-FID spectra of the oxidative stress reaction of 1-Ca-d2 with 2a at 23°C.



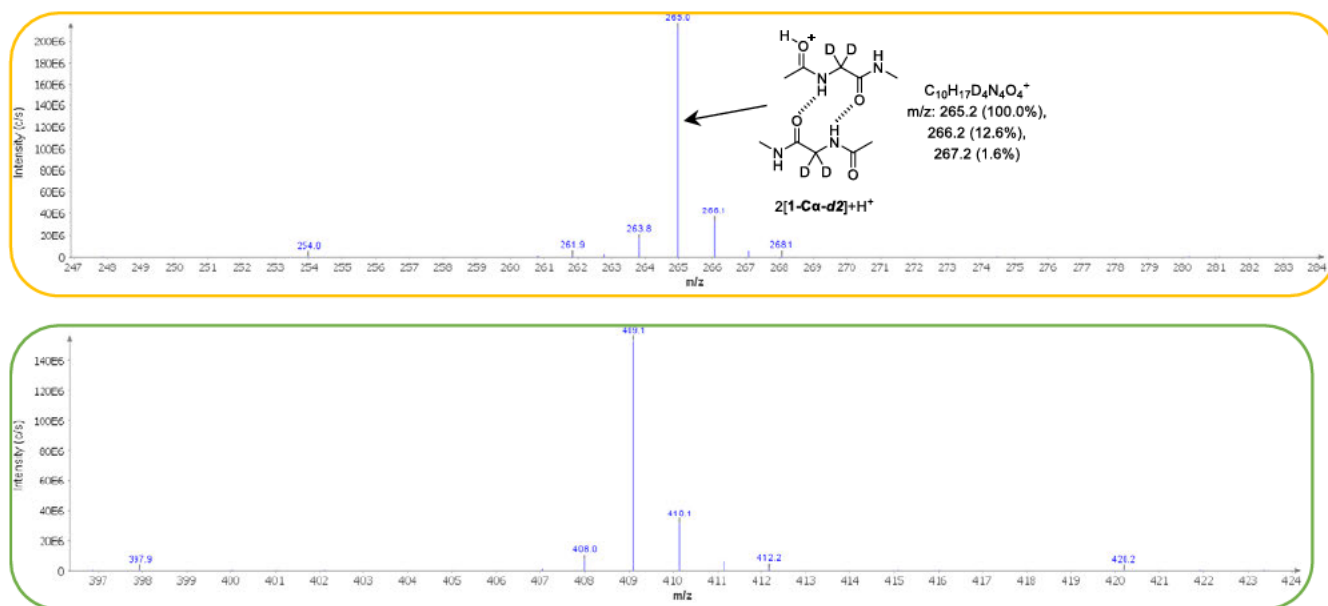
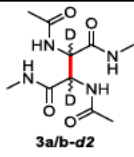
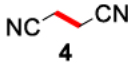
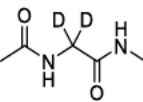
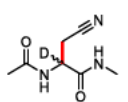
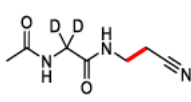
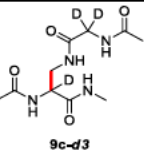


Fig. S26. MS profile of the oxidative stress reaction of **1-C α -d2** with DTBHN **2a** at 23°C.

Table S19. Results of oxidative stress of **1-C α -d2** with DTBHN **2a** at 23°C.

						
Peak area, S ₁	-	78506	228838	13786	17444	-
Added, μ mol	-	-	68.46	24.85	23.67	-
Peak area, S ₂	-	72293	396885	103706	100280	-
Mass, mg	Detected in MS	19.8*	121.0	6.5	8.5	Detected in MS
Yield, %	-	24.8*	91.7	3.8	5.0	-
Mass balance, %	100.5					

*from DTBHN **2a** amount (based on ¹H NMR analysis)

Oxidative stress of **1-NMe-d3** with DTBHN (**2a**) at 23°C.

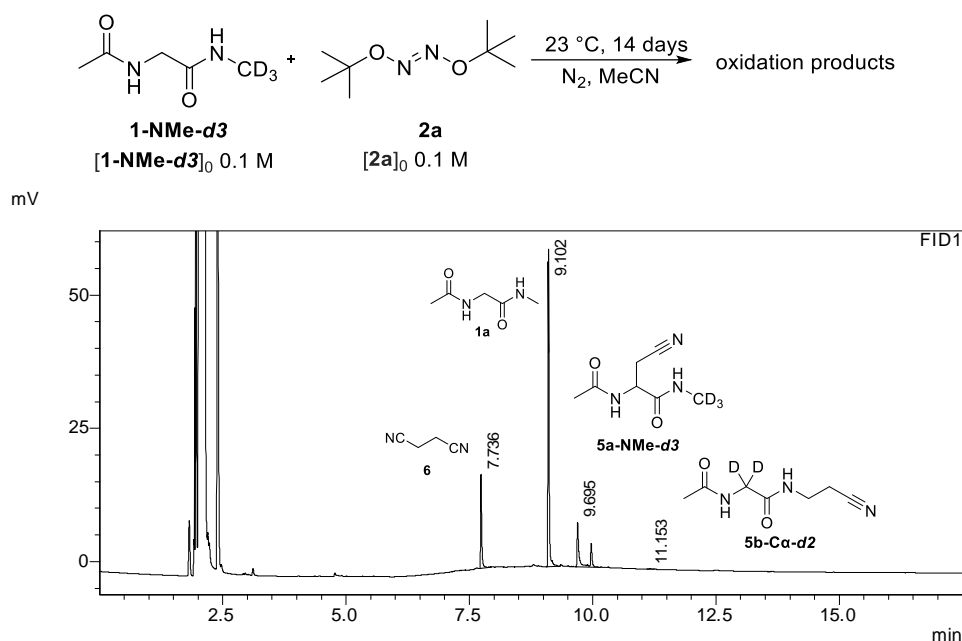
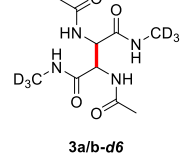
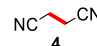
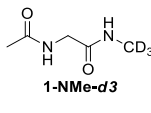

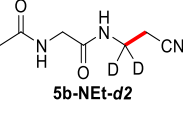
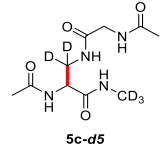


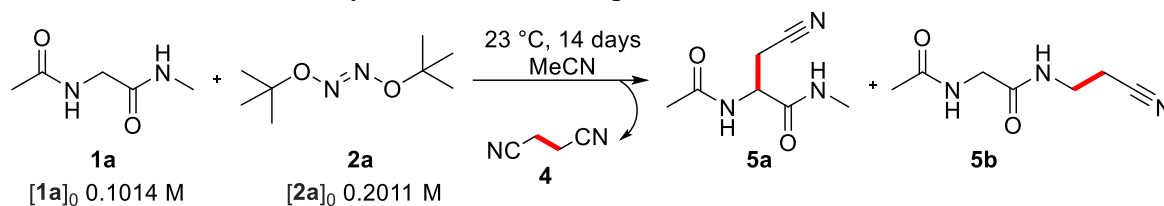
Fig. S27. GC-FID spectra of the oxidative stress reaction of **1-NMe-d3** with **2a** at 23°C.

Table S20. Results of oxidative stress of **1-NMe-d3** with DTBHN (**2a**) at 23°C.

						
	3a/b-d6	4	1-NMe-d3	5a-NMe-d3	5b-NEt-d2	5c-d5
Peak area, S ₁	-	27268	94238	30456	229	-
Added, mg	-	-	10.3	9.6	8.4	-
Peak area, S ₂	-	25383	193803	136928	60883	-
Mass, mg	11.7	15.0*	97.5	21.3	trace	was not isolated
Yield, %	8.9	18.8*	73.3	12.4	trace	was not isolated
Mass balance, %	94.6					

*from DTBHN **2a** amount (based on ¹H NMR analysis)

2.6.3.11. Oxidation of AcGlyNMe (**1a**) with 2 eq of DTBHN (**2a**)



175 mg (1.006 mmol) of DTBHN (**2a**) were dissolved in 5 ml solution of AcGlyNMe (**1a**) (0.1014 M) in dry degassed acetonitrile. 1 ml of the prepared mixture was sealed in a vial under nitrogen atmosphere, wrapped in foil and set in a cryostat at 23 °C for 14 days. Afterwards, it was carefully opened with caution and diluted up to 5 ml with iPrOH (Fig. S28). Yields were obtained by addition of exact amount of known compounds to the crude solution. The results are represented in Table S21.

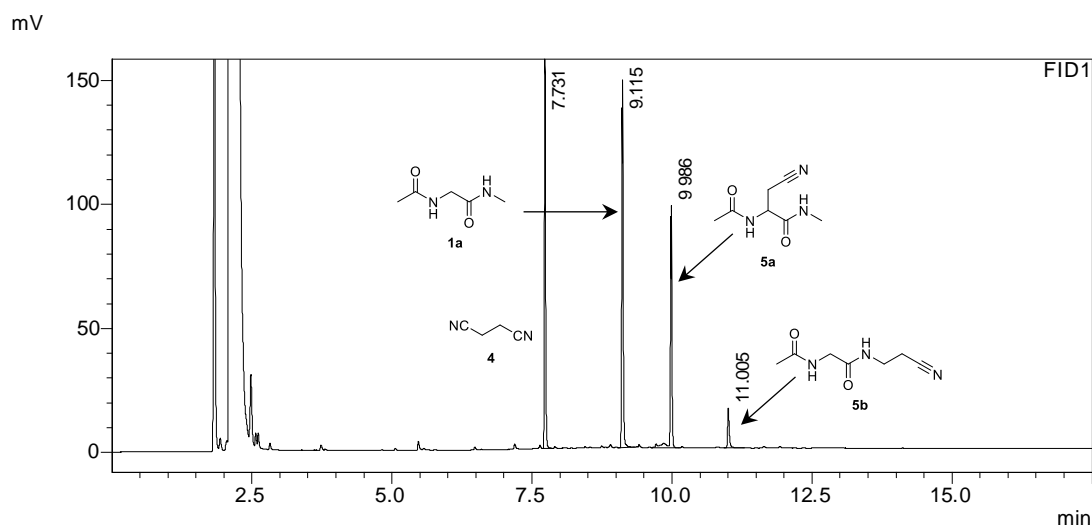
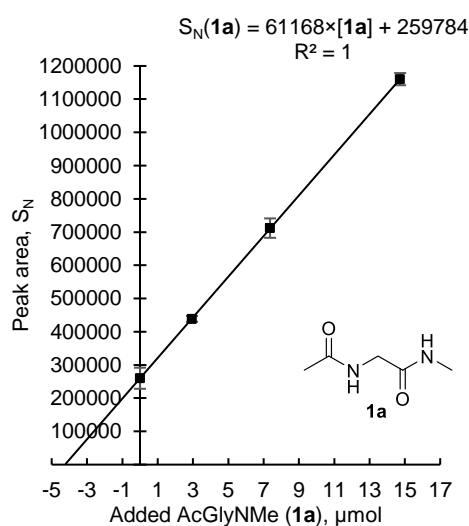


Fig. S28. GC-FID spectra of the oxidative stress reaction of AcGlyNMe (**1a**) with **2a**.

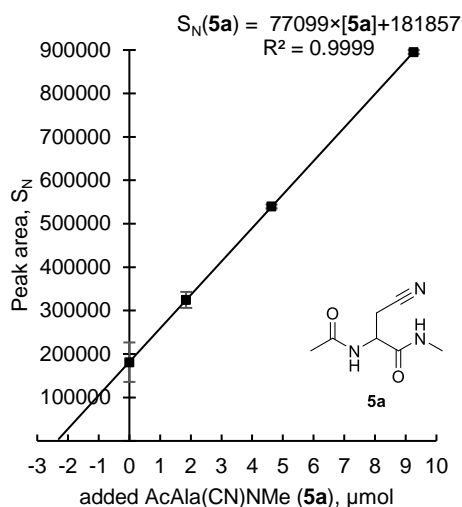
Table S21. Products distribution for oxidation of AcGlyNMe (**1a**) with 2 eq of **2a**.

a) Recovery of AcGlyNMe (**1a**)



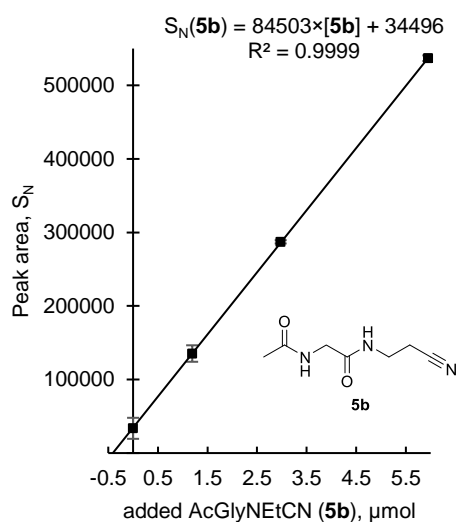
$[\mathbf{1a}]_{\text{Stock}} = 29.46 \text{ mM}$	μmol added	Average peak area, S	DF	Normalized peak area, S_N	Confidence interval, P 0.95
+ 0.00 ml	0.00	259990	1.0	259990	± 31733
+ 0.10 ml	2.95	274209	1.6	438734	± 8875
+ 0.25 ml	7.37	284767	2.5	711916	± 29217
+ 0.50 ml	14.73	290072	4.0	1160286	± 18328
Linear regression equation				$S_N(\mathbf{1a}) = 61168 \times [\mathbf{1a}] + 259784$	
Obtained concentration, $[\mathbf{1a}]$				If $S_N(\mathbf{1a}) = 0$, then $[\mathbf{1a}] = \frac{259784}{61168} \times \frac{5}{0.5 \text{ ml}} = 42.5 \text{ mM}$	
Initial concentration $[\mathbf{1a}]_0$				101.4 mM	
Recovery $\mathbf{1a}$, $[\mathbf{1a}]/[\mathbf{1a}]_0$				42%	

b) Yield of cyanomethylation adduct AcAla(CN)NMe (**5a**)



$[\mathbf{5a}]_{\text{Stock}} = 18.52 \text{ mM}$	μmol added	Average peak area, S	DF	Normalized peak area, S_N	Confidence interval, P 0.95
+ 0.00 ml	0.00	181263	1.0	181263	± 45418
+ 0.10 ml	1.85	203798	1.6	326077	± 18417
+ 0.25 ml	4.63	216579	2.5	541448	± 4384
+ 0.50 ml	9.26	224500	4.0	898000	± 4231
Linear regression equation				$S_N(\mathbf{5a}) = 77099 \times C[\mathbf{5a}] + 181857$	
Obtained concentration				If $S_N(\mathbf{5a}) = 0$, $[\mathbf{5a}] = \frac{181857}{77099} \times \frac{5}{0.5 \text{ ml}} = 23.6 \text{ mM}$	
Initial concentration $[\mathbf{1a}]_0$				101.4 mM	
Yield 5a , $[\mathbf{5a}]/[\mathbf{1a}]_0$				23.2%	

c) Yield of cyanomethylation adduct AcGlyNEtCN (**5b**)



$[\mathbf{5b}]_{\text{Stock}} = 11.83 \text{ mM}$	μmol added	Average peak area, S	DF	Normalized peak area, S_N	Confidence interval, P 0.95
+ 0.00 ml	0.00	33683	1.0	33683	± 14294
+ 0.10 ml	1.18	84464	1.6	135142	± 11219
+ 0.25 ml	2.96	114687	2.5	286718	± 2243
+ 0.50 ml	5.92	134438	4.0	537753	± 3863
Linear regression equation				$S_N(\mathbf{5b}) = 84503 \times C[\mathbf{5b}] + 34496$	
Obtained concentration				If $S_N(\mathbf{5b}) = 0$, $[\mathbf{5b}] = \frac{34496}{84503} \times \frac{5}{0.5 \text{ ml}} = 4.1 \text{ mM}$	
Initial concentration $[\mathbf{1a}]_0$				101.4 mM	
Yield 5b , $[\mathbf{5b}]/[\mathbf{1a}]_0$				4%	

348 mg of hyponitrite **2a** (2 mmol, 2 eq) were added to 1 mmol of AcGlyNMe (**1a**, 1 eq) in 10 ml of dry degassed MeCN under nitrogen atmosphere. The vessel was tightly closed, wrapped in foil to cover the reaction mixture from light and placed in a thermostat at 23 °C. Afterwards, the reaction vessel was opened with caution, the formed white precipitate of **3a/b** was separated via centrifuge, washed with MeCN (3×1 ml), and the organic fractions were dried in vacuo at RT. The crude material was dissolved in 10 ml of EtOH for further GC-FID and NMR analysis. Afterwards, all organic phases were combined and concentrated in vacuo. The crude material was separated on a silica column (DCM/MeOH = 10/1) for further NMR analysis, which shows that these fractions consist of initial solvent dimer **4**, adduct **5a**, dipeptide **1a**, adduct **5b** and dimerization adduct **3c** (in the order of appearance during the column separation). Yields of

dipeptide **1a**, adducts **5a** and **5b** were obtained from quantitative GC-FID analysis (Fig. S29), yield for succinonitrile (**4**) was obtained from ¹H NMR quantitative analysis, yields of dimerization products **3a/b** and **3c** were obtained from gravimetric measurements (Table S22).

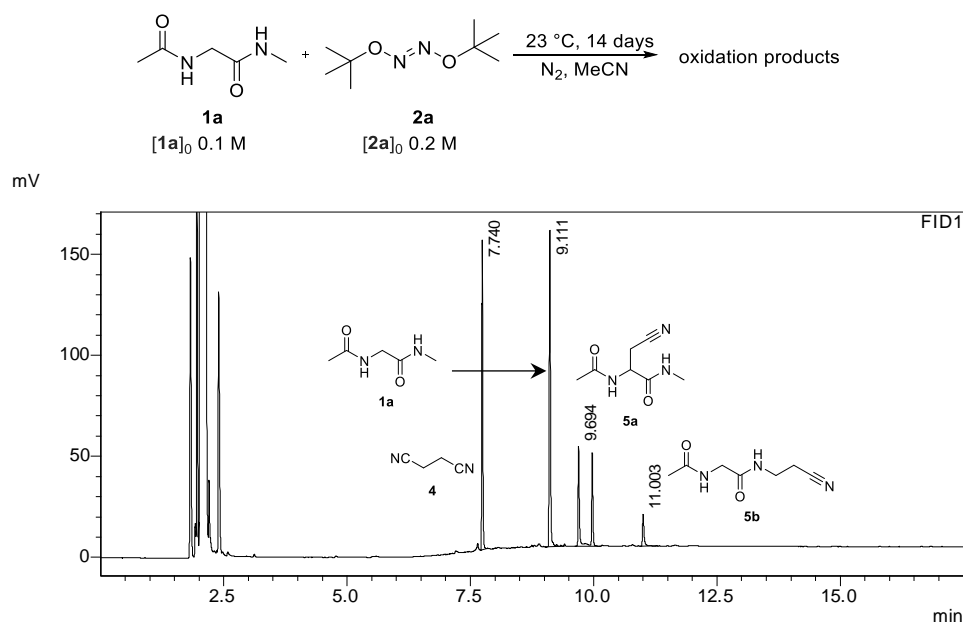


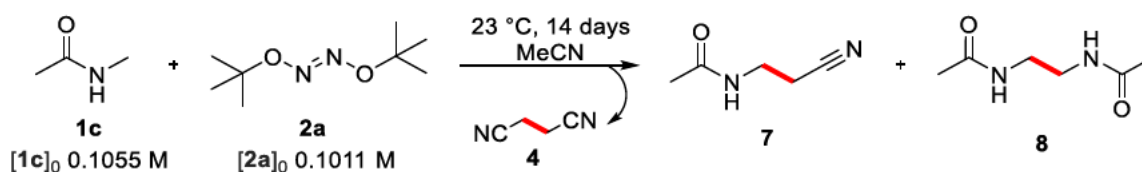
Fig. S29. GC-FID spectra of the oxidative stress reaction of **1a** with 2 eq **2a**

Table S22. Results of oxidative stress of **1a** with 2 eq **2a** at 23°C.

Peak area, S	-	212746	278399	165829	33495	-
Added, mg	-	-	1.300	-	1.044	-
Peak area, S ₂	-	-	345642	166872	81656	-
Conc., M	-	-	0.402	0.215	0.044	-
Mole, n	-	0.271	0.402	0.215	0.044	-
Mass, mg	13.5	21.7	52.3	36.4	7.4	25.7
Yield, %	10.5	13.5*	40.2	21.6	4.4	19.9
Mass balance	96.6 %					

* from DTBHN **2a** amount, from ¹H NMR analysis

2.6.3.12. Oxidation of AcNMe (**1c**) with DTNH (**2a**)



89 mg (0.5055 mmol) of DTBHN (**2a**) were dissolved in 5 ml solution of **1c** (0.1055 M) in dry degassed acetonitrile. 1 ml of prepared mixture was sealed in a vial under nitrogen atmosphere, wrapped in foil and set in cryostat at 23 °C for 14 days. Afterwards, it was carefully opened, then diluted up to 10 ml with iPrOH (Fig. S30 and S31). Yields were obtained by addition of exact amount of known compounds to the crude solution. The results are represented in Table S23 and S24.

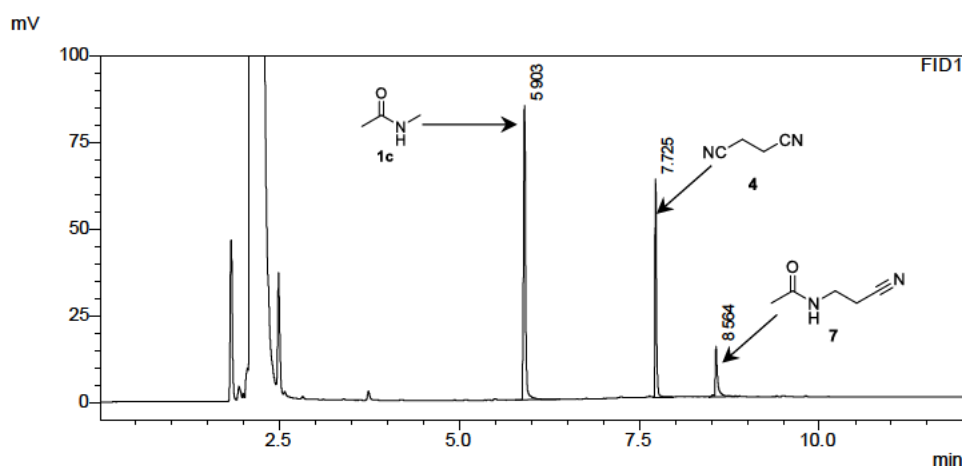


Fig. S30. GC-FID spectra of the oxidative stress reaction of AcNMe (**1c**) with **2a**.

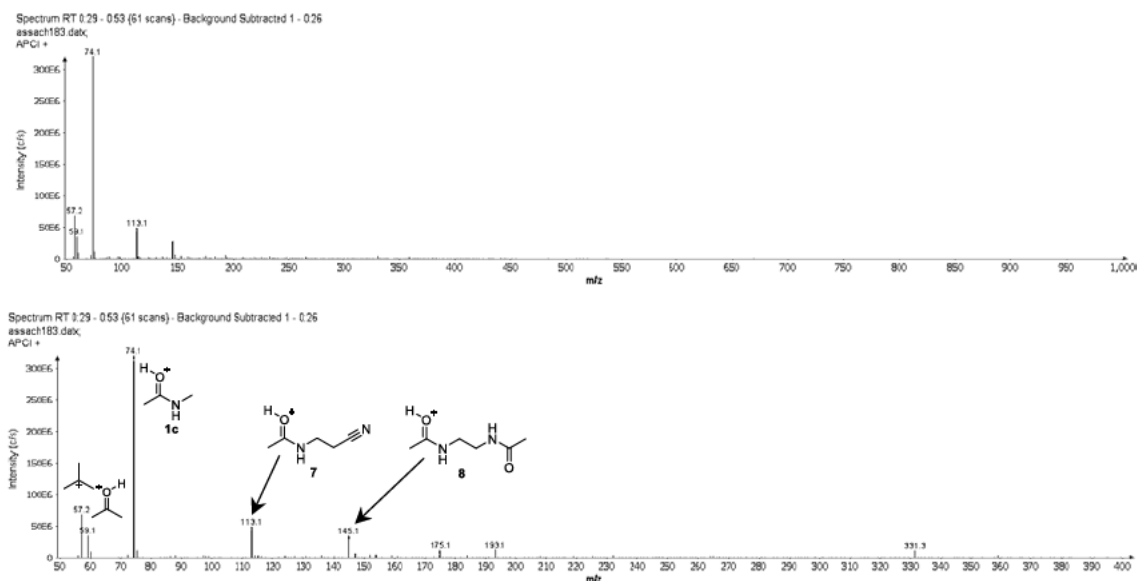
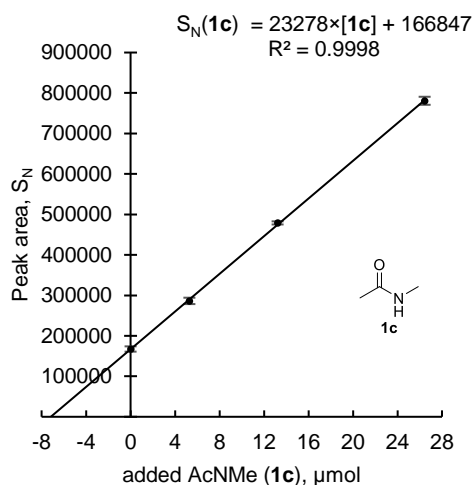


Fig. S31. MS profile of the oxidative stress reaction of AcNMe (**1c**) with **2a**.

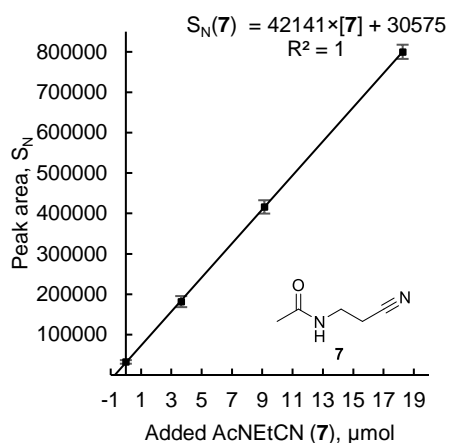
Table S23. Products distribution for the oxidation of AcNMe (**1c**) with **2a**

a) Recovery of AcNMe (**1c**)



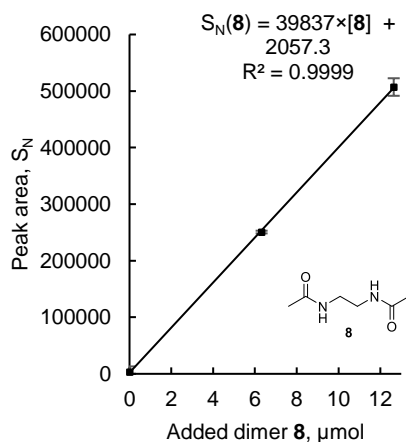
[1c] _{Stock} = 52.88 mM	μmol added	Average peak area, S	DF	Normalized peak area, S _N	Confidence interval, P 0.95
+ 0.00 ml	0.00	167490	1.00	167490	± 6550
+ 0.10 ml	5.29	220276	1.30	286358	± 7897
+ 0.25 ml	13.22	273720	1.75	479009	± 3856
+ 0.50 ml	26.44	312315	2.50	780786	± 9917
Linear regression equation				$S_N(\mathbf{1c}) = 23278 \times [\mathbf{1c}] + 166847$	
Obtained concentration				If $S_N(\mathbf{1c}) = 0$, $[\mathbf{1c}] = \frac{166847}{23278} \times \frac{5}{0.5 \text{ ml}} = 71.7 \text{ mM}$	
Initial concentration [1c] ₀				105.5 mM	
Recovery 1c , [1c]/[1c] ₀				68%	

b) Yield of cyanomethylation adduct AcNEtCN (**7**)



[7] _{Stock} = 36.52 mM	μmol added	Average peak area, S	DF	Normalized peak area, S _N	Confidence interval, P 0.95
+ 0.00 ml	0.00	32369	1.00	32369	± 4371
+ 0.10 ml	3.65	139764	1.30	181693	± 13659
+ 0.25 ml	9.13	237799	1.75	416147	± 16524
+ 0.50 ml	18.26	320062	2.50	800155	± 17560
Linear regression equation				$S_N(\mathbf{7}) = 42141 \times [\mathbf{7}] + 30575$	
Obtained concentration				If $S_N(\mathbf{7}) = 0$, $[\mathbf{7}] = \frac{30575}{42141} \times \frac{5}{0.5 \text{ ml}} = 7.2 \text{ mM}$	
Initial concentration [1c] ₀				105.5 mM	
Yield 7 , [7]/[1c] ₀				6.8%	

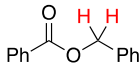
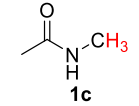
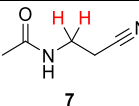
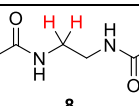
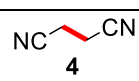
c) Yield of dimerization adduct dimer **8**



[8] _{Stock} = 25.28 mM	μmol added	Average peak area, S	DF	Normalized peak area, S _N	Confidence interval, P 0.95
+ 0.00 ml	0.00	3622	1.00	3622	± 9485
+ 0.25 ml	6.32	143244	1.75	250677	± 2401
+ 0.50 ml	12.64	202849	2.50	507122.5	± 15527
Linear regression equation				$S_N(\mathbf{8}) = 39837 \times [\mathbf{8}] + 2057.3$	
Obtained concentration				If $S_N(\mathbf{8}) = 0$, $[\mathbf{8}] = \frac{2057.3}{39837} \times \frac{5}{0.5 \text{ ml}} = 0.5 \text{ mM}$	
Initial concentration [1c] ₀				105.5 mM	
Yield 8 , [8]/[1c] ₀				<0.5 %	

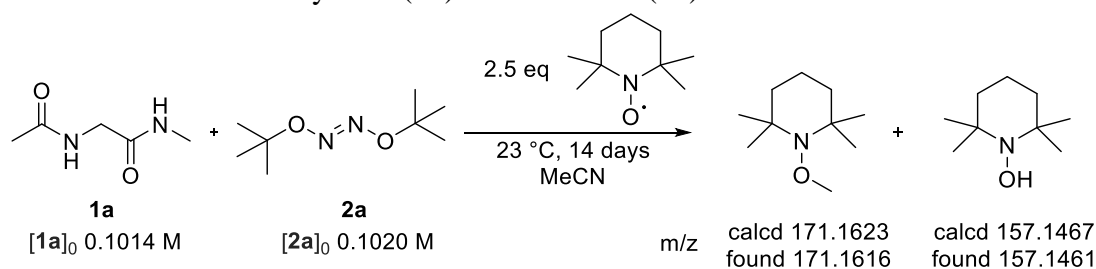
Table S24. Quantitative ^1H NMR of the oxidative stress reaction of AcNMe (**1c**) with **2a**.

12.0 mg of benzyl benzoate solution was added to 2.5 ml of calibrated solution of the crude mixture. All volatiles were evaporated under reduced pressure; the crude material was redissolved in MeOH-*d*₄ and ^1H NMR spectrum was taken.

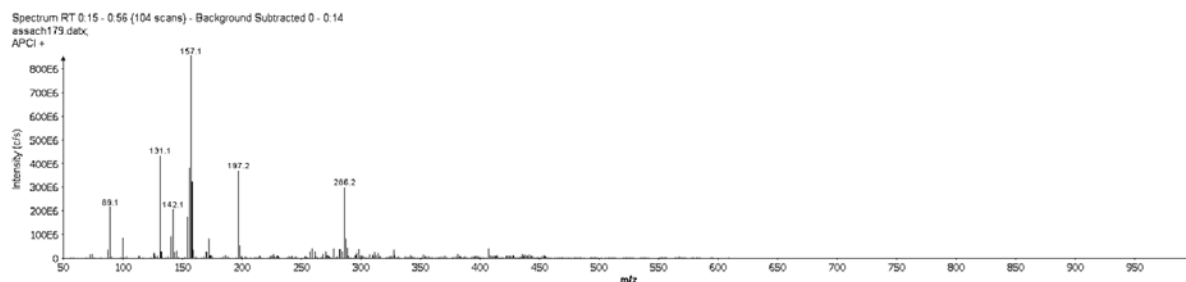
Compound	Peak area	Moles, μmol	Mass, mg	Yield, %
	1.000	56.6	12.0	-
 1c	0.477	45.0	3.34	44 (sublimation)
 7	0.065	9.1	1.01	9
 8	0.011	0.8	0.11	<1 %
 4	0.284	19.8	1.58	20*

*from DTBHN **2a** amount

2.6.3.13. Oxidation of AcGlyNMe (**1a**) with DTBHN (**2a**) and TEMPO



64.2 mg of TEMPO (0.412 mmol) were dissolved in 2 ml of solution of **2a** (0.1040 M) and **1a** (0.1014 M) in dry degassed acetonitrile. 0.8 ml of the prepared mixture was sealed in a vial under nitrogen atmosphere, wrapped in foil and set in cryostat at 23 °C for 14 days. Afterwards, the vial was opened with caution because of increased pressure inside, and the content diluted up to 5 ml with iPrOH (Fig. S32 and S33). Yields were obtained by addition of exact amount of known compounds to 0.5 ml aliquot of the solution. Results are represented in Table S25.



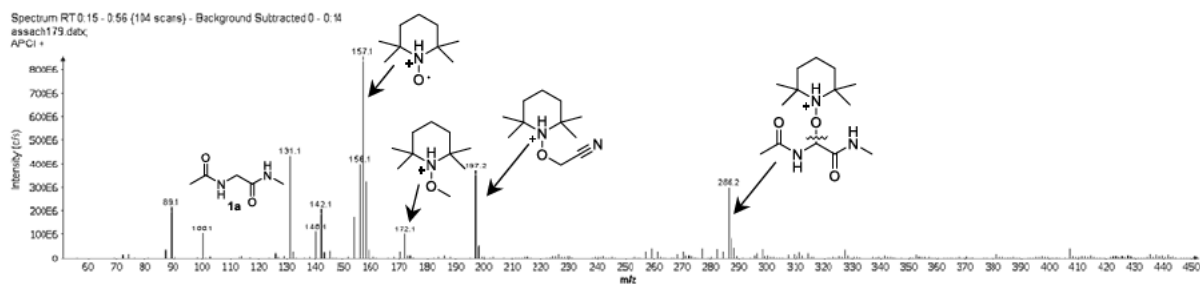


Fig. S32. MS profile of the oxidative stress reaction of **1a** with **2a** and TEMPO.

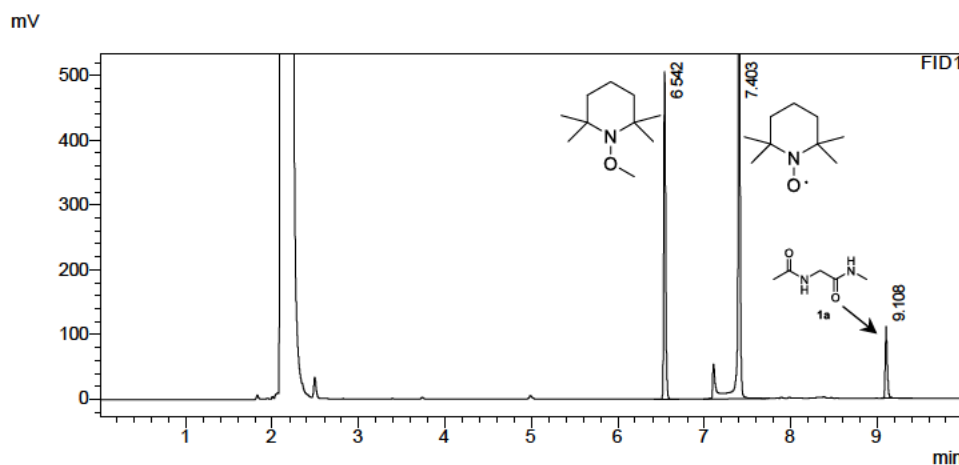
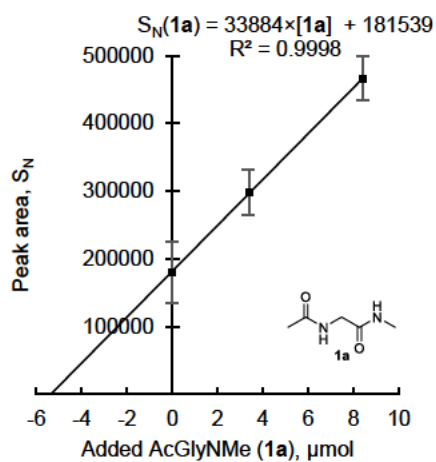


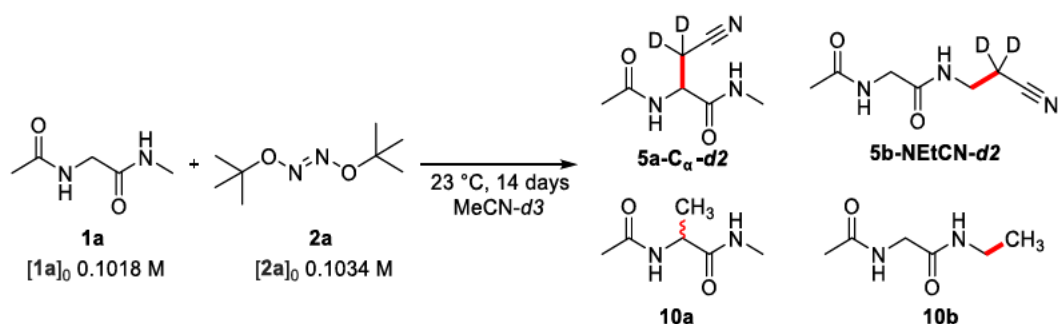
Fig. S33. GC-FID spectra of the oxidative stress reaction of **1a** with **2a** and TEMPO.

Table S25. Recovery of AcGlyNMe (**1a**).



$C_{\text{Stock}}[\mathbf{1a}]$ =33.69 mM	μmol added	Average peak area, S	DF	Normalized peak area, S_N	Confidence interval, P 0.95
+ 0.00 ml	0.00	180120	1.00	180120	± 45437
+ 0.10 ml	3.37	270969	1.10	298066	± 32820
+ 0.25 ml	8.42	372798	1.25	465998	± 32400
Linear regression equation				$S_N(\mathbf{1a}) = 33884 \times [\mathbf{1a}] + 181539$	
Obtained concentration, $[\mathbf{1a}]$				If $S_N(\mathbf{1a}) = 0$, then $[\mathbf{1a}] = \frac{181539}{33884} \times \frac{5}{0.5 \text{ ml} \times 0.8} = 67.0 \text{ mM}$	
Initial concentration $[\mathbf{1a}]_0$				101.4 mM	
Recovery 1a , $[\mathbf{1a}]/[\mathbf{1a}]_0$				66%	

2.6.3.14. Oxidation of AcGlyNMe (**1a**) with DTBHN (**2a**) in MeCN-*d*3



90 mg (0.517 mmol) of DTBHN (**2a**) were dissolved in 5 ml solution of **1a** (0.1018 M) in dry degassed deuterated MeCN. 1 ml of the prepared mixture was sealed in a vial under nitrogen atmosphere, wrapped in foil and set in cryostat at 23 °C for 14 days. Afterwards, it was carefully opened with caution, then diluted up to 5 ml with iPrOH (Fig. S34 and S35). Yields were obtained by addition of exact amount of known compounds to the crude solution.

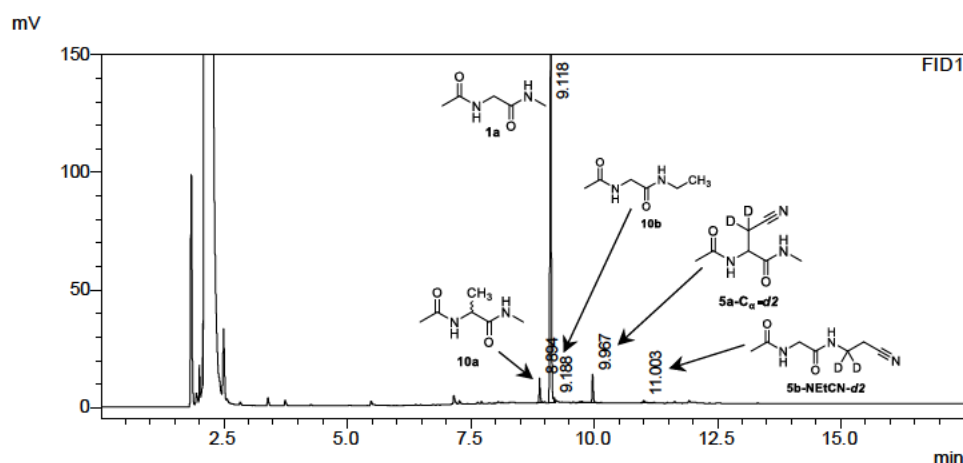


Fig. S34. GC-FID spectra of the oxidative stress reaction of **1a** with **2a** in MeCN-*d*3.

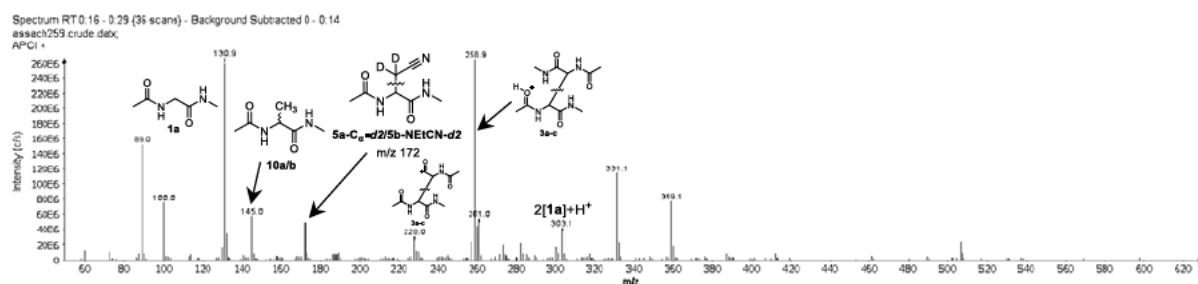


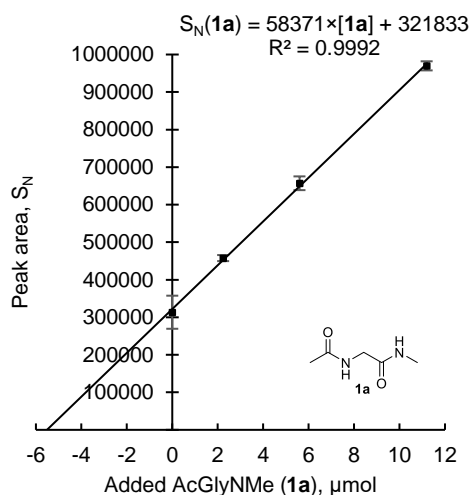
Fig. S35. APCI MS spectrum of the oxidative stress reaction of **1a** with **2a** in MeCN-*d*3.

The rule of equal response per carbon is very important in these measurements and implies that the two isomeric recombination products give the same response per molecule. Due to the identical molecular formula for AcAla(CN)NMe (**5a**) and AcGlyNEtCN (**5b**), DL-

AcAlaNMe (**10a**) and AcGlyNEt (**10b**), the FID determination is suitable to quantify a percentage distribution between the two products. Results are represented in Table S26.

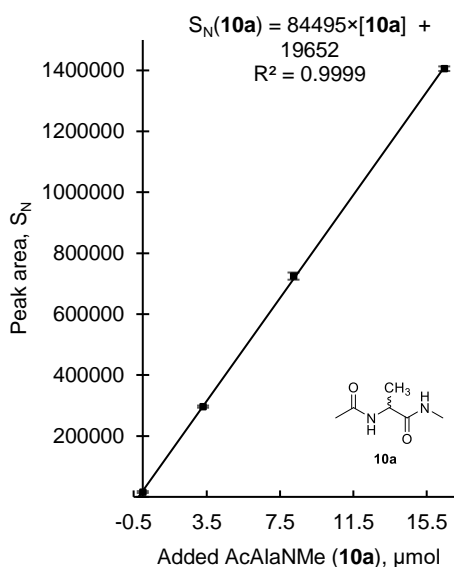
Table S26. Standard addition calibration curves for oxidation products of **1a** with **2a** in MeCN-*d*₃.

a) Recovery of AcGlyNMe (**1a**)



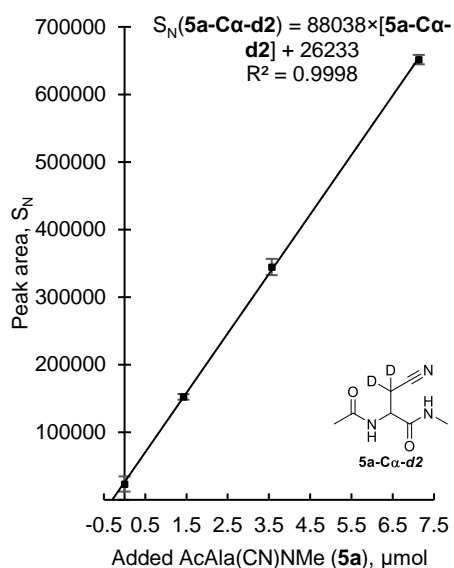
$[\mathbf{1a}]_{\text{Stock}} = 22.38 \text{ mM}$	μmol added	Average peak area, S	DF	Normalized peak area, S_N	Confidence interval, P 0.95
+ 0.00 ml	0.00	313435	1.0	313435	± 44071
+ 0.10 ml	2.24	286034	1.6	457654	± 8043
+ 0.25 ml	5.60	262812	2.5	657029	± 18328
+ 0.50 ml	11.19	242460	4.0	969838	± 12115
Obtained concentration, $[\mathbf{1a}]$				$S_N(\mathbf{1a}) = 58371 \times [\mathbf{1a}] + 321833$	
Initial concentration $[\mathbf{1a}]_0$				If $S_N(\mathbf{1a}) = 0$, then $[\mathbf{1a}] = \frac{321833}{58371} \times \frac{5}{0.5 \text{ ml}} = 55 \text{ mM}$	
Recovery 1a , $[\mathbf{1a}]/[\mathbf{1a}]_0$				101.8 mM	
Obtained concentration, $[\mathbf{1a}]$				54%	

b) Yield of methylation adducts **10a/b**



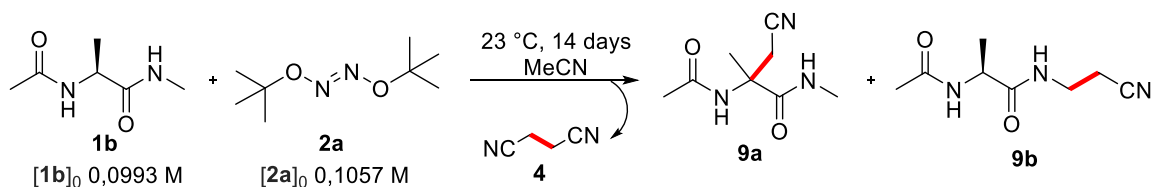
$[\mathbf{10a}]_{\text{Stock}} = 32.92 \text{ mM}$	μmol added	Average peak area, S	DF	Normalized peak area, S_N	Confidence interval, P 0.95
+ 0.00 ml	0.00	15908	1.0	15908	± 2992
+ 0.10 ml	3.29	185232	1.6	296370	± 3499
+ 0.25 ml	8.23	289888	2.5	724719	± 11792
+ 0.50 ml	16.46	351426	4.0	1405704	± 7583
Linear regression equation				$S_N(\mathbf{10a}) = 84495 \times [\mathbf{10a}] + 19652$	
Obtained concentration, $[\mathbf{10a}]$				If $S_N(\mathbf{10a}) = 0$, then $[\mathbf{10a}] = \frac{19652}{84495} \times \frac{5}{0.5 \text{ ml}} = 2.3 \text{ mM}$	
Initial concentration $[\mathbf{1a}]_0$				101.8 mM	
Yield 10a , $[\mathbf{10a}]/[\mathbf{1a}]_0$				2 %	
Obtained concentration, $[\mathbf{10b}]$				If $S_N(\mathbf{10b}) = 0$, then $[\mathbf{10b}] = \frac{4147}{84495} \times \frac{5}{0.5 \text{ ml}} = 0.5 \text{ mM}$	
Yield 10b , $[\mathbf{10b}]/[\mathbf{1a}]_0$				0.5%	

a) Yield of cyanomethylation adducts **5a-C α -d2** and **5b-NEtCN-d2**



[5a] _{Stock} = 14.26 mM	μmol added	Average peak area, S	DF	Normalized peak area, S _N	Confidence interval, P 0.95
+ 0.00 ml	0.00	23430	1.0	23430	± 11238
+ 0.10 ml	1.43	95275	1.6	152439	± 4174
+ 0.25 ml	3.57	137859	2.5	344648	± 12045
+ 0.50 ml	7.13	162889	4.0	651554	± 6969
Linear regression equation				S _N (5a-Cα-d2) = 88038 × [5a-Cα-d2] + 26233	
Obtained concentration, [5a-Cα-d2]				If S _N (5a-Cα-d2) = 0, then [5a-Cα-d2] = $\frac{26233}{88038} \times \frac{5}{0.5 \text{ ml}} = 3.0$ mM	
Initial concentration [1a] ₀				101.8 mM	
Yield 5a-Cα-d2 , [5a-Cα-d2]/[1a] ₀				2.9 %	
Obtained concentration, [5b-NEtCN-d2]				If S _N (5b-NEtCN-d2) = 0, then [5b-NEtCN-d2] = $\frac{3131}{88038} \times \frac{5}{0.5 \text{ ml}} =$ 0.4 mM	
Yield 5b-NEtCN-d2 , [5b-NEtCN-d2]/[1a] ₀				0.4 %	

2.6.3.15. Oxidation of AcAlaNMe (**1b**) with DTBHN (**2a**)



92 mg (0.5287 mmol) of DTBHN (**2a**) were dissolved in 5 ml solution of AcAlaNMe (**1b**) (0.0993 M) in dry degassed acetonitrile. 1 ml of prepared mixture was sealed in a vial under nitrogen atmosphere, wrapped in foil and set in cryostat at 23 °C for 14 days. After, it was carefully opened, then diluted up to 10 ml with iPrOH (Fig. S36 and S37). Yields were obtained by addition of exact amounts of known compounds to 0.5 ml of the crude solution. The rule of equal response per carbon is very important in these measurements: the assumption that the two isomeric recombination products give the same response per molecule. Due to the identical molecular formula for Ac- α -methyl-Ala(CN)NMe (**9a**) and AcAlaNEtCN (**9b**), the FID determination is suitable to quantify a percentage distribution between the two products. Results are represented in Table S27.

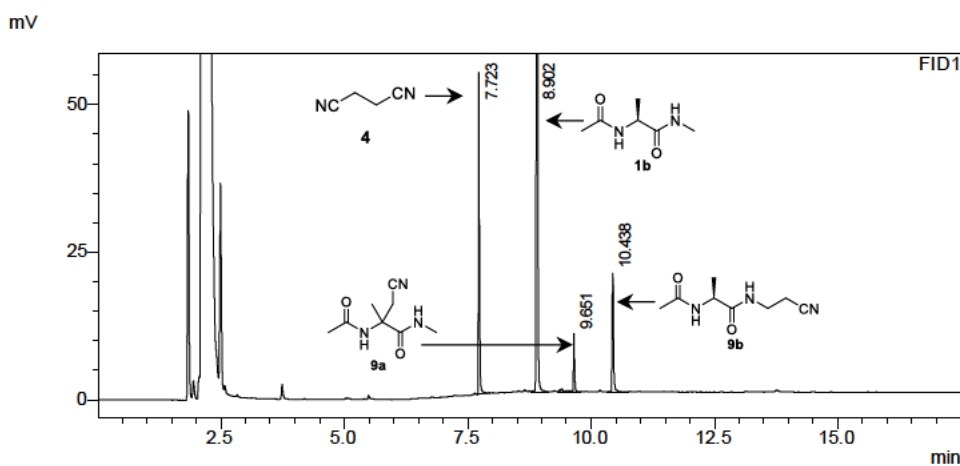


Fig. S36. GC-FID spectra of the oxidative stress reaction of **1b** with **2a** at 23 °C.

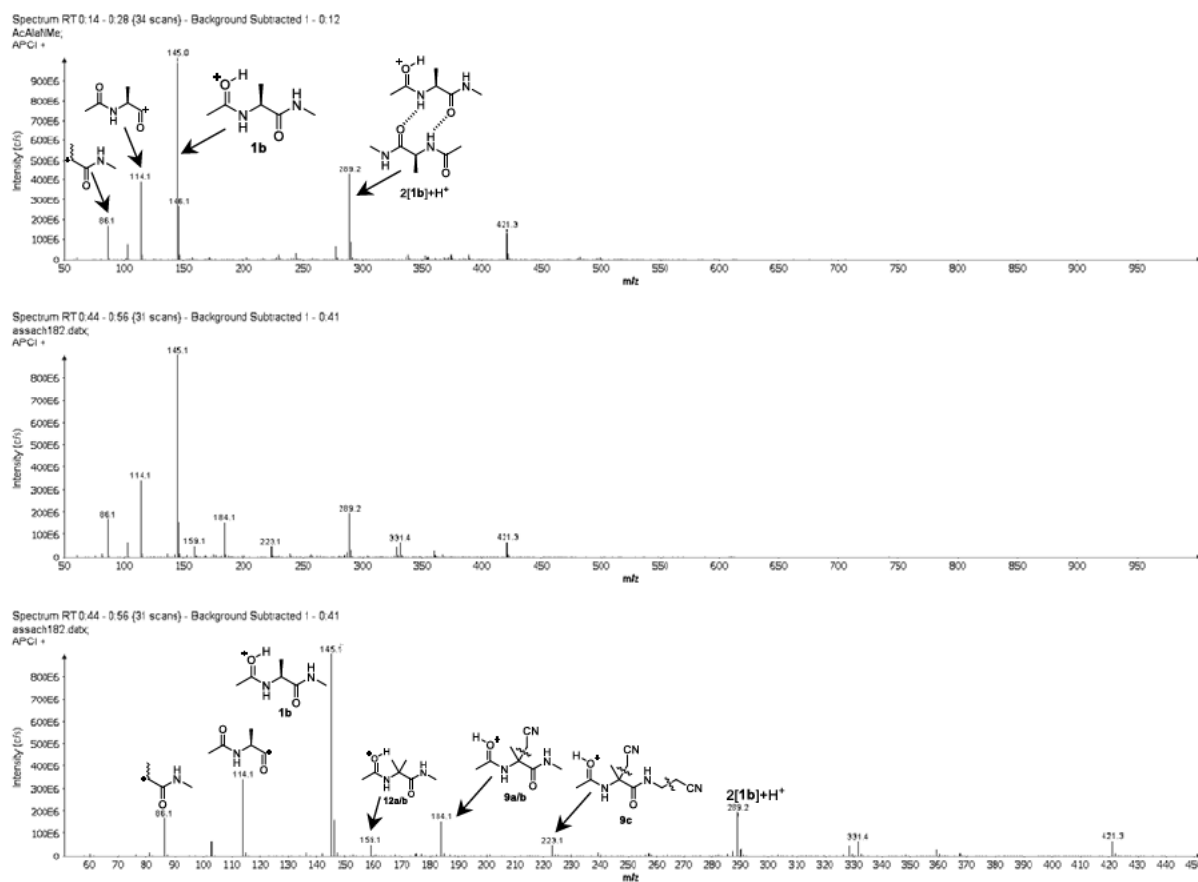
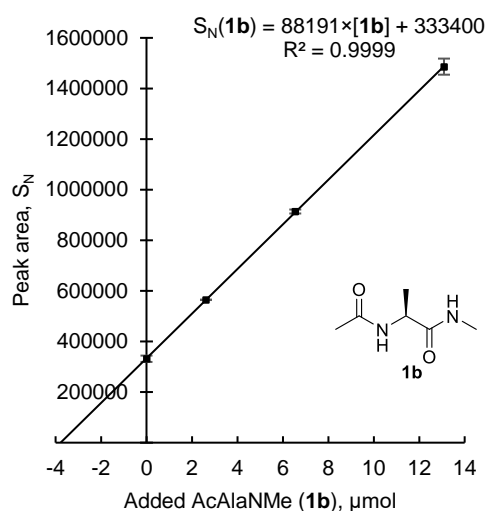


Fig. S37. APCI MS profile of 1) **1b** (top), 2) the oxidative stress reaction of **1b** with **2a** (middle/bottom).

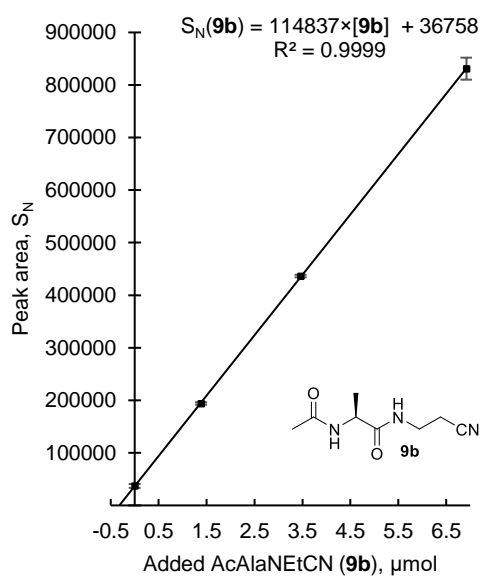
Table S27. Standard addition calibration curves for oxidation products of **1b** with **2a**

a) Recovery of AcAlaNMe (**1b**)

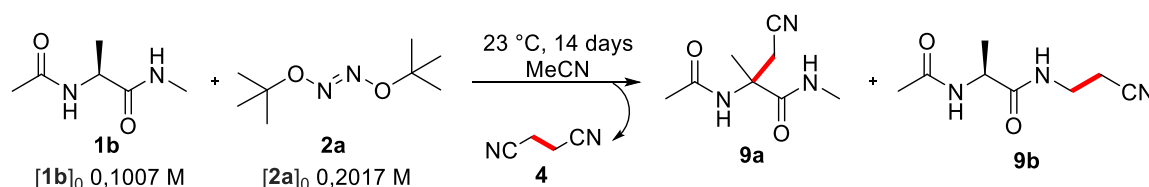


[1b] _{Stock} = 26.18 mM	μmol added	Average peak area, S	DF	Normalized peak area, S _N	Confidence interval, P 0.95
+ 0.00 ml	0.00	331610	1.0	331610	± 12534
+ 0.10 ml	2.62	403279	1.4	564590	± 845
+ 0.25 ml	6.55	456863	2.0	913725	± 7846
+ 0.50 ml	13.09	495414	3.0	1486241	± 31784
Linear regression equation				S _N (1b) = 88191 × [1b] + 333400	
Obtained concentration, [1b]				If S _N (1b) = 0, then [1b] = $\frac{333400}{88191} \times \frac{10}{0.5 \text{ ml}} = 75.6 \text{ mM}$	
Initial concentration [1b] ₀				99.3 mM	
Recovery 1b , [1b]/[1b] ₀				76%	

b) Yield of **9a/b**



[9b] _{Stock} = 13.85 mM	μmol added	Average peak area, S	DF	Normalized peak area, S _N	Confidence interval, P 0.95
+ 0.00 ml	0.00	37030	1.0	37030	± 3710
+ 0.10 ml	1.38	138630	1.4	194081	± 2433
+ 0.25 ml	3.46	218210	2.0	436419	± 2471
+ 0.50 ml	6.92	277016	3.0	831048	± 20927
Linear regression equation				S _N (9b) = 114837 × [9b] + 36758	
Obtained concentration, [9b]				If S _N (9b) = 0, then [9b] = $\frac{36758}{114837} \times \frac{10}{0.5 \text{ ml}} = 6.4 \text{ mM}$	
Initial concentration [1b] ₀				99.3 mM	
Yield 9b , [9b]/[1b] ₀				6.5%	
Obtained concentration, [9a]				If S _N (9a) = 0, then [9a] = $\frac{18562}{114837} \times \frac{10}{0.5 \text{ ml}} = 0.32 \text{ mM}$	
Yield 9a , [9a]/[1b] ₀				3.3%	



351 mg of hyponitrite **2a** (2 mmol, 2 eq) were added to 1 mmol of **1b** (1 eq) in 10 ml of dry degassed MeCN under nitrogen atmosphere. The vessel was tightly closed, wrapped in foil to cover the reaction mixture from the light and placed in a thermostat. After, reaction vessel was

opened with caution, dried in *vacuo* at RT. Crude material was dissolved in 50 ml of *i*PrOH for further GC-FID analysis (Fig. S38).

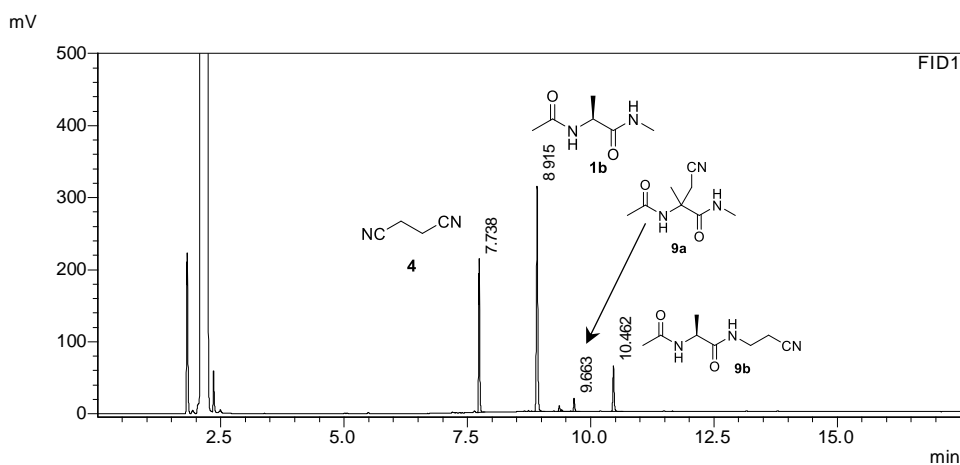


Fig. S38. GC-FID spectra of the oxidative stress reaction of **1b** with 2 eq **2a** at 23 °C.

Table S28. Oxidative stress of **1b** with 2 eq of **2a** at 23 °C.

1. Recovery of **1b**

a. Addition method

[1b] _{Stock} = 9.24 mM	μmol added	Average peak area, S	DF	Normalized peak area, S _N	Confidence interval, P 0.95
+ 0.00 ml	0.00	560613	1.0	560613	-
+ 1.00 ml	9.24	453046	2.0	906092	-
Obtained concentration, [1b]			74.72 mM		
Initial concentration [1b] ₀			100.7 mM		
Recovery 1b , [1b]/[1b] ₀			74.2 %		

b. Direct proportion

Solution	Volume taken, ml	Peak of 1b detected, S
[1b] _{Stock} = 8.653 mM	1.00	340893
[1b] = ??		560613
From direct proportion, n _{reaction} (1b) = 14.23 μmol × 50 => C _{reaction} (1b) = 71.15 mM		
Initial concentration [1b] ₀		100.7 mM
Recovery 1b , [1b]/[1b] ₀		70.7%

2) Yield of cyanomethylation adducts **9a/b**

[9b] _{Stock} = 5.52 mM	μmol added	Average peak area, S	DF	Normalized peak area, S _N	Confidence interval, P 0.95
+ 0.00 ml	0.00	107731	1.0	107731	-
+ 1.00 ml	5.52	191473	2.0	906092	-
Obtained concentration, [9b]			10.82 mM		
Initial concentration [1b] ₀			100.7 mM		

Yield 9b, [9b]/[1b] ₀	10.9 %
Peak area(9a) = 47168 => Yield 9a, [9a]/[1b] ₀	4.5%

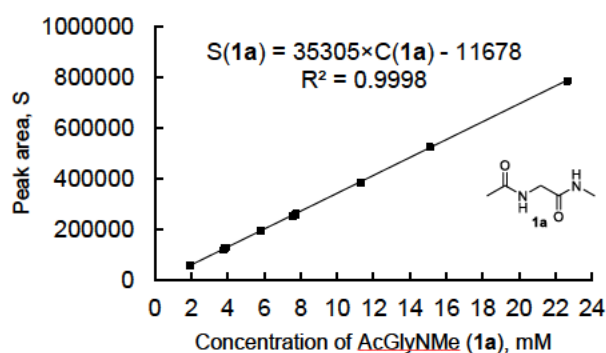
2.6.4. Oxidation Stress Reaction of Ac-AA-NMe (1d-g) and Ac-AA-OMe (14a-c)

2.6.4.1. Matrix effect of solvents during GC-FID analysis

The matrix effect from the presence of MeCN and DMSO in a solution was tested before any quantitative measurements. First, calibration curve for AcGlyNMe (1a) in HPLC grade MeOH is the result of two independent measurements (Table S29).

Table S29. Checking the possible matrix effect during GC-FID analysis.

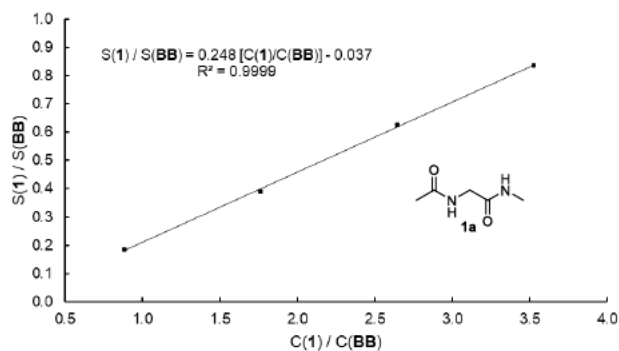
a) Calibration curve for AcGlyNMe (1a) in HPLC MeOH



[1a], mM	Peak area, S
1.93	59144
-	119140
3.86	127801
5.79	192073
-	251173
7.72	260711
-	384156
-	525041
-	786508
S(1a)=35305×[1a] - 11678, R² = 0.9998	

Calibrated solution of AcGlyNMe (1a):	
129.0 mg in 10 ml of dry MeCN	73.8 mg / 66.4 mg in 5 ml of dry DMSO
C ₀ ^{MeCN} (1a) = 9.92 mM	C ₀ ^{DMSO} (1a) = 11.35 mM / 10.22 mM
Obtained solutions were diluted with HPLC MeOH up to 10 times	
S _{av} ^{MeCN} (1a) = 349016	S _{av} ^{DMSO} (1a) = 340709 / 302631
S(1a) = 35305 × C(1a) - 11678, R² = 0.9998	
C ^{MeCN} (1a) = 10.22 mM	C ^{DMSO} (1a) = 9.98 mM / 8.95 mM
Δω = +3%	Δω = -12% / -12%

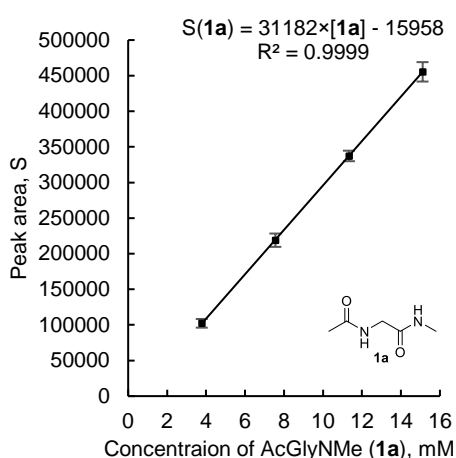
b) Calibration curve for AcGlyNMe (1a) with Benzyl Benzoate (BB) in HPLC MeOH



S(1a) / S(BB)	[1a] / [BB]
0.186	0.88
0.389	1.76
0.624	2.65
0.836	3.53
S(1a)/S(BB) = 0.248 × ([1a]/[BB]) - 0.037, R² = 0.9999	

Calibrated solution of AcGlyNMe (1a):	
129.0 mg in 10 ml of dry MeCN	66.4 mg in 5 ml of dry DMSO
$C_0^{\text{MeCN}}(\mathbf{1a}) = 9.92 \text{ mM}$	$C_0^{\text{DMSO}}(\mathbf{1a}) = 10.22 \text{ mM}$
Obtained solutions were diluted with HPLC MeOH up to 10 times	
1.0 ml of AcGlyNMe (1a) solution + 0.25 ml of BB solution in HPLC MeOH, $C(\mathbf{BB}) = 13.99 \text{ mM}$	
$S^{\text{MeCN}}(\mathbf{1a}) = 264515$, $S^{\text{MeCN}}(\mathbf{BB}) = 394265$	$S^{\text{DMSO}}(\mathbf{1a}) = 241875$, $S^{\text{DMSO}}(\mathbf{BB}) = 390348$
$S(\mathbf{1a})/S(\mathbf{BB}) = 0.248 \times [C(\mathbf{1a})/C(\mathbf{BB})] - 0.037$, $R^2 = 0.9999$	
$C^{\text{MeCN}}(\mathbf{1a}) = 9.98 \text{ mM}$	$C^{\text{DMSO}}(\mathbf{1a}) = 9.26 \text{ mM}$
$\Delta\omega = <1 \%$	$\Delta\omega = -9 \%$

c) Calibration curve for AcGlyNMe (**1a**) in HPLC MeOH/DMSO = 9/1 mixture



[1a], mM	Peak area, S			Average peak area, S		Error
	I	II	III			
3.78	101107	105074	100602	102261		± 6080
7.55	223265	217433	216186	218961		± 9381
11.33	340548	334769	336458	337258		± 7377
15.11	461426	450678	454092	455399		± 13634
Obtained linear equation				$S(\mathbf{1a}) = 31182 \times [\mathbf{1a}] - 15958$, $R^2 = 1.000$		
Substrate	Peak area, S			Average peak area, S	Concentration, mM	$\Delta\omega$, %
	I	II	III			
	340661	345526	335939	340709	11.44	<1 %

Internal standard, benzyl benzoate (**BB**), as an alternative approach, was also tested, but with no success. Whereas influence of MeCN is still neglectable and can be overcome with better sample preparation in future, results clearly indicate the influence of DMSO on peak area. Since the reaction was diluted up to 10 times, the final solution consists of 9 to 1 MeOH/DMSO mixture. Calibrated solution of AcGlyNMe (**1a**) was prepared in MeOH/DMSO = 9/1 solution, which lead to precise quantitative analysis. In future, calibration curves for DMSO containing mixtures were built using 9/1 MeOH/DMSO solution.

2.6.4.2. Blank experiment with AcGlyNMe (**1a**)

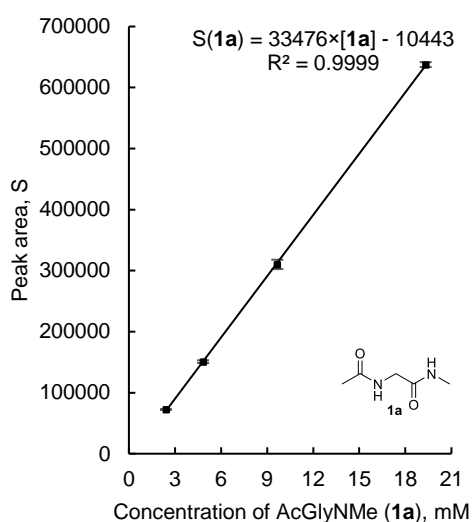
The possibility of dipeptide model degradation was tested. 129 mg (0.9923 mmol) of AcGlyNMe (**1a**) was dissolved in 10 ml of dry degassed MeCN under nitrogen atmosphere, giving final concentration $C[\text{AcGlyNMe}(\mathbf{1a})] = 0.0992 \text{ M}$. Reaction vessel was tightly closed, wrapped in foil and placed in cryostat at 23 °C for 14 days. After, 84.4 mg of Benzyl benzoate (**BB**) was added as an internal standard. GC-FID shows 98% recovery of AcGlyNMe (**1a**), what shows no degradation processes during oxidative stress reaction.

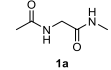
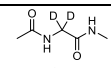
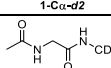
2.6.4.3. Oxidation stress reaction of Ac-AA-NMe **1a-g**

1 mmol of **2a** (1 eq) was added to 1 mmol of Ac-AA-NMe **1a-f** (1 eq) in 10 ml of dry degassed MeCN-*d*₃ under nitrogen atmosphere. The vessel was tightly closed, wrapped in foil to cover the reaction mixture from the light and placed in a thermostat at 23 °C. After, reaction vessel was opened with caution, solution was diluted up to 10 times using HPLC grade MeOH for further GC-FID analysis. Yields of the oxidation products were obtained using absolute calibration curves (Table S30-35). After, all the organic phases were combined and concentrated in *vacuo*. The crude material was separated on a silica column (DCM/MeOH = 10/1) for further NMR analysis. Reaction in DMSO-*d*₆ were scaled down by factor of 2.

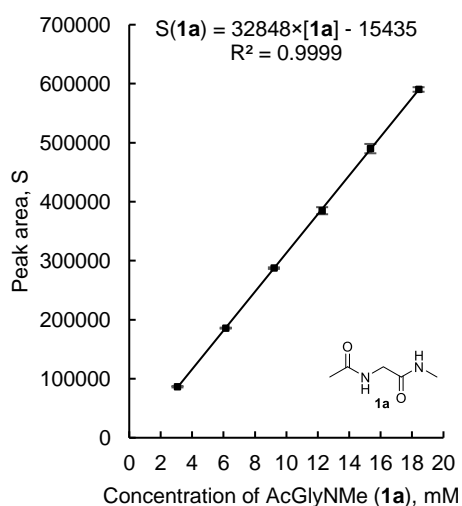
Table S30. Oxidative stress of AcGlyNMe (**1a**) and its deuterated derivatives with **2a**.

a) In MeCN-*d*₃



[1a], mM	Peak area, S			Average peak area, S	Error	
	I	II	III			
2.42	72120	72685	72305	72370	± 715	
4.83	149905	151712	150848	150822	± 2244	
9.66	306766	311275	312672	310238	± 7663	
19.32	636327	637204	639442	637658	± 3988	
Obtained linear equation			S(1a) = 33476 × [1a] - 10443, R ² = 0.9999			
Substrate	Peak area, S			Average peak area, S	Obtained [1a], mM	Turnover, %
	I	II	III			
 1a	158503	159538	160214	159418	50.7	50
 1-C α - <i>d</i> ₂	248717	255325	257114	253719	77.7	23
 1-NMe- <i>d</i> ₃	160955	162665	163127	162249	50.4	50

b) In DMSO-*d*₆



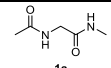
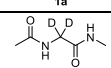
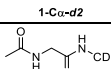
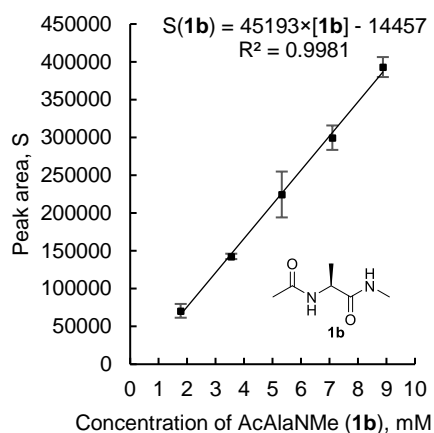
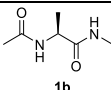
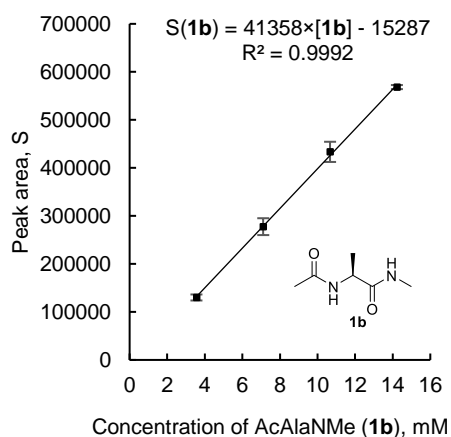
[1a], mM	Peak area, S			Average peak area, S	Error	
	I	II	III			
3.1	85930	86597	86841	86456	± 1171	
6.1	-	185716	185842	185779	± 794	
9.2	288036	287052	287211	287433	± 1311	
12.3	387512	383131	383576	384740	± 5986	
15.3	490553	486545	492852	489983	± 7924	
18.4	589031	589628	591968	590209	± 3854	
Obtained linear equation			S(1a) = 32848 × [1a] - 15435, R ² = 0.9999			
Substrate	Peak area, S			Average peak area, S	Obtained [1a], mM	Turnover, %
	I	II	III			
 1a	119587	118105	117737	118476	40.8	61
 1-C α - <i>d</i> ₂	189740	190949	190266	190318	61.7	39
 1-NMe- <i>d</i> ₃	108458	111395	111808	110554	37.5	63

Table S31. Oxidative stress of AcAlaNMe (**1b**) with DTBHN (**2a**).a) In MeCN-*d*3

[1b], mM	Peak area, S		Average peak area, S	Error		
	I	II				
1.77	71356	69921	70639	± 9117		
3.55	142921	142361	142641	± 3558		
5.32	226895	222122	224509	± 30323		
7.10	298383	300929	299656	± 16175		
8.87	394101	392021	393061	± 13214		
Obtained linear equation			$S(\mathbf{1b}) = 45193 \times [\mathbf{1b}] - 14457, R^2 = 0.9981$			
Substrate	Peak area, S			Average peak area, S	Obtained [1b], mM	Turnover, %
	I	II	III			
	316966	318973	318137	317970	73.6	27

b) In DMSO-*d*6

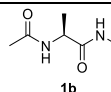
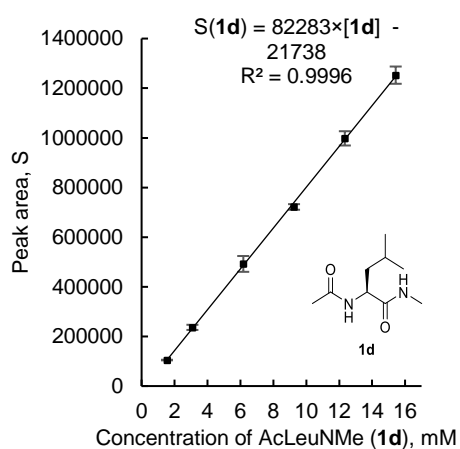
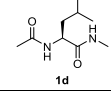
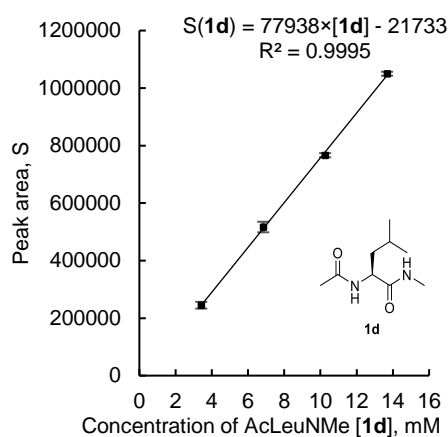
[1b], mM	Peak area, S			Average peak area, S	Error	
	I	II	III			
3.56	132760	127729	129756	130082	± 6284	
7.11	285706	274274	272774	277585	± 17560	
10.67	441079	424297	434734	433370	± 21037	
14.22	569241	569368	566356	568322	± 4229	
Obtained linear equation			$S(\mathbf{1b}) = 41358 \times C(\mathbf{1b}) - 15287, R^2 = 0.9992$			
Substrate	Peak area, S			Average peak area, S	Obtained [1b], mM	Turnover, %
	I	II	III			
	258833	268080	258068	261660	67.0	33

Table S32. Oxidative stress of AcLeuNMe (**1d**) with DTBHN (**2a**).a) In MeCN-*d*3

[1d], mM	Peak area, S			Average peak area, S	Error	
	I	II	III			
1.54	105003	105027	104221	104750	± 1138	
3.09	237748	239842	231793	236461	± 10367	
6.17	502725	495709	477832	492089	± 31865	
9.26	716481	723376	725013	721623	± 11241	
12.34	985174	1000837	1007761	997924	± 28728	
15.43	1259445	1236459	1261841	1252582	± 34791	
Obtained linear equation			$S(\mathbf{1d}) = 82283 \times [\mathbf{1d}] - 21738, R^2 = 0.9996$			
Substrate	Peak area, S			Average peak area, S	Concentration, mM	Turnover, %
	I	II	III			
	561561	560141	552236	557979	70.4	30

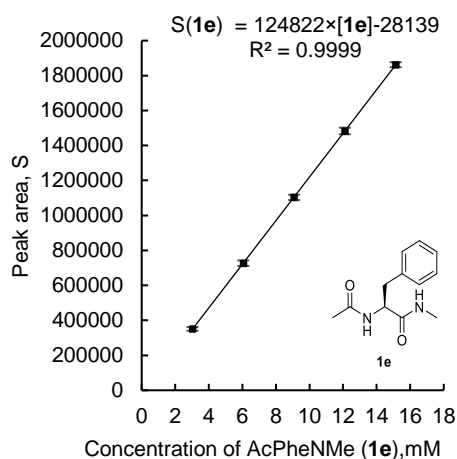
b) In DMSO-*d*₆



[1d], mM	Peak area, S			Average peak area, S	Error	
	I	II	III			
3.42	250226	242536	241718	244827	± 11653	
6.84	511223	513871	525111	516735	± 18306	
10.26	769938	765107	764834	766626	± 7128	
13.68	1050718	1052112	1046733	1049854	± 6930	
Obtained linear equation			$S(1d) = 77938 \times [1d] - 21733, R^2 = 0.9995$			
Substrate	Peak area, S			Average peak area, S	Obtained [1d], mM	Turnover, %
	I	II	III			
	510387	506759	492192	503112	67.3	34

Table S33. Oxidative stress of AcPheNMe (1e) with DTBHN (2a).

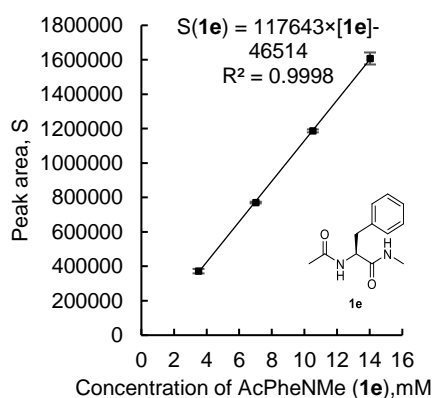
a) In MeCN-*d*₃^a



[1e], mM	Peak area, S			Average peak area, S	Error	
	I	II	III			
3.03	348356	349005	356083	351148	± 10641	
6.05	727639	720502	733306	727149	± 15929	
9.08	1103905	1096920	1109265	1103363	± 15368	
12.11	1487568	1474474	1487736	1483259	± 18890	
15.14	1857165	1861720	1868456	1862447	± 14102	
Obtained linear equation			$S(1e) = 124822 \times [1e] - 28139, R^2 = 0.9999$			
Substrate	Peak area, S			Average peak area, S	Obtained [1e], mM	Turnover, %
	I	II	III			
	1073622	1090075	1068870	1077522	88.6	12

^a Heterogeneous reaction

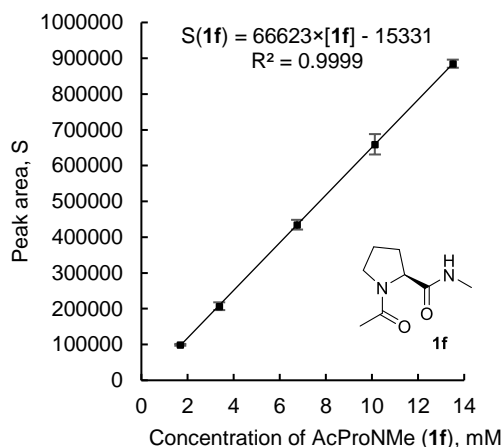
b) In DMSO-*d*₆



[1e], mM	Peak area, S			Average peak area, S	Error	
	I	II	III			
3.50	376745	372873	366333	371984	± 13065	
7.01	769647	772594	769074	770438	± 4689	
10.51	1184069	1185984	1190750	1186934	± 8541	
14.02	1601713	1623445	1597144	1607434	± 34888	
Obtained linear equation			$S(1e) = 117643 \times [1e] - 46514, R^2 = 0.9998$			
Substrate	Peak area, S			Average peak area, S	Obtained [1e], mM	Turnover, %
	I	II	III			
	706245	702727	697701	702224	63.6	37

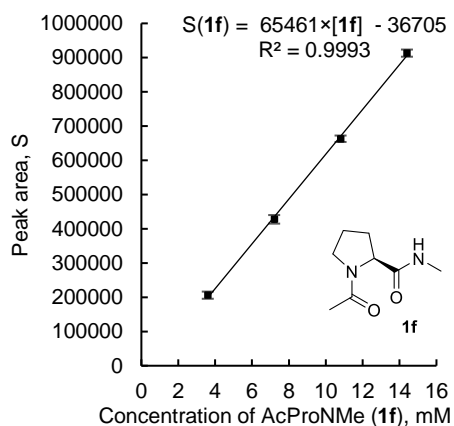
Table S34. Oxidative stress of AcProNMe (**1f**) with DTBHN (**2a**).

a) In MeCN-*d*3



[1f], mM	Peak area, S			Average peak area, S	Error	
	I	II	III			
1.69	101115	99776	99169	100020	± 2472	
3.38	215472	213261	207059	211931	± 10828	
6.75	439781	428870	434870	434507	± 13566	
10.13	678511	657874	659519	665301	± 28474	
13.51	876044	877899	884711	879551	± 11330	
Obtained linear equation			S(1f) = 66623 × [1f] - 15331, R² = 0.9999			
Substrate	Peak area, S			Average peak area, S	Obtained [1f], mM	Turnover, %
	I	II	III			
	317060	322083	308859	316001	49.7	52

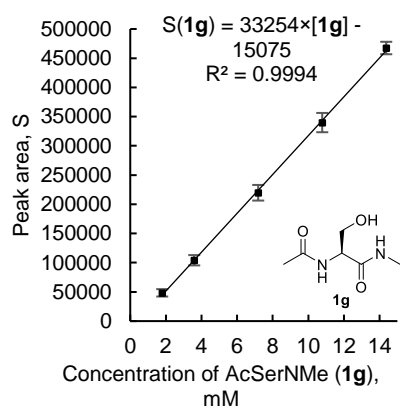
b) In DMSO-*d*6



[1f], mM	Peak area, S			Average peak area, S	Error	
	I	II	III			
3.60	202227	210596	205345	206056	± 10500	
7.20	433042	426632	423103	427592	± 12509	
10.80	658742	664461	665871	663025	± 9373	
14.40	917972	910473	910899	913115	± 10457	
Obtained linear equation			S(1f) = 65461 × [1f] - 36705, R² = 0.9993			
Substrate	Peak area, S			Average peak area, S	Obtained [1f], mM	Turnover, %
	I	II	III			
	293357	296598	283973	291309	50.1	51

Table S35. Oxidative stress of AcSerNMe (**2g**) with DTBHN (**2a**).

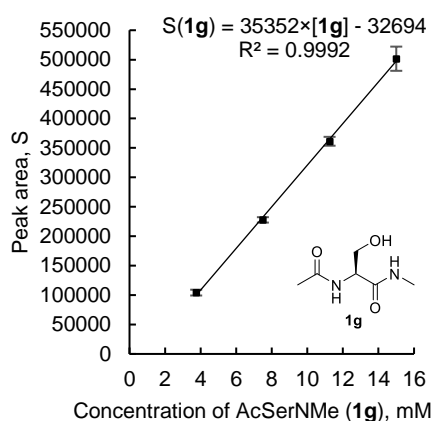
a) In MeCN-*d*3^a



[1g], mM	Peak area, S			Average peak area, S	Error	
	I	II	III			
1.80	45757	48542	50842	48380	± 6322	
3.59	100415	104606	107471	104164	± 8810	
7.19	213580	221709	223778	219689	± 13383	
10.78	332119	343448	343805	339791	± 16500	
14.38	466819	463463	471983	467422	± 10655	
Obtained linear equation			S(1g) = 33254 × [1g] - 15075, R² = 0.9994			
Substrate	Peak area, S			Average peak area, S	Obtained [1g], mM	Turnover, %
	I	II	III			
	247006	252348	235318	244891	78.2	23

^a Heterogeneous reaction

a) In DMSO-*d*₆



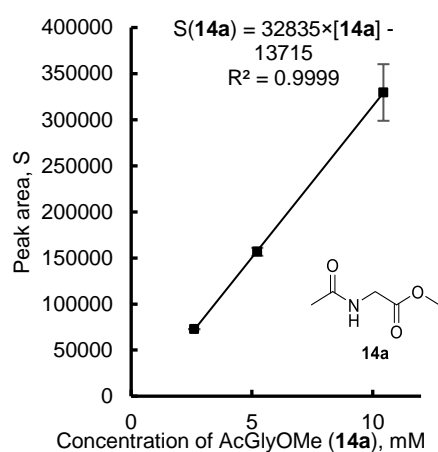
[1g], mM	Peak area, S			Average peak area, S	Error	
	I	II	III			
3.75	104716	105921	102027	104221	± 4949	
7.5	229258	228346	225718	227774	± 4563	
11.25	359486	364830	359666	361327	± 7534	
15	496956	496690	511168	501605	± 20564	
Obtained linear equation			$S(1g) = 35352 \times [1g] - 32694, R^2 = 0.9992$			
Substrate	Peak area, S			Average peak area, S	Concentration, mM	Turnover, %
	I	II	III			
	206540	205708	195225	202491	66.5	35

2.6.4.4. Oxidation stress reaction of Ac-AA-OMe **14a-c**

1 mmol of DTBHN (**2a**, 1 eq) was added to 1 mmol of Ac-AA-OMe (1 eq) in 10 ml of dry degassed MeCN-*d*₃ under nitrogen atmosphere. The vessel was tightly closed, wrapped in foil to cover the reaction mixture from the light and placed in a thermostat at 23 °C. After, reaction vessel was opened with caution, solution was diluted up to 50 ml using HPLC grade MeOH for further GC-FID analysis. Yields of the oxidation products were obtained using absolute calibration curves (Table S36).

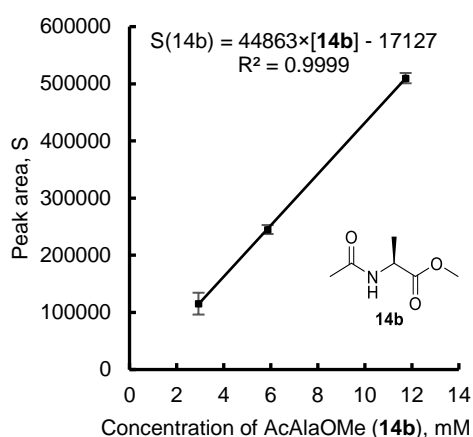
Table S36. Oxidative stress of Ac-AA-OMe (**2g**) with DTBHN (**2a**) in MeCN-*d*₃.

a) Oxidative stress of AcGlyOMe (**14a**)



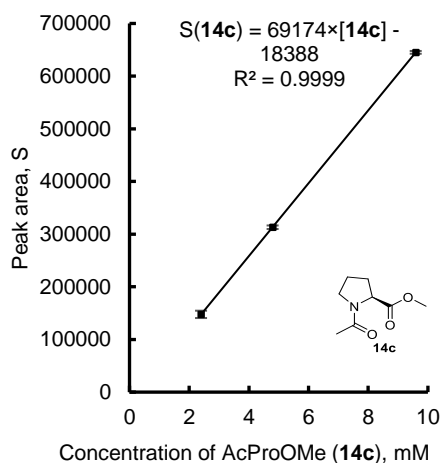
[14a], mM	Peak area, S		Average peak area, S	Error	
	I	II			
2.61	72714	72689	72702	± 159	
5.22	157029	156342	156686	± 4365	
10.44	327103	331935	329519	± 30698	
Obtained linear equation		$S(14a) = 32835 \times [14a] - 13715, R^2 = 0.9999$			
Substrate	Peak area, S		Average peak area, S	Obtained [14a], mM	Turnover, %
	I	II			
	170343	172239	171291	56.3	47.0

b) Oxidative stress of AcAlaOMe (**14b**)



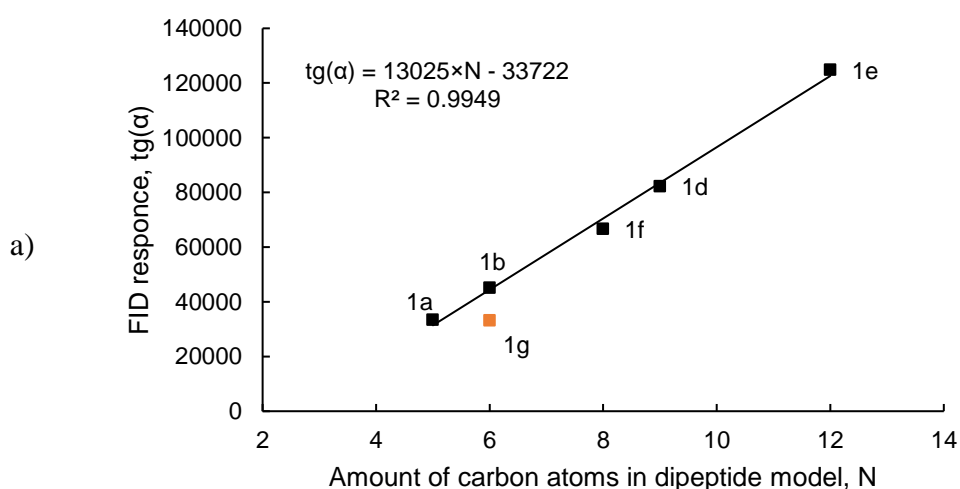
[14b], mM	Peak area, S		Average peak area, S	Error	
	I	II			
2.93	113815	116820	115318	± 19091	
5.87	245597	244361	244979	± 7852	
11.74	510575	509160	509868	± 8989	
Obtained linear equation			$S(14b) = 44863 \times [14b] - 17127, R^2 = 1.000$		
Substrate	Peak area, S		Average peak area, S	Concentration, mM	Turnover, %
	I	II			
14b	349474	348309	348892	81.6	19.9

c) Oxidative stress of AcProOMe (**14c**)



[14c], mM	Peak area, S		Average peak area, S	Error	
	I	II			
2.40	148187	147092	147640	± 6957	
4.80	312799	313328	313064	± 3361	
9.59	645325	644910	645118	± 2636	
Obtained linear equation			$S(14c) = 69174 \times [14c] - 18388, R^2 = 1.000$		
Substrate	Peak area, S		Average peak area, S	Obtained [14c], mM	Turnover, %
	I	II			
14c	319284	321783	321158	49.1	51.8

2.6.4.5. Response factors of GC-FID to number of carbons in the dipeptide models



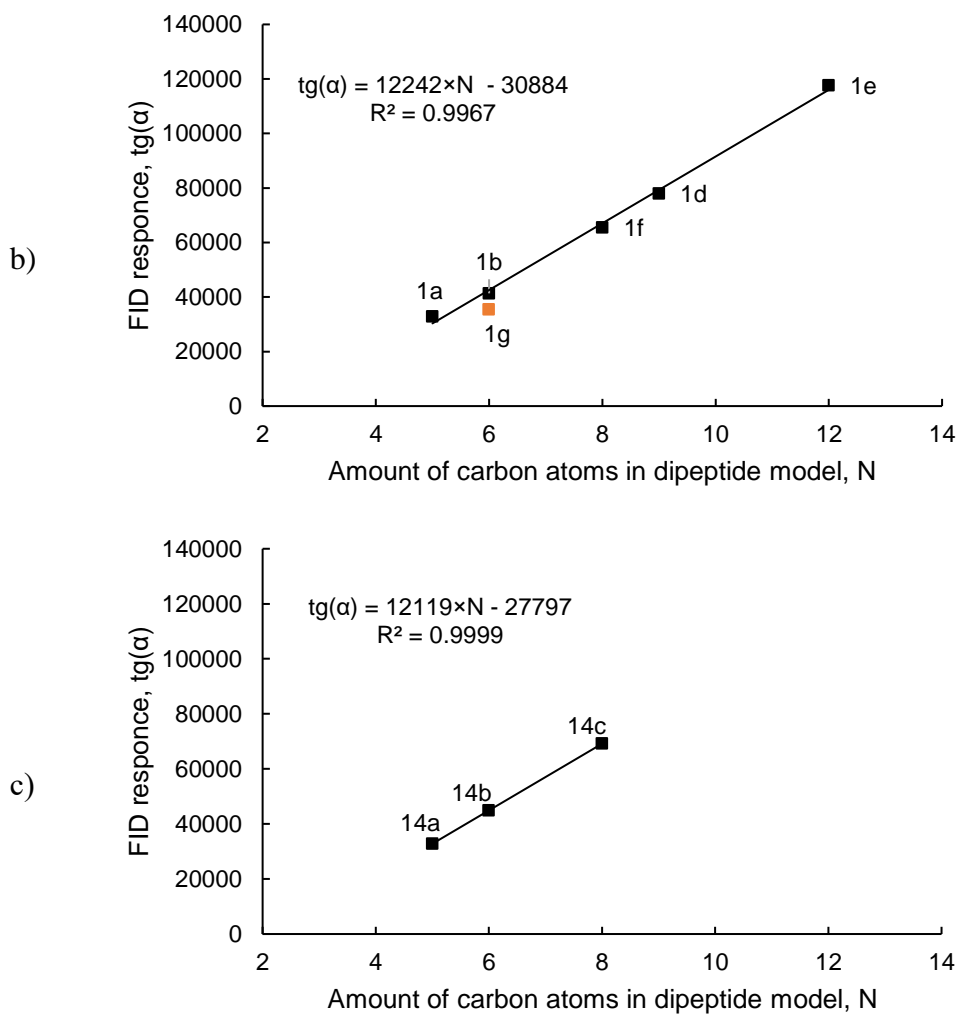


Fig. S39. Dependence of the slope of the calibration curve on the number of carbon atoms in *L*-Ac-AA-NMe **1a-g** in a) MeOH, b) MeOH/DMSO = 9/1 and c) *L*-Ac-AA-OMe **14a-c** in MeOH

GIC-FID shows linear correlation between the detector response and number of carbons in corresponding dipeptide model. This observation validates the previous results, showing the correctness of the obtained calibration curves (Fig. S39). The only exception is AcSerNMe (**1g**), due to partially oxidized carbon in the side chain C-O bond (orange data point).

2.6.5. Analytical Data of the Oxidative Stress Reactions

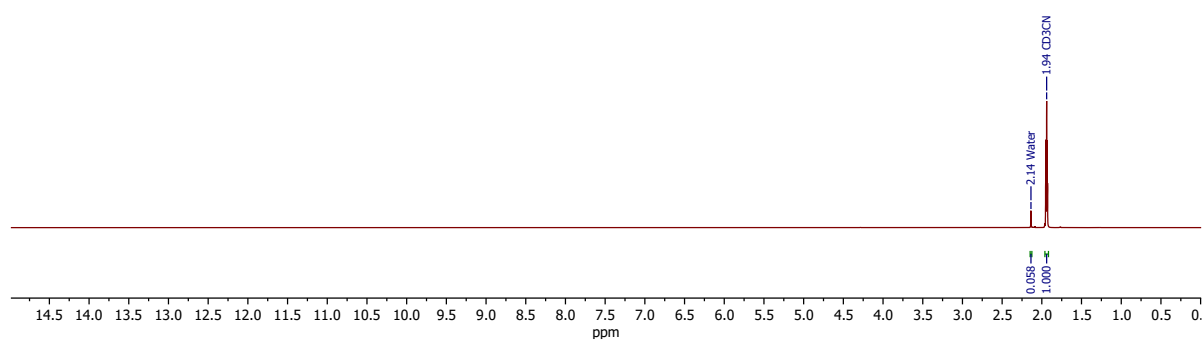


Fig. S40. ^1H NMR spectrum of $\text{MeCN-}d_3$, 400 MHz.

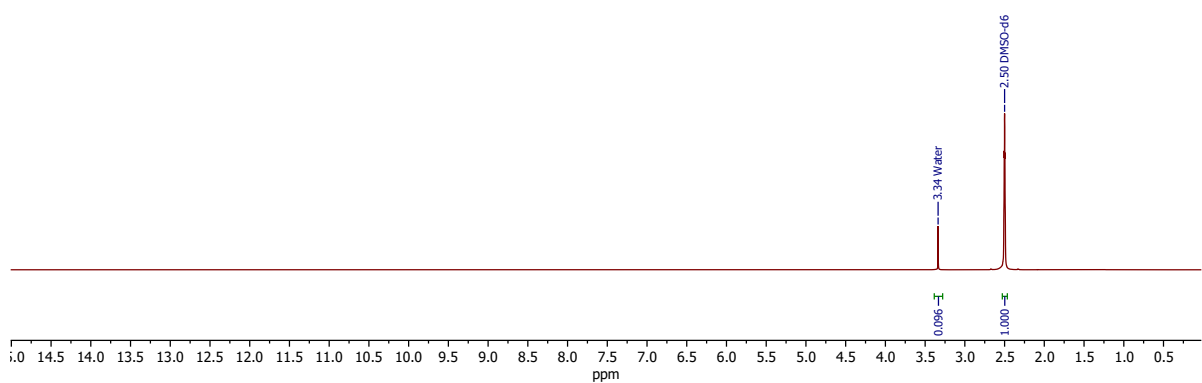


Fig. S41. ^1H NMR spectrum of $\text{DMSO-}d_6$, 400 MHz.

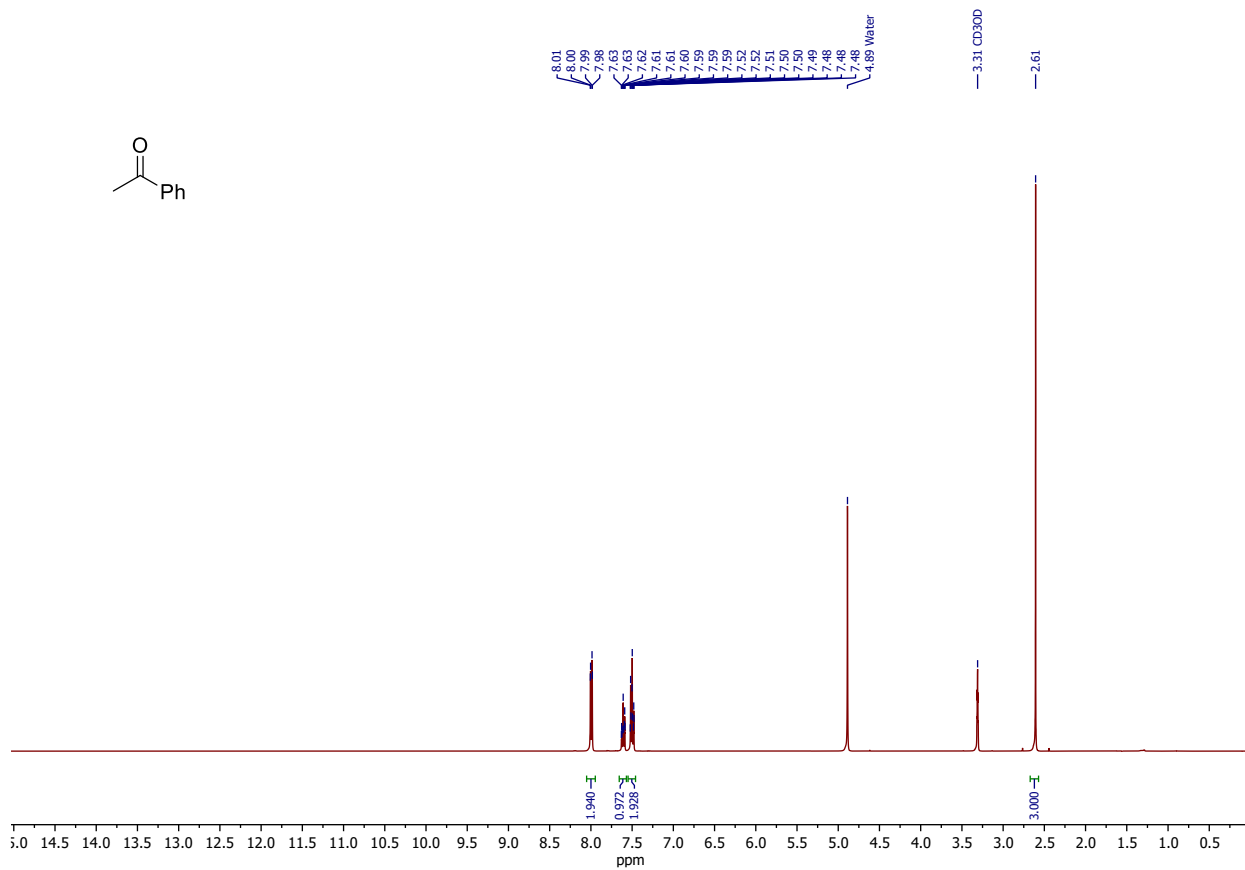


Fig. S44. ¹H NMR spectrum of acetophenone, MeOH-*d*₄, 400 MHz.

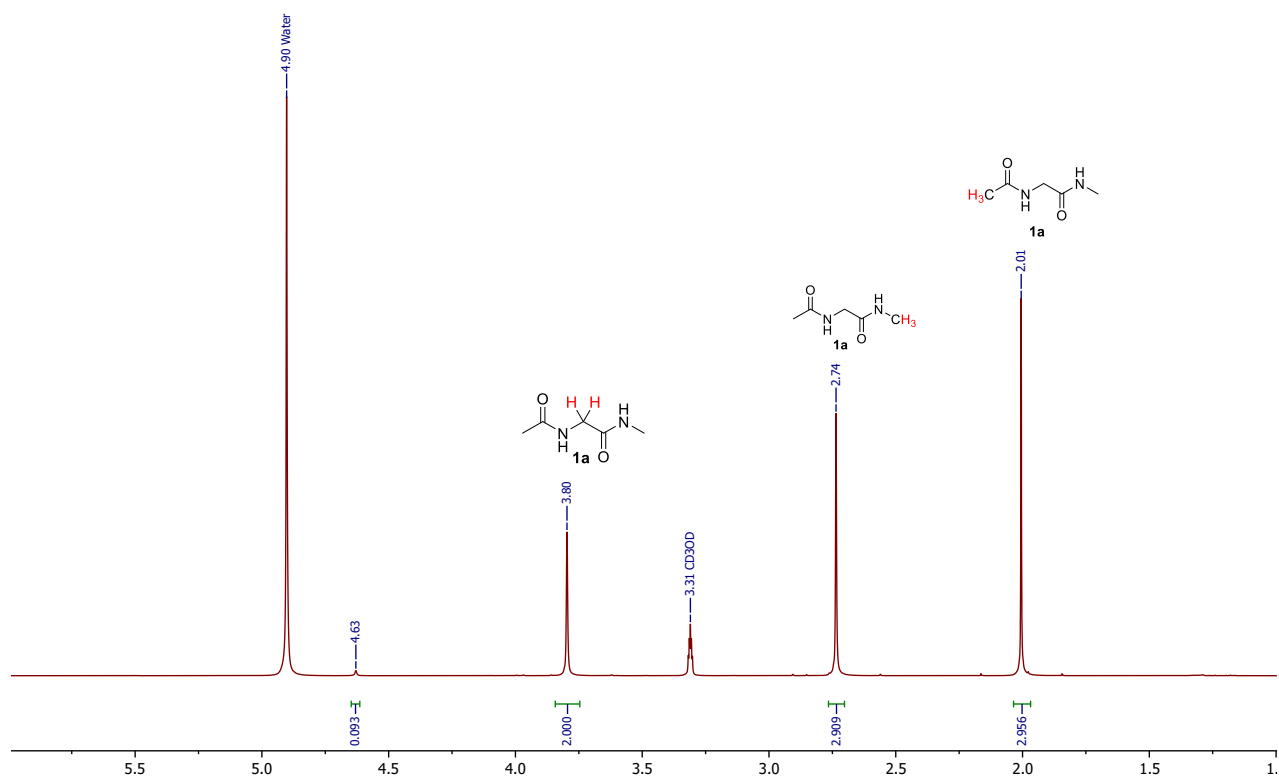


Fig. S45a. ¹H NMR spectrum of AcGlyNMe (1a), MeOH-*d*₄, 400 MHz.

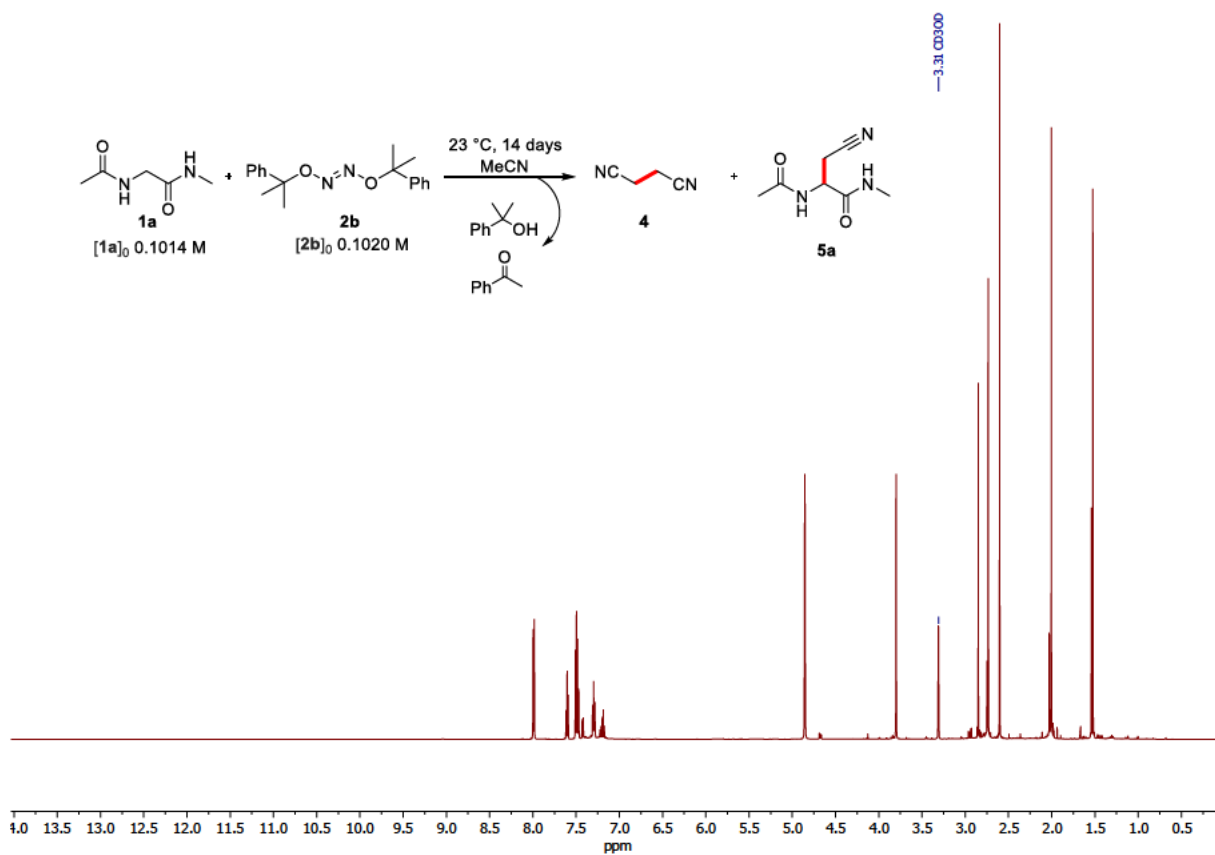


Fig. S45b. ¹H NMR spectrum of the oxidative stress reaction of **1a** with **2b**, MeOH-*d*₄, 600 MHz.

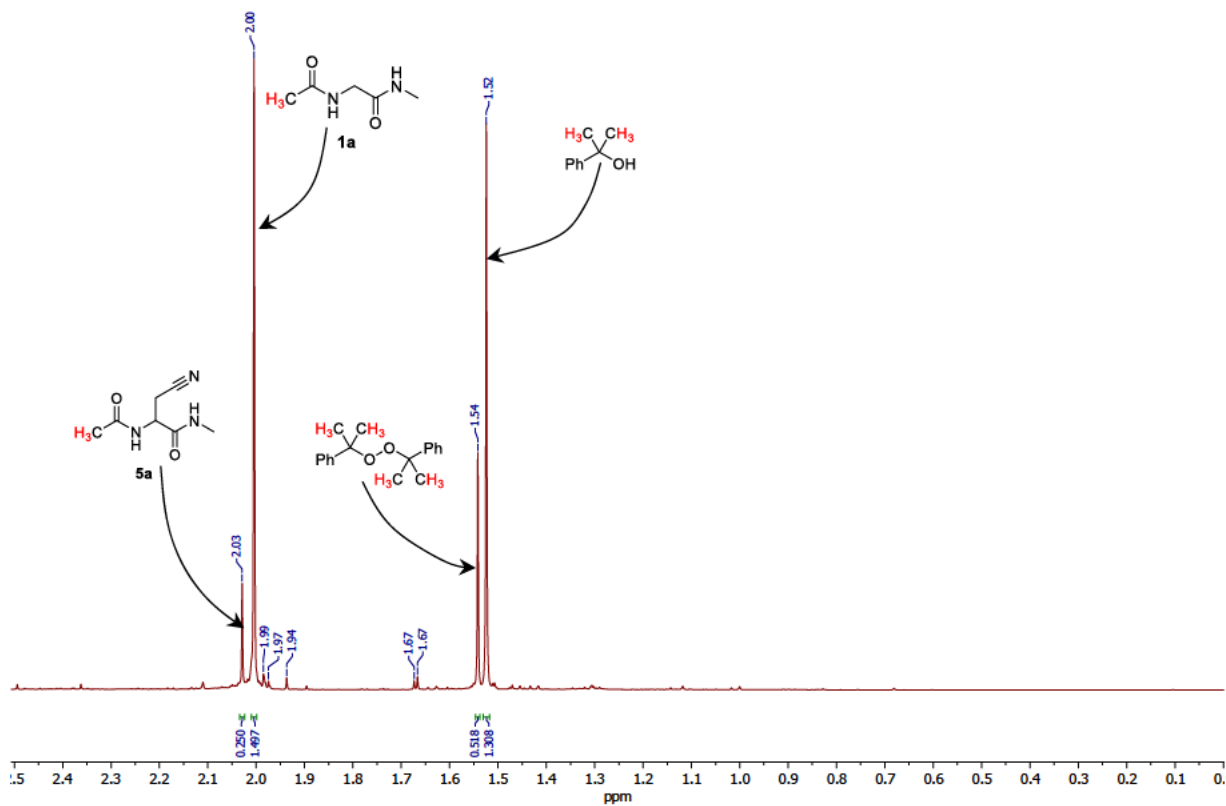


Fig. S45c. ¹H NMR spectrum of the oxidative stress reaction of **1a** with **2b**, MeOH-*d*₄, 600 MHz.

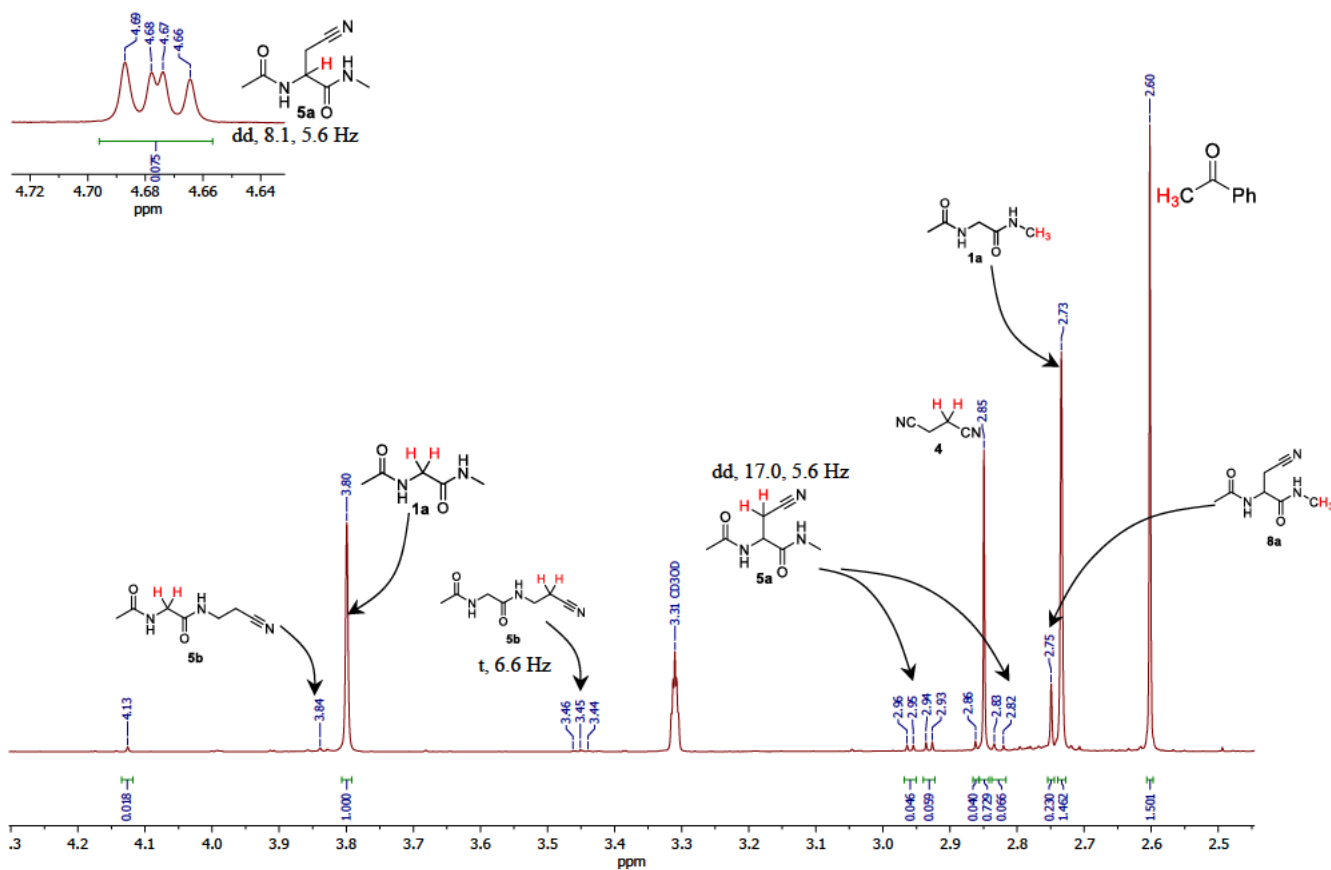


Fig. S45d. ^1H NMR spectrum of the oxidative stress reaction of **1a** with **2b**, $\text{MeOH}-d_4$, 600 MHz.

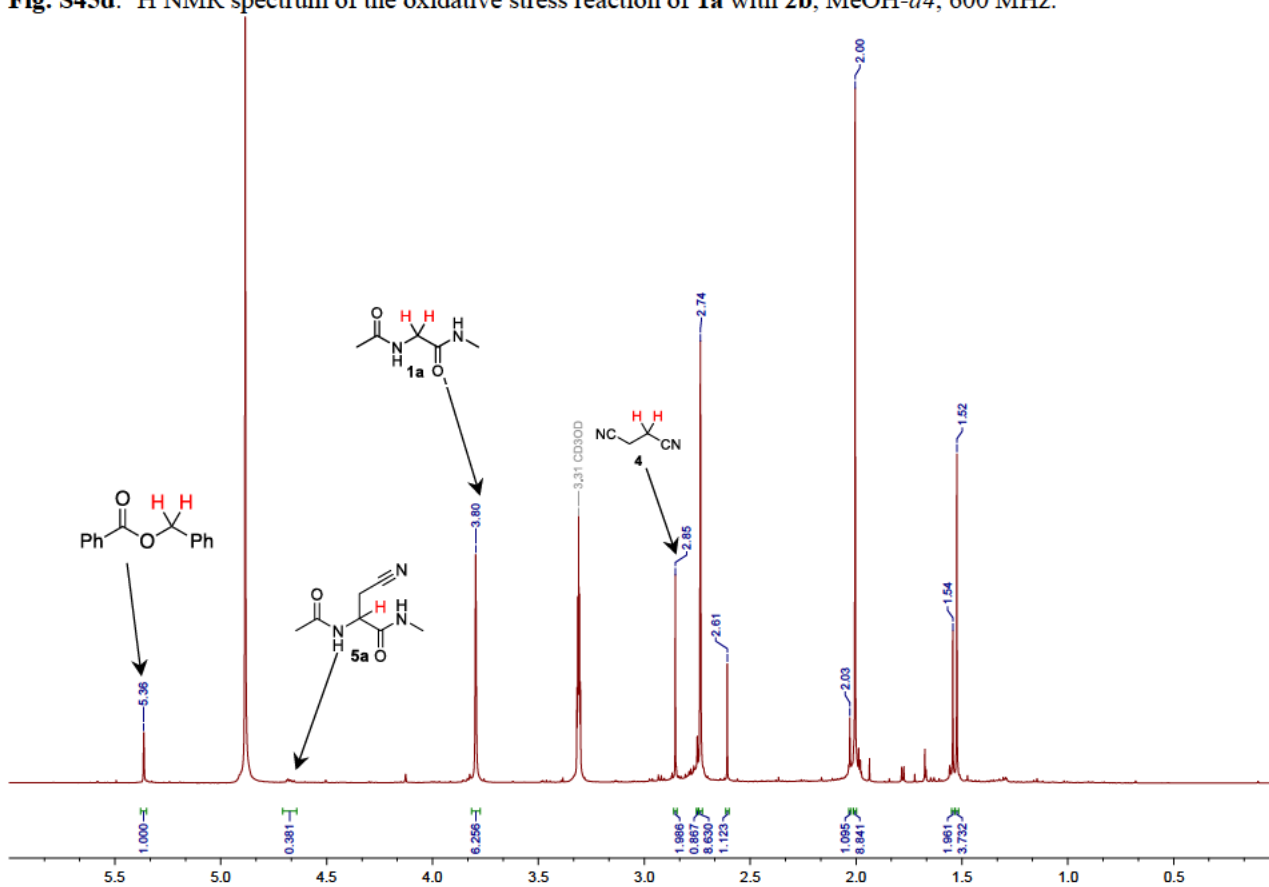


Fig. S45e. Quantitative ^1H NMR spectra of crude mixture after oxidative stress reaction of **1a** with **2b**, $\text{MeOH}-d_4$, 400 MHz.

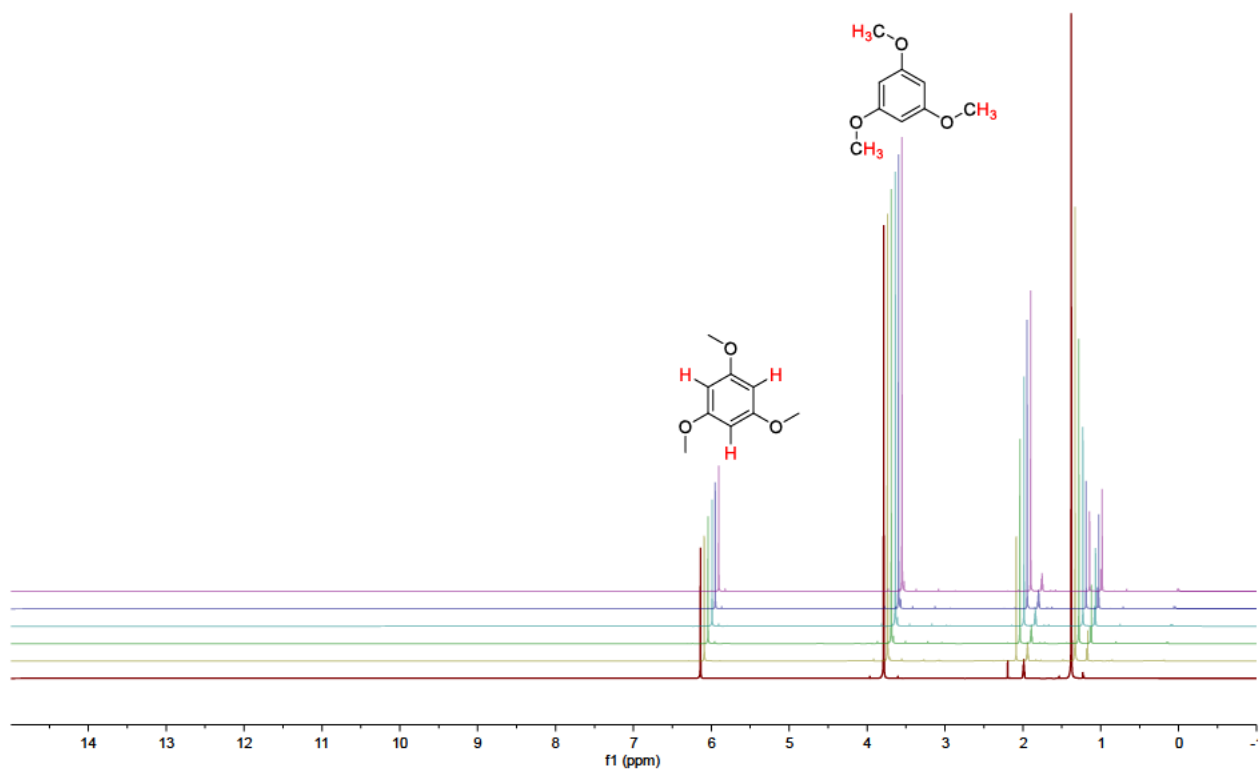


Fig. S46a. ^1H NMR spectrum of DTBHN (2a) decomposition at 65°C , $\text{MeCN-}d_3$, 400 MHz.

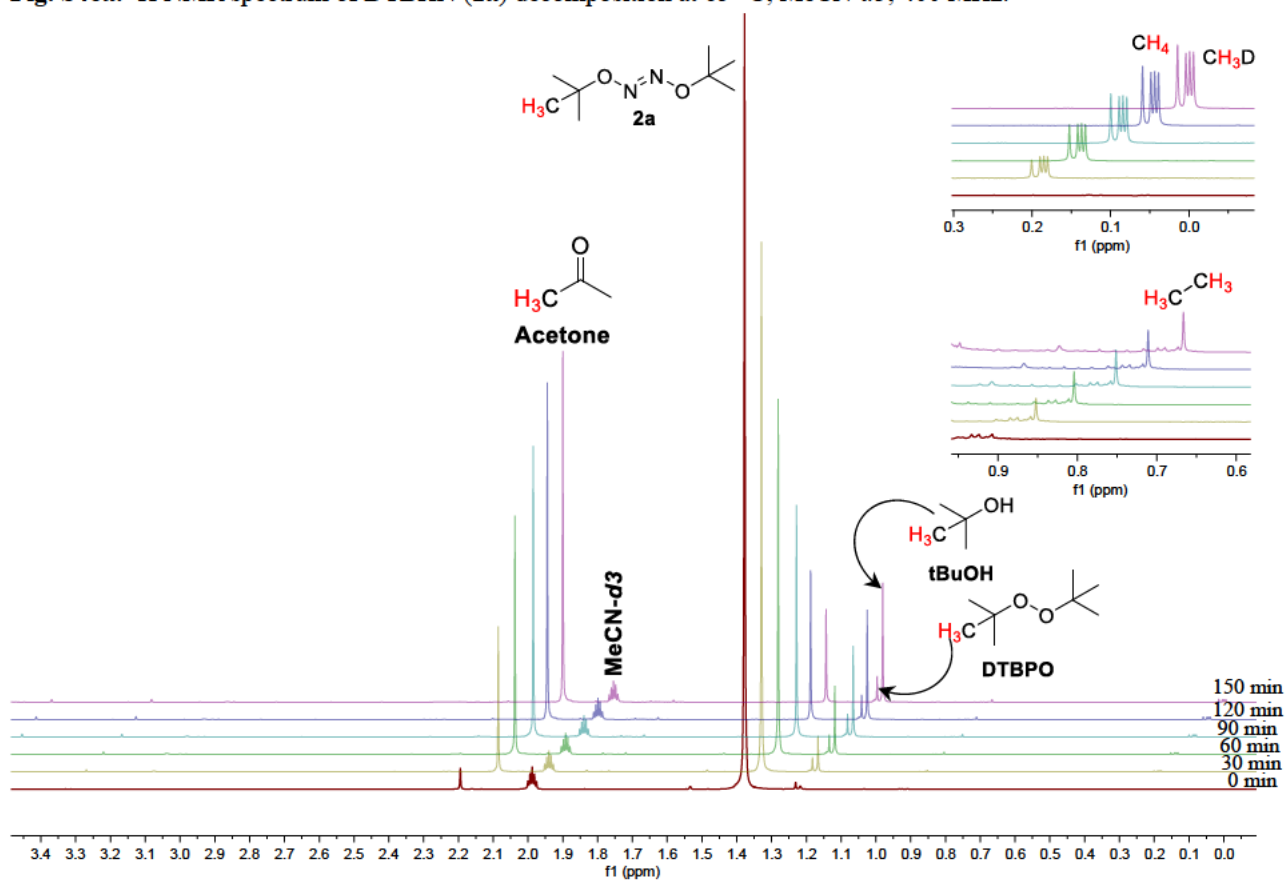


Fig. S46b. ^1H NMR spectrum of DTBHN (2a) decomposition at 65°C , $\text{MeCN-}d_3$, 400 MHz.

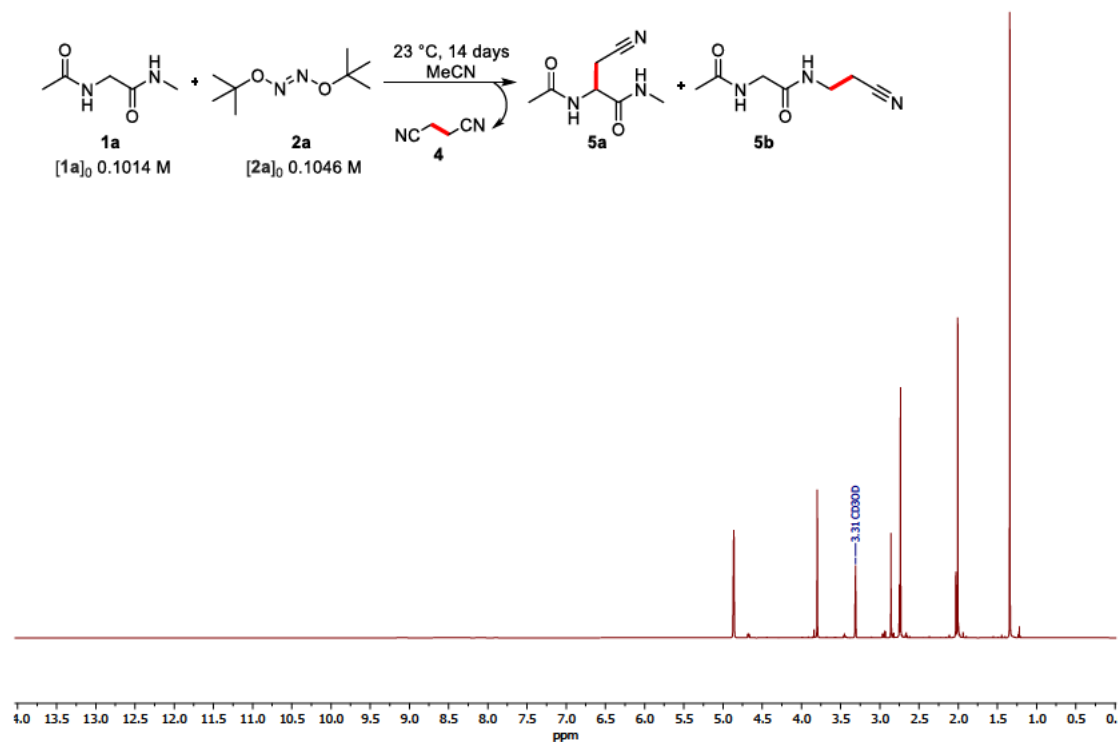


Fig. S47a. ¹H NMR spectrum of the oxidative stress reaction of **1a** with **2a**, MeOH-*d*₄, 600 MHz.

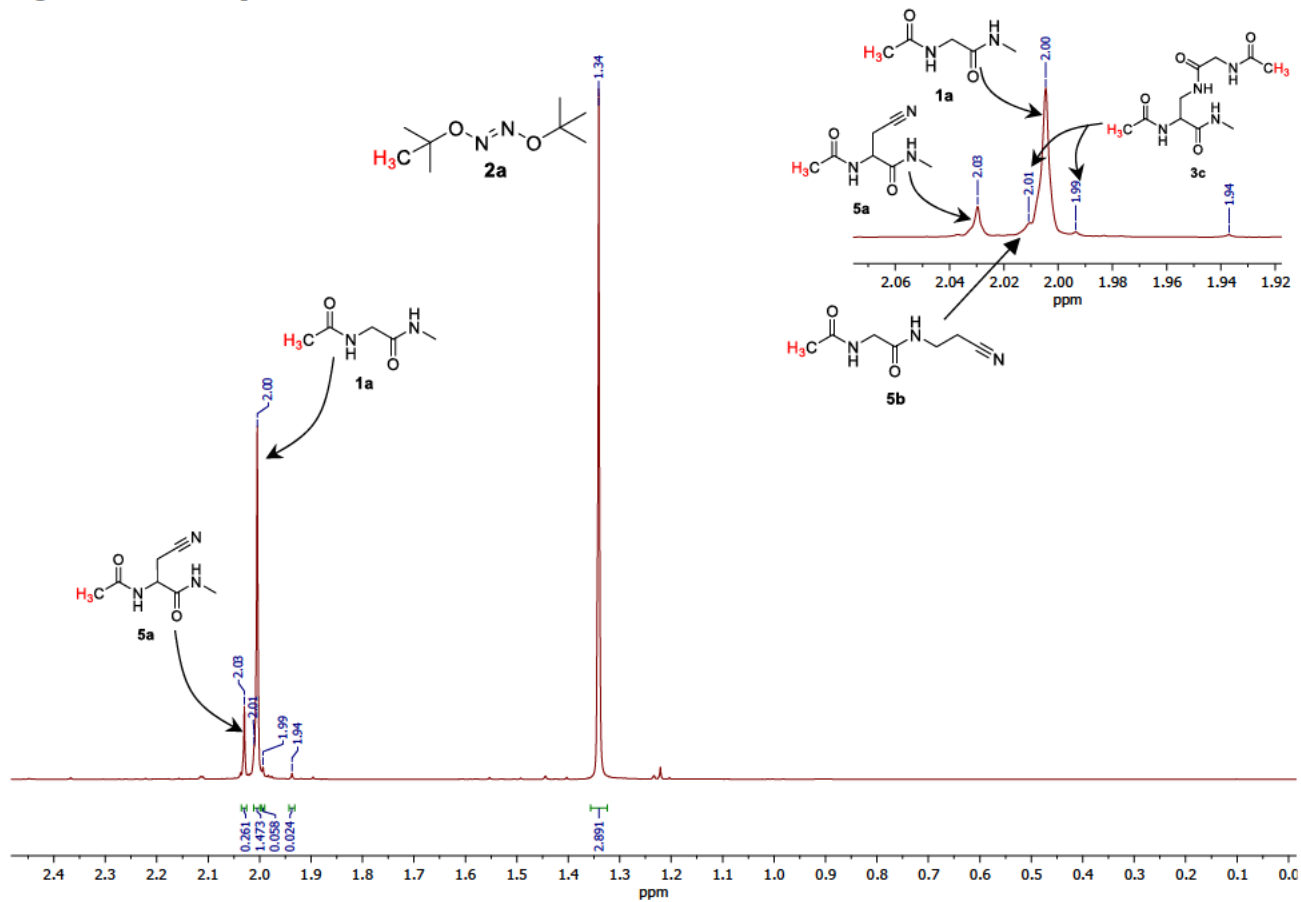


Fig. S47b. ¹H NMR spectrum of the oxidative stress reaction of **1a** with **2a**, MeOH-*d*₄, 600 MHz.

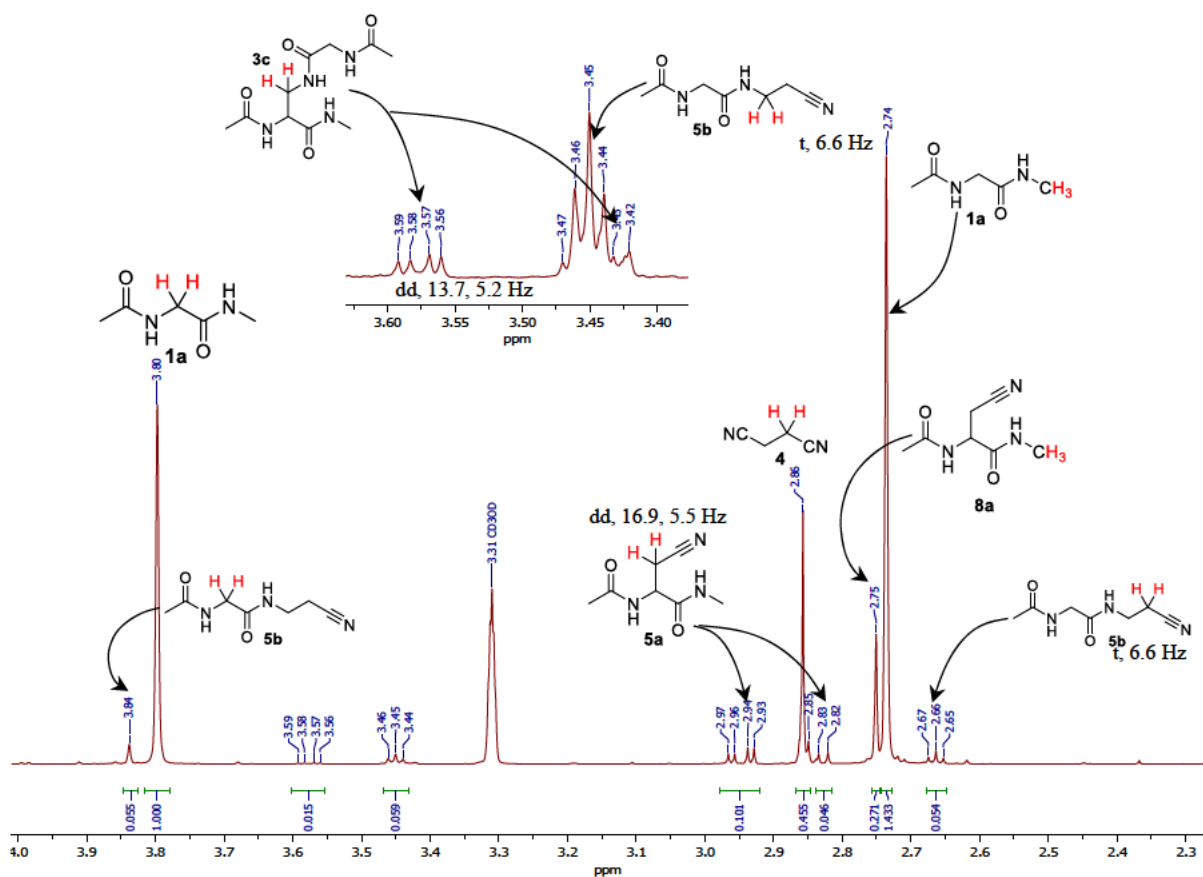


Fig. S47c. ^1H NMR spectrum of the oxidative stress reaction of **1a** with **2a**, $\text{MeOH-}d_4$, 600 MHz.

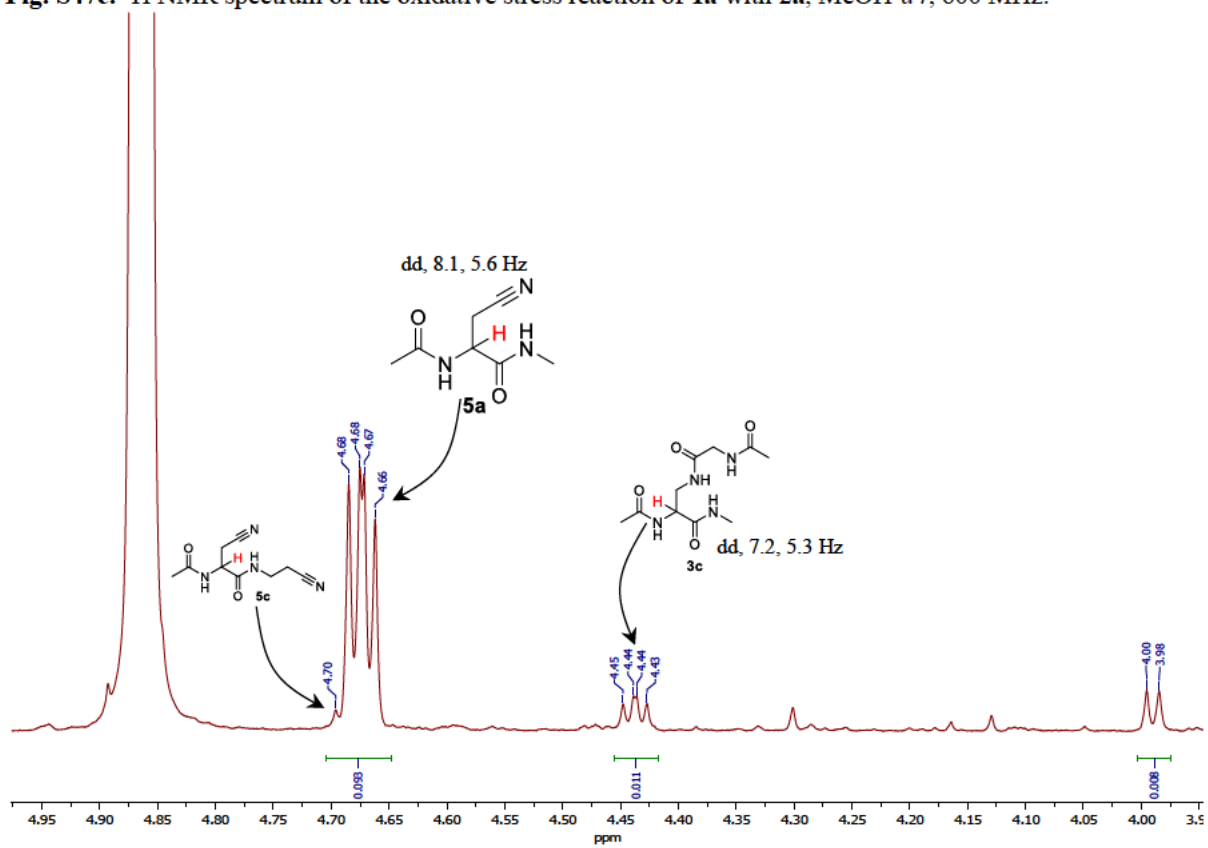


Fig. S47d. ^1H NMR spectrum of the oxidative stress reaction of **1a** with **2a**, $\text{MeOH-}d_4$, 600 MHz.

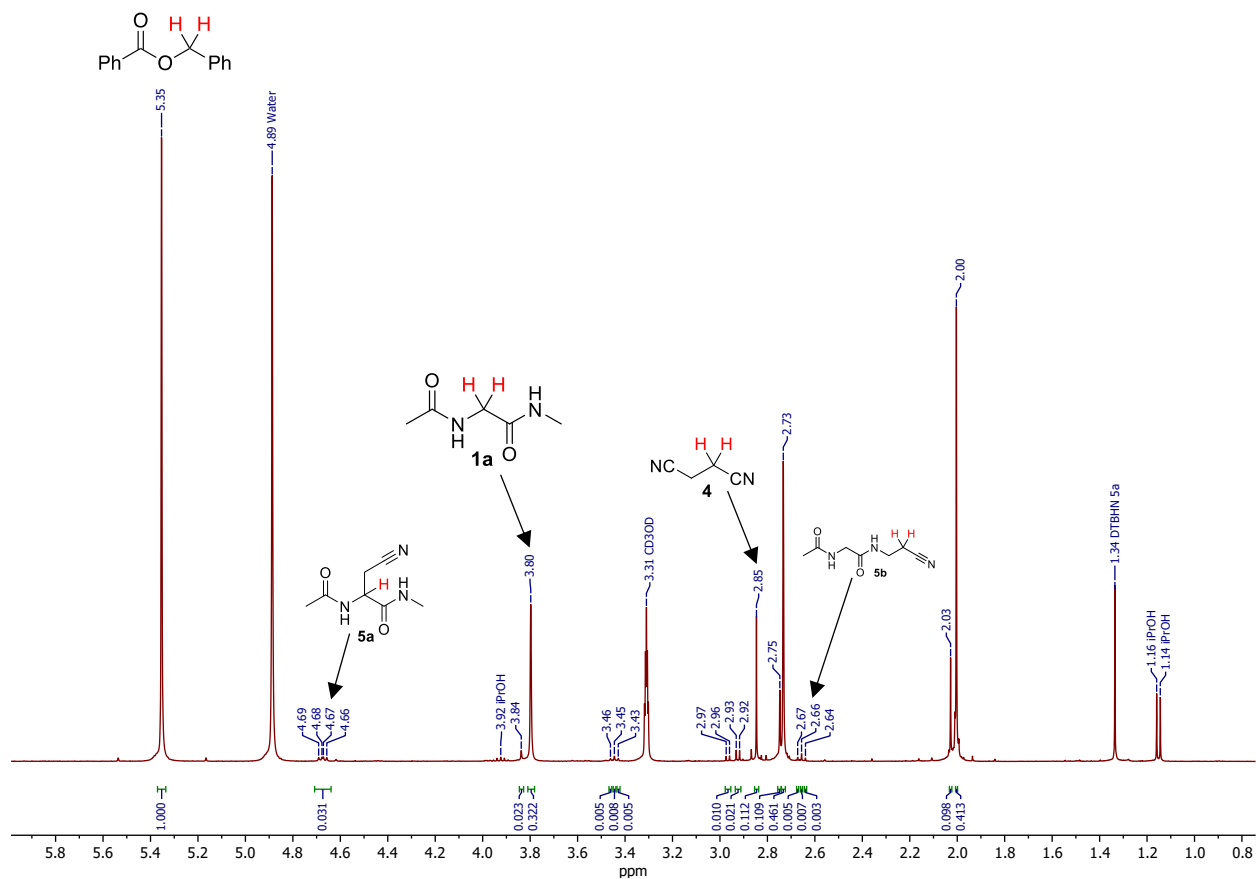


Fig. S47e. Quantitative ^1H NMR spectra of crude mixture after oxidative stress reaction of **1** with **2a**, MeOH-*d*₄, 400 MHz.

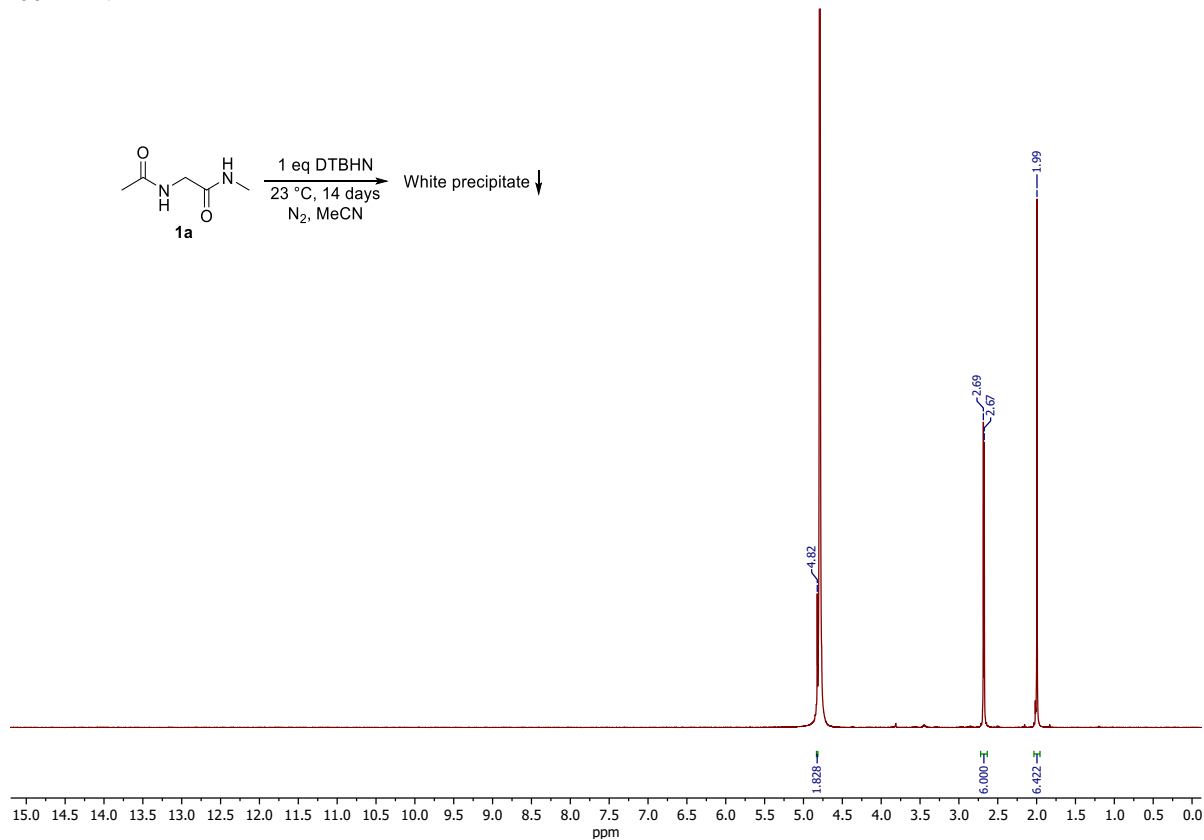


Fig. S48. ^1H NMR spectrum of the precipitate **3a/b** from oxidative stress reaction of **1a** at 23 °C, D₂O, 400 MHz.

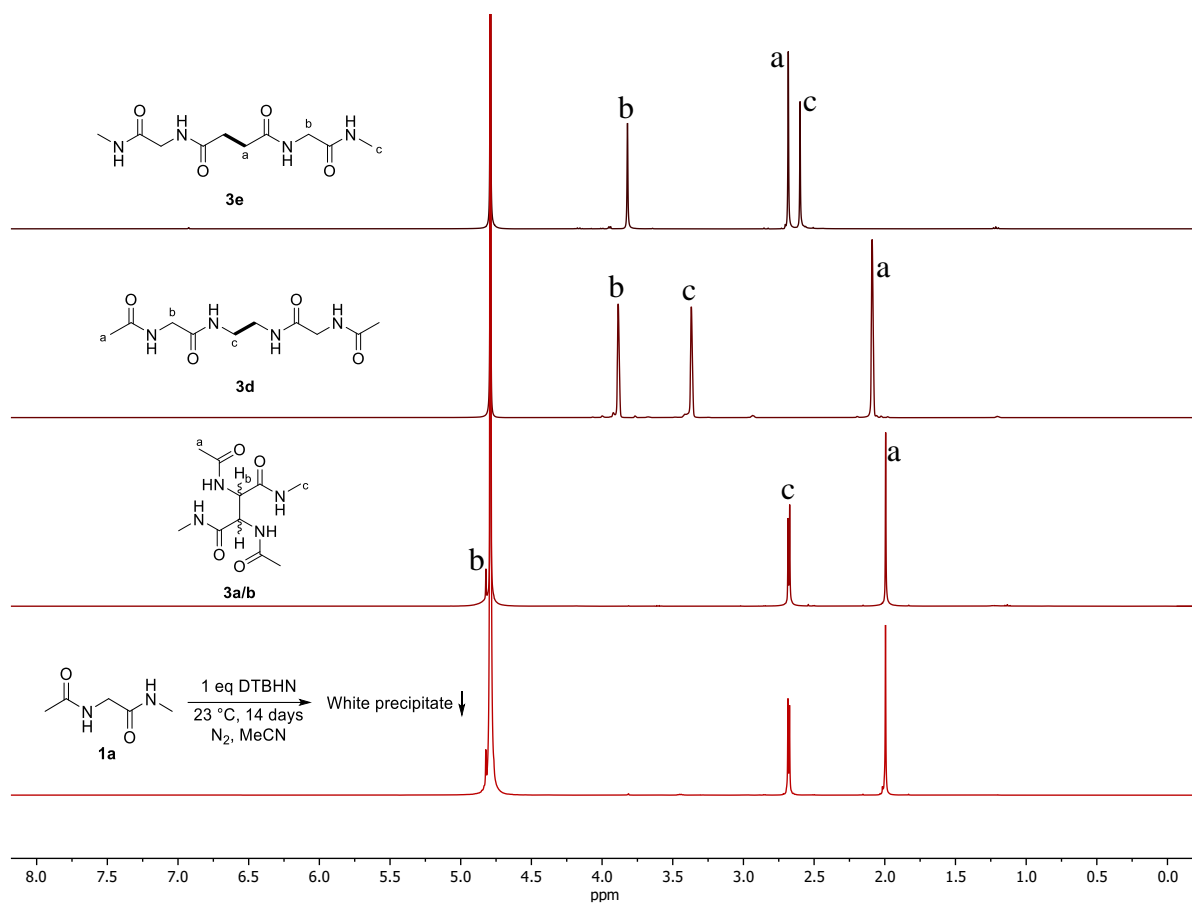


Fig. S49. Comparison of ^1H NMR spectra of different dimers and obtained white precipitate from oxidative stress reaction of **1a** at 23 °C, D_2O , 400 MHz.

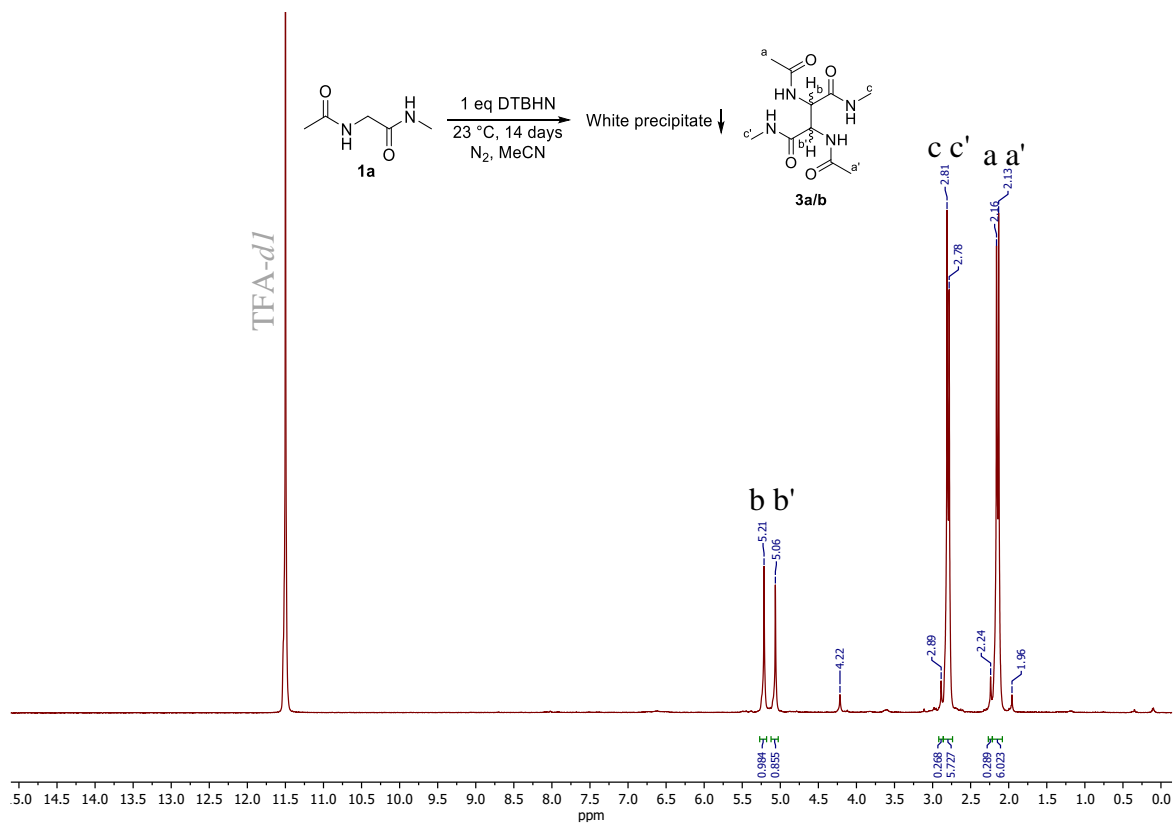


Fig. S50. ^1H NMR-spectra of dimer **3a/b** from oxidative stress reaction of **1a** at 23 °C, TFA-d_1 , 400 MHz.

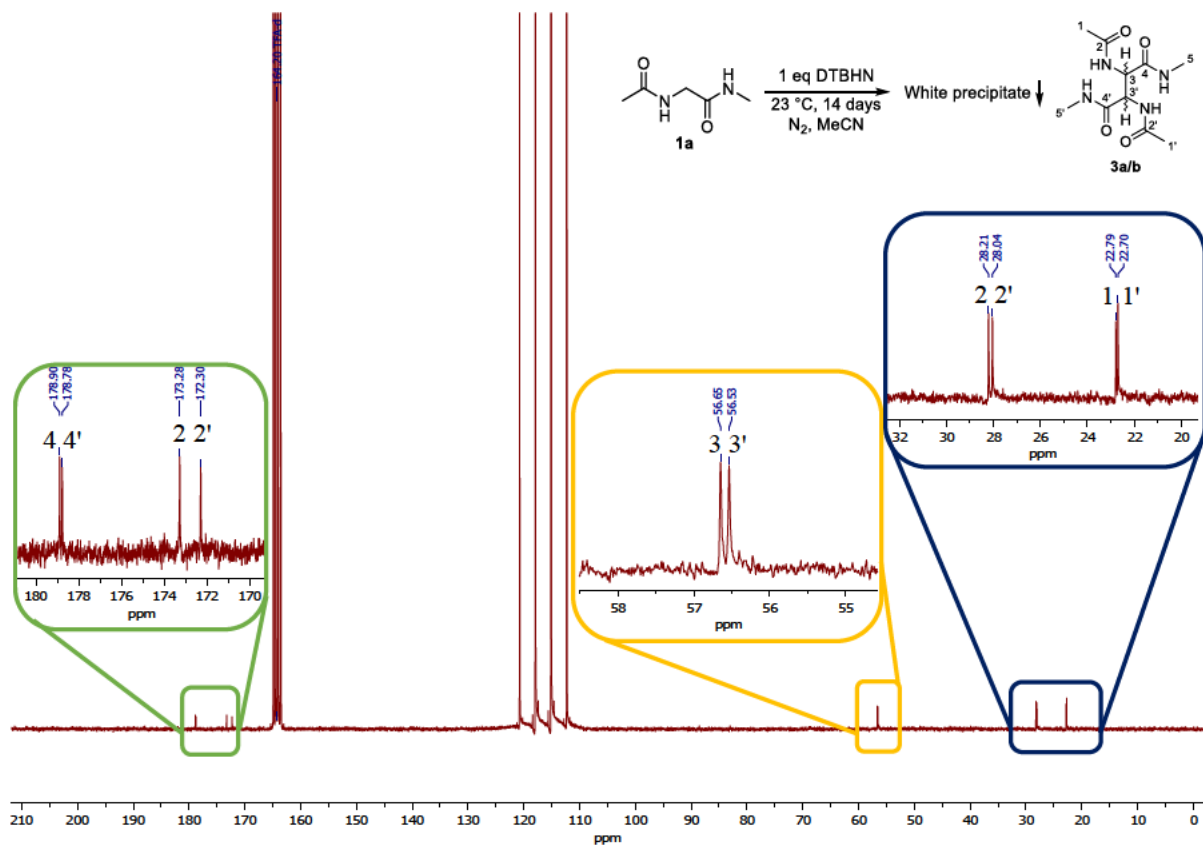


Fig. S51. ^{13}C NMR-spectrum of dimer **3a/b** from oxidative stress reaction of **1a** at 23 °C, TFA-*dl*, 400 MHz.

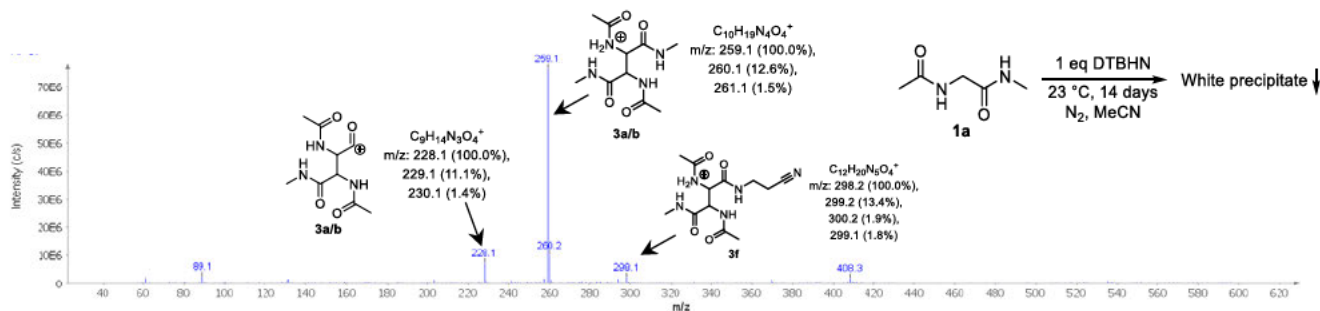


Fig. S52. MS-APCI of the obtained dimer **3a/b** from the oxidative stress reaction of **1a** at 23 °C.

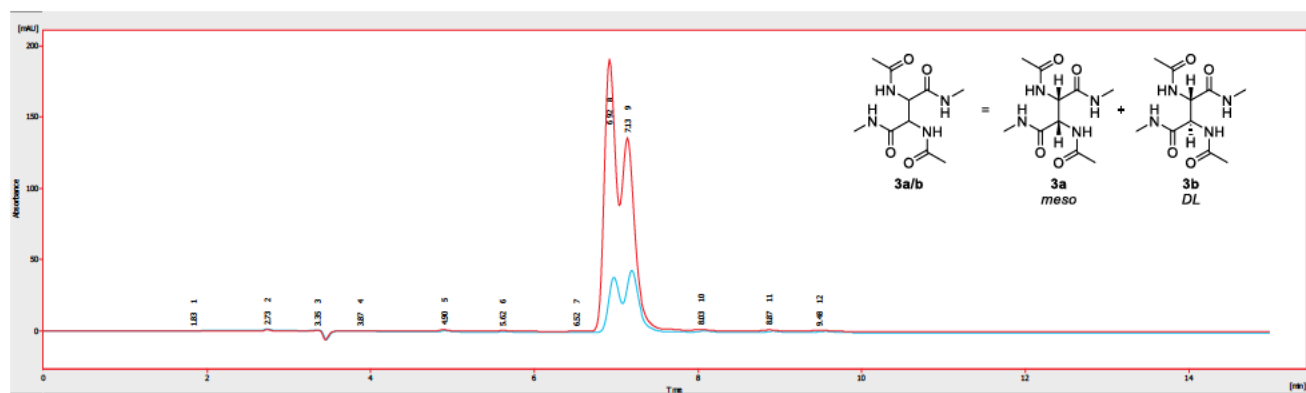


Fig. S53. HPLC-UV spectra of obtained white precipitate and obtained white precipitate + dimer **3a/b**, Eurospher II 100-5 C8A, 250×4.6 mm. 1 ml/min, 100% Water +0.1% TFA, 25 °C, $\lambda = 215$ nm.

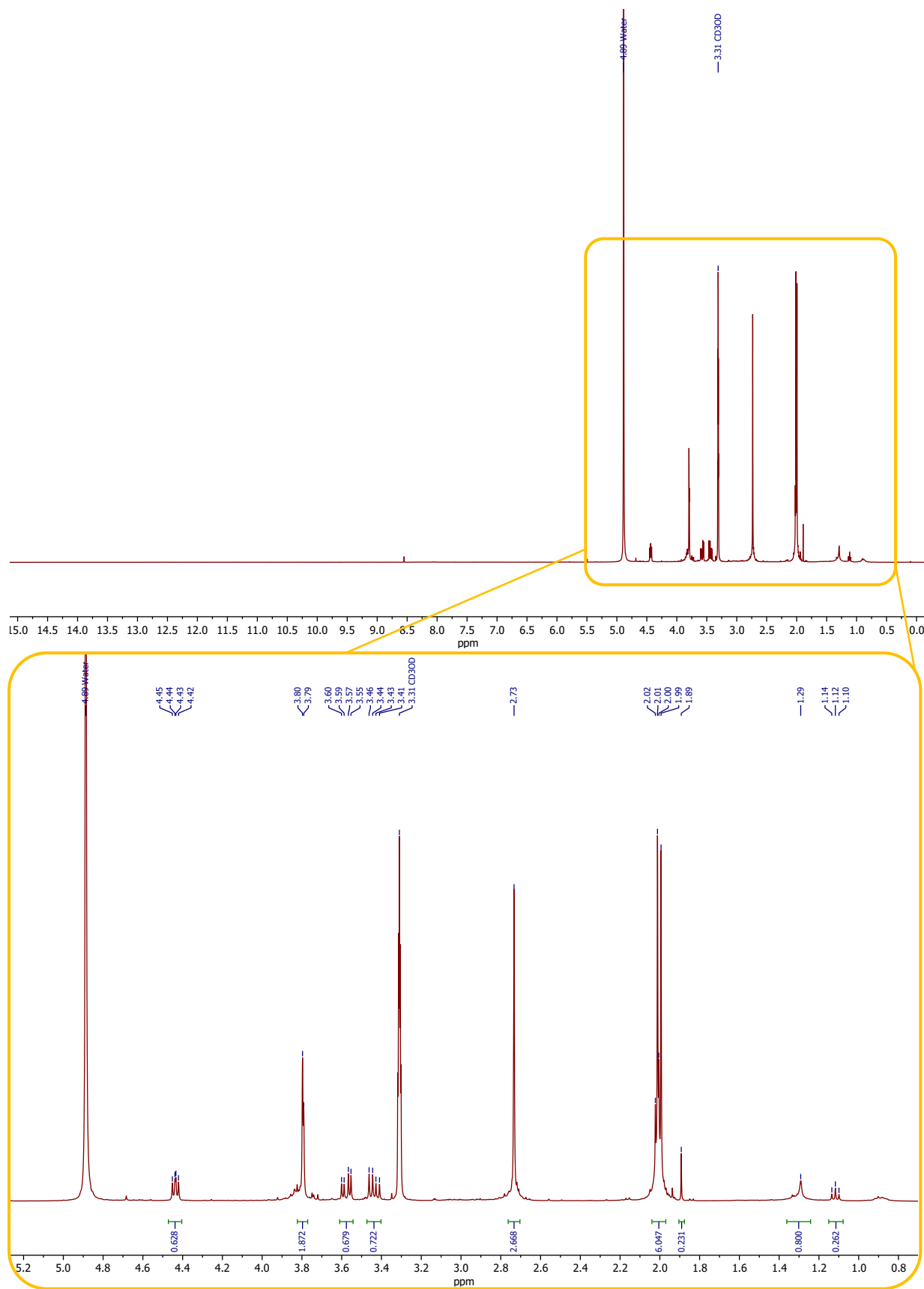


Fig. S54a. ^1H NMR spectrum of unidentified product from oxidative stress reaction of **1a** at 23 °C, $\text{MaOH-}d_4$, 400 MHz.

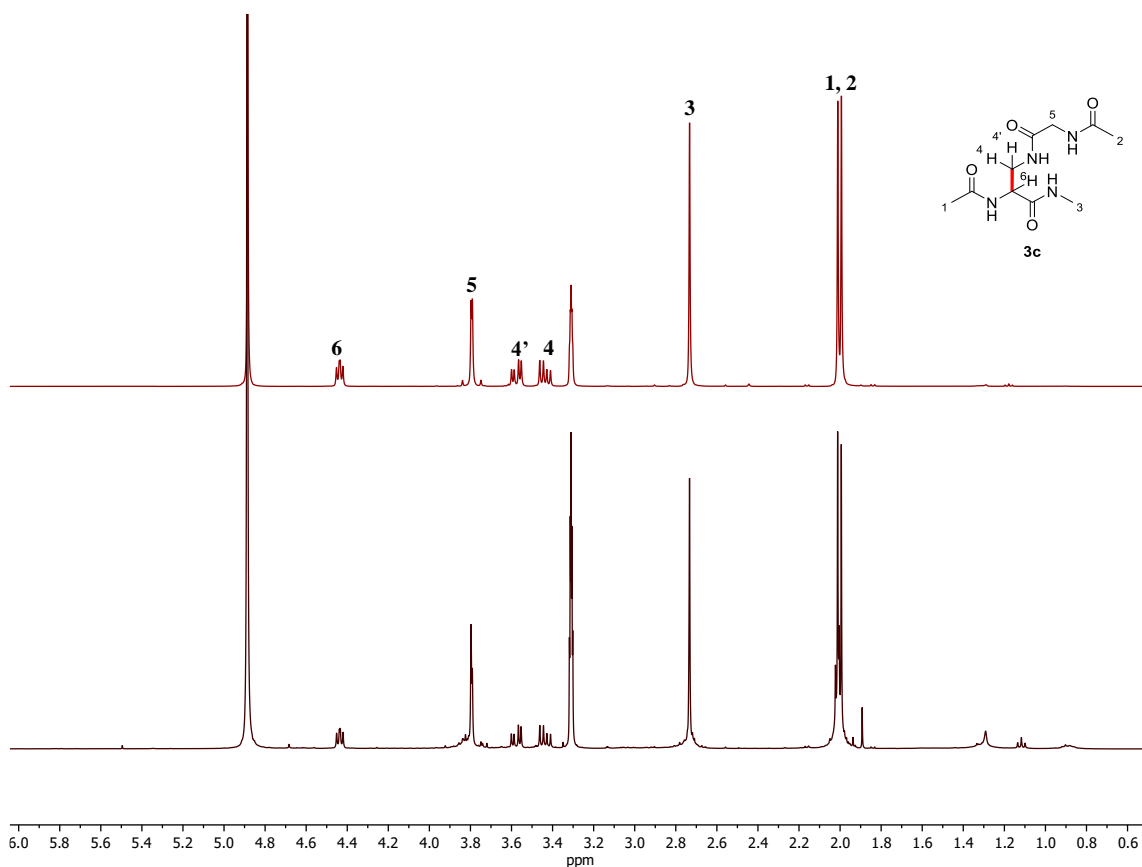


Fig. S54b. ¹H NMR spectra of dimer **3c** (top) and unidentified product from oxidative stress of **1a** at 23°C (bottom), MeOH-*d*₄, 400 MHz.

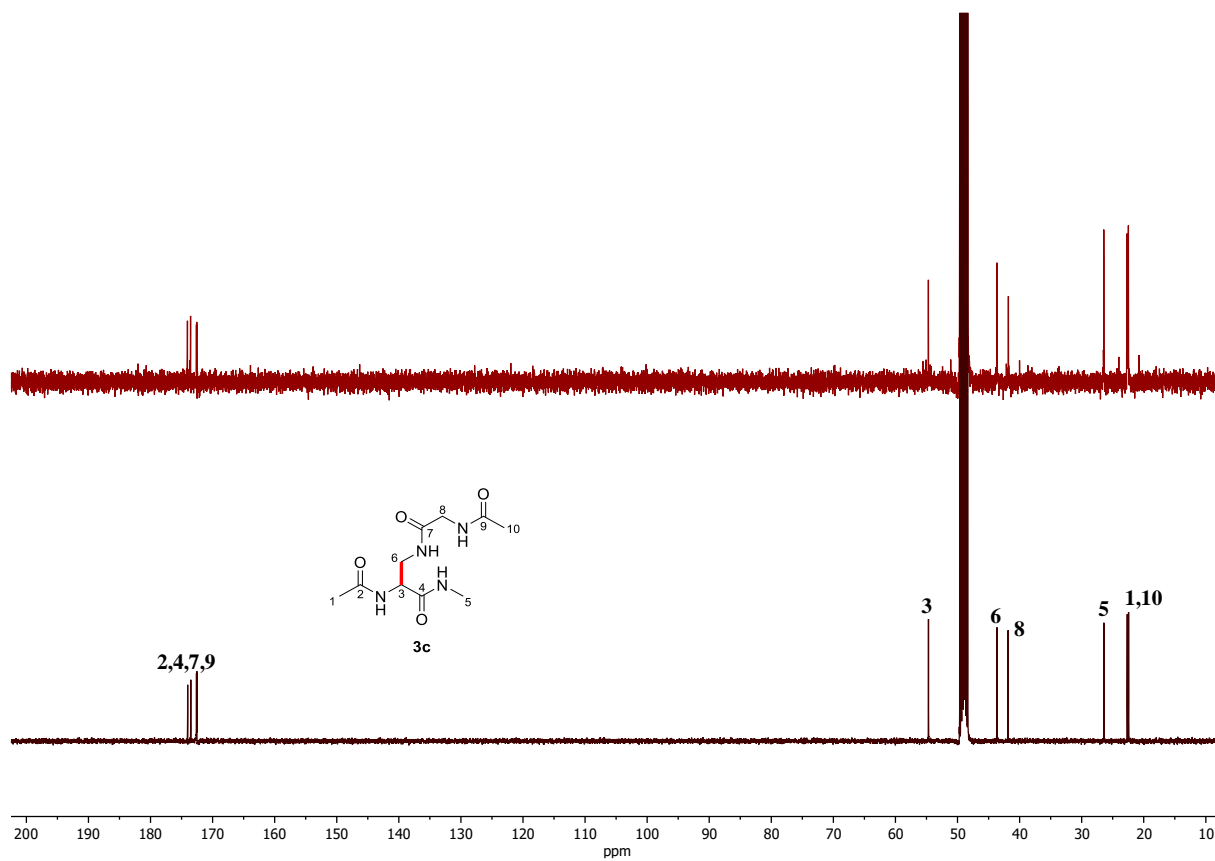


Fig. S54c. ¹³C NMR spectra of unidentified product from oxidative stress of **1a** at 23°C (top) and dimer **3c** (bottom), MeOH-*d*₄, 101 MHz.

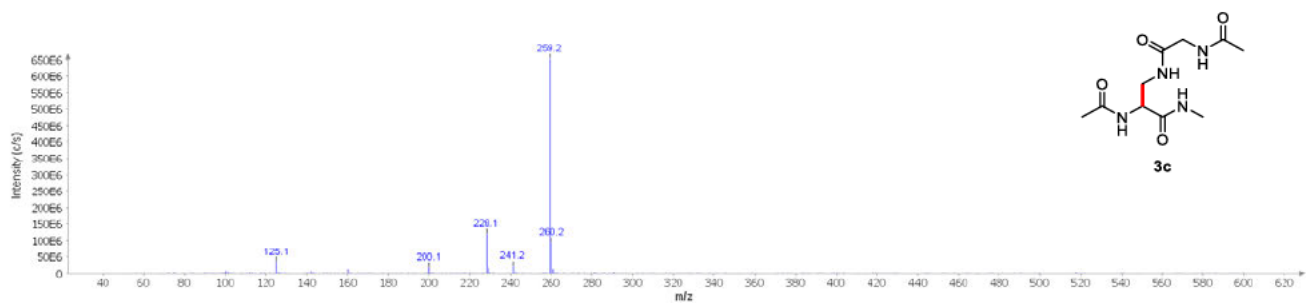


Fig. S55. MS-APCI spectrum of the obtained dimer **3c** from oxidative stress reaction of **1a** at 23°C.

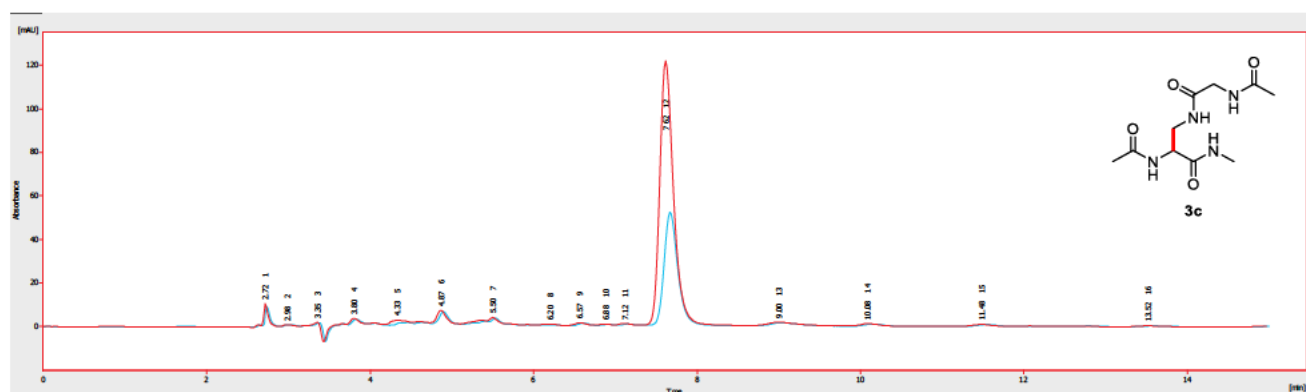


Fig. S56. HPLC-UV spectra of obtained last fractions and obtained last fractions + dimer **3c**, Eurospher II 100-5 C8A, 250×4.6 mm. 1 ml/min, 100% Water +0.1% TFA, 25 °C, $\lambda = 215$ nm

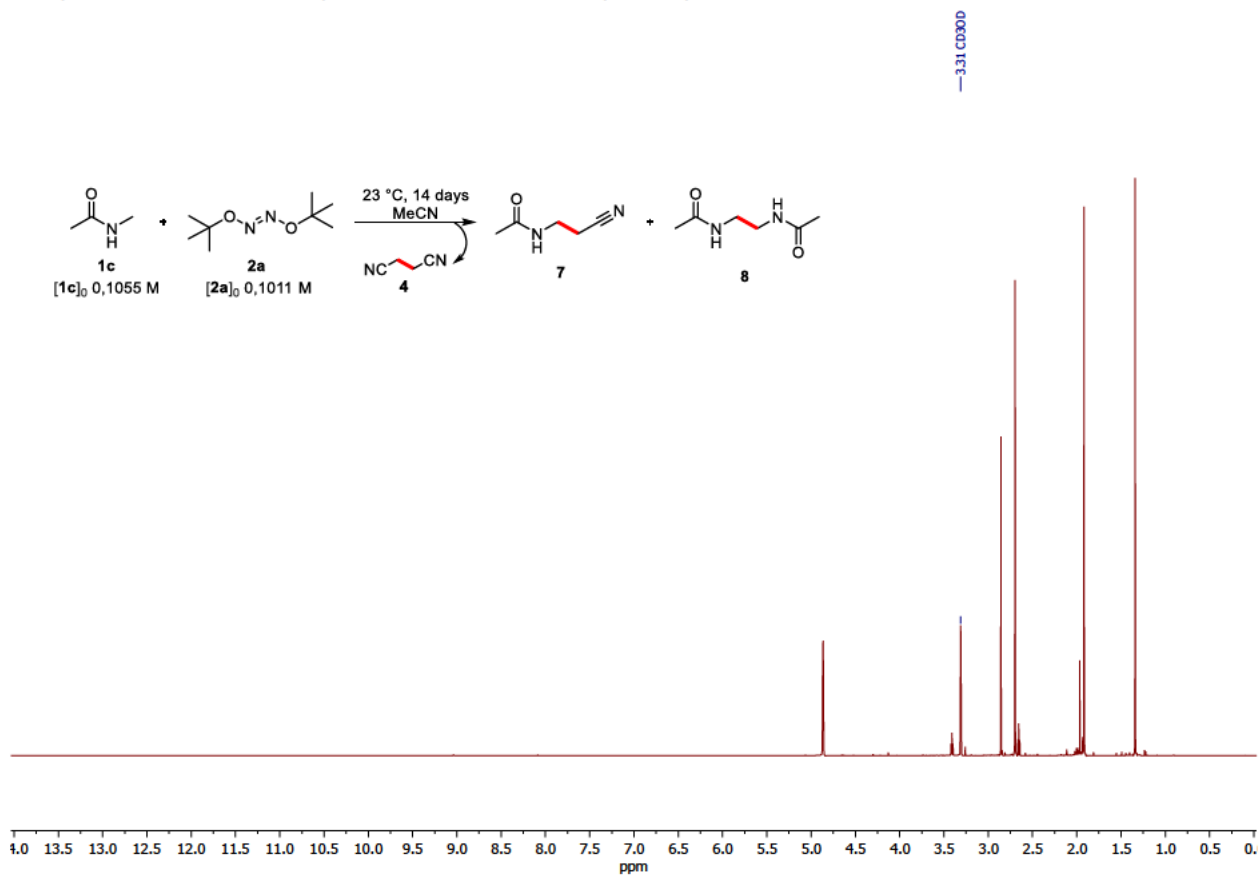


Fig. S57a. ^1H NMR spectrum of crude mixture after oxidative stress reaction of **1c** with **2a**, $\text{MeOH-}d_4$, 600 MHz.

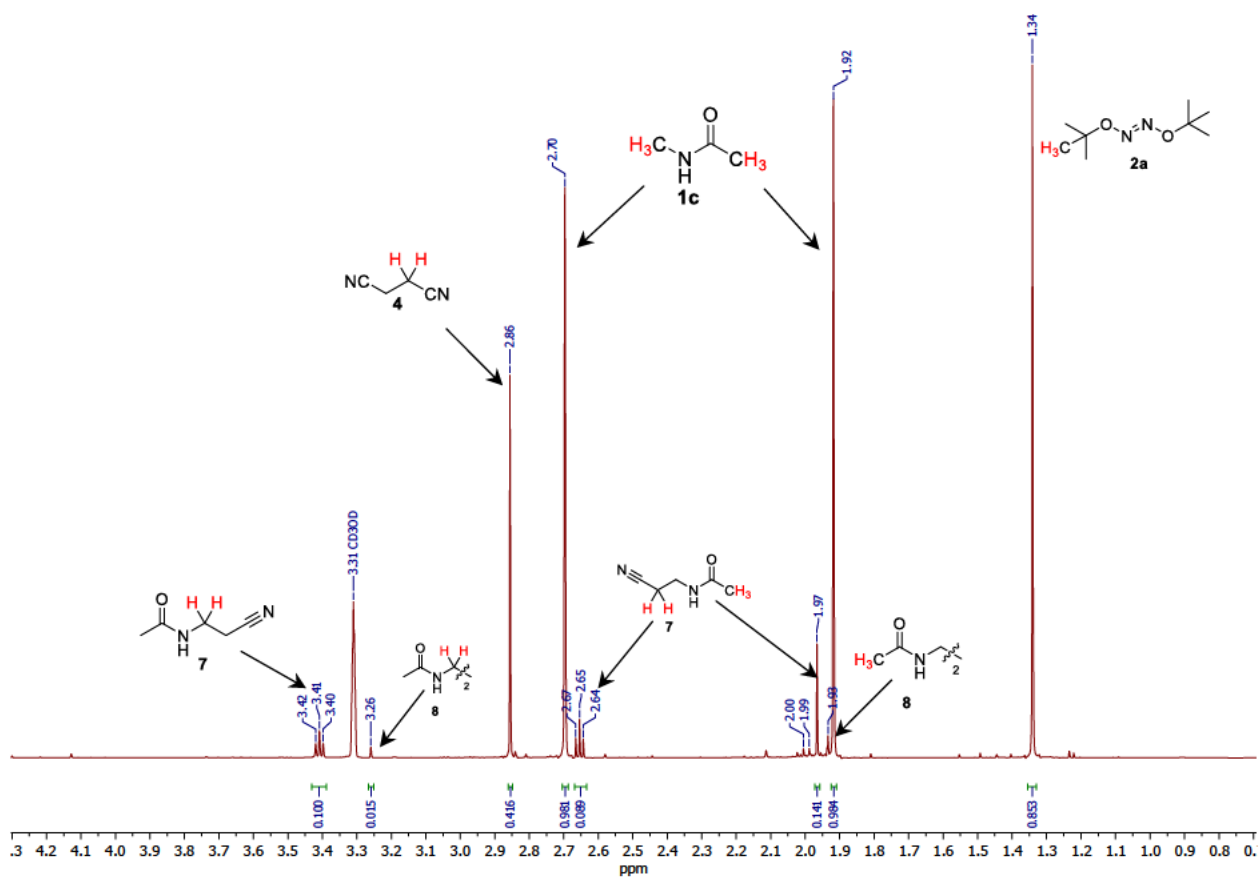


Fig. S57b. ^1H NMR spectrum of crude mixture after oxidative stress reaction of **1c** with **2a**, $\text{MeOH-}d_4$, 600 MHz.

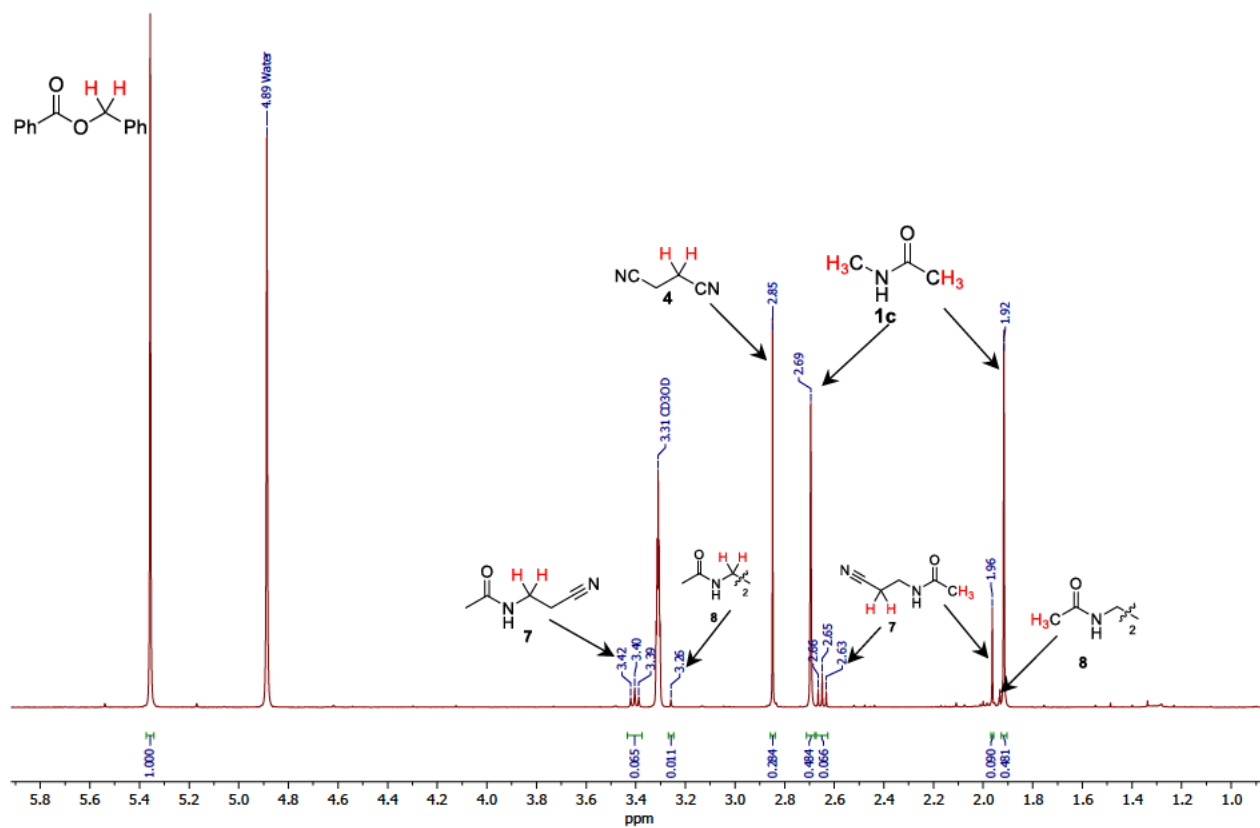


Fig. S57c. Quantitative ^1H NMR spectrum of crude mixture after oxidative stress reaction of **1c** with **2a**, $\text{MeOH-}d_4$, 400 MHz.

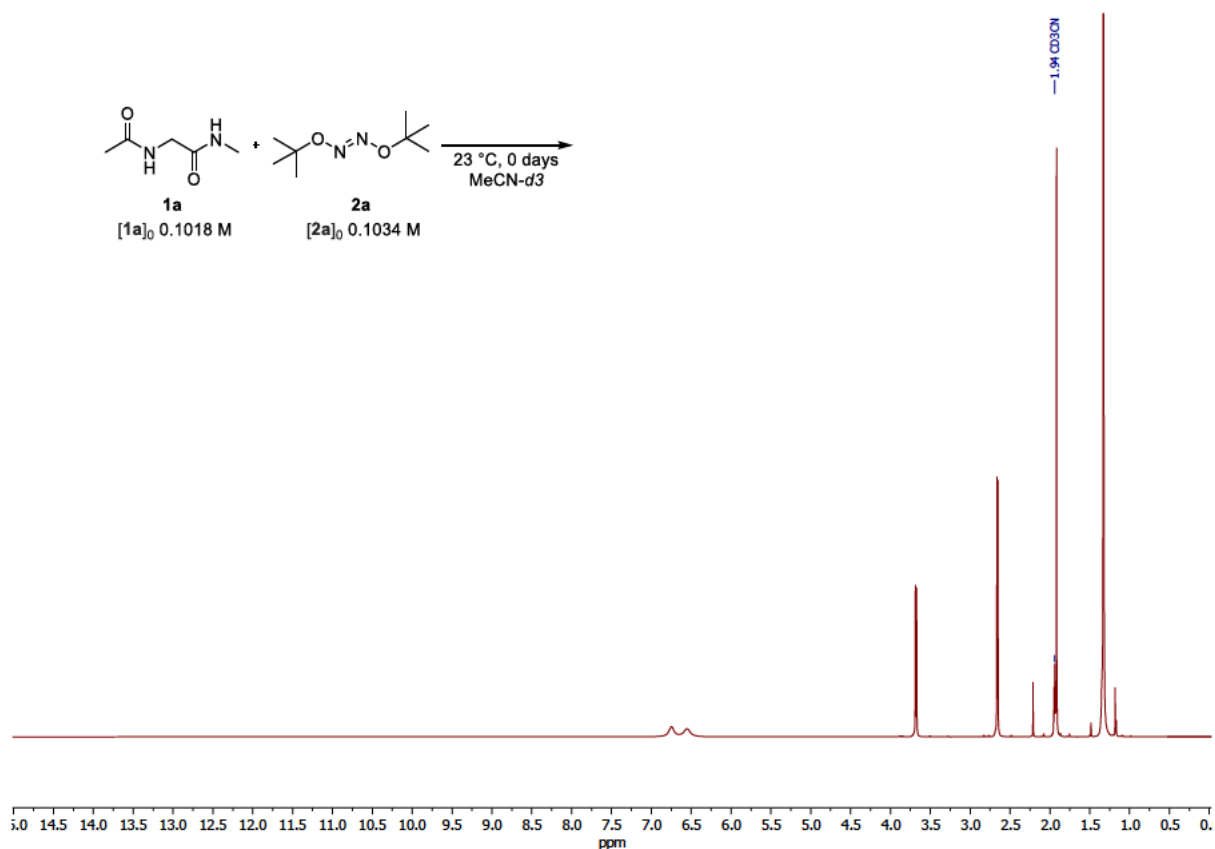


Fig. S58a. *in situ* ^1H NMR spectrum of AcGlyNMe (**1a**) with **2a** (0 day), MeCN- d_3 , 400 MHz.

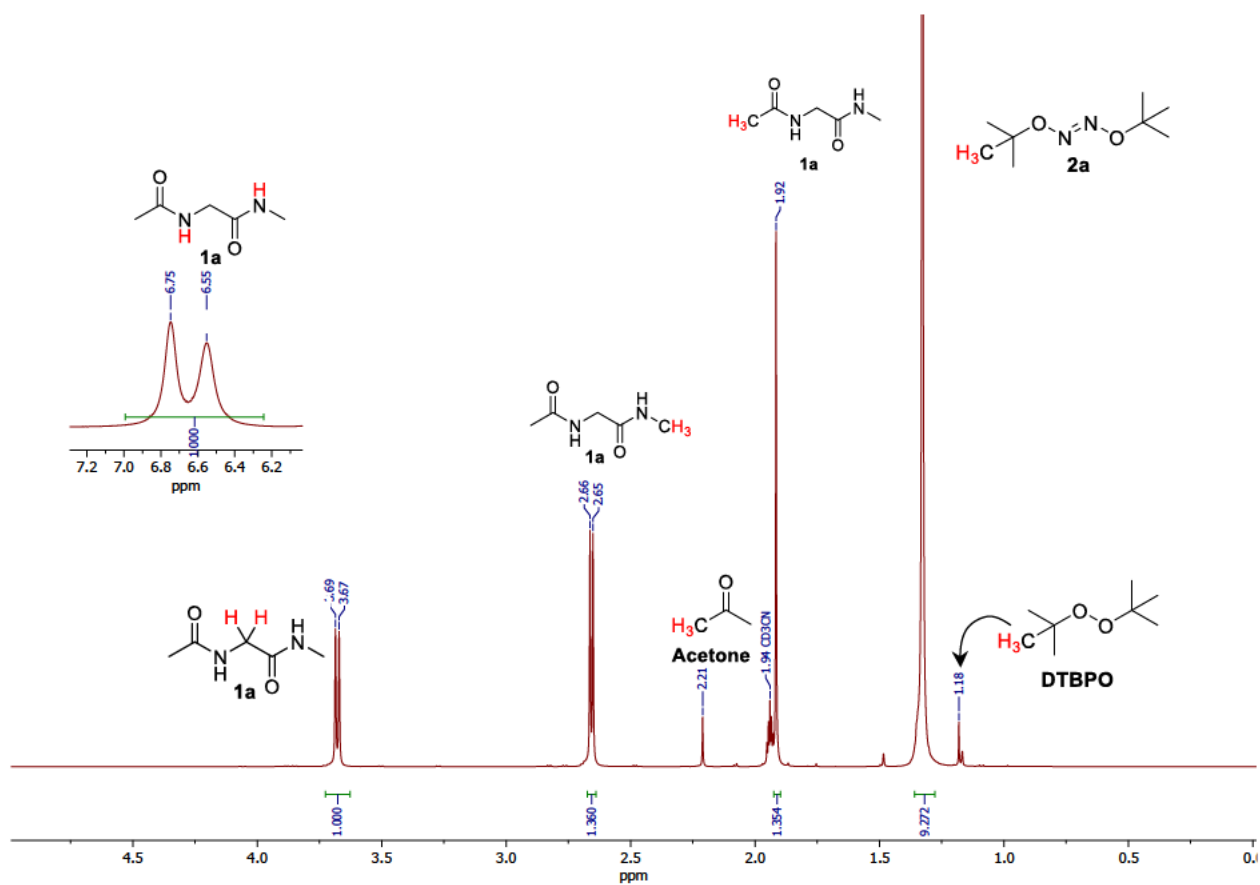


Fig. S58b. *in situ* ^1H NMR spectrum of **1a** with **2a** (0 day), MeCN- d_3 , 400 MHz

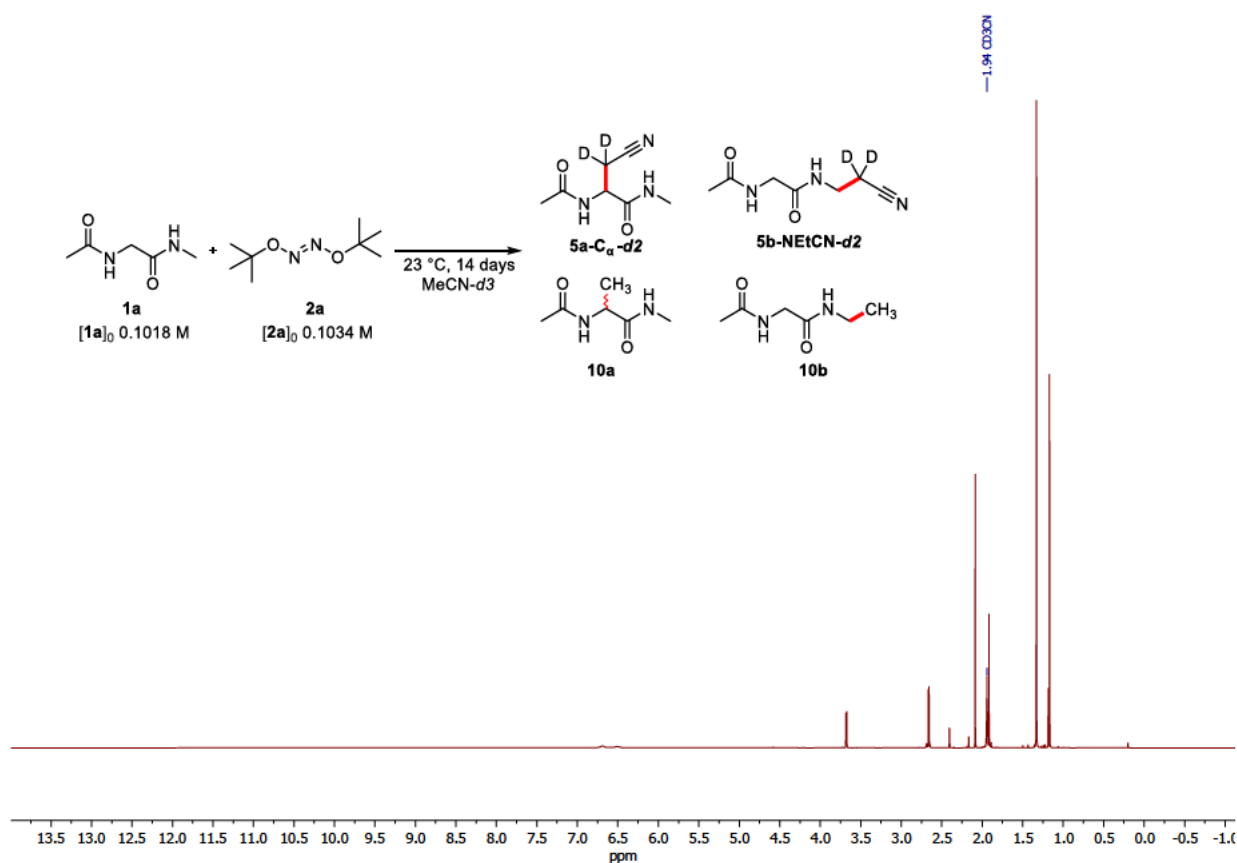


Fig. S58c. *in situ* $^1\text{H NMR}$ spectrum of **1a** with **2a** (14 days), MeCN-d_3 , 400 MHz.

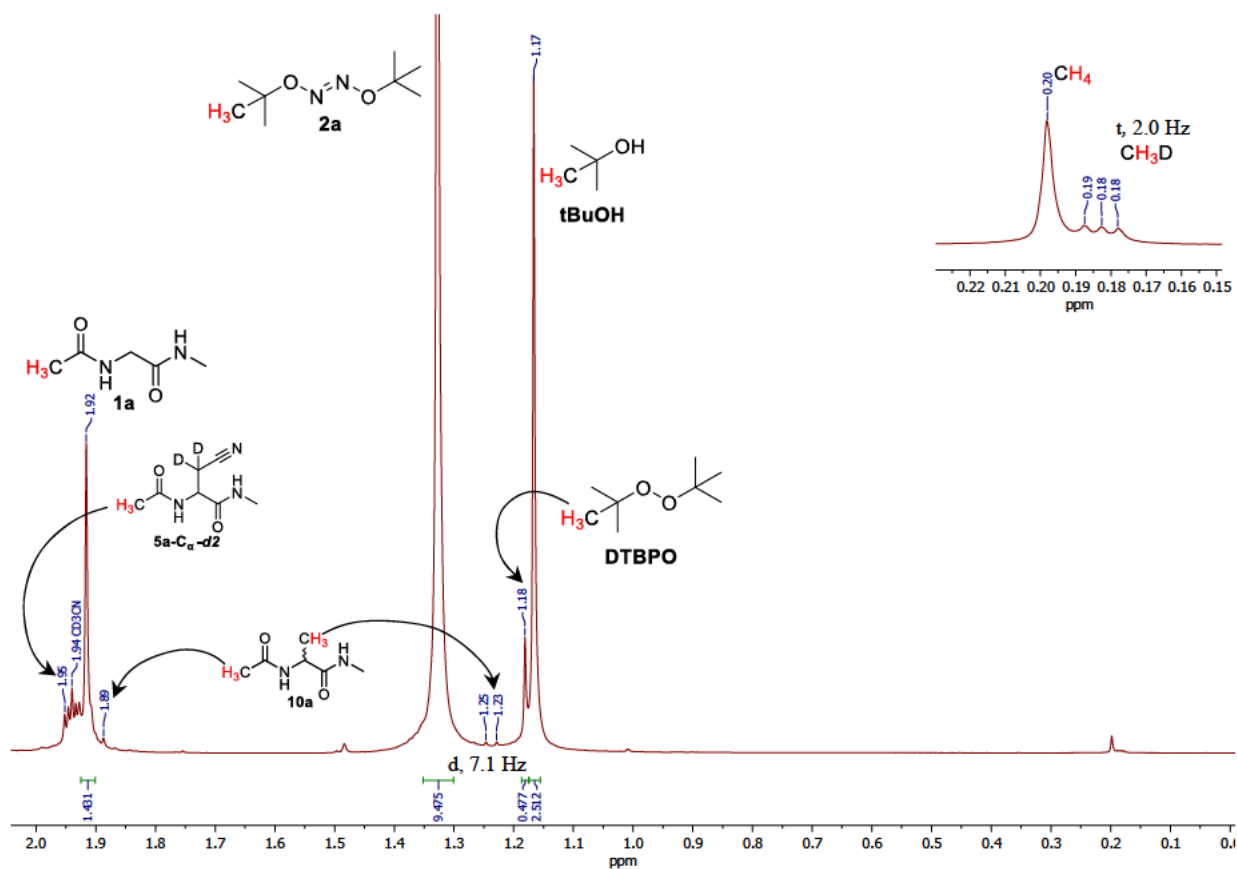


Fig. S58d. *in situ* $^1\text{H NMR}$ spectrum of **1a** with **2a** (14 days), MeCN-d_3 , 400 MHz.

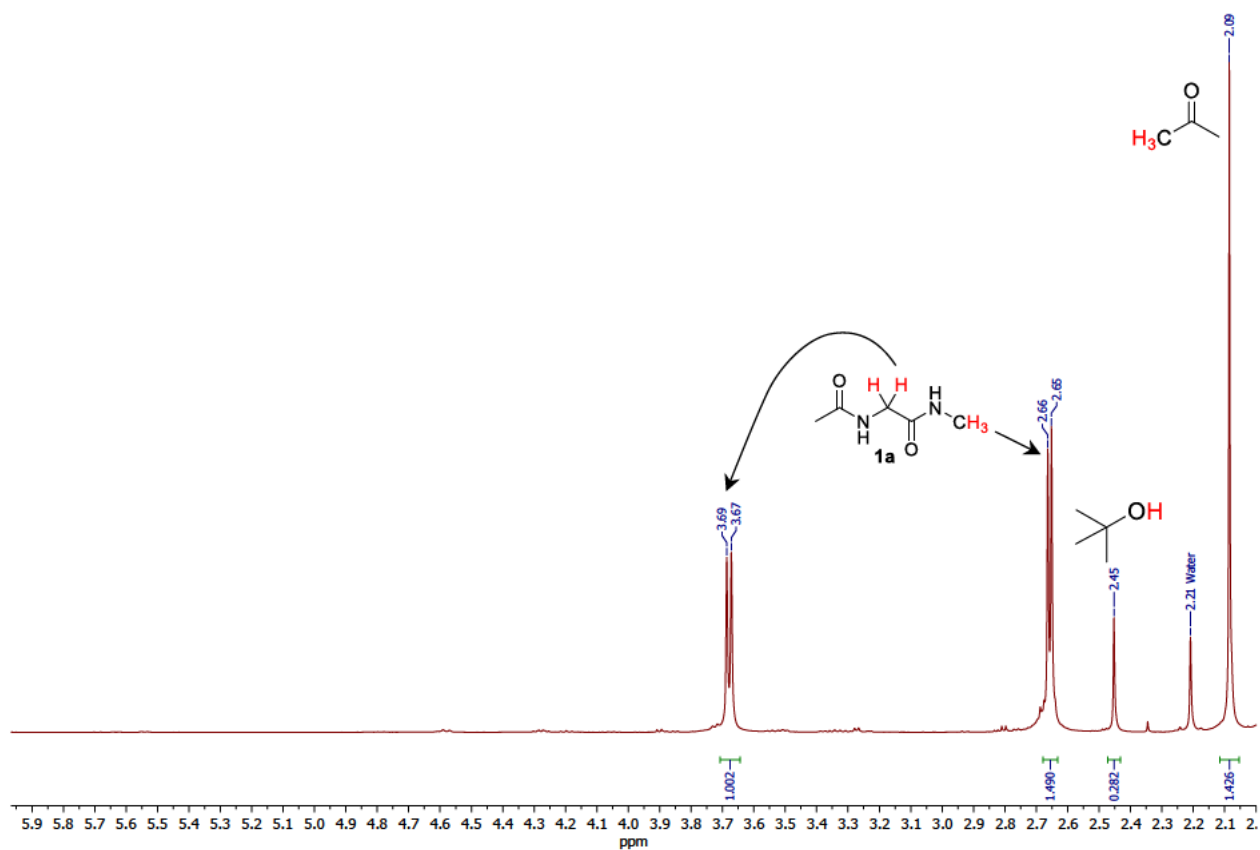


Fig. S58e. *in situ* ^1H NMR spectrum of **1a** with **2a** (14 days), $\text{MeCN-}d_3$, 400 MHz.

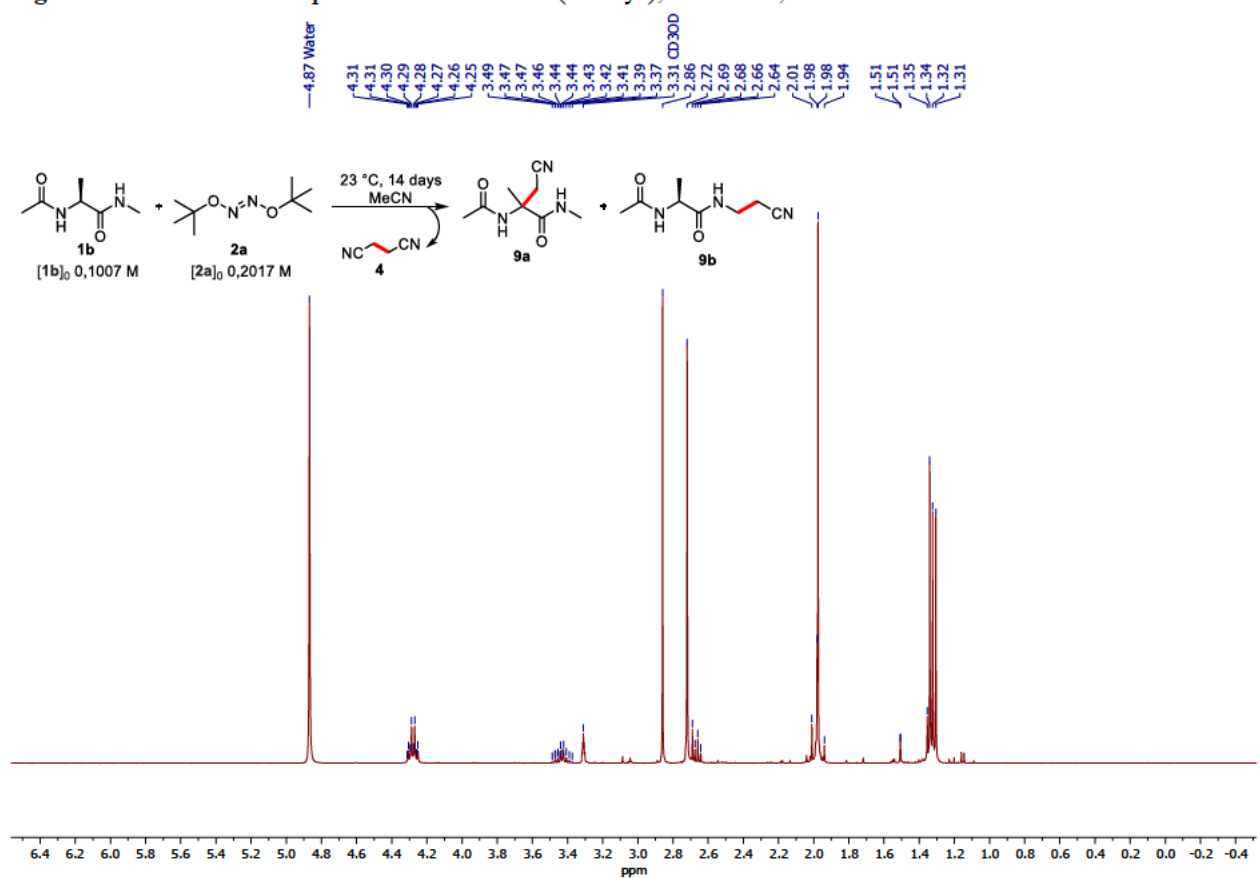


Fig. S59a. ^1H NMR spectrum of crude mixture after oxidative stress reaction of **1b** with 2eq **2a**, $\text{MeOH-}d_4$, 400 MHz.

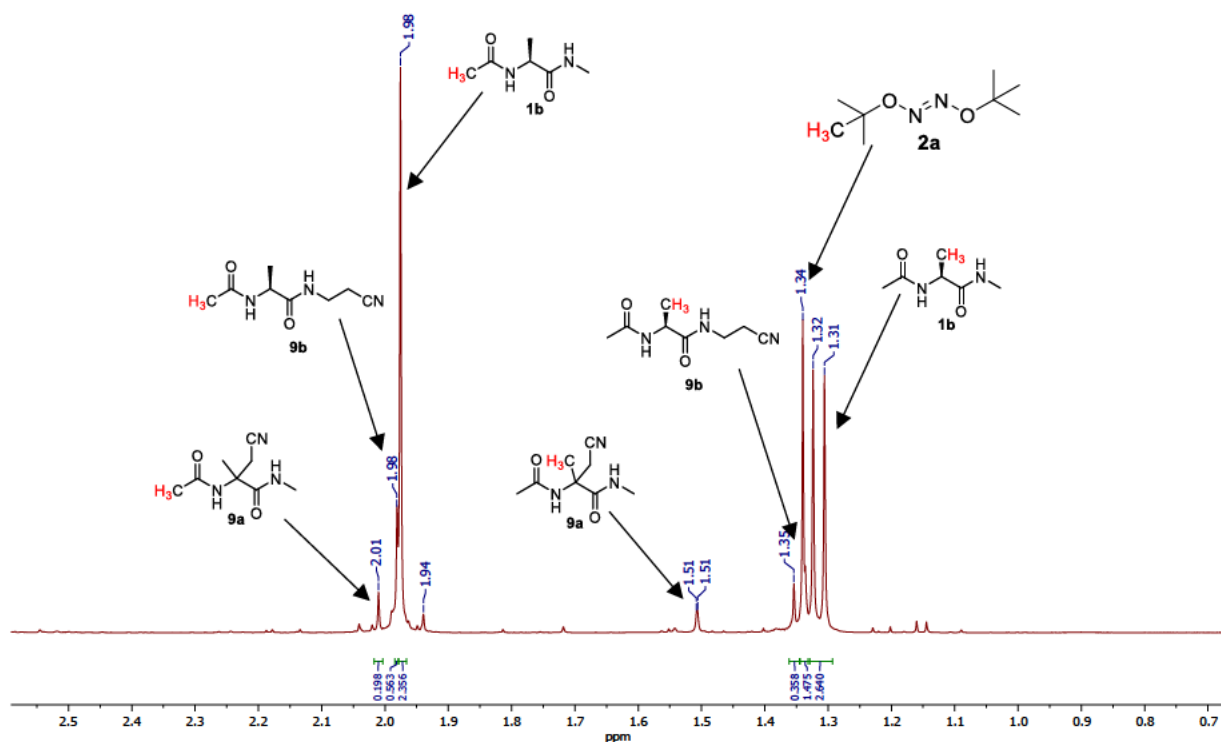


Fig. S59b. ^1H NMR spectrum of crude mixture after oxidative stress reaction of **1b** with 2 eq **2a**, $\text{MeOH-}d_4$, 400 MHz.

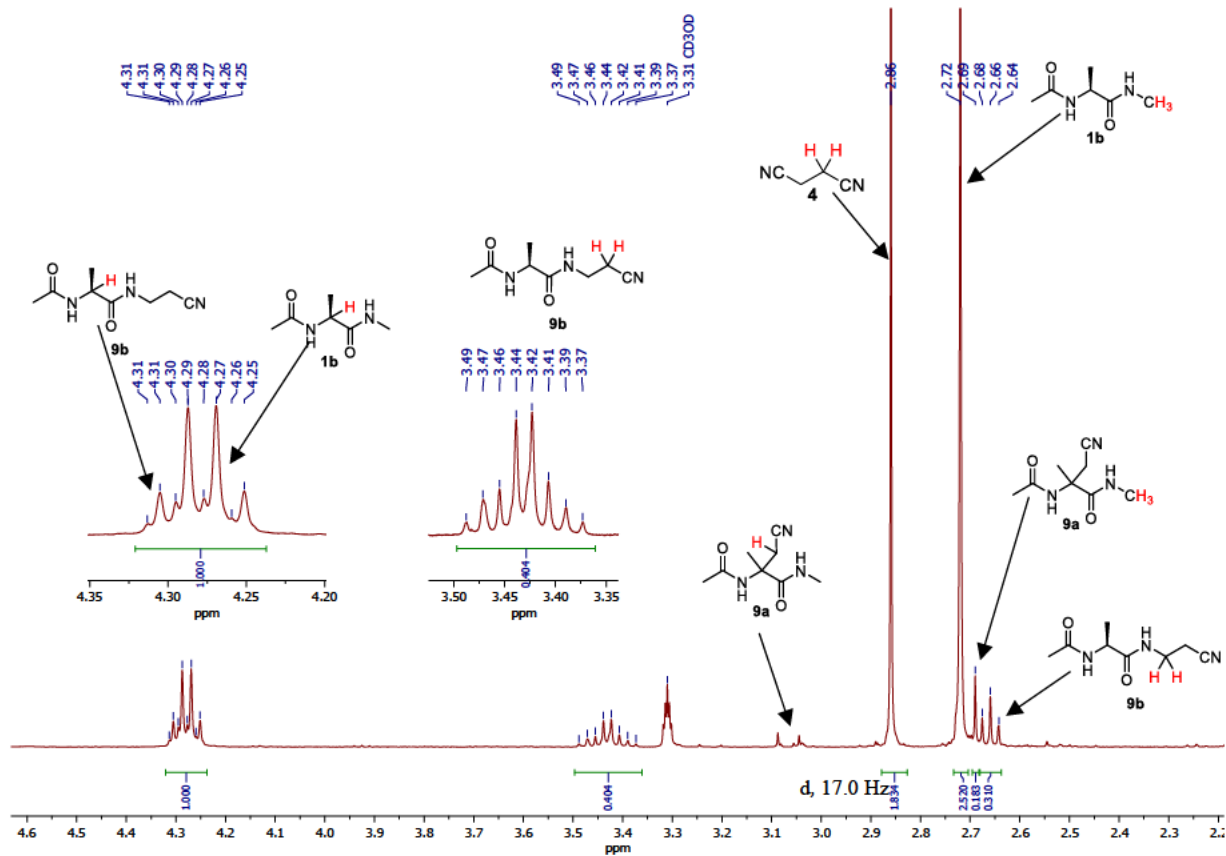


Fig. S59c. ^1H NMR spectrum of crude mixture after oxidative stress reaction of **1b** with 2 eq **2a**, $\text{MeOH-}d_4$, 400 MHz.

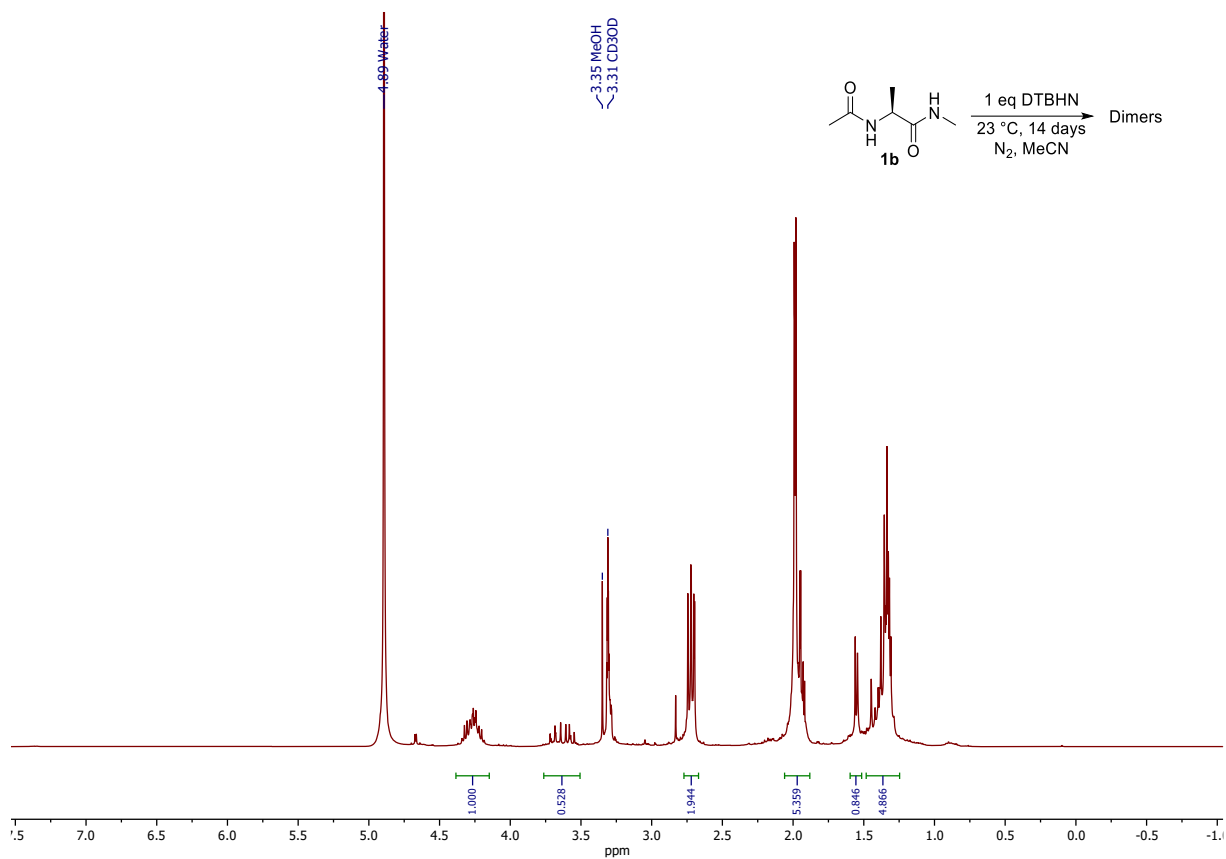


Fig. S60a. ¹H NMR spectrum of unidentified product from oxidative stress reaction of **1b** at 23 °C, MeOH-*d*₄, 400 MHz.

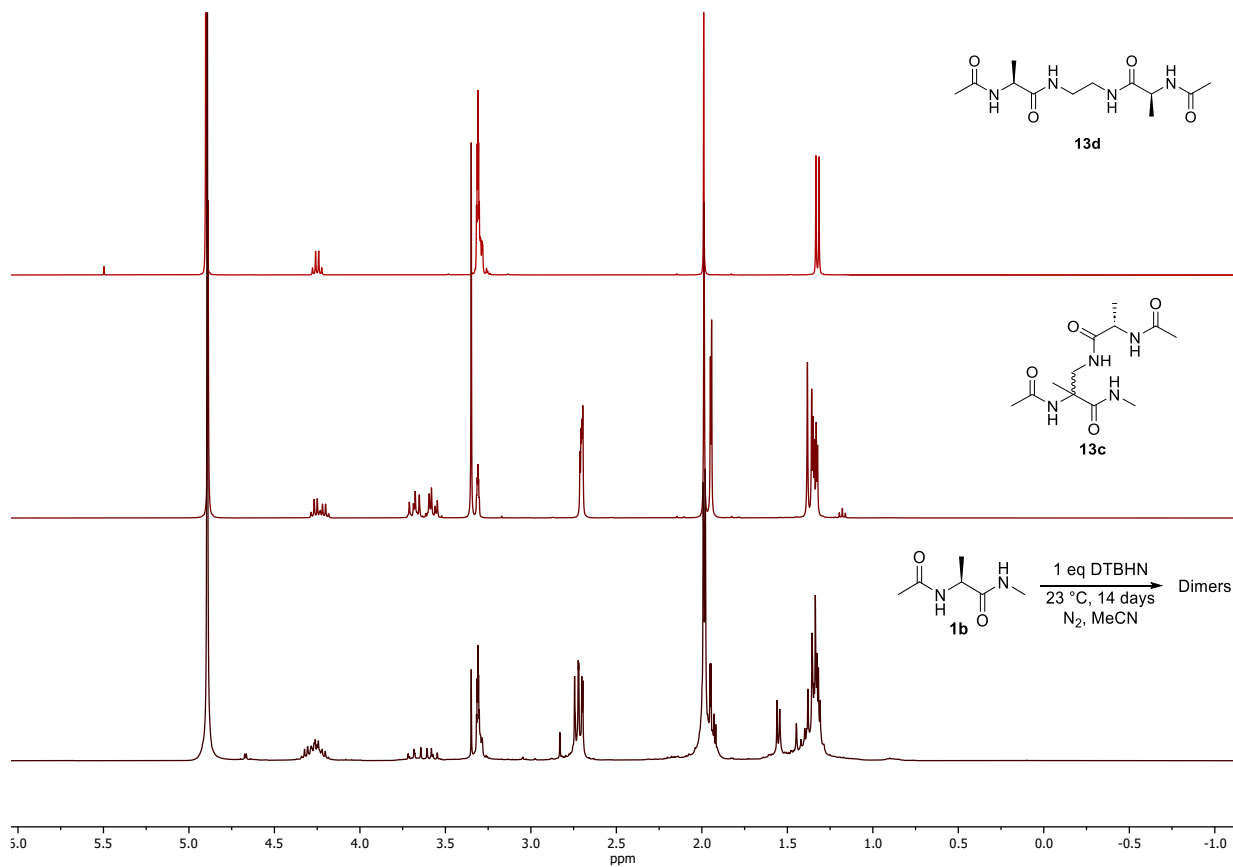


Fig. S60b. ¹H NMR spectra of unidentified product from oxidative stress reaction of **1b** at 23 °C, MeOH-*d*₄, 400 MHz.

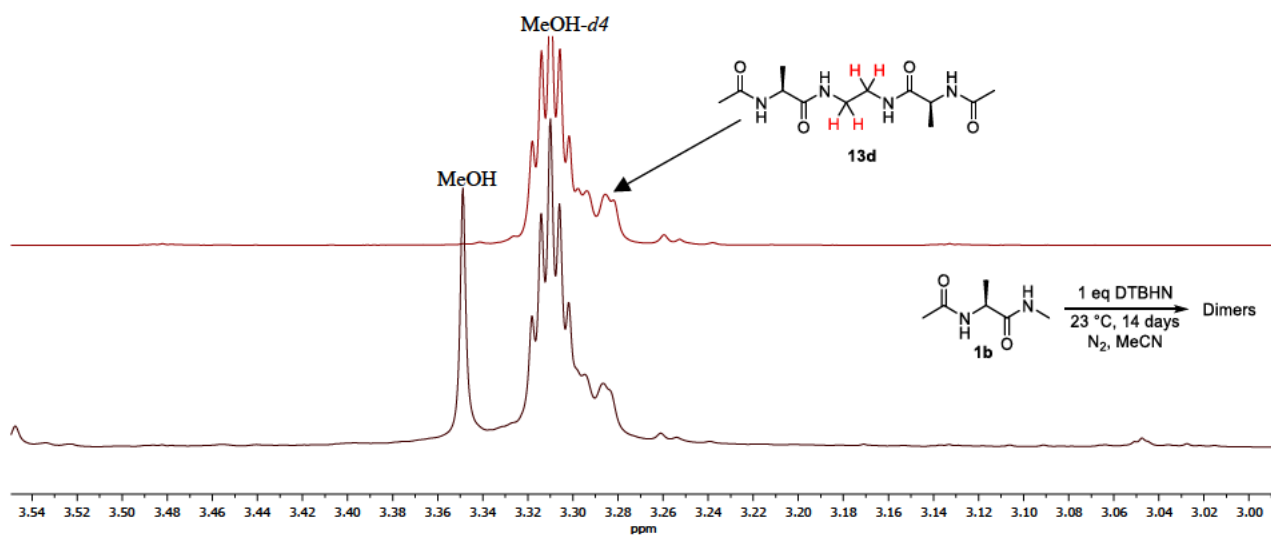


Fig. S61. The overlapping peaks of the dimer **13d** in the polar fractions of **1b** oxidative stress, MeOH-*d*₄, 400 MHz.

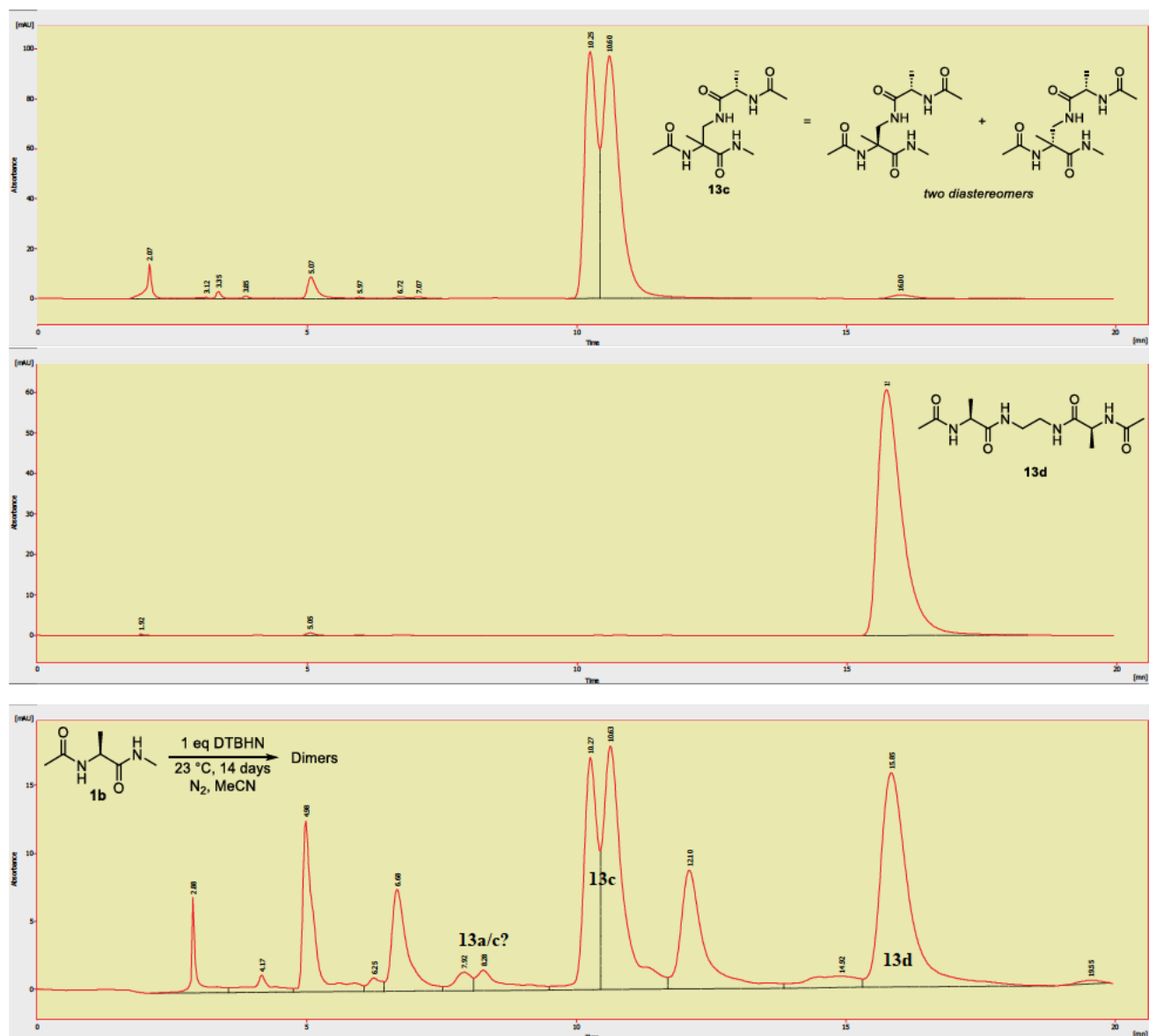


Fig. S62. HPLC-UV spectra of **13a-c** dimers, Eurospher II 100-5 C8A, 250×4.6 mm. 1 ml/min, 100% Water +0.1% TFA, 25 °C, λ = 210 nm.

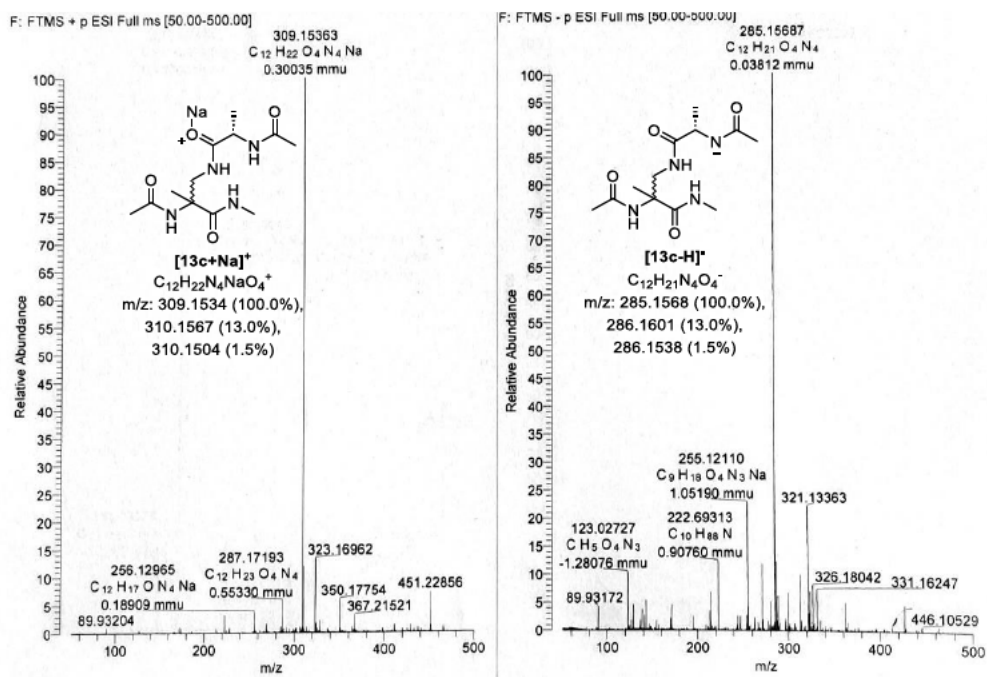


Fig. S63. ESI-MS spectra of the obtained fractions from **1b** oxidative stress.

2.6.6. NMR Spectra of the Synthesized Compounds

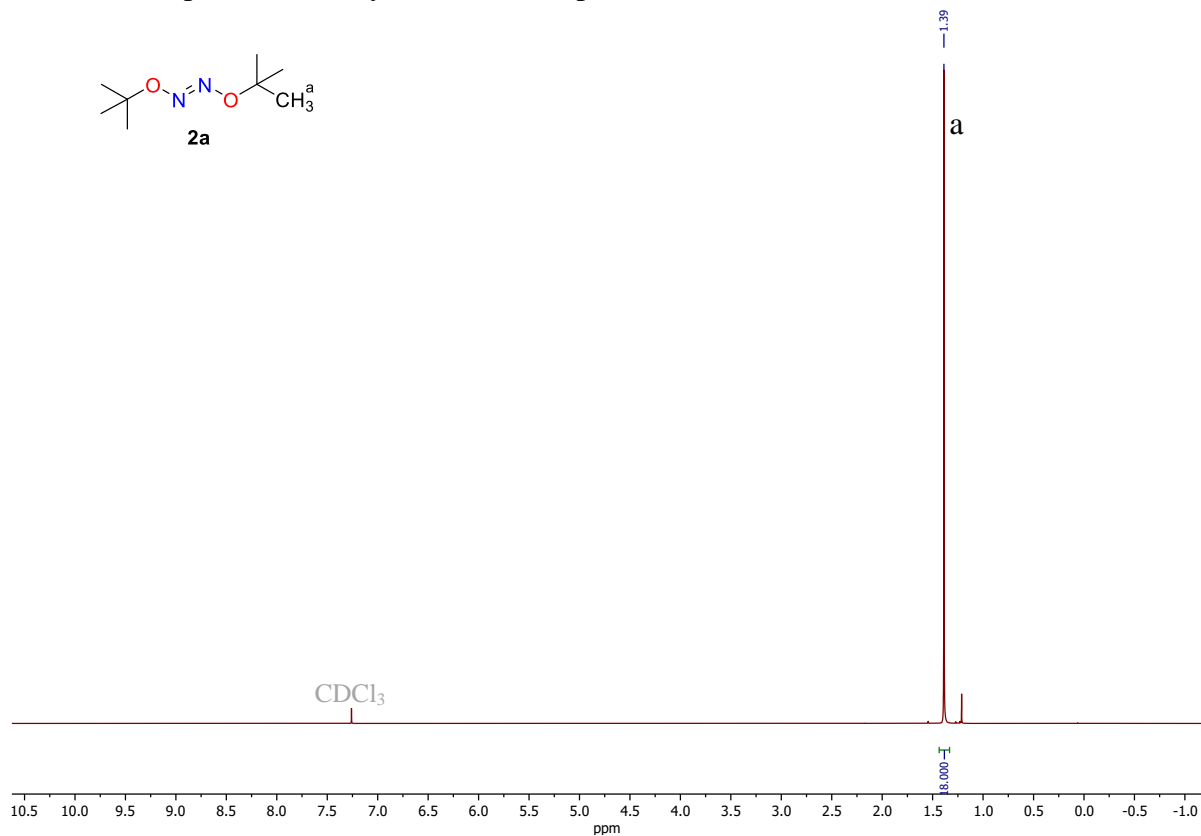


Fig. S64. ¹H NMR spectrum of DTBHN (**2a**), CDCl₃, 400 MHz.

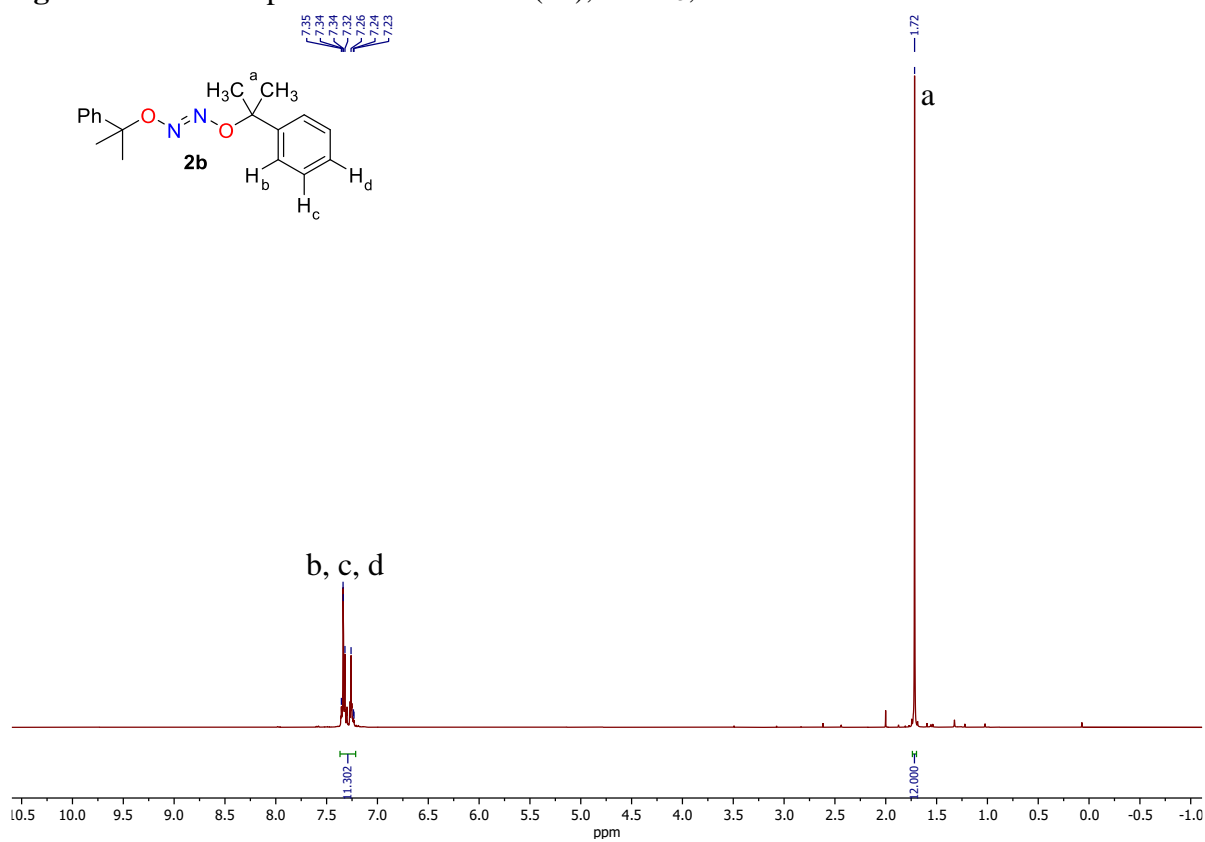
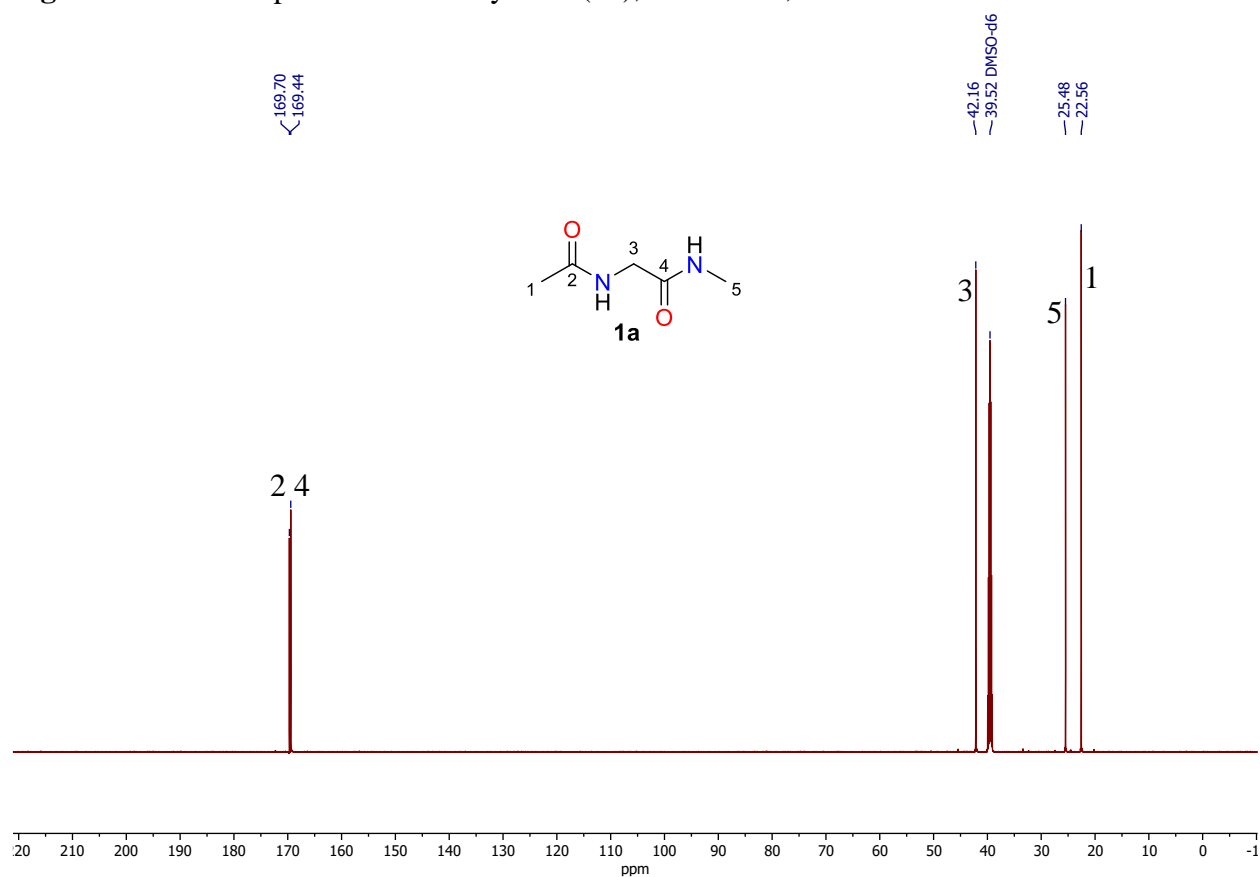
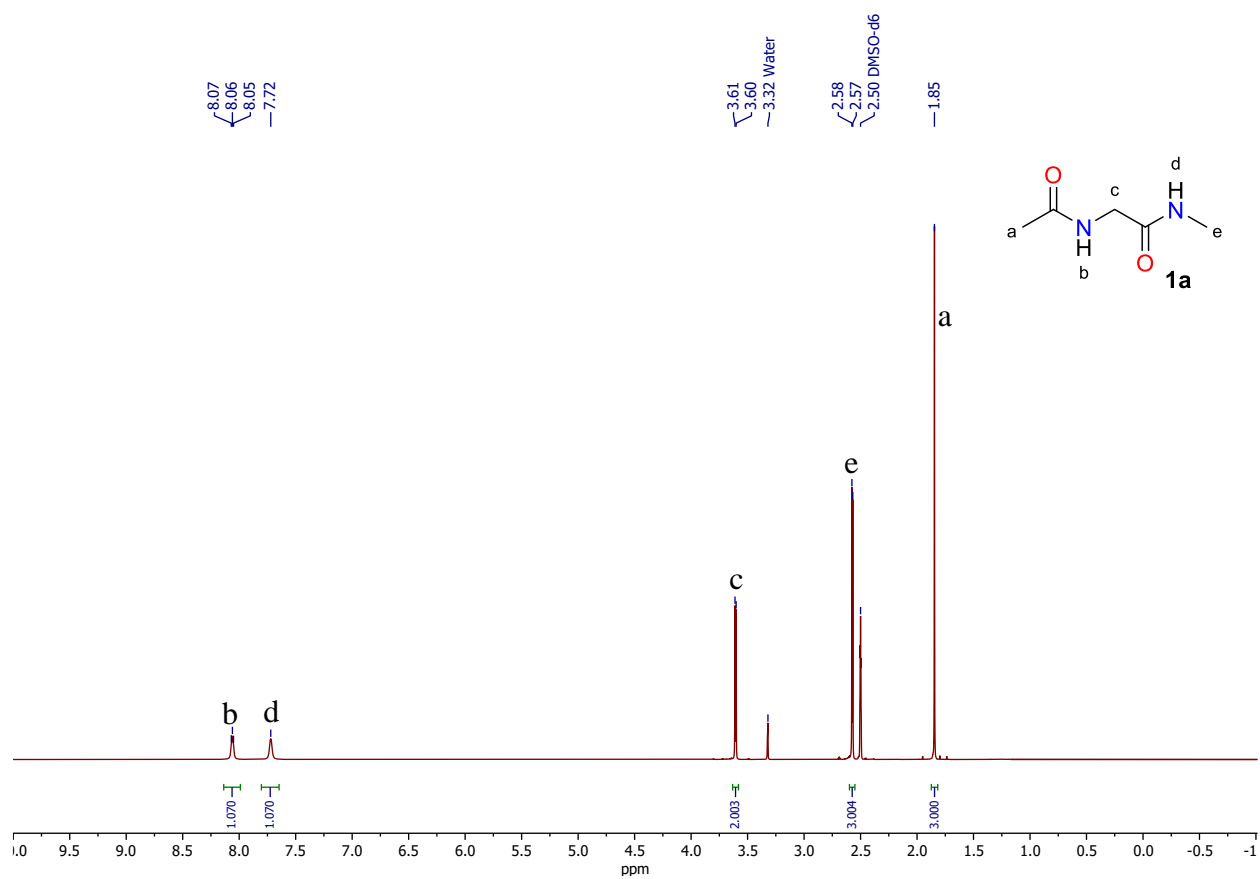


Fig. S65. ¹H NMR spectrum of DCHN (**2b**), CDCl₃, 400 MHz.



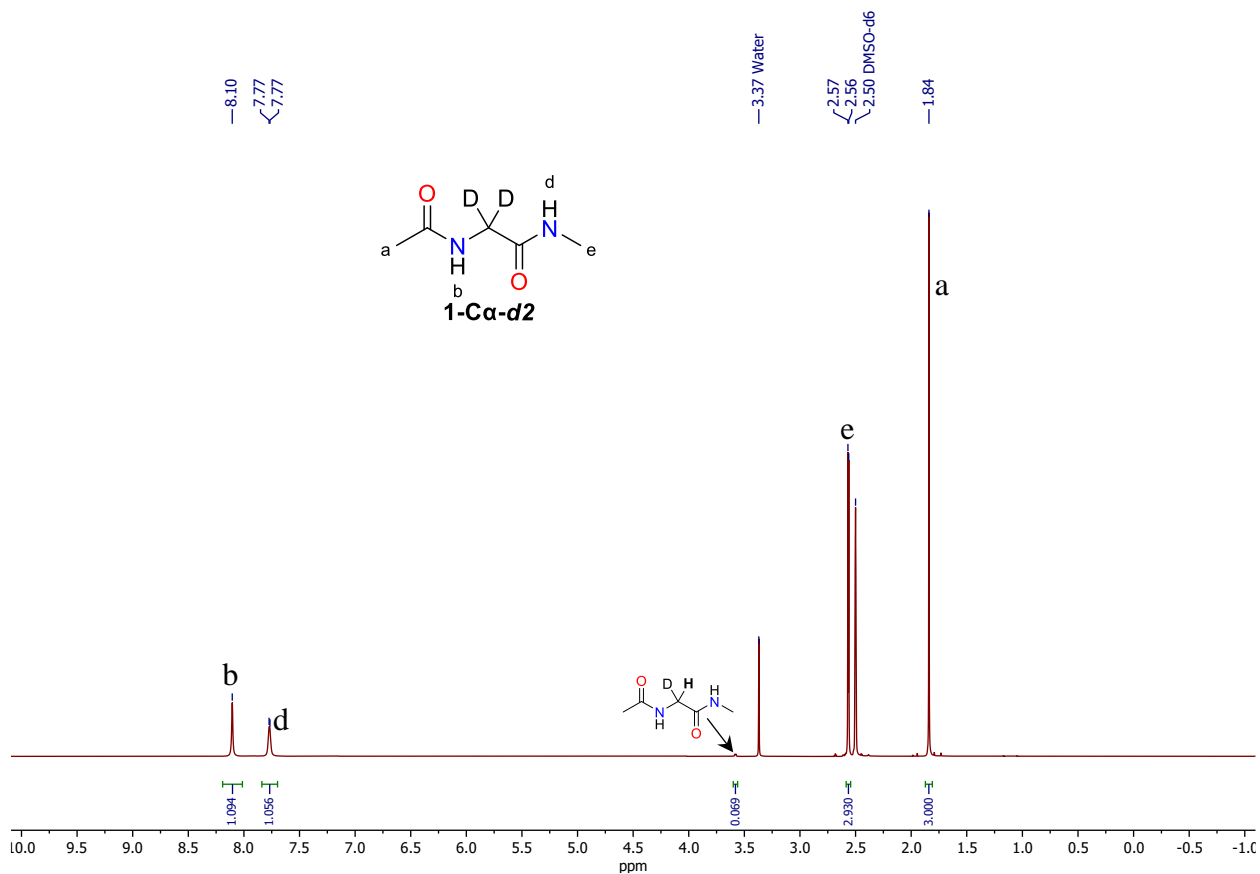


Fig. S68. ^1H NMR spectrum of **1-C α -d₂**, DMSO-*d*₆, 600 MHz.

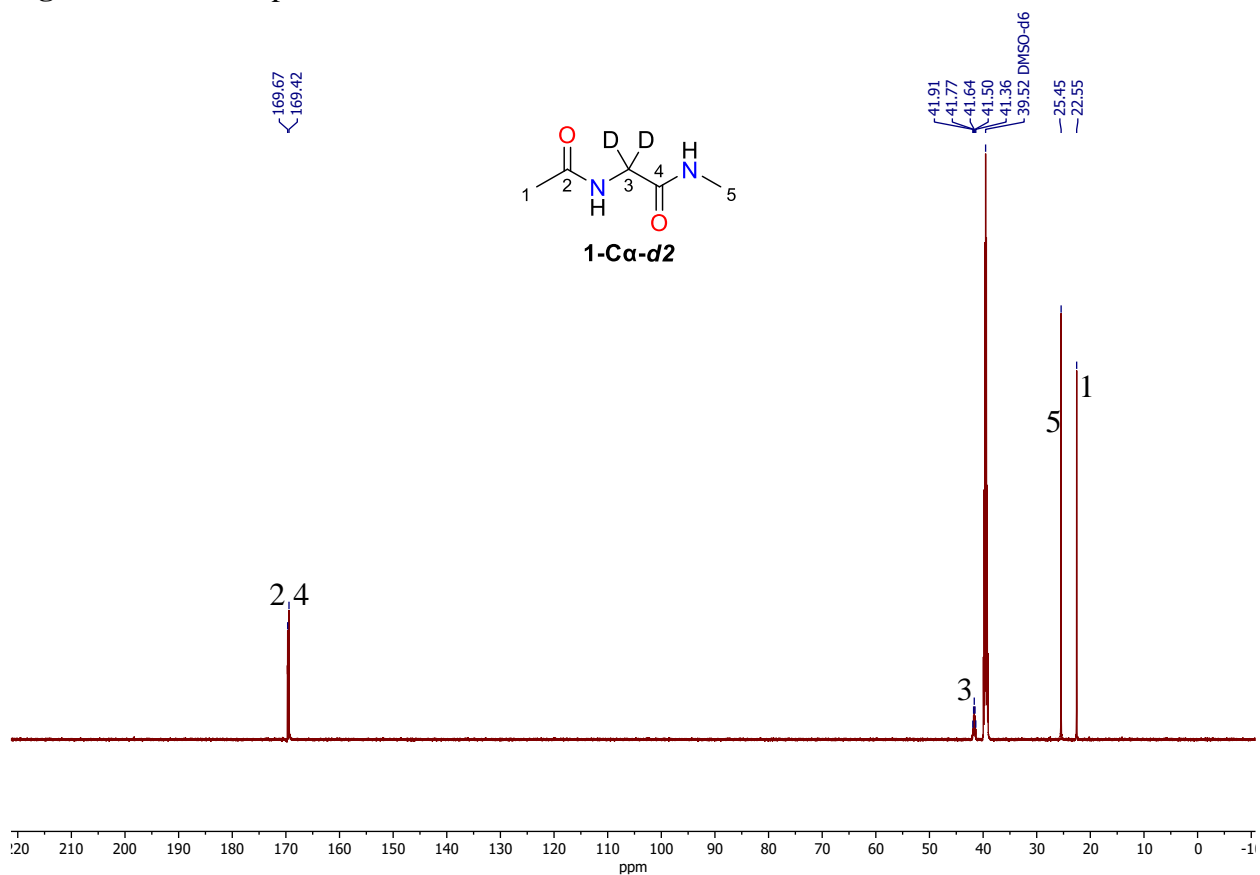


Fig. S69. ^{13}C NMR spectrum of **1-C α -d₂**, DMSO-*d*₆, 150 MHz.

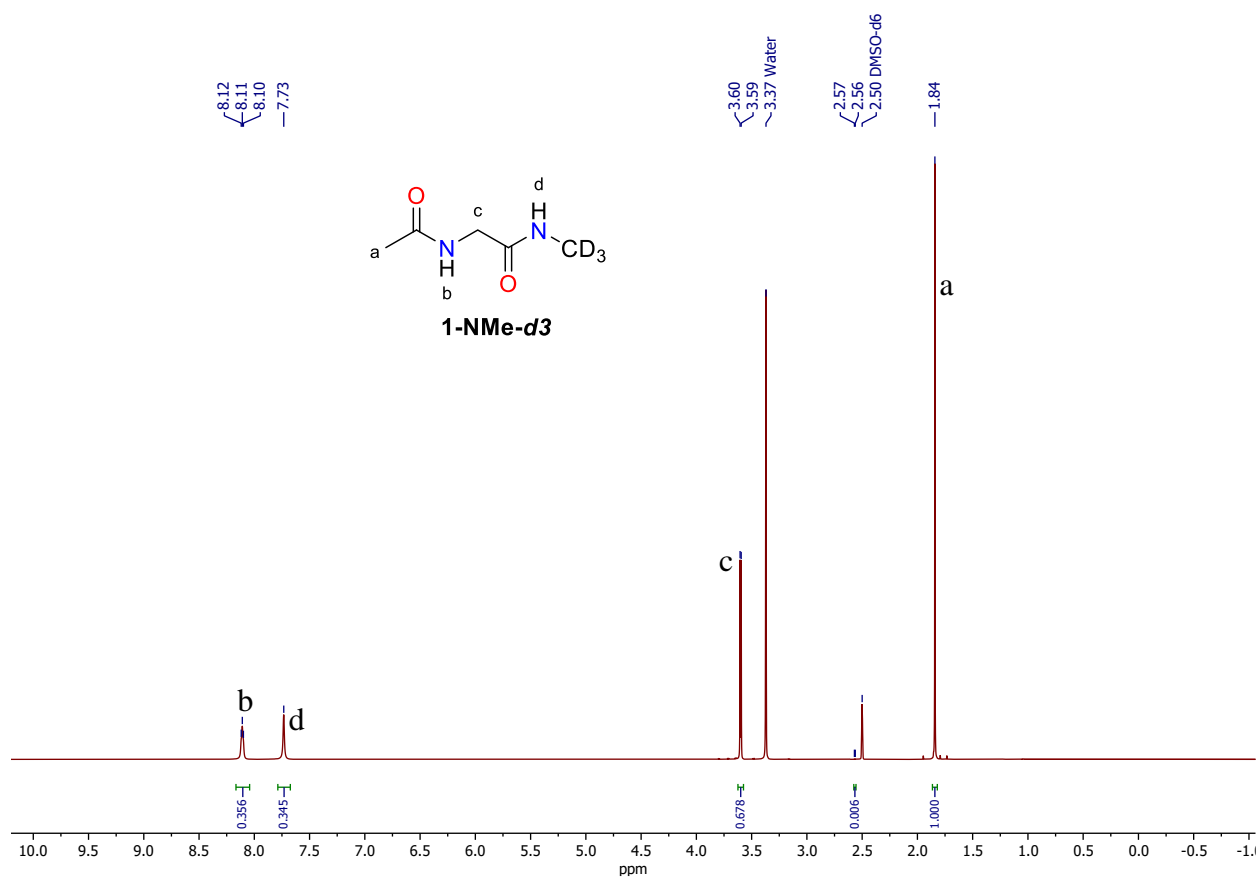


Fig. S70. ^1H NMR spectrum of **1-NMe-d3**, DMSO-d6, 600 MHz.

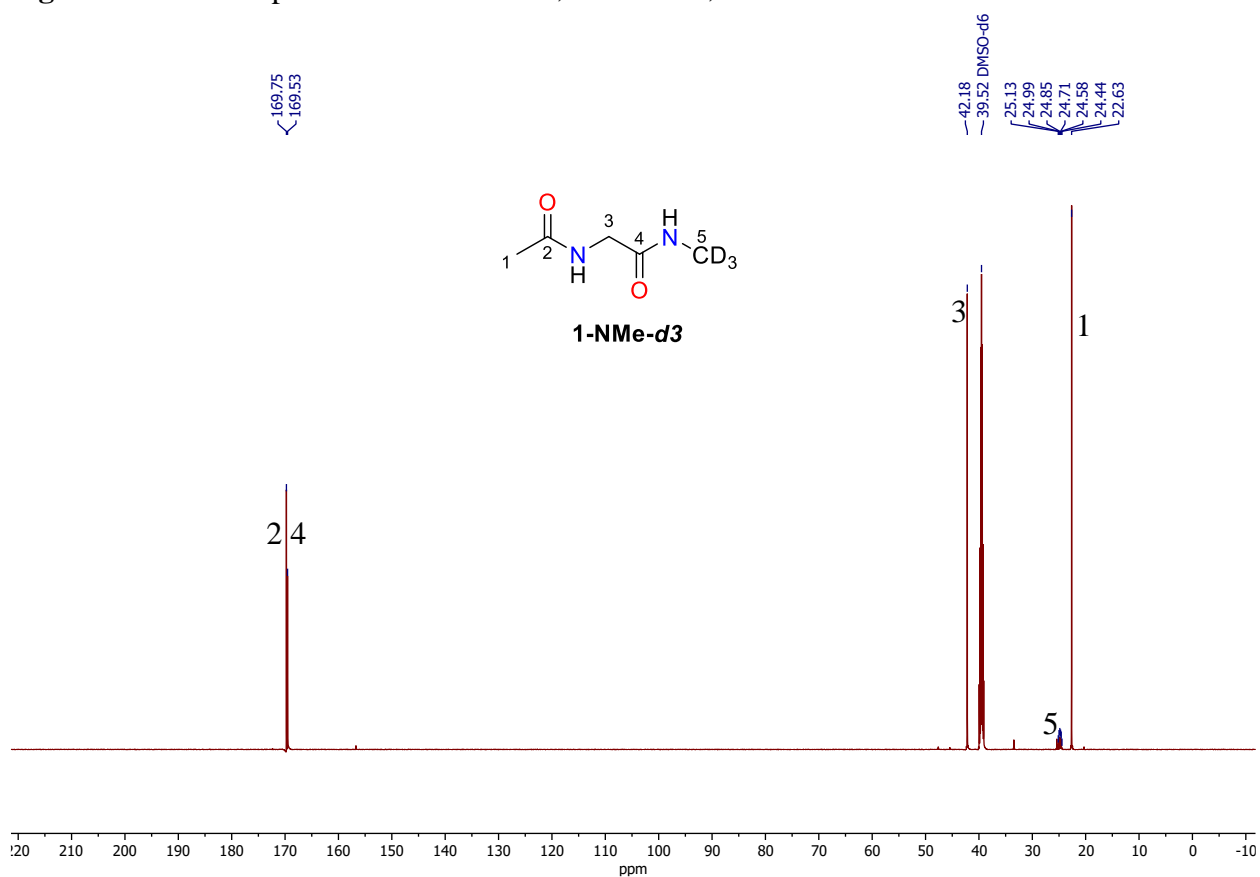


Fig. S71. ^{13}C NMR spectrum of **1-NMe-d3**, DMSO-d6, 150 MHz.

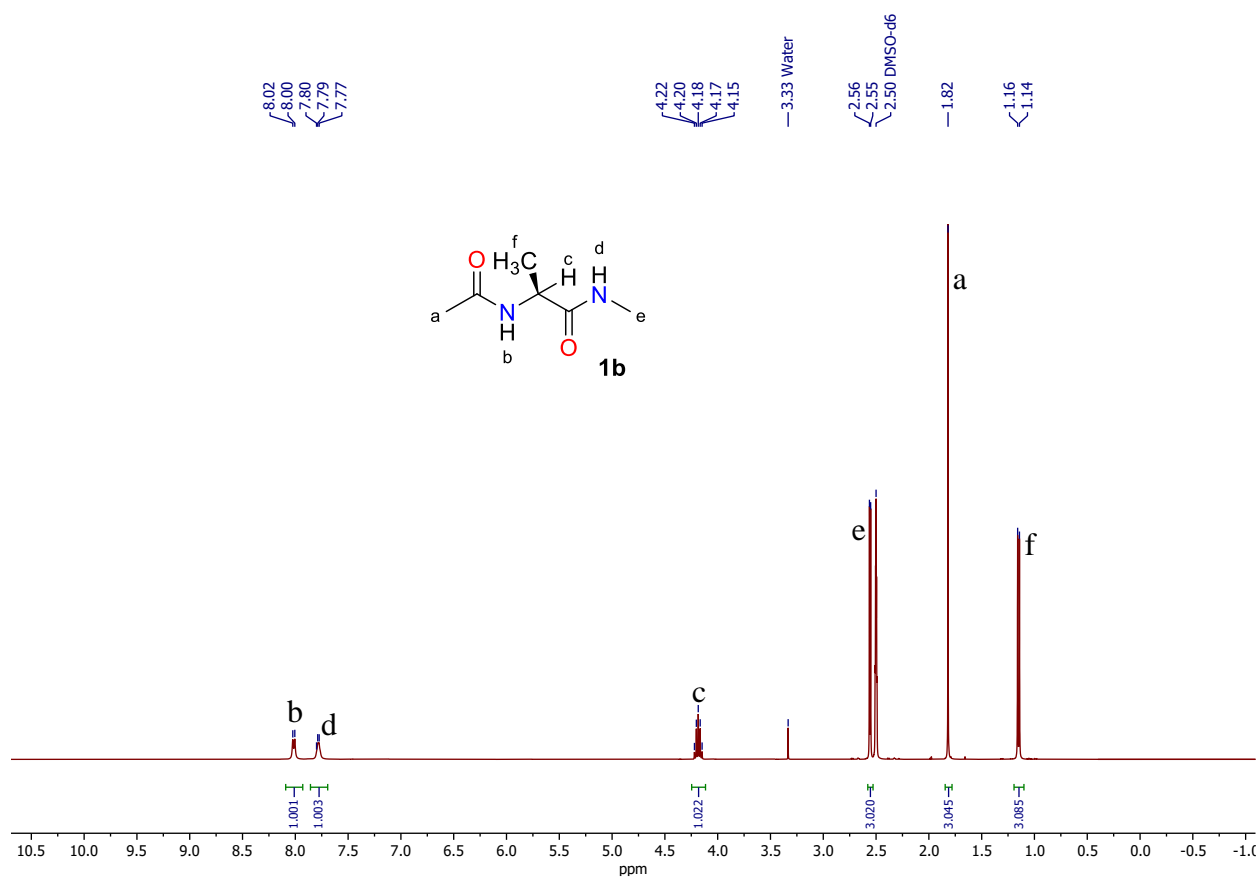


Fig. S72. ¹H NMR spectrum of *L*-AcAlaMe (**1b**), DMSO-*d*₆, 400 MHz.

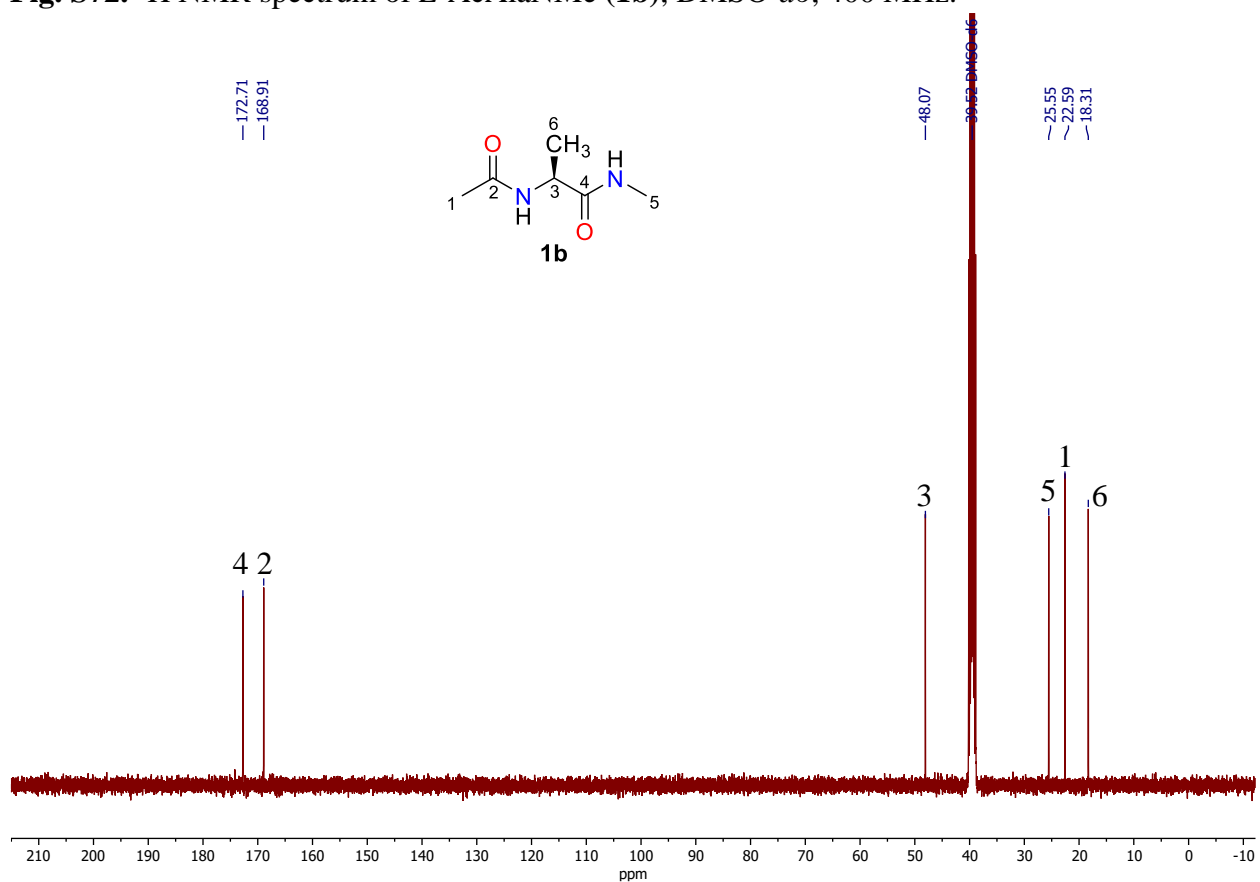
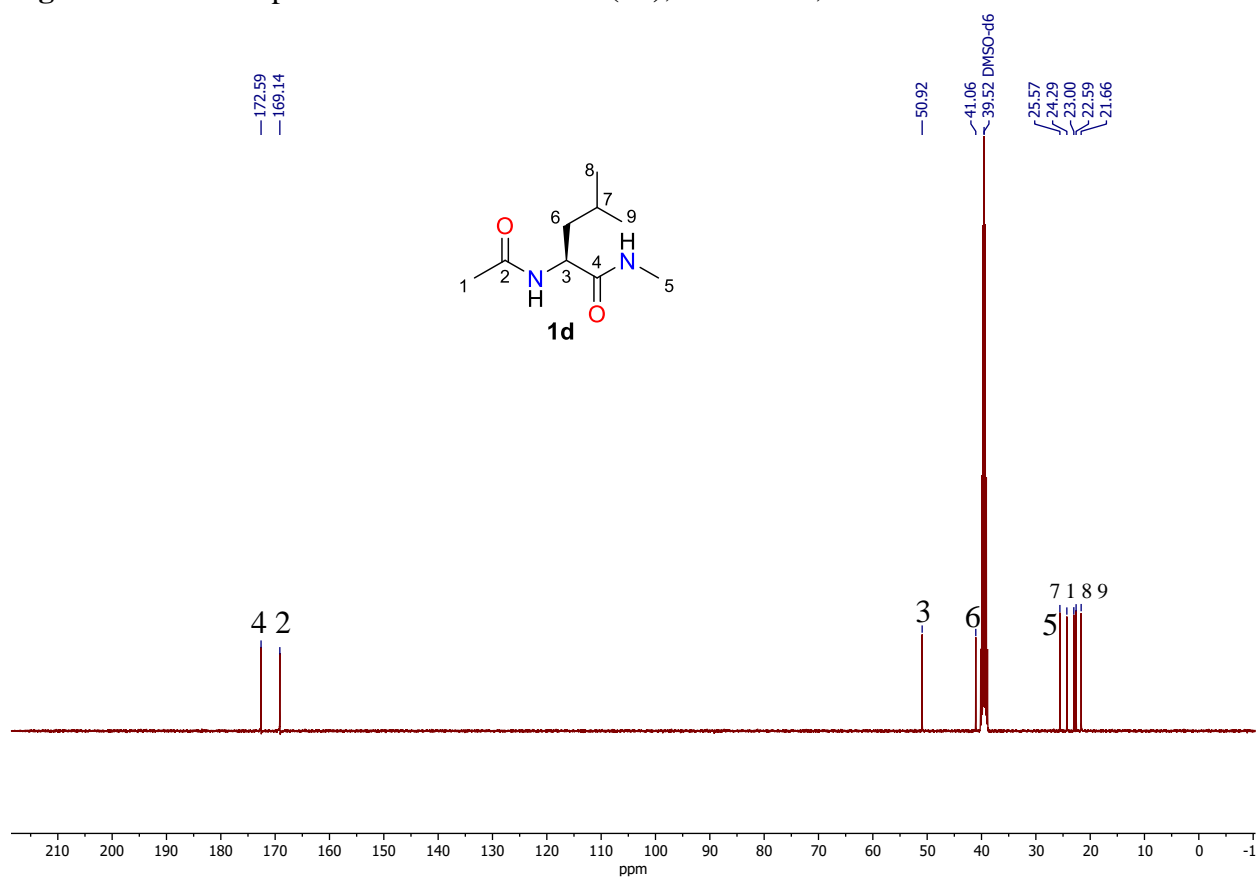
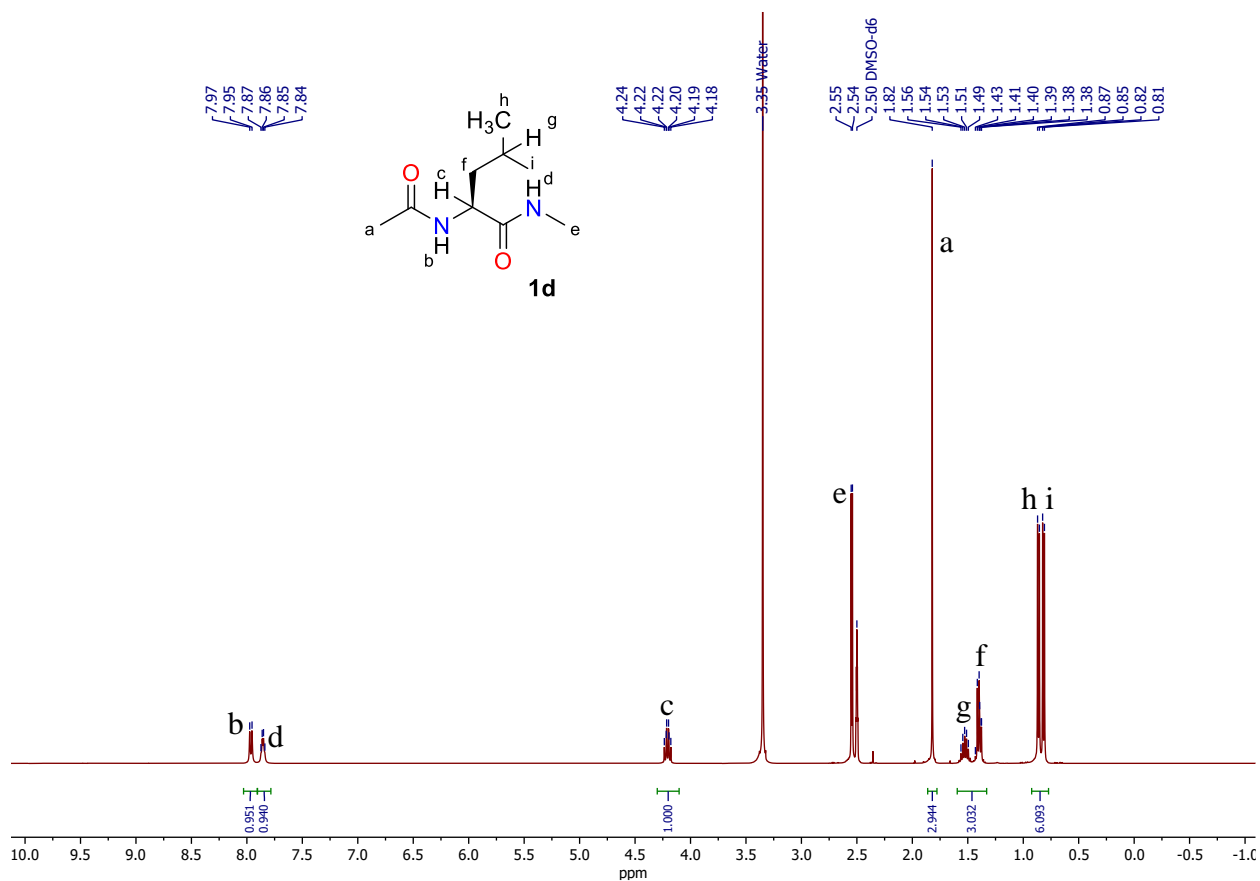


Fig. S73. ¹³C NMR spectrum of *L*-AcAlaMe (**1b**), DMSO-*d*₆, 101 MHz.



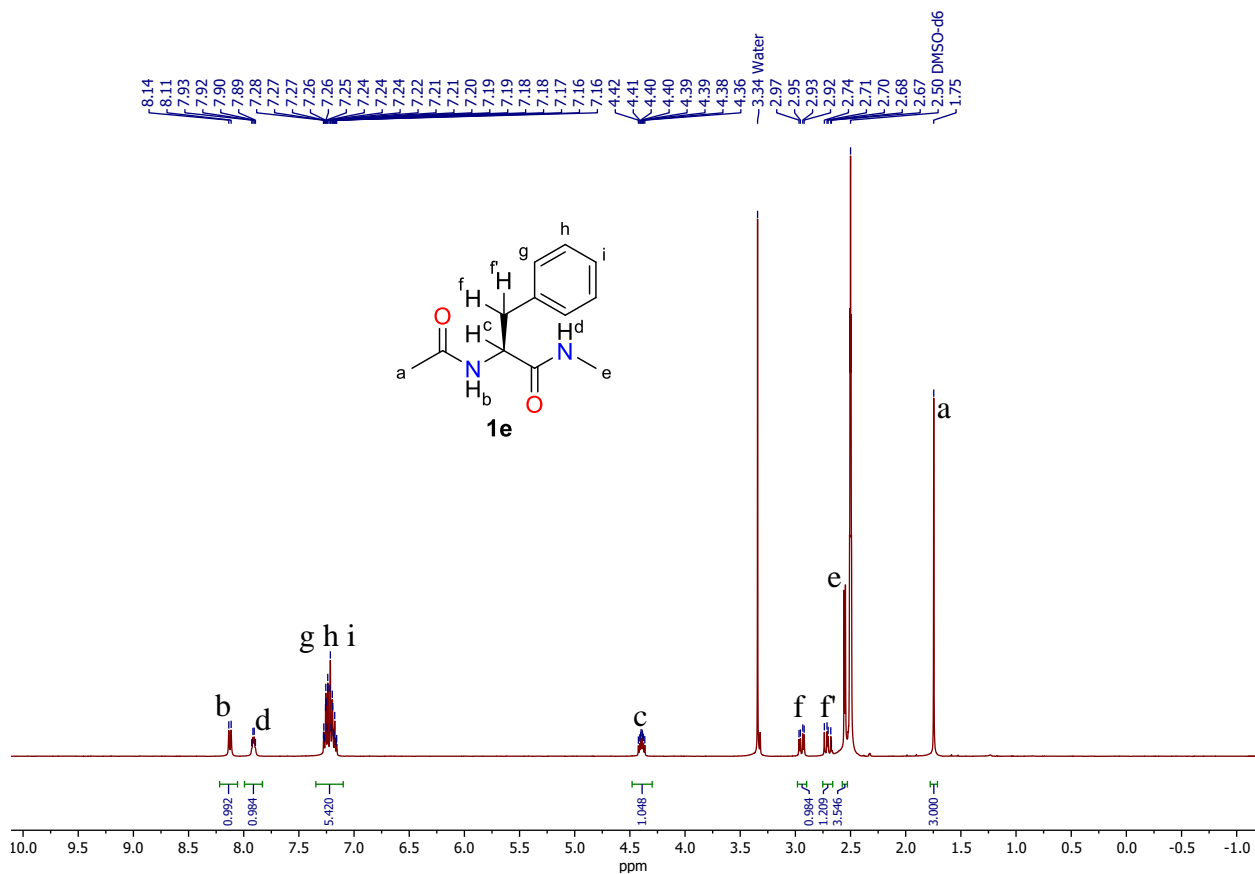


Fig. S76. ¹H NMR spectrum of *L*-AcPhenMe (**1e**), DMSO-*d*₆, 400 MHz.

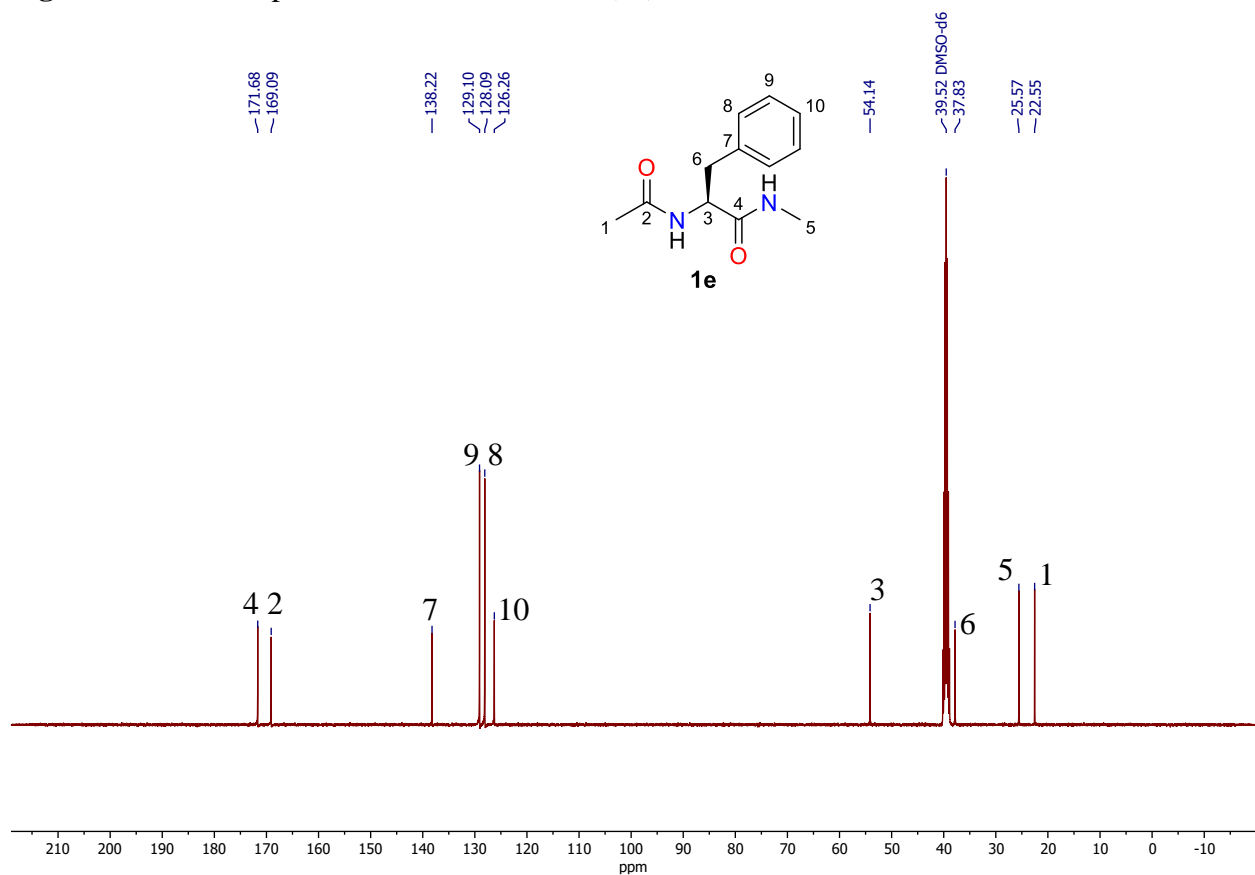


Fig. S77. ¹³C NMR spectrum of *L*-AcPhenMe (**1e**), DMSO-*d*₆, 101 MHz.

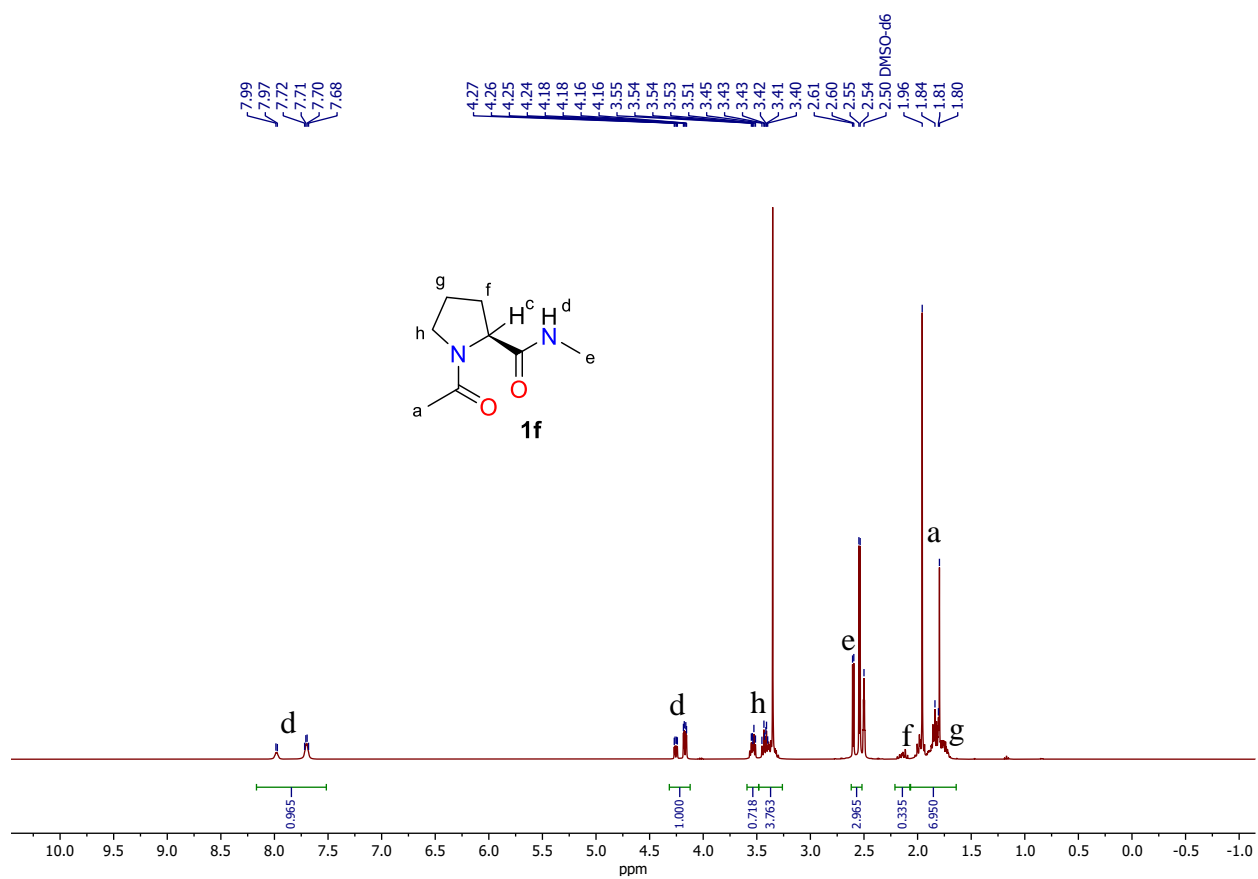


Fig. S78. ^1H NMR spectrum of *L*-AcProNMe (**1f**), DMSO- d_6 , 400 MHz.

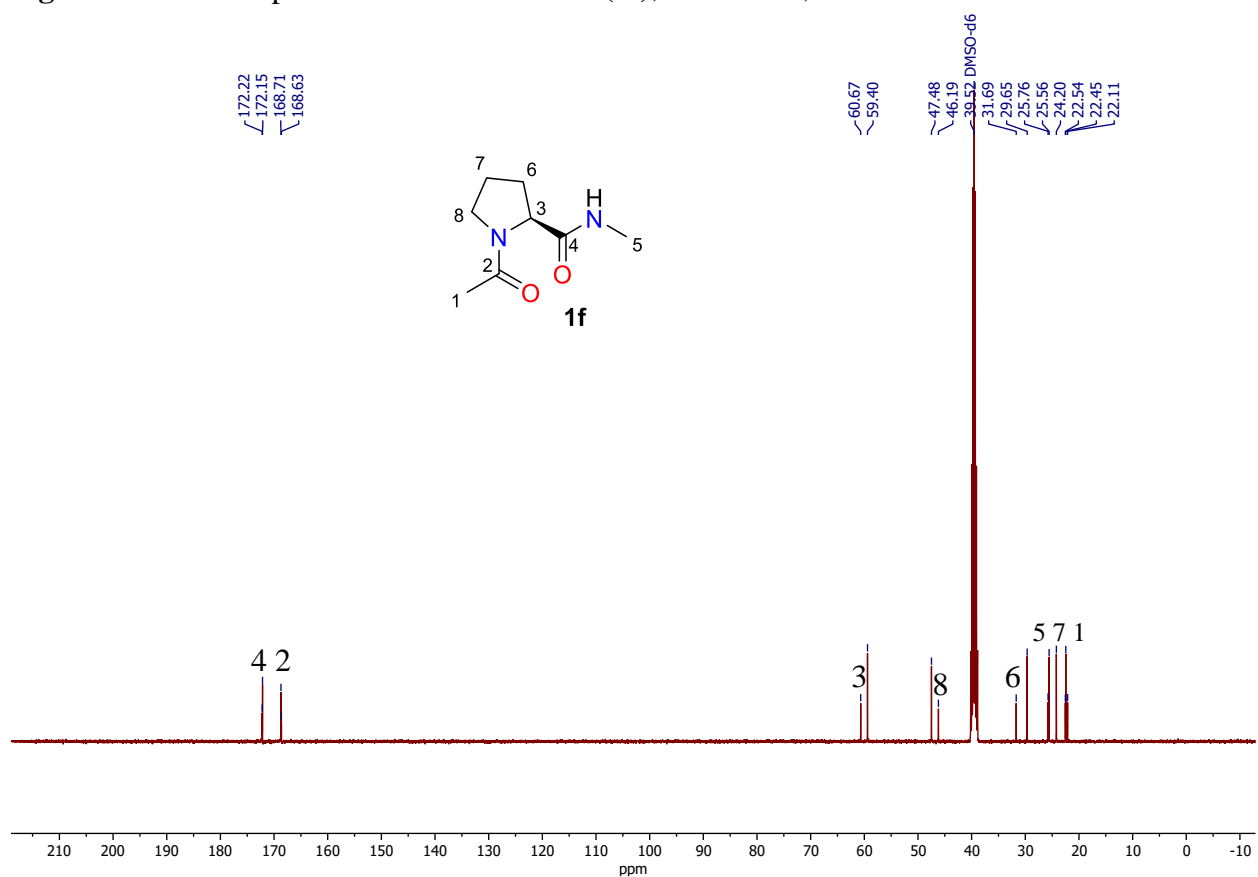


Fig. S79. ^{13}C NMR spectra of *L*-AcProNMe (**1f**), DMSO- d_6 , 101 MHz.

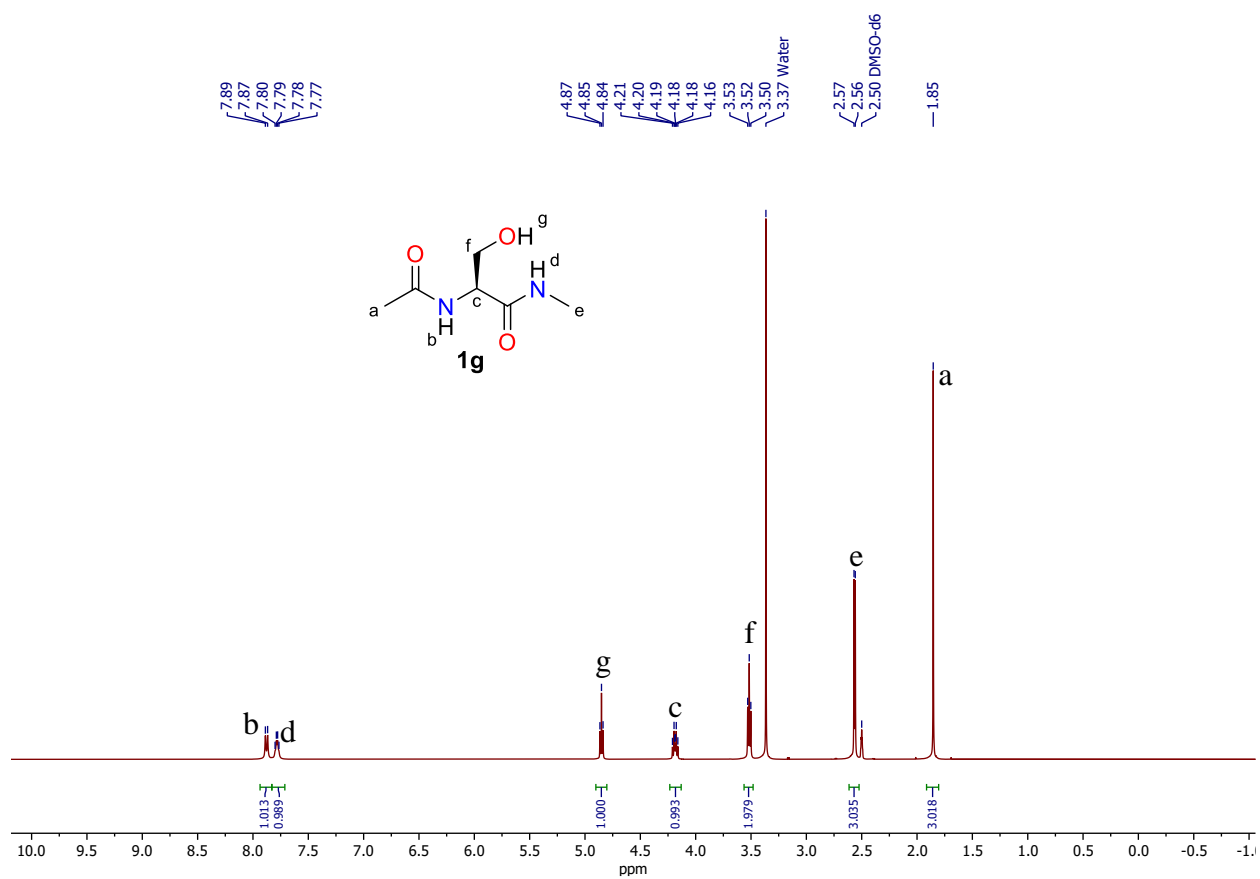


Fig. S80. ¹H NMR spectrum of *L*-AcSerNMe (**1g**), DMSO-*d*₆, 400 MHz.

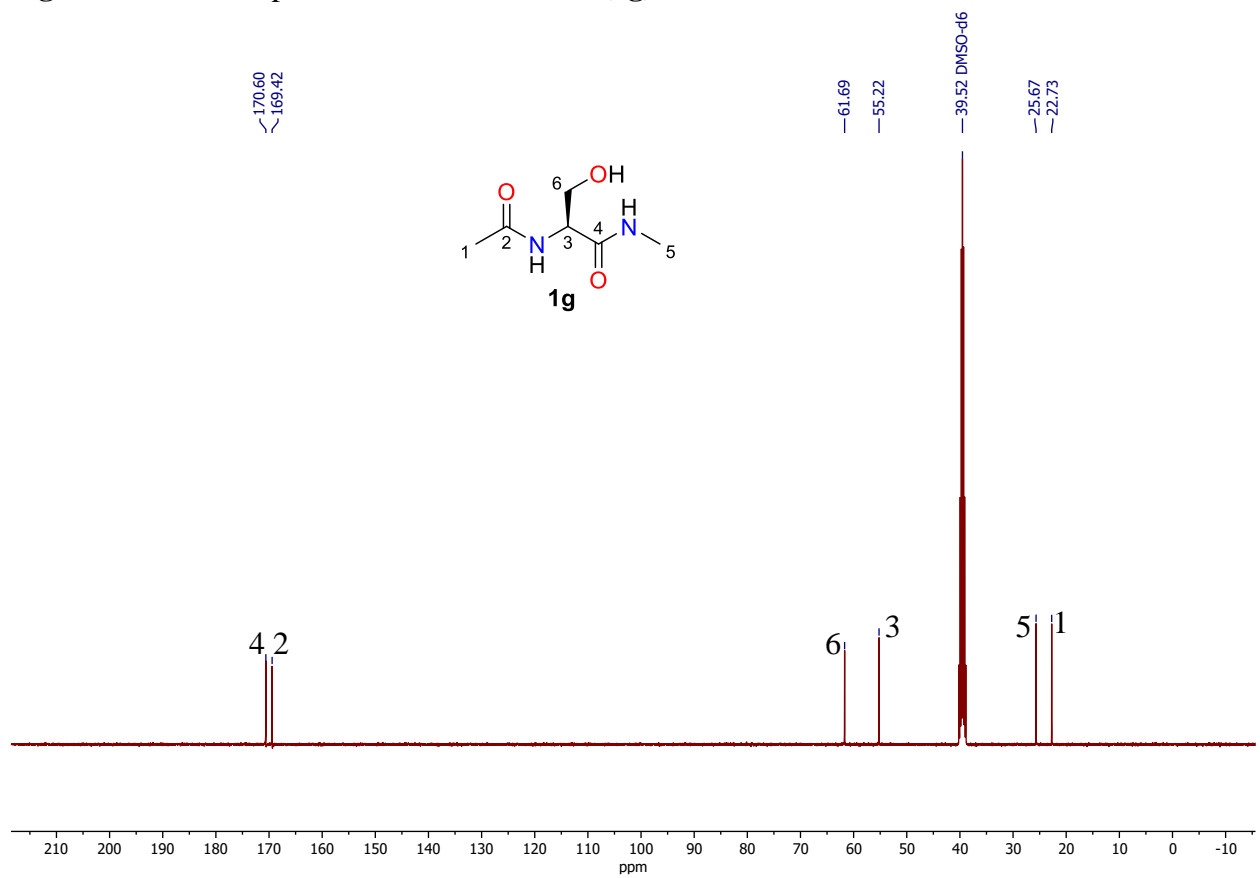


Fig. S81. ¹³C NMR spectrum of *L*-AcSerNMe (**1g**), DMSO-*d*₆, 101 MHz.

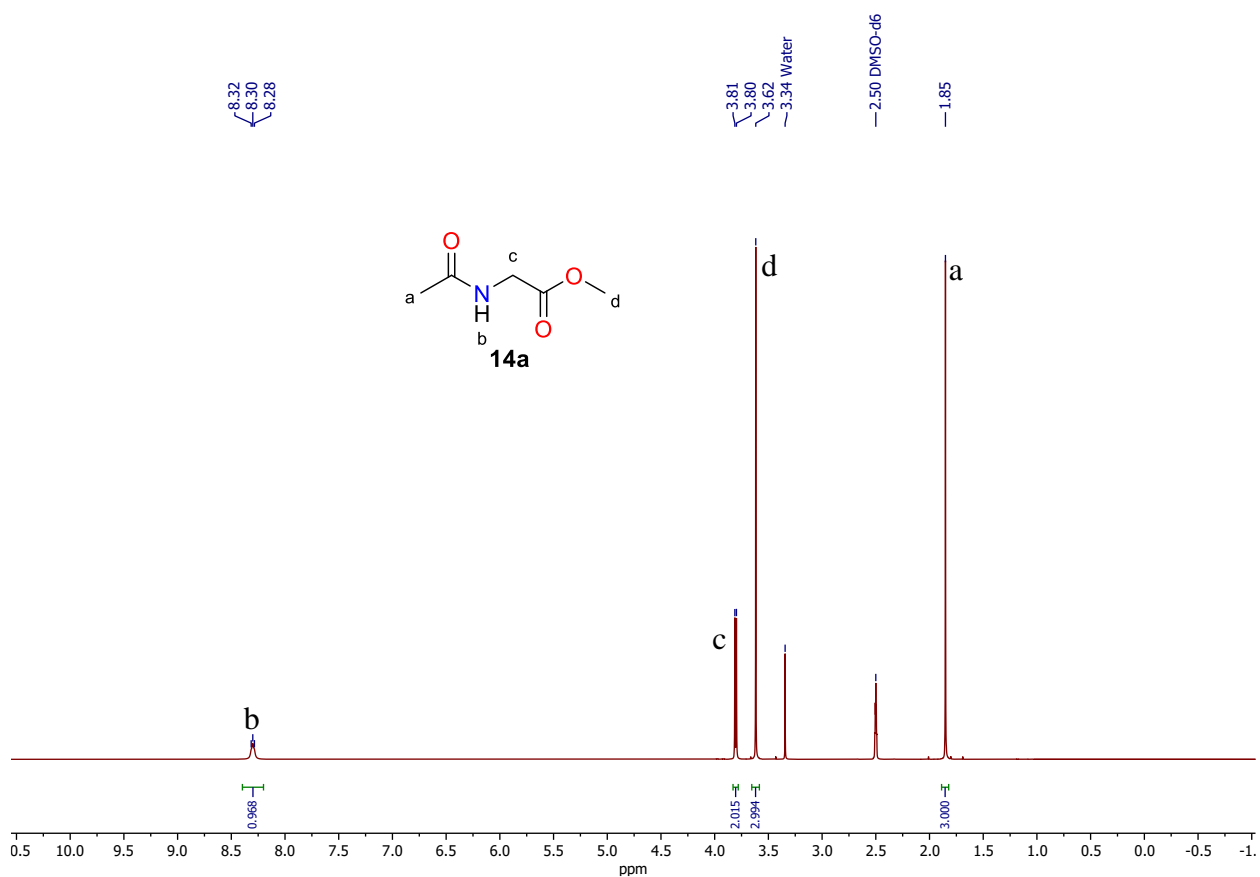


Fig. S82. ^1H NMR spectrum of AcGlyOMe (**14a**), DMSO- d_6 , 400 MHz.

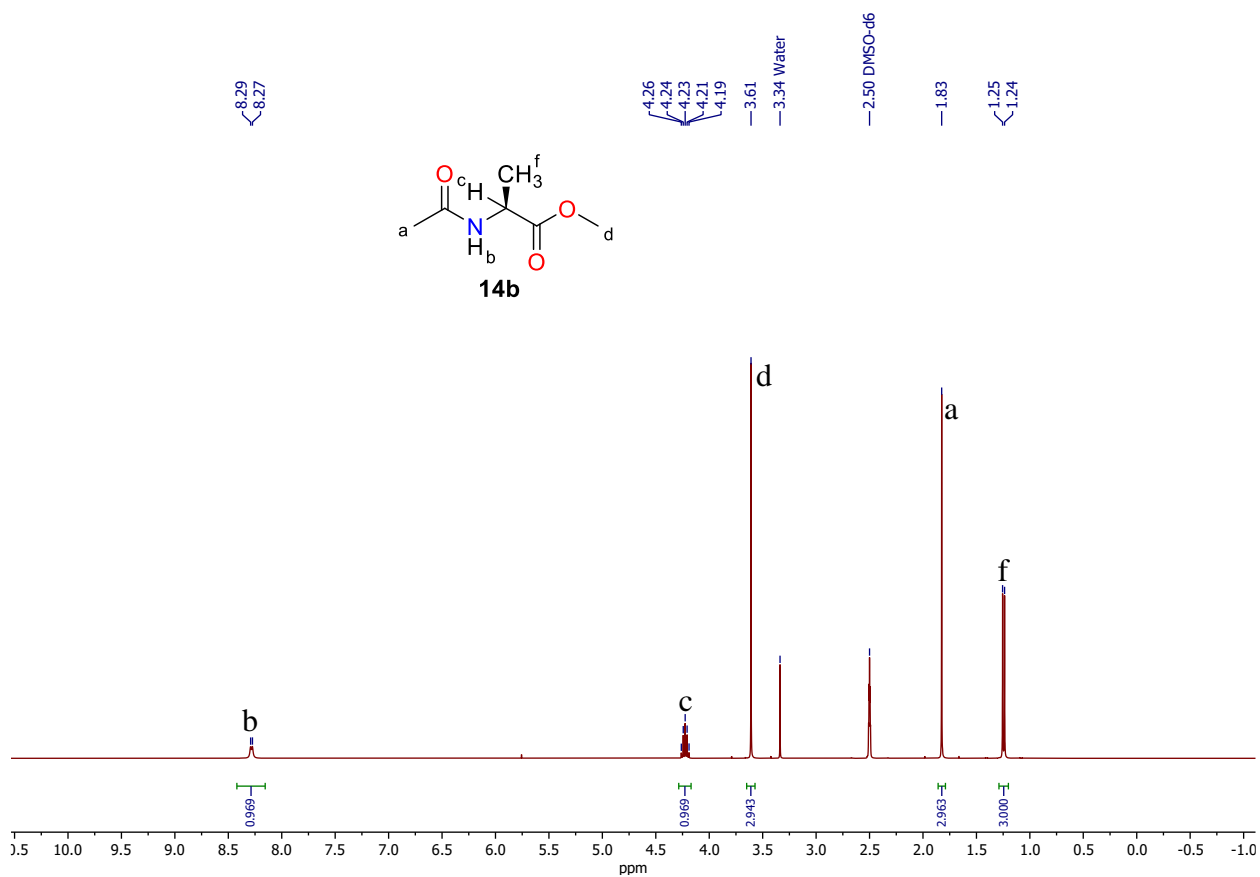


Fig. S83. ^1H NMR spectrum of *L*-AcAlaOMe (**14b**), DMSO- d_6 , 400 MHz.

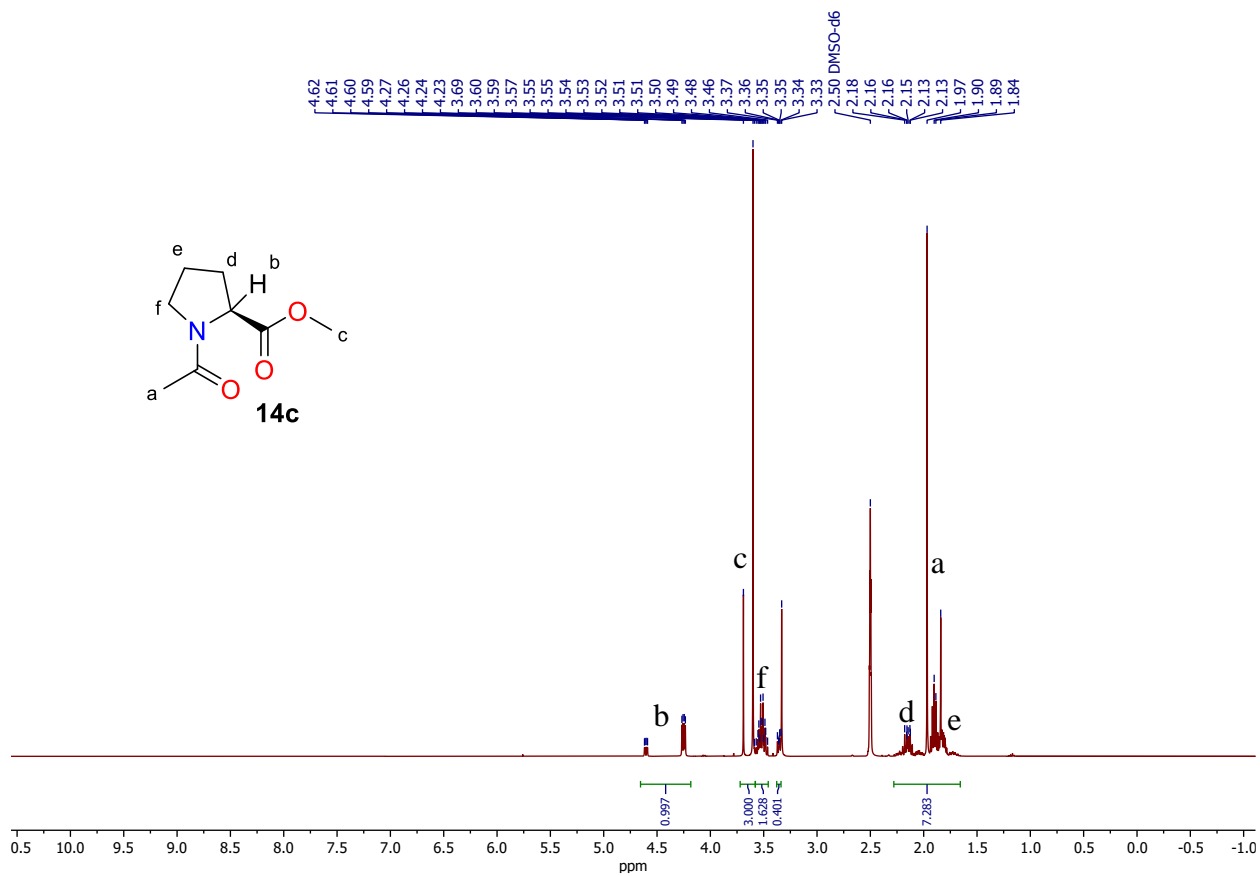
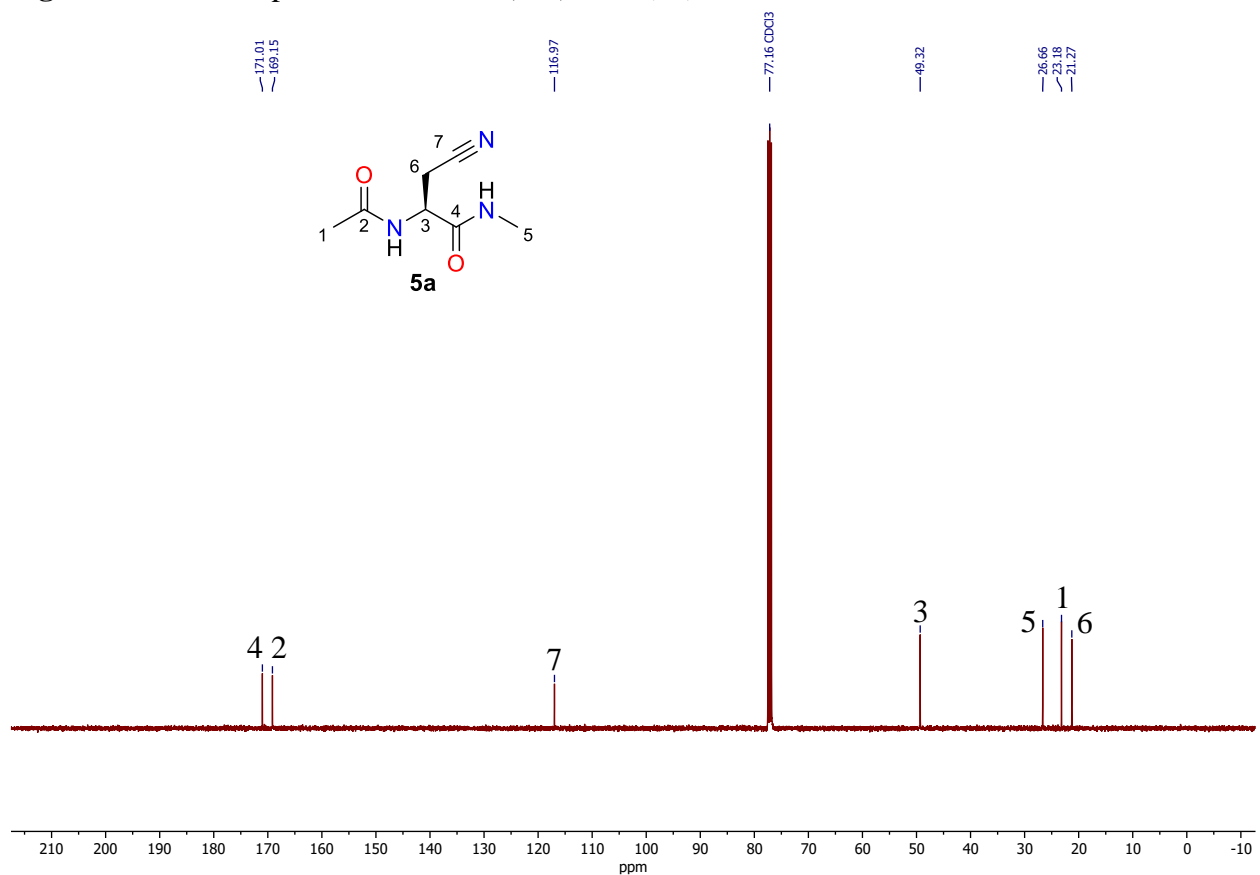
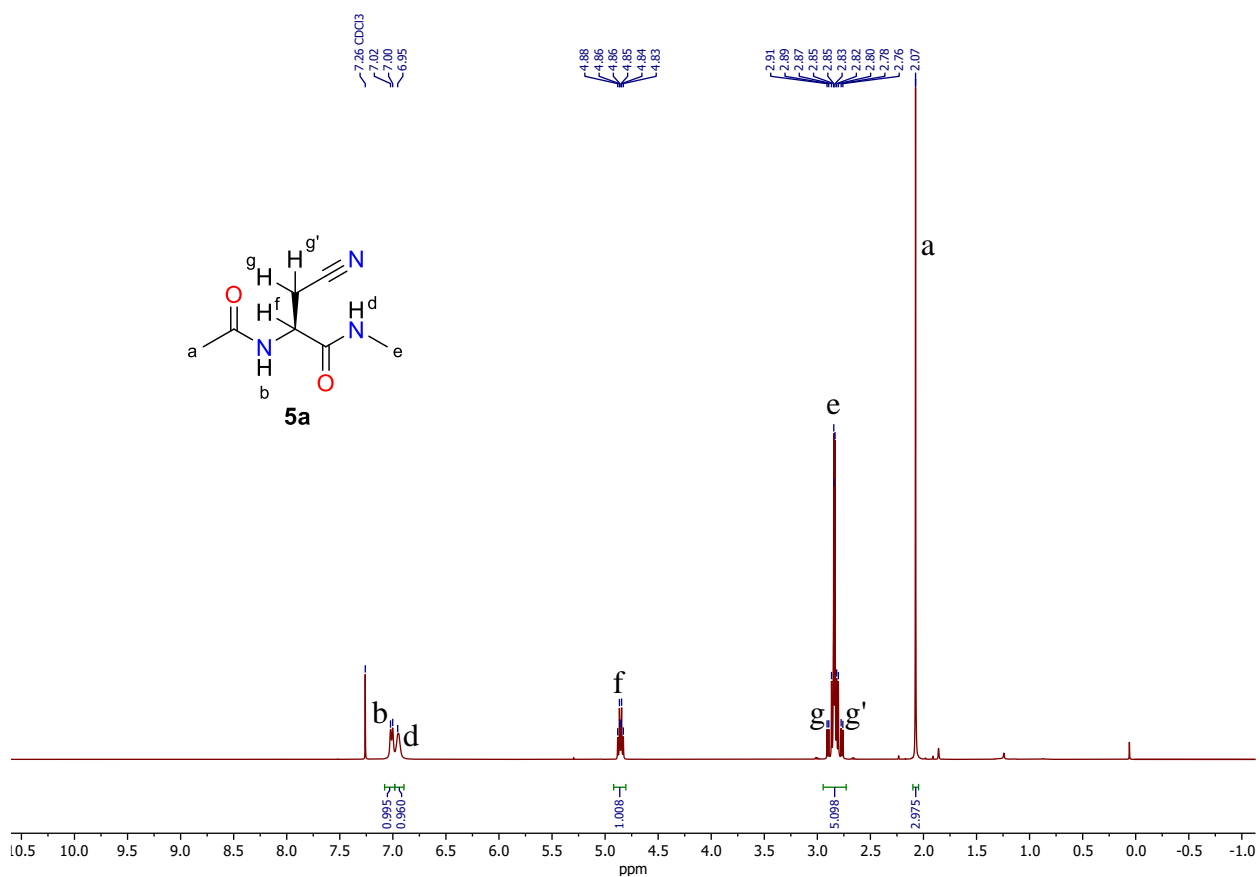


Fig. S84. ¹H NMR spectrum of *L*-AcProOMe (**14c**), DMSO-*d*₆, 400 MHz.



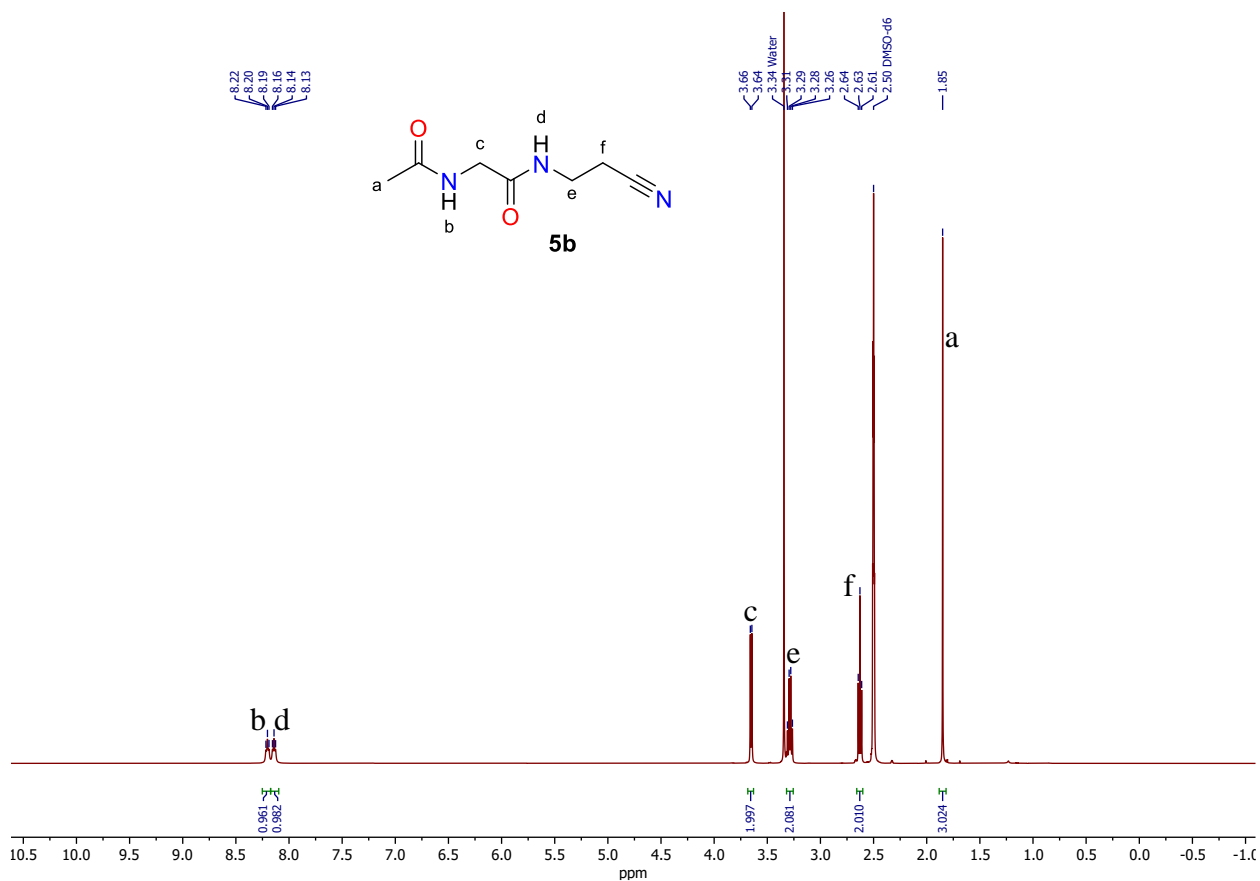


Fig. S87. ¹H NMR spectrum of AcGlyNEtCN (**5b**), DMSO-*d*₆, 400 MHz.

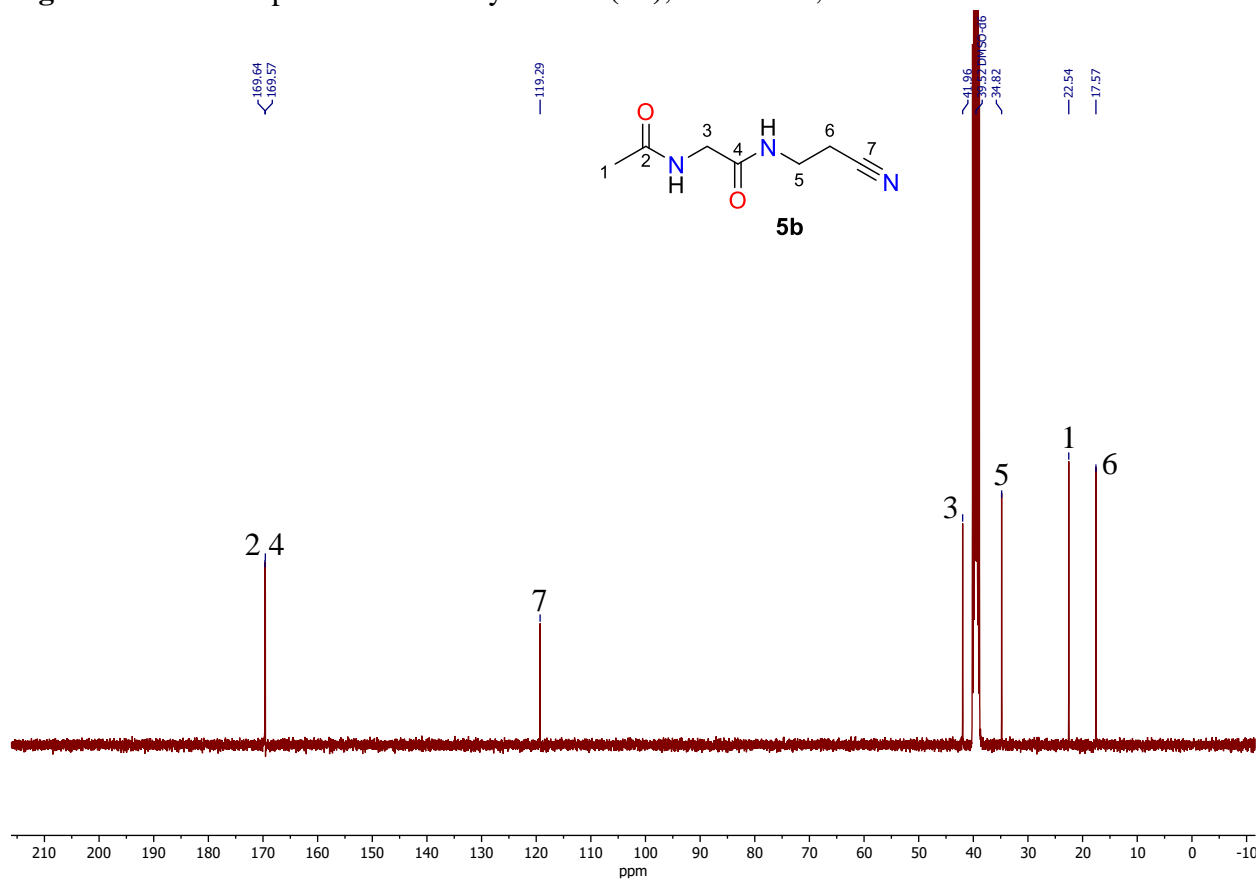
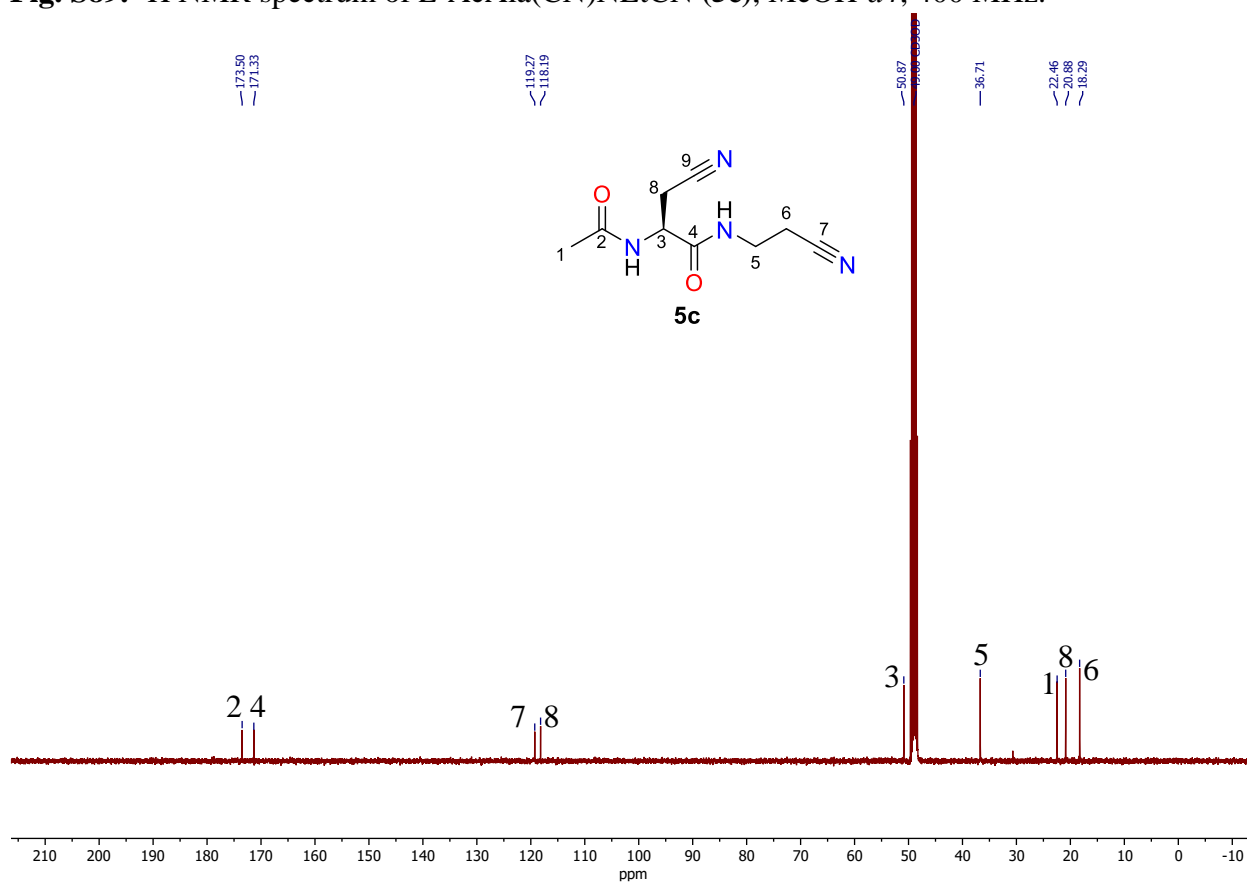
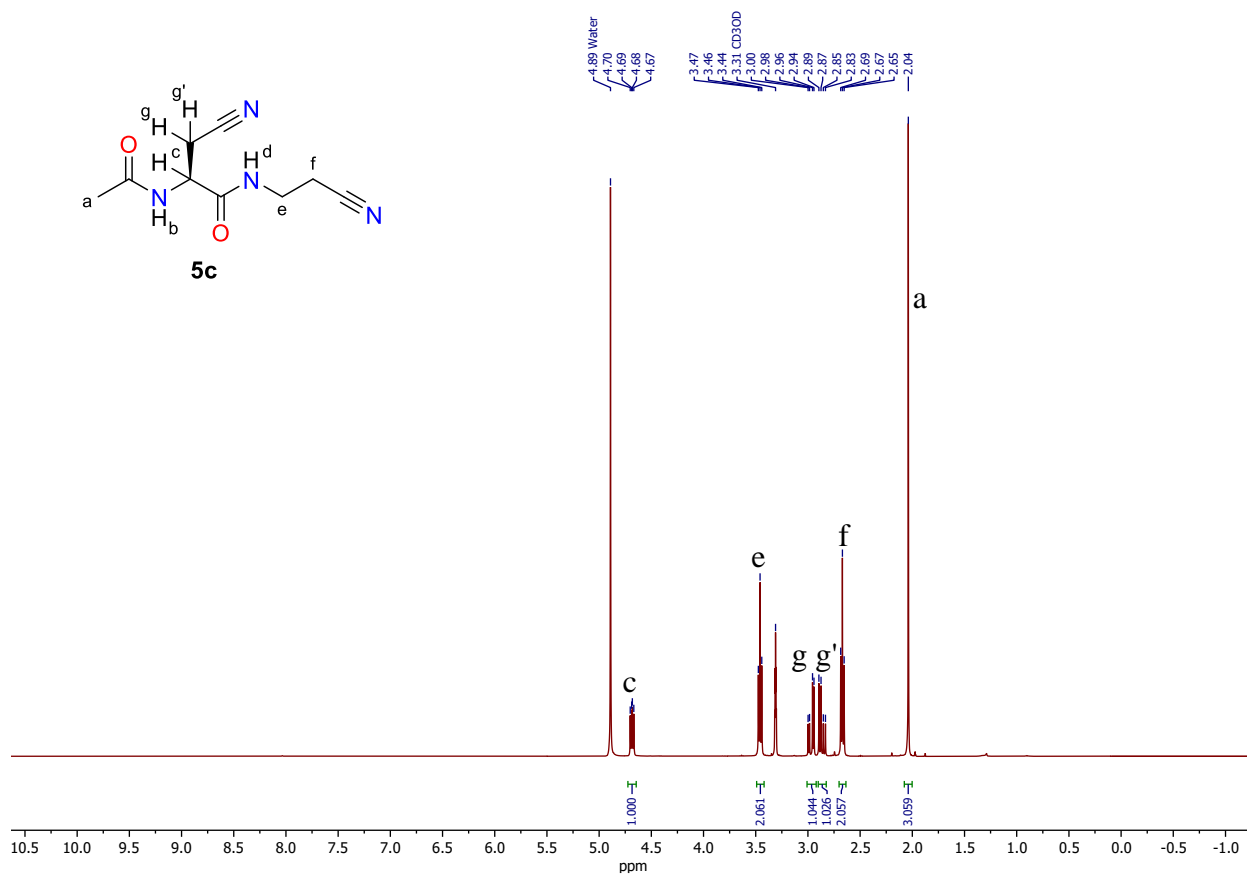


Fig. S88. ¹³C NMR spectrum of AcGlyNEtCN (**5b**), DMSO-*d*₆, 101 MHz.



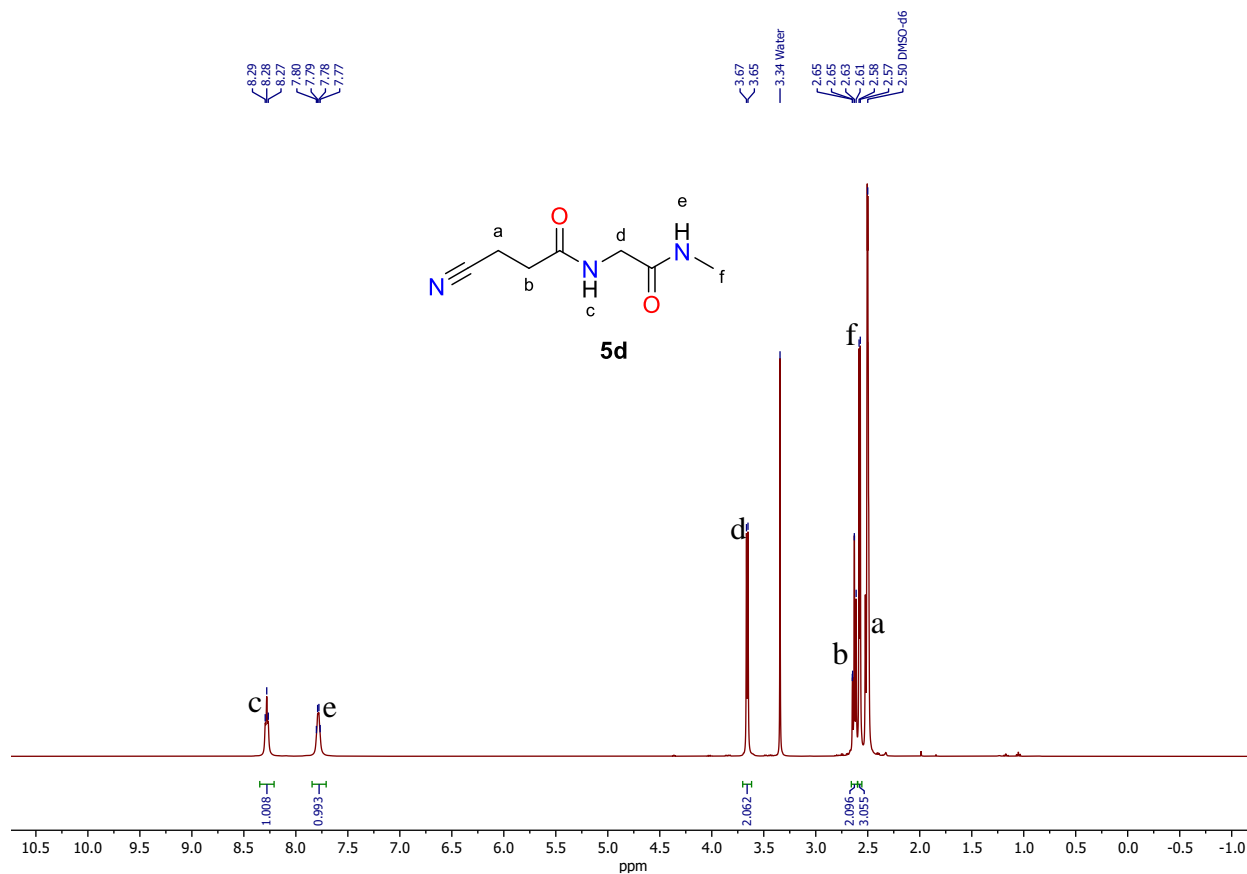


Fig. S91. ^1H NMR spectrum of NCEtCOGlyNMe (**5d**), DMSO- d_6 , 400 MHz.

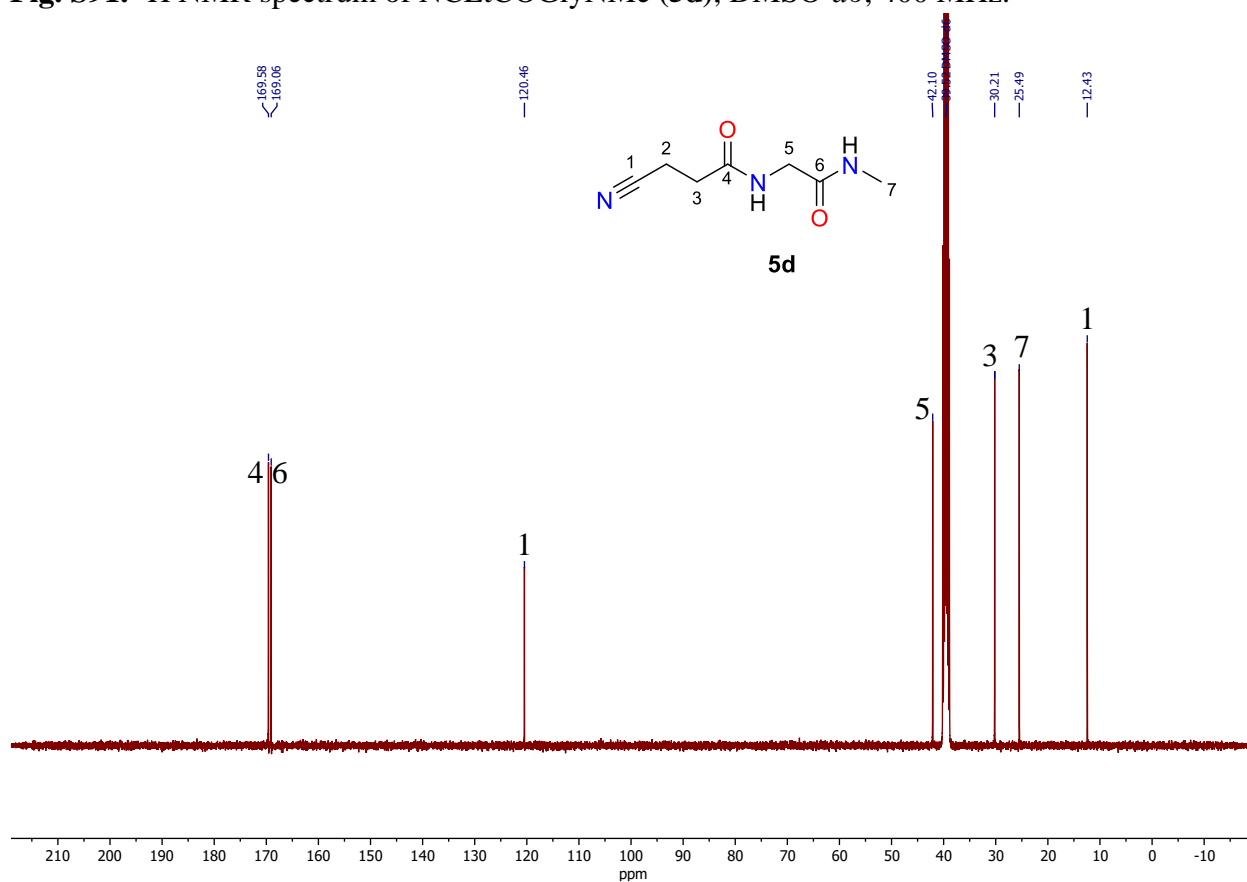


Fig. S92. ^{13}C NMR spectrum of NCEtCOGlyNMe (**5d**), DMSO- d_6 , 101 MHz.

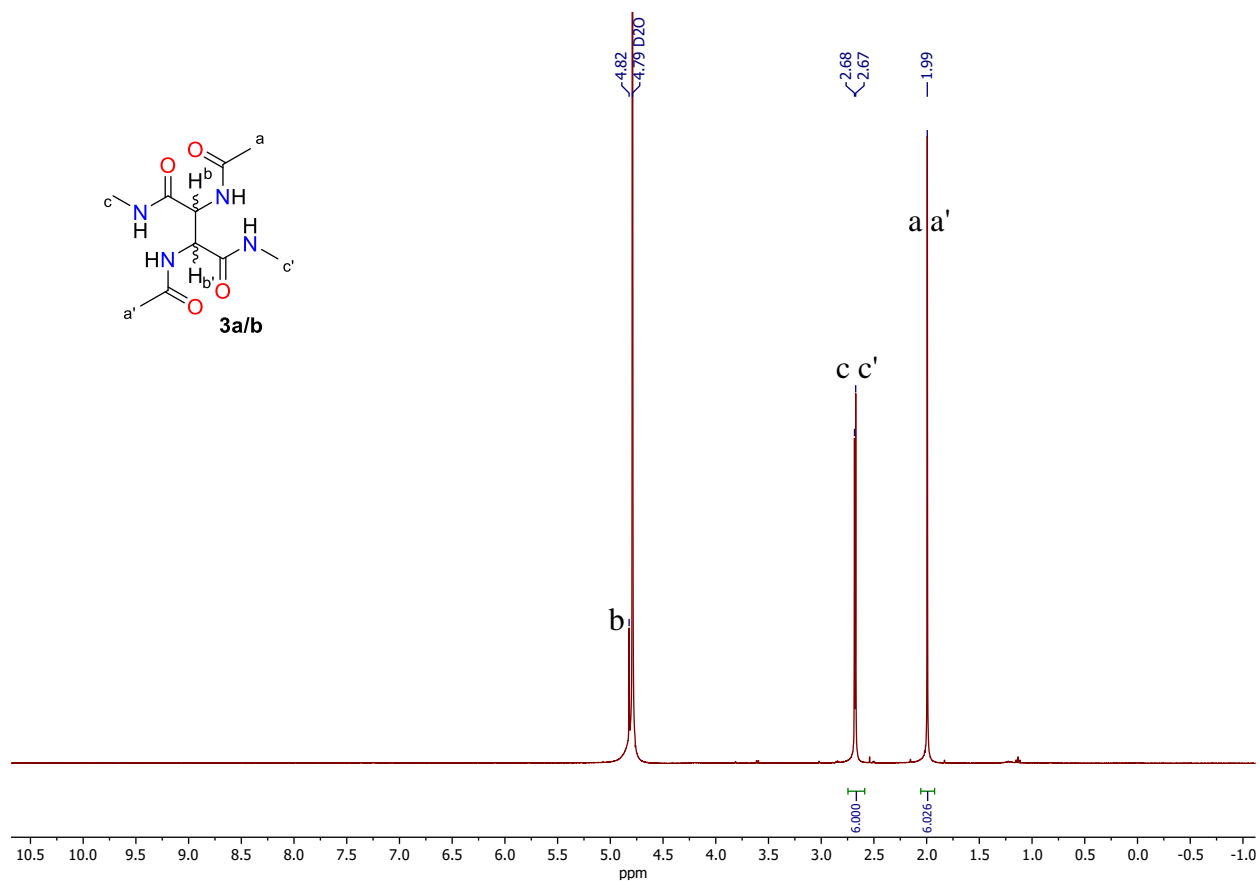


Fig. S93. ^1H NMR spectrum of dimer **3a/b**, D_2O , 400 MHz.

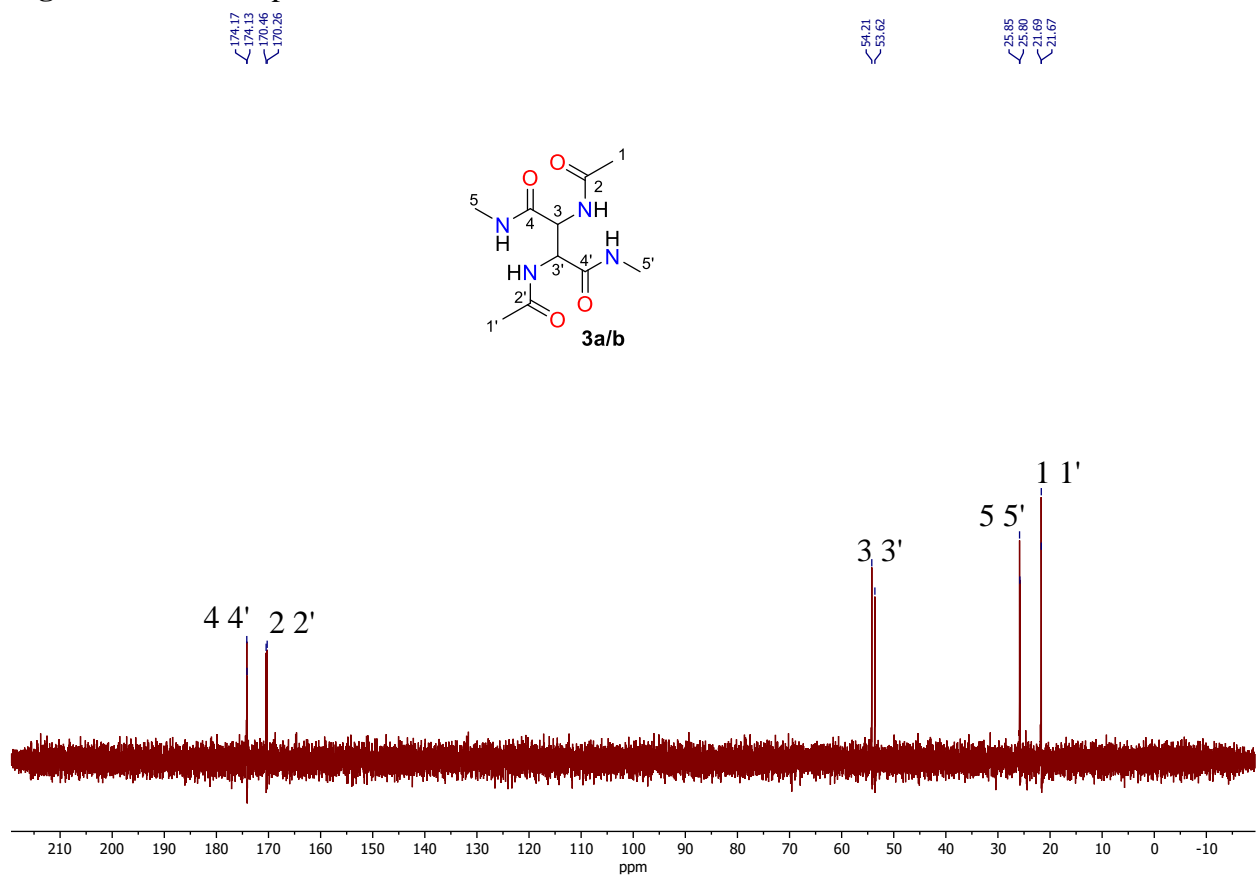


Fig. S94. ^{13}C NMR spectrum of dimer **3a/b**, D_2O , 101 MHz.

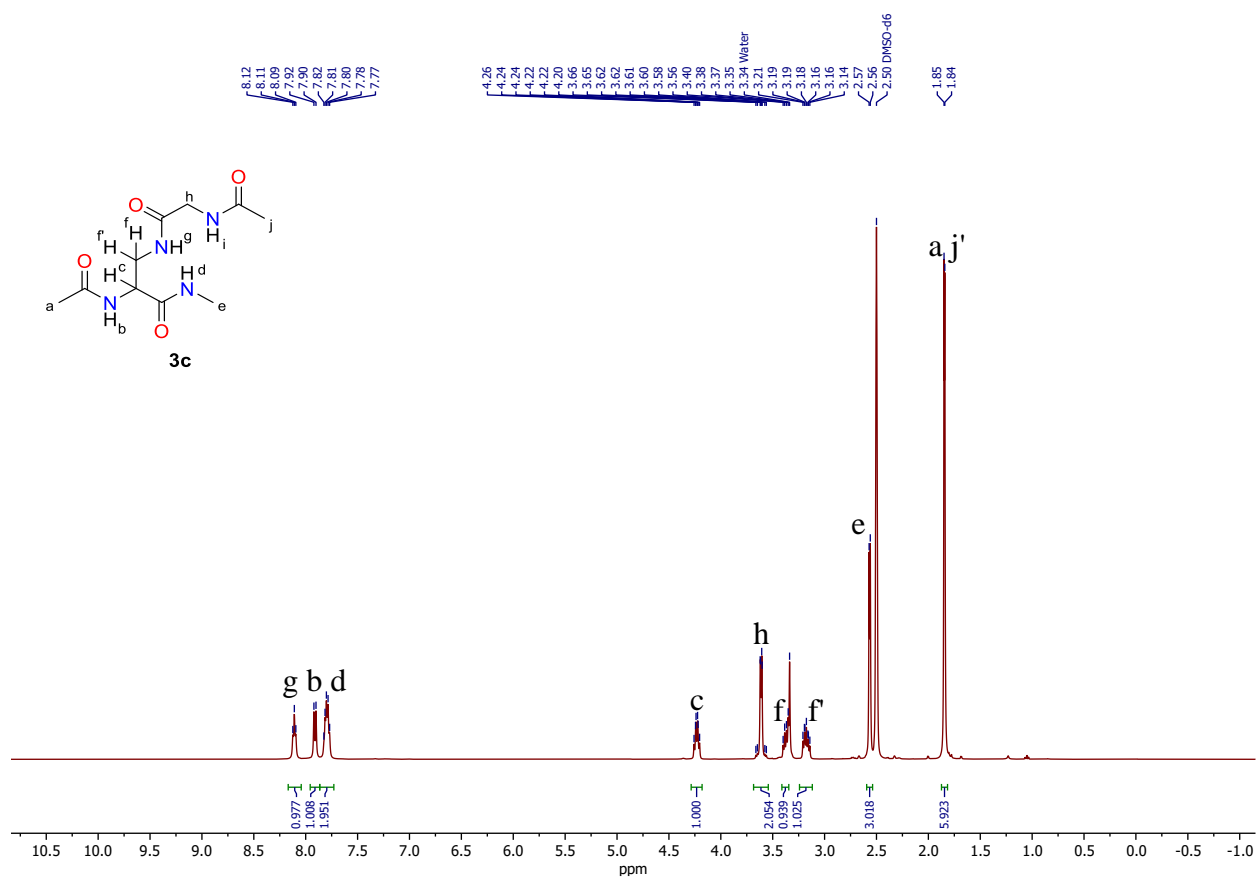


Fig. S95. ¹H NMR spectrum of dimer **3c**, DMSO-*d*₆, 400 MHz.

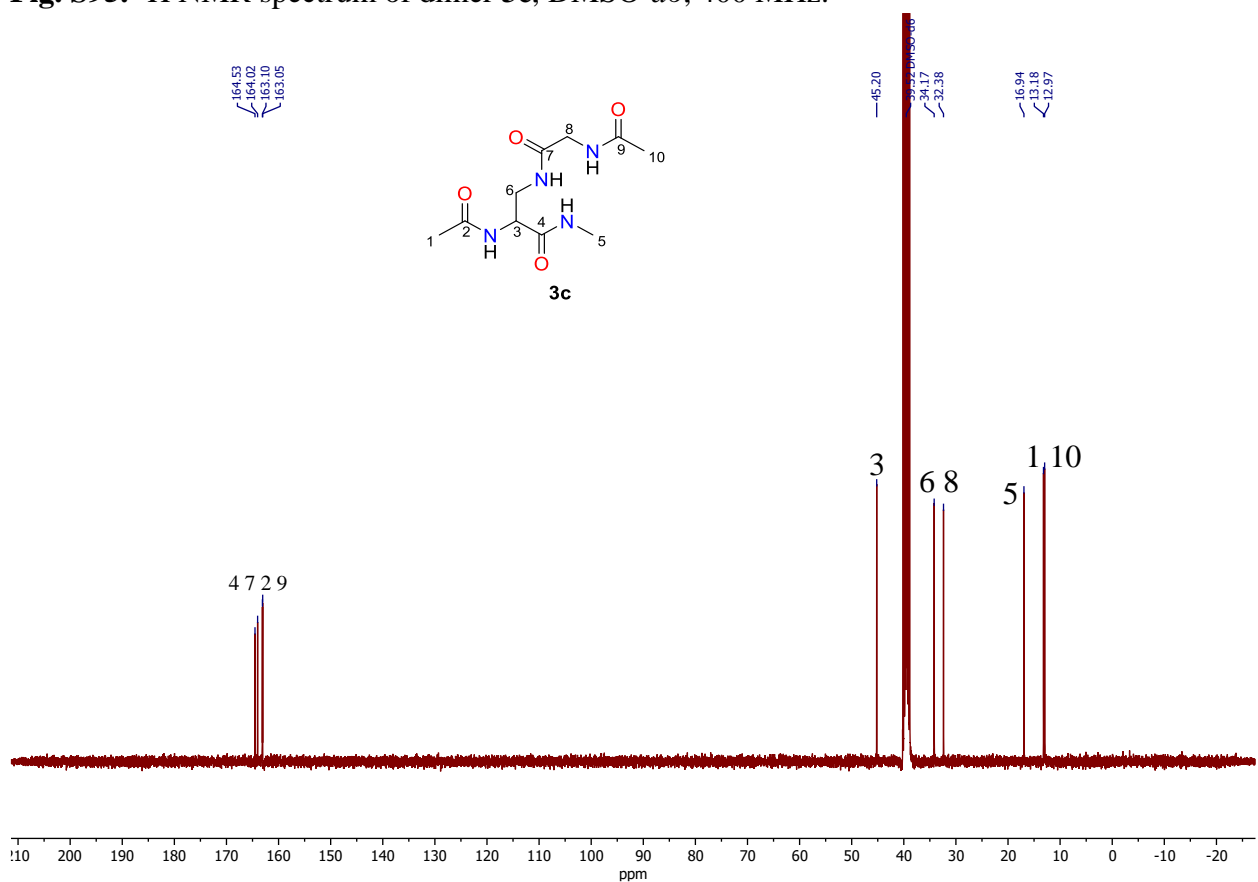
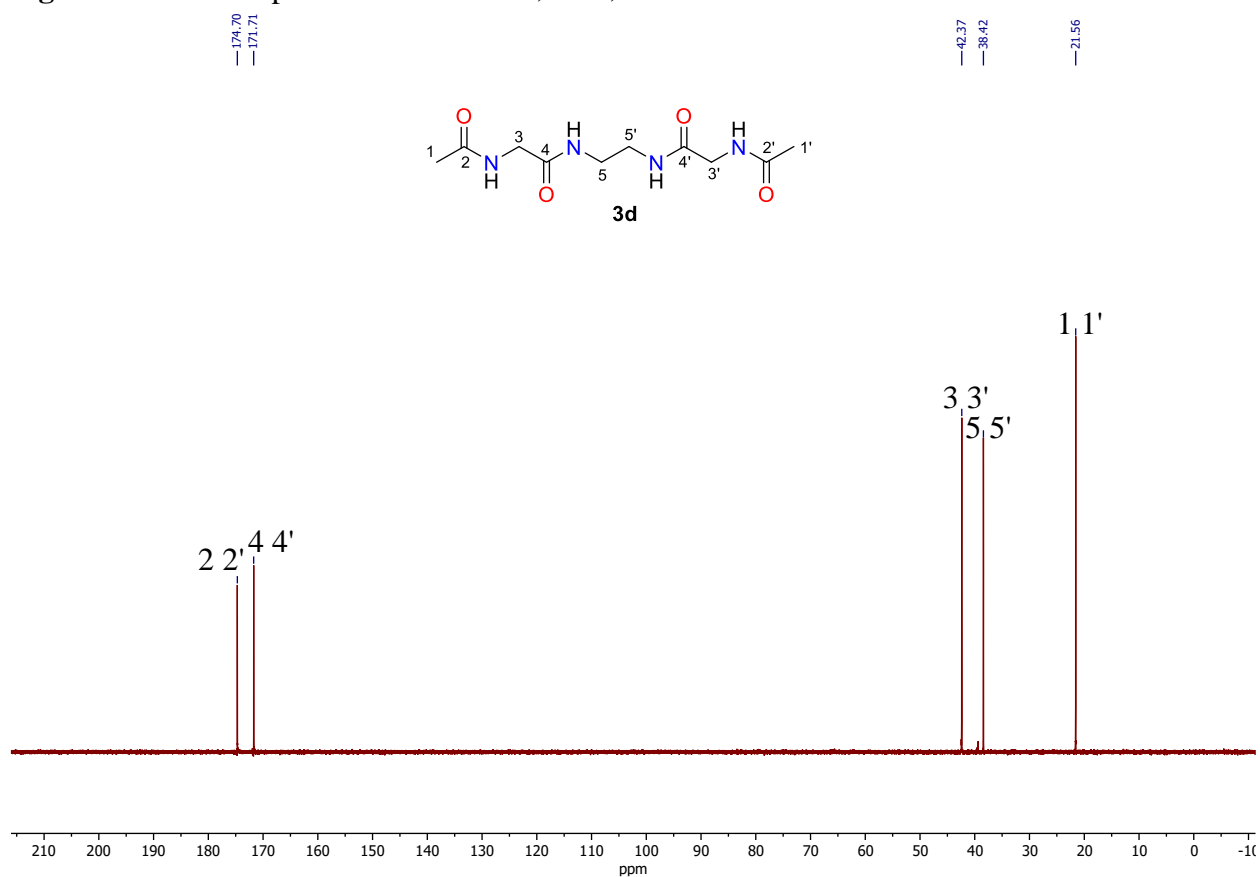
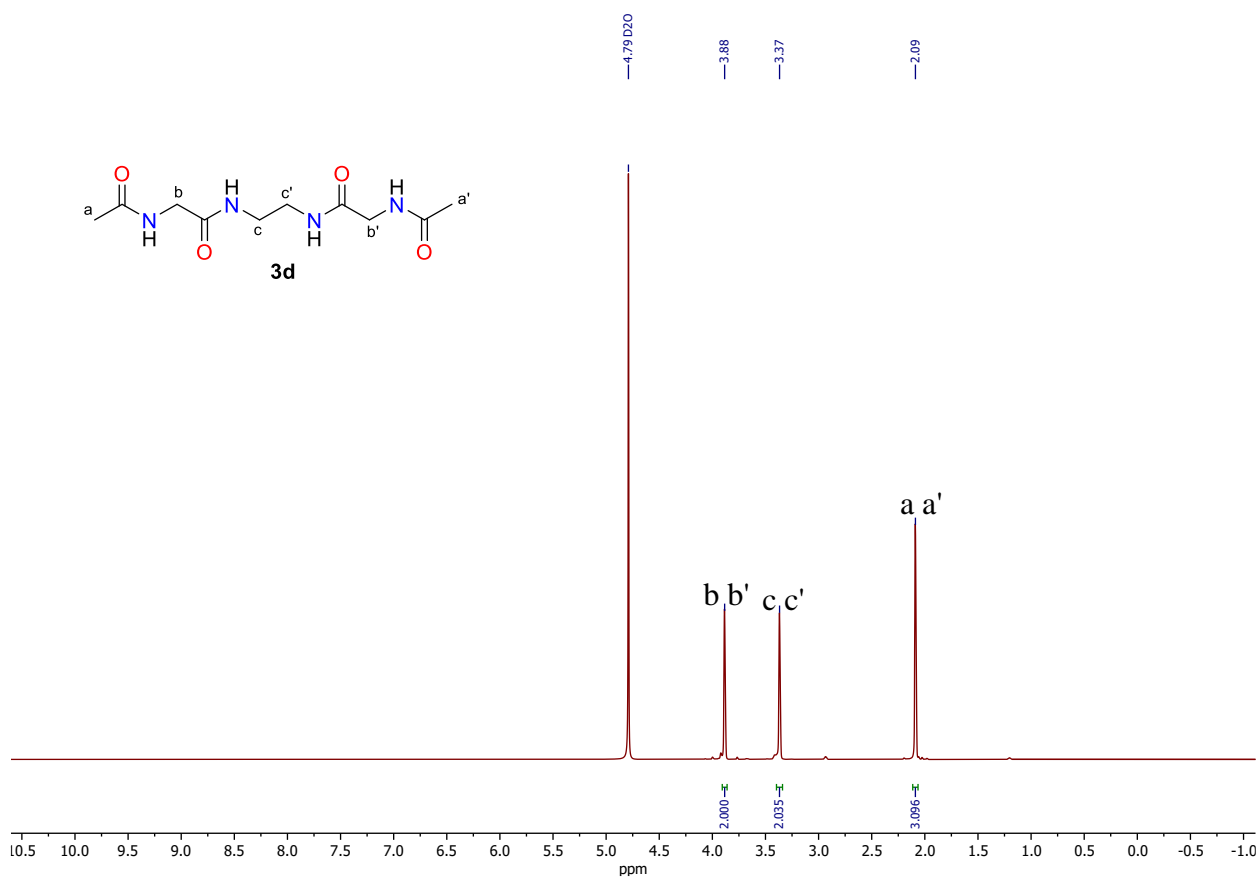


Fig. S96. ¹³C NMR spectrum of dimer **3c**, DMSO-*d*₆, 101 MHz.



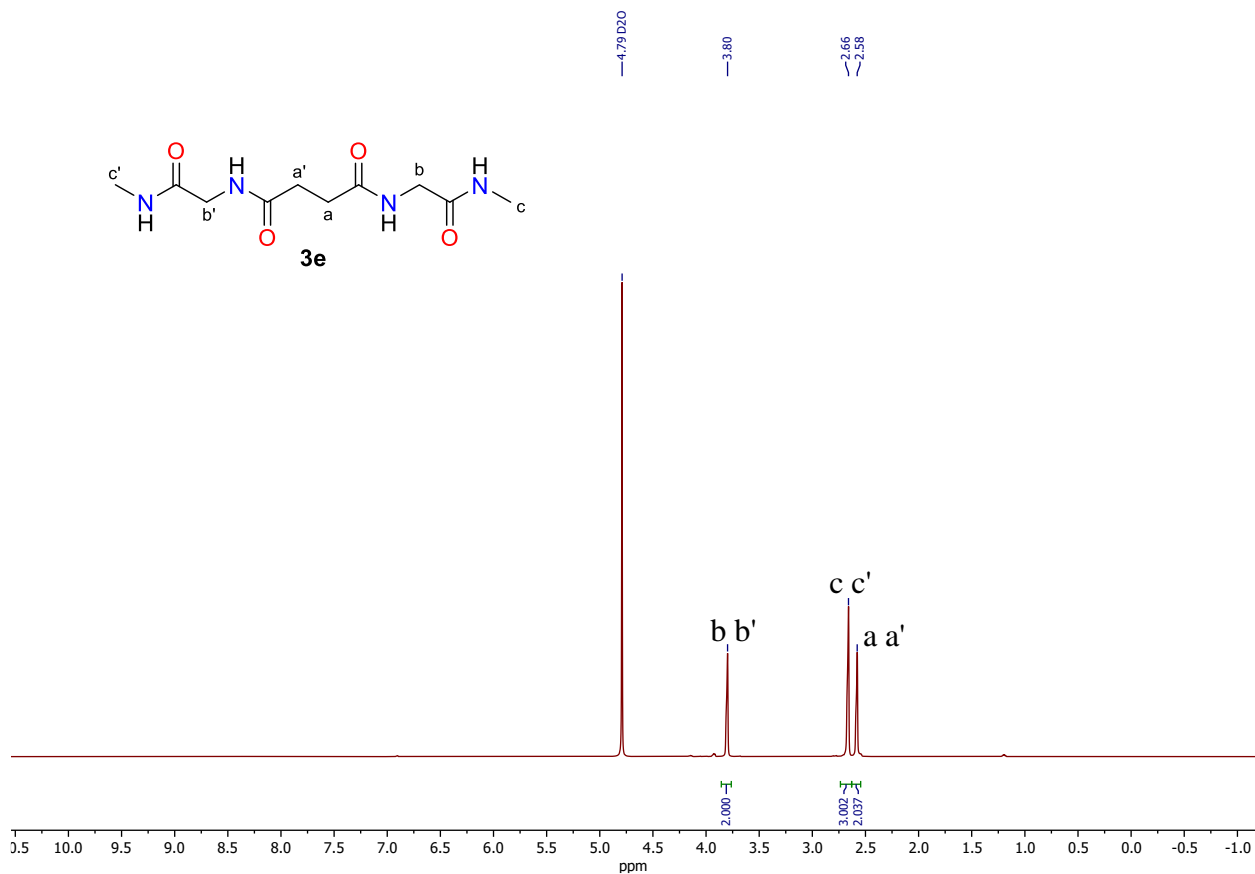


Fig. S99. ^1H NMR spectrum of dimer **3e**, D_2O , 600 MHz.

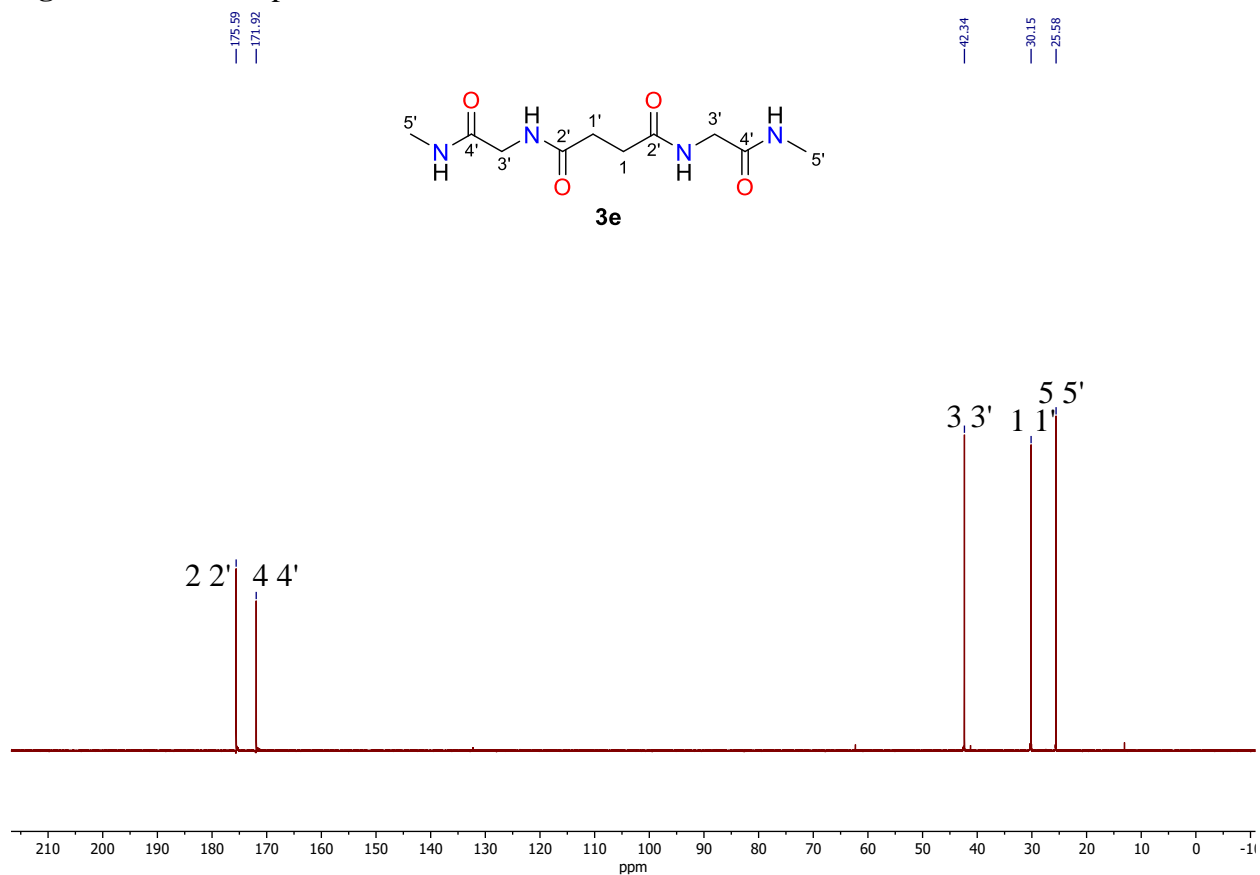


Fig. S100. ^{13}C NMR spectrum of dimer **3e**, D_2O , 150 MHz.

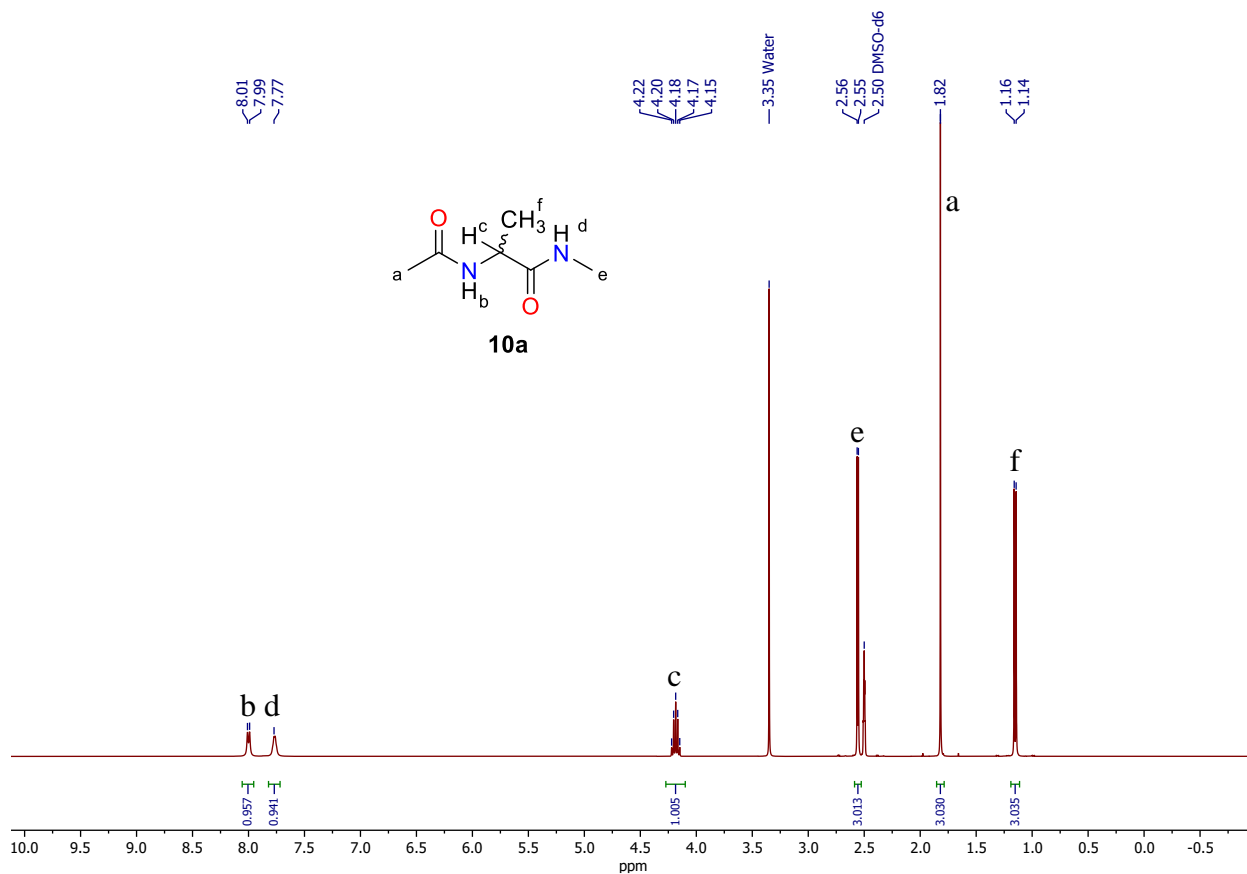


Fig. S101. ¹H NMR spectra of *DL*-AcAlaMe (**10a**), DMSO-*d*₆, 400 MHz.

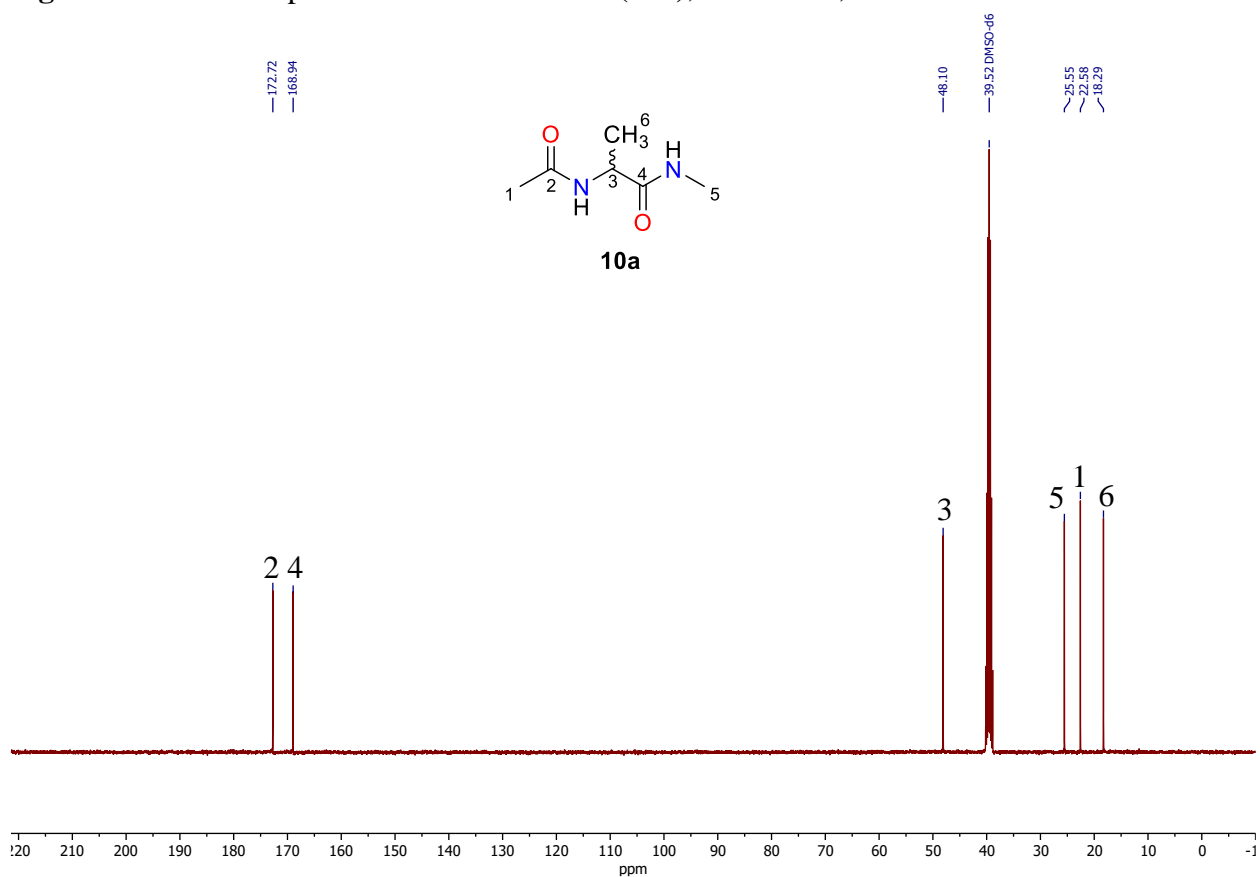


Fig. S102. ¹³C NMR spectrum of *DL*-AcAlaMe (**10a**), DMSO-*d*₆, 101 MHz.

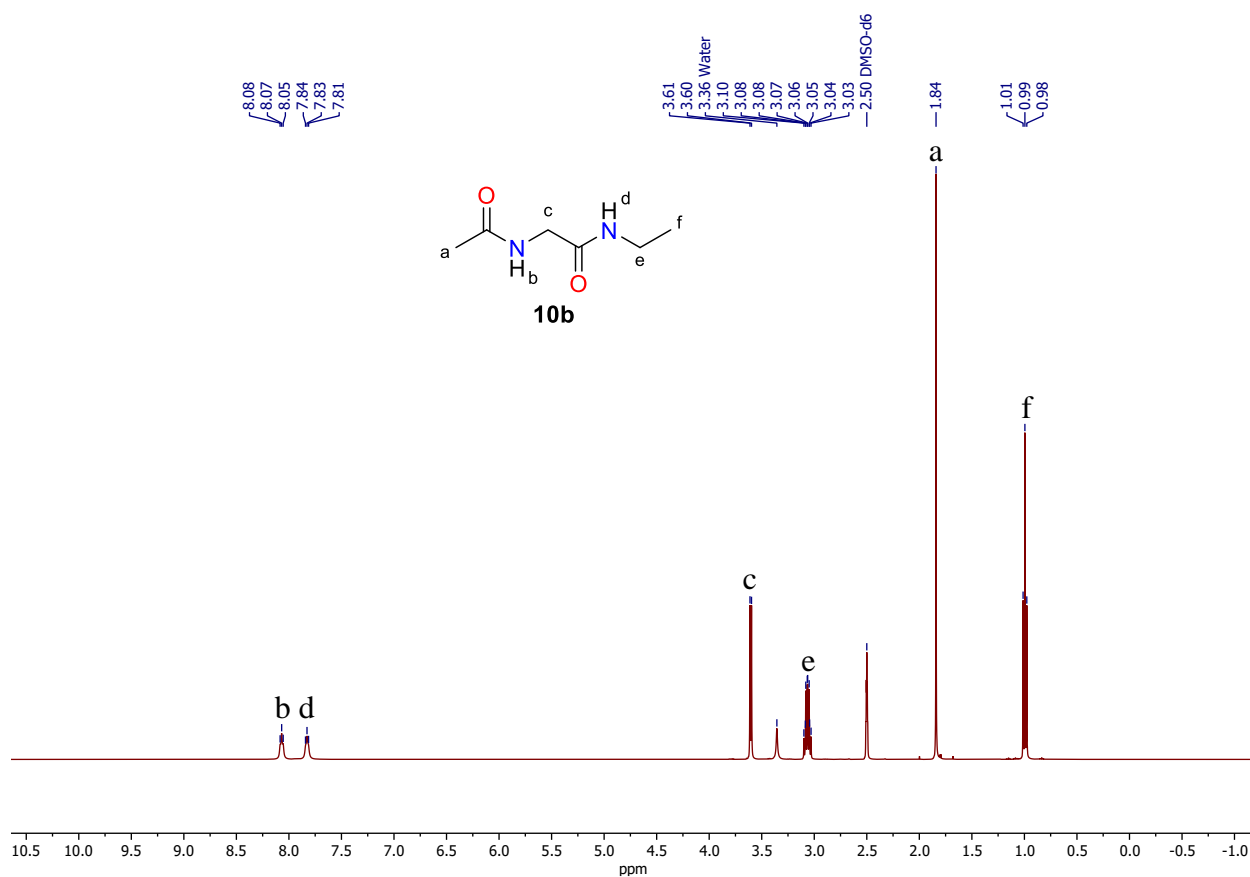


Fig. S103. ¹H NMR spectrum of AcGlyNEt (**10b**), DMSO-*d*₆, 400 MHz.

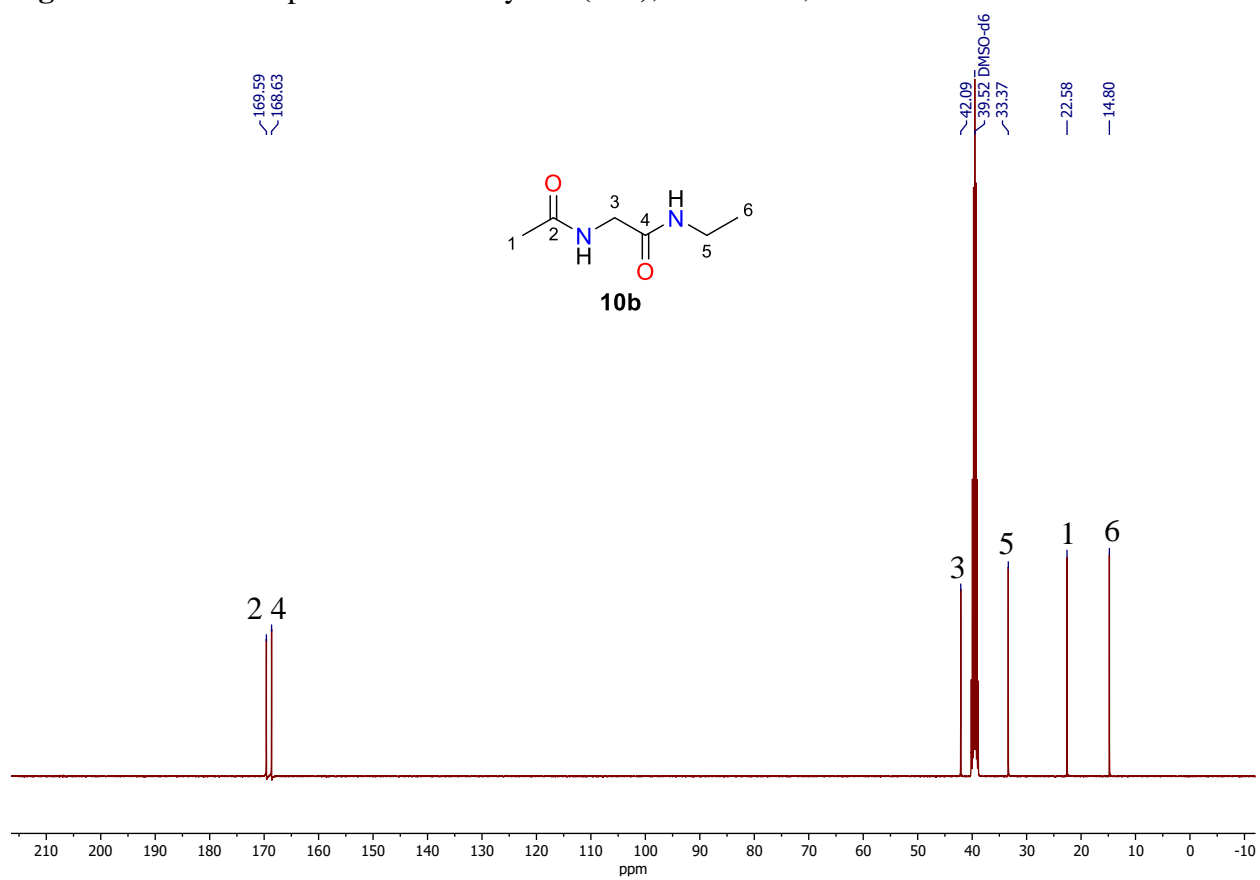


Fig. S104. ¹³C NMR spectrum of AcGlyNEt (**10b**), DMSO-*d*₆, 101 MHz.

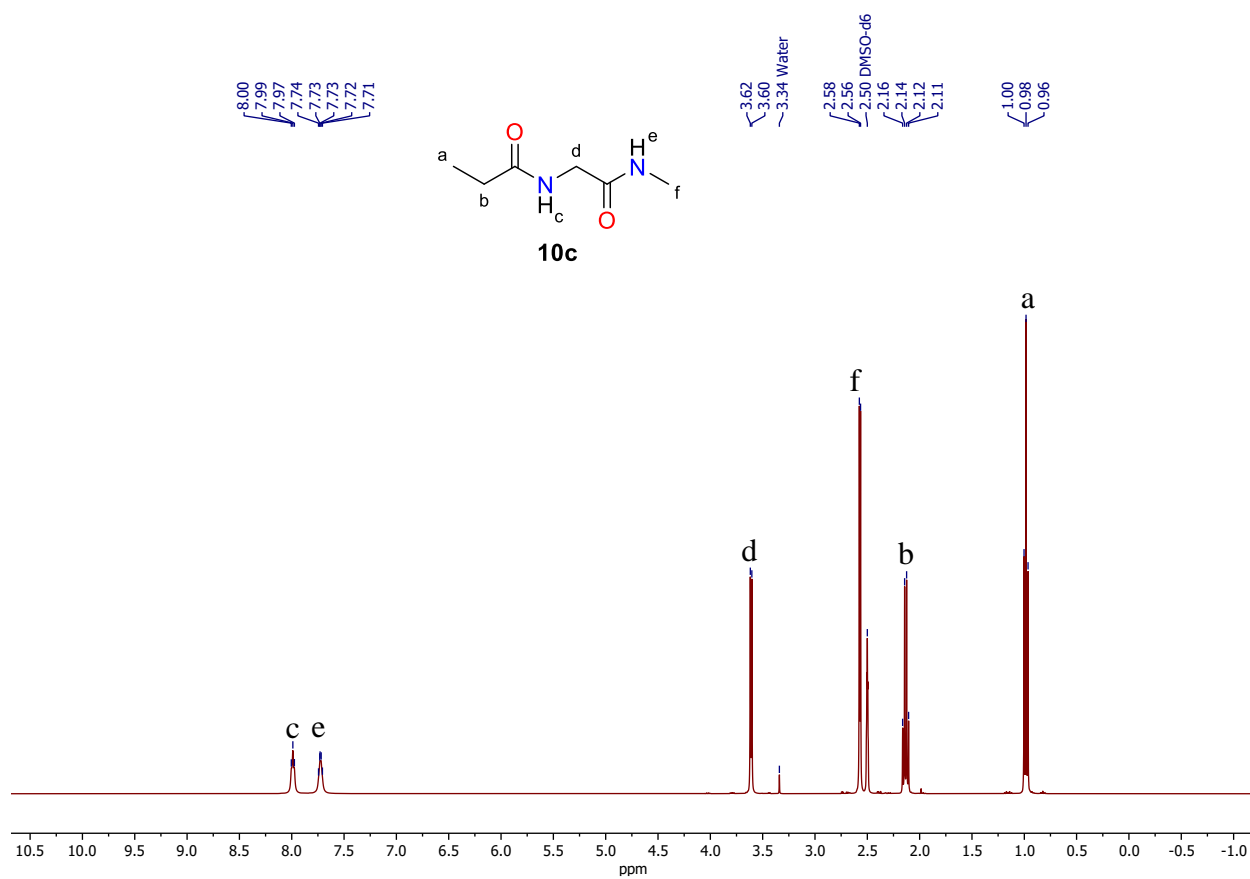


Fig. S105. ¹H NMR spectra of PpGlyNMe (**10c**), DMSO-*d*₆, 400 MHz.

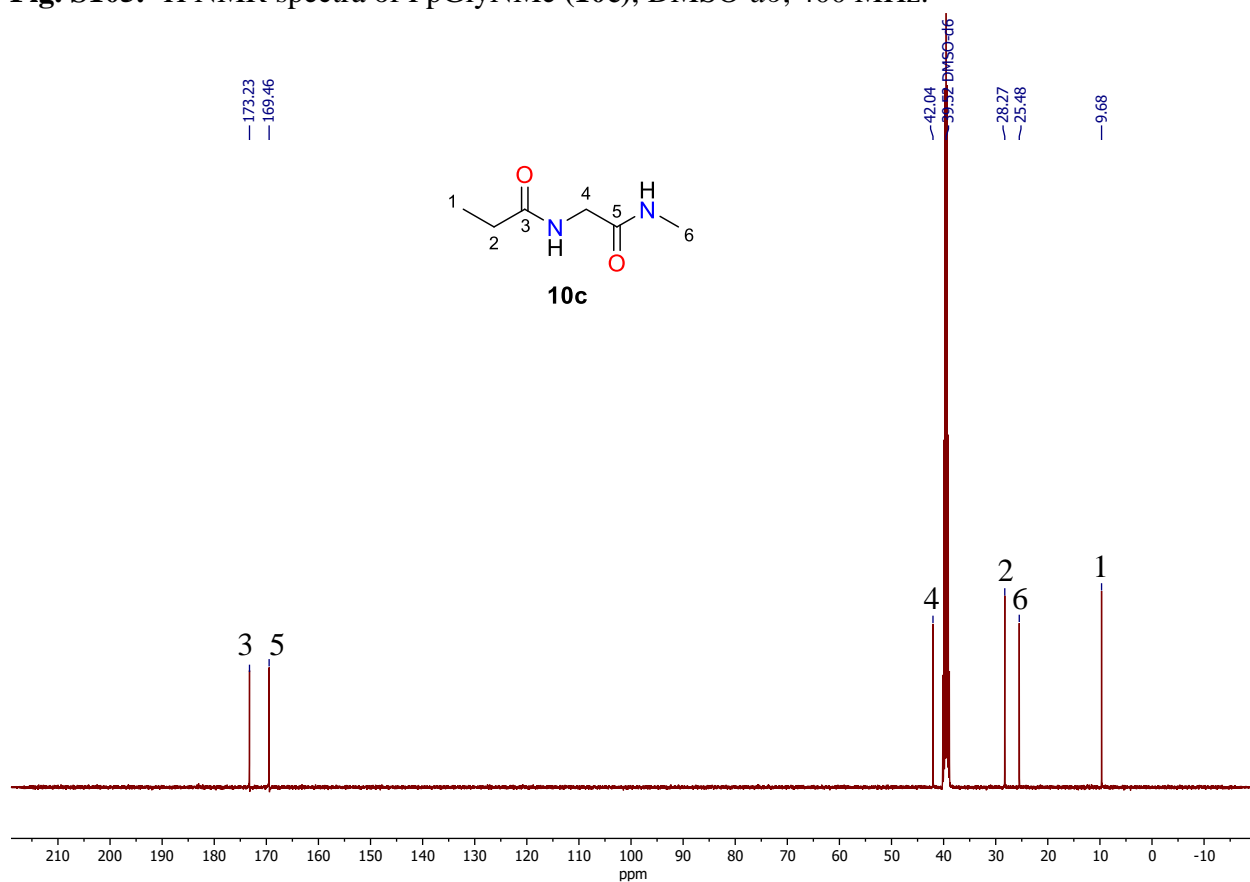


Fig. S106. ¹³C NMR spectra of PpGlyNMe (**10c**), DMSO-*d*₆, 101 MHz.

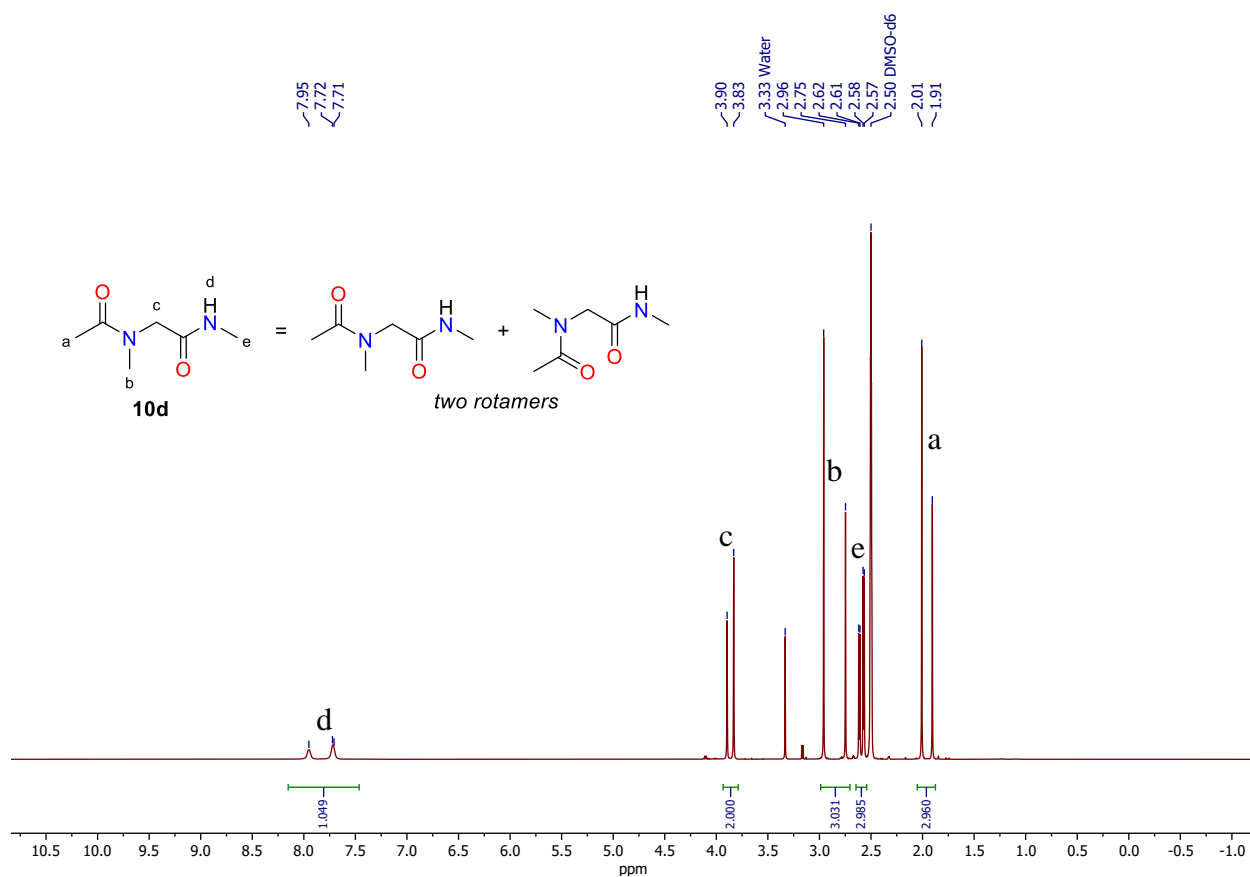


Fig. S107. ¹H NMR spectrum of AcSarNMe (**10d**), DMSO-*d*₆, 400 MHz.

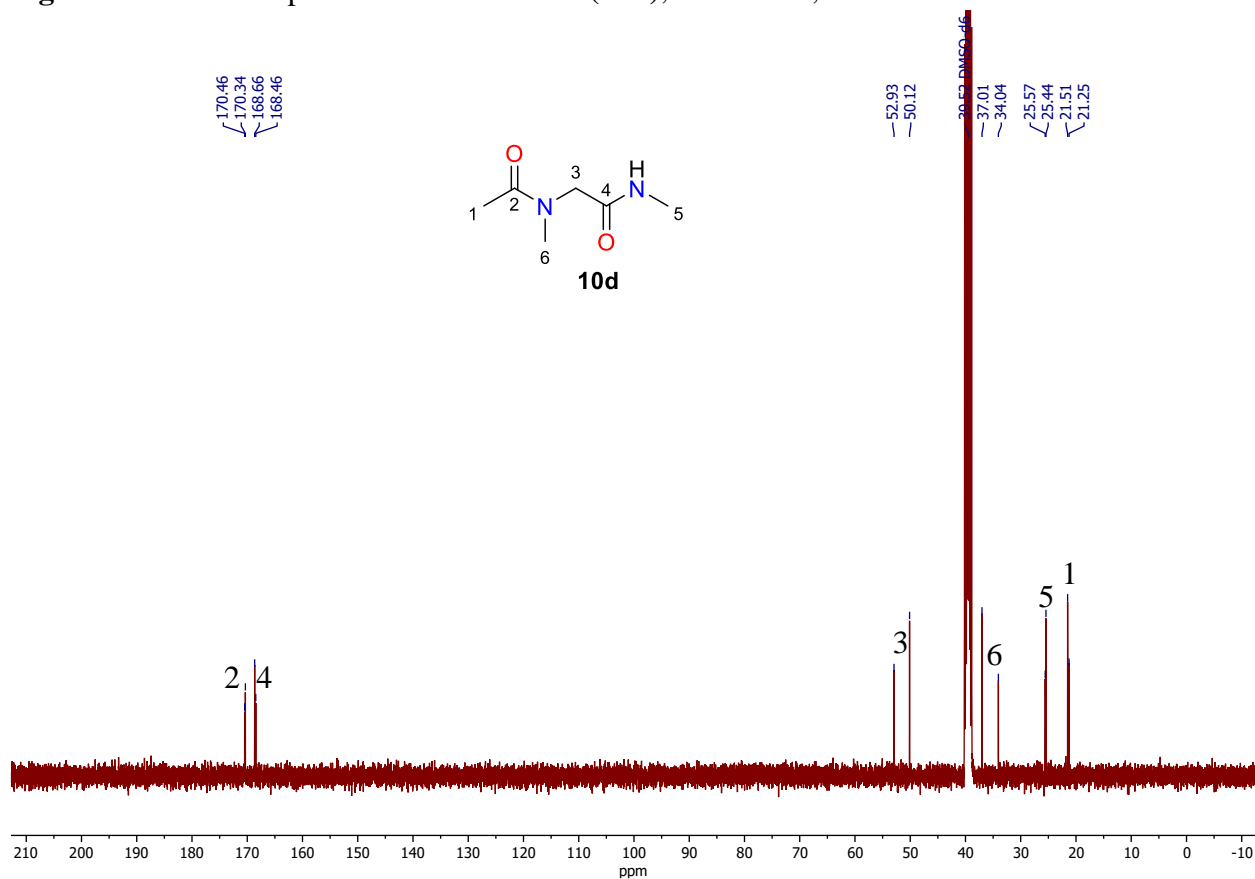


Fig. S108. ¹³C NMR spectrum of AcSarNMe (**10d**), DMSO-*d*₆, 101 MHz.

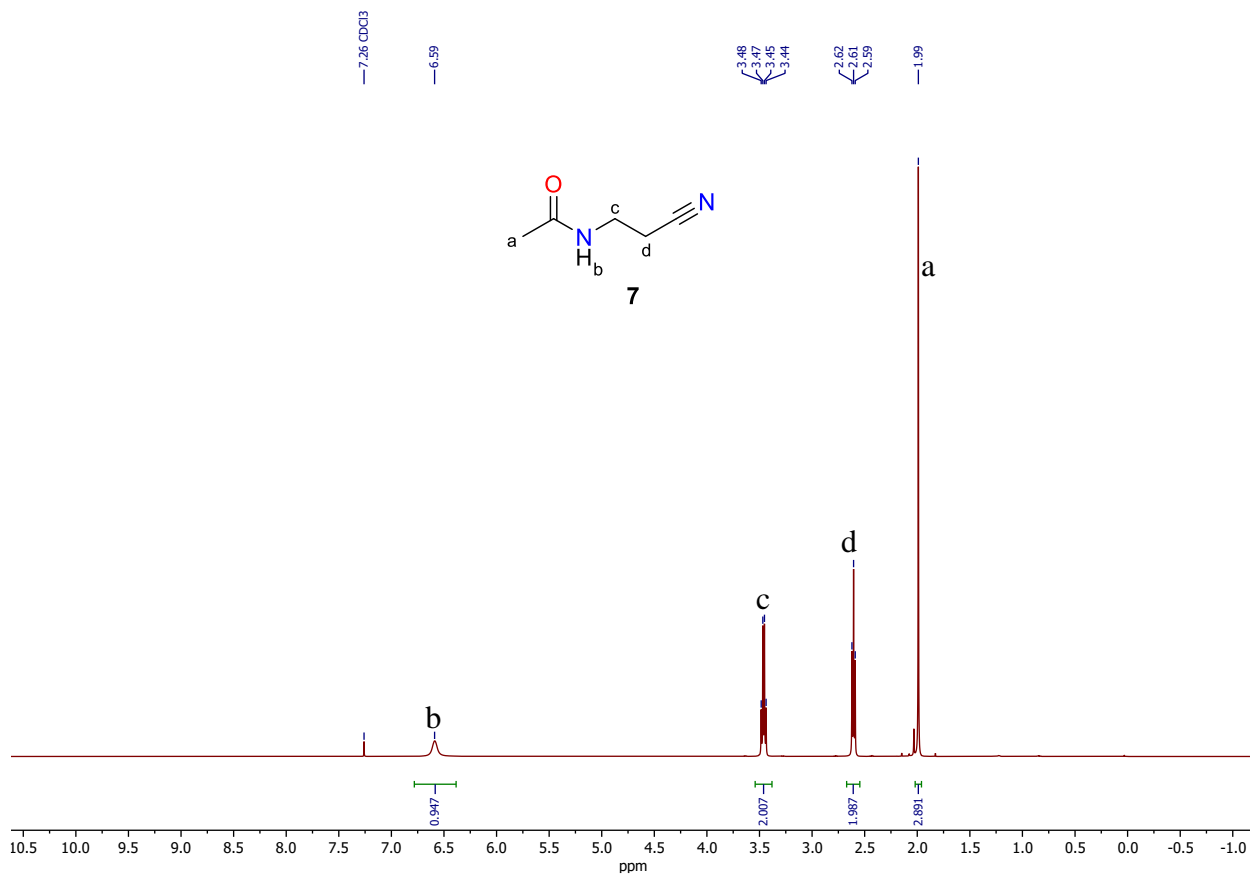


Fig. S109. ^1H NMR spectrum of AcNEtCN (**7**), CDCl_3 , 400 MHz.

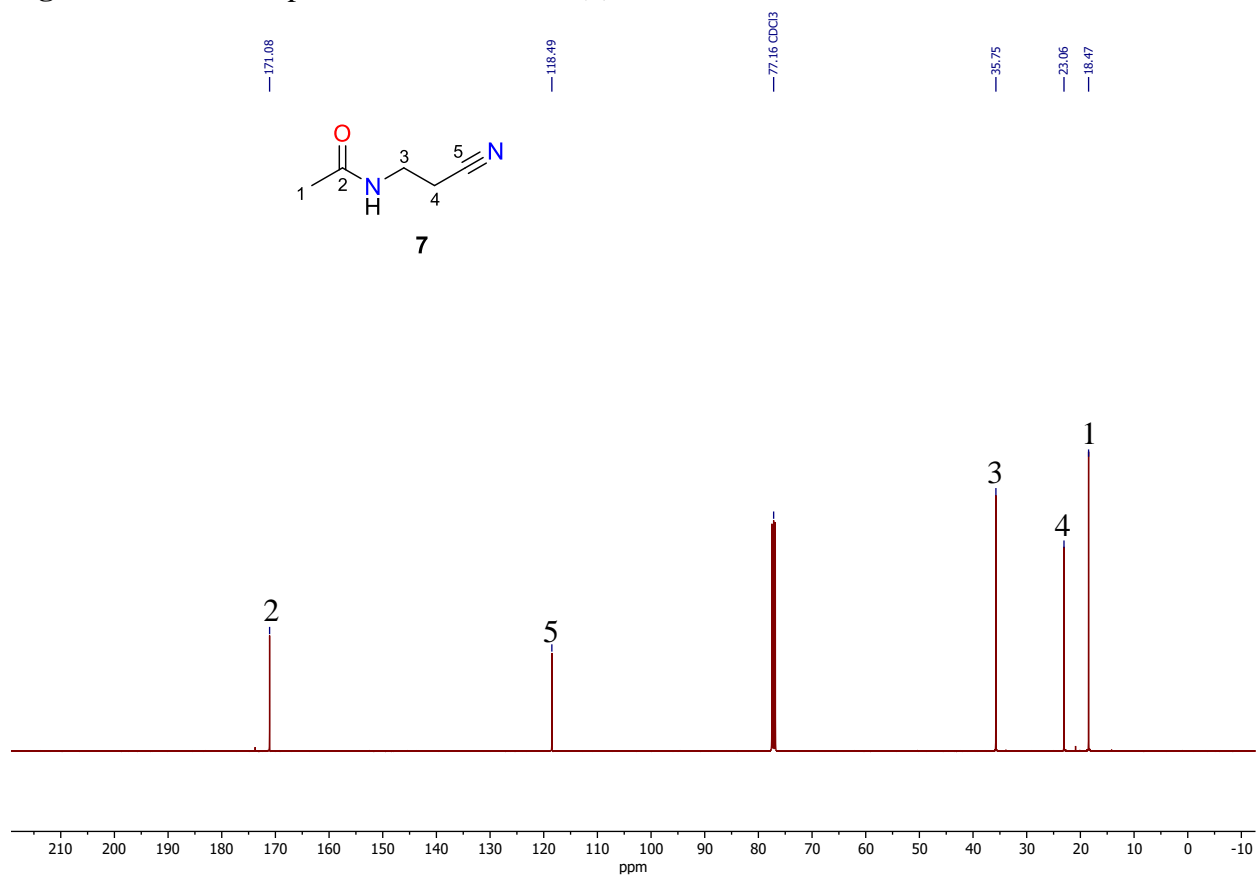


Fig. S110. ^{13}C NMR spectrum of AcNEtCN (**7**), CDCl_3 , 101 MHz.

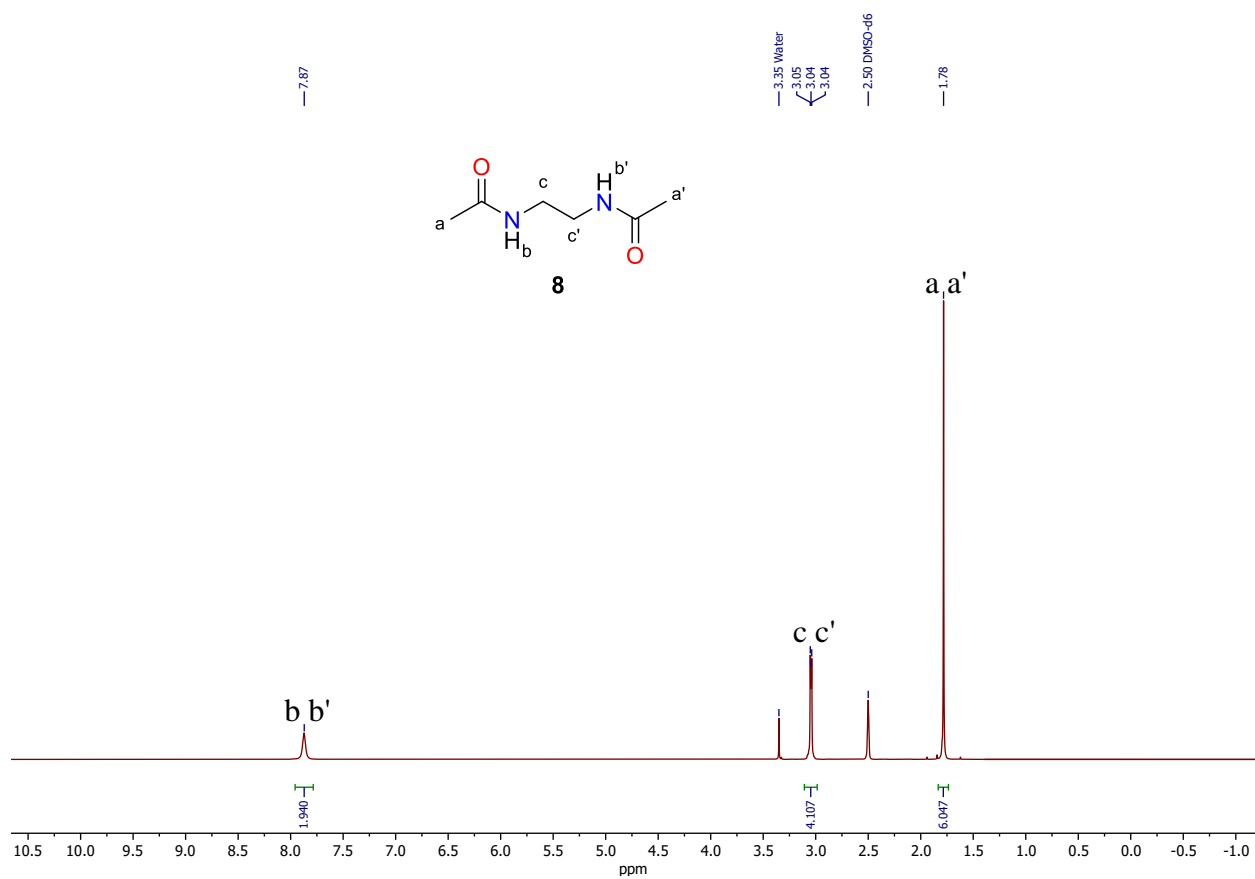


Fig. S111. ^1H NMR spectrum of dimer **8**, DMSO- d_6 , 400 MHz.

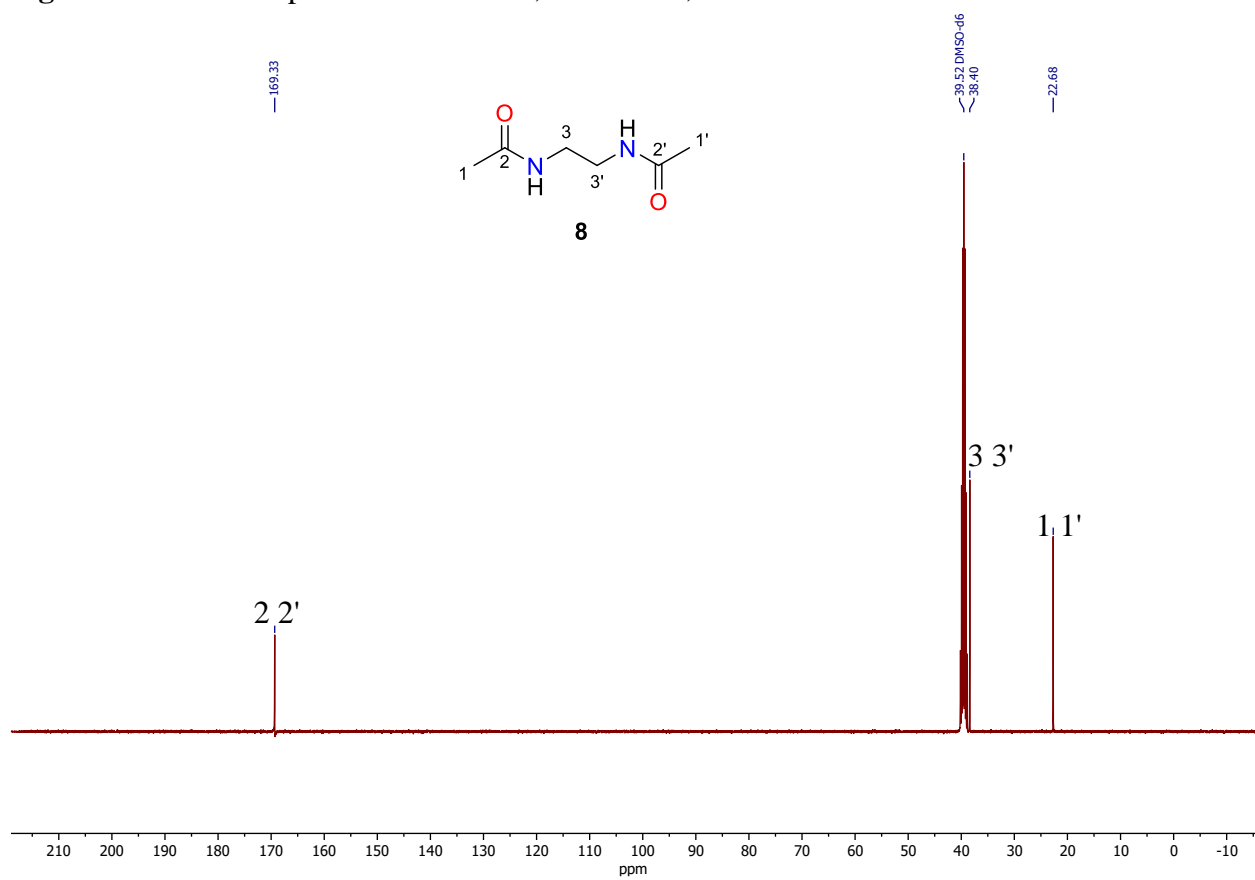


Fig. S112. ^{13}C NMR spectrum of dimer **8**, DMSO- d_6 , 101 MHz.

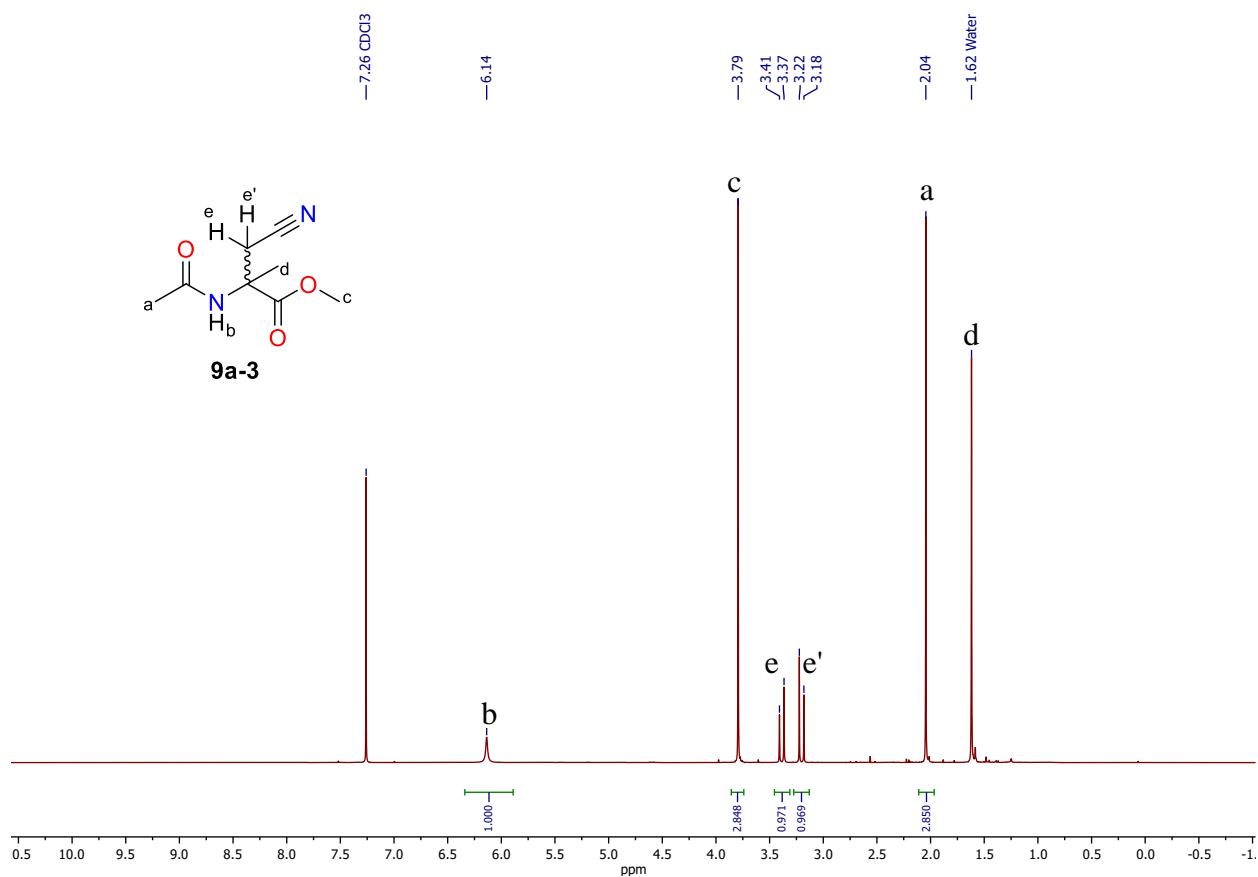


Fig. S113. ¹H NMR spectrum of Ac-(α -Me)-Ala(CN)-OMe (**9a-3**), CDCl₃, 400 MHz.

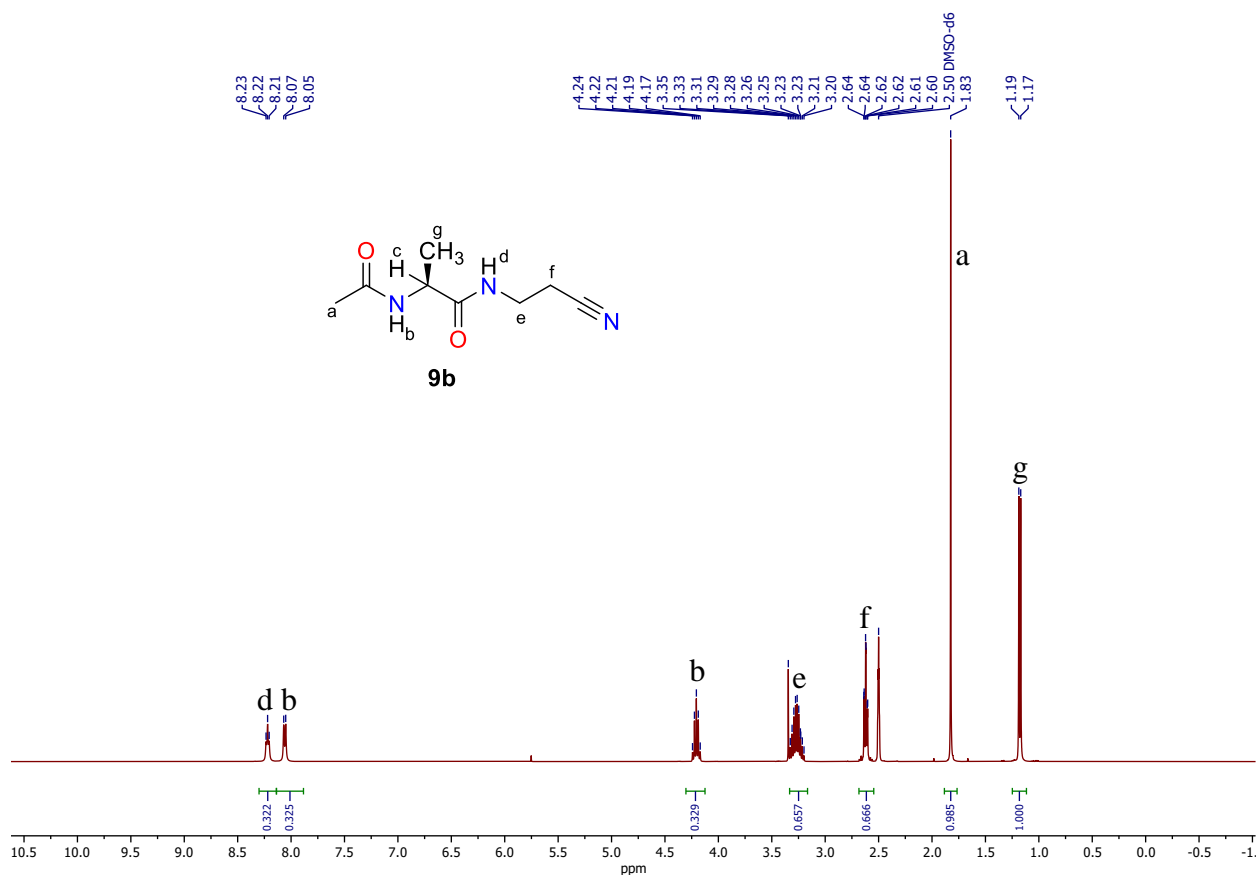


Fig. S114. ¹H NMR spectrum of *L*-Ac-Ala-NEtCN (**9b**), DMSO-*d*₆, 400 MHz.

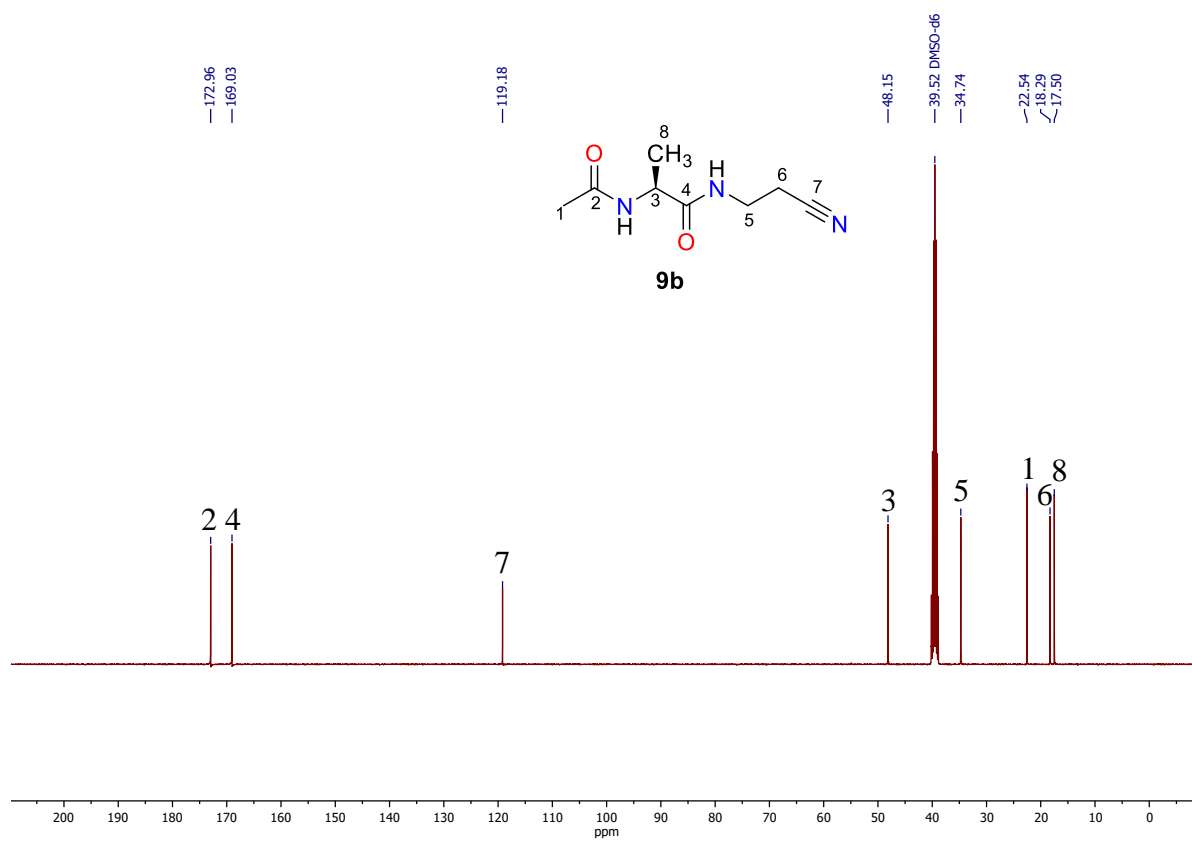


Fig. S115. ^{13}C NMR spectrum of *L*-Ac-Ala-NEtCN **9b**, DMSO- d_6 , 101 MHz.

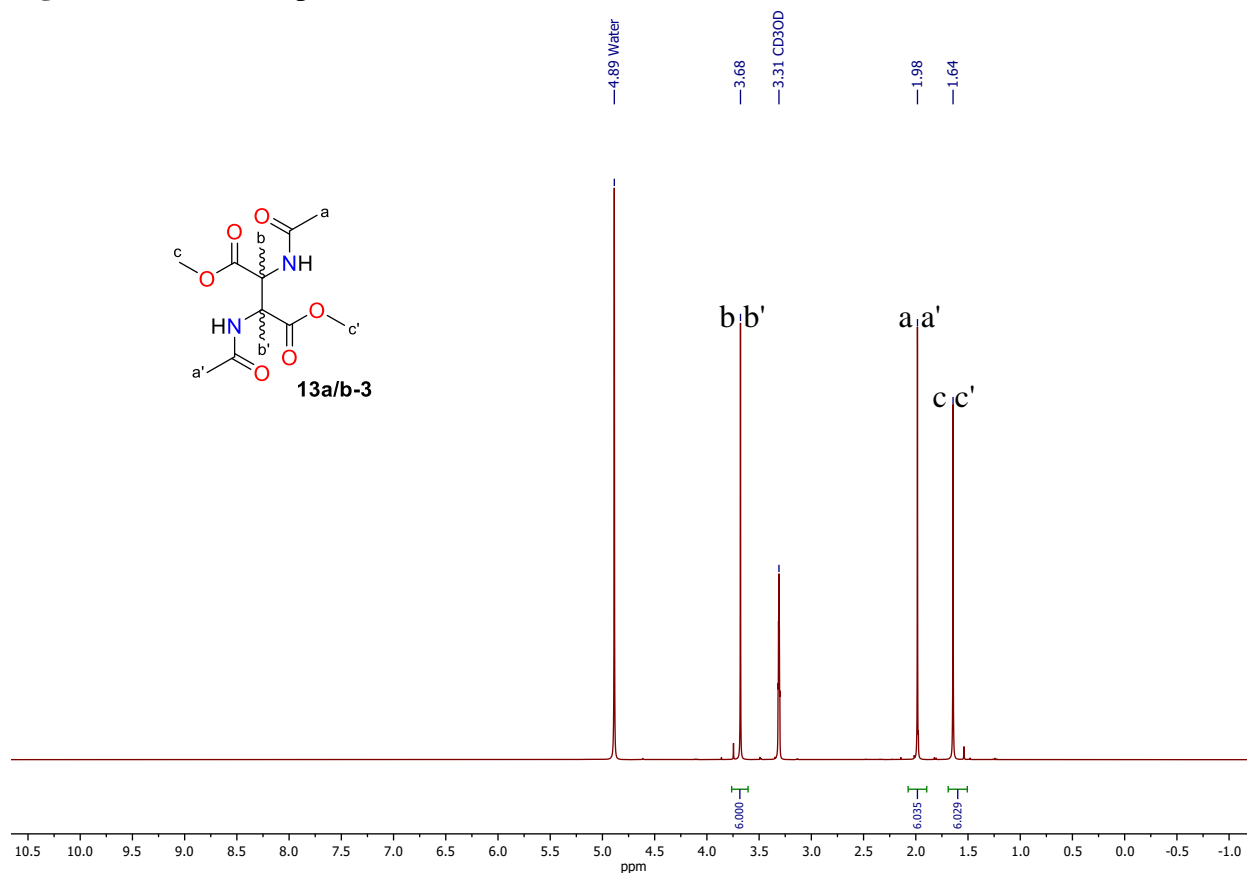


Fig. S116. ^1H NMR spectrum of dimer **13a/b-3**, MeOH- d_4 , 400 MHz.

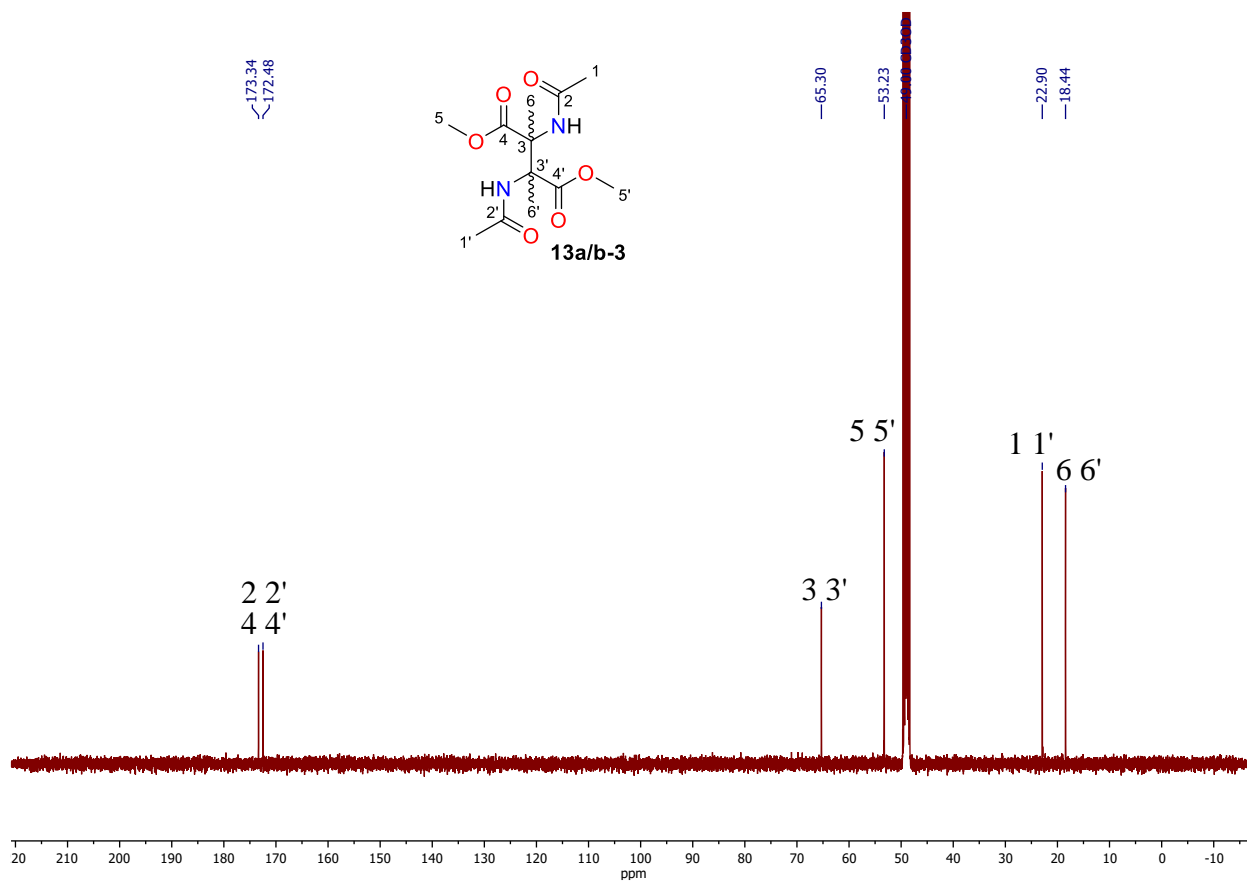


Fig. S117. ^{13}C NMR spectrum of dimer **13a/b-3**, $\text{MeOH-}d_4$, 101 MHz.

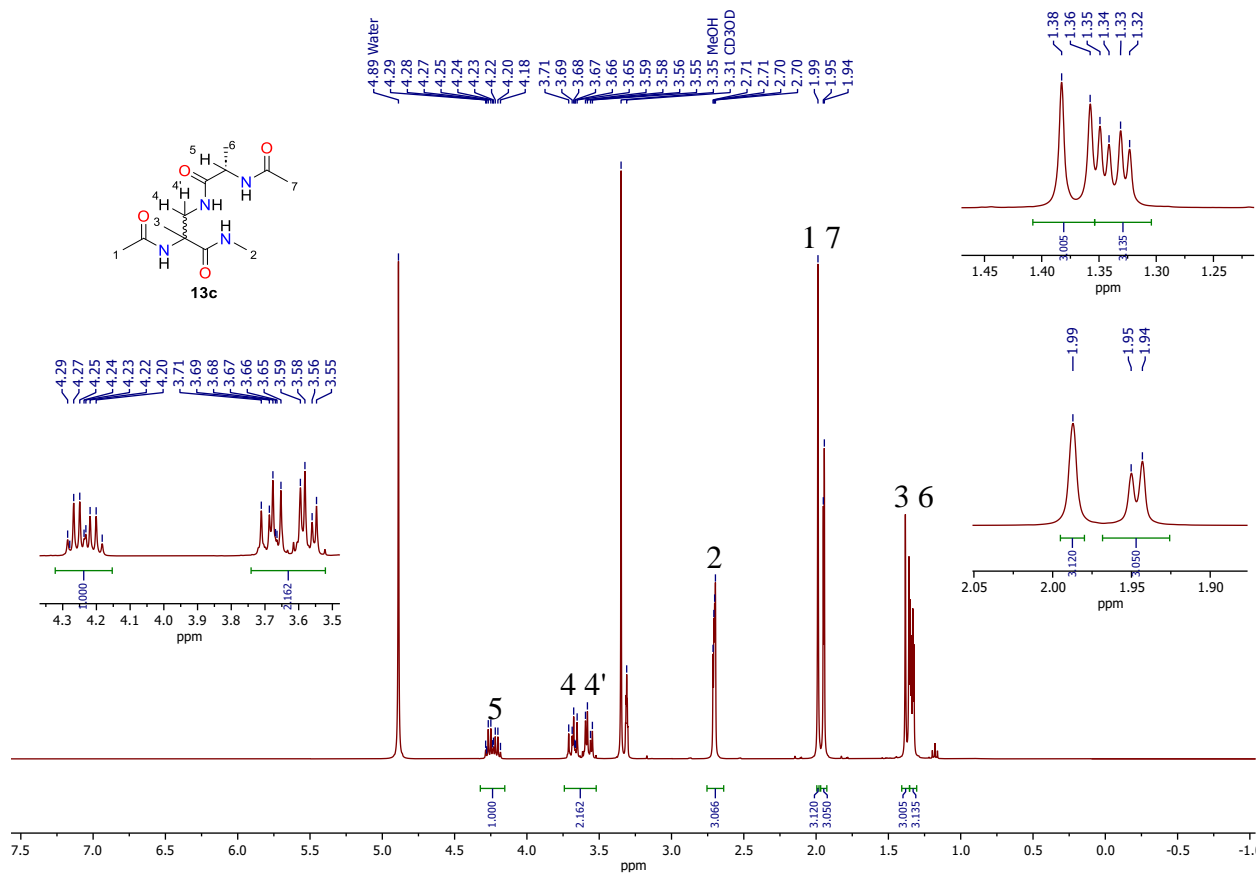


Fig. S118. ^1H NMR spectrum of dimer **13c**, $\text{MeOH-}d_4$, 400 MHz.

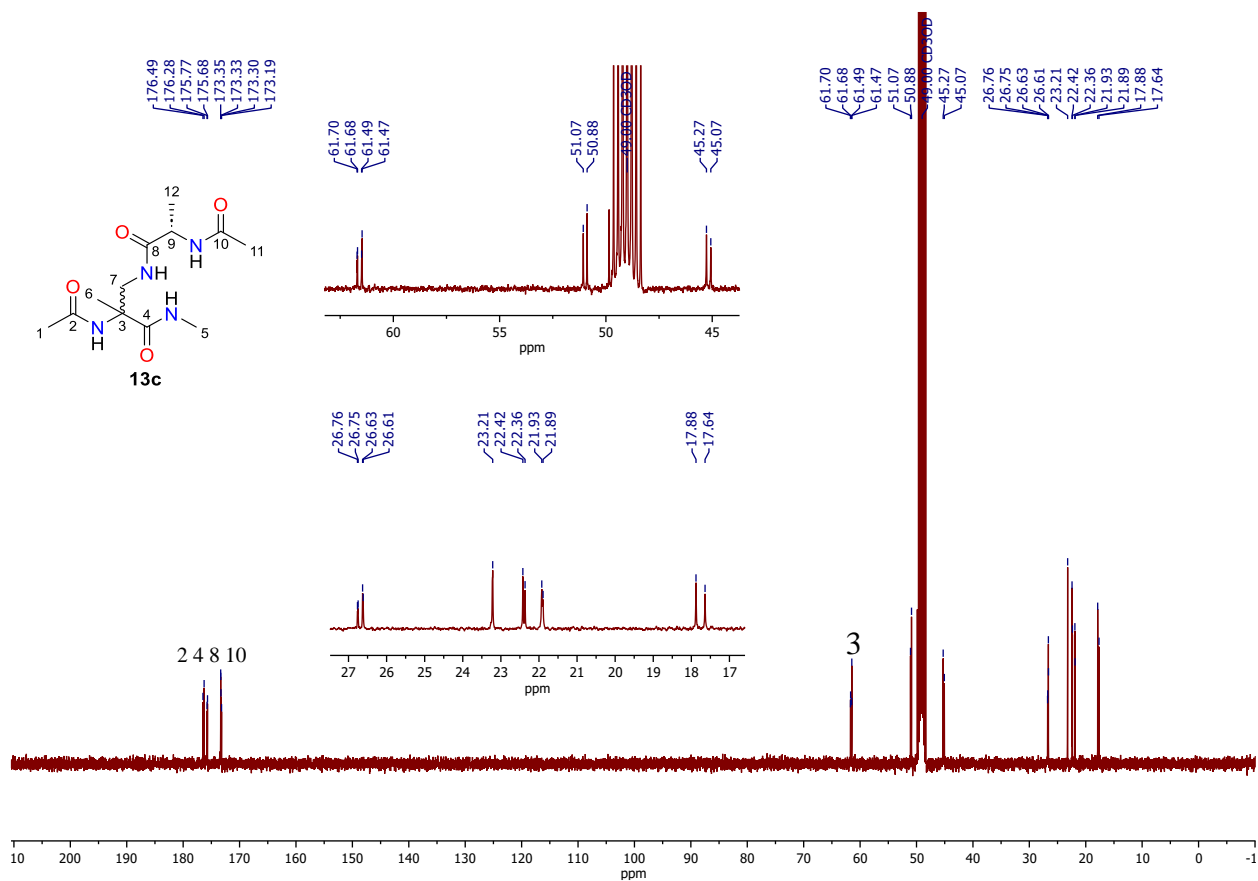


Fig. S119. ^{13}C NMR spectrum of dimer **13c**, $\text{MeOH-}d_4$, 101 MHz.

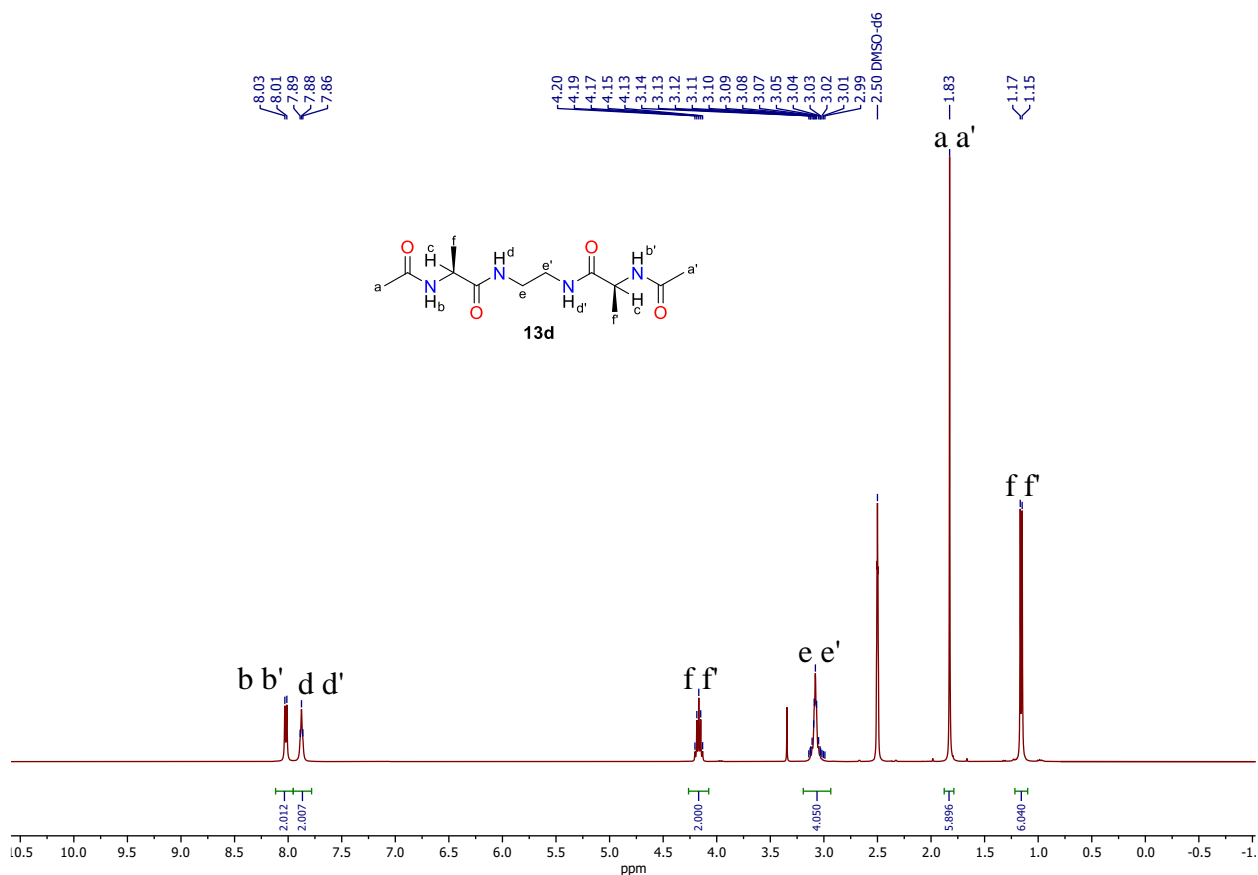


Fig. S120. ^1H NMR spectrum of dimer **13d**, $\text{DMSO-}d_6$, 400 MHz.

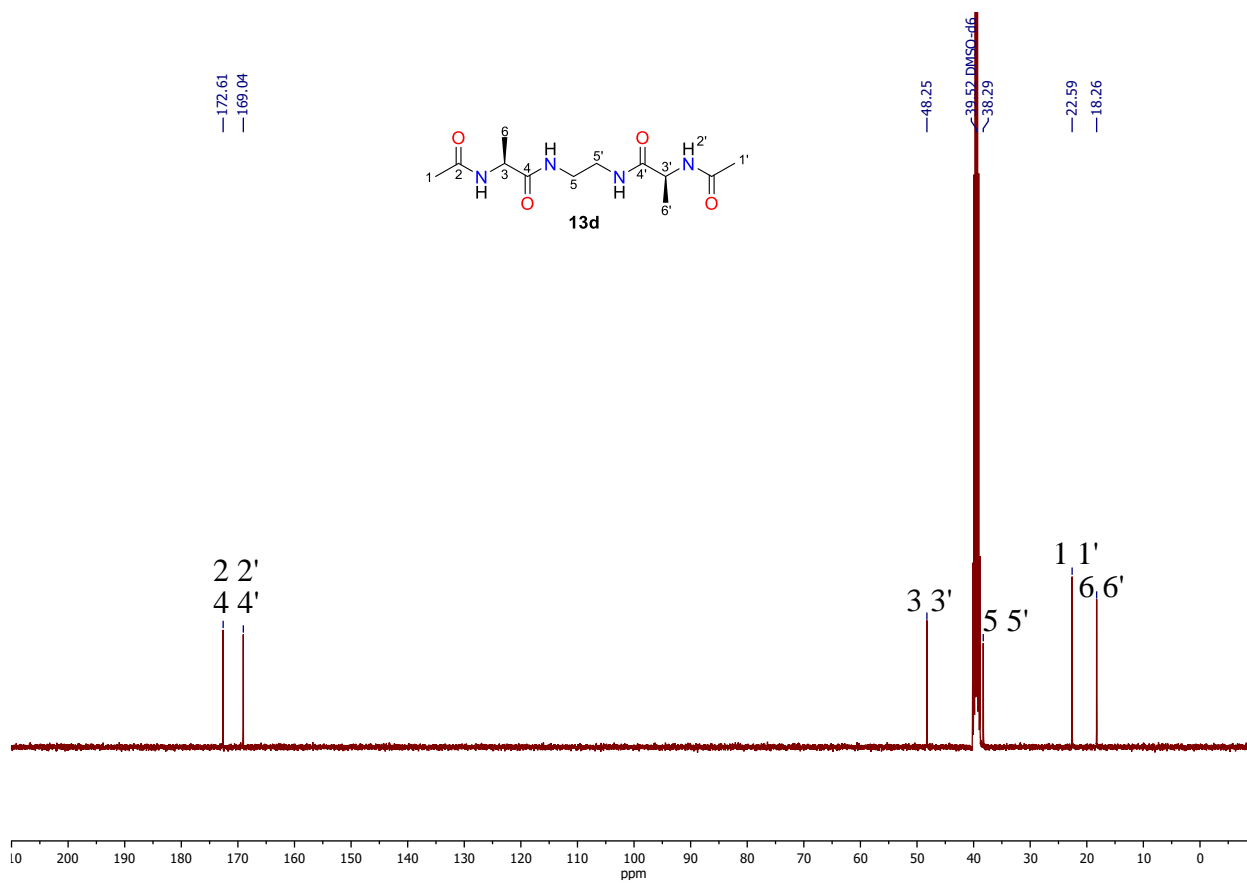


Fig. S121. ^{13}C NMR spectrum of dimer **13d**, $\text{DMSO-}d_6$, 101 MHz.

2.6.7. References

- [1] N. D. C. Tappin, M. Gnägi-Lux, P. Renaud, *Chem. Eur. J.* **2018**, *24*, 11498-11502.
- [2] E. Rizzardo, A. K. Serelis, D. H. Solomon, *Aust. J. Chem.* **1982**, *35*, 2013-2024.
- [3] R. A. Cormanich, R. Rittner, M. Bühl, *RSC Adv.* **2015**, *5*, 13052-13060.
- [4] R. A. Cormanich, M. Bühl, R. Rittner, *Org. Biomol. Chem.* **2015**, *13*, 9206-9213.
- [5] A. H. Sijpkens, G. Somsen, *J. Chem. Soc., Faraday Trans. 1* **1989**, *85*, 2563-2573.
- [6] J. G. Nathanael, U. Wille, *J. Org. Chem.* **2019**, *84*, 3405-3418.
- [7] Y. Koyama, T. Shimanouchi, M. Sato, T. Tatsuno, *Biopolymers* **1971**, *10*, 1059-1074.
- [8] D. N. Reddy, E. N. Prabhakaran, *Biopolymers* **2014**, *101*, 66-77.
- [9] T. H. Applewhite, C. Niemann, *J. Am. Chem. Soc.* **1959**, *81*, 2208-2213.
- [10] K.-K. Lee, E. Kim, C. Joo, J. Song, H. Han, M. Cho, *J. Phys. Chem. B* **2008**, *112*, 16782-16787.
- [11] P. F. Alewood, S. Palma, R. B. Johns, *Aust. J. Chem.* **1984**, *37*, 425-428.
- [12] J. G. Nathanael, J. M. White, A. Richter, M. R. Nuske, U. Wille, *Org. Biomol. Chem.* **2020**, *18*, 6949-6957.
- [13] G. Wang, L. Chen, X. Cai, Z. Li, M. Luo, *Synlett* **2016**, *27*, 309-312.
- [14] M. Maj, C. Ahn, D. Kossowska, K. Park, K. Kwak, H. Han, M. Cho, *Phys. Chem. Chem. Phys.* **2015**, *17*, 11770-11778.
- [15] L.-h. Zhang, G. S. Kauffman, J. A. Pesti, J. Yin, *J. Org. Chem.* **1997**, *62*, 6918-6920.
- [16] M. Radić Stojković, P. Piotrowski, C. Schmuck, I. Piantanida, *Org. Biomol. Chem.* **2015**, *13*, 1629-1633.
- [17] A. Isidro-Llobet, K. Hadje Georgiou, W. R. J. D. Galloway, E. Giacomini, M. R. Hansen, G. Méndez-Abt, Y. S. Tan, L. Carro, H. F. Sore, D. R. Spring, *Org. Biomol. Chem.* **2015**, *13*, 4570-4580.
- [18] K. K. H. Vong, S. Maeda, K. Tanaka, *Chem. Eur. J.* **2016**, *22*, 18865-18872.
- [19] P. Canavelli, S. Islam, M. W. Powner, *Nature* **2019**, *571*, 546-549.
- [20] M. J. O'Donnell, R. L. Polt, *J. Org. Chem.* **1982**, *47*, 2663-2666.
- [21] T. Ikeda, H. Ochiishi, M. Yoshida, R. Yazaki, T. Ohshima, *Org. Lett.* **2022**, *24*, 369-373.
- [22] C. Suzuki, K. Kato, A. B. Tsuji, M.-R. Zhang, Y. Arano, T. Saga, *J. Labelled Compd. Radiopharm.* **2015**, *58*, 127-132.
- [23] C. Alvarez-Ibarra, A. G. Csáky, B. Colmenero, M. L. Quiroga, *J. Org. Chem.* **1997**, *62*, 2478-2482.

- [24] Y. Matsumoto, J. Sawamura, Y. Murata, T. Nishikata, R. Yazaki, T. Ohshima, *J. Am. Chem. Soc.* **2020**, *142*, 8498-8505.
- [25] E. Deseke, Y. Nakatani, G. Ourisson, *Eur. J. Org. Chem.* **1998**, *1998*, 243-251.
- [26] Z. J. Kaminski, M. T. Leplawy, J. Zabrocki, *Synthesis* **1973**, *1973*, 792-793.
- [27] W. Yu, J. McConathy, J. Olson, V. M. Camp, M. M. Goodman, *J. Med. Chem.* **2007**, *50*, 6718-6721.
- [28] A. Olma, A. Kudaj, *Tetrahedron Lett.* **2005**, *46*, 6239-6241.
- [29] T. Fukuyama, L. Xu, *J. Am. Chem. Soc.* **1993**, *115*, 8449-8450.
- [30] A. Kudaj, A. Olma, *Tetrahedron Lett.* **2007**, *48*, 6794-6797.

3. The Effects of Ring Annulation on the Regioselectivity of the Hydrogen Atom Transfer in the Hofmann-Löffler-Freytag Reaction

Salavat S. Ashirbaev^a, Davor Šakić^b, Hendrik Zipse^a

^a*Dept. Chemistry, LMU Muenchen, Butenandtstrasse 5-13, D-81377 Muenchen, Germany*

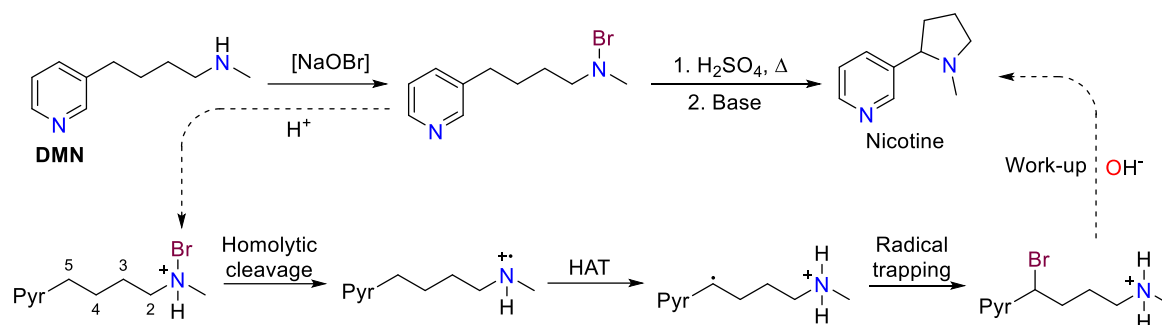
^b*University of Zagreb, Faculty of Pharmacy and Biochemistry, Ante Kovačića 1, 10000 Zagreb, Croatia*

Author contributions:

All experiments were performed by Salavat S. Ashirbaev, all the calculations were performed by Salavat S. Ashirbaev with a help of Dr D. Šakić (for molecule **r3_N**). The manuscript is written jointly by Salavat S. Ashirbaev, Davor Šakić and Hendrik Zipse.

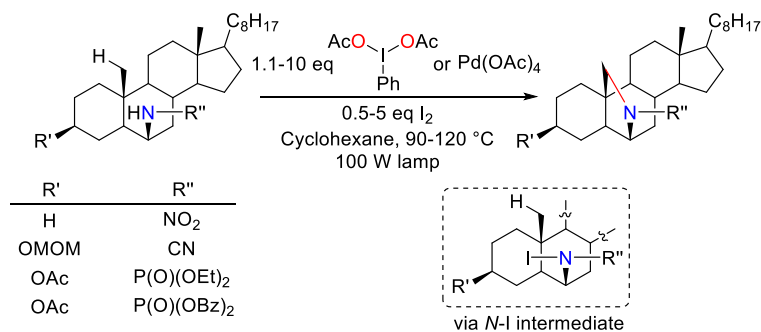
3.1. Introduction

The Hofmann-Löffler-Freytag (HLF) is an organic reaction leading to formation of pyrrolidine ring systems *via* *N*-centered radicals, generated by thermal or photochemical activation of *N*-haloamides. The reaction mechanism can be split into four major steps: a) generation of *N*-haloamine, b) cleavage of the *N*-halogen bond, c) 1,5-hydrogen atom transfer (HAT), d) trapping of the formed radical. One of the first reported reactions was the synthesis of nicotine from dihydrometanicotine (DMN), where the reaction conditions required strongly acidic conditions and elevated temperatures (~135 °C), followed by base work-up (Scheme 1).^[1]



Scheme 1. One of the first examples of the HLF reaction used for the synthesis of the natural compound nicotine.

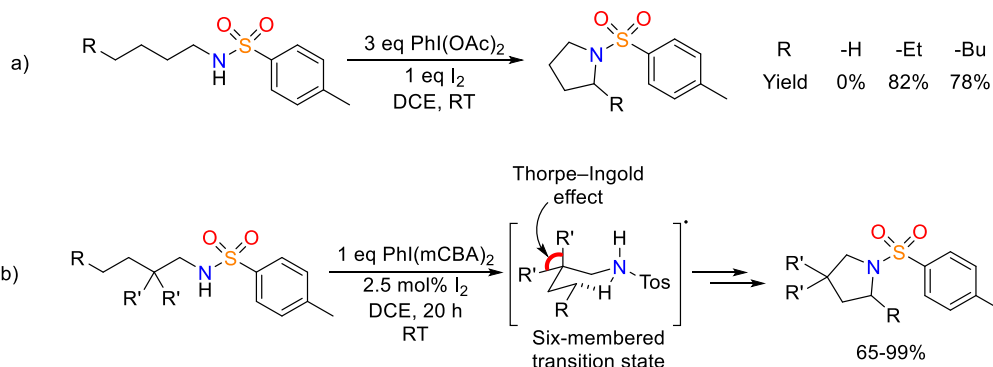
Since the described conditions are not suitable for sensitive substrates or protection groups, the reaction was modified. The most important modification of HLF reaction has been proposed by Suarez, which allows to run a reaction in a mild neutral environment, using a mixture of phenyliodine(III) diacetate (PIDA) or lead (IV) acetate with elemental iodine (Scheme 2).^[2]



Scheme 2. Suarez modification of the HLF reaction.

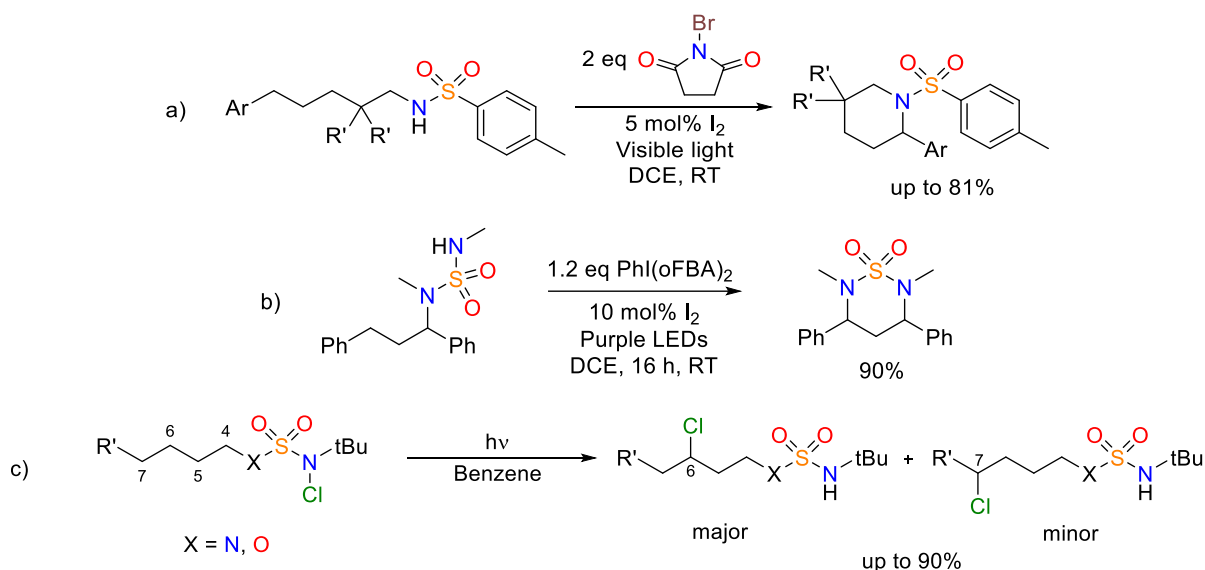
Later, the Suarez modification was improved by Fan *et al.*, who reported an effective functionalization of unmodified alkyl chains (Scheme 3a).^[3] Muniz showed that the HLF reaction can be performed using a catalytic amount of I₂ (2.5 mol), but the scope was limited

to gem-substituted substrates, which can be explained by the Thorpe–Ingold effect that promotes a six membered transition state (Scheme 3b).^[4]



Scheme 3. Fan and Muniz modifications of the HLF reaction.

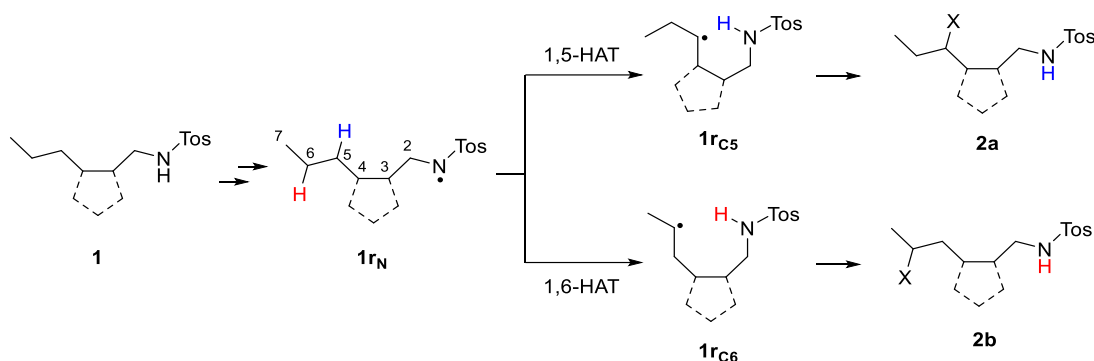
Due to recent developments of the HLF reactions it is possible to obtain also less common products such as those of 1,6-HAT reactions and, in some cases, piperidine derivatives (Scheme 4).^[5]



Scheme 4. 1,6-HAT mediated HLF reactions.

The HLF reaction provides an entry into aminyl-radical mediated C–H bond activation chemistry and has recently received renewed attention due to innovative methods for the generation of nitrogen-centered radicals. From our perspective, the HLF reaction is particularly interesting in the functionalization of otherwise unfunctionalized substrates such as sulfonamide **1** shown in Scheme 5, where the initially generated N-centered radical **1_{rN}** is positioned such that hydrogen abstraction seems feasible at the C5- or C6-position. Currently known experimental results indicate a large kinetic preference for the 1,5-HAT pathway. We now study here how this selectivity is affected by substituents positioned at the C3 and/or C4

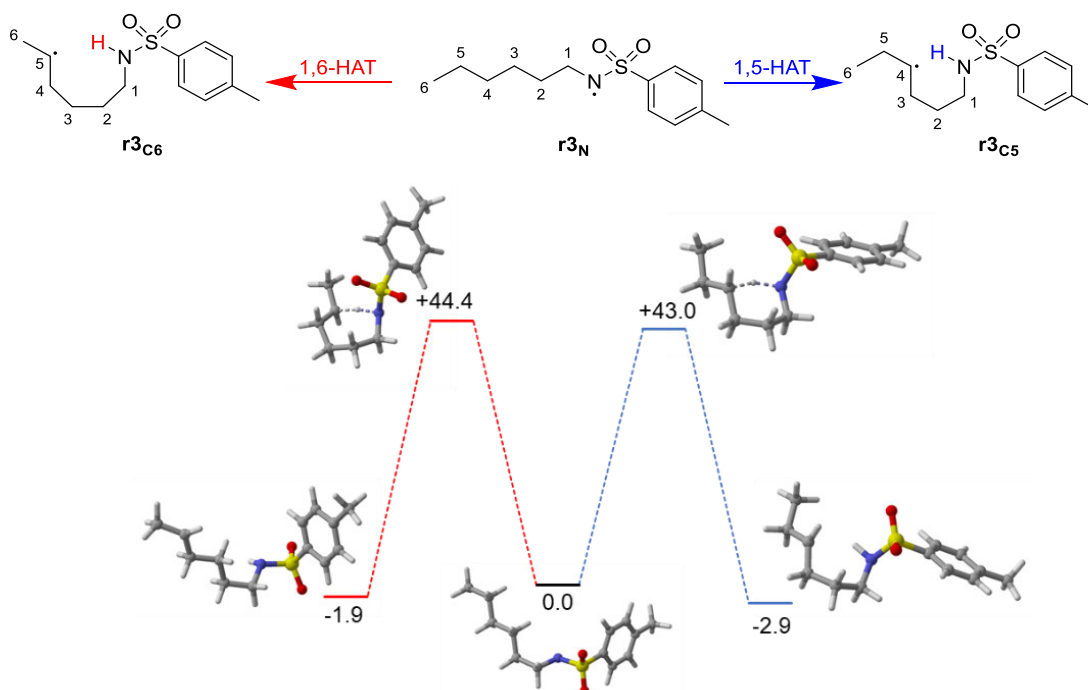
positions, with particular emphasis on the effects of annulated ring systems along these positions.



Scheme 5. HLF reaction of sulfonamide **1** to 1,5- and 1,6-functionalized products **2a** and **2b**.

3.2. Results and Discussions

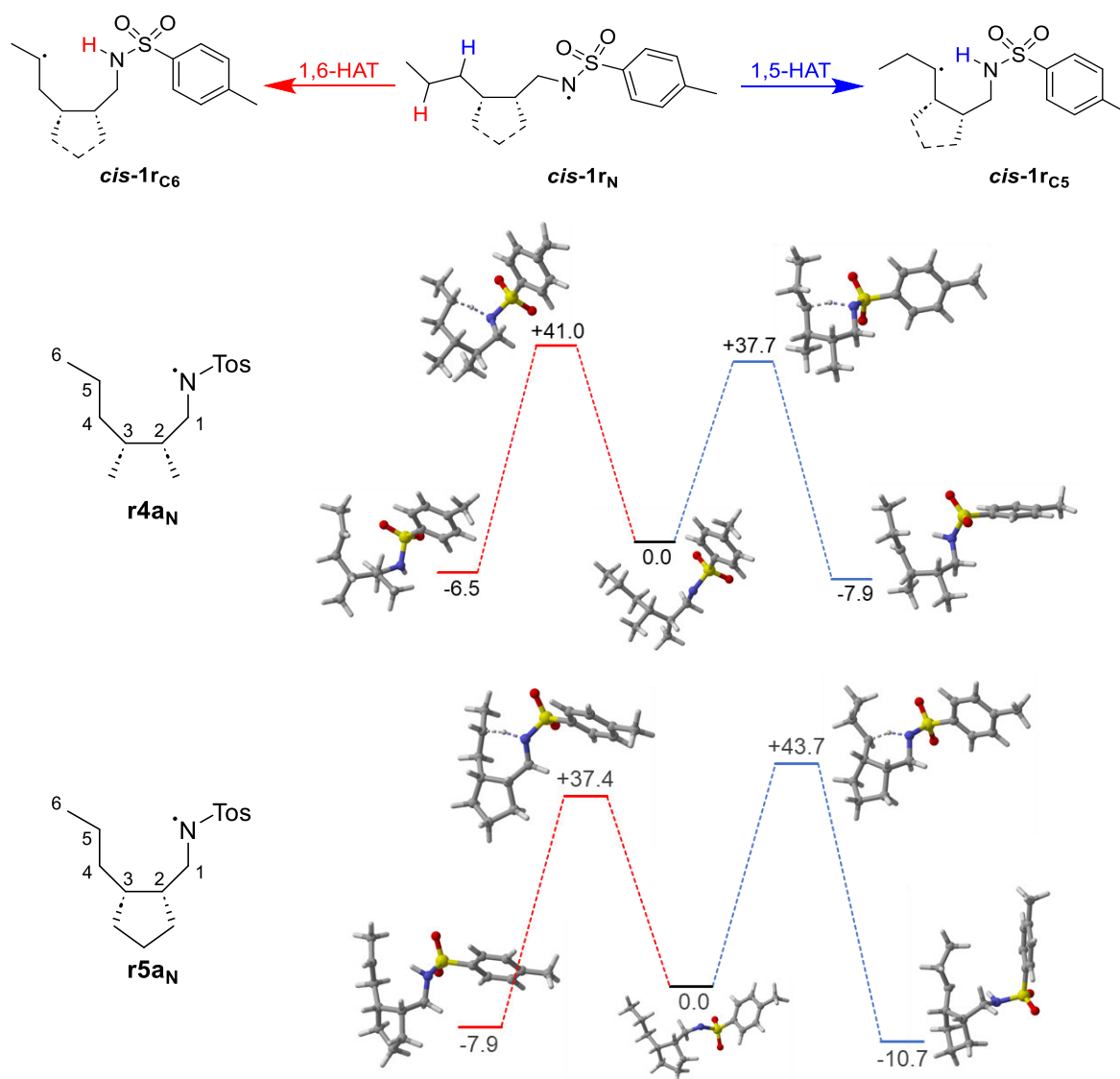
As a first step towards the exploration of the substituent effects outlined in Scheme 5, quantum chemical calculations on the reaction barriers and reaction energies for the respective 1,5- and 1,6-HAT reactions were performed at the DLPNO-CCSD(T)/cc-pVTZ//UB3LYP/6-31G(d) level of theory. The investigation is started from radical **r3_N** as our reference system, which showed no difference in the barriers or reaction enthalpies for the 1,5- or 1,6-HAT steps in the gas phase (Scheme 6).

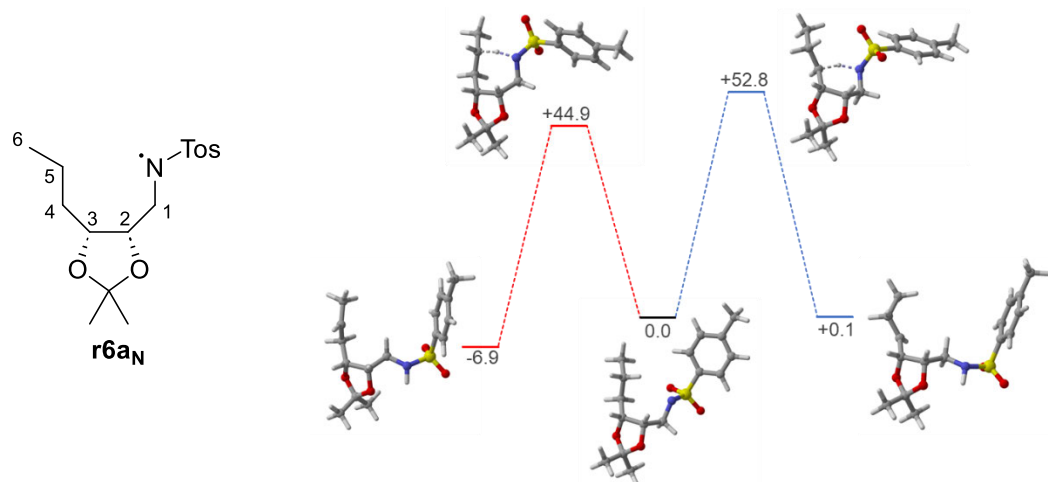


Scheme 6. HAT process of *N*-centered radical **r3_N** to radicals **r3_{c5}** and **r3_{c6}**, calculated at the DLPNO-CCSD(T)/cc-pVTZ//UB3LYP/6-31G(d) level of theory.

It was then decided to modify the unbiased system **r3_N** without any changes at the N-, C5- and C6-positions. Introduction of the 2,3-*cis*-vicinal methyl groups also has no significant influence on the 1,5- or 1,6-HAT barriers in system **r4_{aN}**. But forming a more rigid cyclopentane structure out of 2,3-*cis*-vicinal methyl groups in system **r5_{aN}**, gives lower barrier for previously non-favorable 1,6-HAT process ($\Delta H_{298} = -6.3$ kJ/mol). Since annulated cyclopentyl moiety is rather difficult to implement in the experiments, it was modified to the *cis*-2,2-dimethyl 1,3-dioxolane group, as a *cis*-acetonide protection group, in the system **r6_{aN}**. 1,6-HAT process again was found slightly favorable with $\Delta H_{298} = -7.9$ kJ/mol against 1,5-HAT reaction. The resulting enthalpy data are collected in Table 1.

Table 1. Activation and reaction enthalpies (ΔH_{298} , in kJ/mol) for the 1,5- and 1,6-HAT reactions in N-centered radical ***cis*-r1_N**.^[a]

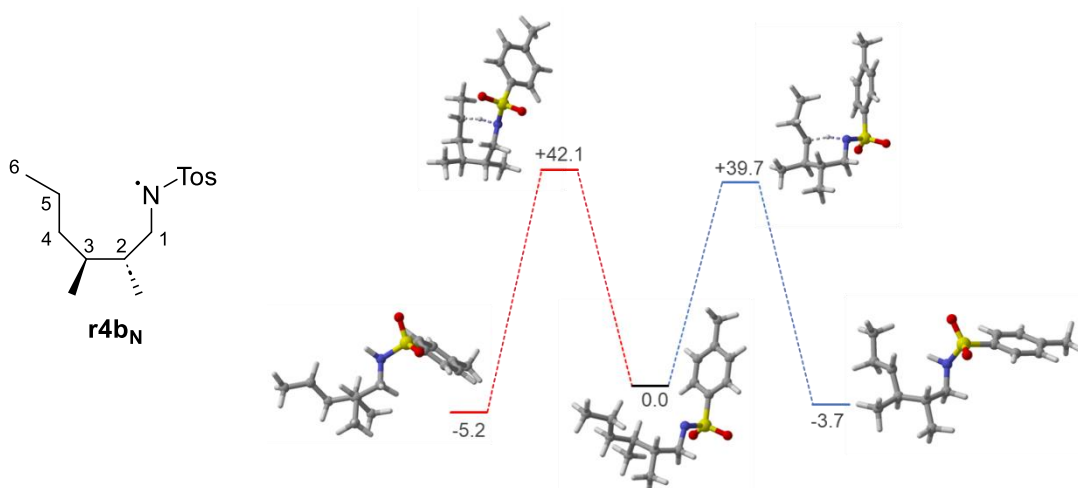
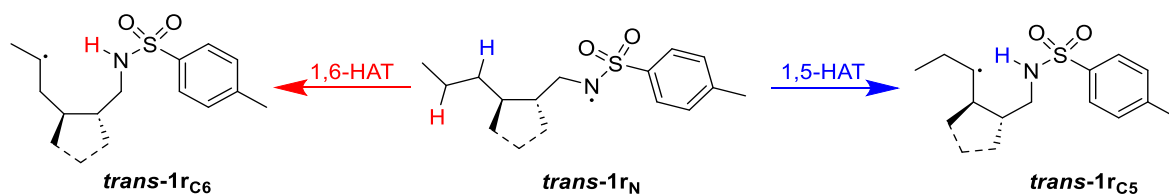


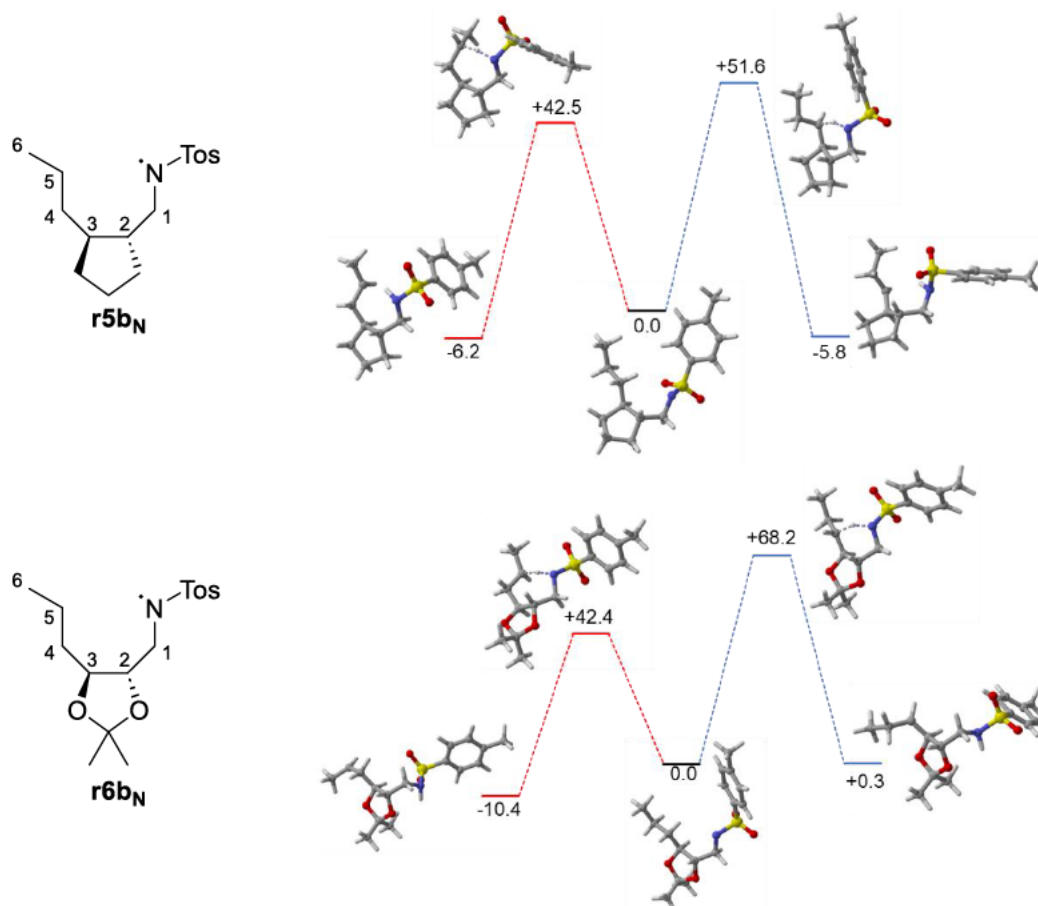


[a] Calculated at the DLPNO-CCSD(T)/cc-pVTZ//UB3LYP/6-31G(d) level of theory.

The same calculations were performed for the same systems, but with 2,3-*trans* configuration of moieties. Results are represented in Table 2. The introduction of both 2,3-*trans*-vicinal dimethyl group, **r4b_N**, and *trans*-annulated cyclopentyl moiety, **r5b_N**, showed almost no difference in comparison to 2,3-*cis*-systems, described above. But the calculation in system **r6b_N** leaves the barrier for the 1,6-HAT step practically unchanged, but increases the barrier for the 1,5-HAT reaction significantly ($\Delta H = -25.8$ kJ/mole).

Table 2. Activation and reaction enthalpies (ΔH_{298} , in kJ/mol) for the 1,5- and 1,6-HAT reactions in N-centered radical *trans*-**r1_N**.^[a]

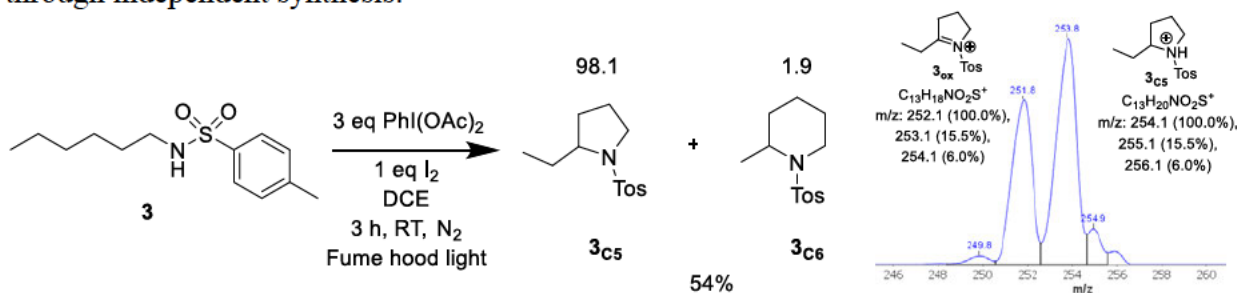




^[a] Calculated at the DLPNO-CCSD(T)/cc-pVTZ//UB3LYP/6-31G(d) level of theory.

Our QM calculations indicate that the 1,6-HAT pathway should be the predominant reaction route in the case of substrate **6b**. This can be explained by the fact that the 2,2-dimethyl 1,3-dioxolane ring, due to its relatively rigid structure, constrains the transition state in such a way that the 1,6-HAT pathway becomes energetically more favorable.

Our preliminary step was to repeat the reaction from Fan *et al.* with unbiased tosylamide **3** (Scheme 7). The resulting yields were lower (54% vs 82% from the yield described in the literature). A more detailed analysis showed that a mixture of the two isomeric products **3c5** and **3c6** (98.1 to 1.9 ratio) had been obtained. The structures of the products were confirmed through independent synthesis.

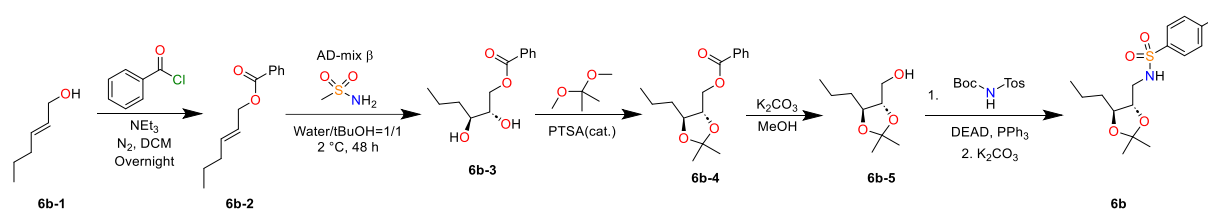


Scheme 7. Fan variation of HLF reaction for **3** with APCI MS spectrum profile (zoomed in).

The APCI MS analysis of the crude reaction mixture showed that use of excess oxidants leads to overoxidation. Almost half of the initial tosylamide **3** went into this pathway, which can explain the observed lower yields. The assumption is based on the detection of product **3_{ox}**, which is 2 m/z units lower than product **3_{c5}**, showing a potential overoxidation process. The observed product ratio is quite surprising, since the QM calculations suggested that the ratio between **3_{c5}** and **3_{c6}** products should be approximately 1 to 1, based on the transition state energies ($\Delta H^{TS} = +43$ and $+44.4$ kJ/mol, correspondingly). The results demonstrate that the formation of **3_{c5}** is a highly favorable pathway as well as the overoxidation of the substrates. This finding suggests that there are some additional factors influencing the reaction outcome, which were not accounted for in the current QM calculations. To answer this questions, further studies are needed to fully understand the underlying reasons for this difference and to adjust the theoretical models accordingly.

3.3. Outlook

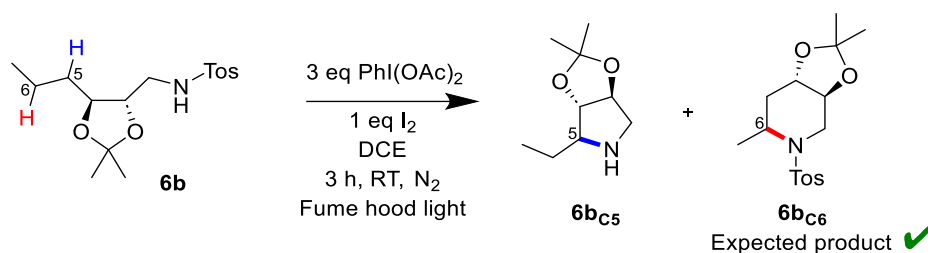
The Fan variation of HLF reaction requires further optimization to achieve the reported yields of 82%. Additionally, it is important to determine the structure of the overoxidation product **3_{ox}** to gain a deeper understanding of the processes occurring during the reaction. An ideal case would be to perform the reaction in a deuterated solvent, DCE-*d4*, for example, allowing for *in situ* monitoring of the reaction progress. To test our assumptions, the actual HLF reaction could be carried out with substrate **6b**. The proposed synthesis begins with the protection of the hydroxyl group of *trans*-2-hexen-1-ol (**6b-1**) using benzoyl chloride (Scheme 8).



Scheme 8. Proposed synthetic route to substrate **6b**.

The next step involves the Sharpless asymmetric dihydroxylation of intermediate **6b-2**, using the commercially available AD-mix- β , which forms diol **6b-3** with two chiral vicinal centers. When the 2,2-dimethyl 1,3-dioxolane ring is created, it also acts as a protecting group, since **6b-4** is treated with K_2CO_3 in MeOH in the next step. The hydroxyl group in **6b-5** is then substituted via the Mitsunobu reaction, using commercially available N-Boc-p-toluenesulfonamide, which is then hydrolyzed again with K_2CO_3 in MeOH. The described

synthetic strategy was successfully implemented to produce the target compound **6b**. The next step will be the HLF reaction with the obtained substrate **6b** to test our hypothesis (Scheme 9).



Scheme 9. Proposed HLF reaction with substrate **6b**.

3.4. References

- [1] a) K. Löffler, C. Freytag, *Ber. Dtsch. Chem. Ges.* **1909**, *42*, 3427-3431; b) K. Löffler, S. Kober, *Ber. Dtsch. Chem. Ges.* **1909**, *42*, 3431-3438.
- [2] P. de Armas, R. Carrau, J. I. Concepción, C. G. Francisco, R. Hernández, E. Suárez, *Tetrahedron Lett.* **1985**, *26*, 2493-2496.
- [3] R. Fan, D. Pu, F. Wen, J. Wu, *J. Org. Chem.* **2007**, *72*, 8994-8997.
- [4] C. Martínez, K. Muñiz, *Angew. Chem. Int. Ed.* **2015**, *54*, 8287-8291.
- [5] a) H. Zhang, K. Muñiz, *ACS Catal.* **2017**, *7*, 4122-4125; b) T. Duhamel, M. D. Martínez, I. K. Sideri, K. Muñiz, *ACS Catal.* **2019**, *9*, 7741-7745; c) M. A. Short, M. F. Shehata, M. A. Sanders, J. L. Roizen, *Chem. Sci.* **2020**, *11*, 217-223.

3.5. Supporting Information

3.5.1. Conformational Analysis and Reaction Energies

Force field-based calculations:

Maestro 10.2 was employed for molecular mechanics (MM)-based conformational search using OPLS_2005 force field (FF) parameters.

Quantum mechanics calculations:

The geometries of all the conformers were optimized at B3LYP/6-31G(d) level of theory in gas phase^[1]. The frequency calculations were performed at the same level of theory and all minima were confirmed with all positive frequencies. Thermochemical corrections to 298.15 K have been calculated at the same level of theory using the rigid rotor/harmonic oscillator model. The solvent correction for ΔG_{solv} was calculated at using IEFPCM in dichloroethane and subsequently added to the single point energy.^[2]

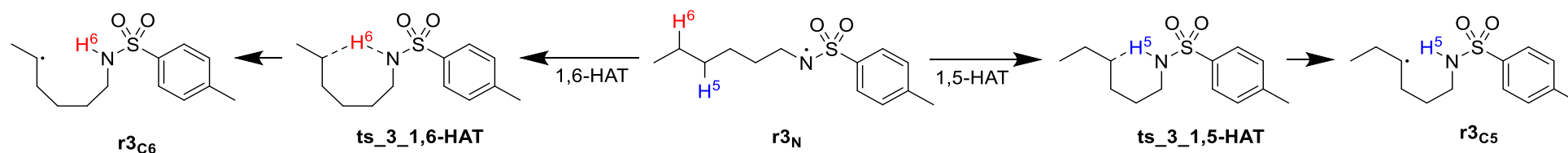


Fig. S1. Rearrangement reactions of *N*-centered radical **r3_N** to radical **r3_{C5}** and **r3_{C6}**.

Table S1a. Energies for all systems shown in Fig. S1.

Molecule	E_{tot} UB3LYP/ 6-31G(d) [Hartree]	$\langle S^2 \rangle$	NIMAG	dH UB3LYP/ 6-31G(d) [Hartree]	dG UB3LYP/ 6-31G(d) [Hartree]	E_{tot} PCM(DCE)/ UB3LYP/ 6-31G(d) ^[a] [Hartree]	dG_{298}^{solv} PCM(DCE)/ UB3LYP/ 6-31G(d) ^[a] [Hartree]	E_{tot} DLPNO-CCSD(T)/ cc-pVTZ ^[a] [Hartree]	G_{298}^{DCE} PCM(DCE) + DLPNO- CCSD(T)/cc-pVTZ ^[a] [Hartree]
r3_N									
TS Nr Cr intra TosHex Nrad MIN	-1110.711852	0.75	-	0.332657	0.260238	-1110.720177	-0.008325	-1109.042606	-1108.790694
TS Nr Cr intra TosHex Nrad MIN ver1	-1110.711673	0.75	-	0.332714	0.260453	-1110.720142	-0.008468	-1109.041909	-1108.789924
TS Nr Cr intra TosHex Nrad MIN ver11	-1110.711326	0.75	-	0.333302	0.260380	-1110.719808	-0.008482	-1109.041907	-1108.790009
1 n-rad	-1110.710732	0.75	-	0.332909	0.260710	-1110.718918	-0.008185	-1109.042669	-1108.790144
TS Nr Cr intra TosHex Nrad MIN ver32	-1110.710308	0.75	-	0.333330	0.260855	-1110.718700	-0.008392	-1109.040963	-1108.788500
TS_Nr_Cr_intra_TosHex_C5_tosrot_ver4_recalc_ircr	-1110.708942	0.75	-	0.333206	0.261450	-1110.716974	-0.008032	-1109.040496	-1108.787077
TS Nr Cr intra TosHex C6 tosrot ver1 recalc ircr o 2	-1110.704811	0.75	-	0.333306	0.262201	-1110.712741	-0.007930	-1109.037588	-1108.783317
ts 3_1,6-HAT									
TS_Nr_Cr_intra_TosHex_C6_tosrot_ver1_recalc	-1110.684442	0.76	-1608	0.327314	0.260990	-1110.693388	-0.008946	-1109.020361	-1108.768318
TS Nr Cr intra TosHex C6 tosrot ver4	-1110.683528	0.76	-1518	0.327107	0.258755	-1110.692659	-0.009131	-1109.018510	-1108.768886

ts 1 1 6-HAT 2	-1110.680990	0.76	-1607	0.327387	0.260536	-1110.690747	-0.009757	-1109.018031	-1108.767253
ts 1 1 6-HAT	-1110.680211	0.76	-1633	0.327369	0.259559	-1110.689504	-0.009293	-1109.016241	-1108.765974
TS_Nr_Cr_intra_TosHex_C6	-1110.679097	0.76	-1519	0.327167	0.261343	-1110.690922	-0.011825	-1109.016470	-1108.766953
r3_{ce}									
TS Nr Cr intra TosHex C6 MIN	-1110.703286	0.75	-	0.332088	0.258413	-1110.713700	-0.010414	-1109.042771	-1108.794771
TS Nr Cr intra TosHex C6 MIN ver32	-1110.702394	0.75	-	0.332219	0.258164	-1110.712159	-0.009765	-1109.041596	-1108.793197
TS Nr Cr intra TosHex C6 tosrot ver1 recalc ircf o	-1110.702375	0.75		0.332449	0.261863	-1110.711001	-0.008625	-1109.042444	-1108.789207
TS Nr Cr intra TosHex C6 MIN ver4 2	-1110.701795	0.75	-	0.332127	0.258040	-1110.712243	-0.010448	-1109.040467	-1108.792875
1 1 6-HAT c-rad	-1110.701557	0.75	-	0.332614	0.259437	-1110.711121	-0.009564	-1109.041796	-1108.791923
ts 3 1,5-HAT									
TS Nr Cr intra TosHex C5 tosrot ver4 recalc	-1110.684737	0.76	-1577	0.327332	0.259432	-1110.367241	-0.009836	-1109.020885	-1108.771289
TS Nr Cr intra TosHex C5 tosrot ver1	-1110.684317	0.76	-1671	0.327336	0.258660	-1110.366661	-0.009681	-1109.020453	-1108.771474
ts_unbiased_1_5_HAT_2	-1110.684044	0.76	-1583	0.327275	0.258666	-1110.367124	-0.010355	-1109.020242	-1108.771931
ts_unbiased_1_5_HAT_preopt	-1110.682674	0.76	-1704	0.327283	0.258546	-1110.366000	-0.010610	-1109.020613	-1108.772677
TS Nr Cr intra TosHex C5	-1110.680907	0.76	-1605	0.327343	0.260227	-1110.365706	-0.012142	-1109.019336	-1108.771251
r3_{cs}									
TS Nr Cr intra TosHex C5 tosrot ver4 recalc ircf	-1110.704253	0.75	-	0.332435	0.259240	-1110.713498	-0.009245	-1109.043480	-1108.793485
TS Nr Cr intra TosHex C5 MIN ver1	-1110.702545	0.75	-	0.332243	0.258267	-1110.714360	-0.011816	-1109.042832	-1108.796380
1 1 5-HAT c-rad	-1110.702391	0.75	-	0.332335	0.257399	-1110.712795	-0.010404	-1109.041974	-1108.794979
TS_Nr_Cr_intra_TosHex_C5_MIN_ver12	-1110.702336	0.75	-	0.332279	0.258660	-1110.712439	-0.010103	-1109.040482	-1108.791925
TS Nr Cr intra TosHex C5 MIN ver11	-1110.702180	0.75	-	0.332207	0.257668	-1110.712379	-0.010199	-1109.040285	-1108.792816
TS Nr Cr intra TosHex C5 MIN ver32	-1110.701837	0.75	-	0.332328	0.258589	-1110.711756	-0.009919	-1109.040856	-1108.792186

[a] Using the gas phase geometry optimized at UB3LY/6-31G(d) level.

Table S1b. Relative energies for all systems shown in Fig. S1 (UB3LYP/6-31G(d) result).

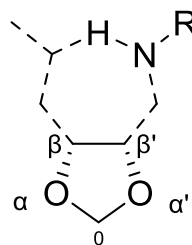
Molecule	UB3LYP/6-31(d)						
	Gas phase			PCM(DiChloroEthane)		DLPNO-CCSD(T)/cc-pVTZ	
	ΔE_{tot} [Hartree]	ΔH_{298} [kJ/mol]	ΔG_{298} [kJ/mol]	ΔH_{298} [kJ/mol]	ΔG_{298} [kJ/mol]	ΔH_{298} [kJ/mol]	ΔG_{298} [kJ/mol]
r3_N							
TS_Nr_Cr_intra_TosHex_Nrad_MIN	+0.0	+0.0	+0.0	+0.0	+0.0	+0.0	+0.0
S_Nr_Cr_intra_TosHex_Nrad_MIN_ver1	+0.5	+0.6	+1.0	+0.2	+0.7	+2.0	+2.4
TS_Nr_Cr_intra_TosHex_Nrad_MIN_ver11	+1.4	+3.1	+1.8	+2.7	+1.3	+3.5	+2.2
1_n-rad	+2.9	+3.6	+4.2	+4.0	+4.5	+0.5	+1.1
TS_Nr_Cr_intra_TosHex_Nrad_MIN_ver32	+4.1	+5.8	+5.7	+5.6	+5.5	+6.1	+5.9
TS_Nr_Cr_intra_TosHex_C5_tosrot_ver4_recalc ircf	+7.6	+9.1	+10.8	+9.9	+11.6	+7.0	+8.7
TS_Nr_Cr_intra_TosHex_C6_tosrot_ver1_recalc ircr_2	+18.5	+20.2	+23.6	+21.2	+24.7	+14.9	+18.3
ts 3 1,6-HAT							
TS_Nr_Cr_intra_TosHex_C6_tosrot_ver1_recalc	+72.0	+57.9	+73.9	+56.3	+72.3	+44.4	+60.4
TS_Nr_Cr_intra_TosHex_C6_tosrot_ver4	+74.4	+59.8	+70.5	+57.7	+68.4	+48.7	+59.4
ts_1_1_6-HAT_2	+81.0	+67.2	+81.8	+63.4	+78.1	+50.7	+65.3
ts_1_1_6-HAT	+83.1	+69.2	+81.3	+66.6	+78.8	+55.3	+67.4

TS_Nr_Cr_intra_TosHex_C6	+86.0	+71.6	+88.9	+62.4	+79.7	+54.2	+71.5
r3_{C6}							
TS_Nr_Cr_intra_TosHex_C6_MIN	+22.5	+21.0	+17.7	+15.5	+12.2	-1.9	-5.2
TS_Nr_Cr_intra_TosHex_C6_MIN_ver32	+24.8	+23.7	+19.4	+19.9	+15.6	+1.5	-2.8
TS_Nr_Cr_intra_TosHex_C6_tosrot_ver1_recalc_ircf_o	+24.9	+24.3	+29.1	+23.5	+28.4	-0.1	+4.7
TS_Nr_Cr_intra_TosHex_C6_MIN_ver4_2	+26.4	+25.0	+20.6	+19.4	+15.1	+4.2	-0.2
1_1_6-HAT_c-rad	+27.0	+26.9	+24.9	+23.7	+21.7	+2.0	+0.0
ts 3 1,5-HAT							
TS_Nr_Cr_intra_TosHex_C6_tosrot_ver1_recalc	+71.2	+57.2	+69.1	+53.2	+65.1	+43.0	+54.9
TS_Nr_Cr_intra_TosHex_C5_tosrot_ver1	+72.3	+58.3	+68.1	+54.8	+64.6	+44.2	+54.0
ts_unbiased_1_5_HAT_2	+73.0	+58.9	+68.9	+53.6	+63.6	+44.6	+54.6
ts_unbiased_1_5_HAT_preopt	+76.6	+62.5	+72.2	+56.5	+66.2	+43.6	+53.3
TS_Nr_Cr_intra_TosHex_C5	+81.2	+67.3	+81.2	+57.3	+71.2	+47.1	+61.1
r3_{C5}							
TS_Nr_Cr_intra_TosHex_C5_tosrot_ver4_recalc_ircf	+19.9	+19.4	+17.3	+17.0	+14.9	-2.9	-4.9
TS_Nr_Cr_intra_TosHex_C5_MIN_ver1	+24.4	+23.3	+19.3	+14.2	+10.1	-1.7	-5.8
1_1_5-HAT_c-rad	+24.8	+24.0	+17.4	+18.5	+11.9	+0.8	-5.8
TS_Nr_Cr_intra_TosHex_C5_MIN_ver12	+25.0	+24.0	+20.8	+19.3	+16.2	+4.6	+1.4
TS_Nr_Cr_intra_TosHex_C5_MIN_ver11	+25.4	+24.2	+18.6	+19.3	+13.7	+4.9	-0.7
TS_Nr_Cr_intra_TosHex_C5_MIN_ver32	+26.3	+25.4	+22.0	+21.2	+17.8	+3.7	+0.3

1) Conformational search for found ts_4_5, ts_4_6 was performed on Maestro 10.2 software as described above.

Conformers are described by 4 parameters: conformation for

1.1 1,3-dioxalane ring conformation:

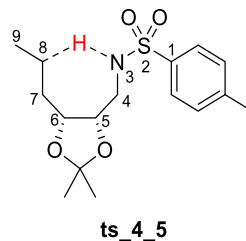


1,3-dioxalane

Envelope (E) conformations are characterized by coplanarity of four adjacent ring atoms (any dihedral angle between 0, α , β , β' , α' $<$ 10°). Arrow shows relative position of the fifth atom: \downarrow - below the plane, \uparrow - above the plane. For example, E $\beta'\uparrow$ means that 0, α , β , α' are on the same plane and atom β' is

above the plane. Twisted conformations were considered when no four adjacent ring atoms were found (dihedral angle between 0, α , β , β' , $\alpha' > 10^\circ$). Two possible twisted conformations are possible $T\uparrow\downarrow$, when α is above the 0, β , β' plane, and $T\downarrow\uparrow$, when α is below the 0, β , β' plane.^[3]

1.2. Torsion angle $\varphi(1-2-3-4)$, $\chi(2-3-4-5)$, $\psi(5-6-7-8)$, $\omega(6-7-8-9)$: s (synperiplannar, $350^\circ-10^\circ$), g1+ (gauche, $10-100^\circ$), e+ (eclipsed, $110-130^\circ$), g2+ (gauche, $140-170^\circ$), a (anti, $170-190^\circ$), g1- (gauche, $190-230^\circ$), e- (eclipsed, $230-250^\circ$), g2- (gauche, $250-350^\circ$)



2) Structures in blue were gotten from 1,5-HAT transition states. Structures in red were gotten from 1,6-HAT transition states.

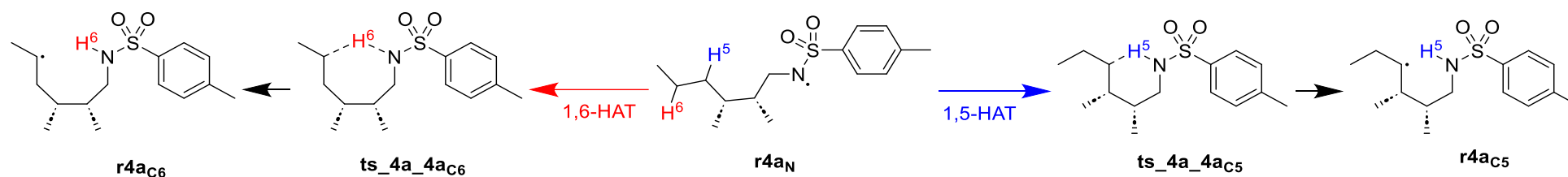


Fig. S2. Rearrangement reactions of *N*-centered radical **r4aN** to radicals **r4aC5** and **r4aC6**

Table S2a. Energies for all systems shown in Fig. S2

Molecule	E_{tot} UB3LYP/ 6-31G(d) [Hartree]	$\langle S^2 \rangle$	NIMAG	dH UB3LYP/ 6-31G(d) [Hartree]	dG UB3LYP/ 6-31G(d) [Hartree]	E_{tot} PCM(DCE)/ UB3LYP/ 6-31G(d) ^[a] [Hartree]	dG_{298}^{solv} PCM(DCE)/ UB3LYP/ 6-31G(d) ^[a] [Hartree]	E_{tot} DLPNO-CCSD(T)/ cc-pVTZ ^[a] [Hartree]	G_{298}^{DCE} PCM(DCE) + DLPNO- CCSD(T)/cc-pVTZ ^[a] [Hartree]
r4aN									
dimet cis N-rad 1	-1189.334741	0.75	-	0.391972	0.313303	-1189.342993	-0.008251	-1187.523100	-1183.909314
dimet cis N-rad 47	-1189.334456	0.75	-	0.391920	0.313230	-1189.342707	-0.008251	-1187.522265	-1183.909062
dimet cis N-rad 4	-1189.333806	0.75	-	0.392322	0.315458	-1189.341737	-0.007930	-1187.523870	-1183.906690
dimet cis N-rad 11	-1189.333753	0.75	-	0.392648	0.315777	-1189.341920	-0.008168	-1187.522462	-1183.904495
ts dimet cis 15HAT 32 ircr	-1189.333212	0.75	-	0.392208	0.315035	-1189.341407	-0.008195	-1187.523315	-1183.904946
dimet cis N-rad 14	-1189.331967	0.75	-	0.392050	0.314178				
dimet cis N-rad 100	-1189.329754	0.75	-	0.392233	0.314752				
ts dimet cis 16HAT 6 ircr	-1189.328936	0.75	-	0.391999	0.313912				
dimet cis N-rad 86	-1189.326872	0.75	-	0.392585	0.314466				
ts_4a_4aC6									
ts dimet cis 16HAT 6	-1189.308816	0.76	-1670	0.386320	0.312496	-1189.318993	-0.010178	-1187.501951	-1183.859556

ts dimet cis 16HAT 2	-1189.308217	0.76	-1552	0.386469	0.313497	-1189.31964	-0.011424	-1187.502377	-1183.860114
ts dimet cis 16HAT 3	-1189.308201	0.76	-1552	0.386458	0.313691	-1189.319629	-0.011429	-1187.502372	-1183.860088
ts_dimet_cis_16HAT_14	-1189.302873	0.76	-1646	0.386683	0.315325	-1189.314715	-0.011842	-1187.497577	-1183.854182
ts dimet cis 16HAT 16	-1189.301926	0.76	-1583	0.386534	0.313803	-1189.318993	-0.010178	-1187.501951	-1183.859556
ts dimet cis 16HAT 7	-1189.301154	0.76	-1607	0.386552	0.313872				
ts dimet cis 16HAT 9	-1189.300146	0.76	-1537	0.386634	0.313429				
ts dimet cis 16HAT 1	-1189.299686	0.76	-1502	0.386372	0.313908				
ts dimet cis 16HAT 20	-1189.295604	0.76	-1610	0.386857	0.314867				
ts dimet cis 16HAT 18	-1189.288964	0.76	-1664	0.386970	0.315374				
r4a_{c6}									
dimet cis C6-rad 29	-1189.327153	0.75	-	0.391418	0.312550	-1189.337438	-0.010284	-1187.524669	-1183.909132
dimet cis C6-rad 4 2	-1189.326460	0.75	-	0.391538	0.312310	-1189.336754	-0.010294	-1187.522829	-1183.908322
dimet_cis_C6-rad_32	-1189.326414	0.75	-	0.391473	0.312797	-1189.335986	-0.009572	-1187.522914	-1183.906852
dimet cis C6-rad 80	-1189.326379	0.75	-	0.391524	0.312310	-1189.336665	-0.010287	-1187.522836	-1183.908232
dimet cis C6-rad 1	-1189.326365	0.75	-	0.391645	0.315592	-1189.335621	-0.009256	-1187.525677	-1183.904993
dimet cis C6-rad 93	-1189.324999	0.75	-	0.391590	0.312740				
ts dimet cis 16HAT 6 ircf	-1189.324485	0.75	-	0.391557	0.312663				
dimet cis C6-rad 8	-1189.323552	0.75	-	0.391556	0.312966				
dimet cis C6-rad 54	-1189.321248	0.75	-	0.391668	0.313330				
ts 4a 4a_{c5}									
ts dimet cis 15HAT 32	-1189.310981	0.76	-1601	0.386543	0.312224	-1189.320849	-0.009867	-1187.503368	-1183.861544
ts dimet cis 15HAT 23	-1189.310895	0.76	-1543	0.386582	0.312216	-1189.320948	-0.010053	-1187.503786	-1183.861669
ts_dimet_cis_15HAT_36	-1189.309764	0.76	-1542	0.386618	0.311717	-1189.320051	-0.010288	-1187.502357	-1183.860774
ts dimet cis 15HAT 14	-1189.309588	0.76	-1680	0.386573	0.312083	-1189.319821	-0.010233	-1187.503733	-1183.861085
ts dimet cis 15HAT 12	-1189.309429	0.76	-1705	0.386591	0.313069	-1189.319504	-0.010074	-1187.502429	-1183.860105
ts dimet cis 15HAT 30	-1189.309212	0.76	-1563	0.386652	0.312475				
ts dimet cis 15HAT 29	-1189.308967	0.76	-1559	0.386797	0.313832				
ts dimet cis 15HAT 10	-1189.308894	0.76	-1598	0.386747	0.312812				
ts dimet cis 15HAT 39	-1189.308640	0.76	-1676	0.386637	0.312017				
ts_dimet_cis_15HAT_38	-1189.308516	0.76	-1558	0.386700	0.311930				
ts dimet cis 15HAT 11	-1189.308197	0.76	-1692	0.386506	0.313035				
ts dimet cis 15HAT 2	-1189.308084	0.76	-1580	0.386463	0.313282				
ts_dimet_cis_15HAT_28	-1189.307815	0.76	-1681	0.386585	0.312439				
ts dimet cis 15HAT 4	-1189.307694	0.76	-1656	0.386714	0.314550				
ts dimet cis 15HAT 46	-1189.307575	0.76	-1539	0.386773	0.313205				
ts dimet cis 15HAT 31	-1189.307454	0.76	-1725	0.386737	0.312802				
ts_dimet_cis_15HAT_34	-1189.307438	0.76	-1693	0.386875	0.312863				
ts dimet cis 15HAT 24	-1189.307129	0.76	-1596	0.386689	0.311399				
ts dimet cis 15HAT 37	-1189.306795	0.76	-1575	0.386759	0.313172				
ts_dimet_cis_15HAT_44	-1189.306561	0.76	-1665	0.386736	0.312258				
ts dimet cis 15HAT 7	-1189.306427	0.76	-1586	0.386674	0.313703				
ts dimet cis 15HAT 41	-1189.306264	0.76	-1580	0.386872	0.312203				
ts dimet cis 15HAT 26	-1189.305268	0.76	-1694	0.386834	0.312615				
ts dimet cis 15HAT 21	-1189.304755	0.76	-1600	0.385714	0.314948				
ts dimet cis 15HAT 16	-1189.304739	0.76	-1615	0.386917	0.314084				
ts dimet cis 15HAT 18	-1189.304603	0.76	-1599	0.386702	0.313457				
ts_dimet_cis_15HAT_22	-1189.304311	0.76	-1670	0.386561	0.313845				
ts dimet cis 15HAT 3	-1189.303861	0.76	-1551	0.386517	0.312030				

ts dimet cis 15HAT 8	-1189.303481	0.76	-1679	0.386696	0.313330				
ts dimet cis 15HAT 6	-1189.303427	0.76	-1640	0.386737	0.313344				
ts dimet cis 15HAT 48	-1189.303408	0.76	-1668	0.387006	0.313160				
ts dimet cis 15HAT 5	-1189.301578	0.76	-1573	0.386923	0.314043				
ts dimet cis 15HAT 15	-1189.300419	0.76	-1519	0.386924	0.313160				
ts dimet cis 15HAT 9	-1189.299106	0.76	-1647	0.386658	0.313835				
ts dimet cis 15HAT 47	-1189.298856	0.76	-1604	0.387047	0.314412				
ts dimet cis 15HAT 40	-1189.294452	0.76	-1702	0.387016	0.314933				
r4acs									
dimet cis C5-rad 102	-1189.329366	0.75	-	0.392025	0.315360	-1189.338946	-0.009579	-1187.524918	-1183.906743
ts dimet cis 15HAT 32 ircf	-1189.329366	0.75	-	0.392025	0.315361	-1189.338945	-0.009579	-1187.524917	-1183.906743
dimet cis C5-rad 27	-1189.329195	0.75	-	0.391623	0.314401	-1189.337934	-0.008739	-1187.526176	-1183.905293
dimet cis C5-rad 69	-1189.328489	0.75	-	0.391873	0.313775	-1189.338578	-0.010089	-1187.526441	-1183.909756
dimet cis C5-rad 83	-1189.328379	0.75	-	0.391723	0.314150	-1189.338354	-0.009975	-1187.525004	-1183.906810
dimet cis C5-rad 15	-1189.327765	0.75	-	0.391997	0.313588				
dimet cis C5-rad 8	-1189.326657	0.75	-	0.391836	0.312581				
dimet cis C5-rad 39	-1189.325467	0.75	-	0.391957	0.314851				
dimet cis C5-rad 47	-1189.321488	0.75	-	0.391563	0.313164				

Table S2b. Energies for all systems shown in Fig. S2 (UB3LYP/6-31G(d) result).

Molecule	UB3LYP/6-31(d)							Conformation $\varphi \chi \psi \omega$
	Gas phase			PCM(DiChloroEthane)		DLPNO-CCSD(T)/cc-pVTZ		
	ΔE_{tot} [Hartree]	ΔH_{298} [kJ/mol]	ΔG_{298} [kJ/mol]	ΔH_{298} [kJ/mol]	ΔG_{298} [kJ/mol]	ΔH_{298} [kJ/mol]	ΔG_{298} [kJ/mol]	
r4an								
dimet cis N-rad 1	0.0	0.0	0.0	0.0	0.0	+0.0	+0.0	a_a_g1-_a
dimet cis N-rad 47	+0.7	+0.6	+0.6	+0.6	+0.6	+2.1	+2.0	a_a_g1-_a
dimet cis N-rad 4	+2.5	+3.4	+8.1	+4.2	+9.0	-1.1	+3.6	a_g1-_g1-_g1+
dimet cis N-rad 11	+2.6	+4.4	+9.1	+4.6	+9.3	+3.4	+8.2	g1-_g2-_g2-_a
ts dimet cis 15HAT 32 ircr	+4.0	+4.6	+8.6	+4.8	+8.7	+0.1	+4.0	a_g2+_g1-_a
dimet cis N-rad 14	+7.3	+7.5	+9.6					a_a_g2-_a
dimet cis N-rad 100	+13.1	+13.8	+16.9					a_g2+_g1-_g2-
ts dimet cis 16HAT 6 ircr	+15.2	+15.3	+16.8					a_a_g2-_a
dimet cis N-rad 86	+20.7	+22.3	+23.7					g1-_g2-_a_g2-
ts_4a_4acs								
ts dimet cis 16HAT 6	+68.1	+53.2	+65.9	+48.2	+60.9	+40.7	+53.4	a_a_g2-_a
ts dimet cis 16HAT 2	+69.6	+55.2	+70.1	+46.9	+61.8	+40.0	+54.9	g2-_a_g2-_g2+
ts dimet cis 16HAT 3	+69.7	+55.2	+70.7	+46.9	+62.4	+39.9	+55.4	g2-_a_g2-_g2+
ts dimet cis 16HAT 14	+83.7	+69.8	+89.0	+60.4	+79.6	+53.1	+72.3	g1+_a_g2-_a
ts dimet cis 16HAT 16	+86.2	+71.9	+87.5					g2-_g1+_g2-_a

ts_dimet_cis_16HAT_7	+88.2	+74.0	+89.7					g1+_a_g1+_g1+
ts_dimet_cis_16HAT_9	+90.8	+76.8	+91.2					g2-_e+_g1+_g1+
ts_dimet_cis_16HAT_1	+92.0	+77.3	+93.6					g1+_e-_g2-_g2+
ts_dimet_cis_16HAT_20	+102.8	+89.3	+106.9					g2-_a_g1+_g1+
ts_dimet_cis_16HAT_18	+120.2	+107.1	+125.6					g1+_e-_g1+_g1+
r4ac6								
dimet_cis_C6-rad_29	+19.9	+18.5	+17.9	+13.1	+12.6	-5.6	-6.1	g1+_a_g1-_g1-
dimet_cis_C6-rad_4_2	+21.7	+20.6	+19.1	+15.2	+13.8	-0.4	-1.9	g1+_a_g1-_g1-
dimet_cis_C6-rad_32	+21.9	+20.6	+20.5	+17.1	+17.1	-0.8	-0.8	g2-_g2-_g1-_g1-
dimet_cis_C6-rad_80	+22.0	+20.8	+19.3	+15.4	+14.0	-0.5	-1.9	g2-_a_g1-_g1-
dimet_cis_C6-rad_1	+22.0	+21.1	+28.0	+18.5	+25.4	-7.6	-0.8	g1+_g2-_g2-_g2+
dimet_cis_C6-rad_93	+25.6	+24.6	+24.1					g2+_g1-_g1-_g1-
ts_dimet_cis_16HAT_6_ircf	+26.9	+25.8	+25.2					g2+_g1-_g2-_g2+
dimet_cis_C6-rad_8	+29.4	+28.3	+28.5					g2-_g2-_g1-_g1-
dimet_cis_C6-rad_54	+35.4	+34.6	+35.5					e-_g2-_g1+_g1-
ts_4a_4acs								
ts_dimet_cis_15HAT_32	+62.4	+48.1	+59.5	+43.9	+55.3	+37.6	+49.0	g1+_g2+_g1-_a
ts_dimet_cis_15HAT_23	+62.6	+48.5	+59.8	+43.7	+55.0	+36.6	+47.9	g2-_g1-_g2-_a
ts_dimet_cis_15HAT_36	+65.6	+51.5	+61.4	+46.2	+56.1	+40.4	+50.3	g2-_g1-_g2-_g2-
ts_dimet_cis_15HAT_14	+66.0	+51.9	+62.8	+46.7	+57.6	+37.0	+56.2	a_g1-_g2-_a
ts_dimet_cis_15HAT_12	+66.5	+52.3	+65.8	+47.5	+61.1	+40.0	+55.6	g2+_g2+_g1-_a
ts_dimet_cis_15HAT_30	+67.0	+53.1	+64.9					g1+_g1+_g2-_g2-
ts_dimet_cis_15HAT_29	+67.7	+54.1	+69.1					g1+_g2+_g1-_g1+
ts_dimet_cis_15HAT_10	+67.9	+54.1	+66.6					g1-_g2-_g1-_a
ts_dimet_cis_15HAT_39	+68.5	+54.5	+65.2					a_g1-_g2-_g2-
ts_dimet_cis_15HAT_38	+68.9	+55.0	+65.2					g1+_g2+_g1-_g2-
ts_dimet_cis_15HAT_11	+69.7	+55.3	+69.0					g2+_g1+_g2-_a
ts_dimet_cis_15HAT_2	+70.0	+55.5	+69.9					g1+_g1-_g2-_a
ts_dimet_cis_15HAT_28	+70.7	+56.6	+68.4					a_g1+_g2-_g2-
ts_dimet_cis_15HAT_4	+71.0	+57.2	+74.3					g2-_g2+_g1-_a
ts_dimet_cis_15HAT_46	+71.3	+57.7	+71.1					g2-_g1-_g2-_g1+
ts_dimet_cis_15HAT_31	+71.6	+57.9	+70.3					a_g2+_g1-_g1+
ts_dimet_cis_15HAT_34	+71.7	+58.3	+70.5					a_g2+_g1-_g2-
ts_dimet_cis_15HAT_24	+72.5	+58.6	+67.5					g1-_g2-_g1-_g1+
ts_dimet_cis_15HAT_37	+73.4	+59.7	+73.0					g1+_g2+_g1+_a
ts_dimet_cis_15HAT_44	+74.0	+60.2	+71.2					a_g1-_g2-_g1+
ts_dimet_cis_15HAT_7	+74.3	+60.4	+75.4					g1+_g1-_g2-_g2-
ts_dimet_cis_15HAT_41	+74.8	+61.4	+71.9					g1-_g2-_g1-_g2-
ts_dimet_cis_15HAT_26	+77.4	+63.9	+75.6					a_g2+_g1+_a

ts_dimet_cis_15HAT_21	+78.7	+62.3	+83.0					g2-_g2+_g1+_a
ts_dimet_cis_15HAT_16	+78.8	+65.5	+80.8					g2-_g2+_g1-_g2-
ts_dimet_cis_15HAT_18	+79.1	+65.3	+79.5					g1+_g1-_g2-_g1+
ts_dimet_cis_15HAT_22	+79.9	+65.7	+81.3					g2-_g1+_g2-_a
ts_dimet_cis_15HAT_3	+81.1	+66.8	+77.7					g1+_e-_g1-_a
ts_dimet_cis_15HAT_8	+82.1	+68.2	+82.1					g2-_a_g1-_g1+
ts_dimet_cis_15HAT_6	+82.2	+68.5	+82.3					g2-_g1+_g2-_g2-
ts_dimet_cis_15HAT_48	+82.3	+69.2	+81.9					a_g2+_g1+_g1+
ts_dimet_cis_15HAT_5	+87.1	+73.8	+89.0					g1+_e-_g1-_g1+
ts_dimet_cis_15HAT_15	+90.1	+76.9	+89.7					g1+_e-_g1-_g2-
ts_dimet_cis_15HAT_9	+93.6	+79.6	+95.0					g2-_e+_g2-_g1+
ts_dimet_cis_15HAT_47	+94.2	+81.3	+97.1					g2-_g2+_g1+_g2-
ts_dimet_cis_15HAT_40	+105.8	+92.8	+110.1					g2-_g1+_a_g1+
r4acs								
dimet_cis_C5-rad_102	+14.1	+14.3	+19.5	+10.8	+16.0	-4.6	+0.6	g1+_g2+_g1-_g2+
ts_dimet_cis_15HAT_32_ircf	+14.1	+14.3	+19.5	+10.8	+16.0	-4.6	+0.6	g1+_g2+_g1-_g2+
dimet_cis_C5-rad_27	+14.6	+13.6	+17.4	+12.4	+16.2	-9.0	-5.2	g1+_g1+_g2-_g2+
dimet_cis_C5-rad_69	+16.4	+16.2	+17.7	+11.3	+12.8	-9.0	-7.5	g1+_a_g1-_g2+
dimet_cis_C5-rad_83	+16.7	+16.1	+18.9	+11.5	+14.4	-5.7	-2.8	g2-_a_g2-_g2+
dimet_cis_C5-rad_15	+18.3	+18.4	+19.1					g1-_g2-_g1-_g2+
dimet_cis_C5-rad_8	+21.2	+20.9	+19.3					g1-_g2+_g1-_g2+
dimet_cis_C5-rad_39	+24.3	+24.3	+28.4					e-_g2-_g1+_g1-
dimet_cis_C5-rad_47	+34.8	+33.7	+34.4					g1+_e+_g2+_a

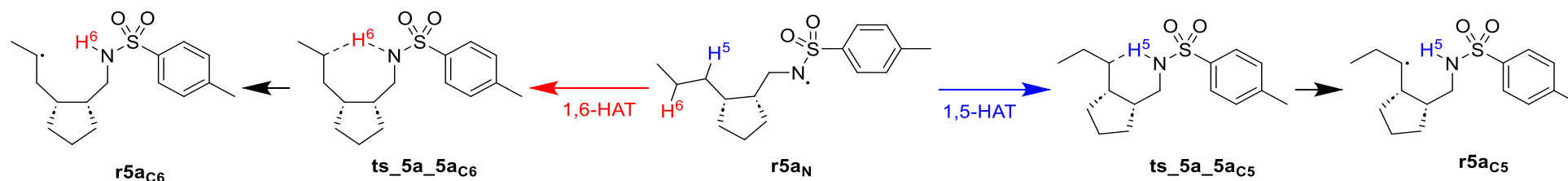


Fig. S3. Rearrangement reactions of N-centered radical $r5a_N$ to radicals $r5a_{C5}$ and $r5a_{C6}$.

Table S3a. Energies for all systems shown in Fig. S3.

Molecule	E_{tot} UB3LYP/ 6-31G(d) [Hartree]	$\langle S^2 \rangle$	NIMAG	dH UB3LYP/ 6-31G(d) [Hartree]	dG UB3LYP/ 6-31G(d) [Hartree]	E_{tot} PCM(DCE)/ UB3LYP/ 6-31G(d) ^[a] [Hartree]	$dG_{298\text{ solv}}$ PCM(DCE)/ UB3LYP/ 6-31G(d) ^[a] [Hartree]	E_{tot} DLPNO- CCSD(T)/ cc-pVTZ ^[a] [Hartree]	$G_{298\text{ DCE}}$ PCM(DCE) + DLPNO- CCSD(T)/cc-pVTZ ^[a] [Hartree]
r5a									
cpen cis n-rad 96	-1227.437348	0.75	-	0.400265	0.322633	-1227.445637	-0.008290	-1221.777802	-1225.242291
cpen cis n-rad 43	-1227.437271	0.75	-	0.399853	0.321687	-1227.445581	-0.008309	-1221.779131	-1225.242886
cpen cis n-rad 67	-1227.437166	0.75	-	0.400229	0.322454	-1227.445480	-0.008313	-1221.777841	-1225.242786
cpen cis n-rad 38	-1227.437143	0.75	-	0.399781	0.321439	-1227.445382	-0.008239	-1221.778980	-1225.243250
cpen cis N-rad 31	-1227.437062	0.75	-	0.400461	0.322586	-1227.445250	-0.008188	-1221.776879	-1225.242345
ts cpen cis 15HAT ircr	-1227.436862	0.75	-	0.399922	0.322836				
cpen_cis_16HAT ircr	-1227.436580	0.75	-	0.399899	0.322656				
cpen cis N-rad 84	-1227.435168	0.75	-	0.399993	0.322233				
cpen cis n-rad 88	-1227.433425	0.75	-	0.400601	0.323505				
cpen_cis_N-rad_64	-1227.432240	0.75	-	0.399961	0.322373				
cpen cis n-rad 93	-1227.425971	0.75	-	0.400829	0.323484				
ts 5a 5a_C6									
ts cpen cis 16HAT	-1227.414131	0.76	-1555	0.394255	0.322077	-1227.424116	-0.009985	-1221.729954	-1225.224646
ts_cpen_cis_16HAT_26	-1227.412990	0.76	-1611	0.394376	0.321309	-1227.422485	-0.009495	-1221.727537	-1225.223660
ts cpen cis 16HAT 10	-1227.410739	0.76	-1610	0.394349	0.323241	-1227.422638	-0.011899	-1221.725891	-1225.223199
ts cpen cis 16HAT 18	-1227.410285	0.76	-1632	0.394387	0.320894	-1227.420208	-0.009924	-1221.726033	-1225.222991
ts_cpen_cis_16HAT_25	-1227.409579	0.76	-1504	0.394404	0.320891	-1227.419231	-0.009653	-1221.724066	-1225.221227
ts cpen cis 16HAT 2	-1227.409422	0.76	-1554	0.394349	0.322034				
ts cpen cis 16HAT 17	-1227.408907	0.76	-1506	0.394495	0.322595				
ts cpen cis 16HAT 15	-1227.408436	0.76	-1485	0.394256	0.321845				
ts cpen cis 16HAT 5	-1227.408409	0.76	-1485	0.394252	0.321934				
ts cpen cis 16HAT 13	-1227.407464	0.76	-1625	0.394481	0.322813				
ts cpen cis 16HAT 19	-1227.405977	0.76	-1568	0.394621	0.323324				
ts_cpen_cis_16HAT_1	-1227.400101	0.76	-1354	0.394331	0.322461				
ts cpen cis 16HAT 11	-1227.395467	0.76	-1536	0.394713	0.323871				
5a_C6									
cpen_cis_6C-rad_21	-1227.431338	0.75	-	0.399516	0.322578	-1227.440904	-0.009566	-1221.774096	-1225.245869
cpen_cis_16HAT ircf	-1227.431317	0.75	-	0.399383	0.322375	-1227.441063	-0.009746	-1221.773640	-1225.245691
cpen cis 6C-rad 18	-1227.430842	0.75	-	0.399644	0.323171	-1227.439794	-0.008952	-1221.774028	-1225.245124

cpen cis 6C-rad 29	-1227.430233	0.75	-	0.399619	0.324055	-1227.439828	-0.009595	-1221.772092	-1225.242829
cpen cis 6C-rad 79	-1227.429852	0.75	-	0.399575	0.321491	-1227.440019	-0.010167	-1221.776905	-1225.246497
cpen_cis_6C-rad_31	-1227.429695	0.75	-	0.399724	0.323484				
cpen cis 6C-rad 26	-1227.428018	0.75	-	0.399571	0.323411				
cpen cis 6C-rad 10	-1227.426534	0.75	-	0.399386	0.320795				
cpen cis 6C-rad 80	-1227.424878	0.75	-	0.399531	0.321431				
ts 5a 5acs									
ts cpen cis 15HAT	-1227.413042	0.76	-1572	0.394493	0.320427	-1227.423284	-0.010241	-1221.728478	-1225.224341
ts cpen cis 15HAT 6	-1227.411416	0.76	-1528	0.394560	0.319787	-1227.421529	-0.010112	-1221.726653	-1225.224696
ts_cpen_cis_15HAT_24	-1227.411363	0.76	-1696	0.394562	0.320480	-1227.421822	-0.010459	-1221.727064	-1225.223680
ts cpen cis 15HAT 20	-1227.411118	0.76	-1526	0.394621	0.320027	-1227.42151	-0.010392	-1221.726726	-1225.223928
ts cpen cis 15HAT 10	-1227.410897	0.76	-1579	0.394641	0.320498	-1227.420167	-0.009270	-1221.723772	-1225.222189
ts_cpen_cis_15HAT_15	-1227.410633	0.76	-1557	0.394407	0.320173				
ts cpen cis 15HAT 23	-1227.410564	0.76	-1648	0.394587	0.319513				
ts cpen cis 15HAT 1	-1227.409557	0.76	-1612	0.394672	0.322582				
ts cpen cis 15HAT 7	-1227.409099	0.76	-1491	0.394696	0.320167				
ts cpen cis 15HAT 17	-1227.408900	0.76	-1565	0.394617	0.320612				
ts cpen cis 15HAT 18	-1227.408888	0.76	-1565	0.394637	0.320902				
ts cpen cis 15HAT 21	-1227.408783	0.76	-1564	0.394692	0.321745				
ts_cpen_cis_15HAT_19	-1227.408765	0.76	-1564	0.394691	0.322060				
ts cpen cis 15HAT 2	-1227.407963	0.76	-1604	0.394808	0.322320				
ts cpen cis 15HAT 25	-1227.407782	0.76	-1661	0.394795	0.321308				
ts_cpen_cis_15HAT_13	-1227.406691	0.76	-1570	0.394536	0.321792				
ts cpen cis 15HAT 8	-1227.405525	0.76	-1655	0.394758	0.321814				
ts cpen cis 15HAT 16	-1227.405424	0.76	-1609	0.394606	0.321449				
ts cpen cis 15HAT 3	-1227.403694	0.76	-1525	0.394900	0.321995				
5arCs									
ts cpen cis 15HAT ircf	-1227.432865	0.75	-	0.399881	0.322528	-1227.442677	-0.009813	-1221.77597	-1225.245480
cpen cis 5C-rad 27 2	-1227.431785	0.75	-	0.399597	0.322018	-1227.441575	-0.009790	-1221.774967	-1225.246248
cpen_cis_5C-rad_48	-1227.431159	0.75	-	0.399672	0.323378	-1227.441964	-0.010805	-1221.776488	-1225.247891
cpen cis 5C-rad 7	-1227.431108	0.75	-	0.399691	0.323153	-1227.442085	-0.010976	-1221.775711	-1225.247721
cpen cis 5C-rad 4	-1227.430992	0.75	-	0.399854	0.322773	-1227.441902	-0.010910	-1221.778002	-1225.247800
cpen_cis_5C-rad_13	-1227.430620	0.75	-	0.399864	0.321843				
cpen cis 5C-rad 38 2	-1227.427419	0.75	-	0.399964	0.321978				
cpen cis 5C-rad 42	-1227.422793	0.75	-	0.399895	0.323060				

Table S3b. Energies for all systems shown in Fig. S3

Molecule	UB3LYP/6-31(d)							Conformation R_φ_χ_ψ_ω
	Gas phase			PCM(DiChloroEthane)		DLPNO-CCSD(T)/cc-pVTZ		
	ΔE_{tot} [Hartree]	ΔH_{298} [kJ/mol]	ΔG_{298} [kJ/mol]	ΔH_{298} [kJ/mol]	ΔG_{298} [kJ/mol]	ΔH_{298} [kJ/mol]	ΔG_{298} [kJ/mol]	
r5a								
cpen cis n-rad 96	0.0	0.0	0.0	0.0	0.0	+0.0	+0.0	Eβ'↓ a g2+ a a
cpen cis n-rad 43	+0.2	-0.9	-2.3	-0.9	-2.3	-0.1	-1.5	Eβ'↓ a a a a
cpen cis n-rad 67	+0.5	+0.4	+0.0	+0.3	-0.1	-0.9	-1.2	Eβ'↓ a g2+ g2- a

cpen_cis_n-rad_38	+0.5	-0.7	-2.6	-0.6	-2.5	-0.8	-2.7	Eβ'↓ a a g2-_a
cpen_cis_N-rad_31	+0.7	+1.3	+0.6	+1.5	+0.9	+0.2	-0.4	Eβ'↓ a g2- g2-_a
ts_cpen_cis_15HAT_ircr	+1.3	+0.4	+1.8					Eα'↓ a a a a
cpen_cis_16HAT_ircr	+2.0	+1.1	+2.1					Eβ'↓ a g1- g2- a
cpen_cis_N-rad_84	+5.7	+5.0	+4.7					Eβ↓ a g2+ a a
cpen_cis_n-rad_88	+10.3	+11.2	+12.6					Eβ'↓ a g2- g1- g2-
cpen_cis_N-rad_64	+13.4	+12.6	+12.7					Eβ↓ a a g1- g2-
cpen_cis_n-rad_93	+29.9	+31.4	+32.1					Eβ'↑ g2+ g1+ g1+ g2-
ts 5a 5ac6								
ts_cpen_cis_16HAT	+61.0	+45.2	+59.5	+40.7	+55.0	+36.5	+50.8	E0↑ g2- a g2- a
ts_cpen_cis_16HAT_26	+64.0	+48.5	+60.5	+45.3	+57.3	+40.1	+52.1	E0↑ g2+ g1+ g2- a
ts_cpen_cis_16HAT_10	+69.9	+54.3	+71.5	+44.9	+62.0	+42.5	+59.6	E0↑ g1+ a g2- a
ts_cpen_cis_16HAT_18	+71.1	+55.6	+66.5	+51.3	+62.2	+44.1	+55.0	Eβ↓ g2+ a g2- a
ts_cpen_cis_16HAT_25	+72.9	+57.5	+68.3	+53.9	+64.8	+48.1	+58.9	Eα'↑ g1+ g1+ g2- a
ts_cpen_cis_16HAT_2	+73.3	+57.8	+71.7					Eβ↓ g2- a g2- a
ts_cpen_cis_16HAT_17	+74.7	+59.5	+74.6					Eβ↓ g1- g2- g2- a
ts_cpen_cis_16HAT_15	+75.9	+60.1	+73.8					E0↑ g2- g1+ g2- a
ts_cpen_cis_16HAT_5	+76.0	+60.2	+74.1					E0↑ g2- g1+ g2- a
ts_cpen_cis_16HAT_13	+78.5	+63.3	+78.9					Eα↑ g1+ g2+ g2- a
ts_cpen_cis_16HAT_19	+82.4	+67.5	+84.2					Eα↓ g2- g1- g1+ g1+
ts_cpen_cis_16HAT_1	+97.8	+82.2	+97.3					Eβ↓ g1+ g2- g2- a
ts_cpen_cis_16HAT_11	+110.0	+95.4	+113.2					Eα'↓ g1+ e- g1+ g1+
r5ac6								
cpen_cis_6C-rad_21	+15.8	+13.8	+15.6	+10.5	+12.3	-7.9	-6.0	Eα↓ g2-_a g2- a
cpen_cis_6C-rad_ircf	+15.8	+13.5	+15.2	+9.7	+11.3	-6.7	-5.1	E0↑ g2-_a g2- g2+
cpen_cis_6C-rad_18	+17.1	+15.5	+18.5	+13.7	+16.8	-8.7	-5.7	Eβ'↓ g2- g1- g2-_a
cpen_cis_6C-rad_29	+18.7	+17.0	+22.4	+13.6	+19.0	-3.4	+2.0	Eα↓ g1-_a g2- g2+
cpen_cis_6C-rad_79	+19.7	+17.9	+16.7	+12.9	+11.8	-4.9	-6.1	Eβ'↓ g2-_a g2- g2+
cpen_cis_6C-rad_31	+20.1	+18.7	+22.3					Eβ↓ g1+ g2+ g2- g2+
cpen_cis_6C-rad_26	+24.5	+22.7	+26.5					Eβ↓ g2- g1- g2-_a
cpen_cis_6C-rad_10	+28.4	+26.1	+23.6					Eα'↓ g1+ g2-_a g1-
cpen_cis_6C-rad_80	+32.7	+30.8	+29.6					Eβ↓ g1+ g2- g2- g2-
ts 5a 5acs								
ts_cpen_cis_15HAT	+63.8	+48.7	+58.0	+43.5	+52.9	+42.9	+52.3	E0↑ g2- g1- g1-_a
ts_cpen_cis_15HAT_6	+68.1	+53.1	+60.6	+48.3	+55.8	+43.5	+51.0	Eβ↓ g1+ g2+ g1- g2-
ts_cpen_cis_15HAT_24	+68.2	+53.2	+62.6	+47.6	+56.9	+45.2	+54.6	Eα↓ g1- g1- g1-_a
ts_cpen_cis_15HAT_20	+68.9	+54.0	+62.0	+48.5	+56.5	+45.8	+53.7	Eα↓ g2- g1- e- g1+
ts_cpen_cis_15HAT_10	+69.4	+54.7	+63.8	+52.1	+61.3	+46.2	+55.4	Eβ↓ g1- g2- g1-_a
ts_cpen_cis_15HAT_15	+70.1	+54.8	+63.7					Eβ↑ g1+ g1- g2-_a
ts_cpen_cis_15HAT_23	+70.3	+55.4	+62.1					Eβ'↓ a g1- g2- g2-

ts_cpen_cis_15HAT_1	+73.0	+58.3	+72.8					Eβ↓ g2- g2+ g1- a
ts_cpen_cis_15HAT_7	+74.2	+59.5	+67.7					Eβ↓ g2- g2- g1- g1+
ts_cpen_cis_15HAT_17	+74.7	+59.9	+69.4					Eβ'↓ g1+ g1- g2- g2-
ts_cpen_cis_15HAT_18	+74.7	+59.9	+70.2					Eβ'↓ g1+ g1- g2- g2-
ts_cpen_cis_15HAT_21	+75.0	+60.4	+72.7					Eα↓ g1+ g1- e- g1+
ts_cpen_cis_15HAT_19	+75.0	+60.4	+73.5					Eα↓ g1+ g1- e- g1+
ts_cpen_cis_15HAT_2	+77.2	+62.8	+76.3					Eβ↓ g2- g2+ g1- g2-
ts_cpen_cis_15HAT_25	+77.6	+63.3	+74.1					E0↓ g2+ g1+ g1- g1+
ts_cpen_cis_15HAT_13	+80.5	+65.4	+78.3					Eα↓ g2- g1+ e- a
ts_cpen_cis_15HAT_8	+83.5	+69.1	+81.4					Eβ↓ g2- a g1- g1+
ts_cpen_cis_15HAT_16	+83.8	+69.0	+80.7					Eβ↑ g2- g1+ g2- g2-
ts_cpen_cis_15HAT_3	+88.4	+74.3	+86.7					Eβ↓ g1+ e- g1- g1+
r5acs								
ts_cpen_cis_15HAT_ircf	+11.8	+10.8	+11.5	+6.8	+7.5	-5.1	-4.4	E0↑ g2- a g1- g2+
cpen_cis_5C-rad_27_2	+14.6	+12.9	+13.0	+8.9	+9.1	-6.6	-6.5	Eβ'↓ g2- a g2- g2+
cpen_cis_5C-rad_48	+16.2	+14.7	+18.2	+8.1	+11.6	-11.6	-8.1	E0↑ g2- g1- g2- g2+
cpen_cis_5C-rad_7	+16.4	+14.9	+17.7	+7.8	+10.7	-10.1	-7.2	Eβ'↓ g1+ g2+ g2- g2+
cpen_cis_5C-rad_4	+16.7	+15.6	+17.1	+8.7	+10.2	-9.0	-7.6	Eβ↓ g2- g1- e- g2+
cpen_cis_5C-rad_13	+17.7	+16.6	+15.6					Eβ'↓ g1+ g1+ g2- g1+
cpen_cis_5C-rad_38_2	+26.1	+25.3	+24.3					Eα↓ g1- g2+ g1- g2+
cpen_cis_5C-rad_42	+38.2	+37.2	+39.3					Eβ'↓ a g1+ g2- g1+

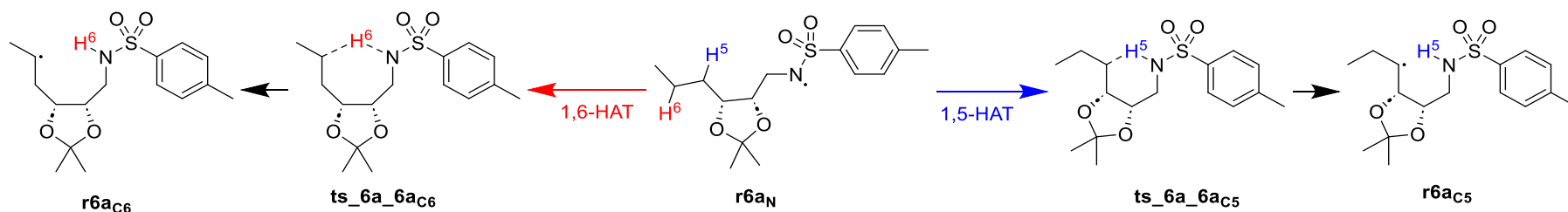


Fig. S4. Rearrangement reactions of *N*-centered radical $r6a_N$ to radicals $r6a_{C5}$ and $r6a_{C6}$.

Table S4a. Energies for all systems shown in Fig. S4.

Molecule	E_{tot} UB3LYP/ 6-31G(d) [Hartree]	$\langle S^2 \rangle$	NIMAG	dH UB3LYP/ 6-31G(d) [Hartree]	dG UB3LYP/ 6-31G(d) [Hartree]	E_{tot} PCM(DCE)/ UB3LYP/ 6-31G(d) ^[a] [Hartree]	dG_{298}^{solv} PCM(DCE)/ UB3LYP/ 6-31G(d) ^[a] [Hartree]	E_{tot} DLPNO-CCSD(T)/ cc-pVTZ ^[a] [Hartree]	G_{298}^{DCE} PCM(DCE) + DLPNO- CCSD(T)/cc-pVTZ ^[a] [Hartree]
$r6a_N$									
dioxalane 8 ircr 2	-1377.878429	0.75	-	0.409484	0.328452	-1377.888169	-0.009741	-1375.811586	-1375.492874
ts_diox_1_5_HAT_6_ircr	-1377.878429	0.75	-	0.409483	0.328448	-1377.888170	-0.009741	-1375.811587	-1375.492880
4 n-rad 1 6-HAT recal	-1377.878426	0.75	-	0.409486	0.328213	-1377.888169	-0.009742	-1375.811577	-1375.493106
ts_4_6_4_ircr	-1377.878358	0.75	-	0.409884	0.329074	-1377.888230	-0.009872	-1375.810128	-1375.490926
diox_n_rad_3	-1377.878116	0.75	-	0.409391	0.327282	-1377.887920	-0.009804	-1375.809867	-1375.492389
diox n rad 66	-1377.876591	0.75	-	0.409261	0.326504	-1377.887726	-0.011134	-1375.807881	-1375.492511
diox n rad 75	-1377.875384	0.75	-	0.409327	0.326413	-1377.886423	-0.011039	-1375.807229	-1375.491855
diox n rad 64	-1377.873624	0.75	-	0.409324	0.327129	-1377.883503	-0.009879	-1375.806456	-1375.489205
diox n rad 43	-1377.872284	0.75	-	0.410009	0.328030	-1377.881817	-0.009533	-1375.804328	-1375.485831
diox n rad 46	-1377.870545	0.75	-	0.410170	0.327669	-1377.879708	-0.009164	-1375.803476	-1375.484970
diox n rad 82	-1377.865760	0.75	-	0.409909	0.330274	-1377.877497	-0.011737	-1375.801237	-1375.482700
ts_{6a_6aC6}									
dioxalane 8	-1377.852945	0.76	-1615	0.403823	0.325595	-1377.539076	-0.011726	-1375.788839	-1375.474970
dioxalane 2	-1377.852585	0.76	-1632	0.403858	0.324948	-1377.538635	-0.010998	-1375.788267	-1375.474317
dioxalane 4	-1377.852209	0.76	-1535	0.403835	0.325529	-1377.538327	-0.011647	-1375.787559	-1375.473677
dioxalane 6	-1377.851799	0.76	-1749	0.403788	0.325427	-1377.538313	-0.011941	-1375.787944	-1375.474458
dioxalane 17	-1377.850083	0.76	-1521	0.403822	0.326153	-1377.535893	-0.011963	-1375.787346	-1375.473878
dioxalane 3	-1377.849636	0.76	-1660	0.403752	0.326439	-	-	-	-
-dioxalane 15	-1377.849075	0.76	-1660	0.403836	0.325884	-	-	-	-
dioxalane 16	-1377.848192	0.76	-1553	0.403626	0.325262	-	-	-	-
dioxalane 1	-1377.848018	0.76	-1585	0.403756	0.325926	-	-	-	-
dioxalane_12	-1377.847157	0.76	-1548	0.403682	0.326468	-	-	-	-
dioxalane 14	-1377.846723	0.76	-1679	0.403715	0.325128	-	-	-	-
dioxalane 10	-1377.844993	0.76	-1595	0.403663	0.326232	-	-	-	-
dioxalane 9	-1377.840290	0.76	-1394	0.403717	0.327514	-	-	-	-
dioxalane 13	-1377.838760	0.76	-1358	0.403759	0.327803	-	-	-	-
$r6a_{C6}$									
diox c rad 23	-1377.873909	0.75	-	0.409057	0.326216	-1377.885883	-0.011974	-1375.813772	-1375.499530

diox c rad 53	-1377.872479	0.75	-	0.408969	0.324607	-1377.884090	-0.011611	-1375.810932	-1375.497935
5 c-rad 1 5-HAT recalc	-1377.872000	0.75	-	0.408920	0.326785	-1377.883416	-0.011417	-1375.812331	-1375.496963
dioxalane_8_ircf_2	-1377.871997	0.75	-	0.408891	0.326264	-1377.883423	-0.011426	-1375.812341	-1375.497503
diox c rad 44	-1377.871217	0.75	-	0.408826	0.324115	-1377.882522	-0.011305	-1375.811014	-1375.498204
diox c rad 69	-1377.870234	0.75	-	0.409107	0.325351	-1377.882211	-0.011976	-1375.812249	-1375.498875
diox c rad 72	-1377.868964	0.75	-	0.409026	0.327398	-1377.882242	-0.013279	-1375.813000	-1375.498881
diox c rad 51	-1377.865699	0.75	-	0.408853	0.327024	-1377.878904	-0.013205	-1375.807278	-1375.493459
ts 6a 6acs									
ts 4 6 4	-1377.850989	0.76	-1643	0.403731	0.325258	-1377.861492	-0.010503	-1375.785721	-1375.470966
ts_diox_1_5_HAT_6	-1377.850306	0.76	-1637	0.403633	0.324106	-1377.862034	-0.011728	-1375.785030	-1375.472652
ts 4 6 9	-1377.850306	0.76	-1637	0.403632	0.324108	-1377.862034	-0.011728	-1375.785030	-1375.472650
ts 4 6 8	-1377.850033	0.76	-1614	0.403781	0.324847	-1377.861025	-0.010992	-1375.785239	-1375.471385
ts 4_6_15	-1377.849226	0.76	-1627	0.403782	0.324004	-1377.861225	-0.011999	-1375.784048	-1375.472043
ts_diox_1_5_HAT_7	-1377.849226	0.76	-1627	0.403782	0.324001	-	-	-	-
ts 4 6 11	-1377.848711	0.76	-1628	0.403733	0.323870	-	-	-	-
ts 4 6 3	-1377.848623	0.76	-1625	0.403610	0.324479	-	-	-	-
ts 4 6 2	-1377.848611	0.76	-1656	0.403723	0.325076	-	-	-	-
ts_diox_1_5_HAT_2	-1377.848326	0.76	-1654	0.403729	0.325310	-	-	-	-
ts_diox_1_5_HAT	-1377.848252	0.76	-1755	0.403629	0.323840	-	-	-	-
ts_diox_1_5_HAT_4	-1377.848156	0.76	-1736	0.403874	0.324151	-	-	-	-
ts 4 6 6	-1377.84803	0.76	-1549	0.403598	0.324315	-	-	-	-
ts 4 6 13	-1377.847955	0.76	-1561	0.403655	0.323188	-	-	-	-
ts_4_6_14	-1377.847246	0.76	-1560	0.403786	0.324730	-	-	-	-
ts 4 6 1	-1377.847052	0.76	-1548	0.403655	0.324448	-	-	-	-
ts_diox_1_5_HAT_3	-1377.846806	0.76	-1667	0.403857	0.325165	-	-	-	-
ts_diox_1_5_HAT_5	-1377.846682	0.76	-1651	0.403902	0.325923	-	-	-	-
ts 4 6 7	-1377.846614	0.76	-1572	0.403681	0.324870	-	-	-	-
r6acs									
diox 1 5 c rad	-1377.873100	0.75	-	0.409161	0.324982	-1377.885311	-0.012211	-1375.811211	-1375.498440
ts_4_6_4_ircf	-1377.872398	0.75	-	0.409021	0.327265	-1377.883422	-0.011024	-1375.810937	-1375.494695
ts_diox_1_5_HAT_6_ircf	-1377.871249	0.75	-	0.408969	0.326145	-1377.883112	-0.011863	-1375.809884	-1375.495602
6_26	-1377.868690	0.75	-	0.409340	0.327082	-1377.881366	-0.012676	-1375.809751	-1375.495345
6_56_a	-1377.862191	0.75	-	0.409674	0.329742	-1377.874644	-0.012453	-1375.802443	-1375.485154

Table S4b. Relative energies for all systems shown in Fig. S4 (UB3LYP/6-31G(d) result).

Molecule	UB3LYP/6-31(d)							Conformation R_φ_χ_ψ_ω
	Gas phase			PCM(DiChloroEthane)		DLPNO-CCSD(T)/cc-pVTZ		
	ΔE_{tot} [Hartree]	ΔH_{298} [kJ/mol]	ΔG_{298} [kJ/mol]	ΔH_{298} [kJ/mol]	ΔG_{298} [kJ/mol]	ΔH_{298} [kJ/mol]	ΔG_{298} [kJ/mol]	
r6as								
dioxalane_8_ircf_2	+0.0	+0.0	+0.0	+0.0	+0.0	+0.0	+0.0	Eβ↑ g1- g1- g2- a
ts_diox_1_5_HAT_6_ircf	+0.0	+0.0	+0.0	+0.0	+0.0	+0.0	+0.0	Eβ↑ g1- g1- g2- a
4_n-rad_1_6-HAT_recalc	+0.0	+0.0	-0.6	+0.0	-0.6	+0.0	-0.6	Eβ↑ g1- g1- g2- a
ts_4_6_4_ircf	+0.2	+1.2	+1.8	+0.9	+1.5	+4.9	+5.5	Eβ↑ g2+ g1+ g2- a
diox_n_rad_3	+0.8	+0.6	-2.2	+0.4	-2.4	+4.3	+1.4	Eβ↑ a g1- a a

diox_n_rad_66	+4.8	+4.2	-0.3	+0.6	-3.9	+9.1	+4.6	Eβ↑ a a a a
diox_n_rad_75	+8.0	+7.6	+2.7	+4.2	-0.8	+11.0	+6.1	Eβ↑ a a a g1+
diox_n_rad_64	+12.6	+12.2	+9.2	+11.8	+8.8	+13.0	+10.0	Eβ↑ a a g2- g2-
diox_n_rad_43	+16.1	+17.5	+15.0	+18.1	+15.6	+20.4	+17.9	Eβ↑ g2+ g1+ g2- g2-
diox_n_rad_46	+20.7	+22.5	+18.7	+24.0	+20.2	+23.1	+19.2	Eα↓ g2+ g1+ g1+ g1+
diox_n_rad_82	+33.3	+34.4	+38.1	+29.1	+32.8	+28.3	+32.0	Eα↓ g2- g1- g1+ g2-
ts 6a 6ac6								
dioxalane 8	+66.9	+52.0	+59.4	+46.8	+54.2	+44.9	+52.2	Eα↓ g2- a g2- a
dioxalane_2	+67.9	+53.1	+58.7	+49.8	+55.4	+46.5	+52.0	Eα↓ g2+ g1+ g2- g2+
dioxalane_4	+68.8	+54.0	+61.2	+49.0	+56.2	+48.3	+55.4	Eα↓ g1+ g1+ g2- a
dioxalane_6	+69.9	+55.0	+62.0	+49.2	+56.2	+47.1	+54.1	Eα↓ a a g2- a
dioxalane_17	+74.4	+59.6	+68.4	+53.7	+62.6	+48.7	+55.7	Eα↓ a a g2- a
dioxalane_3	+75.6	+60.5	+70.3	-	-	-	-	Eβ↑ g1+ a g1+ g1+
dioxalane 15	+77.1	+62.2	+70.3	-	-	-	-	Eα↓ g1+ a g2- a
dioxalane 16	+79.4	+64.0	+71.0	-	-	-	-	Eβ↑ a a g1+ g1+
dioxalane_1	+79.8	+64.8	+73.2	-	-	-	-	Eβ↑ a a g1+ g1+
dioxalane_12	+79.8	+64.8	+73.2	-	-	-	-	Eβ↑ g1+ a g2- a
dioxalane_14	+82.1	+66.9	+76.9	-	-	-	-	Eβ↑ g2- g1+ g2- a
dioxalane_10	+83.2	+68.1	+74.5	-	-	-	-	Eβ↑ g2- g1+ g2- a
dioxalane 9	+87.8	+72.5	+82.0	-	-	-	-	Eβ↑ g2- a g1+ g1+
dioxalane 13	+104.2	+85.0	+97.7	-	-	-	-	Eβ↑ a a g2- a
r6ac6								
diox c rad 23	+11.9	+10.7	+6.0	+4.9	+0.1	-6.9	-11.6	Eβ↑ g1+ a g2- g2+
diox c rad 53	+15.6	+14.3	+5.5	+9.4	+0.6	+0.4	-8.4	Eβ↑ g1- g2- a g2+
5_c-rad_1_5-HAT_recalc	+16.9	+15.4	+12.5	+11.0	+8.1	-3.4	-6.3	Eβ↑ g2- a g2- g2+
dioxalane_8_ircf_2	+16.9	+15.3	+11.2	+10.9	+6.7	-3.5	-7.7	Eβ↑ g2- a g2- g2+
diox_c_rad_44	+18.9	+17.2	+7.6	+13.1	+3.4	-0.2	-9.9	Eβ↑ g1+ g1+ g2- g2+
diox_c_rad_69	+21.5	+20.5	+13.4	+14.7	+7.5	-2.7	-9.9	Eα↓ g2- a g2- g2-
diox c rad 72	+24.9	+23.7	+22.1	+14.4	+12.8	-4.9	-6.5	Eβ↑ g2- a a g2+
diox c rad 51	+33.4	+31.8	+29.7	+22.7	+20.6	+9.7	+7.6	Eβ↑ g1+ g1+ g2- g2+
ts 6a 6ac5								
ts_4_6_4	+72.0	+56.9	+63.7	+54.9	+61.7	+52.8	+59.5	Eβ↑ g1+ g1+ e- a
ts diox 1 5 HAT 6	+73.8	+58.5	+62.4	+53.3	+57.2	+54.4	+58.3	Eβ↑ g2- g1- e- a
ts_4_6_9	+73.8	+58.5	+62.4	+53.3	+57.2	+54.4	+58.3	Eβ↑ g2- g1- e- a
ts_4_6_8	+74.6	+59.6	+65.1	+56.3	+61.8	+54.2	+59.7	Eβ↑ g1+ g1+ g2- g2-
ts_4_6_15	+76.7	+61.7	+65.0	+55.8	+59.1	+57.3	+60.6	Eβ↑ g2- g1- e- g2-
ts_diox_1_5_HAT_7	+76.7	+61.7	+65.0	-	-	-	-	Eβ↑ g2- g2+ e- g2+

ts_4_6_11	+78.0	+62.9	+66.0	-	-	-	-	Eβ↑ g2- g1- e- g1+
ts_4_6_3	+78.3	+62.8	+67.8	-	-	-	-	E0↑ g1+ g2+ g2- a
ts_4_6_2	+78.3	+63.2	+69.4	-	-	-	-	Eβ↑ g1+ g1+ e- g1+
ts_diox_1_5_HAT_2	+79.0	+63.9	+70.8	-	-	-	-	Eβ↑ g1+ a e- a
ts_diox_1_5_HAT	+79.2	+63.9	+67.1	-	-	-	-	Eβ↑ g1- g1- e- a
ts_diox_1_5_HAT_4	+79.5	+64.8	+68.2	-	-	-	-	Eβ↑ a e+ e- g2+
ts_4_6_6	+79.8	+64.4	+69.0	-	-	-	-	Eβ'↑ g1- g2- e- a
ts_4_6_13	+80.0	+64.7	+66.2	-	-	-	-	Eβ'↑ g1+ g2+ e- g2-
ts_4_6_14	+81.9	+66.9	+72.1	-	-	-	-	Eβ'↑ g1- g2- e- g2-
ts_4_6_1	+82.4	+67.1	+71.9	-	-	-	-	Eβ'↑ g1+ g2+ e- g1+
ts_diox_1_5_HAT_3	+83.0	+68.3	+74.4	-	-	-	-	Eβ↑ e+ g1- e- e+
ts_diox_1_5_HAT_5	+83.4	+68.7	+76.7	-	-	-	-	Eβ↑ g1- g1- e- e+
ts_4_6_7	+83.5	+68.3	+74.1	-	-	-	-	Eβ'↑ g1- g2- e- g1+
r6a_{CS}								
diox_1_5_c_rad	+14.0	+13.1	+4.9	+6.7	-1.6	+0.1	-8.1	Eβ↑ g1+ a g2- g2+
ts_4_6_4_ircf	+15.8	+14.6	+12.7	+11.2	+9.3	+0.5	-1.4	Eβ↑ g1+ g1+ g2- g2+
ts_diox_1_5_HAT_6_ircf	+18.8	+17.5	+12.8	+11.9	+7.2	+3.1	-1.6	Eβ↑ g2- a g2- g2+
6_26	+25.6	+25.2	+22.0	+17.5	+14.3	+4.4	+1.2	Eβ↓ g2- g1- g2+ g1-
6_56_a	+42.6	+43.1	+46.0	+36.0	+38.9	+24.5	+27.4	Eβ'↑ g2- g2- g1- g2-

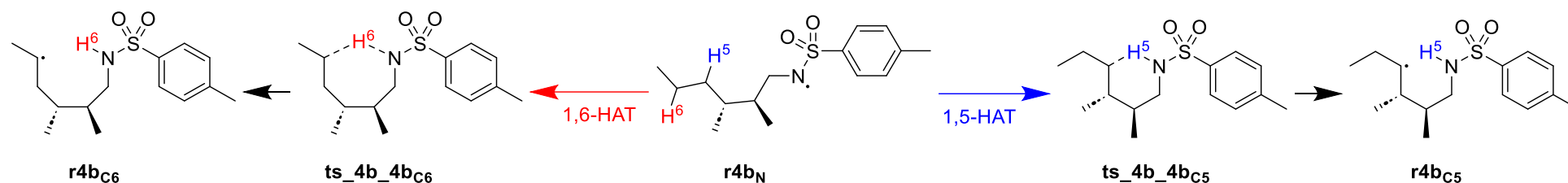


Fig. S5. Rearrangement reactions of *N*-centered radical **r4b_N** to radicals **r4bc₅** and **r4bc₆**.

Table S5a. Energies for all systems shown in Fig. S5.

Molecule	E_{tot} UB3LYP/ 6-31G(d) [Hartree]	$\langle S^2 \rangle$	NIMAG	dH UB3LYP/ 6-31G(d) [Hartree]	dG UB3LYP/ 6-31G(d) [Hartree]	E_{tot} PCM(DCE)/ UB3LYP/ 6-31G(d) ^[a] [Hartree]	$dG_{298\text{ solv}}$ PCM(DCE)/ UB3LYP/ 6-31G(d) ^[a] [Hartree]	E_{tot} DLPNO-CCSD(T)/ cc-pVTZ ^[a] [Hartree]	$G_{298\text{ DCE}}$ PCM(DCE) + DLPNO- CCSD(T)/cc-pVTZ ^[a] [Hartree]
r4b_N									
dimet trans N-rad 13	-1189.335005	0.75	-	0.392101	0.313852	-1189.343216	-0.008211	-1187.523451	-1183.909136
dimet trans N-rad_3_2	-1189.334650	0.75	-	0.392106	0.312997	-1189.342891	-0.008241	-1187.523546	-1183.908886
dimet trans N-rad 12	-1189.334608	0.75	-	0.391915	0.313380	-1189.342930	-0.008322	-1187.522307	-1183.909317
dimet trans N-rad 5_2	-1189.334487	0.75	-	0.392103	0.314572	-1189.342791	-0.008304	-1187.522598	-1183.909055
dimet trans N-rad 25	-1189.334262	0.75	-	0.391888	0.311554	-1189.342522	-0.008261	-1187.522219	-1183.908885
ts dimet trans 15 ircr	-1189.332239	0.75	-	0.392049	0.315324				
dimet trans N-rad 11	-1189.331916	0.75	-	0.392122	0.313005				
dimet trans N-rad 81	-1189.329548	0.75	-	0.392673	0.314924				
ts dimet trans 16HAT 11 ircr	-1189.328622	0.75	-	0.392026	0.314769				
dimet trans N-rad 89	-1189.325740	0.75	-	0.392777	0.314672				
ts 4b 4bc₆									
ts dimet trans 16HAT 16HAT 11	-1189.307622	0.76	-1674	0.386618	0.313452	-1189.317700	-0.010078	-1187.501221	-1183.857973
ts dimet trans 16HAT 16HAT 8	-1189.307022	0.76	-1555	0.386543	0.314055	-1189.318352	-0.011331	-1187.501943	-1183.858736
ts dimet trans 16HAT 16HAT 7	-1189.307006	0.76	-1555	0.386548	0.313935	-1189.318337	-0.011331	-1187.501926	-1183.858692
ts dimet trans 16HAT 16HAT 31	-1189.306046	0.76	-1670	0.386483	0.312400	-1189.316121	-0.010075	-1187.500181	-1183.856612
ts dimet trans 16HAT 16HAT 21	-1189.305664	0.76	-1614	0.386482	0.312954	-1189.315273	-0.009609	-1187.498506	-1183.854130
ts dimet trans 16HAT 16HAT 27	-1189.304652	0.76	-1561	0.386422	0.313922				
ts dimet trans 16HAT 16HAT 30	-1189.304639	0.76	-1561	0.386403	0.313262				
ts dimet trans 16HAT 16HAT 9	-1189.304202	0.76	-1543	0.386438	0.314178				
ts dimet trans 16HAT 16HAT 12	-1189.303772	0.76	-1602	0.386344	0.313839				
ts dimet trans 16HAT 16HAT 32	-1189.303502	0.76	-1592	0.386454	0.313816				
ts dimet trans 16HAT 16HAT 14	-1189.302441	0.76	-1510	0.386627	0.314491				
ts dimet trans 16HAT 16HAT 15	-1189.302421	0.76	-1511	0.386596	0.313720				
ts dimet trans 16HAT 16HAT 4	-1189.301699	0.76	-1397	0.386439	0.313502				
ts dimet trans 16HAT 16HAT 25	-1189.300237	0.76	-1390	0.386442	0.313470				
ts dimet trans 16HAT 16HAT 1	-1189.299007	0.76	-1533	0.386562	0.314295				
ts dimet trans 16HAT 16HAT 16	-1189.293464	0.76	-1362	0.386473	0.313898				
ts dimet trans 16HAT 16HAT 18	-1189.293250	0.76	-1629	0.386660	0.314362				

r4b_{C6}									
dimet trans C6-rad 30 2	-1189.327705	0.75		0.391436	0.312103	-1189.337884	-0.010180	-1187.524853	-1183.909266
dimet trans C6-rad 24	-1189.327601	0.75		0.391412	0.312296	-1189.337875	-0.010274	-1187.524012	-1183.909361
dimet trans C6-rad 15 2	-1189.327390	0.75		0.391515	0.312220	-1189.337649	-0.010259	-1187.524426	-1183.909195
dimet trans C6-rad 27	-1189.327374	0.75		0.391342	0.311588	-1189.337672	-0.010298	-1187.523738	-1183.909454
dimet trans C6-rad 39	-1189.326921	0.75		0.391292	0.312077	-1189.337216	-0.010295	-1187.523452	-1183.908859
dimet trans C6-rad 9	-1189.325104	0.75		0.391454	0.313407				
dimet trans C6-rad 35	-1189.323905	0.75		0.391653	0.313074				
ts dimet trans 16HAT 11 ircf	-1189.323679	0.75	0	0.391859	0.314638				
dimet trans C6-rad 88	-1189.322720	0.75		0.391554	0.312920				
dimet trans C6-rad 79	-1189.320465	0.75		0.391683	0.313690				
ts 4b 4b_{C5}									
ts dimet trans 15HAT 15HAT 15	-1189.308621	0.76	-1663	0.386603	0.312093	-1189.319288	-0.010667	-1187.502939	-1183.861082
ts dimet trans 15HAT 15HAT 4	-1189.308056	0.76	-1573	0.386601	0.313331	-1189.319956	-0.011901	-1187.502873	-1183.861413
ts dimet trans 15HAT 15HAT 35	-1189.306855	0.76	-1682	0.386927	0.314165	-1189.316972	-0.010117	-1187.501192	-1183.857148
ts dimet trans 15HAT 15HAT 6	-1189.306287	0.76	-1540	0.386655	0.312212	-1189.316678	-0.010391	-1187.499362	-1183.857041
ts dimet trans 15HAT 15HAT 32	-1189.305618	0.76	-1631	0.386745	0.314883	-1189.317503	-0.011885	-1187.501277	-1183.857284
ts dimet trans 15HAT 15HAT 14	-1189.304671	0.76	-1544	0.386800	0.313483				
ts dimet trans 15HAT 15HAT 23	-1189.304073	0.76	-1628	0.386893	0.314786				
ts dimet trans 15HAT 15HAT 9	-1189.303956	0.76	-1573	0.386732	0.312891				
ts dimet trans 15HAT 15HAT 1	-1189.303733	0.76	-1649	0.386806	0.314276				
ts dimet trans 15HAT 15HAT 36	-1189.302862	0.76	-1631	0.386740	0.311675				
ts dimet trans 15HAT 15HAT 18	-1189.302748	0.76	-1557	0.386644	0.313942				
ts dimet trans 15HAT 15HAT 26	-1189.302330	0.76	-1712	0.386759	0.313571				
ts dimet trans 15HAT 15HAT 7	-1189.301255	0.76	-1611	0.386833	0.314260				
ts dimet trans 15HAT 15HAT 21	-1189.300937	0.76	-1565	0.386713	0.313308				
ts dimet trans 15HAT 15HAT 33	-1189.298773	0.76	-1752	0.386977	0.315466				
ts dimet trans 15HAT 15HAT 30	-1189.298314	0.76	-1566	0.386929	0.314573				
r4b_{C5}									
dimet trans C5-rad 109	-1189.329271	0.75		0.391746	0.314126	-1189.338954	-0.009683	-1187.524519	-1183.906208
dimet trans C5-rad 110	-1189.328879	0.75		0.391804	0.313703	-1189.338228	-0.009349	-1187.524661	-1183.906039
dimet trans C5-rad 31	-1189.328635	0.75		0.391866	0.312916	-1189.337776	-0.009140	-1187.524038	-1183.904577
dimet trans C5-rad 117	-1189.328480	0.75		0.391748	0.313443	-1189.338706	-0.010226	-1187.523927	-1183.910212
dimet trans C5-rad 46	-1189.328230	0.75		0.391601	0.312867	-1189.337571	-0.009341	-1187.524368	-1183.908481
dimet trans C5-rad 111	-1189.326655	0.75		0.392004	0.311621				
ts dimet trans 15 ircf	-1189.325226	0.75	-	0.392026	0.314794				
dimet trans C5-rad 99_2	-1189.324461	0.75		0.391666	0.312896				
dimet trans C5-rad 73	-1189.321792	0.75		0.391633	0.312631				

Table S5b. Energies for all systems shown in Fig. S5

Molecule	UB3LYP/6-31(d)							Conformation $\varphi_ \chi_ \psi_ \omega$
	Gas phase			PCM(DiChloroEthane)		DLPNO-CCSD(T)/cc-pVTZ		
	ΔE_{tot} [Hartree]	ΔH_{298} [kJ/mol]	ΔG_{298} [kJ/mol]	ΔH_{298} [kJ/mol]	ΔG_{298} [kJ/mol]	ΔH_{298} [kJ/mol]	ΔG_{298} [kJ/mol]	
r4b_N								
dimet trans N-rad 13	0.0	0.0	0.0	0.0	0.0	+0.0	+0.0	a g1- g2+ a
dimet trans N-rad 3 2	+0.9	+0.9	-1.3	+0.9	-1.4	-0.2	-2.5	a g1- g1+ a
dimet trans N-rad 12	+1.0	+0.6	-0.2	+0.3	-0.5	+2.5	+1.8	a a g2+ a
dimet trans N-rad 5 2	+1.4	+1.4	+3.3	+1.1	+3.0	+2.2	+4.1	a a g1+ a
dimet trans N-rad 25	+2.0	+1.4	-4.1	+1.3	-4.2	+2.7	-2.8	a a g2+ a
ts dimet trans 15 ircr	+7.3	+7.1	+11.1					a g1- g2- a
dimet trans N-rad 11	+8.1	+8.2	+5.9					a g2+ a g2-
dimet trans N-rad 81	+14.3	+15.8	+17.1					a g2- g2+ g1+
ts dimet trans 16HAT 11 ircr	+16.8	+16.6	+19.2					a a g2- a
dimet trans N-rad 89	+24.3	+26.1	+26.5					a e- g2- g2-
ts 4b 4bc₆								
ts dimet trans 16HAT 16HAT 11	+71.9	+57.5	+70.8	+52.6	+65.9	+44.0	+57.3	a a g2- g2+
ts dimet trans 16HAT 16HAT 8	+73.5	+58.9	+74.0	+50.7	+65.8	+41.9	+57.0	g2- a g2- g2+
ts dimet trans 16HAT 16HAT 7	+73.5	+58.9	+73.7	+50.7	+65.5	+41.9	+56.7	g2- a g2- g2+
ts dimet trans 16HAT 16HAT 31	+76.0	+61.3	+72.2	+56.4	+67.3	+46.3	+57.3	a a g1+ g1+
ts dimet trans 16HAT 16HAT 21	+77.0	+62.3	+74.7	+58.6	+71.0	+50.7	+63.1	g2+ g1+ g2- a
ts dimet trans 16HAT 16HAT 27	+79.7	+64.8	+79.9					g2- g1- g1+ g1+
ts dimet trans 16HAT 16HAT 30	+79.7	+64.8	+78.2					g2- g1- g1+ g1+
ts dimet trans 16HAT 16HAT 9	+80.9	+66.0	+81.7					g1+ g2+ g1+ g1+
ts dimet trans 16HAT 16HAT 12	+82.0	+66.9	+82.0					g1+ a g2- a
ts dimet trans 16HAT 16HAT 32	+82.7	+67.9	+82.6					g1- g2- g1+ g1+
ts dimet trans 16HAT 16HAT 14	+85.5	+71.1	+87.2					g2- g1+ g2- a
ts dimet trans 16HAT 16HAT 15	+85.6	+71.1	+85.2					g2- g1+ g2- a
ts dimet trans 16HAT 16HAT 4	+87.4	+72.6	+86.5					g2- g1+ g1+ g1+
ts dimet trans 16HAT 16HAT 25	+91.3	+76.4	+90.3					g2- g2- g1+ g1+
ts dimet trans 16HAT 16HAT 1	+94.5	+80.0	+95.7					g1+ e- g2- g2+
ts dimet trans 16HAT 16HAT 16	+109.1	+94.3	+109.2					g1+ g2- g1+ g1+
ts dimet trans 16HAT 16HAT 18	+109.6	+95.3	+111.0					g1+ e- g1+ g1+
r4bc₆								
dimet trans C6-rad 30 2	+19.2	+17.4	+14.6	+12.3	+9.4	-5.4	-8.3	g1+ a g1+ g1-
dimet trans C6-rad 24	+19.4	+17.6	+15.4	+12.2	+9.9	-3.3	-5.6	g2- a g1+ g1-
dimet trans C6-rad 15 2	+20.0	+18.5	+15.7	+13.1	+10.3	-4.1	-6.8	g1+ a g2+ g2+

dimet_trans_C6-rad_27	+20.0	+18.0	+14.1	+12.6	+8.6	-2.7	-6.7	g2- a g2+ g2+
dimet_trans_C6-rad_39	+21.2	+19.1	+16.6	+13.6	+11.1	-2.1	-4.7	g2- a g2+ g2+
dimet_trans_C6-rad_9	+26.0	+24.3	+24.8					g1+ g1+ g2- a
dimet_trans_C6-rad_35	+29.1	+28.0	+27.1					g2- a g2+ g2+
ts_dimet_trans_16HAT_11_ircf	+29.7	+29.1	+31.8					g2+ a g2- g2+
dimet_trans_C6-rad_88	+32.3	+30.8	+29.8					e+ g1+ g2- g2+
dimet_trans_C6-rad_79	+38.2	+37.1	+37.7					g1- g2- g2- g2+
ts_4b_4bcs								
ts_dimet_trans_15HAT_15HAT_15	+69.3	+54.8	+64.7	+48.4	+58.2	+39.4	+49.2	a g1- g2- a
ts_dimet_trans_15HAT_15HAT_4	+70.8	+56.3	+69.4	+46.6	+59.7	+39.6	+52.7	g1+ g1- g2- a
ts_dimet_trans_15HAT_15HAT_35	+73.9	+60.3	+74.7	+55.3	+69.7	+44.9	+59.3	a g2+ g1- g2-
ts_dimet_trans_15HAT_15HAT_6	+75.4	+61.1	+71.1	+55.4	+65.4	+48.9	+58.9	g2- g1- g2- g1+
ts_dimet_trans_15HAT_15HAT_32	+77.2	+63.1	+79.9	+53.4	+70.2	+44.2	+60.9	g2- g2+ g1- a
ts_dimet_trans_15HAT_15HAT_14	+79.6	+65.7	+78.7					g1+ g1- g2- g2-
ts_dimet_trans_15HAT_15HAT_23	+81.2	+67.5	+83.7					g2- g2+ g1- g2-
ts_dimet_trans_15HAT_15HAT_9	+81.5	+67.4	+79.0					g1+ g1- g2- g1+
ts_dimet_trans_15HAT_15HAT_1	+82.1	+68.2	+83.2					g2- g1+ g2- a
ts_dimet_trans_15HAT_15HAT_36	+84.4	+70.3	+78.7					g1- g2- g1- g1+
ts_dimet_trans_15HAT_15HAT_18	+84.7	+70.4	+84.9					g1+ e- g1- a
ts_dimet_trans_15HAT_15HAT_26	+85.8	+71.8	+85.1					a g1+ g2- g1+
ts_dimet_trans_15HAT_15HAT_7	+88.6	+74.8	+89.7					g2- g1+ g2- g2-
ts_dimet_trans_15HAT_15HAT_21	+89.4	+75.3	+88.0					g1+ e- g1- g2-
ts_dimet_trans_15HAT_15HAT_33	+95.1	+81.7	+99.4					g2- g2+ g1- g1+
ts_dimet_trans_15HAT_15HAT_30	+96.3	+82.8	+98.2					g1+ e- g1- g1+
r4bcs								
dimet_trans_C5-rad_109	+15.1	+14.1	+15.8	+10.3	+11.9	-3.7	-2.1	g2- a g2+ g1-
dimet_trans_C5-rad_110	+16.1	+15.3	+15.7	+12.3	+12.7	-4.0	-3.6	g1+ g1+ g2+ a
dimet_trans_C5-rad_31	+16.7	+16.1	+14.3	+13.7	+11.8	-2.2	-4.0	g2+ g1+ g2+ g1-
dimet_trans_C5-rad_117	+17.1	+16.2	+16.1	+10.9	+10.8	-2.2	-2.3	g2- a g2+ g1-
dimet_trans_C5-rad_46	+17.8	+16.5	+15.2	+13.5	+12.2	-3.7	-5.0	g2- g2- g2+ g1-
dimet_trans_C5-rad_111	+21.9	+21.7	+16.1					g1+ g1- g2+ g2-
ts_dimet_trans_15_ircf	+25.7	+25.5	+28.1					g1- a g2- g2+
dimet_trans_C5-rad_99_2	+27.7	+26.5	+25.2					e+ g1+ g2- g2+
dimet_trans_C5-rad_73	+34.7	+33.5	+31.5					g1+ g1+ g1- a

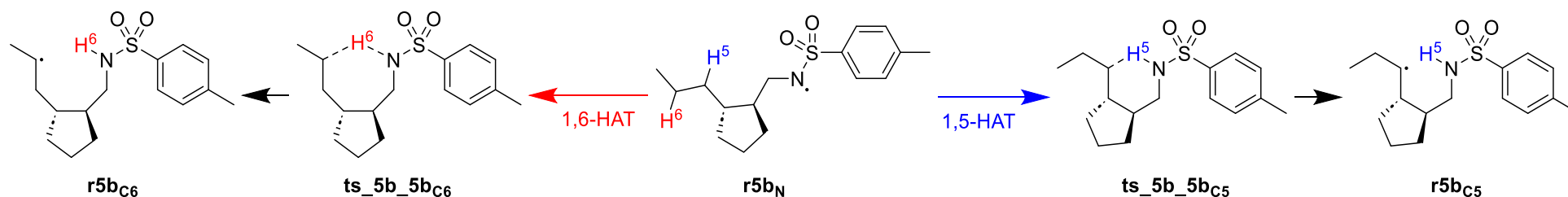


Fig. S6. Rearrangement reactions of *N*-centered radical **r5b_N** to radicals **r5b_{c5}** and **r5b_{c6}**.

Table S6a. Energies for all systems shown in Fig. S6.

Molecule	E_{tot} UB3LYP/ 6-31G(d) [Hartree]	$\langle S^2 \rangle$	NIMAG	dH UB3LYP/ 6-31G(d) [Hartree]	dG UB3LYP/ 6-31G(d) [Hartree]	E_{tot} PCM(DCE)/ UB3LYP/ 6-31G(d) ^[a] [Hartree]	dG_{298}^{solv} PCM(DCE)/ UB3LYP/ 6-31G(d) ^[a] [Hartree]	E_{tot} DLPNO- CCSD(T)/ cc-pVTZ ^[a] [Hartree]	G_{298}^{DCE} PCM(DCE) + DLPNO- CCSD(T)/cc-pVTZ ^[a] [Hartree]
r5b_N									
cpen trans N-rad 20	-1227.440449	0.75	-	0.399807	0.321884	-1227.448586	-0.008138	-1221.782302	-1225.244843
cpen_trans_N-rad_8	-1227.440340	0.75	-	0.399711	0.320539	-1227.448731	-0.008392	-1221.782552	-1225.245605
cpen trans N-rad 3	-1227.440326	0.75	-	0.399711	0.320872	-1227.448707	-0.008381	-1221.782518	-1225.245218
cpen trans N-rad 31	-1227.440210	0.75	-	0.399706	0.321344	-1227.448311	-0.008101	-1221.781982	-1225.244989
cpen trans N-rad 38	-1227.439926	0.75	-	0.400051	0.322536	-1227.448158	-0.008232	-1221.779865	-1225.245081
cpen trans N-rad 91	-1227.438052	0.75	-	0.400274	0.321885				
ts cpen trans 15HAT 1rcr	-1227.437930	0.75	-	0.399982	0.321855				
cpen trans N-rad 70	-1227.436950	0.75	-	0.400543	0.324903				
ts cpen trans 16 HAT10 1rcr	-1227.435286	0.75	-	0.399685	0.321110				
cpen trans N-rad 81	-1227.433470	0.75	-	0.400668	0.324540				
cpen trans N-rad 109	-1227.432987	0.75	-	0.400590	0.324289				
cpen_trans_N-rad_20	-1227.440449	0.75	-	0.399807	0.321884				
cpen trans N-rad 8	-1227.440340	0.75	-	0.399711	0.320539				
ts 5b 5bc₆									
ts cpen trans 16HAT 10	-1227.414985	0.76	-1549	0.394158	0.320670	-1227.424859	-0.009874	-1221.730861	-1225.226491
ts cpen trans 16HAT 7	-1227.413479	0.76	-1503	0.394277	0.321069	-1227.422986	-0.009507	-1221.728180	-1225.223735
ts cpen trans 16HAT 11	-1227.411446	0.76	-1612	0.394233	0.321416	-1227.423473	-0.012028	-1221.727380	-1225.225801
ts cpen trans 16HAT 1	-1227.409605	0.76	-1528	0.394290	0.321663	-1227.42161	-0.012005	-1221.724837	-1225.224962
ts cpen trans 16HAT 3	-1227.409593	0.76	-1528	0.394308	0.321627	-1227.421605	-0.012012	-1221.724801	-1225.224977
ts cpen trans 16HAT 13	-1227.407547	0.76	-1759	0.394541	0.321626				
ts cpen trans 16HAT 12	-1227.405103	0.76	-1638	0.394400	0.320776				
r5bc₆									
cpen trans C6-rad 38 4	-1227.433930	0.75	-	0.399317	0.320628	-1227.443861	-0.009931	-1221.776117	-1225.249066
cpen trans C6-rad 10	-1227.433190	0.75	-	0.399412	0.322289	-1227.44458	-0.011390	-1221.777709	-1225.250204
ts cpen trans 16HAT 10 1rcf	-1227.432974	0.75	-	0.399477	0.323460	-1227.442385	-0.009411	-1221.775469	-1225.245653
cpen trans C6-rad 25 4	-1227.432720	0.75	-	0.399054	0.318336	-1227.44313	-0.010410	-1221.780698	-1225.251180
cpen trans C6-rad 35	-1227.432697	0.75	-	0.399262	0.320387	-1227.44299	-0.010292	-1221.779791	-1225.249244
cpen trans C6-rad 49	-1227.432315	0.75	-	0.399150	0.319937				

cpen trans C6-rad 53	-1227.430978	0.75	-	0.399151	0.319908				
cpen trans C6-rad 14	-1227.429345	0.75	-	0.399346	0.319682				
cpen_trans_C6-rad_23	-1227.428471	0.75	-	0.399509	0.321272				
ts 5b 5b_{CS}									
ts cpen trans 15HAT	-1227.411777	0.76	-1616	0.394703	0.320592	-1227.422255	-0.010478	-1221.726995	-1225.223762
ts cpen trans 15HAT 17	-1227.410593	0.76	-1744	0.394656	0.319650	-1227.421278	-0.010685	-1221.726418	-1225.225359
ts cpen trans 15HAT 4	-1227.409940	0.76	-1646	0.394661	0.320657	-1227.421869	-0.011929	-1221.725608	-1225.225514
ts cpen trans 15HAT 16	-1227.409614	0.76	-1600	0.394689	0.320718	-1227.419305	-0.009691	-1221.723397	-1225.221532
ts cpen trans 15HAT 24	-1227.408380	0.76	-1721	0.394981	0.322300	-1227.418332	-0.009952	-1221.721251	-1225.219052
ts_cpen_trans_15HAT_12	-1227.407436	0.76	-1633	0.394829	0.321797				
ts cpen trans 15HAT 29	-1227.407038	0.76	-1738	0.394787	0.320516				
ts cpen trans 15HAT 26	-1227.406673	0.76	-1611	0.394814	0.321539				
ts_cpen_trans_15HAT_23	-1227.405650	0.76	-1666	0.394805	0.320760				
ts cpen trans 15HAT 2	-1227.405632	0.76	-1721	0.394749	0.322578				
ts cpen trans 15HAT 28	-1227.404112	0.76	-1778	0.394866	0.321497				
ts cpen trans 15HAT 7	-1227.403989	0.76	-1681	0.394884	0.322311				
ts cpen trans 15HAT 11	-1227.398896	0.76	-1710	0.394880	0.322418				
r5b_{CS}									
cpen trans C5-rad 80	-1227.436258	0.75	-	0.399821	0.322430	-1227.445870	-0.009612	-1221.779441	-1225.248056
cpen_trans_C5-rad_76	-1227.435565	0.75	-	0.399804	0.321603	-1227.444904	-0.009339	-1221.779452	-1225.248480
cpen trans C5-rad 55	-1227.435211	0.75	-	0.399866	0.321387	-1227.444400	-0.009189	-1221.777872	-1225.247820
cpen trans C5-rad 26	-1227.434857	0.75	-	0.399982	0.323148	-1227.443634	-0.008777	-1221.777509	-1225.247145
cpen_trans_C5-rad_105	-1227.434829	0.75	-	0.399980	0.320503	-1227.444222	-0.009393	-1221.778208	-1225.248775
ts cpen trans 15HAT ircf	-1227.434141	0.75	-	0.399933	0.322594				
cpen trans C5-rad 12	-1227.431531	0.75	-	0.399686	0.321351				
cpen trans C5-rad 114	-1227.428261	0.75	-	0.399576	0.321155				

Table S6b. Energies for all systems shown in Fig. S6

Molecule	UB3LYP/6-31(d)							Conformation R_φ_χ_ψ_ω
	Gas phase			PCM(DiChloroEthane)		DLPNO-CCSD(T)/cc-pVTZ		
	ΔE_{tot} [Hartree]	ΔH_{298} [kJ/mol]	ΔG_{298} [kJ/mol]	ΔH_{298} [kJ/mol]	ΔG_{298} [kJ/mol]	ΔH_{298} [kJ/mol]	ΔG_{298} [kJ/mol]	
r5b_N								
cpen trans N-rad 20	0.0	0.0	0.0	0.0	0.0	+0.0	+0.0	Eα↑ a a a a
cpen trans N-rad 8	+0.3	+0.0	-3.2	-0.6	-3.9	+1.9	-1.3	Eβ↑ a a a a
cpen trans N-rad 3	+0.3	+0.1	-2.3	-0.6	-3.0	+2.1	-0.3	Eβ↑ a a a a
cpen trans N-rad 31	+0.6	+0.4	-0.8	+0.5	-0.7	+0.7	-0.5	Eβ↑ a a a a
cpen trans N-rad 38	+1.4	+2.0	+3.1	+1.8	+2.8	-1.4	-0.4	Eα↓ a g1- g2+ a
cpen trans N-rad 91	+6.3	+7.5	+6.3					E0↑ g2+ g1+ g1+ a
ts cpen trans 15HAT ircr	+6.6	+7.1	+6.5					Eβ↓ a g1- g2- a
cpen trans N-rad 70	+9.2	+11.1	+17.1					E0↑ a g1+ g1+ g1+
ts cpen trans 16 HAT10 ircr	+13.6	+13.2	+11.5					Eβ↓ a a g1+ g1+
cpen trans N-rad 81	+18.3	+20.6	+25.3					Eα↓ g2+ g1+ g2- g2-

cpen_trans_N-rad_109	+19.6	+21.6	+25.9					E α ↑ a g1+ g2- g2-
ts 5b 5bc₆								
ts cpen trans 16HAT 10	+66.9	+52.0	+63.7	+47.5	+59.1	+41.1	+52.7	E β ↓ g2- g1- g1+ g1+
ts cpen trans 16HAT 7	+70.8	+56.3	+68.7	+52.7	+65.1	+46.6	+59.0	E β ↓ g1+ g1+ g1+ g1+
ts cpen trans 16HAT 11	+76.1	+61.5	+74.9	+51.3	+64.7	+46.8	+60.2	E β ↓ g1+ a g1+ g1+
ts cpen trans 16HAT 1	+81.0	+66.5	+80.4	+56.3	+70.2	+48.4	+62.4	E β ↓ g2- g1+ g1+ g1+
ts cpen trans 16HAT 3	+81.0	+66.6	+80.3	+56.4	+70.2	+48.6	+62.3	E β ↓ g2- g1+ g1+ g1+
ts cpen trans 16HAT 13	+86.4	+72.6	+85.7					E β '↑ g1- g1- g2- a
ts cpen trans 16HAT 12	+92.8	+78.6	+89.9					E β ↓ g2- e+ g2- a
r5bc₆								
cpen_trans_C6-rad_38_4	+17.1	+15.8	+13.8	+11.1	+9.1	-4.4	-6.4	E β ↓ g2- a g1+ g1-
cpen_trans_C6-rad_10	+19.1	+18.0	+20.1	+9.5	+11.6	-7.6	-5.5	E β ↓ g1+ g2+ g1+ g1-
ts_cpen_trans_16HAT_10_ircf	+19.6	+18.8	+23.8	+15.4	+20.4	-3.8	+1.2	E0↓ g2- g1- g1+ g1+
cpen_trans_C6-rad_25_4	+20.3	+18.3	+11.0	+12.3	+5.0	-3.3	-10.7	E α ↑ g2- a a g2+
cpen_trans_C6-rad_35	+20.4	+18.9	+16.4	+13.3	+10.8	-3.4	-5.9	E0↓ g2- a g1+ g1-
cpen_trans_C6-rad_49	+21.4	+19.6	+16.2					E α '↓ g2- g2- a g2+
cpen_trans_C6-rad_53	+24.9	+23.1	+19.7					E0↓ g1+ e+ g1+ g1-
cpen_trans_C6-rad_14	+29.2	+27.9	+23.4					E α ↑ g1+ g2- g1+ g1+
cpen_trans_C6-rad_23	+31.4	+30.7	+29.8					E β ↓ g1+ g2- g2- g2-
ts 5b 5bc₅								
ts_cpen_trans_15HAT	+75.3	+61.9	+71.9	+55.7	+65.7	+51.5	+61.5	E β ↓ g2- g1- g2- a
ts_cpen_trans_15HAT_17	+78.4	+64.9	+72.5	+58.2	+65.8	+50.2	+57.8	E β ↓ a g1- g2- g2+
ts_cpen_trans_15HAT_4	+80.1	+66.6	+76.9	+56.6	+66.9	+50.4	+60.7	E β ↓ g1+ g1- g2- g2+
ts_cpen_trans_15HAT_16	+81.0	+67.5	+77.9	+63.4	+73.8	+54.9	+65.3	E β ↓ g1+ g1+ g2- g2-
ts_cpen_trans_15HAT_24	+84.2	+71.5	+85.3	+66.8	+80.5	+58.7	+72.5	E β ↓ a g1+ g2- g2-
ts_cpen_trans_15HAT_12	+86.7	+73.6	+86.4					E β ↓ g1+ g1- g2- g2-
ts_cpen_trans_15HAT_29	+87.7	+74.5	+84.1					E β '↑ a g1- g2- g1+
ts_cpen_trans_15HAT_26	+88.7	+75.6	+87.8					E β '↑ g1+ g1+ g2- g1+
ts_cpen_trans_15HAT_23	+91.4	+78.2	+88.4					E β '↑ g1+ g1- g2- g1+
ts_cpen_trans_15HAT_2	+91.4	+78.1	+93.2					E β ↓ g2- g1+ g2- a
ts_cpen_trans_15HAT_28	+95.4	+82.4	+94.4					E β '↑ a g1+ g2- g1+
ts_cpen_trans_15HAT_7	+95.7	+82.8	+96.8					E β ↓ g2- g1+ g2- g2-
ts_cpen_trans_15HAT_11	+109.1	+96.2	+110.5					E β '↑ g2- e+ g2- g1+
r5bc₅								
cpen_trans_C5-rad_80	+11.0	+11.0	+12.4	+7.2	+8.6	-6.0	-4.6	E β ↓ g2- g1- g2+ g1-
cpen_trans_C5-rad_76	+12.8	+12.8	+12.1	+9.7	+8.9	-5.7	-6.4	E β ↓ g1+ g1+ g2+ g1-
cpen_trans_C5-rad_55	+13.8	+13.9	+12.4	+11.1	+9.7	-3.6	-5.1	E β ↓ g2+ g1+ g2+ g1-
cpen_trans_C5-rad_26	+14.7	+15.1	+18.0	+13.5	+16.3	-7.2	-4.4	E β ↓ g1+ g1+ g2- g2+
cpen_trans_C5-rad_105	+14.8	+15.2	+11.1	+11.9	+7.8	-2.9	-7.0	E β ↓ g1+ g1+ g2+ g1+
ts_cpen_trans_15HAT_ircf	+16.6	+16.9	+18.4					E β ↓ g2- a g2- g2+

cpen_trans_C5-rad_12	+23.4	+23.1	+22.0						$E\alpha\uparrow$ e+ g1+ g2+ g1-
cpen_trans_C5-rad_114	+32.0	+31.4	+30.1						$E\beta\downarrow$ g2- g1+ g1+ g2+

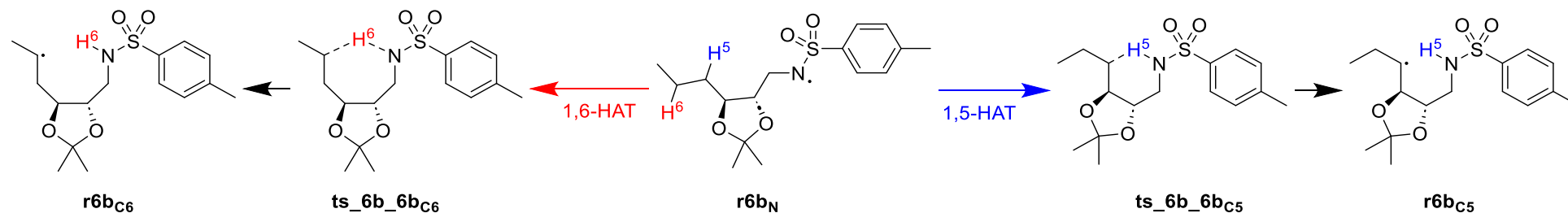


Fig. S7. Rearrangement reactions of *N*-centered radical **r6b_N** to radicals **r6bc₅** and **r6bc₆**.

Table S7a. Energies for all systems shown in Fig. S7.

Molecule	E_{tot}	$\langle S^2 \rangle$	NIMAG	dH	dG	E_{tot}	dG_{298}^{solv}	E_{tot}	G_{298}^{DCE}
	UB3LYP/ 6-31G(d) [Hartree]			UB3LYP/ 6-31G(d) [Hartree]	UB3LYP/ 6-31G(d) [Hartree]	PCM(DCE)/ UB3LYP/ 6-31G(d) ^[a] [Hartree]	PCM(DCE)/ UB3LYP/ 6-31G(d) ^[a] [Hartree]	DLPNO-CCSD(T)/ cc-pVTZ ^[a] [Hartree]	PCM(DCE) + DLPNO-CCSD(T)/cc- pVTZ ^[a] [Hartree]
r6b_N									
7 n-rad 2	-1377.881181	0.75	-	0.409217	0.325553	-1377.891072	-0.009890	-1375.811464	-1375.495801
7 n-rad 2 mirror	-1377.881181	0.75	-	0.409217	0.325553				
ts 7 9 2 2 ircr	-1377.881116	0.75	-	0.409505	0.325489	-1377.890884	-0.009768	-1375.812096	-1375.496375
7 n-rad	-1377.880716	0.75	-	0.409208	0.326203	-1377.891148	-0.010432	-1375.811653	-1375.495882
ts 7 9 2 ircr	-1377.880217	0.75	-	0.409740	0.327064	-1377.890139	-0.009921	-1375.810247	-1375.493104
7 12	-1377.879873	0.75	-	0.409231	0.324899	-1377.889742	-0.009869	-1375.810823	-1375.495794
7 41	-1377.878962	0.75	-	0.409778	0.328055	-	-	-	-
ts 7 8 3 ircr	-1377.878494	0.75	-	0.409253	0.326099	-	-	-	-
ts 7 8 ircr	-1377.878493	0.75	-	0.409254	0.326111	-	-	-	-
7 37	-1377.878449	0.75	-	0.409767	0.325899	-	-	-	-
7_81	-1377.875766	0.75	-	0.410013	0.328524	-	-	-	-
ts 6b 6bc₆									
ts 7 8 3	-1377.855190	0.76	-1648	0.403631	0.325272	-1377.866675	-0.011483	-1375.790071	-1375.476281
ts_7_8_3_mirror	-1377.855192	0.76	-1648	0.403631	0.325272				
ts 7 8	-1377.853177	0.76	-1766	0.403618	0.325006	-1377.865232	-0.012056	-1375.788893	-1375.475942
ts 7 8 2	-1377.853155	0.76	-1624	0.403658	0.325331	-1377.864467	-0.011311	-1375.788168	-1375.474148
ts 7 8 7	-1377.853155	0.76	-1624	0.403658	0.325330	-1377.864466	-0.011311	-1375.788171	-1375.474152
r6bc₆									
8 23	-1377.875877	0.75	-	0.409053	0.326151	-1377.885462	-0.009585	-1375.815588	-1375.499023
8 23 mirror	-1377.875877	0.75	-	0.409053	0.326151				
8_recalc	-1377.874454	0.75	-	0.408953	0.324056	-1377.886270	-0.011816	-1375.813064	-1375.500824
ts 7 8 3 ircf	-1377.874215	0.75	-	0.408813	0.325780	-1377.885950	-0.011736	-1375.812841	-1375.498797
ts 7 8 ircf	-1377.872195	0.75	-	0.408843	0.324824	-1377.884431	-0.012236	-1375.810282	-1375.497695
8_14	-1377.871415	0.75	-	0.408550	0.324192	-1377.882293	-0.010878	-1375.810545	-1375.497231
ts 6b 6bc₅									

ts 7 9 2 2	-1377.845262	0.76	-1816	0.403749	0.324471	-1377.856188	-0.010926	-1375.780372	-1375.466827
ts 7 9 2 2 mirror	-1377.845262	0.76	-1816	0.403749	0.324471				
ts 7 9 1	-1377.844609	0.76	-1761	0.403817	0.324474	-1377.855773	-0.011164	-1375.780254	-1375.466944
ts 7 9 2	-1377.844609	0.76	-1761	0.403817	0.324479	-1377.855773	-0.011164	-1375.780260	-1375.466945
ts 7 9 9	-1377.844562	0.76	-1793	0.403875	0.324056	-1377.855762	-0.011200	-1375.779871	-1375.467015
ts 7 9 10	-1377.844108	0.76	-1769	0.404019	0.324538	-1377.855357	-0.011249	-1375.779694	-1375.466405
ts 7 9	-1377.843621	0.76	-1856	0.403897	0.325040	-	-	-	-
ts 7 9 3	-1377.843045	0.76	-1772	0.403962	0.325277	-	-	-	-
ts 7 9 7	-1377.842699	0.76	-1757	0.404062	0.324617	-	-	-	-
ts 7 9 13	-1377.842145	0.76	-1857	0.403839	0.326329	-	-	-	-
ts 7 9 16	-1377.841396	0.76	-1860	0.404060	0.326157	-	-	-	-
r6b_{C5}									
9 54	-1377.874027	0.75	-	0.409539	0.325882	-1377.885473	-0.011446	-1375.812028	-1375.497592
9 54 mirror	-1377.874027	0.75	-	0.409539	0.325880				
ts 7 9 2 ircf	-1377.872963	0.75	-	0.409010	0.324449	-1377.884159	-0.011196	-1375.811060	-1375.497807
ts 7 9 2 2 ircf	-1377.872537	0.75	-	0.409155	0.326154	-1377.883995	-0.011458	-1375.810190	-1375.495495
9 15	-1377.871171	0.75	-	0.409349	0.325983	-1377.883645	-0.012474	-1375.811315	-1375.497806
9	-1377.870477	0.75	-	0.408962	0.323451	-1377.884046	-0.013569	-1375.808044	-1375.498162
9 22	-1377.869599	0.75	-	0.409371	0.326777	-1377.882002	-0.012403	-1375.810412	-1375.496038

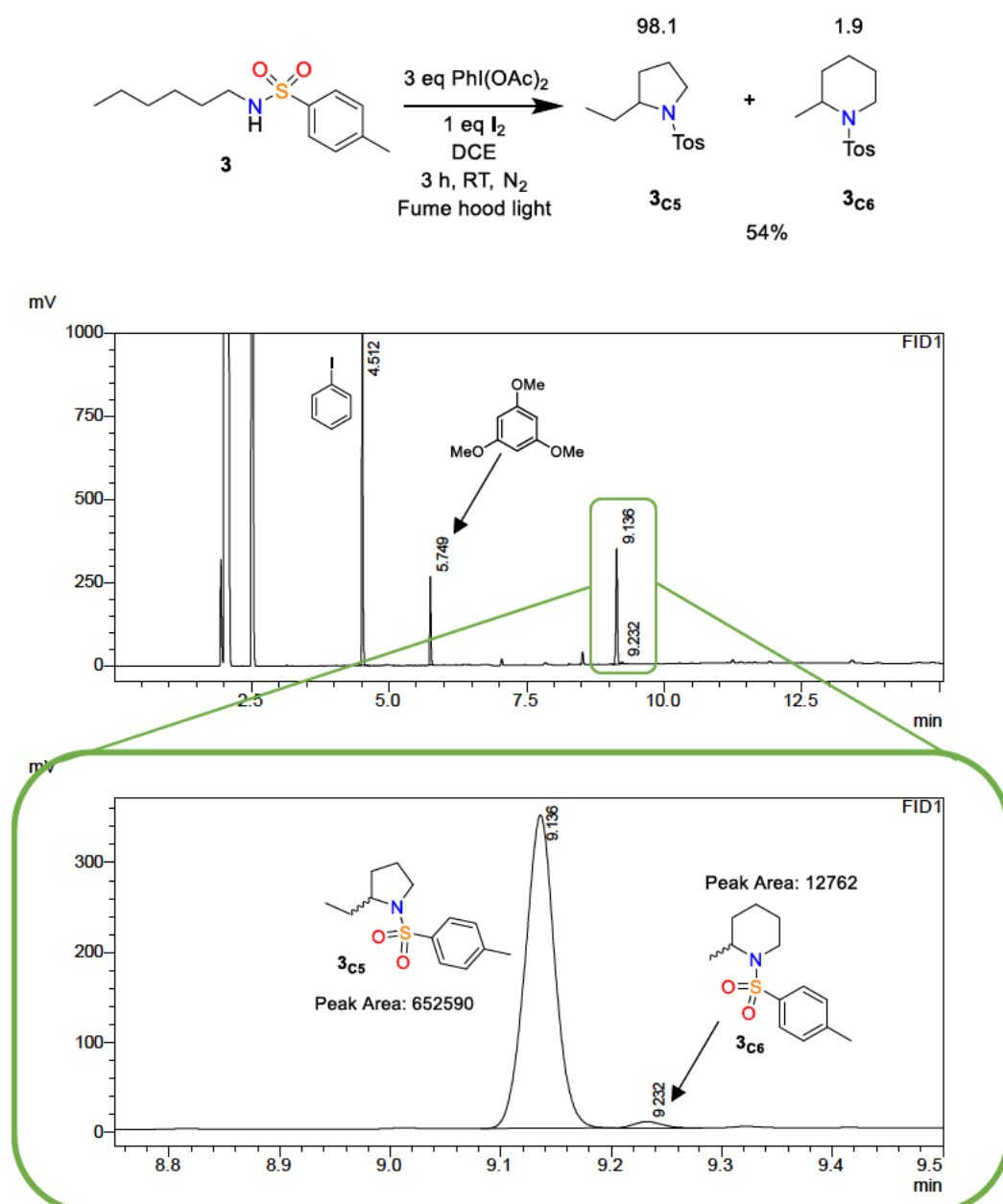
Table S7b. Energies for all systems shown in Fig. S6 (UB3LYP/6-31G(d) result).

Molecule	UB3LYP/6-31(d)							Conformation R_φ_χ_ψ_ω
	Gas phase			PCM(DiChloroEthane)		DLPNO-CCSD(T)/cc-pVTZ		
	ΔE_{tot} [Hartree]	ΔH_{298} [kJ/mol]	ΔG_{298} [kJ/mol]	ΔH_{298} [kJ/mol]	ΔG_{298} [kJ/mol]	ΔH_{298} [kJ/mol]	ΔG_{298} [kJ/mol]	
r6b_N								
7_n-rad_2	+0.0	+0.0	+0.0	+0.0	+0.0	+0.0	+0.0	Eβ↑ a g2+ a a
7 n-rad 2 mirror	+0.0	+0.0	+0.0					
ts_7_9_2_2 ircr	+0.2	+0.9	+0.0	+1.2	+0.3	-0.9	-1.8	Eβ↑ a g2+ a a
7_n-rad	+1.2	+1.2	+2.9	-0.2	+1.5	-0.5	+1.2	Eβ↑ a a a a
ts_7_9_2 ircr	+2.5	+3.9	+6.5	+3.8	+6.4	+4.6	+7.2	Eα↓ g1- g2- a a
7_12	+3.4	+3.5	+1.7	+3.5	+1.8	+1.7	+0.0	Eβ↑ a g2+ a g1+
7 41	+5.8	+7.3	+12.4	-	-	-	-	Eβ↓ g1- g2- g2- a
ts_7_8_3 ircr	+7.1	+7.2	+8.5	-	-	-	-	Eβ↑ a g2+ g2- a
ts_7_8 ircr	+7.1	+7.2	+8.5	-	-	-	-	Eβ↑ a g2+ g2- a
7 37	+7.2	+8.6	+8.1	-	-	-	-	Eα↓ a g2- a g2-
7 81	+14.2	+16.3	+22.0	-	-	-	-	Eα↓ a g2+ g1+ g2-
ts 6b 6b_{C6}								
ts 7 8 3	+68.2	+53.6	+67.5	+49.4	+63.3	+41.5	+55.4	Eβ↑ g1+ g2+ g2- g2+
ts 7 8 3 mirror	+68.2	+53.6	+67.5					
ts_7_8	+73.5	+58.8	+72.1	+53.1	+66.4	+44.6	+57.8	Eβ↑ g2+ g2+ g2- g2+
ts_7_8_2	+73.6	+59.0	+73.0	+55.3	+69.3	+46.6	+60.6	Eβ'↓ g2- g2- g2- g2+
ts_7_8_7	+73.6	+59.0	+73.0	+55.3	+69.3	+46.6	+60.6	Eβ'↓ g2- g2- g2- g2+

r6b _{c6}								
8_23	+13.9	+13.5	+15.5	+14.3	+16.3	-11.3	-9.3	Eβ↑ e- g2- a g2-
8_23_mirror	+13.9	+13.5	+15.5					
8_recalc	+17.7	+17.0	+13.7	+11.9	+8.7	-4.9	-8.1	Eβ↑ g2- a g2- g2-
ts_7_8_3_ircf	+18.3	+17.2	+18.9	+12.4	+14.0	-4.7	-3.0	Eβ↑ g1+ a g2- g2+
ts_7_8_ircf	+23.6	+22.6	+21.7	+16.5	+15.5	+2.1	+1.2	Eβ↑ g2+ a g2- g2+
8_14	+25.6	+23.9	+22.1	+21.3	+19.5	+0.7	-1.2	Eβ↑ e+ g1+ a g2+
ts 6b 6b _{c5}								
ts_7_9_2_2	+94.3	+79.9	+91.5	+77.2	+88.7	+67.3	+78.8	Eβ↑ g1+ g2+ g1- a
ts_7_9_2_2_mirror	+94.3	+79.9	+91.5					
ts_7_9_1	+96.0	+81.8	+93.2	+78.5	+89.8	+67.8	+79.1	Eβ'↓ g2- g2- g1- a
ts_7_9_2	+96.0	+81.8	+93.2	+78.5	+89.9	+67.7	+79.1	Eβ'↓ g2- g2- g1- a
ts_7_9_9	+96.1	+82.1	+92.2	+78.7	+88.8	+68.9	+79.0	Eβ↑ g1+ g2+ g1- g2-
ts_7_9_10	+97.3	+83.7	+94.7	+80.1	+91.1	+69.8	+80.7	Eβ'↓ g2- g2- g1- g2-
ts_7_9	+98.6	+84.6	+97.3	-	-	-	-	Eβ'↓ g1- g2- g1- a
ts_7_9_3	+100.1	+86.3	+99.4	-	-	-	-	Eβ↑ g1+ g2+ g1- g1+
ts_7_9_7	+101.0	+87.5	+98.6	-	-	-	-	Eβ'↓ g2- g2- g1- g1+
ts_7_9_13	+102.5	+88.4	+104.5	-	-	-	-	Eβ'↓ g2- g2+ g1- a
ts_7_9_16	+104.5	+90.9	+106.0	-	-	-	-	Eβ'↓ g2- g2+ g1- g2-
r6b _{c5}								
9_54	+18.8	+19.6	+19.6	+15.5	+15.6	-0.6	-0.6	Eβ↑ g2+ a g1+ g1+
9_54_mirror	+18.8	+19.6	+19.6					
ts_7_9_2_ircf	+21.6	+21.0	+18.7	+17.6	+15.2	+0.5	-1.8	Eβ'↓ g2- g2- g1- g2+
ts_7_9_2_2_ircf	+22.7	+22.5	+24.3	+18.4	+20.2	+3.2	+4.9	Eβ↑ g1+ g2+ g1- g2+
9_15	+26.3	+26.6	+27.4	+19.8	+20.6	+0.7	+1.5	Eβ↑ g1+ e+ g1+ g1+
9	+28.1	+27.4	+22.6	+17.8	+12.9	+8.3	+3.5	Eβ'↓ g1+ a g1- g2+
9_22	+30.4	+30.8	+33.6	+24.2	+27.0	+3.2	+6.0	Eβ'↓ g2- g2- g2- g2-

3.5.2. General Procedure for Fan Variation of HLF Reaction

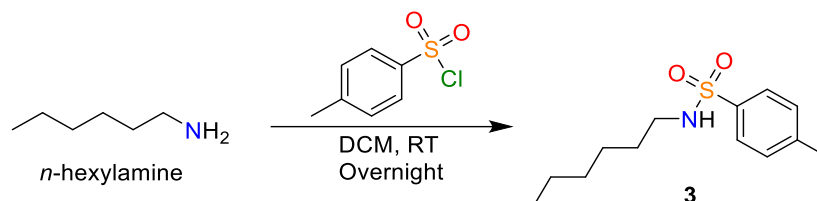
A 10 ml GC vial was charged with $\text{PhI}(\text{OAc})_2$ (212 mg, 0.66 mmol) and sulfonamide (0.22 mmol), evacuated, and backfilled with nitrogen. I_2 (56 mg, 0.22 mmol) and degassed DCE (1.5 mL) were successively added. Then the reaction mixture was stirred at 25 °C under fume hood irradiation. The mixture was quenched with saturated NaHCO_3 and $\text{Na}_2\text{S}_2\text{O}_3$ and extracted by DCM (3×5 ml). Organic phases were combined and dried over MgSO_4 . All volatiles were evaporated, and the crude material was purified by column chromatography ($i\text{Hex}/\text{EtOAc} = 10/1$).



Scheme S1. Fan variation of the HLF reaction results (GC-FID profile).

3.5.3. Synthesis and Analytical Data for Reagents and Products

Synthesis of N-hexyl-4-methylbenzenesulfonamide (**3**)



3.1 ml of n-hexylamine (2.4 g, 24.6 mmol, 2.1 eq) was added dropwise to a solution of 2.0 g TsCl (11.7 mmol, 1 eq) in 40 mL of dry DCM at 0°C and stirred for overnight at RT. The cooling bath was removed and the reaction mixture was allowed to stir overnight. The reaction was quenched with 100 ml of water, extracted with DCM (3 × 50 mL). Organic phases were combined, washed with brine (50 mL), dried over MgSO₄ and evaporated. Crude material was purified by recrystallization from *i*-hexane and **3** was obtained as colorless solid (69%, 2.1 g) Spectral data are in agreement with literature values.^[4]

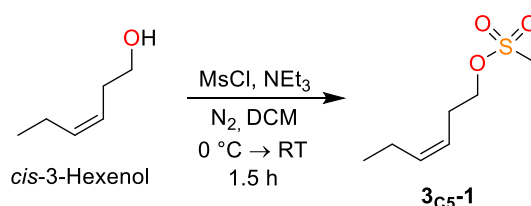
¹H NMR (400 MHz, CDCl₃) δ 7.75 (d, *J* = 8.2 Hz, 2H), 7.31 (d, *J* = 8.2 Hz, 2H), 4.36 (t, *J* = 6.2 Hz, 1H), 2.95 – 2.90 (m, 2H), 2.43 (s, 3H), 1.47 – 1.40 (m, 2H), 1.29 – 1.14 (m, 6H), 0.84 (t, *J* = 7.1 Hz, 3H).

¹³C NMR (101 MHz, CDCl₃) δ 143.5, 137.1, 129.8, 127.3, 43.4, 31.4, 29.7, 26.3, 22.6, 21.7, 14.1.

Elem. Calcd for C₁₃H₂₁NO₂S: C 61.15; H 8.29; N 5.48; S 12.55 Found: C 61.41; H 8.67; N 5.36; S 12.78

Synthesis of 2-Ethyl-1-tosylpyrrolidine (**3c5**)

1. Synthesis of (3*Z*)-hex-3-en-1-yl methanesulfonate (**3c5-1**)



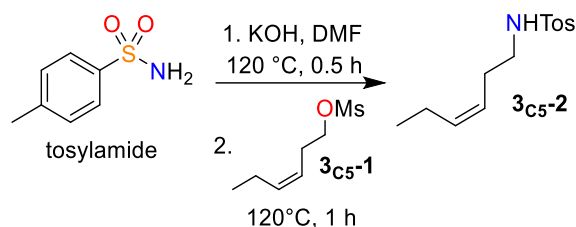
Following the modified literature procedure.^[5]

3.5 ml of triethylamine (2.5 g, 25 mmol, 5 eq) was added to the solution of 0.5 g *cis*-3-Hexenol (5 mmol, 1 eq) in 25 ml of dry DCM. The solution was cooled to 0 °C and 0.46 ml of MsCl (0.69 g, 6 mmol, 1.2 eq) was added dropwise. The solution was stirred for 1.5 h at RT, quenched with 50 ml of saturated NaHCO₃ solution, extracted with DCM (3 × 15 ml). The combined organic layers were dried over MgSO₄. Solvents were evaporated under reduced pressure. The

crude material was passed through a short silica plug (DCM) to afford a pale-yellow oil of **3c5-1** (0.79 g, 88%). Spectral data are in agreement with literature values.^[6]

¹H NMR (400 MHz, CDCl₃) δ 5.61 – 5.53 (m, 1H), 5.37 – 5.25 (m, 1H), 4.20 (t, *J* = 6.9 Hz, 2H), 3.00 (s, 3H), 2.55 – 2.45 (m, 2H), 2.11 – 2.02 (m, 2H), 0.98 (t, *J* = 7.5 Hz, 3H).

2. Synthesis of *N*-((3*Z*)-hex-3-en-1-yl)tosylamine (**3c5-2**)

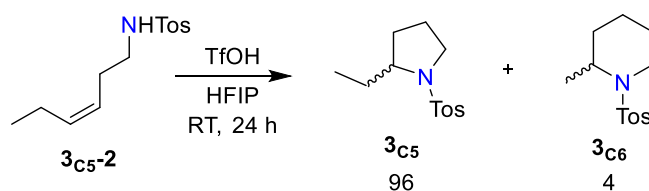


Following the modified literature procedure.^[5]

0.5 g of 85% KOH (7.5 mmol, 1.5 eq) was dissolved in 5 ml of dry DMF at 120 °C, followed by addition of 1.28 g of tosylamide (7.5 mmol, 1.5 eq). The resulting solution was stirred for 30 min at 120 °C. After, a solution of the mesylate **3c5-1**, obtained above in 5 ml of dry DMF was added in one portion. After 1 h of stirring at 120 °C, the reaction was cooled to RT, quenched with water and extracted with DCM (3×10 mL). The combined organic layers were washed with 50 ml of water, dried over MgSO₄ and evaporated. The crude material was passed through a short silica plug (iHex/EtOAc = 10/1) to afford **3c5-2** as colourless oil (45%, 0.51 g). Spectral data are in agreement with literature values.^[7]

¹H NMR (400 MHz, CDCl₃) δ 7.78 – 7.70 (m, 2H), 7.32 – 7.30 (m, 2H), 5.56 – 5.44 (m, 1H), 5.19 – 5.08 (m, 1H), 4.32 (t, *J* = 6.2 Hz, 1H), 2.97 (q, *J* = 6.6 Hz, 2H), 2.43 (s, 3H), 2.25 – 2.15 (m, 2H), 2.02 – 1.94 (m, 2H), 0.94 (t, *J* = 7.5 Hz, 3H).

3. Synthesis of 2-ethyl-1-tosylpyrrolidine (**3c5**)



Following the modified literature procedure.^[8]

0.51 g of the obtained **3c5-2** (2 mmol, 1 eq) was dissolved in 5 ml of HFIP. 0.35 ml of TfOH (0.6 g, 4 mmol, 2 eq) was added dropwise. The resulting solution was stirred for 24 h at RT. Reaction mixture was quenched with saturated aqueous solution of NaHCO₃ and extracted with DCM (3 × 10 mL). The combined organic layers were dried over MgSO₄. Solvents were evaporated under reduced pressure. Crude material was purified by flash chromatography

(*i*Hex/EtOAc= 10/1, R_f 0.25) to give **3**_{C5} (508 mg, 99%) as a white solid. Spectral data are in agreement with literature values.^[8]

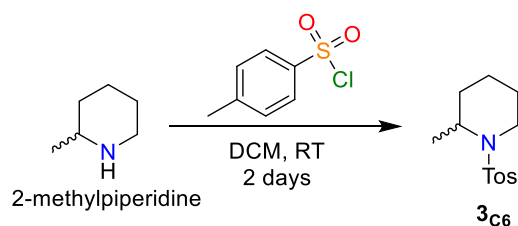
Further ¹H NMR and GC-FID analysis showed that the obtained product consists of 5- and 6-membered adduct **3**_{C5} and **3**_{C6} with ratio 96:4, correspondingly.

¹H NMR (400 MHz, CDCl₃) δ 7.76 – 7.70 (m, 2H), 7.32 – 7.29 (m, 2H), 3.54 (ddd, *J* = 10.3, 7.9, 5.1 Hz, 1H), 3.38 (ddd, *J* = 10.4, 7.0, 5.1 Hz, 1H), 3.19 (dt, *J* = 10.3, 7.2 Hz, 1H), 2.43 (s, 3H), 1.91 – 1.71j (m, 2H), 1.59 – 1.41 (m, 4H), 0.91 (t, *J* = 7.4 Hz, 3H).

¹³C NMR (101 MHz, CDCl₃) δ 143.3, 135.1, 129.7, 127.6, 61.9, 49.1, 30.2, 29.3, 24.2, 21.6, 10.5.

Elem. Calcd for C₁₃H₁₉NO₂S: C 61.63; H 7.56; N 5.53; S 12.65 Found: C 61.64; H 7.57; N 5.51; S 12.64

Synthesis of 2-methyl-1-tosylpiperidine (**3**_{C6})



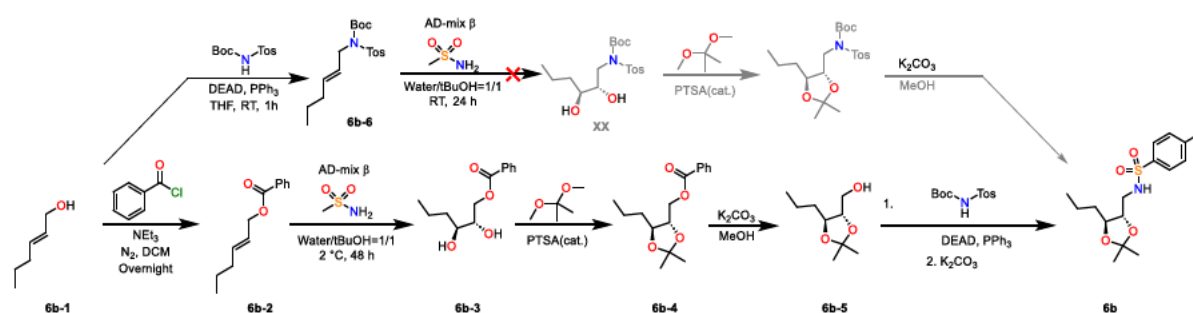
1.4 ml of 2-methylpiperidine (1.15 g, 11.7 mmol, 2.1 eq) was added dropwise to a solution of 1.0 g TsCl (5.8 mmol, 1 eq) in 20 mL of dry DCM at 0°C and stirred for overnight at RT. The cooling bath was removed and the reaction mixture was allowed to stir for 2 days. The reaction was quenched with 50 ml of water, extracted with DCM (3×25 mL). Organic phases were combined, washed with brine (50 mL), dried over MgSO₄ and evaporated. Crude material was purified by recrystallization from *i*Hex and **3**_{C6} was obtained as colorless solid (65%, 0.96 g). Spectral data are in agreement with literature values.^[9]

¹H NMR (400 MHz, CDCl₃) δ 7.71 – 7.68 (m, 2H), 7.28 – 7.25 (m, 2H), 4.26 – 4.19 (m, 1H), 3.72 – 3.67 (m, 1H), 2.96 (td, *J* = 13.0, 2.6 Hz, 1H), 2.41 (s, 3H), 1.66 – 1.46 (m, 4H), 1.46 – 1.30 (m, 2H), 1.05 (d, *J* = 6.9 Hz, 3H).

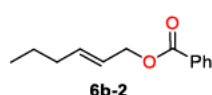
¹³C NMR (101 MHz, CDCl₃) δ 142.9, 138.5, 129.7, 127.1, 48.6, 40.4, 30.5, 25.3, 21.6, 18.3, 15.4.

Elem. Calcd for C₁₃H₁₉NO₂S: C 61.63; H 7.56; N 5.53; S 12.65 Found: C 61.92; H 7.86; N 5.50; S 12.95

Synthesis of annulated substrate **6b**



1. (E)-hex-2-enyl benzoate (**6b-2**)



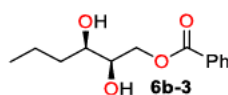
Following the modified literature procedure.^[10]

4.6 ml of Et₃N (3.3 g, 33 mmol, 1.1 eq) were added to stirred solution of *trans*-2-hexen-1-ol **6b-1** (3 g, 30 mmol, 1 eq) in 50 ml of dry DCM at 0 °C. After 10 min, 4.2 ml of freshly distilled benzoyl chloride (4.65 g, 33 mmol, 1.1 eq) were added dropwise. The cooling bath was removed and the reaction mixture was allowed to stir overnight. The reaction was quenched with 50 ml of water, extracted with DCM (3 x 25 mL). Organic phases were combined, washed with brine (50 mL), dried over MgSO₄ and evaporated. Crude material was purified by column chromatography (*i*Hex/EtOAc = 10/1, R_f 0.65). Product was obtained as colorless oil (5.75 g, 28.1 mmol). Spectral data are in agreement with literature value.^[10]

¹H NMR (400 MHz, CDCl₃) δ 8.10 – 8.02 (m, 2H), 7.57 – 7.52 (m, 1H), 7.46 – 7.41 (m, 2H), 5.90 – 5.82 (m, 1H), 5.72 – 5.65 (m, 1H), 4.77 (dd, *J* = 6.4, 1.0 Hz, 2H), 2.07 – 2.03 (m, 2H), 1.43 (h, *J* = 7.4 Hz, 2H), 0.92 (t, *J* = 7.4 Hz, 3H).

¹³C NMR (101 MHz, CDCl₃) δ 166.6, 136.6, 133.0, 130.5, 129.7, 128.4, 124.1, 65.9, 34.5, 22.2, 13.8.

2. (2R,3R)-2,3-Dihydroxyhexyl benzoate (**6b-3**)



Following the modified literature procedure.^[10]

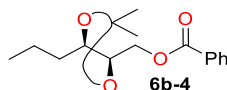
Solution of 2 g of benzoate **6b-2** (9.8 mmol, 1 eq) in 10 ml *t*BuOH was dropwise added to the solution of AD-mix-β (14 g) and 1 g of methansulfonamide (10.5 mmol, 1.05 eq) in *t*BuOH/H₂O (1:1, 30 mL) at 0 °C. The reaction mixture was stirred vigorously for 24 h at 2 °C, 30 ml of *t*BuOH/H₂O (1:1) were added and stirring continued for additional 24 h at 2 °C. The reaction was quenched with 1.5 g of Na₂SO₃ at 2 °C and then it was allowed to stir for 1 h more at RT. The crude mixture was extracted with DCM (3 x 50 mL), organic phases were combined, dried over MgSO₄ and evaporated to give crude material, which was purified by column chromatography (*i*Hex/EtOAc = 1/1, R_f 0.41).

Product **6b-3** was obtained as white solid (1.65 g, 71%). Spectral data are in agreement with literature value.^[10]

¹H NMR (400 MHz, CDCl₃) δ 8.06 – 8.04 (m, 2H), 7.55 – 7.61 (m, 1H), 7.48 – 7.44 (m, 2H), 4.51 (dd, *J* = 11.7, 4.5 Hz, 1H), 4.38 (dd, *J* = 11.7, 6.7 Hz, 1H), 3.80 – 3.86 (m, 1H), 3.69 – 3.65 (m, 1H), 2.58 (d, *J* = 5.8 Hz, 1H), 2.21 (d, *J* = 5.5 Hz, 1H), 1.64 – 1.35 (m, 4H), 0.95 (t, *J* = 7.1 Hz, 3H).

¹³C NMR (101 MHz, CDCl₃) δ 167.2, 133.5, 129.9, 129.8, 128.6, 72.5, 71.3, 66.7, 35.7, 19.0, 14.1.

3. ((4R,5R)-2,2-dimethyl-5-propyl-1,3-dioxolan-4-yl)methyl benzoate (**6b-4**)



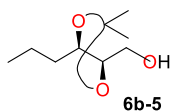
Following the modified literature procedure.^[10]

Catalytic amount of PTSA was dissolved in a solution of 1.5 g of benzoate **6b-3** (6.3 mmol, 1 eq) in 30 ml of dry DCM at 0 °C, followed by dropwise addition of 5 ml 2,2-dimethoxypropane. The cooling bath was removed and the reaction was allowed to stir for 3 h at RT. After the reaction was quenched with 5 ml of Et₃N, evaporated to give crude material, which was purified by column chromatography (*i*Hex/EtOAc = 20/1, R_f 0.24). Product **6b-4** was obtained as colorless liquid (1.66 g, 95 %). Spectral data are in agreement with literature value.^[10]

¹H NMR (400 MHz, CDCl₃) δ 8.08 – 8.05 (m, 2H), 7.59 – 7.55 (m, 1H), 7.47 – 7.42 (m, 2H), 4.50 (dd, *J* = 11.9, 3.4 Hz, 1H), 4.36 (dd, *J* = 11.9, 5.1 Hz, 1H), 4.00 – 3.90 (m, 2H), 1.68 – 1.38 (m, 10H), 0.96 (t, *J* = 7.2 Hz, 3H).

¹³C NMR (101 MHz, CDCl₃) δ 166.5, 133.3, 129.9, 129.8, 128.6, 109.2, 79.1, 77.8, 64.8, 35.3, 27.5, 27.1, 19.4, 14.3.

4. ((4R,5R)-2,2-dimethyl-5-propyl-1,3-dioxolan-4-yl)methanol (**6b-5**)



Following the modified literature procedure.^[10]

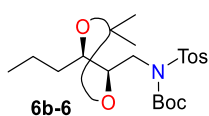
1.6 g of K₂CO₃ (11.5 mmol, 2 eq) were added in one portion to a stirring solution of 1.6 g of benzoate **6b-4** (5.75 mmol, 1 eq) in 30 ml of MeOH at 0 °C. The reaction was allowed to stir for 3 h at RT. After, the reaction mixture was concentrated under reduced pressure at RT, redissolved in 100 ml of water and extracted with EtOAc (3 × 50 ml). Organic layers were combined, dried over MgSO₄ and evaporated to give crude material, which was purified by column chromatography (*i*Hex/EtOAc = 4/1, R_f 0.22).

Product **6b-5** was obtained as colorless oil (0.91 g, 91%). Spectral data are in agreement with literature value.^[10]

¹H NMR (400 MHz, CDCl₃) δ 3.90 – 3.85 (m, 1H), 3.81 – 3.76 (m, 1H), 3.74 – 3.70 (m, 1H), 3.61 – 3.55 (m, 1H), 2.05 (dd, *J* = 7.7, 4.8 Hz, 1H), 1.65 – 1.29 (m, 10H), 0.94 (t, *J* = 7.2 Hz, 3H).

¹³C NMR (101 MHz, CDCl₃) δ 108.7, 81.6, 76.7, 62.1, 35.3, 27.5, 27.2, 19.4, 14.3.

5. Tert-butyl (((4R,5R)-2,2-dimethyl-5-propyl-1,3-dioxolan-4-yl) methyl) (tosyl) carbamate (**6b-6**)



Following the modified literature procedure.^[11]

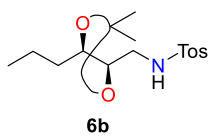
To a stirring solution of 0.85 g of alcohol **6b-5** (4.9 mmol, 1 eq), 1.6 g of triphenylphosphine (5.4 mmol, 1.1 eq), 1.6 g of *N*-Boc-*N*-p-toluenesulfonamide (5.4 mmol, 1.1 eq) was added dropwise 2.5 mL of 2.2 M DEAD (5.4 mmol, 1.1 eq) in THF at 0 °C. The reaction mixture was stirred overnight at RT and evaporated under reduced pressure. Crude material was purified by column chromatography (*i*Hex/EtOAc = 10/1, *R_f* 0.27). Product **6b-6** was obtained as colorless oil (1.8 g, 86%).

¹H NMR (400 MHz, CDCl₃) δ 7.89 – 7.85 (m, 2H), 7.31 – 7.27 (m, 2H), 4.18 – 4.11 (m, 1H), 3.97 – 3.84 (m, 3H), 2.43 (s, 3H), 1.63 – 1.38 (m, 10H), 1.33 (s, 9H), 0.94 (t, *J* = 7.2 Hz, 3H).

¹³C NMR (101 MHz, CDCl₃) δ 151.1, 144.3, 137.5, 129.3, 128.3, 108.9, 84.6, 79.3, 79.2, 48.6, 35.3, 28.0, 27.6, 27.1, 21.8, 19.4, 14.2.

HRMS (ESI): calcd for C₂₁H₃₃NO₆SNa [M + Na]⁺, 450.1921; found 450.1922.

6. *N*-(((4R,5R)-2,2-dimethyl-5-propyl-1,3-dioxolan-4-yl)methyl)-4-methylbenzene sulfonamide **6b**



Following the modified literature procedure.^[12]

1.8 g of obtained carbamate **6b-6** was dissolved in 40 ml of dry MeOH. 3 g K₂CO₃ was added in one portion, the resulting reaction mixture was refluxed for 3 h and cooled down to RT. 50 ml of water was added, the aqueous phase was extracted with DCM (3 x 50 ml). Organic layers were combined, dried over MgSO₄ and evaporated to give crude material, which was purified by column chromatography (*i*Hex/EtOAc = 10/1). Product **6b** was obtained as colorless oil (1.5 g, 94%).

¹H NMR (400 MHz, CDCl₃) δ 7.76 – 7.63 (m, 2H), 7.33 – 7.30 (m, 2H), 4.68 (t, *J* = 6.3 Hz, 1H), 3.76 – 3.72 (m, 1H), 3.65 (ddd, *J* = 8.1, 5.6, 3.3 Hz, 1H), 3.18 (ddd, *J* = 13.0, 6.3, 3.3 Hz, 1H), 2.98 (ddd, *J* = 13.0, 6.2, 5.7 Hz, 1H), 2.43 (s, 3H), 1.57 – 1.19 (m, 10H), 0.93 – 0.90 (m, 3H).

¹³C NMR (101 MHz, CDCl₃) δ 143.8, 136.8, 129.9, 127.2, 108.9, 79.1, 77.7, 44.2, 34.9, 27.4, 27.2, 21.7, 19.3, 14.2.

HRMS (ESI): calcd for C₁₆H₂₅NO₄SNa [M + Na]⁺, 350.1397; found 350.1399.

3.5.4. NMR Spectra of Reagents and Products

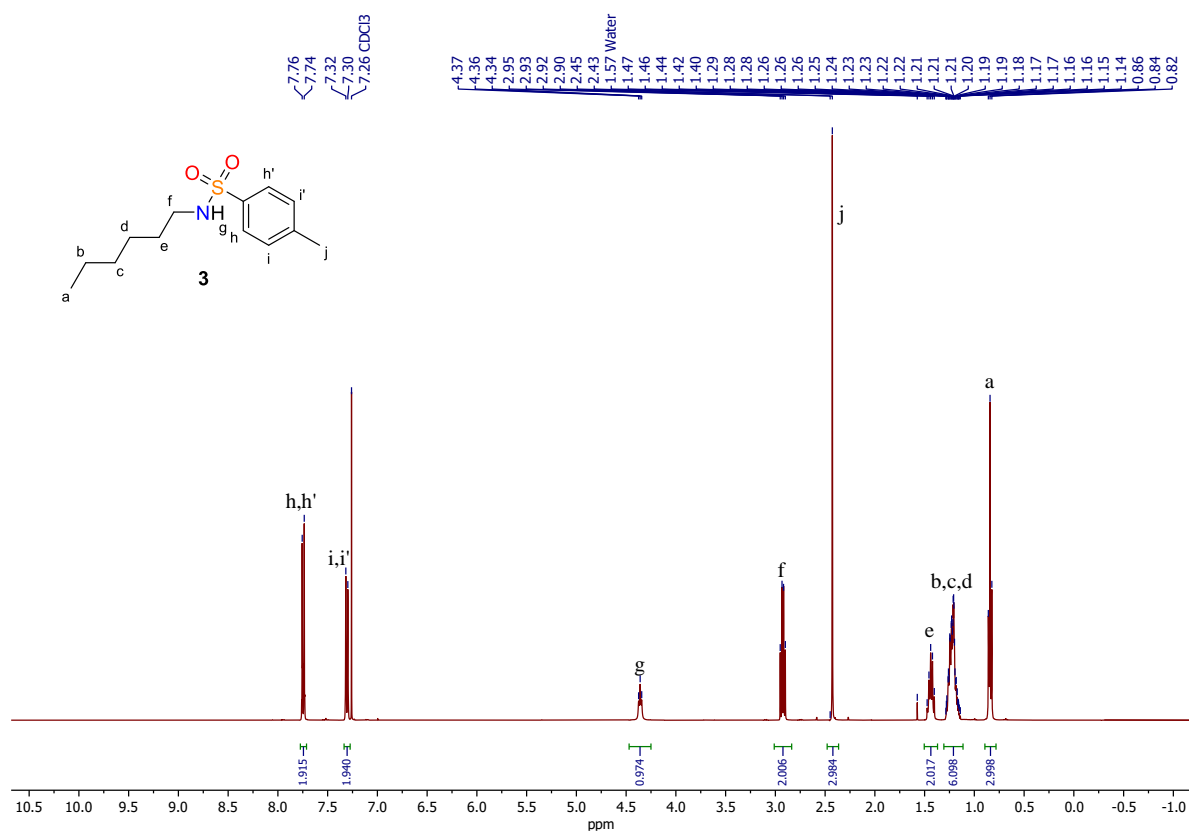


Fig. S8. ¹H NMR spectrum of sulfonamide **3**, CDCl₃, 400 MHz.

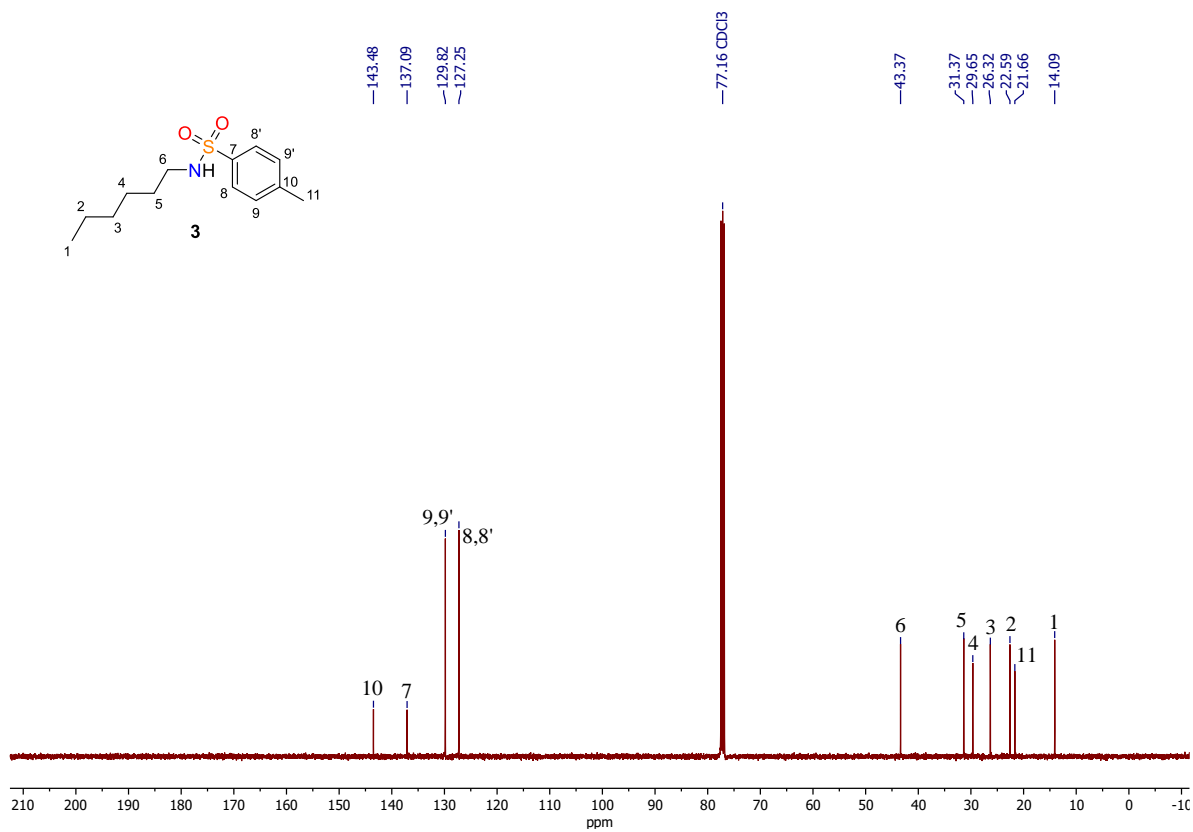


Fig. S9. ¹³C NMR spectrum of sulfonamide **3**, CDCl₃, 101 MHz.

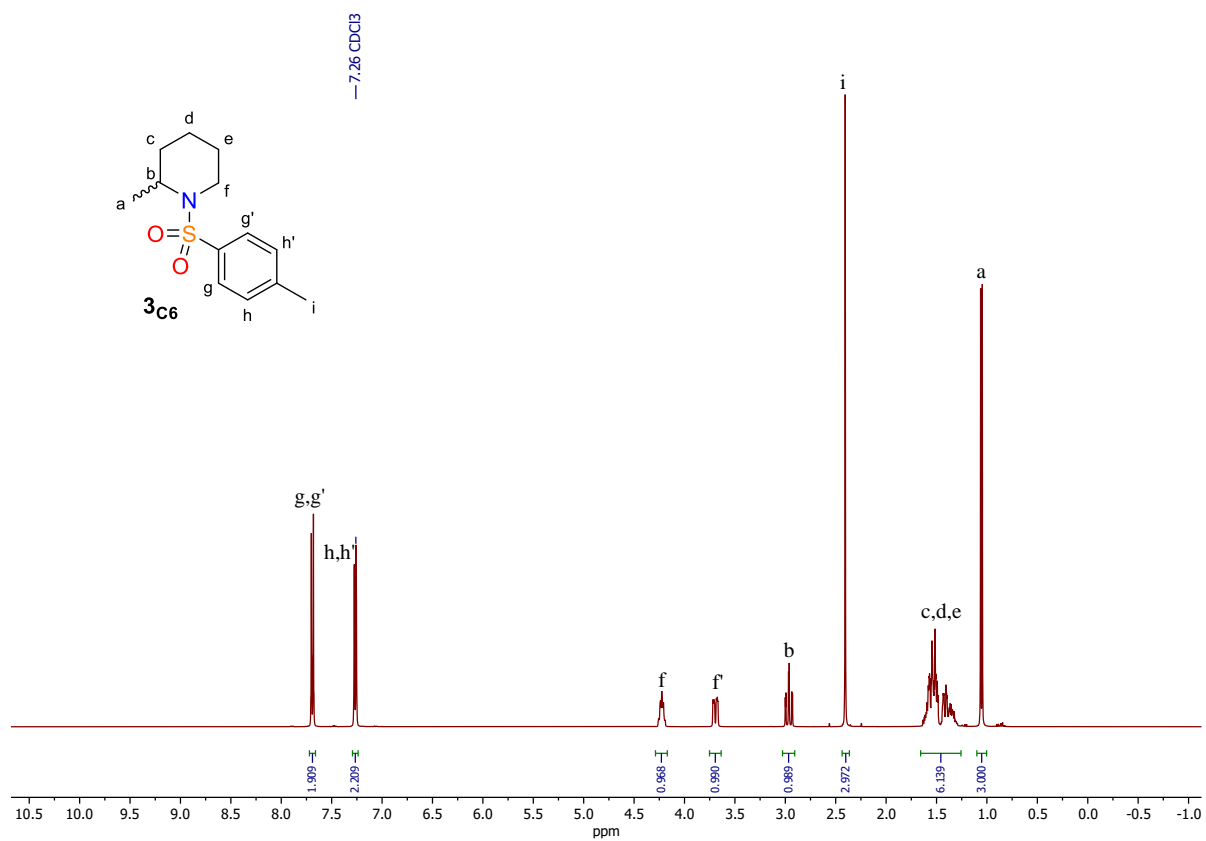


Fig. S14. ^1H NMR spectrum of 2-methylpiperidine **3C6**, CDCl_3 , 400 MHz.

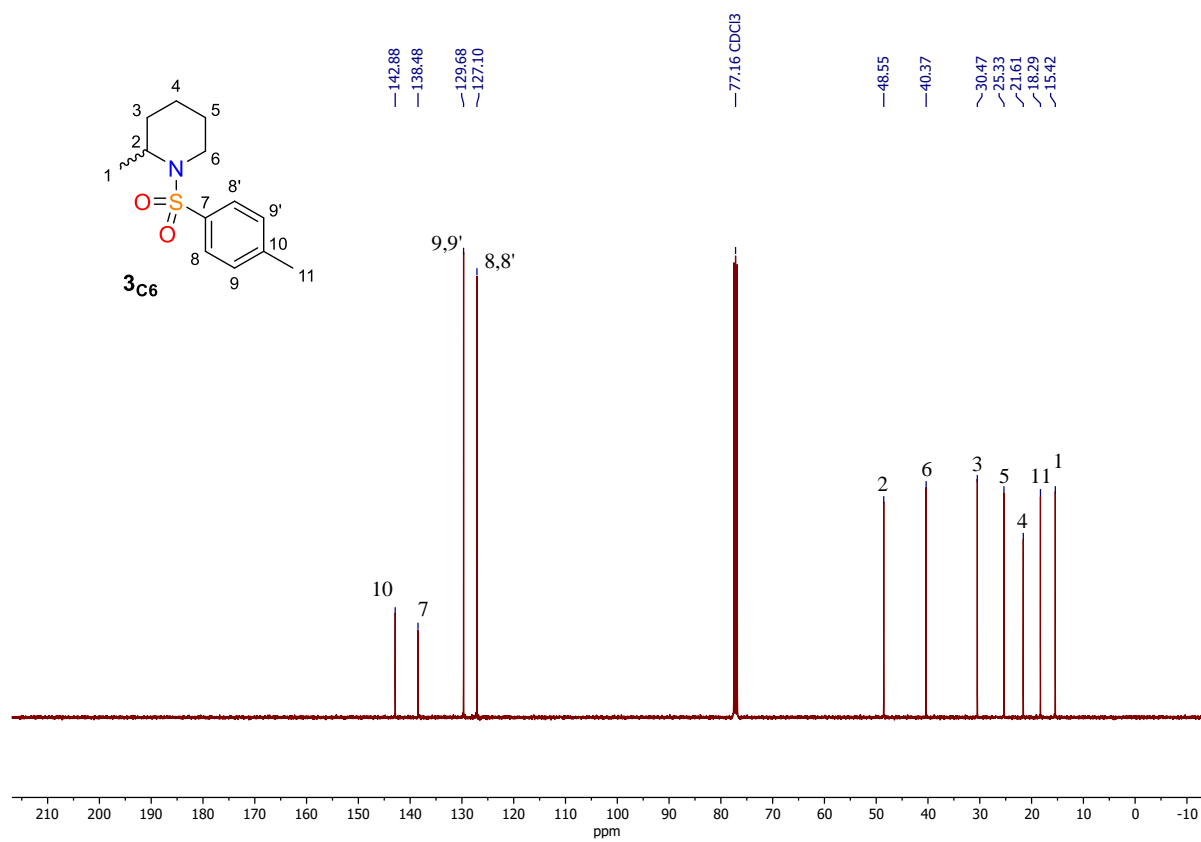


Fig. S15. ^{13}C NMR spectrum of 2-methylpiperidine **3C6**, CDCl_3 , 101 MHz.

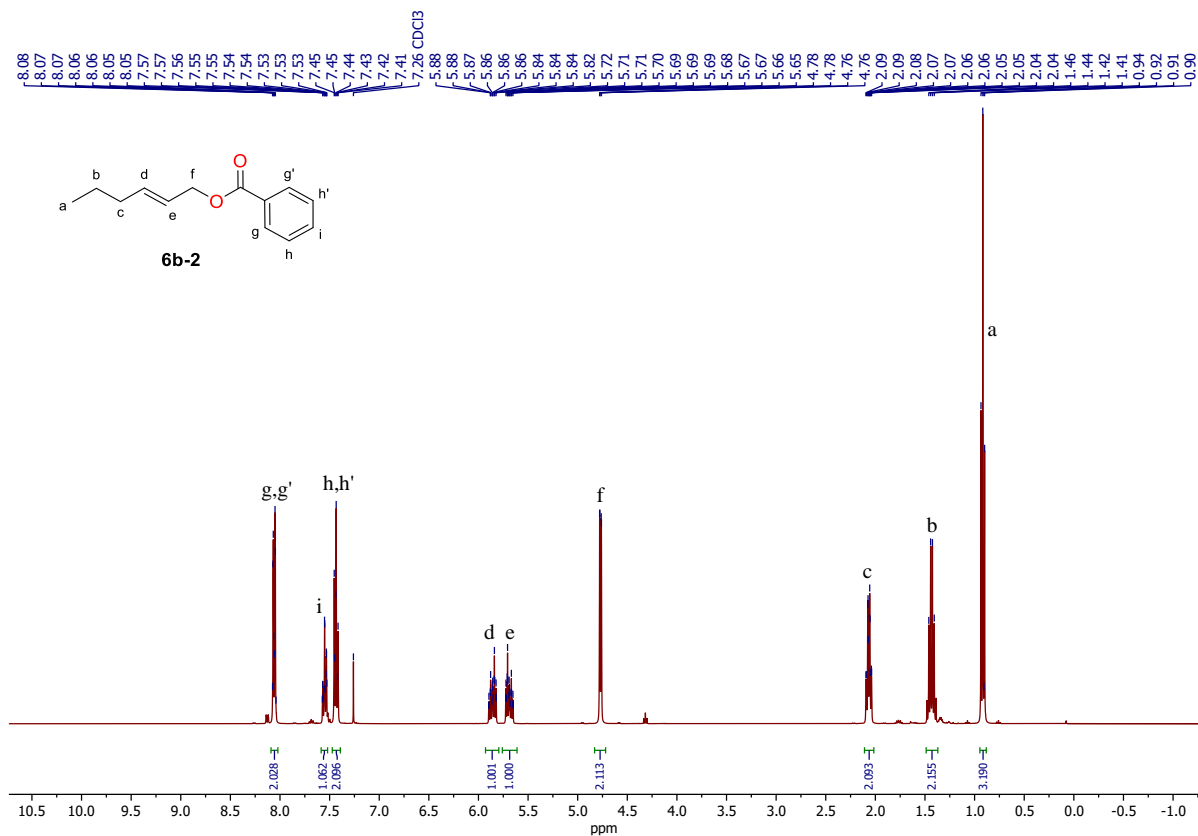


Fig. S16. ¹H NMR spectrum of (E)-hex-2-enyl benzoate **6b-2**, CDCl₃, 400 MHz.

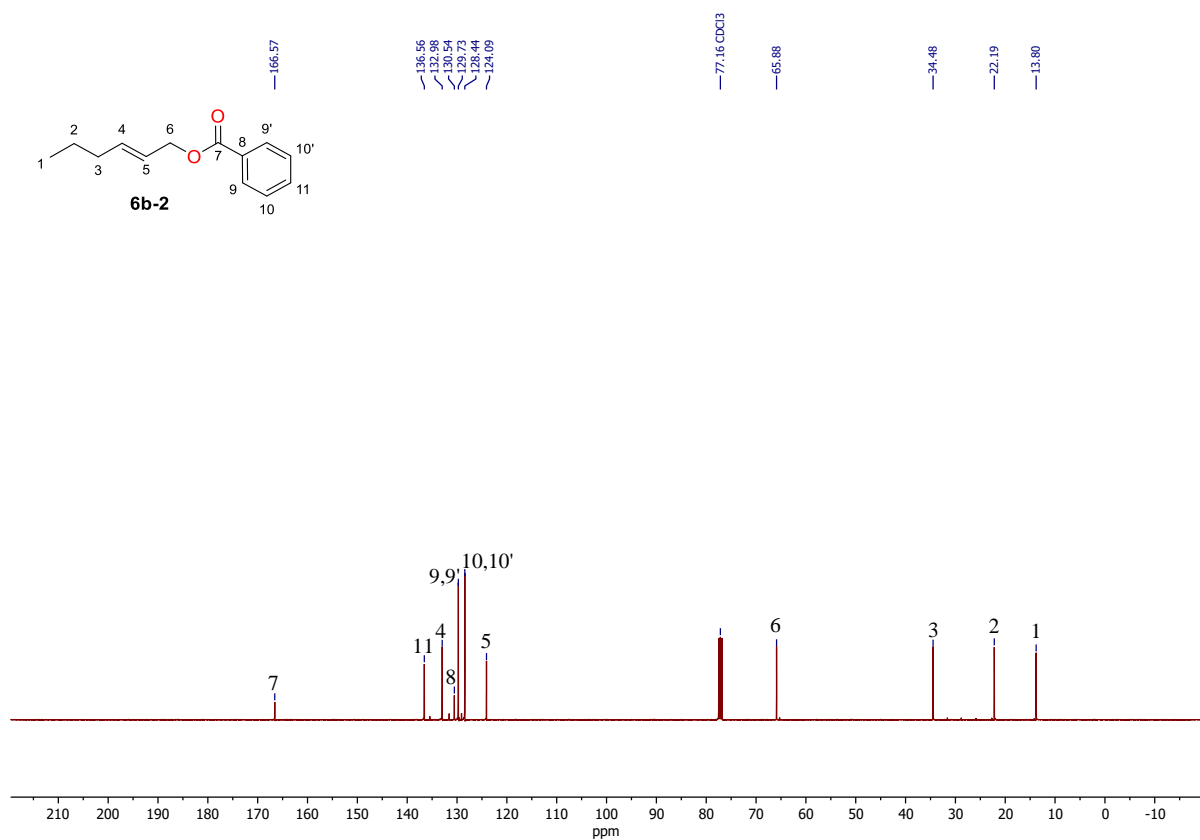
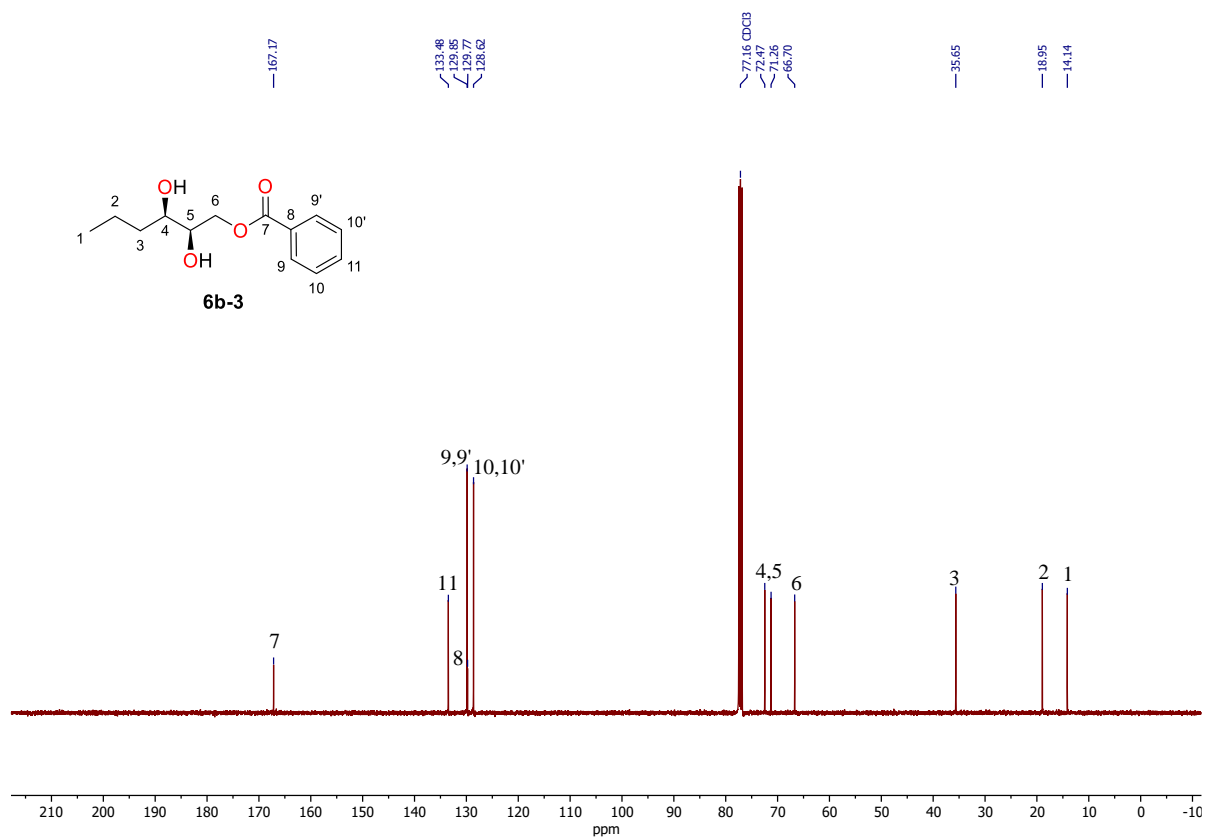
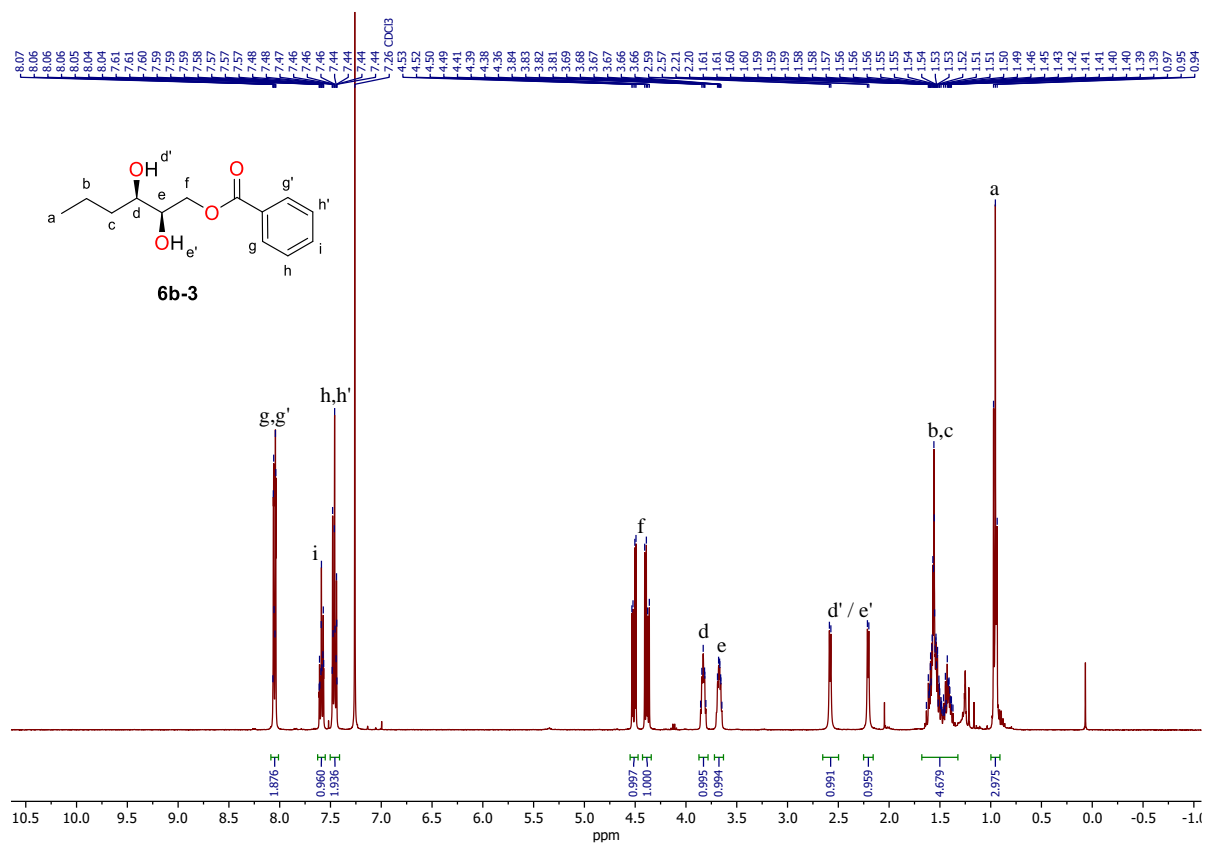


Fig. S17. ¹³C NMR spectrum of (E)-hex-2-enyl benzoate **6b-2**, CDCl₃, 101 MHz.



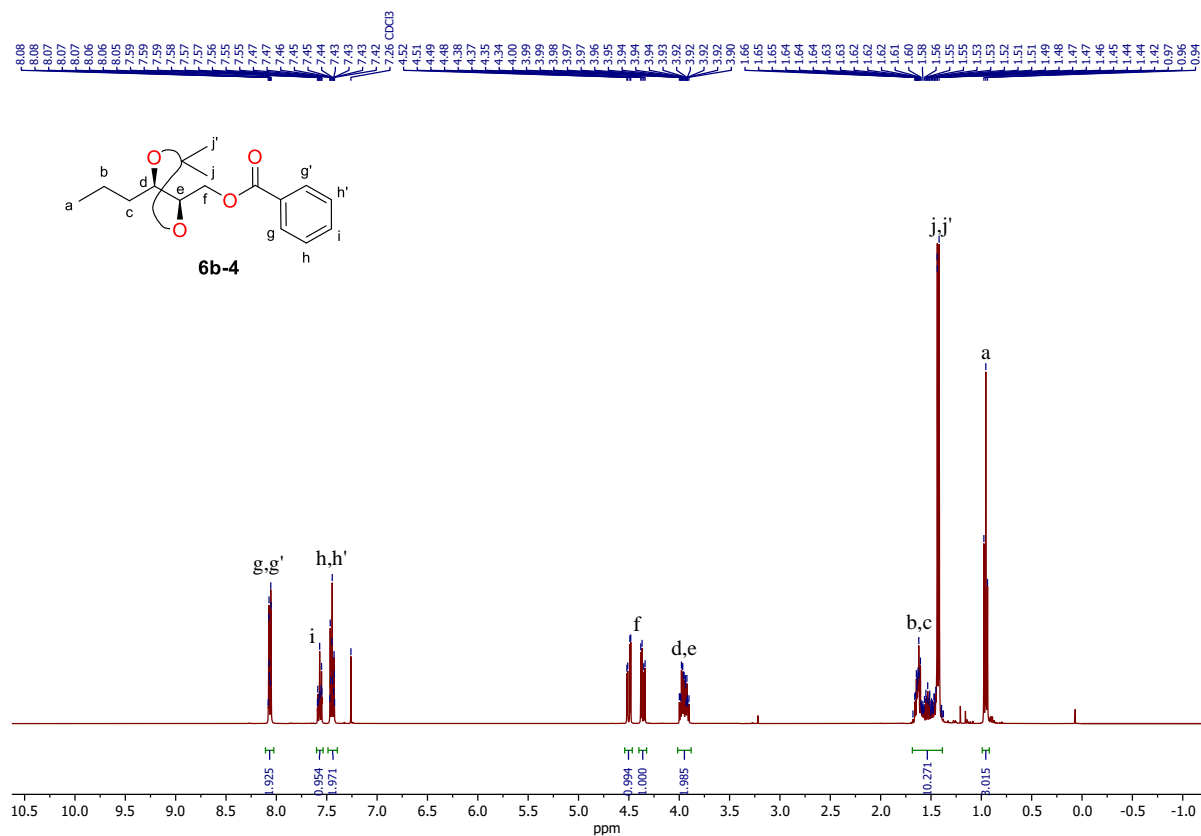


Fig. S20. ^1H NMR spectrum of **6b-4**, CDCl_3 , 400 MHz.

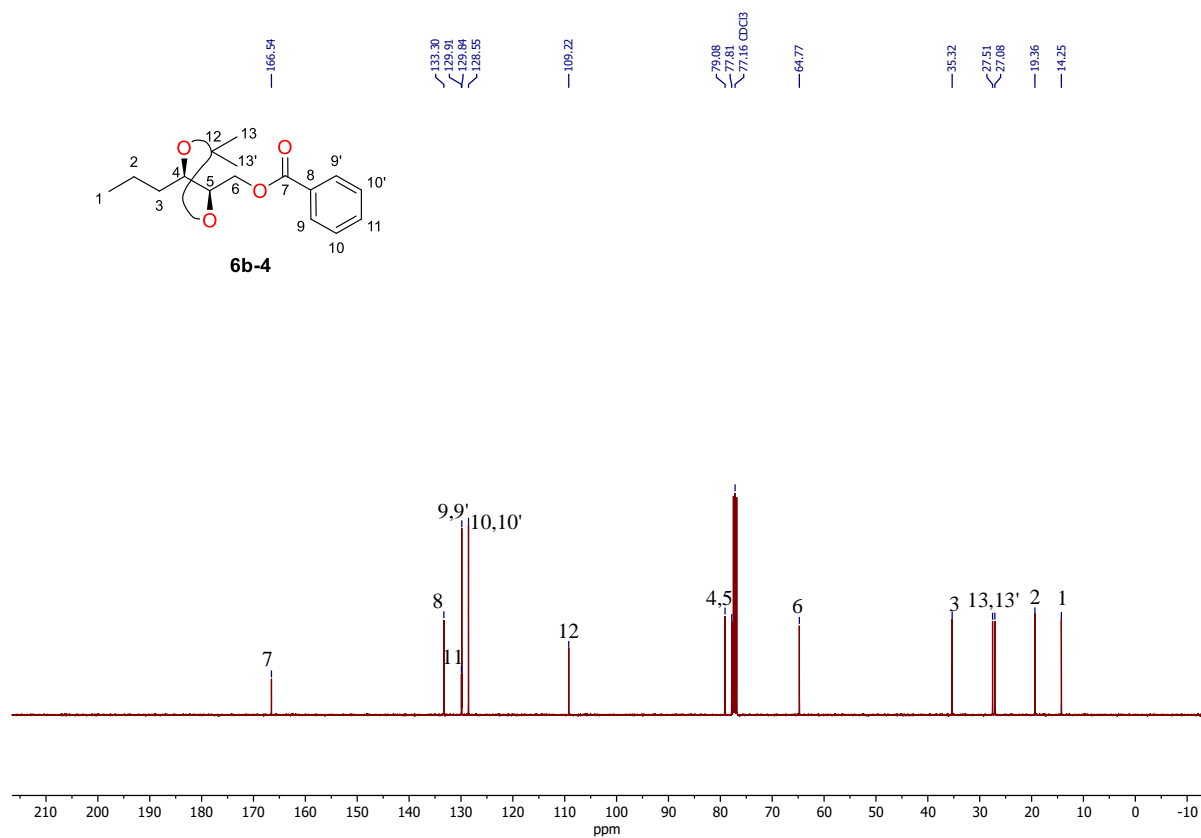


Fig. S21. ^{13}C NMR spectrum of **6b-4**, CDCl_3 , 101 MHz.

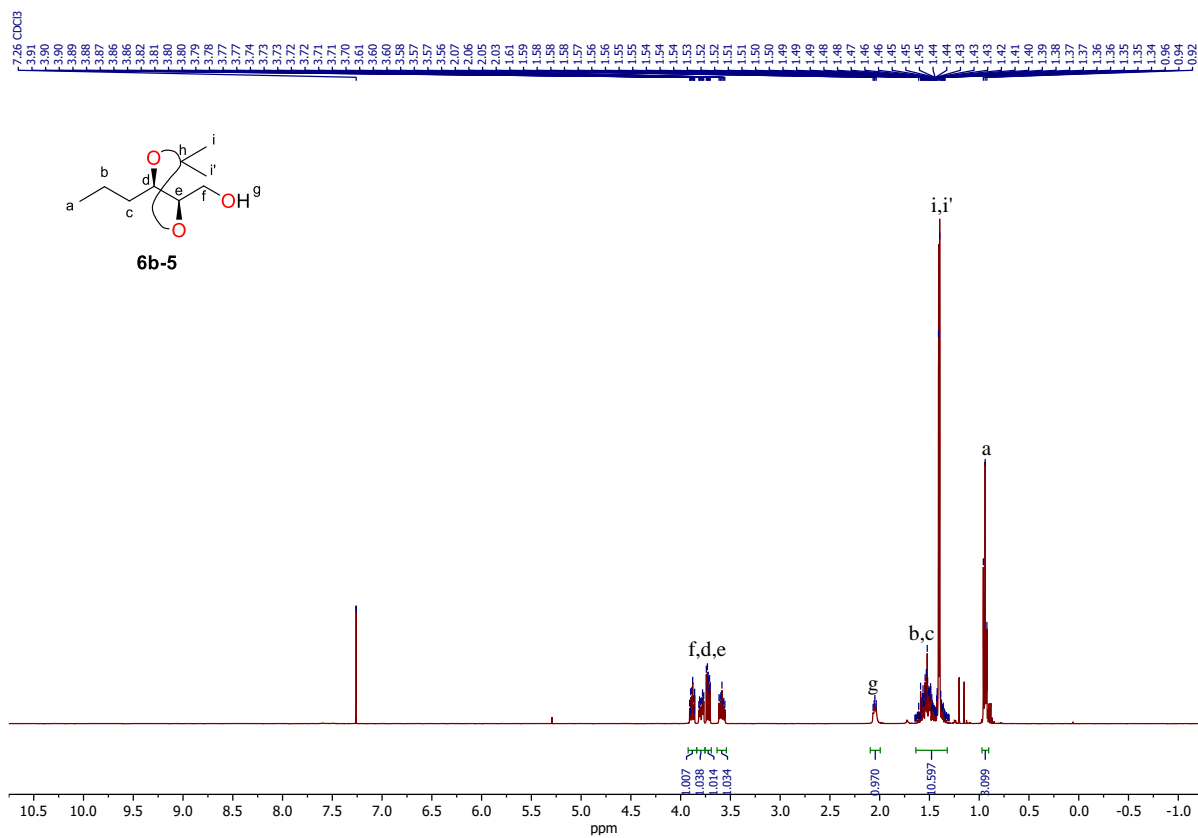


Fig. S22. ¹H NMR spectrum of **6b-5**, CDCl₃, 400 MHz.

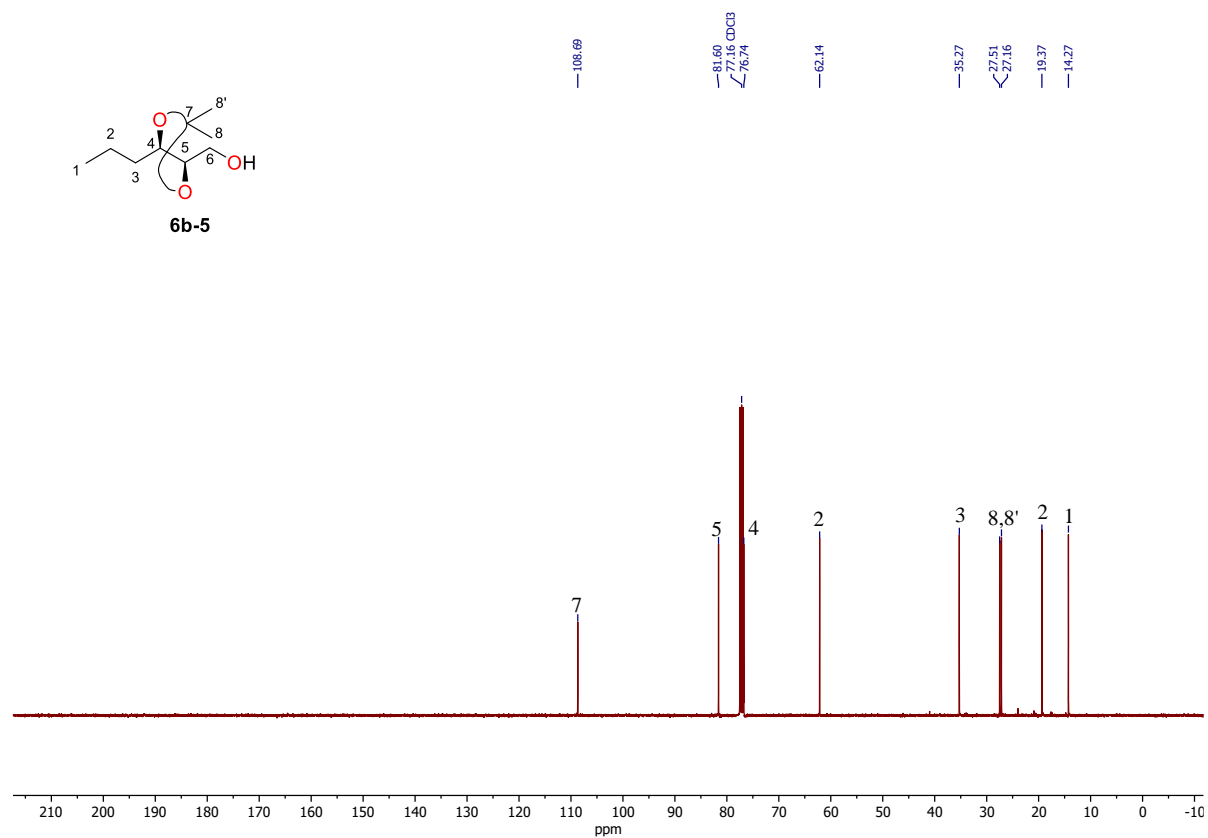
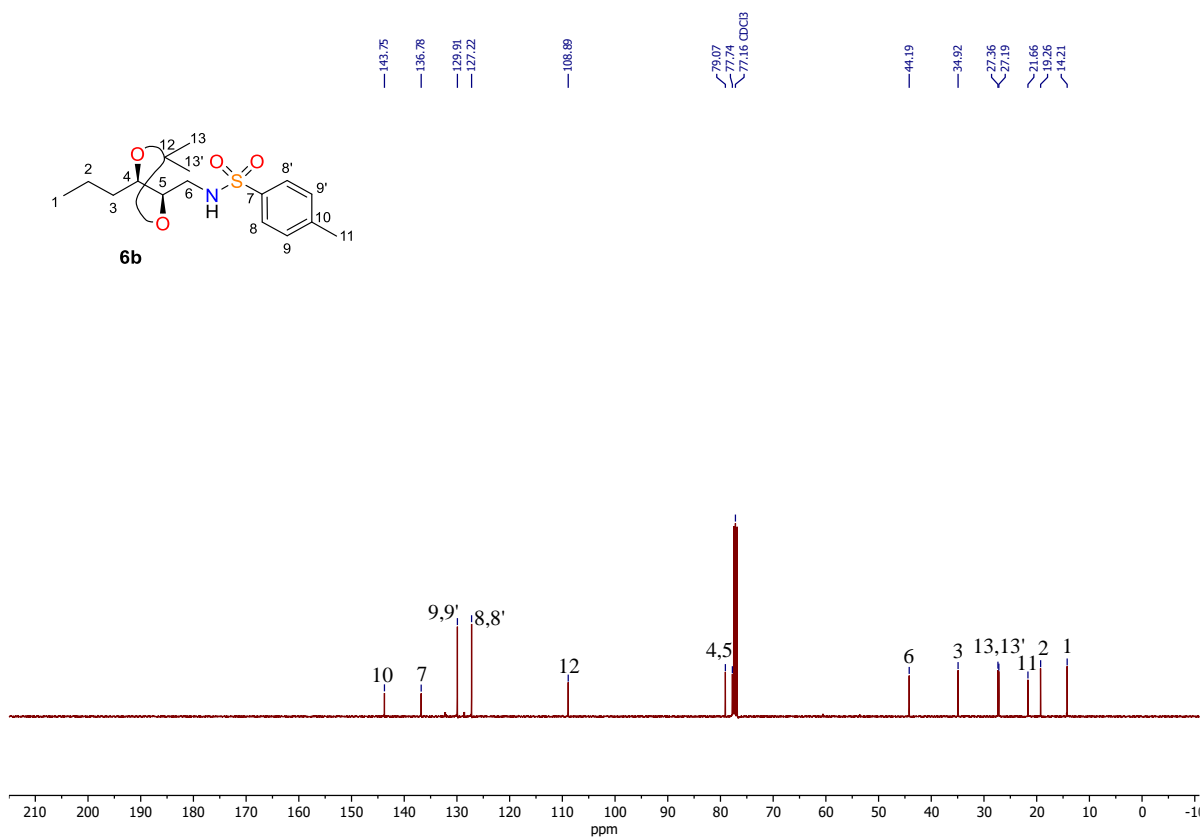
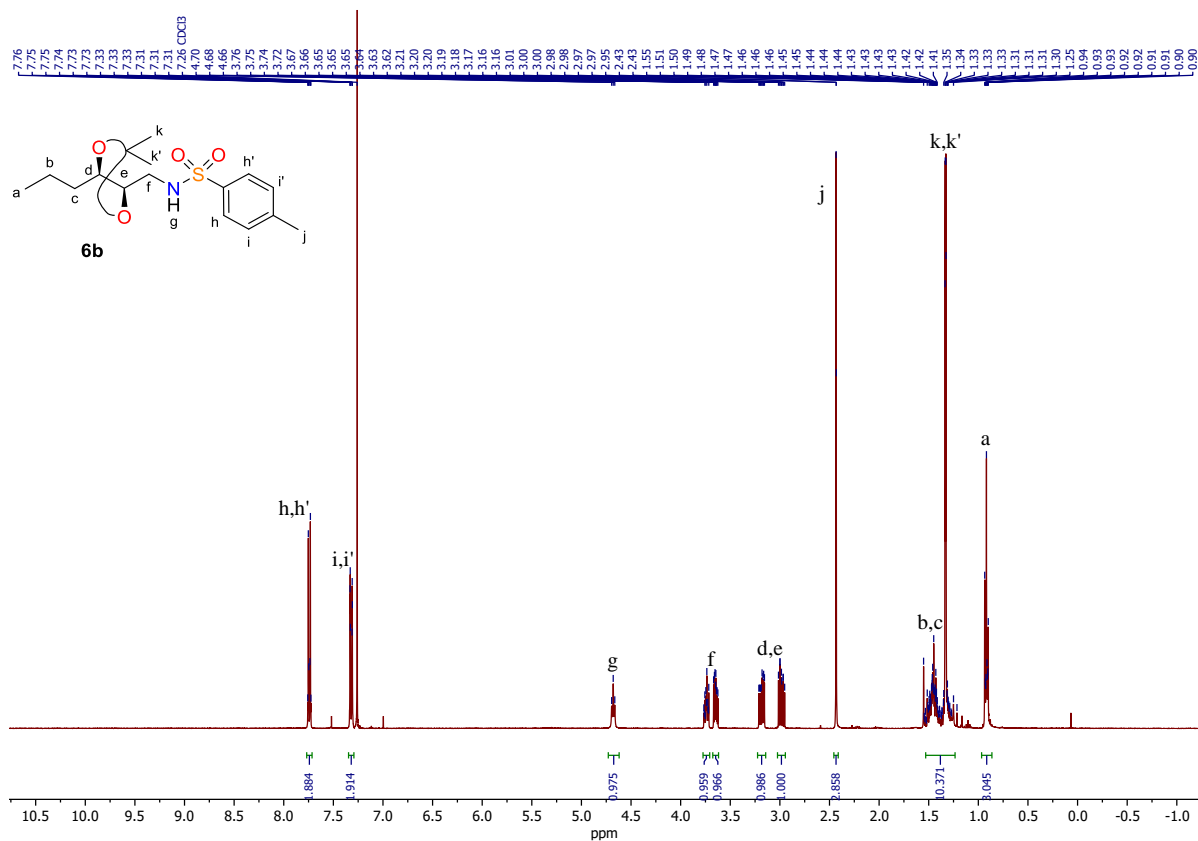


Fig. S23. ¹³C NMR spectrum of **6b-5**, CDCl₃, 101 MHz.



3.5.4. References:

- [1] a) D. J. Henry, M. B. Sullivan, L. Radom, *J. Chem. Phys.* **2003**, *118*, 4849-4860; b) J. Hioe, D. Šakić, V. Vrček, H. Zipse, *Org. Biomol. Chem.* **2015**, *13*, 157-169; c) S. Shkunnikova, H. Zipse, D. Šakić, *Org. Biomol. Chem.* **2021**, *19*, 854-865.
- [2] F. Jensen, *J. Chem. Theory Comput.* **2008**, *4*, 719-727.
- [3] V. M. Rayón, J. A. Sordo, *J. Chem. Phys.* **2005**, *122*, 204303.
- [4] X. Tang, L. Huang, C. Qi, X. Wu, W. Wu, H. Jiang, *Chem. Commun.* **2013**, *49*, 6102-6104.
- [5] M. C. Marcotullio, V. Campagna, S. Sternativo, F. Costantino, M. Curini, *Synthesis* **2006**, *2006*, 2760-2766.
- [6] P. M. Esch, I. M. Boska, H. Hiemstra, R. F. de Boer, W. N. Speckamp, *Tetrahedron* **1991**, *47*, 4039-4062.
- [7] A. D. Jones, D. W. Knight, D. E. Hibbs, *J. Chem. Soc., Perkin Trans. 1* **2001**, 1182-1203.
- [8] S. Lee, H. Lei, T. Rovis, *J. Am. Chem. Soc.* **2019**, *141*, 12536-12540.
- [9] L. F. T. Novaes, J. S. K. Ho, K. Mao, K. Liu, M. Tanwar, M. Neurock, E. Villemure, J. A. Terrett, S. Lin, *J. Am. Chem. Soc.* **2022**, *144*, 1187-1197.
- [10] V. S. Mallula, B. Srinivas, P. Radha Krishna, *Tetrahedron Lett.* **2015**, *56*, 1115-1117.
- [11] T. Go, A. Morimatsu, H. Wasada, G. Tanabe, O. Muraoka, Y. Sawada, M. Yoshimatsu, *Beilstein J. Org. Chem.* **2018**, *14*, 2722-2729.
- [12] G. Zhang, L. Cui, Y. Wang, L. Zhang, *J. Am. Chem. Soc.* **2010**, *132*, 1474-1475.

List of Abbreviations

1,3,5-TMB	1,3,5-trimethoxybenzene	Nva	norvaline
[α] _D	specific rotation	OSu	succinimide ester
Abu	2-aminobutyric acid	PA	1-pentylamine
Ac	acetyl	Phe	Phenylalanine
Ac ₂ O	acetic anhydride	PIDA	phenyliodine(iii) diacetate
AcCl	acetyl chloride	PINO	phthalimide N-oxyl
Ala	alanine	PPh ₃	triphenylphosphine
APCI	atmospheric pressure chemical ionization	ppm	parts per million
BA	baicalein	Pro	proline
Boc	<i>tert</i> -butyloxycarbonyl	pXRD	powder x-ray diffraction
Boc ₂ O	di- <i>tert</i> -butyl dicarbonate	QM	quantum mechanics/mechanical
BSTFA	N,O-bis(trimethylsilyl)trifluoroacetamide	RPM	revolutions per minute
Bz	benzoyl	RT	room temperature
CumO•	cumyloxy radical	Sar	Sarcosine
DBA	dehydrobaicalein	scXRD	single crystal x-ray diffraction
DCC	N,N'-dicyclohexylcarbodiimide	Ser	Serine
DCE	dichloroethane	TAP	2,3,4-trihydroxyacetophenone
DCHN	dicumylhyponitrite	<i>t</i> -BuOH	<i>tert</i> -butyl alcohol
DCM	dichloromethane	TEMPO	(2,2,6,6-tetramethylpiperidin-1-yl)oxyl
DCPO	dicumylperoxide	TFA	trifluoroacetic acid
DCU	1,3-dicyclohexyl urea	THF	tetrahydrofuran
DEAD	diethyl azodicarboxylate	TLC	thin-layer chromatography
DFT	density functional theory	Tle	<i>tert</i> -leucine
DIPEA	N,N-diisopropylethylamine	Val	Valine
DLPNO	domain based local pair natural orbital	μ l	Microliter
DMAP	4-dimethylaminopyridin		
DMF	dimethyl formamid		
DMSO	dimethyl sulfoxide		
DPI	dipentylimine		
dr	diastereomeric ratio		
DTBHN	di- <i>tert</i> -butyl hyponitrite		
DTBPO	di- <i>tert</i> -butyl peroxide		
ECF	ethyl chloroformate		
EDC×HCl	1-ethyl-3-(3-dimethylaminopropyl)carbodiimide hydrochloride		
Elem	elemental analysis		
eq	equivalent(s)		
ESI	electrospray ionization		
<i>et al</i>	"and others"		
Et ₂ O	diethyl ether		
EtOAc	ethyl acetate		
FID	flame ionization detector		
FTIR	Fourier-transform infrared spectroscopy		
GC	gas chromatography		
Gly	glycine		
h	hour(s)		
HAT	hydrogen atom abstraction		
hept	n-heptan		
hIAPP	human islet amyloid polypeptide		
HLF	Hofmann-Löffler-Freytag		
HOBt	hydroxybenzotriazole		
HPLC	high-performance liquid chromatography		
HRMS	high resolution mass spectrometry		
IBCF	isobutyl chloroformate		
<i>i</i> Hex	<i>iso</i> hexane		
<i>i</i> PrOH	isopropyl alcohol		
IS	internal standard		
KIE	kinetic isotope effect		
KOtBu	potassium <i>tert</i> -butylate		
Leu	leucine		
LFP	laser flash photolysis		
MeCN	acetonitrile		
MeI	methyl iodide		
MeOH	methanol		
MS	mass spectrometry		
NEt ₃	triethylamine		
Nle	norleucine		
NMR	nuclear magnetic resonance spectroscopy		